A Color Guide to the Petrography of Carbonate Rocks:
Grains, textures, porosity, diagenesis

Peter A. Scholle

Director, New Mexico Bureau of Geology and Mineral Resources, New Mexico Institute of Mining & Technology, Socorro, NM 87801

Dana S. Ulmer-Scholle

Senior Research Scientist, New Mexico Institute of Mining & Technology, Socorro, NM 87801

AAPG Memoir 77

Published by
The American Association of Petroleum Geologists
Tulsa, Oklahoma, U.S.A.

2003

Printed in Canada

ISBN: 0-89181-358-6

AAPG Editor: John C. Lorenz
Executive director: Richard D. Fritz
Geoscience Director: J. B. "Jack" Thomas

This and other AAPG publications are available from:
The AAPG Bookstore
P. O. Box 979
Tulsa, OK 74101-0979
Phone: 1-918-584-2555 or 1-800-364-AAPG (USA—book orders only)
Fax: 1-918-560-2652 or 1-800-898-2274 (USA)
www.aapg.org • email: bookstore@aapg.org

About the Authors

Peter A. Scholle received his B.S. in Geology from Yale University in 1965. After spending a year on a Fulbright-DAAD fellowship at the University of Munich in Germany, and another year at the University of Texas at Austin (mainly taking petrography classes from Bob Folk), he went to Princeton University, receiving his Ph.D. in geology in 1970. His dissertation work, on deep-water carbonate turbidites in the Italian Apennines, was supervised by Al Fischer.

Peter's professional career has covered a wide range of employment, including state and federal government, the petroleum industry, and academia. He worked for five years for various oil companies (Cities Service, Gulf and Chevron) and consulted for other oil companies for many years. Nine years were spent with the U. S. Geological Survey in Reston (VA) and Denver (CO), including three years as chief of the Oil and Gas Branch. He taught at the University of Texas at Dallas for three years and was Albritton Professor of Geology at Southern Methodist University in Dallas from 1985 to 1999. At SMU, he taught courses in geology, environmental science, and oceanography and developed computer-based instructional media. He also had the good fortune to teach field seminars in carbonate sedimentology and reef ecology in places such as the Cayman Islands, Barbados, and the Bahamas. Since 1999, he has been at the New Mexico Institute of Mining and Technology in Socorro where he is the State Geologist and Director of the New Mexico Bureau of Geology and Mineral Resources (the state geological survey).

Peter also devoted much of his time in those jobs to carbonate research and writing. His major interests were (and remain) in deep-water carbonates (especially chalks) as well as the diagenesis and petroleum potential of Permian carbonate and evaporite deposits in many areas of the world. He has worked in nearly 30 countries and has written, coauthored, or edited eight books, more than 150 papers and abstracts, 23 CD-ROMs, and a number of other computer or audio-visual products. Peter has been a member of AAPG and SEPM since 1976-77; he is a GSA Fellow and a member of IAS, AASG, AIPG, and several local societies. He was an AAPG Distinguished Lecturer (1975-76) and received the AAPG President's award twice, the Sproule Memorial Award, and the AAPG Certificate of Merit. He served as president and special publications editor of SEPM and is now an honorary member of that society.

Dana S. Ulmer-Scholle developed an early love of carbonate rocks and fossils while growing up on the classic Upper Ordovician outcrops around Cincinnati, Ohio. She received a B.S. degree in 1981 from the University of Cincinnati (under the tutelage of Drs. Wayne Pryor and Paul Potter). While at the University of Cincinnati, an Amoco Fellowship provided her with an opportunity to work at Amoco Oil and Gas Co. each summer during her undergraduate career. Dana completed an M.S. degree at Southern Methodist University in Dallas, TX, in 1983, working on the Mississippian Arroyo Peñasco Group of New Mexico (with Robert Laury). After a stint working for ARCO Exploration Co., she returned to SMU for a Ph.D. (received in 1992). Her dissertation research, done with Peter Scholle and Robert Laury, concentrated on evaporite-related diagenesis in upper Paleozoic carbonate rocks from New Mexico, Wyoming and Greenland.

Dana has worked, or consulted, for a number of companies including ARCO Exploration, ARCO International, Mobil Research, and Maersk Oil and Gas. She was the technical editor for SEPM Special Publications from 1994-1997 and managed SMU's student computer labs for several years where she developed an interest in computer-based learning. She had co-led student trips to the Cayman Islands as well as AAPG Field Seminars (with Peter and Robert Goldstein) to the Permian Reef Complex in West Texas/New Mexico and Mississippian and Pennsylvanian bioherms in New Mexico. Dana is a Senior Research Scientist at the New Mexico Institute of Mining and Technology and is an adjunct faculty member in the Department of Earth and Environmental Sciences. She currently teaches carbonate-related courses including petrography, depositional/diagenetic models, and field studies. Her research interests continue to include carbonate sedimentology and diagenesis, petrography, low-temperature isotope and trace element geochemistry, fluid inclusion analysis, and fluid flow histories in carbonate rocks. Since arriving at New Mexico Tech, however, she has also become involved in environmental investigations that include heavy-metals bioremediation.

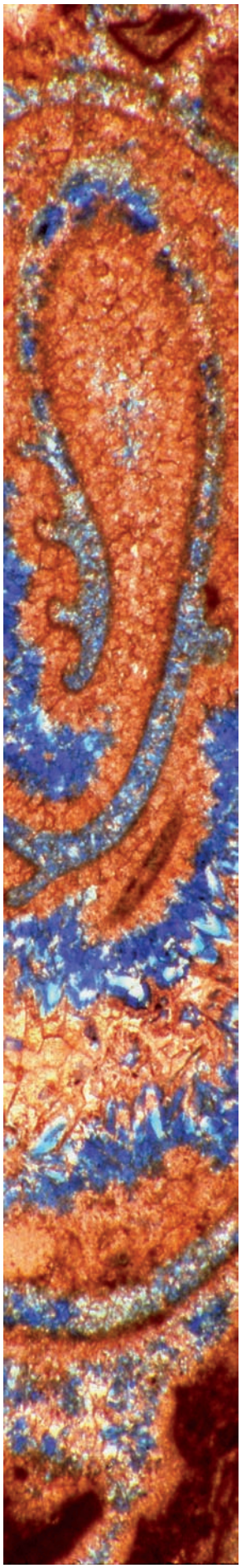

Table of Contents

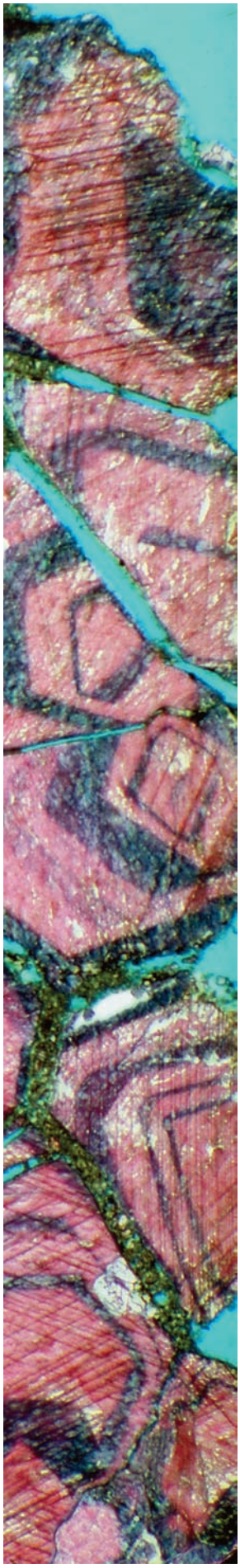

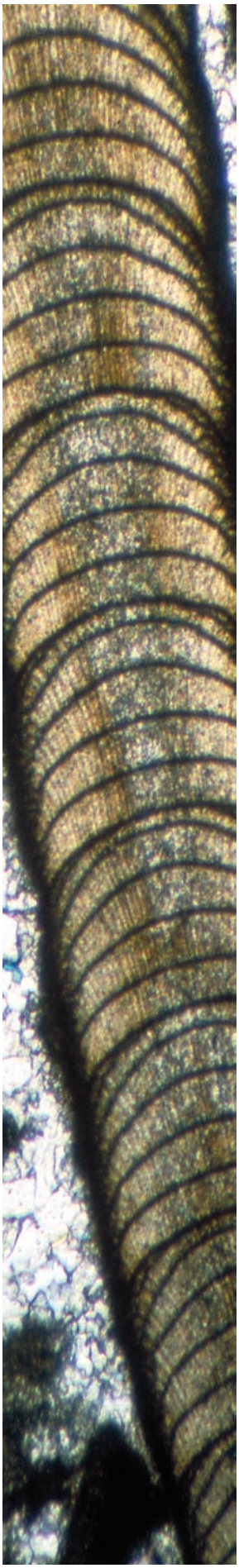

INTRODUCTION

Carbonate petrography — the study of limestones, dolomites and associated deposits under optical or electron microscopes —greatly enhances field studies or core observations and can provide a frame of reference for geochemical studies. Petrography is an especially powerful tool because it enables the identification of constituent grains, the detailed classification of sediments and rocks, the interpretation of environments of deposition, and the determination of the often complex history of post-depositional alteration (diagenesis). The last of these, the ability to determine the timing of diagenetic events such as cementation or secondary porosity development relative to the emplacement of hydrocarbons or metallic ores, makes petrography an important component of geochemical and sedimentologic studies in energy- and mineral-resource exploration applications as well as in academic research.

The petrographic study of carbonate rocks is particularly useful because carbonate grains, unlike clastic terrigenous ones, normally are produced in close proximity (from less than a meter to hundreds of meters) to the site of their ultimate deposition. In addition, carbonate grains are formed mainly by organisms, and thus the grains convey ecological information about the environment of formation as well as stratigraphical information on the age of the deposit.

In some ways, carbonate petrography is not a very complex undertaking, especially when compared to the petrography of clastic terrigenous deposits. Most carbonate rocks are dominated by just one or two common carbonate minerals (mainly calcite and dolomite) plus a limited number of accompanying minerals — silica, detrital grains, phosphate, glauconite, and a few evaporite precipitates. The diagram below shows the general compositions of the full spectrum of carbonate minerals found in modern and ancient strata.

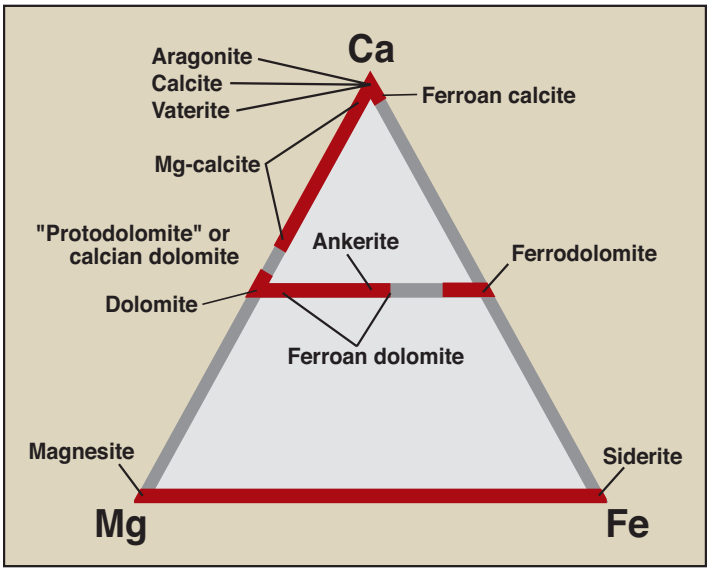

In other ways, however, carbonate petrography can be quite complicated. Many different organisms produce carbonate material and that requires learning how to recognize a wide variety of shell morphologies and wall structures. The changing assemblages of organisms through time (see diagram near the end of this introduction), coupled with the randomness of thin section cuts through complex shell forms, add to the difficulty of identifying skeletal grains. Furthermore, because many primary carbonate grains are composed of unstable minerals (especially aragonite and high-Mg calcite), diagenetic alteration commonly is quite extensive in carbonate rocks. The variability of inorganic and biogenic carbonate mineralogy through time, however, complicates prediction of patterns of diagenetic alteration.

This book is designed to help deal with such challenges. It is by no means a complete treatise or textbook — that would be essentially impossible in a single volume. It does, however, include a wide variety of examples of commonly encountered skeletal and nonskeletal grains, cements, fabrics, and porosity types. It also encompasses a number of noncarbonate grains, that occur as accessory minerals in carbonate rocks or that may provide important biostratigraphic or paleoenvironmental information in carbonate strata. With this guide, students and other workers with little formal petrographic training should be able to examine thin sections or acetate peels under the microscope and interpret the main rock constituents and their depositional and diagenetic history.

Carbonate petrography is primarily a qualitative skill. One must learn to recognize the distinguishing characteristics of skeletal grains of various ages, cut in various orientations, and preserved in various stages of alteration. There are no simple diagnostic tests (such as measuring birefringence or an optic figure) that can be used to identify a bryozoan, for example. It is simply a question of experience. Comparison of grains in thin sections with photographs of identified grains, in this and other books, allows geologists to readily identify the majority of the rock-forming grains in their samples. A selected bibliography is provided to permit the interested reader to pursue details that are only briefly covered in this book and to supplement the interpretive aspects of petrographic work. A chart is also provided at the end of this chapter to facilitate accurate estimation of abundances of grains. For greater accuracy, however, quantitative point counting or image analysis should be done and references to these methods are provided in the Techniques chapter.

Most pictures in this book were chosen to illustrate typical rather than spectacular, but unusual, examples of grains and fabrics. For example, grains that were originally composed of aragonite normally undergo wholesale diagenetic alteration and extensive destruction of primary structural features. Therefore, we show examples of these grains in their extensively altered state because that is the norm for what the user will encounter. Introductory text in each chapter provides the reader with details about original grain mineralogies in order to help the reader anticipate such preservation problems. Examples also were specifically chosen from a variety of countries, basins, and units to provide a sense of the global consistency of carbonate fabrics. Furthermore, examples have been included from rocks of Precambrian to

Holocene age because of the enormous evolutionary changes in organisms (and, therefore, carbonate deposits and their alteration) through time.

In terms of the overall costs of energy exploration or academic geoscience today, the financial investment needed for petrographic work is relatively insignificant. A basic polarizing microscope can be purchased currently for $2000 to $25,000 depending on optical quality, accessories, and other factors. Thin sections can be purchased for $8 to $20 each from a number of commercial labs. Acetate peels (see technique section of the bibliography) can be made in any office in minutes from polished rock slabs, and can provide a remarkable amount of information. Outcrop samples, conventional cores, sidewall cores, and cuttings samples all can be examined microscopically, although the quality of textural information decreases with decreasing sample size. Even the investment of time involved in petrographic work need not be great relative to the potential for problem solving. Few other techniques are as valuable and accurate for the identification of preserved, destroyed, or created porosity, or the prediction of depositional and diagenetic trends.

Research conducted over the past several decades has outlined many principles of deposition and diagenesis in carbonate sediments. Facies models have been established for modern (as well as ancient) reefs and other bank-margin deposits, for tidal-flat and sabkha sedimentation, for basinal deposition, and for other environments. Diagenetic studies have pointed out the influence of syndepositional marine cementation, early freshwater diagenesis, and later subsurface compaction-dissolution phenomena. This work has clearly shown that, although carbonate depositional and diagenetic patterns may be complex, commonly there is a large volume of information recorded in the rocks, which can be used to decipher this record.

Petrography, when used in close conjunction with well-log analysis, seismic interpretation, regional geology, and other studies, can be an invaluable tool for applying these recently developed principles of carbonate sedimentology to ancient rocks. Furthermore, it is best applied by the explorationist who is deeply involved in techniques other than petrography, for that person is in the best position to ask the right questions — questions that petrography may be able to answer. That is the goal of this volume.

Explanation of Captions

Each photograph in this book has a description in standard format. The first lines give the stratigraphic unit (including geologic age) and state or country of origin. Sample localities are in the United States of America unless otherwise noted. This is followed by a description of the photograph. The last line of the caption gives the type of lighting used, any staining or impregnation of the thin section, and the scale of the photograph. The following **caption abbreviations** are used:

PPL - plane-polarized light
XPL - cross-polarized light
PXPL - partially cross-polarized light
RL - reflected light
GP - gypsum plate (Quartz Red I plate) inserted
OS - organic matter stained
AS - calcite stained red with Alizarin Red S
AFeS - stained with a combination of Alizarin Red S and potassium ferricyanide
CYS - stained with Clayton Yellow for Mg-calcite
BSE - blue- or green-dyed epoxy filling porosity
CL - cathodoluminescence photomicrograph
FL - fluorescence photomicrograph
MP - microprobe (back-scattered electron image)
SEM - scanning electron micrograph image
Mac - macroscopic photograph of rock slab or outcrop

Photographic Scales

All dimensions are given as HA = xx where HA is the full horizontal axis of the photograph (including, for the sake of uniformity, any borders within the picture area). L and R are used where left and right pictures occupy the frame; T and B refer to top and bottom pictures. Dimensions are given in micrometers (µm) or millimeters (mm). There are 1000 micrometers in a millimeter.

Acknowledgments

Enormous thanks go to Philip W. Choquette, Alfred G. Fischer, Robert L. Folk, Noel P. James, L. Greer Price, and William D. Raatz for reviewing the entire book or large portions thereof. Individual chapters were reviewed by Jack A. Babcock (algae), Merlynd and Galina Nestell (foraminifers), Jeremy Young (miscellaneous microfossils), Stanley A. Kling (siliceous microfossils), Carl W. Stock (stromatoporoids), Ronald A. Johns (sponges), James E. Sorauf (corals), Roger J. Cuffey (bryozoans), Jed E. Day (brachiopods), G. Lynn Brewster-Wingard (mollusks), Bruce R. Wardlaw (conodonts), Leanne Pyle (skeletal grains), H. Curtis Monger (soil fabrics), and Nelia W. Dunbar (techniques). Both groups of reviewers caught many potential errors and made excellent suggestions for improvements. Noel P. James was an invaluable help in sending large numbers of pictures, in helping to organize the book, and as a partner in the production of interactive digital products that will supplement this volume. Roger J. Cuffey (bryozoans), Reinhold R. Leinfelder (*Lithocodium*), Carl W. Stock (stromatoporoids), and Graham R. Young (tabulate corals) were wonderfully generous in providing materials for the digital projects and allowing us to use them in this book — those sections owe much to their guidance. Many other scientists also very kindly contributed photographs (each acknowledged individually in specific figure captions). Finally, we would like to express our appreciation to the petrographers who spent many hours looking down a microscope with us and whose teaching and research dedication made this volume possible: A. G. Fischer, R. L. Folk, and R. G. C. Bathurst for P. A. S. and P. E. Potter, R. B. Koepnick, and D. E. Eby for D. S. U.-S. We can only hope that this book will aid another generation of petrographers as effectively as we were helped.

Some photographs in this book have been electronically edited or enhanced to accentuate contrast, improve focus, or remove unwanted blemishes (air bubbles or scratches, for example). None of the relevant structures, however, were altered.

Useful General References

These books provide general background information on carbonate petrography, carbonate sedimentation, paleontology and related subjects that are useful for working with carbonate rocks and sediments under the microscope and interpreting their origin and significance.

Adams, A. E., and W. S. MacKenzie, 1998, A Color Atlas of Carbonate Sediments and Rocks Under the Microscope: New York, John Wiley & Sons, 180 p.

Bathurst, R. G. C., 1975, Carbonate Sediments and their Diagenesis [Developments in Sedimentology 12]: New York, Elsevier, 658 p.

Blatt, H., 1982, Sedimentary Petrology: San Francisco, W. H. Freeman & Co., 564 p.

Boardman, R. S., A. H. Cheetham, and A. J. Rowell, eds., 1987, Fossil Invertebrates: Palo Alto, Blackwell Scientific Publications, 713 p.

Brasier, M. D., 1980, Microfossils: Boston, George Allen & Unwin, 193 p.

Carozzi, A. V., 1989, Carbonate Rock Depositional Models: A Microfacies Approach: Englewood Cliffs, Prentice-Hall, 604 p.

Carozzi, A. V., 1993, Sedimentary Petrography: Englewood Cliffs, Prentice-Hall, 330 p.

Cayeux, M. L., 1935, Les Roches Sédimentaires de France. Roches Carbonatées (calcaires et dolomies): Paris, Masson, 436 p.

Cayeux, L., 1970, Carbonate rocks (limestones and dolomites) Sedimentary rocks of France [translated and updated by A. V. Carozzi]: Darien, CT, Hafner Publishing Company, 394 p.

Clarkson, E. N. K., 1998, Invertebrate Paleontology and Evolution [4th Edition]: Oxford, Blackwell Science, 452 p.

Elf-Aquitaine with A. Reeckmann, and G. M. Friedman, 1982, Exploration for Carbonate Petroleum Reservoirs: New York, John Wiley & Sons, 213 p.

Fischer, A. G., S. Honjo, and R. E. Garrison, 1967, Electron Micrographs of Limestones and their Nannofossils: Princeton, NJ, Princeton University Press, 141 p.

Flügel, E., 1982, Microfacies Analysis of Limestones: New York, Springer-Verlag, 633 p.

Gubler, Y., J. P. Bertrand, L. Mattavelli, A. Rizzini, and R. Passega, 1967, Petrology and petrography of carbonate rocks, in G. V. Chilingar, H. J. Bissell, and R. W. Fairbridge, eds., Carbonate Rocks: Origin, Occurrence and Classification: Developments in Sedimentology 9A: New York, Elsevier, p. 51-86.

Harwood, G., 1988, Microscopical techniques: II. Principles of sedimentary petrography, in M. Tucker, ed., Techniques in Sedimentology: Oxford, Blackwell Scientific Publications, p. 108-173.

Horowitz, A. S., and P. E. Potter, 1971, Introductory Petrography of Fossils: New York, Springer-Verlag, 302 p.

Johnson, J. H., 1951, An introduction to the study of organic limestones: Colorado School of Mines Quarterly, v. 46 (2), p. 1-185.

Johnson, J. H., ed., 1952, Studies of organic limestones and limestone building organisms: Colorado School of Mines Quarterly, v. 47, 1-94 p.

Lippmann, F., 1973, Sedimentary Carbonate Minerals: New York, Springer-Verlag, 228 p.

Majewske, O. P., 1969, Recognition of Invertebrate Fossil Fragments in Rocks and Thin Sections [Internat. Sed. Petrog. Series v. 13]: Leiden, E. J. Brill, 101 p.

Milliman, J. D., 1974, Marine Carbonates. Part 1, Recent Sedimentary Carbonates: New York, Springer-Verlag, 375 p.

Moore, C. H., 1989, Carbonate Diagenesis and Porosity [Developments in Sedimentology, 46]: New York, Elsevier, 338 p.

Moore, C. H., 2001, Porosity Evolution and Diagenesis in a Sequence Stratigraphic Framework [Developments in Sedimentology, 55]: New York, Elsevier, 460 p.

Moore, R. C., C. G. Lalicker, and A. G. Fischer, 1952, Invertebrate Fossils: New York, McGraw-Hill Book Co., 766 p.

Morse, J. W., and F. T. Mackenzie, 1990, Geochemistry of Sedimentary Carbonates [Developments in Sedimentology, 48]: New York, Elsevier Scientific Publ. Co., 696 p.

Murray, J. W., ed., 1985, Atlas of Invertebrate Macrofossils: New York, John Wiley & Sons, 241 p.

Reeder, R. J., ed., 1983, Carbonates: Mineralogy and Chemistry: Washington, D.C., Mineralogical Society of America, Reviews in Mineralogy, Vol. 11, 394 p.

Scholle, P. A., 1978, A Color Illustrated Guide to Carbonate Rock Constituents, Textures, Cements, and Porosities: Tulsa, OK, American Association of Petroleum Geologists Memoir 27, 241 p.

Scoffin, T. P., 1987, An Introduction to Carbonate Sediments and Rocks: New York, Chapman & Hall, 274 p.

Sorby, H. C., 1879, On the structure and origin of limestones: Proceedings of the Geological Society of London, v. 35, p. 56-95. [The original work in this field]

Tucker, M. E., and V. P. Wright, 1990, Carbonate Sedimentology: Oxford, Blackwell Scientific Publications, 482 p.

Tucker, M. E., 1991, Carbonate Petrology: An Introduction: 2nd edition: Oxford, Blackwell Scientific Publications, 272 p.

Wilson, J. L., 1975, Carbonate Facies in Geologic History: New York, Springer Verlag, 471 p.

The following books are more limited in their temporal or areal scope, but have many high-quality petrographic plates that effectively show assemblages of organisms through time.

Bissell, H. J., 1970, Petrology and Petrography of Lower Triassic Marine Carbonates of Southern Nevada, in [Int. Sed. Petrog. Ser., v. 14]: Leiden, E. J. Brill, p. 27.

Carozzi, A. V., and D. A. Textoris, 1967, Paleozoic Carbonate Microfacies of the Eastern Stable Interior (U.S.A.) [Int. Sed. Petrog. Ser., v. 11]: Leiden, E. J. Brill, 41 p.

Cita, M. B., 1965, Jurassic, Cretaceous and Tertiary Microfaunas from the Southern Alps (Northern Italy) [Int. Sed. Petrog. Ser., v. 8]: Leiden, E. J. Brill, 99 p.

Cuvillier, J., 1961, Stratigraphic Correlation by Microfacies in Western Aquitaine [Int. Sed. Petrog. Ser., v. 2]: Leiden, E. J. Brill, 34 p.

Fabricius, F. H., 1966, Beckensedimentation und Riffbildung an der Wende Trias/Jura in den Bayerisch-Tiroler Kalkalpen [Int. Sed. Petrog. Ser., v. 9]: Leiden, E. J. Brill, 143 p.

Ford, A., and J. J. H. C. Houbolt, 1963, The Microfacies of the Cretaceous of Western Venezuela [Int. Sed. Petrog. Series, v. 6]: Leiden, E. J. Brill, 55 p.

Glintzboeckel, C., and J. Rabaté, 1964, Microfaunes et Microfacies du Permo-Carbonifere du Sud Tunisien [Internat. Sed. Petrog. Ser., v. 7]: Leiden, E. J. Brill, 45 p.

Grunau, H. R., 1959, Mikrofazies und Schichtung Ausgewählter, Jungmesozoischer, Radiolarit-Führender Sedimentserien der Zentral-Alpen [Int. Sed. Petrog. Ser., v. 4]: Leiden, E. J. Brill, 179 p.

Hagn, H., 1955, Fazies und Mikrofauna der Gesteine der Bayerischen Alpen [Int. Sed. Petrog. Ser., v. 1]: Leiden, E. J. Brill, 27 p.

Hanzawa, S., 1961, Facies and Micro-Organisms of the Paleozoic, Mesozoic and Cenozoic Sediments of Japan and her Adjacent Islands [Int. Sed. Petrog. Ser., v. 5]: Leiden, E. J. Brill, 117 p.

Longman, M. W., C. T. Siemers, and C. F. Jordan, Jr., eds., 1993, Modern Carbonates and their Ancient Counterparts in Indonesia: A Guide to Interpreting and Understanding Carbonate Reservoirs: Jakarta, Indonesian Petroleum Association, 123 p.

Perconig, E., 1968, Recognition of the Triassic and Jurassic Sediments of Spain [Int. Sed. Petrog. Ser., v. 10]: Leiden, E. J. Brill, 63 p.

Rey, M., and G. Nouet, 1958, Microfacies de la Région Prérifaine et de la Moyenne Moulouya (Maroc Septentional) [Int. Sed. Petrog. Ser., v. 3]: Leiden, E. J. Brill, 44 p.

Sampò, M., 1969, Microfacies and Microfossils of the Zagros Area, Southwestern Iran (from Pre-Permian to Miocene) [Int. Sed. Petrog. Ser., v. 12]: Leiden, E. J. Brill, 102 p.

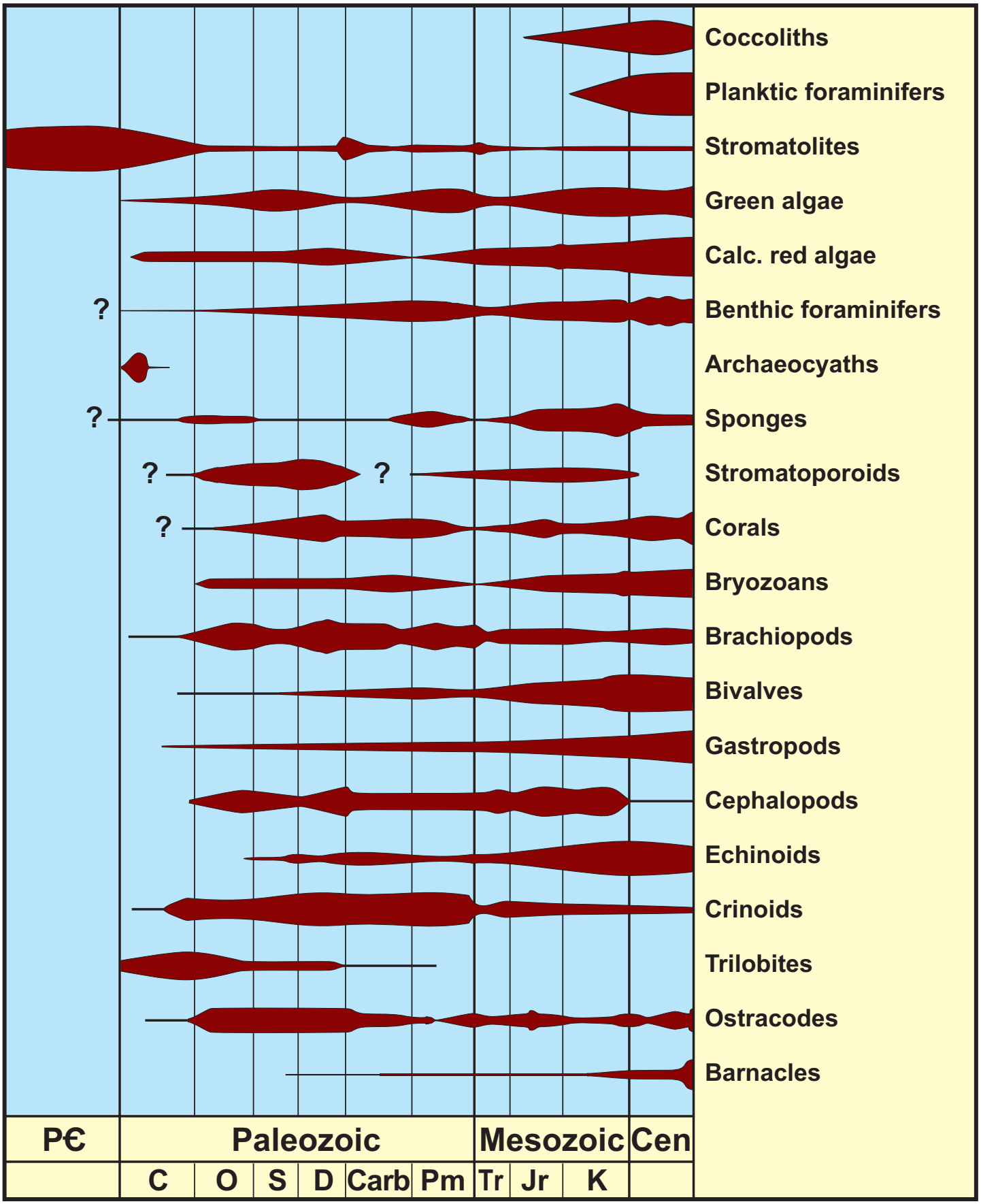

A diagram summarizing the fluctuations in approximate diversity and abundance of the major groups of marine carbonate-producing organisms through time. The diagram was adapted from Horowitz and Potter (1971 and other sources. It should be used only as a general guide to the types of organisms likely to be encountered in rocks of any particular age.

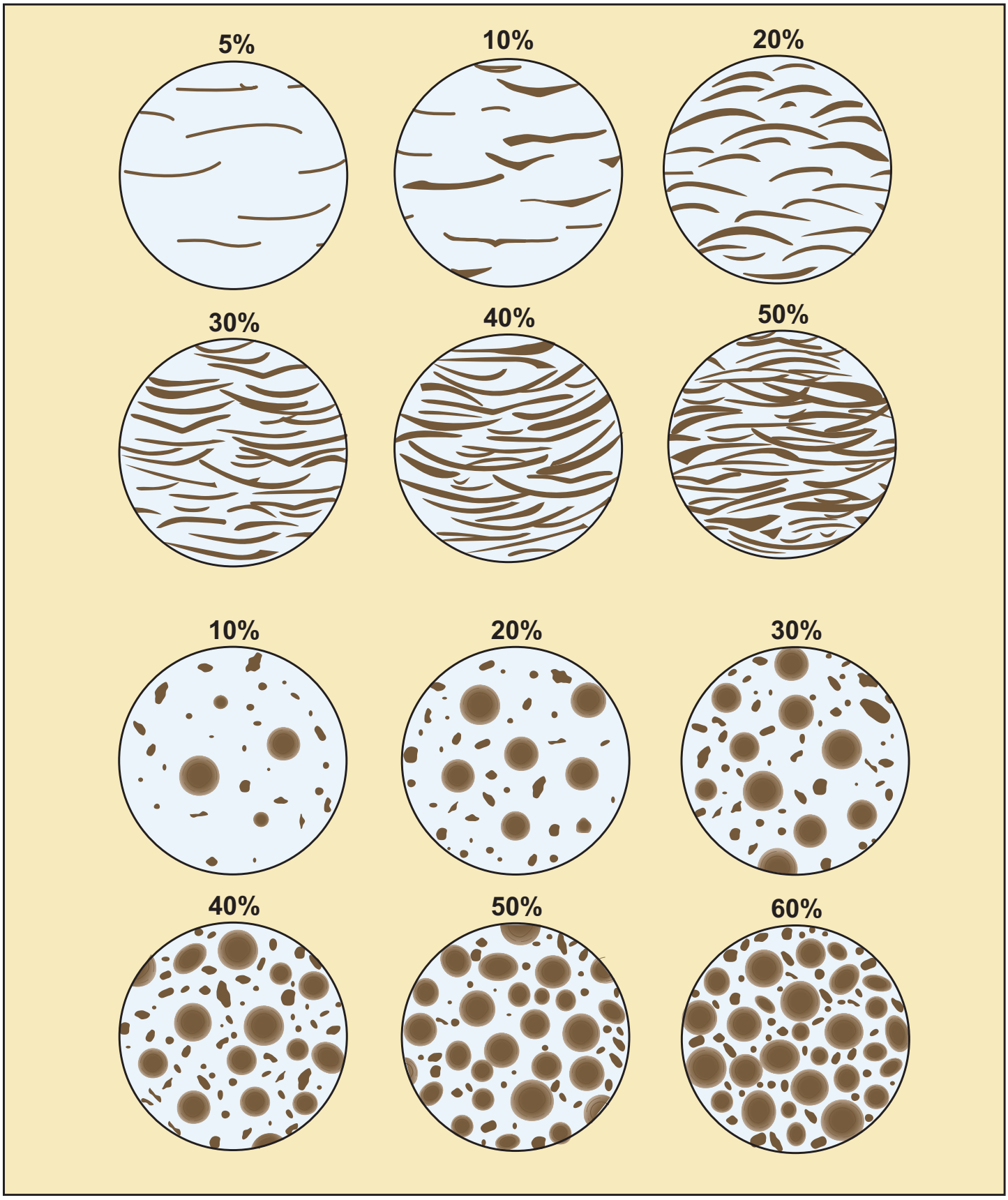

Visual comparison charts for estimating abundances of constituents in thin section, peels, and photographic or digital images. Adapted from Baccelle and Bosellini (1965). Other such charts can be found in Flügel (1982) and Swanson (1981). All citations given at the end of Chapter 30 - Techniques.

Facing Page: Modern domal, subtidal to lower intertidal, microbial stromatolites from Carbla Point, Shark Bay, Western Australia. Stromatolite heads are 30-60 cm in diameter.

GRAINS: Skeletal Fragments

Calcimicrobes and calcareous algae

CHAPTER 1

Calcimicrobes/ cyanobacteria

Marine green algae

Charophytes

Red algae

Phylloid algae

CALCIMICROBES/CYANOBACTERIA (BLUE-GREEN ALGAE)

Taxonomy and Age Range:

Cyanobacterial stromatolites usually are grouped in the Phylum Cyanophyta — Precambrian (Archean)-Recent

Classification of other microbes is complex, uncertain, and ever changing (generally placed under the Prokaryotes, but most of these organisms are really best considered as "microproblematica"). Organisms once termed blue-green algae are now generally termed cyanobacteria.

Ranges of some specific calcimicrobes depicted in this section:

Girvanella — Cambrian-mid. Cretaceous (Eocene?)

Epiphyton — Cambrian-Devonian

Renalcis — Cambrian-Devonian

Frutexites — Latest Cambrian-Devonian

Environmental Implications:

Many are photosynthetic and therefore require light; non-photosynthetic microbes also are important, especially in cryptic settings. Recognition of photosynthetic forms is especially critical in paleoenvironmental studies.

Wide salinity tolerance from strongly hypersaline to freshwater; rare as dominant sediment formers in modern, normal-salinity marine environments.

Wide temperature tolerance: sub-glacial to hot springs settings; most common in temperate- to warm-water marine settings.

Marine stromatolites range from subtidal to intertidal settings — intertidal forms predominate today.

A progressive shift occurred from normal-salinity environments in the Precambrian to highly stressed environments today, possibly due to the Phanerozoic increase in grazing organisms or interspecific competition. Cenozoic microbial carbonate deposits are predominantly peritidal.

Skeletal Mineralogy:

Marine forms are mainly aragonitic; incorporated detrital components can have any carbonate or terrigenous mineralogy; lacustrine forms are mostly calcitic.

Morphologic Features:

Most are uncalcified and the remainder have "nonskeletal" or "extraskeletal" calcification largely incidental to their growth. Calcification results from biochemical processes (removal of CO_2), but generally is not necessary for, or beneficial to, the organism's survival.

Calcimicrobial deposits, thus, have no clearly defined and consistent skeletal morphologies (hence the difficulty of classifying these microproblematica). Calcimicrobial deposits are recognized by overall sediment structure, by externally calcified filaments or spherical bodies, and by trapped sediment. Flat-lying laminated sediment, domal stromatolites, or clotted, finger-like thrombolite structures are characteristic — shapes vary with environmental conditions (water depth, current strength, and others).

Lamination in stromatolites reflects microbial growth through day-night cycles and tidal cycles; those organic laminae commonly are interspersed with micritic or peloidal carbonate or terrigenous detritus that was deposited during episodic storms.

Non-stromatolitic calcimicrobes typically form lumpy encrustations or small upright "shrubs".

Keys to Petrographic Recognition:

1. Size: Stromatolites are cm to meters in height; laminae are mm- to cm-sized.
2. A general absence of well-defined skeletal features other than possible carbonate-encased filaments or tubules.
3. Stromatolites can have an abundance of trapped grains, especially pellets/peloids but also clastic terrigenous materials in many cases.
4. Stromatolites are characterized by planar or contorted laminations with alternations of organic-rich and grainy or micritic layers; others have vaguely clotted (thrombolitic) structure.
5. Stromatolites commonly have fenestral fabrics (elongate pores paralleling lamination).
6. Planar stromatolites are associated (in Phanerozoic arid settings) with early diagenetic evaporites.
7. Many microbes can form branching growths of micritic peloids or micritic tubules.
8. Some form finely laminated micritic or phosphatic encrustations with digitate structure.
9. Some calcimicrobes form coated grains (oncoids) with scalloped or irregular coatings and with or without tubular or filamentous structure.
10. Calcimicrobes also can form lumpy, micritic, localized encrustations of other organisms.

Recent algal preparation

A stained biological preparation of *Anabaena* sp. These spherical cyanobacterial bodies (formerly termed blue-green algae) are linked up into chains. Such coccoid microbes, in combination with filamentous forms, are common in modern stromatolites. The oversized purple-stained cells are nitrogen-fixing heterocysts.

PPL, OS, HA = 0.13 mm

Recent algal preparation

A stained biological preparation of *Rivularia* sp. — a filamentous cyanobacteria. The individual cells are stained purple and the mucilaginous sheaths are stained green. A meshwork of such interlocking filaments is effective in the trapping of terrigenous and/or carbonate particles in microbial mats through a baffling effect as well as by adhesion to the slightly sticky mucilaginous sheaths.

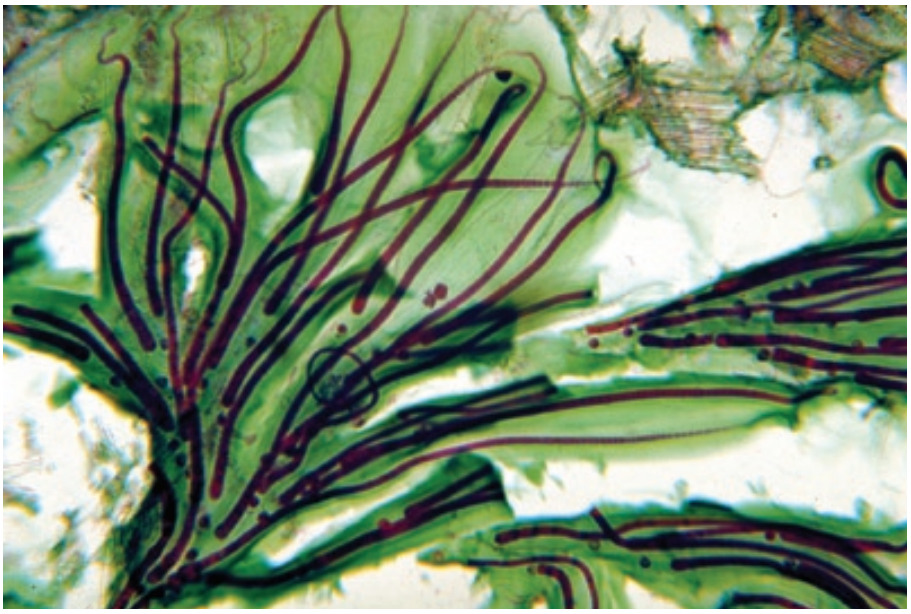

PPL, OS, HA = 0.24 mm

Holocene travertine, north of Durango, Colorado

An SEM image of an aragonitic "dumb-bell" that is believed to have formed around a clump of bacteria. Similar structures have been produced by bacterial action under controlled laboratory experiments. Large calcite crystals are visible in the background. Photograph courtesy of Henry S. Chafetz (from Chafetz et al., 1991).

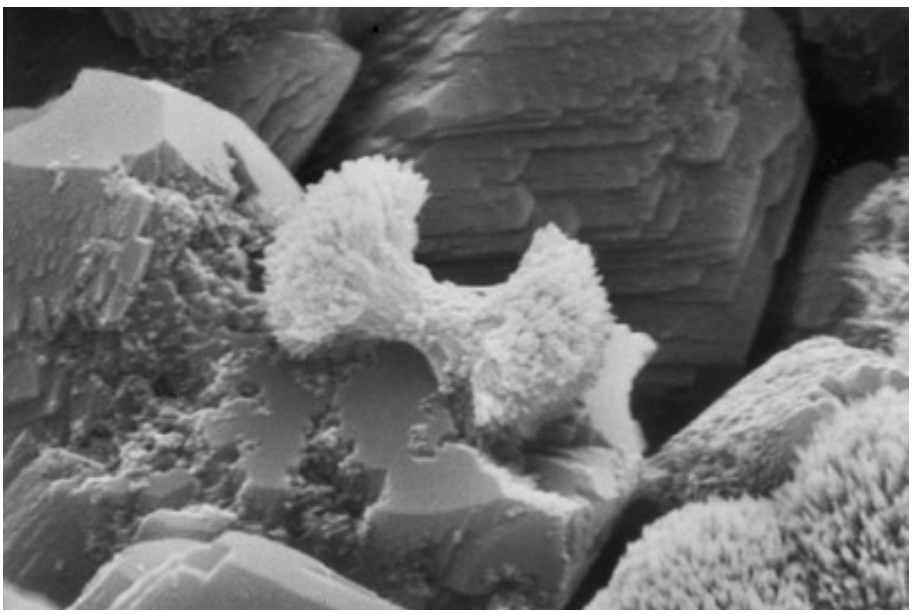

SEM, HA = 32 µm

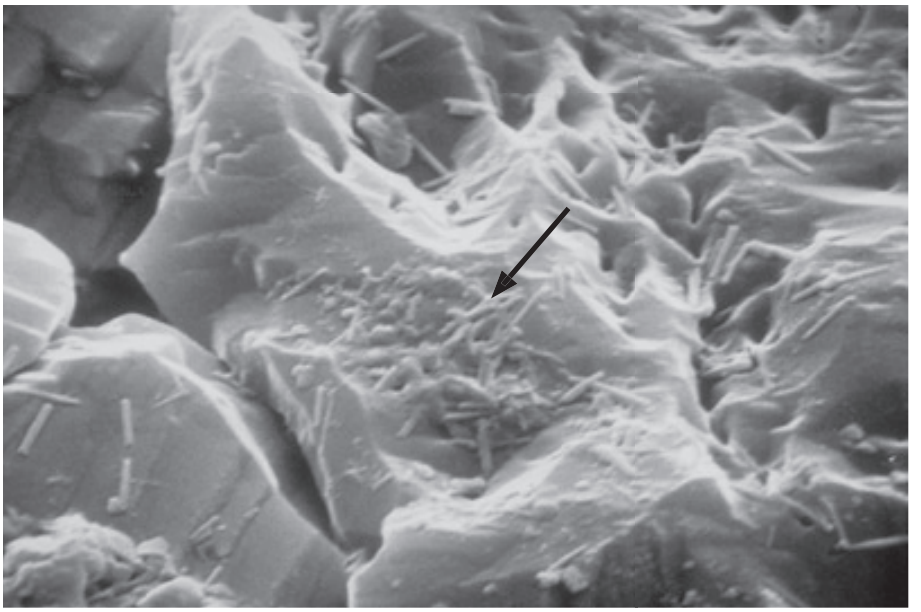

Holocene travertine, Clark County, Idaho

An SEM image of a lightly etched travertine displaying probable bacterial rods (well displayed in the area indicated by the black arrow) that were encased within calcite crystals. Bacterial fossils are relatively rare, their preservation potential is poor, and they have been conclusively identified only in shrub and shrub-related structures; thus, shrubs (shown later) are the most diagnostic bacterial structures. Photograph courtesy of Henry S. Chafetz (from Chafetz and Folk, 1984).

SEM, HA = 18 μm

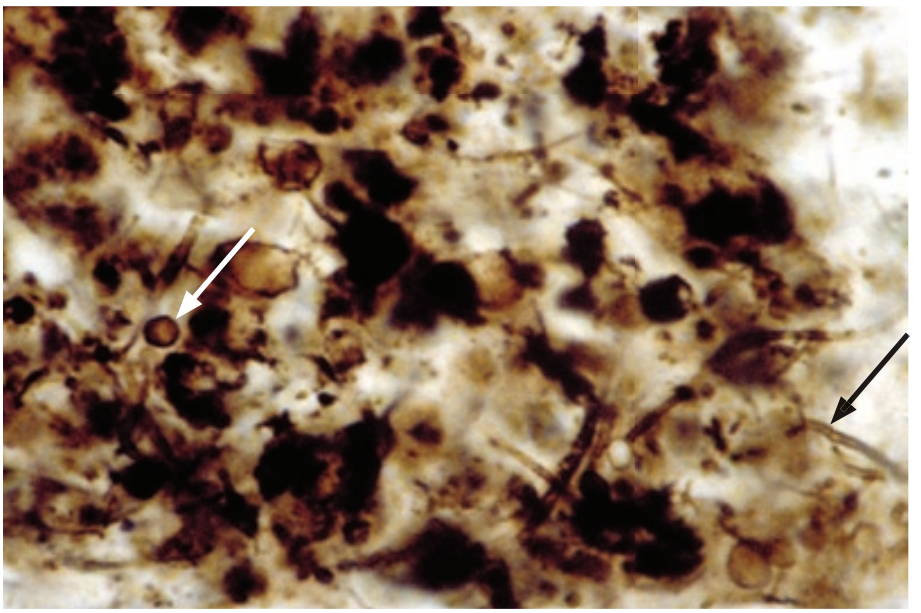

Neoproterozoic Shaler Gp., Glenelg Fm., Victoria Island, Northwest Territories, Canada

A chert nodule from a supratidal microbial laminite showing silicified cyanobacterial filaments (black arrow points to one of many examples) and coccoid cells (white arrow). Microbial remains have been identified from many localities in Precambrian rocks extending well back into the Archean. Photograph courtesy of Brian R. Pratt.

PPL, HA = 0.17 mm

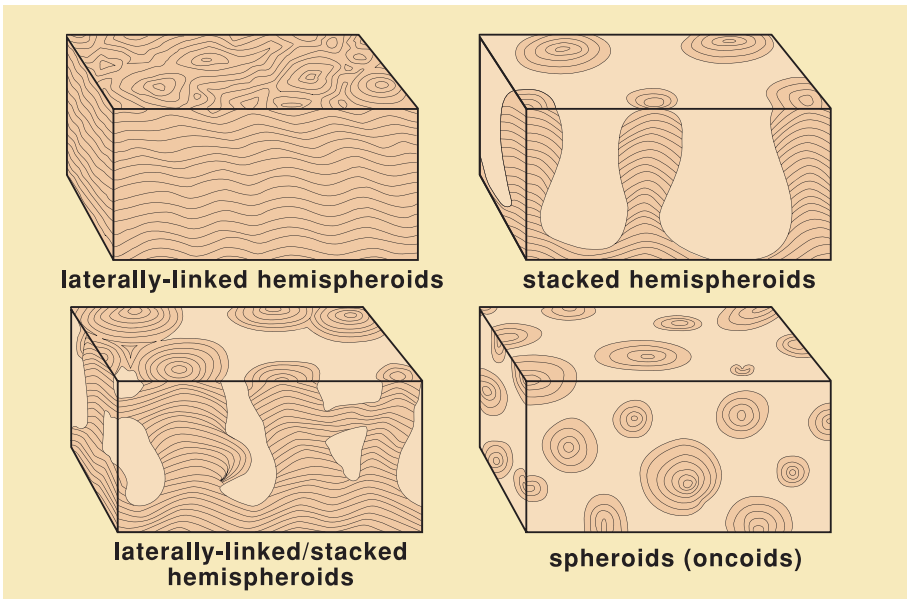

Common microbial stromatolite growth forms

Modern and ancient stromatolitic structures are found in a wide variety of growth forms. The main types are shown schematically in this classification by Logan et al. (1964). Most stromatolites are composed of laminae of trapped carbonate and/or terrigenous sediment; generally they are easier to recognize on outcrop, or in polished slabs, than in thin section. Skeletal elements are rarely found in stromatolites although they are organosedimentary structures probably created primarily by sediment-trapping microbial mats.

Triassic Dachstein Ls., Lofer facies, Tirol, Austria

A well developed ancient example of a laminated and contorted stromatolite (loferite). The dark reddish-brown color (reflecting significant preservation of organic matter), slightly pelletal texture, irregular lamination, and elongate ("birdseye" or fenestral) pores are characteristic of stromatolites, but are not always this clearly displayed. Although the stromatolite fabric most likely represents growth and sediment trapping in and on a microbial mat, no microbes were recognizable in this deposit (as in most such stromatolites).

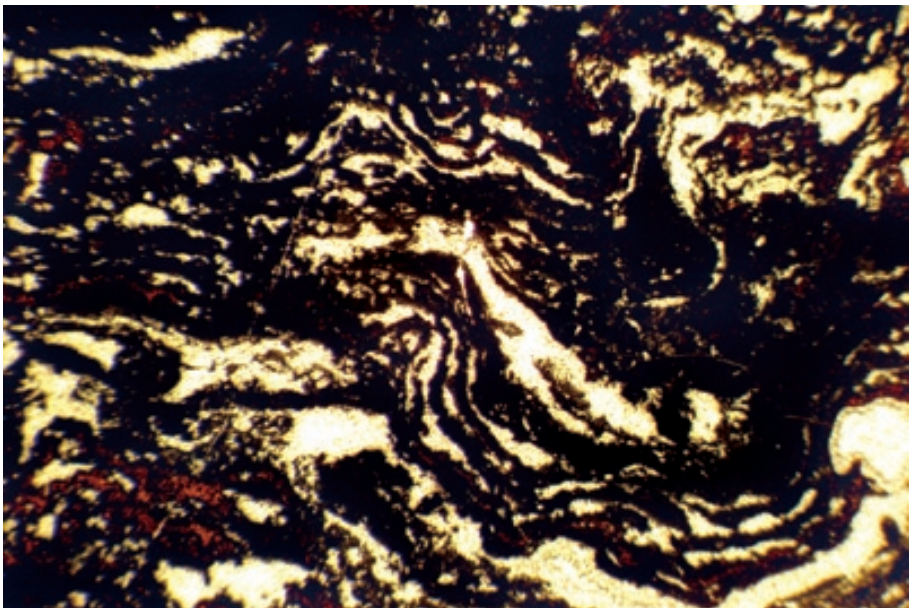

PPL, HA = 5.8 mm

Recent sediment, Crane Key, Florida Bay, Florida

Detailed texture of a typical intertidal stromatolite with interlamination of organic zones (cyanobacterial filaments, mangrove remains, and other organic detritus) and zones of transported and trapped detritus. The trapped materials include carbonate fecal pellets and microbial peloids as well as various skeletal fragments, especially bivalves, gastropods, and benthic foraminifers. Note the pronounced fenestral fabric that is characteristic of such intertidal stromatolite deposits.

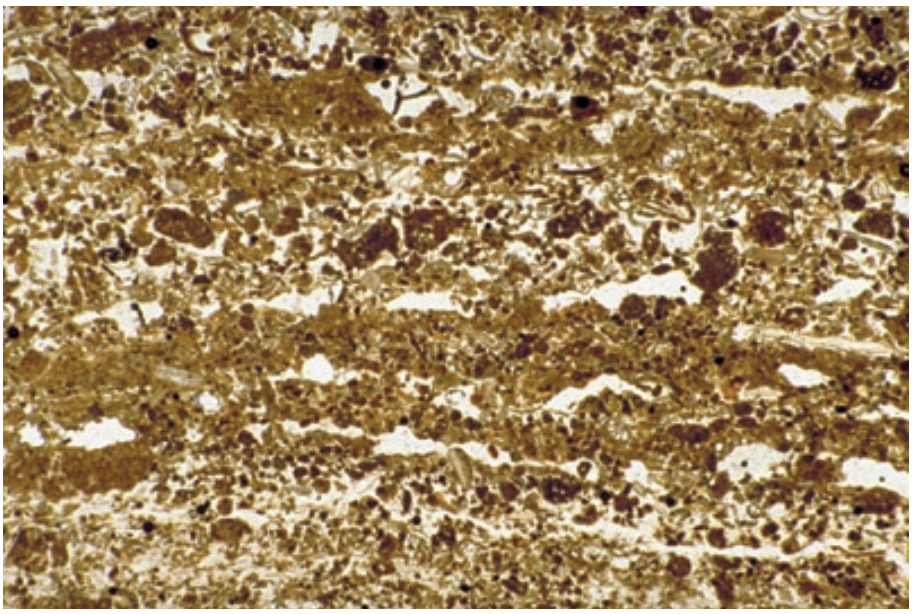

PPL, HA = 5.7 mm

Recent sediment Deep Lake, Yorke Peninsula, South Australia

A stromatolite from a hypersaline lake (a coastal salina). Note microbial peloids and encrusted filaments forming small, incipient branching structures. Peloidal "shrubs" normally are not so well preserved, but more typically disaggregate, contributing to the peloid content of such mat deposits.

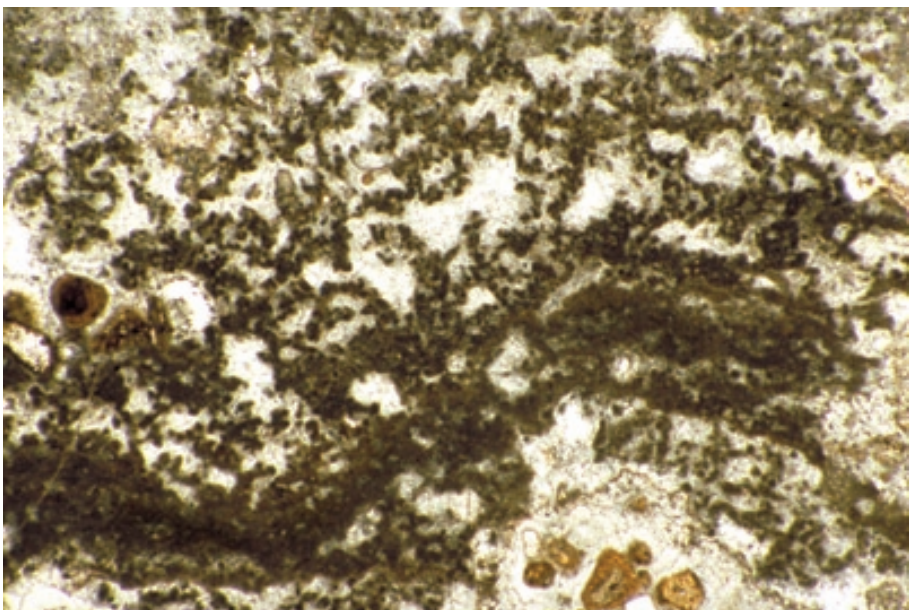

PPL, HA = 3.5 mm

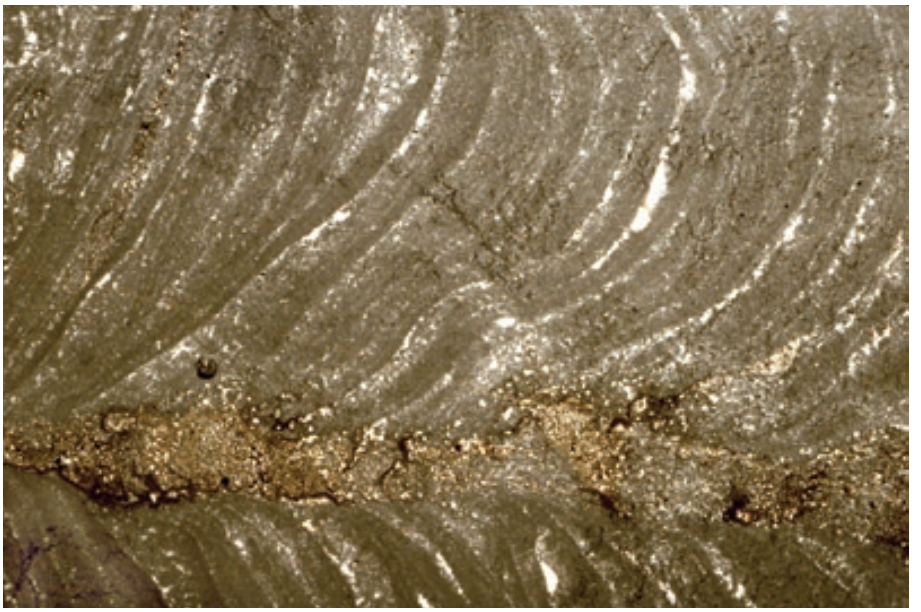

Precambrian, northern Wisconsin

A columnar, stromatolitic boundstone or biolithite (original up direction toward the right). Digitate or columnar stromatolites are typically of subtidal origin, unlike the nearly planar mats of previous images that form primarily in intertidal settings. The lamination in both types of mats, however, results mainly from alternating episodes of microbial growth and entrapment of transported sediment. Sample from Robert Laury.

PPL, HA = 16 mm

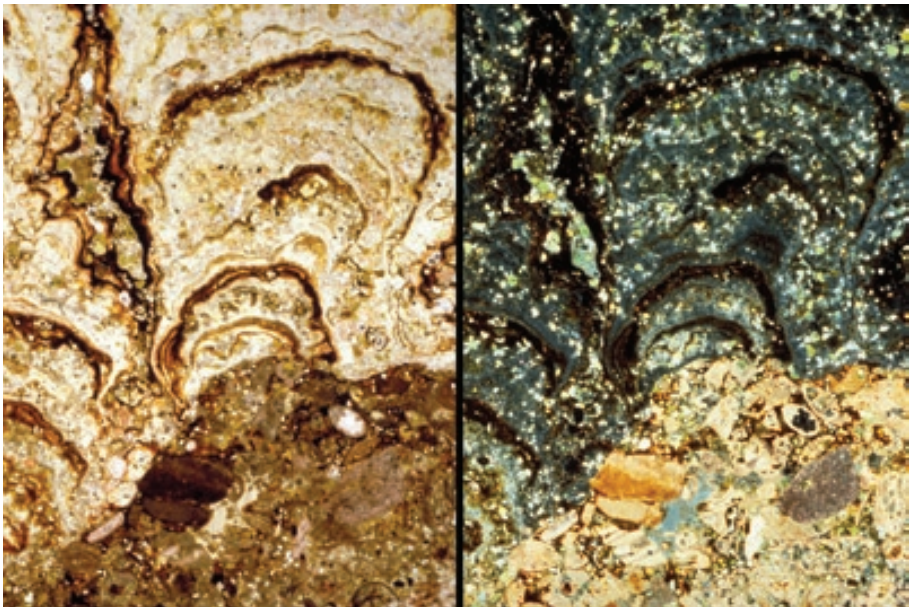

Oligocene-Miocene hardground, Oamaru, Otago, New Zealand

A stromatolitic crust atop a marine hardground. The lumpy, digitate, laminated crust is largely phosphatic, hence the brownish color in plane-polarized light and the nearly isotropic appearance in cross-polarized light. Although a biotic origin of such structures is likely, it is difficult to prove in the absence of preserved microbial remains.

PPL/XPL, HA = 7.1 mm each

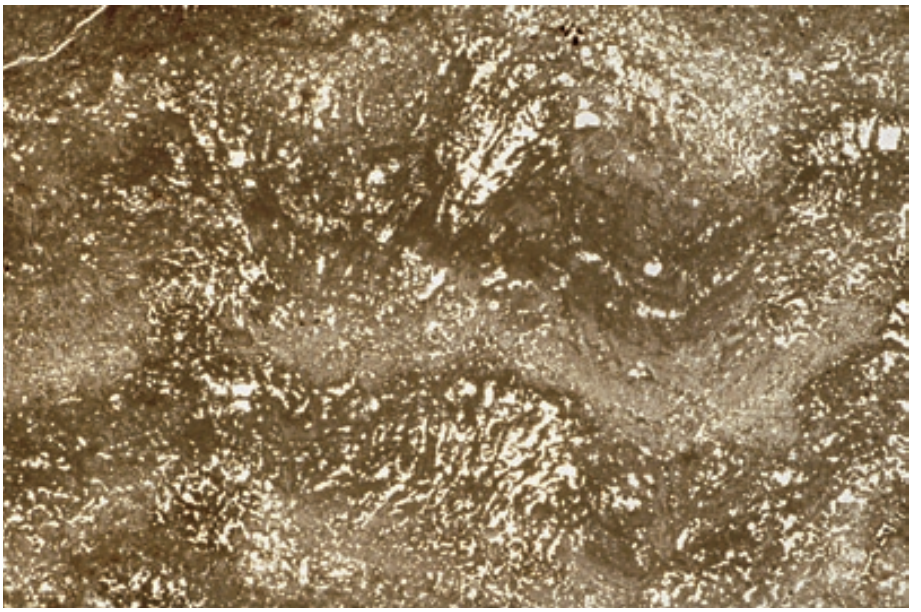

Up. Permian (lo. Ufimian) Lower Solikamskaya Suite, Perm Region, Russia

A stromatolitic or thrombolitic deposit showing typical contorted laminations that were substantially disrupted by the growth of evaporites. Intertidal stromatolites that grow in arid regions are commonly associated with gypsum, anhydrite or halite crystals or crystal fragments formed by the evaporative concentration and infiltration of water trapped on original mat surfaces.

PPL, HA = 14.5 mm

Up. Devonian (Frasnian) Sadler Fm., Canning Basin, Western Australia

Microbial growth can form nodular structures, as in this *Girvanella* oncoid (a pisoid of bacterial/algal origin), particularly in areas of at least episodically strong wave or tidal action. The irregularity and contortion of laminations and the preservation of internal filamentous fabrics (see following photograph) are the main clues to a microbial (probably cyanobacterial) origin of such grains.

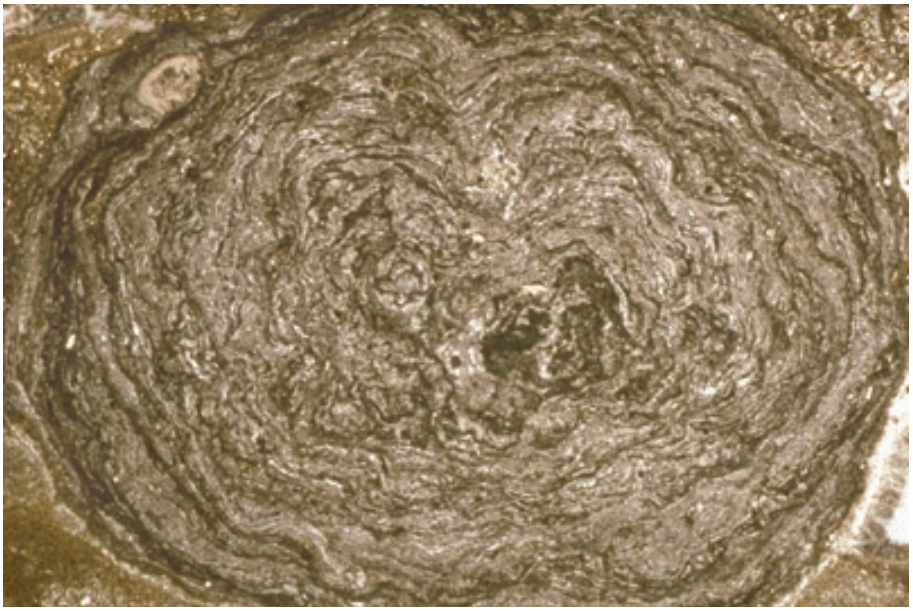

PPL, HA = 16 mm

Up. Devonian (top Frasnian) Simla-Blue Ridge Fm., Alberta, Canada

A close-up view of a *Girvanella* oncoid displaying well developed tubular structure. Note the interfingering of individual filaments and the selective precipitation of dense, micritic carbonate around the filament sheaths. It is necessary to view thin sections at maximum magnifications in order to see such filamentous structures and demonstrate a probable microbial origin for particular pisoids.

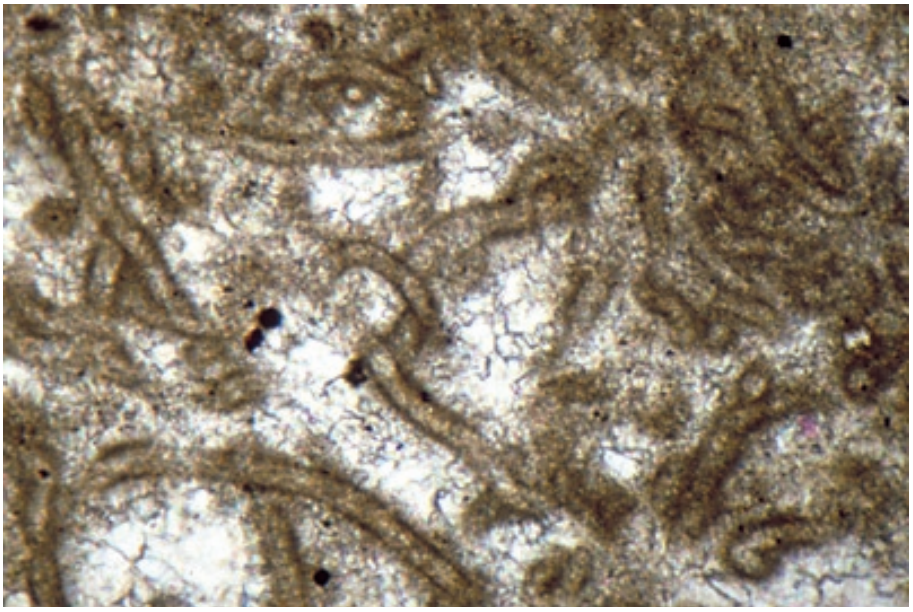

PPL, HA = 0.55 mm

Oligocene Deborah Volcanic Fm., Oamaru, Otago, New Zealand

These are peloidal, calcitic, probably microbial branching growths that formed in association with basaltic pillow lavas. The microbes grew atop glassy, zeolitic, pillow rinds (the yellow material at the bottom of the photograph) and extended into open inter-pillow cavities. These shrub-like growths were later encased in sparry calcite cement, but where uncemented they commonly fall apart, generating large volumes of small micritic peloids.

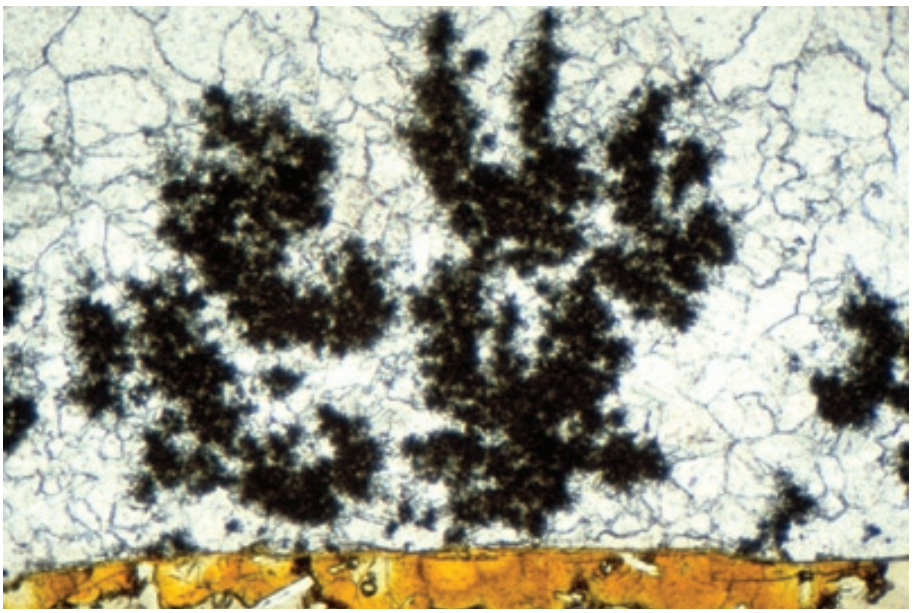

PPL, HA = 2.4 mm

Lo. Cambrian (Tommotian) Pestrotsvet Fm., Siberian Platform, Russia

Dendritic growth forms of the widespread calcimicrobe or microproblematic organism, *Epiphyton*. This genus has distinctively thick, solid branches. It commonly forms unusually large growths that can be a substantial rock-forming element in association with other framework organisms. Sample from Noel P. James.

PPL, HA = 4.5 mm

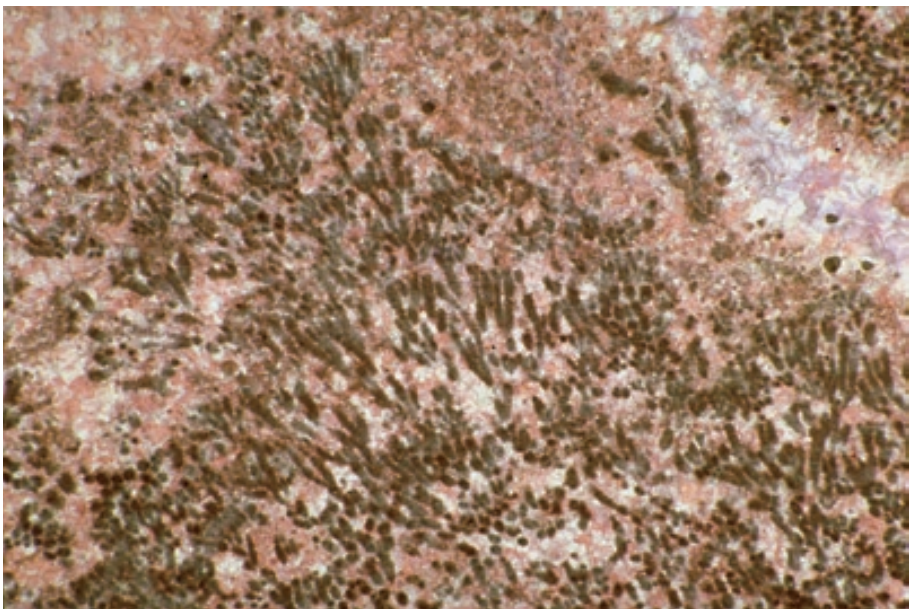

Lo.-Mid. Ordovician Cow Head Gp., Newfoundland, Canada

Another view of dendritic growths of *Epiphyton*, a possible cyanobacterial organism. This genus is quite common in Cambrian and Ordovician carbonate strata and has been described from rocks as young as Devonian. Sample from Noel P. James.

PPL, AFeS, HA = 6 mm

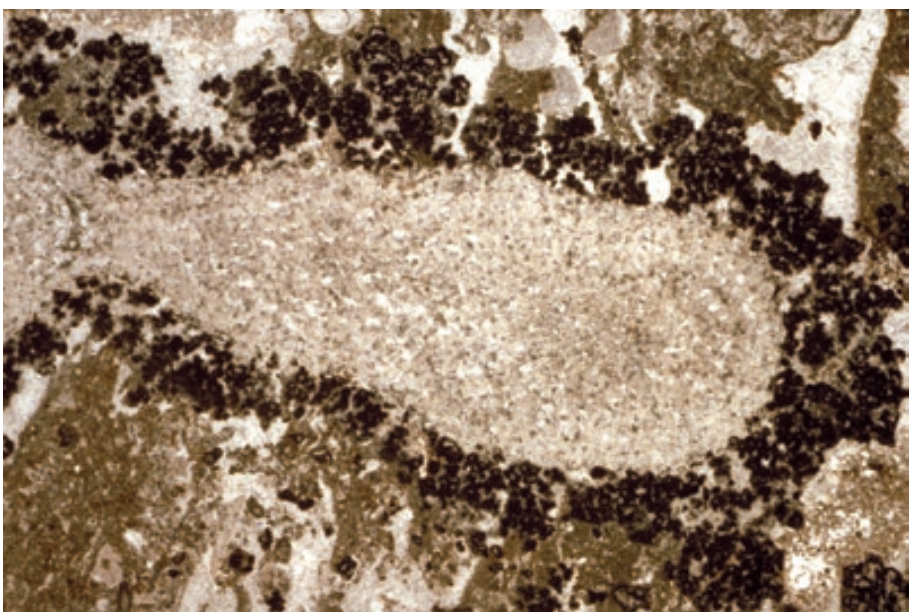

Up. Devonian (Frasnian) Pillara Ls., Canning Basin, Western Australia

Lumpy, peloidal accumulations of the microproblematic genus *Renalcis*, a possible cyanobacterial organism, here encrusting a finger-shaped stromatoporoid. This genus is widespread in Cambrian through Devonian strata and formed small, self-supporting growths as well as encrustations that may have helped to bind other framework organisms.

PPL, HA = 16 mm

Up. Devonian (Famennian) Piker Hills Fm., Canning Basin, Western Australia

A small branching cluster of *Renalcis* in an allochthonous block of reef within marginal-slope deposits. Note the characteristic dense micrite within the stacked, branching, domal growth stages. Photograph courtesy of Phillip E. Playford.

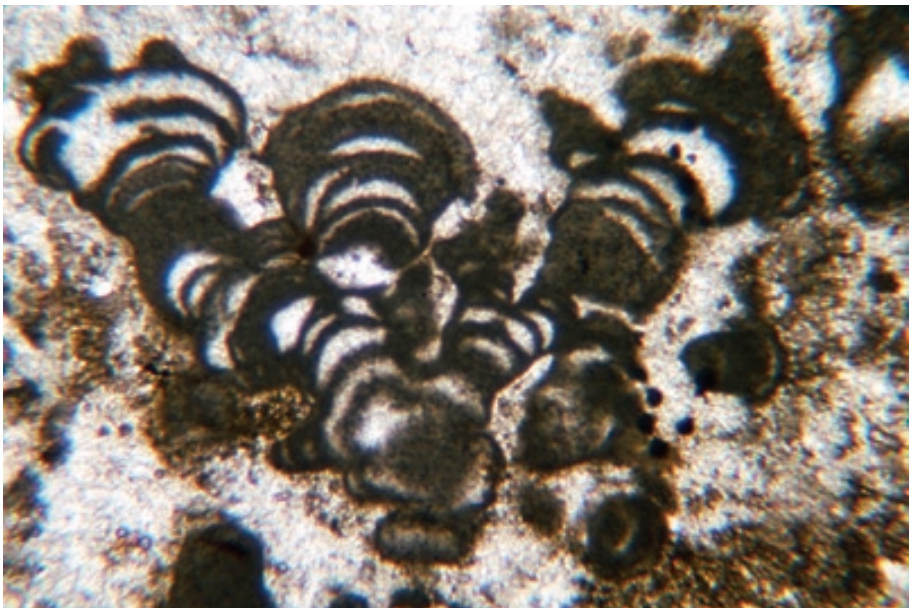

PPL, HA = 4 mm

Up. Devonian (basal Famennian) Virgin Hills Fm., Canning Basin, Western Australia

A biolithite with iron- and iridium-rich, calcified digitate growths of *Frutexites*, a possible cyanobacterial form. This deposit formed just above the Frasnian-Famennian boundary, a time of widespread extinction of many higher organisms.

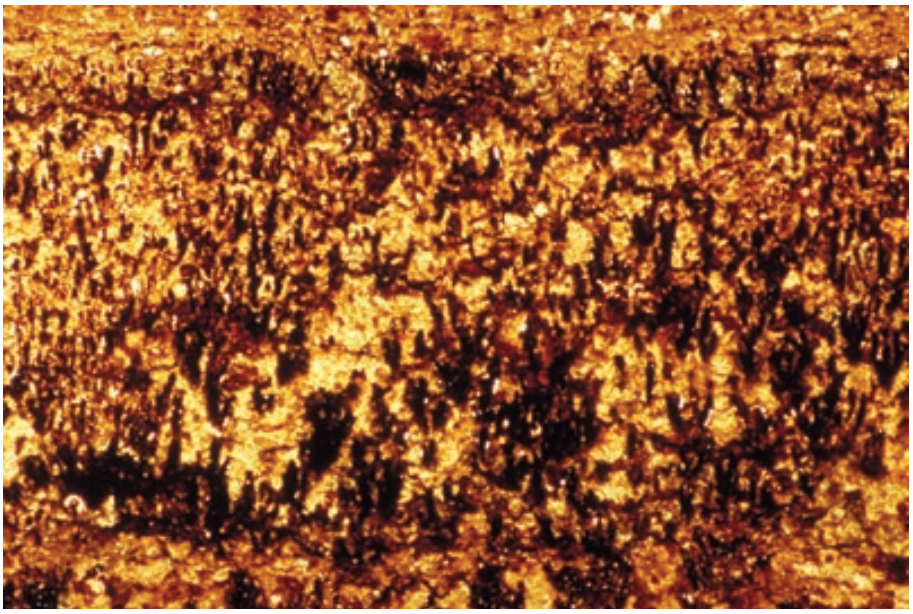

PPL, HA = 6 mm

Up. Permian (Kazanian?) Karstryggen Fm., Jameson Land, East Greenland

Calcified. microproblematic, densely branching growths. Such calcified arborescent remains have been considered as microbial by some workers and as green algal by others. The examples shown here were formed and preserved in shallow-marine areas with exceptionally high rates of marine cementation.

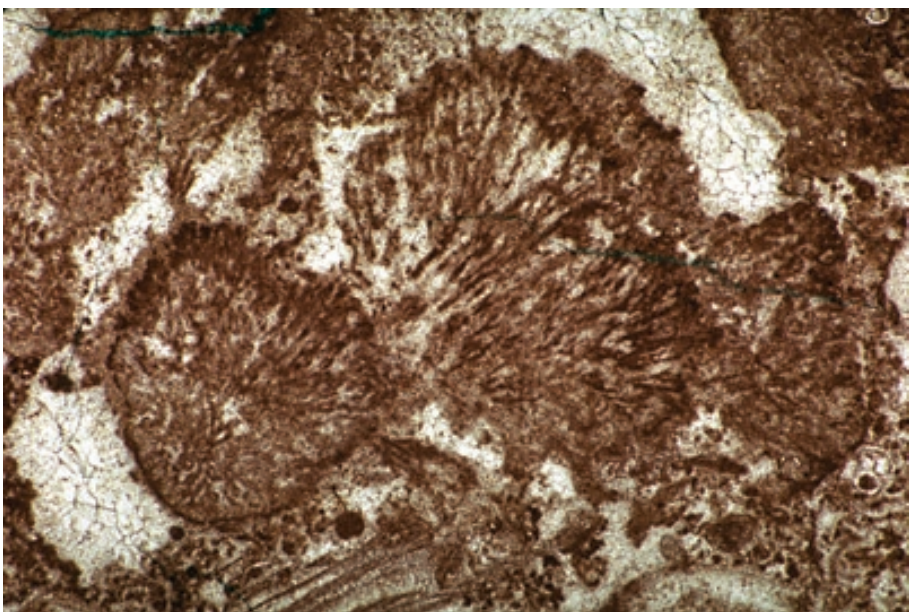

PPL, AS, HA = 8 mm

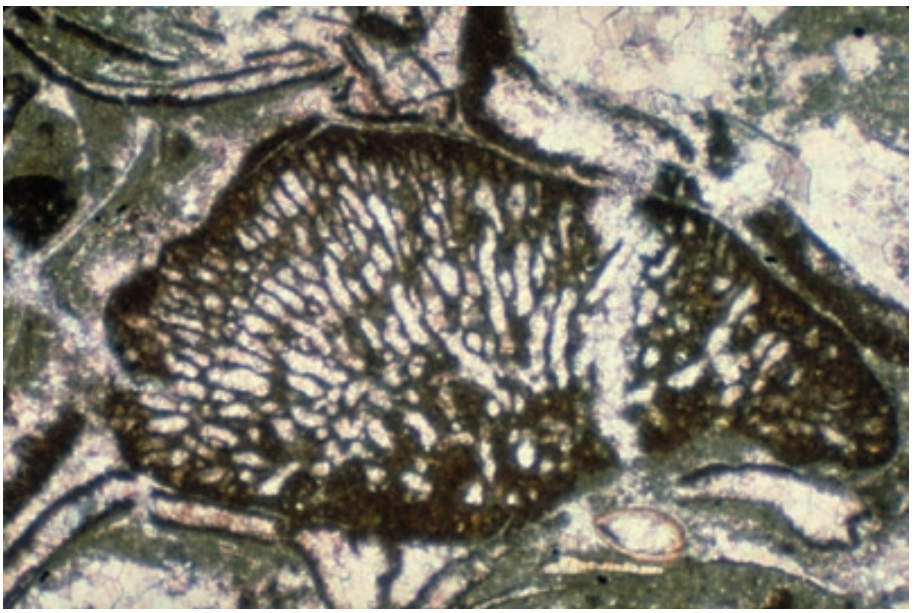

Jurassic Morrison-Sundance Fms., Park Co., Wyoming

Many structures formed by microbial organisms have problematic phyletic assignments. As noted earlier, some of the most characteristic microbial fabrics are branching or shrub-like features. In this example, an *Ortonella*-type alga has formed a radiating cluster of calcified tubules. A number of similar species with tubular structures are differentiated mainly by their branching patterns and are classed by some as microbial structures, but by most workers as codiacean green algae (see Wray, 1977).

PPL, AFeS, HA = 3.6 mm

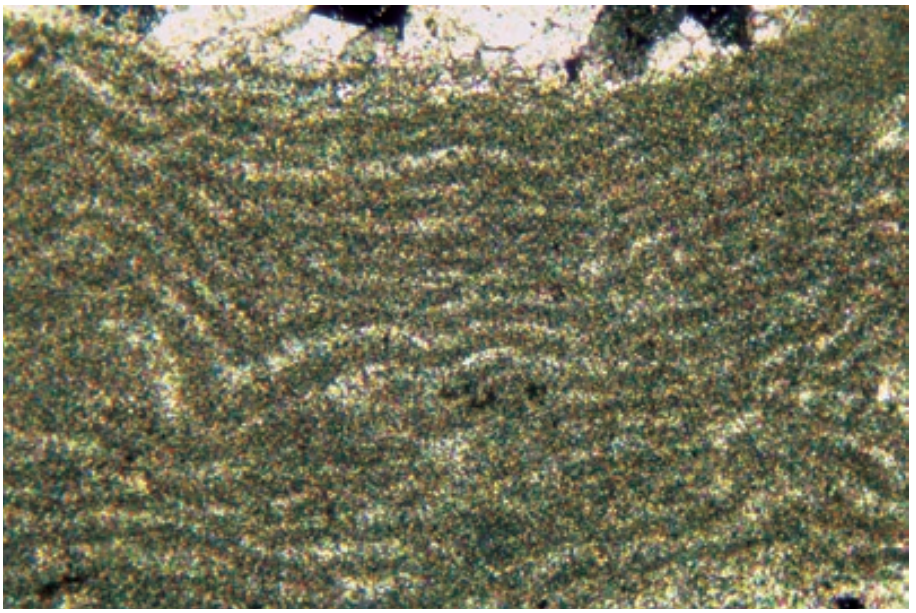

Up. Permian (Guadalupian) Capitan Fm., Eddy Co., New Mexico

A close-up view of *Archaeolithoporella*, an important encrusting microproblematic organism in Permian reefs (commonly in close association with *Tubiphytes* and interlaminated with synsedimentary marine cements). It has been classed as a calcimicrobial deposit by some workers, and as a red alga by others. Photograph courtesy of Sal J. Mazzullo.

XPL, HA = 5.0 mm

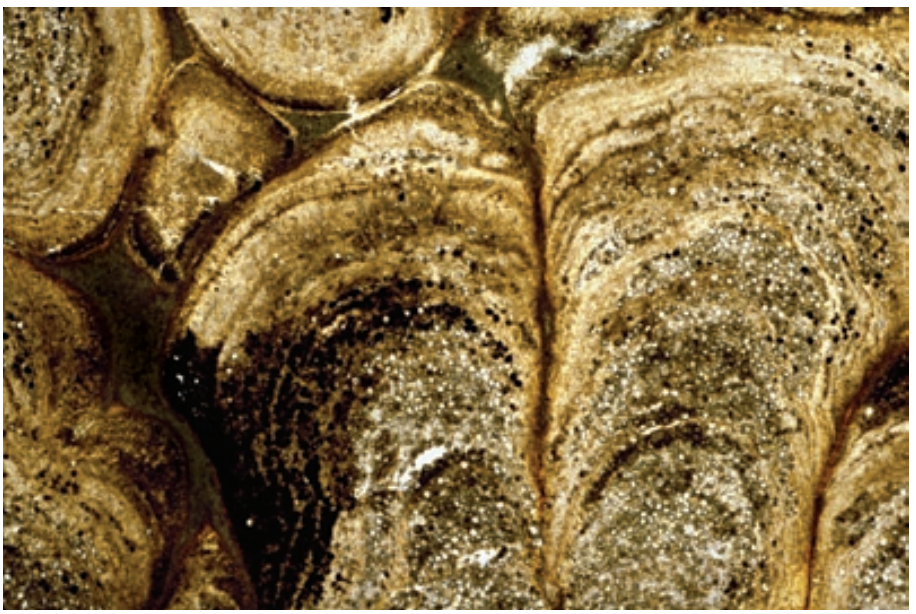

Eocene Green River Fm., Laney Mbr., Sweetwater Co., Wyoming

Finger-shaped to domal stromatolites of a lacustrine alga, *Chlorellopsis coloniata* (described as formed by unicellular coccoid algae of uncertain affinities by Bradley, 1929). The laminated, domal or digitate structures are typical of stromatolites created by the trapping and binding action of organic mats, even if the sporangial features (the layers of small spherical bodies visible throughout the columns) are not. The entire rock has been replaced by chert in this example.

PPL, HA = 14.5 mm

Up. Permian (Guadalupian) Tansill Fm., Eddy Co., New Mexico

A colony of *Collenella guadalupensis* forming a finger-like or domal skeletal structure that is part of the reef to near-backreef framework. The columns, which are composed of precipitated, not trapped calcium carbonate, are surrounded by typically fossiliferous, shelf margin carbonate detritus. Although viewed as a microbial deposit by some, it has been described as a probable stromatoporoid by others (J. A. Babcock, 2003, written commun.). This genus is known only from Upper Permian strata.

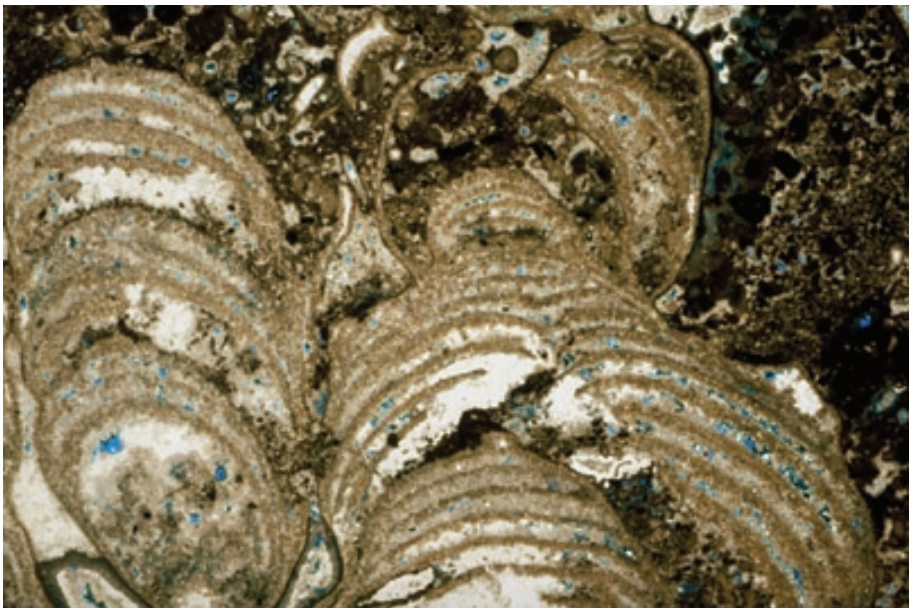

PPL, BSE, HA = 16 mm

Lo. Jurassic (mid. Liassic) limestone, Central High Atlas region, Morocco

An example of "clotted" fabric — possible bacterial crusts — in a sponge reef. Patchy, dark, micritic or peloidal accumulations, commonly found in association with sponges or other framework organisms are frequently interpreted as microbial precipitates although absolute evidence of a microbial origin is very hard to find. The darker patches of microbial material are surrounded here by normal micritic carbonate sediment.

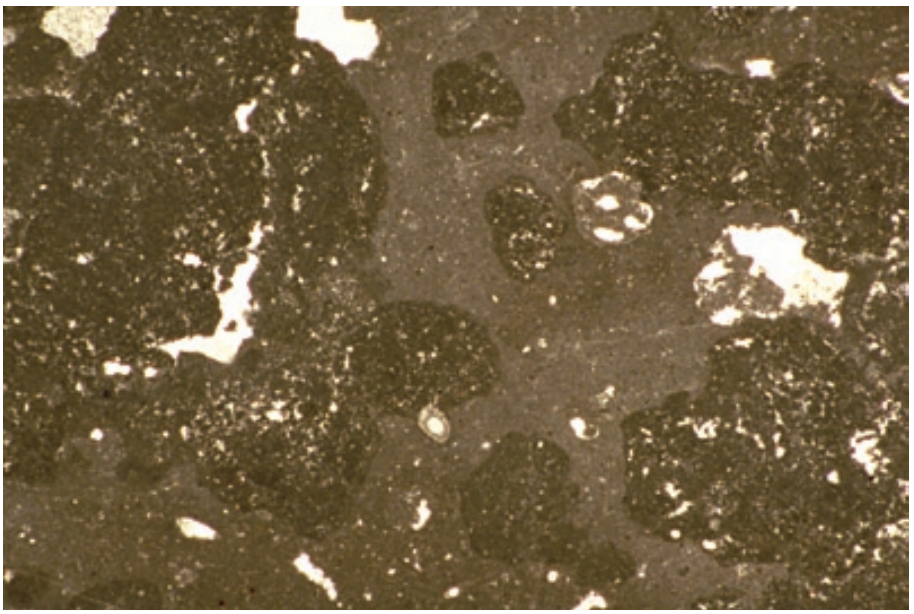

PPL, HA = 8 mm

Up. Permian (Kazanian?) Wegener Halvø Fm., Jameson Land, East Greenland

Dense, micritic masses (dark material) that may have formed around now-leached or decomposed grains. This microproblematicum has been classified as *Thartharella* sp. and it may be a cyanobacterial product (although, as with most problematic forms, it could also have other origins). Such micritic and peloidal encrustations are especially common in rocks of this age although they can be found essentially throughout the Phanerozoic rock record.

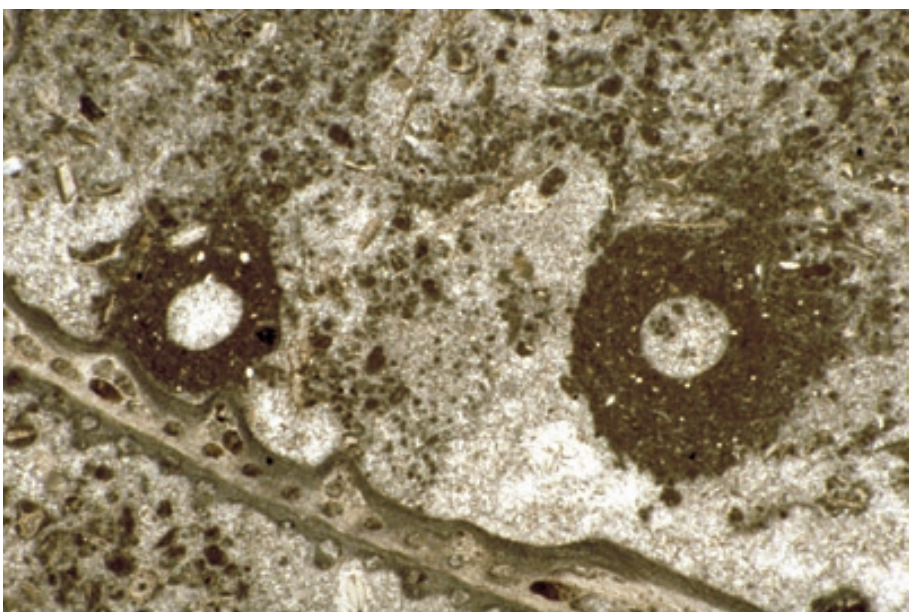

PPL, HA = 6 mm

MARINE GREEN ALGAE

Taxonomy and Age Range:

Phylum Chlorophyta
Family Codiaceae — Ordovician-Recent
Family Dasycladaceae — Cambrian-Recent
Ranges of some specific genera depicted in this section:
***Halimeda* - Cretaceous-Recent**
***Mizzia* - Permian**
***Mastopora* - Ordovician**

Environmental Implications:

Photosynthetic and thus require light. Green algae generally are most common at depths of 2 to 30 m, but some heavily calcified modern codiaceans are most abundant at depths of 50-100 m; a few forms extend into water depths greater than 100 m.

Wide salinity tolerance ranging from strongly hypersaline to brackish. Most calcified forms grow mainly in warm temperate to tropical areas with near-normal salinity waters. Also common in reef and near-backreef areas and can even form biohermal thickets or mounds.

Important contributors to sand- and mud-sized fractions of modern and ancient carbonate deposits of warm-water regions.

Skeletal Mineralogy:

Virtually all aragonite, but some calcitic forms may have existed in the past.

Morphologic Features:

Modern codiacean green algae (*Halimeda*, *Penicillus* and others) form upright, typically segmented, shrubby plants about 5-15 cm high. The segments are composed of extremely small, needle-like aragonite crystals (about 5 µm long), especially in surficial areas. The needles may be dispersed into the sediment upon death, forming a major source of carbonate mud (micrite). Other codiaceans disaggregate into intact, elongate plates with organized tubular or filamentous structure that may or may not be preserved after diagenesis. Paleozoic codiaceans also included nodular or crustose forms.

Dasycladacean green algae (e.g., *Cymopolia*) also consist of segmented, branching shrubs that stand several centimeters tall. Most segments separate on death of the organism and form isolated, generally spherical, hollow grains with radially-oriented tubules or wall perforations (utricles).

Keys to Petrographic Recognition:

1. **Aragonitic mineralogy generally results in poor preservation in ancient limestones.**
2. **Typically found as molds or filled molds with only traces of the original tubular fabric or other internal structures. Recognition is facilitated where tubules were filled with Mg-calcite marine cement or where micritic sediment infiltrated the plates and was lithified prior to dissolution of aragonite from the plates. In such cases, the structure of green algal grains may be a reverse of the original one — pores filled with carbonate material and former plates leached to produce voids or secondarily-filled former voids.**
3. **Generally found as small (mm-sized), disarticulated segments rather than complete plants.**
4. **Well-defined tubular and/or filamentous structures, where preserved.**
5. **Different structures occur in the cortex and medulla regions of many codiacean green algae.**
6. **Radial symmetry in dasycladaceans; outwardly-oriented utricles in some codiaceans.**
7. **Some calcispheres (small, spherical, single- or double-walled calcareous bodies) and large volumes of carbonate mud may be of green algal origin.**

PHOTO SCALES AND ABBREVIATIONS ARE EXPLAINED IN THE BOOK'S INTRODUCTION

Typical codiacean green algal structure

This diagrammatic view of *Halimeda* sp. depicts an individual plate segment and its relationship to the full plant. Plate walls (cortex areas) are perforated with small tubes (utricles) and are heavily calcified. The plate centers (medulla regions) are only weakly calcified and have complexly intertwined filaments. Adapted from Wray (1977) and other sources. The approximate scale of the whole bush (left) is apparent from the photograph below.

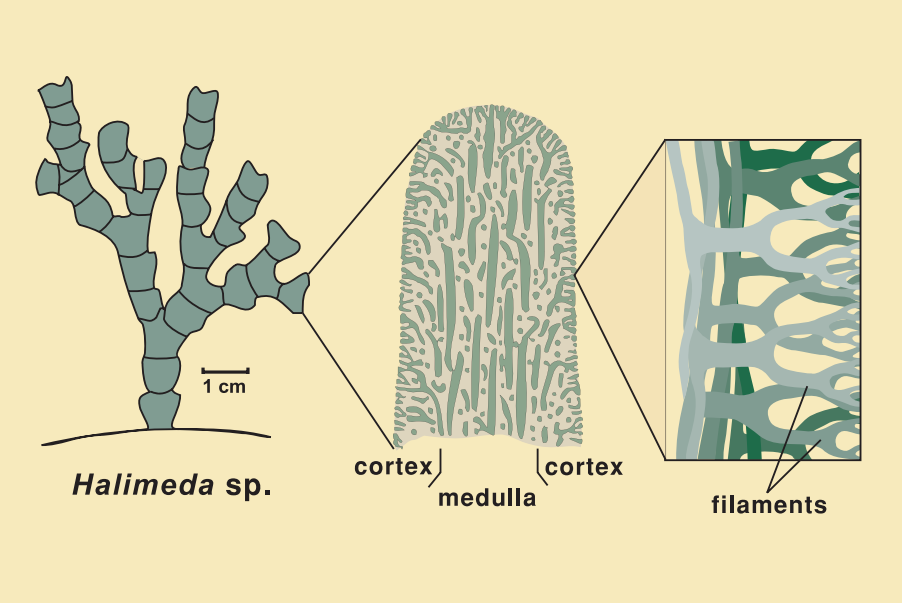

Recent sediment, Florida reef tract, southern Florida

Dried samples of four common green algae that are significant sediment producers in modern Caribbean shelf settings. From left to right: *Halimeda*, *Penicillus*, *Udotea*, *Rhipocephalus*. *Halimeda* is a prolific carbonate sand former, *Penicillus* is a major carbonate mud former, and the other two are more weakly calcified minor mud producers.

Mac, HA = 21 cm

Holocene sediment (beachrock), Grand Cayman, Cayman Islands, B.W.I.

A complete single plate shed by *Halimeda* sp., a green alga (left side in picture above). Note the characteristic yellowish to reddish-colored material that is filled with minute aragonite needles and a series of tubules (utricles) — large ones in the center of the grain (mainly oriented parallel to the long axis of the grain) and smaller ones near the edges (oriented largely perpendicular to the grain margins). The tubules have been partially filled with syndepositional marine cement.

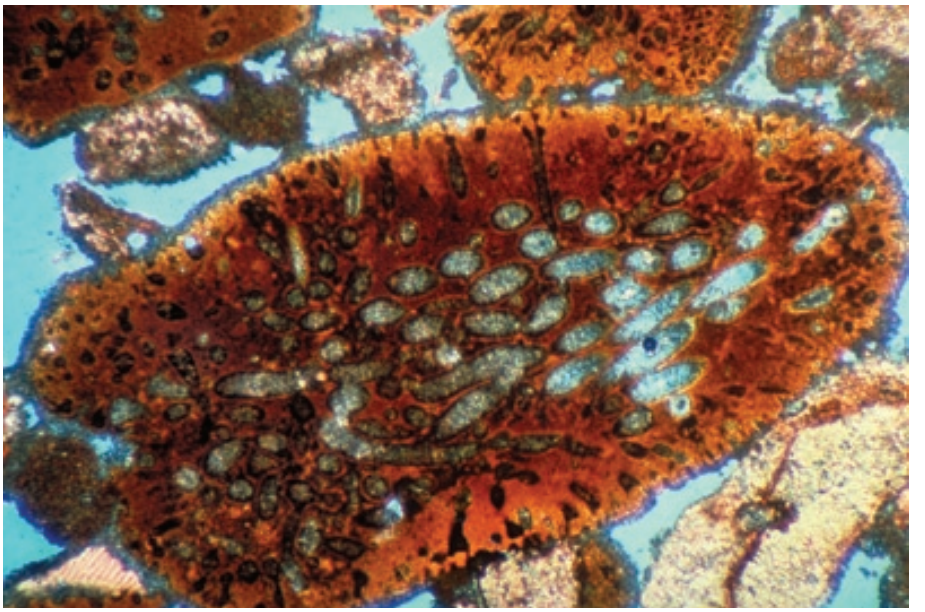

PPL, BSE, HA = 2.4 mm

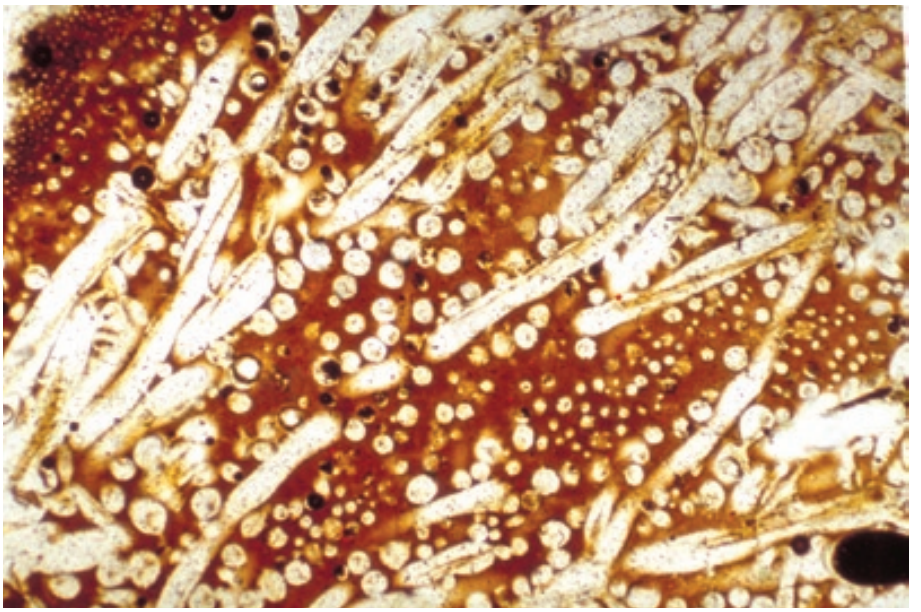

Recent sediment, Great Bahama Banks, Bahamas

A close-up view of a *Halimeda* sp. plate. The reddish-brown organic tissue is substantially calcified, but consists of extremely small crystals of aragonite (a mineral likely to be dissolved during later diagenesis). The utricles are clearly visible and here have not been filled with syndepositional marine cement.

PPL, HA = 2.0 mm

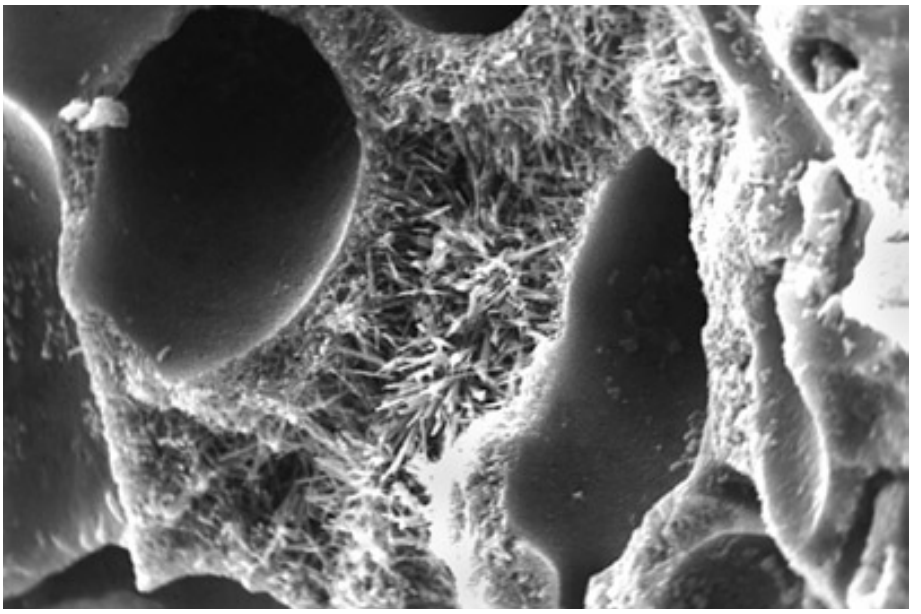

Recent sediment, Belize

An SEM image showing a cross section through a broken *Halimeda* sp. plate. Note the tubular passageways (utricles), originally occupied by plant tissues and intervening calcified areas (equivalent to the brownish-colored areas in previous photographs). The calcified areas consist of abundant, interlocked, predominantly randomly-oriented aragonite needles that constitute the preservable portion of the *Halimeda* plate.

SEM, HA = 113 μm

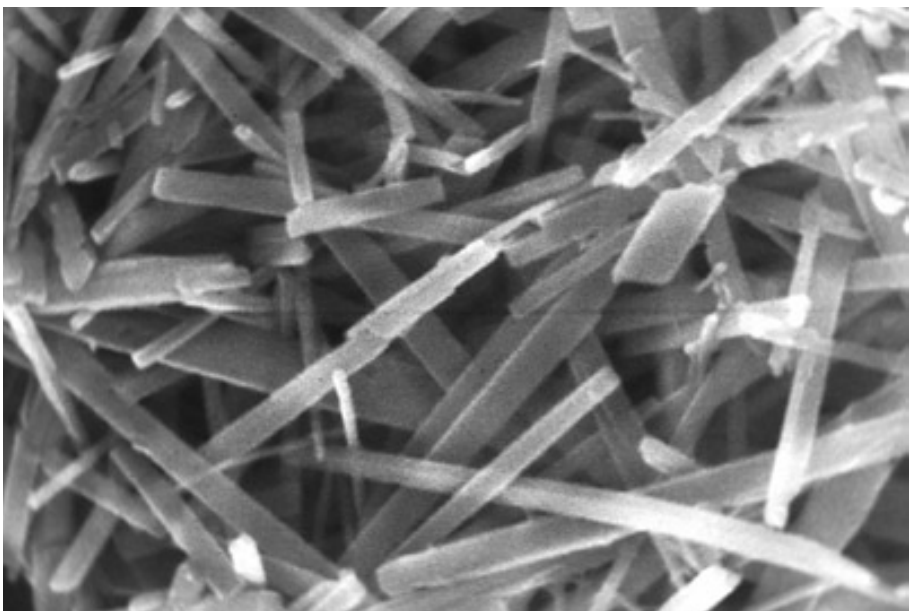

Recent sediment, Belize

A higher magnification SEM image of a *Halimeda* sp. plate showing details of the interlocking aragonite needles seen in the previous photograph. Needles such as these are found in many species of green algae including *Penicillus*, *Udotea*, *Halimeda* and others. When the algae decompose, the needles may be scattered and add significantly to the local production of clay-sized particles (carbonate mud). The porous structure, the unstable mineralogy and the small crystal size make it likely that *Halimeda* plates will be substantially altered during diagenesis.

SEM, HA = 11.3 μm

Pleistocene Miami Ls., Dade Co., Florida

An extensively altered, roughly 120,000 year-old *Halimeda* sp. plate. Note the filling of original tubules (utricles) with blocky meteoric calcite but retention of dark, organic-rich inclusions in areas of neomorphosed aragonite.

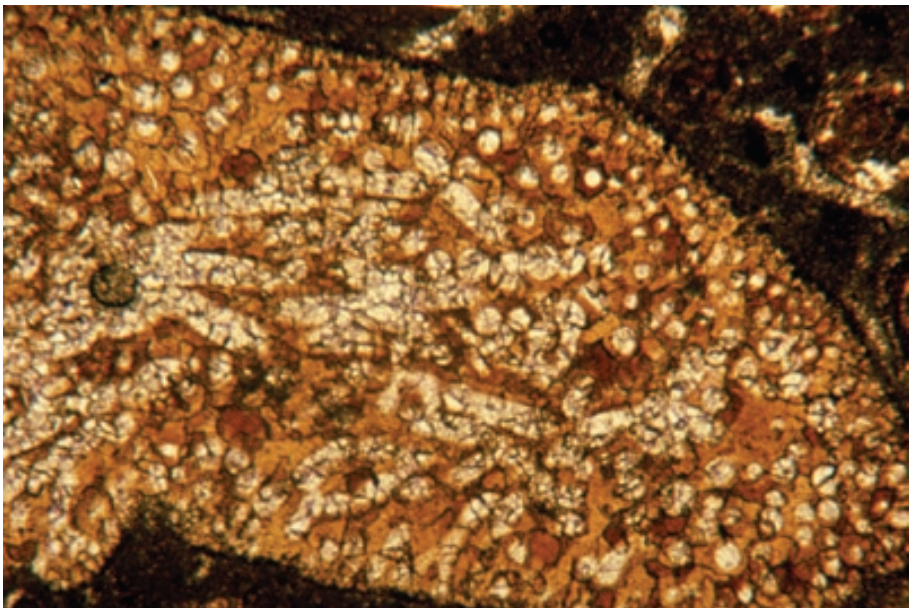

PPL, HA = ~14 mm

Pleistocene Key Largo Ls., Florida Keys, Monroe Co., Florida

A close-up view of an even more altered *Halimeda* sp. plate, again from a 120,000 year-old unit. Here, the tubules and grain exterior are outlined with cement, but the entire original mineralized part of the grain has been leached, generating substantial intragranular secondary porosity. Structural preservation in this example largely was due to the synsedimentary formation of micrite envelopes created by epiphytic or epilithic cyanobacteria after the *Halimeda* plates fell to the sea floor.

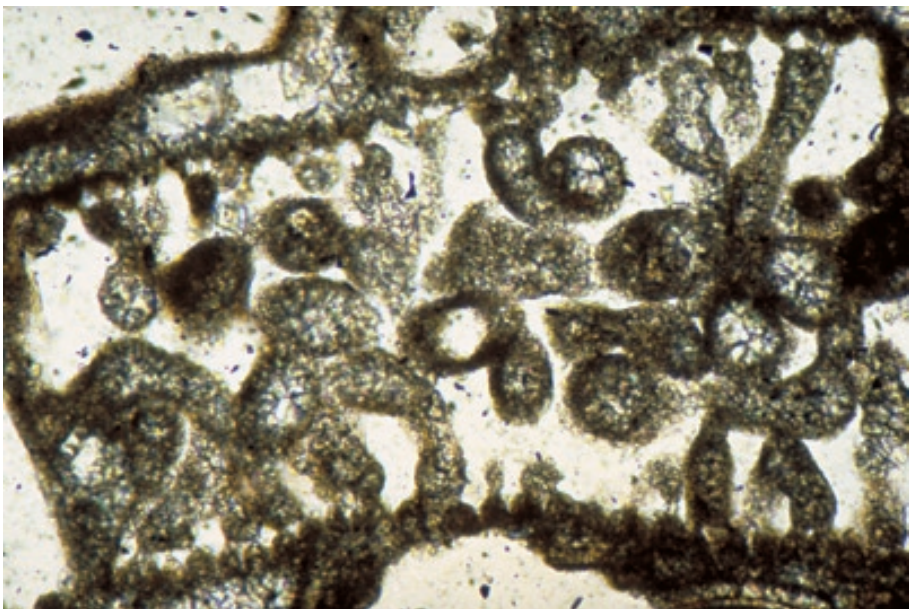

PPL, HA = 0.65 mm

Up. Miocene (Messinian) Upper Coralline Limestone Fm., Ghar Lapsi, Malta

An older example of leached *Halimeda* grains in a limestone in which green algal plates form a substantial part of the total sediment. Note the partial preservation of utricles and grain outlines that still allow the identification of the grains despite the complete leaching and porosity formation in the areas of original aragonite mineralization. Such leached platy algal deposits can be prolific hydrocarbon reservoirs.

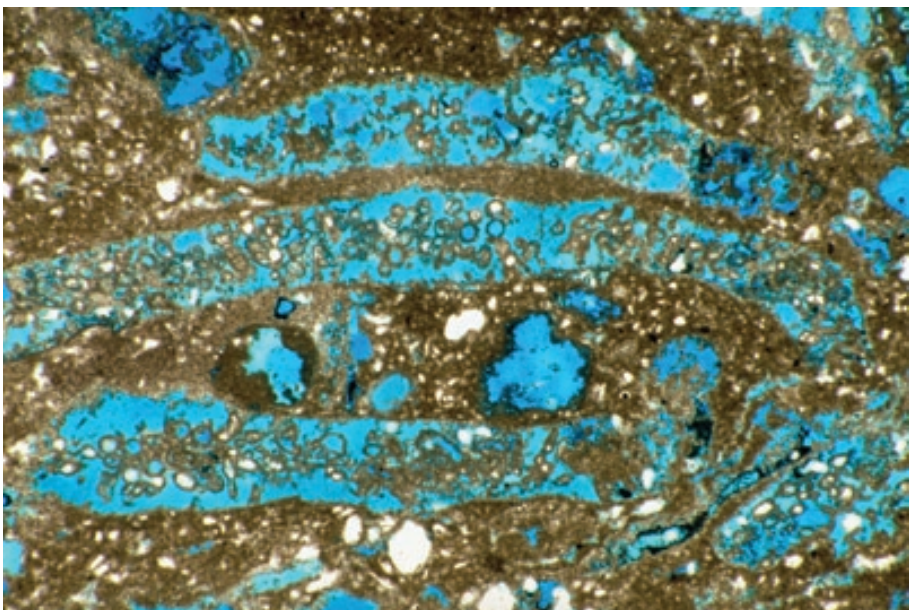

PPL, BSE, HA = 5 mm

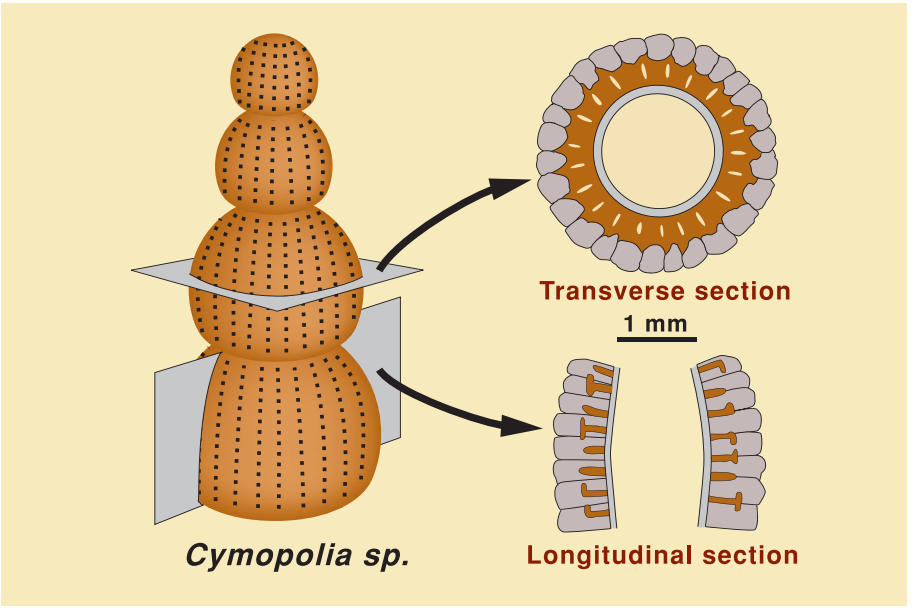

Typical dasycladacean green algal structure

Dasycladacean algae are far more widely recognized in the geologic record than codiacean forms. This diagram (adapted from Wray, 1977) of *Cymopolia* sp. shows common characteristics of dasycladaceans — a small, upright plants having its thallus or body structure radially arranged around a central axis with whorls of lateral branches. Whole plants can disarticulate into individual segments.

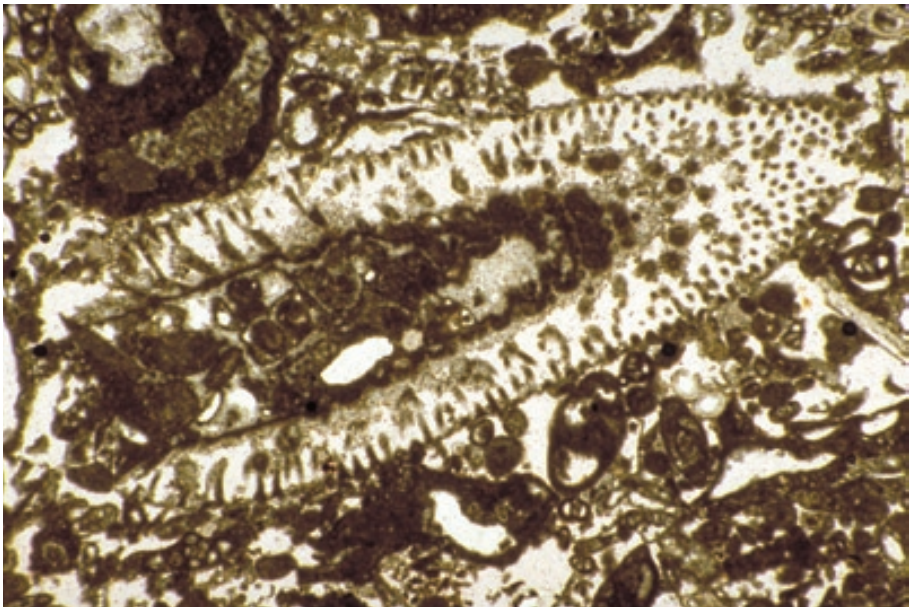

Oligocene Suwanee Ls., Citrus Co., Florida

A probable dasycladacean green algal grain. Note the infilling of original pores and outlining of the grain with micritic sediment or precipitates that allows recognition of the grain. In the absence of such "pore casting" of the structure prior to dissolution, the origin of this grain would probably not be discernable.

PPL, HA = 5 mm

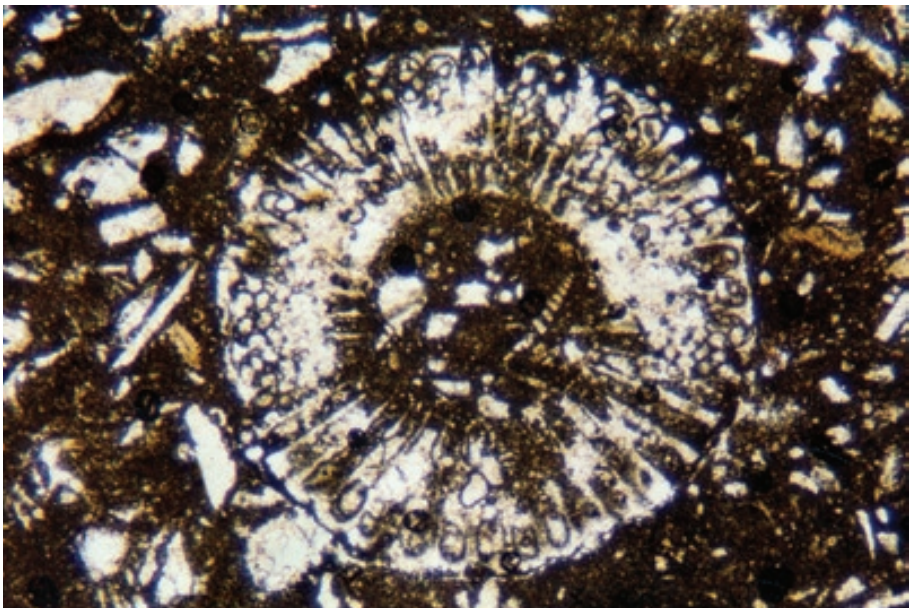

Cretaceous, Albian-Cenomanian Tamabra Ls., San Luis Potosi, Mexico

A transverse cross section through a dasycladacean green alga. Shows the radial symmetry of elements about the central cavity. The characteristic features which allow identification are the presence of radiating tubes and a central cavity, coupled with poor preservation of wall structure.

PPL, HA = 5.5 mm

Up. Permian (Guadalupian) Tansill Fm., Eddy Co., New Mexico

A cluster of segments of *Mizzia* sp., another dasycladacean green algae. This alga has hollow, spherical segments perforated by tubules that are oriented perpendicular to the inner and outer walls. Preservation is due to synsedimentary infill of the tubules and coating of the grain walls rather than the presence of mineralized parts of the original organism.

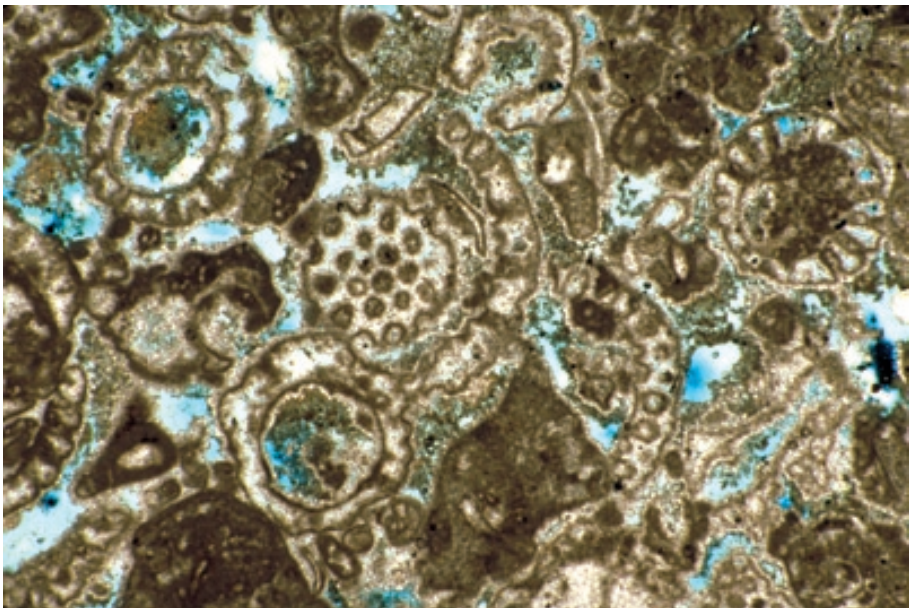

PPL, BSE, HA = 5.8 mm

Up. Permian (Guadalupian) Tansill Fm., Culberson Co., Texas

Three *Mizzia* green algal grains with substantial intraparticle porosity. Note the radially-symmetrical tubules that characterize dasycladacean algal remains. This species was a major carbonate sand producer in the near-back-reef setting, a setting similar to that occupied by some species of modern codiacean algal genus, *Halimeda*.

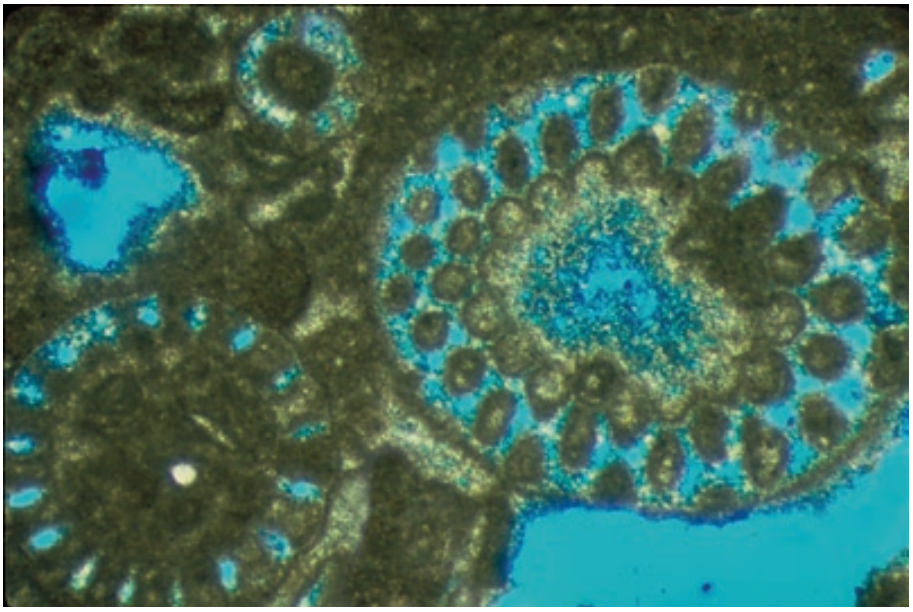

PPL, BSE, HA = 3.6 mm

Ordovician Chambersburg Ls., Shenandoah Co., Virginia

An early dasycladacean green alga, *Mastopora* sp., showing radially-arranged cortical cups along the grain margin, but with no preservation of any other wall structure. Note the large, sparry calcite-filled, central cavity of this alga.

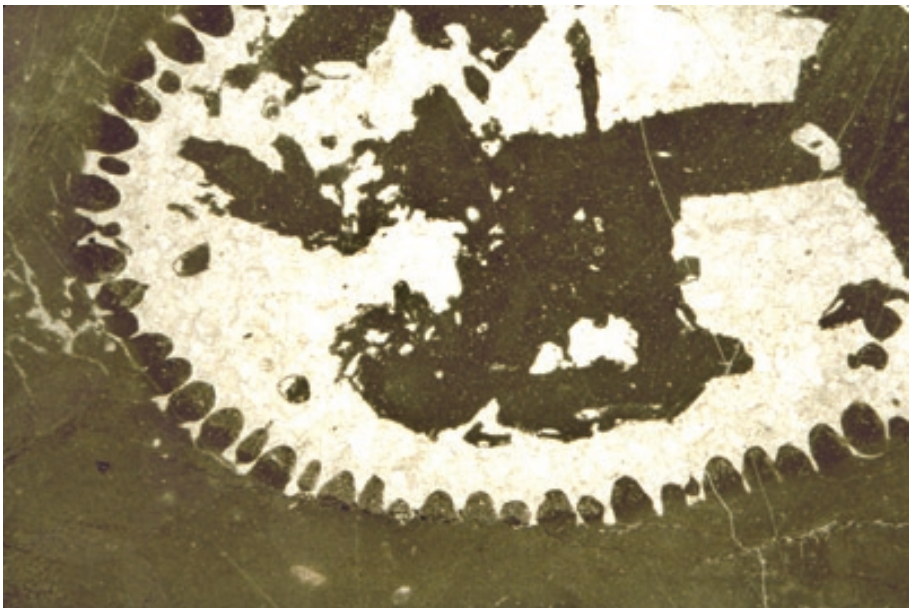

PPL, HA = 23 mm

CHAROPHYTES

Taxonomy and Age Range:

Charophytes are a group of green algae that apparently share a common ancestor with land plants; RNA and DNA evidence indicates that charophytes are the closest non-plant relative of land plants.

Traditionally placed in the Phylum Charophyta, and separated from other green algae by placement in the Class Charophyceae — Late Silurian-Recent.

Environmental Implications:

Photosynthetic and thus require light for growth.

Modern examples are found in fresh to brackish waters (with rare occurrences in saline waters); charophytes are most common in lacustrine settings, especially clear-water, alkaline/calcium-rich lakes. Fossil forms are widely distributed in nonmarine rocks, especially in shales and limestones, but also extend into rocks deposited in brackish and perhaps even more saline environments (Racki, 1982). It should also be remembered that calcified reproductive parts (oogonia) can be readily transported into marine waters by rivers and streams.

Charophytes can be significant rock-forming elements as well as useful biostratigraphic markers, especially in Cenozoic lacustrine deposits.

Skeletal Mineralogy:

Almost all are low-Mg calcite, but aragonite has also been recorded; low-Mg calcite is also the dominant inorganic cement around plant stems in lacustrine settings.

Morphologic Features:

Modern charophytes, commonly known as stoneworts or brittleworts, grow as bushy plants up to 60 cm tall with whorls of short branches and attached oogonia.

Carbonate can be precipitated as plant stem encrustations (in the same way that many other plants may get encrusted in shoreline or spring-related travertines), but the reproductive organs (termed oogonia or gyrogonites) are the only parts that are substantially calcified by the organism themselves.

Keys to Petrographic Recognition:

1. **Calcified oogonia are generally the only clearly identifiable charophyte forms.**
2. **Oogonia are recognizable as ovoid to circular bodies, roughly 0.5 to 1 mm in diameter, with spirally arranged tubules that form external ridges.**
3. **Most common appearance is as a large central cavity ringed by smaller circular to ovoid features (that represent cuts through the external spiral tubules). Wide separations between adjacent charophyte tubules and their spiral arrangement help to distinguish charophyte remains from those of dasycladacean green algae.**
4. **When found, they commonly occur in large numbers.**

Characteristic features of a typical charophyte alga

The structure of a modern charophyte, *Chara* sp., is shown on this diagram, adapted from Wray (1977). The oogonia are calcified, and thus they are the most likely parts to be preserved in sediments. Stems may also be encased in externally precipitated calcite (travertine, for example) and thus may be preserved as casts. Scale of plant is illustrated in photograph below.

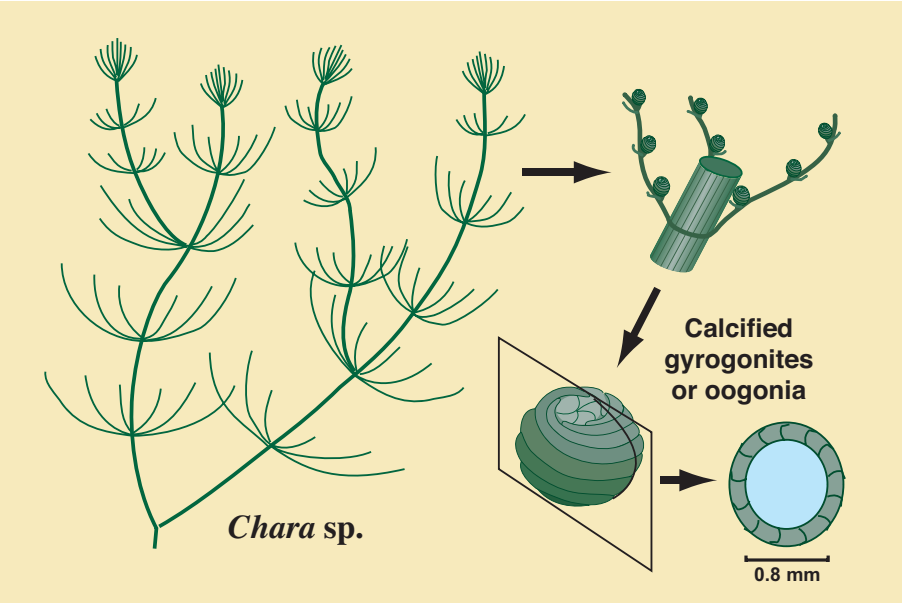

Holocene of Green Lake, Fayetteville, New York and Blue Hole, Ohio

Macroscopic views of charophyte deposits: a living charophyte (*Chara* sp.) containing about 50% dry weight $CaCO_3$ (right) and carbonate mud that consists mostly of low-Mg calcite derived from charophytes (left). The right-hand picture shows low-Mg calcite encrustations around charophyte stems. Photographs courtesy of Walter E. Dean.

Mac, L: HA = ~18 cm; R: HA = ~3 cm

Up. Pleistocene lacustrine sediment, U.S.A.

An SEM image of the calcareous outer cover of the female reproductive structure (oogonium) of a charophyte. Note the spirally arranged external cortical tubes that give the grain a ribbed appearance. Photograph courtesy of Walter E. Dean (taken by Richard M. Forester).

SEM, HA = 0.78 mm

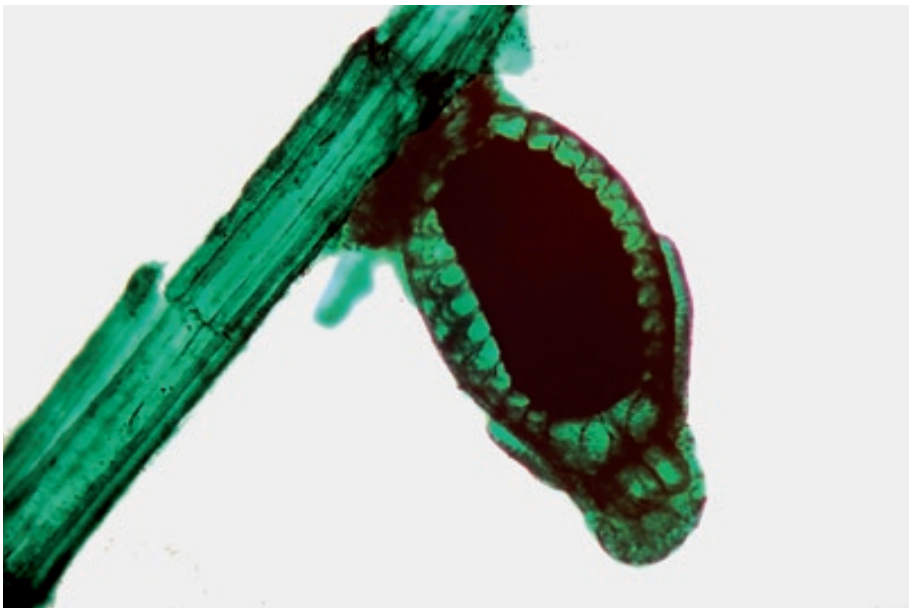

Recent lacustrine sediments, U.S.A.

A cross-section through a single organically stained oogonium of *Chara* sp. that is still attached to the plant stem. Note the hollow central cavity (black) surrounded by cortical tubes that are spirally arranged around the oogonium.

PPL, OS, HA = 1.8 mm

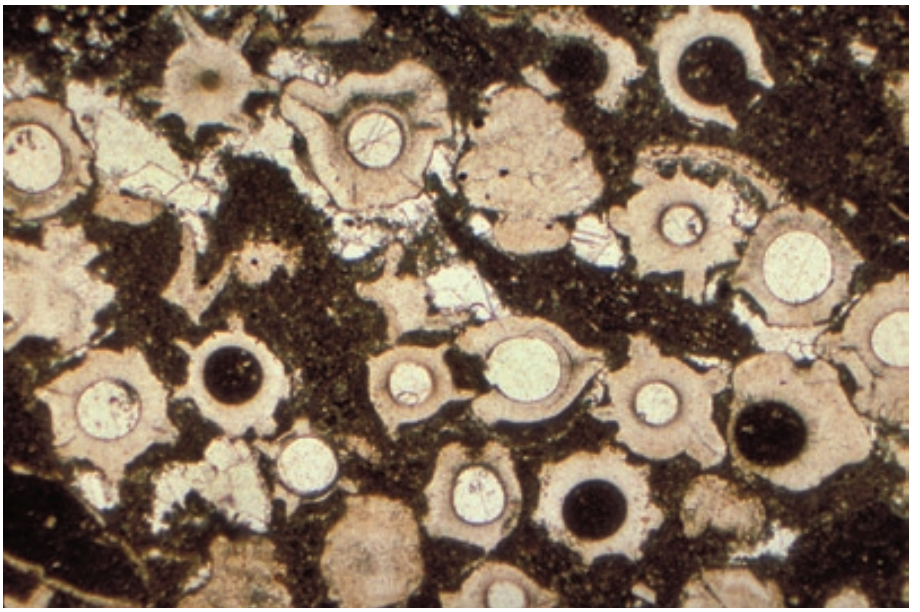

Up. Devonian Yaosoo Fm., Dushan, Guizhou Province, People's Republic of China

Calcified gyrogonites (oogonia) are also recognizable in thin section. These are examples of some very early probable charophytes; they show distinctive outlines with vertical ribbing and the well-preserved fabric of originally calcitic grains. Photograph courtesy of Albert V. Carozzi (see Carozzi, 1993; reference given in reference list at end of this book's Introduction).

PPL, HA = 3 mm

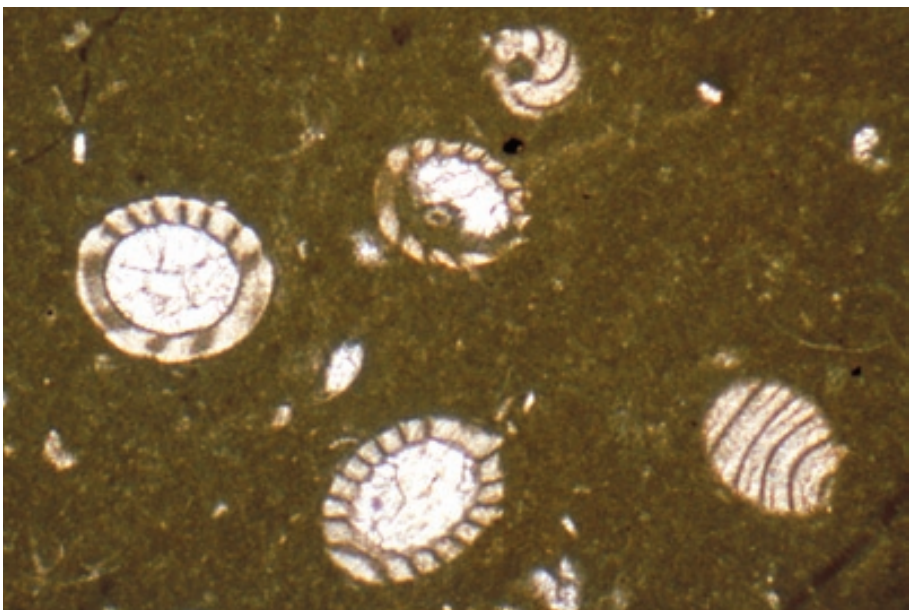

Up. Jurassic, Portlandian (Purbeckian), Salève, France

A calcareous mudstone with *Chara* sp. oogonia showing characteristic wall structure with spiral arrangement of cortical tubes. Photograph courtesy of Albert V. Carozzi (see Carozzi, 1993; reference given in the Introduction section of the book).

PPL, HA = 2 mm

Lo. Cretaceous Newark Canyon Fm., Nevada

A transverse section through a calcified gyrogonite (oogonium) of a charophyte, showing the characteristic central tube with surrounding cortical tubes. The distinctness of the individual cortical tube walls and the quality of their preservation helps to distinguish such charophyte grains from similar appearing dasycladacean green algal remains. In this section and the one below, however, the characteristic spiraling of the tubules is not discernable.

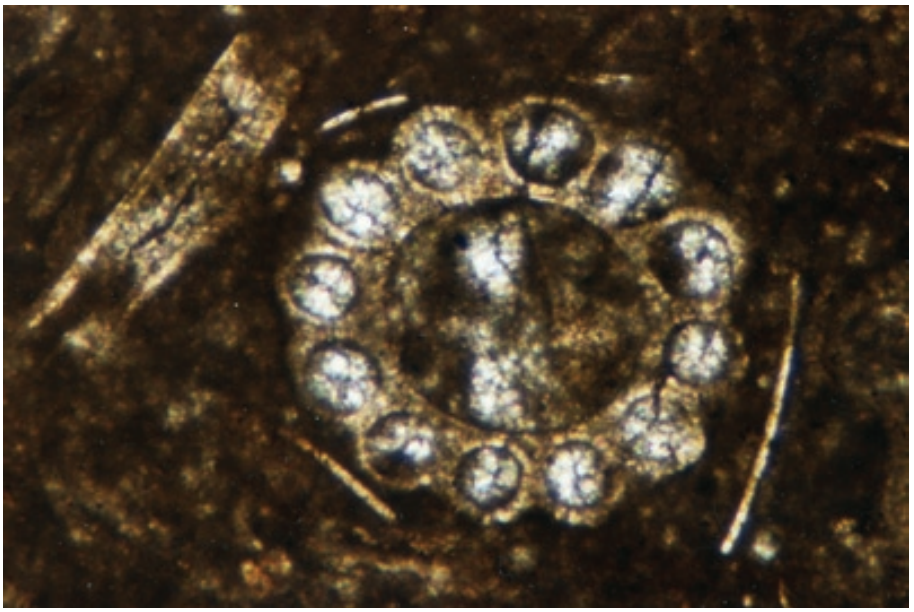

PPL, HA = 2.1 mm

Lo. Cretaceous Newark Canyon Fm., Nevada

Oblique sections through the reproductive parts of two charophytes again showing variations in views of the central cavity and surrounding cortical tubes.

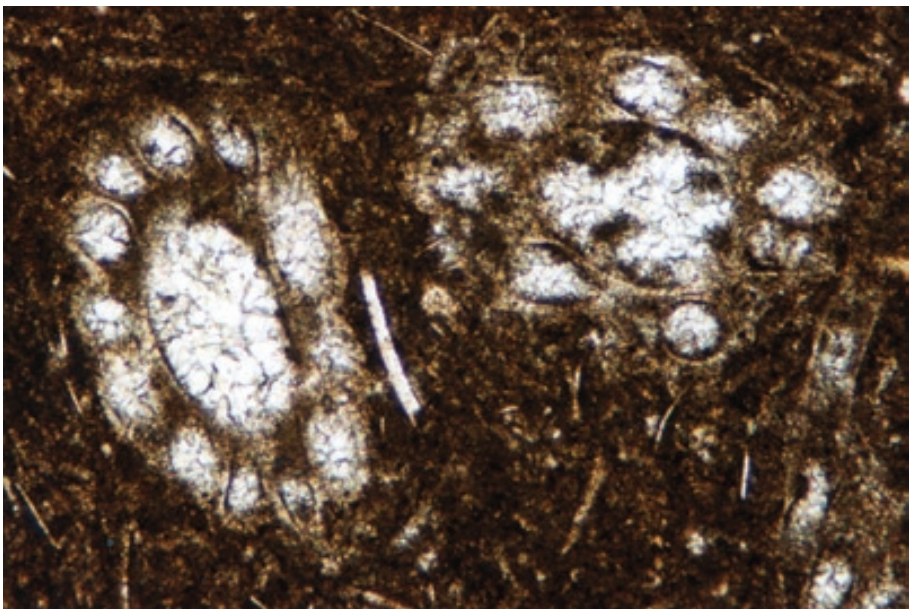

PPL, HA = 2.7 mm

Recent sediment, Elk Lake, Clearwater Co., Minnesota

An SEM image of *Phacotus* sp., a planktonic, lacustrine organism. Although not a charophyte, it is both a green alga and one of the few calcareous planktonic organisms that contributes carbonate to lacustrine sediments. It thus is commonly found in association with charophytes in such deposits. Photograph courtesy of Walter E. Dean.

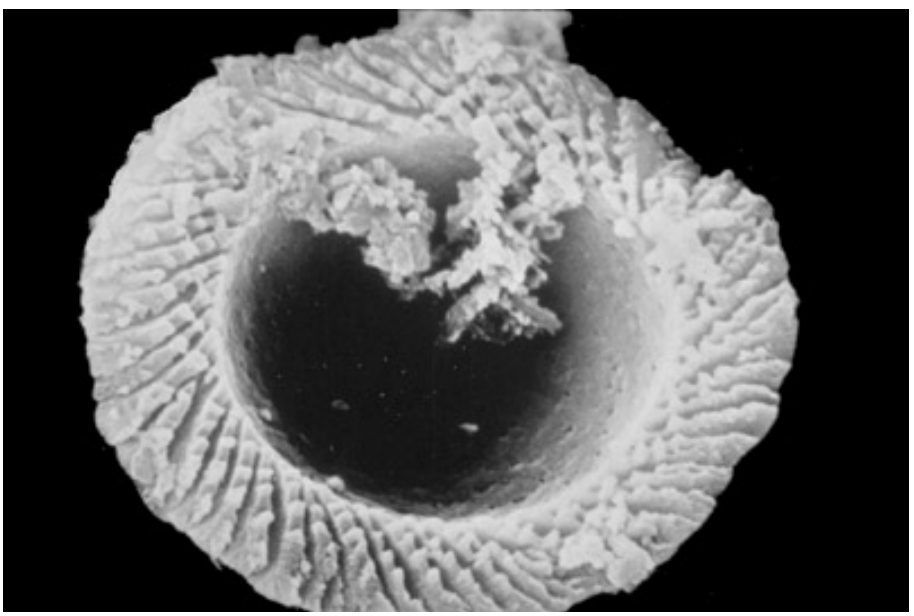

SEM, HA = 15 μm

RED ALGAE

Taxonomy and Age Range:

Phylum Rhodophyta: Cambrian - Recent

Family Corallinaceae: Jurassic-Holocene (possible late Paleozoic forms)
Family Solenoporaceae: Cambrian-Paleocene (Miocene??)
Family Squamariaceae: Pennsylvanian?-Holocene
Family Gymnocodiaceae: Permian-Cretaceous

Environmental Implications:

Photosynthetic — require light, but are the algal group best adapted to use the blue light that penetrates into deep waters. Thus, some may be found to depths of 125 m or more.

Dominantly marine (about 2% live in fresh water); most live in waters with salinities ranging from 33-42 ppt.

Wide temperature latitude — allows them to be an important component of both cold- and warm-water carbonates and therefore makes them difficult to use as paleoclimate indicators.

Fragile, branching forms are found in moderate wave energy areas. Encrusting, nodular, and robust branching forms can withstand very high wave energy. Indeed, red algal encrusters are the dominant binding organisms in most Cenozoic to modern reefs.

Skeletal Mineralogy:

Coralline red algae are/were composed of very high-Mg calcite (8 to >30 mole% Mg); squamariaceans are dominantly aragonite.

Morphologic Features:

Red algal grains typically are cm-sized although crustose forms can reach decimeter size.

Members of the red algae have several growth habits: a) as fragments of encrusting, nodular and rigid, branching plants, b) as erect, articulated, branching or arborescent forms, c) as massive encrusters and binders, and d) as coatings on other grains (forming rhodoids or rhodoliths).

Keys to Petrographic Recognition:

1. **The heavy calcification and original high-Mg calcite composition of many red algae leads to very good preservation of both internal structures and external outlines.**
2. **Coralline red algae (and most other red algae) are most easily identified by their very fine-scale reticulate, cellular or latticework internal structure that reflects the filamentous fabric of these organisms. High magnification and/or ultra-thin sections may be needed for recognition of this structure.**
3. **Reproductive (spore producing) bodies commonly are present in coralline red algae. Small, individual, spherical cavities are termed sporangia; sometimes these can be merged into a larger cavity, termed a conceptacle.**
4. **There is a clear differentiation between external (perithallus) and internal (hypothallus) structural layers in many coralline red algae.**
5. **Solenoporoids are characterized by radiating or sub-parallel tubular or filamentous structures; cells show polygonal shapes in transverse section; they lack conceptacles and are found as encrusting, rounded or nodular masses.**
6. **Squamariacean red algae have poorly-preserved structure due to their aragonitic composition — structure is visible mainly where early sediment infiltration or cementation occurred (illustrated in the following section on phylloid algae).**

PHOTO SCALES AND ABBREVIATIONS ARE EXPLAINED IN THE BOOK'S INTRODUCTION

Characteristic structures of a representative coralline red alga

The crustose coralline algae, illustrated here by *Lithophyllum* sp., are the most heavily calcified of the modern red algae. They have a reticulate cellular (filamentous) structure with an exterior layer (perithallus) that is differentiated from the interior (hypothallus), as seen in this diagram adapted from Wray (1977). Reproductive organs (sporangia or conceptacles) may also be present. Coralline red algae were important sediment formers from the Jurassic to the Recent.

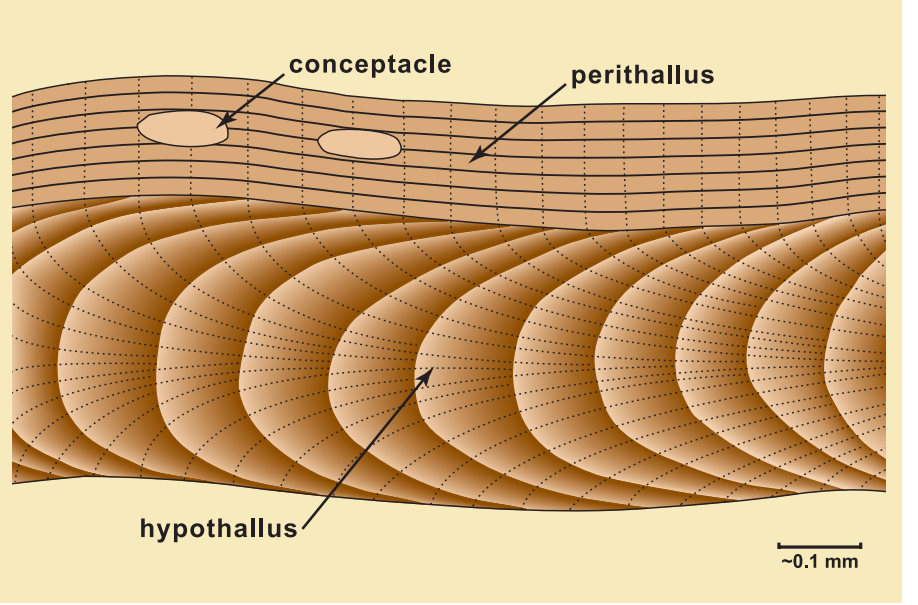

Characteristic structures of a representative segmented red alga

Not all coralline algae are encrusters or rigidly branched — articulated forms, such as the *Corallina* sp. shown here in a diagram adapted from Wray (1977), also are common. Their calcified segments disarticulate upon death and are contributed to the sediment.

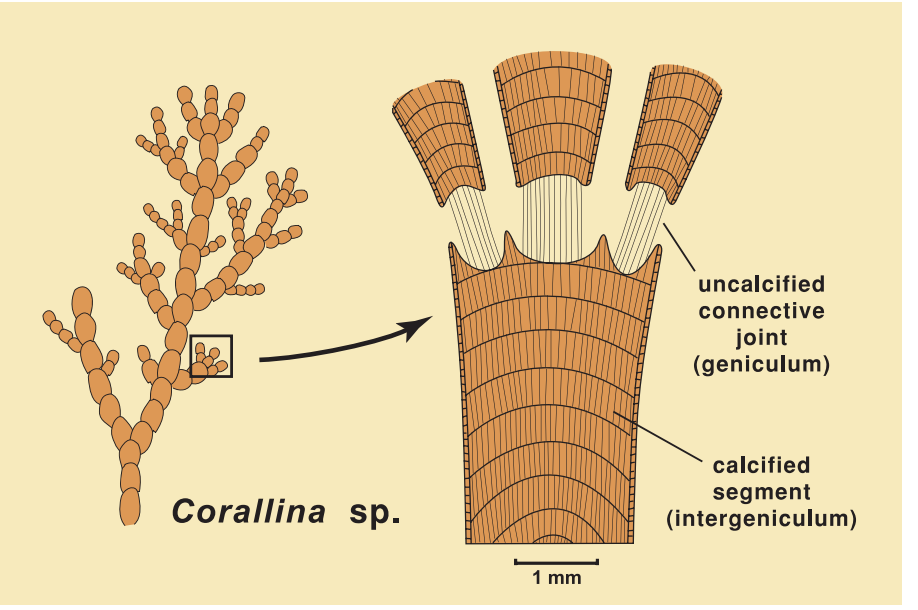

Recent sediment, St. Peter's Parrish, Barbados

This modern crustose coralline red algal grain shows differentiation of cellular structure in inner and outer layers. The outer layer (perithallus) has denser structure and cells oriented outward; the inner layer (hypothallus) has a series of light and dark bands and cell structure oriented parallel to the long axis of the grain. Compare with diagram at top of page.

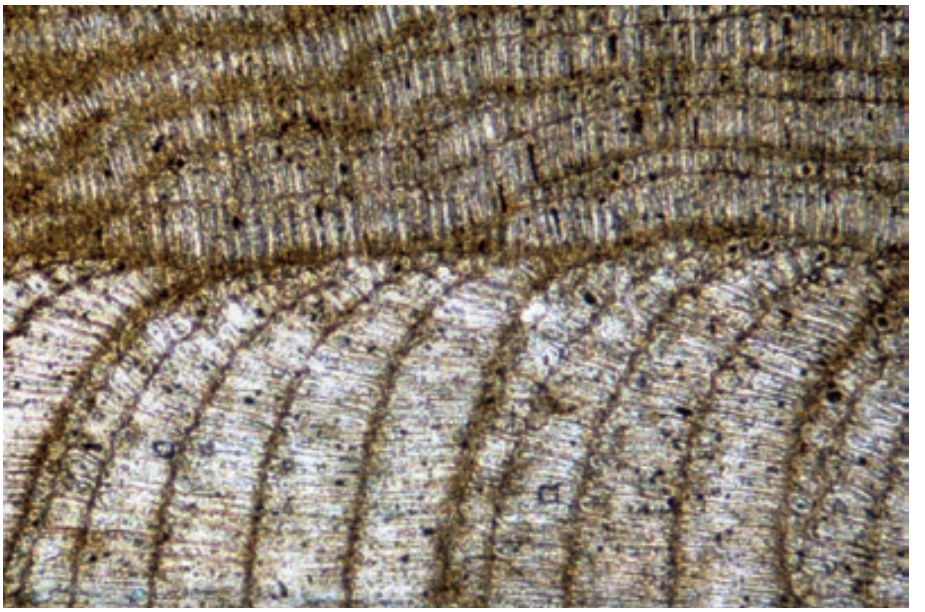

PPL, BSE, HA = 0.6 mm

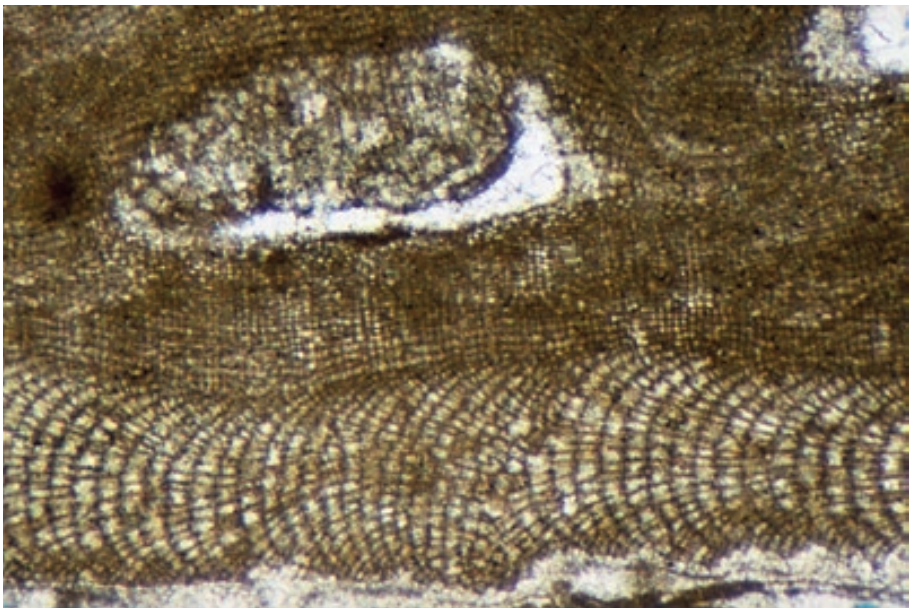

Pliocene-Pleistocene limestone, Boca Grandi, Aruba

A crustose coralline red algal grain showing differentiation of cellular structure — the hypothallus in the lower part of the photograph and the perithallus with a reproductive organ (termed a conceptacle) in the upper part. The regular, and extremely small-scale boxwork structure of both layers is the most diagnostic feature for recognition of red algae.

PPL, HA = 1.6 mm

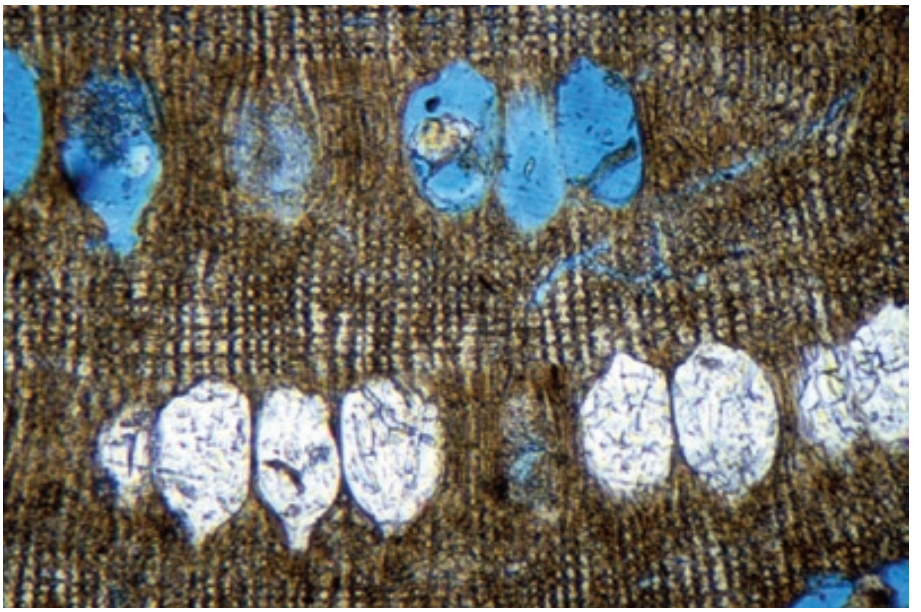

Recent sediment, Grand Cayman, Cayman Islands, B.W.I.

A modern crustose coralline red algal grain showing both diagnostic cellular structure and a series of reproductive bodies (sporangia), some of which are porous whereas others have been filled with sparry calcite. The high-Mg calcite composition of coralline red algae generally leads to excellent preservation of their skeletal structure.

PPL, BSE, HA = 0.65 mm

Oligocene Lower Coralline Limestone Fm., Malta

An irregularly-shaped crustose coralline red algal nodule (termed a rhodoid) showing characteristic fine-scale cellular structure with distinct, lighter-colored rows of small, spore-bearing reproductive bodies (sporangia).

PPL, BSE, HA = 14.5 mm

Eocene Totara Fm., Up. Rhodolith Ls., northern Otago, New Zealand

A close-up view of irregular, sheet-like, crustose coralline red algal encrustations in a rhodoid. The spar-filled gaps between successive layers of red algal encrustations are quite common in rhodoids. The spherical rhodoid grains in the rock from which this example is taken are 2 to 4 cm in diameter

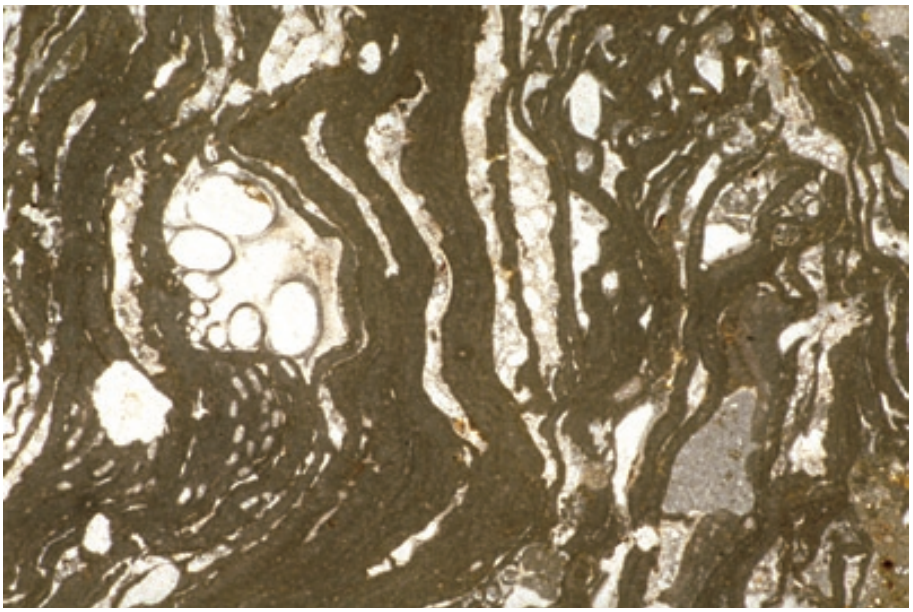

PPL, HA = 10 mm

Up. Miocene (Tortonian-Messinian) Upper Coralline Limestone Fm., Malta

A cool-water sediment with multiple layers or plates of red algal material (probably *Mesophyllum* or *Lithophyllum*) forming sheet-like seafloor encrustations. Crustose coralline red algae are a very important contributor to cool-water carbonate deposits (extending even into polar waters). Despite being photosynthetic organisms, red algae are found even at water depths in excess of 100 m. The surrounding sediment is a silty, detrital limestone.

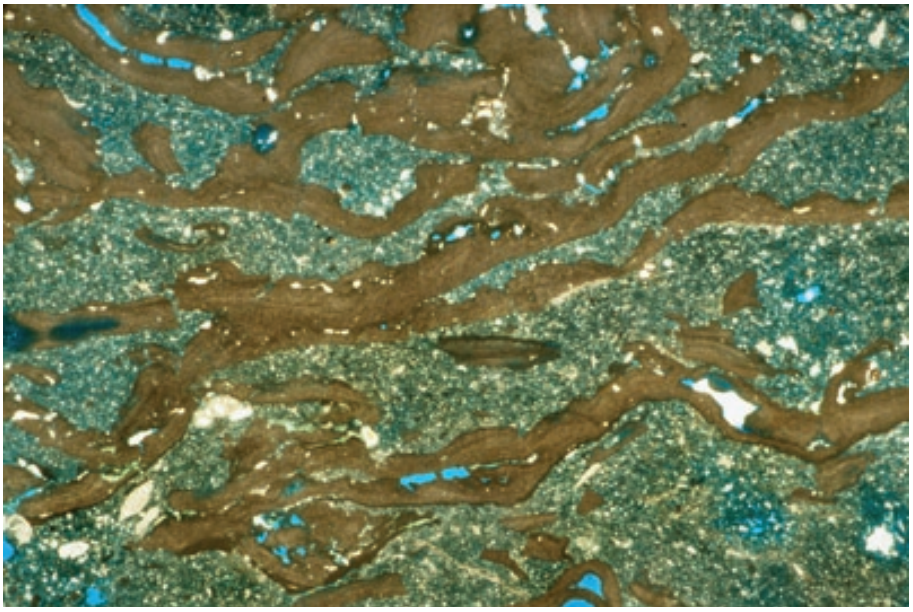

PPL, BSE, HA = 12.5 mm

Mid. Eocene Naranjo Fm., Coamo Springs Mbr., Ponce-Coamo area, Puerto Rico

An example of a branching crustose coralline red alga. Such forms are quite brittle and subject to breakage, making them substantial contributors of fragmental material in reef-slope, back-reef, or shelfal settings. Sample from E. A. Pessagno, Jr.

PPL, HA = 5 mm

Recent sediment, San Juan harbor, Puerto Rico

Some genera of red algae, the segmented corallines, are articulated, with individual hard segments held together by soft tissue (see diagram at the beginning of the red algal section). This example shows both longitudinal and transverse cuts through an intact modern segmented red alga, probably *Jania* sp. These organisms can be prolific contributors to the sand-sized fraction of carbonate sediments.

PPL, BSE, HA = 3.2 mm

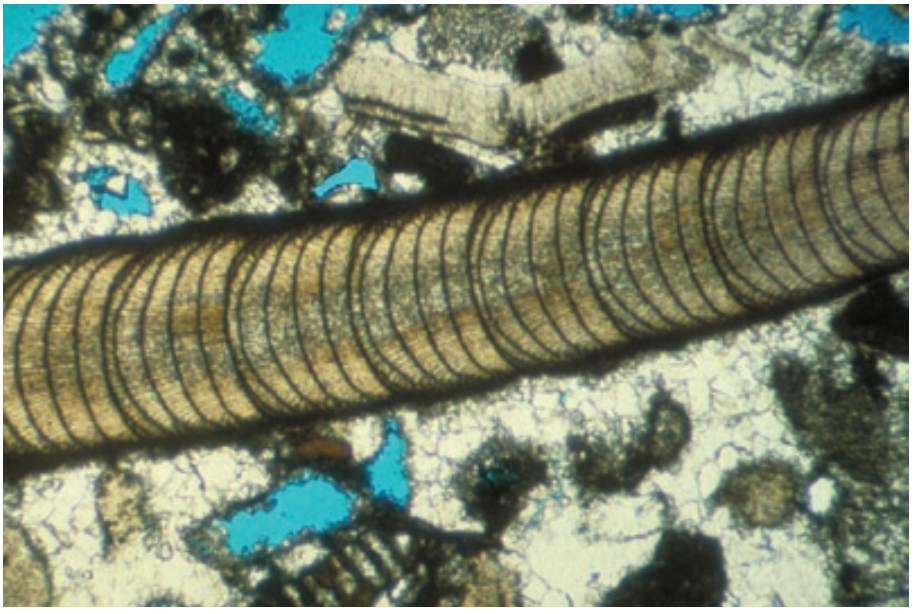

Pleistocene (125 ky) Coral Rock Fm., St. Philip Parish, Barbados

An example of pieces of a possible segmented red alga in near-reef sediment. Note the pronounced growth banding and fine-scale cellular structure.

PPL, BSE, HA = 2.4 mm

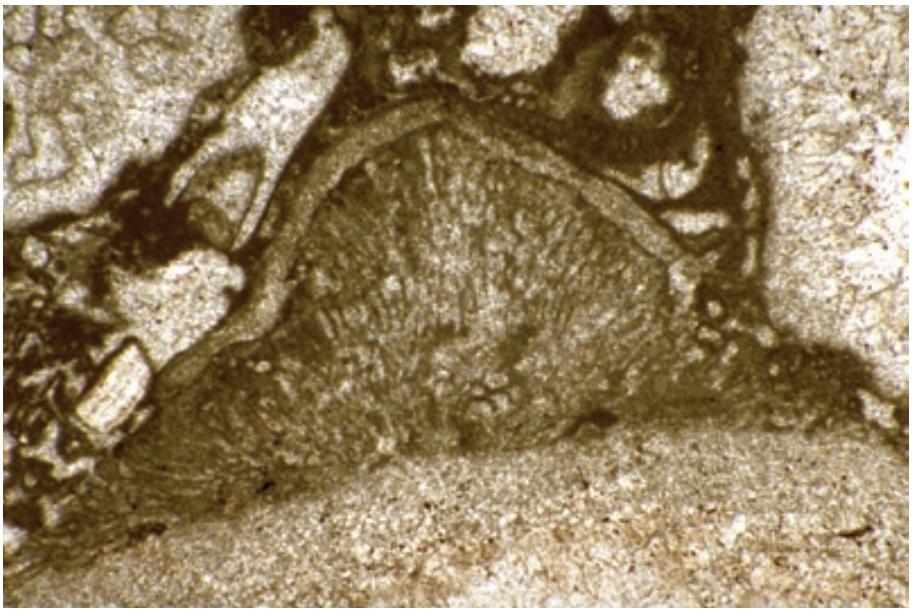

Cretaceous (Albian-Cenomanian) Tamabra Ls., San Luis Potosi, Mexico

Not all preserved ancient red algae are corallines. This example shows several types of encrusting algae. The large tubular, encrusting form may be a solenoporoid red alga, whereas the dark, micritic, irregular forms above and to the left are other red algal, cyanobacterial, and possibly other encrustations. This illustrates the complex intergrowth of algal types and their importance in stabilizing reef material (such as the poorly preserved rudistid fragments seen along the bottom edge and the upper left and right corners of the image).

PPL, HA = 4.5 mm

Mid. Ordovician Black River Gp., Kingston, Ontario, Canada

The characteristic simple (undifferentiated) elongate cellular or tubular fabric of the red alga *Solenopora* sp. is well shown in this example of a relatively early form. Sample from Noel P. James.

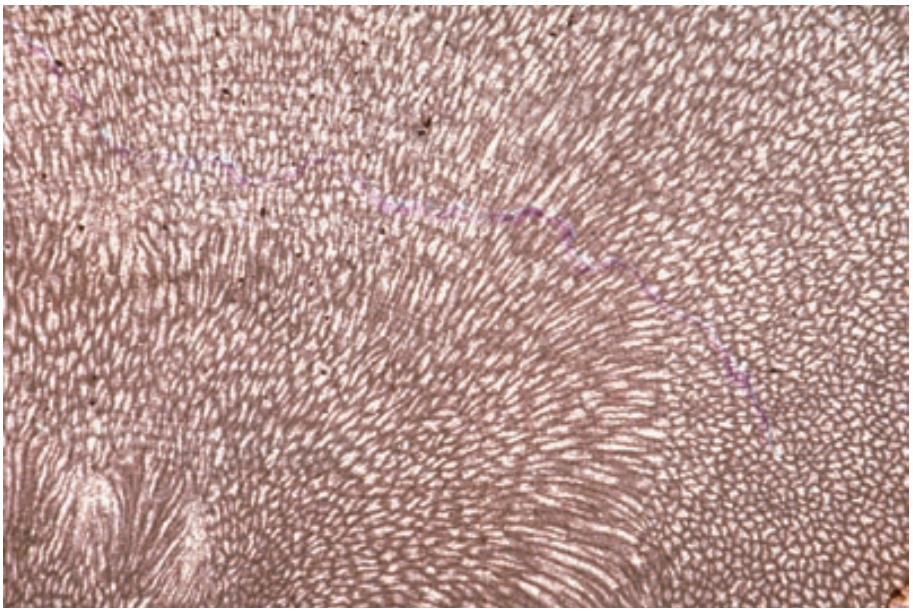

PPL, AS, HA = 12.5 mm

Cretaceous (Albian-Cenomanian) Tamabra Ls., San Luis Potosi, Mexico

Preservation in some calcareous algae is poor, indicating a probably aragonitic original composition. Although most red algae were calcitic, a few modern and ancient forms are (or were) aragonitic. This poorly preserved grain is clearly of algal origin but could be either a red or a green alga.

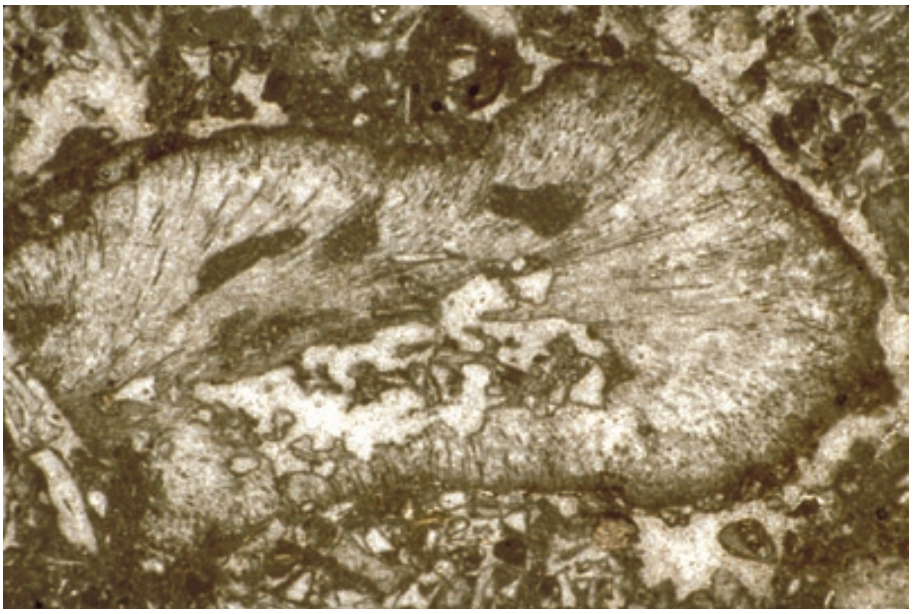

PPL, HA = 9 mm

Pennsylvanian Marble Falls Ls., San Saba Co., Texas

A view of a branching (ramifying) microproblematic organism, *Mazloviporidium* sp. (syn. *Cribroporidium*, *Contortoporidium*), considered by some workers to be a red alga. It is confined to Middle Carboniferous strata and probably formed upright, branching thickets. Despite the moderately good preservation of this sample, it is considered to have been originally aragonitic (Groves and Mamet, in Toomey and Nitecki, 1985).

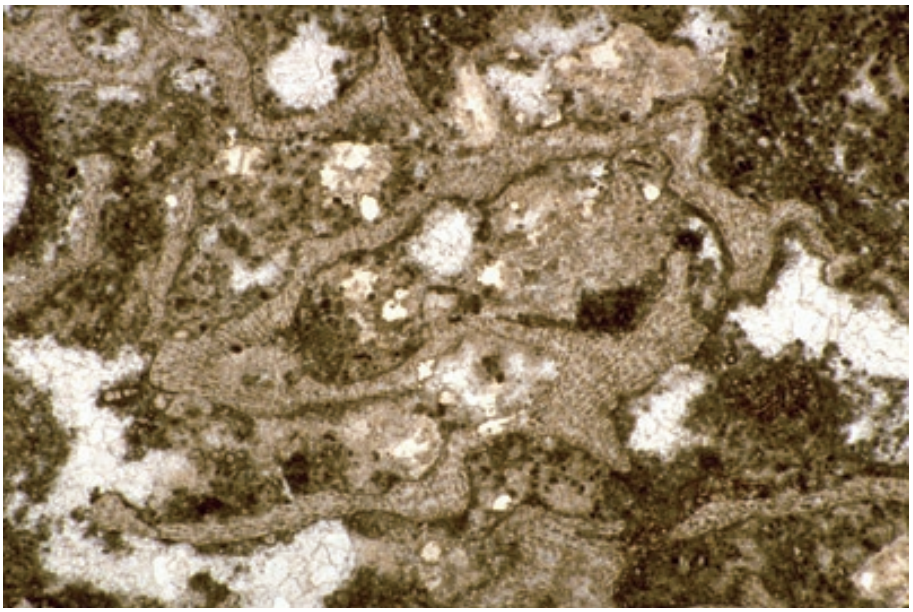

PPL, HA = 6 mm

PHYLLOID ALGAE

Taxonomy and Age Range:

Complex and problematic taxonomy — some may have been related to modern squamariacean red algae; others may have been codiacean green algae; because of their abundance and significance as reservoir rock-formers, they are presented here as a separate grouping. The term phylloid algae, is descriptive rather than genetic, and is especially useful because such algae generally were strongly altered by diagenesis and exhibit few diagnostic features. Indeed, the term "phylloid algae" was specifically coined to describe the full spectrum of Late Paleozoic, poorly preserved, platy, calcareous algal remains that cannot be identified to generic level.

Pennsylvanian (Late Carboniferous)-Late Permian

Environmental Range:

Photosynthetic — required light and probably grew in very shallow water; some modern codiacean green algae of similar shape, however, are found in abundance in water depths greater than 50 m.

All are marine, generally in normal salinity environments.

Common in shallow-shelf settings; formed biohermal to biostromal buildups and are also found isolated within shelf sediments.

Skeletal Mineralogy:

Mainly aragonite, but a few forms are inferred to have been high-Mg calcite.

Morphologic Features:

Grew as individual, platy (leaf-like) or cup-shaped structures (probably much like the modern green alga, *Udotea* sp., illustrated on p. 13), typically a 2 to 10 cm in length and only about 0.5 to 1 mm in thickness.

Most phylloid algae apparently stood upright, but are only preserved that way where stabilized by extensive marine cementation. More typically they are found as fallen and/or as reworked and fragmented plates. Reconstructions of some of the more elaborate growth forms are shown below, but most phylloid algae had much simpler leaf-like or bladed forms.

Keys to Petrographic Recognition:

1. **Thin, platy grains typically a few cm long and a mm or less in thickness.**
2. **Phylloid algal grains are similar to bivalve fragments; however, phylloid algal grains have more irregular shapes (wavy, corn flake or potato chip-like forms, rather than the regular curvature of bivalves) and do not have the hinge structures seen in bivalves.**
3. **Ends of phylloid algal plates in some species thicken slightly (unlike bivalve shells that thin at non-hinge edges).**
4. **Generally little or no preservation of internal structure due to original aragonite mineralogy — most often only a micritic rim is visible, but in some cases, one can still see a series of mud- or cement-filled tubules within the exterior portions of the grains.**

Reconstructions of complex phylloid algae

Left: Artist's reconstruction of complex, cup-like phylloid algae that formed biohermal buildups in the Lower Permian (Wolfcampian) of New Mexico. Other phylloid algae most likely had simpler, platy or leaf-like morphologies. Courtesy of Robert B. Halley.

Right: Reconstruction of a phylloid alga, *Eugonophyllum*. External shape of organism supplied by Cross and Klostermann (1981) based on serial slabbing of neomorphosed thalli. Internal morphology added by Kirkland et al. (1993), based on thin sections of broken, still aragonitic thalli.

Characteristic fabrics of three common phylloid algae

The originally aragonitic phylloid algae typically show poor structural preservation, regardless of whether they had green or red algal affiliations. This diagram, adapted from Wray (1977) shows three important phylloid algal genera of probable green algal affinity. *Calcifolium* had a simple, undifferentiated (monostromatic) arrangement; *Eugonophyllum* and *Ivanovia* were differentiated into medullary and cortical regions. The darker colors on the diagram represent areas with more intense calcification, and therefore greater probability of structural preservation, although most preserved structure resulted from secondary micritic infilling of primary tubules.

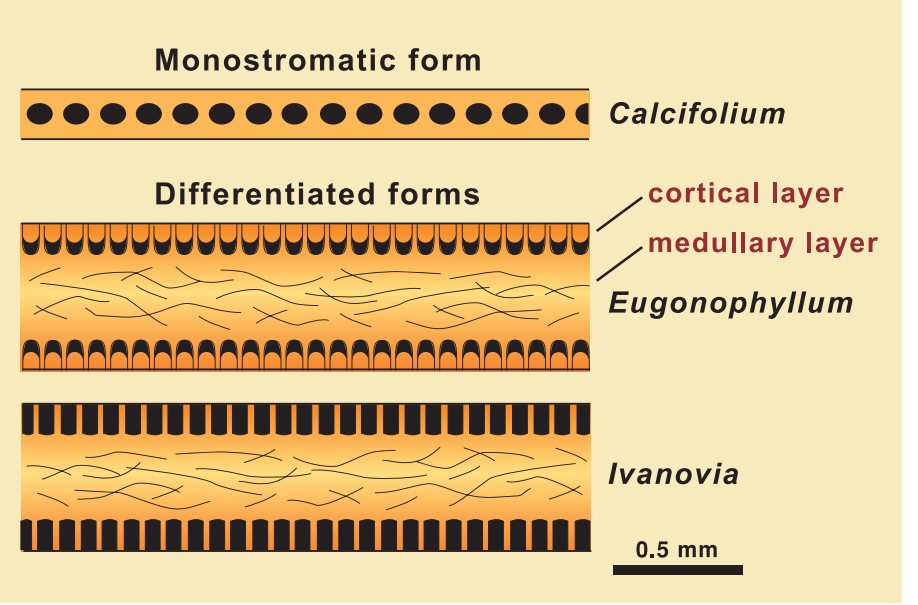

Up. Pennsylvanian (Virgilian) Upper Magdalena Gp., El Paso Co., Texas

A moderately well preserved phylloid alga showing several characteristic features — filled primary tubules preserved along some of the grain margins, a flared end to one of the plates, and somewhat irregular grain shapes and sizes. These grains clearly were originally aragonitic, and the structure was preserved only through filling of tubules and or outlining of external forms by micritic sediment or cement.

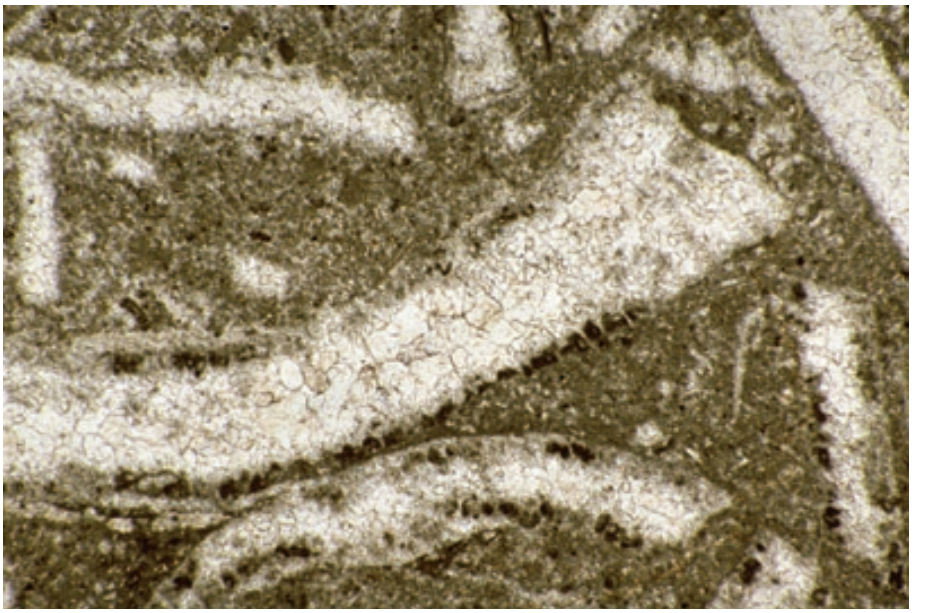

PPL, HA = 4.5 mm

Up. Pennsylvanian (Virgilian) Upper Magdalena Gp., El Paso Co., Texas

Another example of a fairly well preserved phylloid alga. Extensive infilling of marginal tubules with micritic sediment or aphanocrystalline cement has given the more calcified grain margin a characteristic scalloped appearance.

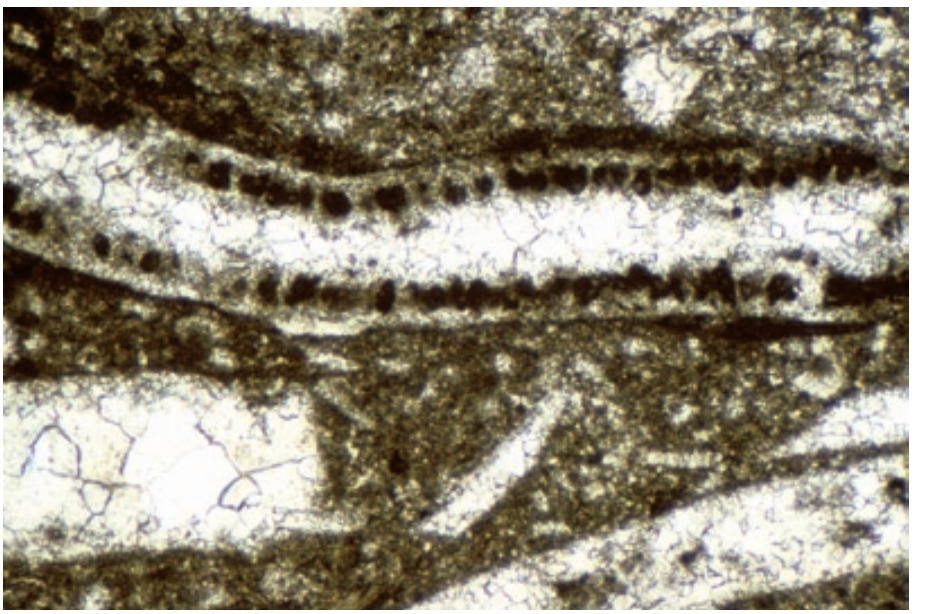

PPL, HA = 2.4 mm

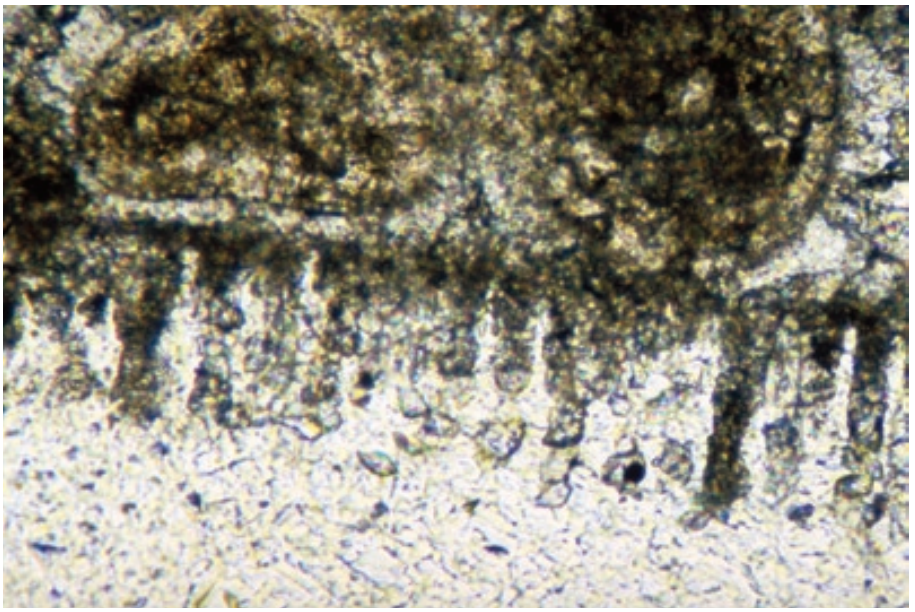

Up. Pennsylvanian (Missourian) Canyon Gp., Winchell Ls., near Ranger, Texas

A close-up view showing details of a moderately well-preserved phylloid algal plate. In this species, long and straight marginal tubules were partially cemented at an early stage. Subsequent dissolution of the primary aragonite of the algal plate left the tubules hanging into void space. That space was later filled with sparry calcite cement but, in other examples, leached phylloid algal plates were not infilled and now make outstanding hydrocarbon reservoirs. Sample from Robert Laury.

PPL, HA = 0.5 mm

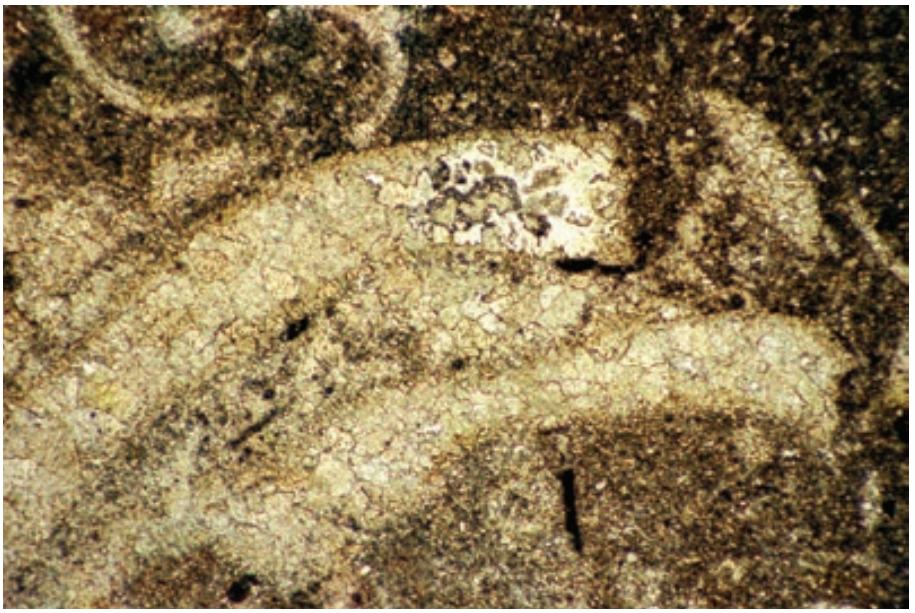

Pennsylvanian (Desmoinesian) Minturn Fm., Robinson Mbr., Eagle Co., Colorado

A more typical example of possible phylloid algae with very poorly-preserved wall structure. Despite the absence of internal fabrics, the squared and slightly flaring ends of the grains allow their differentiation from otherwise similar-looking, neomorphosed (originally aragonitic) bivalve shells.

PPL, HA = 3.5 mm

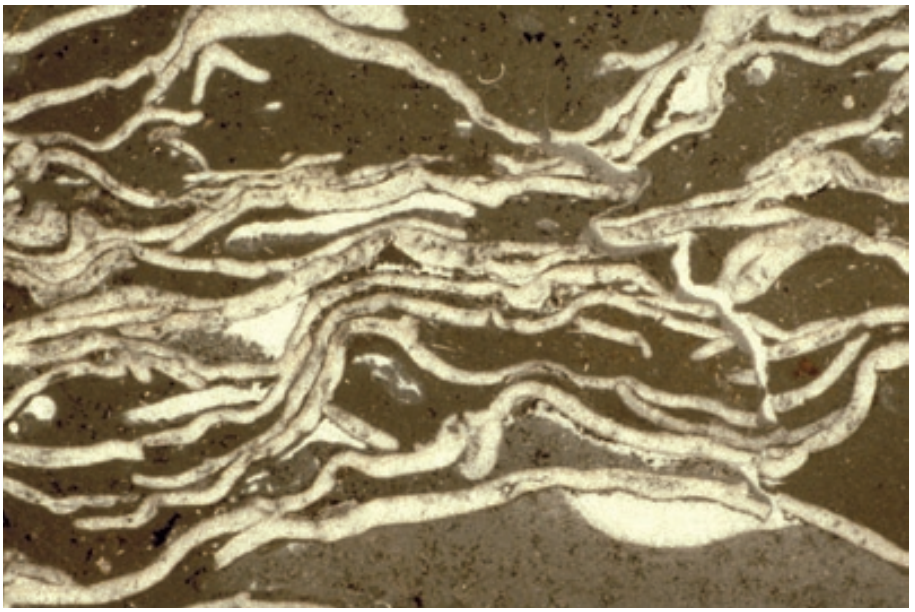

Lo. Permian (Wolfcampian) Hueco Ls., Doña Ana Co., New Mexico

The relationships between phylloid algae and other algal groups are problematic — some probably were red algae, others most likely were green algae, and many are impossible to classify definitively. This nodule (rhodoid or rhodolith), for example, was constructed by an unusual encrusting, platy, ancestral coralline red alga, *Archaeolithophyllum lamellosum*. Such irregular, platy forms are very similar to some free-standing phylloid algae, showing a probable linkage between red algae and at least some phylloid algae.

PPL, HA = 12.5 mm

Pennsylvanian limestone, west of Fort Worth, Texas

A view of two probable *Archaeolithophyllum* sp. plates (the same genus as shown in the previous photograph). These red algae have fairly well-preserved internal cellular structure. These examples, however, are not encrusting but rather had the free-standing, platy morphology typical of phylloid algae.

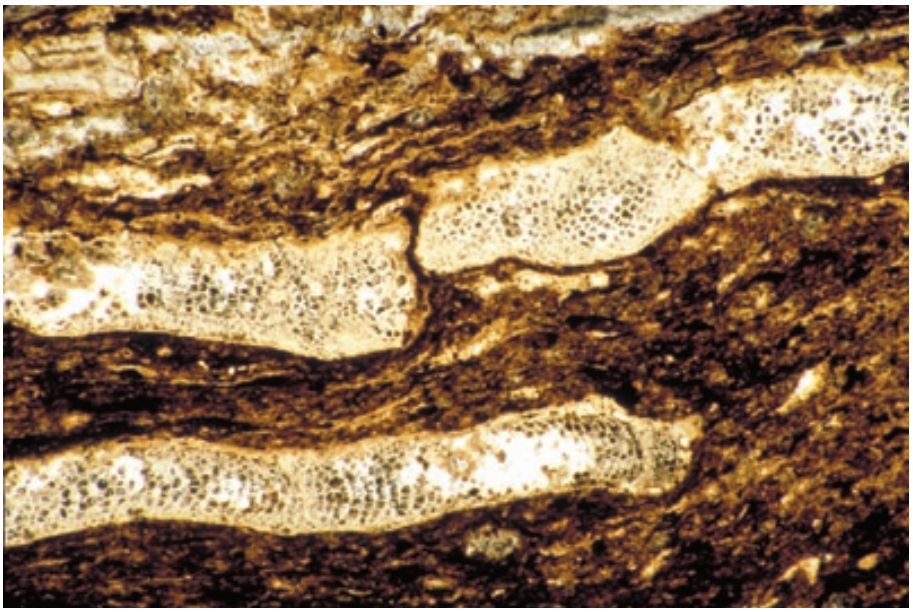

PPL, HA = 4 mm

Pennsylvanian limestone, west of Fort Worth, Texas

A closer view of an example of the *Archaeolithophyllum* sp., from the same thin section depicted in the previous photograph. Note the excellent preservation of internal cellular structure (which does not closely resemble the marginal tubules of the phylloid algae depicted earlier).

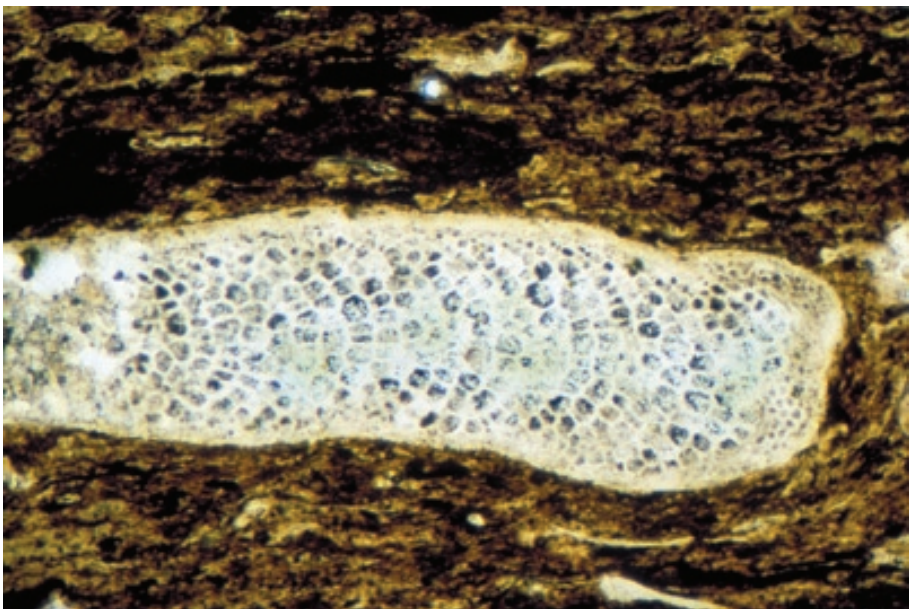

PPL, HA = 2.0 mm

Recent sediment, Bermuda

A plan view of the overlapping foliose sheets of living squamariacean red algae (of the genus *Peyssonnelia*) from 5-m water depth. These aragonitic algae are considered by some workers to be the closest modern relatives of Paleozoic phylloid algae. Photograph courtesy of Noel P. James (James et al., 1988).

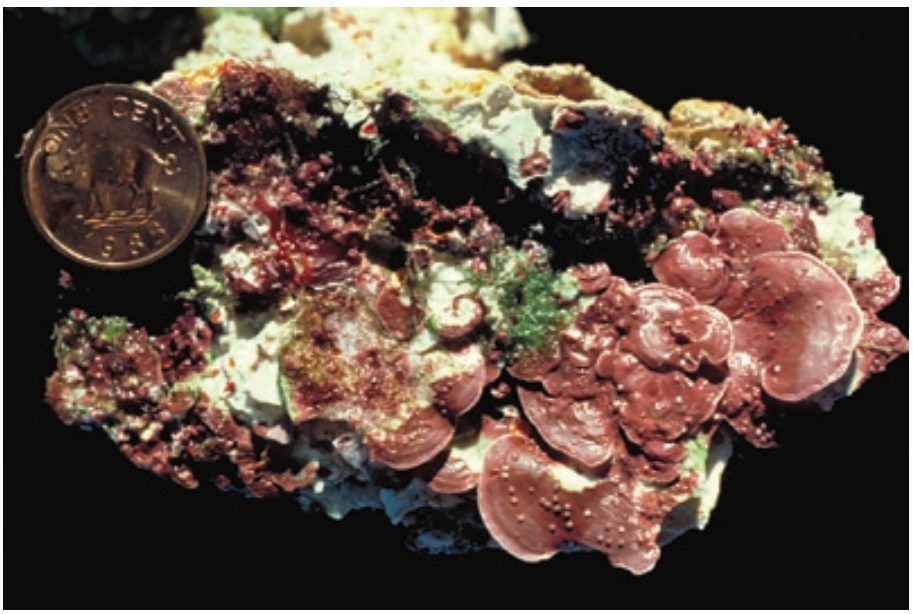

Mac, HA = 9.7 cm

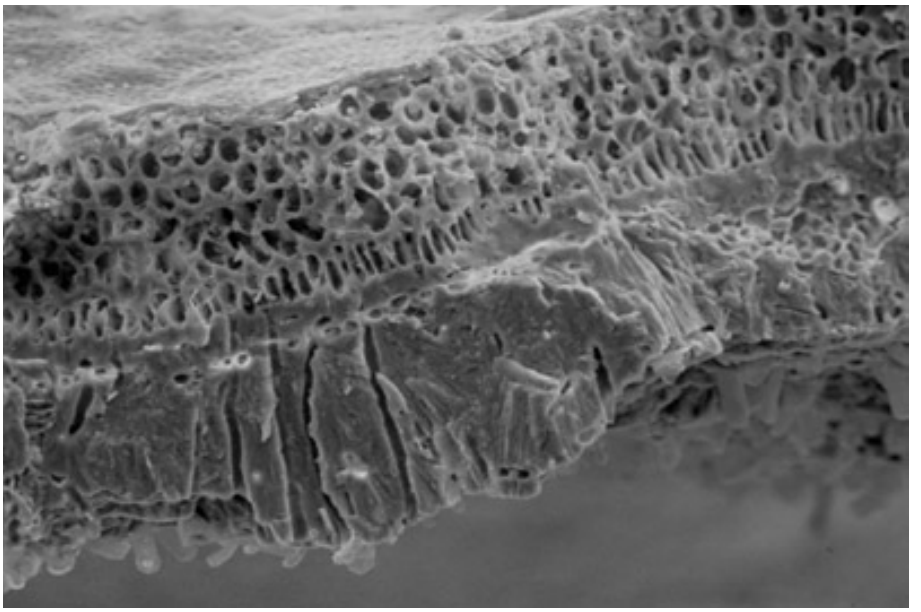

Recent sediment, Bahamas

An SEM image of *Peyssonnelia* sp., a modern squamariacean red alga. Shown are a vertical section of cellular thallus above (perithallium and basal hypothallium) and dense hypobasal aragonite below. The holes in the hypobasal layer are tubular rhizoids. Photograph courtesy of Noel P. James (James et al., 1988).

SEM, HA = 0.58 mm

Cited References and Additional Information Sources

Adey, W. H., and I. G. Macintyre, 1973, Crustose coralline algae: a re-evaluation in the geological sciences: Geological Society of America Bulletin, v. 84, p. 883-904.

Awramik, S. M., 1984, Ancient stromatolites and microbial mats, *in* Y. Cohen, R. W. Castenholz, and H. O. Halvorson eds., Microbial Mats: Stromatolites: New York, Alan R. Liss Inc., p. 1-22.

Bosence, D. W. J., 1983, Description and classification of rhodoliths (rhodoids, rhodolites), *in* T. M. Peryt, ed., Coated Grains: New York, Springer-Verlag, p. 217-224.

Bradley, W. H., 1929, Algal reefs and oolites of the Green River Formation: Washington, D.C., U. S. Geological Survey Professional Paper 154-G, p. 203-223.

Buchbinder, B., and R. B. Halley, 1985, Occurrence and preservation of Eocene squamariacian and coralline rhodoliths: Eua, Tonga, *in* D. F. Toomey, and M. H. Nitecki, eds., Paleoalgology: Contemporary Research and Applications: New York, Springer-Verlag, p. 248-256.

Chafetz, H. S., and C. Buczynski, 1992, Bacterially induced lithification of microbial mats: Palaios, v. 7, p. 277-293.

Chafetz, H. S., and R. L. Folk, 1984, Travertines: depositional morphology and the bacterially constructed constituents: Journal of Sedimentary Petrology, v. 54, p. 289-316.

Chafetz, H. S., P. F. Rush, and N. M. Utech, 1991, Microenvironmental controls on mineralogy and habit of $CaCO_3$ precipitates: an example from an active travertine system: Sedimentology, v. 38, p. 107-126.

Cross, T. A., and M. J. Klosterman, 1981, Autoecology and development of a stromatolitic-bound phylloid algal bioherm, Laborcita Formation (Lower Permian), Sacramento Mountains, New Mexico, USA, *in* C. L. Monty, ed., Phanerozoic Stromatolites: New York, Springer-Verlag, p. 45-59.

Flajs, G., 1977, Die Ultrastrukturen des Kalkalgenskelettes: Palaeontographica, Abteilung B (Paläophytologie), v. 160 (4-6), p. 69-128.

Flügel, E., 1977, Fossil Algae: Recent Results and Developments: New York, Springer-Verlag, 375 p.

Ginsburg, R. N., R. Rezak, and J. L. Wray, 1971, Geology of Calcareous Algae: Short Course Notes, Comparative Sedimentology Laboratory, University of Miami, 62 p.

James, N. P., J. L. Wray, and R. N. Ginsburg, 1988, Calcification of encrusting aragonitic algae (Peyssonneliaceae): implications for the origin of Late Paleozoic reefs and cements: Journal of Sedimentary Petrology, v. 58, p. 291-303.

Johnson, J. H., 1961, Limestone-building algae and algal limestones: Golden, CO, Colorado School of Mines, 297 p.

Johnson, J. H., 1963, Pennsylvanian and Permian Algae: Colorado School of Mines Quarterly, v. 58 (3), p. 1-211.

Johnson, J. H., 1964, The Jurassic Algae: Colorado School of Mines Quarterly, v. 59 (2), p. 1-129.

Kirkland, B. L., C. H. Moore, Jr., and J. A. D. Dickson, 1993, Well preserved, aragonitic phylloid algae (*Eugonophyllum*, Udoteaceae) from the Pennsylvanian Holder Formation, Sacramento Mountains, New Mexico: Palaios, v. 8, p. 111-120.

Logan, B. W., R. Rezak, and R. N. Ginsburg, 1964, Classification and environmental significance of algal stromatolites: Journal of Geology, v. 72, p. 68-83.

Macintyre, I. G., and R. P. Reid, 1995, Crystal alteration in a living calcareous alga (*Halimeda*): implications for studies in skeletal diagenesis: Journal of Sedimentary Research, Section A: Sedimentary Petrology and Processes, v. A65, p. 143-153.

Marszalek, D. S., 1971, Skeletal ultrastructure of sediment producing green algae, *in* O. Johari, and I. Corvin eds., Scanning Electron Microscopy/ 1971, Part I, Proceedings of the 4th Annual Electron Microscopy Symposium: Chicago, IL, IIT Research Institute, p. 273-280.

Monty, C., 1981, Phanerozoic Stromatolites: New York, Springer-Verlag, 249 p.

Peck, R. E., 1934, The North American trochiliscids, Paleozoic Charophyta: Journal of Paleontology, v. 8, p. 83-119.

Peck, R. E., 1957, North American Mesozoic Charophyta: U.S. Geological Survey Professional Paper 294-A, 44 p.

Racki, G., 1982, Ecology of primitive charophyte algae: a critical review: Neues Jahrbuch für Geologie und Paläontologie, Abhandlungen, v. 162, p. 388-399.

Riding, R., ed., 1991, Calcareous Algae and Stromatolites: New York, Springer-Verlag, 530 p.

Riding, R., 2000, Microbial carbonates: the geological record of calcified bacterial-algal mats and biofilms: Sedimentology, v. 47, p. 179-214.

Toomey, D. F., and J. A. Babcock, eds., 1983, Precambrian and Paleozoic algal carbonates, west Texas-southern New Mexico: Golden, Colorado School of Mines Professional Contributions, v. 11, 345 p.

Toomey, D. F., and M. H. Nitecki, 1985, Paleoalgology: Contemporary Research and Applications: New York, Springer-Verlag, 376 p.

Walter, M. R., ed., 1976, Stromatolites [Developments in Sedimentology 20]: New York, Elsevier, 790 p.

Wray, J. L., 1977, Calcareous Algae [Developments in Palaeontology and Stratigraphy 4]: New York, Elsevier Publ. Co., 185 p.

Facing Page: Top: Photomicrograph of *Hastigerina pelagica*, a planktic foraminifer. The test (without spines) is about 500 μm in diameter. Photograph courtesy of David A. Caron.
Bottom: Dry mount of whole foraminifers from modern sediments of the Mediterranean Sea and the Miocene of Malta. Courtesy of Wim van Egmond (www.micropolitan.tk).

GRAINS: Skeletal Fragments

FORAMINIFERS

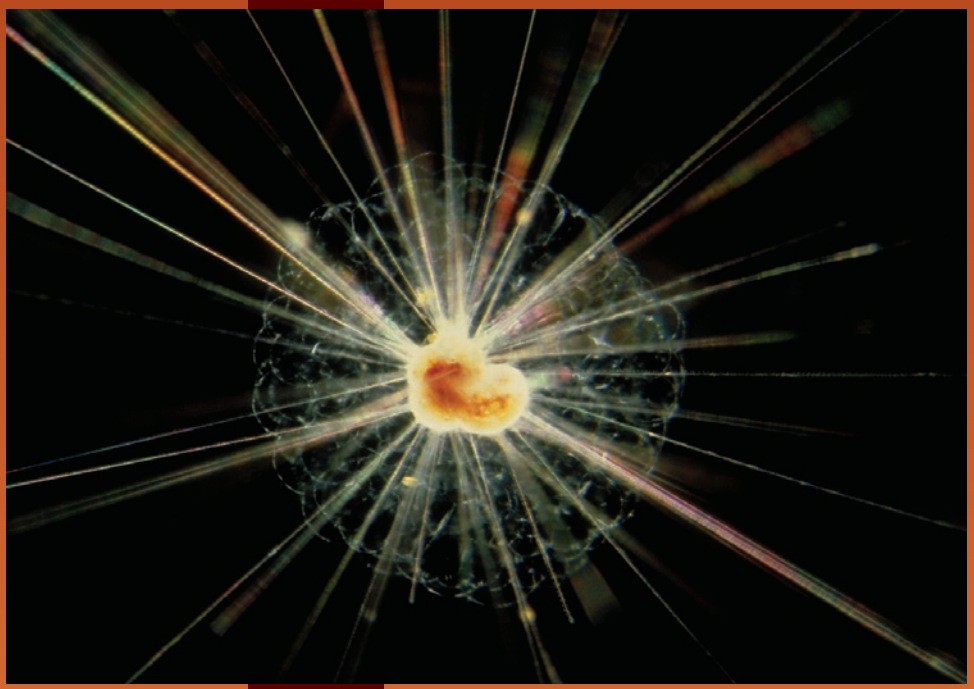

CHAPTER 2

FORAMINIFERS

Taxonomy and Age Range:

Kingdom Protista, Phylum Sarcomastigophora, Subphylum Sarcodina, Superclass Rhizopoda, Class Granuloreticulosea, Order Foraminiferida — Basal Cambrian-Recent

Benthic foraminifers: Cambrian-Recent (early forms were exclusively agglutinating)

Calcareous benthic foraminifers — Ordovician-Recent; large forms from Late Carboniferous-Recent

Planktic foraminifers: Middle Jurassic-Recent

Despite being single-celled protozoans, this is a very complex group of organisms, with 12 suborders recognized by Loeblich and Tappan (1984) and some 60-80,000 species identified from Phanerozoic strata. So many shape, size, and wall-structure varieties exist, however, that this chapter can provide only the minimal information needed to identify the most important groups.

Environmental Implications:

Modern foraminifers are fully marine to marginal marine organisms, extending from the intertidal zone to abyssal oceanic depths and from cold-water polar settings to warm tropical environments. Some genera live in marginal-marine hypersaline or subsaline water bodies where they are commonly found in great numbers (but low species diversity).

Most foraminifers are benthic organisms (of the roughly 4,000 modern species, only about 40 are planktic).

Some of the largest living benthic species harbor symbiotic algae in their tissues and thus live primarily in the photic zone; the vast majority, however, are not light dependent.

For reasons related mainly to food supply, most planktic foraminifers live in the upper 300 m of the water column, although after death, their tests fall to the underlying, deeper seafloor.

Foraminifers can be major rock forming elements in open- or restricted-shelf as well as deeper marine deposits. In some cases, foraminiferal abundances reach tens of thousands of individuals per m^3 of sediment.

Skeletal Mineralogy:

The tests of all planktic species and most benthic species are composed of calcite (planktic forms are low-Mg calcite; both high-Mg and low-Mg calcite are common in benthics); some benthic species construct tests of aragonite, silica, or organic matter (a proteinaceous mucopolysaccharide); yet other benthic forms construct their tests of cemented (agglutinated) clastic terrigenous or calcareous sediment grains. Among agglutinators, some are indiscriminate in their selection of building materials, whereas others carefully select calcareous grains, sponge spicules, mica flakes or other specific constituents for their tests.

Morphologic Features:

Foraminiferal tests typically range in size from less than 0.1 mm to 1 mm; the largest fossil forms reach nearly 20 cm in length.

Tests consist of hollow chambers, separated from each other by partitions with small openings (foramina). The last chamber has one or more exterior openings (apertures). Species with multiple chambers are termed *multilocular*; the rarer species that construct single chambered tests are termed *unilocular*.

Multichambered tests may have chambers arranged in a single linear chain (*uniserial*) or in double (*biserial*) or triple (*triserial*) rows. Others have chambers arranged in a coil within a single plane (*planispiral*) or as a snail-like helical spire (*trochospiral*). More complex arrangements of chambers such as *milioline* (chambers arranged in a series where each extends the length of the test, and each later chamber forms at an angle of up to 180° from the previous one) or *fusiform* (a planispiral coil elongated along the coiling axis) are common. Simple tubes (*tubular*), branching tubes (*arborescent*), and *irregular* forms without consistent arrangement of chambers are also found. Some species switch from one growth form to another during life.

Encrusting foraminifers are widespread throughout the Phanerozoic geologic record; they commonly have irregular, multichambered forms and may be interlaminated in complex consortia with algae and other organisms.

Keys to Petrographic Recognition:

1. **Most tests are multichambered, with chambers arranged in a variety of distinctive patterns described above. Simple forms typically are smaller than similarly-chambered mollusks (gastropods or cephalopods); larger**

forms have distinctive morphologies.

2. **Three basic wall compositions: organic, agglutinated and calcareous (the latter two also have an organic inner layer or substrate).**
3. **Three major calcareous wall textures: a) *microgranular* — equidimensional, subspherical calcite crystals closely packed and held together by cryptic carbonate cement, yielding a dark-colored wall (found mainly in Late Paleozoic forms, including fusulinids); b) *porcelaneous* — imperforate, multilayered wall made of apparently randomly arranged microscopic rods or laths of calcite, with ordered inner and outer surface layers (found in miliolids); and c) *hyaline* — interlocking crystals of calcite about 1 µm in diameter with two types of optical behavior (optically radial forms have calcite c-axes oriented normal to the test wall and display a pseudo-uniaxial cross under cross-polarized light; optically granular forms that appear speckled with color flecks under cross-polarized light). Most hyaline forms also exhibit a lamellar wall structure that is perforated by small (1-15 µm) pores. Many of the Cretaceous-Tertiary larger foraminifers and planktic groups have hyaline walls (orbitoids, discocyclinids, lepidocyclinids, nummulitids, globigerinids, and others).**
4. **Planktic forms typically have spines and large, simple, thin-walled, globular chambers with highly perforated walls (all features designed to minimize settling rates). Some keeled and thicker-walled forms also exist.**

PHOTO SCALES AND ABBREVIATIONS ARE EXPLAINED IN THE BOOK'S INTRODUCTION

Common test morphologies of foraminifers

Some common external shapes and chamber arrangement patterns in foraminiferal tests. Some organisms follow a single test construction pattern throughout their life; others can change patterns during their life cycle, switching, for example, from uniserial to biserial chambering or from evolute to involute coiling. Adapted from Moore et al. (1952), Loeblich and Tappan (1964), and Culver (1987).

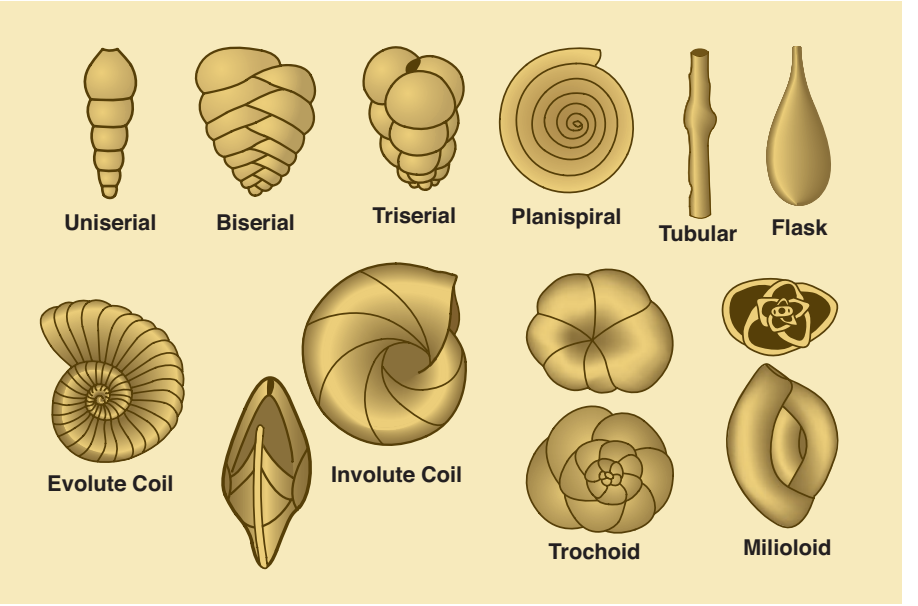

Major foraminiferal calcareous wall structures

Diagrammatic view of the main types of secreted calcareous wall structures of foraminiferal tests. The dashed lines represent the c-axis orientation of constituent microcrystalline calcite crystals in hyaline wall structures. The lamellar growth structure of most hyaline tests is not illustrated here. Adapted from Haynes (1981).

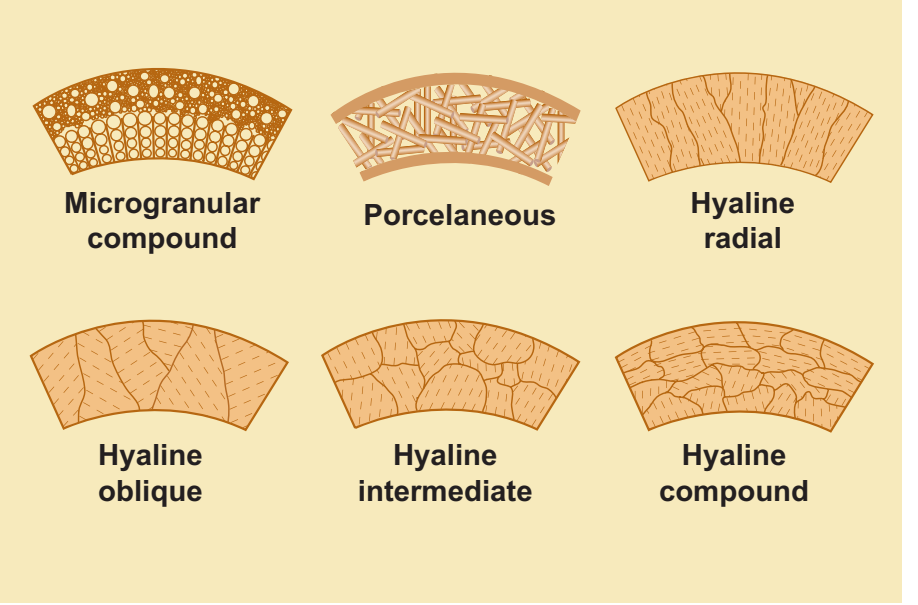

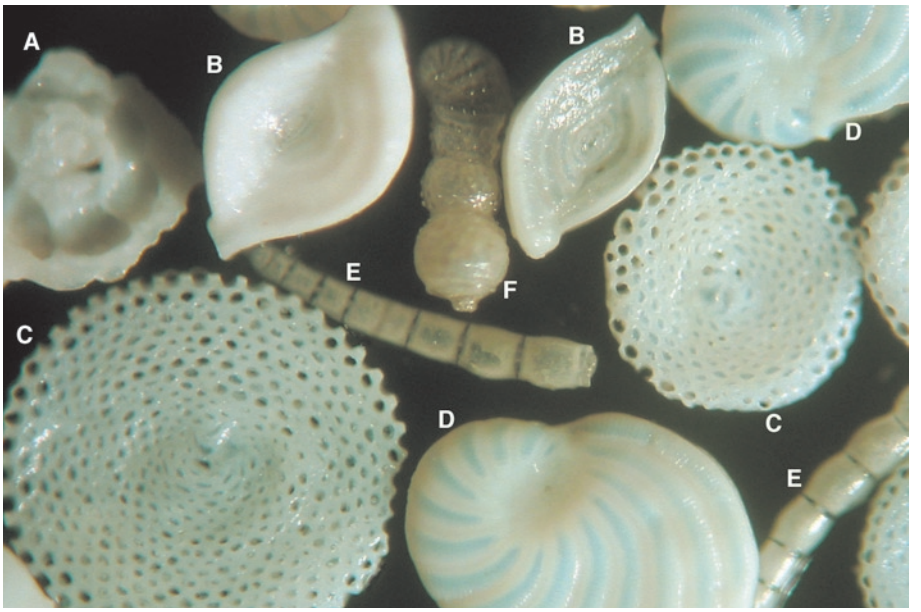

Recent sediment, Mediterranean Sea, and Miocene of Malta

A dry mount of whole foraminifers showing some of the remarkable variation of test morphologies in this group.
A=*Nubecularia lucifuga*
B=*Spiroloculina depressa*
C=*Sorites orbiculus*
D=*Peneroplis planatus*
E=*Dentalia subsoluta*
F=*Marginulina hirsuta*
E and F are Miocene uniserial forms; the others are modern examples. Photograph courtesy of Brian Darnton (http://www.microscopy-uk.org.uk).

Mac, HA = ~3.25 mm

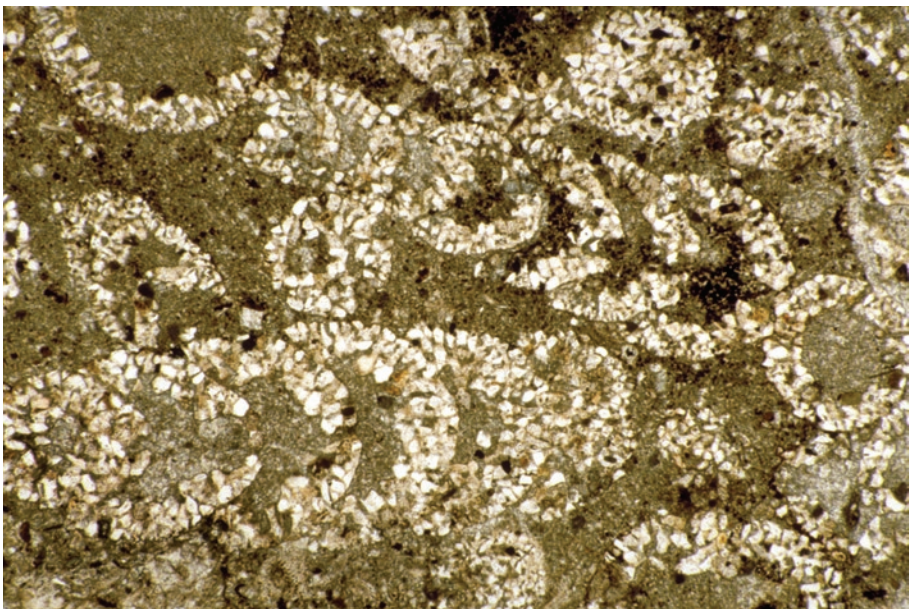

Up. Cretaceous (Cenomanian) Del Rio Fm., Big Bend area, west Texas

A limestone packed with multilocular, uniserial, agglutinated (arenaceous) foraminifers — *Cribratina texana*. This species, found only in Albian-Cenomanian strata, carefully selected clastic terrigenous (mainly quartz) grains of a consistent size to construct its tests, despite the predominantly carbonate sediment composition. The individual quartz grains are held together with an organic cement.

PPL, HA = 5.7 mm

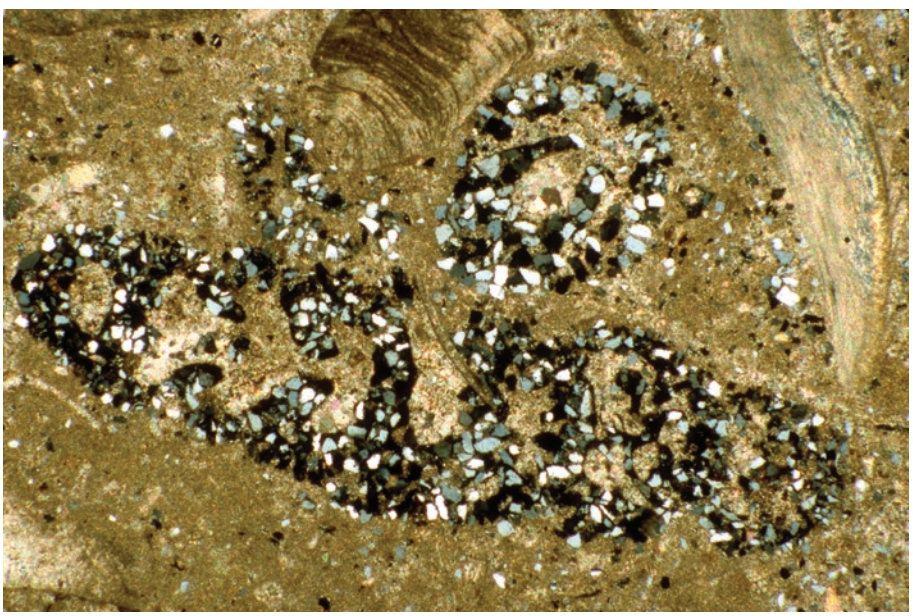

Up. Cretaceous (Cenomanian) Del Rio Fm., Val Verde Co., Texas

The same types of agglutinated (arenaceous) foraminifers seen in the previous photograph, but here shown under cross-polarized light, allowing the quartzose nature of the walls to be seen more clearly. It often requires careful observation to distinguish arenaceous foraminifers from concentrations of terrigenous grains in burrows or other sedimentary structures. The chambered shape of foraminifers clearly is a key to their recognition.

XPL, HA = 4.5 mm

Up. Cretaceous Lower Chalk, Buckinghamshire, England, U.K.

A cross-section through a single agglutinated foraminifer — in this case, one that selected both carbonate and non-carbonate grains to build its test. These foraminifers are recognizable by the chamber-shaped grain arrangements rather than the otherwise random distribution of grains in the rest of the rock. The angular white grains are detrital quartz silt.

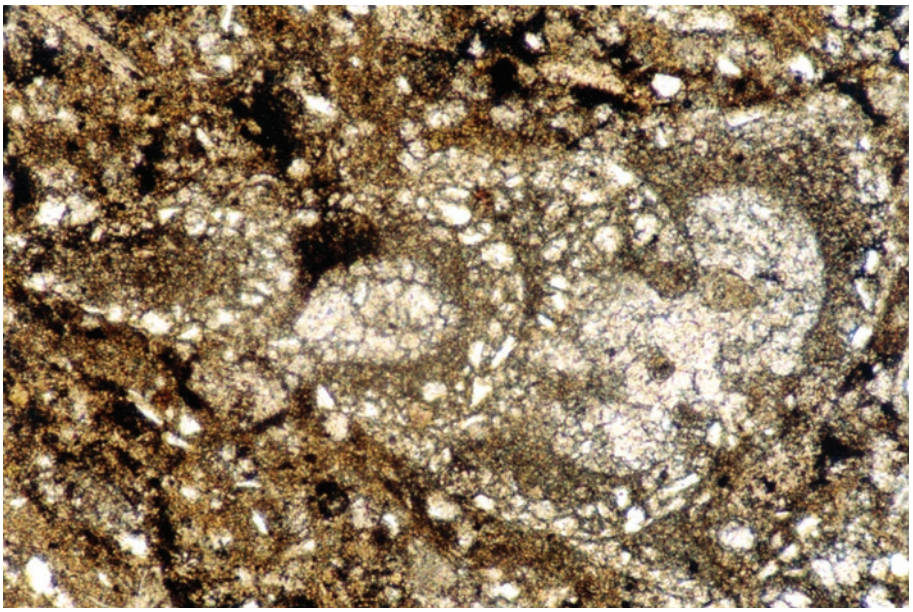

PPL, HA = 0.9 mm

Up. Eocene limestone, Zakinthos, Ionian Islands, Greece

An agglutinated foraminifer with a wall composed primarily of fine-grained carbonate fragments held together with microcrystalline calcareous cement. The walls of the foraminifer are outlined with precipitated sparry calcite cement. If this grain were surrounded by calcilutite or calcisiltite, it would be much harder to recognize.

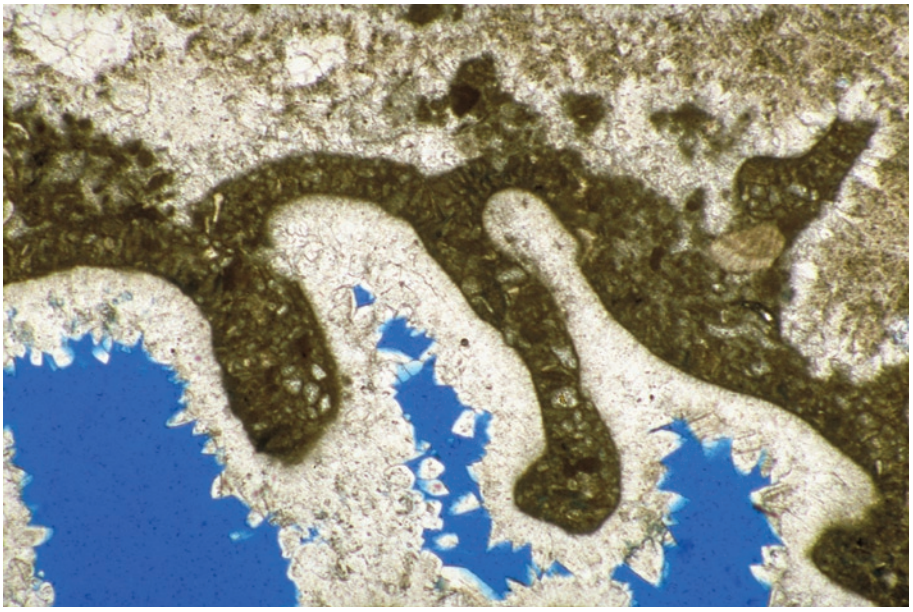

PPL, BSE, HA = 3.2 mm

Recent sediment, Grand Cayman, Cayman Islands, B.W.I.

There is a complete spectrum of agglutinated wall structures in benthic foraminifers, ranging from grain-rich tests with some organic cement to tests with nearly completely organic walls containing just a few agglutinated grains. This example shows a dominantly calcareous (porcelaneous) wall incorporating scattered agglutinated quartz and other grains. This coiling pattern is typical of miliolids.

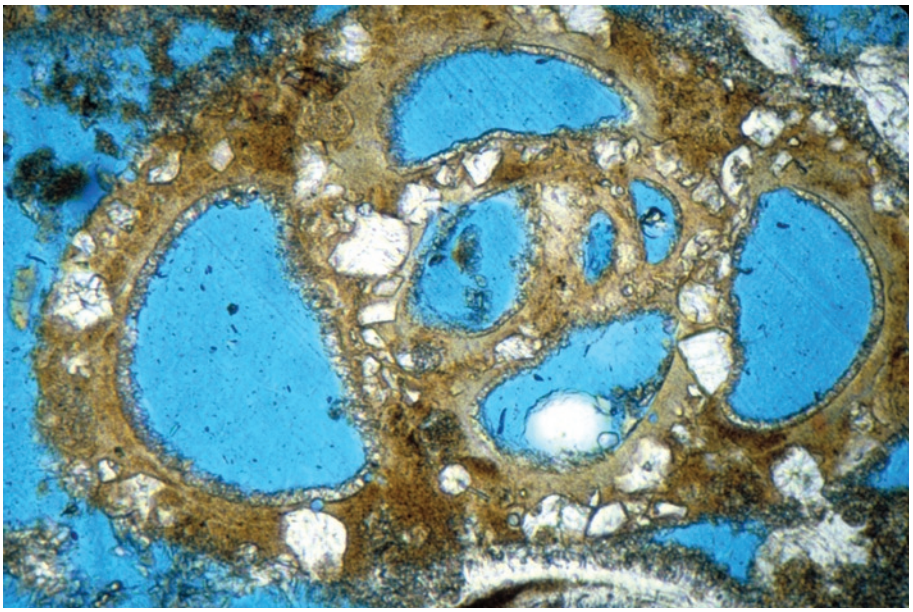

PPL, BSE, HA = 0.65 mm

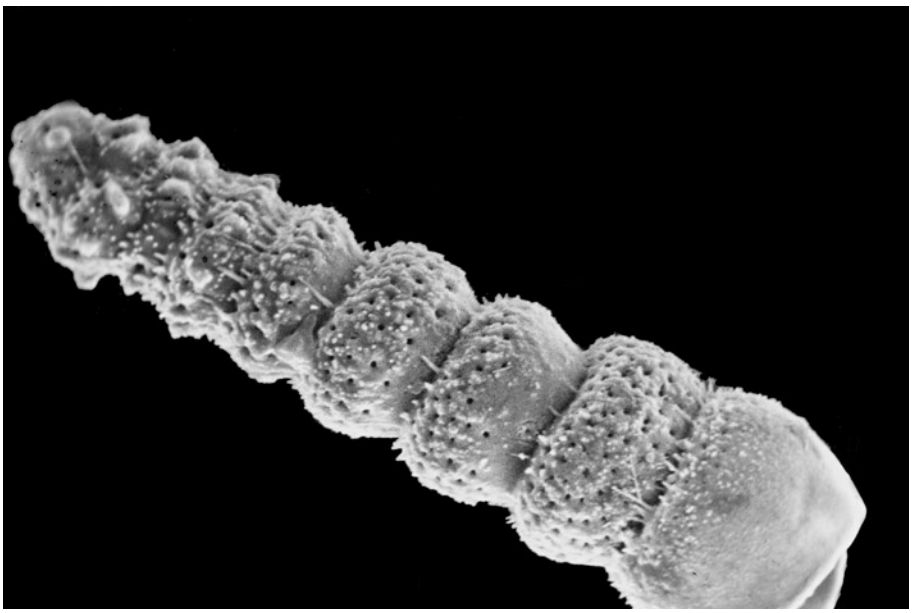

Recent sediment, Belize

A complete specimen of *Rectobolivina* sp. This uniserial foraminifer has porous walls and short attached spines. At any given time, the protozoan organism itself lives in all but the last-constructed chamber.

SEM, HA = ~385 μm

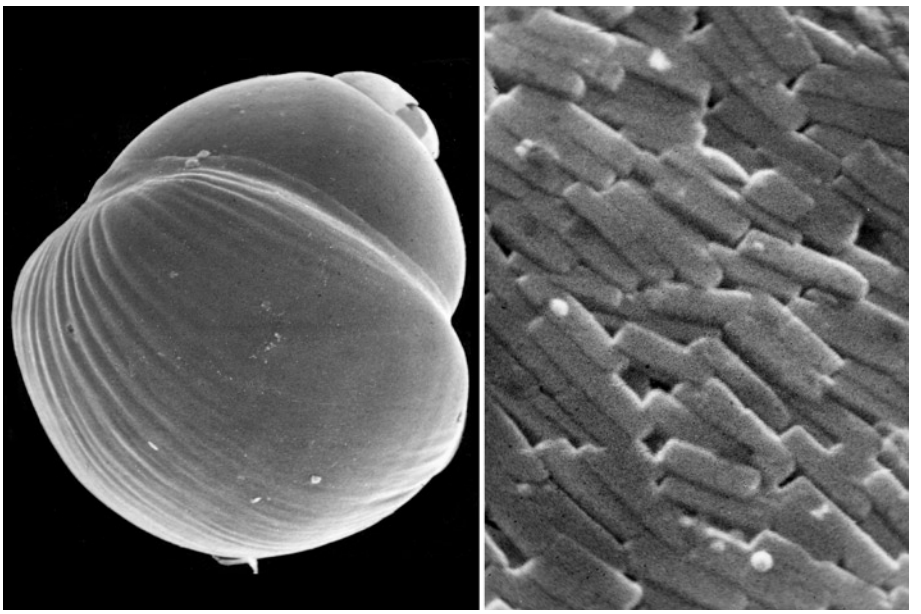

Recent sediment, Belize

A whole specimen and close-up view of a modern, calcareous, benthic foraminifer, *Pyrgo* sp. Note the tightly packed, oriented laths of high-Mg calcite that make up the porcelaneous wall. With degradation of the organic binding material, or abrasion of the shell by natural processes, these laths could contribute to the supply of clay-sized carbonate particles (carbonate mud) in shelfal sediments.

SEM, L: HA = 775 μm; R: HA = ~5 μm

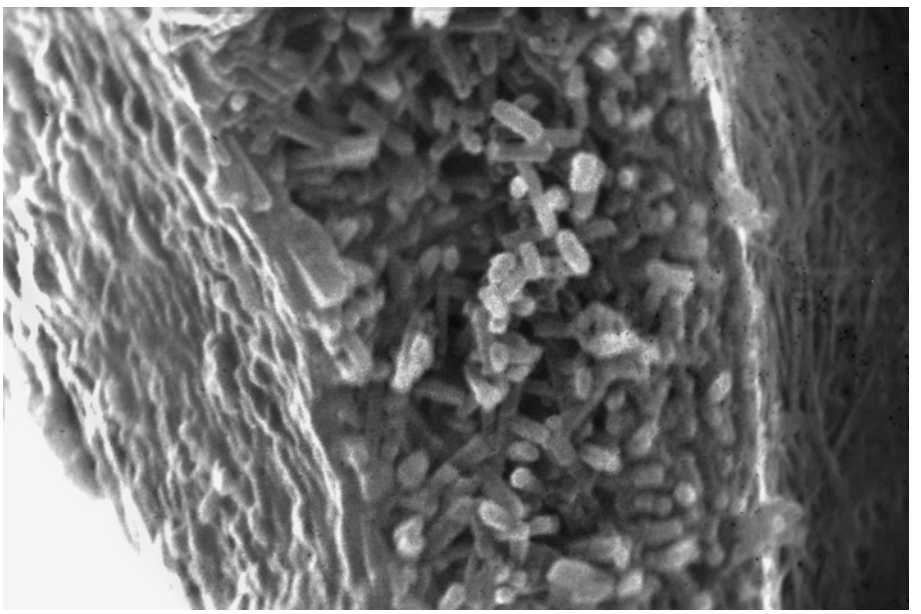

Recent sediment, Belize

A view of the fractured wall of a modern benthic foraminifer, *Spiroloculina* sp. It shows the inner and outer test surfaces, as well as a cross section of the wall itself. Note the bladed crystals that make up the porcelaneous wall and their changing orientation toward the test surface. The short, round-ended crystals appear very similar to the nannobacterial "batons" illustrated in Folk and Lynch (2001), perhaps indicating bacterial involvement in the calcification process.

SEM, HA = ~11.3 μm

Oligocene-Miocene, Top McDonald Ls., northern Otago, New Zealand

An example of a calcareous uniserial benthic foraminifer in a ferruginous hardground. In this example, the chambers are easily seen because they have been filled with precipitated, very finely crystalline phosphatic cements.

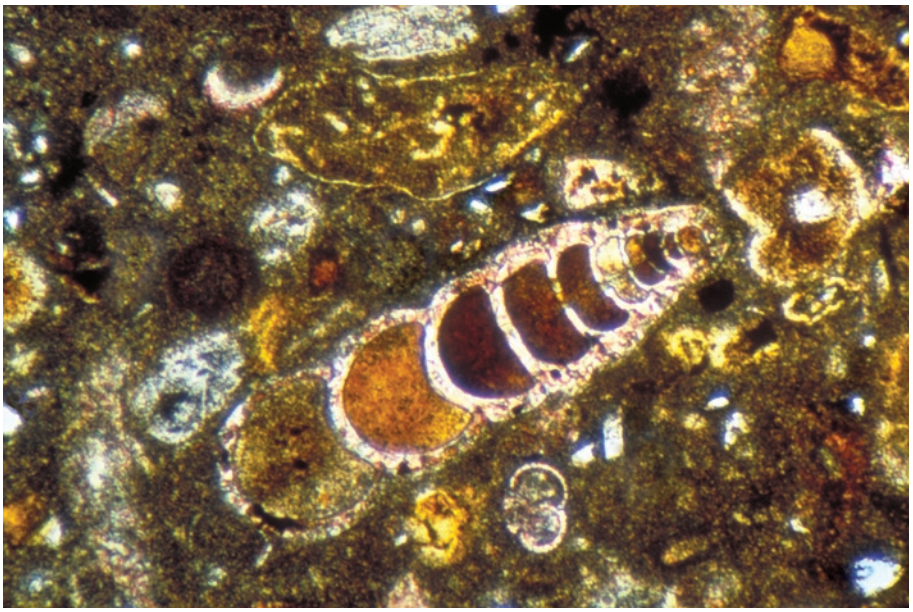

PPL, HA = 1.6 mm

Mid. Pennsylvanian Paradox Fm., southeastern Utah

Sections through a biserial foraminifer (probably of the genus *Deekerella*). The left section is a tangential cut through a different specimen of the same species. Note the typical palaeotextulariid, double-walled, calcareous test structure. The two layers are distinguished by differing crystal orientations. The matrix of this rock is composed of pellets and small skeletal fragments (mainly echinoderms).

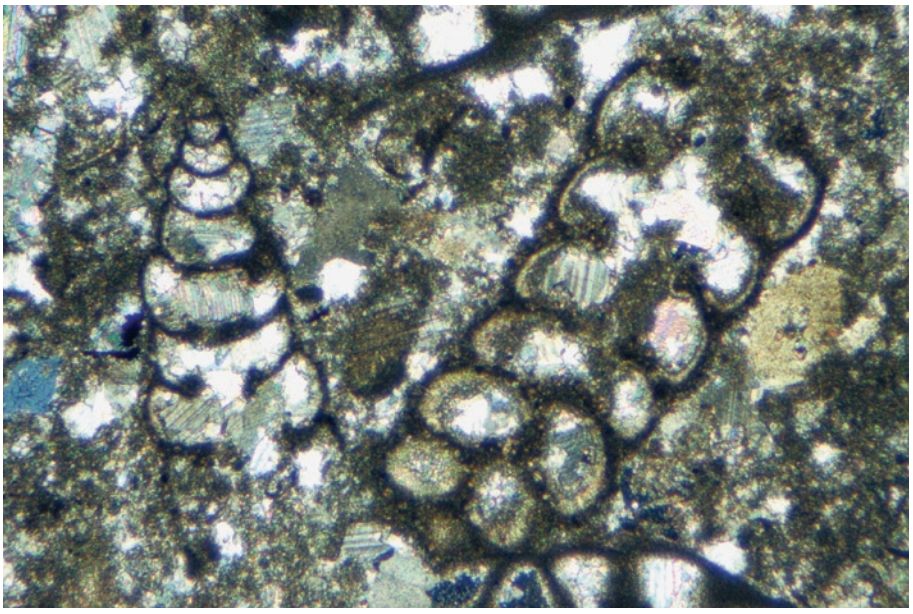

XPL, HA = 2.2 mm

Up. Mississippian (Visean) Arroyo Peñasco Gp., Terrero Fm., San Miguel Co., New Mexico

An endothyrid foraminifer (a member of the Suborder Fusulinina) in a carbonate grainstone to packstone. The characteristic streptospiral test and granular to micro-fibrous two-layer wall are visible.

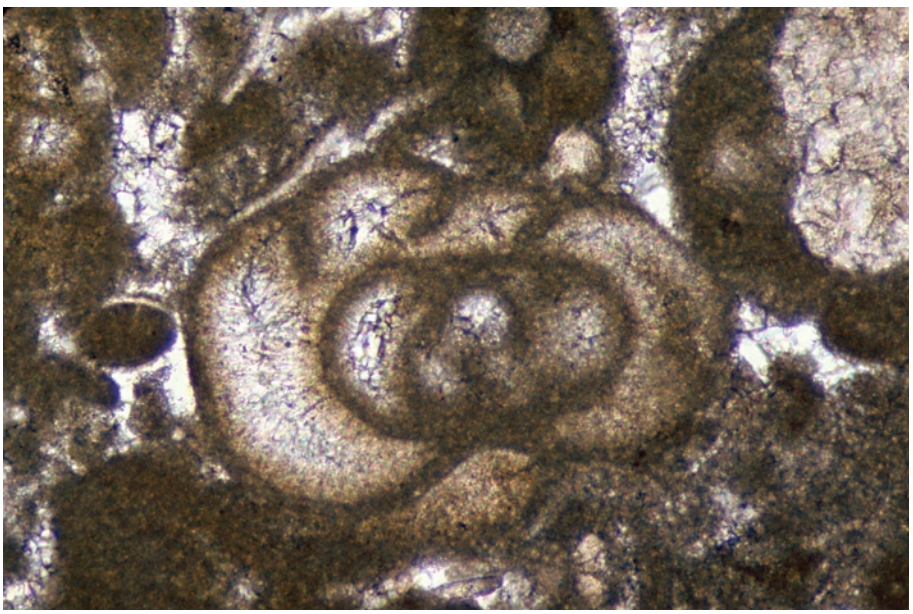

PPL, HA = 0.28 mm

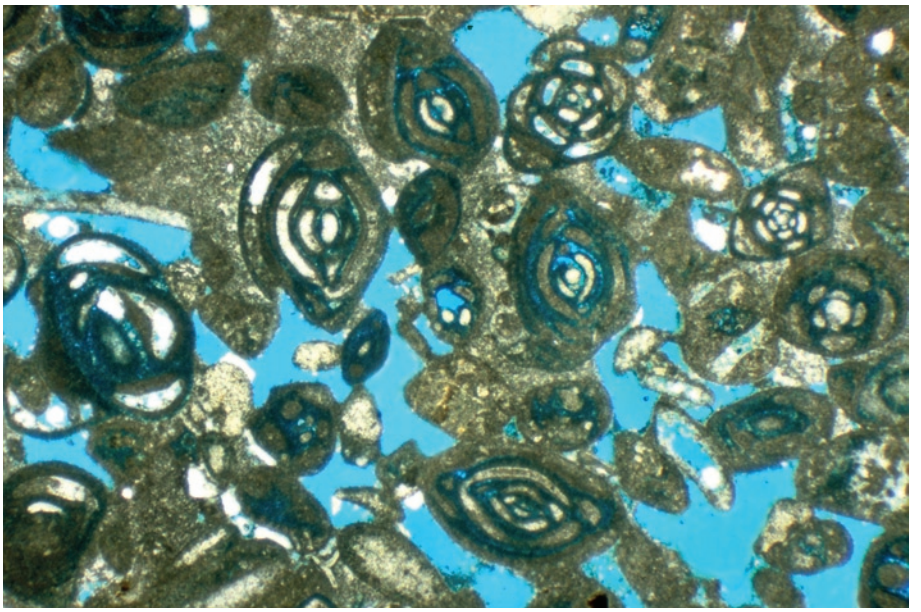

Eocene Ocala Gp., Inglis Fm., Levy Co., Florida

A limestone (packstone) in which miliolid foraminifers are a major component of the total sediment. The tests have non-laminar, porcelaneous calcareous walls and complex (miliolid) chamber coiling patterns. The original walls were high-Mg calcite, although some of the walls may have been partially dissolved in this example.

PPL, BSE, HA = 5.1 mm

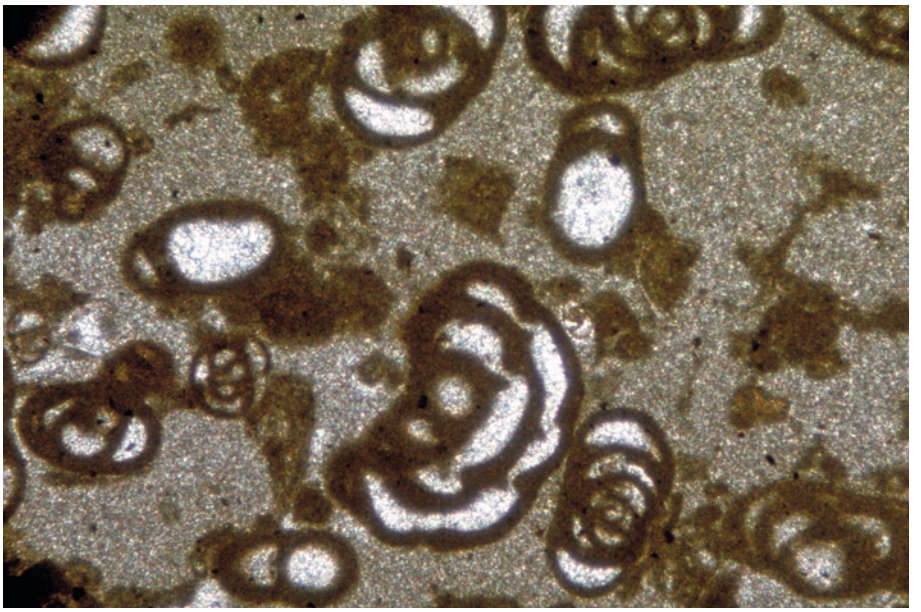

Mid-Cretaceous El Abra Ls., Tamaulipas, Mexico

A shelf limestone (wackestone) with abundant miliolid foraminifers in a lime-mud matrix. The foraminiferal tests and part of the matrix mud are oil stained, accentuating the dark color of the porcelaneous test walls in this group. Photograph courtesy of Paul Enos.

PPL, HA = 3 mm

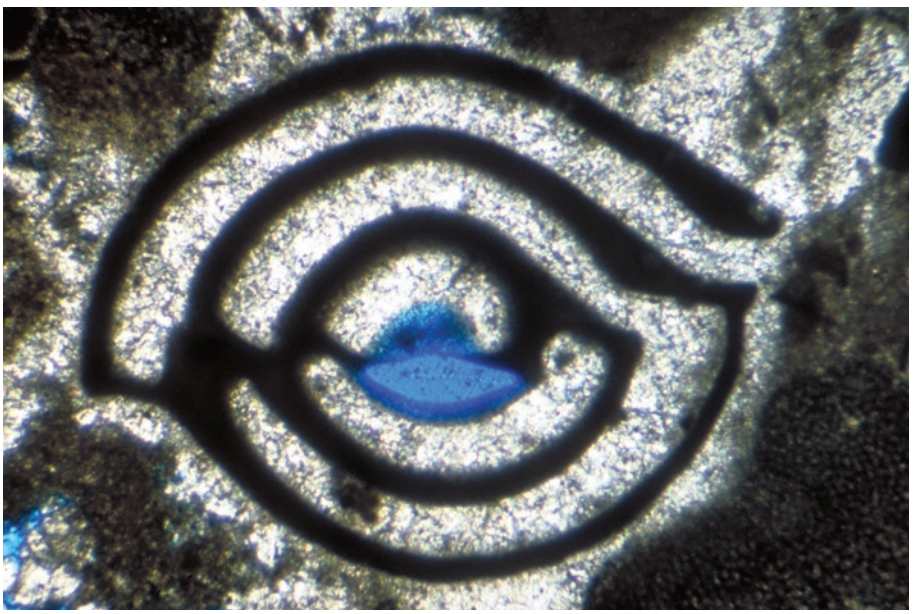

Eocene limestone, Zakinthos, Ionian Islands, Greece

An example of microgranular, imperforate, carbonate test walls and complex (biloculine or spiroloculine) chamber coiling in a spiroloculinid-like benthic foraminifer.

PPL, BSE, HA = 2.4 mm

Pleistocene Belmont calcarenite, Belmont, Bermuda

Cross-sectional views of two specimens of *Peneroplis* sp., a large benthic foraminifer with characteristic color and "fingerprint-like" chambering. Peneroplid foraminifers are important sediment formers in modern carbonate shelf deposits, especially in restricted lagoonal settings with variable salinity where they can be the dominant faunal element. Photograph courtesy of Clif Jordan.

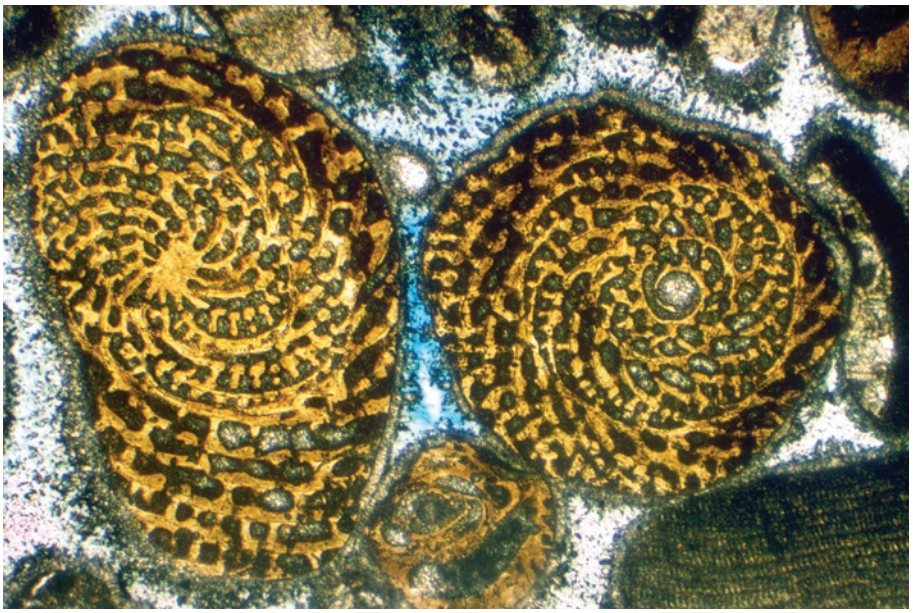

PPL, BSE, HA = ~1.0 mm

Recent sediment, Grand Cayman, Cayman Islands, B.W.I.

A medial cross-sectional view of *Peneroplis* sp. The peneroplids are an Eocene to Recent group of foraminifers of the Suborder Miliolina. The largely imperforate, porcelaneous calcareous walls have a characteristic amber to reddish color and the coiling patterns are predominantly planispiral, but may vary through the life cycle of the organism. The dark color of the test is largely the result of its micrometer-scale nannoporous structure.

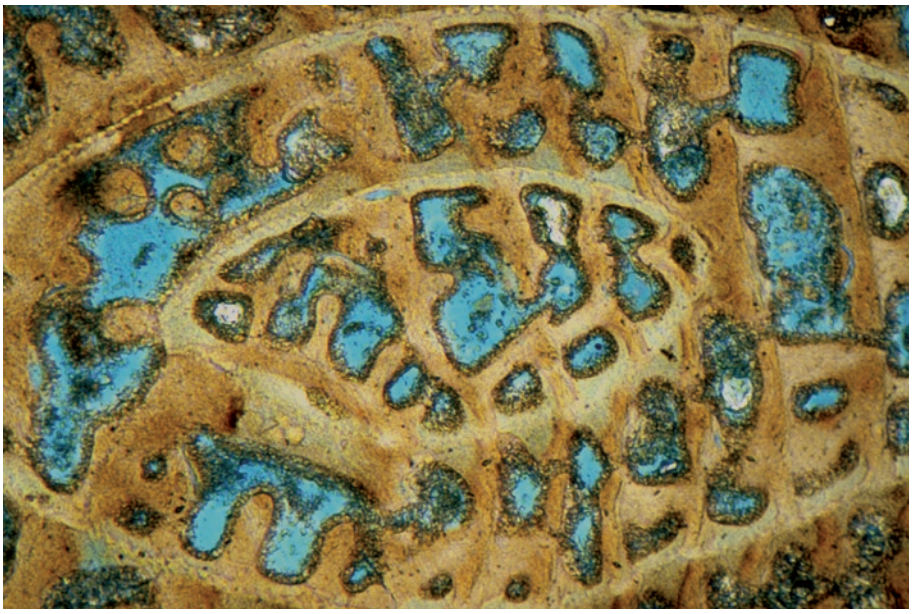

PPL, BSE, HA = 0.65 mm

Recent sediment, Yorke Peninsula, South Australia

This section of restricted lagoonal sediment shows a microgranular-walled benthic foraminifer. Note the presence of a thin, but distinct, outer wall in this test.

PPL, HA = 0.65 mm

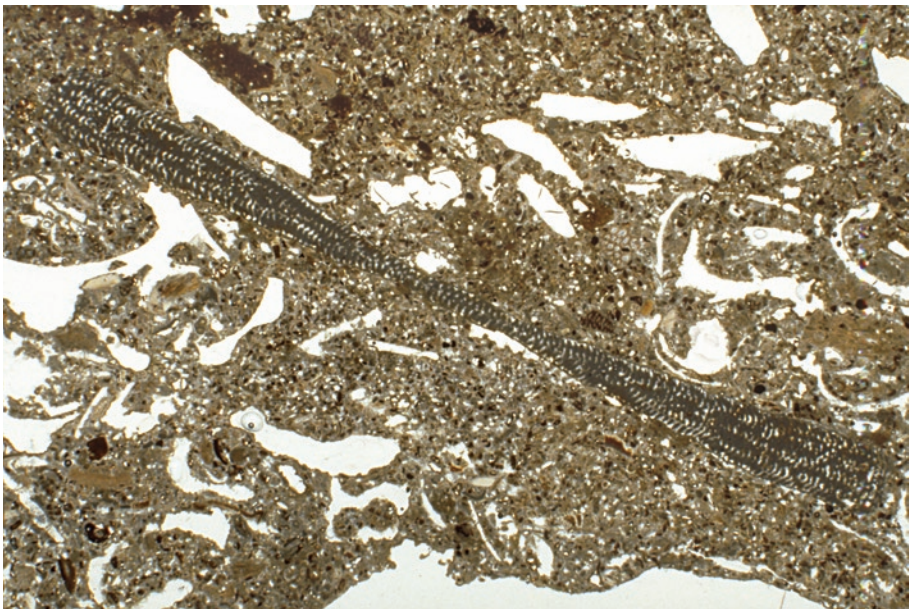

Miocene Pata Ls., Murray Basin, South Australia

Some benthic foraminiferal tests can reach very large sizes, especially considering that they are constructed by single-celled organisms. This single *Marginopora* sp. is an excellent example of a large foraminifer with planispiral coiling. It has small, early-formed chambers in the center and increasingly larger chambers toward the margins. The irregular molds in this rock (white) represent leached aragonitic skeletal fragments. Sample from Noel P. James.

PPL, HA = 16 mm

Eocene-Oligocene? Hanmer Marble, northern Canterbury, New Zealand

Plane- and cross-polarized light views of the same nummulite foraminifer. Nummulites are a group of large, thick, coin- or discus-shaped benthic foraminifers. They are classed in the Suborder Rotaliacea and are especially widespread in Eocene strata (although they range from Paleocene to Recent). Note the robust walls, the V-shaped gaps or cavities between chambers, and the pronounced extinction bands that result from the optically-radial calcite crystal structure.

PPL/XPL, HA = 1.2 mm each

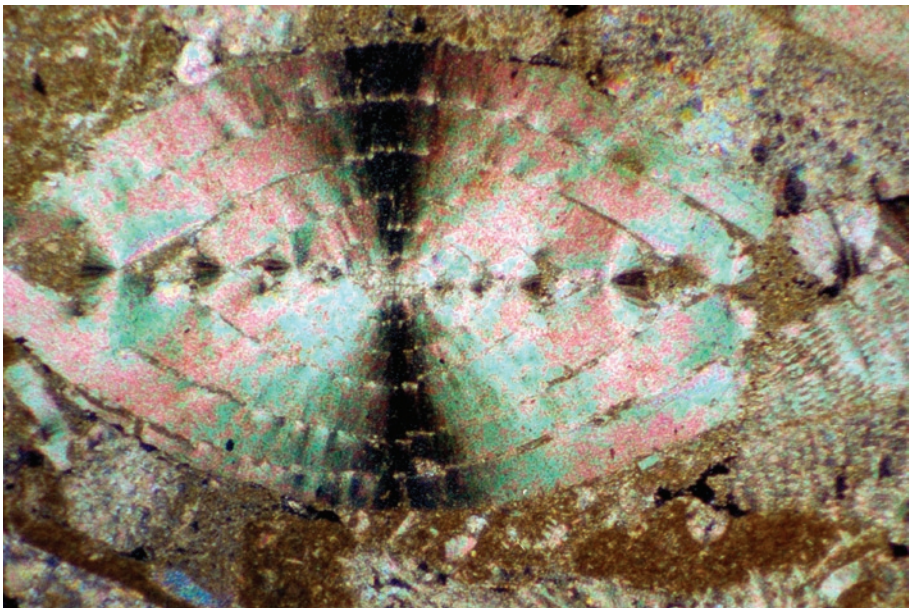

Eocene Nummulite Ls., near Split, Croatia

A longitudinal axial section of a single nummulite foraminifer, *Nummulites* sp. Note again the large size, robust radial hyaline walls, extinction bands, biconvex planispiral coiling, and traces of perforations that characterize this important foraminiferal group. Individual nummulitid foraminifers can reach a maximum diameter of 19 cm (and commonly are 4-6 cm in diameter). The excellent preservation of these tests indicates that they originally has a high- or low Mg calcite composition.

XPL, HA = 3.4 mm

Mid. Eocene Naranjo Fm., Coamo Springs Mbr., Ponce-Coamo area, Puerto Rico

This limestone is packed with orbitoid foraminifers — discocyclinids — as well as numerous red algal fragments. Discocyclinids are benthic foraminifers belonging to the Superfamily Orbitoidacea, are restricted to Eocene deposits, reach cm-size, and have optically-radial hyaline calcitic tests. Orbitoids as a whole range from Late Cretaceous to Miocene. Sample from E. A. Pessagno, Jr.

PPL, HA = 8 mm

Mid. Eocene Naranjo Fm., Coamo Springs Mbr., Ponce-Coamo area, Puerto Rico

A higher magnification view of a *Discocyclina* sp. benthic foraminifer. The characteristic radiating calcite pillars and small chambers are clearly visible at this magnification. Sample from E. A. Pessagno, Jr.

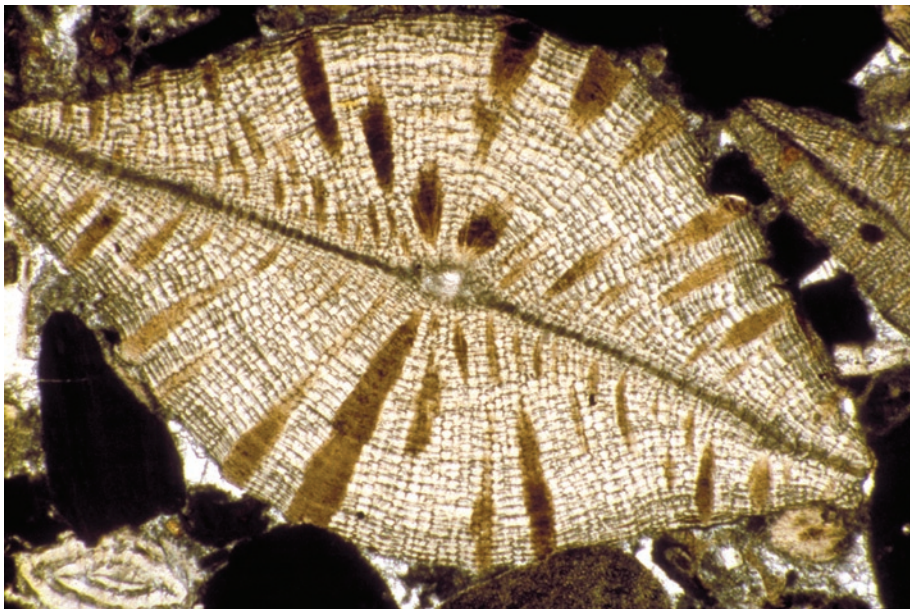

PPL, HA = 3.75 mm

Up. Oligocene (Chattian) Lower Coralline Limestone Fm., Malta

This cool-water shelfal limestone shows whole and fragmented giant *Lepidocyclina* sp. benthic foraminifers. This is another member of the suite of orbitoid foraminifers that are important sediment formers in mid-Tertiary limestones (the genus ranges from Eocene to middle Miocene). The calcitic walls of these large, discoidal tests are generally well preserved and can retain substantial volumes of intraparticle porosity, as in this example.

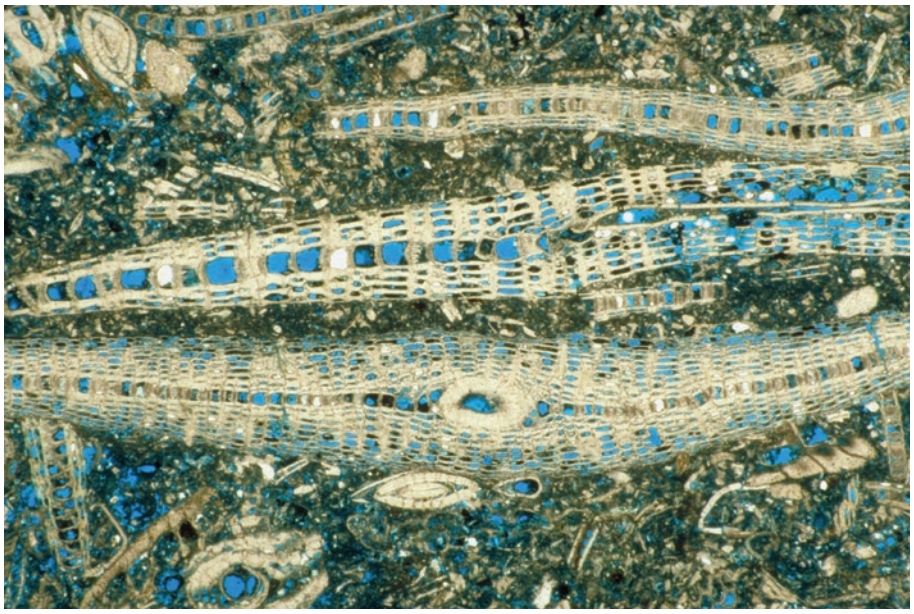

PPL, BSE, HA = 8 mm

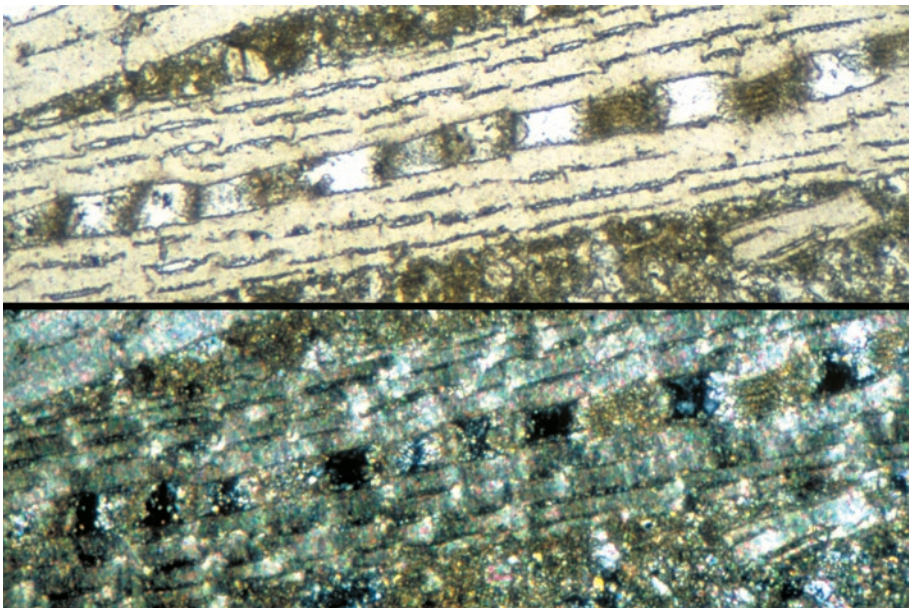

Tertiary Marianna Ls., Marianna, Florida

These close-up views under plane- and cross-polarized light of large lepidocyclinid foraminifers show the distinctive extinction patterns created by the combination of elongate chambers and massive walls. The walls show a characteristically textured extinction pattern related to the radial hyaline crystal structure.

PPL/XPL, HA = 1.6 mm

Lo. Cretaceous (Aptian) Shuaiba Fm., offshore Qatar

Another large foraminifer of very different shape and wall structure — a pyrite-impregnated calcite-stained *Orbitolina* sp. in a peloidal shelf limestone. Note the typical conical shape in this longitudinal section. Orbitolinids range from the Cretaceous to the Eocene, although this genus is found only in Cretaceous rocks.

PPL, AFeS, HA = 3.0 mm

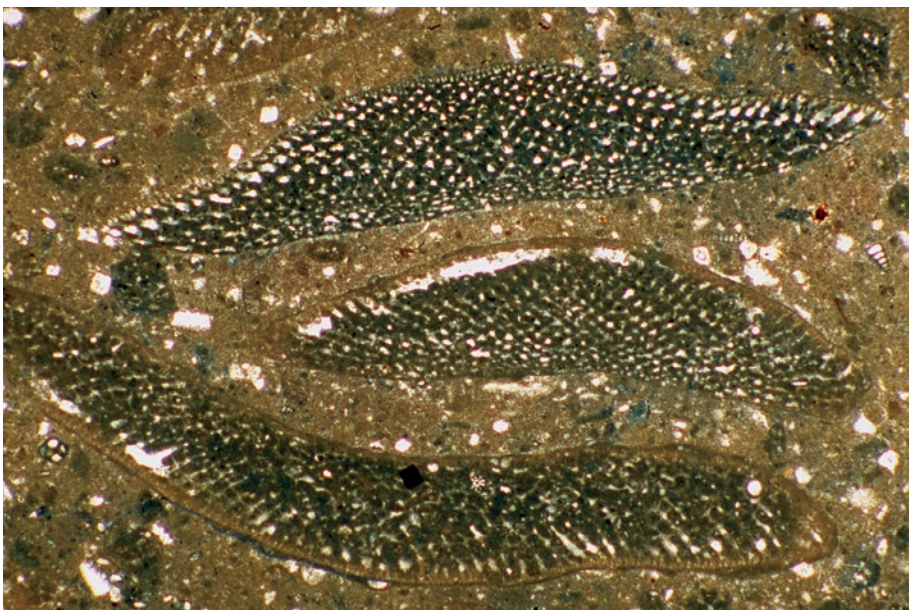

Lo. Cretaceous (Aptian) Shuaiba Fm., offshore Qatar

A variety of cuts through three large orbitolinid foraminifers. As in this example, these benthic foraminifers can be important rock-forming elements (and important biostratigraphic markers), especially in Lower Cretaceous open-shelf and deep-shelf sediments.

PPL, HA = 4.5 mm

Up. Cretaceous (Cenomanian) limestone, Tirol, Austria

A cross-section through a single, large *Orbitolina* sp. foraminifer. The conical to domal shape, elongate to saucer-shaped chambers, and pores or cellules in the dark, micritic marginal zone are characteristic of orbitolinids. Like all other members of the Suborder Textulariina, orbitolinids have agglutinated walls. Recognizing the agglutinated fabric requires careful observation, however, largely because the constituent grains are small and the chamber structure is so complex.

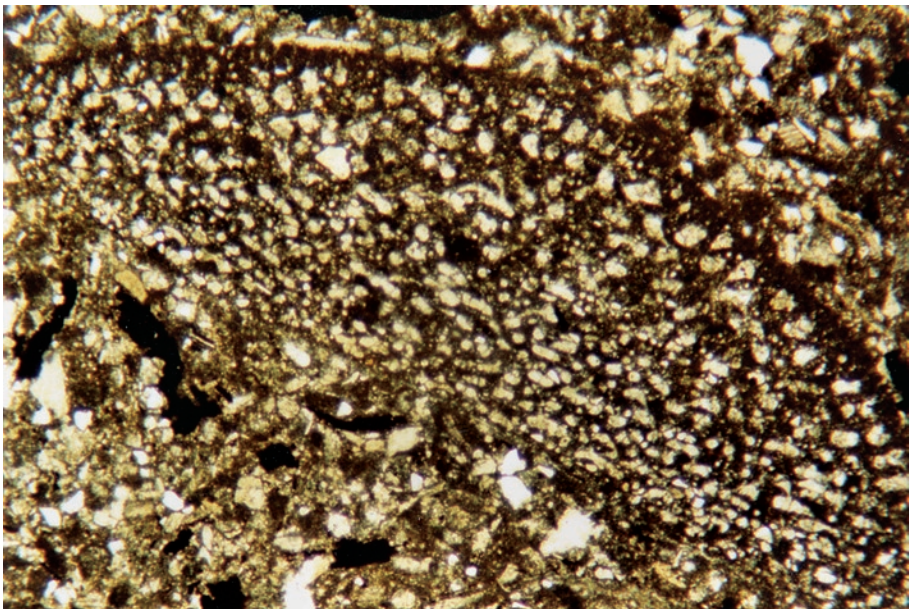

PPL, HA = 3.3 mm

Morphology and wall structure of a typical fusulinid foraminifer

A diagrammatic view of the chamber arrangement and wall structure of a typical fusulinid foraminifer, based on the general morphological shape of *Parafusulina*, *Fusulinella*, and *Schwagerina*. Note the multilayered calcareous microgranular walls that have abundant perforations. Adapted from Brasier (1980) and Moore et al. (1952); citations given at end of book introduction. The full fusulinid is aprroximately a centimeter in length.

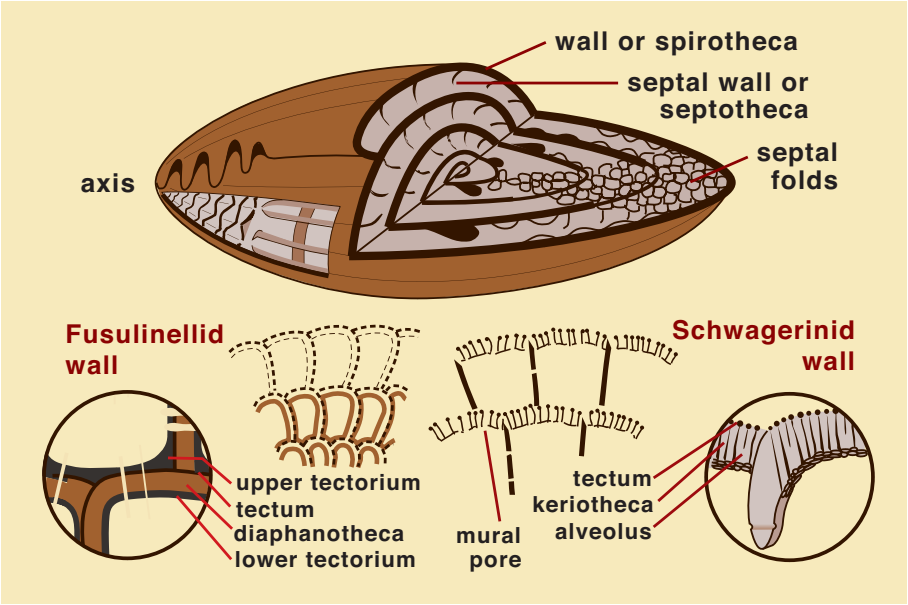

Up. Pennsylvanian (Virgilian) Holder Fm., Otero Co., New Mexico

An example of a limestone in which fusulinid foraminifers (*Tricites* sp.) are not just the dominant, but essentially the only, constituent. The circular to cigar-shaped cross-sections of these spiral forms, the chambered structure, and the microgranular walls with barely visible perforations all are characteristic of this group. Although these are relatively small fusulinids, some Permian forms can reach 6 cm in length.

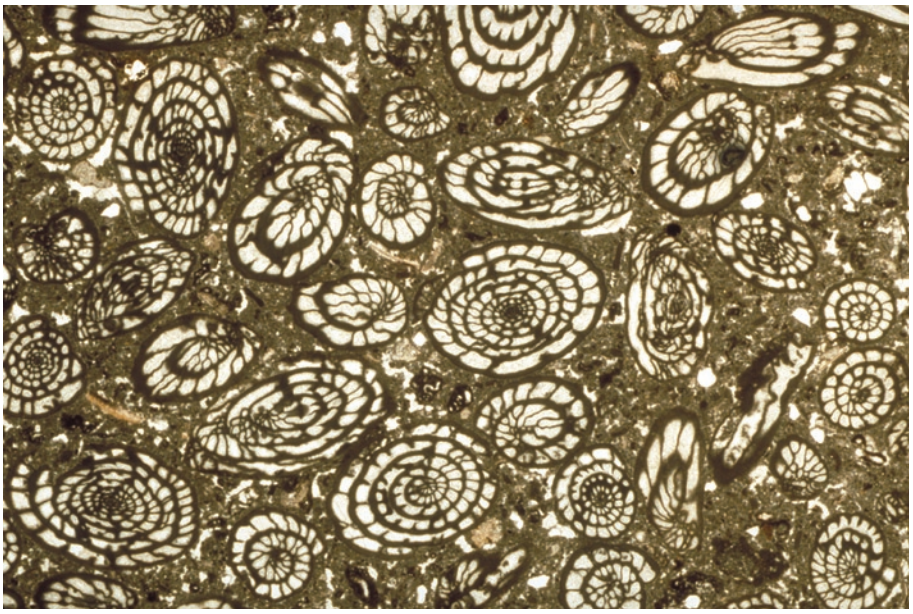

PPL, HA = 16 mm

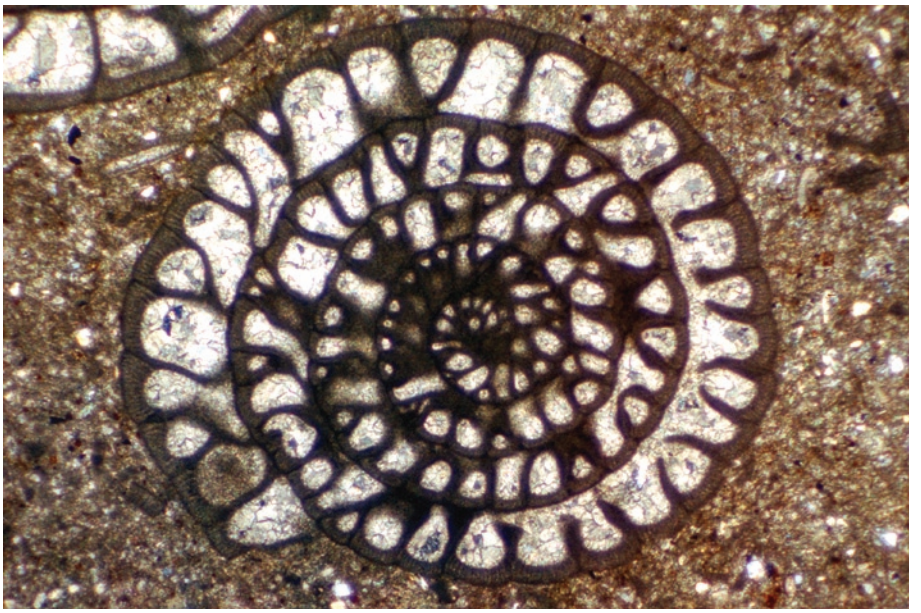

Lo. Permian (Leonardian) Bone Spring Ls., Apache Canyon, Texas

A fusulinid foraminifer (*Parafusulina schucherti*) in transverse section across its circular axis. Note the distinctive chamber shapes and radially perforated wall structure. Although fusulinids are found only in Pennsylvanian and Permian strata, they were prolific sediment producers in open shelf and shelf margin (including reefal) deposits. The rounded, cigar-shaped exteriors of these grains made them easy to transport and orient, and as such they can be useful paleocurrent indicators.

PPL, HA = 3.4 mm

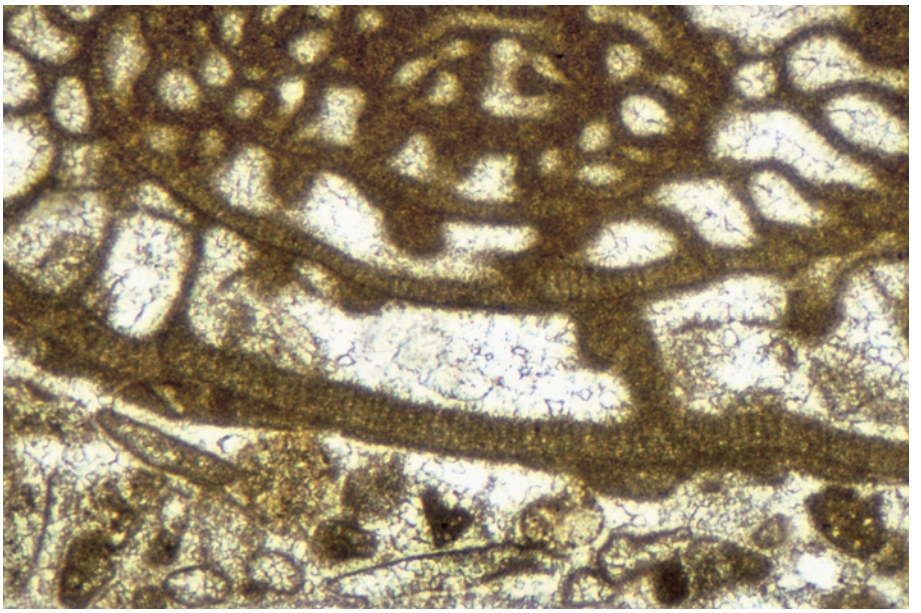

Lo. Permian (Wolfcampian) Abo Gp., Laborcita Fm., Otero Co., New Mexico

A high-magnification view of a fusulinid foraminifer showing the numerous, closely-spaced pores that perforate the microgranular calcite of the test wall. In lower magnification views, these pores are essentially invisible.

PPL, HA = 1.6 mm

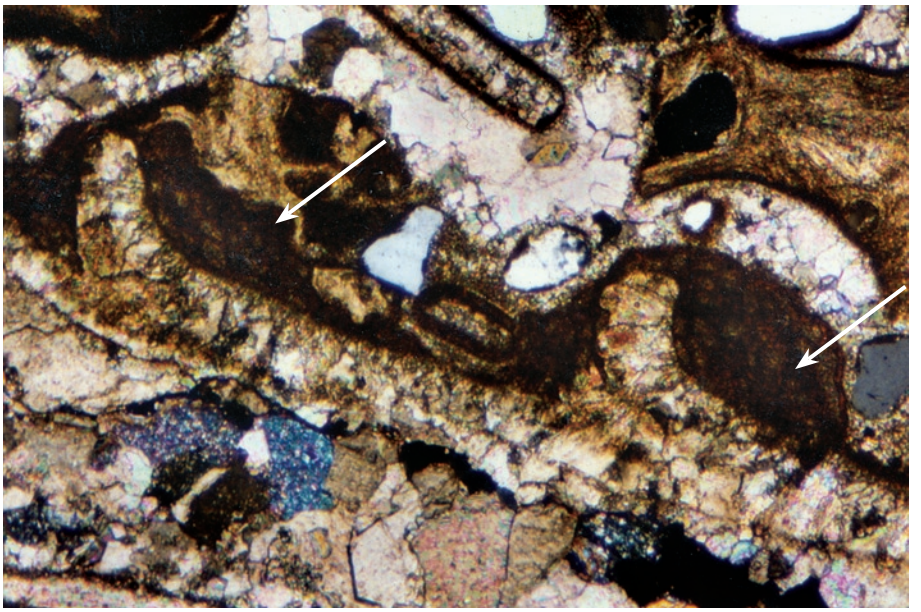

Pennsylvanian (Morrowan) Bloyd Fm., Mayes Co., Oklahoma

Encrusting foraminifers (arrows) on a neomorphosed, highly ornamented bivalve shell. The globular, chambered, foraminiferal structure is barely visible within the dense, micritic encrustation. For this reason, among others, encrusting foraminifers are often misidentified as encrusting algae (most encrusting red algae, however, have finer-scale, more rectangular, cellular structures).

XPL, HA = 2.0 mm

Recent sediment, Cay Corker, Belize

A cross-section of the large encrusting foraminifer, *Homotrema rubrum*. The reddish hue is the natural (unstained) color characteristic of this species. These foraminifers are found as bright reddish, centimeter-sized encrustations on other carbonate grains in modern tropical shelf carbonates in many areas of the world. The heavy, durable walls of this species and its remarkable adhesion to its substrates make it a very successful encruster in high-energy settings. *Homotrema* encrustations are so prolific in coastal settings that many carbonate beach sands (Bermuda, for example) have a pink color from their tests.

PPL, HA = 3.5 mm

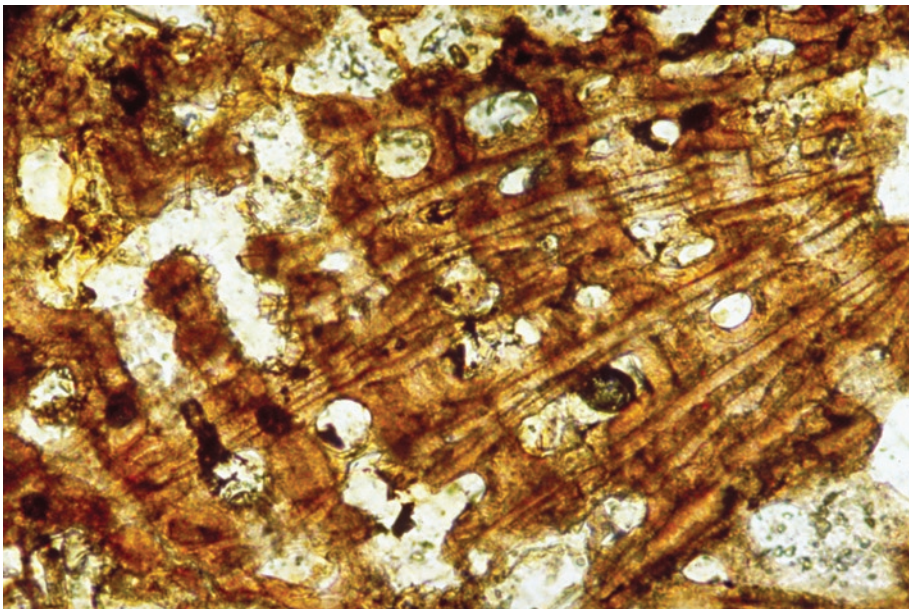

Up. Permian (Kazanian) Wegener Halvø Fm., Jameson Land, East Greenland

The irregular chambers of a possible encrusting tubular foraminifer are seen here forming part of a bryozoan-foraminiferal bioherm. Late Paleozoic and some Mesozoic deposits, in particular, have intricate intergrowths (possibly symbiotic consortia) of encrusting foraminifers and algae, bryozoans and other organisms. Some workers have classified forms similar to this one with the algae rather than with foraminifers.

PPL, HA = 2.4 mm

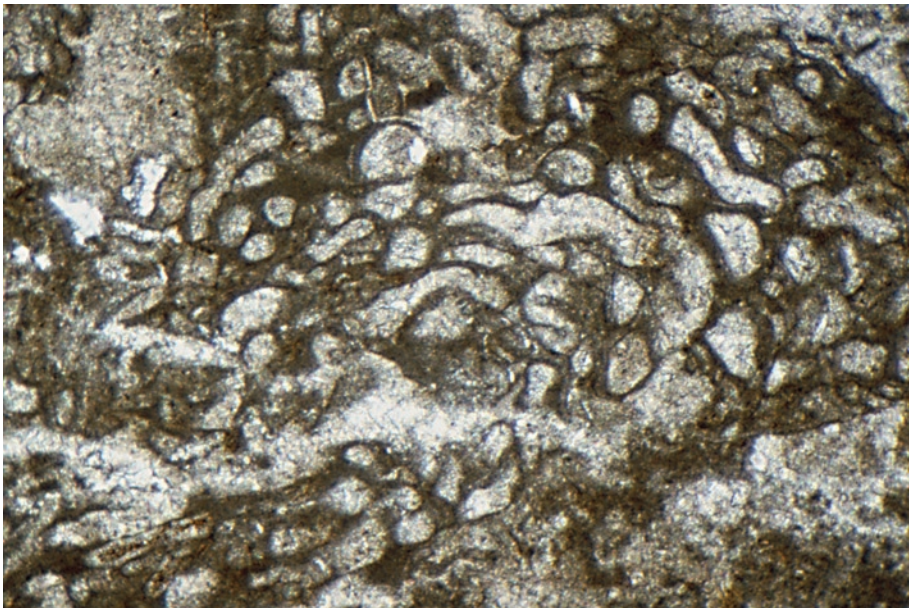

Holocene Reef wall limestone, Belize

An encrusting foraminifer in a tropical reef limestone, probably *Gypsina* sp. This robust species has large, regularly arranged chambers. Sample from Noel P. James.

PPL, CYS, HA = 3.0 mm

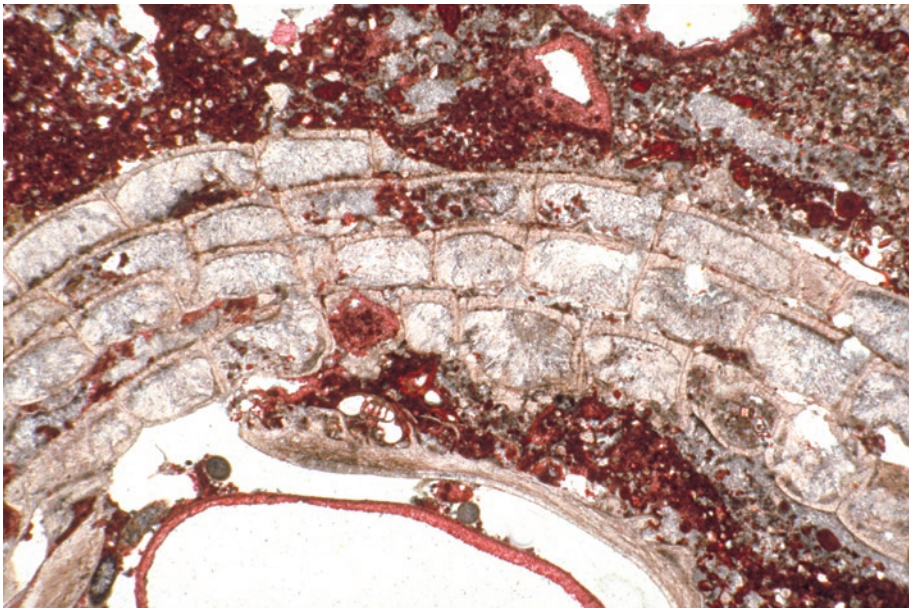

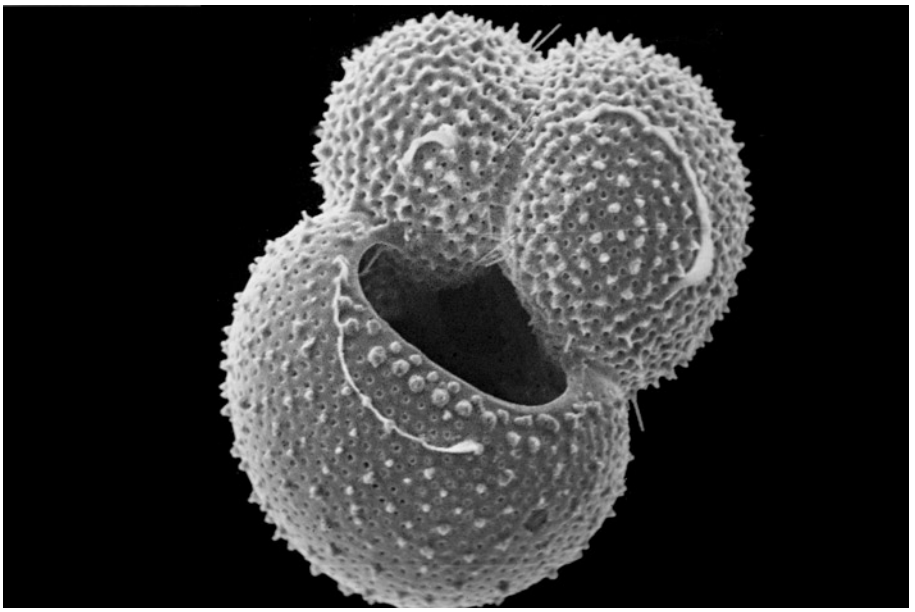

Holocene sediment, Southern Shelf, Belize

A specimen of *Globigineroides rubra*, a planktic foraminifer. This species is characterized by highly globular chambers, a large aperture, short spines and numerous wall pores.

SEM, HA = ~775 μm

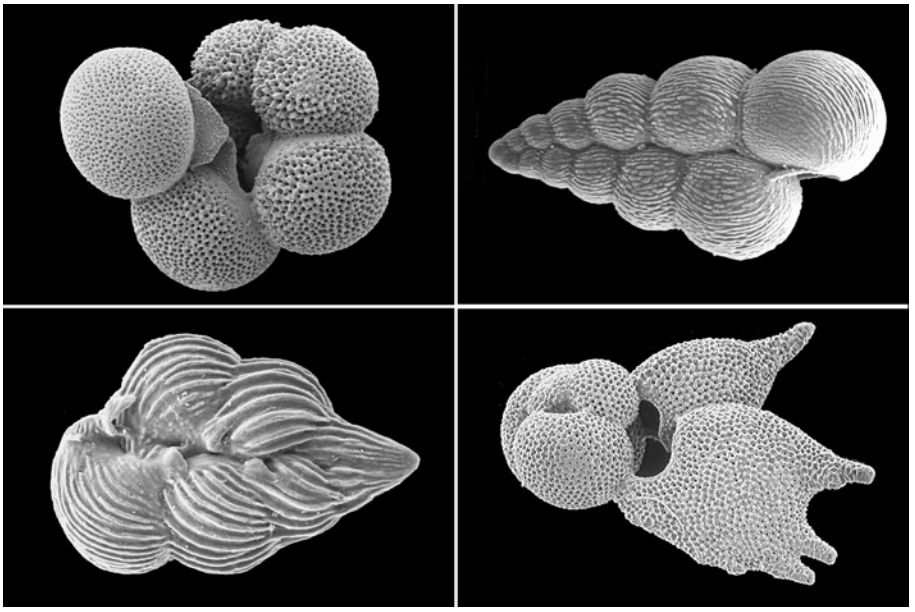

SEM views of calcareous planktic foraminifers

UL: Up. Paleocene, North Atlantic.
Parasubbotina variospira. HA = ~170 μm
UR: Up. Cretaceous (Maastrichtian), Alabama.
Heterohelix crinata. HA = ~400 μm
LL: Up. Cretaceous (Maastrichtian), North Atlantic.
Pseudoguembelina excolata. HA = ~325 μm
LR: Up. Pliocene, Eastern equatorial Pacific.
Globigerinoides sacculifer. HA = ~1000 μm

All photographs courtesy of Richard Norris.

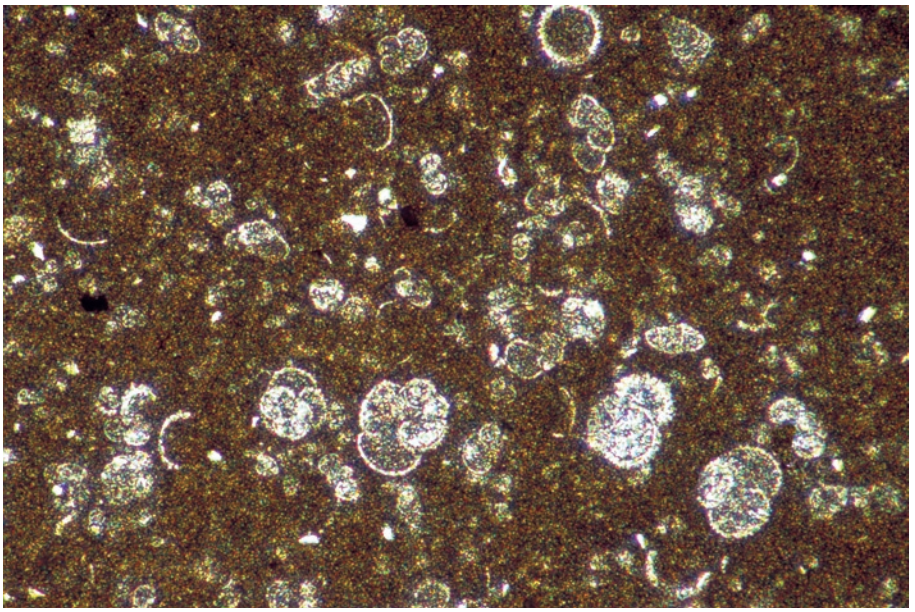

Lo. Tertiary Amuri Ls., Marlborough, New Zealand

A low-magnification view of a typical planktic foraminiferal (globigerinid) biomicrite. Such deposits are distinguished from calcisphere limestones by the fact that most of the grains show multiple chambers (and even the grains showing a single chamber probably represent tangential cuts through one chamber of a multi-chambered organism).

PPL, HA = 2.0 mm

Up. Cretaceous (Cenomanian-Turonian) Greenhorn Ls., Denver Basin, Colorado

A deep-shelf chalk containing globigerinid planktic foraminifers with spar-filled chambers. This example shows thin-walled, unornamented tests without visible pore structure. As in many planktic foraminiferal limestones, the matrix consists largely of nannofossil debris, recognizable at higher magnifications of in SEM.

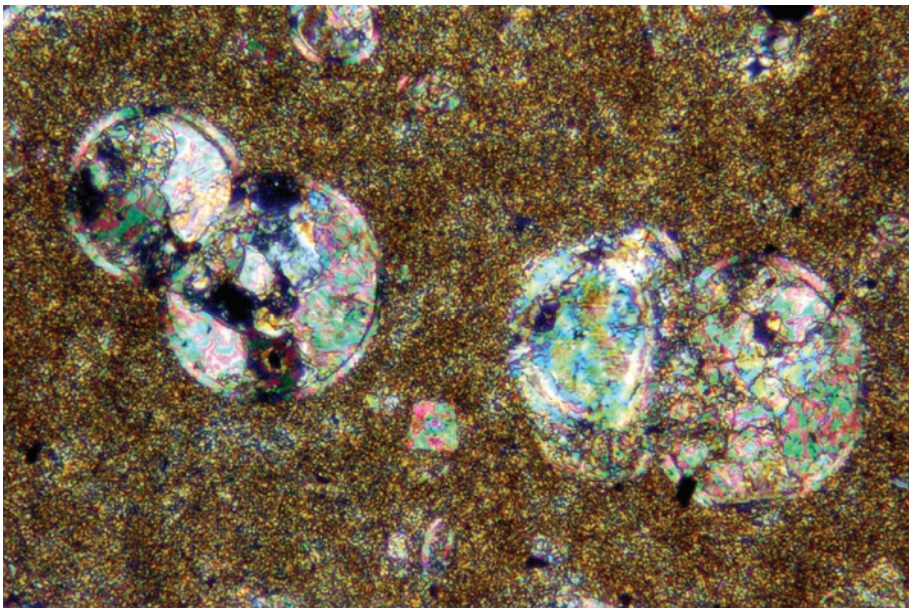

XPL, HA = 0.54 mm

Pleistocene (?) sediment, Miami Terrace, offshore Florida

A modern planktic foraminiferal ooze containing a rich fauna of globorotaliid foraminifers. The tests have well-preserved porous radial wall structure and micrite filling of their chambers. These organisms are planktonic and are abundant in outer shelf, slope, and deeper oceanic sediments.

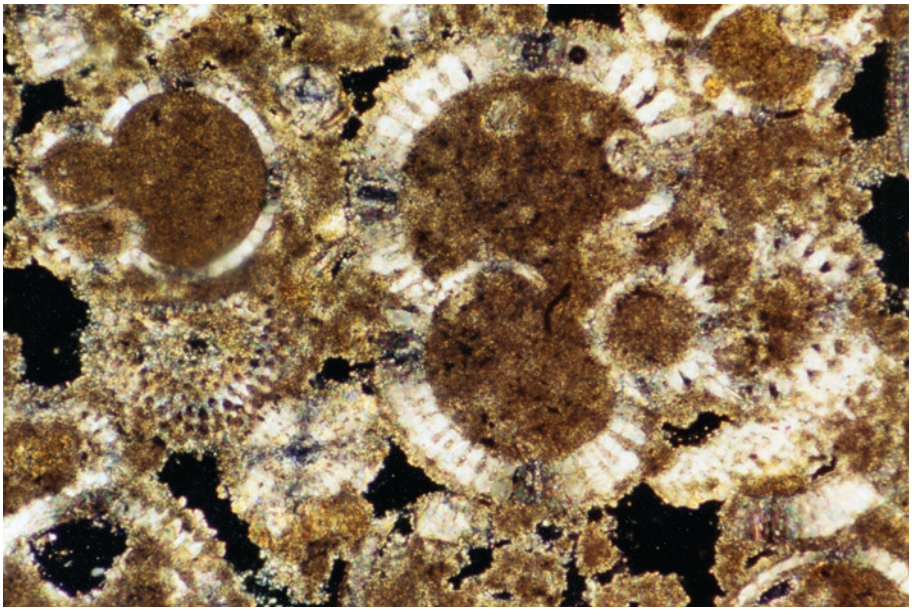

XPL, HA = 0.90 mm

Miocene (Aquitanian-Burdigalian) Middle Globigerina Limestone Fm., Gozo, Malta

A high-magnification view showing large pores in relatively thick planktic foraminiferal walls. The blue-stained epoxy has penetrated and accentuated the pores. The low-Mg calcite composition of planktic foraminiferal tests generally leads to good preservation of structure. Cementation, however, can obscure features such as these pores.

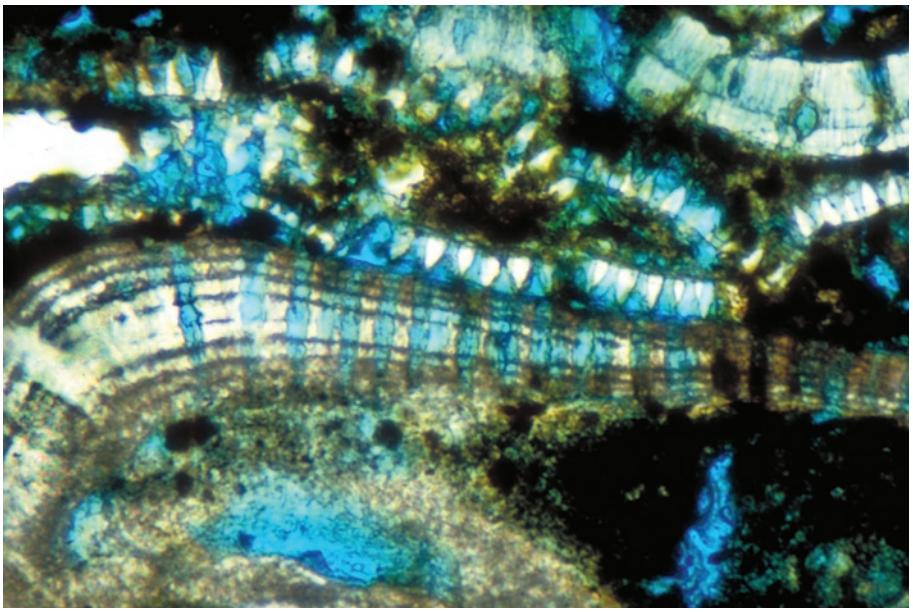

PPL, BSE, HA = 0.42 mm

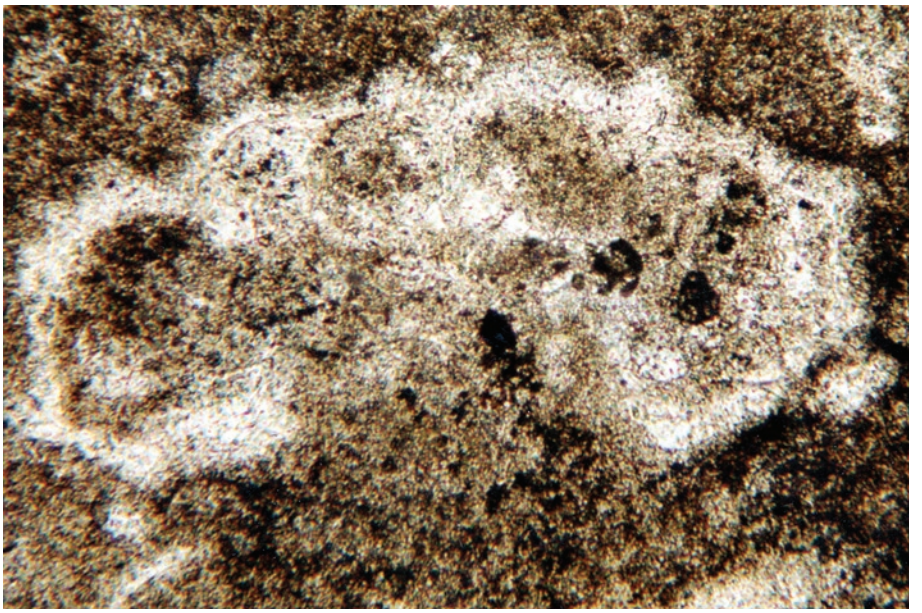

Up. Cretaceous Upper Chalk, Kent, England, U.K.

A *Globotruncana* sp. planktic foraminifer. These are common in Cretaceous open shelf and deeper marine deposits. Note the keeled chambers diagnostic for this genus and the relatively poor preservation of wall structure, an exception to the norm in planktic foraminifers.

PPL, HA = 0.36 mm

Cited References and Additional Information Sources

Banner, F. T., and C. P. G. Pereira, 1981, Some biserial and triserial agglutinated smaller foraminifera: their wall structure and its significance: Journal of Foraminiferal Research, v. 11, p. 85-117.

Banner, F. T., R. Sheehan, and E. Williams, 1963, The organic skeletons of rotaline foraminifera: a review: Journal of Foraminiferal Research, v. 3, p. 30-42.

Bathurst, R. G. C., 1975, Carbonate Sediments and their Diagenesis [2nd Edition]: New York, Elsevier Science Publ. Co., 658 p. [see section on p. 39-49].

Bé, A. W. H., and L. Lott, 1964, Shell growth and structure of planktonic Foraminifera: Science, v. 145, p. 823-824.

Bignot, G., and M. Neumann, 1962, La structure des tests des foraminiferes. Analyse bibliographique: Revue de Micropaléontologie, v. 4, p. 237-248.

Blackmon, P. D., and R. Todd, 1959, Mineralogy of some foraminifera as related to their classification and ecology: Journal of Paleontology, v. 33, p. 1-15.

Buzas, M. A., R. C. Douglass, and R. A. Smith, 1987, Kingdom Protista, *in* R. S. Boardmann, A. H. Cheetham, and A. J. Rowell, eds., Fossil Invertebrates: Palo Alto, CA, Blackwell Scientific Pubs., p. 67-106.

Culver, S. J., 1987, Foraminifera, *in* J. H. Lipps, ed., Fossil Prokaryotes and Protists: Notes for a Short Course: University of Tennessee, Department of Geological Sciences, Studies in Geology 18, p. 169-212.

Folk, R. L., and F. L. Lynch, 2001, Organic matter, putative nannobacteria and the formation of ooids and hardgrounds: Sedimentology, v. 48, p. 215-229.

Glaessner, M. F., 1963, Major trends in the evolution of the Foraminifera, *in* G. H. H. Koenigswald, et al., eds., Evolutionary Trends in Foraminifera: Amsterdam, Elsevier Publishing Company, p. 9-24.

Hay, W. W., K. M. Towe, and R. C. Wright, 1963, Ultrastructure of some selected foraminiferal tests: Micropaleontology, v. 9, p. 171-195.

Haynes, J., 1981, Foraminifera: New York, John Wiley & Sons, 433 p.

Hedley, R. H., and C. G. Adams, 1974, Foraminifera: New York, Academic Press, 276 p.

Hemleben, C., 1969, Ultrastrukturen bei kalkschaligen Foraminiferen: Naturwissenschaften, v. 56, p. 534-538.

Hofker, J., 1962, Studien an planktonischen Foraminiferen: Neues Jahrbuch für Geologie und Paläontologie, Abhandlungen, v. 114, p. 81-134.

Hofker, J., 1967, Hat die feinere Wandstruktur der Foraminiferen supragenerische Bedeutung?: Paläontogische Zeitschrift, v. 41, p. 194-198.

Hohenegger, J., and W. Piller, 1975, Wandstrukturen und Großgliederung der Foraminiferen: Sitzungsberichte der Österreichische Akademie der Wissenschaften, Mathematisch-Naturwissenschaftliche Klasse, Abteilung I, v. 184, p. 67-96.

Jørgensen, N. O., 1977, Wall structure of some arenaceous Foraminifera from the Maastrichtian White Chalk (Denmark): Journal of Foraminiferal Research, v. 7, p. 313-321.

Loeblich, A. R., Jr., and H. Tappan, 1964, Sarcodina, chiefly "Thecamoidians" and Foraminiferida, *in* R. C. Moore, ed., Treatise on Invertebrate Paleontology, Part C, Protista 2: Geological Society of America and University of Kansas Press, 2 vols., 900 p.

Loeblich, A. R., Jr., and H. Tappan, 1968, Suprageneric classification of the Foraminiferida (Protozoa): Micropaleontology, v. 30, p. 1-70.

Loeblich, A. R., Jr., and H. Tappan, 1988, Foraminiferal Genera and their Classification: New York, Van Nostrand, v. 1, 970 p.; v. 2, 212 p.

Moore, R. C., C. G. Lalicker, and A. G. Fischer, 1952, Invertebrate Fossils: New York, McGraw-Hill Book Co., 766 p. [Foraminifers, p. 39-72]

Norling, E., 1968, On Liassic nodosariid Foraminifera and their wall structures: Sveriges Geologiska Undersökning, ser. C, no. 623, Årsbok 61, no. 8, 75 p.

Podobina, V. M., 1990, Composition and microstructure of agglutinated foraminifer wall, *in* C. Hemleben, M. A. Kaminski, W. Kuhnt, and D. B. Scott, eds., Paleoecology, biostratigraphy, paleoceanography and taxonomy of agglutinated foraminifera, v. 327, D. Reidel Publishing Company, p. 19-23.

Thompson, M. L., 1964, Fusulinacea, *in* R. C. Moore, ed., Treatise on Invertebrate Paleontology, Part C, Protista 2: Geological Society of America and the University of Kansas Press, p. C358-C436.

Towe, K. M., and I. Cifelli, 1967, Wall ultrastructure in the calcareous Foraminifera: crystallographic aspects and a model for calcification: Journal of Paleontology, v. 41, p. 742-762.

Wood, A., 1949, The structure of the wall of the test in the Foraminifera; its value in classification: Quarterly Journal of the Geological Society of London, v. 104, p. 229-255.

Facing Page: Top: An SEM image of a calcareous heterococcolith, *Discosphaera tubifer*, with trumpet-like projections. Photograph courtesy of Jeremy R. Young.
Bottom: A phytoplankton bloom in the waters of the Cabot Strait, south of Newfoundland, on 29 July 2002. Terra MODIS true-color image provided by Jacques Descloitres, MODIS Land Rapid Response Team, NASA/GSFC.

GRAINS: Skeletal Fragments

Other micro- and nannofossils

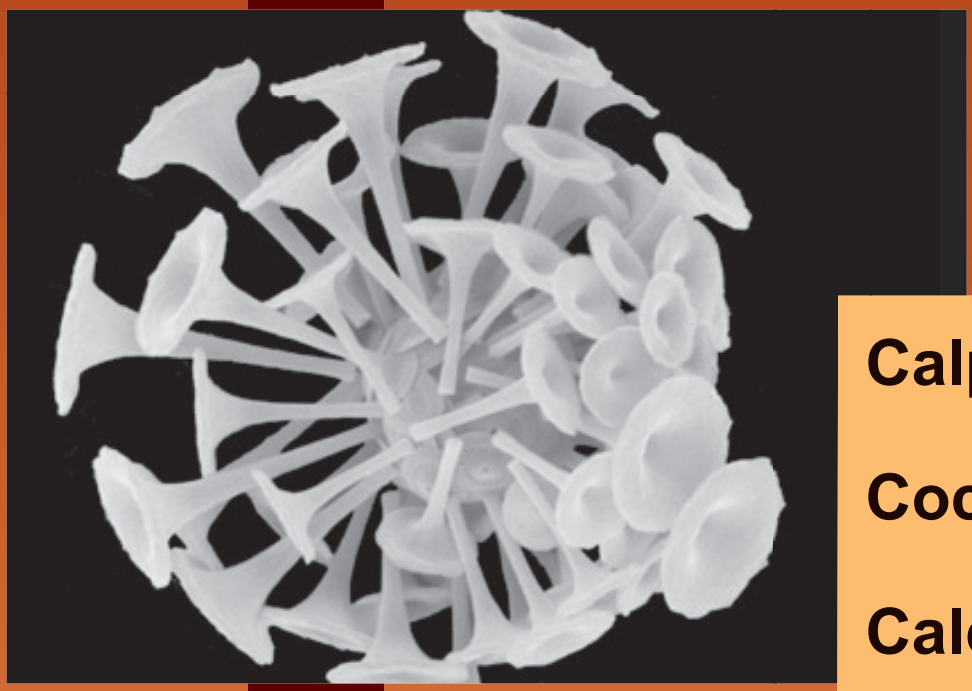

CHAPTER 3

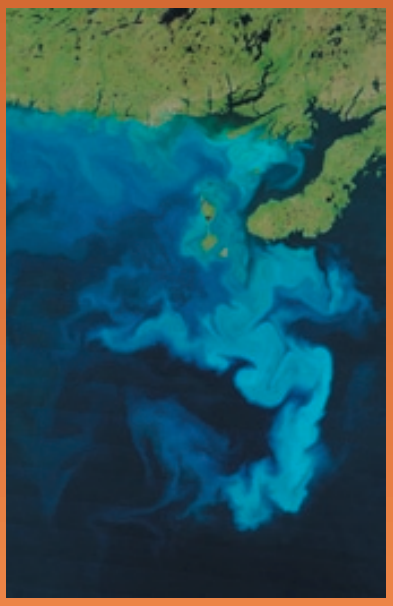

- Calpionellids
- Coccolithophores
- Calcispheres
- Tunicate spicules
- Siliceous groups (radiolarians, diatoms and others)
- Organic-walled groups

CALPIONELLIDS

Taxonomy and Age Range:

Often grouped with the tintinnids (pelagic ciliate protozoans of the subclass Spirotheca), although modern tintinnids are organic-walled and calpionellids had calcareous walls. Thus, calpionellids are grouped by other workers as Protozoa *incertae sedis*.

Calpionellids — Late Jurassic (Tithonian) to Early Cretaceous (Valanginian; possibly into Albian)

Tintinnids — Jurassic-Recent (but with possible record extending into the Paleozoic, perhaps even to the Cambrian)

Environmental Implications:

These open marine organisms are significant contributors to pelagic limestones and chalks in the Late Jurassic. Their distribution is largely restricted to the warm-water Tethyan region, within about 30-35° of the paleo-equator.

Skeletal Mineralogy:

All calpionellids apparently were composed of low-magnesium calcite; thus, generally well preserved. The TEM studies conducted by Fischer et al. (1967; cited at end of book's introduction) showed that some calpionellids built two-layered tests in which the main layer incorporated carbonate detritus (including coccoliths) and was lined by an inner, secreted layer.

Morphologic Features:

Small size (typically 45 to 150 µm in length and 30 to 90 µm in width), spherical to elongate, U- or V-shaped grains with a large opening rimmed, in some cases, by a narrowed, slightly thickened collar.

Keys to Petrographic Recognition:

1. **Small size (comparable to small calcispheres or planktic foraminifers).**
2. **Characteristic single-chambered cup or vase shape, commonly with a distinctive neck or collar, when seen in long-axis section.**
3. **Typically good preservation of overall outline and wall structure due to originally calcitic composition.**
4. **Can be mistaken for calcispheres or small planktic foraminifers if seen in sections through the short axis; thus, it is important to look for multiple examples.**
5. **Have a distinctive fabric of helicoidally arranged radial calcite crystals which can be distinguished in well preserved samples when viewed with SEM. Some may have a multi-layered structure as noted above.**

PHOTO SCALES AND ABBREVIATIONS ARE EXPLAINED IN THE BOOK'S INTRODUCTION

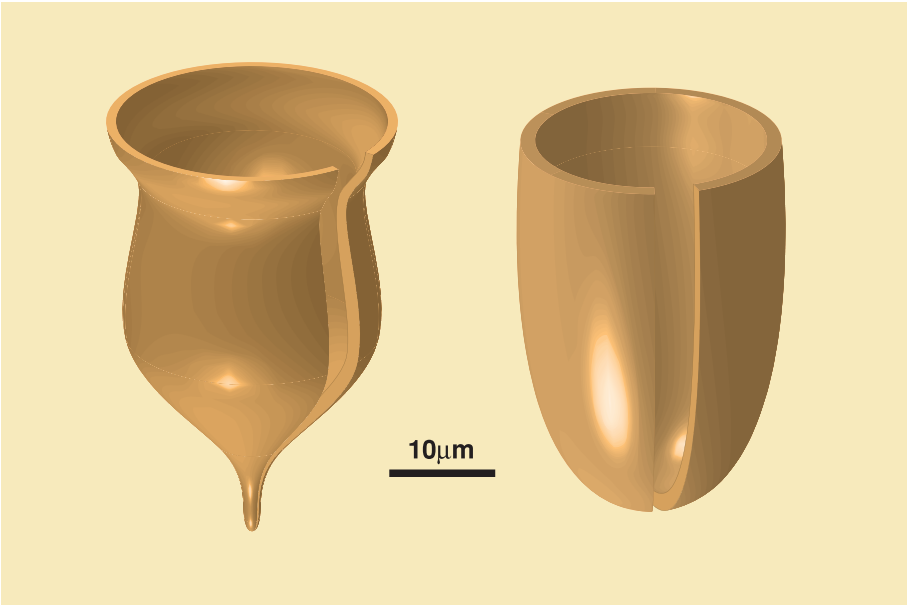

Typical three-dimensional calpionellid morphologies

Reconstructions of some typical calpionellids (redrawn after Remane, 1971). Note the characteristic cup- or vase-shapes, the large opening, the thin wall, and the presence of a collared neck in one case.

Diagram showing outlines of major calpionellid genera

Longitudinal cross-sectional outlines of some of the major calpionellid genera. Thin-section examination still provides the best method for identifying these organisms. Redrawn from Brasier (1980, p. 300).

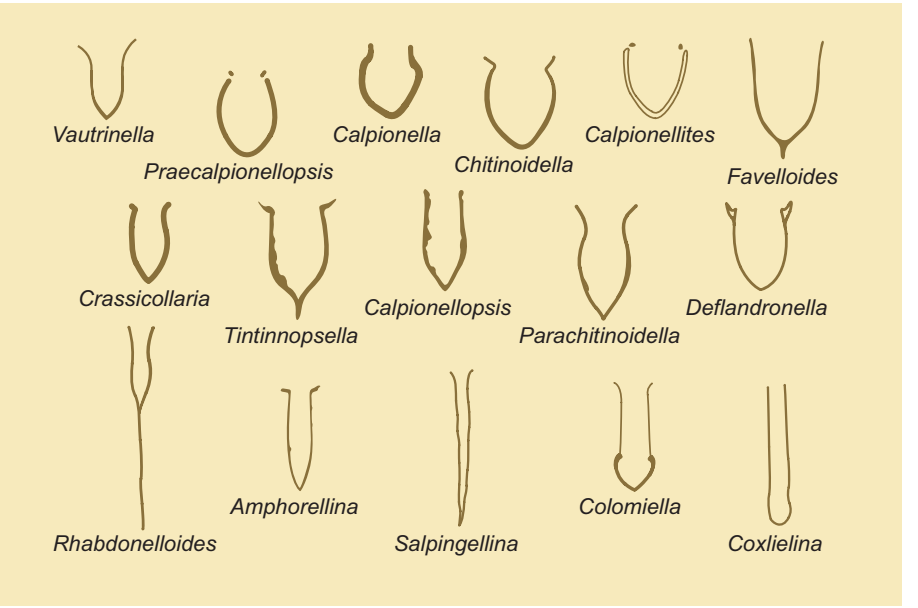

Up. Jurassic-Lo. Cretaceous "Vigla" Ls., Epirus, Greece

A calpionellid-rich limestone. Although in most cuts one only sees a single chambered, simple walled spherical (calcisphere-like grain), other sections show the single large opening with a U-shaped or characteristic vase-shaped body. Thus, to confidently identify calpionellids, one generally needs to examine multiple grains.

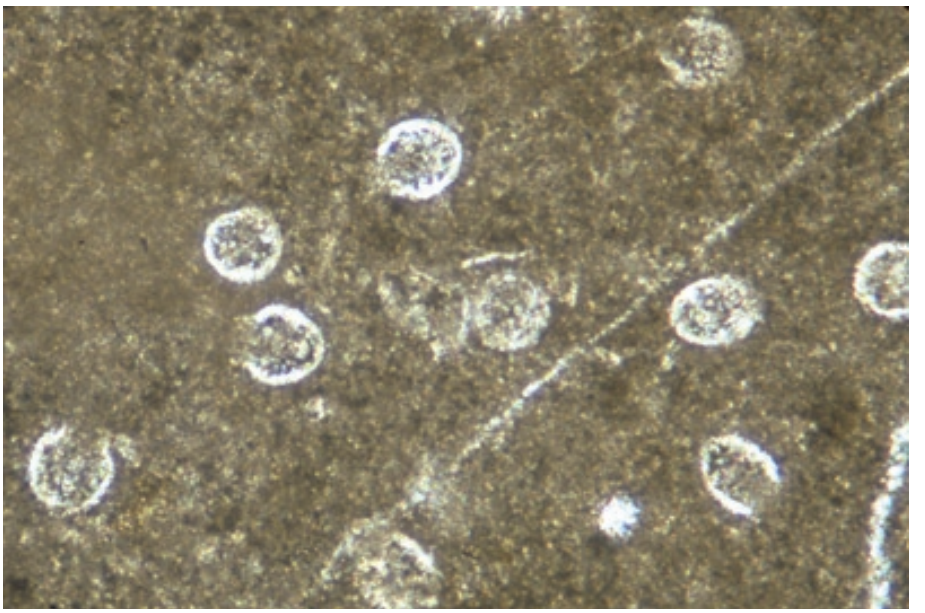

PPL, HA = 0.55 mm

Up. Jurassic-Lo. Cretaceous "Vigla" Ls., Epirus, Greece

Magnified longitudinal views of two calpionellids showing the distinctive, slightly thickened neck or collar that rims the chamber opening. The U- or V-shaped tests are readily recognizable in longitudinal sections but are very hard to distinguish from calcispheres and small planktic foraminifers in transverse sections.

PPL, HA = L: 0.11 mm; R: 0.17 mm

COCCOLITHOPHORES AND OTHER CALCAREOUS NANNOPLANKTON

Taxonomy and Age Range:

Coccolithophores are planktic unicellular algae belonging to the division (or phylum) Haptophyta which produce coccoliths — calcareous exoskeletal plates. The Haptophyta are characterized by possession of two flagellae and a third flagellum-like organelle, the Haptonema. The phylum includes many non-mineralizing algae, but these have no fossil record.

Coccolithophores are in the class Coccolithophyceae — Coccolithophores first occur in the Late Triassic (putative Paleozoic records are regarded as spurious by most authorities) and are abundant from the Early Jurassic to the Recent.

There are two basic types of coccoliths: heterococcoliths and holococcoliths. Heterococcoliths are formed of radial arrays of complex-shaped crystal units whereas holococcoliths are formed of large numbers of minute (roughly 0.1-0.5 µm) euhedral crystallites arranged in hexagonal or rhombohedral arrays. These two coccolith types are now thought to be characteristic of different phases in the life-cycle of coccolithophores. The typical coccolithophore life-cycle has an alternation of a diploid heterococcolith-producing phase and a haploid holococcolith producing phase, both of which reproduce asexually.

Additionally, many calcareous fossils exist, of similar size to coccoliths, but lacking the characteristic features of either holococcoliths or heterococcoliths — these are termed nannoliths. Since nannoliths and coccoliths co-occur, they usually are studied together and are collectively termed nannoliths.

Environmental Implications:

Exclusively planktic photoautotrophs — thus, they require light and live in surface waters, although they accumulate as rock-forming constituents primarily in deep shelf to oceanic areas that are above the calcite compensation depth (CCD) and have low terrigenous influx. Most are normal marine, but some species live over a broad salinity range (<18 to >40 ppt salinity). They also span a wide range of water temperatures from cool-water to tropical settings (coccolithophores can grow in waters as cold as 7.5°C, but generally are out-competed in cold waters by siliceous microplankton). Form the main constituents of chalk (the dominant Cretaceous to Recent calcareous oceanic sediment).

Skeletal Mineralogy:

Composed of low-magnesium calcite; thus generally well preserved, except where corroded by undersaturated (generally deep) oceanic waters or altered during diagenesis. One modern genus (*Polycrater*) has aragonitic coccoliths, but none has been identified in fossil forms.

Morphologic Features:

Extremely small flagellate organisms, termed "coccolithophores", form spherical to ellipsoidal tests (coccospheres) composed of interlocking shields (coccoliths). Some forms may have spines (especially rhabdosphaerids); related groups (e.g., discoasters) can have radiating arms or star-like morphologies).

Coccospheres typically are less than 25 µm in diameter (and in some cases, less than 5 µm in diameter); individual coccolith shields are commonly 1-15 µm across; constituent crystals are typically in the sub-micrometer size range.

Because of their small sizes, coccoliths and coccolithophores are best studied using strew- or smear-slides or the Scanning Electron Microscope (SEM). In standard (30 µm) petrographic thin sections, multiple coccoliths are likely to overlie each other, making recognition difficult or impossible. By using ultra-thin sections (or by looking at the especially thin edges of standard sections) one can sometimes see the characteristic pseudo-uniaxial cross (pinwheel pattern) of coccoliths under cross-polarized light. The SEM is often used for the study of these organisms, but standard microscopy of smear-mounts remains the norm for biostratigraphers.

There are many possibly related problematic groups (e.g., nannoconids, an exclusively Mesozoic group of cone-shaped nannofossils composed of tiny, radially arranged, wedge-shaped crystals forming conical structures).

Keys to Petrographic Recognition:

1. Very small size that, in some cases, approaches the resolution limits of optical microscopy.
2. Characteristic circular to ovoid outlines with cross-shaped or pinwheel-shaped interiors.
3. Distinctive sweeping extinction pattern when rotated under cross-polarized light.
4. Far more detail and easier identification is available by using strew- or smear mounts and/or SEM.

Diagrammatic representation of a typical coccosphere

A drawing of a typical coccosphere based on the genus *Coccolithus* (adapted from Lehmann and Hillmer, 1983). Coccospheres consist of a variable number of overlapping calcite shields that, in turn, are composed of a large number of radiating single crystals of calcite. Coccospheres are only rarely found in sediments because they typically disaggregate into their individual shields or constituent crystals. Typical coccospheres are between 5 and 25 µm in diameter. Adapted from Scoffin (1987, p. 49; citation provided in book introduction).

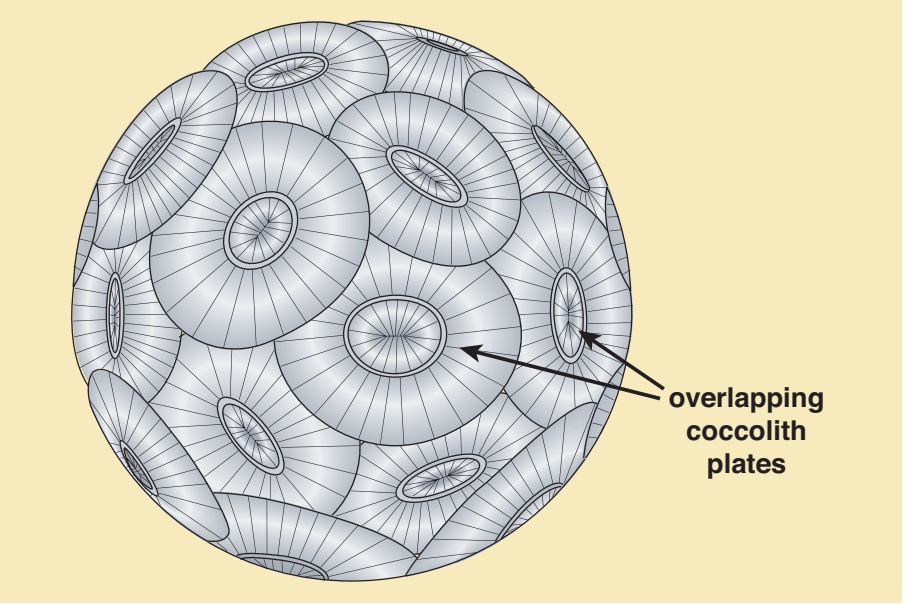

Diagrammatic representation of the structure of coccoliths

These drawings provide a cross-sectional view showing how double-layered coccoliths partially overlap and weakly interlock. Upon death, most coccospheres disaggregate into individual coccoliths and, in many cases, individual coccoliths further disaggregate into shield fragments (crystal elements) or individual sub-micrometer-sized crystals. Adapted from Scoffin (1987, p. 49; citation provided in book introduction).

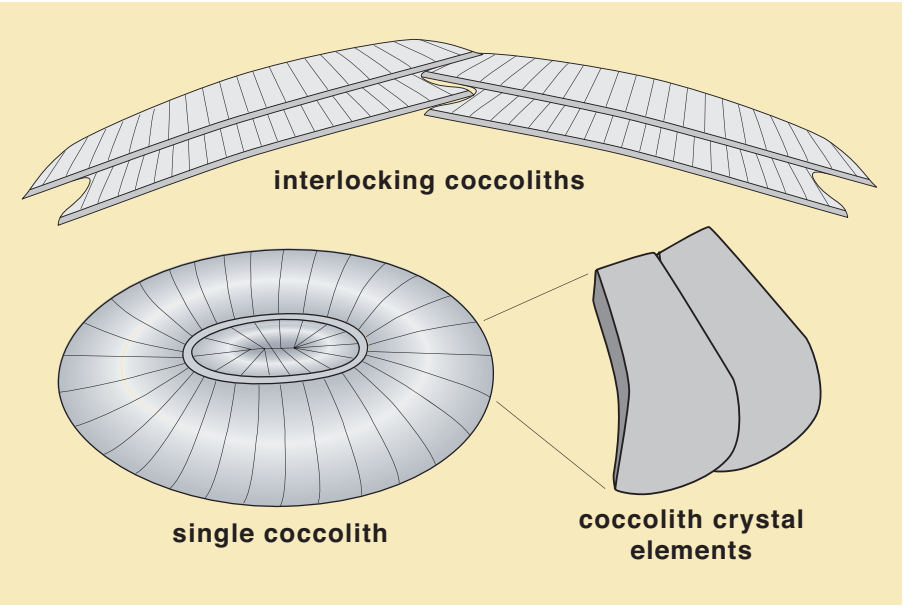

Eocene chalk, Bermuda Rise, North Atlantic Ocean

Photomicrograph of a smear mount depicting abundant coccoliths with characteristic curved-cross (or curved-swastika) extinction patterns. Coccoliths are the dominant constituent of most Cretaceous and younger chalks, but are not easily seen in standard thin sections (a typical coccolith is less than a few micrometers in thickness and many would overlap in a standard 30 µm section). Wedge-edges of sections, specially ground ultra-thin sections, smear mounts or SEM examination normally are required to adequately image coccoliths.

XPL, HA = 0.13 mm

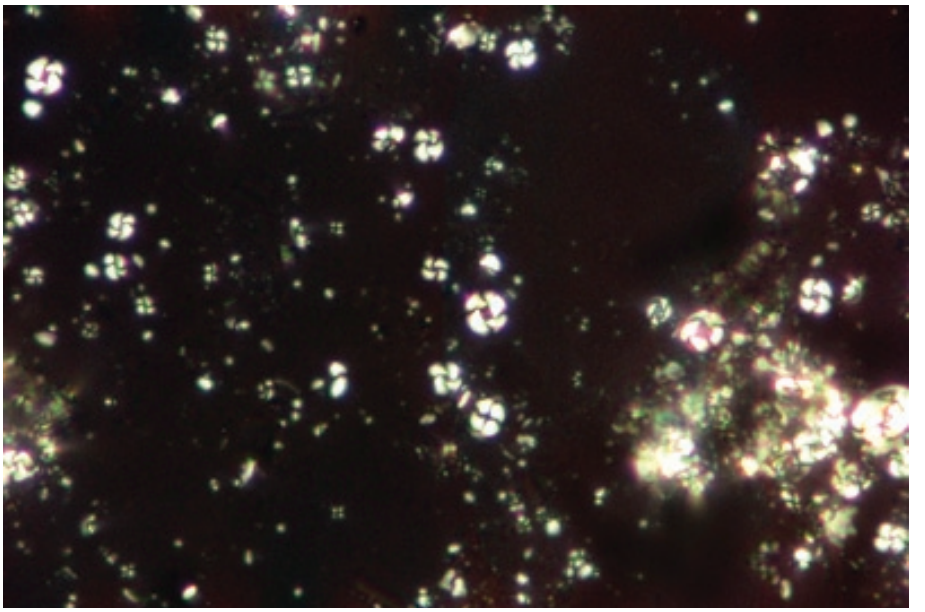

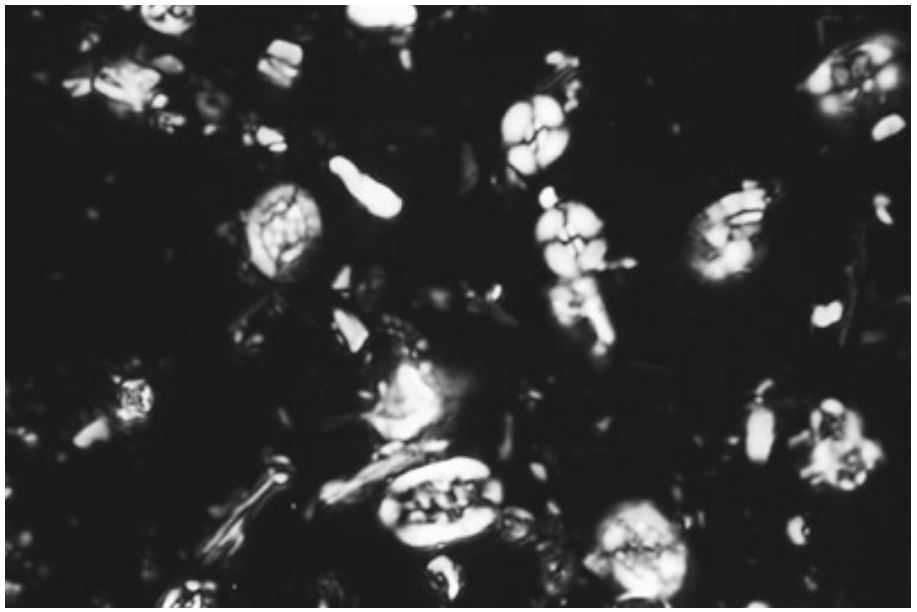

Up. Cretaceous (up. Maastrichtian) chalk, ODP Leg 171B, Hole 1052E, Blake Nose, Atlantic Ocean

A high-magnification view of a smear mount. Note the distinctive oval outlines and pseudo-uniaxial crosses formed by the radial arrangements of calcite crystals in these minute coccoliths. A number of different coccolith types are clearly distinguishable. Photograph courtesy of Jean M. Self-Trail.

XPL, HA = 50 μm

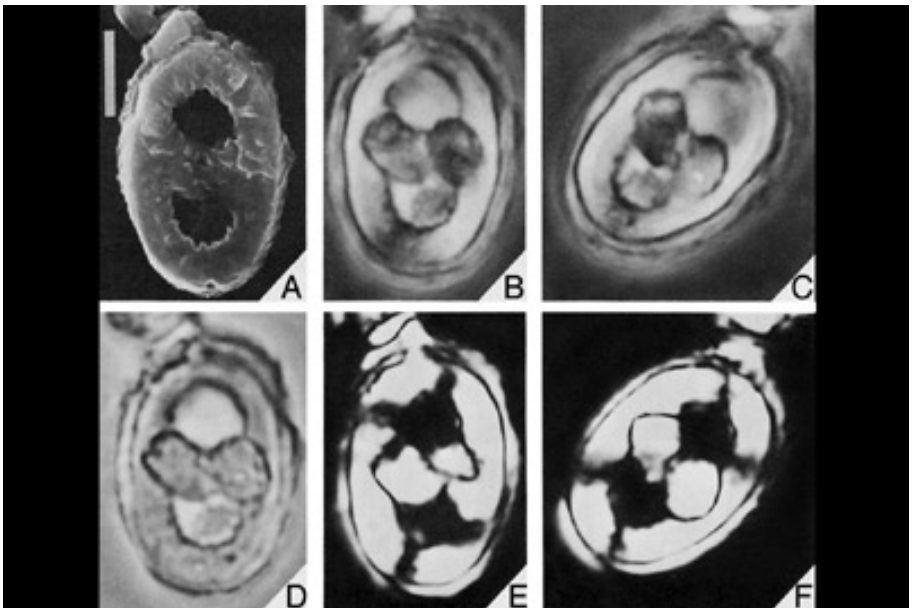

Up. Cretaceous (up. Turonian) Boquillas Fm., Langtry, Kinney County, Texas

High-magnification views of a single coccolith — *Zeugrhabdotus embergeri* (Noel 1958). Fig. A is an SEM view; Figs. B and C were taken in phase contrast illumination; Fig D is a transmitted light image; and Figs. E and F show two orientations under cross-polarized lighting. The bar scale on Fig. A is 4 μm in length and applies to all six images. This shows the comparative degree of detail that can be obtained for coccoliths using various petrographic techniques. Photograph courtesy of Charles C. Smith (from Smith, 1981).

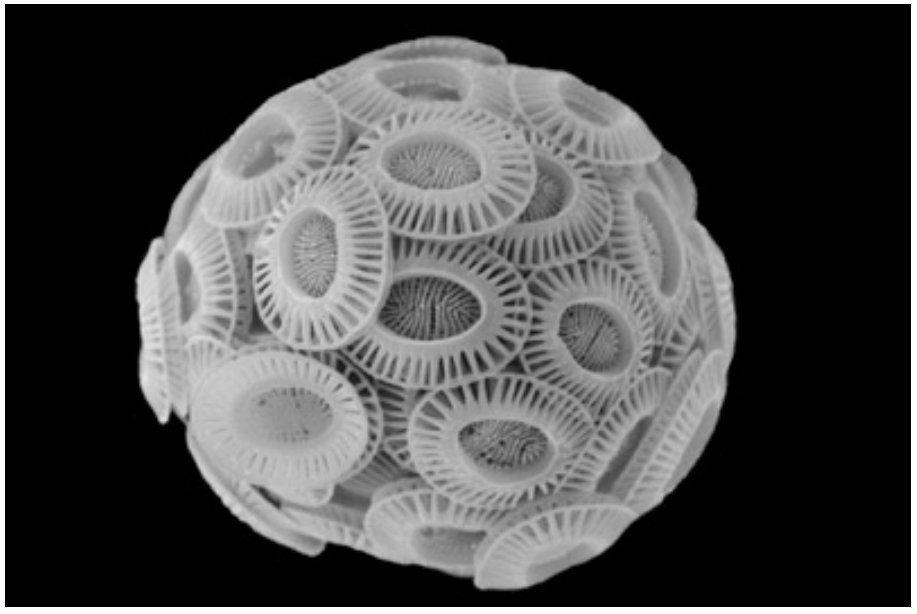

Recent sediment, North Atlantic Ocean, 26°N

An SEM image of the calcareous heterococcolith, *Emiliania huxleyi*, one of the most ubiquitous species of modern coccolithophorids. Note the overlapping coccoliths that constitute the full coccosphere. Photograph courtesy of Jeremy R. Young.

SEM, HA = ~15 μm

Recent sediment, North Atlantic Ocean, 54°N

An SEM image of the calcareous heterococcolith, *Coccolithus pelagicus*. Note the more robust construction and lesser number of coccoliths on this coccosphere as compared with the previous example. Photograph courtesy of Jeremy R. Young.

SEM, HA = ~19 µm

Recent sediment, southern Belize lagoon, Belize

An SEM image of a broken coccosphere of *Emiliania huxleyi* with several missing coccoliths. This view clearly shows the interlocking of adjacent coccoliths to form a complete coccosphere.

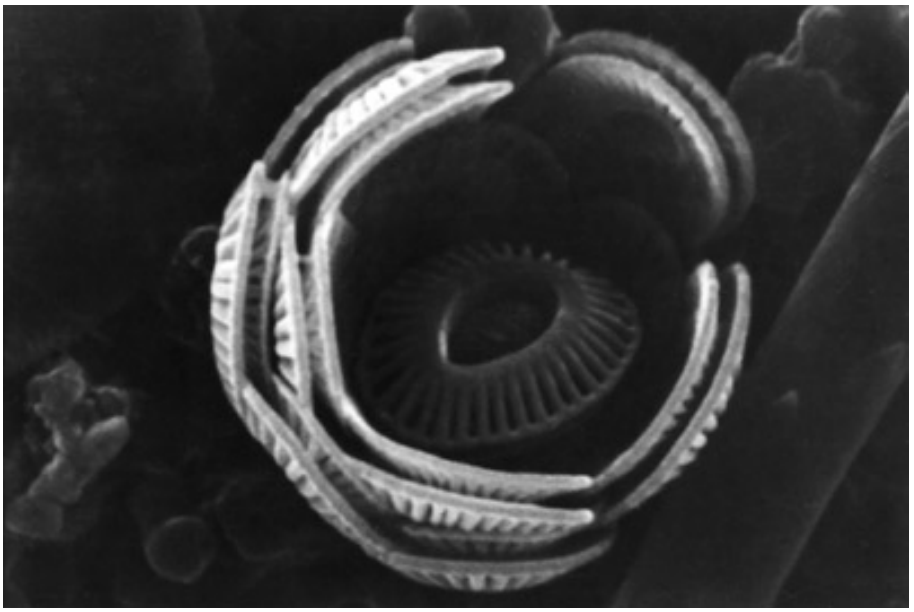

SEM, HA = ~16 µm

Lo. Paleocene (Danian) Ekofisk Fm. chalk, Danish North Sea

An SEM image of a deep shelf chalk that shows an unusual mix of whole coccospheres of *Prinsius* sp., intact coccoliths, and fully disaggregated coccolith crystal elements. The extensive porosity (~45%) is common in clay-poor coccolith chalks that have not been deeply buried and is, at least partly, due to the diagenetically stable nature of primary sediment composed of virtually pure calcite with little or no aragonite admixture. This is an excellent example of the sediment-forming capabilities of coccolithophores. Sample courtesy of Maersk Olie og Gas A.S.

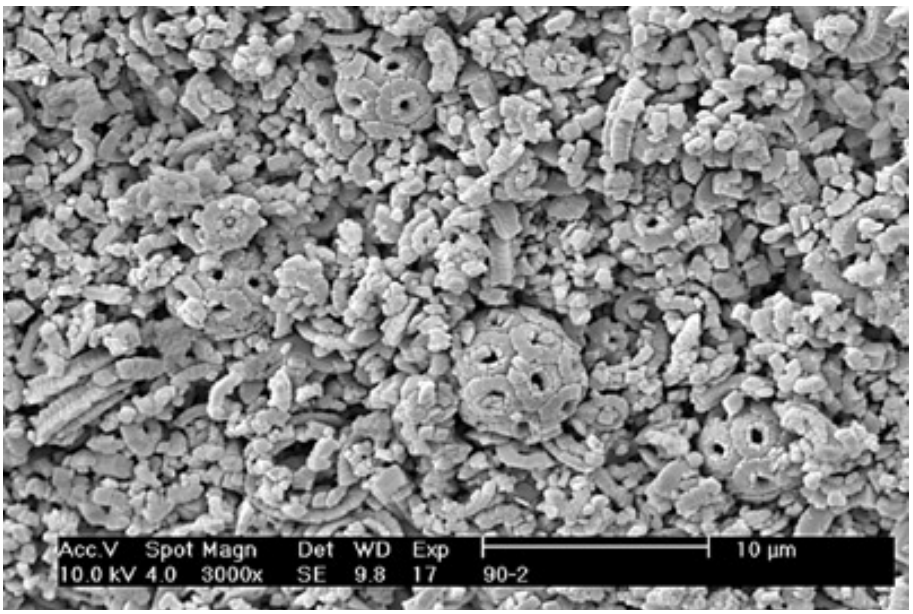

SEM, HA = 38 µm

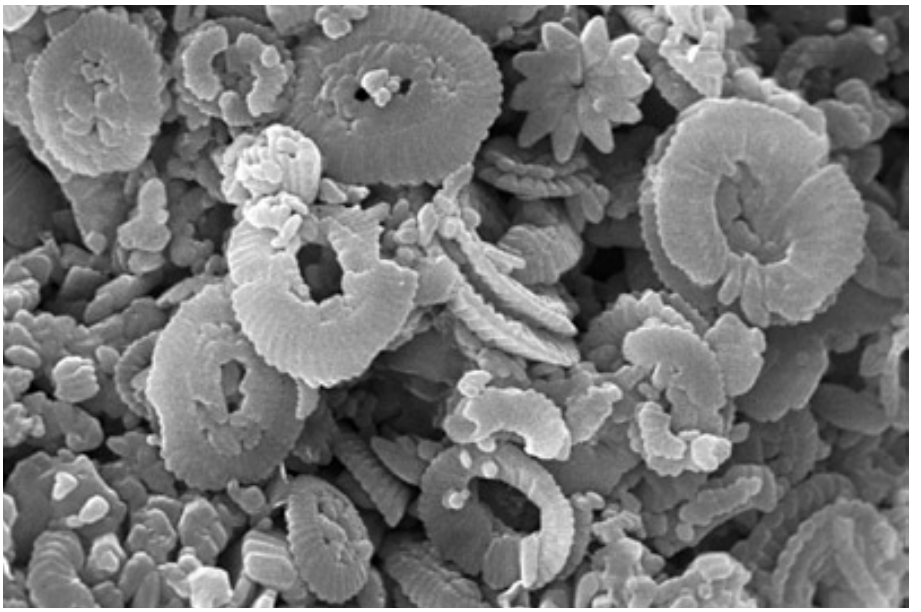

Mid. Miocene chalk, Hatton-Rockall Basin, North Atlantic Ocean

An SEM image of an oceanic coccolith ooze. Sediment is composed almost entirely of coccolith plates and fragments with subordinate discoasters (star-shaped grain at upper right). Virtually no cement is visible, and sediment still has about 60 percent porosity. Some corrosion of coccoliths is evident, a common syn- and post-depositional feature in deep sea sediments.

SEM, HA = ~22 μm

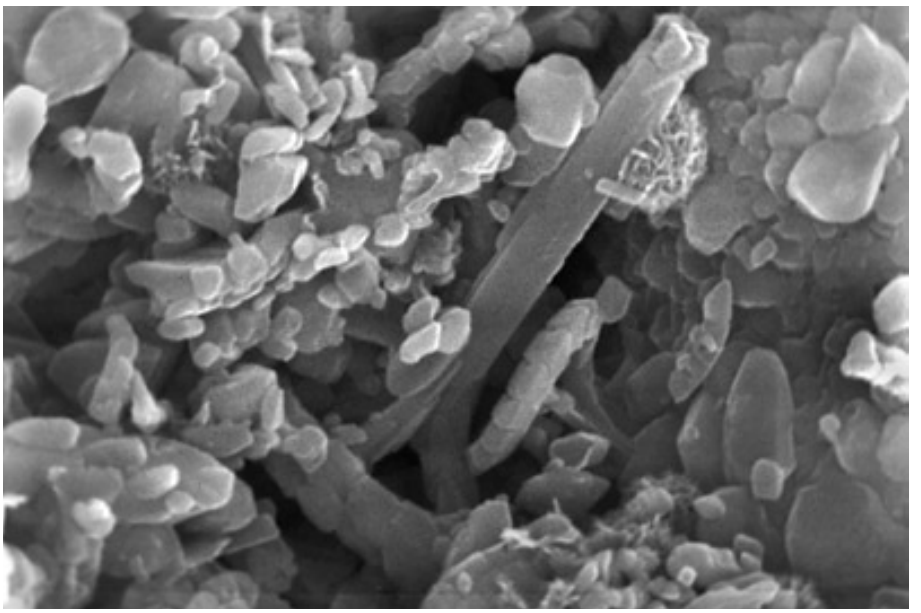

Up. Cretaceous (Maastrichtian) Tor Fm. chalk, Denmark

An SEM image of a chalk containing a coccolith (center) with an elongate central spine attached to its outer surface. It is quite common to find the spines broken off, and such spines can compose a significant portion of some chalks.

SEM, HA = ~20 μm

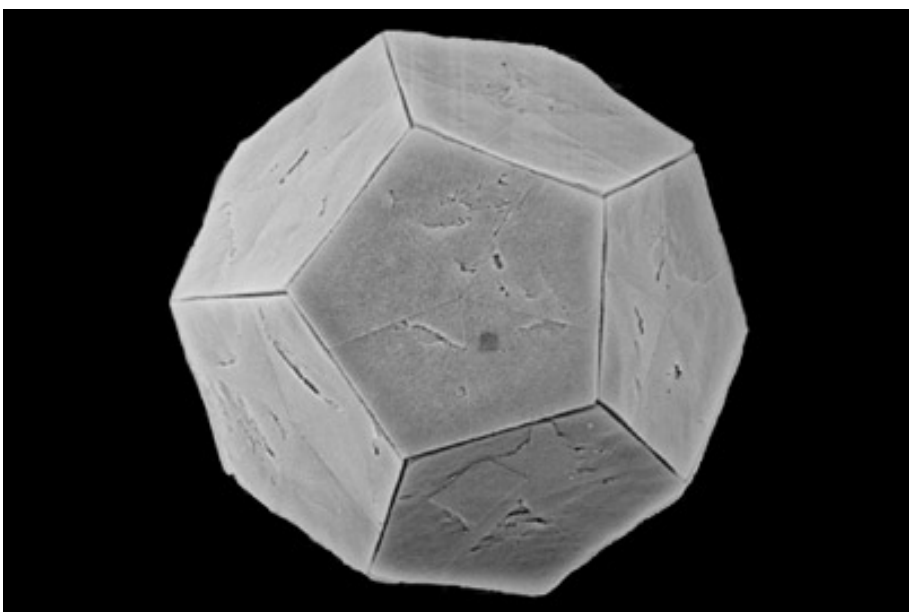

Recent sediment, Gulf of Maine, offshore Maine

An SEM image of *Braarudosphaera bigelowii*, an extant species of unknown affinity. The test is formed of 12 pentagonal plates, each composed of five crystal units. Braarudosphaerid pentaliths are occasionally found in enormous abundances in Mesozoic to Recent sediments and are thought to represent forms that flourished primarily during times of unusual environmental stresses. Photograph courtesy of Jeremy R. Young.

SEM, HA = 18 μm

Recent sediment, North Atlantic Ocean, 26°N

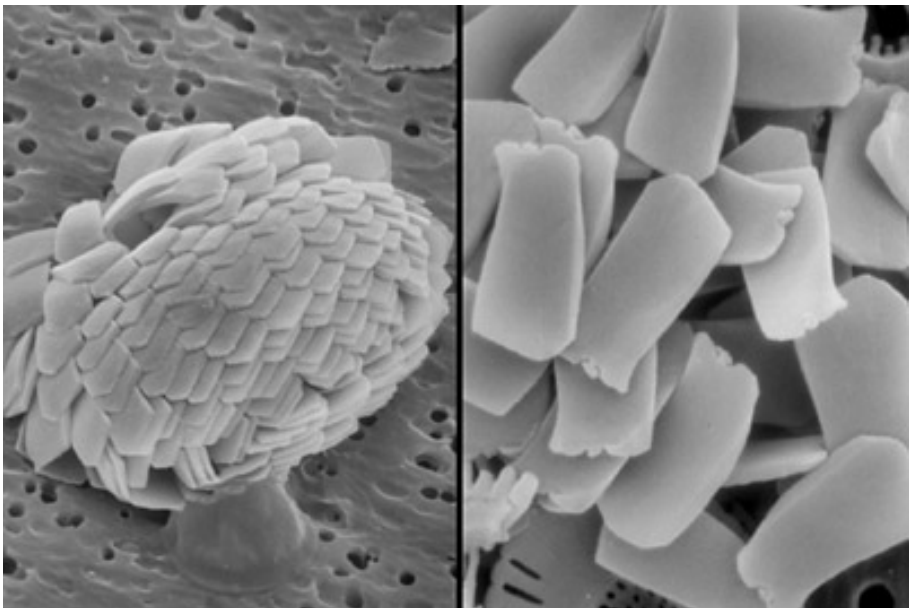

An SEM image (left) of the calcareous heterococcolith, *Florisphaera profunda*. This is an extremely abundant deep-photic zone (50-150 m) species and an invaluable paleoceanographic indicator of oligotrophic conditions. The individual coccoliths are plates formed of a single calcite crystal. The left hand image shows a complete coccosphere, the right hand image a collapsed coccosphere. Photograph courtesy of Jeremy R. Young.

SEM, HA = L, ~8 µm; R, ~2 µm

Recent sediment, North Atlantic Ocean, 26°N

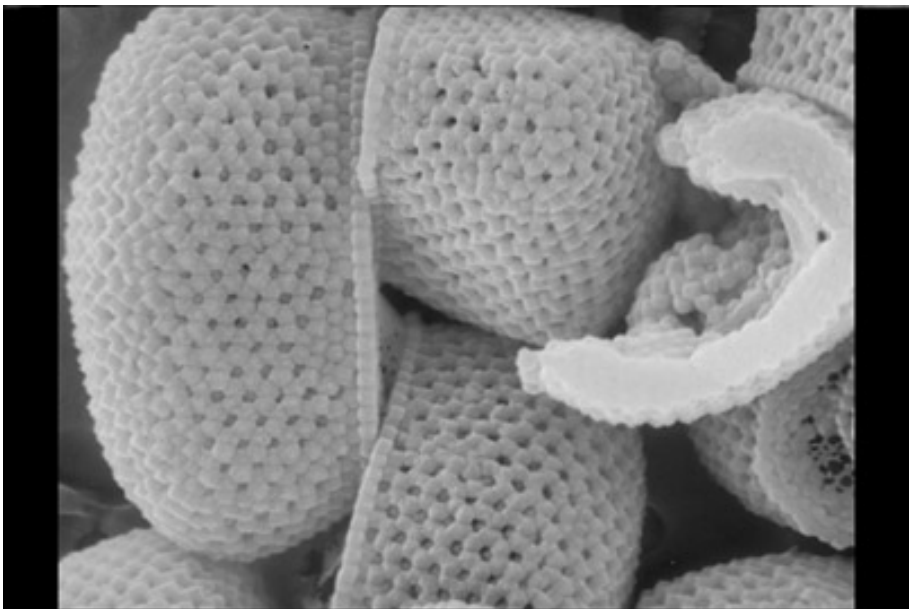

An SEM image of the calcareous holococcolith, *Calyptrosphaera oblonga*. The characteristic holococcolith construction from an array of minute euhedral crystallites is nicely shown. Holococcoliths are often abundant in the plankton, but have very low preservation potential. Photograph courtesy of Jeremy R. Young.

SEM, HA = ~4.2 µm

Lo. Cretaceous (Aptian) Shuaiba Fm., offshore Qatar

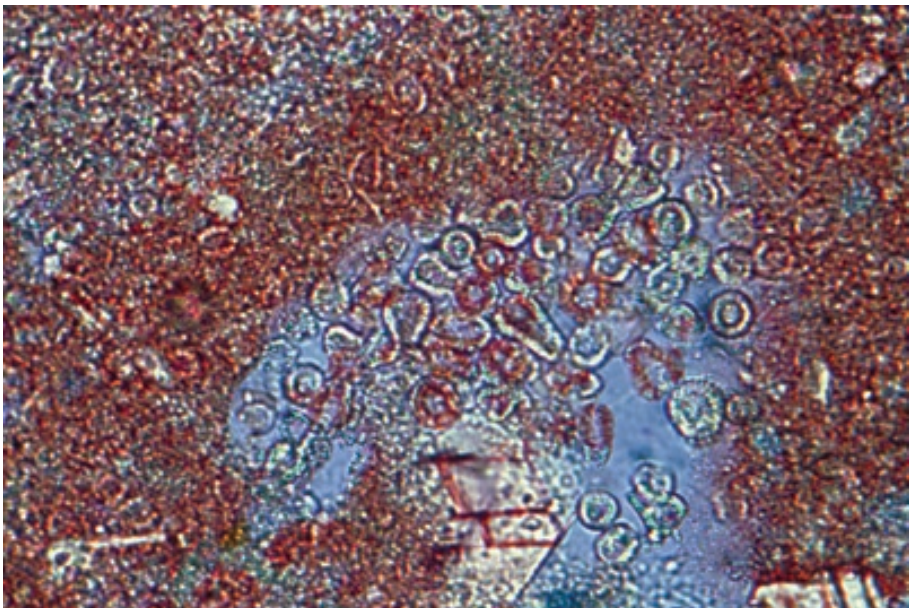

A shallow shelf chalky micrite with high concentrations of nannoconids visible in a leached area as well as in surrounding unleached matrix. Note the conical longitudinal sections and circular transverse ones. The transverse sections also show traces of the wedge-shaped calcite crystals that make up the nannoconid wall. Large bluish-purple areas are epoxy-impregnated pores.

PPL, AFeS, BSE, HA = 0.25 mm

CALCISPHERES

Taxonomy and Age Range:

Calcispheres are problematic grains that have, in most instances, no certain origin. Several types of calcispheres exist and most are attributed to algal sources. Mesozoic to Recent calcispheres are predominantly the remains of dinoflagellates.

Precambrian calcisphere-like organisms exist (*Eosphaera*); true calcispheres range from Cambrian to Recent and are common from Devonian to Recent.

Environmental Implications:

The lack of a clearly defined origin for most calcispheres makes environmental interpretation difficult. Even when one attributes calcispheres to an algal (i.e., photic zone) source, the calcispheres themselves may be transported far from their site of formation.

Some calcispheres are largely restricted to coastal, lagoonal settings; others are associated mainly with open shelf to ocean pelagic deposits. Thus one needs to identify specific calcispheres before drawing environmental conclusions.

Skeletal Mineralogy:

Many calcispheres have well preserved wall structures and thus probably had calcitic mineralogy (or represent calcite permineralization of organic-walled structures); those with poorly preserved walls (and some modern green algal reproductive bodies) had or have aragonitic composition.

Morphologic Features:

Calcispheres are small hollow grains with single or double walls with or without perforations or openings. Single calcispheres are typically tens to hundreds of micrometers in diameter. Most have no other major openings in the walls.

Radiosphaerid calcispheres have prominent external spines and a radial wall microstructure of calcite crystals; non-radiosphaerids have smooth surfaces and a microgranular wall structure.

Some calcispheres from Cretaceous pelagic limestones (e.g., *Pithonella ovalis*) have an elliptical shape, a single opening, and a shingled calcite wall structure. These grains, known to be dinoflagellate cysts, may have a very different origin from other calcispheres.

Keys to Petrographic Recognition:

1. **Walled, hollow grains generally without openings. May have any of a number of wall types including ones with single or multiple layers.**
2. **Walls may be uniform, dark and micritic, may consist of radial crystals, may have imbricate brick-like calcite crystals, or may have still other fabrics.**
3. **The most common forms are without spines, but spined forms are known.**
4. **Diameters (external) of 60-250 µm; wall thicknesses of 3-30 µm; spined forms may be up to 500 µm in total diameter including spines.**
5. **Commonly occur in great numbers in particular horizons (perhaps indicative of episodic blooms of calcispheres or unusually stressful conditions that eliminated growth of other planktic organisms).**

PHOTO SCALES AND ABBREVIATIONS ARE EXPLAINED IN THE BOOK'S INTRODUCTION

Up. Cretaceous Chalk, Netherlands North Sea

An SEM image of calcispheres (mainly *Pithonella ovalis*) in a shelf chalk. Most calcispheres have uncertain origins, but these are known to be calcareous dinoflagellate cysts. Note the characteristic ovoid shape and brick-like construction of the calcite walls formed of elements with their c-axes oblique to the wall and sub-parallel to each other.

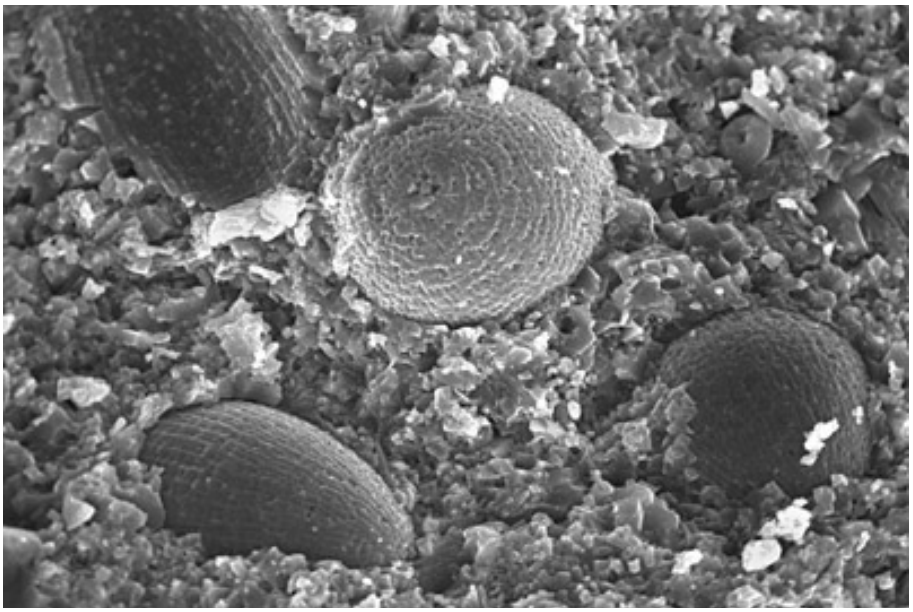

SEM, HA = ~30 μm

Up. Cretaceous Lower Chalk, Kent, England, U.K.

A calcisphere-rich shelf chalk. The bulk of the microfossils in this section are from the dinoflagellate genus *Pithonella*. Although a few multi-chambered planktic foraminifers are also visible, this is a good example of a chalk in which calcispheres predominate over planktic foraminifers. Such deposits generally are thin and represent short-lived events relative to the far more widespread foraminiferal chalks.

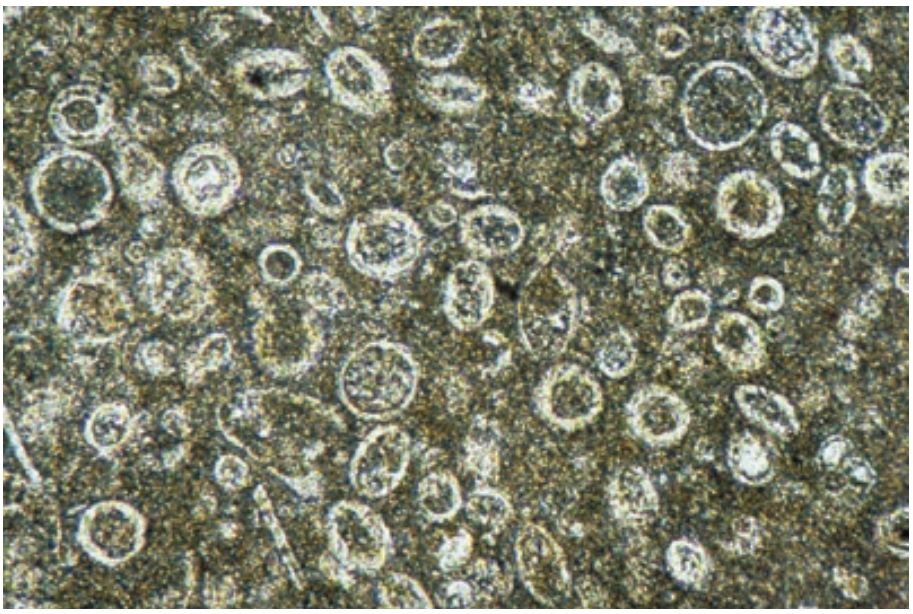

PPL, HA = 1 mm

Cretaceous (Albian-Cenomanian) Tamaulipas Ls., San Luis Potosi, Mexico

Abundant calcispheres in a basinal limestone. These calcispheres have varied sizes and moderately thick walls composed of finely granular (micritic) calcite, a very common wall type in ancient calcispheres. These too are probable calcareous dinoflagellate cysts.

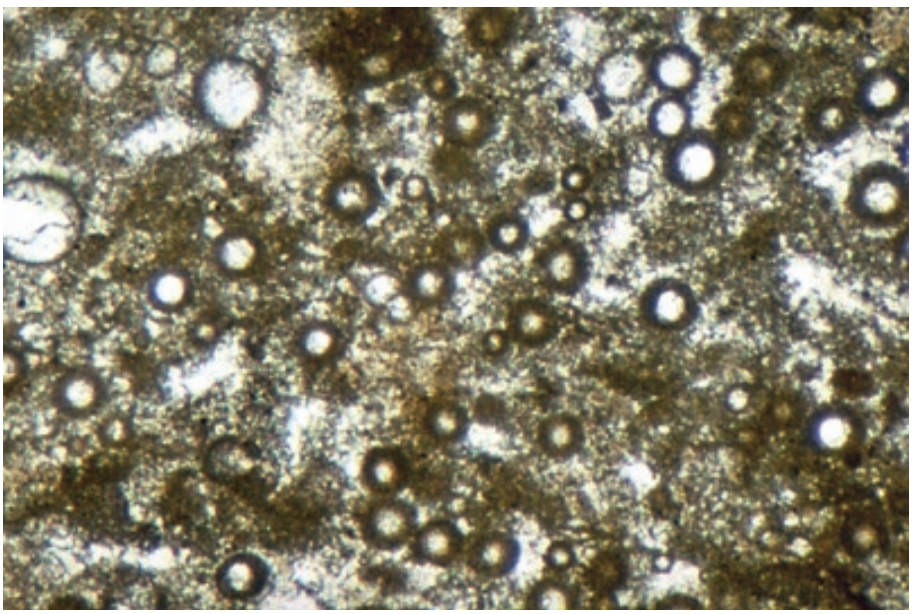

PPL, HA = 1.5 mm

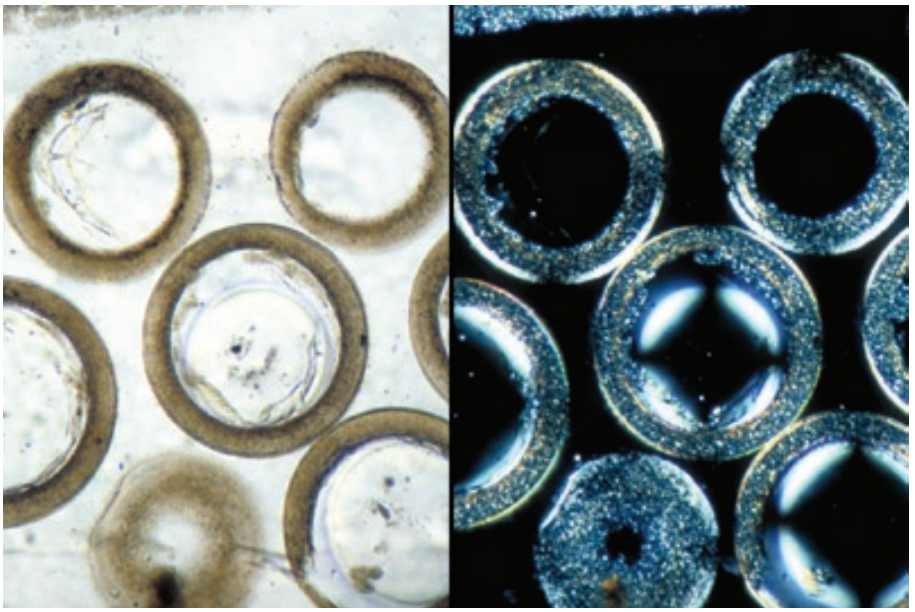

Recent sediment, Florida Keys, Florida

These modern, weakly calcified calcispheres have walls composed of organic matter plus fine-grained aragonite. They are reproductive cysts from the dasycladacean green alga, *Acetabularia* sp. The cysts are shed into modern shelf carbonates in large numbers by these marine algae.

PPL/XPL, HA = 0.3 mm each

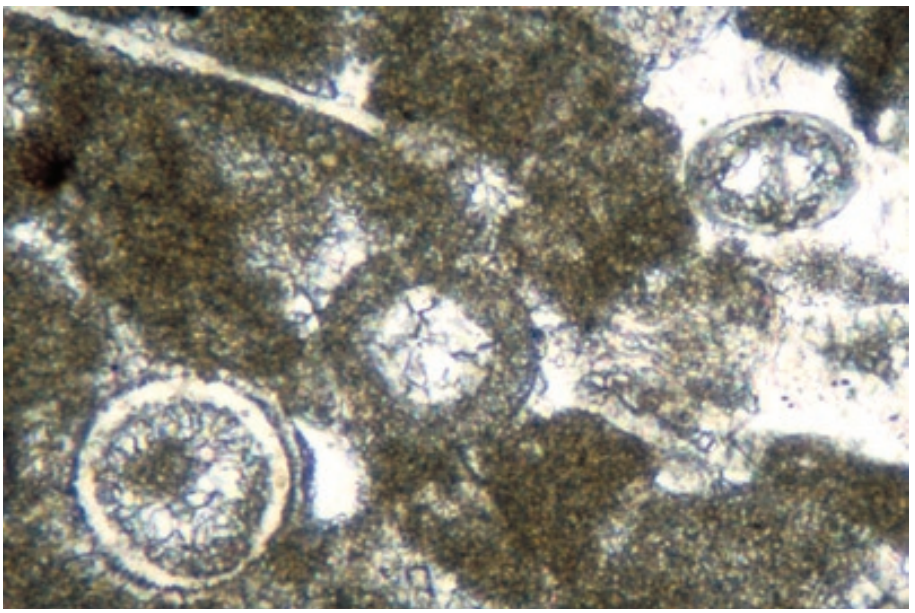

Up. Mississippian (Visean) Arroyo Peñasco Gp., Manuelitas Fm., Taos Co., New Mexico

Several types of calcispheres from a cherty shelfal limestone. Note particularly the variety of wall types in a single sample, probably reflecting a variety of origins for these different grains.

PPL, HA = 0.4 mm

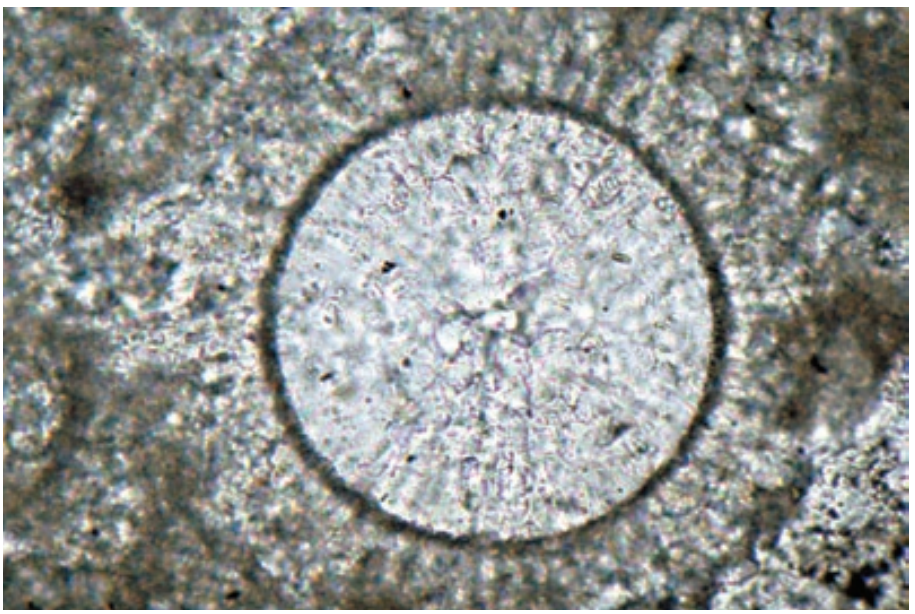

Lo. Carboniferous (Visean) limestone, west of Krakow, Poland

A calcisphere with two concentric skeletal layers and radial perforations penetrating the wall. This clearly is a very different type of calcisphere from those shown in the previous photographs, but its exact origin is not known.

PPL, HA = 0.2 mm

Tunicate Spicules

Taxonomy and Age Range:

Phylum Chordata, Subphylum Urochordata, Superclass Tunicata — sparse fossil record but at least Jurassic-Recent; may extend much farther back in time since possible/questionable forms have been described from the Precambrian.

Environmental Implications:

Both sessile and pelagic tunicates (salps) exist; sessile forms (often called sea squirts) are generally shallow-water, open-marine forms.

Skeletal Mineralogy:

Modern tunicate dermal spicules are composed of aragonite; older tunicate spicules may also have been aragonitic, but this is speculative due to a sparse fossil record.

Morphologic Features:

Larvae exhibit chordate features including a notochord, a dorsal nerve cord, and pharyngeal slits.

Adults have simple body form consisting of a large chamber or sack with two siphons through which water enters and exits.

Tissues of adult (non-larval) tunicates contain embedded calcareous spicules that serve to stiffen the soft tissue.

Keys to Petrographic Recognition:

1. **Small spicules, roughly 75-150 µm in diameter, are the only calcified remains, and they typically are very minor sediment constituents.**
2. **Spicules consist of thick radiating spikes forming a variety of mace-like carbonate grains.**
3. **Spicules are virtually never recognized in thin section, but are quite easily identifiable in grain mounts of Holocene sediments.**

Recent sediment, Florida Keys, Florida; Colson Cay, Belize

Although not really microfossils, tunicate spicules are included here because they are comparable in size and morphology to microfossils and represent the only preserved parts of tunicates. Such spiny aragonitic spicules are embedded in the soft tissue of the tunicates and are shed into sediment after death of the organism. They are readily recognizable in sediment grain mounts (such as these), but are very difficult to identify in thin sections of lithified sediment.

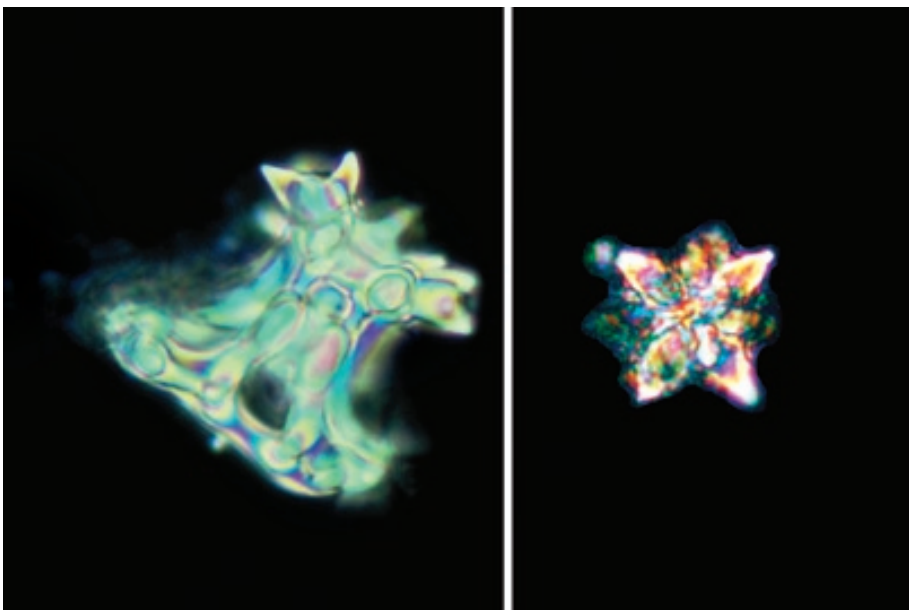

XPL, HA = L: 0.06 mm; R: 0.04 mm

SILICEOUS MICROFOSSILS - RADIOLARIANS

Taxonomy and Age Range:

Radiolarians are classed in the Phylum Protozoa as a subclass of the Class Actinopoda
Post-Paleozoic siliceous forms are mainly from the superorder Polycystina.
Spumellarians (radially-symmetrical forms) — Middle-Late Cambrian to Recent
Nassellarians (helmet-shaped forms) — Triassic to Recent

Environmental Implications:

Radiolarians are fully marine plankton; they are most common and shallow water but are found at all depths in modern oceans. They are common constituents of pelagic deposits throughout the Phanerozoic.

Individual species are depth zones and occupy provinces defined by the physical and chemical properties of oceanic water masses. Radiolarians as a whole are found in polar to tropical settings, especially in upwelling areas.

Skeletal Mineralogy:

Most radiolarians had skeletons composed of amorphous (opaline) silica. These skeletons typically are recrystallized to chert or other stable forms of quartz or are replaced by other minerals in pre-Tertiary (or younger) deposits.

Morphologic Features:

Radiolarians have solitary, highly porous, hard skeletons (with or without spines) that are embedded in the organism's soft tissues. Spumellarian skeletons commonly occur as nested spheres and normally have radial symmetry; most nassellarians are characterized by axial symmetry.

Radiolaria occur in a wide range of sizes from less than 100 µm to more than 2 mm.

Keys to Petrographic Recognition:

1. **Originally siliceous (opal-A) mineralogy, but generally dissolved or replaced by more stable forms of silica in older or more deeply buried samples.**
2. **Radiolarians and silicoflagellates can be distinguished from each other on the basis of size and skeletal geometry.**
3. **Both groups have rather open tests; radiolarians have a great variety of shapes, but many are shaped like spiked spheres or like bullets and spacecraft.**

PHOTO SCALES AND ABBREVIATIONS ARE EXPLAINED IN THE BOOK'S INTRODUCTION

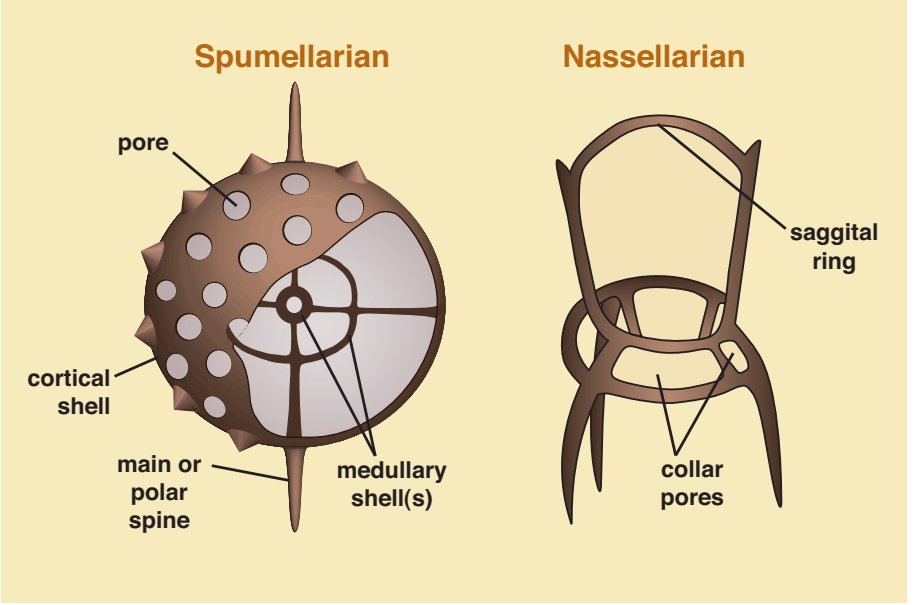

Diagram showing the two major radiolarian skeletal types

Left: Partial external and internal views of a representative spumellarian radiolarian (redrawn from Brasier, 1980). Note radial symmetry of this form and nesting of internal and external structural spheres.

Right: Diagrammatic view of a representative helmet-shaped nassellarian radiolarian (redrawn from Kling, 1978, p. 215).

Up. Oligocene ooze, Caroline Ridge, Pacific Ocean

An SEM image of opaline silica tests from a diverse assemblage of well-preserved nassellarian radiolarians. This deposit represents a deep sea siliceous ooze in 2,850-m water depth (present-day). Photograph courtesy of Stanley A. Kling.

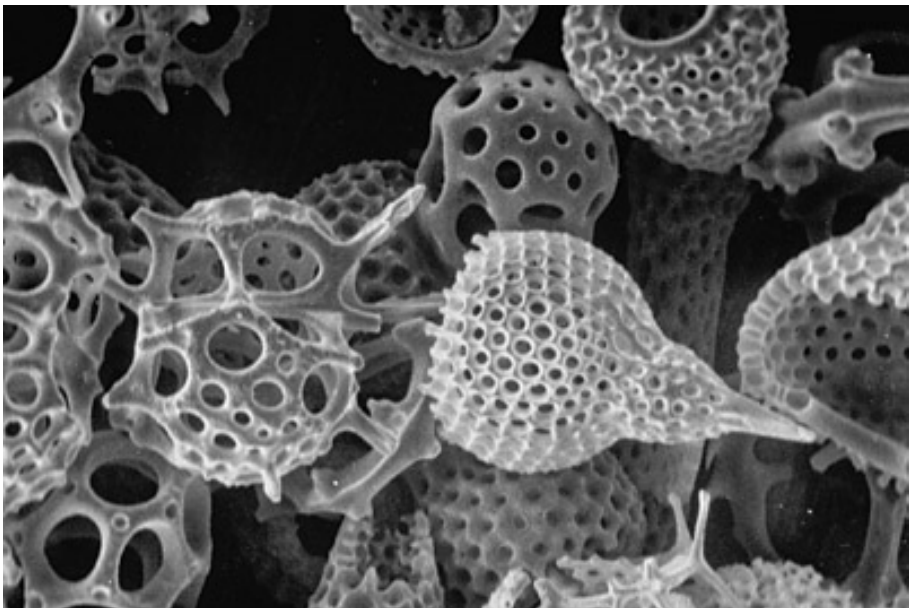

SEM, HA = ~375 µm

Modern siliceous ooze, Pacific Ocean

An SEM image of a spumellarian radiolarian, *Hexacontium* sp., showing inner and outer capsules, coarsely porous structure, and a number of external spines. Photograph courtesy of Stanley A. Kling.

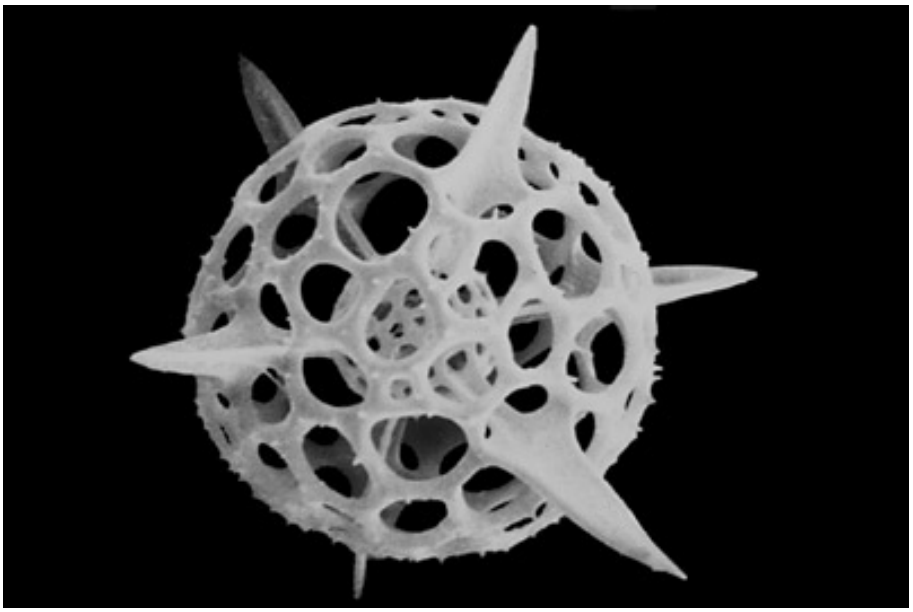

SEM, HA = ~250 µm

Up. Jurassic-Cretaceous Radiolarite, Oman

A moderately well preserved assemblage of radiolarians (and subordinate sponge spicules) in an oceanic radiolarite. Spherical and bullet-shaped forms are readily visible, as are the coarse pores that typify radiolarian skeletons.

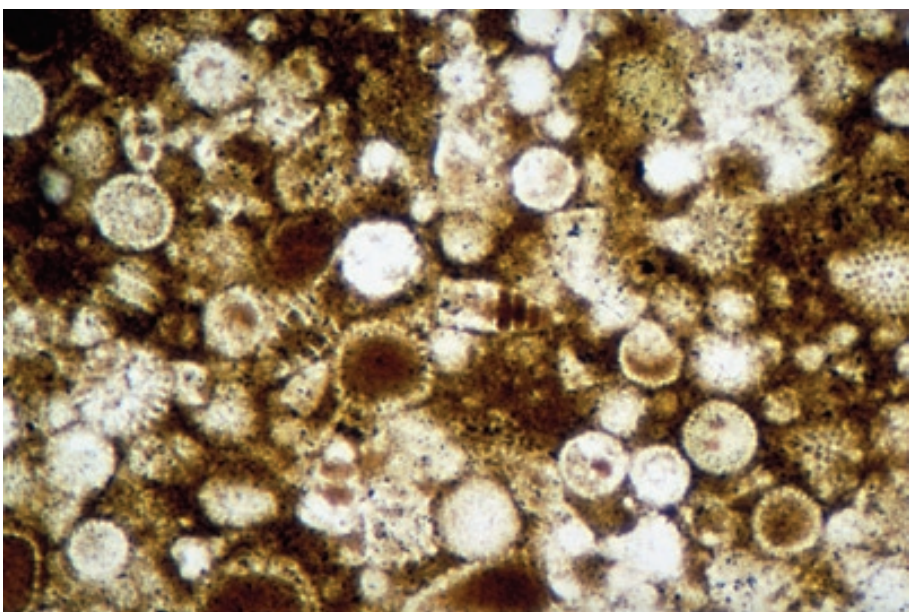

PPL, HA = 1.6 mm

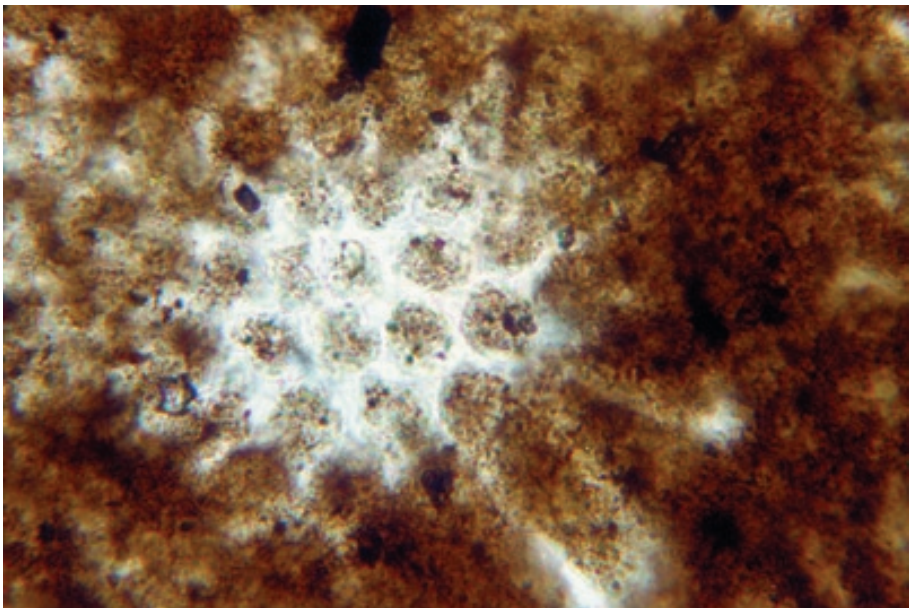

Up. Jurassic-Cretaceous Radiolarite, Oman

A tangential section through the moderately well preserved outer wall of a radiolarian. In the alteration of opal-A tests to cristobalite and finally to quartz, much of the structural detail may be obscured. In this example, however, the coarse radiolarian pore structure is still clearly visible.

PPL, HA = 0.25 mm

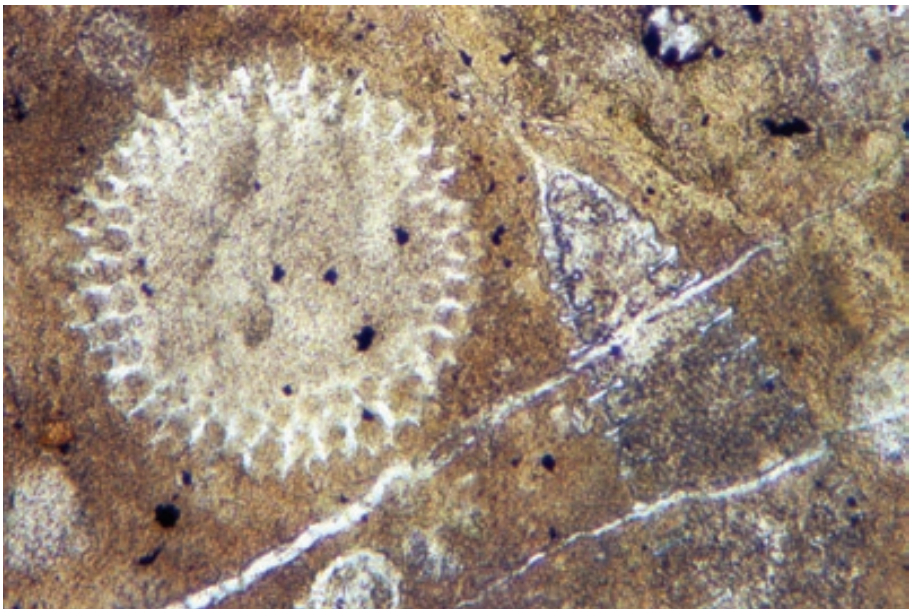

Up. Jurassic (Tithonian) Franciscan Gp., Point Sal ophiolite, Santa Barbara Co., California

Cross sections through two spumellarian radiolarians showing good preservation of tests despite alteration from opal to quartz. Coarse pore structures, in addition to size and shape of tests, are the main criteria for identification of these grains as radiolarians.

PPL, HA = 0.62 mm

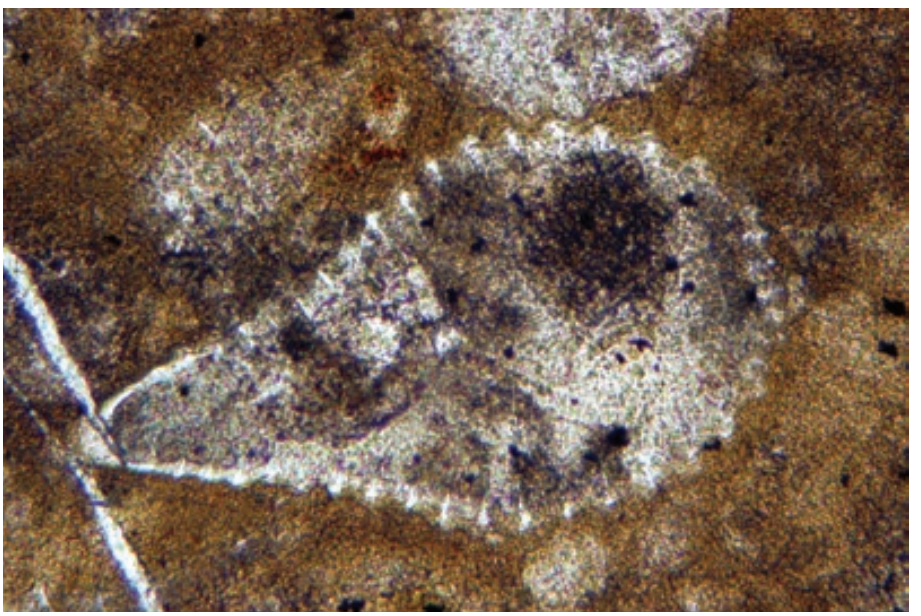

Up. Jurassic (Tithonian) Franciscan Gp., Point Sal ophiolite, Santa Barbara Co., California

A longitudinal cross section through a single spumellarian radiolarian test. Originally opal, this example has been diagenetically altered to quartz (chert) but still shows the coarse pore structure in the outer skeleton. Radiolarians are wide ranging and extremely important in the formation of deep-water siliceous deposits.

PPL, HA = 0.62 mm

Siliceous Microfossils - Diatoms and Other Algal Groups

Taxonomy and Age Range:

Unicellular, non-flagellate algae of the class Bacillariophyceae.

They are divided into the order Centrales (forms that typically have radial symmetry) and the order Pennales (elongate forms, generally with bilateral symmetry).

Marine diatoms — Early Jurassic (Toarcian) to Recent (examples older than Late Cretaceous are rare, but molecular (DNA/RNA) data indicates that the group arose in Precambrian).

Freshwater forms — Paleocene to Recent.

Chrysophytes are a complex, possibly polyphyletic, group of marine algae. Forms with silica plates are separately grouped by some workers as Synurophyceae. Fossil record: Cretaceous-Recent.

Silicoflagellates are unicellular algae with a single flagellum. Fossil record: Early Cretaceous-Recent

Environmental Implications:

Diatoms are photosynthetic algae and thus are restricted to the photic zone. They can be planktic or sessile, and marine forms range from open marine settings to coastal (brackish as well as hypersaline); non-marine forms are common in lacustrine environments.

Marine diatoms are especially prevalent in high latitude, deep-water deposits, but are also present in equatorial sediments, especially in nutrient-rich (upwelling) areas.

In general, centric diatoms are marine, planktic forms; pennate diatoms are predominantly motile benthic forms that live in coastal to lacustrine settings.

Diatom fossil assemblages are affected by preferential preservation of heavily silicified forms.

Skeletal Mineralogy:

Diatom hard parts, termed frustules, are and were composed of amorphous (opaline) silica. Older (fossil) forms may have undergone dissolution, recrystallization (to more stable forms of silica such as opal-CT or quartz), or replacement by calcite or other minerals.

Morphologic Features:

Diatoms secrete external shells (frustules) that consist of two overlapping valves (similar to a Petri dish) and a girdle that helps to bind them together. Diatom frustules can have radial symmetry (in centric forms) or bilateral symmetry (in pennate forms).

Diatom frustules typically are perforated by many, regularly arranged openings (termed areolae) and other, smaller pores, giving them the appearance of tiny sieves (a property that makes diatomaceous earth useful in filtration applications).

Centric forms may be circular, triangular or oblong, but surface markings in all these shape varieties radiate from a central zone; pennate forms have a long axis and two short axes, with surface markings perpendicular to the long axis.

Diatoms range in size from about 4 µm to more than 1 mm.

Silicoflagellates are small (generally 20-50 µm; rarely up to 100 µm), unicellular marine microplankton structures ranging from simple rings with spines to more complex domal forms. They are far less abundant than radiolaria or diatoms.

Keys to Petrographic Recognition:

1. **Siliceous (opal-A) primary composition; thus commonly dissolved (sometimes leaving molds) or replaced by quartz or calcite in Cenozoic and older strata.**
2. **Shaped like Petri dishes, triangles, or banana-like oblongs (and thus different from the typical conical- or spherical-shaped, helmet-like forms of radiolarians).**
3. **Distinctive, porous, sieve-like fabric produced by abundant, regularly arranged punctae perforating both valves.**

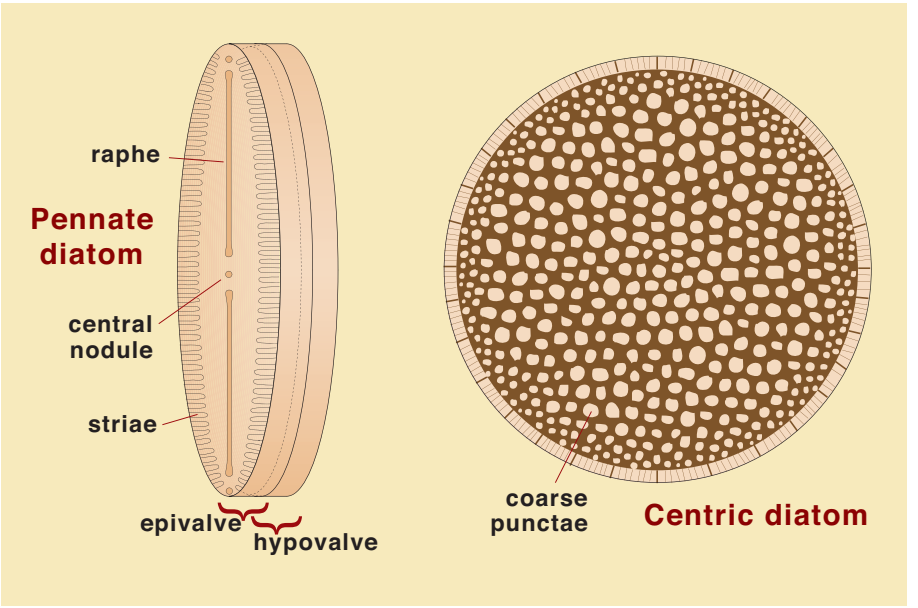

Diagram showing the two major diatom skeletal types

Left: oblique diagrammatic view of a representative pennate diatom (*Pinnularia* sp.) showing the paired valves and the bilateral symmetry that characterizes this group. Redrawn from Brasier (1980, p. 42, after Scagel et al., 1965).

Right: diagrammatic view of a representative centric diatom (*Coscinodiscus* sp.) showing the radial symmetry of this group. Valve is about 45 µm in diameter. Redrawn from Brasier (1980, p. 43).

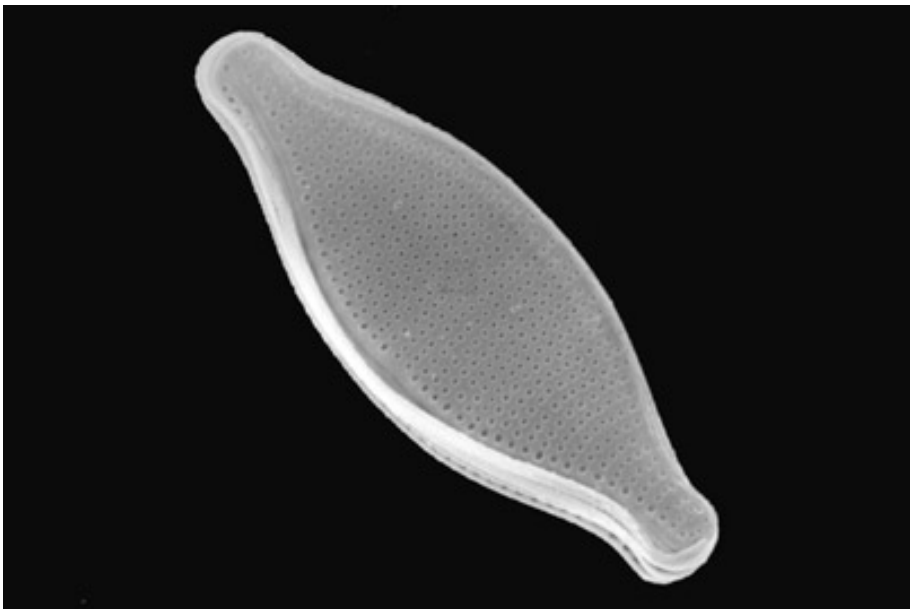

Recent sediment, North Atlantic Ocean

An SEM image of a typical pennate diatom with bilateral symmetry. Photograph courtesy of Jeremy R. Young.

SEM, HA = ~21 µm

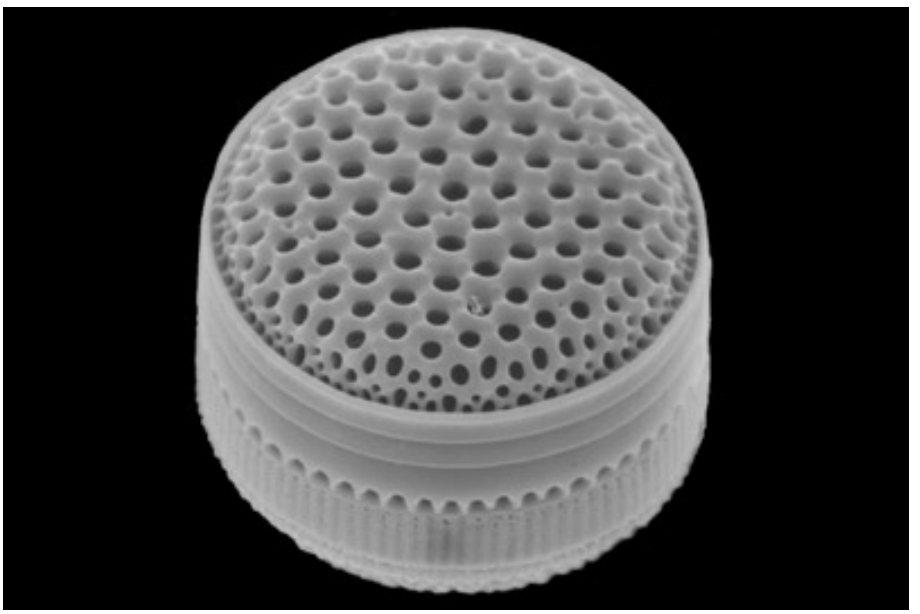

Recent sediment, North Atlantic Ocean, 54°N

An SEM image of a typical centric diatom with radial symmetry. Shows a common shape with upper and lower valves held together by a central girdle. The minute pores found in all diatoms explain why diatomaceous sediments are so widely used as filtration material (for swimming pools and many other applications). Photograph courtesy of Jeremy R. Young.

SEM, HA = ~26 µm

Tertiary sediment, U.S.A.

The effective study of diatoms using standard light microscopy typically involves strew mounts or grain mounts in which isolated diatoms are scattered into a mounting medium on the slide. This allows the viewing of relatively uniformly oriented grain with minimal overlap of individual specimens. This strew mount shows a variety of well-preserved, mainly centric diatoms. Note the simple circular shapes and the radially arranged, sieve-like pore structure of these organisms.

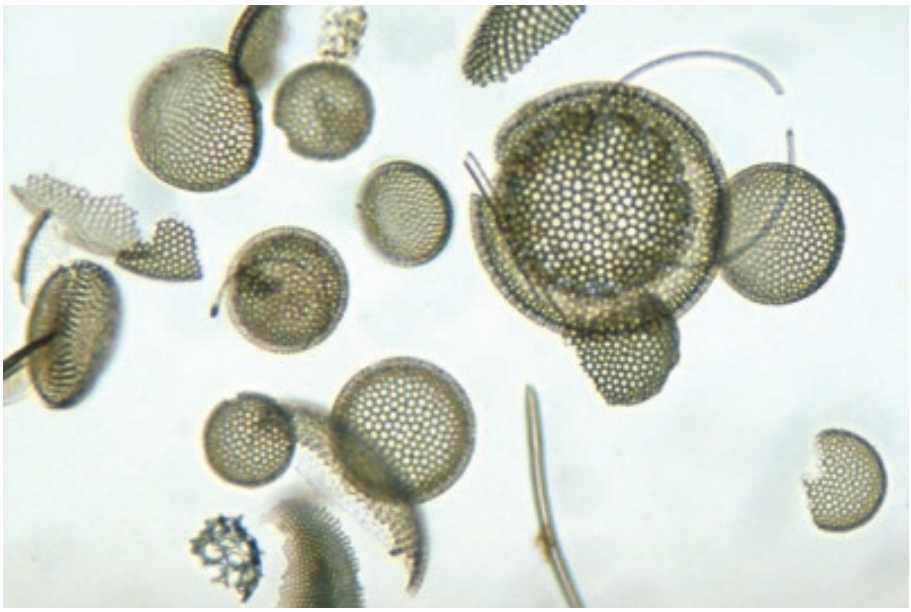

PPL, HA = 0.6 mm

Tertiary sediment, Calvert Co., Maryland

A grain-mount photomicrograph showing top views of three well preserved specimens of a large centric diatom (*Actinoptychus* sp.). Note the simple circular shapes and the complexly patterned, radially arranged, sieve-like pore structure.

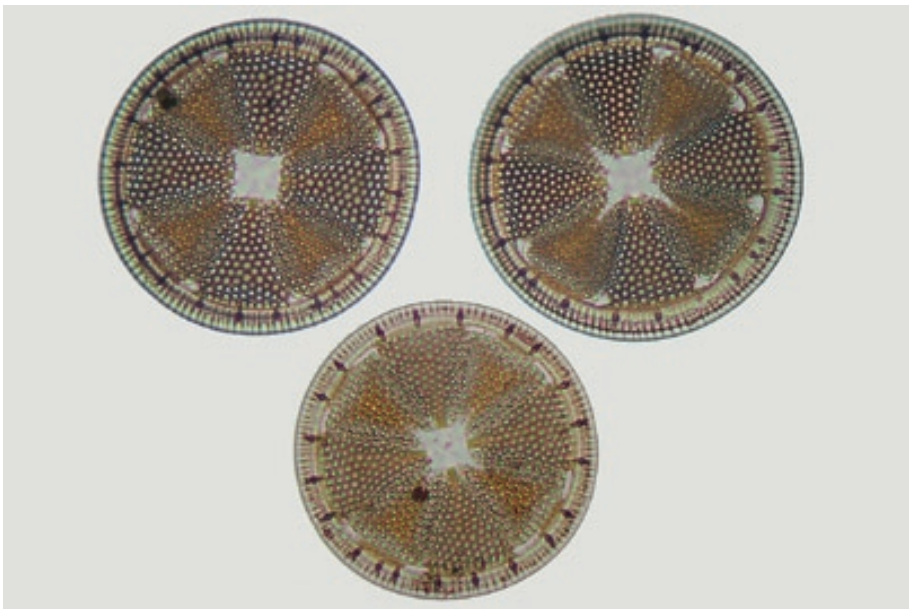

PPL, HA = 0.51 mm

Recent sediment, Florida

Close-up view of two specimens of a centric diatom, *Trinacria excavata*. The triangular shapes of these grains are common diatom growth forms. Photograph courtesy of Jeremy R. Young.

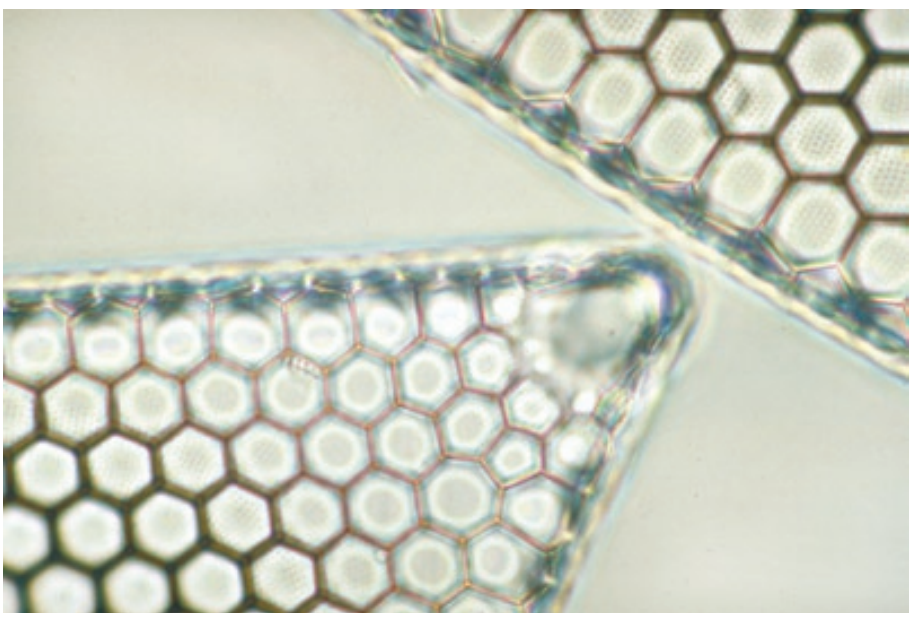

PPL, HA = 15 µm

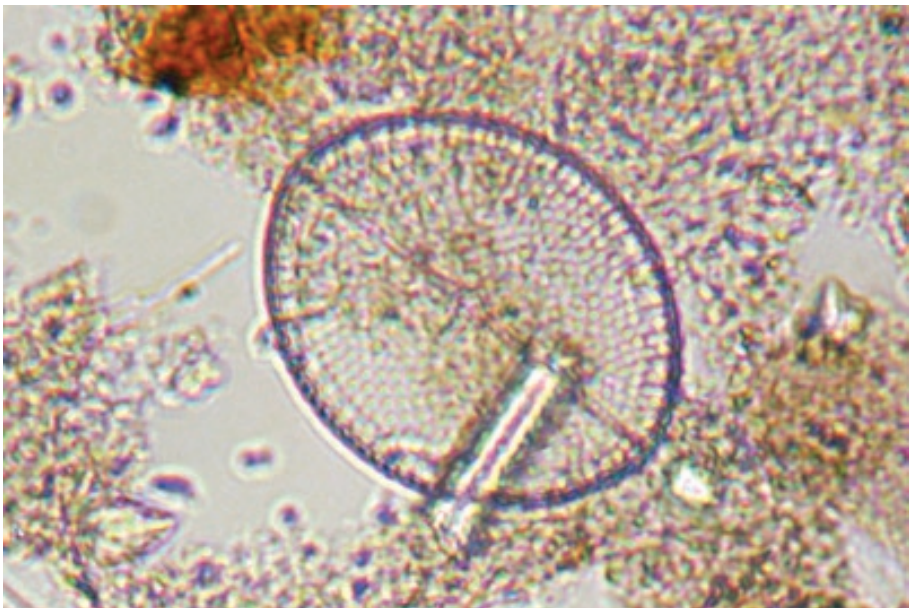

Recent sediment, Cancun lagoon, Quintana Roo, Mexico

A smear-mount image showing an opaline diatom test (*Cocconeis* sp.). Diatoms are important in Cretaceous to Recent sediments from a number of environments. Originally composed of opal-A, they alter to other forms of silica, often with considerable loss of textural detail. Note a small fragment of a sponge spicule which overlaps the diatom.

PPL, HA = 0.16 mm

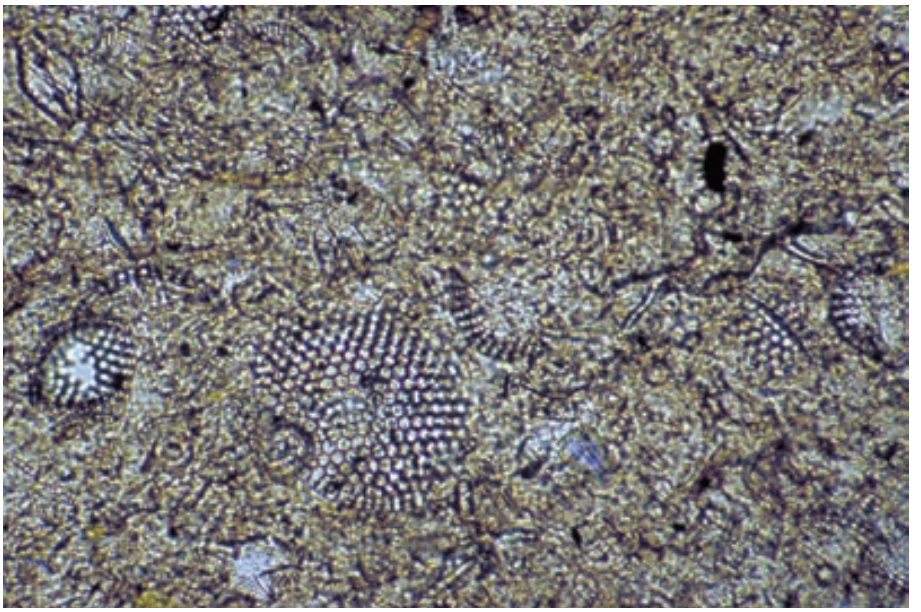

Eocene Oamaru Diatomite, Otago, New Zealand

Abundant, partially fragmented diatoms in a siliceous marine sediment. Note the simple circular to ovoid shapes and the small, regularly arranged pores that give the grains the distinctive appearance of small sieves.

PPL, BSE, HA = 0.7 mm

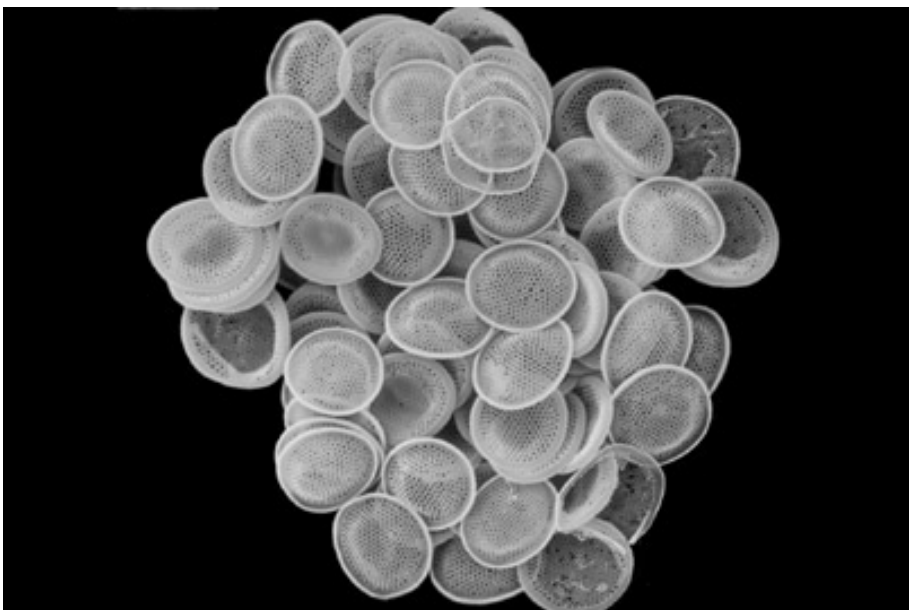

Recent sediment, North Atlantic Ocean, 26°N

An SEM image of chrysophytes, a relatively uncommon group of siliceous, marine phytoplanktonic organisms. Photograph courtesy of Jeremy R. Young.

SEM, HA = ~45 μm

Recent sediment, North Atlantic Ocean, 26°N

An SEM image showing a more detailed view of the chrysophyte shields depicted in the previous image. Photograph courtesy of Jeremy R. Young.

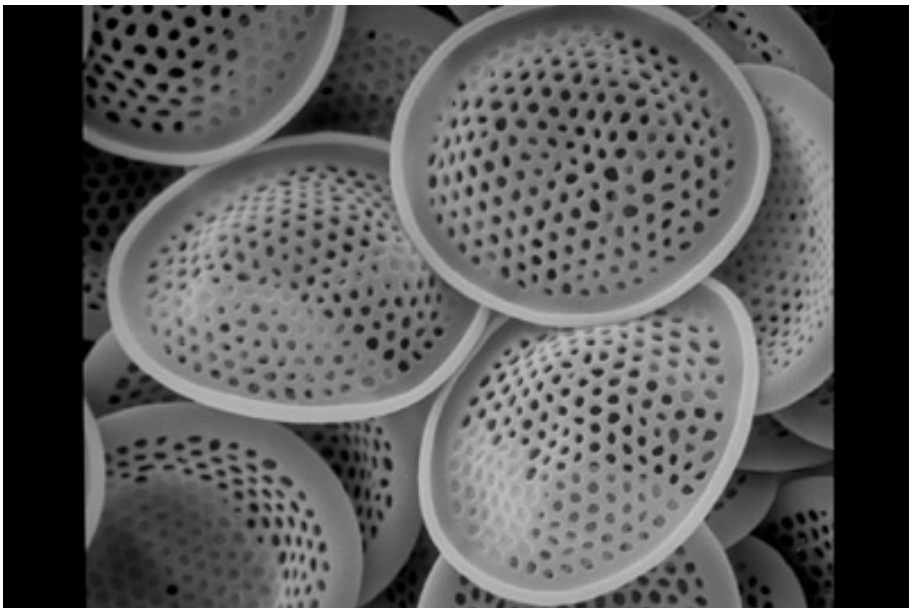

SEM, HA = ~14 μm

Recent sediment, North Atlantic Ocean, 26°N

An SEM image of the opaline silica skeleton of a silicoflagellate, *Dichtyocha fibula*. These are the opaline remains of unicellular algae with a single flagellum — this species has a very simple test morphology. Silicoflagellates generally are far less common in marine sediments than diatom or radiolarian remains, but they can be locally abundant. Photograph courtesy of Jeremy R. Young.

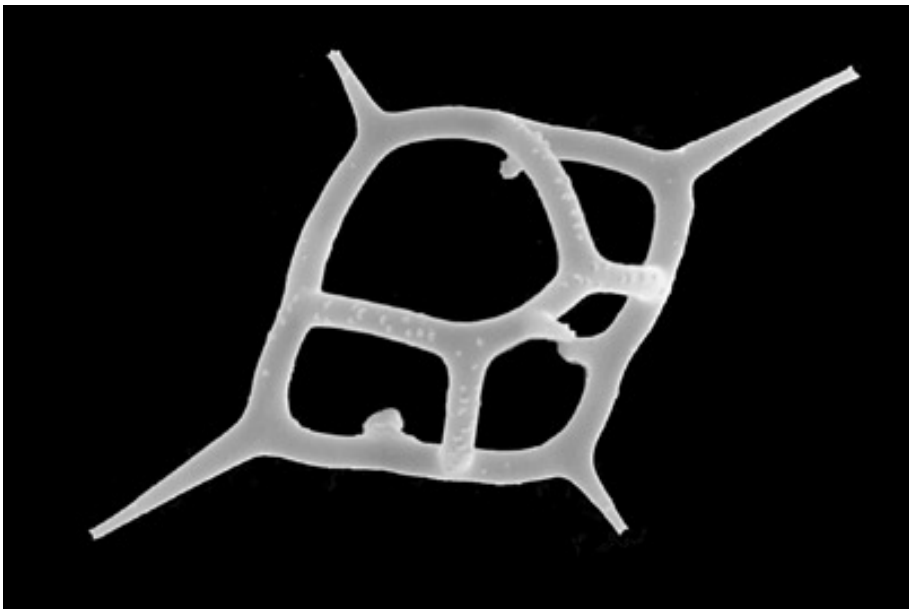

SEM, HA = ~32 μm

Recent sediment, North Sea

An SEM image of a silicoflagellate, *Dichtyocha speculum* (sometimes placed in the genus *Distephanus*). This species shows a slightly more complex morphology than the one shown above. Photograph courtesy of Jeremy R. Young.

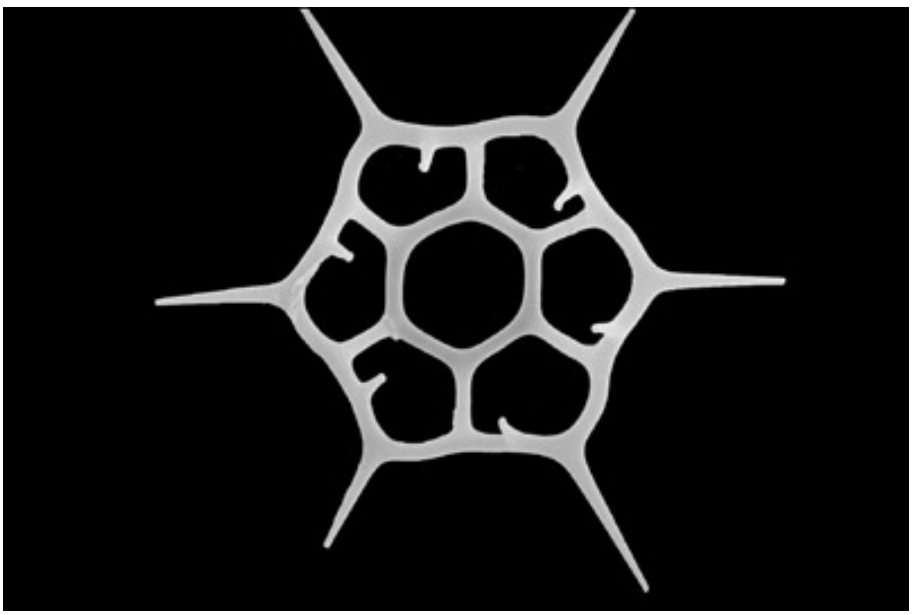

SEM, HA = ~38 μm

DINOFLAGELLATES AND OTHER ORGANIC-WALLED GROUPS

Taxonomy and Age Range:

These flagellate protists have both animal- and plant-like characteristics, but for nomenclatural purposes are classified as algae in the Kingdom Protista, Division Pyrrhophyta, class Dinophyceae.

Silurian precursors are known (and Paleozoic acritarchs may be related to this group), but the main fossil record is Permian to Recent.

Environmental Implications:

Modern dinoflagellates are mainly open marine to coastal, but some nonmarine (mainly lacustrine) forms exist; relatively few pre-Pleistocene nonmarine forms are known, however.

The most abundant dinoflagellate assemblages are found in sediments from middle neritic to upper bathyal settings.

Dinoflagellates often occur in blooms or "red tides" associated with nutrient availability, and thus are often found in great numbers within individual sediment layers.

Individual species are temperature-constrained, but dinoflagellates, as a whole, range from boreal to tropical settings.

Skeletal Mineralogy:

Some dinoflagellates have an encysted stage (dinocysts) designed to withstand adverse conditions. It is these dinocysts that form the fossil record, because many have a tough, dissolution-resistant wall composed of complex organic matter (sporopollenin).

Some organisms with calcitic tests (thoracosphaerids, for example) have been proven to be dinoflagellates, despite their non-organic shell composition, and are included in this section.

Morphologic Features:

Most fossil dinocysts have a moderate range of sizes from about 25 µm to 250 µm.

Dinocysts can be spherical, ellipsoidal or elongate; open-ocean species typically have long "horns" or ornamented "wings" (increasing flotation), whereas neritic forms are simpler and less ornamented. Most horns are about 50 µm in length.

Keys to Petrographic Recognition:

1. Sporopollenin (organic-walled) remains of small size and without the sutures of spores or shapes and sculptural features of pollen.
2. Most have spherical, ellipsoid, or elongate outlines; many have exterior collars, horns or spines.
3. Wall structure consists of one or more layers, and wall layering is an important component in group taxonomy.
4. Although dinocysts can be seen in thin section, they are almost impossible to distinguish from other organic remains. Thus, they are most commonly studied in separates produced by HCl and HF acid dissolution followed by heavy liquid concentration.
5. Differentiated from spores and pollen in grain mounts or SEM by overall morphology and surface features. Dinoflagellates generally are heavily ornamented, with horns, collars and spines; spores generally are less ornamented, lobate grains with relatively subdued surface sutures; pollen are saccate grains again with more subdued ornamentation than most dinoflagellates. Both spores and pollen tend to be slightly smaller than dinoflagellates, averaging 20-80 µm (although pre-Cenozoic spores may be up to 2 mm in diameter).

Recent sediment, North Sea

An SEM image of an organic-walled dinoflagellate, *Dinophysis norvegica*. The sporopollenin walls of these cysts are very durable and quite readily fossilized. Photograph courtesy of Jeremy R. Young.

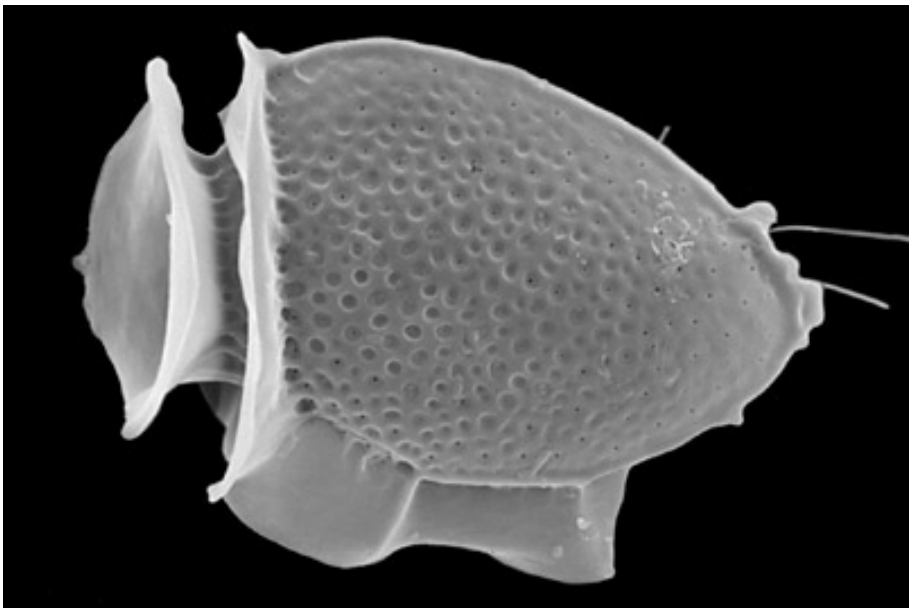

SEM, HA = ~50 μm

Recent sediment, North Atlantic Ocean

An SEM image of an organic-walled dinoflagellate, *Ceratium* cf. *compressum*. Photograph courtesy of Jeremy R. Young.

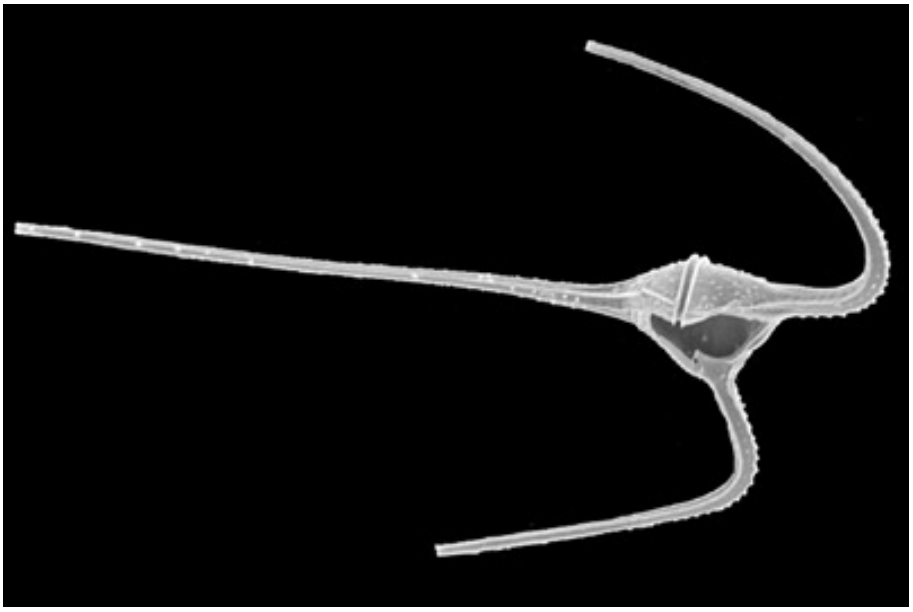

SEM, HA = ~330 μm

Up. Cretaceous Red Bank Fm. (L) and Mount Laurel Fm. (R), New Jersey

Left: a stained preparation of a dinoflagellate *Deflandria diebeli*. Central portion (endocyst) and spinose appendages (horns) are stained differentially. Dinoflagellates can be useful in correlation of marine sediments of Triassic to Recent age.

Right: stained preparation of the dinoflagellate *Spiniferites ramosus*. The central portion has taken a dark stain and the multiple, radiating, splay-tipped or trumpet-like appendages are clearly visible. These resting cysts are formed of noncalcified sporopollenin.

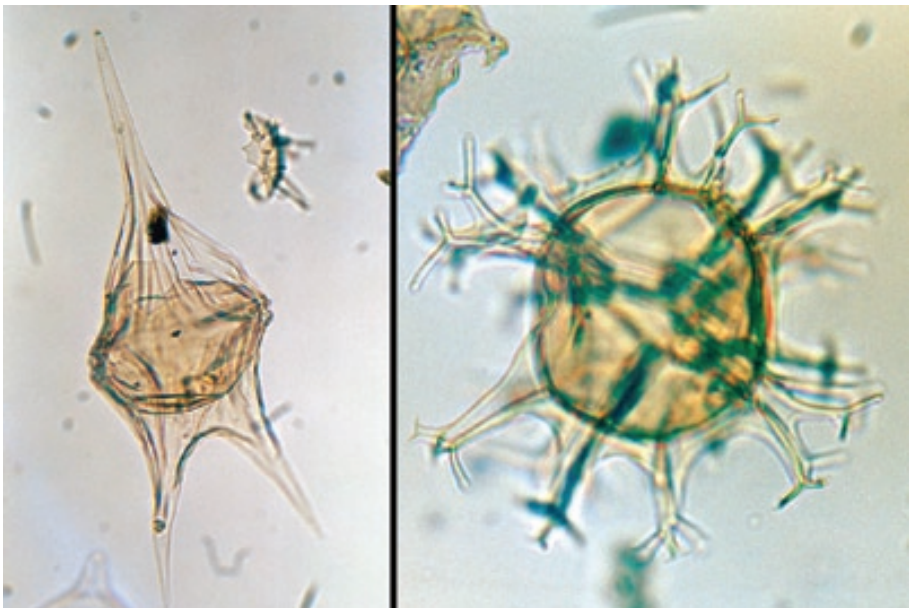

PPL, OS, HA = L: 0.13mm, R: 0.11mm

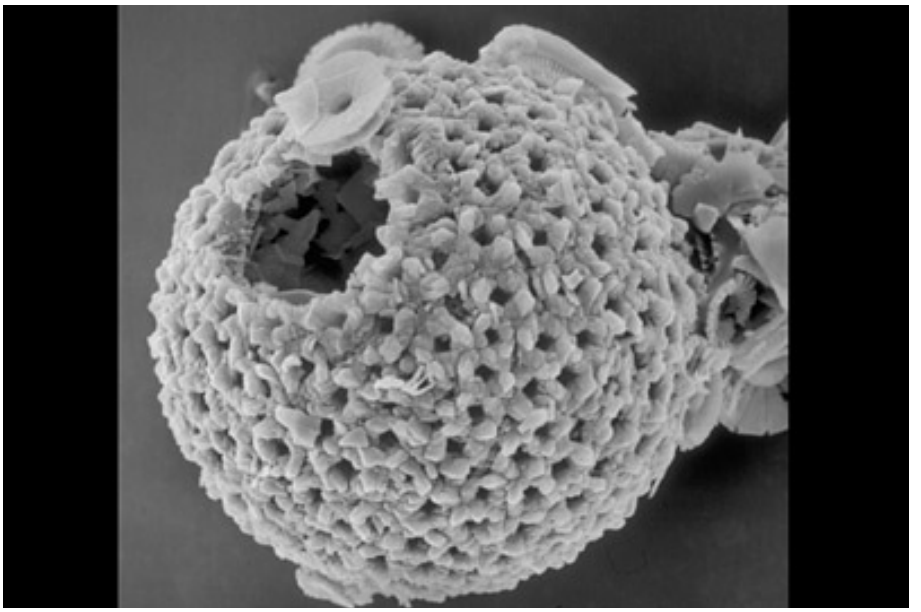

Recent sediment, South Atlantic Ocean

An SEM image of a possible calcareous dinoflagellate, *Thoracosphaera albatrosiana*. This sample is from modern sediment recovered by the H.M.S. "Challenger" expedition. The fossil record of thoracosphaerids, however, goes back to the Mesozoic. This organism is now thought to be a vegetative stage dinophyte (and thus most likely is related to, yet is somewhat different from, the Cretaceous calcareous dinophyte cysts shown earlier under the calcispheres). Photograph courtesy of Jeremy R. Young.

SEM, HA = ~25 μm

Cited References and Additional Information Sources

Banner, F. T., 1972, *Pithonella ovalis* from the early Cenomanian of England: Micropaleontology, v. 18, p. 268-284.

Baxter, J. W., 1960, Calcisphaera from the Salem (Mississippian) limestone in southwestern Illinois: Journal of Paleontology, v. 34, p. 1153-1157.

Black, M., 1963, The fine structure of the mineral parts of Coccolithophoridae: Proc. of the Linnean Society of London, v. 174, p. 41-46.

Blome, C. E., P. M. Whalen, and K. M. Reed (Convenors), 1995, Siliceous Microfossils: Short Courses in Paleontol. 8, Paleontological Society, 185 p.

Bonet, F., 1956, Zonificacion microfaunistica de las calizas Cretacicas del este de Mexico: Boletín del Asociación Mexicana de Geologos Petroleros, v. 8, p. 389-488.

Brasier, M. D., 1980, Microfossils: Boston, George Allen & Unwin, 193 p.

Burckle, L. H., 1978, Marine diatoms, *in* B. U. Haq and A. Boersma, eds., Introduction to Marine Micropaleontology: New York, Elsevier, p. 245-266.

Campbell, A. S., 1954, Radiolaria, *in* R. C. Moore, ed., Treatise on Invertebrate Paleontology, Part D: Geological Society of America and University of Kansas Press, p. D11-D163.

Campbell, A. S., 1954, Tintinnina, *in* R. C. Moore, ed., Treatise on Invertebrate Paleontology. Part D: Geological Society of America and University of Kansas press, p. D166-D180

Casey, R.E., 1993, Radiolaria, *in* J. H. Lipps, ed., Fossil Prokaryotes and Protists: Oxford, Blackwell Scientific Publ., p. 249-284.

Colom, G., 1948, Fossil tintinnids: loricated infusoria of the order of the Oligotricha: Journal of Paleontology, v. 22, p. 233-266.

Colom, G., 1965, Essais sur la biologie, la distribution géogeographique et stratigraphique des Tintinnoidiens fossiles: Eclogae geologicae Helvetiae, v. 58, p. 319-334.

Deflandre, G., 1936, Tintinnoidiens et Calpionelles. Comparaison entre les Tintinnoldiens, Infusoires loriqués pélagiques des mers actuelles et les Calpionelles, microfossiles de l'époque secondaire: Bull. Société Français Microscop., v. 5, p. 112-122.

Edwards, L.E 1993, Dinoflagellates, *in* J. H. Lipps, ed., Fossil Prokaryotes and Protists: Oxford, Blackwell Scientific Publ., p. 105-130.

Jones, D. J., 1956, Introduction to Microfossils: New York, Harper & Brothers, 406 p.

Kling, S. A., 1978, Radiolaria, *in* B. U. Haq, and A. Boersma, eds., Introduction to Marine Micropaleontology: New York, Elsevier, p. 203-244.

Lipps, J. H., ed., 1992, Fossil Prokaryotes and Protists: Cambridge, MA, Blackwell Science, 342 p.

Loeblich, A. R., Jr., and H. Tappan, 1966, Annotated index and bibliography of the calcareous nannoplankton: Phycologia, v. 5, p. 81-216.

Loeblich, A. R., Jr., and H. Tappan, 1968, Annotated index to the genera, subgenera and suprageneric taxa of the ciliate Order Tintinnida: Journal of Protozoology, v. 15, p. 185-192.

Marszalek, D. S., 1975, Calcisphere ultrastructure and skeletal aragonite from the alga *Acetabularia antillana*: Journal of Sedimentary Petrology, v. 45, p. 266-271.

Masters, B. A., and R. W. Scott, 1978, Microstructure, affinities, and systematics of Cretaceous calcispheres: Micropaleontology, v. 24, p. 210-211.

Noël, D., 1978, Les Calcaires à Nannoconus (dits Calcaires à Calpionelles) de l'Ermitage d'Esparron (Isère), au passage Tithonique-Berriasien: Note du Laboratoire de Paléontologie, Université de Genève, v. 13, p. 109-113.

Remane, J,. 1963, Les Calpionelles dans les couches de passage Jurassique-Crétacé de la fosse vocontienne: Univ. Grenoble Laboratoire de Géologie fac. sci. Travaux, v. 39, p. 25-82.

Remane, J., 1978, Calpionellids, *in* B. U. Haq, and A. Boersma, eds., Introduction to Marine Micropaleontology: New York, Elsevier, p. 161-170.

Sandgren, C. D., J. P. Smol, J. Kristiansen, eds., 1995, Chrysophyte Algae: Ecology, Phylogeny and Development: Cambridge, Cambridge University Press, 413 p.

Siesser, W.G., 1993, Calcareous nannoplankton, *in* J. H. Lipps, ed., Fossil Prokaryotes and Protists: Oxford, Blackwell Scientific Publ., p. 169-202.

Smith, C. C., 1981, Calcareous Nannoplankton and Stratigraphy of Late Turonian, Coniacian, and Early Santonian Age of the Eagle Ford and Austin Groups of Texas: U. S. Geol. Survey Prof. Paper 1075, 98 p.

Stanton, R, J., Jr., 1967, Radiosphaerid calcispheres in North America and remarks on calcisphere classification: Micropaleontology, v. 13, p. 465-472.

Tappan, H., 1993, Tintinnids, *in* J. H. Lipps, ed., Fossil Prokaryotes and Protists: Oxford, Blackwell Scientific Publ., p. 285-303.

Trejo H., Mario, 1960, La familia Nannoconidae y su alcance-estratigrafico en America (Protozoa, *Incertae Saedis*): Boletín del Asociación Mexicana de Geologos Petroleros, v. 12, p. 315-318.

Williams, G. L., 1978, Dinoflagellates, acritarchs and tasmanitids, *in* B. U. Haq, and A. Boersma, eds., Introduction to Marine Micropaleontology: New York, Elsevier, p. 293-326.

Winter, A., and W. G. Siesser, eds, 1994, Coccolithophores: Cambridge, Cambridge University Press, 242 p.

Facing Page: Underwater view of Christmas tree worms (*Spirobranchus giganteus*) with their tubes encased in a *Montastrea* sp. coral from the Bonaire reef front. Photograph courtesy of Woody Mayhew.

GRAINS: Skeletal Fragments

Annelids and related groups

CHAPTER 4

Serpulids

Sabellariids

Problematic conical forms:
Cornulites
Tentaculites
Styliolina

ANNELID WORMS (SERPULIDS AND SABELLARIIDS)

Taxonomy and Age Range:

Worm remains are known from Precambrian to Recent — most are soft-bodied, but preserved fossil forms include some segmented worms that built solid housing structures. These generally belong to the:

Phylum Annelida: Proterozoic-Recent

Class Polychaeta: (Proterozoic?) Cambrian-Recent

The most important sediment-producing or sediment-influencing groups in Phylum Annelida include three groups or families within the order Sabellida:

Serpulids and spirorbids (groups that precipitate solid calcareous tubes)

Sabellariids (producers of agglutinated tubes)

A variety of soft-bodied burrowers and pellet producers

Environmental Implications:

Most preserved forms lived in fully marine to hypersaline-water settings; rare in freshwater and even rarer in terrestrial settings (although non-calcified forms can produce pellets in those environments).

Serpulids are most common in shallow to coastal waters (largely as hard-substrate encrusters) but extend into deeper shelf waters as well. Especially common in slightly hypersaline settings (where they may form small reef-like masses) or at hiatus surfaces.

Skeletal Mineralogy:

Serpulid worm tubes are composed of high-Mg calcite (typically 6-16 mole% Mg), aragonite, or a combination of aragonite and calcite. Other tubes may be entirely chitinous or a mix of chitin and phosphate.

Sabellariid worm tubes consist of agglutinated, oriented, calcareous or terrigenous clastic sand grains with a wide variety of compositions.

Morphologic Features:

Worm-built calcareous or agglutinated tubes that are typically from <1 to 10 cm long and 1 cm in diameter. They have smoothly circular to elliptical interior tubes and smooth or ornamented exterior surfaces. Tubes can be free-standing, but quite commonly are found as encrustations on hard surfaces, especially other shells. Tubes may be isolated (straight, sinuous, or spiral) or can form intergrown clusters resembling piles of spaghetti.

Keys to Petrographic Recognition:

1. **Distinctive tubular external and internal shape (generally with a circular to ovoid cross-section and commonly with an encrusting morphology). These attributes differentiate them from most organisms other than vermetid gastropods, scaphopods, and some tubular foraminifers.**
2. **One or two-layer walls with a type of foliated microstructure. Wall consists of concentric, very fine (0.005 mm or less in thickness) laminations, sometimes with thin, lenticular gaps between layers (due to parabolic of cone-in-cone outer layer construction). Thus, they differ from vermetid gastropods and scaphopods that typically have radial-prismatic or crossed-lamellar outer shell layers (see Schmidt, 1951).**
3. **Some examples with two-layer walls show a discordance in lamination angles between inner and outer walls (reminiscent of brachiopod material).**
4. **Aragonitic forms (or aragonitic layers in mixed-mineralogy forms) usually have little or no preserved primary wall structure.**

PHOTO SCALES AND ABBREVIATIONS ARE EXPLAINED IN THE BOOK'S INTRODUCTION

Morphology and wall structure of serpulid tubes

A diagram showing the wall structure and external morphology of calcified annelid worms (partially adapted from Majewske, 1969, Plate 13). The individual forms in the upper tier show a variety of coiling morphologies. The colonial form has intergrown tubes with some external ornamentation. Both types have a two-layered wall with concentrically laminated, foliated microstructure in the interior part and darker, more microgranular, but still laminated microstructure in the outer part. The outer part also has lenticular spar zones in small, parabolic separations between successive laminae. Scales differ among the five drawings.

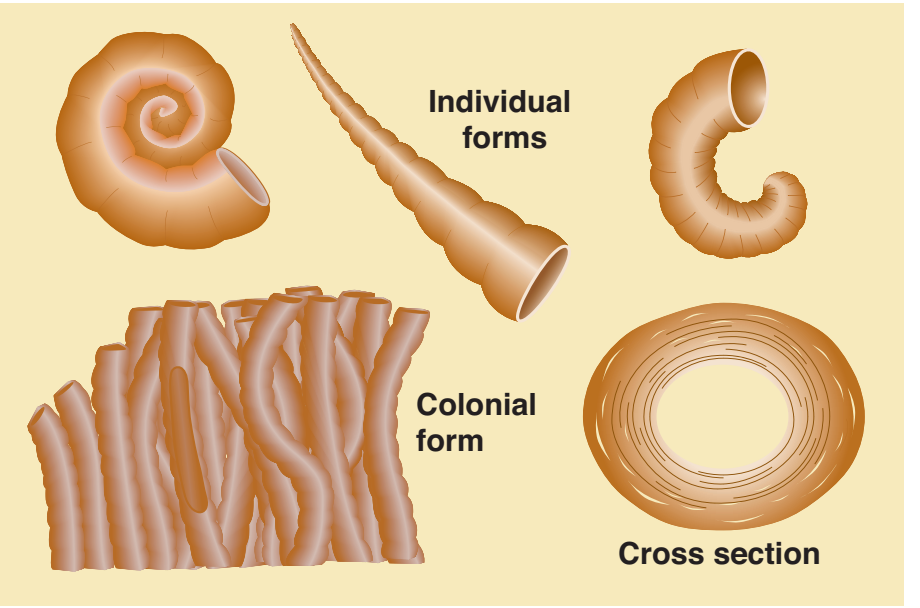

Lo. Cretaceous (Albian) Glen Rose Ls., central Texas

A cluster of serpulid worm tubes encrusting on a mollusk shell (not in field of photograph) and upon each other. Note the concentrically laminated microgranular wall structure, the smooth morphology of the interior and exterior surfaces of the tubes, and the way they are attached to neighboring tubes. As a result of this structure, encrusting serpulids can form small, but very stable and wave resistant patch reefs.

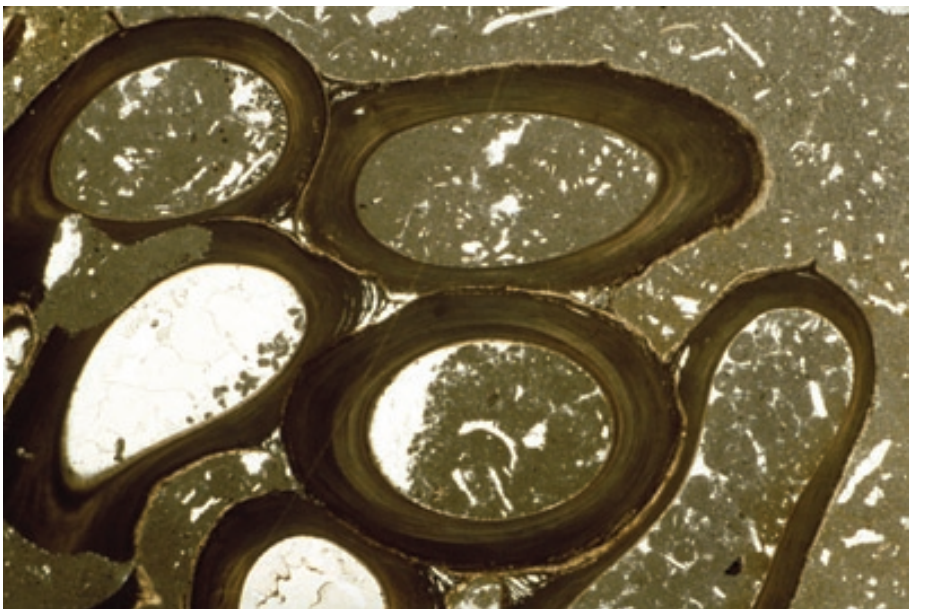

PPL, HA = 13.5 mm

Lo. Cretaceous (Albian) Glen Rose Ls., central Texas

A more detailed view of the dense, laminar wall structure in serpulid worm tubes from the same unit as shown in the previous photograph. The microgranular fabric, the concentric laminations, and the characteristic localized, lenticular gaps between successive laminae (resulting from parabolic structure of the precipitates of the outer layer) are all clearly visible. The excellent fabric preservation indicates a primary calcitic wall composition.

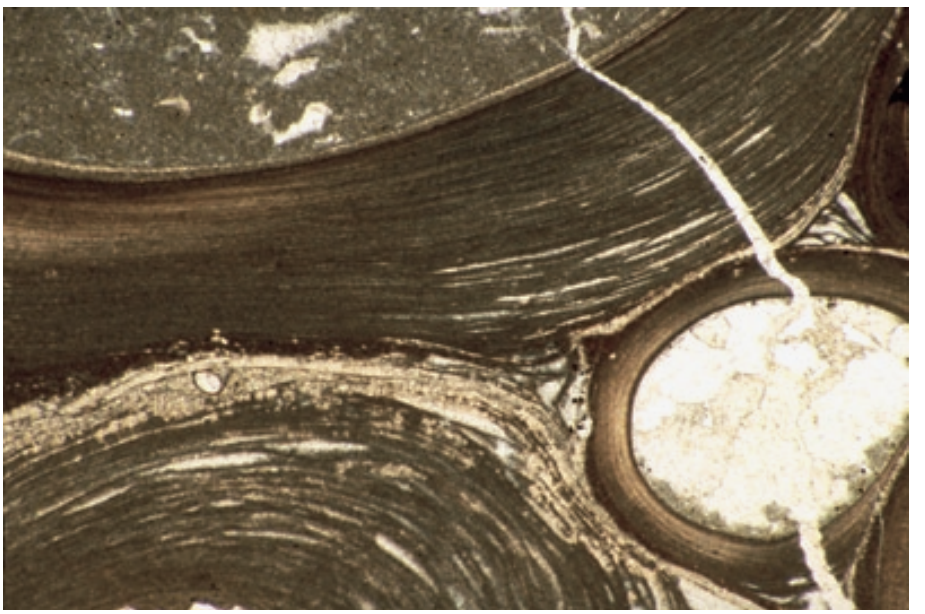

PPL, HA = 4 mm

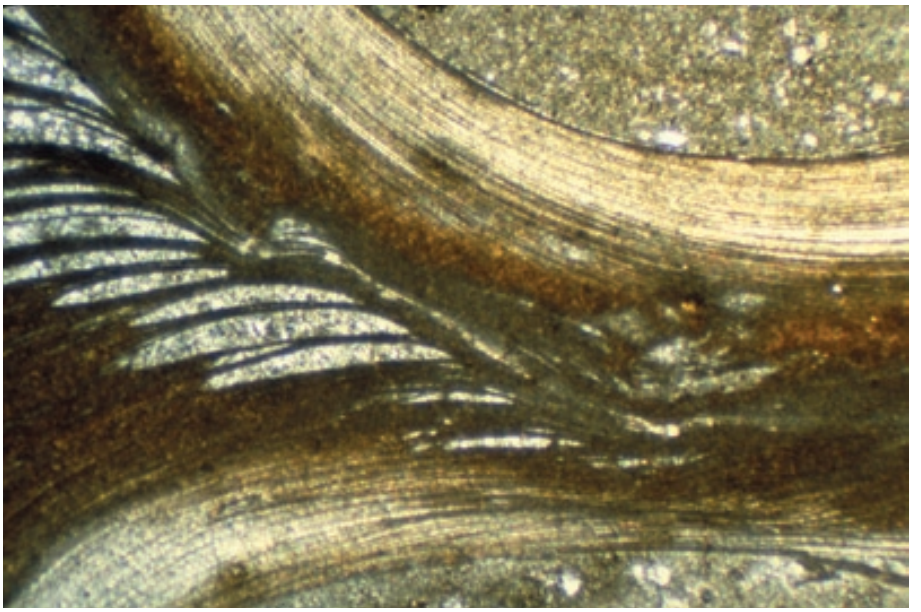

Up. Pliocene Greta Fm., northern Canterbury, New Zealand

A close-up of encrusting serpulid worm tubes showing two distinctly different wall layers: an inner, lighter-colored, parallel-laminated (foliated) zone, and an outer, darker, more microgranular zone with lenticular spar zones. The elongate spar-filled lenses paralleling the laminar shell structure are the most uniquely diagnostic characteristic of most serpulid worm tubes.

PPL, HA = 4.1 mm

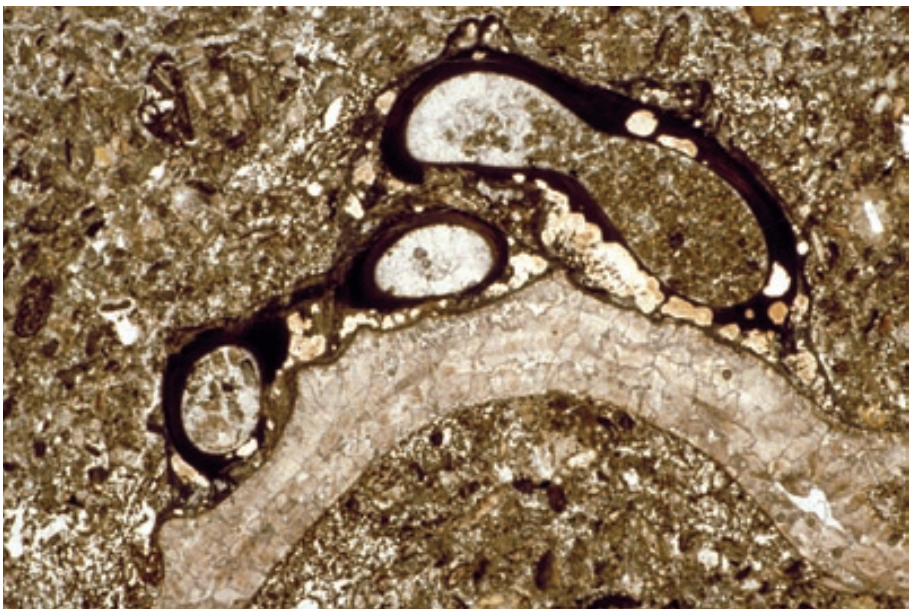

Jurassic Trigonia beds, Dorset, England, U.K.

The encrusting habit of serpulid worm tubes is well shown in this example in which the serpulids have grown on a bivalve shell. Note the differences in wall structure preservation between the originally aragonitic bivalve and the calcitic serpulid. The serpulid has, however, been partially and selectively replaced by silica (rounded, white patches within the serpulid wall).

PPL, HA = 11 mm

Mid. Jurassic (Bajocian) Calcaire Corniche, Central High Atlas region, Morocco

Serpulid worm tubes showing poorly preserved wall structure. These tubes show the same shapes and encrusting habit as was seen in previous photographs, but the walls have been extensively altered (dissolution of primary carbonate and reprecipitation of sparry calcite). This suggests a primary aragonitic wall structure for this group of serpulids. The serpulid tubes in this example were further encrusted by foraminifers (dark material).

PPL, AFeS, HA = 2.4 mm

Up. Pennsylvanian Panther Seep Fm., Doña Ana Co., New Mexico

A worm tube boundstone from a dark calcareous mudstone facies. Worm tubes and peloids are dolomitized (unstained) and dolomite cement lines the tubes; coarse calcite (pink) fills pore space. The generally poor preservation of the wall structure indicates an at least partially aragonitic primary composition. Photograph courtesy of Gerilyn S. Soreghan.

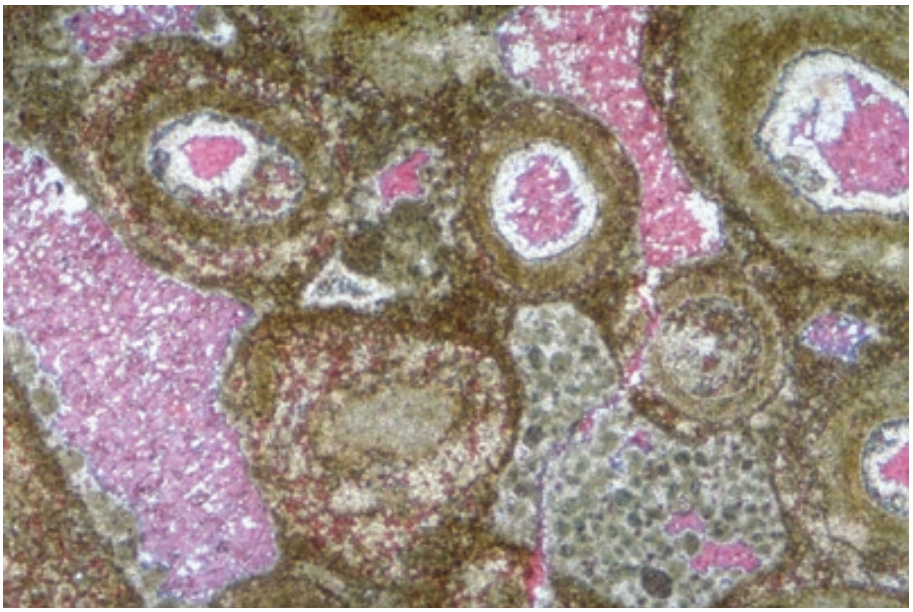

PPL, AFeS, HA = 2.0 mm

Recent sediment, Key Biscayne, Dade Co., Florida

Sabellariid worm tubes associated with mangrove roots (not shown). The tubes consist of agglutinated, cemented, and imbricated grains of mixed clastic terrigenous and carbonate sediment from the surrounding environment. These organisms form moderately rigid patch reefs composed of parallel agglutinated tubes on wave-protected but otherwise normal marine coastlines. These agglutinated worm tubes are larger than most arenaceous foraminifers and do not have the internal chambers found in foraminiferal tests.

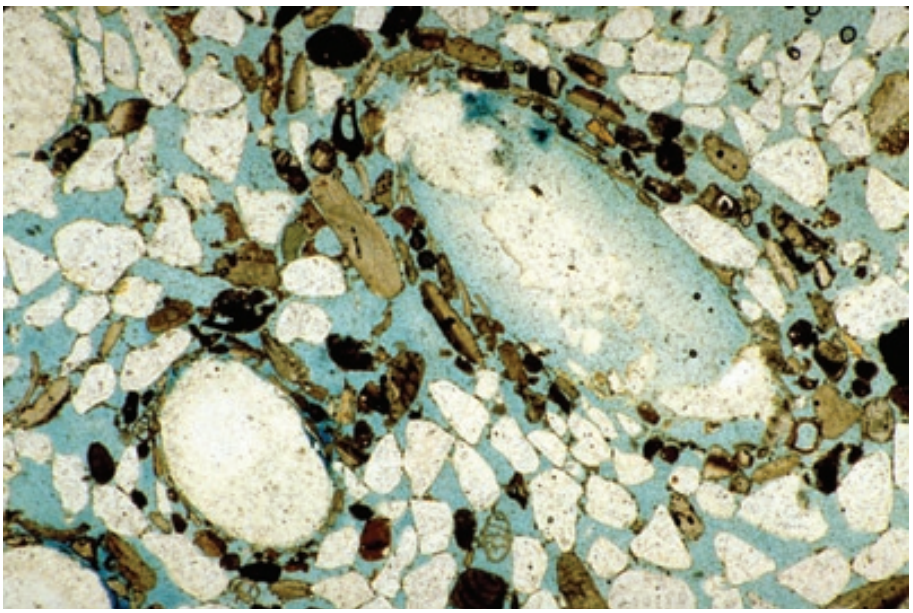

PPL, BSE, HA = 7 mm

Recent sediment, Key Biscayne, Dade Co., Florida

An enlarged view of a single sabellariid worm tube showing the nonselective use of several types of grains, their orientation with long axes tangential to the tube outline, and the very sparse binding material. Bluish-green-stained areas are filled with a stained impregnating medium.

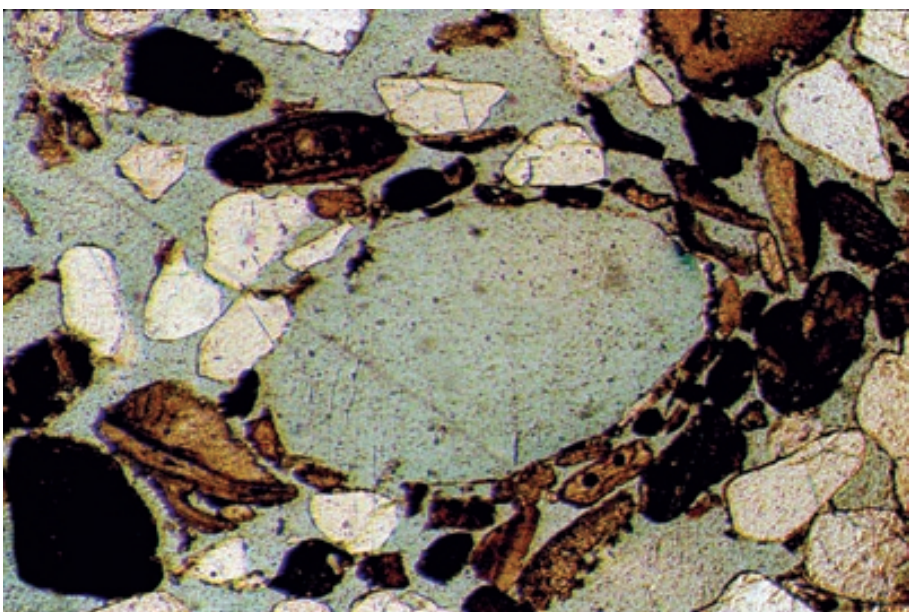

PPL, BSE, HA = 3 mm

CORNULITES, TENTACULITES, AND STYLIOLINIDS

Taxonomy and Age Range:

Problematic small conical organisms that sometimes have been placed with the annelids, the mollusks (pteropods), or as a separate phylum (perhaps related to the annelids or mollusks); also sometimes grouped with the conulariids. Cornulites is more commonly accepted as an annelid.

Sometimes grouped in the Class Coniconchia (syn. Cricoconarida).

Cornulites — Ordovician-Devonian
Tentaculitids — Ordovician-Devonian (common Silurian-Devonian)
Styliolinids — Devonian

Environmental Implications:

Cornulites were benthic, and in some cases encrusting.
Tentaculitids may have had a nektic/benthic lifestyle.
Styliolinids are thought to have been pelagic/planktic organisms.
All are fully marine.

Skeletal Mineralogy:

Tentaculitids and styliolinids are generally well preserved and thus most likely had primary calcite shells; cornulites may have been aragonite and/or calcite.

Morphologic Features:

All have small, conical shells. Tentaculitids have roughly 5-25 mm long shells, with roughly 0.5-1 mm circular openings, strong external ribbing (transverse rings) and internal septa; styliolinids have broader, smoother external ribs and no internal septa and are smaller than tentaculitids (1-5 mm in length); Cornulites can be up to 1-2 cm long and have strong, broad external ribbing.

Keys to Petrographic Recognition:

1. **Tapering, conical, ribbed forms in longitudinal section; circular or flattened ovoid shape in transverse section.**
2. **External shell ribbing or plications give wavy appearance to transverse cuts through shells, especially for the tentaculitids.**
3. **Typically have a size range from mm to 2 cm and a large percentage of intact shells.**
4. **Cornulites are often found attached to (encrusting on) brachiopod shells.**
5. **Tentaculitids and styliolinids are thinner walled than many other conical shells (scaphopods, for example) and can be major rock-forming elements, especially in Devonian strata.**

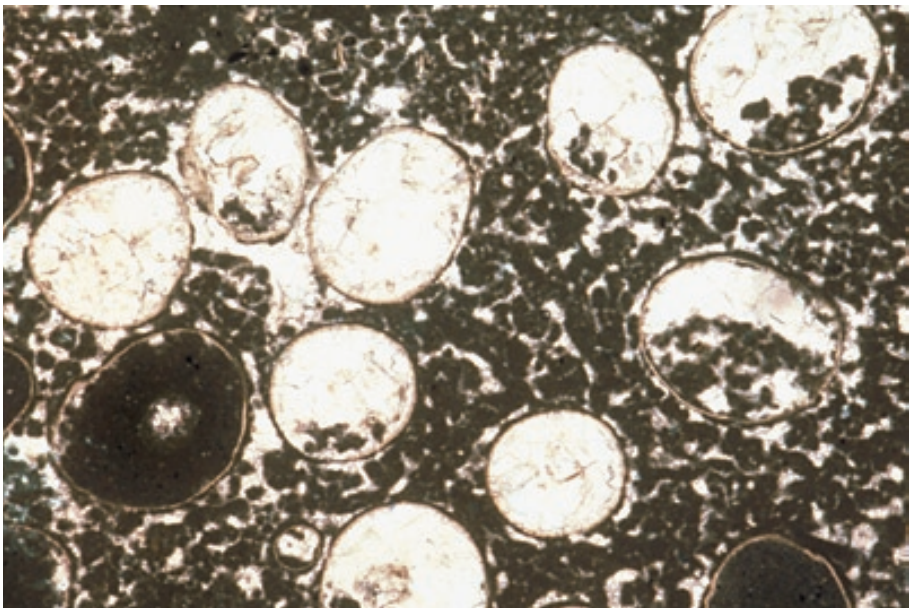

Mid. Ordovician Black River Gp., Lowville Fm., near Kingston, Ontario, Canada

Oriented calcareous tubes of *Cornulites* sp., a possible early serpulid? worm, in stromatospongia microbial fabric of a thrombolite. Cornulites were benthic, commonly encrusting, conical organisms, here seen in transverse section. Sample from Noel P. James.

PPL, HA = 4.5 mm

Devonian, unidentified unit, U.S.A.

Close-up macrophotograph of a calcareous sandstone with a tentaculite exposed on a bedding plane. Note the conical shape and the pronounced transverse ribbing on the exterior of the small shell.

Mac, HA = ~8 mm

Devonian Tentaculiten Knottenkalk, Frankenwald, Bavaria, Germany

A slice through part of a tentaculite parallel to its long axis, showing the conical shape and characteristic crenulate or corrugate exterior (the tentaculite is the grain that extends diagonally from the upper left corner to the lower right corner of the image). These fossils are similar to *Styliolina* except for the external ornamentation, and are classed by some as belonging to the worms; others place them with the mollusks.

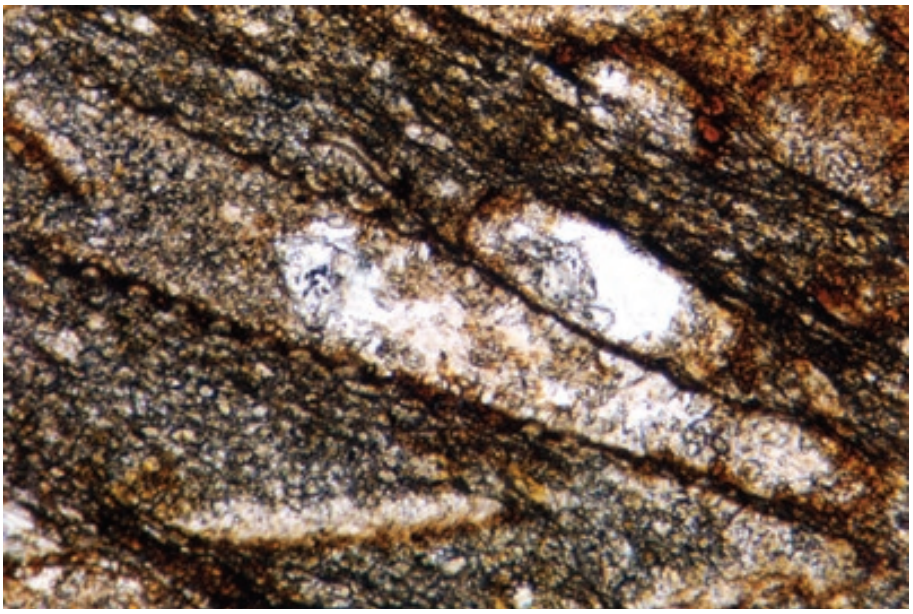

PPL, HA = ~1.5 mm

Up. Devonian Genundewa Ls., New York

Abundant examples of *Styliolina fissurella* in transverse section. Note the very thin, but well preserved walls. These conical microfossils are similar to tentaculitids and have unknown faunal affinities; they are sometimes grouped as Conulariids. *Styliolina* and other similar genera are important rock-formers in the Devonian.

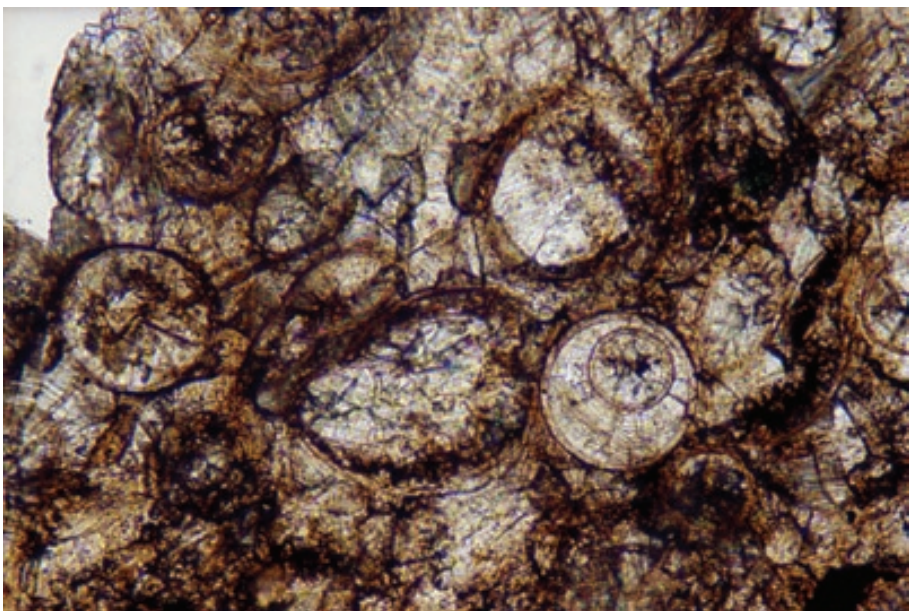

PPL, HA = ~1.1 mm

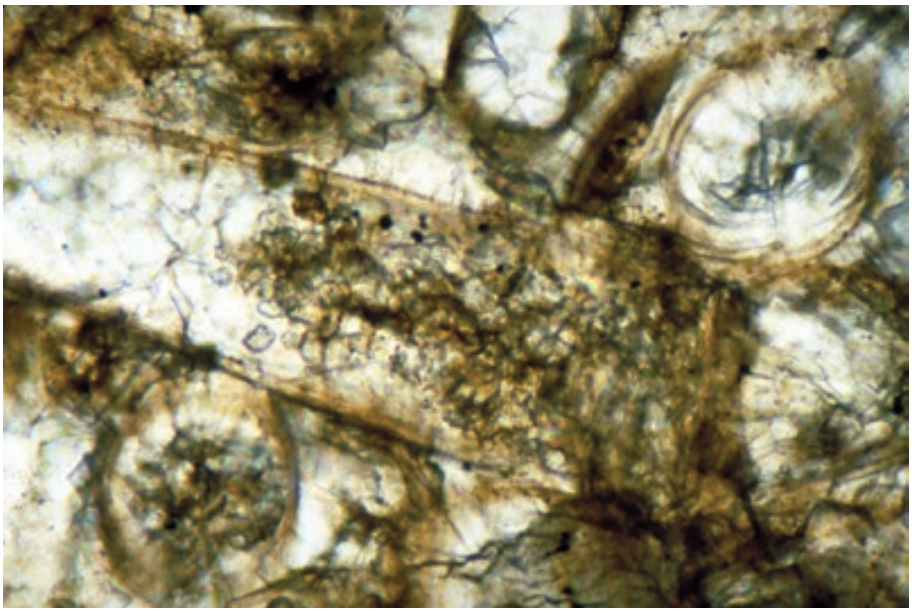

Up. Devonian Genundewa Ls., New York

A more detailed view of *Styliolina fissurella*. Note the circular (transverse) and conical (longitudinal) sections and the reverse-feathered aspect produced by twinning of the calcite. The dark (organic-rich) shell wall shows preservation indicative of an original calcite mineralogy. The longitudinal section shows almost no plications (unlike tentaculitids).

PPL, HA = 0.65 mm

Cited References and Additional Information Sources

Bailey-Brock, J. H., 1987, The polychaetes of Fanga'Uta lagoon and coral reefs of Tongatapu, Tonga, with discussion of the serpulidae and spirorbidae: Bulletin of the Biological Society of Washington, v. 7, p. 280-294.

Barnard, T., 1956, An unusual worm tube from the lower Lias: Journal of Paleontology, v. 30, p. 1273-1274.

Beauchamp, B., J. C. Harrison, W. W. Nassichuk, and L. S. Eliuk, 1988, Lower Cretaceous (Albian) serpulid-bivalve carbonate "mounds" related to hydrocarbon seeps, Canadian Arctic Archipelago, *in* H. H. J. Geldsetzer, N. P. James, and G. E. Tebbutt, eds., Reefs, Canada and Adjacent Areas: Calgary, Alberta, Canadian Society of Petroleum Geologists Memoir 13, p. 706-712.

Beus, S. S., 1980, Devonian serpulid bioherms in Arizona: Journal of Paleontology, v. 54, p. 1125-1128.

Bornhold, B. D., and J. D. Milliman, 1973, Generic and environmental control of carbonate mineralogy in serpulid (polychaete) tubes: Journal of Geology, v. 81, p. 363-373.

Broennimann, P., and L. Zaninetti, 1972, On the occurrence of the serpulid *Spirorbis* Daudin, 1800 (Annelida, Polychaetia, Sedentarida) in thin sections of Triassic rocks of Europe and Iran: Rivista Italiana di Paleontologia e Stratigrafia, v. 78, p. 67-84.

Ekdale, A. A., and D. W. Lewis, 1993, Sabellariid reefs in Ruby Bay, New Zealand: A modern analogue of *Skolithos* "Piperock" that is not produced by burrowing activity: Palaios, v. 8, p. 614-620.

Goedert, J. L., J. Peckmann, and J. Reitner, 2000, Worm tubes in an allochthonous cold-seep carbonate from lower Oligocene rocks of western Washington: Journal of Paleontology, v. 74, p. 992-999.

Götz, G., 1931, Bau und Biologie fossiler Serpuliden: Neues Jahrbuch für Mineralogie, Geologie, und Paläontologie, v. 65, Beil. Band, Abt. B, p. 385-438.

Gram, R., 1968, A Florida Sabellariidae reef and its effect on sediment distribution: Journal of Sedimentary Petrology, v. 38, p. 863-868.

Howell, B. F., 1962, Worms, *in* R. C. Moore, ed., Treatise on Invertebrate Paleontology, Part W, Miscellanea: Geological Society of America and University of Kansas Press, p. W144-W177.

Kirtley, D. W., and W. F. Tanner, 1968, Sabellariid worms: builders of a major reef type: Journal of Sedimentary Petrology, v. 38, p. 73-78.

Leeder, M. R., 1973, Lower Carboniferous serpulid patch reefs, bioherms and biostromes: Nature, v. 242, p. 41-42.

Mistiaen, B., and J. Poncet, 1983, Stromatolithes, serpulidés et Trypanopora (Vers?), associés dans les petits biohermes Givétiens du Boulonnais (France): Palaeogeography, Palaeoclimatology, Palaeoecology, v. 41, p. 125-138.

Palmer, C. P., 2001, *Dentalium giganteum* Phillips; a serpulid worm tube: Proceedings of the Yorkshire Geological Society, v. 53, p. 253-255.

Pillai, T. G., 1993, A review of some Cretaceous and Tertiary serpulid polychaetes of the genera *Cementula* and *Spiraserpula* Regenhardt 1961, *Laqueoserpula* Lommerzheim 1979 and *Protectoconorca* Jaeger 1983: Palaeontologische Zeitschrift, v. 67, p. 69-88.

Robison, R. A., 1987, Annelida, *in* R. S. Boardman, A. H. Cheetham, and A. J. Rowell, eds., Fossil Invertebrates: Palo Alto, CA, Blackwell Scientific Publications, p. 194-204.

Schmidt, W. J., 1951, Die Unterscheidung der Röhren von Scaphopoda, Vermetidae und Serpulidae mittels mikroskopischer Methoden: Mikroskopie, v. 6, p. 373-381.

Schmidt, W. J., 1955, Die tertiären Würmer Osterreichs: Osterreichs Akademie der Wissenschaften, Mathematisch-naturwissenschaftliche Klasse Denkschriften, v. 109, no. 7, 121 p.

Ten Hove, H. A., and P. van den Hurk, 1993, A review of Recent and fossil serpulid "reefs"; actuopalaeontology and the "upper Malm" serpulid limestones in NW Germany: Geologie en Mijnbouw, v. 72, p. 23-67.

Tucker, M. E., and A. C. Kendall, 1973, The diagenesis and low-grade metamorphism of Devonian styliolinid-rich pelagic carbonates from West Germany: possible analogues of Recent pteropod oozes: Journal of Sedimentary Petrology, v. 43, p. 672-687.

Wrigley, A., 1950, The differences between the calcareous tubes of vermetids and of serpulids: Journal de Conchyliologie, v. 90, p. 118-121.

Zibrownius, H., 1990, A propos des prétendus "Récifs de Serpulidae" de l'ile Rousse, Corse (méditerranée nord-occidentale: Mésogée, v. 50, p. 71-74.

Facing Page: Underwater view of an azure vase sponge, *Calyspongia plicifera*, among other tube sponges on the Bonaire reef front. Photograph courtesy of Woody Mayhew.

GRAINS: Skeletal Fragments

SPONGES AND RELATED GROUPS

CHAPTER 5

Archaeocyaths

Calcareous sponges

Siliceous sponges

Stromatoporoids

ARCHAEOCYATHS

Taxonomy and Age Range:

This short-lived but widespread group have been classed by various as sponges, corals, or calcareous algae. Archaeocyaths now are almost universally considered as subphylum of the Porifera (possibly related to the demosponges); a few workers still group them in a separate phylum (Phylum Archaeocyatha). They range mainly from basal Cambrian to late Early Cambrian (a few forms persisted to Middle and Late Cambrian).

Environmental Implications:

One of the earliest groups to secrete substantial skeletal calcium carbonate and the first reef-building organism.

Sessile, benthic, filter feeders. Exclusively marine organisms that lived in tropical, normal salinity (ca. 30-40 ppt) waters at depths from the intertidal zone to a few tens of meters, mainly in areas with relatively low influx of terrigenous sediments (see Debrenne and Reitner, 2001).

Constructed small bioherms in association with calcimicrobes. They also are found in lesser abundance, size and diversity in inter-bioherm areas.

Skeletal Mineralogy:

The good preservation of most archaeocyath skeletal material indicates a primary calcitic composition.

Morphologic Features:

Most archaeocyaths have a solitary cup- or bowl-shaped skeleton that has a pair of porous walls enclosing a large central cavity. The inner and outer walls have a series of spherical perforations and are connected by numerous perforate or imperforate partitions (vertical septa and horizontal tabulae).

Less commonly, archaeocyaths had branched, massive, or chain-like colonial forms.

The average size of archaeocyath cups is 1 to 2.5 cm in diameter and 15 cm in height. Cups as small as 2-3 mm or as large as 60 cm in diameter are known, however.

Closely associated with calcimicrobial encrusters such as *Renalcis* and/or *Epiphyton*, and external morphology is commonly outlined by such encrusters.

Keys to Petrographic Recognition:

1. **Distinctive double-walled cup shape with a large central cavity — similar to solitary rugose (cup) corals, but distinguished by presence of perforations in archaeocyath walls and, in some cases, septa. Distinguished from many early sponges by the absence of the characteristic spicular networks that are found in sponge walls.**
2. **Large size — typically cups are 1 to 2.5 cm in diameter and approximately 10 to 15 cm in height.**
3. **Generally good preservation of wall morphology and its laminated microstructure that consists of "a very fine granular mosaic of calcite, the crystals being about 0.02 mm in diameter" (Hill, 1965, p. 25).**
4. **Distribution limited to Lower and lower Middle Cambrian strata (prior to the occurrence of rugose corals).**
5. **Very commonly encrusted with peloidal or filamentous microbial material (*Renalcis* or *Epiphyton*).**

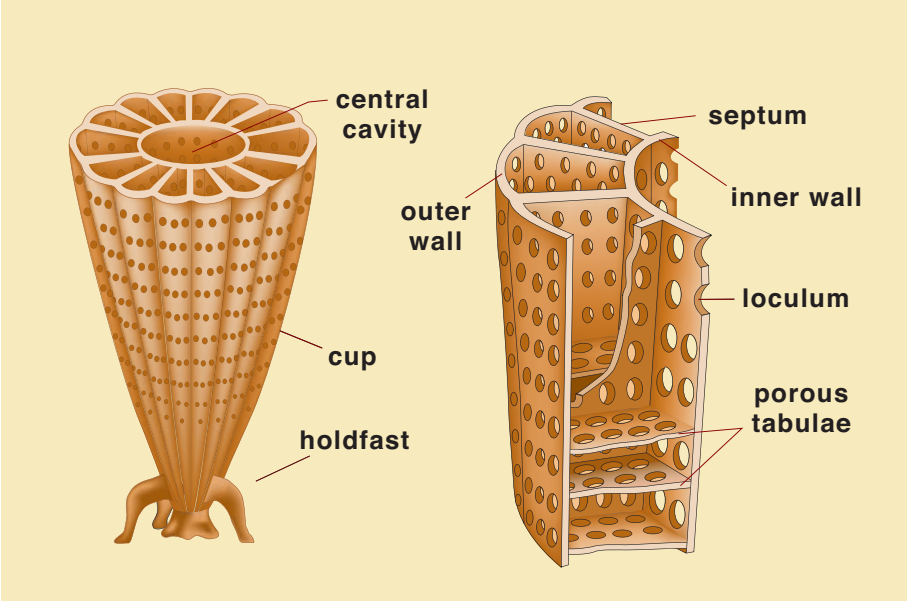

Morphology and wall structure of a typical archaeocyath

A diagram showing a typical archaeocyath morphology, with a cup-shaped, double-walled skeleton made more structurally rigid by a series of vertical and horizontal partitions (septa and tabulae, respectively). Other patterns of internal supports (curved dissepiments and rod-like synapticulae) are commonly found in archaeocyaths but are not depicted here. Redrawn from Rigby and Gangloff (1987).

Cross-sections of regular and irregular archaeocyaths

Longitudinal and transverse sections through typical examples of the two major groups of archaeocyaths showing some of the structural features that can be seen in the walls at various ontogenetic stages. Adapted from Rigby and Gangloff (1987).

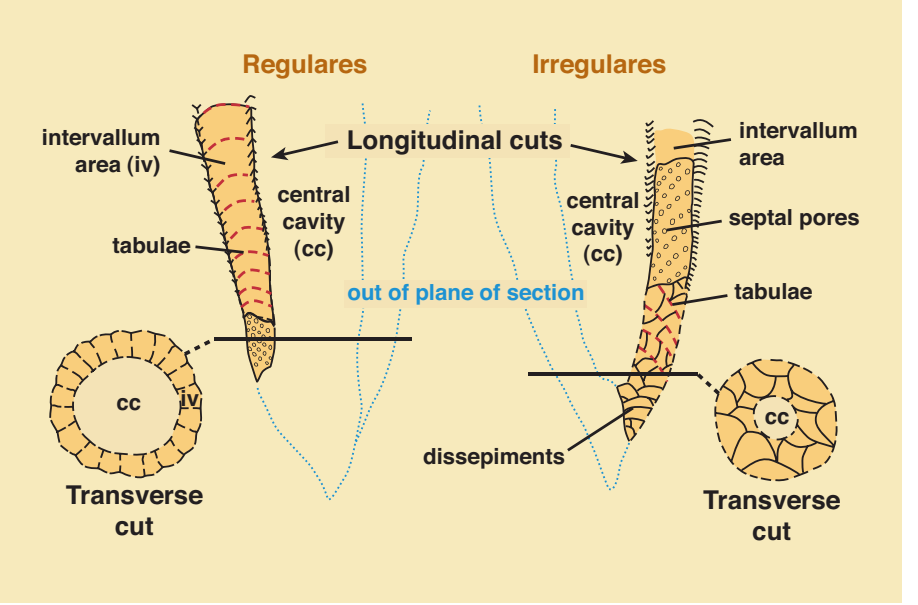

Lo. Cambrian (Tommotian) Pestrotsvet Fm., southeastern Siberian Platform, Russia

Three regular archaeocyaths encrusted with *Renalcis* and encased in marine cement. The cup-shaped, double-walled, perforated skeletal material and central cavity are well represented in this view, as are the septa that provide structural support. Sample from Noel P. James.

PPL, HA = 16 mm

Lo. Cambrian (Tommotian) Pestrotsvet Fm., southeastern Siberian Platform, Russia

A transverse section through a regular archaeocyath illustrating the cup-shaped morphology and the numerous pores that pass through the inner and outer skeletal walls as well as the supporting septa. Sample from Noel P. James.

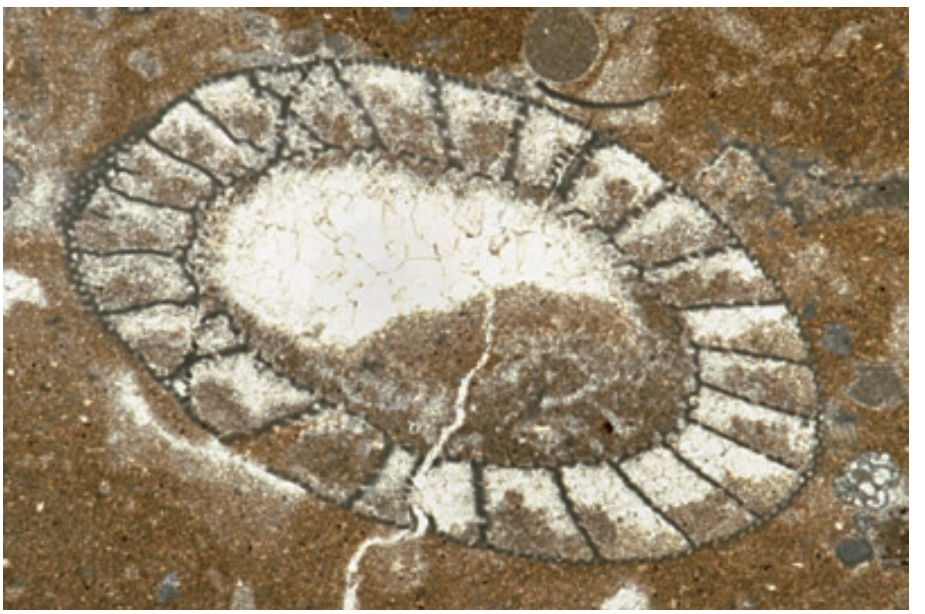

PPL, HA = 4.5 mm

Lo. Cambrian (Tommotian) Pestrotsvet Fm., southeastern Siberian Platform, Russia

An oblique cut through the lower part of an archaeocyath cup. The quite characteristic large pores that perforate inner and outer walls as well as septa are clearly visible here (producing a "dashed line" effect in the walls) and represent one of the best criteria for recognition of archaeocyath material. Sample from Noel P. James.

PPL, HA = 5.5 mm

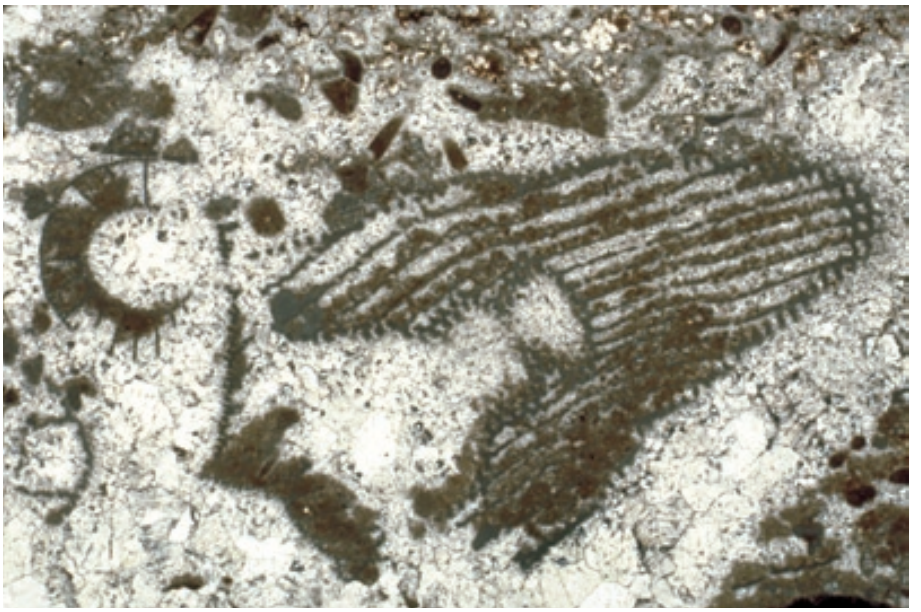

Lo. Cambrian (Tommotian) Pestrotsvet Fm., southeastern Siberian Platform, Russia

A slightly oblique longitudinal cut through an archaeocyath showing the U-shaped external morphology and the perforate internal septal partitions. Sample from Noel P. James.

PPL, HA = 16 mm

Cambrian Ajax Ls., Beltana, Australia

A magnified section through an archaeocyathan wall. The granular microcrystalline wall structure is typical for archaeocyaths. The inner and outer walls and the connecting structural supports (septa) are visible. The septa in this example do not show pores — recent studies have shown that archaeocyaths with pores were the dominant forms in settings with low-energy currents; forms with aporous septa predominated in areas with higher-energy currents (Savarese, 1992).

PPL, HA = 8 mm

Lo. Cambrian (Tommotian) Pestrotsvet Fm., southeastern Siberian Platform, Russia

Longitudinal and transverse cross-sections through two irregular archaeocyaths showing complex patterns of internal structure. Sample from Noel P. James.

PPL, HA = 12.5 mm

Lo. Cambrian, Labrador, Canada

A photomicrograph of an oblique cross-section of an archaeocyath skeleton (*Archaeocyathus atlanticus*) illustrating the complex internal structure and the laminated, finely crystalline nature of the skeleton. Photograph courtesy of Noel P. James.

PPL, AS, HA = 4.0 mm

Lo. Cambrian, Labrador, Canada

A photomicrograph of the archaeocyath *Metaldytes profundus*, illustrating its finely crystalline, somewhat laminated skeletal wall and dissepiments. Photograph courtesy of Noel P. James.

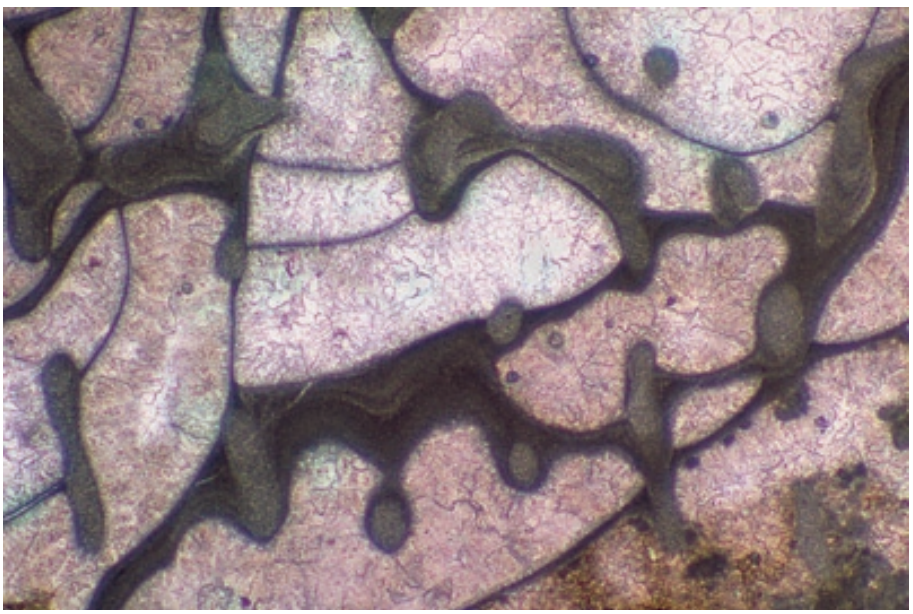

PPL, AS, HA = ~1.0 mm

SPONGES

Taxonomy and Age Range:

Phylum Porifera – Early Vendian (Precambrian) to Recent

Class Demospongea (including former Class Sclerospongea) — Cambrian-Recent
Class Hexactinellida — latest Precambrian (Vendian)-Recent
Class Calcarea — Cambrian-Recent

Sponge taxonomy is complex and contested; for the purposes of this book we will simply divide sponges into calcareous and siliceous forms because this grouping is petrographically convenient, even if it is not at all taxonomically accurate.

Environmental Implications:

A group characterized by great variability and adaptability. Sponges are/were generally sessile, benthic organisms; preserved forms are predominantly marine (freshwater sponges are fairly common, but almost never are preserved as fossils). Cryptic (cavity dwelling) sponges also are/were common and can be important components of reefal assemblages.

Most Paleozoic and early Mesozoic forms were shallow-shelf dwellers; later forms ranged from shallow- into deeper-water environments (but were rare in water depths greater than 1000 m).

Important reef components, especially in the Ordovician, Silurian, Devonian, Permian, Triassic and Jurassic.

Skeletal Mineralogy:

Different groups of sponges have/had skeletons composed entirely of spongin (a tough organic compound that readily decomposes after death), entirely of silica (opal-A) in the form of siliceous spicules, of both spongin and silica, or of calcium carbonate (in the form of spicules or as layered and cross-supported walls). In the calcareous groups, many were originally aragonitic, but calcitic forms (both low- and high-Mg calcite) also were (and still are) common.

Generally, demosponges and hexactinellids were siliceous; Calcarea and sclerosponges were calcareous.

Morphologic Features:

Although sponges are biologically simple, they were the first multicellular organism to advance from a colony of identical cells to one containing specialized cells fulfilling specific purposes. Sponges are sessile and most have simple, porous walls through which water is drawn and a large central cavity through which the water is expelled. Overall morphologies are highly variable, but common exterior shapes include cylindrical tubes, spheres, discoids, fans, as well as irregular, crustose or branching forms. Many are/were encrusters.

Overall sizes of both modern and ancient sponges range from a few mm to well over 1 m.

Individual spicules fall into two groups: large forms (megascleres) with diameters greater than 0.003 mm and microscleres with diameters typically 0.001 mm or less. These spicules can be simple single rays (monaxons), pointed at each end, or they can be more complex, multi-rayed forms (triaxon, tetraxon, hexaxon, and higher). Most siliceous spicules are formed with a central canal, although it is not always well preserved during diagenetic alteration; calcareous spicules do not have central canals.

Keys to Petrographic Recognition:

1. **Calcareous forms are found as intact or only slightly fragmented specimens. Most lack well defined external morphologies but do retain some internal fabric. Some have a well-defined central body cavity; many have irregular, meandering passages; most sphinctozoans (common in Carboniferous-Triassic strata) were segmented and had chambers irregularly clustered or arranged in series (like uniserial foraminifers, but with larger chambers). Structures are less consistently organized into regular patterns and hierarchical wall structures than corals, and generally lack the fibrous wall structures of bryozoans.**
2. **Siliceous forms are characterized by having spicule networks with intervening passages. Spicular forms commonly are disaggregated, forming spicule-rich sediment. Many well preserved specimens are associated with microbial encrustations that helped to hold the skeletal material together.**
3. **Disaggregated siliceous sponge spicules are recognizable by having a central canal (not always preserved) and distinctive monaxon or polyaxon shapes; original opaline silica normally converts to chert or chalcedony or is replaced by calcite.**

PHOTO SCALES AND ABBREVIATIONS ARE EXPLAINED IN THE BOOK'S INTRODUCTION

The generalized structure of a sponge

The basic body plan of a sponge is remarkably simple but effective. The cup- or vase-shaped wall is perforated by a series of pores that allow water inflow. Flagellate collar cells draw water through the wall where nutrients are filtered out and the waste water is expelled through the "chimney" at the top of the sponge. The walls are stiffened by embedded loose spicules or spicule networks (right). Adapted from Moore et al. (1952) and other sources.

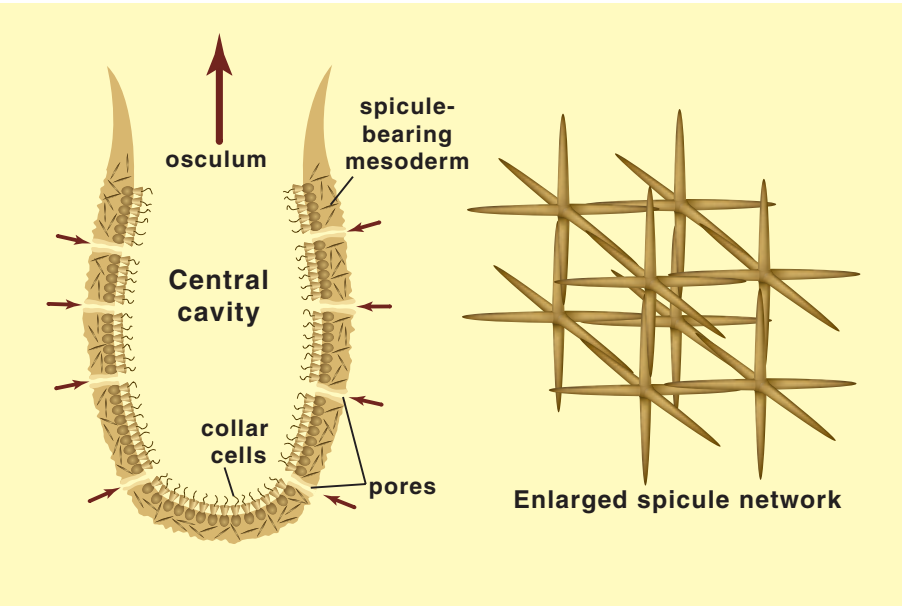

Wall morphologies of some segmented sponges

A diagrammatic view of the cross-sectional morphologies of some segmented (sphinctozoan) calcareous sponges from the Alpine Middle Triassic. Elongate to bulbous skeletons with well-defined growth forms, large serially-arranged chambers (with or without pores), and a variety of internal partitions characterize these sponges. Some forms also have a distinctive central cavity (right). Aporate sphinctozoans have a single or rare large openings in each chamber, whereas porate sphinctozoans have numerous small openings in each chamber. Sphinctozoan skeletons are either aragonite or high-Mg calcite and that is why they are often recrystallized or replaced. Adapted from Ott (1967).

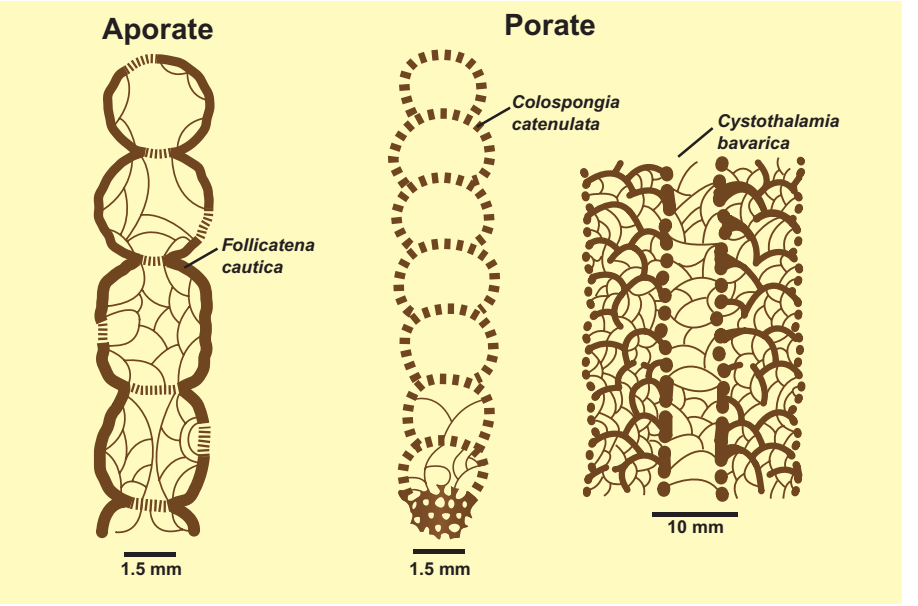

Permian (Leonardian-Lo. Guadalupian) Road Canyon Fm., Brewster Co., Texas

A chambered calcareous (sphinctozoan) sponge. Note the elongate shape and the serially arranged chambers that are much larger than those of uniserial foraminifers. Although there is poor preservation of wall fabric in this specimen, the connecting pores between the segment chambers remain clearly visible (compare with the diagram above).

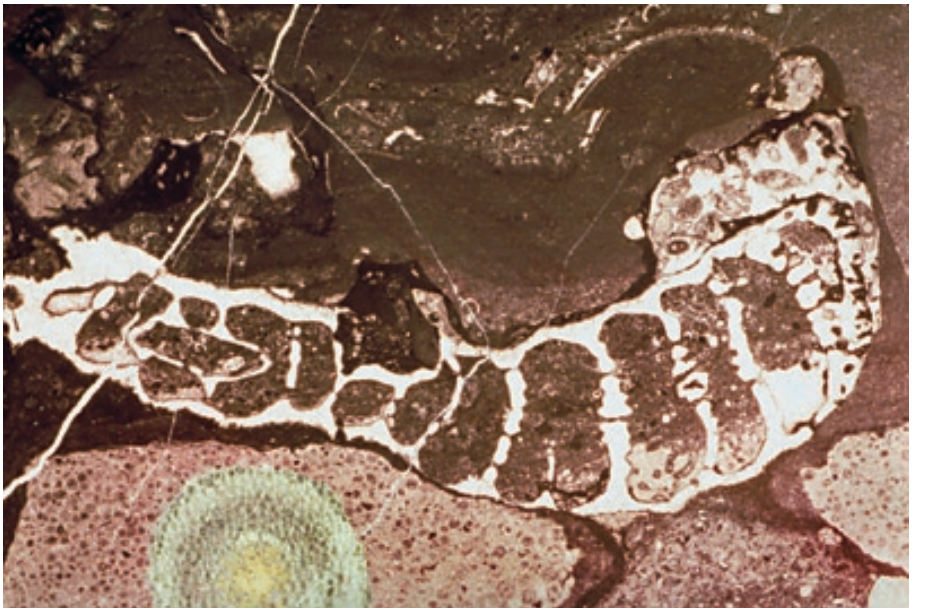

PPL, AS, HA = 15.5 mm

Up. Permian (Guadalupian) Cherry Canyon Fm., Getaway Ls. Mbr., Culberson Co., Texas

A chambered calcareous sponge with silica (chert and chalcedony) replacement of its walls and much of the surrounding sediment. The overall uniserially chambered morphology enables recognition as a calcareous sponge, but detailed (species level) identification generally requires whole specimen examination. Selective silica replacement of sponges often helps in identification of sponges, because it allows acid dissolution of matrix material and extraction of the sponge remains. Indeed, some of the finest Permo-Carboniferous sponge collections come from partially silicified strata.

PPL, HA = 12.5 mm

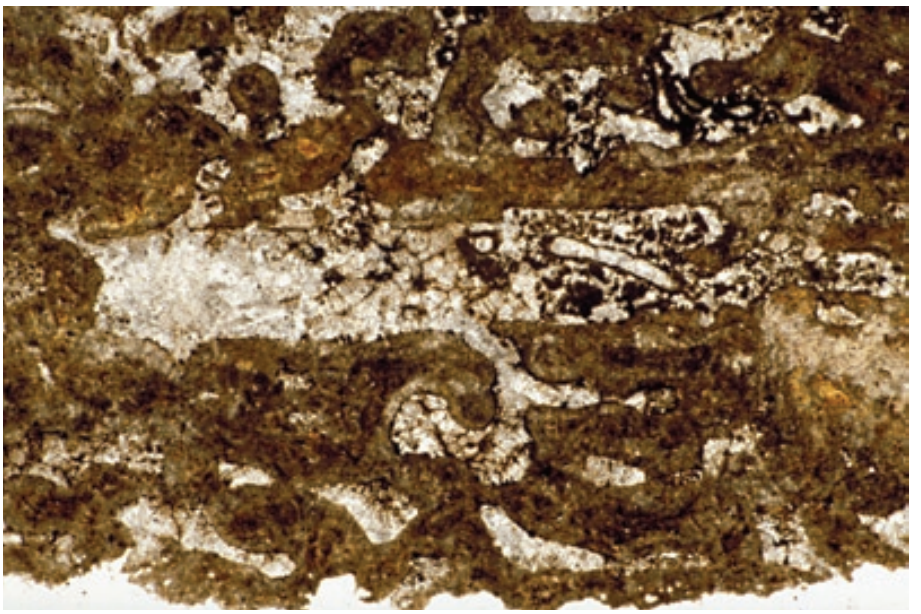

Pennsylvanian Graford Fm., Wise Co., Texas

A moderately well preserved calcareous sponge, *Maeandrostia* sp.(?). Note the dark brown coloration of the skeletal walls due to incorporated organic matter, the labyrinthine pore structure, and the central cavity that was intersected in this longitudinal section.

PPL, HA = 10 mm

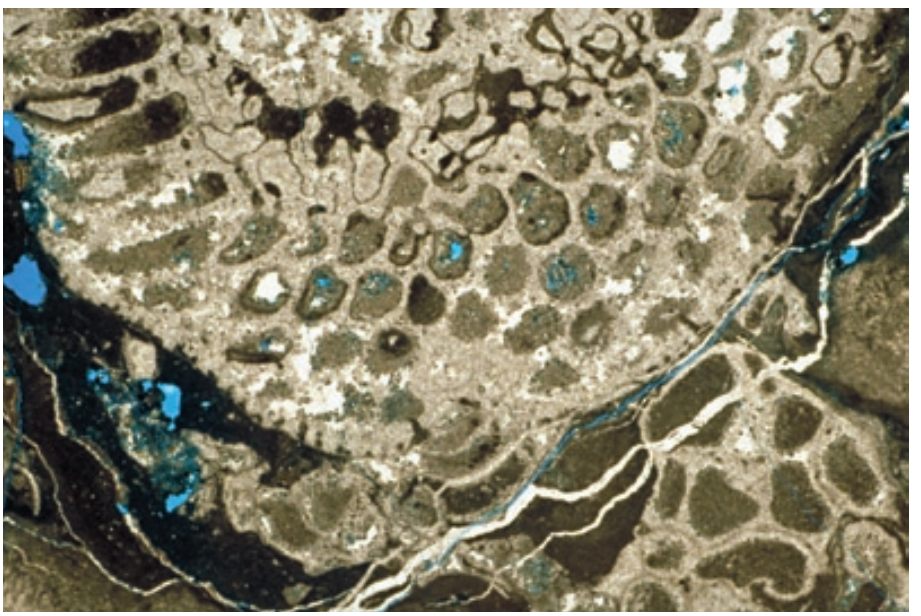

Up. Permian (Guadalupian) Capitan Fm., Culberson Co., Texas

A large, chambered calcareous sponge forming part of the framework of this world-renowned reef complex. Note the preservation of marginal pores and a variety of chambers despite poor preservation of details of the wall structure. Infiltration or precipitation (perhaps microbially influenced) of micritic material in cavities greatly enhanced the preservation of the general skeletal outlines of this sponge.

PPL, BSE, HA = 12.5 mm

Up. Permian (Guadalupian) Capitan Fm., subsurface, Eddy Co., New Mexico

Another calcareous sponge from the Capitan reef. In this case, only the margins of the sponge chambers were selectively dolomitized, probably quite early in the history of this deposit. The rest of the sponge was leached, and the resulting pores were extensively filled with anhydrite cement (now hydrated to gypsum, the large white patches in this photograph).

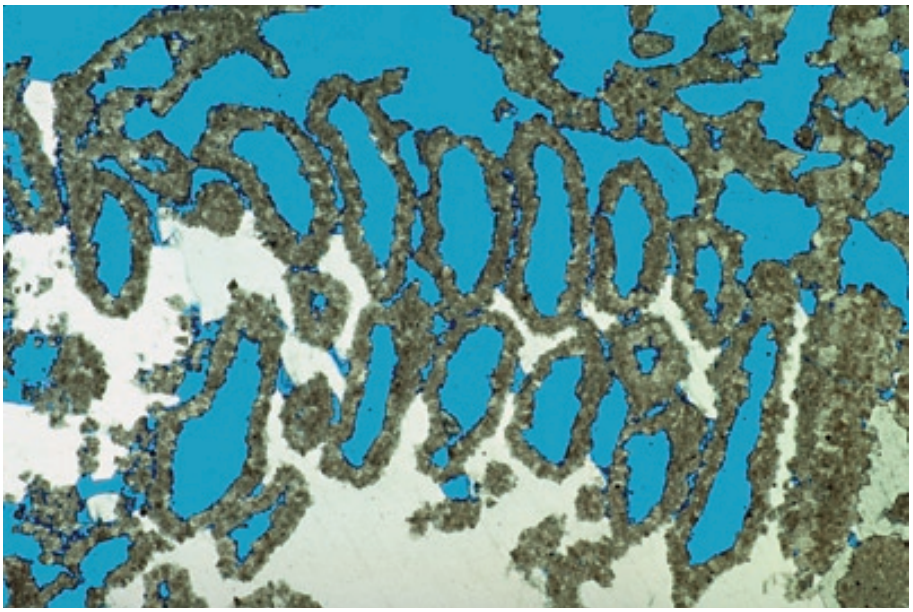

PPL, BSE, HA = 11 mm

Up. Permian Middle reef complex, Djebel Tebaga, Tunisia

Calcareous sponges were major framework components of Permian and Triassic reefs, in part because of the demise or decline of many competitive groups. These finger-like calcareous sponges from the reefs of Tunisia show labyrinthine, chambered walls and relatively distinct central cavities. The skeletal structure here too is visible largely due to infill or precipitation of micritic material.

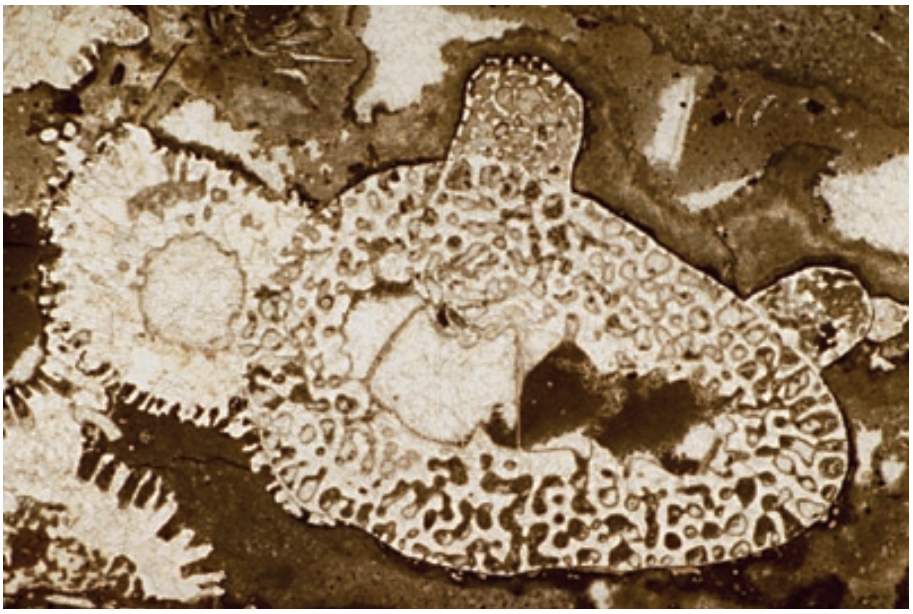

PPL, HA = 11 mm

Up. Permian Middle reef complex, Djebel Tebaga, Tunisia

Another framework builder in the Tunisian reefs, this calcareous sponge has geopetal micrite fills of its chambers and a well preserved network of labyrinthine or maze-like pores in its walls.

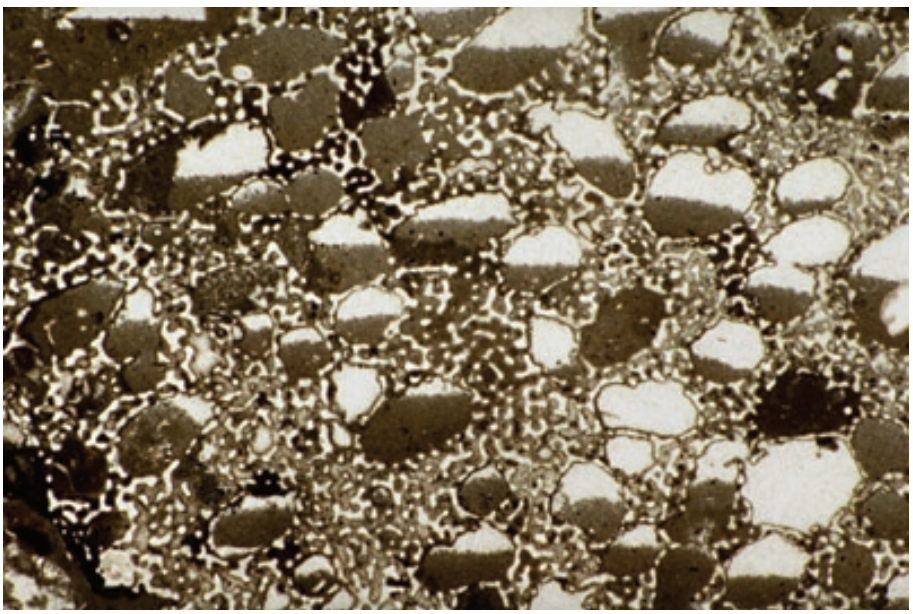

PPL, HA = 8.0 mm

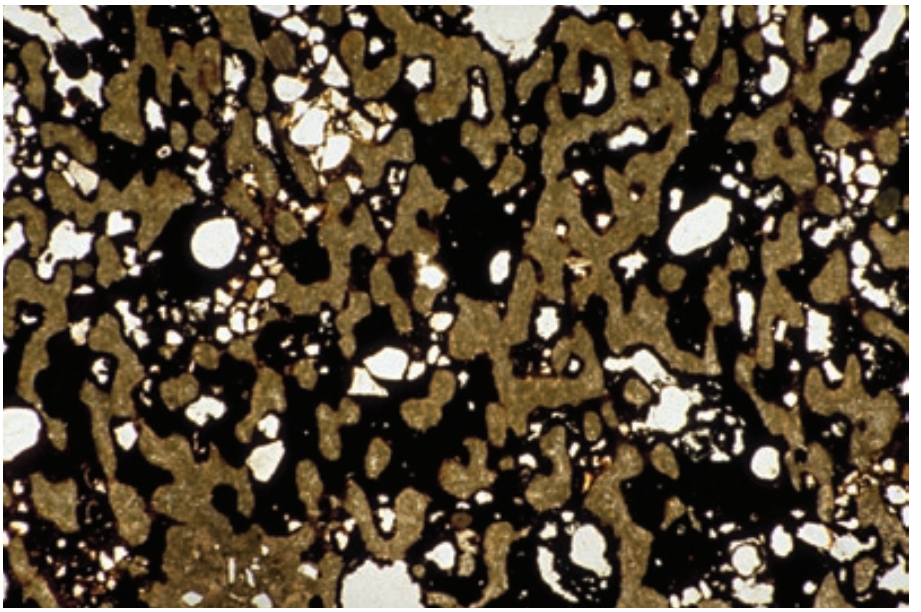

Up. Cretaceous (Aptian) Greensand (reworked into Pliocene Lenham Beds), Folkestone, Kent, England, U.K.

A small, vase-like calcareous sponge (a member of the Calcarea), probably *Raphidonema faringdonensis*, partially filled with ferruginous material during weathering and resedimentation into a sinkhole. Note the meandering, cavernous wall structure that contains spicules visible at higher magnifications.

PPL, HA = 6.0 mm

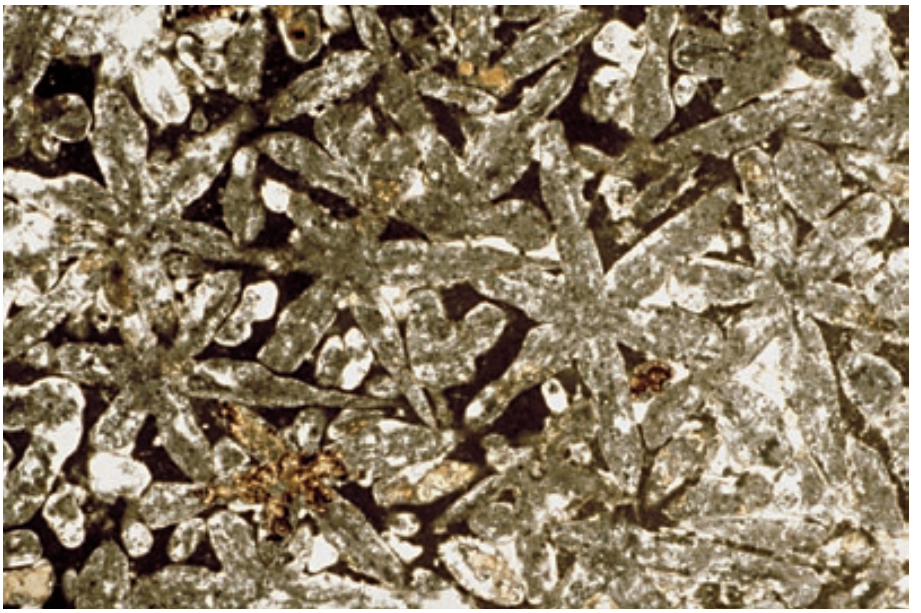

Up. Silurian Brownsport Fm., Perry Co., Tennessee

The wall structure of this bowl-shaped, calcareous heteractinellid sponge, *Astraeospongium meniscum*, shows an interlocking fabric of in-situ, unfused, octactine spicules (eight-rayed spicules with six rays visible in this plane of section). These sponges were adapted to open marine, shallow water, soft bottom environments with high nutrient supplies (Mehl and Reitner, 1996). Sponges of this genus range from at least the Late Ordovician to Late Devonian.

PPL, HA = 14.5 mm

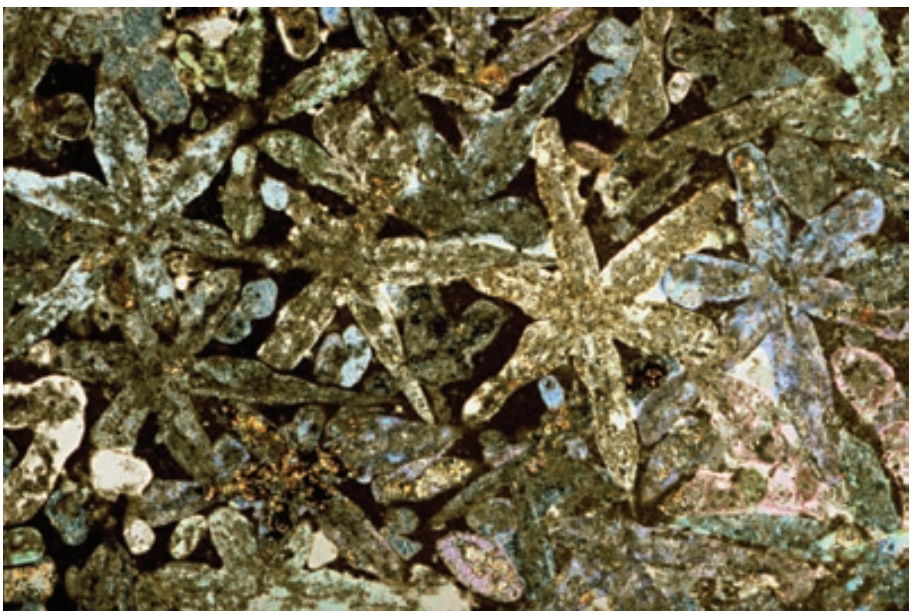

Up. Silurian Brownsport Fm., Perry Co., Tennessee

A cross-polarized light view of the same area shown in the photograph above. The extinction patterns show that each of the spicules acts optically as a single crystal of calcite. These originally calcareous sponge spicules, unlike siliceous ones, do not have a central canal.

XPL, HA = 14.5 mm

Recent sediment, Florida Keys, Monroe Co., Florida

A cross-polarized light view of the wall structure of a modern sponge with a relatively intact network of triaxon calcareous spicules. These spicules are not fused together, but nevertheless serve to stiffen the tissue of the sponge. In plane-polarized light, these spicules are colorless and essentially transparent. Some disturbance of the fabric and breakage of spicules occurred during sampling and sectioning.

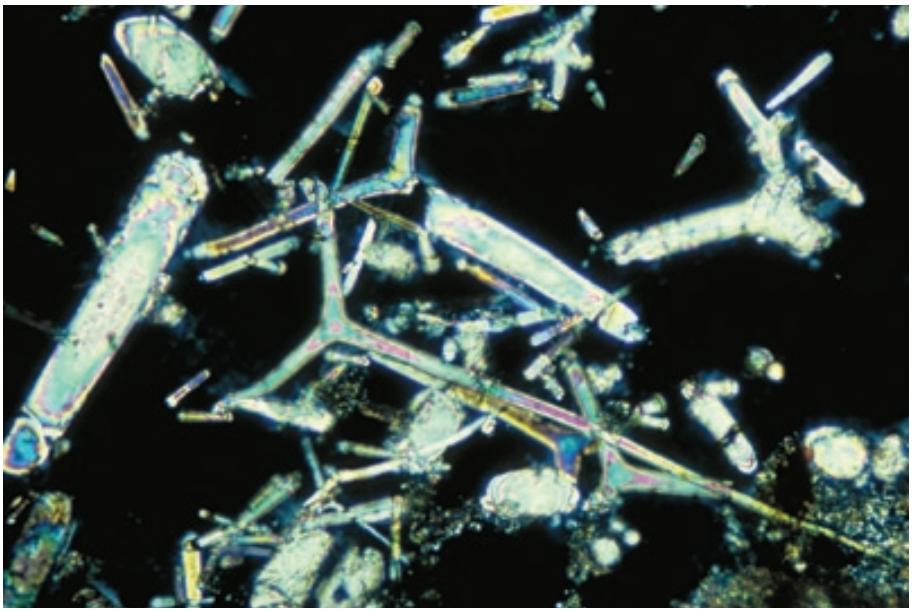

XPL, HA = 0.6 mm

Recent sediment, Belize

An SEM image of a modern siliceous sponge showing smooth, interlocked, diversely oriented opaline spicules. Upon death of the sponge, these spicules may be widely dispersed; loose spicules are commonly found in modern sediments from both shallow- and deep-water environments.

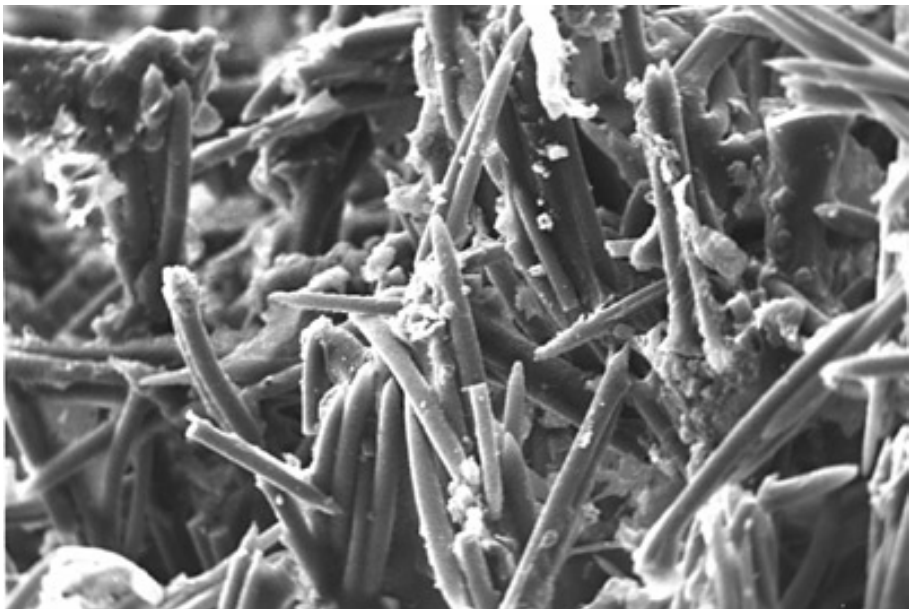

SEM, HA = 380 μm

Lo. Ordovician (Canadian) Arbuckle Gp., West Spring Creek Ls., Murray Co., Oklahoma

A view of a sponge with a well-preserved multi-axoned spicule network embedded in its wall structure. Note the difference between these thin and isolated spicule remains and the more robust, continuous walls of the calcareous sponges illustrated earlier.

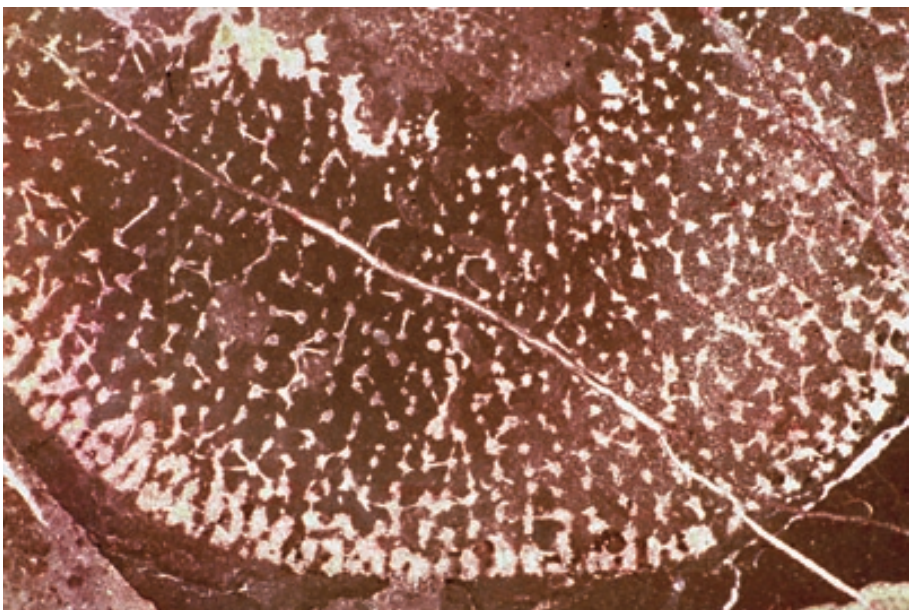

PPL, AFeS, HA = 11 mm

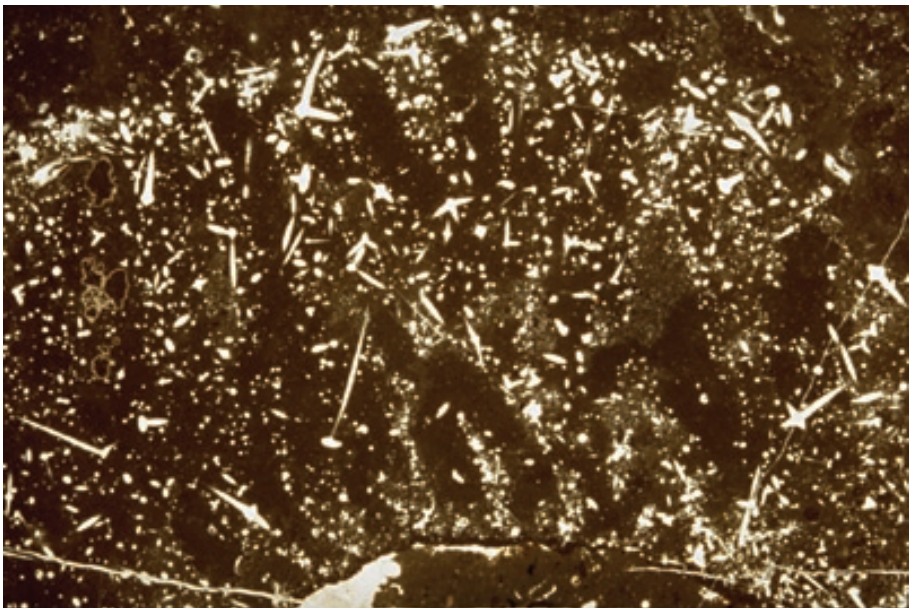

Lo. Jurassic (mid. Liassic) limestone, Central High Atlas region, Morocco

Exceptional wall preservation of a sponge showing an in-place spicule network and intervening pores passing through the wall (later infilled with dark micrite). The exterior of the sponge is at the top of this photograph and the well-defined central cavity is at the bottom. Note the variations in size and shape of spicules within a single sponge.

PPL, HA = 25 mm

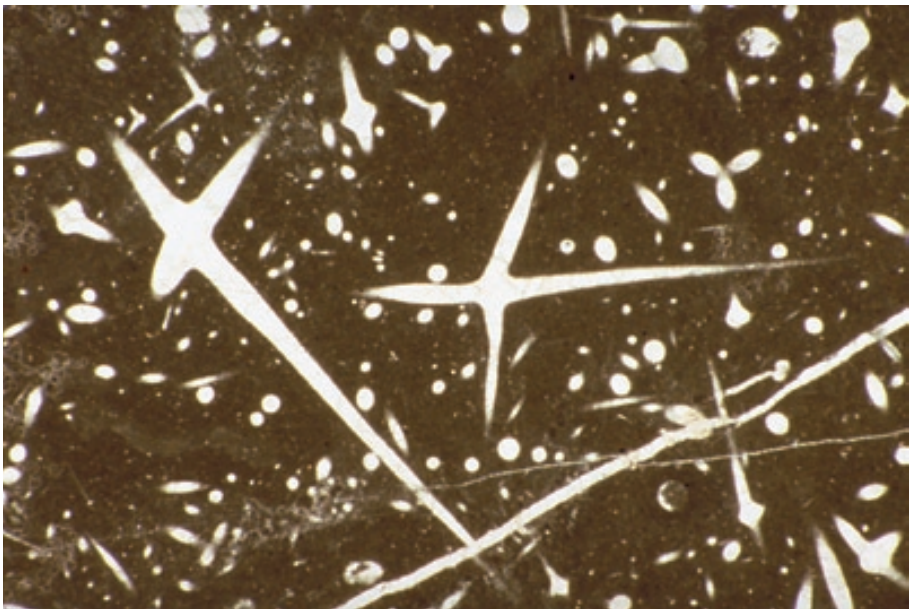

Lo. Jurassic (mid. Liassic) limestone, Central High Atlas region, Morocco

A magnified wall structure view of the sponge shown in the previous image. The now-calcitic multi-axoned spicules embedded in the walls compose a loose meshwork of unfused rigid elements that serve to strengthen the porous, predominantly organic spongin material that constitutes the main part of the wall

PPL, HA = 5.5 mm

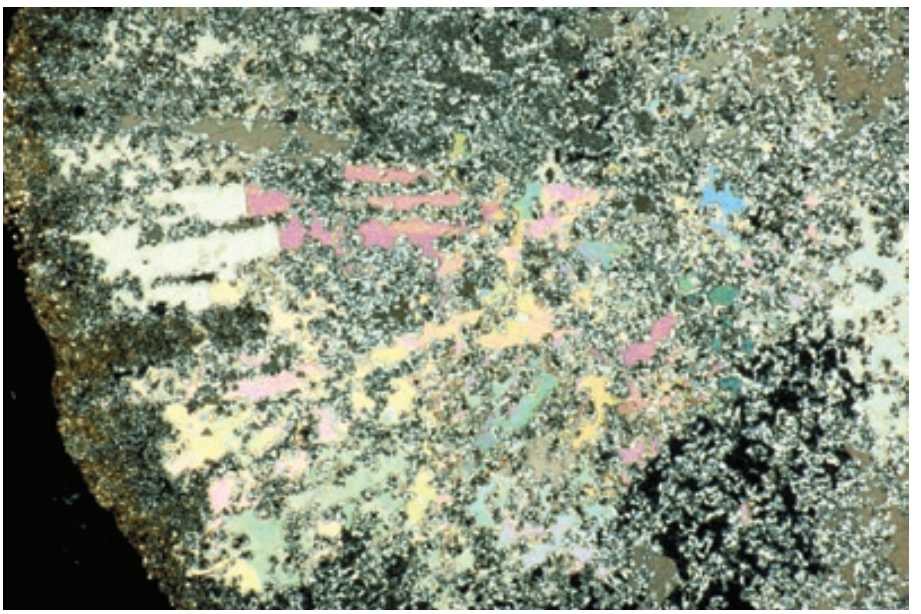

Devonian Onondaga Ls., Ontario, Canada

A demosponge — *Microspongia* [=*Hindia*] *sphaeroidalis*. This specimen shows chertified walls surrounding large, labyrinthine pores filled with coarsely crystalline (almost poikilotopic) calcite. The original opaline silica of siliceous sponge spicules is normally dissolved and can reprecipitate within the walls as more stable quartz (chert, chalcedony, or megaquartz).

XPL, HA = 3.5 mm

Pennsylvanian Marble Falls Ls., Burnet Co., Texas

Longitudinal and transverse sections through a multitude of siliceous sponge spicules in a shelf limestone. Some spicules have been replaced by calcite, but almost all still show the central canal characteristic of most, but not all, sponge spicules that were originally siliceous. All appear to be monaxon spicules (single, hollow rods tapering to a point at each end).

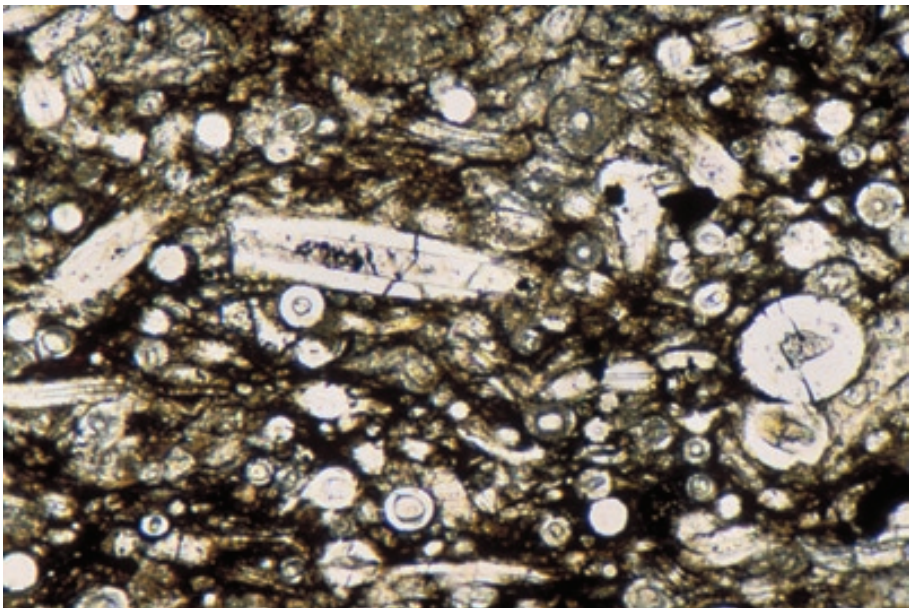

PPL, HA = 0.6 mm

Lo. Pennsylvanian Dimple Ls., Marathon Mountains, west Texas

A moderately deep-water shelf limestone containing abundant siliceous sponge spicules. These monaxon spicules were originally composed of opaline silica that was later replaced, partially by calcite and partially by chert. Despite the replacement, most grains still show the central canal characteristic of most originally-siliceous sponge spicules. Sample from Robert Laury.

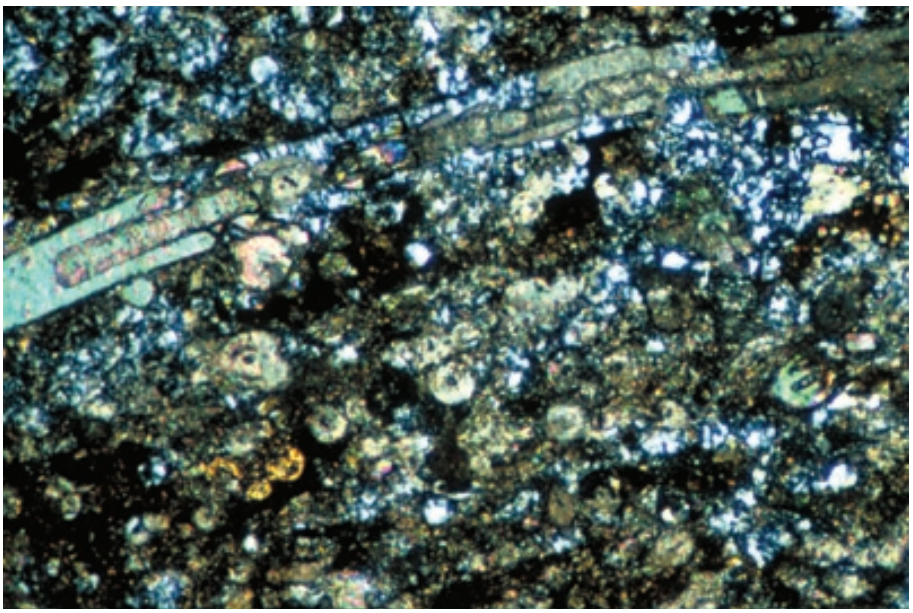

XPL, HA = 1.6 mm

Lo. Pennsylvanian limestone, Mora Co., New Mexico

Numerous leached siliceous monaxon sponge spicules (one longitudinal section and several in transverse section) in a dolomite. The original opaline silica was leached, and the moldic voids were filled, probably much later, with highly ferroan calcite (stained dark blue). In the absence of preserved central canals, recognition of the spicules in longitudinal or oblique sections is clearly easier than for those in transverse sections.

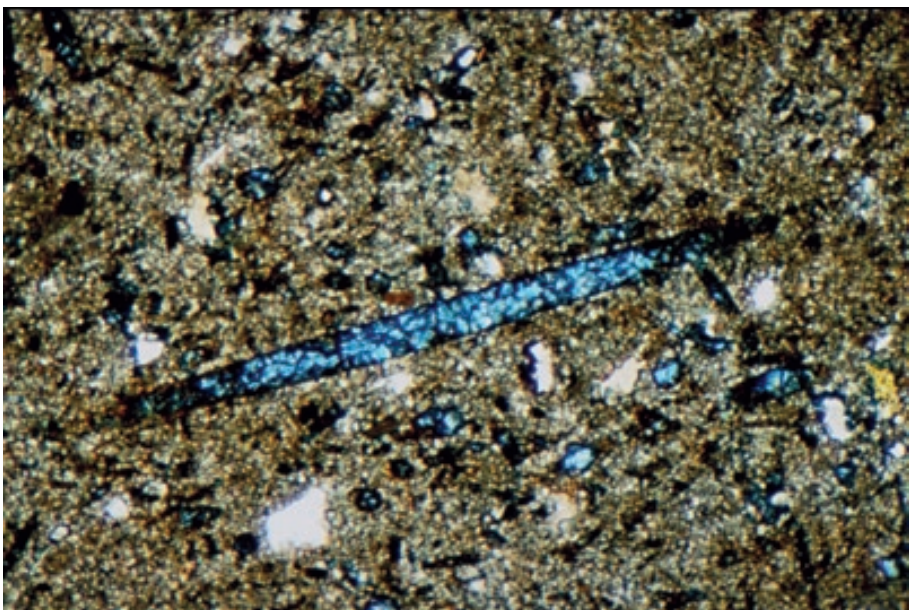

PPL, AFeS, HA = 2.0 mm

STROMATOPOROIDS

Taxonomy and Age Range:

A group with uncertain affinities once grouped with coelenterates (and still thought by a few to be coelenterates), but now widely considered to be more closely related to sponges (probably the demosponges).

Phylum Porifera, Class Stromatoporoida — Early Ordovician to Late Devonian; Cretaceous (Cenozoic?)

True stromatoporoids were extremely common from Ordovician to Devonian. All later forms assigned to the stromatoporoids are thought to have resulted from convergent evolution toward the stromatoporoid skeletal morphology (Stearn et al., 1999). Post-Devonian stromatoporoids remain in a state of nomenclatural uncertainty.

Environmental Implications:

Exclusively marine organisms that generally favored clear-water, well oxygenated environments; widespread in shelf and high-energy shelf margin settings. Mesozoic forms found mainly in warm-water areas.

Stromatoporoids were major contributors to reefs (many of which are or were hydrocarbon reservoirs) in the time interval from the Middle Ordovician to the Late Devonian (and again in the uncertainly assigned forms of the Jurassic to Early Cretaceous time interval).

Branching, finger-like forms were widespread in the Devonian where they commonly formed biostromes in back-reef and lagoonal settings.

Skeletal Mineralogy:

Primarily calcitic; but some groups apparently were aragonitic.

Morphologic Features:

Stromatoporoid skeletal remains range in size from less than a centimeter to more than a meter. Most had massive, sheet-like, encrusting forms, but globular and branching, finger-like forms also were common.

Stromatoporoids have mamelons (protuberances) of varying size that give the surface a bumpy or knobby texture.

Stromatoporoids were ecophenotypic, with the same species exhibiting different growth morphologies due to environmental factors (e.g., discoid or encrusting, laminar forms developed in high energy settings and more delicate branching forms developed in lower energy settings).

Keys to Petrographic Recognition:

1. **Most stromatoporoid skeletons are characterized by a cellular or latticework pattern composed of horizontal laminae and vertical pillars that partially enclose galleries. In some cases, either the laminae or pillars are more prominent and impart a dominant grain to the pattern. Some forms have pillars that continue through several laminae forming a very regular latticework; in other groups, the pillars are irregularly placed and do not extend through the laminae, yielding a more irregular and open latticework of galleries. Overall, the presence of pillars, rather than solid walls, yields more open (or partially open) look to galleries than is found in latticework of red algae or foraminifers. In many cases, the stromatoporoid latticework is warped in gentle undulations.**
2. **Stromatoporoid skeletal material generally has a pale brownish color due to the incorporation of organic matter in the skeletal carbonate.**
3. **Stromatoporoid wall structures have been described as compact, cellular, microreticulate (containing three subtypes: orthoreticular, acosmoreticular, and clinoreticular), melanospheric, fibrous, tubulate, striated, and ordinicellular (see Lecompte, 1956; and especially Stearn et al., 1999).**
4. **Some stromatoporoids (see diagram at top of next page) have "astrorhizae" composed of astrorhizal canals that are mainly horizontally oriented. They can be stacked vertically into an astrorhizal column. Mamelon columns can also be developed. Astrorhizae can occur without mamelons and mamelons can occur without astrorhizae, but in the majority of cases the occur together.**
5. **Large colonial forms help to differentiate stromatoporoids from foraminifers; very regular structure, presence of astrorhizae and absence of spicules help to differentiate stromatoporoids from other groups of sponges; the latticework of stromatoporoids is generally coarser and more open-chambered than the cellular structure of red algae.**

Morphology and structure of a typical Paleozoic stromatoporoid

Diagrammatic representation of the generalized structural features of a massive, laminated, mid-Paleozoic stromatoporoid. The open latticework structure results from the intersection of vertical pillars and horizontal laminae. The thicker laminae (termed latilamina) add emphasis to the horizontal fabric of this stromatoporoid. Mamelons, the knobby protrusions on the surface, are tied into the structure by a series of canals or tubes (termed astrorhizae). Adapted from Moore et al. (1952; citation given in reference list at end of book introduction) and others.

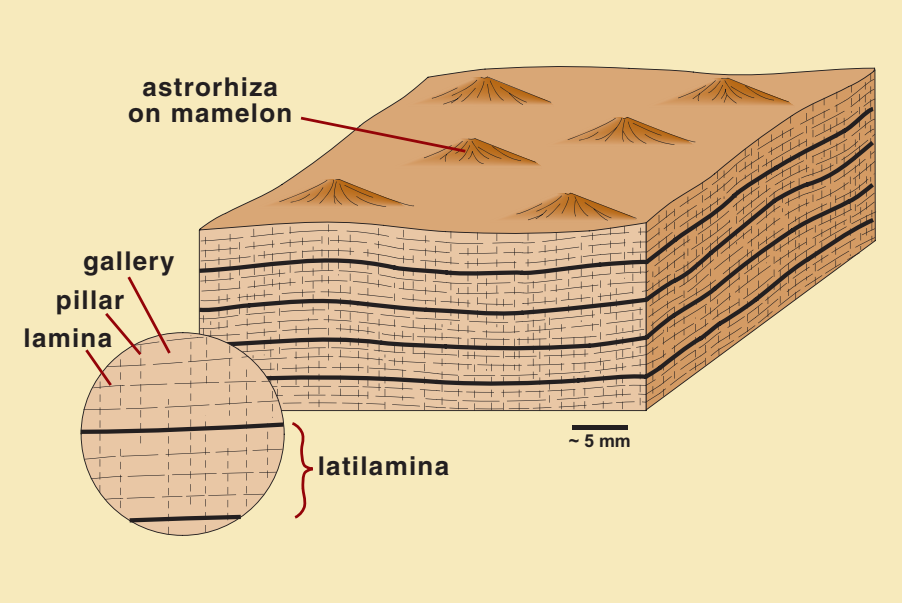

Mid. Ordovician Black River Gp., Lowville Fm., Kingston, Ontario, Canada

An early stromatoporoid — *Stromatocerium* sp. The skeleton shows strong development of vertical pillars and large, horizontally elongate galleries. The pillars have undergone substantial neomorphism. Sample from Noel P. James.

PPL, AFeS, HA = 5.2 mm

Up. Devonian Lime Creek Fm., Cerro Gordo Co., Iowa

A laminar stromatoporoid, *Stromatopora incrustans*, with well preserved, and very characteristic, latticework fabric with mid-scale reticulate microstructure. The horizontal laminae and vertical pillars of the latticework are clearly visible, as are the varied gallery shapes. Note the very large astrorhizal canals punctuating the skeletal structure. The excellent structural preservation implies originally calcitic mineralogy.

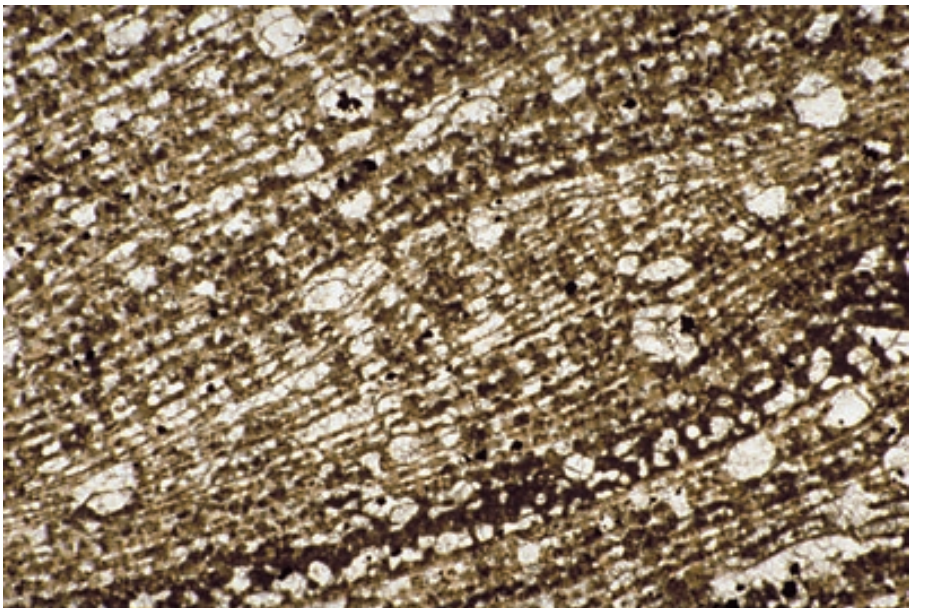

PPL, HA = 6 mm

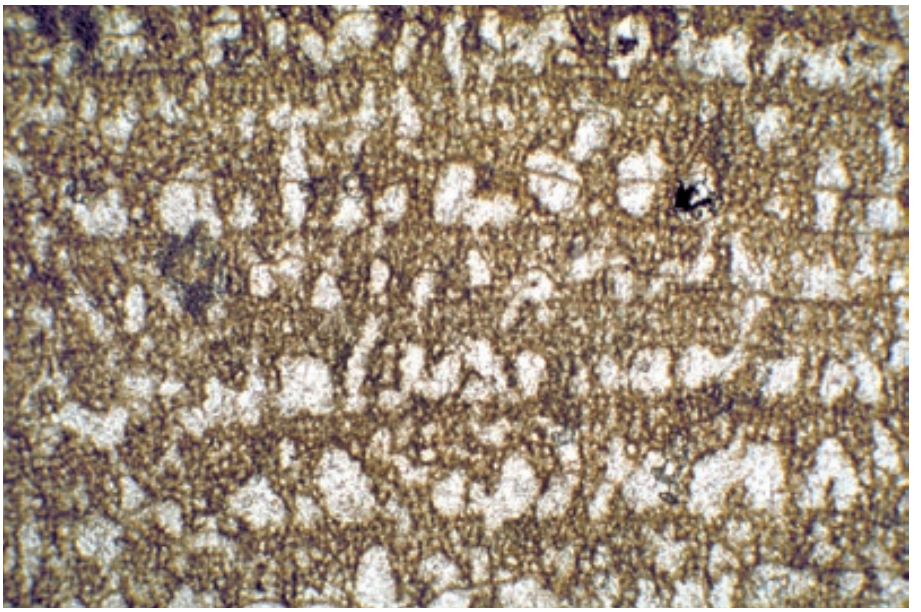

Up. Silurian Rondout Fm., Glasco Mbr., Ulster Co., New York

A detailed view of *Habrostroma kaugatomicum.* The laminae and pillars are composed of acosmoreticular microstructure. The presence of micropillars and microcolliculi are most apparent in tangential section rather than in this longitudinal section. Photograph courtesy of Carl W. Stock.

PPL, HA = 3.4 mm

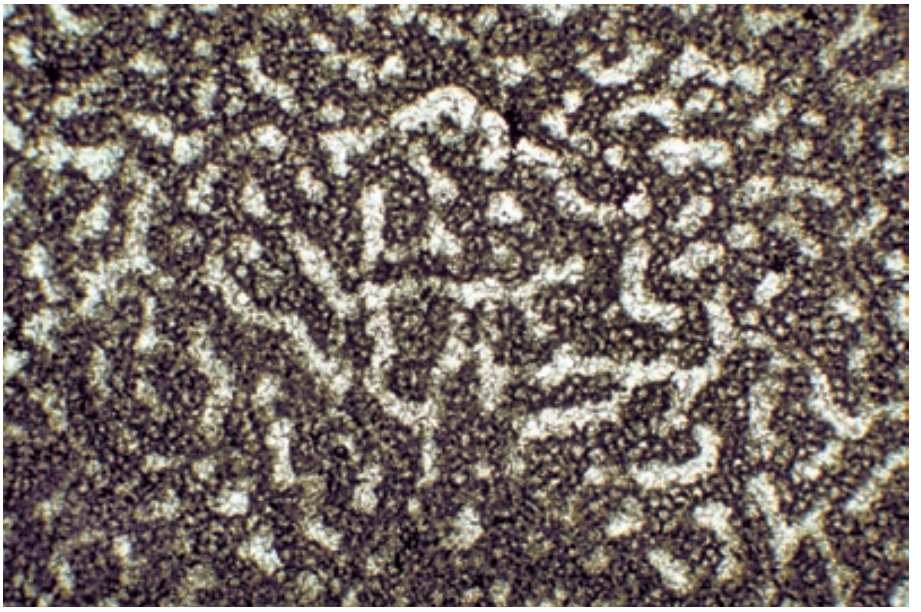

Mid. Devonian, Columbus Ls., Kelleys Island, Ohio

A tangential section of a stromatoporoid. The large, long, thick pillars of *Syringostroma* display clinoreticular microstructure. This is best seen in the pillars to the right. Photograph courtesy of Carl W. Stock.

PPL, HA = 3.4 mm

Up. Devonian (Frasnian) limestone, Holy Cross Mountains, Poland

A laminar stromatoporoid showing the pillar and lamina structure and gallery patterns typical of this group. The folds or undulations are common in these knobby to bulbous, encrusting forms. Such stromatoporoids are common encrusters of other organisms and thus are major contributors to the binding of reef constituents as well as the generation of reef frameworks.

PPL, AS, HA = 11 mm

Up. Devonian Shell Rock Fm., Nora Mbr., Cerro Gordo Co., Iowa

This vertical section through the skeleton of *Actinostroma expansum* is composed of long pillars that are connected by colliculi. The colliculi are horizontally aligned, giving the impression of continuous laminae in longitudinal thin sections; however, transverse (tangential) thin sections reveal the "hexactinellid" pattern formed by the colliculi where they radiate from pillars (colliculi are horizontal rods protruding from pillars). *Actinostroma* has compact microstructure. Photograph courtesy of Carl W. Stock.

PPL, HA = 9.0 mm

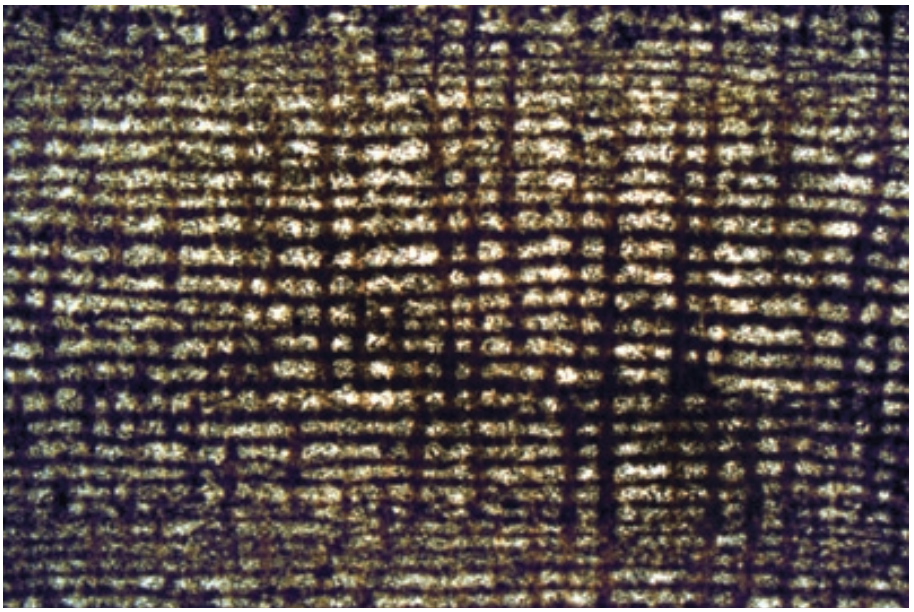

Up. Devonian (Frasnian) Pillara Ls., Canning Basin, Western Australia

These finger-like stromatoporoids (*Idiostroma* sp.) have well preserved radial, chambered structure. The stromatoporoids are encrusted by *Renalcis* colonial calcimicrobial growths, a common association in Devonian strata.

PPL, HA = 23 mm

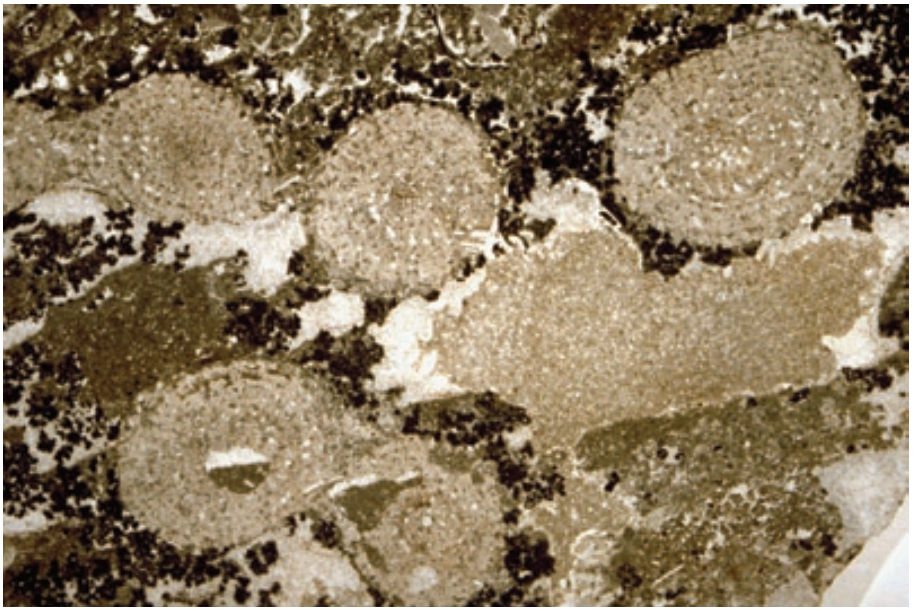

Up. Devonian Shell Rock Fm., Nora Mbr., Cerro Gordo Co., Iowa

Here several specimens of *Amphipora* are surrounded by an organic-rich matrix. The skeletons are small and twig-like. Both longitudinal sections and cross sections can be seen here. The internal skeletal structure is irregular, but in some specimens an axial canal with a circular cross section is developed; several of the upper specimens display this structure (for example, at arrowhead). Photograph and caption courtesy of Carl W. Stock.

PPL, HA = 11 mm

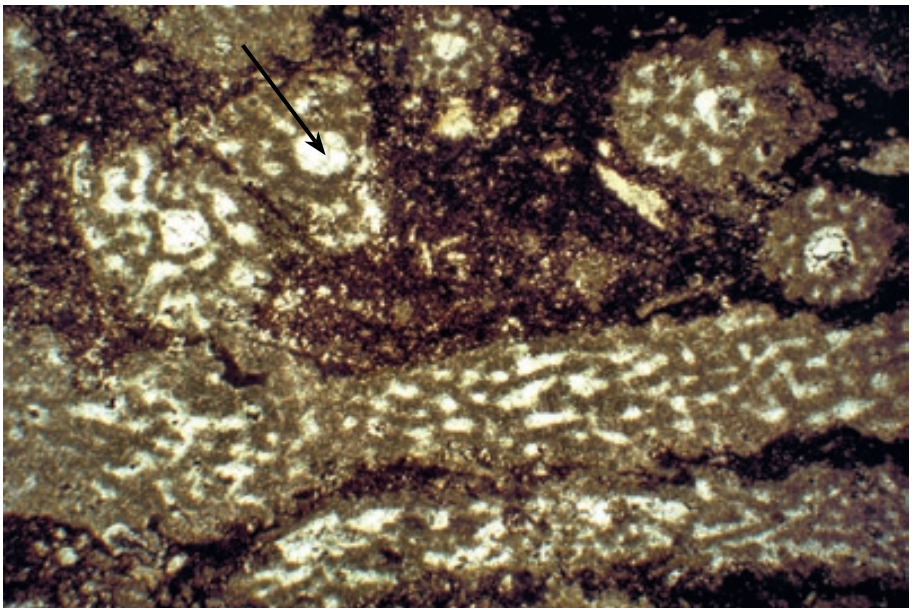

Cited References and Additional Information Sources

Aldinger, H., 1968, Ecology of algal-sponge-reefs in the Upper Jurassic of the Schwäbische Alb, Germany, *in* G. Müller, and G. M. Friedman, eds., Recent Developments in Carbonate Sedimentology in Central Europe: New York, Springer-Verlag, p. 250-253.

Bergquist, P. R., 1978, Sponges: Berkeley, CA, University of California Press, 268 p.

Brunton, F. R., and O. A. Dixon, 1994, Siliceous sponge-microbe biotic associations and their recurrence through the Phanerozoic as reef mound constructors: Palaios, v. 9, p. 370-387.

Debrenne, F., and N. P. James, 1981, Reef-associated archaeocyathans from the Lower Cambrian of Labrador and Newfoundland: Palaeontology, v. 24, p. 343-378.

Debrenne, F., and Reitner, J., 2001, Sponges, cnidarians and ctenophores, *in* A. Yu. Zhuravlev, and R. Riding, eds., The Ecology of the Cambrian Radiation: New York, Columbia University Press, p. 301-325.

Debrenne, F., and J. Vacelet, 1984, Archaeocyatha: is the sponge model consistent with their structural organization?: Palaeontographica Americana, v. 54, p. 358-369.

De Laubenfels, M. W., 1955, Porifera, *in* R. C. Moore, ed., Treatise on Invertebrate Paleontology, Part E: Geological Society of America and University of Kansas Press, E21-E122.

Flügel, E., J. K. Ribgy, and B. Senowbari-Daryan, 1996, Inozoid sponges from Upper Permian of Djebel Tebaga, Tunisia, *in* J. Reitner, F. Neuweiler, and F. Gunkel, eds., Global and regional controls on biogenic sedimentation, Göttinger Arbeiten zur Geologie und Paläontologie [Geol. Inst., Univ. Göttingen] Nr. SB2, p. 313-315.

Galloway, J. J., 1957, Structure and classification of Stromatoporoidea: Bulletin of American Paleontology, v. 37, no. 164, p. 341-480.

Hartman, W. D., 1977, Sponges as reef builders and shapers, *in* S. H. Frost, M. P. Weiss, and J. B. Saunders, eds., Reefs and Related Carbonates — Ecology and Sedimentology: Tulsa, OK, American Association of Petroleum Geologists Studies in Geology No. 4, p. 127-134.

Hartman, W. D., J. W. Wendt, and F. Wiedenmayer, eds., 1980, Living and Fossil Sponges — Notes for a Short Course: Miami, FL, University of Miami, Comparative Sedimentology Laboratory, 274 p.

Hill, D., 1965, Archaeocyatha from Antarctica and a review of the phylum: Trans-Antarctic Expedition 1955-1958, Scientific Report (Geology No. 3), v. 10, p. 1-151.

Hill, D., 1972, Archaeocyatha, *in* C. Teichert, ed., Treatise on Invertebrate Paleontology Part E [2nd edition]: Geological Society of America and University of Kansas Press, p. 2-158.

Kershaw, S., 1984, Patterns of stromatoporoid growth in level bottom environments: Palaeontology, v. 27, p. 113-130.

Kershaw, S., 1998, The application of stromatoporoid paleobiology in paleoenvironmental analysis: Palaeontology, v. 41, p. 509-544.

Knight, J. B., et al., 1960, Mollusca 1, *in* R. C. Moore, ed., Treatise on Invertebrate Paleontology Part I: Geological Society of America and University of Kansas Press, 351 p.

Kruse, P. D., and F. Debrenne, 1989, Review of archaeocyathan microstructure, *in* P. A. Jell, and J. W. Pickett, eds., Proceedings of the Fifth International Symposium on Fossil Cnidaria including Archaeocyatha and Spongiomorphs, Memoirs of the Association of Australasian Palaeontology Nr. 8, p. 133-141.

Lecompte, M., 1956, Stromatoporoidea, *in* R. C. Moore, ed., Treatise on Invertebrate Paleontology, Part F, Coelenterata: Geological Society of America and University of Kansas Press, p. F107-F144.

Mastandrea, A., and F. Russo, 1995, Microstructure and diagenesis of calcified demosponges from the Upper Triassic of the northeastern Dolomites (Italy): Journal of Paleontology, v. 69, p. 416-431.

Mehl, D., and J. Reitner, 1996, Observations on *Astraeospongium meniscum* (Roemer, 1848) from the Silurian of western Tennessee: constructional morphology and palaeobiology of the Astraeospongiidae (Calcarea, Heteractinellidae): Berliner geowissenschaftliche Abhandlungen, v. 18, p. 243-255.

Okulitch, V. J., 1955, Archaeocyatha, *in* R. C. Moore, ed., Treatise on Invertebrate Paleontology, Part F: Geological Society of America and University of Kansas Press, p. E1-E20.

Ott, E., 1967, Segmentierte Kalkschwämme (Sphinctozoa) aus der alpinen Mitteltrias und ihre Bedeutung als Riffbildner im Wettersteinkalk: Abhandlungen Bayerische Akademie der Wissenschaften, Mathematisch-Naturwissenschaftliche Klasse, Neue Folge, v. 131, p. 1-96.

Reitner, J., and H. Keupp, eds., 1991, Fossil and Recent Sponges: Berlin, Springer-Verlag, 595 p.

Rigby, J. K., 1971, Sponges and reefs and related facies through time, *in* J. K. Rigby, and N. D. Newell, eds., Reef Organisms Through Time, Symposium Volume: Chicago, IL, Proceedings of the North American Paleontological Convention, Part J, p. 1374-1388.

Rigby, J. K., 1987, Phylum Porifera, *in* R. S. Boardman, A. H. Cheetham, and A. J. Rowell, Fossil Invertebrates: Palo Alto, CA, Blackwell Scientific Publications, p. 116-139.

Rigby, J. K., J. Fan, and W. Zhang, 1989, Sphinctozoan sponges from the Permian reefs of South China: Journal of Paleontology, v. 63, p. 404-439.

Rigby, J. K., J. Fan, and W. Zhang, 1989, Inozoan calcareous Porifera from the Permian reefs of China: Journal of Paleontology, v. 63, p. 778-799.

Rigby, J. K., and Gangloff, R. A., 1987, Phylum Archaeocyatha, *in* R. S. Boardman, A. H. Cheetham, and A. J. Rowell, eds., Fossil Invertebrates: Palo Alto CA, Blackwell Scientific, p. 107-115.

Savarese, M., 1992, Functional analysis of archaeocyathan skeletal morphology and its paleobiological implications: Paleobiology, v. 18, p. 464-480.

Senowbari-Daryan, B., 1991, "Sphinctozoa": an overview, *in* J. Reitner, and H. Keupp, eds., Fossil and Recent Sponges: Berlin, Springer-Verlag, p. 224-241.

Stearn, C. W., 1966, The microstructure of stromatoporoids: Paleontology, v. 9, p. 74-124.

Stearn, C. W., 1972, The relationship of the stromatoporoids to the sclerosponges: Lethaia, v. 5, p. 369-388.

Stearn, C. W., 1977, Studies of stromatoporoids by scanning electron microscopy, Proceedings of the 2nd International Symposium on Corals and Fossil Coral Reefs: Paris, Mémoires du Bureau de Recherches Géologiques et Minières (France) 89, p. 33-40.

Stearn, C. W., 1980, Classification of the Paleozoic stromatoporoids: Journal of Paleontology, v. 54, p. 881-902.

Stearn, C. W., and A. J. Mah, 1987, Skeletal microstructure of Paleozoic stromatoporoids and its mineralogical implications: Palaios, v. 2, p. 76-84.

Stearn, C. W., B. D. Webby, H. Nestor, and C. W. Stock, 1999, Revision and terminology of Palaeozoic stromatoporoids: Acta Palaeontologica Polonica, v. 44, p. 1-70.

Wendt, J., 1974, Der Skelettbau aragonitischer Kalkschwämme aus der alpinen Obertrias: Neues Jahrbuch für Geologie und Paläontologie Monatshefte, v. 8, p. 498-511.

Wendt, J., 1976, Der Skelettbau mesozoischer und rezenter Kalkschwämme: Zentralblatt für Geologie und Paläontologie, Teil 2 - Paläontologie, v. 1976, p. 321-325.

Wendt, J., 1978, Skelettbau und entwicklung der massiven Kalkschwämme vom Jungpaläozoikum bis in die Gegenwart: Neues Jahrbuch für Geologie und Paläontologie, Abhandlungen, v. 157, p. 91-98.

Wendt, J., 1984, Skeletal and spicular mineralogy, microstructure and diagenesis of coralline calcareous sponges, *in* W. A. Oliver, Jr., W. J. Sando, S. D. Cairns, A. G. Coates, I. G. Macintyre, F. M. Bayer, and J. E. Sorauf, eds., Fourth International Symposium on fossil Cnidaria (and Archaeocyathids and Stromatoporoids): Palaeontographica Americana, v. 54, Paleontological Research Institution, p. 326-336.

Facing Page: Underwater view of an orange cup coral (*Tubastrea coccinea*) with emergent polyps; Bonaire reef at night. Photograph courtesy of Woody Mayhew.

GRAINS: Skeletal Fragments

Corals, octocorals, and hydrozoans

CHAPTER 6

Tabulate corals

Rugose corals

Scleractinian corals

Octocorals

Hydrozoans

TABULATE CORALS

Taxonomy and Age Range:

Phylum Cnidaria, Class Anthozoa

Subclass Zoantharia — Ordovician (Cambrian ?)- Recent

Order Tabulata — Early Ordovician-Late Permian

Possible tabulate corals have been reported from the Early Cambrian (Sorauf and Savarese, 1995). The group was widespread and diverse from Late Ordovician to Middle Devonian, but declined in Late Devonian and into the Carboniferous. The group became extinct during the great end-Permian faunal crisis.

Environmental Implications:

Tabulate corals were fully marine, sessile organisms and were contributors to stromatoporoid and microbial reefs and bioherms of Ordovician to Carboniferous age. Although substantial contributors to some reefs, tabulates rarely were dominant reef framework formers. Tabulate corals did build smaller, isolated bioherms that are widely distributed in muddy, open shelf carbonate rocks.

Many tabulate corals were attached to their substrates, others were unattached, rolling free on the sea floor.

Whether tabulate corals had a symbiotic relationship with zooxanthellate analogs, and therefore were restricted to living in the photic zone, is an open question because such soft tissues are not preserved. Environmental reconstructions, however, indicate that tabulates lived at shallow marine depths within the photic zone, so an analogous symbiotic relationship is possible, but has neither been proven nor refuted.

Skeletal Mineralogy:

Virtually all tabulate corals probably were originally calcitic; very few (probably on the Tetradiidae, a group that is not universally classed with the tabulates) may have been aragonitic. Determination of original mineralogy is based mainly on the quality of structural preservation.

Morphologic Features:

Exclusively colonial corals characterized by having slender (typically 0.2-5 mm diameter), polygonal, oval or circular tubes (corallites) with perforate or more rarely imperforate walls. The corallite tubes are partitioned by horizontal interior platforms (termed "tabulae"); vertical corallite partitions (septa), if present at all, are very short and almost spine-like. Corallites can parallel each other and be closely packed, or can be loosely packed and joined only by cross-tubes (stolons); corallites can also diverge in bud-like or branch-like fashion; yet others form in linear chains.

Tabulate coral colonies range in size from a few mm to as much as 4 m in width and height.

Keys to Petrographic Recognition:

1. **Exclusively colonial corals with slender corallite tubes that are commonly closely packed and have circular, oval, or polygonal shapes in transverse sections.**
2. **Horizontal tabulae are prominent and vertical septa are subordinate, if present at all (septa commonly are reduced to small stubs or spines).**
3. **Calcitic forms generally are well preserved and have a "fuzzy" fibrous wall structure with fibers apparently oriented normal to the plane of tabulae (Majewske, 1969). Some forms have a thin, external carbonate layer around the skeleton (the epitheca) that appears structureless; other forms have wall structure similar to the radiating fiber bundles (fascicles) that constitute trabecular fabric (described later for scleractinian corals); yet others have clear, compact calcite crystals within their walls (see Majewske, 1969) for further details. Many tabulate corals, however, have a lamellar wall structure, regarded by some to be original and biogenic, but thought by others to be diagenetic. Many of these tabulates with lamellar walls (lamellae parallel to growth lines and exterior surface) have yet to be found with any other (pre-existing) fibrous structure.**
4. **Tabulate corals generally form larger colonies and have larger individual living chambers than bryozoans; tabulate partitions and small septal structures also differentiate these corals from bryozoans. The skeletal (corallite) arrangement is very different from, and coarser than that found in, stromatoporoids or red algae.**

PHOTO SCALES AND ABBREVIATIONS ARE EXPLAINED IN THE BOOK'S INTRODUCTION

Morphologies of some common tabulate corals

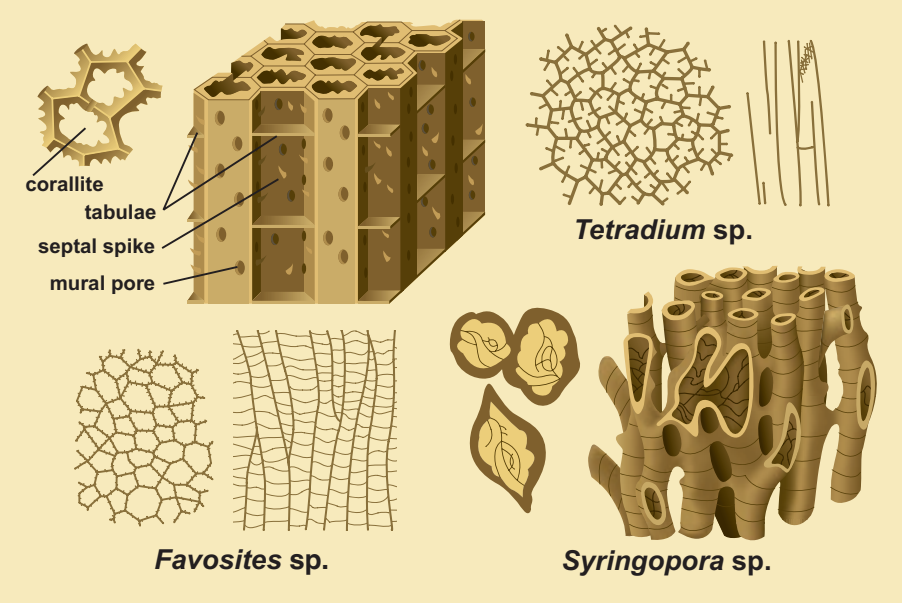

A block diagram showing the basic arrangement of structural elements in a tabulate coral colony (upper left); transverse and longitudinal cross sections of two common genera of tabulate corals (*Tetradium* and *Favosites*), and a block diagram and longitudinal cross section (lower right) of *Syringopora*, a tabulate coral with isolated, thick-walled corallites connected by stolons. In general, horizontal tabulae and vertical corallite walls dominate the architecture of tabulate corals and septal partitions within individual corallites generally are small, reduced to spikes, or non-existent. Adapted from Moore et al. (1952) and Majewske (1969).

Mid. Ordovician Black River Gp., Kingston area, Ontario, Canada

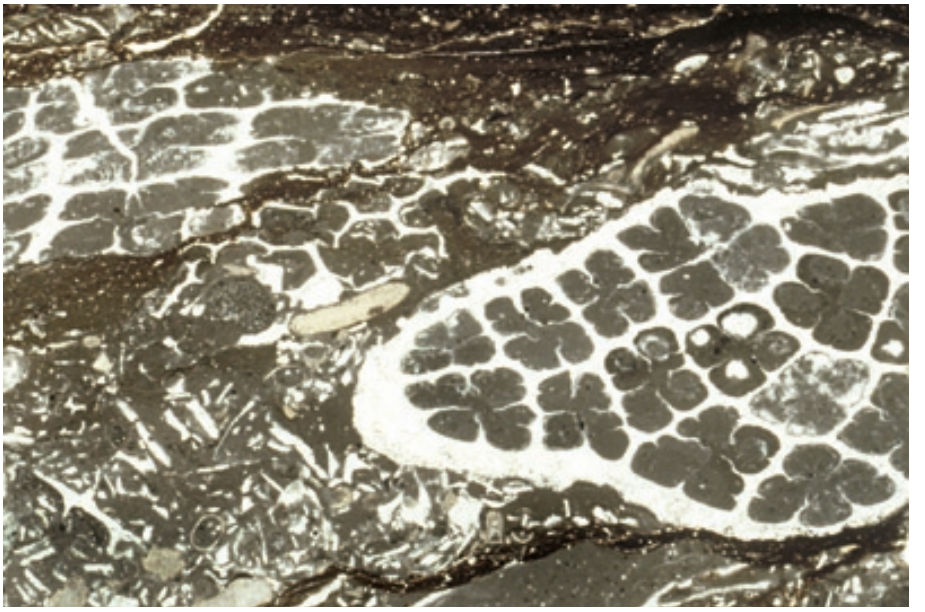

A transverse section of an early tabulate coral — *Tetradium* sp., Order Tetradiida. The packed, slender, quadrate corallites are readily distinguishable. Note also the broken fragments of compacted *Tetradium* throughout the sediment matrix. Internal structure is never preserved in this group, so this likely was the only group of tabulate corals that had primary aragonitic mineralogy. On the other hand, this group may not belong with the tabulate corals at all, and indeed, many workers do not classify them in that order. Sample from Noel P. James.

PPL, HA = 9.0 mm

Mid. Ordovician Black River Gp., Kingston area, Ontario, Canada

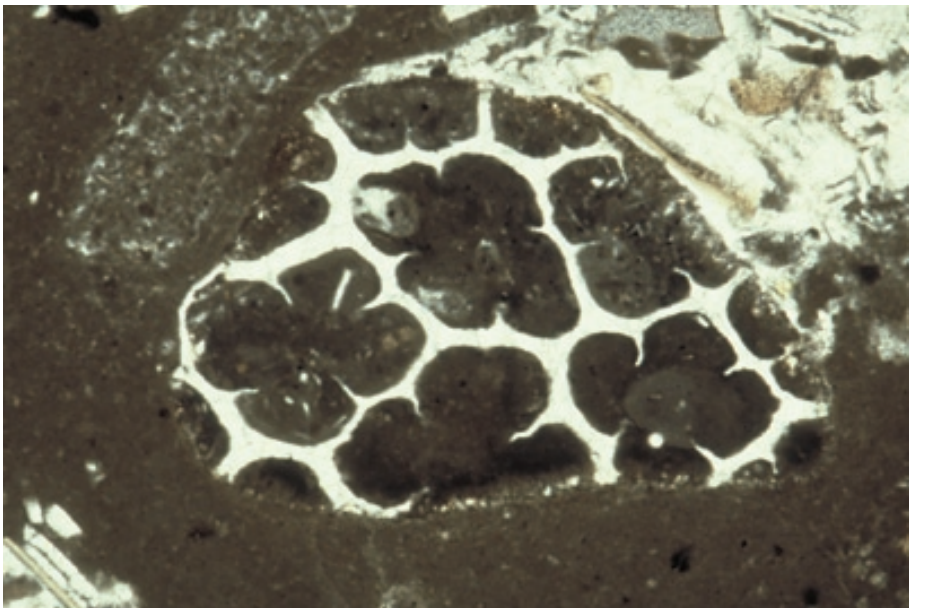

A magnified view of the early tabulate coral shown in the previous example — *Tetradium* sp. The quadrate corallites produce a distinctive appearance like a clover leaf in this fragmental grain. This order of tabulate corals was confined to Ordovician strata where it commonly formed small bioherms. Sample from Noel P. James.

PPL, HA = 5.0 mm

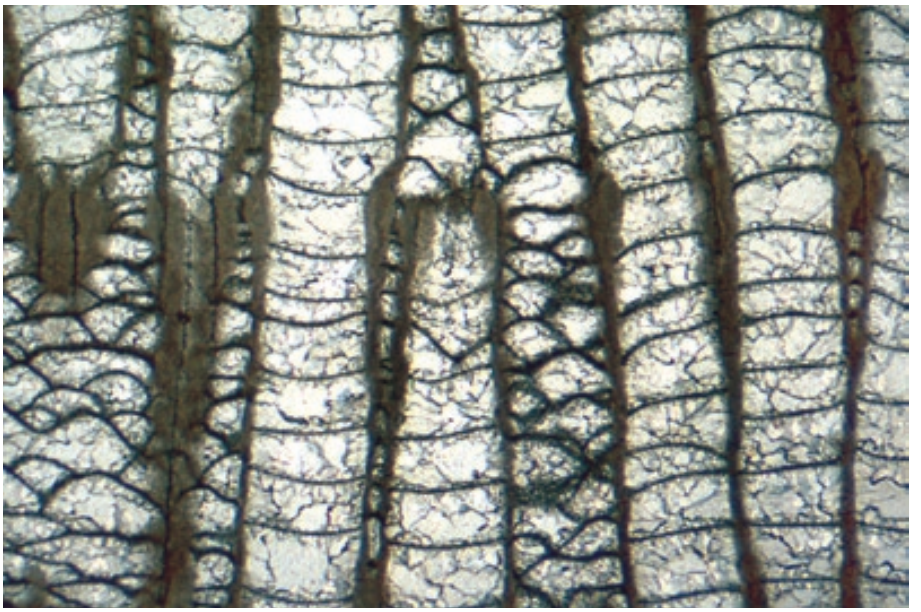

Up. Ordovician Keel Fm., Pontotoc Co., Oklahoma

The tabulate coral *Propora thebesensis* (Foerste) — Order Heliolitida. This longitudinal section shows that the calcite of the corallite walls is composed of septal trabeculae (fiber bundles). The microstructure within the thinner tabulae and coenenchymal dissepiments is not distinct. Photograph courtesy of Graham Young.

PPL, HA = 7.5 mm

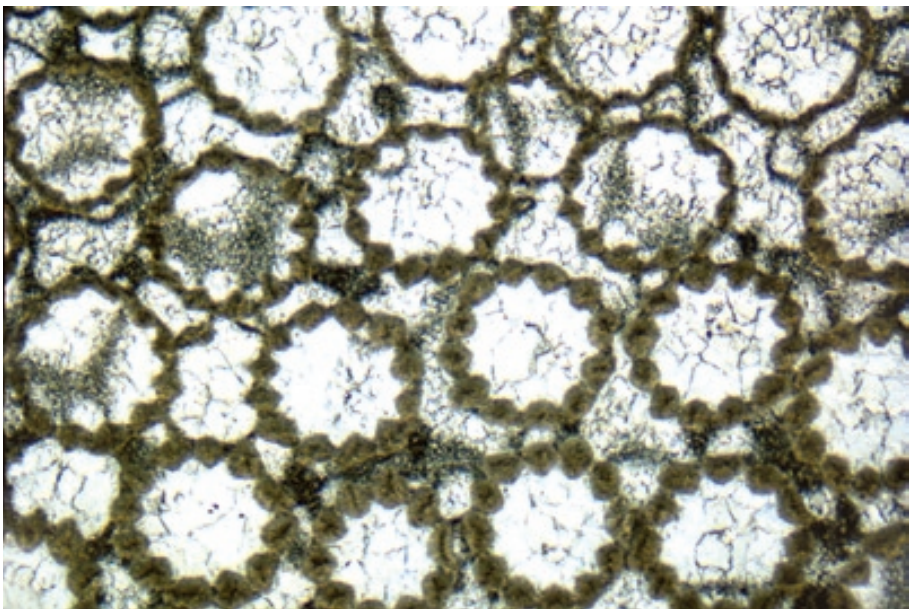

Up. Ordovician Keel Fm., Pontotoc Co., Oklahoma

The tabulate coral *Propora thebesensis* (Foerste) —Order Heliolitida. This transverse section shows a contrast between the thickened and unthickened parts of the skeleton. Septal trabeculae are well developed in the thickened parts. Photograph courtesy of Graham Young.

PPL, HA = 5.5 mm

Lo. Silurian?, (lo. Llandovery?) Bryant Knob Fm., Pike Co., Missouri

The tabulate coral *Paleofavosites subelongus* (Savage) — Order Favositida. A longitudinal section showing abundant septal spines. Photograph courtesy of Graham Young.

PPL, HA = 15.5 mm

Up. Ordovician Keel Fm., Pontotoc Co., Oklahoma

A transverse section of two chain-like ranks of the tabulate coral *Halysites alexandricus* (Young and Elias) — Order Halysitida. This Ordovician-Silurian group has round to elliptical corallites that are arranged in uniserial ranks that diverge and rejoin at various point, enclosing large internal spaces. Note the relatively thick, brown, originally calcitic walls that have prismatic wall structure (termed fibro-normal) with crystals oriented perpendicular to the exterior surface of the wall. Photograph courtesy of Graham Young.

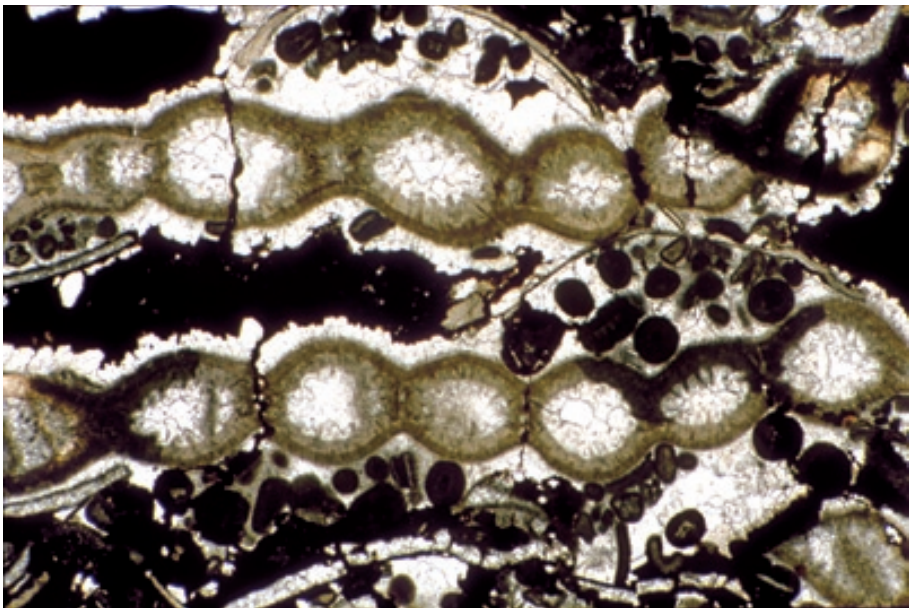

PPL, HA = ~9 mm

Devonian limestone, midcontinent, U.S.A.

A longitudinal section through a colonial tabulate coral showing slight thickening of wall structure at the margin of the colony. The typically dark and "fuzzy" fibrous microfabric of the wall is apparent here as is the simple arrangement of tabulae.

PPL, HA = 5.0 mm

Devonian limestone, midcontinent, U.S.A.

A transverse section through the same colonial tabulate coral shown in the previous photograph. The close packing of polygonal corallites, the lack of internal septal partitions, and the well preserved brownish calcite of the corallite walls are readily visible in this example.

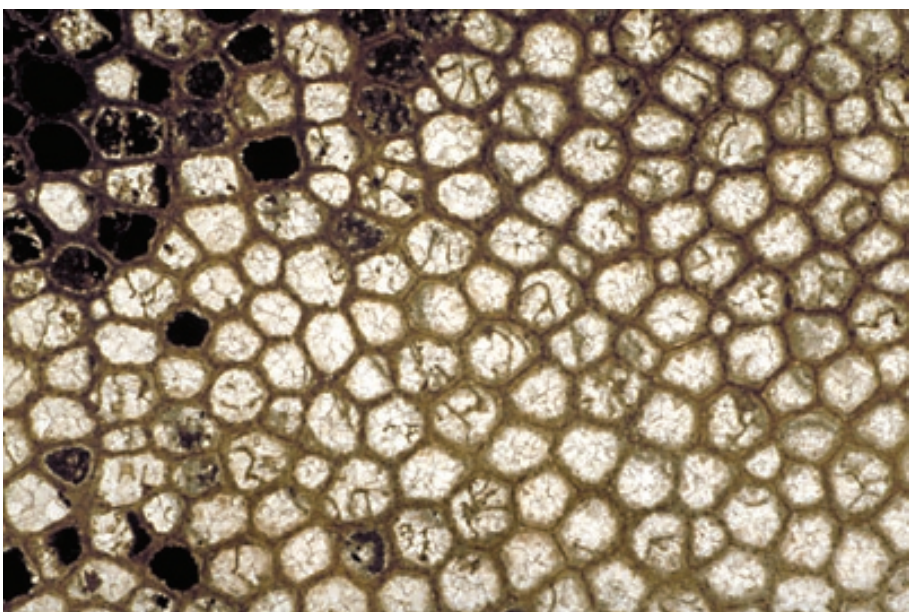

PPL, HA = 12.5 mm

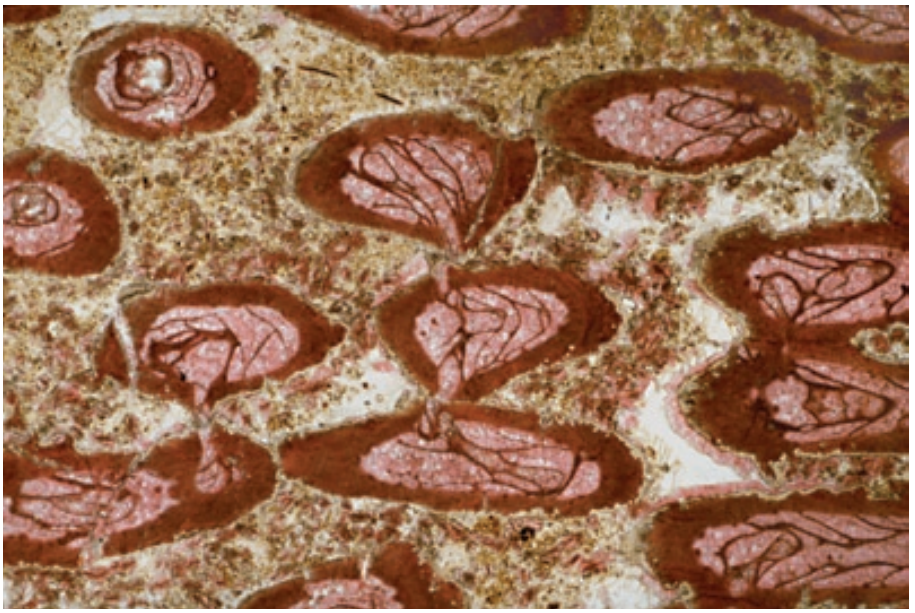

Lo. Permian (Sakmarian) Tastubsky Horizon, Gubakha, Perm Region, Russia

A cut through a colonial coral, *Syringopora* sp. This widespread and long-ranging group has long, cylindrical, thick-walled corallites that are separate from each other and are joined only in a few places by connecting tubes (stolons or tubuli). They also have funnel-shaped (infundibuliform) tabulae that extended through the tubuli.

PPL, AFeS, HA = 14.5 mm

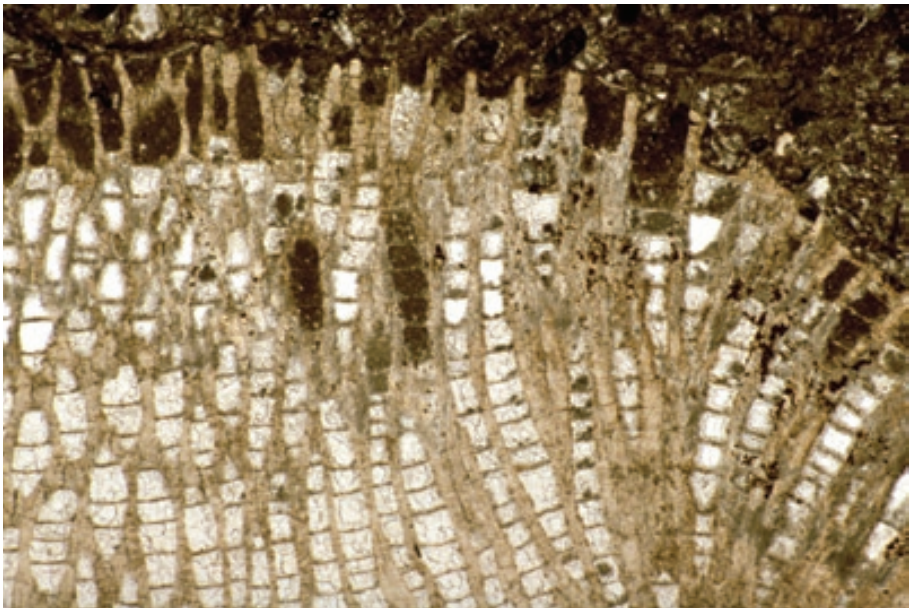

Pennsylvanian Magdalena Gp., El Paso Co., Texas

The well preserved margin of a colony of *Chaetetes* sp. Long classified as tabulate corals, this group is now definitively placed with the sponges by most current workers. The sponge assignment is based on the discovery of possible modern relative, *Acanthochaetetes wellsi*, that has the spicules and soft tissues typical of demosponges. Spicules are not yet known in fossil chaetetids, however, so we have continued to include this group with the tabulate corals for now. The skeleton of *Chaetetes* is known to have been high-Mg calcite.

PPL, HA = 8.0 mm

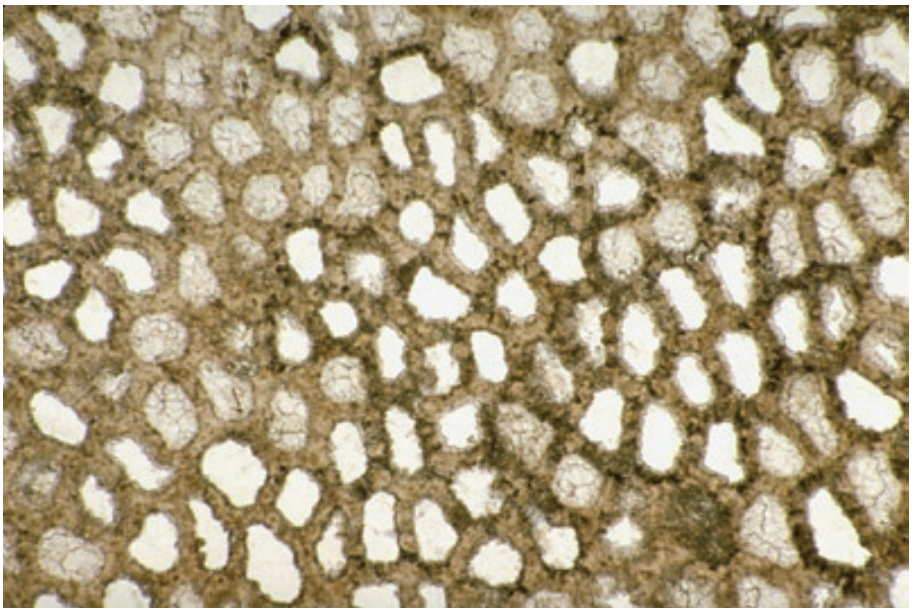

Pennsylvanian Magdalena Gp., El Paso Co., Texas

This transverse section of a colony of *Chaetetes* sp. shows the simple, interlocked, non-septate living chambers of this colonial organism. Chaetetid colonies range from sheet-like encrustations to upright columns and some colonies reach a diameter of three meters.

PPL, HA = 12.5 mm

Rugose Corals

Taxonomy and Age Range:

Phylum Cnidaria, Class Anthozoa, Subclass Zoantharia
Order Rugosa — Middle Ordovician-Late Permian

Environmental Implications:

Rugose corals (tetracorals) are a fully marine group that is found predominantly in warm, shallow water strata (although there is no evidence that they had photosynthetic symbionts or were confined to photic water depths).

They were significant contributors to reefs during the Paleozoic, but were rarely the predominant reefal framework formers (perhaps because they had very high skeletal calcite requirements or a lack of effective means of attachment). In addition, although banding studies on rugose corals indicate growth rates comparable to those of some modern scleractinian corals, none of the rugosans had the remarkable growth rates of modern reef-forming scleractinians (especially the main reef-front species of *Acropora*).

Rugose corals were common in clear-water, hard-bottomed, carbonate shelf settings; colonial forms constructed small (meter-scale) bioherms.

Some forms apparently were adapted to living in basinal, low-oxygen settings with soft, muddy seafloors.

Skeletal Mineralogy:

Rugose corals were originally composed of calcite and have well preserved skeletal structure; most were low-Mg calcite, although some Carboniferous and Permian forms had moderately high-Mg calcite compositions (6-8 mole% Mg).

Morphologic Features:

Rugose corals include both solitary (about 2/3rd) and colonial (about 1/3rd) forms. Colonial rugosans typically formed cm to m-sized domal structures, with some reaching 4-m diameter; solitary forms typically are cm- to dm-sized and have horn-shaped corallites.

Colonial forms had varied architectural patterns, including: irregular branching forms; massive forms where corallites touched and formed polygonal contact surfaces; looser packed corallites with localized connections; clusters in which corallite walls are completely or partially lost; and forms in which adjacent corallite walls are lost and septa of adjacent corallites merge.

In some forms, the septa may branch or unite near the center of the corallite to form an elongate axial structure (the columella or axial vortex).

Keys to Petrographic Recognition:

1. **Rugose corals can be solitary or colonial; solitary forms have distinctive horn shape in longitudinal sections (unique in the Paleozoic); colonial forms can look very similar to tabulate corals, but differ from most other groups in the large size of rugosan living chambers and their patterns of organization.**
2. **Rugosans have a distinctive, bilaterally symmetrical, pattern of septal arrangement. Most rugosans have longer and better developed septa, but less well-developed tabulae, than tabulate corals. Rugosans also have a unique pattern of septal insertion: septa are inserted at four loci, and major and minor septa of differing length are usually developed during successive growth stages (see second diagram on next page for details). The septal projections into living chambers of rugosans help to differentiate rugose corals from bryozoans.**
3. **Rugose corals have a well developed outer wall (epitheca) that commonly shows strong ribbing (the name of this group refers to the growth ridges, or "rugae", which wrinkle the exterior of the coral — these are not the same as septal ridges).**
4. **Wall structures generally are well preserved, are distinctly brownish (possibly due to incorporated organic material), and have a "fuzzy" fibrous fabric (Majewske, 1969). Some forms have septal structural fabrics similar to the radiating fiber bundles (fascicles) that constitute trabecular fabric (described later for scleractinian corals); yet others have clear, compact calcite crystals within their walls (see Majewske, 1969) for further details; high-Mg forms commonly have "zigzag microstructure".**

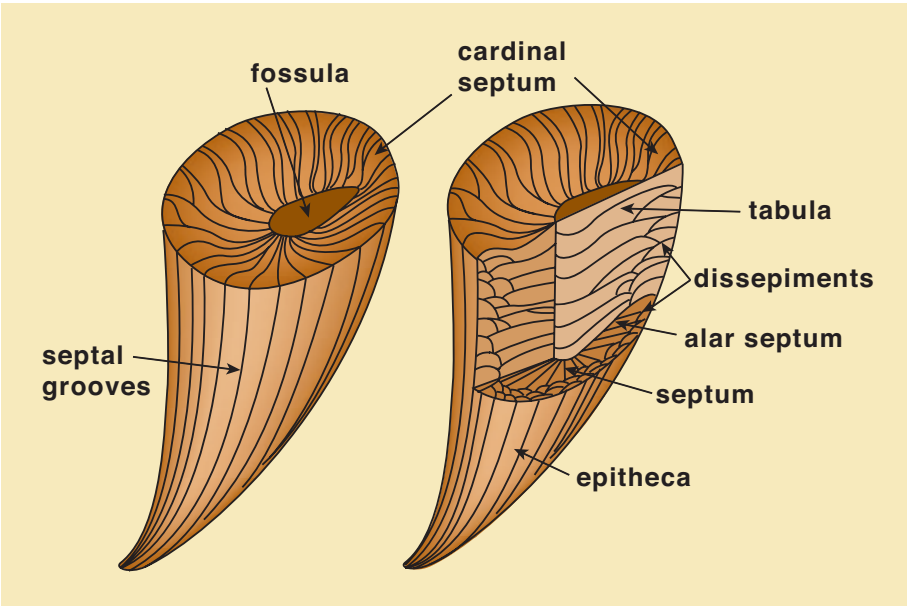

Major morphologic features of a typical rugose coral

A simplified model of a rugose coral (with minor septa omitted). The sliced section shows the relationship between septa, tabulae, and dissepiments. External grooves mark the position of internal septa. Adapted from Boardman et al. (1987; reference given in citations at end of book introduction).

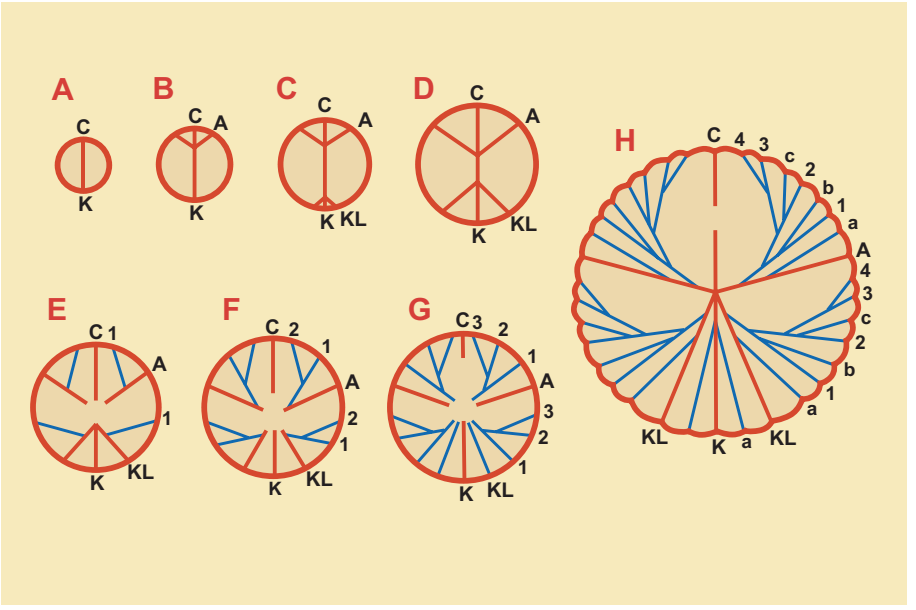

Sequence of septal addition in rugose corals

Rugosans are differentiated from other corals by the sequence in which they add septa through their growth history, and the pattern and symmetry of those septa. This diagram shows eight stages in rugosan growth as well as the sequential addition of the cardinal septum (C), the counter septum (K), the alar septa (A), the counterlateral septa KL, the metasepta (1-4), and mature-stage minor septa (a-c). Adapted from Oliver (1980).

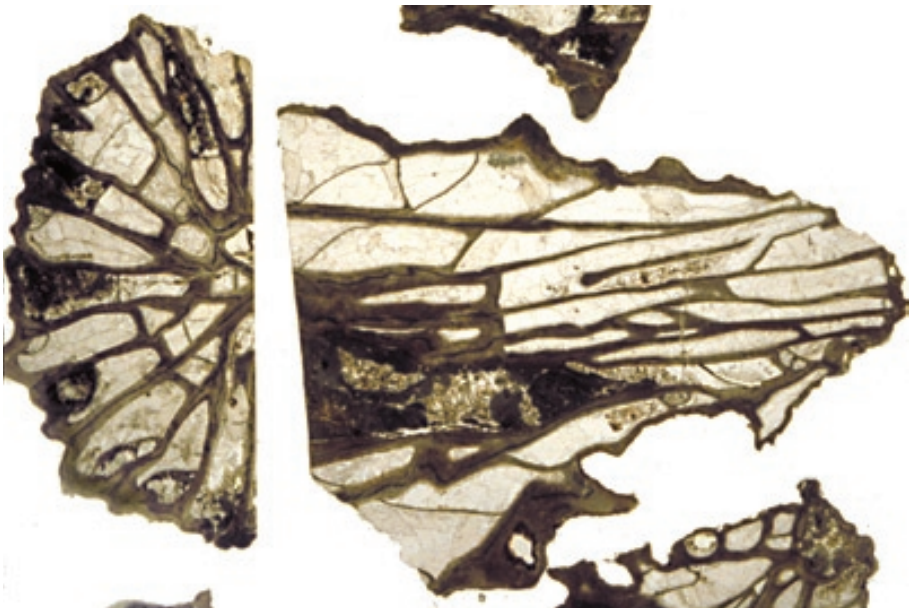

Pennsylvanian limestone, north-central Texas

Longitudinal and transverse sections through a solitary rugose coral, probably *Zaphrentites* sp. The transverse section shows half of the cup-shaped corallite with radiating, brownish calcite septal walls. The longitudinal section shows the conical (horn shaped) outline of a solitary rugosan, with thick septal partitions and thinner supporting dissepiments.

PPL, HA = 20 mm

Pennsylvanian limestone, north-central Texas

An enlargement showing the septa and walls of the solitary rugose coral (*Zaphrentites* sp.) shown in the previous photograph (rotated 90° clockwise). Note the thick septa and walls that retain much of their original dark color and radiating fibrous calcite fabric. This preservation is typical of rugose coral material, supporting the idea that this group had primary calcite composition.

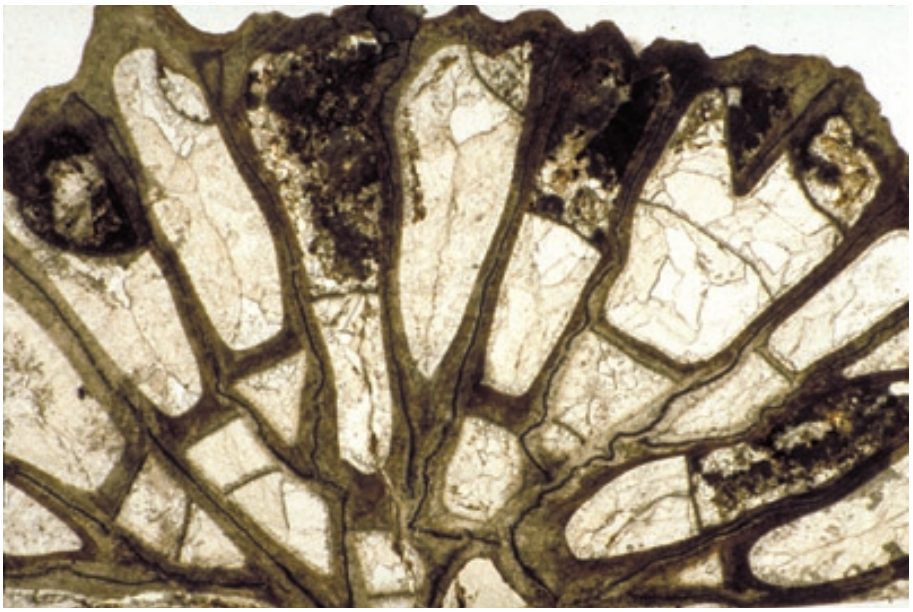

PPL, HA = 8.0 mm

Carboniferous limestone, England, U.K.

A longitudinal section through a solitary rugose coral (with fragment of additional rugosans on each side. This cut nicely shows the horn-shaped skeleton with septa that paralleled the long-axis and a complex series of curved dissepiments and more planar tabulae that provided internal support.

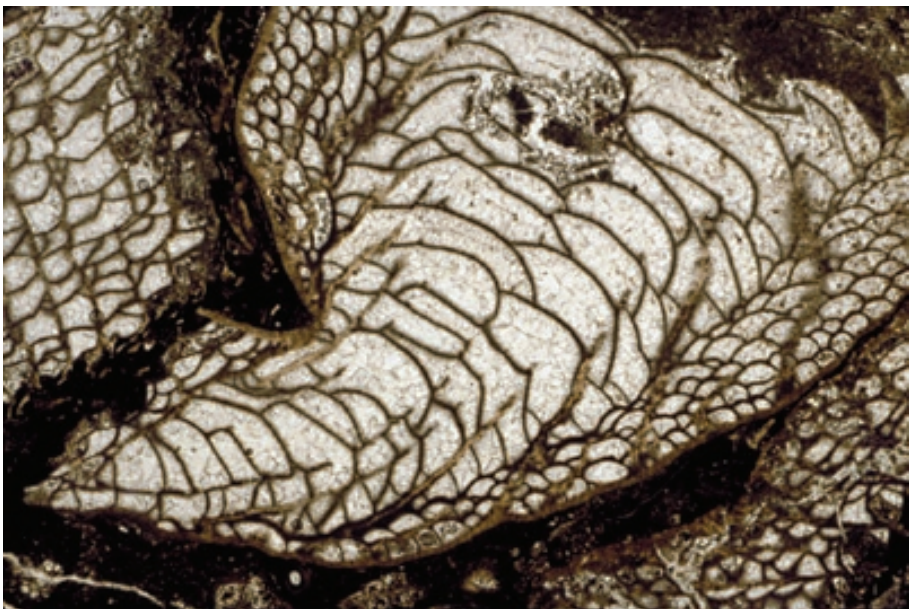

PPL, HA = 16 mm

Carboniferous limestone, England, U.K.

A magnified view of the longitudinal section through a solitary rugose coral shown in the previous photograph. The complex shapes of the dark, calcitic partitions are readily apparent here, and are organized quite differently from the internal structure of bryozoans, one of the groups sometimes mistaken for corals in thin section.

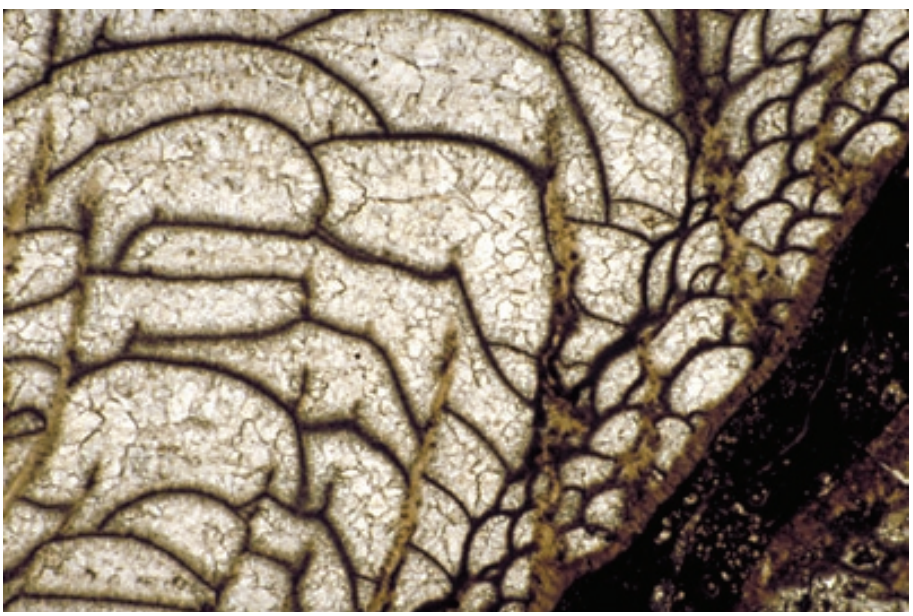

PPL, HA = 7.0 mm

Pennsylvanian Graham Fm., Coleman Co., Texas

A transverse section through a solitary rugose coral, *Lophophyllidium proliferum*. Note the near-circular shape in this section, the large central columella, and the broad, fairly well preserved septa and epitheca. The wall structure, however, has undergone some diagenetic alteration. Geochemical studies have shown elevated Mg contents and microdolomite inclusions, probably indicating an original intermediate- to high-Mg calcite composition (up to about 6-8 mole% Mg; see Sorauf & Webb (2003, Jour. Paleo., v. 77, p. 16-30).

PPL, HA = 11 mm

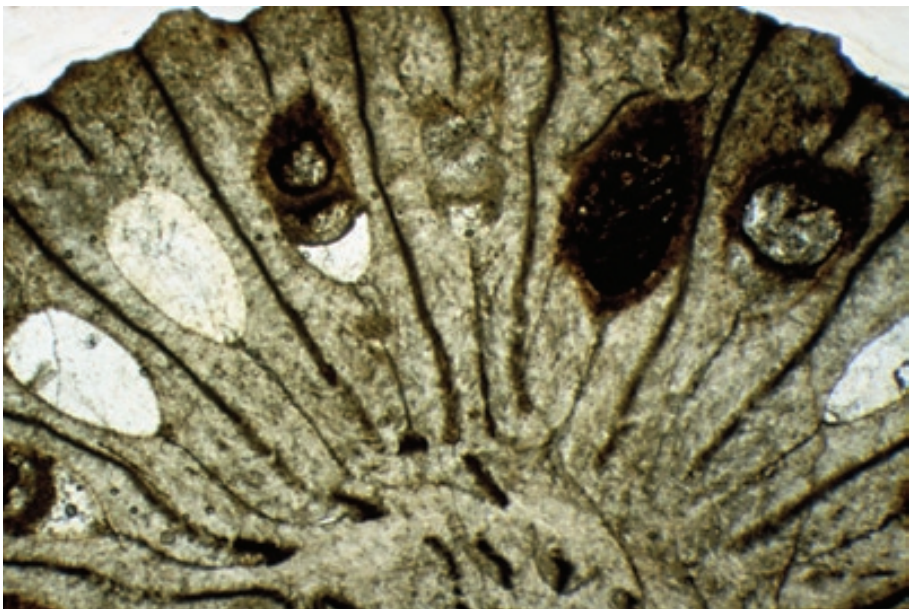

Pennsylvanian Graham Fm., Coleman Co., Texas

An enlarged view of the transverse section through a solitary rugose coral, *Lophophyllidium proliferum*, shown in the previous photograph. Major and minor septa are clearly distinguishable and both types of septa show dark calcification centers surrounded by bundles of fibrous calcite. The thickened marginal epitheca nicely shows the relationship between the correspondence between internal septa and external grooves in the rugosan wall. The chevron-like septal wall fabric has been termed "zigzag microstructure" and appears to be characteristic of rugosan forms with moderately high-Mg calcite skeletons.

PPL, HA = 5.1 mm

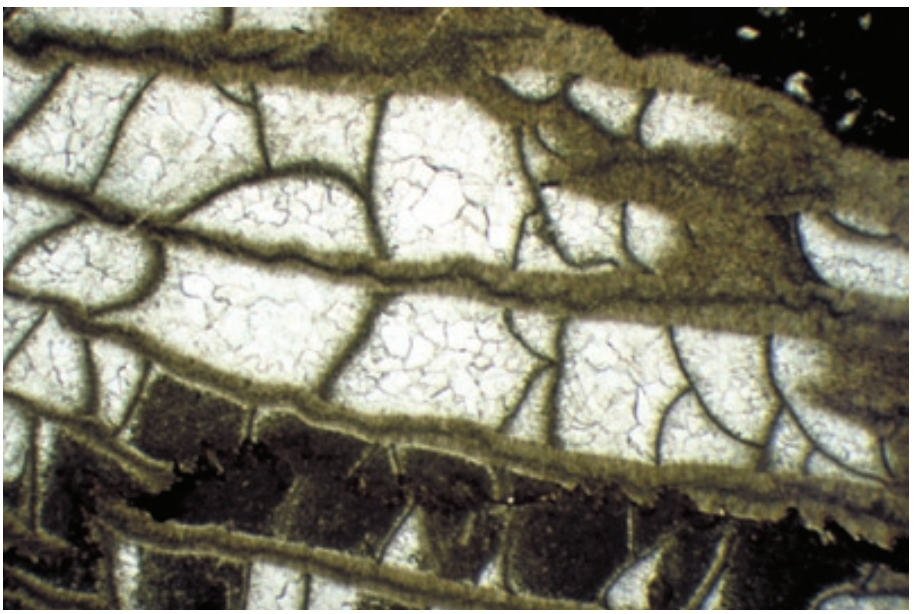

Up. Devonian (Frasnian) Sadler-Pillara Ls., Canning Basin, Western Australia

A longitudinal section through the wall of a rugose coral. The septa extend roughly parallel to the long axis of the picture and show a dark central stripe that represents centers of calcification from which fibers of calcite radiate (the lighter brown areas of the septa). The tabulae and dissepiments that divide the chambers are also composed of fibrous calcite; interstitial pores have been filled with diagenetic sparry calcite cement.

PPL, HA = 5.1 mm

Lo. Permian (Sakmarian) Tastubsky Horizon, Perm Region, Russia

A higher magnification view of a colonial rugose coral showing the microstructure of the coral wall. The dark calcification center in the large septum is surrounded by bundles of cloudy, organic-rich calcite fibers; the thinner dissepiments also contain organic-rich calcite, but with a less identifiable microfabric. Pore space is filled with three generations of cement, and the orientation of the first generation may have been influenced by the orientation of the calcite fibers in the coral walls.

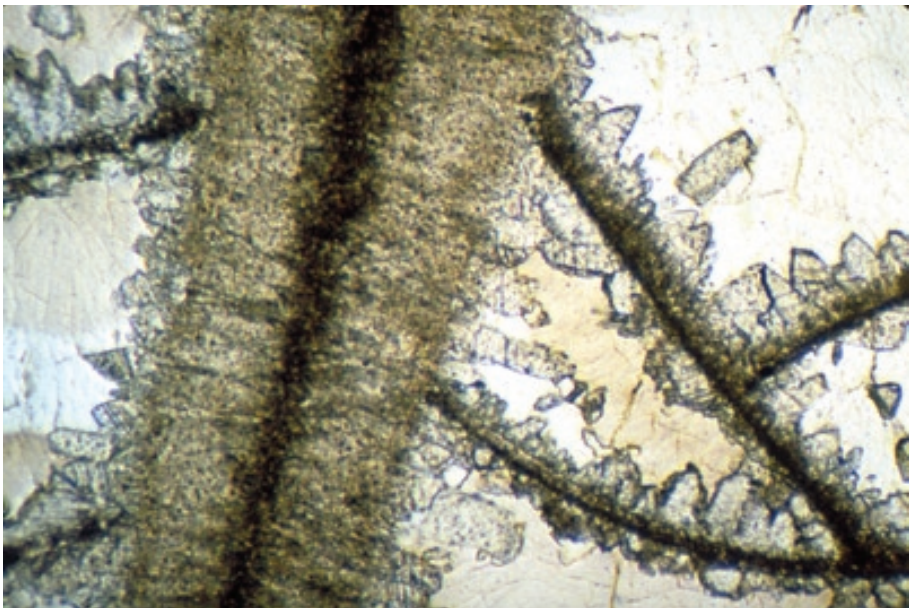

PPL, HA = 2.0 mm

Middle Devonian Blue Fjord Fm. Ellesmere Island, Arctic Islands, Canada

A transverse section through a colonial rugose coral (*Spongonaria* sp.) with packed corallites forming polygonal boundaries. Relatively short septa surround a central area of dissepiments. Note the offset of rugose grooves and corresponding septa from one corallite to the next. Sample from Noel P. James.

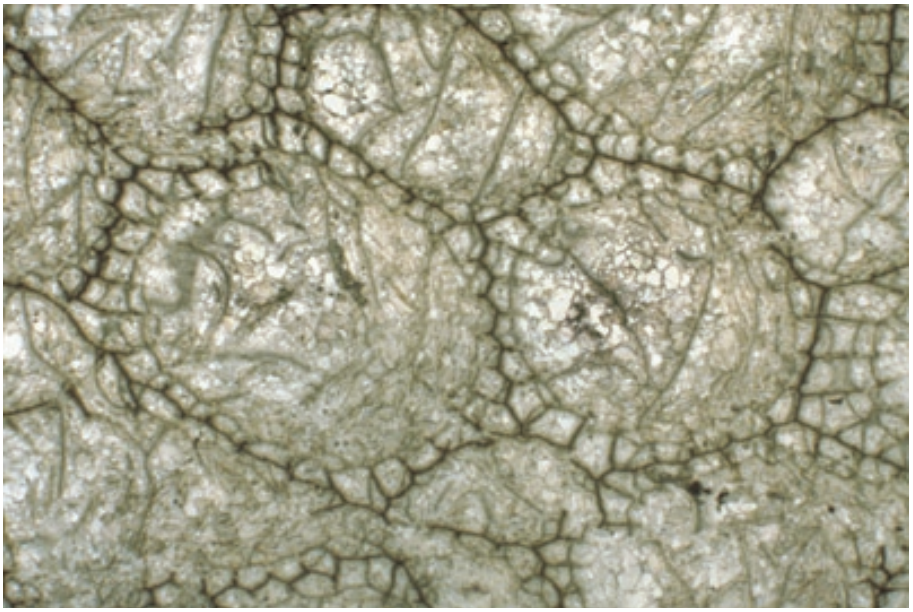

PPL, HA = 16 mm

Devonian limestone, Iowa

A transverse section through a colonial rugose coral, *Pachyphyllum woodmani*. This specimen shows the dark central cores of thin septa, with excellent differentiation of major and minor septa. It also shows that in this group, the corallite walls were lost and septa of adjacent corallites were joined.

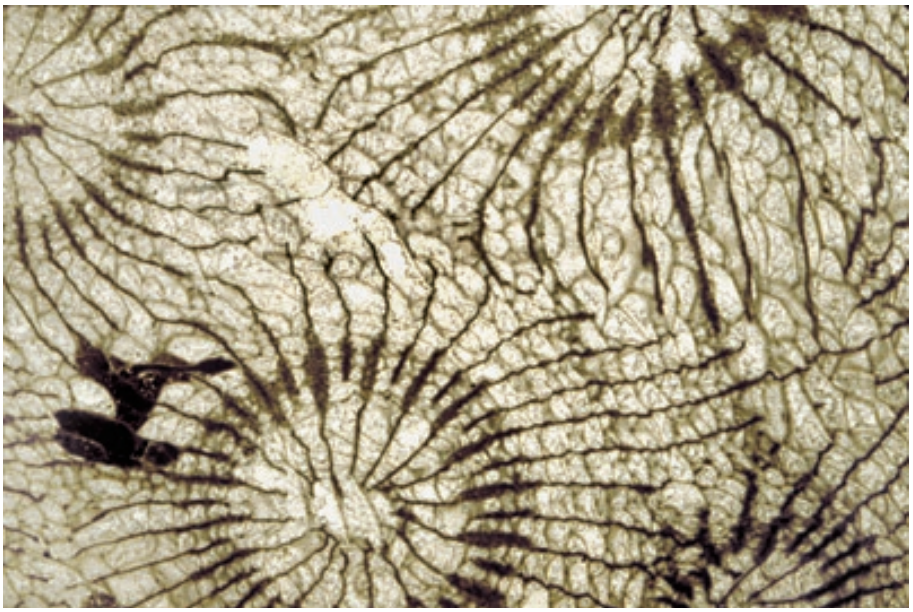

PPL, HA = 25 mm

Up. Devonian (up. Frasnian) Simla-Blue Ridge Fm., Alberta, Canada

An oblique transverse section through another colonial rugose coral (*Peneckiella* sp.) that had separated corallites. It has a series of relatively short septa surrounding a large central area divided by tabulate partitions. The corallite internal voids have been filled with multiphase calcite cements.

PPL, AFeS, HA = 16 mm

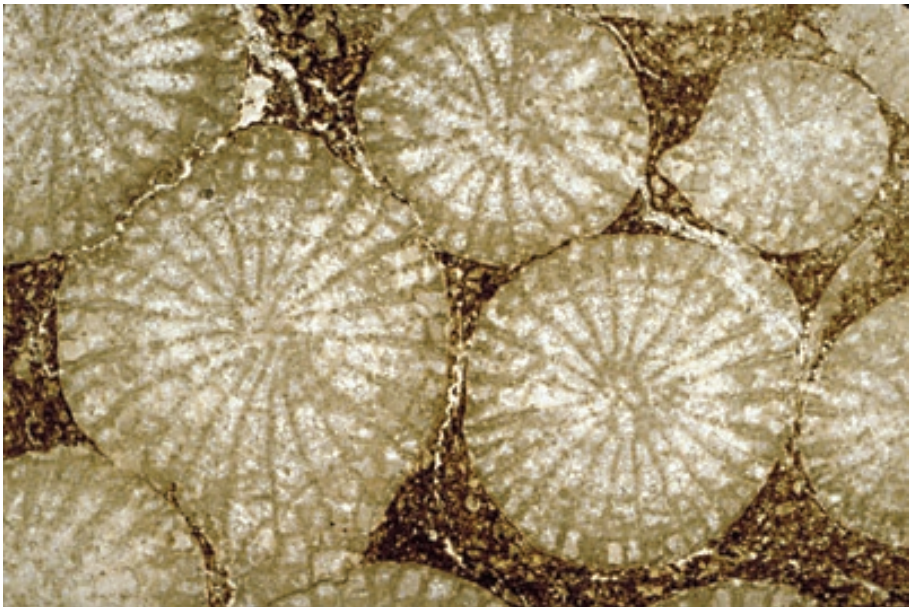

Up. Devonian Mt. Hawk Fm., Alberta, Canada

A colonial rugose coral with moderately well preserved corallite structure of the genus *Disphyllum* (possibly *D. fasciculatum*). Although these corallites touch in places (and have undergone some pressure-solution at those contacts), they were not closely packed originally and thus show inter-corallite sediment pockets.

PPL, HA = 16 mm

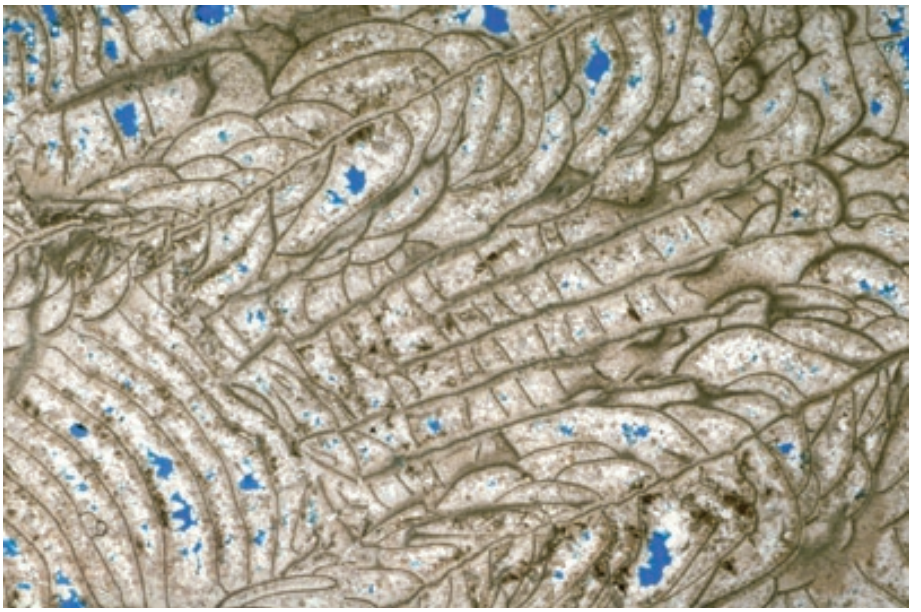

Lo. Permian (Sakmarian) Tastubsky Horizon, Perm Region, Russia

A longitudinal section through a colonial rugose coral showing complex internal structure consisting of septa (oriented from lower left to upper right), small tabulae normal to the septa, and curved dissepiments.

PPL, BSE, HA = 14.5 mm

Scleractinian Corals

Taxonomy and Age Range:

Phylum Cnidaria, Class Anthozoa, Subclass Zoantharia
Order Scleractinia — Middle Triassic-Recent

Environmental Implications:

Scleractinian corals (hexacorals) are fully marine, sedentary organisms with planktic larvae.

Most modern forms are stenohaline (generally 34-36‰ salinity) and are restricted to warm waters (about 16°C minimum; 25-29°C optimum range). Thus, scleractinian corals typically are found in waters between 30° N and S latitudes (except where extended by warm ocean currents).

Most scleractinians have a low tolerance for suspended sediment so they are found mainly in clear-water, carbonate depositional settings.

Most scleractinians have the ability to firmly attach to substrates allowing growth in high-energy areas — thus, they are major reef framework contributors (especially in Miocene to Recent reefs). A few scleractinian corals, such as *Siderastrea radians*, are non-attached, rolling free on the sea floor

Zooxanthellate scleractinian corals have polyp tissues that contain photosynthetic dinoflagellate symbionts (zooxanthellae) — thus, they are limited to euphotic waters (90 m in exceptionally clear waters; 50 m or less in normal waters). Zooxanthellate corals have robust morphologies, heavily calcified skeletons, and rapid growth rates and most commonly are reef dwelling (hermatypic) forms.

Azooxanthellate (or nonzooxanthellate) scleractinians lack dinoflagellate symbionts (zooxanthellae) and thus can extend from warm, photic, shallow-water settings into cold (4°C) and very deep (>6,000 m) aphotic waters. They typically are delicate, lightly calcified, branching, ahermatypic forms that grow as isolated colonies or form small biohermal thickets.

Skeletal Mineralogy:

Modern scleractinian corals are aragonitic and fossil forms, based on quality of preservation, were aragonitic as well.

Morphologic Features:

This group includes both solitary and colonial forms. Colonial forms can be robust and domal, flat and encrusting, or branching into fingers or plates — these growth forms reflect specific adaptations to wave energy, light availability, growth rates of competitive organisms, and other environmental factors.

Scleractinian skeletons have well developed septa that are generally arranged in six cycles, thus dividing the tubular corallites into six areas and have hexameral symmetry. The dissepiments are better described as "shelf like", providing resting places for the base of the polyp, seen forming series of these shelves, as new dissepiments are formed at the base of the polyp, retracting upwards during growth. These dissepiments are formed centripetally, and are generally labeled as endothecal or exothecal, depending on their position within the corallite wall (endothecal) or in colonial skeleton between corallites (exothecal).

Keys to Petrographic Recognition:

1. **Found as large solitary or colonial skeletons (typically cm-scale or larger); commonly also found as fragmented and abraded grains because many scleractinians live in high-energy environments.**
2. **Aragonitic composition means that most pre-Pleistocene fossil remains have poorly preserved skeletal microstructure. Those specimens are recognizable by their radiating septal structure (often preserved mainly though infilling of the living chambers with micrite or microcrystalline calcite cement).**
3. **The poor preservation of the aragonitic scleractinians actually helps to distinguish them from three calcitic groups with which they might otherwise be confused — rugose corals, tabulate corals, and bryozoans.**
4. **Scleractinian corals preserved as aragonite are known as far back in the geologic column as the Middle Triassic. They show excellent trabecular septal structures — finely fibrous aragonite crystals that radiate outward in bundles from isolated point calcification centers. The constituent fibers typically are only 1-2 µm in thickness. The points from which the fibers radiate commonly look darkly granular and line up along the centerline of the septal walls.**

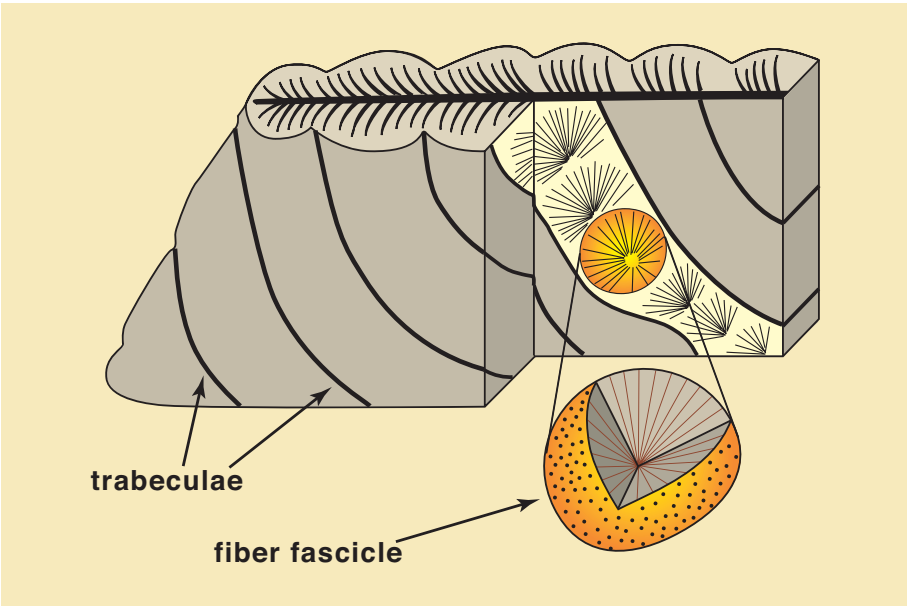

A diagrammatic view of scleractinian coral septal structure

A representation of the trabecular crystal structure found in the septa of scleractinian corals. Finely fibrous aragonite crystals are arranged in radiating bundles (termed fascicles) that grow from isolated but linearly arranged point calcification centers. This produces a splayed fibrous microtexture. The biologically grown crystal fibers radiate out from the axes of the trabeculae, but are not fully radial. In other words, growth is radial in the transverse view, but extends upward and outward in a longitudinal view. The constituent crystal fibers typically are only 1-2 μm in thickness. Adapted from Majewske (1969) and Hill (1981).

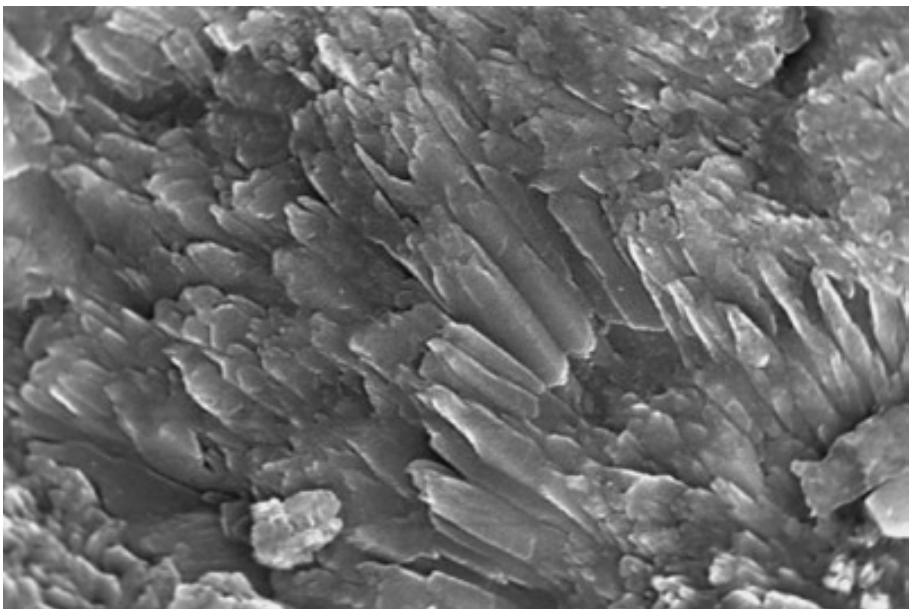

Recent sediment, Belize

An SEM image of a broken portion of the scleractinian coral *Agaricia agaricites*. One can see a radiating bundle of fibrous aragonite crystals, termed a "fascicle" — the basic building block of trabecular wall structure.

SEM, HA = 37 μm

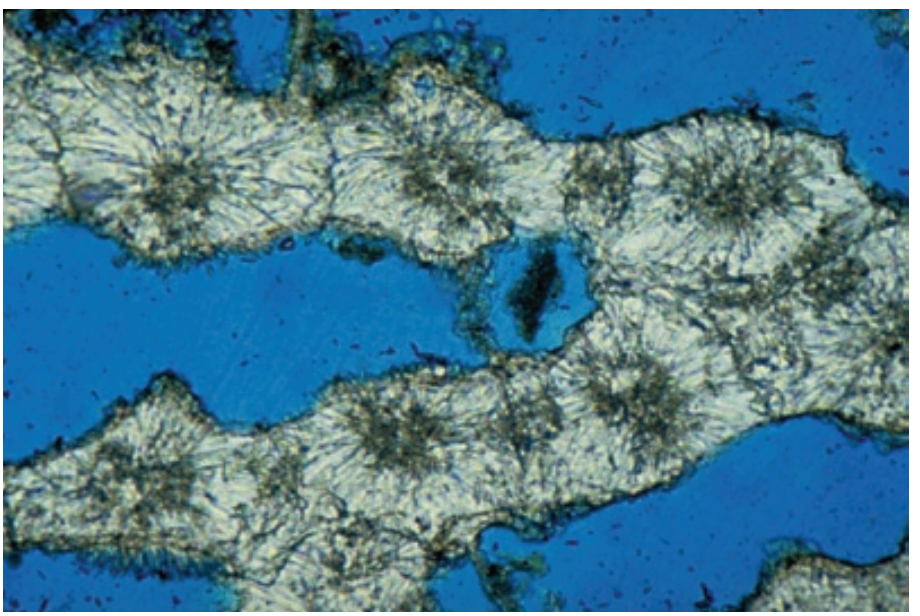

Recent sediment, Grand Cayman, Cayman Islands. B.W.I.

A modern, colonial scleractinian coral, probably *Siderastrea radians*, showing coarse trabecular structure in its septa. Note the series of dark growth centers that are the starting points for the growth of radiating aragonite fiber fascicles (also visible). Although this aragonitic fabric is diagnostic of scleractinian corals, it rarely is preserved in pre-Neogene (or even pre-Pleistocene) samples. Blue epoxy fills the empty corallites.

PPL, BSE, HA = 0.65 mm

Recent sediment, Grand Cayman, Cayman Islands. B.W.I.

A cross-polarized view of the same modern scleractinian coral, probably *Siderastrea radians*, shown in the previous photograph. The radiating bundles of aragonite fibers (fascicles) constituting trabeculae within septa are readily visible. The aragonitic skeleton of such corals is rarely preserved in porous reef limestones of pre-Neogene age, but is preserved as such in more impermeable strata, even in strata as old as Triassic.

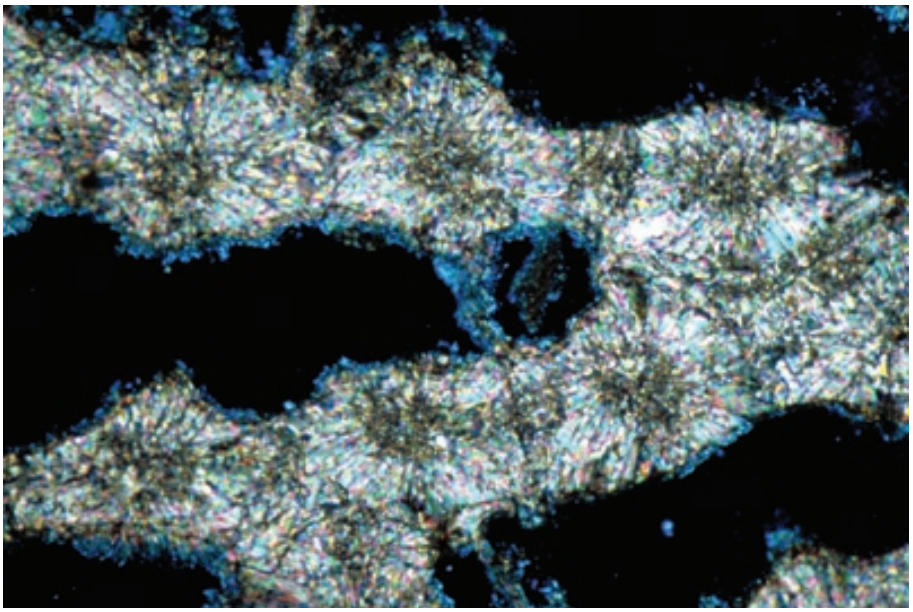

XPL, BSE, HA = 0.65 mm

Recent sediment, Grand Cayman, Cayman Islands. B.W.I.

A further enlarged view of the wall of a modern, colonial scleractinian coral showing trabecular septal structure. The details of the fiber fascicles are visible as is the line of microcrystalline growth centers that runs down the axis of each septum.

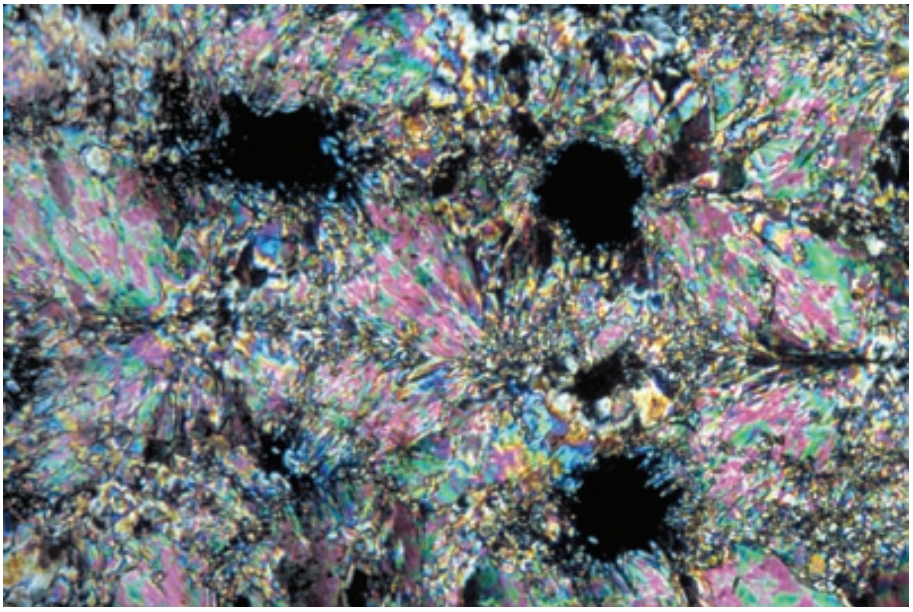

XPL, BSE, HA = 1.6 mm

Recent sediment, Grand Cayman, Cayman Islands. B.W.I.

A fragment of a modern, colonial scleractinian coral, *Siderastrea radians*, showing the tightly packed arrangement of adjacent corallites and the pattern of radiating septa. The aragonitic septal structure of this coral is still pristine.

PPL, BSE, HA = 16 mm

Pleistocene Key Largo Ls., Windley Key, Monroe Co., Florida

Because all scleractinian coral skeletons originally were composed of aragonite, they are generally strongly affected by diagenesis (either relatively rapidly altered during subaerial or freshwater diagenesis, or more slowly altered in marine settings). This scleractinian coral, *Diploria strigosa*, has experienced about 120,000 years of meteoric diagenesis. It has undergone some dissolution, but most of the wall structure is still aragonitic.

PPL, HA = 14.5 mm

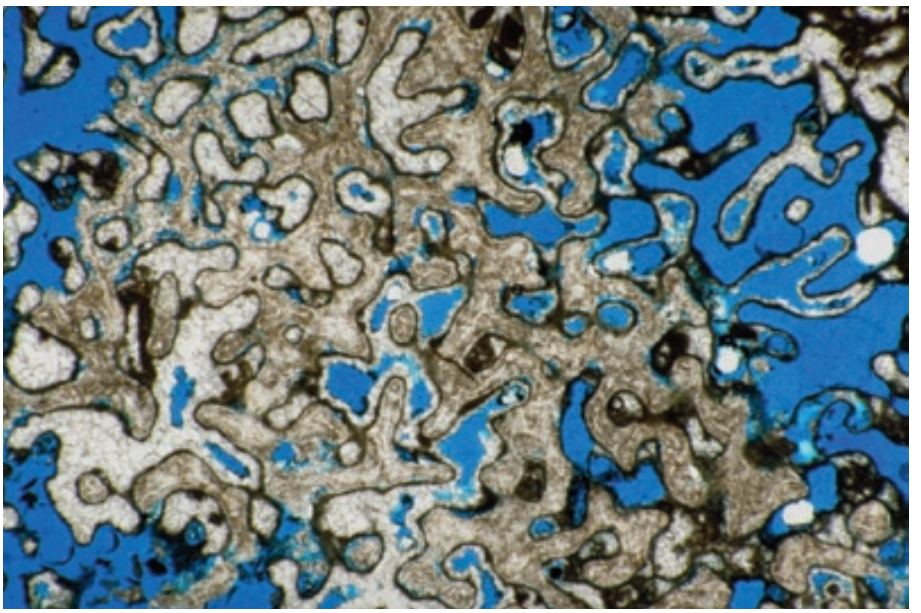

Pleistocene (120 ky) Coral Rock Fm., St. Peter Parish, Barbados

This scleractinian coral (probably *Porites porites*) has also undergone roughly 120,000 years of meteoric alteration, but suffered more extensive dissolution or neomorphism of its originally aragonitic skeleton. The difference in the degree of alteration between this sample and the previous one may be related to coral structure — *Porites* has an extremely porous and permeable skeleton formed of thin elements that are easily altered, while *Diploria* has more solid septa and is less easily altered. An additional factors may be the volume of fresh water that has contacted the two corals (a function of rainfall and permeability)

PPL, BSE, HA = 5.0 mm

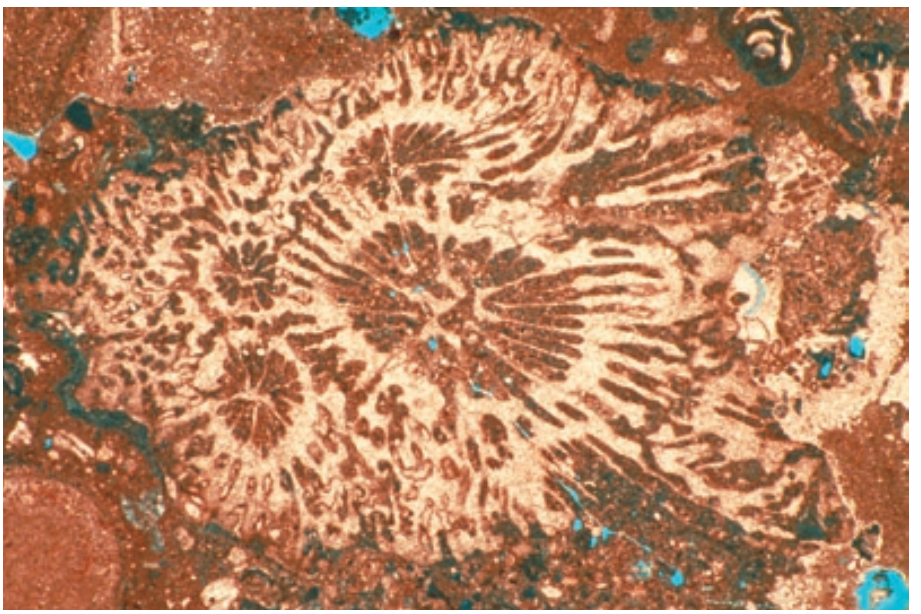

Up. Cretaceous (Maastrichtian?) limestone, Paxos, Ionian Islands, Greece

This fragment of a roughly 65 million year old colonial scleractinian coral has been completely neomorphosed. It remains quite recognizable as scleractinian coral material, however, because the skeletal outlines have been preserved through infilling by micritic sediment matrix. Commonly, such poor preservation of internal structure of septa and walls can be a criterion for recognition of scleractinian corals and help to distinguish their remains from those of other (calcitic) groups of corals and bryozoans.

PPL, BSE, AFeS, HA = 9.0 mm

Mid. Jurassic (Bajocian) limestone, Central High Atlas region, Morocco

This page gives three examples of completely neomorphosed scleractinian corals. This solitary corallite remains recognizable because of a combination of sediment infill and microbial encrustation (the dark brown, irregular coatings).

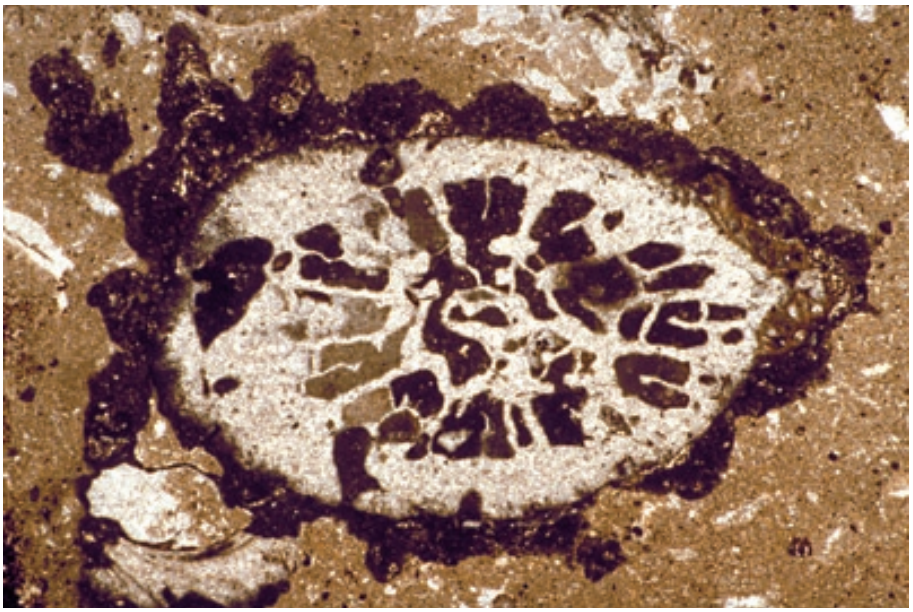

PPL, HA = 10 mm

Lo. Jurassic (Liassic) limestone, Central High Atlas region, Morocco

This neomorphosed colony of finger-like scleractinian corals shows highly variable preservation of two adjacent specimens. In the left-hand specimen, internal morphology has been preserved, perhaps through early cementation. The right-hand specimen, however, has undergone leaching of the septal structures and later infill of the pores by coarse calcite spar.

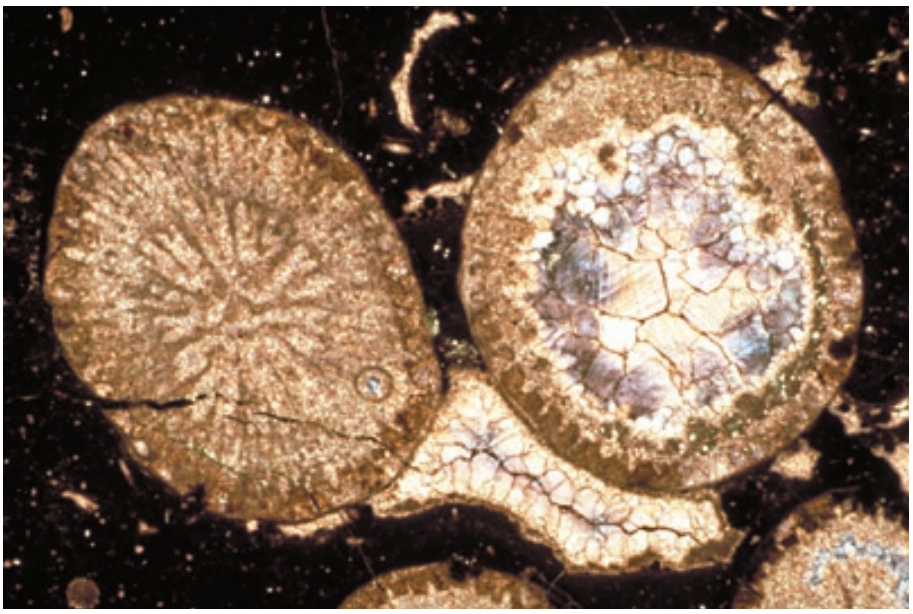

PPL, AFeS, HA = 12.5 mm

Lo. Jurassic (Liassic) limestone, Central High Atlas region, Morocco

This final example of a neomorphosed group of scleractinian corals shows very poor preservation of structure. Nevertheless, gross morphological preservation of size and shape of corallites allows general identification of this material as being of scleractinian origin.

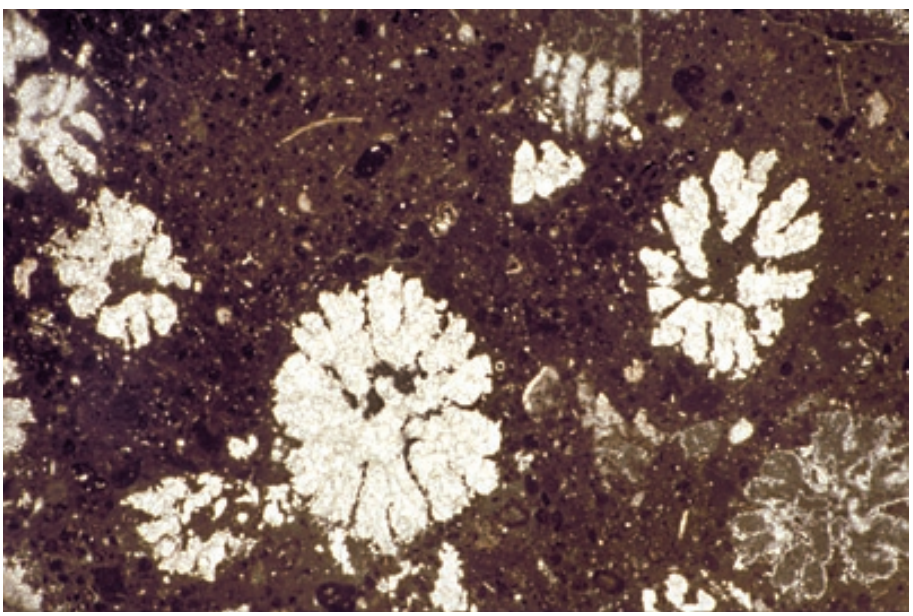

PPL, HA = 9.0 mm

OCTOCORALS

Taxonomy and Age Range:

Phylum Cnidaria, Class Anthozoa

Subclass Octocorallia (=Alcyonaria) — Late Proterozoic-Recent (but with many stratigraphic gaps)

Order Gorgonacea — including the sea whips and sea fans, Cretaceous-Recent.

Environmental Implications:

This group includes sea fans, sea whips, and soft corals that are commonly found on tropical reefs. It also includes the order Stolonifera or "organ-pipe" corals and the order Helioporaceae (including *Heliopora*, the "blue coral" of the Indian and Pacific Oceans). These organisms (with some exceptions) are weakly calcified and thus leave little record in reefs.

Non-zooxanthellate forms (sea pens, for example) can extend to great depths (>6000 m) and very cold waters.

Skeletal Mineralogy:

Octocorals generally have high-Mg calcite spicules, but a few (Holaxonia, a suborder of the Gorgonacea) have aragonitic or mixed aragonite and calcite components. Fossil gorgonian holdfasts apparently were calcitic (probably high-Mg calcite). *Tubipora musica* is hi-Mg calcite, with 14-16 mole% Mg. *Heliopora coerula* is composed of aragonite.

Morphologic Features:

Octocorals are so named because they have eight-fold symmetry; for example, each polyp in the colony has eight tentacles. They are exclusively colonial anthozoans.

Most octocorals have tissues of relatively hard (horn-like) organic material that decomposes after death. Many, however, have calcareous spicules (sclerites) contained within their organic tissues, and some groups produce calcified holdfast structures or long, slender internal supports — these calcareous constituents can be preserved as fossils but are found only rarely in thin section.

Keys to Petrographic Recognition:

1. **Alcyonarian spicules (sclerites) are small (0.01-0.1 mm), straight to slightly curved, spindle-shaped rods that are pointed at both ends and are covered with small spines or protrusions. They are commonly seen in grain mounts of modern carbonate sediment, but rarely are recognized in thin sections of ancient rocks.**
2. **Modern alcyonarian spicules have a distinctly reddish-purple color and slightly undulose extinction (unlike holothurian sclerites).**
3. **Gorgonian holdfasts have barrel-like shapes and a dense, well preserved structure with a radially-oriented, plicated fibrous fabric.**
4. ***Tubipora*, strictly speaking, does not have an exoskeleton, but rather has fused and cement covered spicules.**

Recent sediment, Florida Keys, Monroe Co., Florida

An impregnated sample of a gorgonian coral (a sea whip) showing the embedded, lenticular, high-Mg calcite spicules (sclerites). Note the general length-parallel orientation of the sclerites within the alcyonarian tissues. A slight reddish-purple color is seen in some of the sclerites.

XPL, BSE, HA = 7.0 mm

Recent sediment, Florida Keys, Monroe Co., Florida

A detailed view of alcyonarian coral (soft coral; sea whip) tissues showing the embedded high-Mg calcite sclerites with their characteristic reddish-purple color. These sclerites are massive and lenticular and have relatively smooth exterior surfaces. Upon death of the organism, the organic tissue decomposes, releasing these spicules as isolated sediment grains.

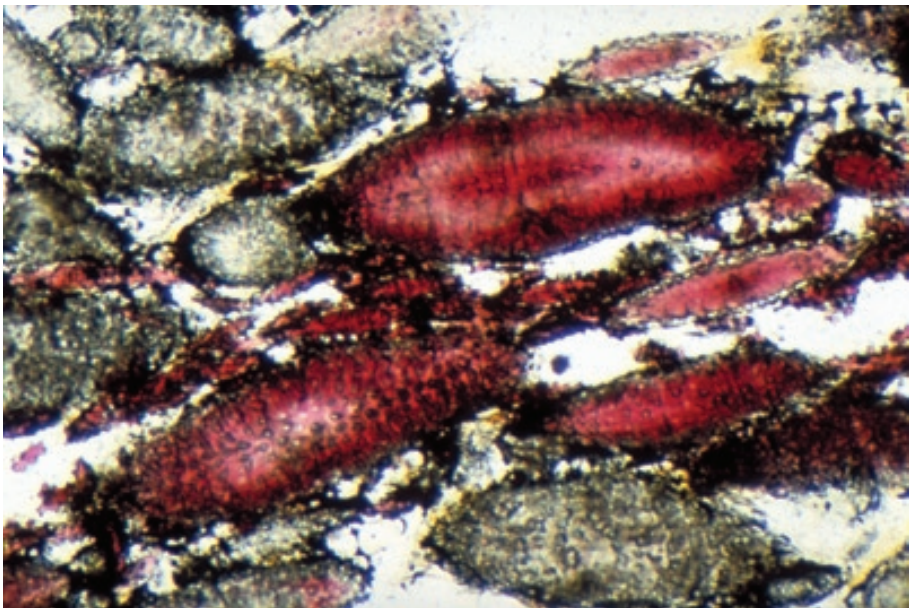

PPL, HA = 2.0 mm

Recent sediment, St. Croix, U.S. Virgin Islands

Spicules (sclerites) of a gorgonian as loose sediment particles. These calcitic sclerites have a more slender shape with more pronounced club-like surface protrusions that are characteristic of many species of gorgonians. Photograph courtesy of Lee Gerhard.

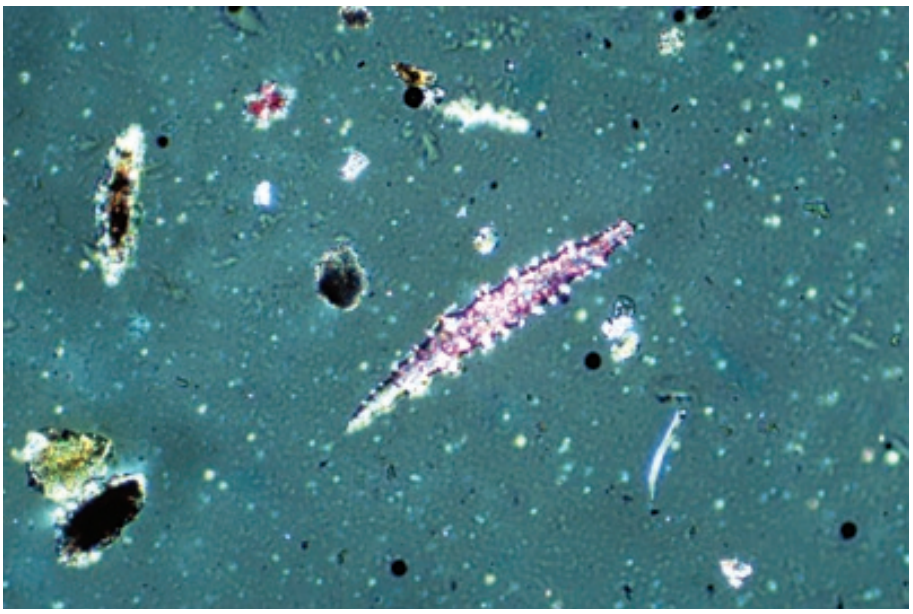

PXPL, HA = ~0.8 mm

Oligocene-Miocene hiatal surface atop McDonald Ls., Oamaru, Otago, New Zealand

This grain has been described as a gorgonian holdfast that was attached to a phosphatic hardground. The particles are barrel-shaped, with nearly rectangular outlines in axial sections and circular outlines in transverse sections such as this one. The well preserved radiating plications are characteristic features of these originally calcitic grains.

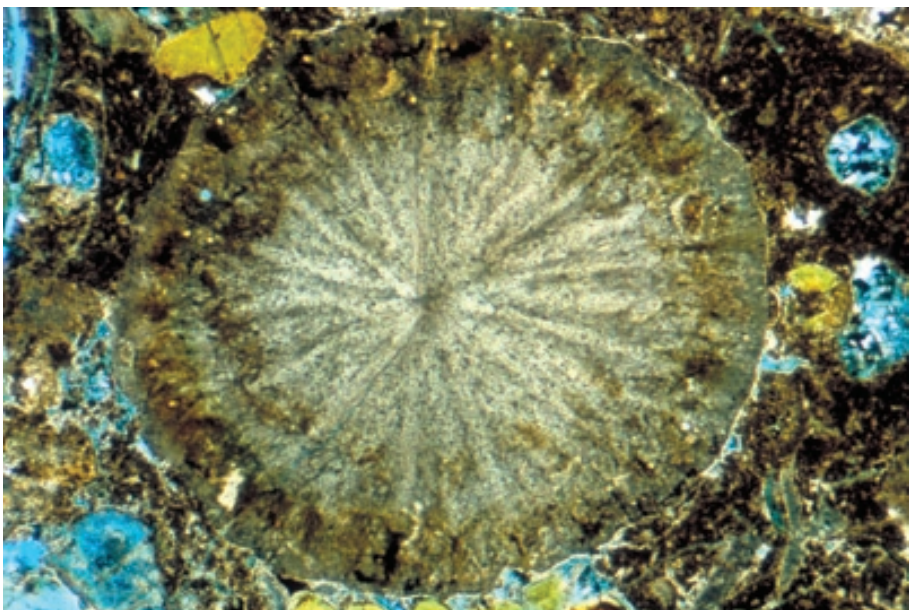

PPL, BSE, HA = 2.4 mm

Oligocene-Miocene hiatal surface atop McDonald Ls., Oamaru, Otago, New Zealand

Under cross-polarized illumination, the radial, plicated structure of this gorgonian holdfast is more clearly visible than it is with plane-polarized lighting.

XPL, HA = 4.1 mm

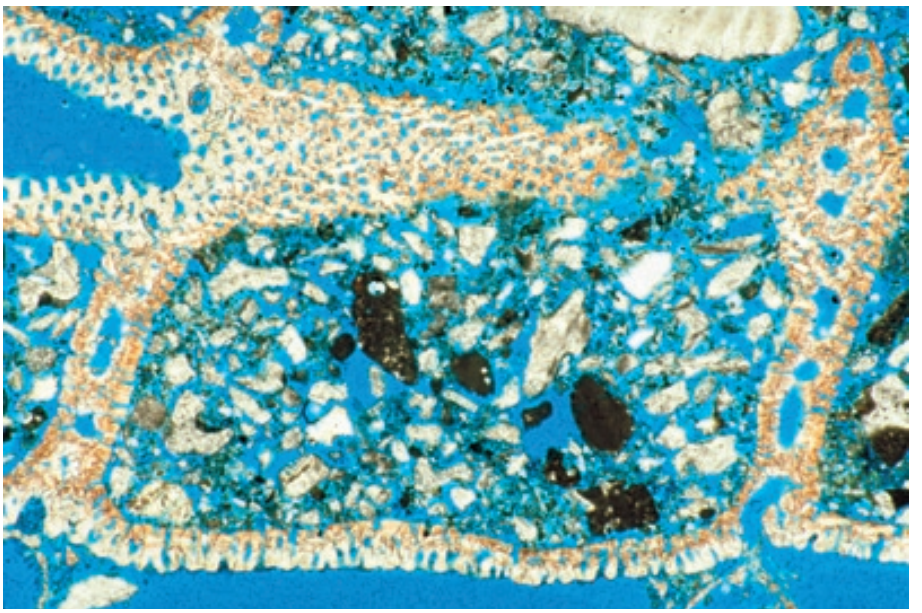

Recent sediment, Pacific region

A longitudinal cross section through a modern "organ pipe" coral — *Tubipora musica*. The skeletal remains of this member of the Stolonifera consist of densely packed fascicles (bundles of radiating fibers), actually fused and cemented-encased spicules. The relatively high content of organic matter in the skeleton gives it a yellowish color in thin section (and a deep red color in hand sample).

PPL, BSE, HA = 6.0 mm

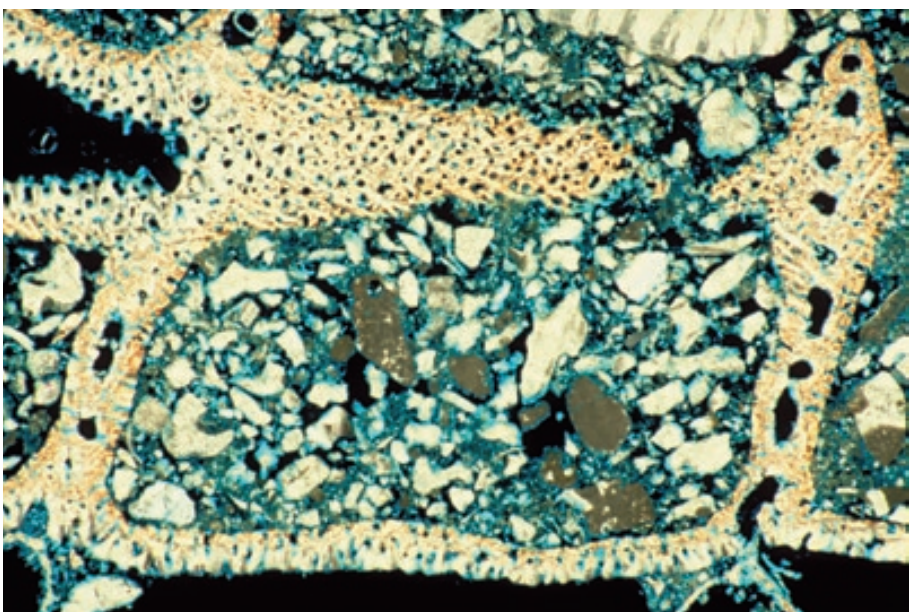

Recent sediment, Pacific region

The same view of a modern organ pipe coral — *Tubipora musica* — under cross-polarized illumination. Even though this coral builds large, hard skeletons, it is a member of the Octocorallia (the "soft" corals) because of the spicular nature of the skeletal material, quite unlike the solid exoskeletons of members of the Scleractinia.

XPL, BSE, HA = 6.0 mm

Hydrozoans

Taxonomy and Age Range:

Phylum Cnidaria, Class Hydrozoa
Order Hydroida — Late Proterozoic-Recent (but with many stratigraphic gaps)
Order Hydrocorallina (includes the Milleporina and Stylasterina) — Tertiary (Cretaceous?)-Recent
Order Spongiomorphida — Triassic-Jurassic

Environmental Implications:

This is an extremely complex group of organisms, and we will only present a single modern form here, *Millepora*, (other possible hydrozoans are included under "Problematica"). *Millepora* is a common framework builder and encruster in high-energy (upper reef front) settings in modern, warm water (tropical) reefs. *Millepora* tissues contain zooxanthellae so they are found only in euphotic water depths.

Skeletal Mineralogy:

Various groups of modern hydrozoans have either aragonitic or calcitic skeletons. Members of the Milleporina are aragonitic: members of the Stylasterina are predominantly aragonitic with some possible admixture of calcite in settings with low water temperatures.

Morphologic Features:

***Millepora* (the "fire coral") generally has finger-like to bladed, very hard and brittle growth forms. It is different from true corals in that its calyces appear as minute holes, with neither septa nor tentacles visible. The pores are divided into two functional categories: gastropores house feeding polyps (gastrozoids) that have four to six tentacles that are rarely emergent. Numerous smaller pores (dactylopores) surround the gastropores and house the stinging cells for which the "fire coral" is named.**

Triassic-Jurassic spongiomorphids formed substantial colonies with radiating pillars that are joined by horizontal bars. As their name implies, they can appear very similar to sponges, especially when poorly preserved.

Keys to Petrographic Recognition:

1. ***Millepora* has no central cup or body cavity.**
2. ***Millepora* has a labyrinthine-appearing, aragonitic wall structure that is perforated with numerous small pores with two distinct size modes.**
3. **The aragonitic composition of *Millepora* makes good preservation of skeletal microstructure unlikely in pre-Pleistocene samples.**

Recent sediment, Grand Cayman, Cayman Islands. B.W.I.

A section showing the wall structure of the modern hydrozoan, *Millepora alcicornis*. Note the characteristic wall fabric consisting of a few large pores (gastropores) surrounded by more numerous smaller pores (dactylopores). The pores here have been filled with blue-dyed epoxy.

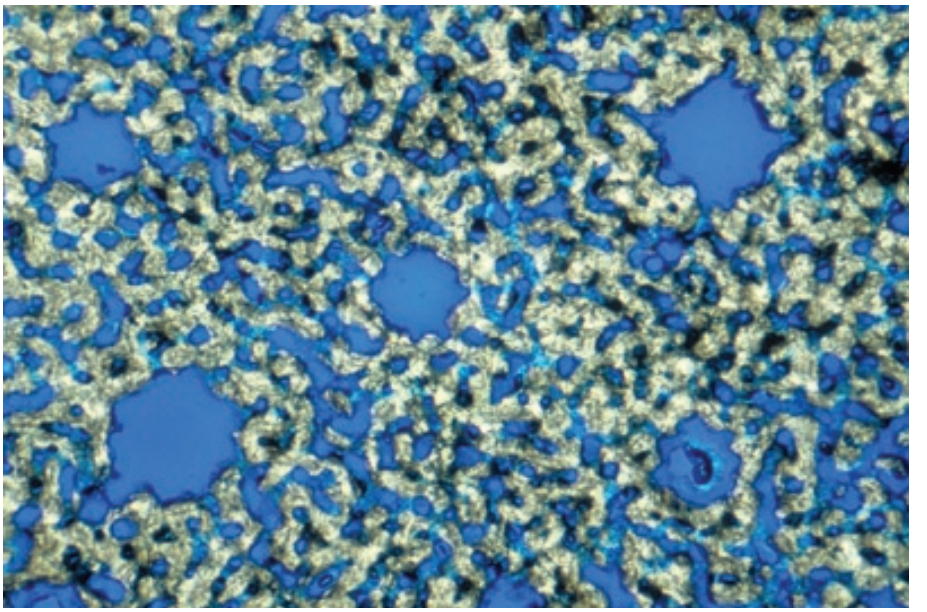

PPL, BSE, HA = 2.4 mm

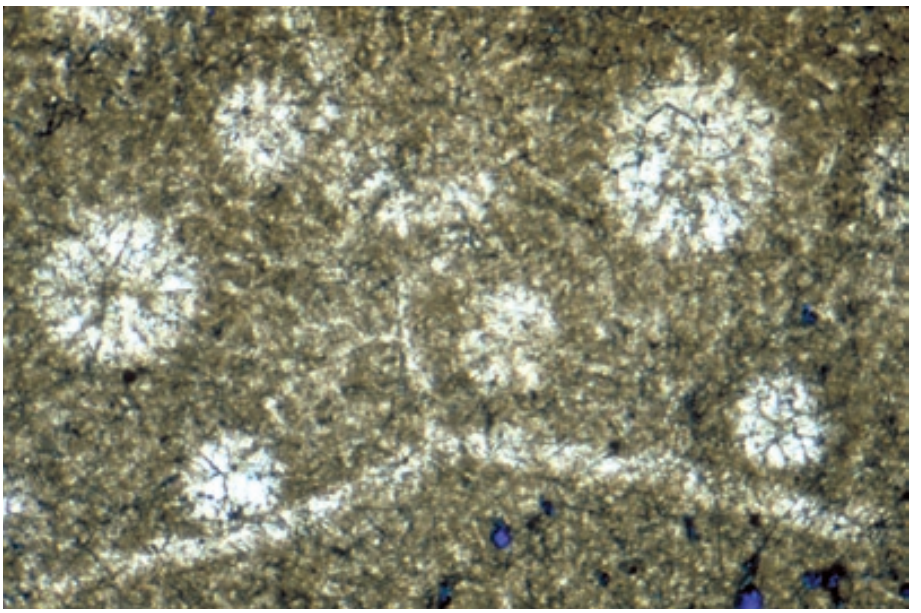

Recent sediment, Grand Cayman, Cayman Islands, B.W.I.

A view of a sedimentary fragment of the modern hydrozoan, *Millepora alcicornis*, with significant marine cementation in its intraparticle pores. Although such cementation makes it more difficult to recognize the distinctive structure of large pores surrounded by small ones, it may help to preserve those pores during later diagenesis.

PPL, HA = 2.4 mm

Cited References and Additional Information Sources

Bayer, F. M., 1956, Octocorallia, *in* R. C. Moore, ed., Treatise on Invertebrate Paleontology, Part F, Coelenterata: Geological Society of America and University of Kansas Press, p. F166-F230.

Bryan, W. H., and D. Hill, 1940, Spherulitic crystallization as a mechanism of skeletal growth in the hexacorals: Royal Society of Queensland Proceedings, v. 52, p. 78-91.

Flügel, H.W., 1975, Skelettenentwicklung, Ontogenie und Funktionsmorphologie rugoser Korallen: Paläontologische Zeitschrift, v. 49 (4), p. 407-431.

Hill, D., 1981, Rugosa and Tabulata, *in* C. Teichert, ed., Treatise on Invertebrate Paleontology, Part F, Coelenterata, Supplement 1: Geological Society of America and University of Kansas Press.

Hill, D., and Stumm, E. C., 1956, Tabulata, *in* R. C. Moore, ed., Treatise on Invertebrate Paleontology, Part F, Coelenterata: Geological Society of America and University of Kansas Press, p. F233-F324.Hudson, R. G. S., 1956, Tethyan Jurassic hydroids of the family Milleporidiidae: Journal of Paleontology, v. 30, p. 714-730.

Kato, M., 1963, Fine skeletal structures in Rugosa: Journal of the Faculty of Science of Hokkaido University, Series 411, p. 571-630.

Majewske, O. P., 1969, Recognition of Invertebrate Fossil Fragments in Rocks and Thin Sections: Leiden, E. J. Brill, 101 p.

Oliver, W. A., Jr.,1980, The relationship of the scleractinian corals to the rugose corals: Paleobiology, v. 6, p. 146-160.

Oliver, W. A., Jr., and A. G. Coates, 1987, Phylum Cnidaria, *in* R. S. Boardman, A. H. Cheetham, and A. J. Rowell, Fossil Invertebrates: Palo Alto, CA, Blackwell Scientific Publications, p. 140-193.

Roniewicz, E., 1996, The key role of skeletal microstructure in recognizing high-rank scleractinian taxa in the stratigraphical record, *in* G. D. Stanley, Jr., ed., Geological Society of America, annual meeting, v. 1, Paleontological Society, p. 187-206.

Scrutton, C. T., 1997, The Palaeozoic corals, 1: Origins and relationships: Proceedings of the Yorkshire Geological Society, v. 51, p. 177-208.

Scrutton, C. T., and B. R. Rosen, 1985, Cnidaria, in J. W. Murray, Atlas of Invertebrate Macrofossils: New York, John Wiley & Sons, p. 11-46.

Sorauf, J. E., 1972, Skeletal microstructure and microarchitecture in Scleractinia (Coelenterata): Palaeontology, v. 15, p. 88-107.

Sorauf, J. E., 1996, Biocrystallization models and skeletal structure of Phanerozoic corals, *in* G. D. Stanley, Jr., ed., Geological Society of America, annual meeting, v. 1, The Paleontological Society, p. 159-185.

Sorauf, J. E., 1999, Skeletal microstructure, geochemistry, and organic remnants in Cretaceous scleractinian coals; Santonian Gosau beds of Gosau, Austria: Journal of Paleontology, v. 73, p. 1029-1041.

Sorauf, J. E., and Cuif, J.-P., 2001, Biomineralization and diagenesis in the Scleractinea: part 2, diagenesis: Bulletin Tohoku University Museum (Japan), no. 1, p. 152-163.

Sorauf, J. E., and W. A. Oliver, Jr., 1976, Septal carinae and microstructure in middle Devonian *Heliophyllum* (Rugosa) from New York State: Journal of Paleontology, v. 50, p. 331-343.

Sorauf, J. E., and N. Podoff, 1977, Skeletal structure in deep water ahermatypic corals, *in* Proceedings of the 2nd International Symposium on Corals and Fossil Coral Reefs: Paris, Mémoires du Bureau de Recherches Géologiques et Minières (France) 89, p. 2-11.

Sorauf, J.E., and M. Savarese, 1995, A Lower Cambrian coral from South Australia: Palaeontology, v. 38, p. 757-770.

Stehli, F. G., 1956, Shell mineralogy in Paleozoic invertebrates: Science, v. 123, p. 1031-1032.

Strel'nikov, S. I., 1965, Microstructure of septal system in some Silurian tetracorals: International Geology Review, v. 7, p. 910-917. [Translated from Russian article in Paleont. Zhumal, no. 3, p. 10-17.

Sultanbekova, Z. S., 1991, The significance of skeletal microstructure for the systematics of ancient streptelasmids (Rugosa): Paleontological Journal, v. 25, p. 144-149.

Wang, H. C., 1950, A revision of the Zoantharia Rugosa in the light of their minute skeletal structures: Philosophical Transactions, Royal Society of London, Series B, Biological Sciences, v. 234, no. 611, p. 175-246.

Wells, J. W., 1956, Scleractinia, *in* R. C. Moore, ed., Treatise on Invertebrate Paleontology, Part F, Coelenterata: Geological Society of America and the University of Kansas Press, p. F161-F164.

Wells, J. W., and Hill, D., 1956, Anthozoa - General features, *in* R. C. Moore, ed., Treatise on Invertebrate Paleontology, Part F, Coelenterata: Geological Society of America and the University of Kansas Press, p. F328-F444.

Wise, S. W., Jr., 1970, Scleractinian coral exoskeletons: surface microarchitecture and attachment scar patterns: Science, v. 169, p. 978-980.

Young, G. A., and R. J. Elias, 1997, Patterns of variation in Late Ordovician and Early Silurian tabulate corals. Boletin Real Sociedad Española de Historia Natural, Seccion Geologica, v. 91, p. 193-204.

Facing Page: Top - Underwater view of branching bryozoan colonies (the fawn-green "bushes"), 20 m water depth, Three Kings platform, northern New Zealand. Photograph courtesy of Campbell S. Nelson and Roger V. Grace.

Bottom - Bryozoan-rich, gravel-sized fraction of Holocene skeletal carbonate sediment, 122 m water depth, Three Kings platform, northern New Zealand. Photograph courtesy of Campbell S. Nelson and Roger V. Grace.

GRAINS: Skeletal Fragments

Bryozoans

CHAPTER 7

BRYOZOANS

Taxonomy and Age Range:

Phylum Bryozoa
- **Subphylum Entoprocta — Middle Cambrian?, Late Jurassic-Recent**
- **Subphylum Ectoprocta**
  - **Class Phylactolaemata — Middle Jurassic-Recent**
  - **Class Gymnolaemata — Early Ordovician-Recent (dominates Mesozoic-Recent)**
    - **Order Ctenostomida — Early Ordovician-Recent**
    - **Order Cheilostomida — Late Jurassic-Recent**
  - **Class Stenolaemata — Early Ordovician-Recent (dominates Ordovician-Permian)**
    - **Order Cyclostomida — Early Ordovician-Recent**
    - **Order Cystoporida — Early Ordovician-Late Triassic**
    - **Order Trepostomida — Early Ordovician-Late Triassic**
    - **Order Cryptostomida — Early Ordovician-Late Triassic**

Environmental Implications:

Bryozoans are sessile, filter-feeding organisms with a wide salinity tolerance — most are marine, but a few species (from the Entoprocta, Phylactolaemata, and Ctenostomida) inhabit fresh water and a few others (from the Cheilostomida) are found in brackish-water environments.

Bryozoans have wide latitudinal (tropical to polar), temperature, and depth ranges (0 to 8.5 km). They can be the main constituents in Mesozoic and Cenozoic temperate- and cold-water shelf carbonates, as well as in deeper shelf and slope settings; in the Paleozoic, they were more conspicuous in tropical to subtropical habitats.

Many bryozoans require a firm substrate on which to encrust; some are free living, and others have roots extending into sandy substrates. Massive and encrusting varieties are found in high-energy environments; delicate, erect varieties are indicative of low-energy environments.

Skeletal Mineralogy:

Entoproct bryozoans are soft bodied and, therefore, are rarely preserved.

Most ectoproct bryozoan zooecial walls are composed of calcite (usually low-Mg calcite; a few consist of high-Mg calcite and others are partially aragonitic). Some species have chitinous or gelatinous walls.

Morphologic Features:

Bryozoans are colonial, polyp-like, lophophorate invertebrate animals that are distinguished by their U-shaped digestive track. Entoproct bryozoans have an anal opening inside their circle of tentacles; ectoproct bryozoans are characterized by having an anal opening outside or below the tentacles.

Each zooid inhabits a hardened exoskeleton (zooecium) and forms encrusting thread-like or sheet-like, massive, nodular, hemispherical, ramose, bifoliate, fenestrate, or tuft-like colonies.

Keys to Petrographic Recognition:

1. **Bryozoans are colonial organisms with full colonies ranging in size from mm up to cms.**
2. **Individual zooecia typically are less than 1 mm in diameter and length.**
3. **Zooecial wall structures consist of laminar, foliated or granular crystals of calcium carbonate.**
4. **Cheilostomes have a regular, box-like to random arrangement of zooecia; zooecial walls are composed of calcite or mixed calcite-aragonite. Zooecia usually do not contain diaphragms (partitions).**
5. **Stenolaemates have elongate, tubular zooecia.**

   • Cyclostomes have very elongate zooecia. Zooecial walls are very thin (finely granular to thinly laminated) and may contain small pores (interzooecial pores). Growth habits are varied (encrusting, branching, disks). Diaphragms (partitions) are uncommon.

   • Cystoporida have thin-walled, short to long zooecia. Zooecia may contain diaphragms. Ceramoporina have long empty tubes (exilapores) parallel to zooecia. Walls are laminated and contain interzooecial pores. Fistuliporina contain bubble-like pores (cystopores) between zooecia. Wall structure is granular to massive.

• Trepostomes have long slender zooecia and can form large branching to nodular masses. The central zooecial walls are thin and fused together. Towards the exterior, zooecial walls thicken significantly. May contain small tubes (mesopores) between zooecia and diaphragms within or between zooecia. Well-developed wall lamination. May have low spines (acanthorods) that in tangential sections appear as circular structures.
• Cryptostomes have short tubes that form delicate colonies. Zooecial walls are well laminated, thinner in the center and becoming thicker outward. Many zooecium are empty except for a single diaphragm (those may partially cross the zooecium). Rhabdomesina (or rhomboporoid) bryozoans form slender cylindrical branches; zooecia radiate outward from the long axis. They have complete and/or partial diaphragms. Tangential cuts may have acanthorods that vary in size. Ptilodictyina bryozoans (bifoliates) form thin, flat branches that exhibit bilateral symmetry along a plane. Fenestrina bryozoans form mesh-like fronds that contain a single layer of zooecia. Zooecia may appear linear and unconnected in some sections.

6. **The main differences between bryozoans and corals are the typically smaller size of bryozoan colonies and individual living chambers, and the outward thickening of bryozoan living chamber (zooecial) walls. Unlike red algae or corals, bryozoans have acanthorods and mesopores.**

PHOTO SCALES AND ABBREVIATIONS ARE EXPLAINED IN THE BOOK'S INTRODUCTION

Morphologic features of bryozoans

A diagram illustrating the common morphologic features of bryozoans. These elements may or may not be present in all bryozoans. Trepostomes are the only group in which specimens routinely show all of these features. The diagram is modified from Moore et al. (1952) and other sources.

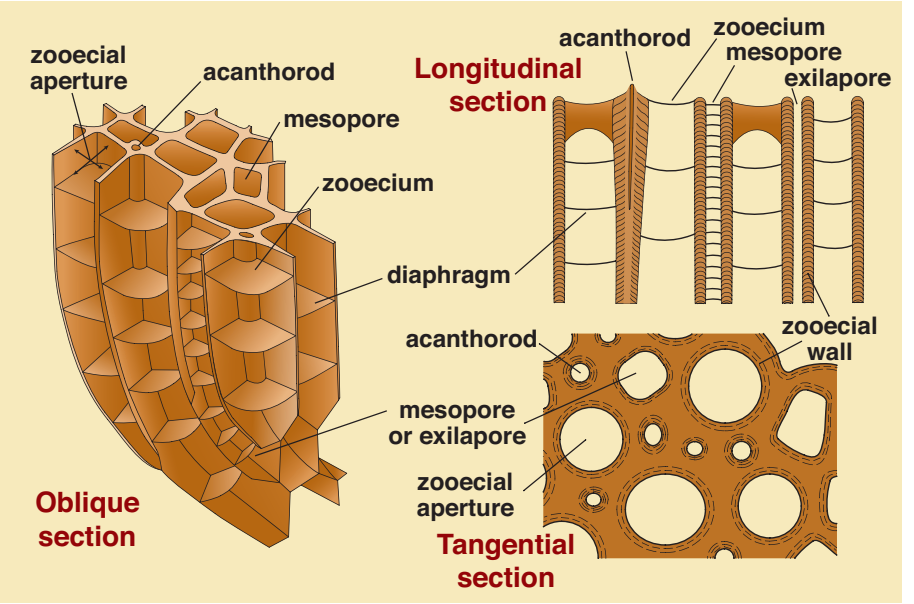

Oligocene Nile Gp., Karamea, Westland, New Zealand

In this bryozoan-rich temperate-water limestone, a variety of common bryozoan growth habits are visible: encrusters, sheets, branches (ramose), and fenestrate. These specimens are cheilostome and cyclostome bryozoans.

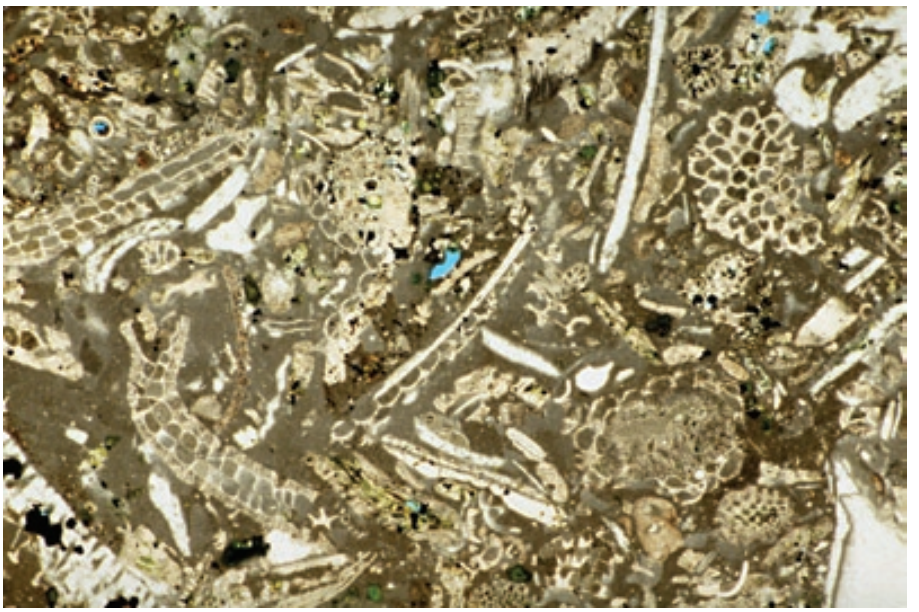

PPL, BSE, HA = 10 mm

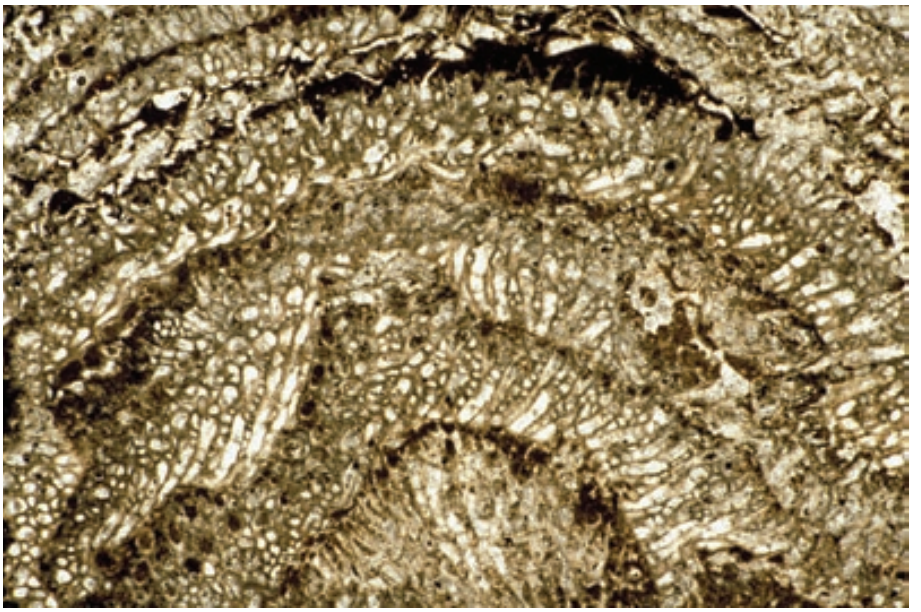

Up. Ordovician (Cincinnatian) Fairview Fm., Hamilton Co., Ohio

Another growth form common to bryozoans, these hemispherical mounds, with a few centimeters of relief, were formed by several generations of encrusting bryozoans. This bryozoan exhibits the typical pore structure of fistuliporoids (order Cystoporida).

PPL, HA = 10 mm

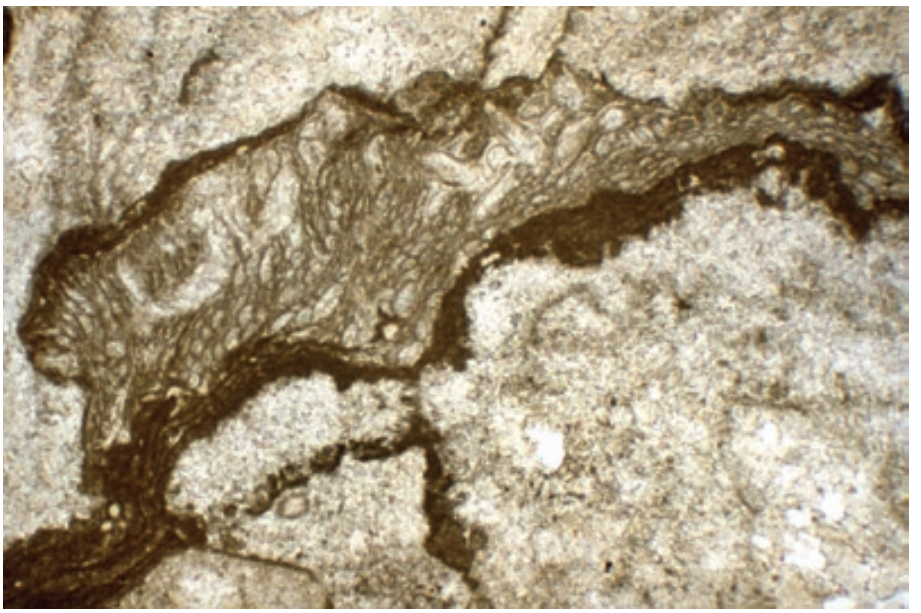

Up. Permian (Guadalupian) Capitan Fm., Eddy Co., New Mexico

Most bryozoans require a hard substrate on which to attach. Here a possible fistuliporoid bryozoan has attached to early (synsedimentary) marine cements within the sponge-algal reef of the Capitan complex.

PPL, HA = 5.1 mm

Up. Permian (Kazanian?) Wegener Halvø Fm., Jameson Land, East Greenland

Trepostome bryozoans commonly formed large, branching (or ramose) masses. In Late Paleozoic carbonates, trepostomes (along with fenestrate bryozoans) were the dominant framework contributors in many large biohermal mounds. These mounds reached several tens of meters of synoptic relief, and the cross-sectional diameters of the mounds could reach nearly a kilometer. This is the tip of a trepostome bryozoan branch, and it shows a slightly oblique cut through the long axis of the colony.

PPL, HA = 12.5 mm

Mississippian (Tournaisian-Visean) Waulsortian Ls., Co. Dublin, Ireland

Fenestrate bryozoans formed upright, fan- or cone-shaped colonies with a coarse, lattice-like appearance, and can be up to a few tens of centimeters tall. Fenestrate bryozoans can be remarkably inconspicuous in thin section, because cuts through piles of these window-screen-like grains can have close to 90% porosity (only a few "wires" in each "screen" are cut). This fenestrate bryozoan biosparite, despite its appearance, is actually a grain-supported rock. The large fenestrate bryozoans (*Fenestella* sp.) are surrounded by radial, fibrous to bladed sparry marine calcite cements.

PPL, HA = 16 mm

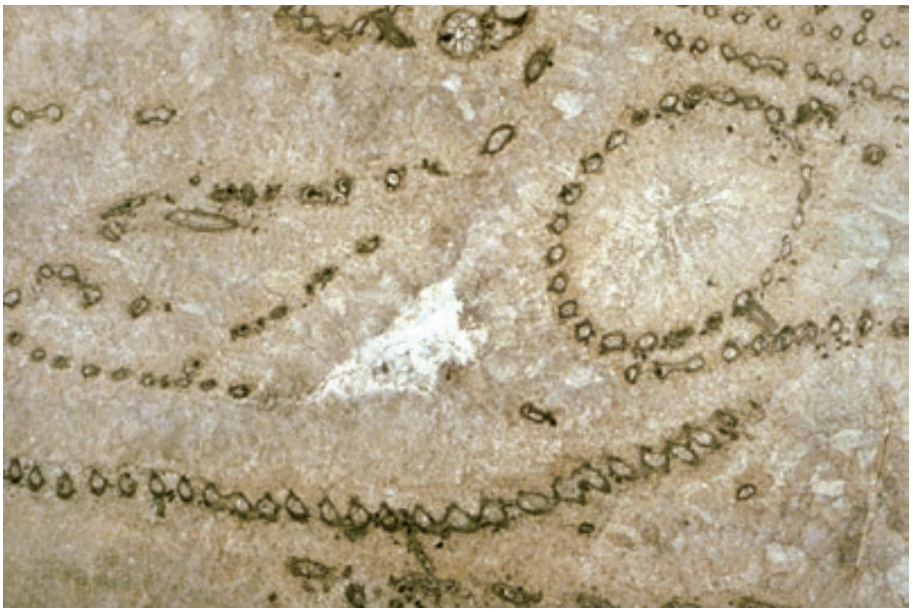

Pleistocene Key Largo Ls., Dade Co., Florida

Cheilostomes are the dominant class of bryozoans in modern carbonate sediments. Cheilostomes typically have thick zooecial walls and a regular box-like arrangement of their zooecia. This is a specimen of *Schizoporella errata*, an encrusting cheilostome that forms nodular or robustly branching colonies. Many of the zooecia are filled with blocky calcite cements.

PPL, HA = 10 mm

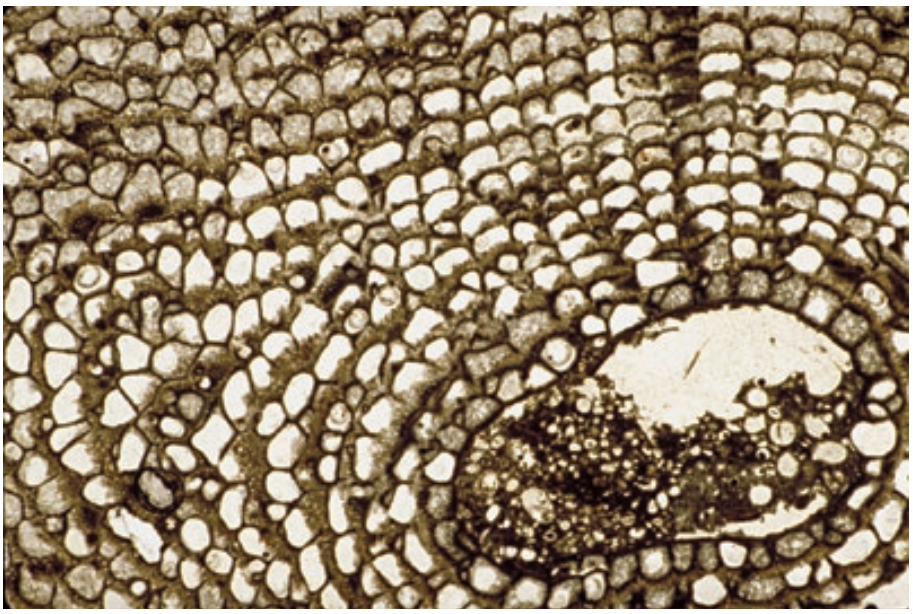

Pleistocene Key Largo Ls., Dade Co., Florida

A close-up view of the previous specimen's (*Schizoporella errata)* zooecia. Note the regular boxlike arrangement of zooecia and the thickened wall structure between successive generations. The complex zooecial relationship between successive generations show zooecia forming and pinching-out during growth, but an overall box-like arrangement is maintained.

PPL, HA = 5.0 mm

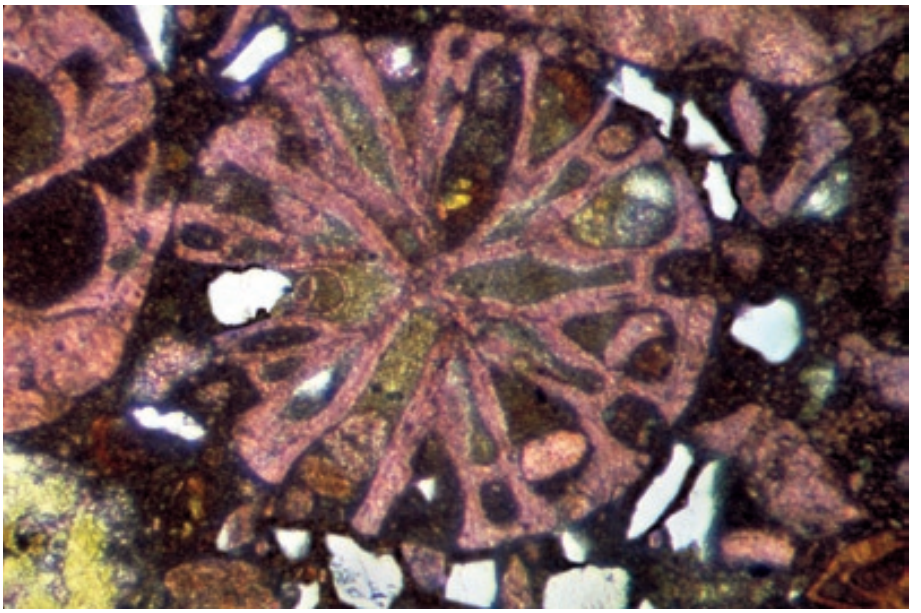

Oligocene Nile Gp., Karamea, Westland, New Zealand

Unlike the bryozoans shown in the previous two photomicrographs, this cheilostome bryozoan forms delicate branches. This transverse cut through a branch shows the empty zooecia that are typical of cheilostomes. Some zooecia are partially filled with precipitated phosphatic material; others have infills of micrite containing both carbonate and terrigenous clastic grains.

PPL, AFeS, HA = 1.6 mm

Oligocene Nile Gp., Karamea, Westland, New Zealand

This cheilostome bryozoan encrusts a bivalve (oyster) shell fragment. The transverse cut through this specimen does not exhibit an orderly box-like arrangement.

PPL, BSE, HA = 6.0 mm

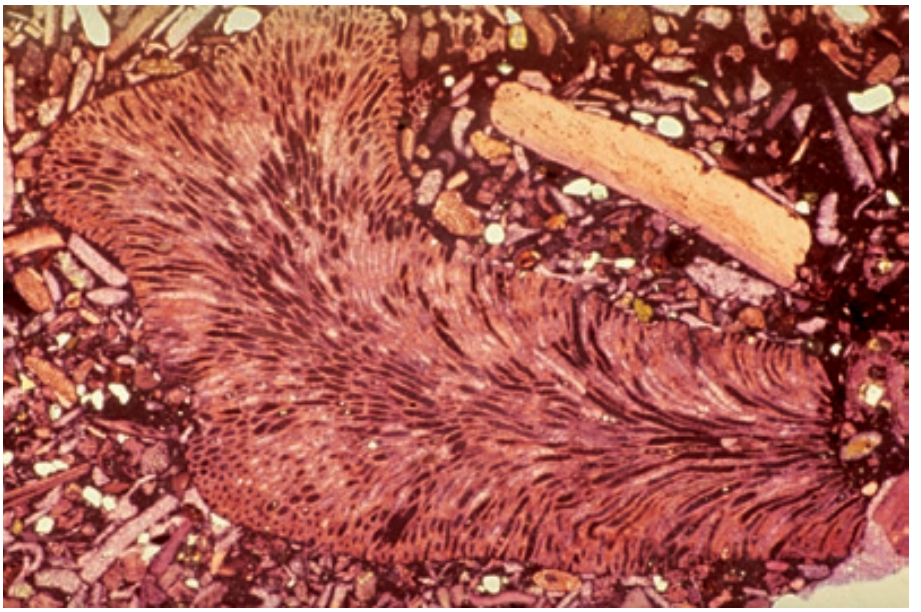

Oligocene Nile Gp., Karamea, Westland, New Zealand

This longitudinal section through a cyclostome (a cerioporoid) bryozoan branch exhibits some of the typical characteristics of cyclostomes: very elongated zooecia, thin zooecial walls, and no diaphragms.

PPL, AFeS, HA = 5.1 mm

Oligocene Nile Gp., Karamea, Westland, New Zealand

A transverse section through a cerioporoid cyclostome bryozoan. Near the center of the colony, the zooecia appear smaller than at the edge because the zooecia bend from the center of the colony outward; thus, near the edge of the sample, the zooecial walls are nearly normal to the exterior wall.

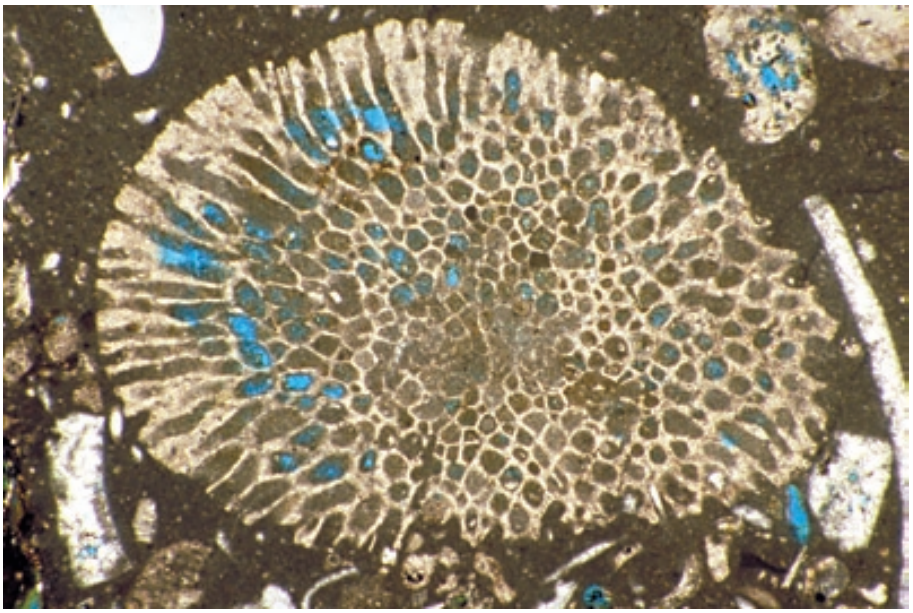

PPL, BSE, HA = 3.9 mm

Oligocene Nile Gp., Karamea, Westland, New Zealand

This longitudinal section through a cerioporoid cyclostome bryozoan colony shows elongate, empty zooecia. The large holes in the structure are possibly ovicells — shelter chambers used by developing larvae. Alternatively, they may be tunnels or borings cut by worms or arthropods living inside the bryozoan colony.

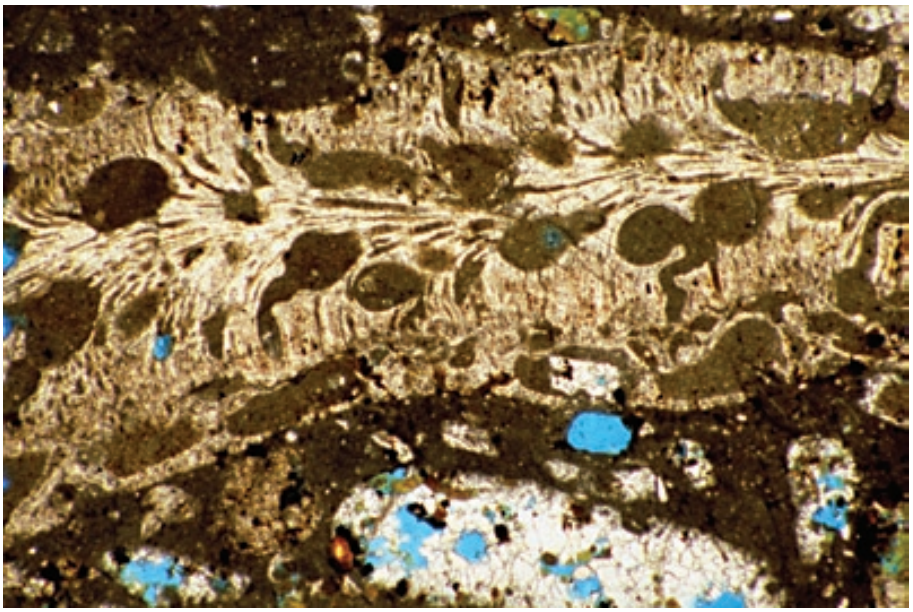

PPL, BSE, HA = 5.1 mm

Oligocene Thomas Fm., Canterbury, New Zealand

A transverse section through a cyclostome bryozoan branch, like the previous sample, has large pores that are possible ovicells or borings. Note the granular or blocky nature of the zooecial walls, a typical feature of cyclostomes. The very large pore in the lower half of bryozoan may have been enlarged by boring organisms.

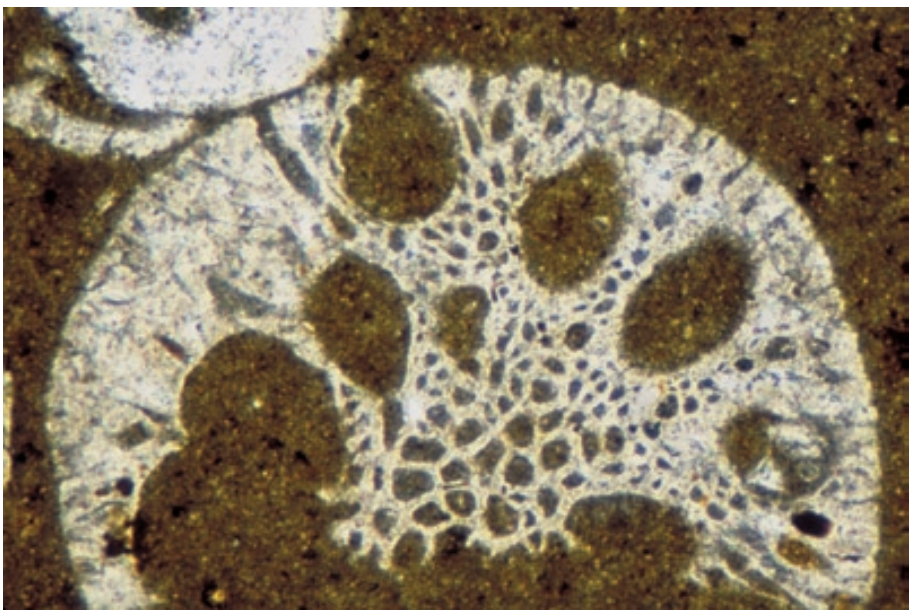

PPL, HA = 3.6 mm

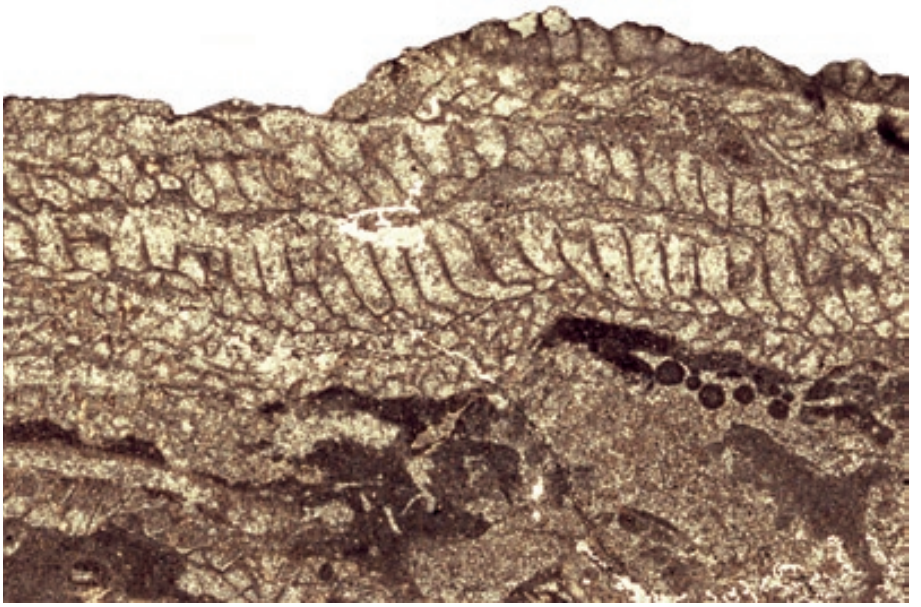

Mid. Ordovician Mingan-Chazyan Ls., Mingan Islands, Quebec, Canada

This ceramoporoid bryozoan boundstone depicts both transverse (lower) and longitudinal (upper) cross sections through the encrusting organisms. The specimen is *Cheiloporella* sp. and it exhibits a thin, finely-crystalline wall structure that lacks diaphragms within the zooecia. Photograph courtesy of Roger J. Cuffey.

PPL, HA = 10.0 mm

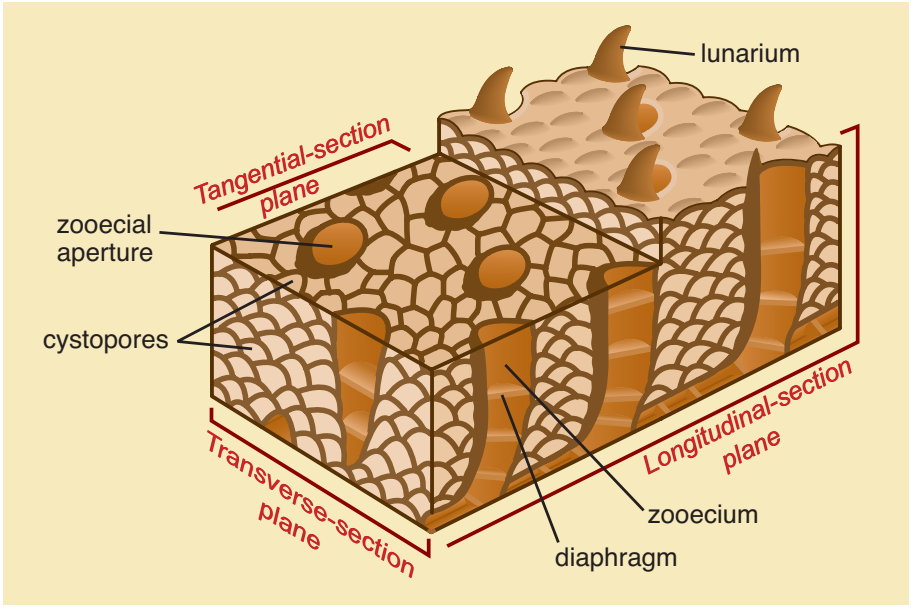

Morphology of typical fistuliporoid bryozoans

A block diagram showing longitudinal, tangential and transverse sections through a typical fistuliporoid bryozoan. Fistuliporoids generally are among the easier bryozoans to identify in thin section, because of the large zooecia surrounded by numerous small, bubble-like cystopores. The diagram is modified from Warner and Cuffey (1973).

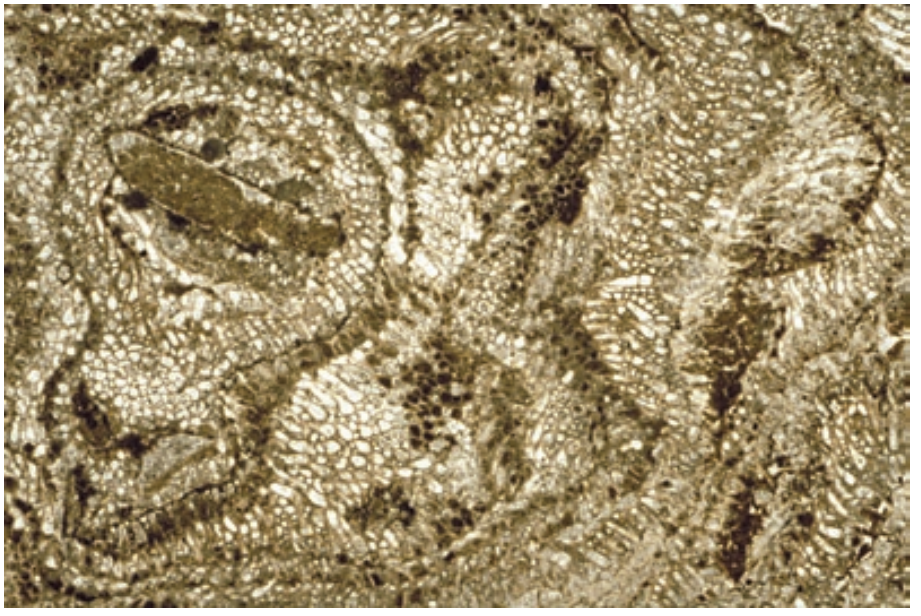

Up. Ordovician (Cincinnatian) Fairview Fm., Hamilton Co., Ohio

This is an example of an encrusting fistuliporoid bryozoan. Because of its nodular shape, a variety of orientations are visible in this sample of *Fistulipora* sp. This provides an example of typical fistuliporoid structure, with large, elongate zooecia containing diaphragms; the zooecia are separated by smaller cystopores. Fistuliporids can form large irregular masses or nodules.

PPL, HA = 16 mm

Up. Permian (Kazanian?) Wegener Halvø Fm., Jameson Land, East Greenland

This thin-section photomicrograph is a tangential to transverse section through a branch of a fistuliporoid bryozoan. Within the larger, elongate zooecia, some partitions are visible. The cystopores and zooecia are filled with a slightly ferroan calcite cement. This bryozoan biosparite is from the flank facies of a deep-water bioherm.

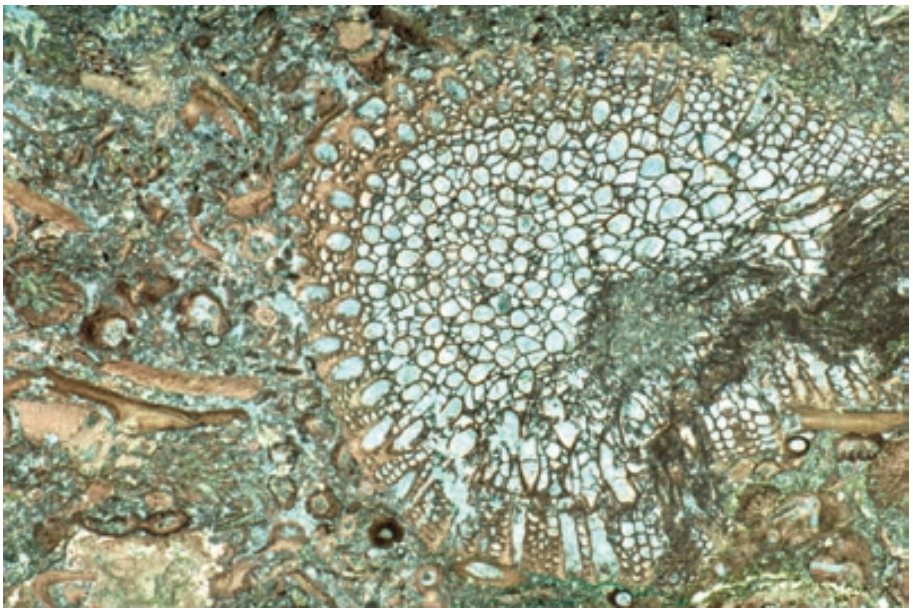

PPL, AFeS, BSE, HA = 12.5 mm

Mid. Permian (Leonardian) Skinner Ranch Fm., Glass Mountains, Texas

A longitudinal section through a branch of a fistuliporoid bryozoan, possibly *Meekopora* sp. The exterior surface consists of solid skeletal calcite, punctuated with large zooecia and surrounding small cystopores. In *Meekopora*, the solid exterior portion develops secondarily as the bryozoan polyps deposit skeletal calcite that fills the bubble-like cystopores that were produced during initial growth.

PPL, HA = 4.7 mm

Mid.-Up. Permian (Leonardian-Guadalupian) Road Canyon Fm., Glass Mountains, Texas

This is a transverse section through an encrusting fistuliporoid bryozoan, probably *Fistulipora* sp. This thin-section photomicrograph shows well preserved zooecia (containing diaphragms — the thin lines of microcrystalline carbonate crossing the zooecia). The zooecia are separated by numerous small cystopores.

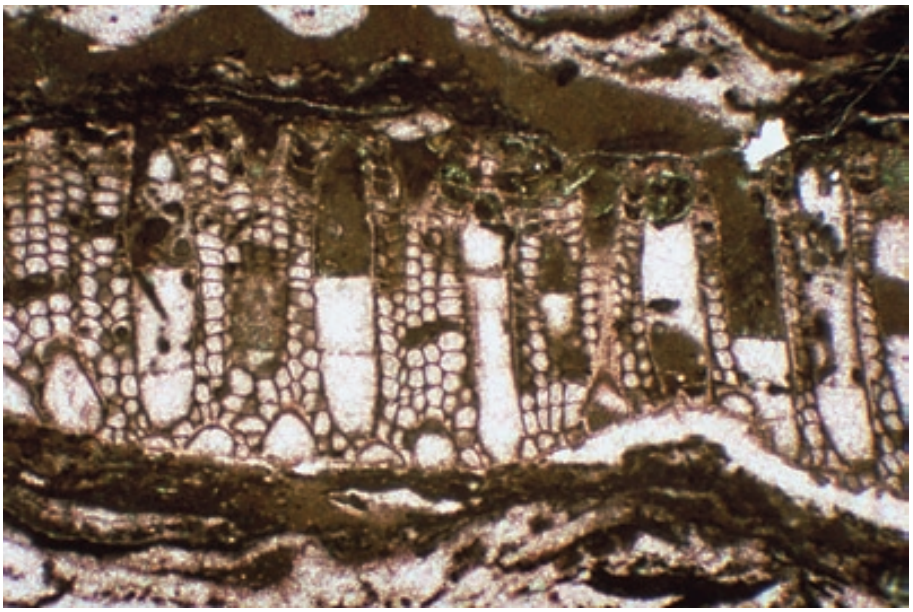

PPL, HA = 5.1 mm

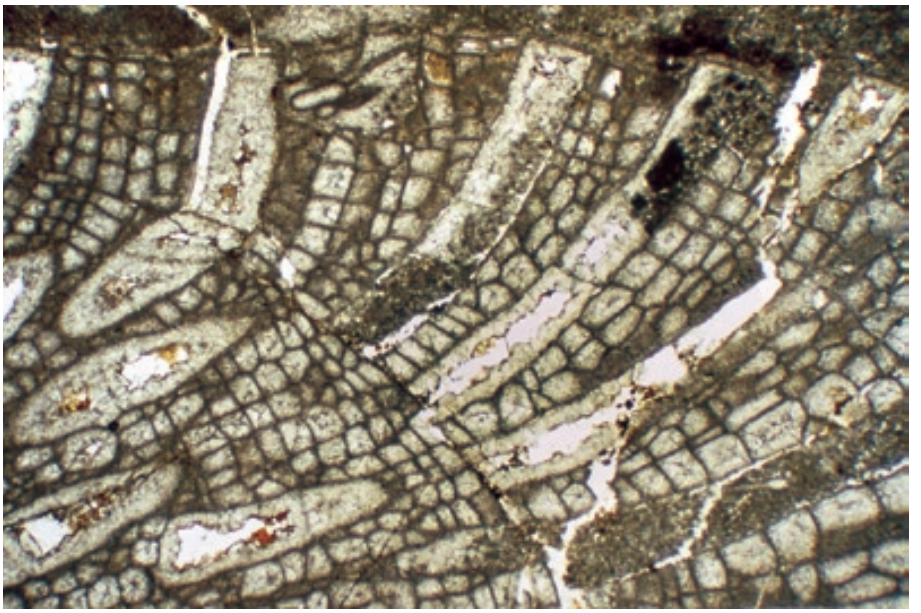

Up. Permian (Guadalupian) Bell Canyon Fm., Rader Ls. Mbr., Culberson Co., Texas

This longitudinal section through *Fistulipora* sp., a fistuliporoid bryozoan, has well-preserved zooecia (containing a few diaphragms) separated by numerous cystopores. The zooecia are largely filled with calcite cement.

PPL, HA = 5.1 mm

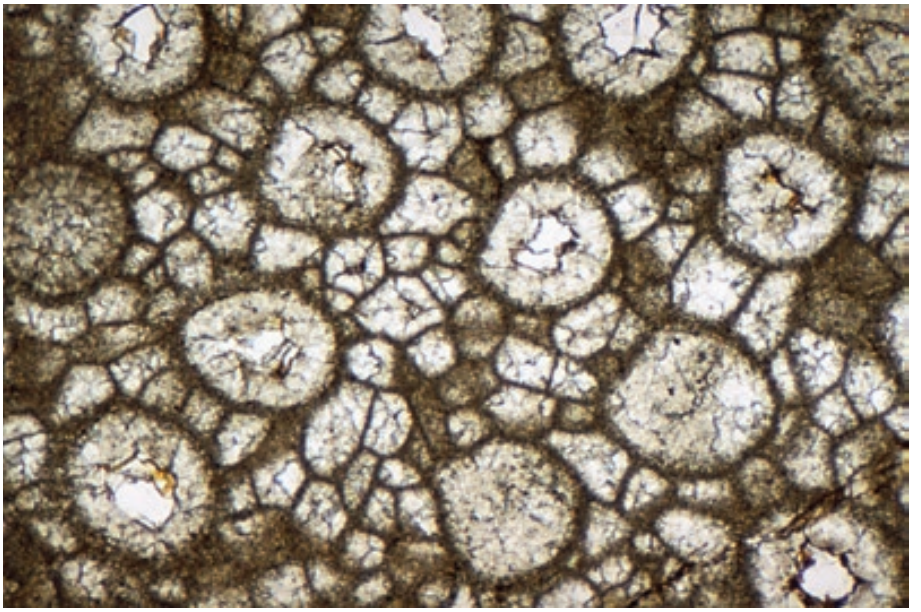

Up. Permian (Guadalupian) Bell Canyon Fm., Rader Ls. Mbr., Culberson Co., Texas

This tangential section through *Fistulipora* sp. shows well preserved large circular zooecia surrounded by numerous smaller cystopores. The zooecia are partially filled with sparry calcite cement, whereas the cystopores are completely spar filled.

PPL, HA = 2.4 mm

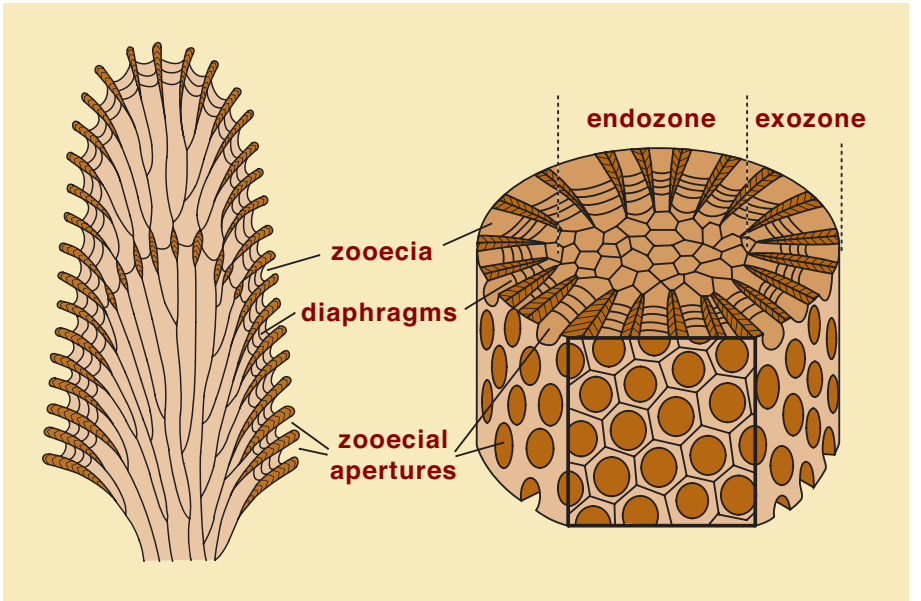

Morphology of typical trepostome bryozoans

Trepostome bryozoans range from branching to encrusting colonies. In thin section, some key elements to help in the identification of trepostomes include: zooecial walls that thicken and bend outward, the presence of mesopores and acanthorods (neither shown on diagram), and common to abundant diaphragms in the zooecia. Diagram modified from Boardman and Cheetham (1987).

Up. Ordovician (Cincinnatian) Fairview Fm., Hamilton Co., Ohio

A transverse section through a trepostome bryozoan colony. The zooecia in the exozone contain numerous diaphragms that are characteristic of trepostomes. Note the excellent preservation and the fine lamination within the zooecial wall structure. Other common features of trepostome bryozoans that are present in this photomicrograph are mesopores (narrower pores with more numerous diaphragms than the zooecia), acanthorods (see next photograph) embedded in the zooecial walls, and the thickening of the zooecial walls outward.

PPL, HA = 3.0 mm

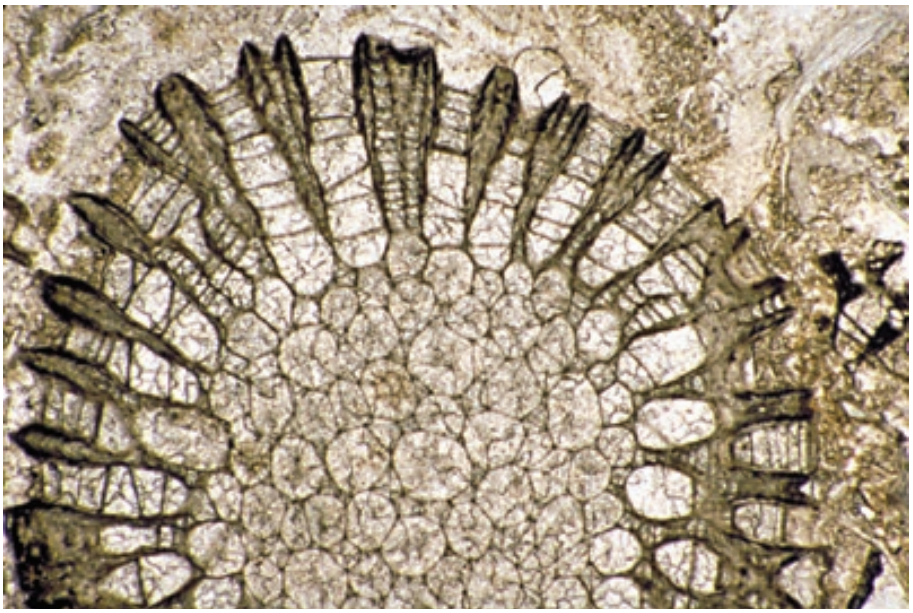

Up. Permian (Ufimian?) Schuchert Dal Ss., Jameson Land, East Greenland

This transverse section of a trepostome bryozoan branch shows details of the zooecial walls. The zooecia in this specimen have only a few preserved diaphragms, but embedded within the zooecial walls are acanthorods. Acanthorods are very small, thin calcite rods, the walls of which extend beyond the exterior of the bryozoan as projecting spines. In this view, the surrounding acanthorod walls disturb or deflect the rest of zooecial wall fabric forming a "high" or bend in the wall structure, both internally and externally.

PPL, AFeS, BSE, HA = 1.6 mm

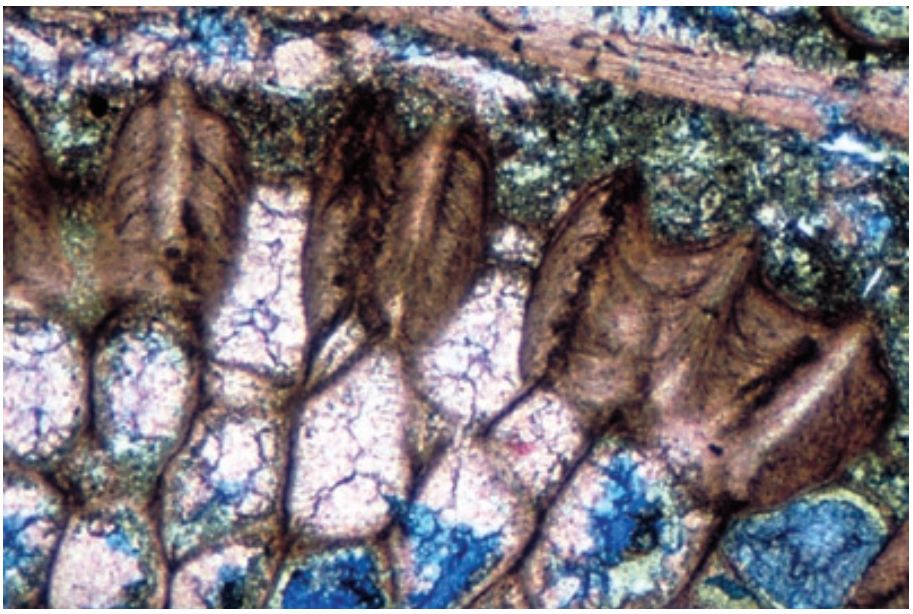

Up. Permian (Kazanian?) Wegener Halvø Fm., Jameson Land, East Greenland

Transverse cross sections through two trepostome bryozoan fragments from the flank facies of a deep-water bioherm. These bryozoans have few diaphragms in the zooecia, but acanthorods are present. The zooecia are well preserved because they were filled early with a combination of non-ferroan marine calcite cements and glauconite; blocky, ferroan calcite cement filled the remaining voids during deeper burial.

PPL, AFeS, BSE, HA = 8.5 mm

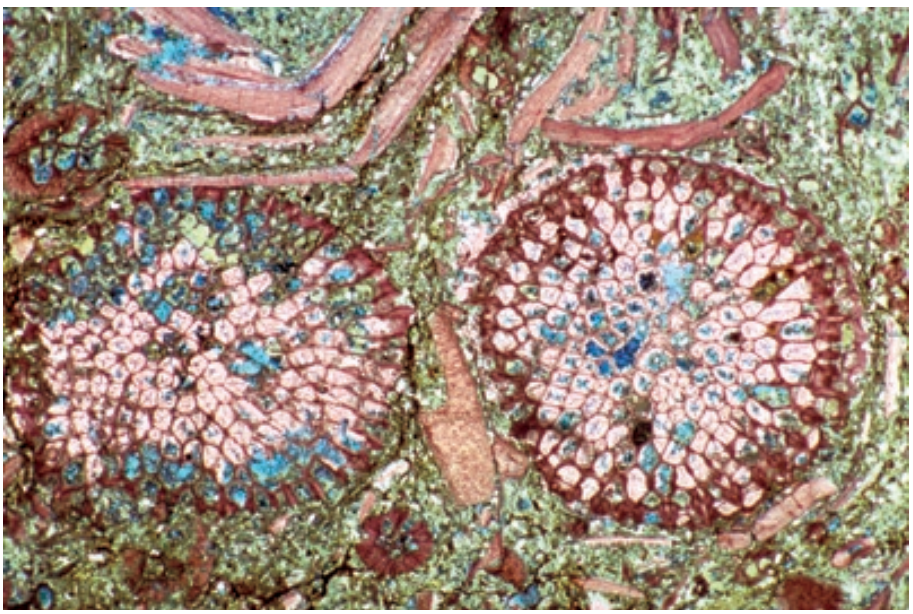

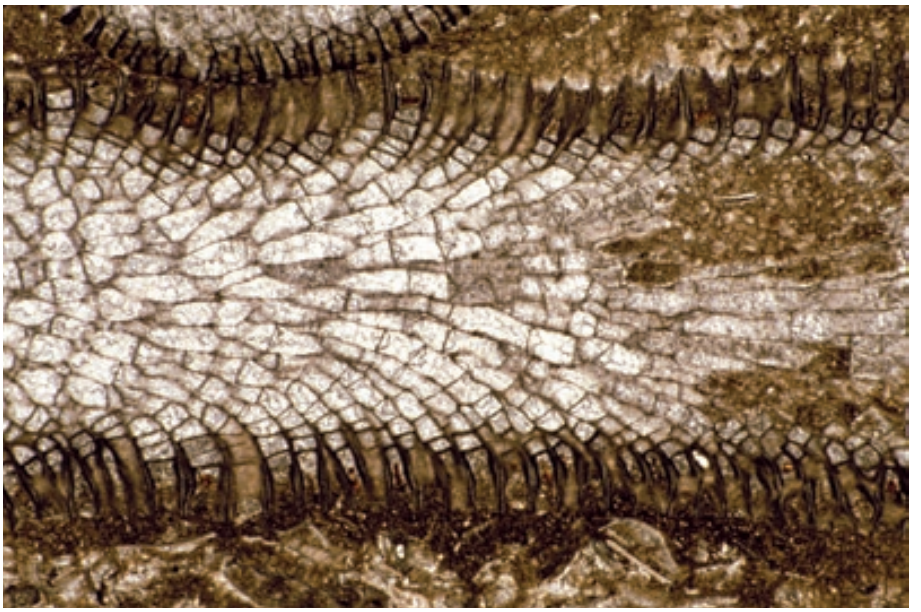

Up. Ordovician (Cincinnatian) Fairview Fm., Hamilton Co., Ohio

A longitudinal section through a trepostome bryozoan branch (possibly *Heterotrypa* sp.). The zooecia contain numerous diaphragms, a characteristic of trepostomes. Note the excellent preservation and finely fibrous lamination of the walls showing the outward-thickening of zooecial walls. Other common trepostome bryozoan features visible in this example are acanthorods embedded in the zooecial walls (the light lines) and a few mesopores. A part of the interior (endozone) of the bryozoan was destroyed by boring or later diagenesis (brown, finely crystalline calcite at right).

PPL, HA = 8.0 mm

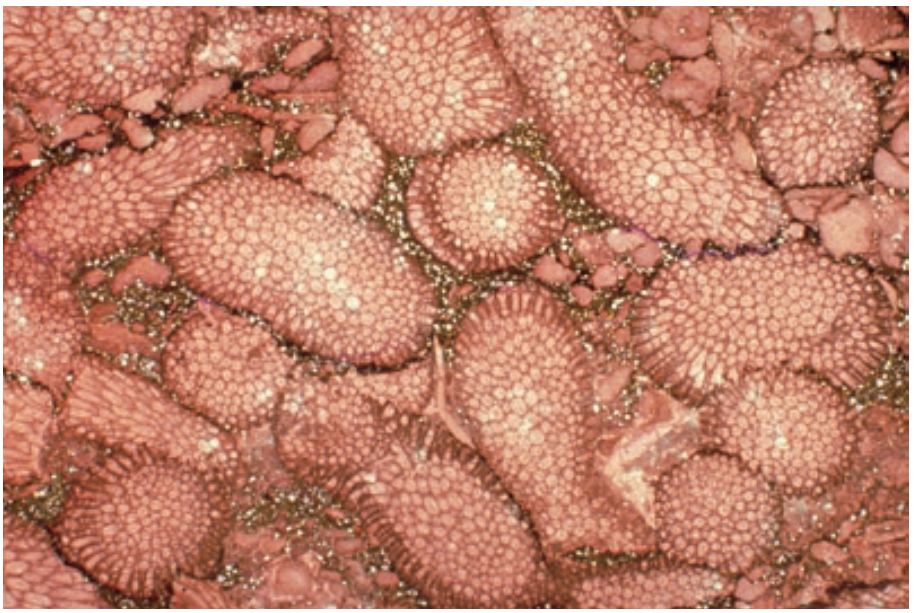

Mid. Ordovician Black River Gp., Lowville Fm., Kingston, Ontario, Canada

This view shows a variety of cross sections through trepostome bryozoan branches in a bryozoan rudstone. The bryozoans in this example are well preserved, probably due to early cementation, and contain zooecia with numerous diaphragms and abundant mesopores. Sample from Noel P. James.

PPL, AS, HA = 16 mm

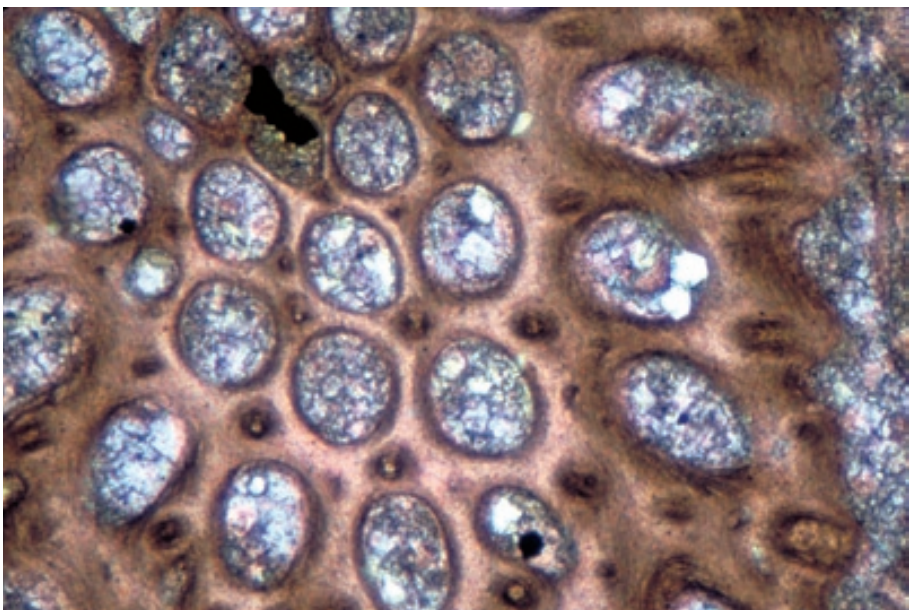

Up. Permian (Kazanian?) Wegener Halvø Fm., Jameson Land, East Greenland

A tangential section through a trepostome bryozoan showing the placement of acanthorods at the corners of most of the zooecia. Along the edges of this bryozoan fragment, small mesopores also are visible. The smaller openings that look similar to the zooecia are either mesopores or early stages of full-fledged zooecia ("baby" zooecia can be difficult to distinguish from mesopores in some cases).

PPL, AFeS, HA = 1.6 mm

Up. Silurian Tonoloway-Keyser Ls., Mifflin Co., Pennsylvania

A trepostome bryozoan with acanthorods and a few mesopores. If you look closely, you can see a few preserved diaphragms in the zooecia near the top of the specimen. Diaphragms can be destroyed prior to diagenesis if the clast is transported and abraded.

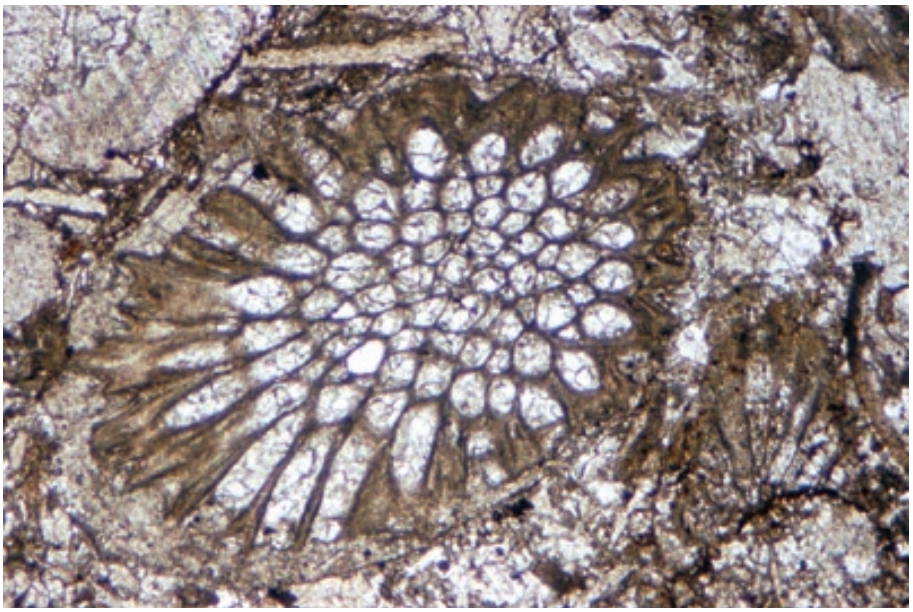

PPL, HA = 2.7 mm

Pennsylvanian Graham Fm., Young Co., Texas

A transverse section through a branch of a rhabdomesid/rhomboporoid bryozoan, *Megacanthopora* sp. Rhabdomesid bryozoans can be quite difficult to differentiate from trepostome bryozoans as a result of convergent evolution. If the external pores form a rhombic surface pattern, then the sample is likely to be a rhabdomesid. In this example, the walls are well laminated and contain acanthorods but no mesopores (mesopores are lacking in many rhabdomesids).

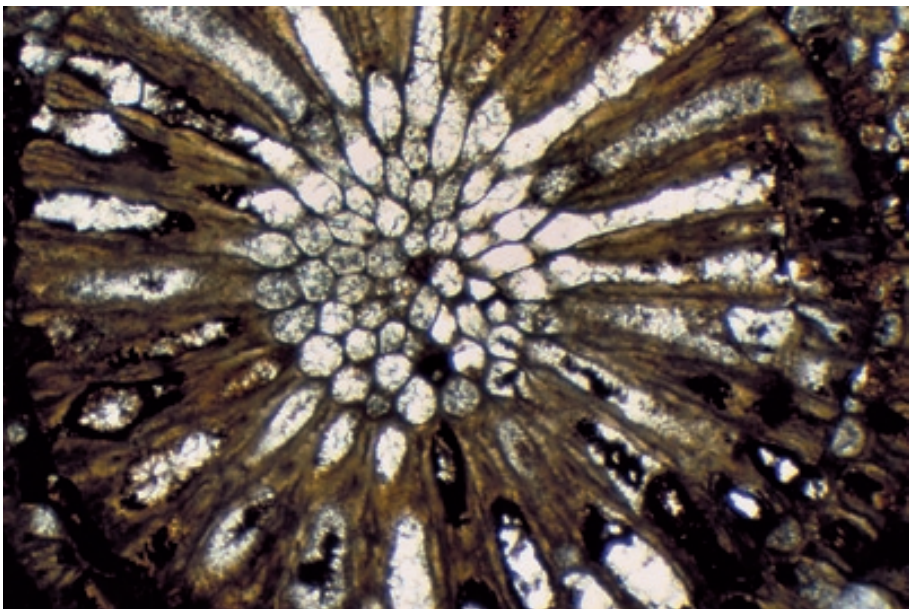

PPL, HA = 4.1 mm

Up. Permian (Kazanian?) Wegener Halvø Fm., Jameson Land, East Greenland

A transverse section of a possible rhabdomesid/ rhomboporoid or thin-branching trepostome bryozoan. The zooecial walls are well laminated and contain acanthorods that are clearly visible in this specimen.

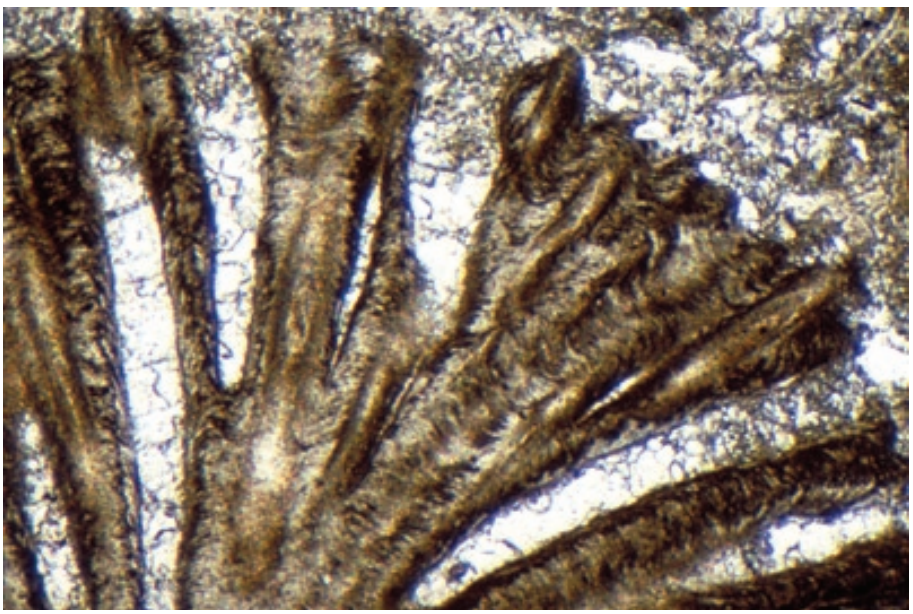

PPL, HA = 2.0 mm

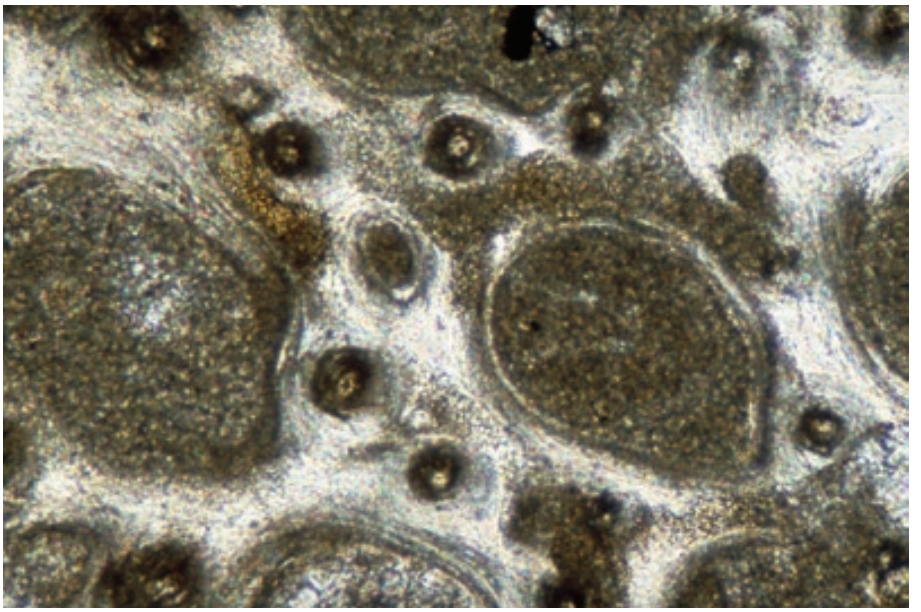

Up. Permian (Kazanian?) Wegener Halvø Fm., Jameson Land, East Greenland

A tangential cross section through a possible rhabdomesid/rhomboporoid bryozoan. Such bryozoans commonly contain acanthorods, but unlike trepostomes, they may vary greatly in size. Note the wall structure and acanthorods that are preserved in this specimen.

PPL, HA = 1.65 mm

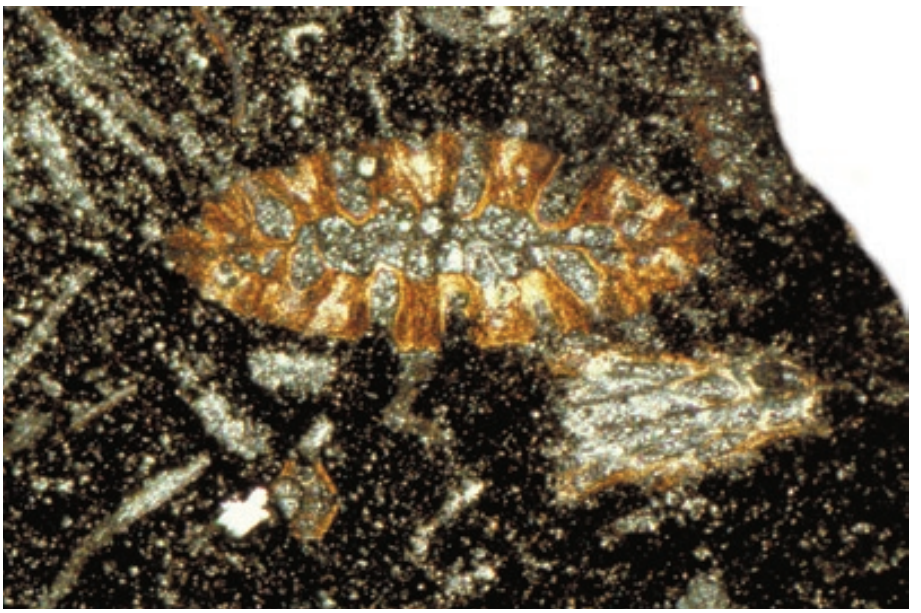

Mid. Ordovician Coburn Ls., Pennsylvania

A transverse section through a Ptilodictyina bryozoan, *Stictopora fenestrata*. These bryozoans are more commonly called bifoliates because of their bi-lateral symmetry. They form flattened branches and have zooecial walls that are laminated and thicken outward. Photomicrograph courtesy of Roger J. Cuffey.

PPL, HA = 4.5 mm

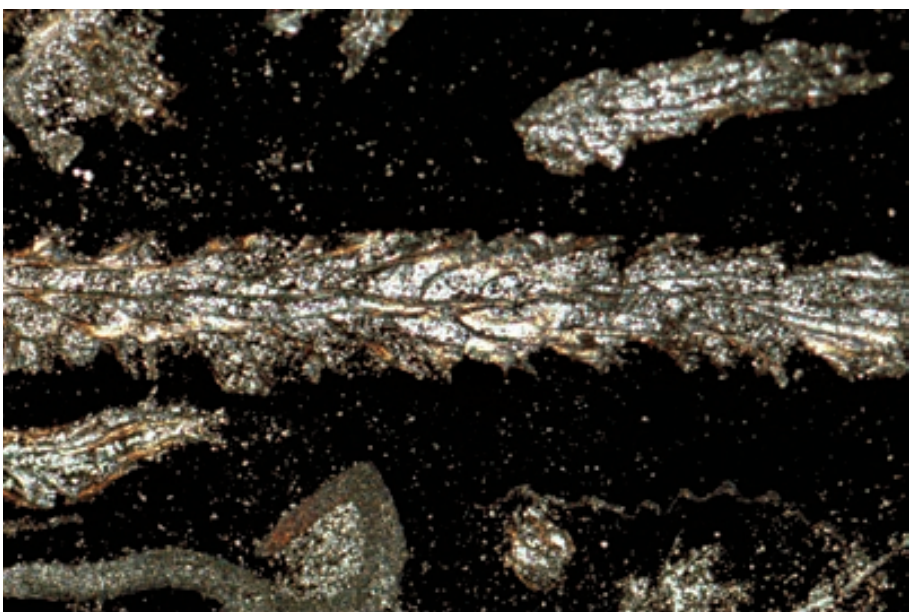

Mid. Ordovician Coburn Ls., Pennsylvania

A longitudinal section through the same species as in the previous photomicrograph (*Stictopora fenestrata*). The zooecia are usually short and form from a plane extending through the center of the colony. Note how the zooecial walls thicken outward. Photograph courtesy of Roger J. Cuffey.

PPL, HA = 4.5 mm

Morphology of fenestrate bryozoans

Fenestrate bryozoans, unlike other bryozoans, have zooecia that all face outward in a single direction. The zooecial walls can be extremely thick, laminated to foliated, contain acanthorods, and form spine-like protrusions near the zooecial aperture. When seen in thin section, these spines appear to be star-like masses of finely crystalline calcite. The open spaces enclosed by the vertically extending branches (containing zooecia) and the solid cross bars (termed dissepiments) are known as fenestrules. Modified from Majewske (1969, plate 35).

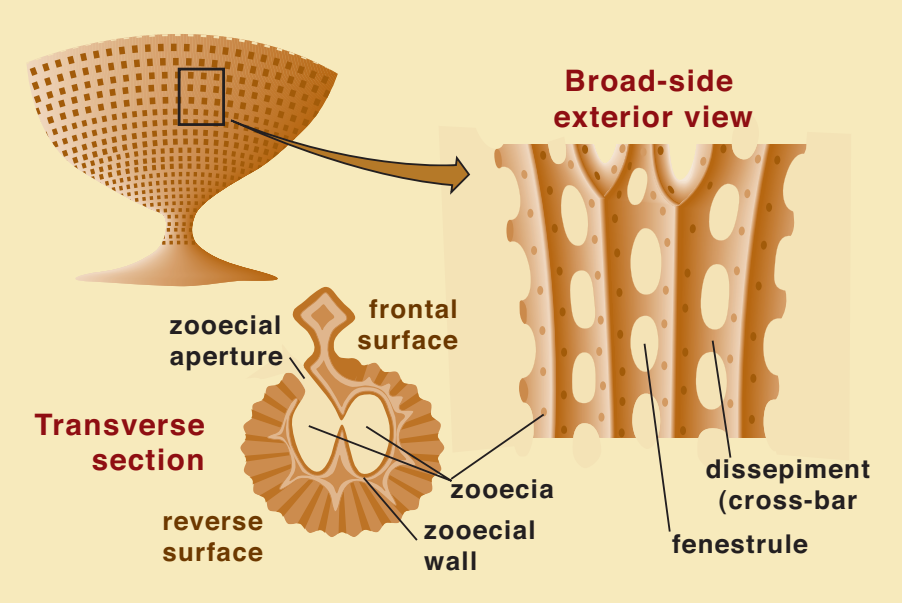

Mississippian Chester Gp., Fayetteville Sh., Vinita, Oklahoma

A tangential section through the fenestrate bryozoan, *Archimedes communis* Ulrich. Most fenestrate bryozoans form fan-shaped or simple cone-shape colonies, but *Archimedes* bryozoans form a complex cone-shaped colony that spirals around a central axis. Also unlike other fenestrate bryozoans, *Archimedes* is more massive, indicating it probably grew in higher energy environments than most of the more delicate fenestrate bryozoans.

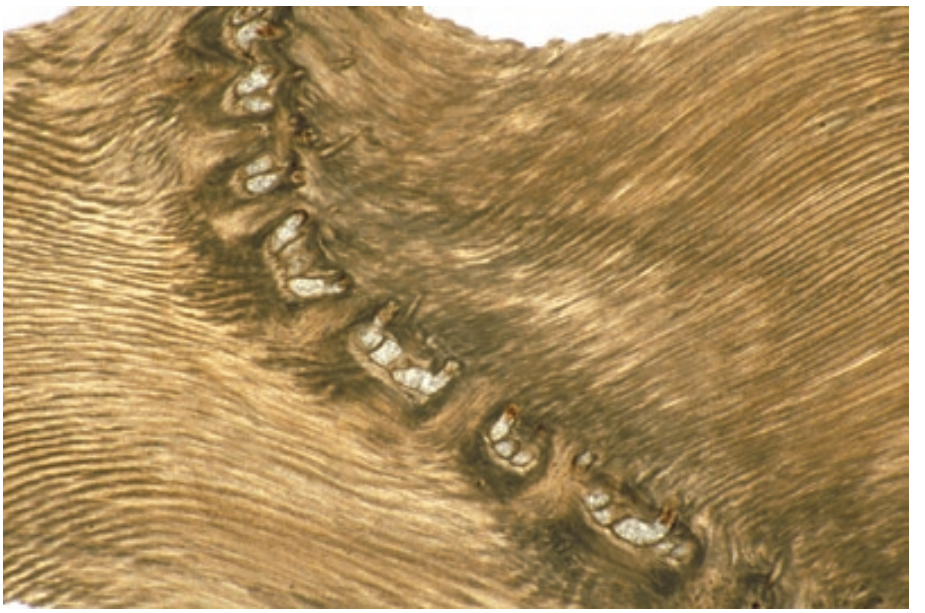

PPL, HA = 5.2 mm

Mississippian (Chesterian) Pitkin Ls., Ft. Gibson Dam, Oklahoma

These transverse and longitudinal cuts through fenestrate bryozoan fronds (*Fenestella* sp.) in a micritic matrix show the variety of appearances a window-screen-like fenestrate bryozoan may have depending on the direction of sectioning. Some of the bryozoans show connected zooecia that form chains; others appear as isolated zooecia arranged linearly. Sample from Robert Laury.

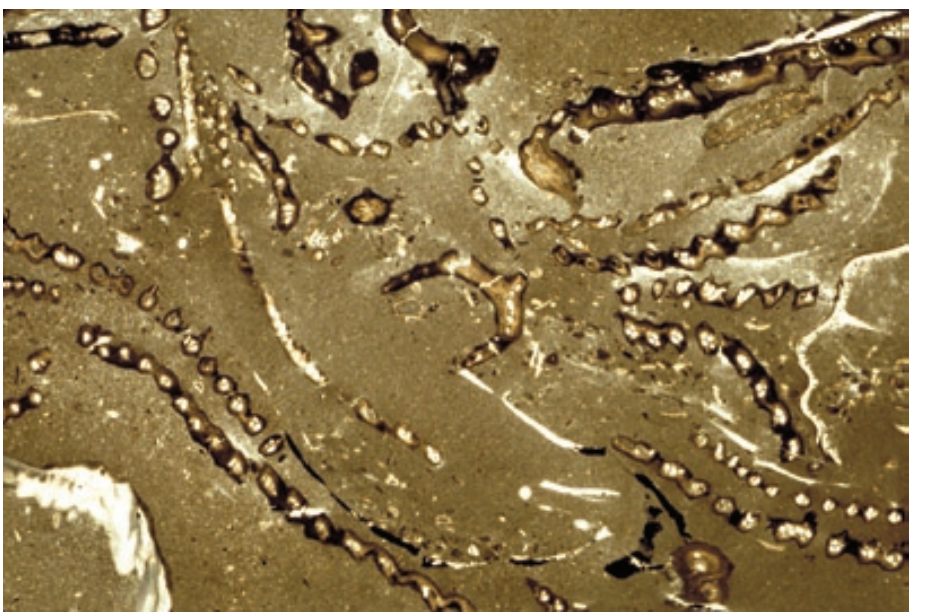

PPL, HA = 16 mm

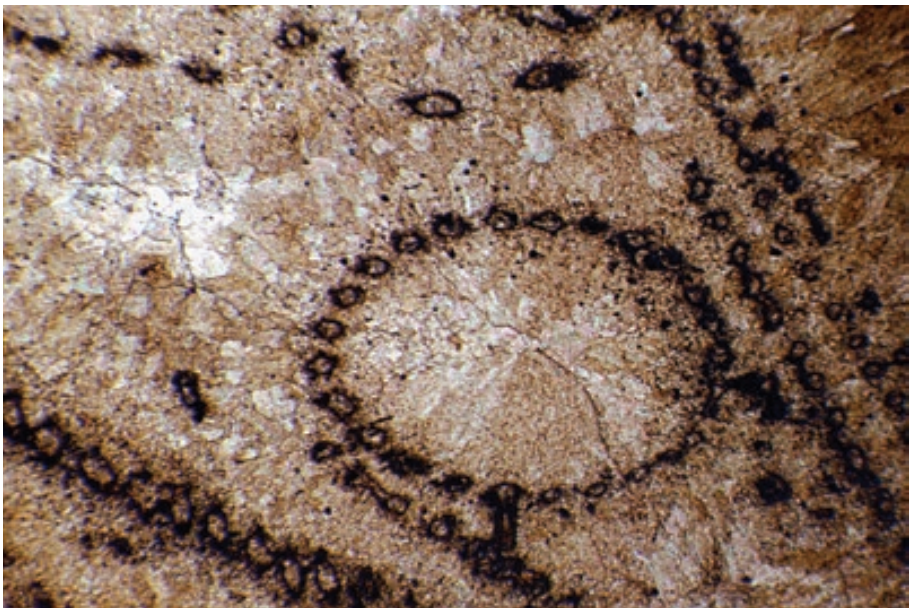

Mississippian (Tournaisian-Visean) Waulsortian Ls., Co. Dublin, Ireland

These large fenestrate bryozoans, *Fenestella* sp., are surrounded by radial, fibrous to bladed, sparry calcite cements. The circular ring of isolated bryozoan "grains" represents a transverse cut through a single cup-shaped fenestrate colony.

PPL, HA = 8.0 mm

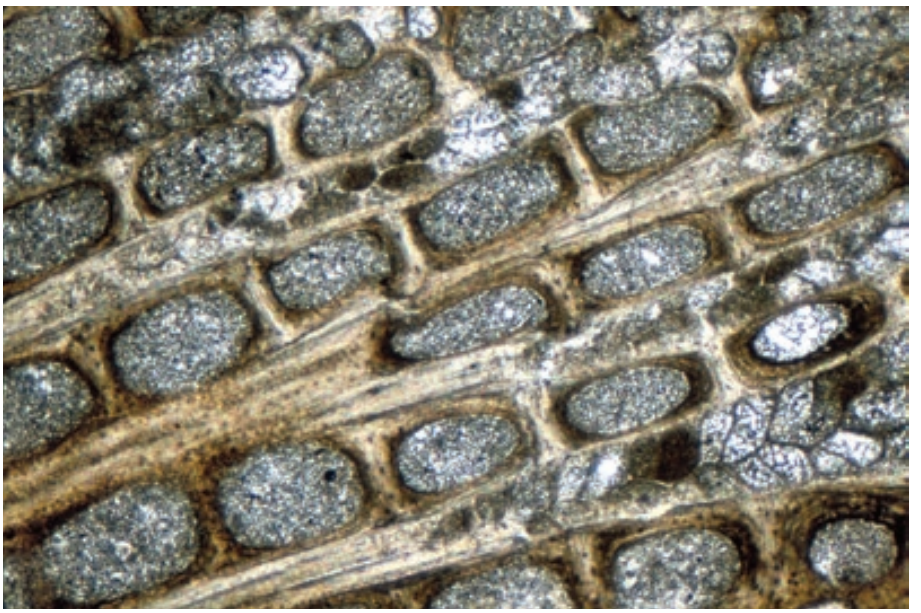

Mid. Mississippian Warsaw Ls., Illinois

In this tangential longitudinal section, the lattice-like appearance of fenestrate bryozoans is clearly visible. The thick laminated zooecial walls and acanthorods are also common in fenestrate bryozoans. In this example, the zooecia are filled with micrite or microcrystalline calcite cements; the fenestrate openings (fenestrules) are filled with microspar. Sample from Robert Laury.

PPL, HA = 1.65 mm

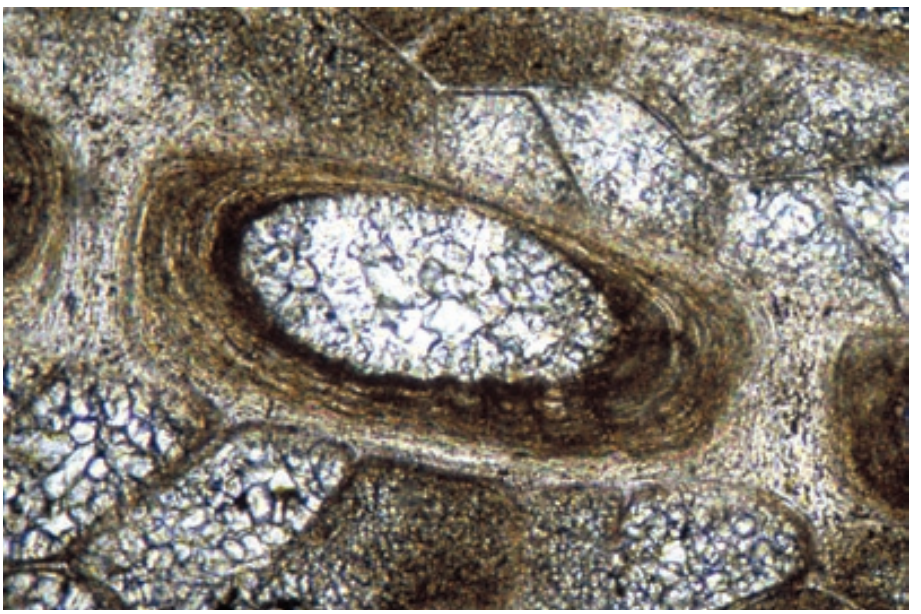

Mid. Mississippian Warsaw Ls., Illinois

A close-up view of the sample shown in the previous photograph. Note the laminated (and slightly crenulate) wall structure surrounding the fenestrule, the large oval opening in the center of the image that lies between the branches (horizontal) and the dissepiments (vertical). The zooecia are the polygonal openings at the top and bottom of the picture. Sample from Robert Laury.

PPL, HA = 0.65 mm

Up. Permian (Kazanian?) Wegener Halvø Fm., Jameson Land, East Greenland

This transverse section of zooecia and wall structure in fenestrate bryozoans illustrates the laminated, crenulate exterior of the zooecial wall.

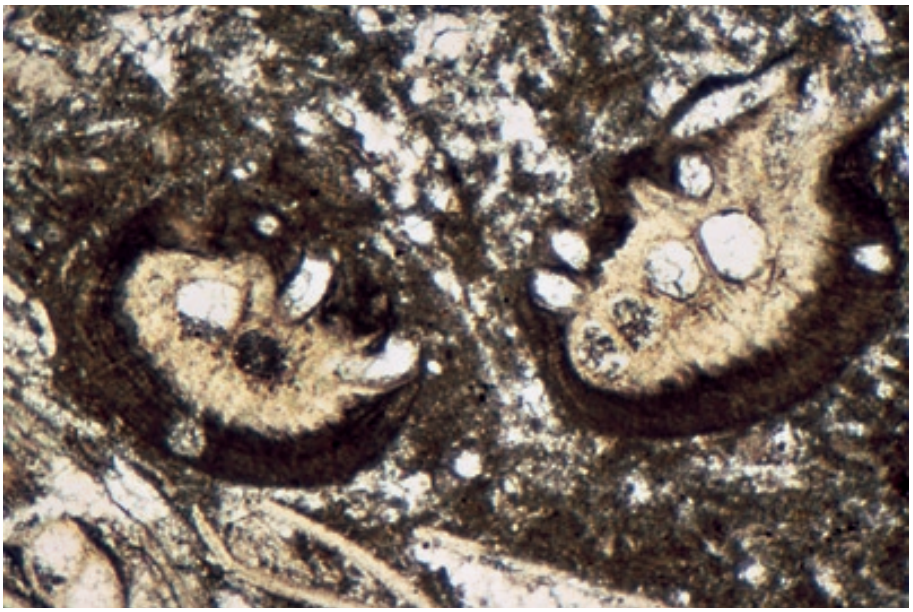

PPL, HA = 2.4 mm

Up. Permian (Guadalupian) Capitan Fm., Eddy Co., New Mexico

An oblique cut through part of a probable fenestrate bryozoan (possibly *Acanthocladia* sp.). Oblique cuts produce some unusual fabrics and can make identification of small fenestrate bryozoan grains difficult.

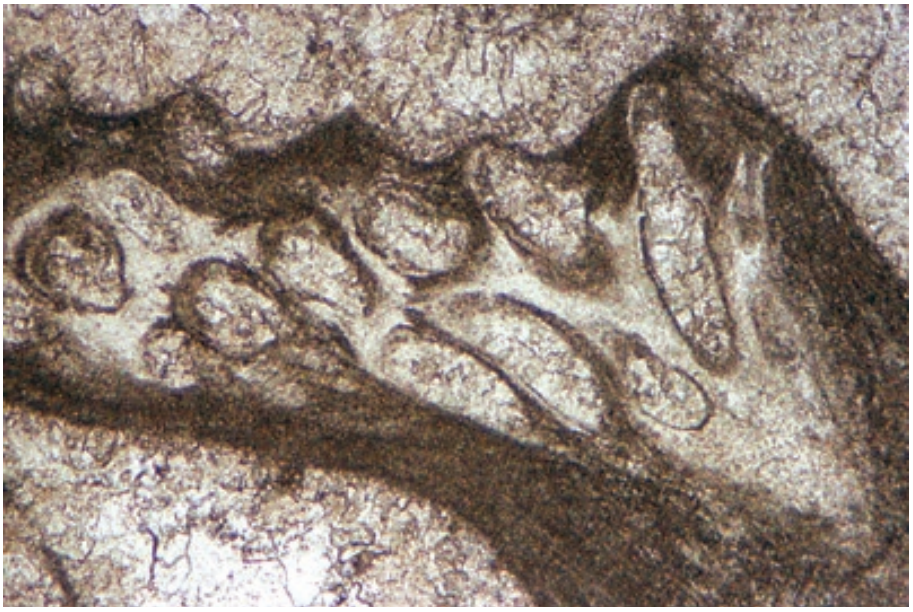

PPL, HA = 3.42 mm

Paleozoic limestone, southwestern U.S.A.

Transverse and oblique sections of fenestrate bryozoan fronds (*Fenestella* sp.) showing zooecia within the individual fronds which are stacked upon one another in this rock. The branches forming any particular frond are the lines of similar zooecia extending horizontally across this image. Sample from Robert Laury.

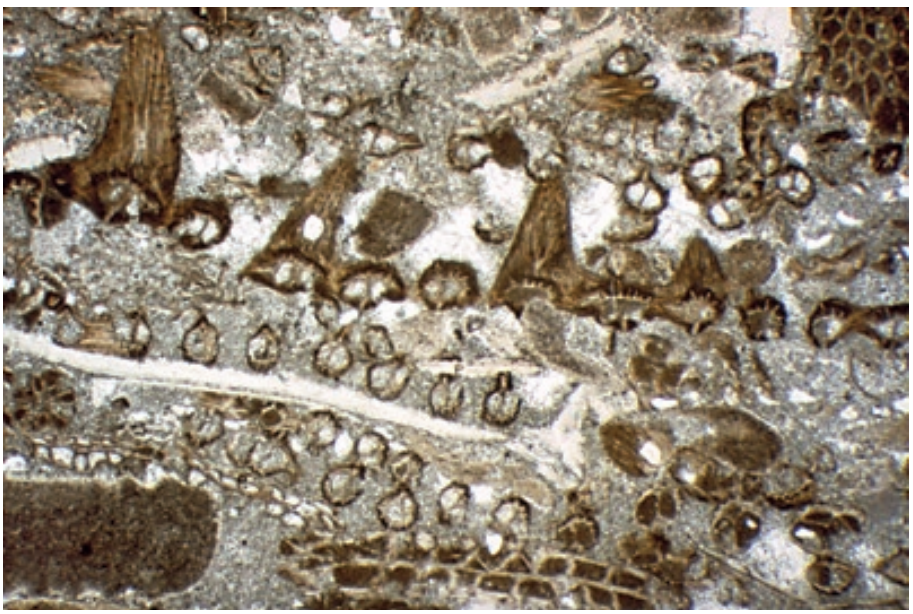

PPL, HA = 5.1 mm

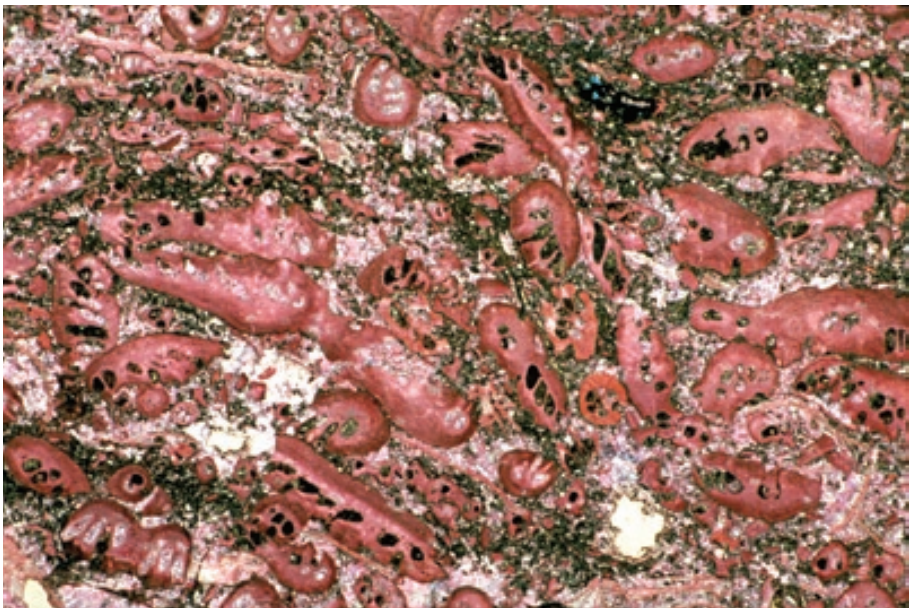

Up. Permian (Kazanian?) Wegener Halvø Fm., Jameson Land, East Greenland

A thin-section photomicrograph showing a packstone composed of broken fragments of fenestrate bryozoans in various orientations. Without early marine cements to stabilize the relatively fragile fenestrate fronds, they break up easily into smaller clasts.

PPL, AS, BSE, HA = 10 mm

Cited References and Additional Information Sources

Bassler, R. S., 1953, Bryozoa, *in* R. C. Moore, ed., Treatise on Invertebrate Paleontology, Part G, Bryozoa: Lawrence, University of Kansas Press, 253 p.

Boardman, R. S., 1960, Trepostomatous Bryozoa of the Hamilton Group of New York State: U. S. Geological Survey Professional Paper 340, 87 p.

Boardman, R. S., and A. H. Cheetham, 1969, Skeletal growth, intracolony variation, and evolution in Bryozoa; a review: Journal of Paleontology, v. 43, p. 205-233.

Boardman, R. S., and A. H. Cheetham, 1987, Phylum Bryozoa, *in* R. S. Boardman, A. H. Cheetham, and A. J. Rowell, eds., Fossil Invertebrates: Palo Alto, CA, Blackwell Scientific Publications, p. 497-549.

Bone, Y., and N. P. James, 1993, Bryozoans as carbonate sediment producers on the cool-water Lacepede Shelf, southern Australia: Sedimentary Geology, v. 86, p. 247-271.

Cheetham, A. H., J. B. Rucker, and R. E. Carver, 1969, Wall structure and mineralogy of the cheilostome bryozoan *Metrarabdotos*: Journal of Paleontology, v. 43, p. 129-135.

Cuffey, R. J., 1970, Bryozoan-environment interrelationships—an overview of bryozoan paleoecology and ecology: Earth and Mineral Sciences Bulletin, Pennsylvania State University, v. 39, p. 41-45.

Cuffey, R. J., 1974, Delineation of bryozoan constructional roles in reefs from comparison of fossil bioherms and living reefs, *in* A. M. Cameron, et al., eds., Proceedings of the Second International Coral Reef Symposium, v. 1: Brisbane, Australia, Great Barrier Reef Committee, p. 357-364.

Cuffey, R. J., 1977, Bryozoan contributions to reefs and bioherms through geologic time, *in* S. H. Frost, M. P. Weiss, and J. B. Saunders, eds., Reefs and Related Carbonates — Ecology and Sedimentology: Tulsa, OK, American Association of Petroleum Geologists Studies in Geology No. 4, p. 181-194.

Cuffey, R. J., and J. E. Utgaard, 1999, Bryozoans, *in* R. Singer, Encyclopedia of Paleontology, 2nd ed., Chicago, IL, Fitzroy Dearborn Publishers, vol. 1, p. 204-216.

Hageman, S. J., Y. Bone, B. McGowran, and N. P. James, 1997, Bryozoan colonial growth-forms as paleoenvironmental indicators: Evaluation of methodology: Palaios, v. 12, p. 405-419.

James, N. P., D. A. Feary, F. Surlyk, J. A. T. Simo, C. Betzler, A. E. Holbourn, Q. Y. Li, H. Matsuda, H. Machiyama, G. R. Brooks, M. S. Andres, A. C. Hine, and M. J. Malone, 2000, Quaternary bryozoan reef mounds in cool-water, upper slope environments: Great Australian Bight: Geology, v. 28, p. 647-650.

Larwood, G. P., 1973, Living and Fossil Bryozoa: Recent Advances in Research [2nd International Bryozoology Association Conference, Proceedings]: New York, Academic Press, 634 p.

Majewske, O. P., 1969, Recognition of Invertebrate Fossil Fragments in Rocks and Thin Sections: Leiden, Neth., E. J. Brill, 101 p.

McKinney, F. K., 1986, Historical record of erect bryozoan growth forms: Proceedings of the Royal Society of London, v. B 228, p. 133-149.

Moore, R. C., C. G. Lalicker, and A. G. Fischer, 1952, Invertebrate Fossils: New York, McGraw-Hill Book Co., 766 p.

Nelson, C. S., F. M. Hyden, S. I. Keane, W. I. Leask, and D. P. Gordon, 1988, Application of bryozoan zooarial growth-form studies in facies analysis of non-tropical carbonate deposits in New Zealand: Sedimentary Geology, v. 60, p. 301-322.

Nye, O. B., 1969, Aspects of microstructure in post-Paleozoic Cyclostomata: Atti della Società Italiana di Scienze Naturali e del Museo Civile di Storia Naturale di Milano, v. 108, p. 111-114.

Ross, C. A., and J. R. P. Ross, 1990, Late Palaeozoic bryozoan biogeography, *in* W. S. McKerrow, and C. R. Scotese, eds., Palaeozoic Palaeogeography and Biogeography: London, Geological Society (London) Memoir No. 12, p. 353-362.

Tavener-Smith, R., 1969, Skeletal structure and growth in the Fenestellidae (Bryozoa): Palaeontology, v. 12, p. 281-309.

Tavener-Smith, R., 1969, Wall structure and acanthopores in the bryozoan *Leioclema asperum*: Lethaia, v. 2, p. 89-97.

Taylor, P., and P. Allison, 1998, Bryozoan carbonates through time and space: Geology, v. 26, p. 459-462.

Warner, D. J., and R. J. Cuffey, 1973, Fistuliporacean bryozoans of the Wreford Megacyclothem (Lower Permian) of Kansas: University of Kansas Paleontological Contributions, Paper 65, p. 1-24.

Facing Page: Top - Underwater view of two examples of a brachiopod, *Terebratella sanguinea*, living on fjord walls at 20 m (60 ft) depth in Doubtful Sound, Westland, New Zealand. Photograph courtesy of Dick Singleton, New Zealand National Institute of Water and Atmosphere.

Bottom - A selectively silicified spiriferid brachiopod from Permian (Leonardian) lower slope deposits from the Glass Mountains, of west Texas. Note the remarkable fidelity of preservation of delicate ornamentation and internal spiralia. Sample from Smithsonian Institution collections.

GRAINS: Skeletal Fragments

Brachiopods

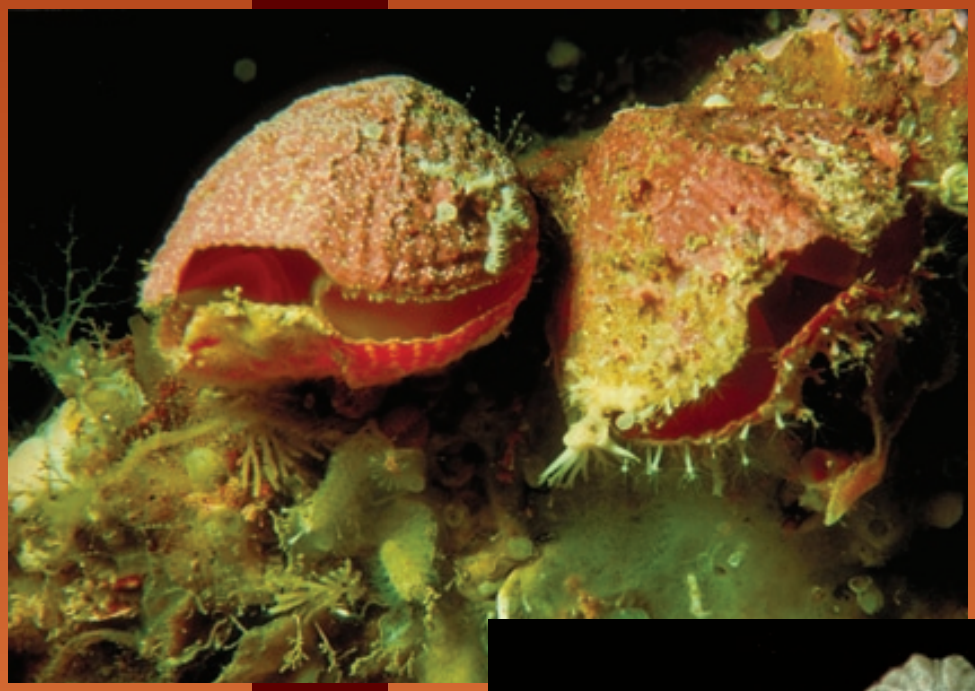

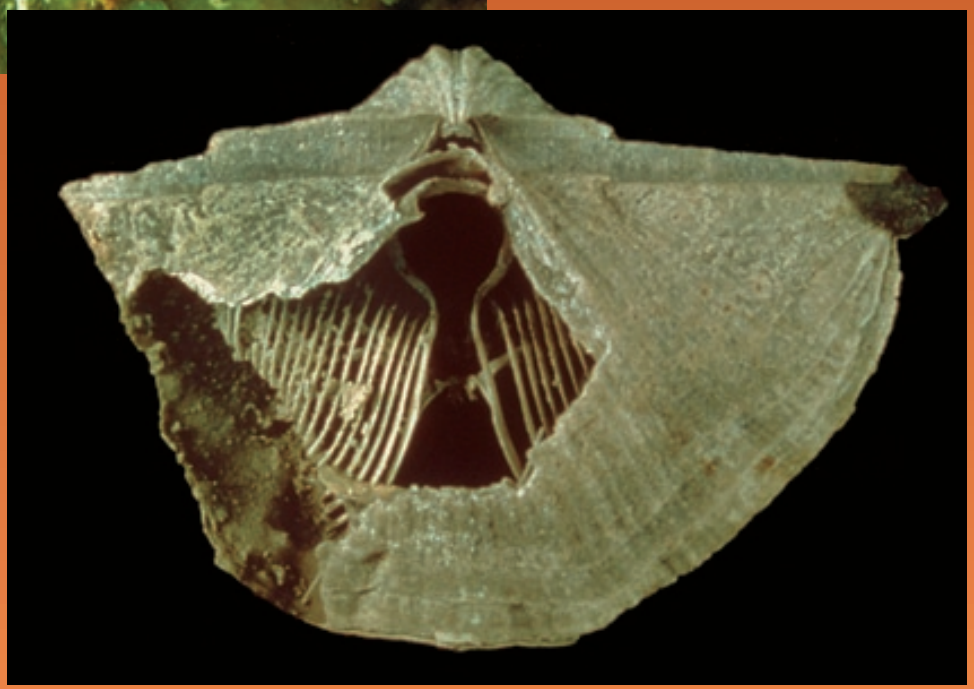

Chapter 8

BRACHIOPODS

Taxonomy and Age Range:

Phylum Brachiopoda — earliest Cambrian-Recent

Subphylum Linguliformea (Early Cambrian-Recent): shells lack skeletal articulation structures; shells are chitinophosphatic with laminar microstructure; pedicle usually present, emerging between valves or from opening in ventral valve.

Class Lingulata (Early Cambrian-Recent): brachiopods with chitinophosphatic shells lacking teeth and sockets; pedicle usually present emerging from shell between valves or from apex of one of the valves.

Class Paterinata (Early Cambrian-Late Ordovician): shell rounded to elliptical with straight posterior margin with pseudointerarea; delthyrium often closed by plates; pedicle reduced or absent.

Subphylum Craniiformea (Early Cambrian-Recent): calcareous shells; valves lack hinge teeth and sockets; shell usually attached to substrate by cementation of pedicle (ventral) valve.

Class Craniata (Mid. Cambrian-Recent): features as above for subphylum.

Subphylum Rhynchonelliformea (Early Cambrian-Recent): Brachiopods with calcitic shells that have endopunctate, impunctate, pseudopunctate, or tabular microstructure; crura usually present extended to form a brachidium (spiralia or loops) in some groups; articulated valves with hinge teeth and sockets are the norm, but in some forms, reduced or modified types of articulation structures are present; the vast majority of known rhynchonelliform brachiopods are included in the classes Strophomenata and Rhynchonellata.

Class Chileata (Early Cambrian only): short-lived early group, see features in Clarkson (1998, p. 181).

Class Obolellata (Early-Mid. Cambrian): short-lived early group, see features in Clarkson (1998).

Class Kutorginida (Early-Mid. Cambrian): short-lived early group, see features in Clarkson (1998).

Class Strophomenata (Mid. Cambrian-Triassic): Shell usually concavo-convex or planoconvex; shell usually pseudopunctate; straight hinge with simple teeth (often lost); some groups with spines, pedicle opening usually closed by plate(s). Includes the Orders: Strophomenida (six suborders), and Productida (two suborders).

Class Rhynchonellata (Early Cambrian-Recent): Biconvex shells with both strophic and nonstrophic hinges; impunctate and punctate shells; crura usually present; brachidium often present. Includes the orders: Orthida (shell usually impunctate); Rhynchonellida; Pentamerida; Athyrida (spiralia present, usually impunctate); Atrypida (spiralia present, impunctate); Spiriferida (spiralia present, punctate and impunctate shells); Spiriferinida (spiralia present, impunctate and punctate shells), and Terebratulida (loop present, punctate shell).

In general, brachiopods were especially abundant in the Paleozoic where they reached their peak diversity in the Devonian. In many settings, they were among the main rock-forming organisms. Although they are much less abundant in Mesozoic and Cenozoic strata, they retain considerable biostratigraphic value in those deposits.

Environmental Implications:

All brachiopods are/were marine organisms, but the group exhibits a significant salinity range into both brackish (hyposaline) and slightly hypersaline settings.

Virtually all brachiopods are sessile, attached organisms that live in shelf waters ranging from high- to low-latitude settings. A few modern species extend to >1500 m water depths.

Warm- and shallow-water forms tend to have thicker shells than cold- or deeper-water forms.

Skeletal Mineralogy:

All rhynchonelliform brachiopod shells are calcitic, with 0 to 7 mole% Mg (low-Mg calcite). Linguliform brachiopod shells are composed of interlaminated chitin and calcium phosphate. Craniform brachiopods have either calcitic or aragonitic shells.

Morphologic Features:

Brachiopods have shells with pairs of curved valves that are markedly unequal in size and shape; each shell, however, is bilaterally symmetrical and may have a smooth, corrugated or spiny exterior. The symmetry characteristics help to distinguish brachiopod from bivalve shells in hand specimens, but rarely can be applied in thin sections. Shells typically have a rounded, elongate central elevation (the fold), generally on the brachial

(dorsal) valve, and a corresponding central depression (the sulcus) on the pedicle (ventral) valve — these structures affect both inner and outer shell surfaces (see top diagram, next page).

Rhynchonelliform brachiopods (the vast majority) are held together by a hinge (with a teeth-and-socket mechanism); linguliform and craniform shells are held together only by musculature.

Many brachiopods have some form of calcified internal support for their feeding organs (lophophores) — these are termed crura, brachidia, or spiralia, depending on the geometry of the structures.

Morphologic features of specific classes and orders are given above under "Taxonomy and Age Range".

Keys to Petrographic Recognition:

1. **The shell shapes of brachiopods are similar to bivalves; in terms of wall structure, they are most easily confused with mollusks that have foliated shell structure and with some cuts through (or small fragments of) bryozoans.**
2. **Brachiopods are found as articulated shells, single valves, or shell fragments. They typically are in the mm- to cm-size range and have smoothly curved to strongly plicated (corrugated) or spinose margins.**
3. **Microstructures are well preserved. Most shells have two layers and some have three. The thin outer (primary) layer has fine calcite fibers oriented with their long axes (and optic axes) perpendicular to the shell margin; this layer is difficult to see in poorly preserved specimens. The thicker inner (secondary) layer is composed of long calcite fibers arranged at a low angle (average 15 degrees) to the shell wall. Pentamerids and some spiriferids commonly have an additional innermost layer composed of coarse calcite prisms oriented with their long axis (and optic axis) perpendicular to the shell surface.**
4. **Brachiopod shells can have five types of shell microstructure: laminar, impunctate, punctate/endopunctate, pseudopunctate, or tabular. The first four are the most common and are illustrated below. Laminar shells consist of interlaminated sheets of collophane (phosphate) and chitin. Impunctate shells have primary and secondary layers lacking perforations and taleolae. Punctate (endopunctate) shells have small holes — punctae up to 100 µm wide — that perforate the wall and are oriented perpendicular to the shell surface. Pseudopunctate shells have stacked, conical plications (taleolae or pseudopunctae) in the fibers of the secondary layer that look somewhat like punctae. These microstructural variations have some taxonomic significance: for example, most spiriferids and nearly all rhynchonellids and orthids are impunctate; terebratulids are punctate; virtually all strophomenids are pseudopunctate, and all linguliform brachiopods have chitinophosphatic laminar shells. For more detailed discussions of shell structure of brachiopods see Clarkson (1998, p. 168-171, 176) and Williams (1997).**
5. **Brachiopod shells can be highly plicated, giving the shells and internal structures a very wavy appearance.**
6. **Distinctive, specialized structures such as a pedicle opening or foramen, a spondylum, and internal lophophore supports (crura, brachidia or spiralia) may be visible, but generally are rare except where complete shells are sectioned.**
7. **Detached spines may be abundant. They are hollow and have a distinctive two-layer fibrous structure.**

Anatomical features of a typical articulate brachiopod

A median longitudinal section through an articulate brachiopod (redrawn from Moore et al., 1952). The pedicle opening allows for attachment of the organism to rocks or other substrates by a muscular stalk, termed the pedicle. The lophophore is the feeding organ whose sidearms are folded or enrolled into loops or spirals. The inequality of size and shape between the pedicle and brachial valves is clearly shown in this diagram.

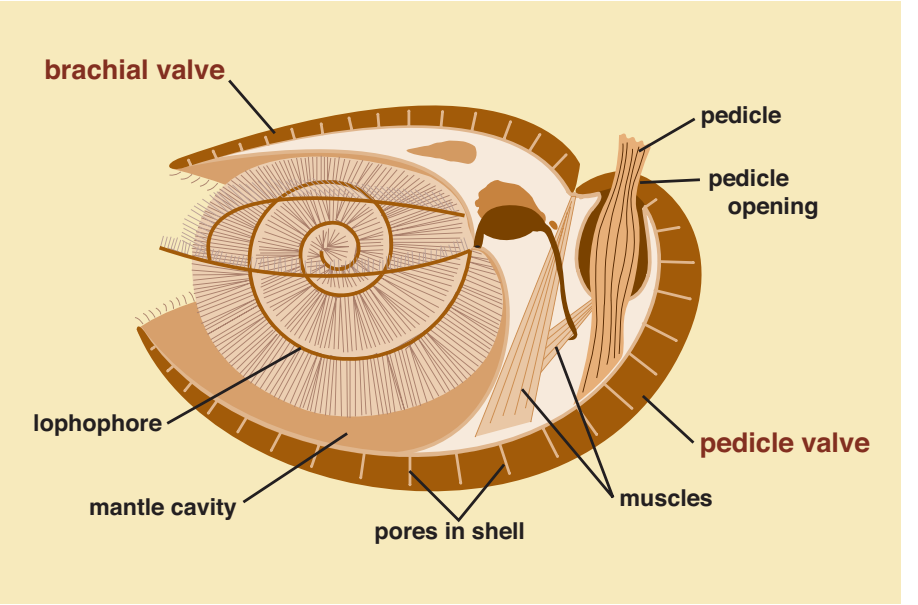

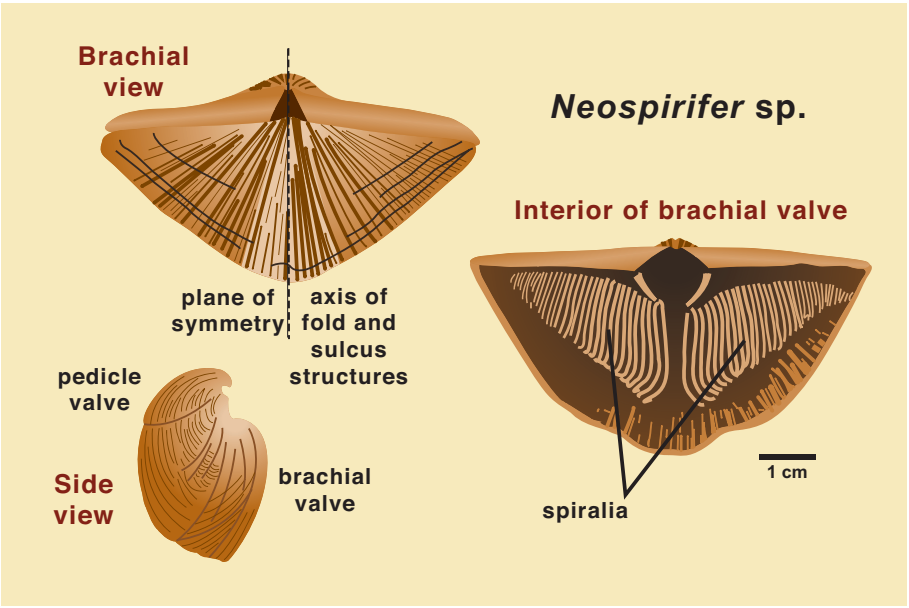

Morphology of a typical spiriferid brachiopod

Two surface views and an interior view of the brachial valve of *Neospirifer* sp., a representative spiriferid brachiopod (redrawn from Moore et al., 1952). Spiriferids developed specialized internal lophophore support structures (termed spiralia). These are sometimes encountered in thin-section views of whole or nearly whole spiriferid brachiopod shells. See also the lower photograph on the title page of this section.

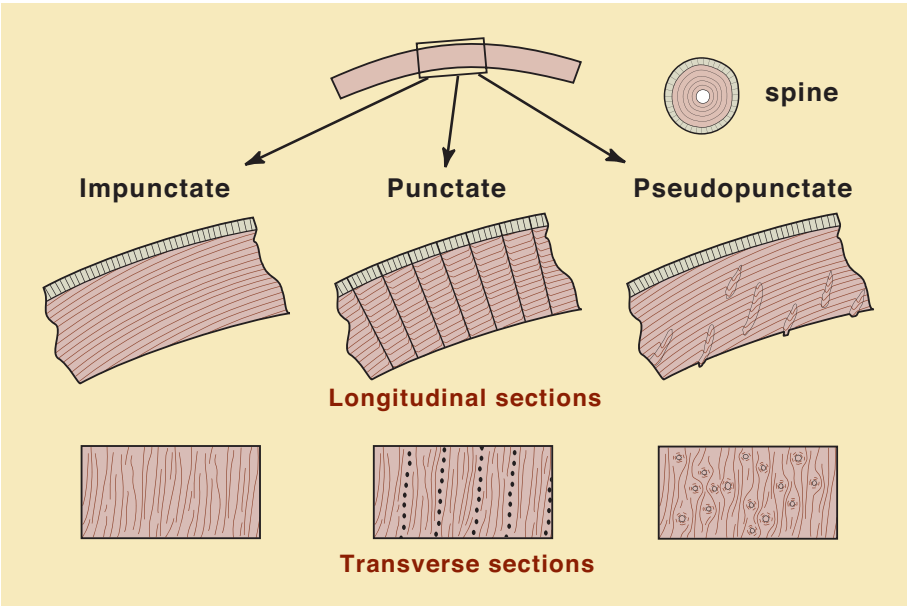

Variations in typical articulate brachiopod shell structures

Diagrammatic representations of variations in articulate brachiopod shell structures as adapted from Scoffin (1987) and other sources. Most shells have a thin, primary outer layer (not always preserved) of fine prisms oriented perpendicular to the shell exterior and a thick secondary inner layer with fibers inclined obliquely (roughly 15° relative to the shell surface). Spines have comparable two-layered structure. Shells can also have true punctae or pores that penetrate the shell wall, pseudopunctae (stacked plications in the secondary layer that mimic pores), or no punctae or pseudopunctae (termed an impunctate shell).

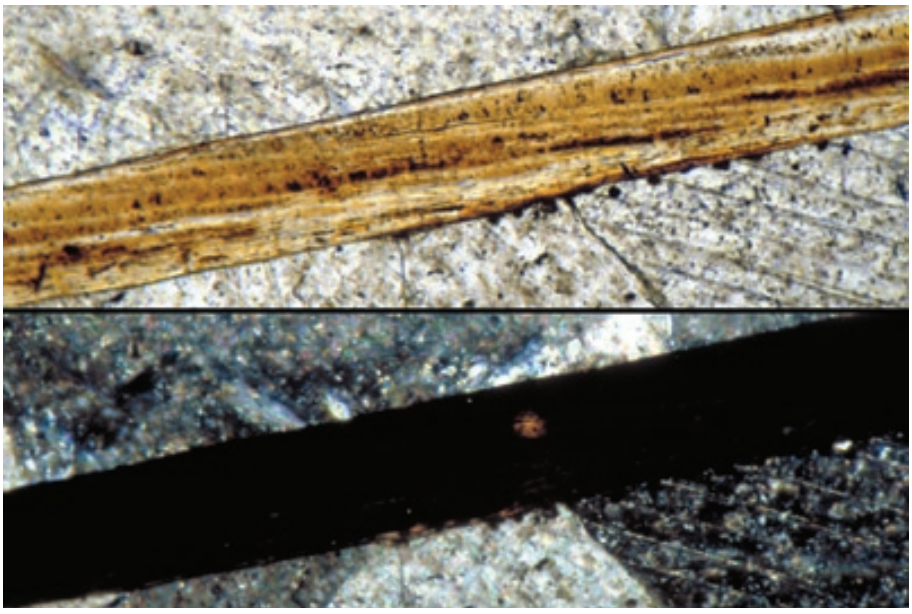

Mid.-Up. Cambrian Riley Fm., Lion Mountain Ss. Mbr., Burnet Co., Texas

Two views of an early, chitinophosphatic, inarticulate brachiopod shell. Characteristic features include the inclined laminae within the shell, the brownish color of the chitinous and phosphatic shell in plain-polarized light, the extremely slight curvature of the shell, and the isotropic or near-isotropic behavior under cross-polarized light.

PPL/XPL, HA = 0.65 mm each

Up. Mississippian Hindsville Ls., Mayes Co., Oklahoma

A variety of micrite-coated brachiopod grains (and crinoid ossicles) are visible in this slide. All the brachiopods have a low-angle fibrous wall structure, one of the most important criteria for identification of these grains. The long impunctate shell in the center clearly shows both the thick, fibrous, secondary layer and the outer primary layer that has fibers oriented perpendicular to the shell surface. The shell above it is a punctate brachiopod with micritic fillings of the individual punctae. A third (heavily micrite encrusted) shell below has impunctate structure with wavy shell contortions.

PPL, HA = 1.9 mm

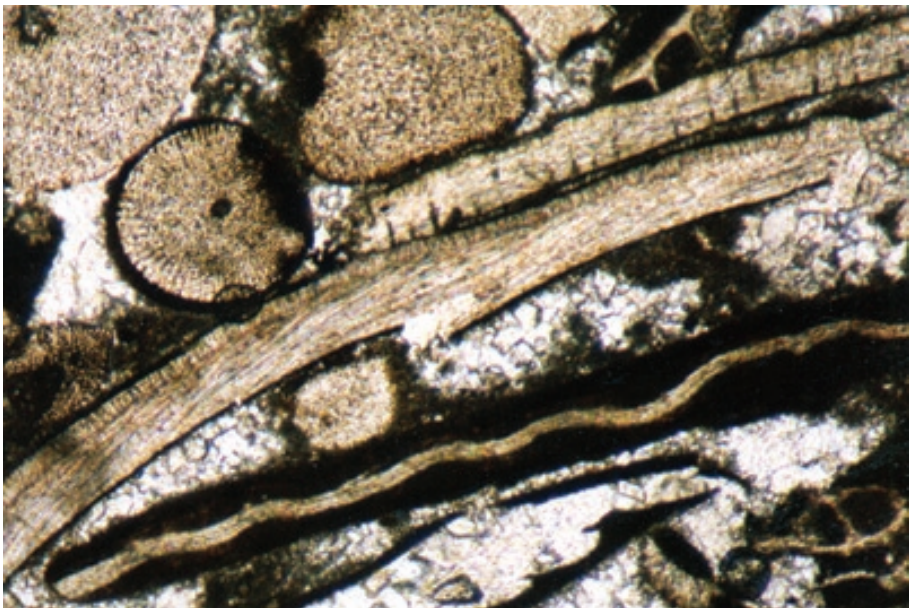

Up. Ordovician limestone, Kentucky

An example of an impunctate shell wall in the brachiopod *Platystropha cypha*. This shell has an extremely thin (or diagenetically altered) primary layer and a thick secondary layer. Note the typical low-angle fibrous structure and the substantial lateral variations in shell thickness.

PPL, HA = 3.0 mm

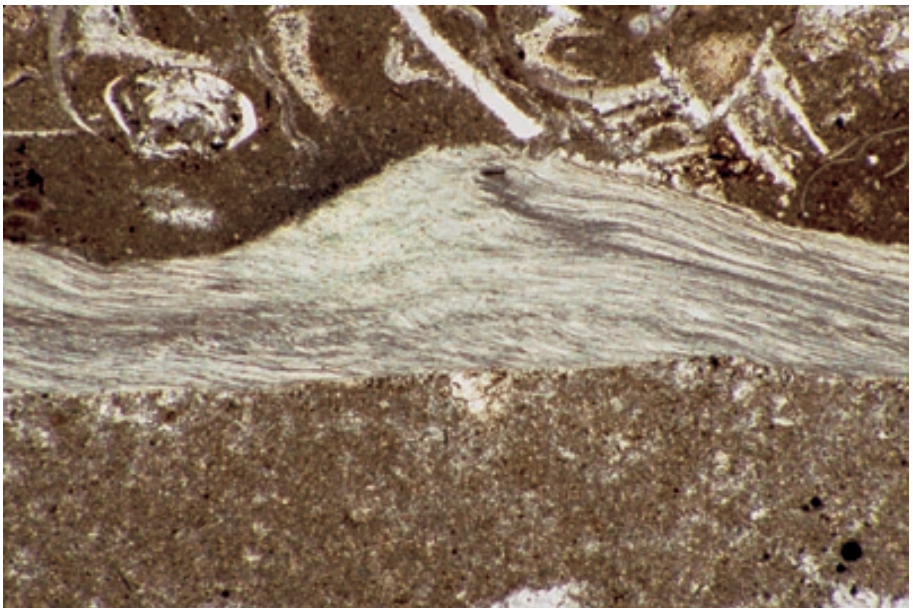

Miocene Mount Brown Beds, Canterbury, New Zealand

An example of a punctate brachiopod shell. The vertical punctae were holes that penetrated the shell wall from the interior almost to the outer surface of the shell. They are easily visible here because they have been filled with micritic material (most likely precipitated *in-situ*). Although other organisms (trilobites, ostracodes and a few bivalves, for example) also have pores that may completely penetrate the shell wall, the combination of the low-angle fibrous wall structure and punctae is diagnostic for the recognition of brachiopod material.

PPL, BSE, HA = 2.0 mm

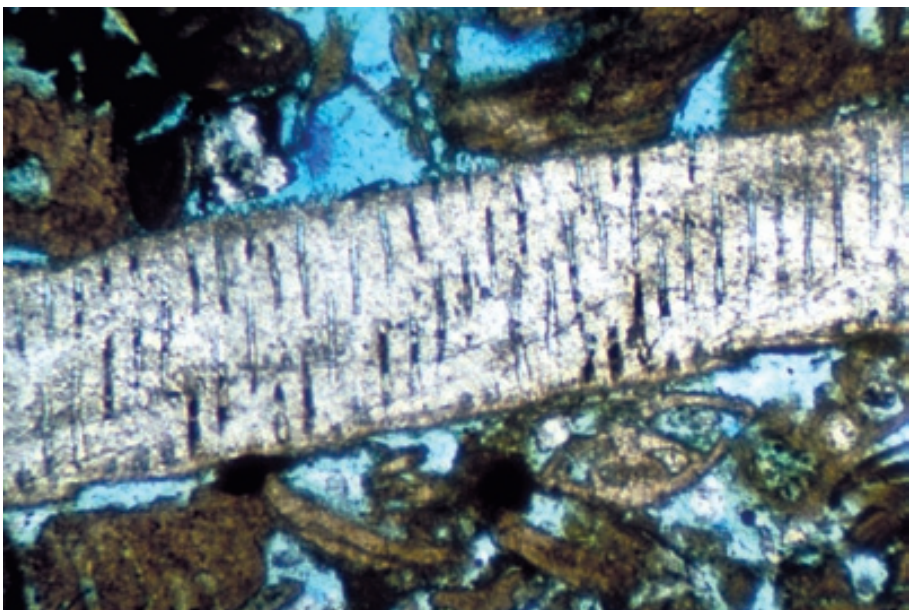

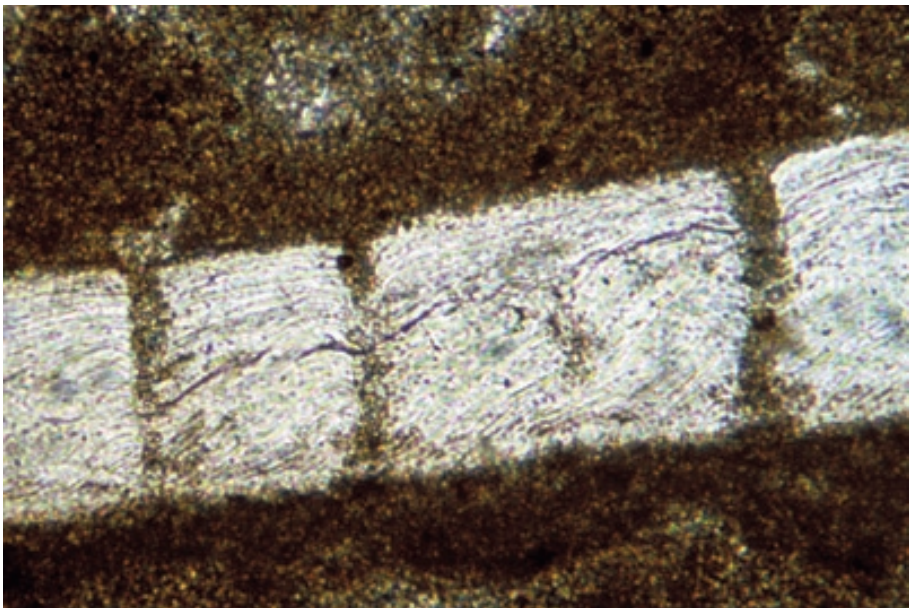

Up. Permian Middle reef complex, Djebel Tebaga, Tunisia

An enlarged view of a punctate brachiopod wall. Clearly, the individual punctae completely penetrate the shell wall and, once again, have been made visible through the infiltration or precipitation of micrite in the openings. In life, small finger-like projections of the body covering (mantle) extended through these openings.

PPL, HA = 3.5 mm

Oligocene Nile Gp., Karamea, Westland, New Zealand

A punctate brachiopod in which the punctae have been filled with calcite cement. Fortunately, the cements were slightly ferroan and thus stained pale purple, contrasting with the pink-stained non-ferroan calcite of the rest of the shell. In the absence of such differential staining, recognition of the cemented pores would be difficult.

PPL, AFeS, HA = 2.4 mm

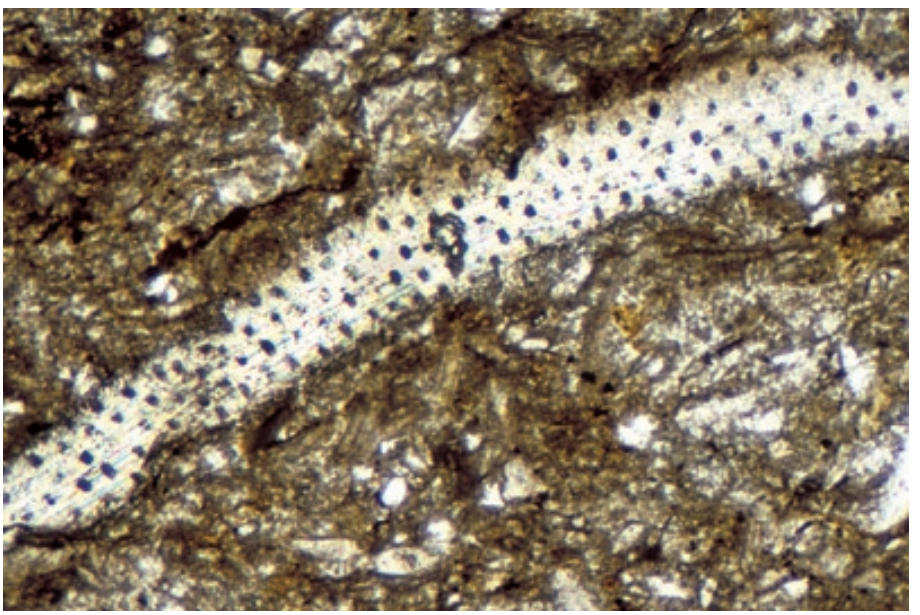

Up. Permian (Ufimian?) Schuchert Dal Ss., Jameson Land, East Greenland

An oblique or tangential cross section through a punctate brachiopod that shows circular to elliptical shapes of the punctae (now seen as micrite-filled former pores).

PPL, HA = 2.0 mm

Up. Permian (Kazanian?) Wegener Halvø Fm., Jameson Land, East Greenland

A detailed view of a pseudopunctate brachiopod shell. Although pseudopunctae, at first glance, may look like true punctae, they are quite different. They are stacked columns of cone-shaped plications or granular zones in the fibrous structure of the secondary wall layer. They mimic pores (punctae) but were never actually open spaces. They are unique to brachiopods; however, they are found in only a few groups, primarily the strophomenids.

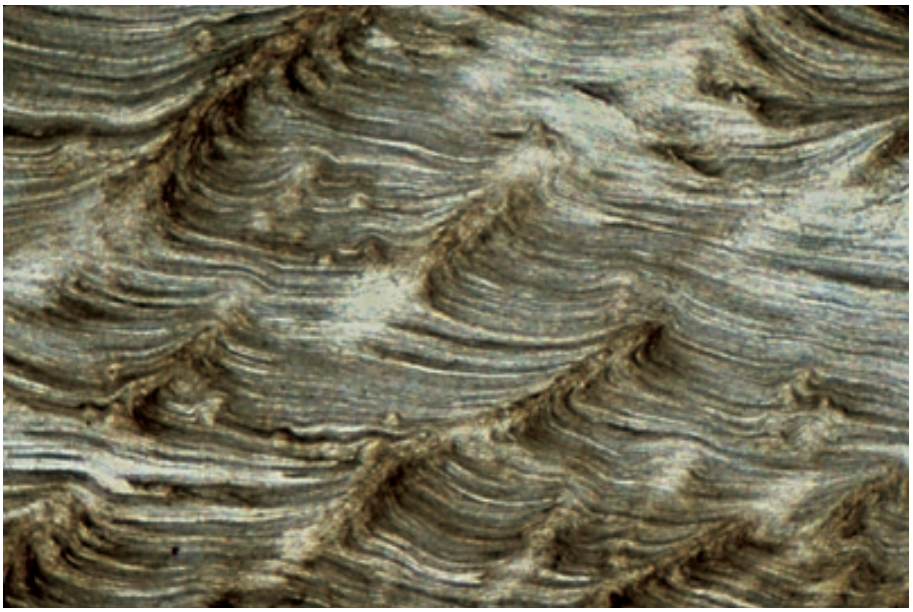

PPL, HA = 2.4 mm

Lo. Devonian Becraft Ls., Schoharie Co., New York

A high-magnification, longitudinal section through a pseudopunctate brachiopod shell. Note the parallel fibrous wall structure oriented at a low angle to the shell margin. These pseudopunctae consist of very small fiber plications, oriented perpendicular to the shell exterior.

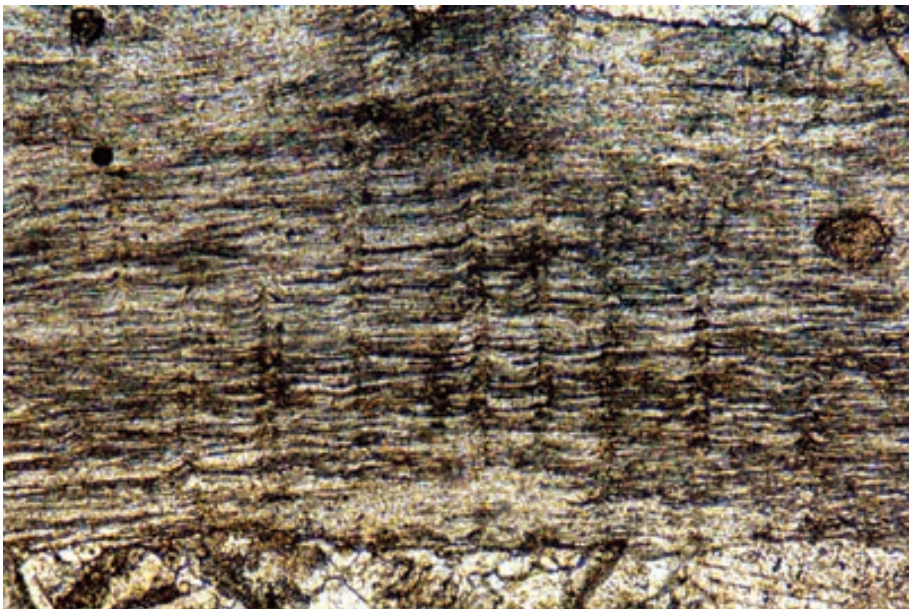

PPL, HA = 1.0 mm

Up. Permian (Kazanian?) Wegener Halvø Fm., Jameson Land, East Greenland

This oblique, nearly transverse cut through a pseudopunctate brachiopod shell nicely shows the irregularly spaced stacks of plications and circular or slightly elliptical shape of these distinctive features.

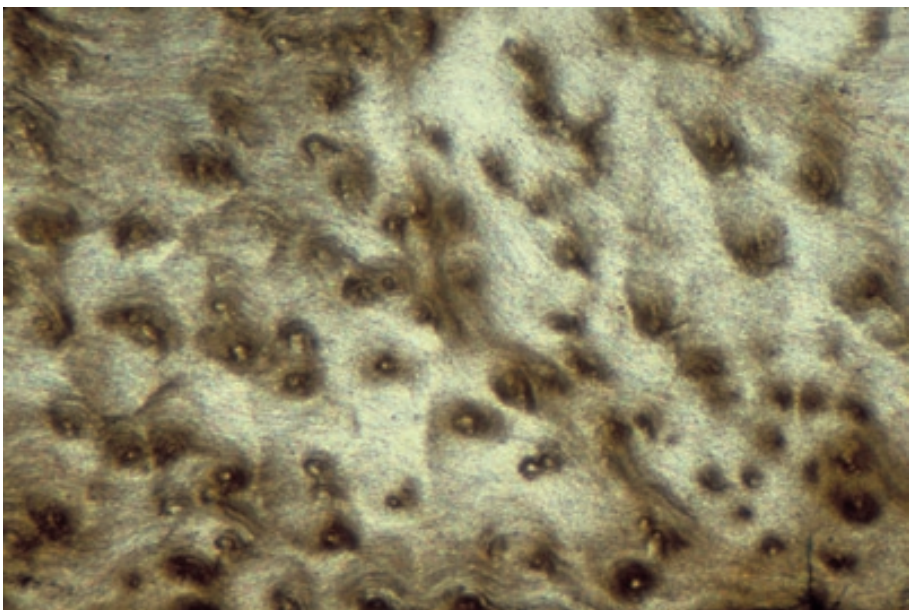

PXPL, BSE, HA = 2.0 mm

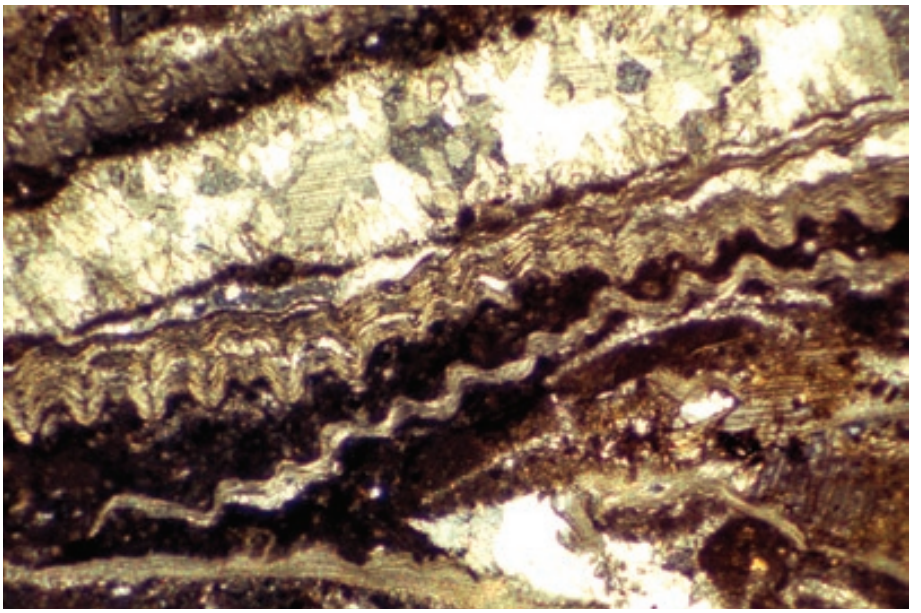

Mid. Ordovician Chazy-Black River Fms., Mifflin Co., Pennsylvania

The longitudinal sections through several shells in this slide illustrate the highly crenulate shape of many brachiopods. The contorted fabric within the shells does not represent pseudopunctae, but rather is caused by plications and shell ornamentations that affect the entire wall structure.

XPL, HA = 3.4 mm

Up. Permian (Kazanian?) Wegener Halvø Fm., Jameson Land, East Greenland

Several groups of brachiopods were extensively "armored" with long spines, most of which are broken off during transport and deposition of the shells. This example shows a brachiopod shell with a portion of an attached spine.

PPL, AFeS, HA = 2.0 mm

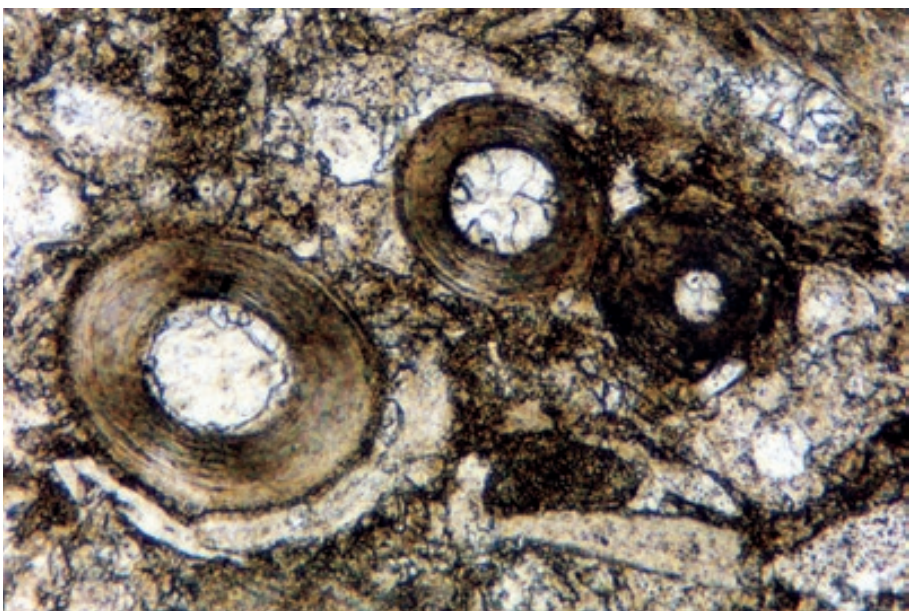

Lo. Carboniferous Glencar Ls., County Sligo, Ireland

Individual broken productid brachiopod spines in a shelf limestone. Here, three brachiopod spines lie in close proximity to each other. Each displays a characteristic hollow center and concentric, two-layer wall structure — a margin-parallel fibrous inner zone, and a thin, radially-oriented, fibrous outer zone. The oriented crystal structure in both layers produces a distinctive "pseudo-uniaxial cross" under cross-polarized light (a hint of which is even seen in this view).

PPL, HA = 0.8 mm

Up. Permian (Kazanian?) Wegener Halvø Fm., Jameson Land, East Greenland

An enlarged view of a two-layered productid brachiopod spine. The relatively large size, the central canal, and the thick, two-layered wall with oriented crystal structure are unique to brachiopod spines. In transverse cuts like this one, they could most easily be mistaken for ooids.

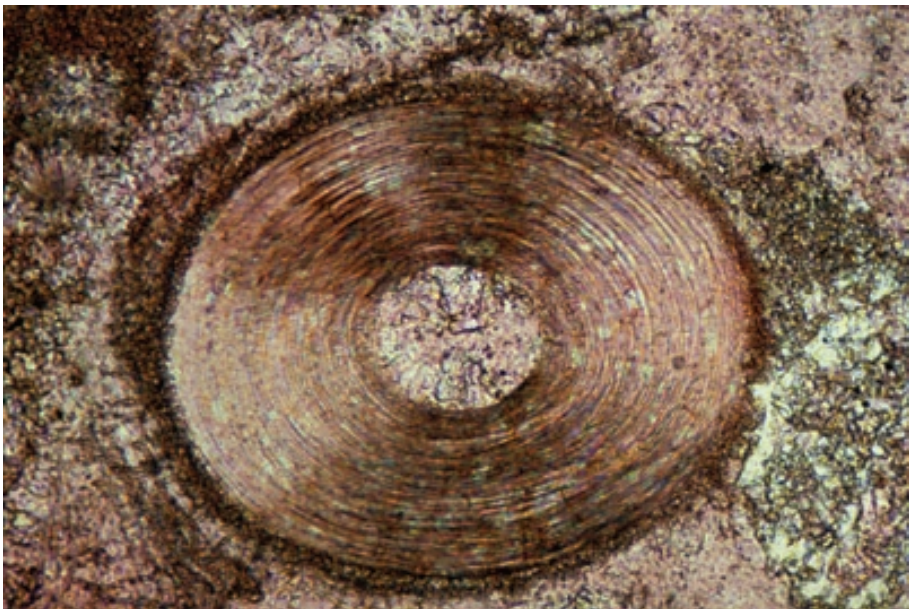

PPL, AFeS, HA = 0.65 mm

Lo. Carboniferous Glencar Ls., County Sligo, Ireland

An oblique longitudinal cross section of a brachiopod spine. The two-layered, fibrous wall structure is characteristic of such grains and serves (along with the relatively large size) to distinguish these spines from a variety of conical microfossils or spherical ooids.

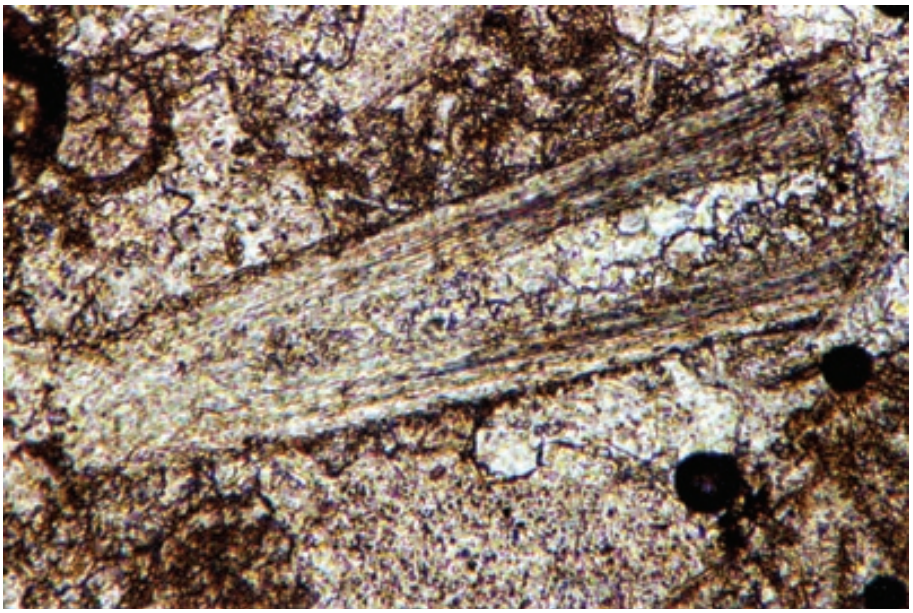

PPL, HA = 0.75 mm

Permian (Leonardian-Guadalupian) Park City Fm., Franson Mbr., Bear Lake Co., Idaho

An example of a sandy shelf limestone in which brachiopod spines are the predominant faunal constituent, at least in some intervals. The consistent near-circular outlines of these detached spines indicates a strong orientation of the grain long axes, a result of transport and current orientation. Pressure solution and mechanical compaction during burial-stage diagenesis has led to interpenetration of adjacent grains and thus has modified their shapes.

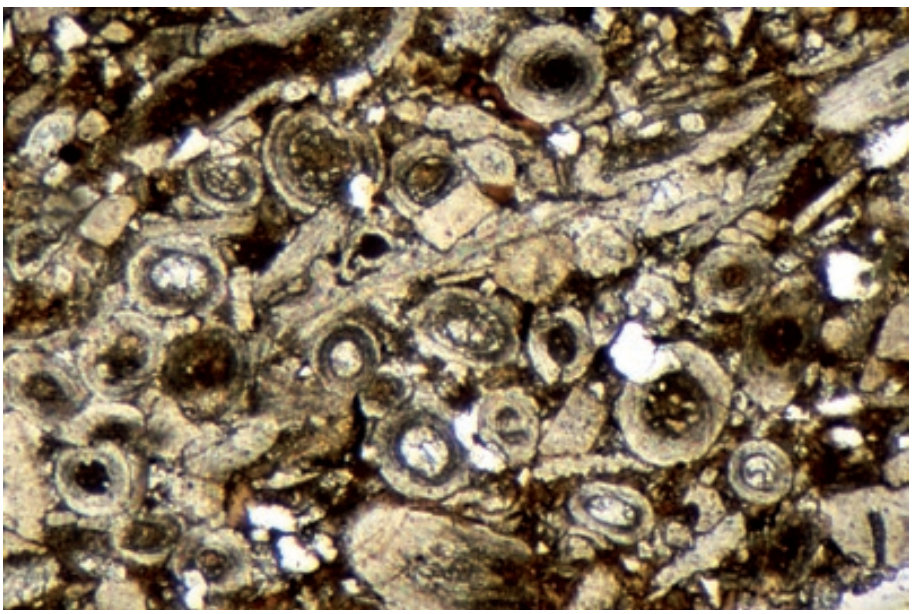

PPL, HA = 3.6 mm

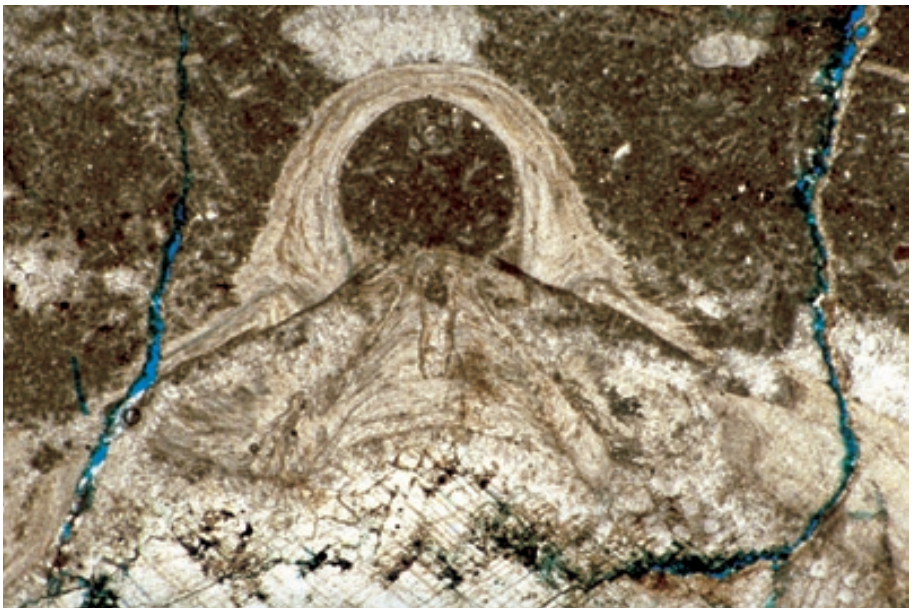

Up. Permian (Kazanian?) Wegener Halvø Fm., Jameson Land, East Greenland

An unusual, but very distinctive, cut through a largely intact pedicle valve of a brachiopod showing its pedicle opening. This is the opening through which the pedicle extends that allows the brachiopod to attach itself to its substrate. Where recognizable, it helps to distinguish brachiopods from bivalves.

PPL, BSE, HA = 8.0 mm

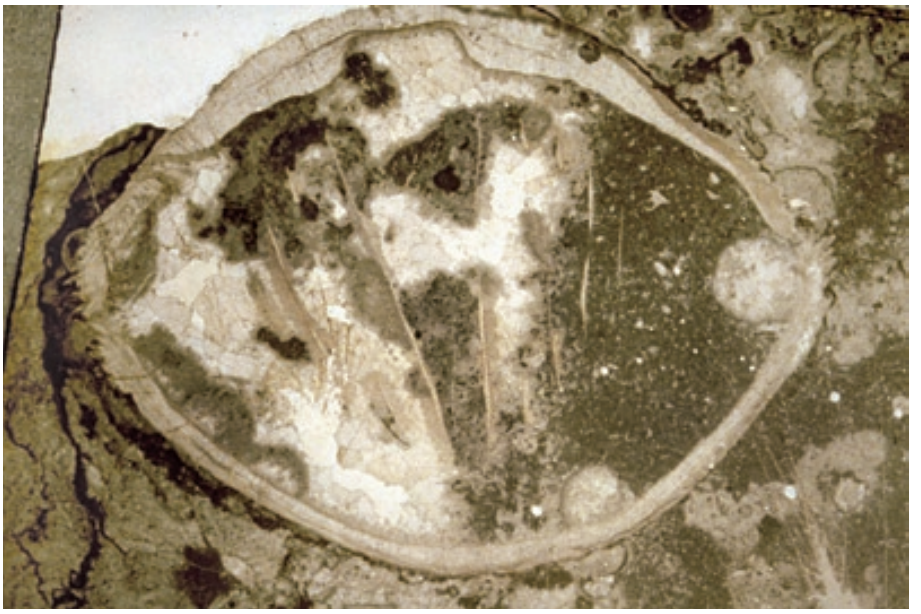

Up. Permian (Guadalupian) Capitan Fm., Eddy Co., New Mexico

A transverse section through a complete spiriferid brachiopod showing the internal spiralia (elaborate spiral brachidia) — the slightly V-shaped lines of shell material within the internal cavity of the organism. These spiral-shaped calcareous growths (see second diagram in this chapter) served as internal supports for the organism's feeding structure (termed the lophophore).

PPL, HA = 25 mm

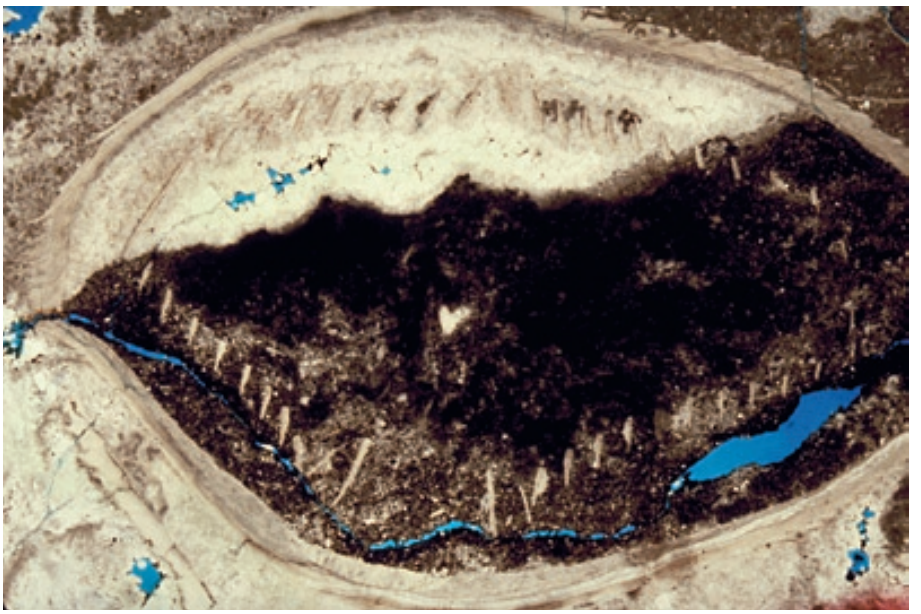

Up. Permian (Kazanian?) Wegener Halvø Fm., Jameson Land, East Greenland

A slightly oblique, longitudinal section through both valves of an articulated brachiopod shell that has internal spiralia. The multilayered fibrous wall of the shell and the orientation of the sectioned loops of the spiralia are well shown. The shell has a geopetal fill that consists of internal sediment (impregnated with asphaltic residues) in the lower part and calcite pore-filling cements in the upper portion.

PPL, BSE, HA = 25 mm

Lo. Permian limestone, Axel Heiberg Island, Canada

A longitudinal cut through a spiriferid brachiopod with both valves intact showing elongate sections through the internal spiralia. The spiralia later acted as substrates for oriented growth of cement crystals within the mantle cavity. Note also the preferential replacement of parts of the shell by silica, a common phenomenon in brachiopod material. Sample from Noel P. James.

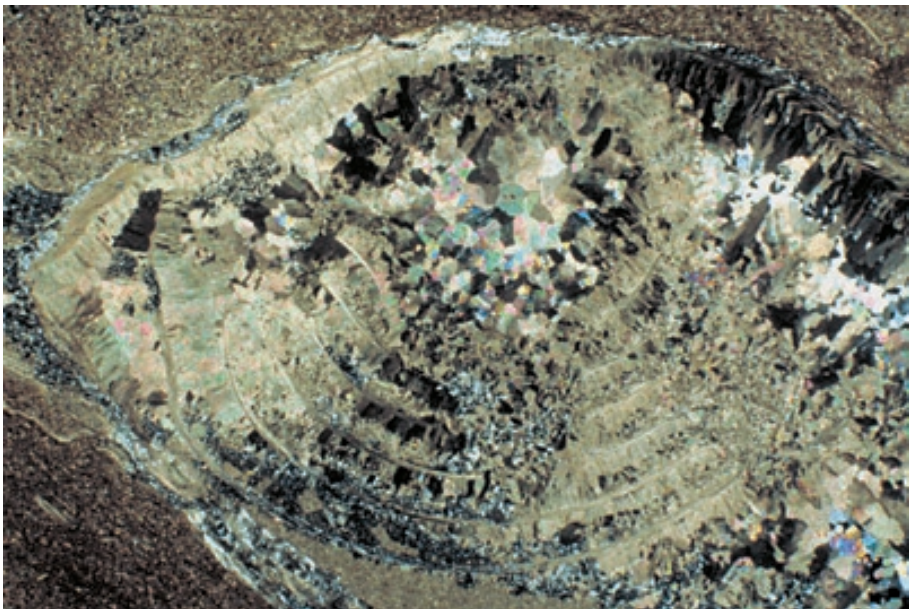

XPL, HA = 16 mm

Lo. Permian limestone, Axel Heiberg Island, Canada

An enlarged view of the spiriferid brachiopod shown in the previous image. The curved spiralia and their fibrous wall structure are clearly visible, as are the cloudy, bladed burial-stage calcite cements that nucleated on, and grew outward from, the spiralia. Silica replacement (the low birefringence crystals with gray to white extinction colors) affects both the spiralia and the calcite cement crystals. Sample from Noel P. James.

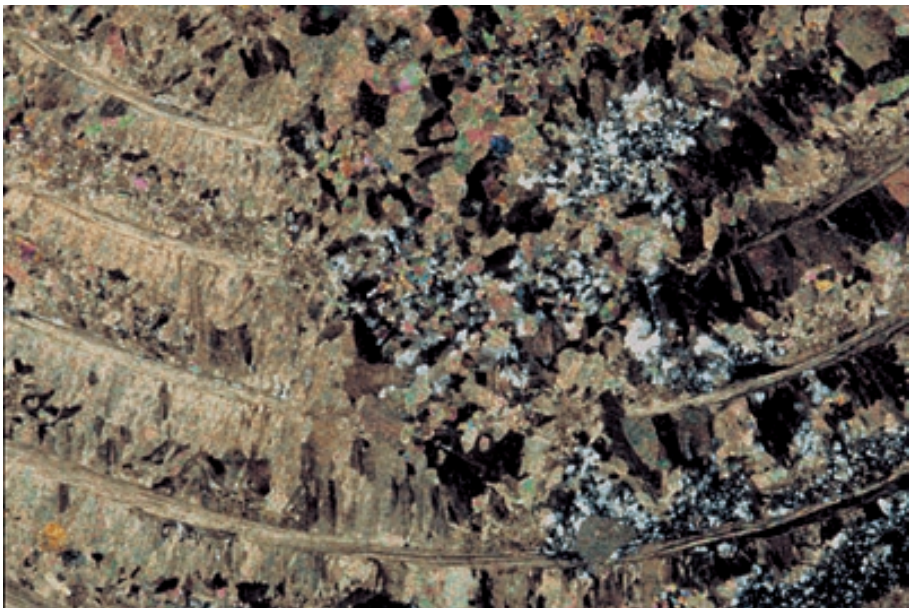

XPL, HA = 5.5 mm

Up. Permian (Guadalupian) Capitan Fm., Eddy Co., New Mexico

A portion of the wall of *Composita* sp., a brachiopod with an atypical wall structure. The fibrous prismatic inner and outer layers are here sandwiched around a thick, coarsely crystalline zone with prisms oriented perpendicular to the shell margin. This particular group of brachiopods is restricted to Carboniferous and Permian strata. *Composita* shells can be differentiated from prismatic bivalve shells on the basis of the presence of internal calcareous spires in *Composita* (although those are not always preserved or intersected in every section).

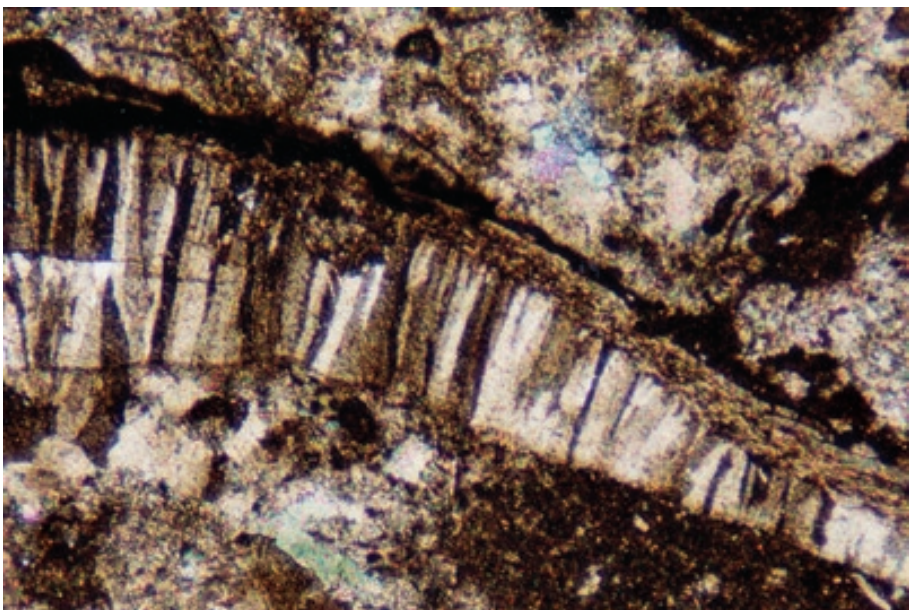

XPL, HA = 4.6 mm

Cited References and Additional Information Sources

Ager, D. V., 1967, Brachiopod paleoecology: Earth-Science Reviews, v. 3, p. 157-179.

Biernat, G., and A. Williams, 1971, Shell structure of the siphonotretacean Brachiopoda: Palaeontology, v. 14, p. 423-430.

Boucot, A. J., 1971, Practical taxonomy, zoogeography, paleoecology, paleogeography, and stratigraphy for Silurian-Devonian brachiopods: Proceedings of the North American Paleontological Convention, Chicago, 1969 (F), p. 566-611.

Brunton, C. H. C., 1972, The shell structure of chonetacean brachiopods and their ancestors: Bulletin of the British Museum Natural History Geology Series, v. 21, p. 3-25.

Clarkson, E. N. K., 1998, Invertebrate Palaeontology and Evolution [4th Edition]: Oxford, Blackwell Scientific, 452 p.

Dagys, A. S., and T. N. Smirnova, 1984, Peculiarities of the shell structure of Mesozoic and Cenozoic brachiopods, *in* N. A. Bogdanov, ed., Mezhdunarodnyy geologicheskiy kongress; 27, International Geological Congress, v. 27, p. 248-249.

Daley, R. L., and D. W. Boyd, 1996, The role of skeletal microstructure during selective silicification of brachiopods: Journal of Sedimentary Research, Section A: Sedimentary Petrology and Processes, v. 66, p. 155-162.

Elliott, G. F., 1955, Shell structure of thecidean brachiopods: Nature, v. 175, p. 1124.

Gauri, K. L., and A. J. Boucot, 1968, Shell structure and classification of Pentameracea M'Coy, 1844: Palaeontographica, Abt. A, v. 131, p. 79-135.

Hall, J., 1884, Preliminary note on the microscopic shell structure of the Paleozoic Brachiopoda: American Association for the Advancement of Science, Proceedings, p. 266-268.

Isogai, F., 1970, (Shell structure of brachiopods; part 3): Chishitsugaku Zasshi [Journal of the Geological Society of Japan], v. 76, p. 96.

Iwata, K., 1981, Fine structure and calcification of shells of inarticulate brachiopod shells: I, Case of the *Lingula unguis* shell: Chishitsugaku Zasshi [Journal of the Geological Society of Japan], v. 87, p. 405-415.

Jaanusson, V., 1966, Fossil brachiopods with probable aragonitic shells: Geologiska Föreningen Stockholm Förhandlingar, v. 88, p. 279-281.

Kats, Y. I., A. M. Popov, and E. S. Tkhorzhevskiy, 1973, New techniques in the study of the internal structure and microstructure of brachiopod shells: Paleontological Journal, v. 7, p. 541-548.

MacKinnon, D. I., 1974, The shell structure of spiriferide Brachiopoda: Bulletin of the British Museum Natural History Geology Series, v. 25, p. 189-261.

MacKinnon, D. I., and A. Williams, 1974, Shell structure of terebratulid brachiopods: Palaeontology, v. 17, p. 179-202.

Popp, B. N., T. F. Anderson, and P. A. Sandberg, 1986, Brachiopods as indicators of original isotopic compositions in some Paleozoic limestones: Geological Society of America Bulletin, v. 97, p. 1262-1269.

Rowell, A. J., and R. E. Grant, 1987, Phylum Brachiopoda, *in* R. S. Boardman, A. H. Cheetham, and A. J. Rowell, Fossil Invertebrates: Palo Alto, CA, Blackwell Scientific Publications, p. 445-496.

Rudwick, M. J. S., 1959, The growth and form of brachiopod shells: Geological Magazine, v. 96, p. 1-24.

Rudwick, M. J. S., 1970, Living and Fossil Brachiopods: London, Hutchinson, 199 p.

Rush, P. F., and H. S. Chafetz, 1990, Fabric-retentive, non-luminescent brachiopods as indicators of original $\delta^{13}C$ and $\delta^{18}O$ composition: Journal of Sedimentary Petrology, v. 60, p. 968-981.

Sass, D. B., 1967, Electron microscopy, punctae, and the brachiopod genus *Syringothyris* WINCHELL, 1863: Journal of Paleontology, v. 41, p. 1242-1246.

Vachard, C., and C. Tellez-Giron, 1978, Espines de Brachiopodes reticulacriacea dans les microfacies du Paléozoique supérieur: Rev. Inst. Mexicano Petrol., v. 10, no. 2, p. 16-30.

Veizer, J., P. Fritz, and B. Jones, 1986, Geochemistry of brachiopods: oxygen and carbon isotopic records of Paleozoic oceans: Geochimica et Cosmochimica Acta, v. 50, p. 1679-1696.

Westbroek, P., 1967, Morphological observations with systematic implications on some Paleozoic Rhynchonellida from Europe, with special emphasis on the Uncinulidae: Leidse Geol. Mededeel., v. 41, p. 1-82.

Williams, A., 1956, The calcareous shell of the Brachiopoda and its importance to their classification: Biological Reviews of the Cambridge Philosophical Society, v. 31, p. 243-287.

Williams, A., 1968, A history of skeletal secretion in brachiopods: Lethaia, v. 1, p. 268-287.

Williams, A., 1968, Evolution of the shell structure of articulate brachiopods: Palaeontological Association, Special Papers in Palaeontology, no. 2, 55 p.

Williams, A. 1997, Shell structure, *in* Williams, A., M. A. James, C. C. Emig, S. Mackay, M. C. Rhodes, B. L. Cohen, A. B. Gawthrop, L. S. Peck, G. B. Curry, A. D. Ansell, M. Cusack, D. Walton, C. H. C. Brunton, D. I. MacKinnon, and J. R. Richardson, Treatise on Invertebrate Paleontology, Part H, Revised Brachiopoda, Volume 1: Introduction: Boulder, Geological Society of America and University of Kansas, p. 267-320.

Williams, A., M. A. James, C. C. Emig, S. Mackay, M. C. Rhodes, B. L. Cohen, A. B. Gawthrop, L. S. Peck, G. B. Curry, A. D. Ansell, M. Cusack, D. Walton, C. H. C. Brunton, D. I. MacKinnon, and J. R. Richardson, 1997, Treatise on Invertebrate Paleontology, Part H, Revised Brachiopoda, Volume 1: Introduction: Boulder, Geological Society of America and University of Kansas, 539 p.

Williams, A., and A. J. Rowell, 1965, Morphology, *in* R. C. Moore, ed., Treatise on invertebrate paleontology, Part H Brachiopoda: Geological Society of America and University of Kansas Press, p. H57-H138.

Williams, A., and A. D. Wright, 1970, Shell structure of the Craniacea and other calcareous inarticulate brachiopods: Palaeontological Association, Special Papers in Palaeontology, no. 7, 51 p.

Facing Page: Underwater view of *Tridacna* sp. Note the brilliantly hued mantle on this giant (1.5 m long) bivalve from the Australian Great Barrier Reef. Photograph courtesy of Woody Mayhew.

GRAINS: Skeletal Fragments

MOLLUSKS

CHAPTER 9

Gastropods

Bivalves (pelecypods)

Cephalopods

Scaphopods

GASTROPODS

Taxonomy and Age Range:

Phylum Mollusca, Subphylum Cyrtosoma

Class Gastropoda — Early Cambrian-Recent

Order Thecosomata (pteropods) — Cretaceous-Recent (possible precursors Cambrian?-Permian?)

Gastropods are the largest class of both living and fossil mollusks (with nearly 8,000 genera), although they are rarely major rock-forming organisms.

Environmental Implications:

Gastropods (snails) are a remarkably wide-ranging group of organisms. They are found at all latitudes and in normal marine, brackish, hypersaline, and fresh water as well as subaerial environments. They rarely are major sediment formers, however, except in stressed (especially hypersaline or freshwater) settings.

Warm-water forms generally are thicker shelled than cold-water forms.

Pteropods are open-marine, predominantly warm-water, nektic organisms that contribute mainly to deep-sea oozes on seafloors shallower than about 3,000 m (because of aragonite dissolution effects).

Skeletal Mineralogy:

Gastropod shells have a thin outer coating of organic material (conchiolin) plus a thick carbonate layer generally consisting of only aragonite. Some families, however, have shells with separate layers of calcite and aragonite. Where present, the calcite layer normally is thicker than the aragonite layer. Gastropod calcite has a low Mg content (typically less than 0.3 mole% Mg; rarely exceeding 1 mole% Mg). Pteropods have aragonite shells.

Morphologic Features:

Both shell-bearing and non-shell-bearing gastropods exist. The shelled forms are univalves that have an unchambered cone, most commonly coiled about a central axis. Some forms are able to withdraw fully into their shell and have a plate (an operculum) that they can draw behind themselves to close the shell opening; opercula can be composed entirely of conchiolin (proteinaceous organic material that is rarely preserved) or aragonite.

Diverse coiling patterns exist: high-spired, conical, and planispiral forms are common; some groups (such as the vermetids) have very open spirals and form shells that resemble serpulid worm tubes.

Adult gastropods typically are about 2-3 cm in length (modern forms of up to 60 cm length are known, however). Fragments typically mm- to cm-sized.

Pteropods are nektic gastropods and although the majority are shell-less, some have slender, conical, generally uncoiled, thin-walled shells, typically less than 1-2 cm in length.

Keys to Petrographic Recognition:

1. **Gastropod shells or fragments are typically in the mm to cm size range — larger than most foraminifers, especially those that have similarly shaped tests.**
2. **Strongly curved, smooth to somewhat ornamented shell fragments predominate — those that are large enough may have distinctively spiraled shapes. Coiled gastropod shells differ from cephalopods in that they generally are smaller and lack the internal chambering of cephalopods (although gastropods may falsely appear chambered in some sections).**
3. **Most gastropods are/were entirely aragonitic and such shells generally lose all internal microstructure during diagenesis; originally calcitic shell layers, found in some gastropods, typically retain primary fabrics. Mixed-mineralogy gastropod shells tend to have thicker calcite layers that are well preserved and aragonitic layers that are thinner and poorly preserved.**
4. **Aragonitic shell microstructures of gastropods include: crossed-lamellar (very common), finely prismatic, homogeneous (also termed homogeneous prismatic), and nacreous fabrics. Calcitic microstructures include: prismatic (common), foliated (rare), and crossed-lamellar (rare) fabrics. Crossed-lamellar structure is characterized by a distinctive "zebra striping" in cross-polarized illumination.**
5. **Well preserved gastropod and bivalve (pelecypod) fragments sometimes can be distinguished from each other on the basis of distinctive combinations of layering, but shape is generally the simplest and most reliable method of identification.**

PHOTO SCALES AND ABBREVIATIONS ARE EXPLAINED IN THE BOOK'S INTRODUCTION

Morphology and wall structure of a typical high-spired gastropod

Diagrammatic view of typical longitudinal (A) and transverse (B) cross sections through a high-spired gastropod with the names of the most prominent structural features. Also shown are some typical aragonitic wall fabrics found in gastropods (mainly crossed-lamellar along with homogeneous or nacreous) and their appearance after typical diagenetic alteration by dissolution of unstable aragonite and reprecipitation of void-filling calcite. Wall structural depictions were partially adapted from Tucker (1981). Although the shell appears chambered in this vertical section, no actual partitions divide the continuous spiral of the internal tube in which the animal lives.

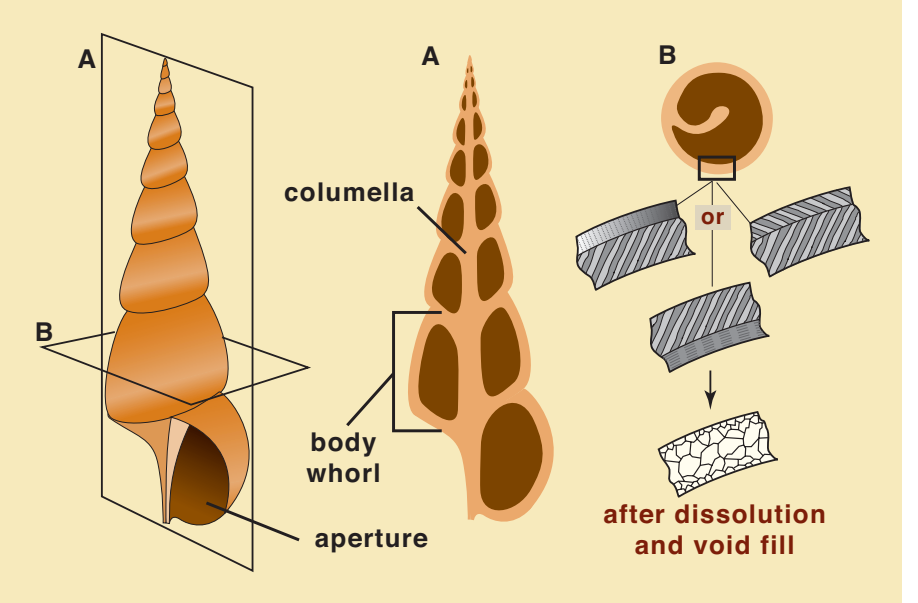

Recent sediment, Abu Dhabi, coastal United Arab Emirates

Oblique and longitudinal sections through modern high-spired cerithid gastropods in a hardground. The longitudinal section is slightly off the center of the grain — thus, the central columella is not shown as a continuous structure. This genus of gastropods is well adapted to variable and high salinity environments and is a dominant faunal element in many lagoonal deposits.

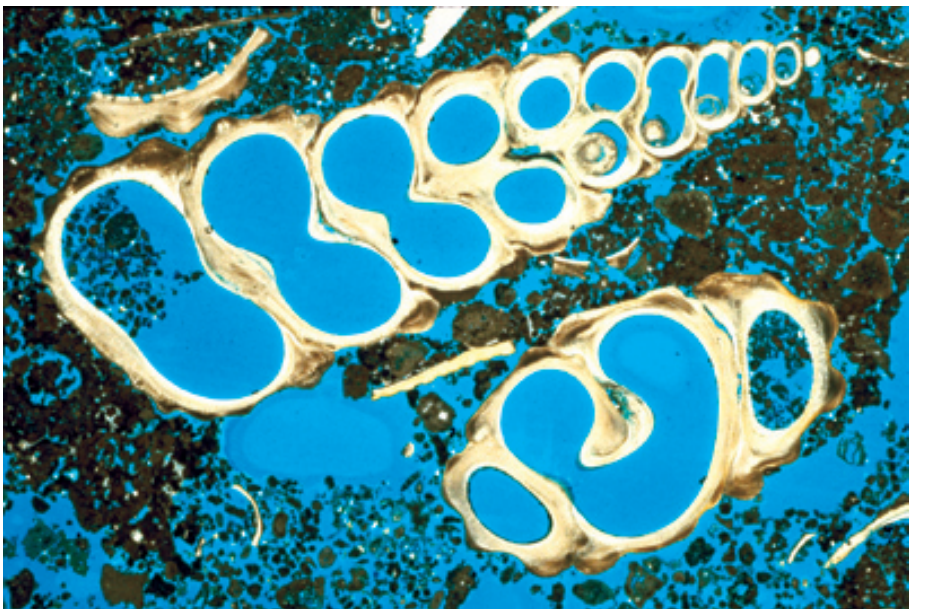

PPL, BSE, HA = 16 mm

Recent sediment, Grand Cayman, Cayman Islands, B.W.I.

Another longitudinal section through an aragonitic gastropod shell. This shell has a more conical (lower spired) form. It shows the early stages of marine diagenesis that help to preserve at least the outlines of gastropods in the geologic record. The exterior of the shell has been encrusted with high-Mg calcite and aragonite cement; the body chamber has been extensively filled with fibrous aragonite. Both may prove less soluble than the shell itself during diagenesis and thereby allow later mold-filling cements to preserve the shell form.

PPL, BSE, AFeS, HA = 1.6 mm

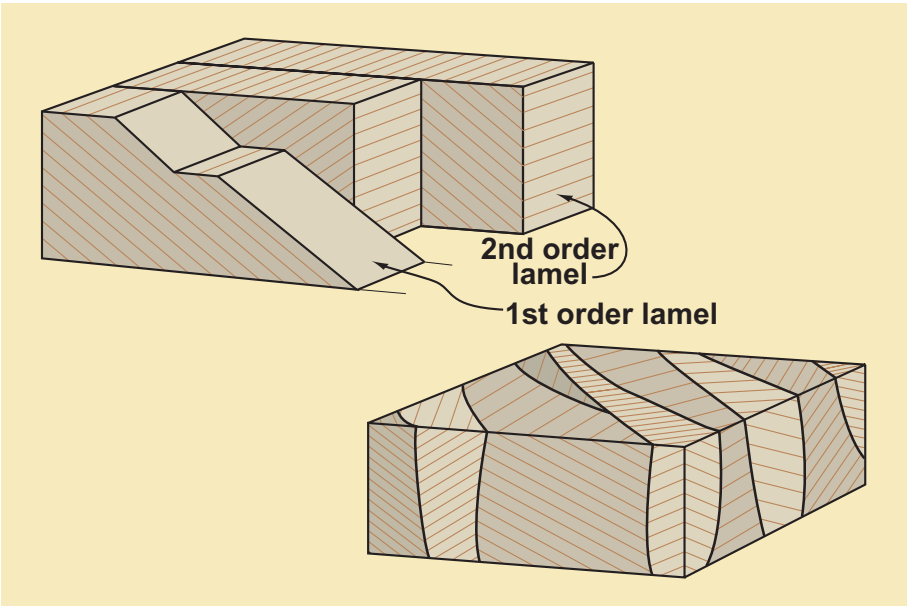

Diagrammatic views of crossed-lamellar shell structure

Crossed-lamellar structure is the dominant wall type in aragonitic gastropods (and is also common in bivalves). The first block shows an idealized model with parallel layering of crystals in individual lamellae and a plywood-like arrangement of adjacent lamellae with different crystal orientations, a fabric with remarkable strength. The second block presents a less idealized view with an interlocking fabric of somewhat lenticular domains of differentially oriented aragonite crystals. Redrawn from Bathurst (1975). It should be remembered that although this aragonitic fabric is common in modern gastropods, it is rarely observed (preserved) in pre-Pleistocene samples.

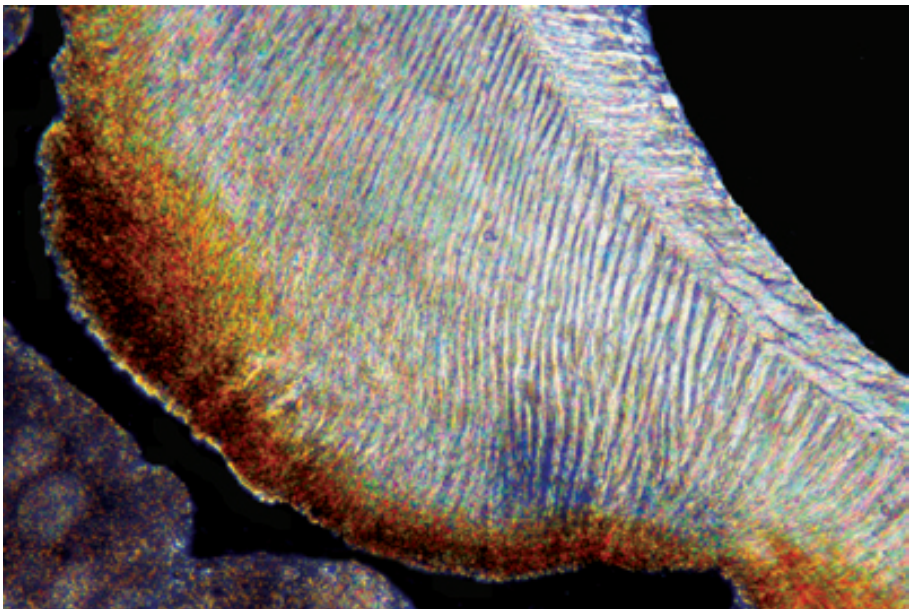

Recent sediment, Bimini, Bahamas

An example of crossed-lamellar wall structure in a gastropod fragment. Note the distinctive, "zebra striping" consisting of alternating light and dark extinction bands that wedge out laterally. Note the two distinct layers of crossed-lamellar fabric with differing orientations, further strengthening the shell wall. This fabric is most clearly visible under cross-polarized or partially cross-polarized lighting.

XPL, HA = 0.8 mm

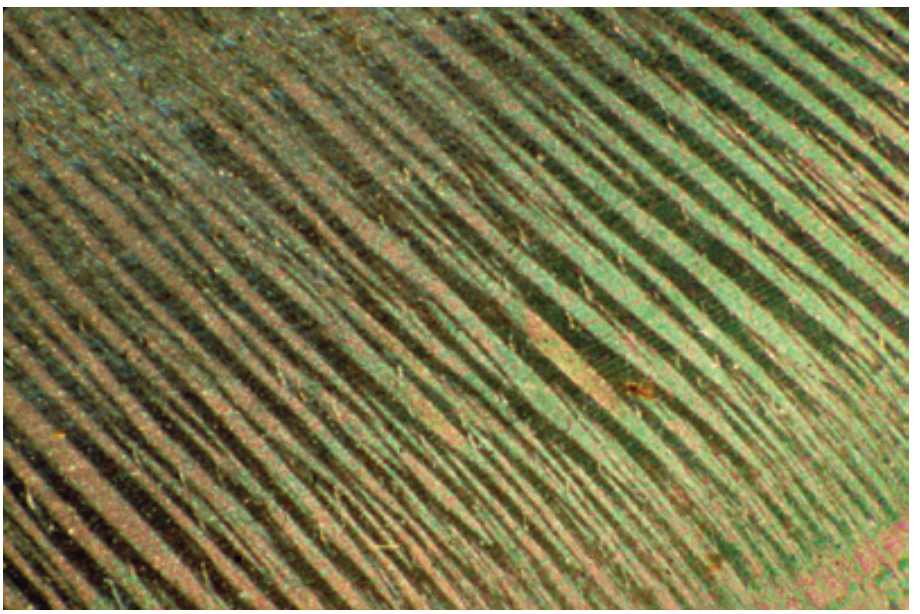

Recent sediment, Bimini, Bahamas

A detailed view of crossed-lamellar structure in a modern aragonitic gastropod (a conch shell, *Strombus* sp.). The alternating, slightly wedge-shaped, light and dark bands reflect the differing orientations of constituent aragonite crystals. This fabric, although quite distinctive, must be differentiated from coarsely fibrous or prismatic structures.

XPL, HA = 3.8 mm

Eocene Green River Fm., Laney Mbr., Sweetwater Co., Wyoming

Large numbers of a single species of gastropod from a lacustrine environment. These thin-walled organisms dominated the fauna in this restricted, freshwater setting. The excellent preservation of the wall material is relatively unusual because most modern lacustrine gastropods are aragonitic. The quality of preservation may indicate that these shells were originally calcitic or that the incorporated conchiolin microlayers (brownish organic material) and/or the low permeability of the surrounding sediments allowed exceptional retention of primary skeletal aragonite.

PPL, HA = 13.5 mm

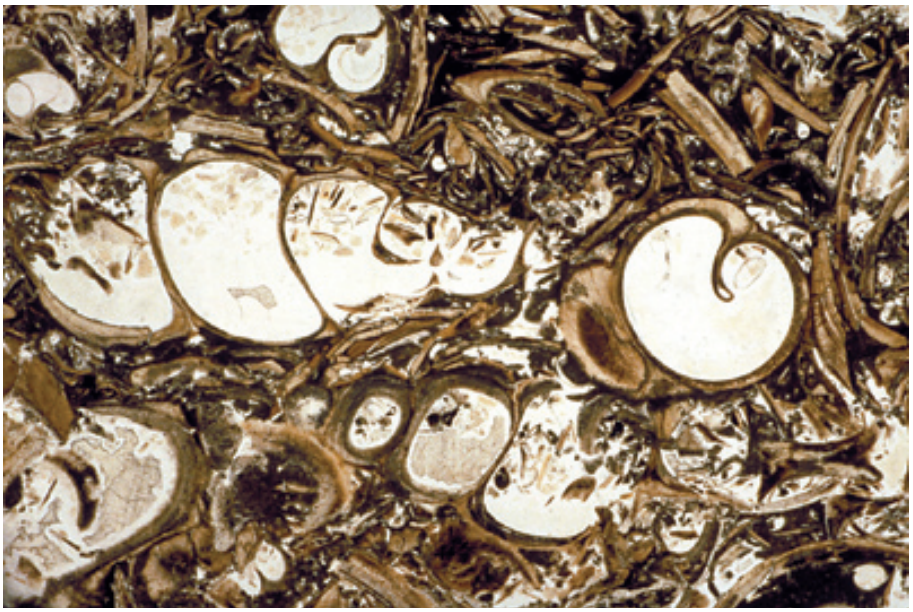

Mid. Jurassic (Bajocian) limestone, Central High Atlas region, Morocco

A fragmented, abraded, and neomorphosed gastropod shell that still is recognizable by shape (another specimen is visible in the lower right). Although some organic-rich internal layers are still visible, most of this originally aragonitic shell was dissolved and the mold was later filled with sparry calcite. This is the norm for most gastropod remains and in the absence of diagnostic shell shapes it would be impossible to differentiate from leached neomorphosed remains of other organisms (bivalves or phylloid algae, for example).

PPL, AFeS, HA = 5.0 mm

Lo. Cretaceous Cupido Fm., Coahuila, Mexico

A longitudinal section through an originally aragonitic gastropod. All wall structure was diagenetically obliterated, but the distinctive external and internal outlines were preserved, largely due to early diagenetic (probably synsedimentary) infilling of chambers with fibrous cement crusts and formation of an external micrite envelope.

PPL, HA = 2.25 mm

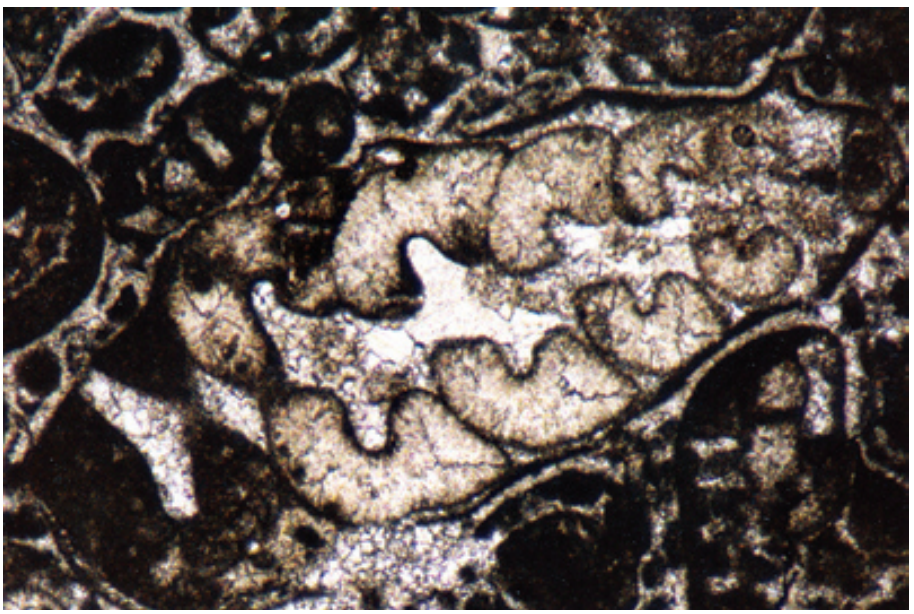

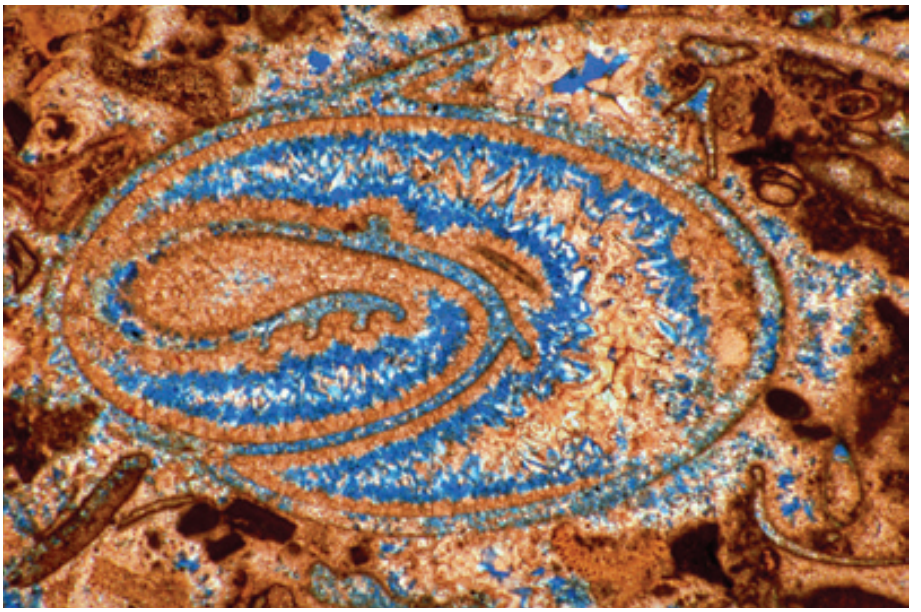

Up. Eocene limestone, Zakinthos, Ionian Islands, Greece

An example of an intermediate stage in the diagenesis of an aragonitic gastropod. Here the shell wall was entirely removed by dissolution, and the mold remains partially open pore space that is outlined by an early generation of cement. An intermediate generation of cement has also been dissolved, leaving a curious fabric of preserved early and late cements sandwiched by moldic porosity in the shell wall and in areas of intermediate-stage cement.

PPL, BSE, AFeS, HA = 4.5 mm

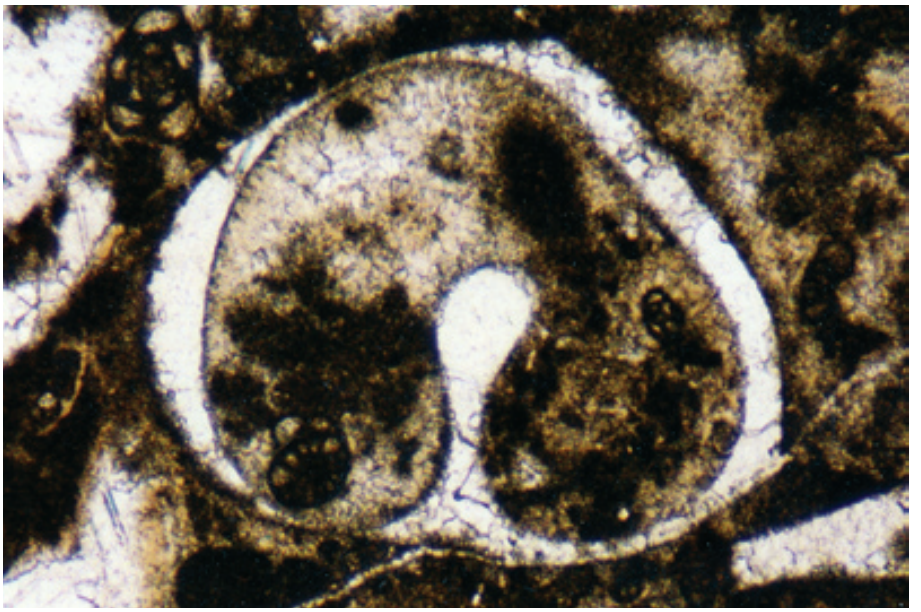

Lo. Cretaceous Cupido Fm., Coahuila, Mexico

A transverse section through a single, originally aragonitic, gastropod. All trace of original wall structure has been obliterated during inversion to calcite, but a recognizable outline (sometimes termed "baby-bottom structure") is preserved by internal and external sediment plus cement. Some selective areas of compactional deformation appear to have affected the shell outline during the void phase before calcite filling of the gastropod mold (upper left). Alternatively, parts of the shell may have been thinned by abrasion prior to deposition and diagenesis.

PPL, HA = 1.9 mm

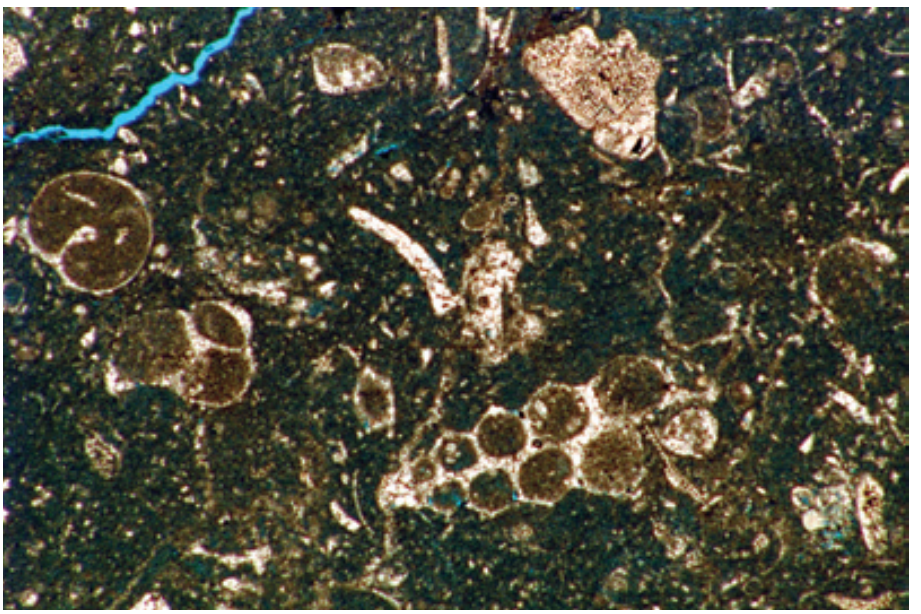

Lo. Cretaceous (Aptian) Shuaiba Fm., offshore Qatar

A molluscan packstone in which gastropods are a major sediment contributor. This shows some of the wide variety of geometrical shapes that can be generated by random cuts through complicated shell forms. It also shows the progressively greater difficulty of identifying small fragments of formerly aragonitic gastropod shells.

PPL, BSE, HA = 3.2 mm

Holocene sediment, Coral Sea, Pacific Ocean

Pteropods are an important group of nektic gastropods that are important contributors to oceanic sediments. This example shows a modern globigerinid-pteropod ooze (from >1000-m water depth) showing remains of both planktic foraminifers and pteropods. The multi-chambered organisms are the foraminifers; the larger, circular grains without chambers are pteropods, almost all cut in transverse section. The oriented aragonite crystals in the wall structure yield a pseudo-uniaxial cross in cross-polarized light.

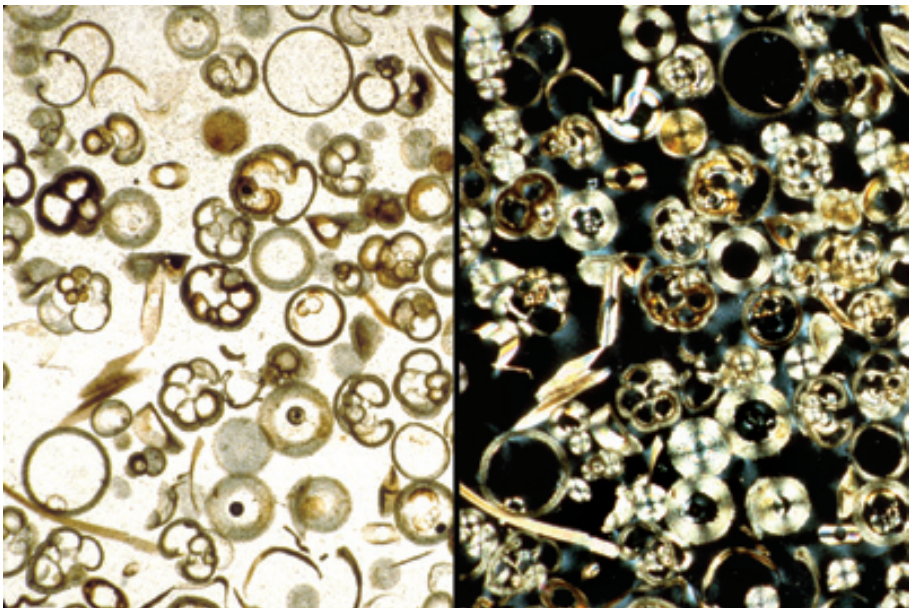

PPL/XPL, HA = 3.5 mm each

Up. Oligocene, North Atlantic Ocean

Pteropods are seen in transverse and longitudinal sections in this pteropod-globigerinid ooze. The longitudinal section shows the narrow V shape and very thin, aragonitic wall of this type of pteropod; the transverse section (upper left) shows a circular cross section with some cementation on the interior wall.

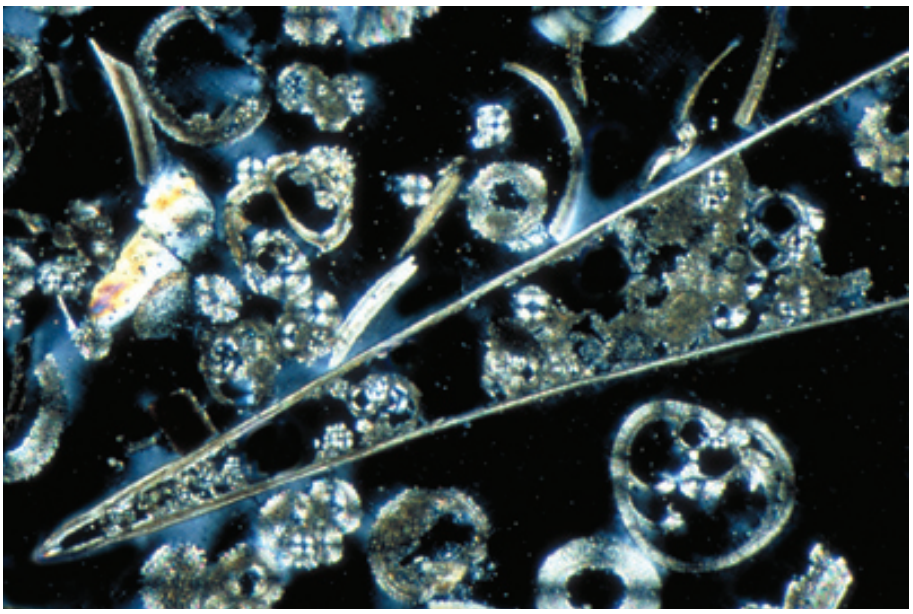

XPL, HA = 2.4 mm

Holocene sediment, Coral Sea, Pacific Ocean

A higher magnification view of a modern pteropod ooze (from >1000-m water depth). These transverse and oblique sections show the conical shape, homogeneous prismatic wall structure, and pseudo-uniaxial extinction bands of pteropod shell material.

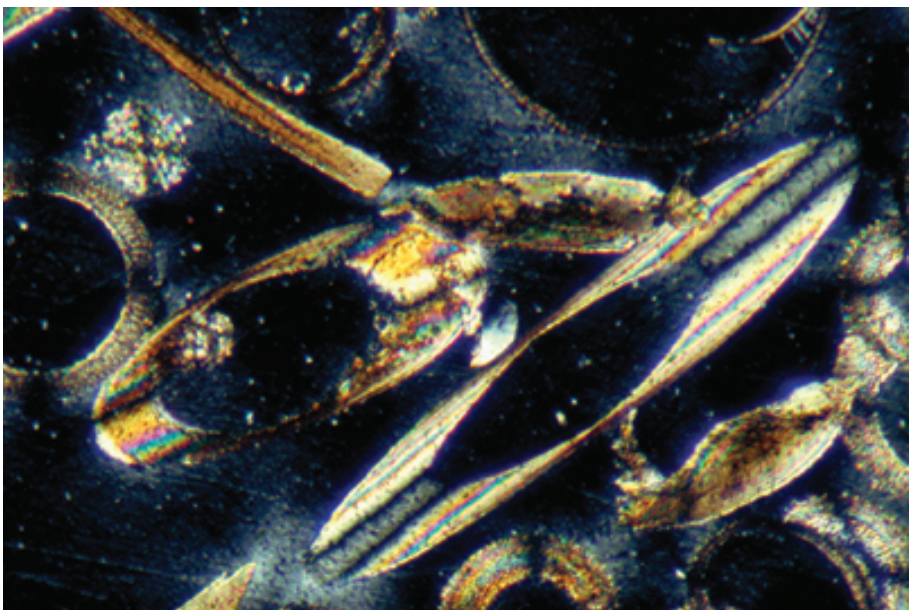

XPL, HA = 1.5 mm

BIVALVES (PELECYPODS)

Taxonomy and Age Range:

Phylum Mollusca; Subphylum Diasoma

Class Pelecypoda (sometimes classed as Bivalvia) — Early-Mid. Cambrian-Recent.

Pelecypods had significant faunal diversity from the Ordovician onward, although individual species can be abundant even in the Cambrian. Evolution of specialized groups (such as the rudistids, oysters and inoceramids) in the Mesozoic gave the group even greater significance during that time period; they remain one of the major sediment producing groups today.

Environmental Implications:

Most are bottom-dwelling infaunal burrowers or attached benthic epifauna. Many are deposit or suspension feeders; some can even bore into wood or rock substrates.

The vast majority inhabit shallow-marine settings, but representatives are found in almost all aqueous environments from fresh water (from the Middle Devonian onward), through brackish and hypersaline coastal regions, to deep-water areas. Some bivalves (especially the now-extinct rudistids) even were important bioherm and reef builders.

There is a general correlation between greater shell thickness and higher environmental energy levels.

Skeletal Mineralogy:

Bivalve skeletons vary in composition at family and lower levels. Most are purely aragonite; some have interlayered calcite and aragonite; a few are completely calcitic. The calcite has less than 1 mole% Mg.

Morphologic Features:

Bivalves have paired, generally identical (bilaterally symmetrical), calcareous shells joined at a hinge by soft muscle tissue. Some groups, especially the rudistids, had aberrant shells with one massive valve shaped like horn coral and the other shaped like a cover plate on the top of the horn.

Shell exteriors are generally smooth to slightly ribbed; some have heavier ornamentation.

Adult bivalves range in length from less than 1 mm to nearly 2 m (in the case of some inoceramids). The largest known living clam (*Tridacna*) reaches 90 cm in length and weighs more than 180 kg. Most commonly, however, bivalves are between 1 and 10 cm in length.

Keys to Petrographic Recognition:

1. **The remains of robust bivalves are typically in the mm to cm size range — larger than most ostracodes which have somewhat similarly shaped (but overlapping) valves.**
2. **Gently curved, smooth to somewhat ornamented shell fragments predominate; one end may have a thickened hinge area. Some bivalves, especially the rudistids had more complex cup- or horn-shaped shells.**
3. **Most bivalves have/had aragonitic shells that typically lose their internal microstructure during meteoric or burial diagenesis; originally calcitic shells retain their primary fabrics; mixed-mineralogy shells show selective preservation of originally calcitic layers.**
4. **The most fundamental structure of bivalve walls consists of an inner lamellar layer and an outer prismatic layer, but the group shows enormous variability of wall structure. The most common aragonitic microstructures are nacreous and crossed-lamellar; the calcitic oysters have foliated microstructure, but prismatic, complex-crossed-lamellar, and homogeneous fabrics also occur. Vesicular prismatic fabrics are common in some of the thicker-walled groups (oysters and rudistids, for example). Shells with mixed mineralogy, and thus mixed fabric, are common. Most modern work on molluscan shell structure relies on SEM examination and it is difficult to find direct correspondence between SEM-determined structures and the traditional petrographic classifications of shell structures (summarized in Majewske, 1969, and Bathurst, 1975).**
5. **Shells may show tidal, diurnal or other periodic growth lines (not found in ostracodes); others may show perforations similar to brachiopod punctae.**
6. **Bivalves lack the internal structural features of some brachiopods (e.g., spiralia, dental lamellae, a pedicle opening) or the grain-margin cellular structures found in well preserved phylloid algae.**

Morphology and wall structure of a typical bivalve

Diagrammatic view of the morphology and wall structure of a typical bivalve, based on the freshwater clam, *Anodonta* sp. Adapted from Moore et al. (1952) and other sources. Note how the shell symmetry differs from that of the brachiopods shown earlier (useful when examining sections that include articulate shell pairs). The multilayered nacreous and prismatic wall fabrics illustrate the complex and varied structures found in bivalve shells.

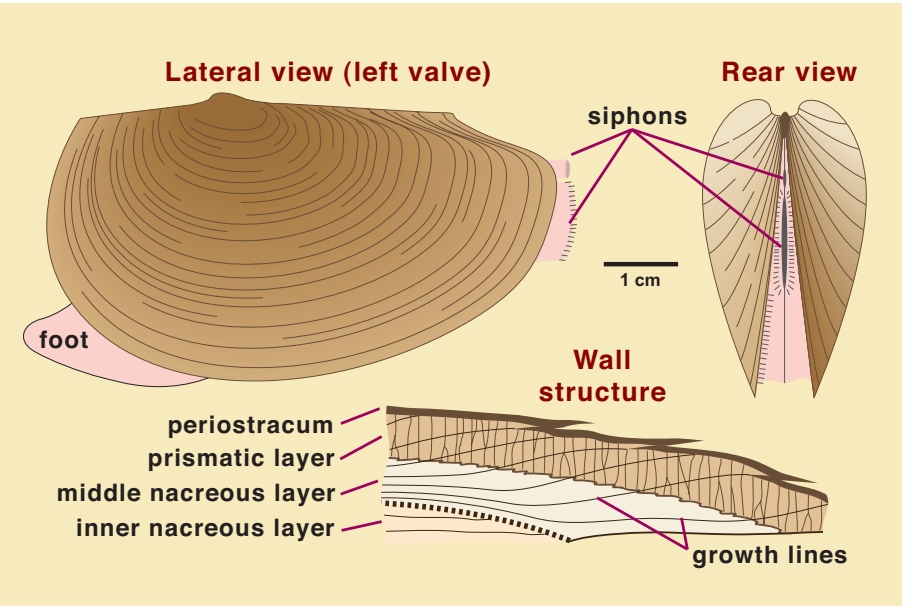

Variations in bivalve shell structure and preservation

A diagrammatic representation of some of the different bivalve shell compositions and structures, and some of the possible patterns of fabric preservation or loss during diagenesis. Modified from Tucker (1981). In general, primary calcitic layers remain well preserved throughout the history of the grain; aragonitic layers are well preserved only in modern or relatively young deposits or in special situations in which diagenetic alteration is inhibited. Under normal circumstances, aragonite is dissolved and the resulting voids may be filled with sparry calcite.

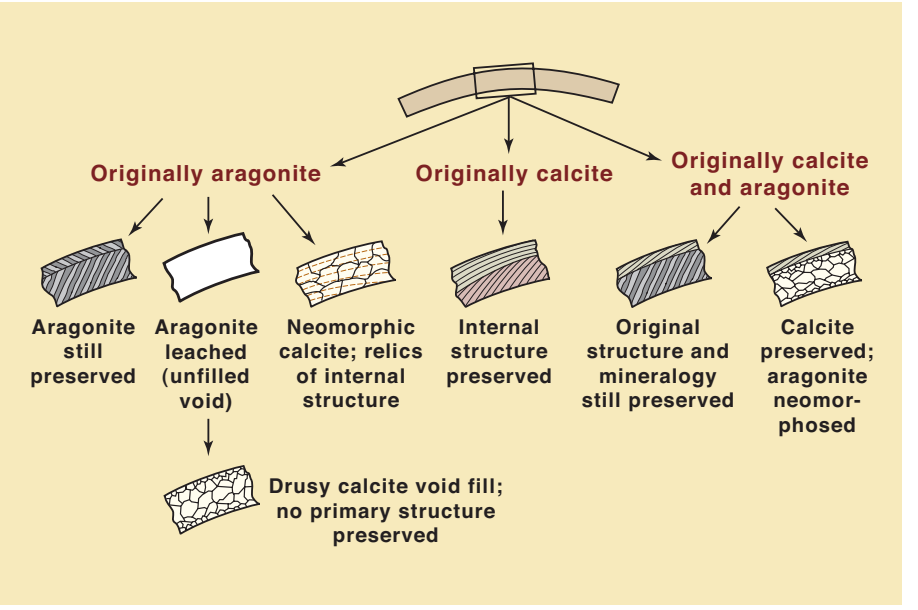

Holocene beachrock, Grand Cayman, Cayman Islands, B.W.I.

Aragonitic crossed-lamellar structure in a molluscan (possibly a bivalve) fragment. This is a very common fabric in both bivalves and gastropods and in small, gently curved fragments, such as this one, it can be very difficult to distinguish between those two groups. Because aragonitic crossed-lamellar fabric is almost certain to be obliterated during diagenesis, it becomes even harder to determine the exact origin of such grains in older strata.

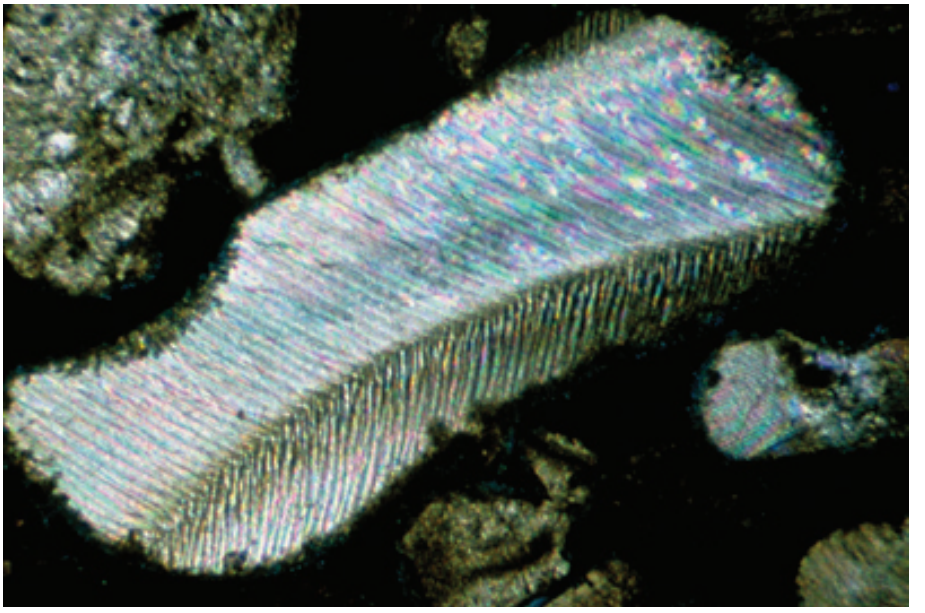

XPL, HA = 2.4 mm

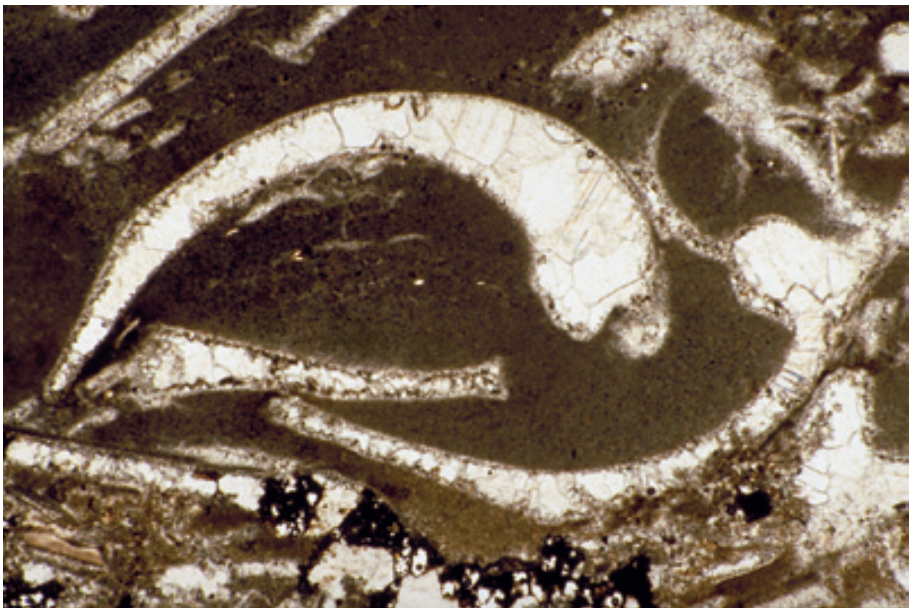

Mid. Triassic Muschelkalk, Western Silesia, Poland

This is an example of the normal appearance of formerly aragonitic bivalve shells after diagenetic alteration. The bivalve shells were dissolved and the molds were later filled with sparry calcite. The bivalve origins remain clear, however, based on shell shapes — smoothly curved and thickening toward the still discernible hinge structures. Less complete fragments would provide greater identification problems.

PPL, HA = 7.0 mm

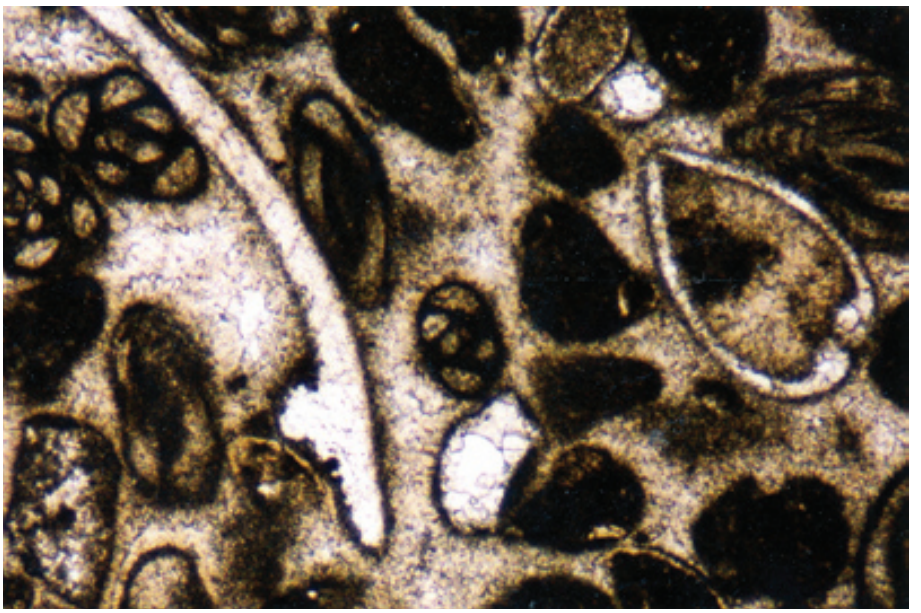

Lo. Cretaceous Cupido Fm., Coahuila, Mexico

Two additional examples of bivalves showing neomorphic alteration (inversion) of their originally aragonitic shells. The alteration here, as in the example above, involved dissolution of aragonite and reprecipitation of more stable calcite spar. This obliterated all relict internal shell structure, so grains are identifiable only on the basis of characteristic shapes (symmetrical shells with distinctive hinge structures) outlined by micrite envelopes. The numerous miliolid foraminifers also present have better-preserved wall structure than the mollusks because of their originally high-Mg calcite test composition.

PPL, HA = 2.0 mm

Mid. Triassic Muschelkalk, Western Silesia, Poland

These incomplete fragments of probable bivalve shells underwent complete dissolution, a likely indication of an originally aragonitic structure. The molds of the leached fossil were filled with non-ferroan and moderately ferroan calcite cements. Shape is the only remaining criterion for identification of these grains, but other organisms (phylloid algae, for example), may have similar shapes. In this Triassic example, however, phylloid algae are not a reasonable possibility. Thus, bivalve fragments are the most likely grains with this shape and originally aragonitic compositions.

PPL, AFeS, HA = 5.5 mm

Up. Triassic (Carnian) Halstatt Ls., Bavaria, Germany

Numerous thin shells of the pectinoid dysodont pelecypod, *Halobia* sp. This may have been a motile bivalve or one that used its thin, broad shells to "float" on soft sediments. The smooth to slightly plicate shells have virtually no preserved wall structure and are recognizable mainly on the basis of shape and shell thickness.

PPL, HA = 12.5 mm

Cretaceous (Albian-Cenomanian) El Abra Ls., San Luis Potosi, Mexico

A shell of *Toucasia* sp. (a thin-shelled rudistid bivalve) showing differential fabric preservation in a two-layer wall structure. The outer layer was originally calcitic; the inner layer aragonitic. Note organic remnants in the calcitic layer and absence of remnants in the neomorphosed formerly aragonitic layer, the edge of which is marked by contact with micrite and miliolid grains.

PPL, HA = 8.0 mm

Cretaceous (Albian-Cenomanian) El Abra Ls., San Luis Potosi, Mexico

An enlarged view of the *Toucasia* sp. rudistid wall shown in the previous photograph. Note the brownish color reflecting organic remnants and growth banding in the calcitic layer.

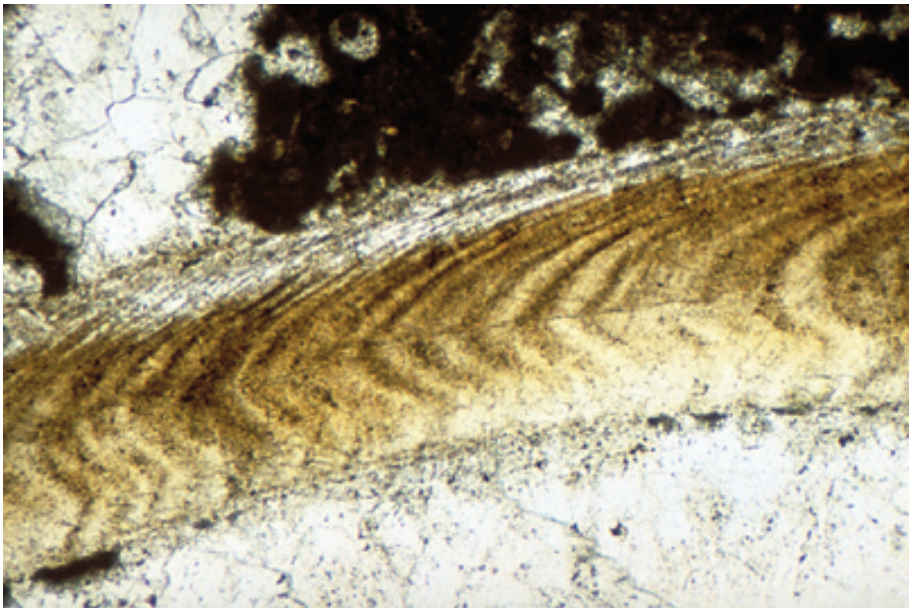

PPL, HA = 2.4 mm

Up. Oligocene (Chattian) Molasse, Bavaria, Germany

Part of a large *Cyrenia* shell easily recognizable as a bivalve by its shell shape. This genus has a homogeneous (sometimes termed homogeneous prismatic) calcite wall structure. Because the minute crystals are oriented with their c-axes perpendicular to the shell margin, extinction bands (also oriented perpendicular to outer shell wall) sweep through the length of the shell as stage is rotated. This wall structure is also found in trilobites, ostracodes, and some foraminifers so these groups must be distinguished on other criteria, generally shell or test morphology.

XPL, HA = 7.0 mm

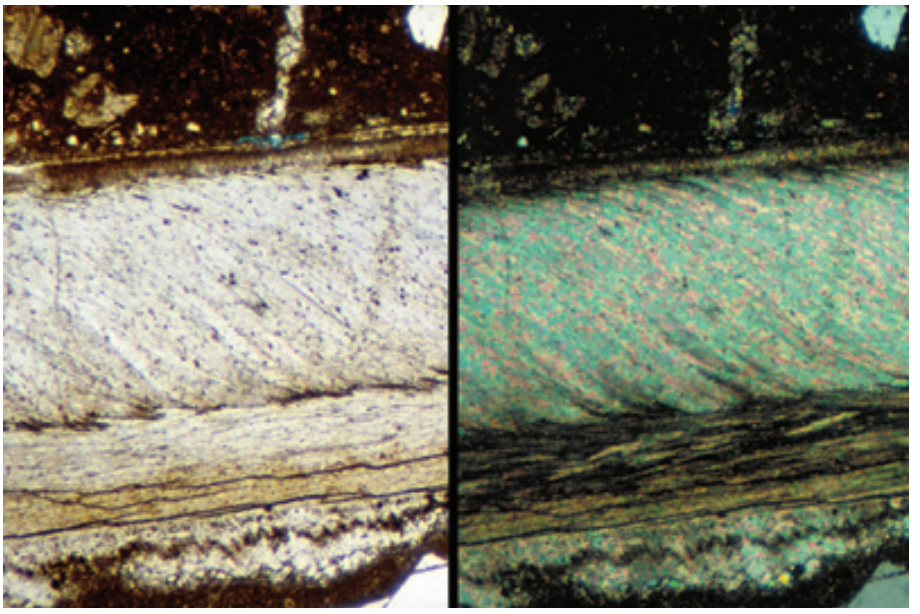

Oligocene Nile Gp., Westland, New Zealand

A multi-layered bivalve shell showing at least two types of foliated wall structure. Multiple layers with different foliation orientations, as seen here, add considerably to the structural strength of bivalve shells. The foliated structure depicted here is calcitic; essentially the same structure in aragonitic layers is termed "nacreous" fabric. Foliated structure is found in mollusks, brachiopods, some bryozoans, and some worm tubes.

PPL/XPL, HA = 1.0 mm each

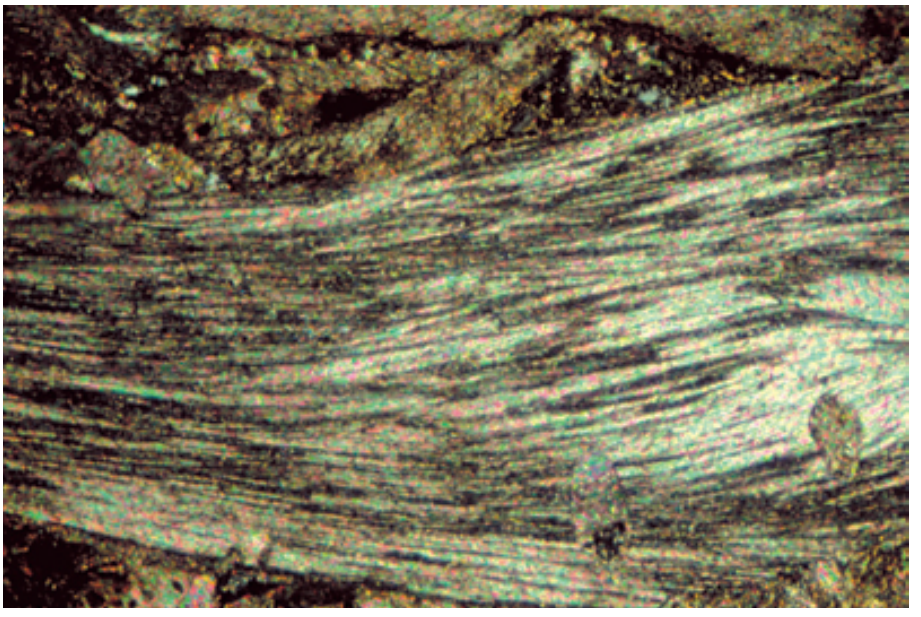

Lo. Cretaceous Paw Paw Fm., Quarry Ls., Grayson Co., Texas

This section provides a more detailed view of foliated structure in a probable *Gryphaea* shell. The stacked bundles of calcite crystals with differing orientations are clearly visible in this example. The ovoid disturbances in the wall structure are borings.

XPL, HA = 1.6 mm

Lo. Cretaceous (Albian) Glen Rose Ls., Somervell Co., Texas

A view of more irregular foliated structure in a *Gryphaea* shell. Foliated structure consists of more or less "randomly oriented bundles of calcite lamellae producing an effect similar to cross-bedding" (Majewske, 1969, Plate 7). It is particularly common in oysters and oyster-like (ostreid) groups, which include *Gryphaea*, *Exogyra*, *Ostrea* and other genera.

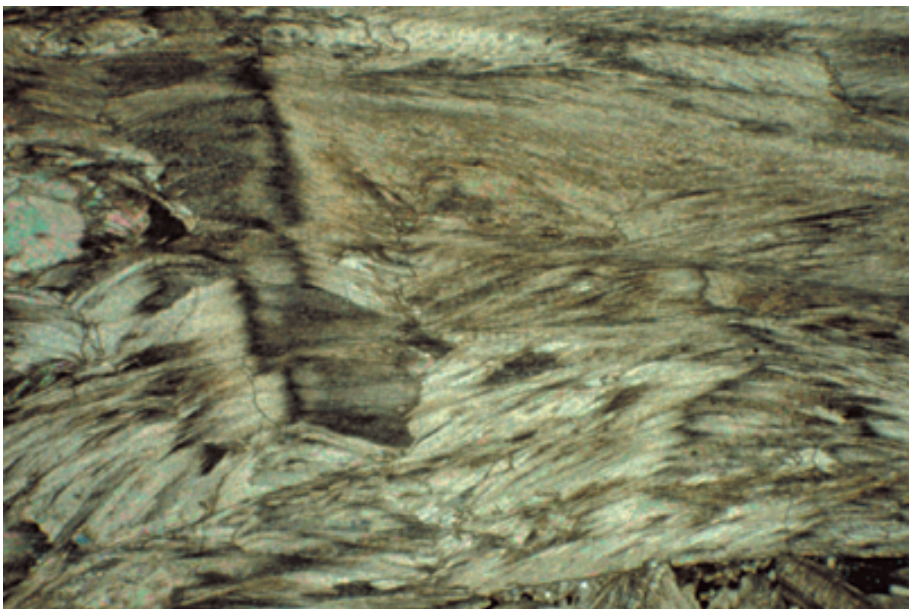

XPL, HA = 2.4 mm

Up. Cretaceous Selma Chalk, Alabama

An example of multilayered structure in an ostreid (oyster-like) shell. Although it appears varied, all the fabric shown here is actually foliated structure. Standard foliations pass laterally into areas where the foliations diverge and rejoin, thus surrounding open spaces now filled with diagenetic sparry calcite. This structure is termed "vesicular" and it reflects the same principle as corrugated cardboard — great strength with minimal use of materials. It allows the organism to build a thick shell (thus enabling it to resist boring organisms) without having to secrete massive quantities of calcite.

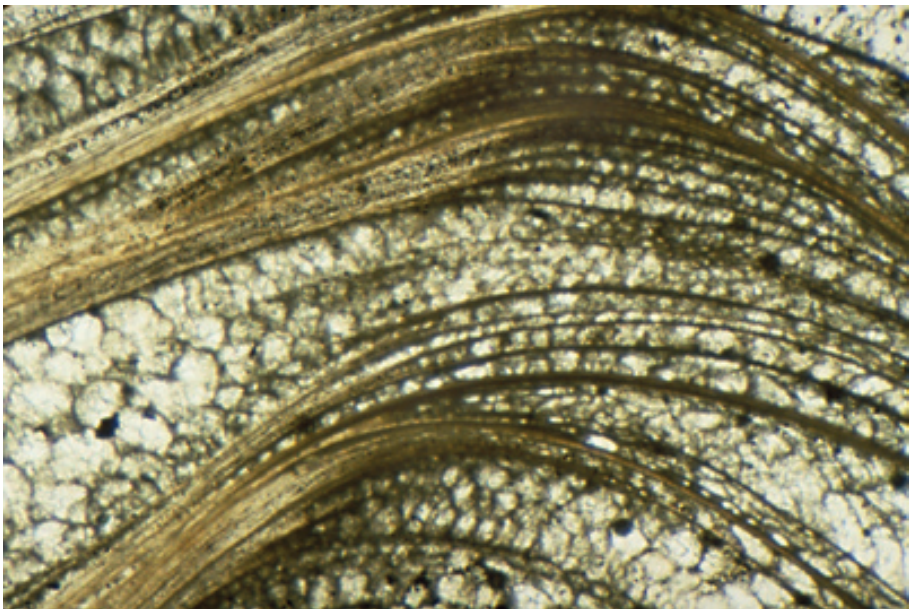

PPL, HA = 2.4 mm

Plio-Pleistocene Caloosahatchee Fm., Hendry Co., Florida

A fragment of an oyster shell cut by large sponge(?) borings. The borings (dark patches) are filled with carbonate mud (micrite). The shell is complexly multilayered, with alternating layers of near-horizontally foliated (or nacreous) and normal prismatic fabrics.

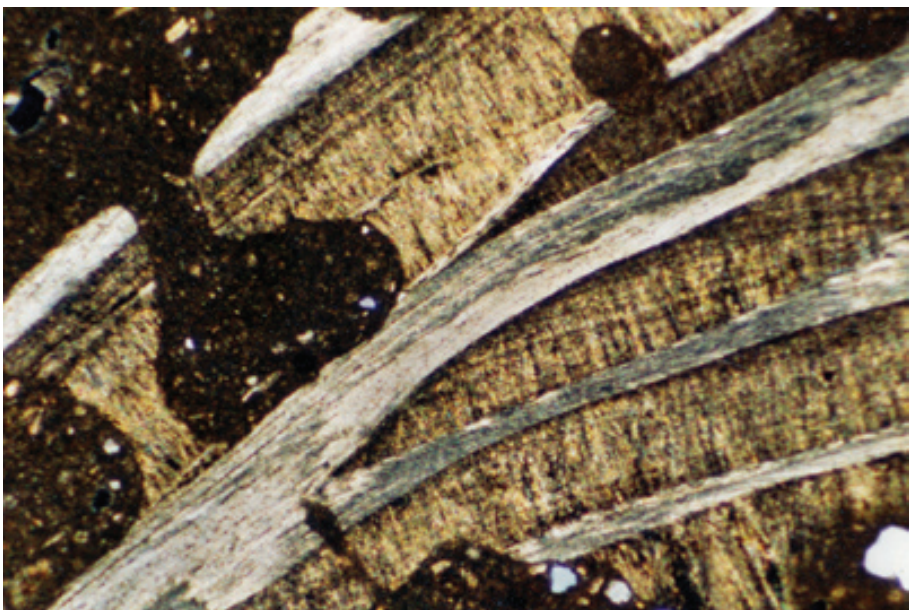

XPL, HA = 3.3 mm

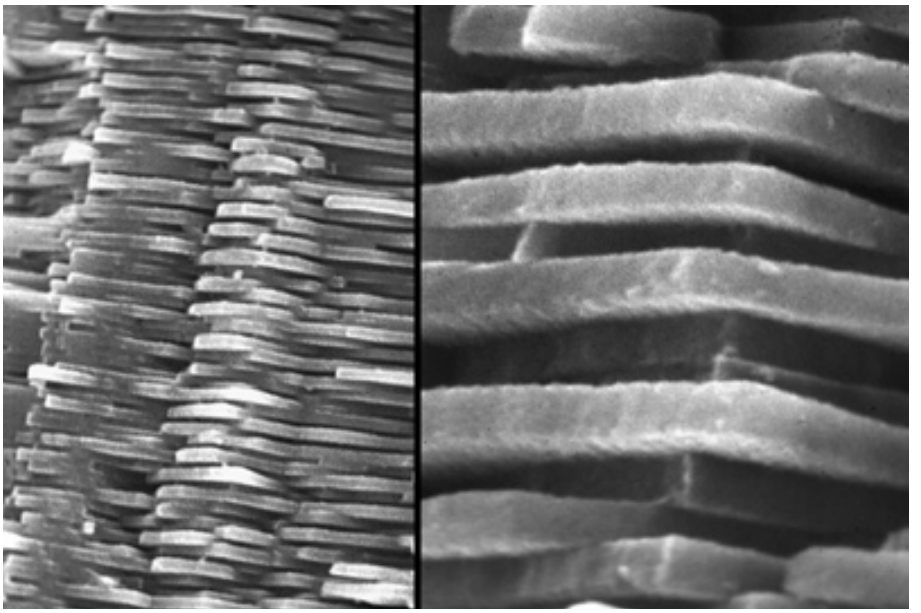

Recent shell material, Belize

Two SEM images showing the structure of the nacreous layer of a bivalve shell at different magnifications. Nacre represents the pearly material found in some mollusks (pearl "oyster" shells and pearls, pearly nautiloids, and a variety of aragonitic bivalves including *Nucula*, *Nuculana*, *Pinctada*, and *Pteria*). As can be seen here, nacre consists of stacked, overlapping, vertical columns of tabular aragonite crystals that are separated by extremely thin sheaths of organic material. Although this structure is lost during diagenesis, it is useful in identification of modern shell fragments.

SEM, L: HA = 22 μm; R: HA = 5.8 μm

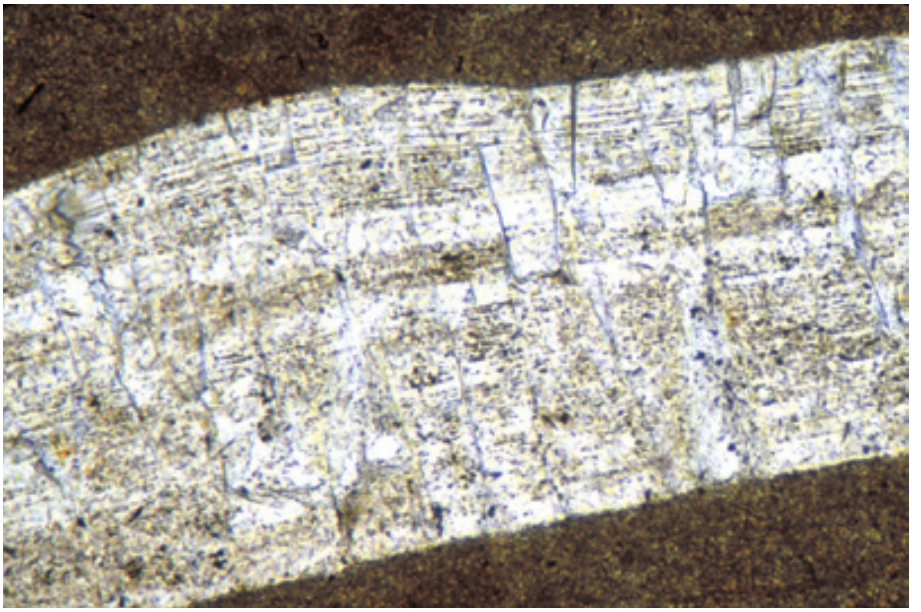

Mid. Triassic Muschelkalk limestone, Malogoszcz, Poland

A plane-polarized light view of a bivalve shell with coarsely prismatic structure. Margin-parallel lines of inclusions mark original layering within the shell; more subtle margin-normal inclusion traces mark the edges of the individual prisms.

PPL, HA = 0.6 mm

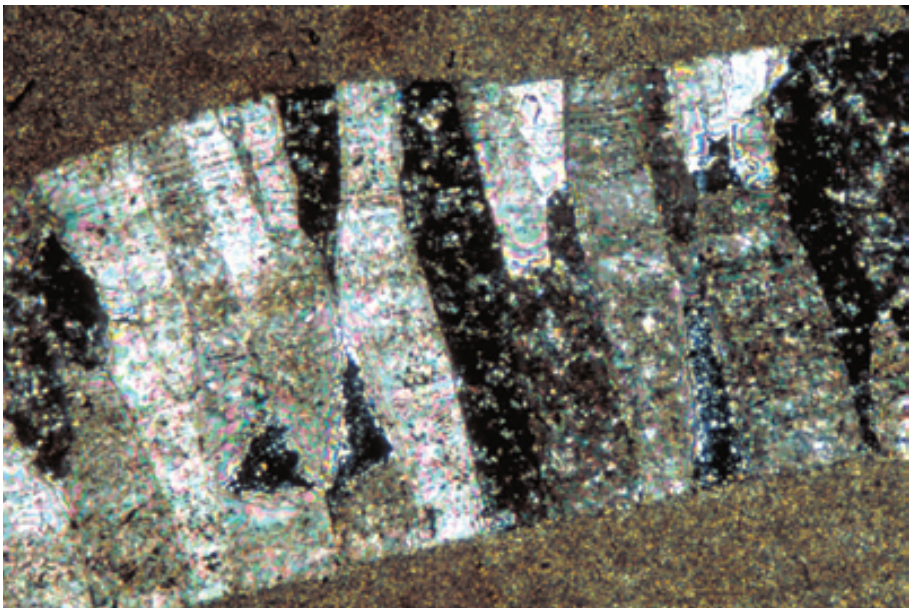

Mid. Triassic Muschelkalk limestone, Malogoszcz, Poland

A view of the same area as in the previous photograph, but under cross-polarized illumination. The coarse prisms that compose the shell wall can be seen to extend from one shell margin to the other (probably indicating complete diagenetic removal of a secondary, presumably aragonitic, shell layer). The coarseness and inclusion-rich nature of the prisms may indicate that they too have undergone some diagenetic modification.

XPL, HA = 0.6 mm

Up. Cretaceous San Carlos Fm., Presidio Co., Texas

This *Inoceramus* shell has a distinctive, unrecrystallized, originally calcitic, prismatic wall structure, here cut by a number of borings along the shell margin. Inoceramids are restricted to Cretaceous strata, but comprise a biostratigraphically important group, especially in shelf chalks. They had a mixed-mineralogy shell with a thin, nacreous, aragonitic layer and a thick, prismatic calcite layer. The aragonitic layer is rarely preserved and may have been lost, in many cases, prior to burial. Thus, inoceramid shells commonly broke up into individual prisms that may constitute an important fraction of some deposits.

XPL, HA = 3.4 mm

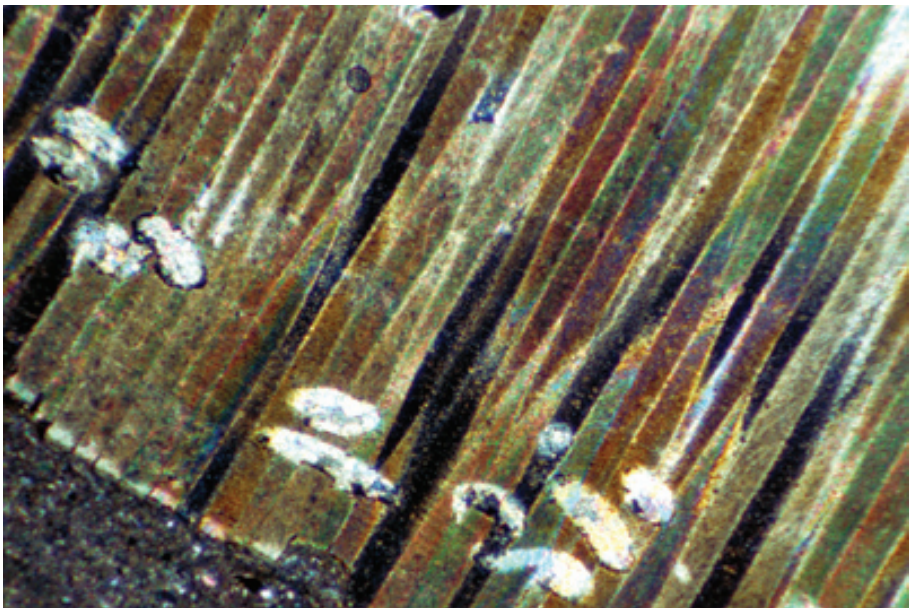

Cretaceous block in Tertiary allochthon, Toa Toa, Northland, New Zealand

This is a sediment composed essentially entirely of individual calcite prisms from disaggregated inoceramid shells. The prisms have a distinctive polygonal (generally hexagonal) outline in transverse section and a tapering or blunt wedge shape in longitudinal section. Although it is rare to find a deposit so packed with prisms, isolated inoceramid prisms are common constituents in many Cretaceous shelf chalks.

XPL, HA = 3.2 mm

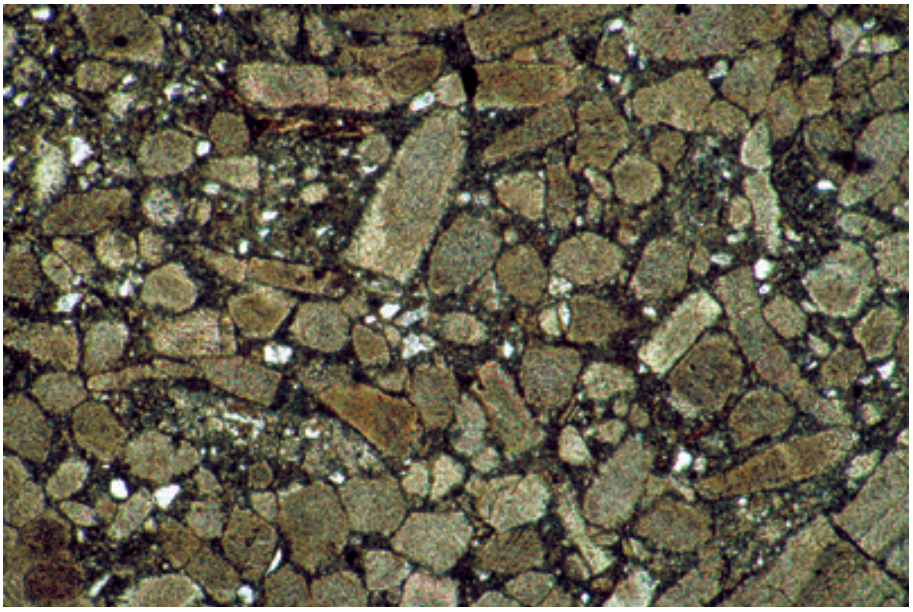

Eocene Barton Beds, Barton, England, U.K.

A portion of the shell of a pachydont bivalve *Chama squamosa*, with a punctate shell wall (the pores are visible as small white circles). Punctate structure is rare in bivalves, but it is common in brachiopods; punctate shells of the two groups can be differentiated on other characteristics — for example, the well developed growth lines seen in this bivalve that would not be seen in a brachiopod.

PPL, HA = 4.0 mm

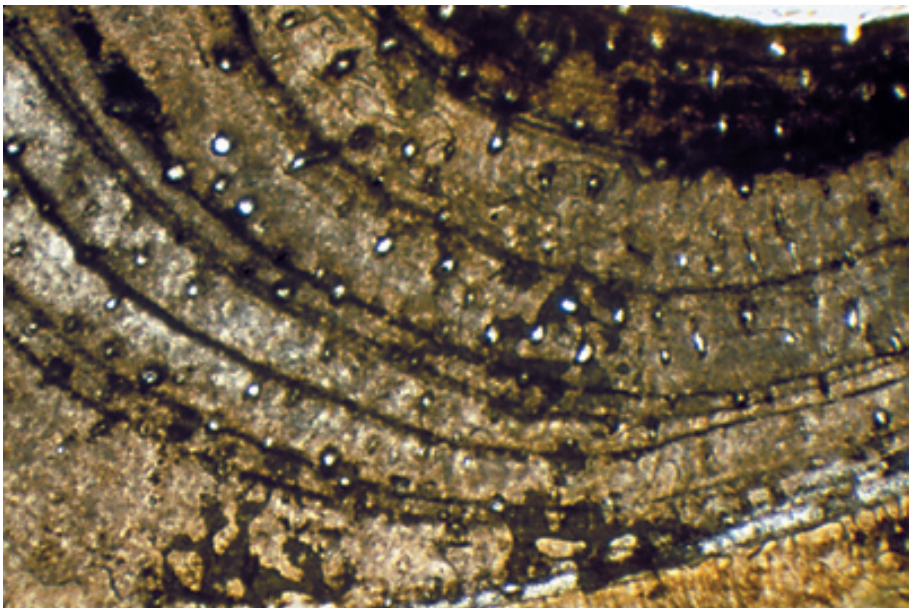

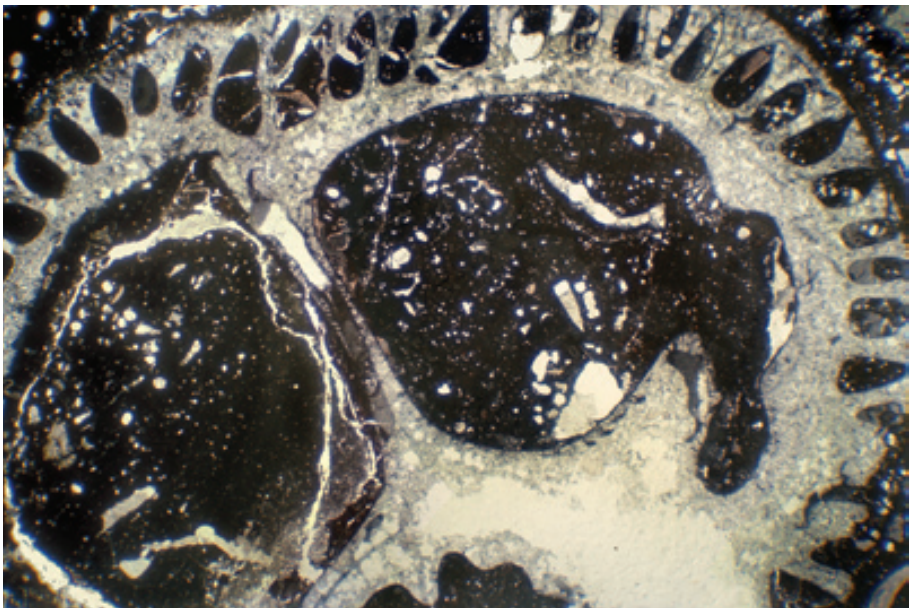

Lo. Cretaceous Rodessa Fm., subsurface, Duke Field, Houston Co., Texas

Arguably the most aberrant of all bivalves are the pachydont rudistids. This image shows a transverse cut through an intact, thick walled, horn shaped, lower valve of *Planocaprina* sp., a caprinid rudistid — large canals, characteristic of caprinids, run through the walls. Rudistids were a short-lived group (Cretaceous with Late Jurassic precursors), found primarily in warm-water areas (0-35° lat.). Their large size (some are greater than 30 cm long) and robust walls enabled them to act as major bioherm formers and sediment producers. Photograph courtesy of Robert W. Scott.

PPL, HA = 13 mm

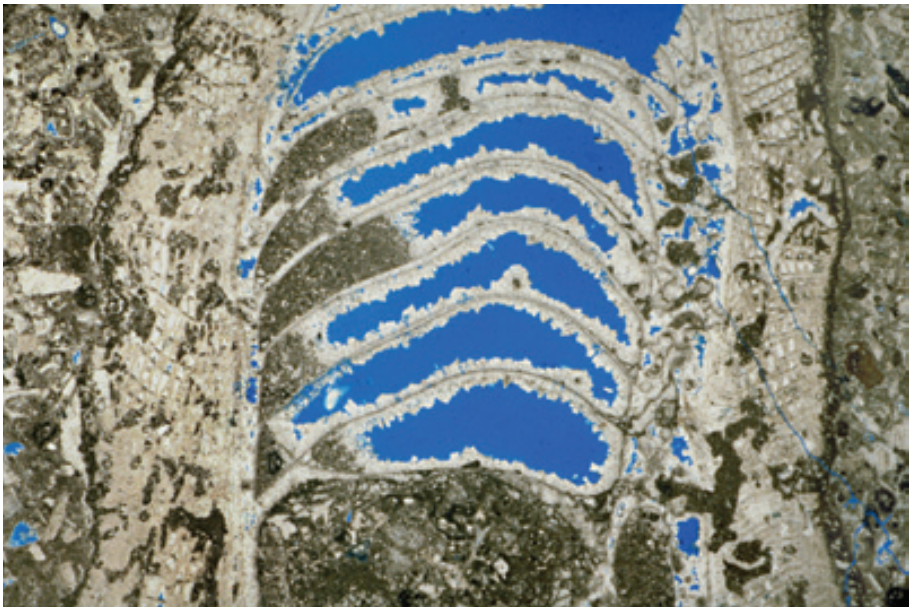

Up. Cretaceous limestone, Zakinthos, Ionian Islands, Greece

A longitudinal section of a large rudistid shell showing internal partitioning within the horn- or tube-shaped main valve and vesicular fabric in the walls. Rudistids did not encrust or actively cement to each other and so were not true reef builders. Some stood upright in packed clusters, whereas others lived recumbent on the seafloor. Isolated rudistids probably were frequently reoriented by wave action, and rudistid bioherms in high energy shelf margins were stabilized primarily through encrustation by corals, algae and other organisms, as well as through syndepositional marine cementation.

PPL, BSE, HA = 13.5 mm

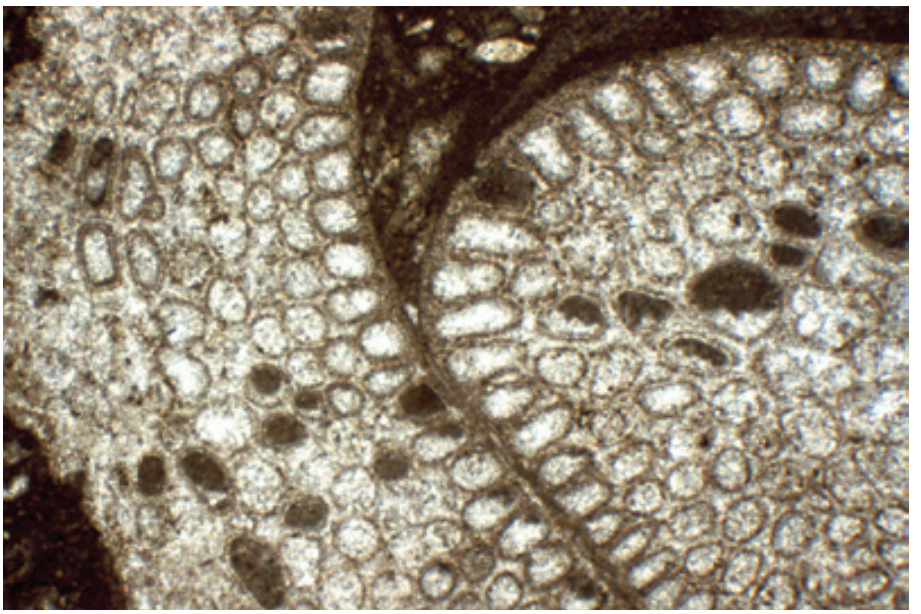

Cretaceous (Albian-Cenomanian) Tamabra Ls., San Luis Potosi, Mexico

Most rudistid walls had exterior ribbing and highly vesicular walls to strengthen their shells. This example, probably from a radiolitid rudistid, shows relatively poor structural preservation typical of aragonitic composition.

PPL, HA = 5.1 mm

Up. Cretaceous (Turonian?) limestone, Cephalonia, Ionian Islands, Greece

A longitudinal section through the wall of fragmented rudistid shell showing the elongate morphology of the main valve, the corrugated construction (vesicular structure), and traces of external ribbing. Even in smaller fragments, these features remain recognizable and allow the identification of rudistid debris.

PPL, AFeS, BSE, HA = 9.0 mm

Up. Cretaceous limestone, Cephalonia, Ionian Islands, Greece

An example of extremely vesicular structure in a fragment of a rudistid wall. Note compactional crushing of parts of the wall. Such lightly mineralized rudistids are more prevalent in protected shelf interior or back-reef settings.

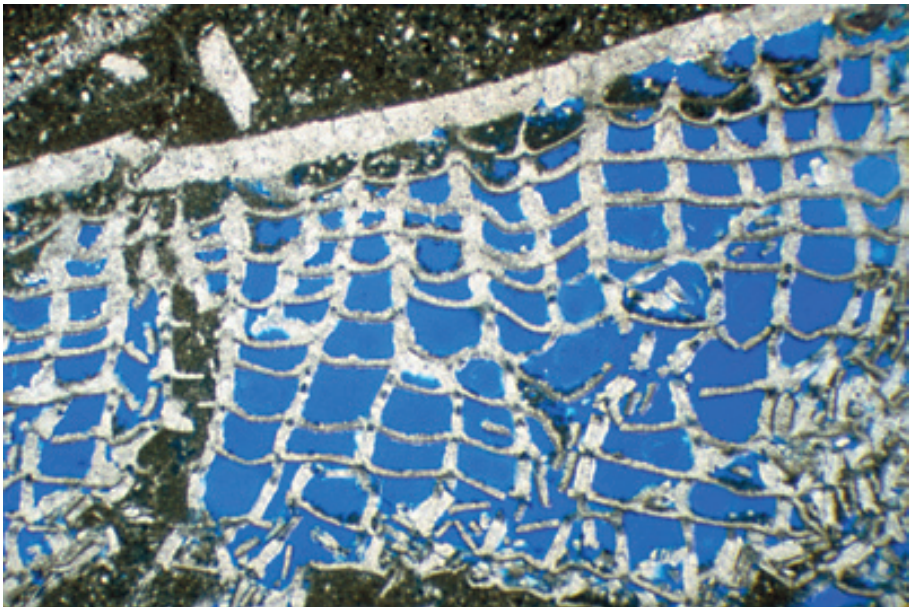

PPL, BSE, HA = 5.1 mm

Up. Cretaceous top Edwards Fm., Bell Co., Texas

A limestone composed of rounded rudistid fragments. Rudistid debris is very common in Cretaceous limestones. The vesicular structure, lack of adhesion between adjacent organisms, and growth in high-energy settings led to extensive fragmentation and reworking of rudistid shells. Although identification of each grain may be difficult, recognition of vesicular and canal-bearing fragments, as in this example, makes it likely many other grains are also of rudistid origin.

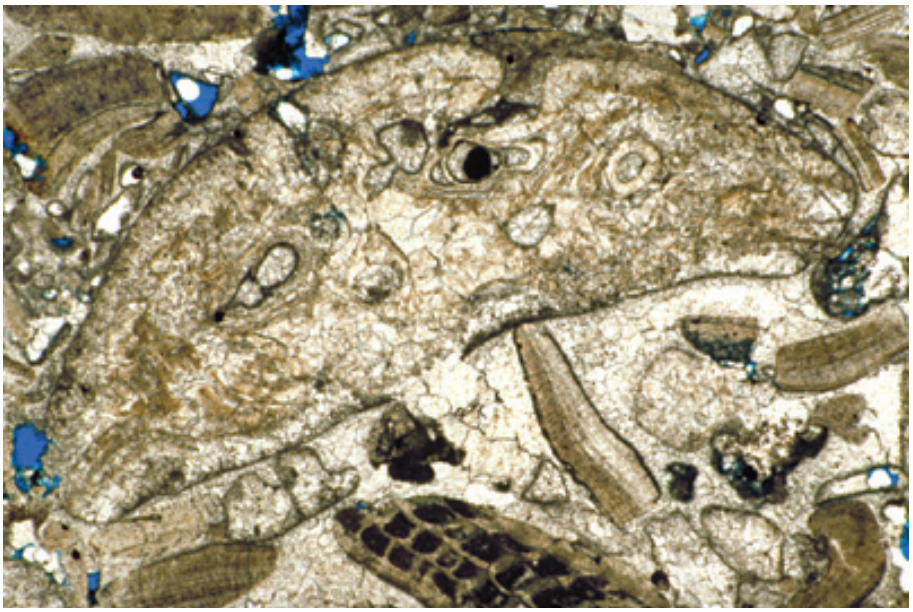

PPL, BSE, HA = 8.0 mm

CEPHALOPODS

Taxonomy and Age Range:

Phylum Mollusca, Subphylum Cyrtosoma

Class Cephalopoda — Late Cambrian-Recent

Commonly divided into six subclasses of which only three are listed here:

Subclass Nautiloidea — Late Cambrian-Holocene (modern representatives reduced to a single genus)

Subclass Ammonoidea — Early Devonian-Late Cretaceous

Subclass Coleoidea — Early Devonian-Holocene (includes the order Belemnitida — Late Mississippian-Late Cretaceous)

Encompasses several important calcified groups including nautiloids, ammonites, goniatites, baculites, and belemnites as well as uncalcified organisms such as squid and octopi.

Cephalopods only rarely are significant sediment formers in Paleozoic and Mesozoic strata, but they are among the most important stratigraphic index macrofossils in many rocks.

Environmental Implications:

Cephalopods are a diverse group of highly developed mollusks. Most were nektic creatures with moderate to high mobility; some were benthic, but still mobile, organisms. All modern and ancient forms are interpreted as fully marine. Although cephalopods are found washed into marginal marine settings, they are most common in open shelf and deeper-water deposits. Their remarkable buoyancy controls, propulsion mechanisms, intelligence, and eyesight enabled the cephalopods to be formidable predators throughout their history.

Skeletal Mineralogy:

Modern nautilus shells (and probably most fossil ammonoids and nautiloids) are/were entirely aragonitic. Some thin layers or parts were composed of organic material (conchiolin) or calcium phosphate; cameral deposits precipitated in life also were aragonitic, sometimes with alternating layers of clear and organic-rich carbonate. Most cephalopod aptichi, on the other hand, were low-Mg calcite. Belemnite rostra also were entirely low-Mg calcite with some organic interlayers, although Triassic coleoid rostra probably were aragonitic.

Morphologic Features:

The calcified cephalopods have an external, typically conical, chambered skeleton that may be straight, tightly planispirally coiled, or partially coiled. Chambers are walled by septa that may be straight and smooth or highly convolute and attached to the shell wall by ornate sutures of varying complexity. Some groups also have an aptichus (or an anaptichus), used to close the external opening of the shell (comparable to the operculum of a gastropod).

Many nautiloids and ammonoids have a siphuncle (a tube that runs through each of the internal chambers). Nautiloids also commonly have calcium carbonate cameral deposits lining, or completely filling, posterior chambers and parts of their siphuncle (for buoyancy control).

Whole cephalopods are typically centimeter- to decimeter-sized; some can be more than 2 m in length. Most are thus larger than a thin section; most recognizable fragments are in the mm to cm size range.

Belemnites had solid internal rostra that are conical in shape, straight, and hollow at the larger end.

Keys to Petrographic Recognition:

1. **Cephalopod shells can be up to 3 m in length. Fragments are typically in the cm or larger size range, have conical (straight or coiled) shapes, and are internally chambered (septate) throughout their length (unlike gastropods). The partitioned chambers are connected by a small tube (the siphuncle) that may be visible in some sections.**
2. **Nautiloids typically have smoothly curved septa whereas ammonites have convolute septa and sutures.**
3. **Modern nautiloids have very thin-walled aragonitic shells with one to three layers (a thin, porcelaneous layer of aragonite prisms, the ostracum, on the outside); a thicker middle layer composed of nacreous aragonite and organic matter (termed the nacreous layer); and a thin inner layer of prismatic aragonite. Fossil ammonoids most likely had the same composition and wall structure (aragonitic wall structure generally is lost during diagenesis except in unusual circumstances where aragonite has been preserved). A few fossil nautiloids have excellent preservation of some or all of their wall structure and may have been partially calcitic.**
4. **Belemnites have a very distinctive structure with a very thick, solid, tapering, partially hollow, calcitic rostrum that is normally very well preserved. The rostra of belemnites are composed of radially arranged, extremely long and thin calcite prisms; this produces a pseudo-uniaxial cross in cross-polarized light.**

Morphology of a typical nautiloid cephalopod

Diagrammatic sections through a coiled nautiloid cephalopod, based on the only surviving externally-shelled cephalopod, the pearly nautilus (adapted from Moore et al. (1952) and other sources. The coiled shell is divided into chambers (camera) by smooth, septal partitions. The living, squid-like organism occupies only the outermost chamber at each stage in its development. The shell in this example (and in many but not all fossil forms) is aragonitic and consists mainly of nacre with a significant organic content. The nacre is sandwiched between very thin inner and outer layers composed of tiny aragonite prisms.

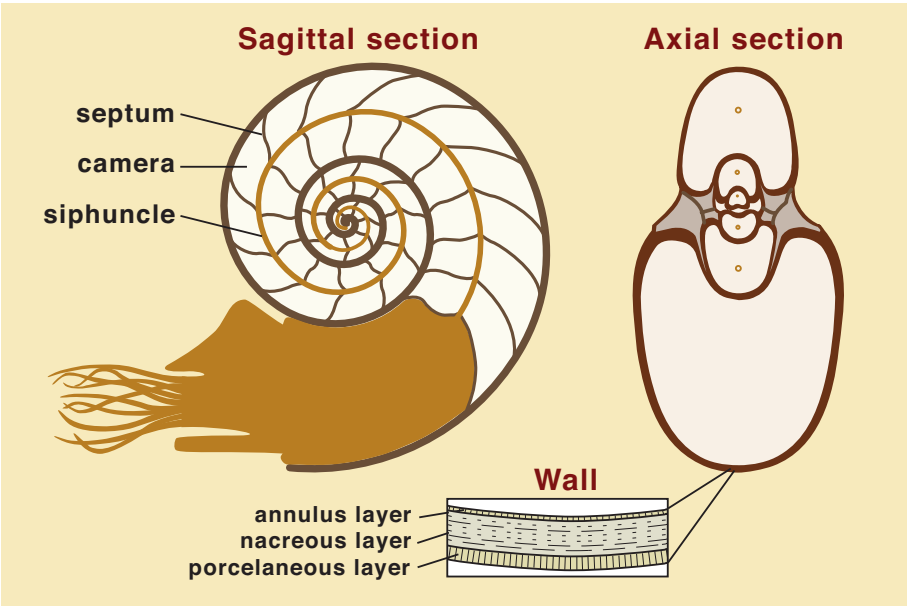

Mid. Ordovician Holston Fm., eastern Tennessee

A polished slab of orthoconic (uncoiled) nautiloid-rich sediment. Note the smooth septa and thin walls typical of nautiloids. The complex internal sediment fillings in the orthocones indicate a complex, and probably long, period of exposure on the sea floor. The lighter gray areas within shells consist of fibrous calcite cement of probable marine origin. Photograph courtesy of Andrew Stefaniak.

Mac, HA = ~28 cm

Up. Permian Middle reef complex, eastern Djebel Tebaga, Tunisia

A cross-section through a small ammonoid cephalopod (center) showing a progressive increase in chamber sizes from its initial whorls to the final ones. The typically thin walls of this nektic organism have been completely neomorphosed — the norm for originally aragonitic shell material. Several other formerly aragonitic molluscan fragments, mainly from bivalves, also are visible.

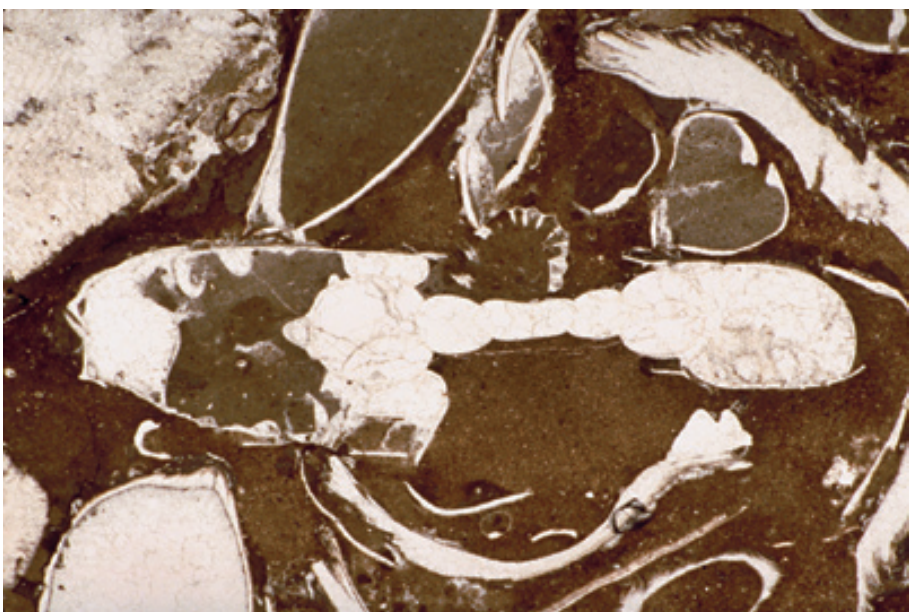

PPL, HA = 10 mm

Lo. Carboniferous Dartry Ls., near Sligo, Ireland

A cut through a nautiloid cephalopod with well-preserved internal chambers. The uniformly curved septa and the trace of a siphuncle (the ovoid feature toward the left of center) serve as distinguishing features of nautiloid material. Although the calcareous wall structure is not well preserved, the wall areas have a dark color that may represent preservation of at least a fraction the organic matter that once was a component of the shell wall.

PPL, HA = 25 mm

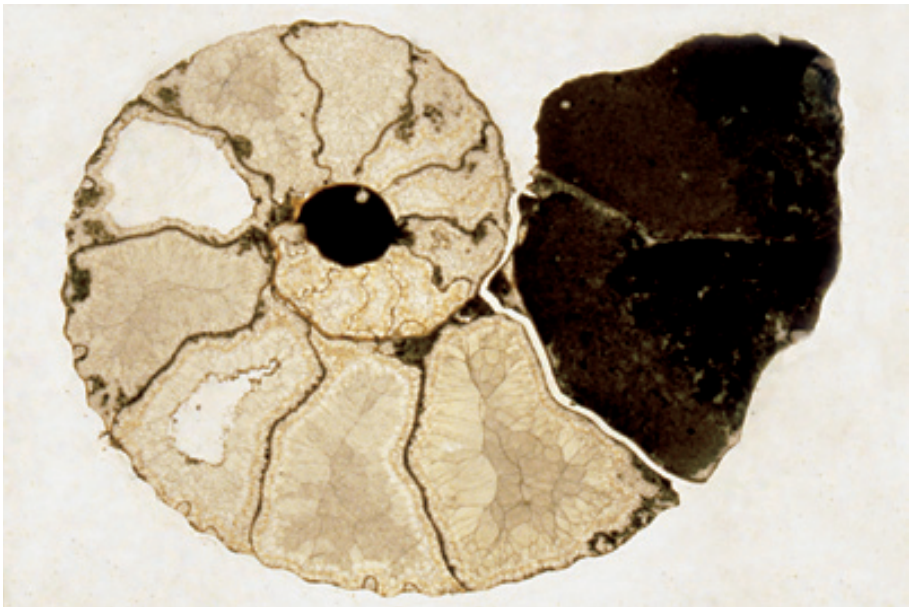

Up. Cretaceous Carlisle Shale (?), South Dakota

A low-magnification view of a sagittal section through a complete ammonite — *Acanthoceras* sp. The spiral, chambered form, the large size, and the thin walls with remnants of brownish organic matter all serve to identify this a coiled cephalopod. The wavy or plicate septa distinguish this as an ammonite (rather than a nautiloid that would have non-plicate septa).

PPL, HA = 35 mm

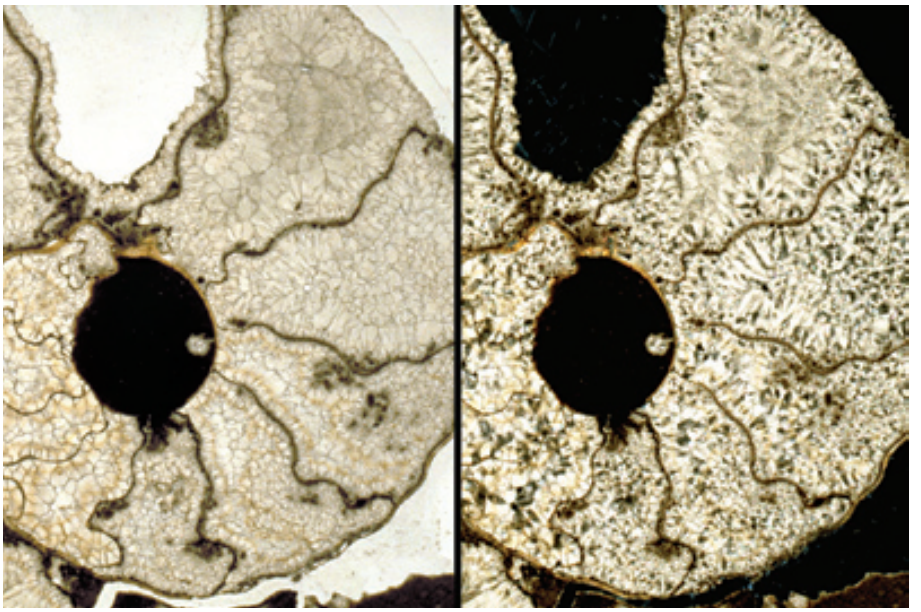

Up. Cretaceous Carlisle Shale (?), South Dakota

Enlarged plane- and cross-polarized views of the same complete ammonite shown in the previous photograph. The details of the septa, the external wall, and the cameral precipitates are more clearly visible. As in many such shells, the marine or early burial cements that fill cephalopod body cavities contain traces of brownish organic matter, perhaps reflecting the remnants of soft organic tissues or the influence of microbes that colonized the shell interiors after death of the organism.

PPL/XPL, HA = 8 mm each

Up. Cretaceous Fox Hills Ss., Dewey Co., South Dakota

A thin-walled ammonite with uncharacteristic preservation of the original, thin, aragonitic wall. The preservation of aragonite for 70 million years resulted from encasement in an impermeable concretion during early diagenesis. The shell has nacreous structure (the original thin prismatic layers are not preserved here). Note also the fibrous to bladed marine calcite infill of the ammonite chambers, a common feature in most preserved, undeformed cephalopods.

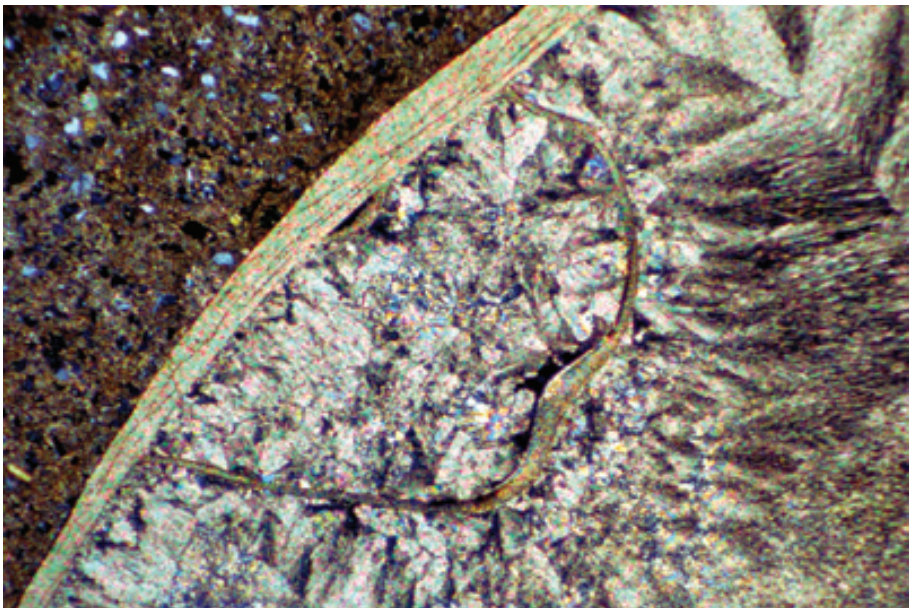

XPL, HA = 3.4 mm

Pennsylvanian Buckhorn Asphalt, Murray Co., Oklahoma

An example of preserved aragonite walls in crushed cephalopod shells. This is some of the oldest preserved primary skeletal aragonite (nacre); the unusual preservation results from early impregnation of the sediment by crude oil (now heavy oil or asphalt that has given the rock a yellowish-brown color). Such exceptional occurrences of preserved material allow a better understanding of the mineralogy and structure of the now extinct or nearly extinct externally-shelled cephalopods.

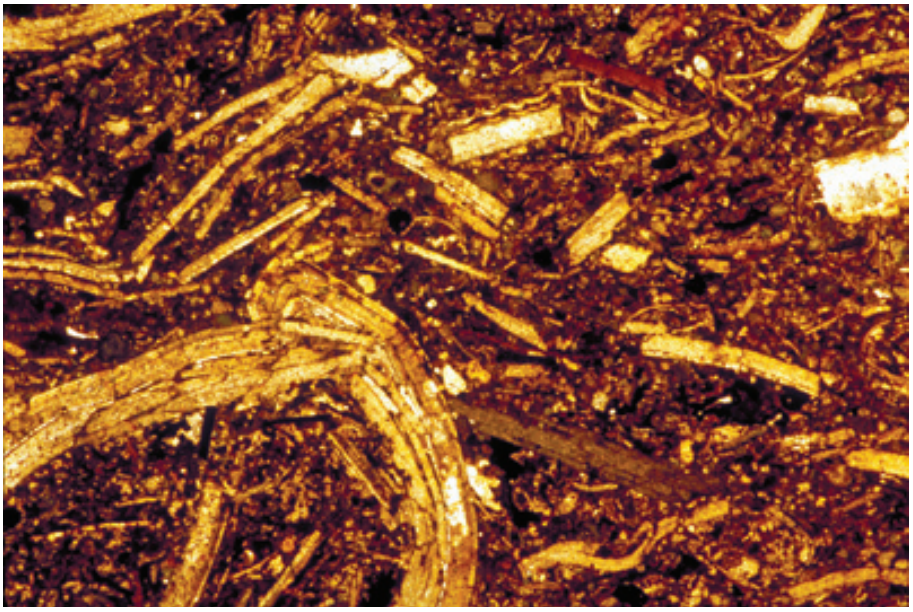

PPL, HA = 8 mm

Cretaceous, coastal plain, New Jersey

A transverse cross-section through a belemnite rostrum. The rostrum was a massive, elongate, conical structure with a conical cavity at one end. It is the most commonly preserved portion of belemnites; the phragmocone is much more delicate and rarely is well preserved. Belemnite rostra consist of radiating fibers or prisms of calcite that produce a strong pseudo-uniaxial cross under cross-polarized light. Although not seen in this specimen, many belemnites also show tree-ring-like growth lines marked by layers of brownish organic matter within the rostrum.

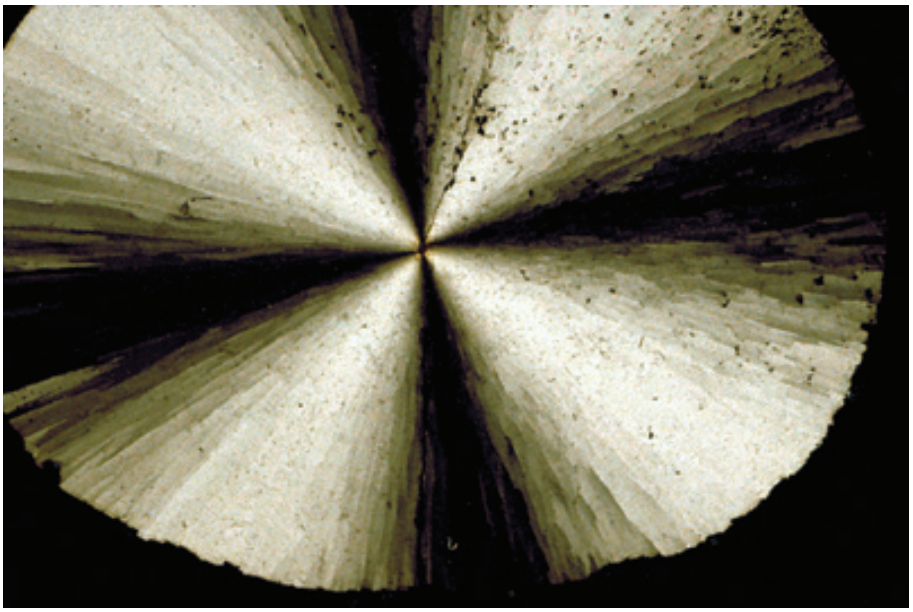

XPL, HA = 16 mm

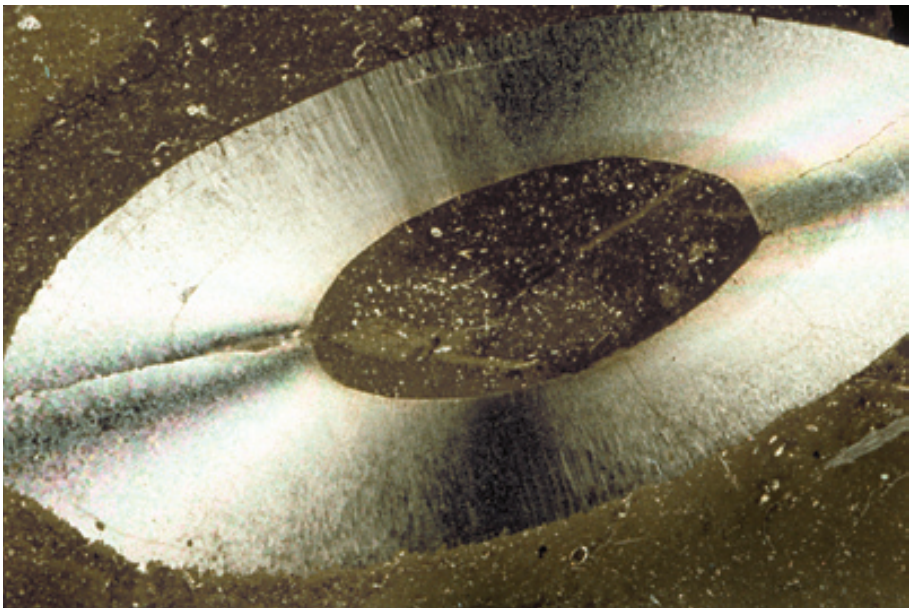

Up. Cretaceous (Senonian) White Ls., Ballycastle, Northern Ireland

An oblique section through the part of a belemnite rostrum with a conical cavity that once held the phragmocone. Note the pseudo-uniaxial cross, the clearly visible radial calcite fibers, and the weakly visible growth lines. Belemnites are important biostratigraphic fossils and significant carbonate contributors in Mesozoic (especially Jurassic and Cretaceous) strata.

XPL, HA = 16 mm

SCAPHOPODS

Taxonomy and Age Range:

Phylum Mollusca; Subphylum Diasoma
Class Scaphopoda — Mid. Ordovician-Recent

Environmental Implications:

Modern scaphopods are fully marine and all fossil examples are thought to have lived in the same conditions.
Modern forms are benthic, infaunal deposit feeders that inhabit soft bottoms from shelfal waters to depths greater than 6 km. They feed primarily on benthic foraminifers.
Rarely are dominant rock-forming constituents.

Skeletal Mineralogy:

Shells are composed of aragonite with low Sr (and Mg) content.

Morphologic Features:

Scaphopods are univalve mollusks with a tapering, slightly curved, conical shell that is open at both ends.
Shells of adult forms typically are 2 cm or shorter in length and a few mm in width.

Keys to Petrographic Recognition:

1. **Scaphopod shells or fragments are typically in the size range from mm to a few cm.**
2. **Curved, smooth to somewhat ornamented shell fragments predominate — most have circular, to elliptical internal shapes and circular to polygonal exteriors. Cuts parallel to the long axis show two sub-parallel lines of material representing the walls of a simple, unchambered, tapering cone.**
3. **Because they are aragonitic, shell walls of fossils typically are poorly preserved.**
4. **Well preserved shells have extremely thin inner and outer walls sandwiched around a middle layer with crossed-lamellar fabric. Toward the smaller end of the shell, this microstructure becomes indistinguishable. It is this distinctive microstructure, where preserved, that allows distinction from annelid worm tubes and other tubular to conical grains.**
5. **Scaphopods lack septa which helps to distinguish them from small nautiloids.**

Comparison of wall structures of scaphopods and other tube-shaped fossils

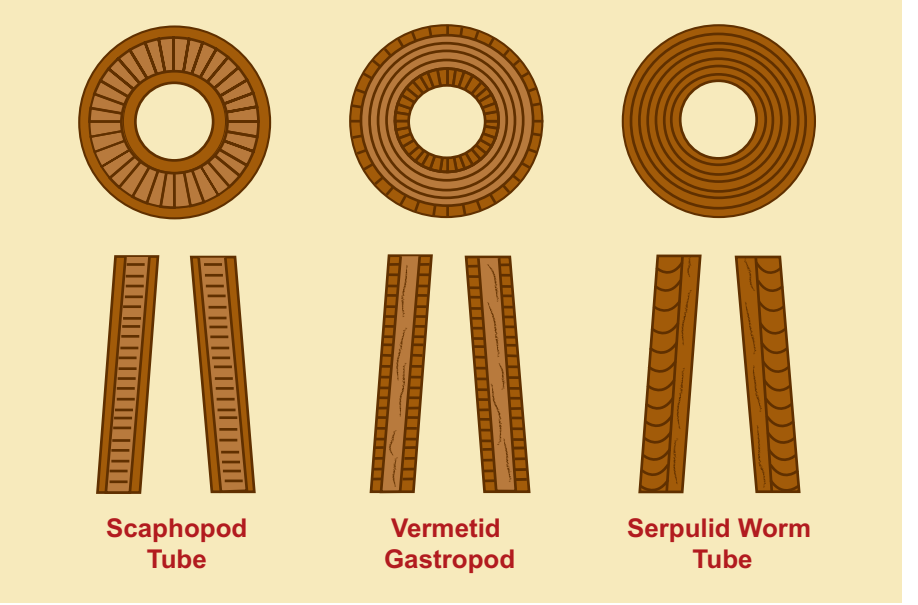

Schematic transverse and longitudinal sections through a scaphopod, a vermetid gastropod, and a serpulid worm tube. The scaphopod has thin, clear inner and outer layers, with a thick, commonly crossed-lamellar or prismatic middle layer that also may be concentrically laminated. The vermetid gastropod shell has a prismatic inner and outer layer and a laminated middle layer. The serpulid worm tube has a laminated inner layer and a cone-in-cone structure in its outer layer. In practice, however, those wall-structural differences are not always easy to distinguish. After Schmidt (1955) and Horowitz and Potter (1971).

Pliocene, Sarteano, Italy

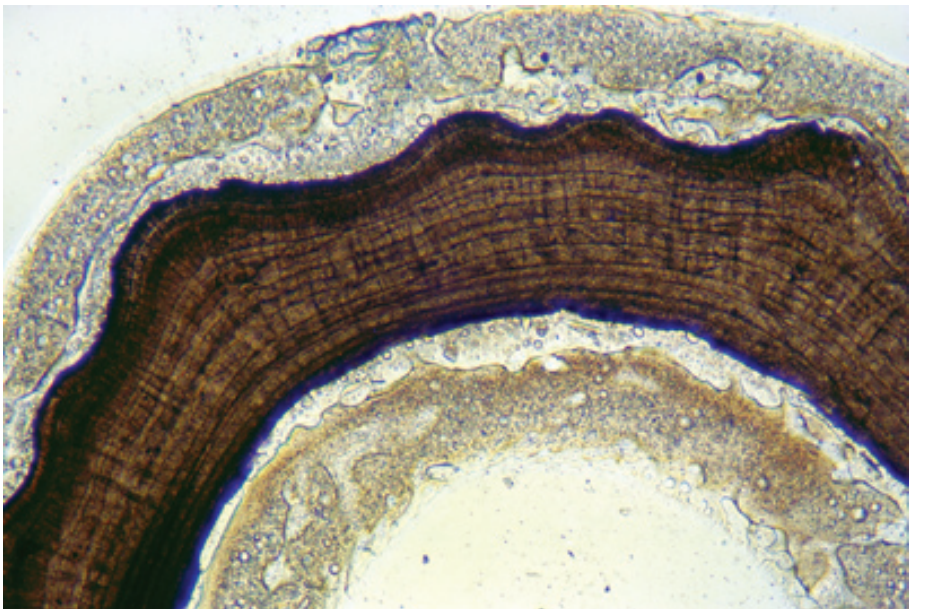

A transverse section through part of the wall of a scaphopod, *Dentalium sexangulare*. This genus is characterized by its conical shape, aragonitic shell with extensive external ribbing (unusual for the usually smooth-walled scaphopods). Although the shell is composed of three layers (see above), the inner and outer layers are normally very thin, compared to the thick central layer. The central zone may have prismatic, homogeneous, or crossed-lamellar wall structure (Bøggild, 1930). One can also distinguish numerous dark growth bands within the shell wall. To add complexity, some members of this genus have recently been reclassified as worm tubes (Yochelson and Goodison, 1999).

PPL, HA = 5.7 mm

Pliocene, Sarteano, Italy

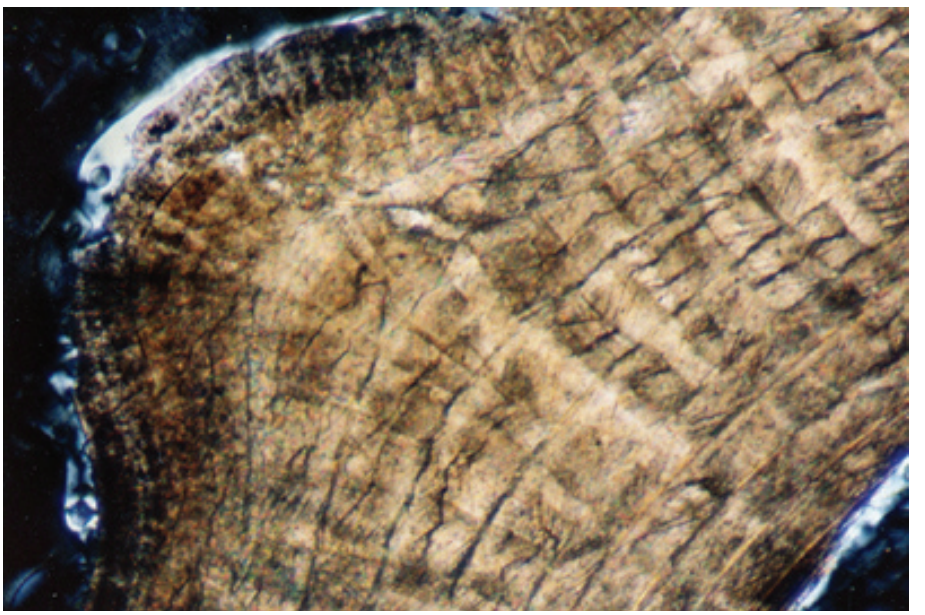

An cross-polarized light image showing details of the wall structure of the scaphopod, *Dentalium sexangulare*. The concentrically laminated, homogeneous (or very finely crystalline crossed-lamellar) structure of the central band of the shell is visible but not dramatic in this section — it generally is more pronounced in longitudinal sections. A thin outer shell layer is also present.

XPL, HA = 1.4 mm

Cited References and Additional Information Sources

Bandel, K., 1981, Struktur der Molluskenschale im Hinblick auf ihre Funktion: Funktionsmorphologie, v. 1, p. 25-47.

Bathurst, R. G. C., 1964, The replacement of aragonite by calcite in the molluscan shell wall, *in* J. Imbrie, and N. D. Newell, eds., Approaches to Paleoecology: New York, John Wiley & Sons, p. 357-375

Bathurst, R. G. C., 1975, Carbonate Sediments and their Diagenesis: New York, Elsevier Science Publ. Co., 658 p. [Mollusks: p. 2-20.]

Batten, R. L., 1982, The origin of gastropod shell structure, *in* B. Mamet, and M. J. Copeland, eds., Third North American paleontological convention, v. 3, North American Paleontological Convention, p. 35-39.

Birkelund, T., 1981, Ammonoid shell structure, *in* M. R. House, and J. R. Senior, eds., Systematics Association symposium on the Ammonoidea; the evolution, classification, mode of life and geological usefulness of a major fossil group, v. 18: New York, Academic Press, p. 177-214.

Blind, W., 1988, Comparative investigations on the shell morphology and structure of *Nautilus pompilius*, *Orthoceras* sp., *Pseudorthoceras* sp., and *Kionoceras* sp., *in* J. Wiedmann, and J. Kullmann, eds., Cephalopods; Present and Past [2nd international cephalopod symposium], v. 2: Stuttgart, E. Schweizerbart'sche Verlagsbuchhandlung, p. 273-289.

Bøggild, O. B., 1930, The shell structure of the Mollusks: Kongelige Danske Videnskabernes Selskab Skrifter, 9 Raekke, Naturvidens Kunde og Mathematisk Afdeling, v. 2, p. 231-326.

Carter, J. G., and F. G. Stehli, 1980, Environmental and biological controls of bivalve shell mineralogy and microstructure, *in* C. C. Rhoads, and R. A. Lutz, eds., Skeletal Growth of Aquatic Organisms: biological records of environmental change: New York, Plenum Press, p. 69-113.

Carter, J. G., and F. G. Stehli, 1980, Appendix 2; Bivalve shell mineralogy and microstructure; Part A, Selected mineralogical data for the Bivalvia, *in* C. C. Rhoads, and R. A. Lutz, eds., Skeletal Growth of Aquatic Organisms: biological records of environmental change: New York, Plenum Press, p. 627-643.

Carter, J. G., and F. G. Stehli, 1980, Appendix 2; Bivalve shell mineralogy and microstructure; Part B, Guide to bivalve shell microstructures, *in* C. C. Rhoads, and R. A. Lutz, eds., Skeletal Growth of Aquatic Organisms: biological records of environmental change: New York, Plenum Press, p. 645-673.

Cox, L. R., 1960, Gastropoda - General characteristics of Gastropoda, *in* R. C. Moore, ed., Treatise on Invertebrate Paleontology, Part I, Mollusca 1: Geological Society of America and University of Kansas Press, p. 1 84-1 169.

Cuif, J. P., Y. Dauphin, A. Denis, P. Gautret, A. Lawniczak, and A. Raguideau, 1987, Résultats récents concernant l'analyse des biocristaux carbonatés: implications biologiques et sédimentologiques: Bulletin de la Société géologique de France, Série 8, v. 3, p. 269-288.

Davies, T. T., 1965, The shell structure and composition of Recent molluscs from the Atlantic coasts: Maritime Sediments, v. 1, p. 30-31.

Dodd, J. R., 1966, The influence of salinity on mollusk shell mineralogy: a discussion: Journal of Geology, v. 74, p. 85-89.

Horowitz, A. S., and P. E. Potter, 1971, Introductory Petrography of Fossils: New York, Springer-Verlag, 302 p.

Herman, Y., 1978, Pteropods, *in* B. U. Haq and A. Boersma, eds., Introduction to Marine Micropaleontology: New York, Elsevier, p. 151-159.

Kennedy, W. J., N. J. Morris, and J. D. Taylor, 1970, The shell structure, mineralogy, and relationships of the Chamacea (Bivalvia): Palaeontology, v. 13, p. 379-413.

Kennedy, W. J., and J. D. Taylor, 1968, Aragonite in rudistids: Proceedings of the Geological Society of London, no. 1645, p. 325-331.

Kennedy, W. J., J. D. Taylor, and A. Hall, 1969, Environmental and biological controls on bivalve shell mineralogy: Biological Reviews of the Cambridge Philosophical Society, v. 44, p. 499-530.

Knight, J. B., et al., 1960, Mollusca 1, *in* R. C. Moore, ed., Treatise on Invertebrate Paleontology Part I: Geological Society of America and University of Kansas Press, 351 p

Kulicki, C., 1979, The ammonite shell: its structure, development and biological significance: Palaeontologia Polonica, no. 39, p. 97-142.

MacClintock, C., 1967, Shell structure of patelloid and bellerophontoid gastropods (Mollusca): Peabody Museum of Natural History Yale University, Bulletin 22, 140 p.

Majewske, O. P., 1969, Recognition of Invertebrate Fossil Fragments in Rocks and Thin Sections [Internat. Sed. Petrog. Series v. 13]: Leiden, E. J. Brill, 101 p.

Moore, R. C., C. G. Lalicker, and A. G. Fischer, 1952, Invertebrate Fossils: New York, McGraw-Hill Book Co., 766 p.

Mutvei, H., 1967, On the microscopic shell structure in some Jurassic ammonoids: Neues Jahrbuch für Geologie und Paläontologie, Abhandlungen, v. 129, p. 157-166.

Oberling, J. J., 1964, Observations on some structural features of the pelecypod shell: Naturforschungs Gesellschaft Bern, Mitteilungen, Neue Serie v. 20, p. 1-63.

Pojeta, J., Jr., B. Runnegar, J.S. Peel, and G. Mackenzie, Jr. 1987, Phylum Mollusca, *in* R. S. Boardman, A. H. Cheetham, and A. J. Rowell, eds., Fossil Invertebrates: Palo Alto, Blackwell Sci. Publ., p. 270-435.

Schenk, H. G., 1934, literature on the shell structure of pelecypods: Bulletin du Muséum Royale d'Histoire Naturelle de la Belgique, v. 10, No. 34, 20 p.

Schmidt, W. J., 1951, Die Unterscheidung der Röhren von Scaphopoda, Vermetidae und Serpulidae mittels mikroskopischer Methoden: Mikroskopie, v. 6, p. 373-381.

Skelton, P. W., 1974, Aragonitic shell structure in the rudistid Biradiolites and some palaeobiological inferences: Géologie Méditerranéenne, v. 1, p. 53-74.

Skelton, P.W., 1978, The evolution of functional design in rudistids (Hippuritacea) and its taxonomic implications: Philosophical Transactions, Royal Society of London, Ser. (B), v. 284, p. 305-318.

Taylor, J. D., W. J. Kennedy, and A. Hall, 1969, The shell structure and mineralogy of the Bivalvia; introduction; Nuculacea-Trigonacea: London, British Museum (Natural History), 115 p.

Taylor, J. D., W. J. Kennedy, and A. Hall, 1973, The shell structure and mineralogy of the Bivalvia. II. Lucinacea-Clavagellacea, conclusion: British Museum (Natural History) Bulletin, Zoology, v. 22, p. 255-294.

Teichert, C., B. Kummel, W. C. Sweet, H. B. Stenzel, W. M.Furnish, B. F. Glenister, H. K. Erben, R. C. Moore, and D. E. N, Zeller, 1964, Mollusca 3, *in* R. C. Moore, ed., Treatise on Invertebrate Paleontology, Part K: Geological Society of America and University of Kansas Press, 519 p.

Tucker, M. E., 1981, Sedimentary Petrology: An Introduction: New York, John Wiley & Sons (Halsted Press), 252 p.

Wilbur, K. M., 1964, Shell structure and mineralization in molluscs. Calcification in biological systems, *in* R. F. Sognnaes, ed., Calcification of biological systems—A symposium: Washington, D.C., American Association for the Advancement of Science, Publication 64, p. 15-40.

Wise, S. W., Jr., 1969, Study of molluscan shell ultrastructures, *in* O. Johari, ed., Scanning Electron Microscopy/1969, Proceedings 2nd Annual Scanning Electron Microscopy Symposium: Chicago, IL, IIT Research Institute, p. 205-216.

Wise, S. W., Jr., 1970, Microarchitecture and mode of formation of nacre (mother-of-pearl) in pelecypods, gastropods, and cephalopods: Eclogae geologicae Helvetiae, v. 63, p. 775-797.

Wise, S. W., Jr., 1971, Shell ultrastructure of the Taxodont pelecypod *Anadara notabilis* (Roding): Eclogae geologicae Helvetiae, v. 64, p. 1-12.

Wise, S. W., Jr., and W. W. Hay, 1968, Scanning electron microscopy of molluscan shell ultrastructures. II. Observations of growth surfaces: Transactions of the American Microscopical Society, v. 87, p. 419-430.

Yochelson, E. L., and R. Goodison, 1999, Devonian *Dentalium martini* Whitfield, 1882, is not a mollusk but a worm: Journal of Paleontology, v. 73, p. 634-640.

Zakharov, Y. D., 1996, Orthocerid and ammonoid shell structure; its bearing on cephalopod classification: Bulletin of the National Science Museum (Japan) Series C: Geology and Paleontology, v. 22, p. 11-35.

Facing Page: Underwater photograph of a crinoid perched atop a reef-front coral head on the Great Barrier Reef, Australia. Photograph courtesy of Woody Mayhew.

GRAINS: Skeletal Fragments

ECHINODERMS

CHAPTER 10

- Echinoids
- Crinoids
- Blastoids
- Holothurians
- Asteroids and ophiuroids

ECHINOIDS

Taxonomy and Age Range:

Phylum Echinodermata
Subphylum Echinozoa
Class Echinoidea — Late Ordovician-Recent

Environmental Implications:

Echinoids (sea urchins) live in normal marine environments because they with a very limited range of salinity tolerance (generally only a few ppm).

They occur mainly as grazers or burrowers in sandy shelf areas or as grazers and bioeroders along rocky shorelines. They occur in deeper waters as well, extending to abyssal depths. Fossil forms are most common in normal marine, open shelf or platform deposits.

Echinoids are common in both warm- and cold-water settings, although they rarely are major rock-forming organisms (i.e., they rarely exceed 10-15% of the total sediment).

Skeletal Mineralogy:

Modern and ancient echinoids are/were composed of moderate- to high-Mg calcite. Modern forms contain between 2 and 17 mole% Mg; the Mg content varies with generic group and increases with increasing water temperature (see Milliman, 1974, p. 130-134, for details and citations).

Morphologic Features:

Echinoids, like all echinoderms at some stage in their life cycle, show pentameral (five-fold) symmetry. They have heavily calcified, globular to discoidal, hollow, endoskeletal tests (coronas) that are composed of individual sutured, interlocking or imbricated calcite plates. The calcitic coronal plates are porous and sponge-like; echinoids with rapid growth rates have spongier plates (with more holes and less calcification) than slow-growing counterparts. Thus, slow growing, cold-water forms can be more heavily calcified than those from warmer waters (Raup. 1958)

In life, echinoid tests are covered with elongate, moveable spines (in some species extremely short, but in others longer than 8 cm). The spines normally detach after death and can themselves be significant sediment contributors.

Generally, each plate of an echinoid behaves optically as a single, extensively perforated, calcite crystal (see comments below). Echinoid teeth, however, are polycrystalline.

Keys to Petrographic Recognition:

1. **Whole echinoids range from less than 1 cm to more than 10 cm in diameter; most plates or plate fragments are 30 mm or smaller.**
2. **With few exceptions, each individual echinoid plate or spine appears to be a single crystal of calcite and displays unit extinction (although in reality, at least the outer margins of each plate consist of a mass of submicroscopic crystals with very closely aligned c-axes; Towe, 1967). Echinoid fragments are easy to distinguish from the skeletal remains of other phyla on this basis alone, but unit extinction is a characteristic shared with virtually all other echinoderms.**
3. **Plates and spines are perforated with a regularly arranged meshwork or honeycomb of 15 to 25µm-diameter pores. Where the pores are filled with contrasting material (such as organic matter, micrite or glauconite), they are readily visible in thin section and at low magnifications give echinoid fragments a "dusty" appearance. The regular arrangement of these pores yields a "checkerboard" appearance at higher magnifications. This characteristic is shared with other echinoderm groups, specifically crinoids and asteroids/ophiuroids.**
4. **Echinoid spines have pores arranged with radial symmetry; thus, in circular cross-sections, echinoid spines have a distinctive lobate or flower-like appearance.**
5. **Plates and spines commonly have large, single-crystal syntaxial overgrowths (cements in optical continuity with their skeletal substrate). The presence of micritic matrix or oolitic coatings can inhibit the formation of such overgrowths.**

PHOTO SCALES AND ABBREVIATIONS ARE EXPLAINED IN THE BOOK'S INTRODUCTION

Diagrammatic view of typical echinoids

This diagram (adapted from Moore et al., 1952) emphasizes some of the features of echinoid tests as exemplified by *Hyattechinus* (a Lower Mississippian lepidocentroid form) and *Encope tamiamensis* (a Pliocene clypeastroid species). In particular, it shows their pentameral (five-fold) symmetry and interlocking calcareous plates, each of which acts optically as a single calcite crystal. Most echinoids disaggregate into particles that consist of whole single plates and/or spines or broken pieces of those components.

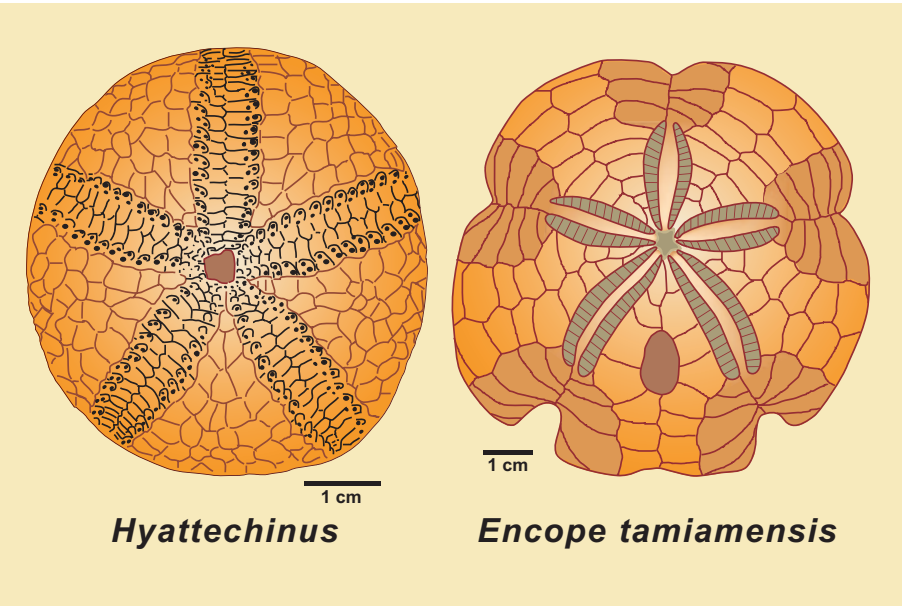

Up. Cretaceous (Maastrichtian) Tor Fm. chalk, Skjold Field, Danish North Sea

Most whole echinoids are so large that only small portions are seen in normal-sized thin sections. This unusual plan view of a whole juvenile echinoid is visible in a "thick section", cut for fluid-inclusion studies. The echinoid displays the group's diagnostic five-fold skeletal symmetry composed of multiple single-crystal plates.

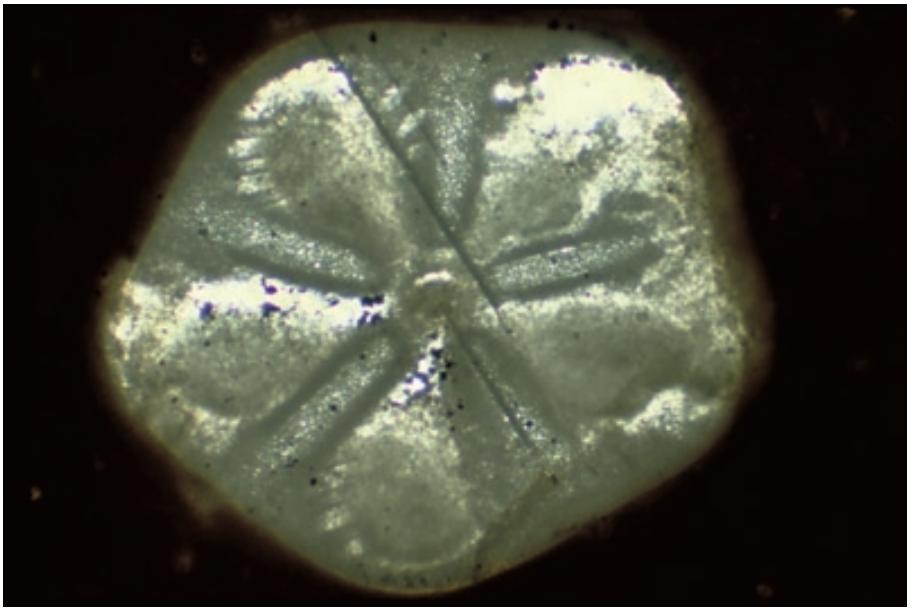

PPL, HA = 5 mm

Oligocene Nile Gp., north of Karamea, Westland, New Zealand

An unusual cut through a small but complete echinoid. The test (or corona) consists of numerous interlocked calcite plates surrounding the central cavity. The mouth opening (peristome) is visible at the bottom. The numerous large pores passing through the walls were passageways for the water-vascular system that operated the organism's tube feet.

PPL, BSE, HA = 8 mm

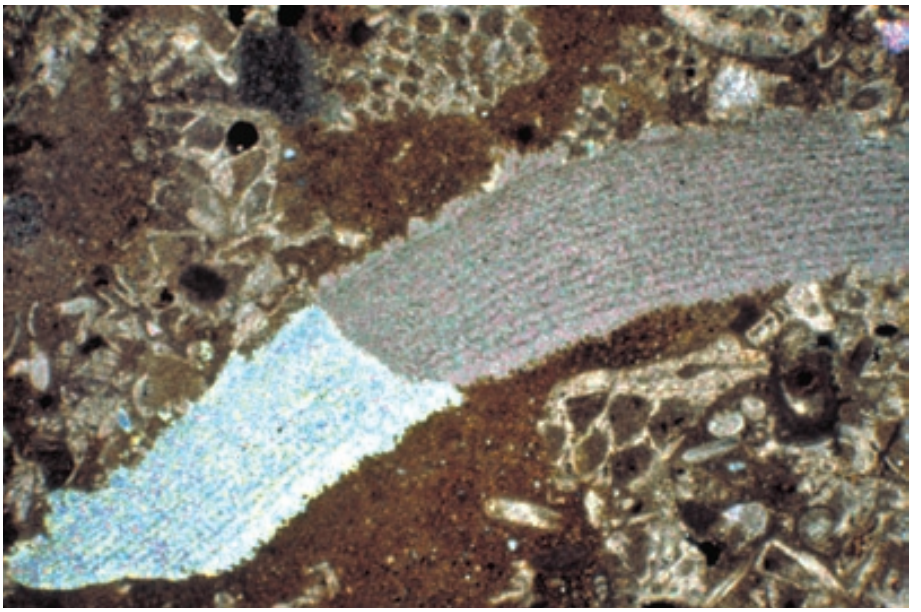

Oligocene Thomas Fm., western Canterbury, New Zealand

Two joined plates from a fragmented echinoid corona. Note the fact that each plate has separate unit extinction and shows (weakly in this case) the regular pattern of intraplate pores that permeate all echinoid material.

XPL, HA = 5.1 mm

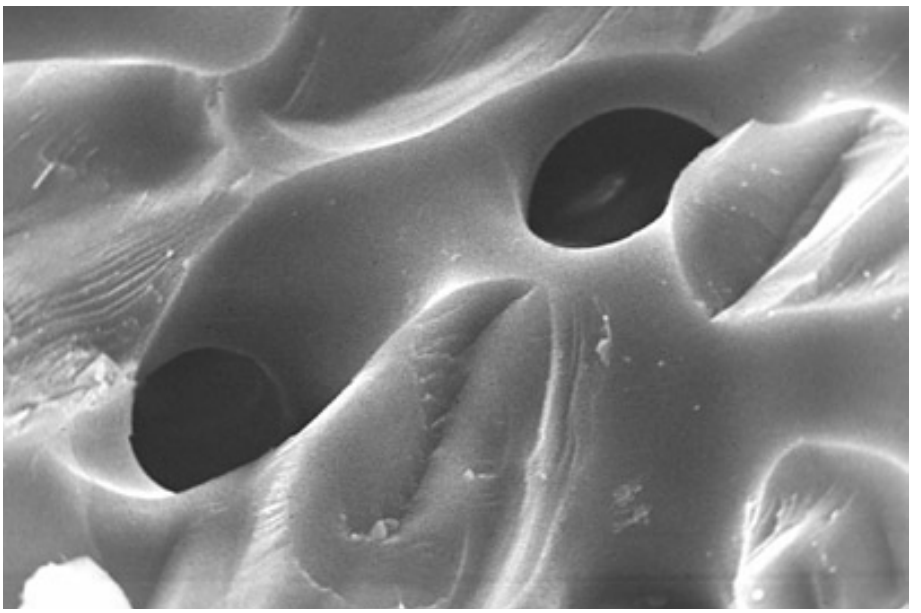

Recent sediment, Belize

An SEM image of a fractured piece of echinoid wall. It illustrates the massive construction of echinoid tests and the network of large pores which transect the structure. In many cases, the intraplate pore space exceeds 50% of the total volume of the plate. Despite the single crystal appearance of the plate, it consists of a mass of microcrystals so small that they are only visible at extreme magnifications.

SEM, HA = 70 μm

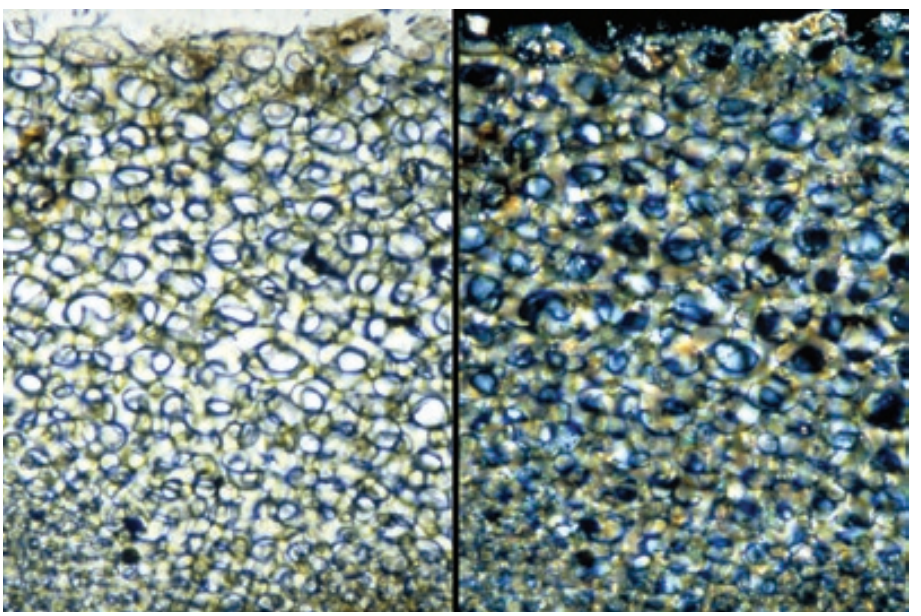

Recent echinoid, Florida Keys, Florida

A close-up view of a single echinoid plate. Note predominantly single-crystal extinction (also termed unit extinction) of each plate as well as regular spongy or "holey" fabric produced by tunnels through the otherwise solid high-Mg calcite plates. During diagenesis, these pores typically are either filled with syntaxial calcite cement (in which case they become virtually impossible to see) or with micritic matrix, organic matter or other contrasting material that allows the pores to remain visible.

PPL/XPL, each HA = 3.2 mm

Up. Eocene Ocala Gp., Citrus Co., Florida

A large echinoderm fragment with characteristic single-crystal or unit extinction and uniform "honeycomb" microtexture (small pores filled with micrite). Also note the fact that the grain is surrounded by calcite overgrowths that formed in optical continuity with the grain and predate later silica cement. The irregular shape and lack of a central canal help to distinguish it from a crinoid columnal.

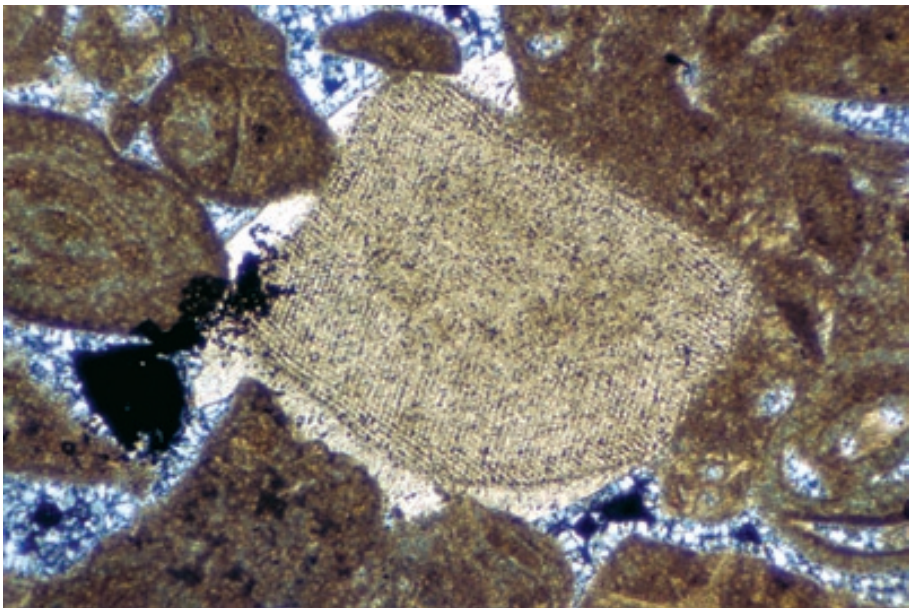

XPL, HA = 2.7 mm

Eocene Ocala Gp., Inglis Fm., Levy Co., Florida

An unusual example of a strongly ornamented and very porous echinoid plate. Here the pores were filled with micritic material that contrasts with the optically clear calcite of the echinoid.

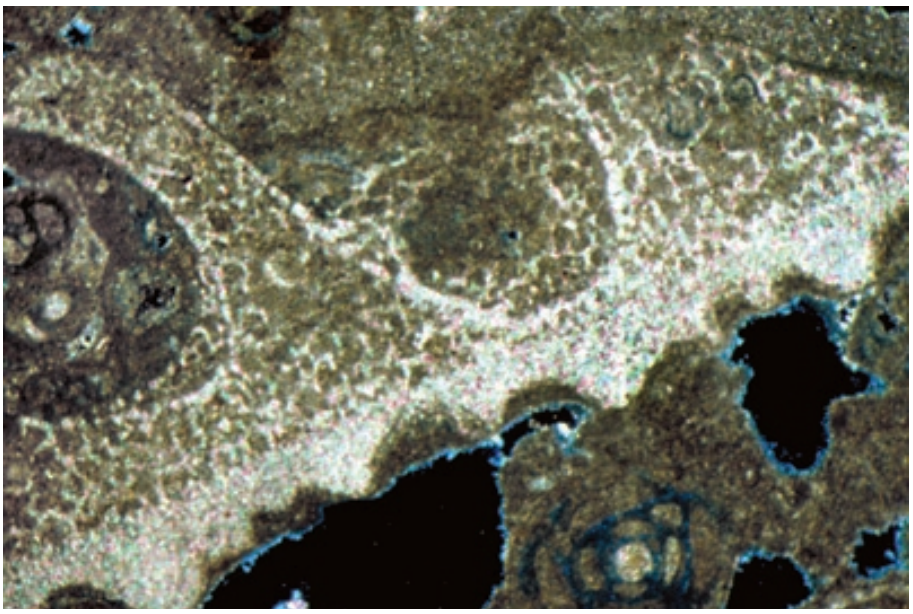

XPL, HA = 2.4 mm

Up. Silurian Tonoloway-Keyser Ls., Mifflin Co., Pennsylvania

An echinoderm fragment with optical single-crystal structure and a large overgrowth in optical continuity (syntaxial cement). The optical continuity is especially apparent here because the twinning lamellae of the calcite crystal are continuous from grain to cement.

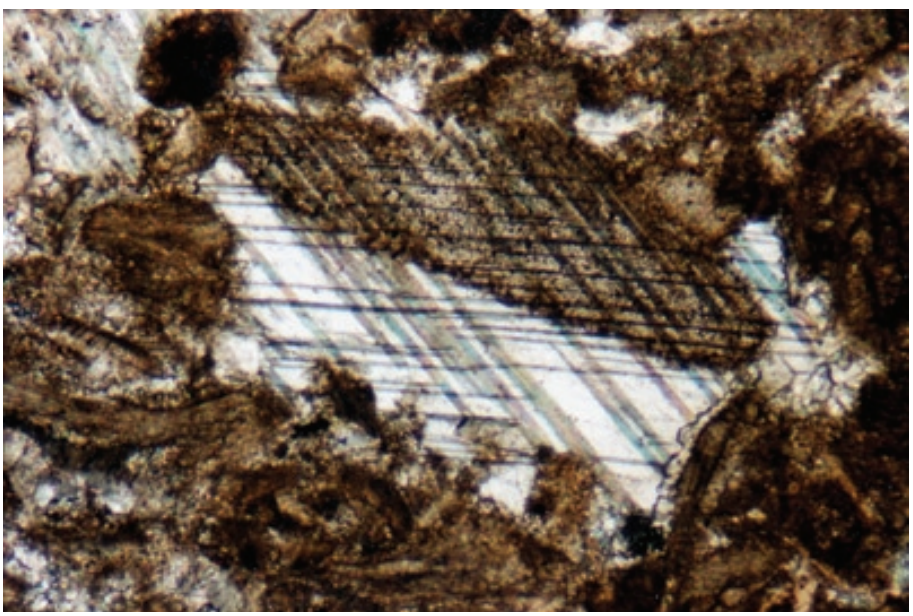

PPL, HA = 2.1 mm

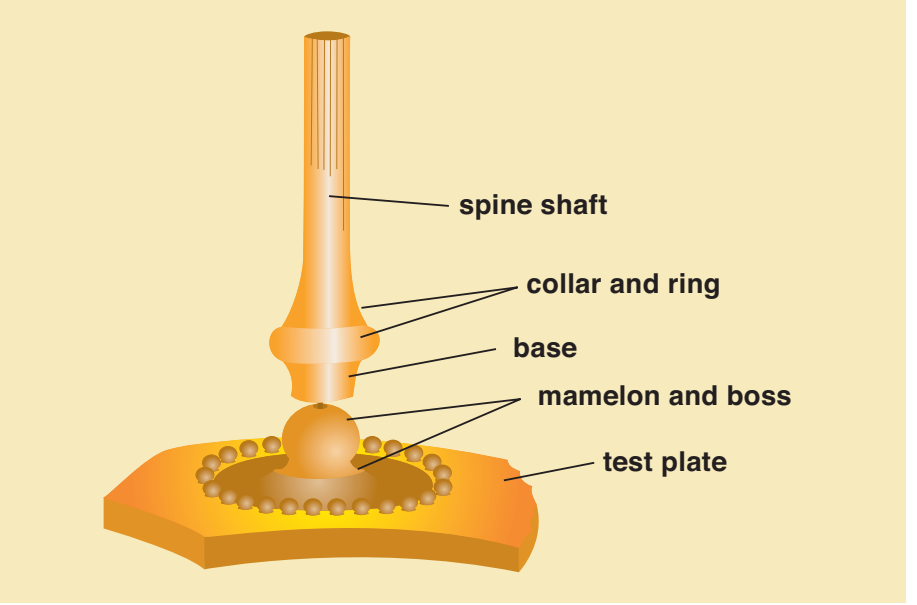

Diagram of an echinoid spine and its attachment

Echinoid spines are attached to the body of the organism with a type of ball and socket structure depicted here (redrawn from Moore et al., 1952, p. 678). This linkage is held together in life by surrounding organic tissue, but with death of the organism, decomposition of the organic material, and mechanical or biological reworking of the sediment, spines almost always become detached from the echinoid coronal plates.

Up. Cretaceous chalk, Limburg, The Netherlands

An SEM image of an echinoid spine in a calcarenitic chalk. The entire spine appears as a single calcite crystal (although, again, it is a mass of submicroscopic crystals with virtually identical optical orientation). Note both the strong ribbing on the exterior of the spine and the characteristic attachment socket at the left end.

SEM, HA = ~ 6 mm

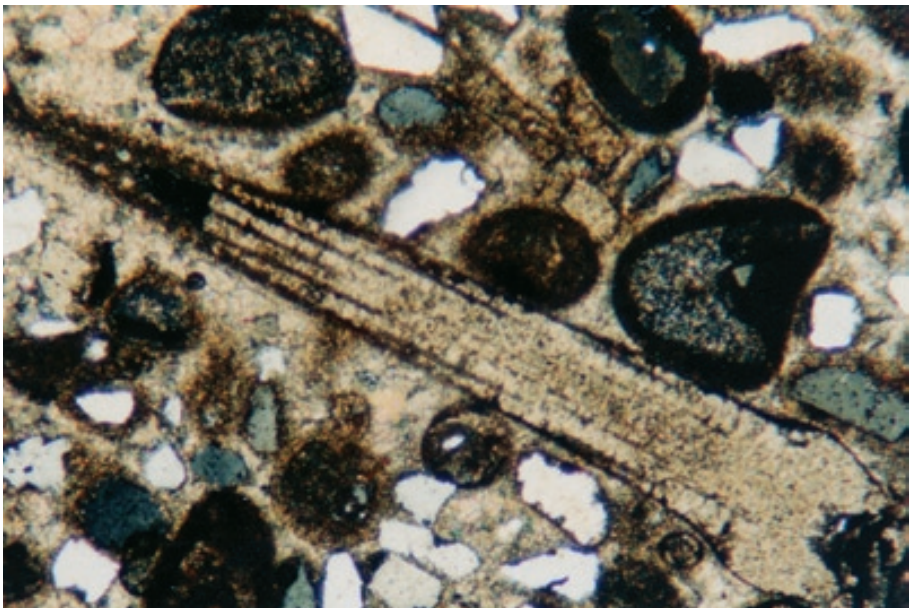

Lo.-Mid. Pennsylvanian Bloyd Fm., Mayes Co., Oklahoma

A longitudinal section through an echinoid spine. Note the bulbous attachment socket at one end and the elongate, ribbed, tapering spine itself. As with other echinoid grains, the entire spine acts like a single calcite crystal with unit extinction. The external ribbing visible on the spine in the SEM above reveals the origin of the micrite-filled stripes that parallel the long axis of the thin-sectioned spine.

XPL, HA = 1.8 mm

Mid. Jurassic (Bajocian) limestone, Central High Atlas region, Morocco

An echinoid spine showing the characteristic attachment "ball" at its base. The elongate shape of the grain, the apparent single-crystal structure (with unit extinction), and the presence of regularly arranged "dirt-filled" pores also help to identify the echinoid origin of this grain.

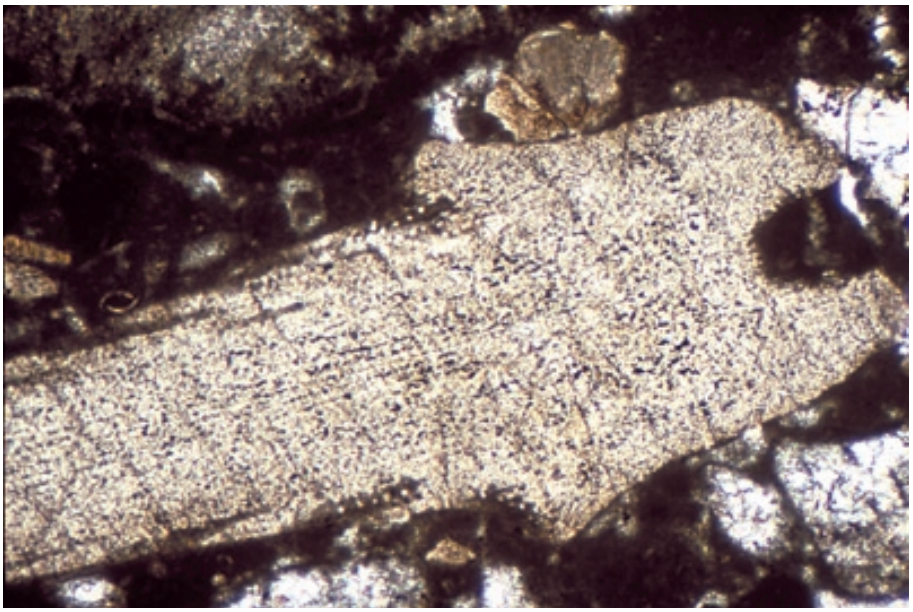

PPL, HA = 2.4 mm

Recent sediment, Cary Cay, Belize

Cross section of an echinoid spine showing single-crystal optical behavior (unit extinction) and a very characteristic lacy or flower-like pattern produced by the regular, radial arrangement of large pores within the spine.

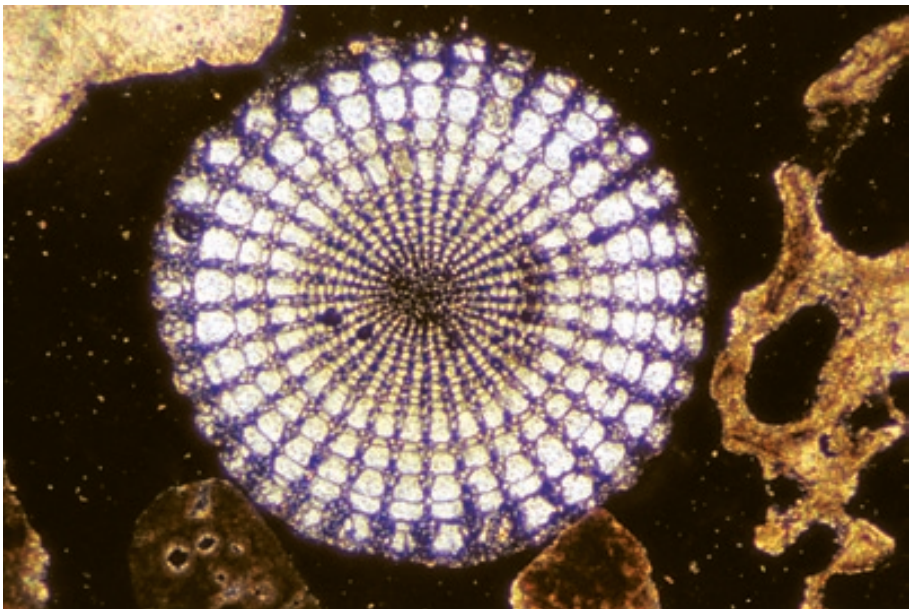

XPL, HA = 2.1 mm

Plio-Pleistocene coastal sediment, Crete, Greece

A transverse section through a single echinoid spine showing the characteristic lobate outline and flower-like structure. The structure of the spine is delineated because of micritic infill and/or cementation that helps to distinguish the spine from its extensive diagenetic overgrowth (syntaxial calcite cement that has grown in optical continuity with its echinoid substrate).

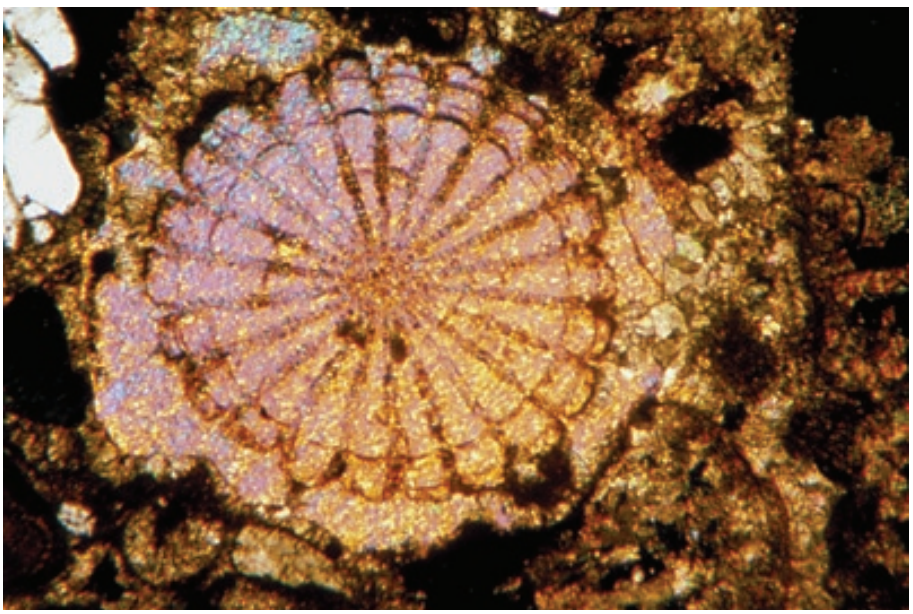

XPL, HA = 2.4 mm

CRINOIDS

Taxonomy and Age Range:

Phylum Echinodermata
Subphylum Pelmatozoa (= Crinozoa) — Early Cambrian-Recent
Class Eocrinoidea — Early Cambrian through Silurian
Class Crinoidea — Basal Ordovician-Recent

Environmental Implications:

Crinoids are fully marine, normal salinity organisms.

Crinoids (also known as sea lilies) were extremely important rock-forming constituents in Paleozoic (especially Devonian to Pennsylvanian) strata. Paleozoic forms occurred mainly as attached or "rooted" organisms (pelmatozoans) in shelf and shelf-margin settings (although they also lived in deeper water).

Post-Paleozoic distribution is/was much reduced and has shifted somewhat to deeper waters (modern forms extend to about 4 km depth). However, modern motile forms, commonly known as feather stars, are found in reefs and other shallow shelf settings.

Planktic forms also existed, especially in the Mesozoic.

Crinoids are common in both warm- and cold-water settings, even extending into Arctic and Antarctic waters.

Skeletal Mineralogy:

Composed of high-Mg calcite; modern forms contain 3 to 8 mole% Mg.

Morphologic Features:

Crinoids are heavily calcified; most consist of three parts: a root-like attachment, a long stem, and a calyx with radiating, feathery arms. Most ancient post-larval crinoids were attached (rooted) forms; most living species, however, are rootless, mobile forms.

All three parts (root, stem and calyx) are formed of individual calcite plates assembled like stacks of poker chips. Most sediment occurrences, however, consist of disarticulated plates.

Keys to Petrographic Recognition:

1. **Whole crinoids range from less than 10 cm to more than 1 m in size; however, they normally disaggregate into mm- to cm-sized plates or ossicles that have considerable diversity in size and shape.**
2. **Stem plates (columnals) typically have a circular, ovoid, or pentagonal outline with an axial canal (the lumen) that also can be circular or pentagonal; arm plates typically have a "U" shape. It is mainly on the basis of the size and shapes of grains that crinoid remains are distinguished from echinoid fragments — echinoid remains tend to have more elongate or irregular shapes; crinoid columnals have uniform shapes and sizes with axial canals visible in transversely oriented cuts).**
3. **Each individual skeletal component (columnal or arm plate) effectively acts as a single crystal of calcite and displays unit extinction.**
4. **Crinoid plates are perforated with small, regularly arranged pores which may be visible in thin section where they are filled with contrasting material (most commonly micrite or organic matter). These filled pores give crinoid fragments a distinctive "dusty" appearance at low magnification and a regular "checkerboard" appearance at higher magnifications.**
5. **The single-crystal crinoid plates commonly have syntaxial overgrowths, some of which can form coarse, even poikilotopic, cements. Indeed, in the absence of micritic coatings on crinoid fragments, most crinoidal limestones become heavily cemented by overgrowths relatively early in their diagenetic history.**

Typical crinoid structure

This diagrammatic view of a crinoid (adapted from Boardman et al. (1988, p. 558) and other sources. Crinoid stems consist of a series of corrugated circular or pentagonal plates (columnals) that resemble a stack of poker chips and easily disarticulate upon death of the crinoid. These columnals also have a readily recognizable central canal, termed a lumen. The arms that radiate from the calyx or head of the crinoid (not shown) have an ambulacral groove that gives the plates a characteristic U- or V-shape.

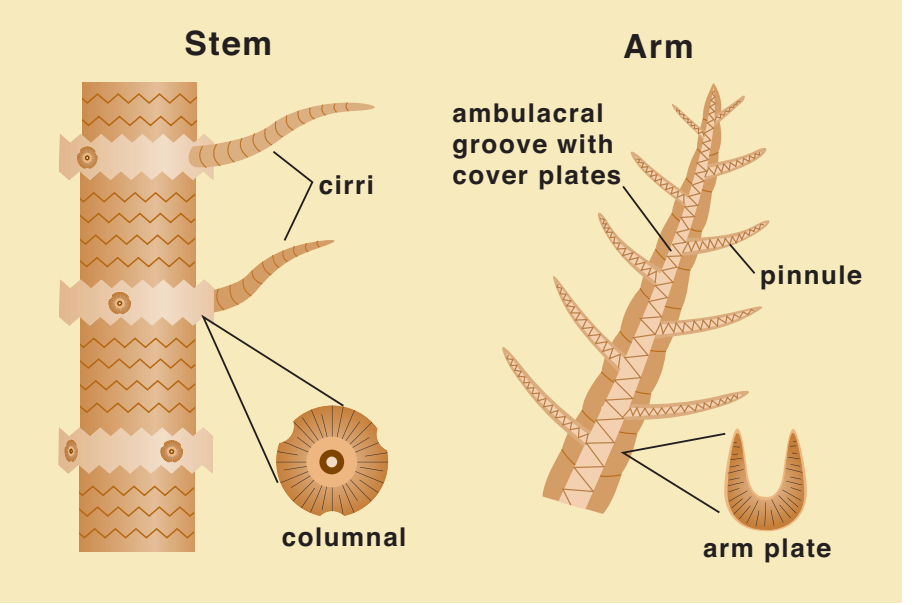

Up. Mississippian Salem Ls., Lawrence Co., Indiana

A longitudinal section of a crinoid stem showing a series of connected stem segments (columnals). It is relatively unusual to find crinoid columnals still articulated. Also note the partial cut through the axial canal (lumen) in the center of some of the columnals, and the unit extinction of the columnals, each of which acts optically as though it were a single calcite crystal with unit extinction.

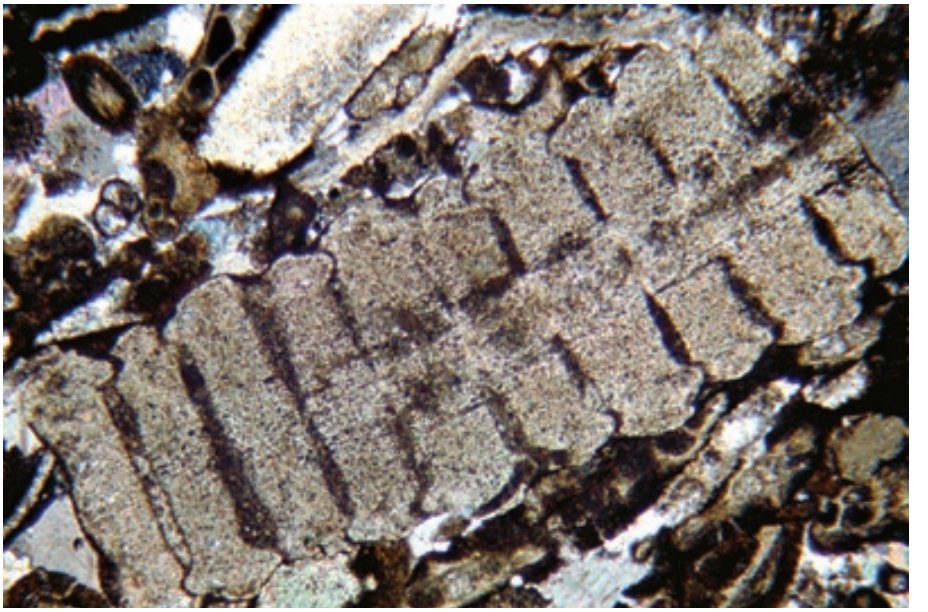

XPL, HA = 3.3 mm

Lo. Mississippian Lake Valley Fm., Otero Co., New Mexico

A longitudinal section showing three articulated crinoid columnals with slightly varying unit extinction. The poker-chip shape of the columnals is clear, but the section is sufficiently off-center that it misses the lumen (axial canal).

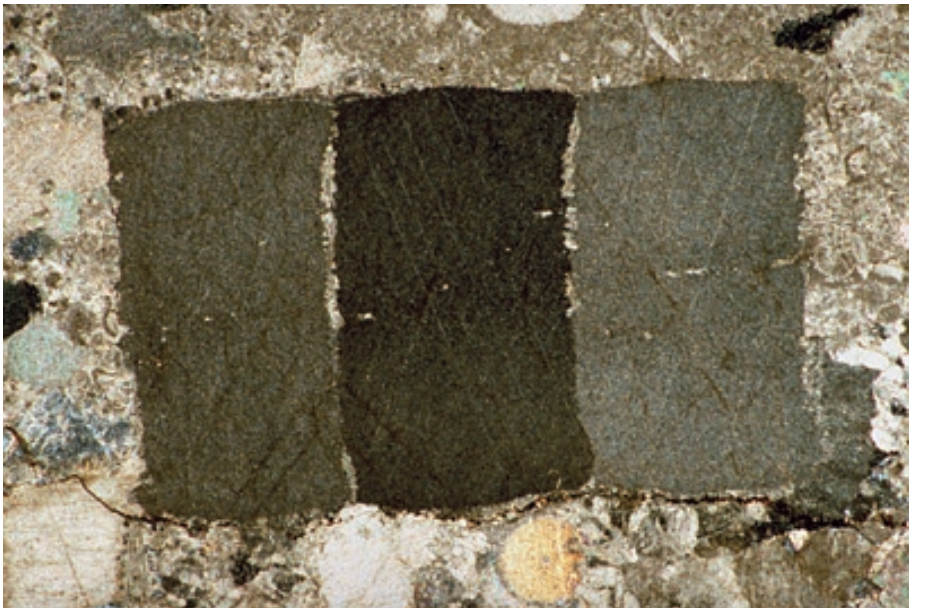

XPL, HA = 8 mm

Mid. Ordovician Black River Gp., Lowville Fm., Kingston, Ontario, Canada

Random cuts through stacks of crinoid columnals with large lumens. The grain shapes and the unit extinction serve to uniquely identify these grains as being of crinoidal origin.

PPL, HA = 10 mm

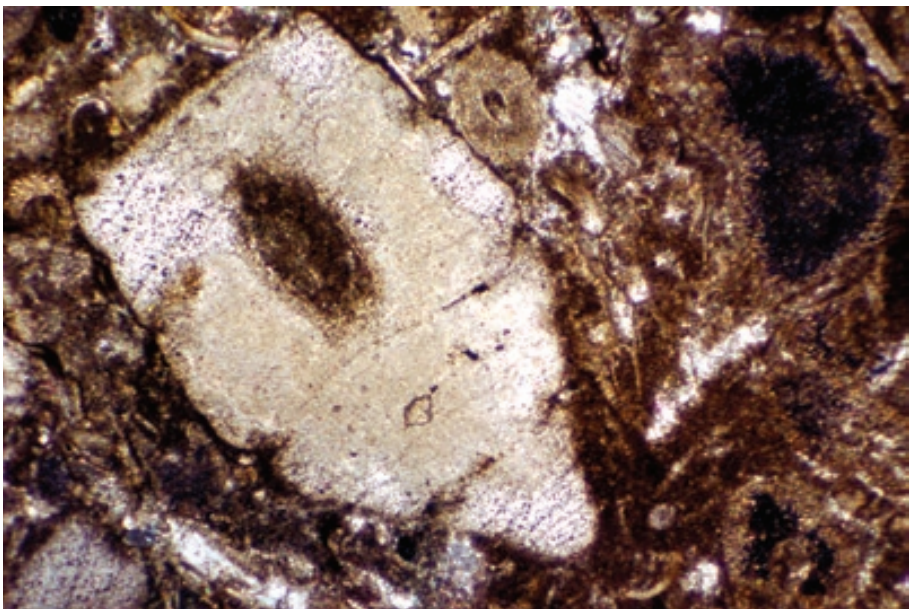

Up. Silurian Tonoloway-Keyser Ls., Mifflin Co., Pennsylvania

A crinoid fragment with single-crystal structure, a clearly displayed lumen (central canal) and much of the internal structure replaced by chert. Crinoid fragments are quite susceptible to this type of replacement.

PXPL, HA = 3.4 mm

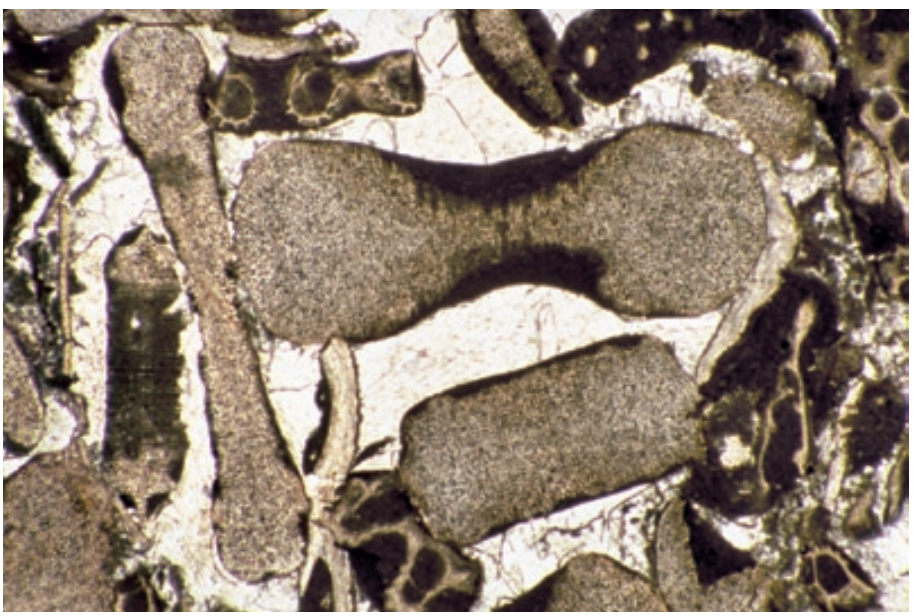

Up. Mississippian Hindsville Ls., Mayes Co., Oklahoma

A crinoidal limestone in which the discoidal crinoid plates are thickest at their margins and thinner in their interiors. The internal pores are completely filled with micritic carbonate giving the grains a characteristic "dusty" or speckled appearance at this magnification. At higher magnification, the regular arrangement of pores becomes more apparent.

PPL, HA = 3 mm

Pennsylvanian Marble Falls Ls., Burnet Co., Texas

A crinoid-rich sediment showing grains with circular and pentameral outlines. Five-fold symmetry is common to all members of the Echinodermata but is apparent in only a minority of crinoid grains. Note the "dusty" appearance of the crinoids due to micritic infills of the pores. The absence of syntaxial overgrowths also is a result of the presence of extensive micrite matrix around the grains.

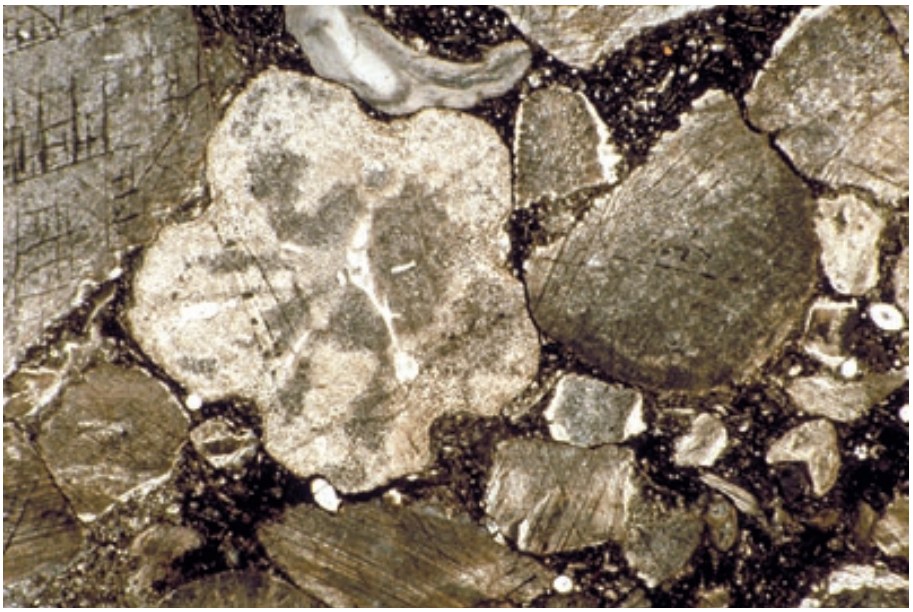

PPL, HA = 6 mm

Pennsylvanian Marble Falls Ls., Burnet Co., Texas

A crinoid showing the unit extinction (single-crystal extinction), traces of pore structure, and the axial canal common to this group. The grain has been substantially altered by cementation within pores, by organic boring (and filling of those borings with micrite), and by pressure solution along grain margins. All three of these alteration processes can complicate grain identification.

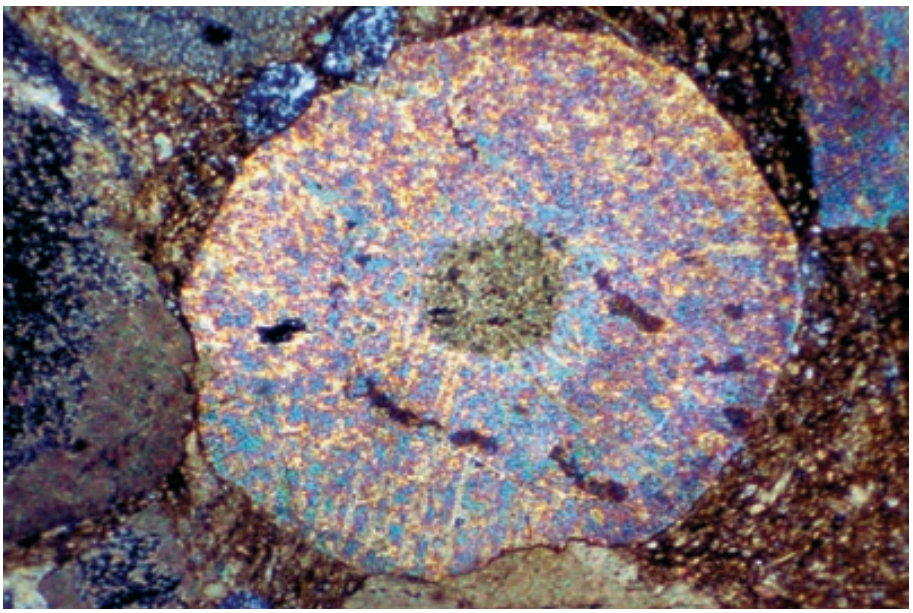

XPL, HA = 3.5 mm

Paleozoic limestone, midcontinent U.S.A.

A crinoid arm plate forms the nucleus of this ooid. Crinoid arm plates curve around an ambulacral groove which gives them their characteristic U-shape. Coupled with unit extinction and coarse pore structure, the shape definitively marks the grain as being of crinoidal origin. The presence of synsedimentary oolitic coatings on the grain prevented later diagenetic formation of syntaxial overgrowth cements.

PPL, HA = 0.52 mm

Up. Silurian Tonoloway-Keyser Ls., Mifflin Co., Pennsylvania

A crinoidal biomicritic limestone. Crinoids are commonly found as the dominant rock-forming element in both high- and low-energy shelfal strata. In this example, crinoids and bryozoans are the major faunal contributors and the crinoids are marked by their "dusty" appearance, five-fold symmetry elements, central lumen, and susceptibility to silica replacement (upper left).

PPL, HA = 12.5 mm

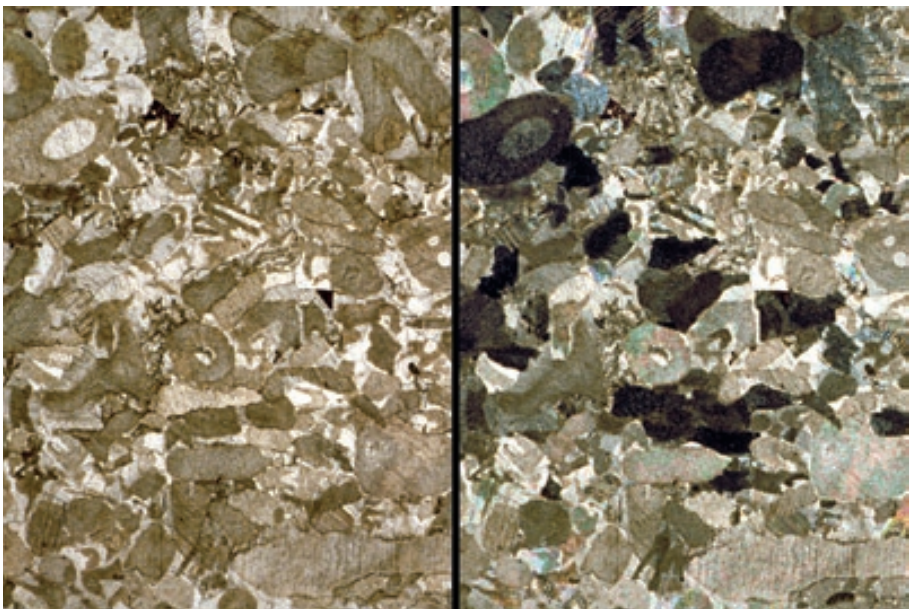

Up. Silurian Tonoloway-Keyser Ls., Mifflin Co., Pennsylvania

Plane- and cross-polarized views of a crinoidal grainstone (encrinite) fully cemented with syntaxial calcite overgrowths. The coarse, essentially single-crystal nature of crinoids (and other echinoderms) makes them extremely susceptible to syntaxial overgrowth cementation. Thus, crinoidal limestones are commonly marked by nearly complete porosity destruction, as in this example.

PPL/XPL, HA = 6.2 mm each

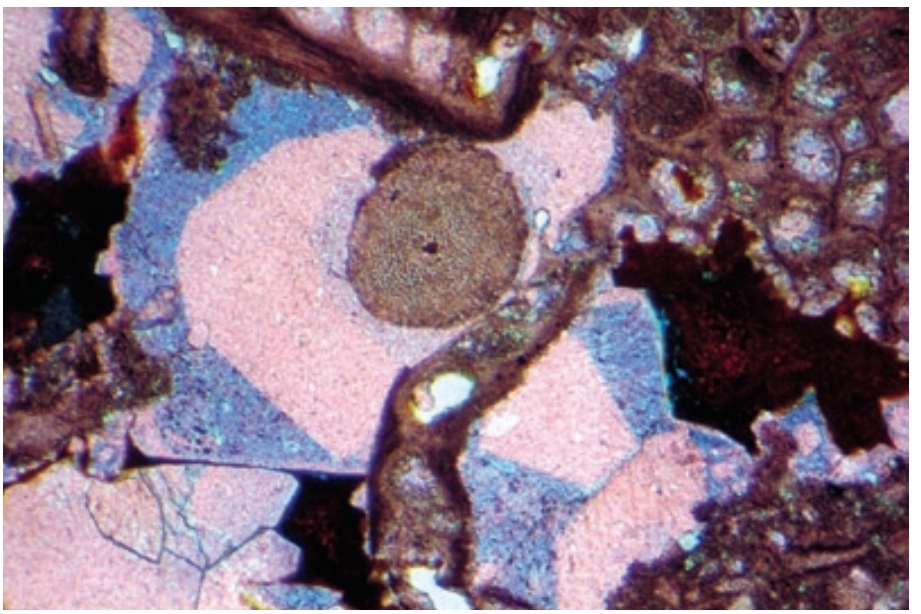

Up. Permian Park City Fm., Tosi Chert Mbr., Thermopolis, Wyoming

A bryozoan-crinoid packstone that is cemented by highly zoned, syntaxial overgrowths that formed preferentially on the crinoids. The zonation of iron content (marked by the differential staining) indicates that overgrowth formation probably took place over an extensive period of progressive burial. In this example, calcite cementation was followed by hydrocarbon filling of the remnant porosity (reddish-brown to opaque material).

PPL, AFeS, HA = ~ 5 mm

BLASTOIDS

Taxonomy and Age Range:

Phylum Echinodermata; Subphylum Blastozoa — Cambrian-Late Permian.
Class Blastoidea — Mid. Ordovician (but most commonly Mid. Silurian)-Late Permian.

Environmental Implications:

Blastoids are fully marine, open-shelf organisms with a very limited salinity range.

Skeletal Mineralogy:

Composed of calcite (probably originally high-Mg calcite).

Morphologic Features:

Blastoids were small, heavily calcified, relatively primitive, attached, stalked echinoderms with small pentagonal "heads" consisting of numerous calcite plates. Rarely a major rock-forming element and generally identified as crinoidal remains in thin section.

Carboniferous blastoid, midcontinent, U.S.A.

A complete head of a blastoid — *Pentremites godoni* (Defrance). The coarsely crystalline, cloudy calcite of the margins shows unit extinction (with slight undulosity due to the curvature of the test) under cross-polarized light. In this example, the blastoid test wall has been extensively replaced by authigenic silica (patchy brownish to white areas). The large area of coarse, unreplaced calcite at the center is pore- filling cement within the blastoid interior. The "up" position in life is at the left side of this image.

PPL, HA = 18 mm

Carboniferous blastoid, midcontinent, U.S.A.

Detailed view of the side margin of the partially silicified blastoid — *Pentremites godoni* (Defrance) — shown in the previous photograph. The calcite of the blastoid wall is cloudy due to the primary pore structure of the skeleton and shows unit extinction. The partial silica (chert and chalcedony) replacement appears gray and black in this cross-polarized light view.

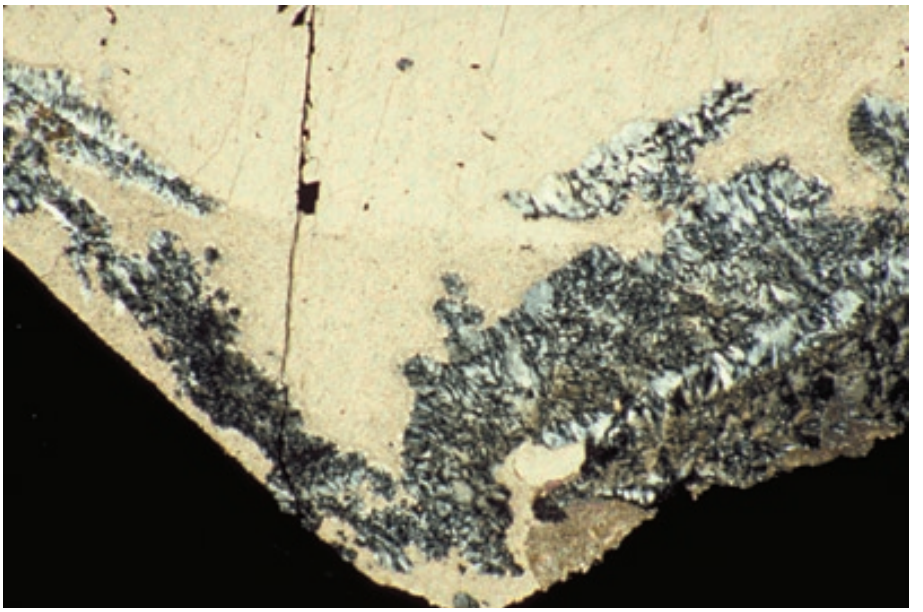

XPL, HA = 3.5 mm

HOLOTHURIANS

Taxonomy and Age Range:

Subphylum Echinozoa

Class Holothuroidea — Mid. Ordovician (possibly Mid. Cambrian)-Recent

Environmental Implications:

Holothurians (sea cucumbers) are fully marine organisms with a very limited salinity range and are widespread in both shallow- and deep-water environments.

Most are free-living (eleutherozoan), grazing or burrowing, sediment-ingesting echinoderms; pelagic/nektic and attached forms exist but are much less common.

Skeletal Mineralogy:

Sclerites are composed of intermediate- to high-Mg calcite; most modern forms contain 3 to 4 mole% Mg.

Morphologic Features:

Holothurians are tube- or sausage-like organisms. Unlike previously discussed echinoderms, they do not have a hard skeleton. Instead, their soft tissues contain microscopic calcite bodies (termed dermal plates or sclerites) that serve to stiffen the organism. Individual holothurians can contain millions of individual sclerites that are released into the sediments upon death of the organism.

Keys to Petrographic Recognition:

1. **Holothurian dermal plates occur in a variety of shapes including hooks, wheels, tables, anchors, perforated plates, rods and others.**
2. **Sclerites are small (typically 0.05 to 2 mm) and composed of single crystals of calcite. Rarely identifiable in thin section, but commonly found in washed samples and grain mounts of modern sediments; they are more rarely found in disaggregated samples of older strata.**
3. **Identification of ancient holothurian sclerites is based largely on comparison with modern forms; no absolute identification criteria exist.**

ASTEROIDS AND OPHIUROIDS

Taxonomy and Age Range:

Subphylum Asterozoa — Late Cambrian or Early Ordovician-Recent

Class Asteroidea (starfish) — Early Ordovician-Recent

Class Ophiuroidea (brittle stars) — Early Ordovician-Recent

Environmental Implications:

Marine grazing organism; modern forms have a wide range of life settings, from intertidal to abyssal water depths. Coastal forms can tolerate greater salinity variations than other echinoderms.

Skeletal Mineralogy:

High-Mg calcite as for other echinodermal groups.

Morphologic Features:

Relatively soft-bodied, most commonly five-armed organisms that have internal stiffening from numerous weakly calcified and very porous plates and spines

Keys to Petrographic Recognition:

1. **Plates are more variably and irregularly shaped than the plates of most other types of echinoderms.**
2. **Asteroids/ophiuroids have highly porous skeletal plates with unit extinction under cross-polarized light.**
3. **Plates normally are completely disarticulated and rarely form a significant percentage of total sediment volume.**

Representative forms of holothurian sclerites

The major types of sclerites found in modern holothurians (adapted from Frizzel and Exline, 1955, and Boardman et al., 1987). These microscopic ossicles are found embedded in the soft body of holothurians where they serve to stiffen the tissue. They range in size from 0.05 to 2 mm and have a wide variety of distinctive shapes.

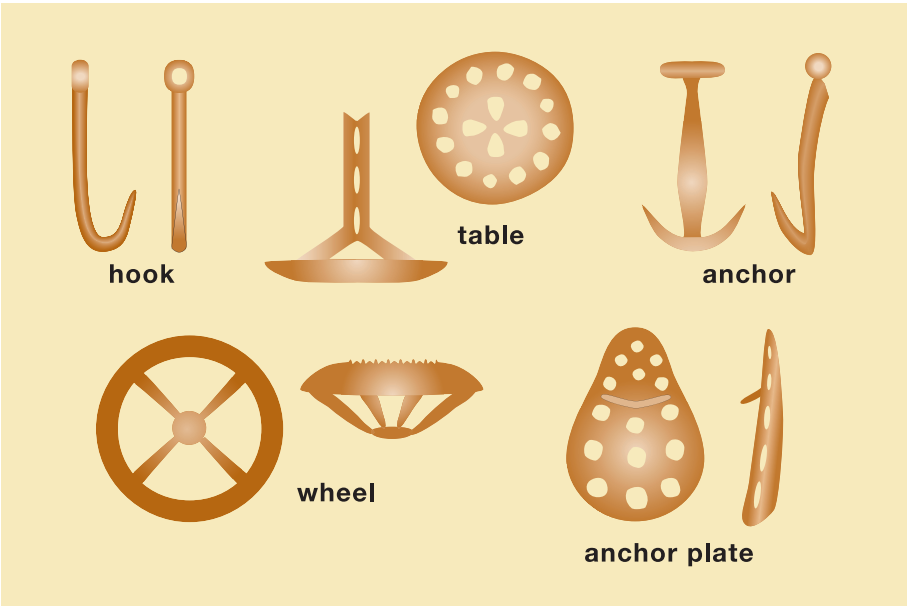

Recent sediment, Florida Keys, Monroe Co., Florida

A smear-mount photomicrograph depicting a variety of sclerites (dermal plates) obtained from the disaggregation of a single modern holothurian (sea cucumber), *Stichopus* sp. These calcitic plates are only rarely identified in ancient sedimentary rocks (although they are known from rocks at least as old as Mississippian). When they are found, it is primarily in grain mounts of disaggregated material, rather than in thin sections.

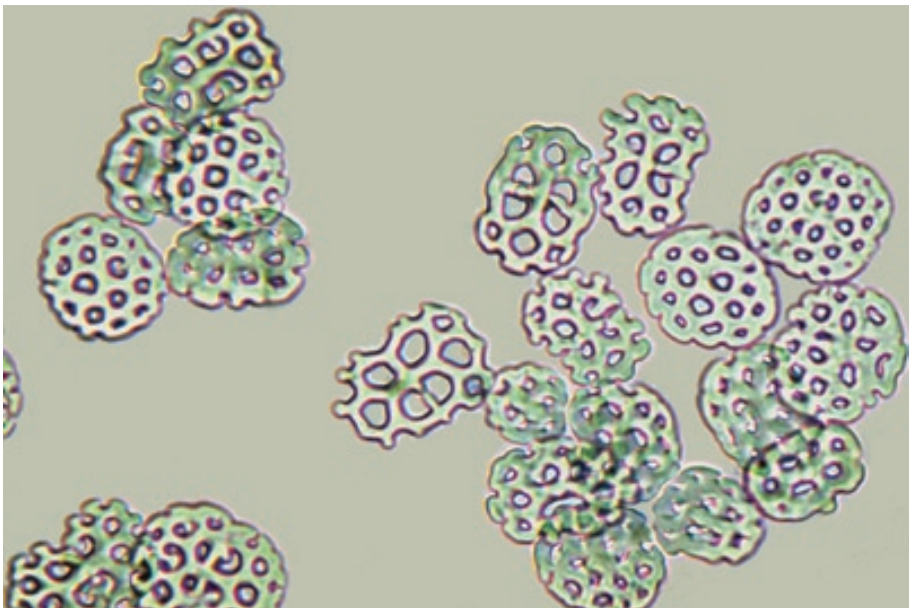

PPL, HA = 0.16 mm

Recent starfish, U.S.A.

Internal plates and spicules derived from the disaggregation of a single specimen of the starfish *Asterias* sp. Note the great variety of plate and spicule shapes and sizes. The blue color is due to the dyed epoxy that has penetrated the spongy (more than 50% intraparticle porosity) fabric of these single-crystal plates.

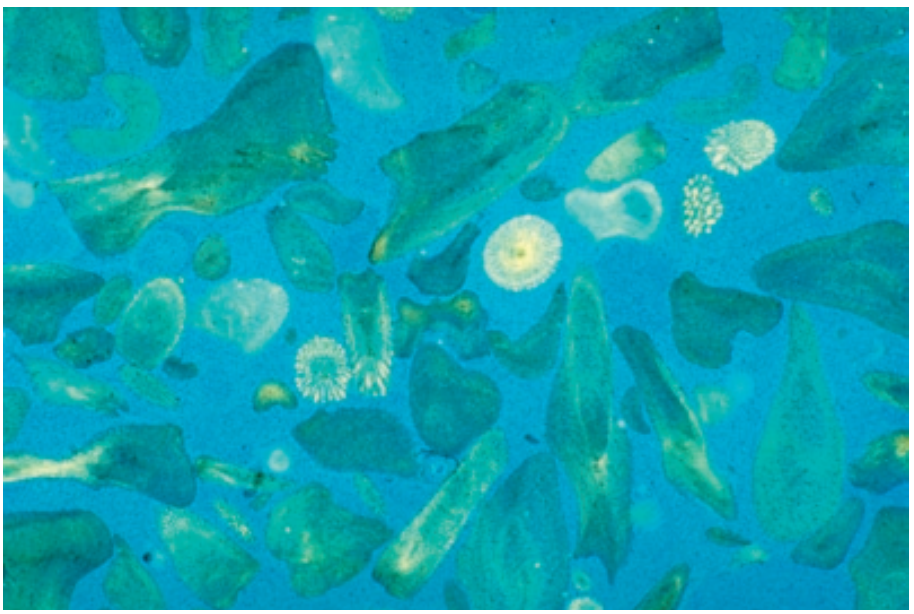

PPL, BSE, HA = 8 mm

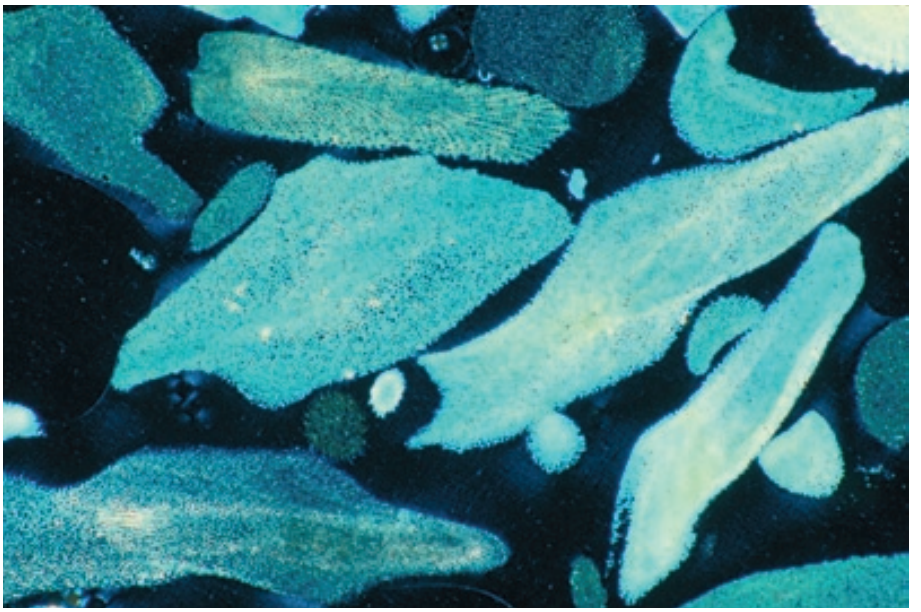

Recent starfish, U.S.A.

Detailed view of the internal plates and spicules derived from the disaggregation of a single specimen of the starfish *Asterias* sp. Note the great variety of plate shapes and sizes. The blue color is due to the dyed epoxy that has penetrated the spongy fabric of these single-crystal plates.

XPL, BSE, HA = 4 mm

Cited References and Additional Information Sources

Beaver, H. H., ed., 1967, Treatise on Invertebrate Paleontology, Part S, Echinodermata 1, General characters, Homalozoa, Crinozoa (except Crinoidea): Geological Society of America and University of Kansas Press, 296 p.

Blake, D. F., and D. R. Peacor, 1981, Biomineralization of crinoid skeletal elements using TEM and STEM microanalysis: Scanning Electron Microscopy, III, p. 321-328.

Dickson, J. A. D., 1995, Paleozoic Mg calcite preserved: Implications for the Carboniferous ocean: Geology, v. 23, p. 535-538.

Dickson, J. A. D., 2001, Diagenesis and crystal caskets: echinoderm Mg calcite transformation, Dry Canyon, New Mexico, U.S.A: Journal of Sedimentary Research, v. 71, p. 764-777.

Donnay, G., and D. L. Pawson, 1969, X-ray diffraction studies of echinoderm plates: Science, v. 166, p. 1147-1150.

Durham, J. W., 1966, Asterozoa-Echinozoa, *in* R. C. Moore, ed., Treatise on Invertebrate Paleontology, Part U, Echinodermata 3: Geological Society of America and University of Kansas Press, 366 p.

Evamy, B. D., and D. J. Shearman, 1965, The development of overgrowths from echinoderm fragments: Sedimentology, v. 5, p. 211-233.

Evamy, B. D., and D. J. Shearman, 1969, Early stages in development of overgrowths on echinoderm fragments in limestones: Sedimentology, v. 12, p. 317-322.

Frizzell, D. L., and H. Exline, 1955, Monograph of fossil holothurian sclerites: University of Missouri School of Mines and Metallurgy Bulletin No. 89, 203 p.

Glazek, J., and A. Radwanski, 1968, Determination of brittle star vertebrae in thin sections: Bulletin de l'Academie Polonaise des Sciences. Serie des Sciences Geologiques et Geographiques, v. 16, no. 2, p. 91-96.

Groiss, J. T., 1964, Echinodermenreste in Schlaemmproben aus dem Weissen Jura der Franken-Alb: Geologische Blätter für Nordost-Bayern und Angrenzende Gebiete, v. 14, no. 2, p. 45-53.

Hyman, L. H., 1955, The Invertebrates: Echinodermata IV: New York, McGraw-Hill Book Co., 763 p.

Manze, U., and D. K. Richter, 1979, Die Veränderung des C^{13}/C^{12}-Verhältnisses in Seeigelcoronen bei der Umwandlung von Mg-Calcit in Calcit unter meteorisch-vadosen Bedingungen: Neues Jahrbuch für Geologie und Palaeontologie, Abhandlungen, v. 158, no. 3, p. 334-345.

Milliman, J. D., 1974, Marine Carbonates. Part 1, Recent Sedimentary Carbonates: New York, Springer-Verlag, 375 p.

Moore, R. C., C. G. Lalicker, and A. G. Fischer, 1952, Invertebrate Fossils: New York, McGraw-Hill Book Co., 766 p.

Mostler, H., 1971, Ophiurenskelettelemente (äussere Skelettanhänge) aus der alpinen Trias: Geologisch-Paläontologische Mitteilungen Innsbruck, v. 1, no. 9, p. 1-35.

Mostler, H., 1972, Holothuriensklerite der alpinen Trias und ihre stratigraphische Bedeutung: Nachbargebiete Mitteilungen der Gesellschaft der Geologie- und Bergbaustudenten in Oesterreich, v. 21, no. 2, p. 729-744.

Nissen, H. U., 1969, Crystal orientation and plate structure in echinoid skeletal units: Science, v. 166, p. 1150-1152.

Raup, D. M., 1958, The relation between water temperature and morphology in *Dendraster*: Journal of Geology, v. 66, p. 668-677.

Raup, D. M., 1959, Crystallography of echinoid calcite: Journal of Geology, v. 67, p. 661-674.

Raup, D. M., 1962, The phylogeny of calcite crystallography in echinoids: Journal of Paleontology, v. 36, p. 793-810.

Raup, D. M., 1966, Crystallographic data for echinoid coronal plates: Journal of Paleontology, v. 40, p. 555-568.

Richter, D. K., 1974, Zur subaerischen Diagenese von Echinidenskeletten und das relative Alter pleistozäner Karbonatterrassen bei Korinth (Griechenland): Neues Jahrbuch für Geologie und Palaeontologie, Abhandlungen, v. 146, no. 1, p. 51-77.

Rioult, M., 1965, Sclerites d'holothuries tertiaires (eocene du bassin de Paris et miocene du bassin d'Aquitaine): Revue de Micropaleontologie, v. 3, p. 165-174.

Schroeder, J. H., E. J. Dwornik, and J. J. Papike, 1969, Primary protodolomite in echinoid skeletons: Geological Society of America Bulletin, v. 80, p. 1613-1616.

Sprinkle, J., and P. M. Kier, 1987, Phylum Echinodermata, *in* R. S. Boardman, A. H. Cheetham, and A. J. Rowell, eds., Fossil Invertebrates: Palo Alto, CA, Blackwell Scientific Publications, p. 550-611.

Strimple, H. L., 1972, Porosity of a fossil crinoid ossicle: Journal of Paleontology, v. 46, p. 920-921.

Towe, K. M., 1967, Echinoderm calcite: single crystal or polycrystalline aggregate: Science, v. 157, p. 1048-1050.

Facing Page: Macrophotograph of a trilobite, *Phacops* sp., from the Devonian of Morocco. Sample from the New Mexico Museum of Natural History and Science, courtesy of Spencer Lucas.

GRAINS: Skeletal Fragments

ARTHROPODS

CHAPTER 11

Trilobites

Ostracodes

Barnacles

TRILOBITES

Taxonomy and Age Range:

Phylum Arthropoda
Superclass Trilobitomorpha
Class Trilobita — Early Cambrian (late Proterozoic?)-Late Permian

Environmental Implications:

Most trilobites were mobile, benthic, detritus feeding, fully marine organisms with a limited salinity tolerance (they are not found in inferred salinity-stressed settings). A few groups of pelagic trilobites are known.

Although most common in shallow shelf settings, trilobites, especially eyeless forms, are also found in deeper-water environments. They are major rock-forming elements mainly in shallow shelf deposits of Cambro-Ordovician age.

Skeletal Mineralogy:

Trilobite carapaces were composed of chitin with large amounts of calcium carbonate and variable amounts of calcium phosphate (up to 30% in some species). The carbonate consisted of calcite, probably with moderate to high Mg content.

Morphologic Features:

Trilobites were characterized by exoskeletal carapaces with three lobes that extended the length of the organism. Carapaces were divided into a head shield (cephalon), an abdominal section (thorax) with 2 to 40 segments (sclerites), and a tail shield (pygidium).

The shields and segments were sharply recurved inwards along the margins of the organism. Carapaces were shed during growth stages (molting behavior) adding to the large numbers of trilobite grains in many sedimentary deposits.

Adult trilobites ranged in length from 0.1 to 75 cm; they average about 5 cm in length and 1-3 cm in width.

Keys to Petrographic Recognition:

1. **The segmented nature of the carapaces, coupled with trilobite molting behavior, means that these organisms are normally found as fragmentary remains. Individual segments typically are in the mm to cm length range and are less than a mm in thickness.**
2. **The recurved margins of trilobite shields and the multidirectionally curved forms of thoracic segments (sclerites) yielded fragments that commonly have characteristic "hook" or "shepherd's crook" shapes.**
3. **Skeletal fragments have a homogeneous prismatic microstructure, with extremely fine (micrometer-scale) calcite prisms oriented perpendicular to the carapace surface. Typically, the wall appears smooth and uniform with no obvious crystals; trilobite fragments, however, show sweeping (undulose) extinction when rotated under cross-polarized light. Some trilobites may also have finely lamellar layers.**
4. **Many specimens show small perforations (canaliculi) that trend perpendicular to the skeletal walls.**
5. **Fine growth lines may be visible — they parallel the carapace surface but do not interrupt the continuity of calcite prisms**
6. **Trilobite fragments can be visibly multilayered, with thin inner or outer layers over the main carapace wall. Outer layer can be organic rich with a dark coloration in transmitted light.**
7. **Homogeneous prismatic wall structure (and consequent extinction behavior) of trilobites is similar to that shown by ostracodes and a few bivalves. Trilobite fragments, however, generally are larger than ostracodes and are more irregular in curvature than either ostracodes or bivalves.**

PHOTO SCALES AND ABBREVIATIONS ARE EXPLAINED IN THE BOOK'S INTRODUCTION

Characteristic features of trilobite carapaces

This diagram (adapted from Majewske, 1969) illustrates the main features of trilobite carapaces. It clearly shows the three-lobed body construction (in plan view), the details of both the head and tail shields (the cephalon and pygidium, respectively), and the thoracic segments or sclerites. Because these parts were held together with soft tissue, trilobites disarticulated relatively readily.

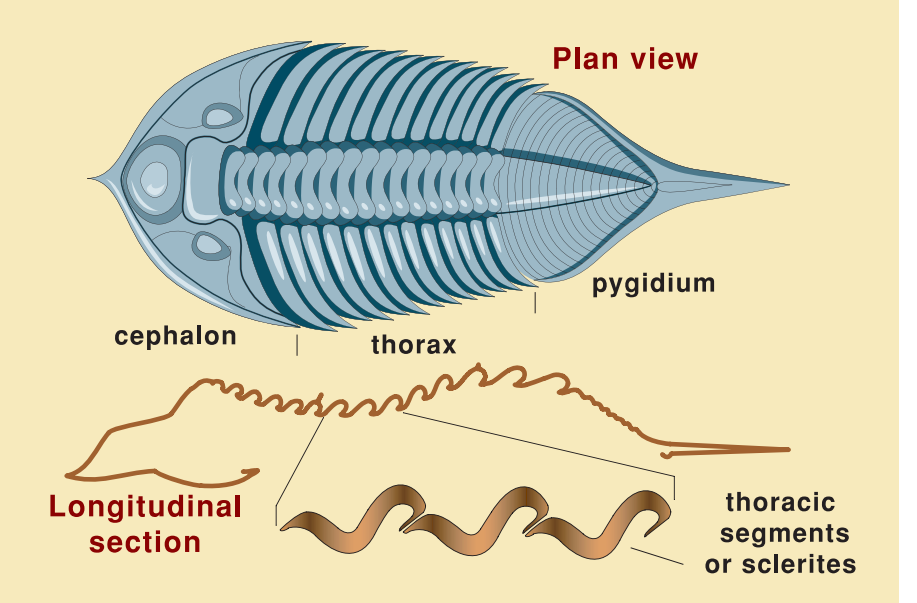

Lo. Ordovician El Paso Gp., Franklin Mountains, Texas

A transverse cut through an unusually complete trilobite carapace showing the highly recurved nature of the calcitic skeleton. These fossils are more commonly found broken into smaller fragments that show shapes like boomerangs or shepherd's crooks. Note also the very finely homogeneous nature of the carapace wall.

PPL, HA = 6.0 mm

Lo. Ordovician El Paso Gp., Franklin Mountains, Texas

Same field of view as previous photograph. Note the characteristic extinction bands that sweep through the grain as the stage is rotated under cross-polarized light. Such extinction behavior results from the uniform orientation of minute calcite prisms perpendicular to the carapace margin.

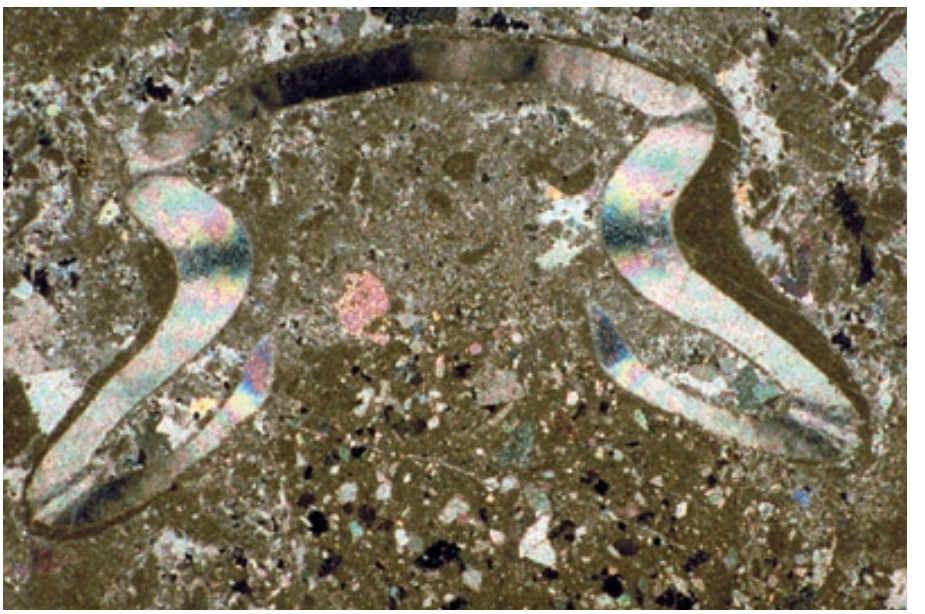

XPL, HA = 6 mm

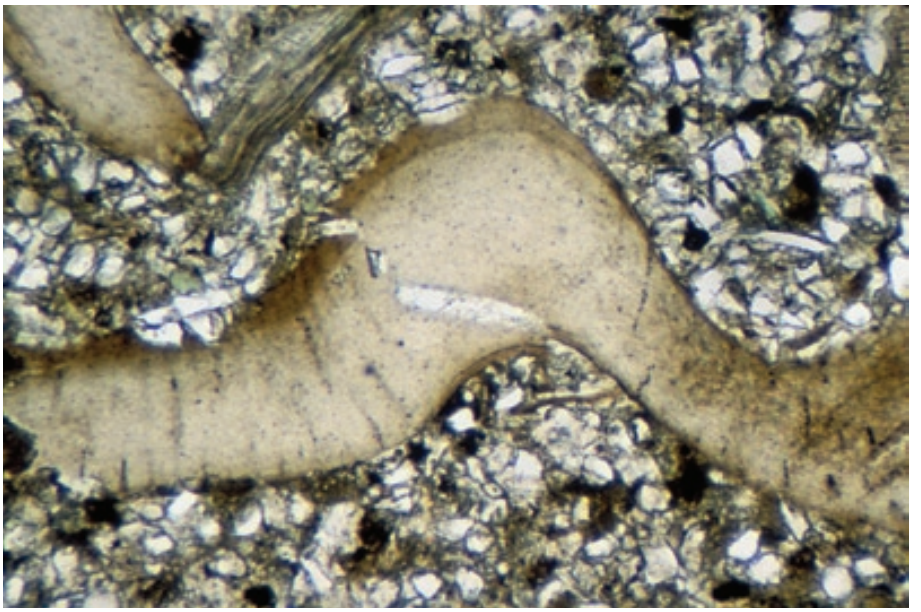

Mid, Ordovician Reedsville Fm., Mifflin Co., Pennsylvania

This trilobite fragment shows characteristic complex curvature of the shell and homogeneous prismatic shell structure (essentially showing no visible crystal structure at this magnification). The presence of tubular pores and a slightly brownish carapace color (due to the chitinous and organic constituents of the shell) are also characteristic of trilobites.

PPL, HA = 3.5 mm

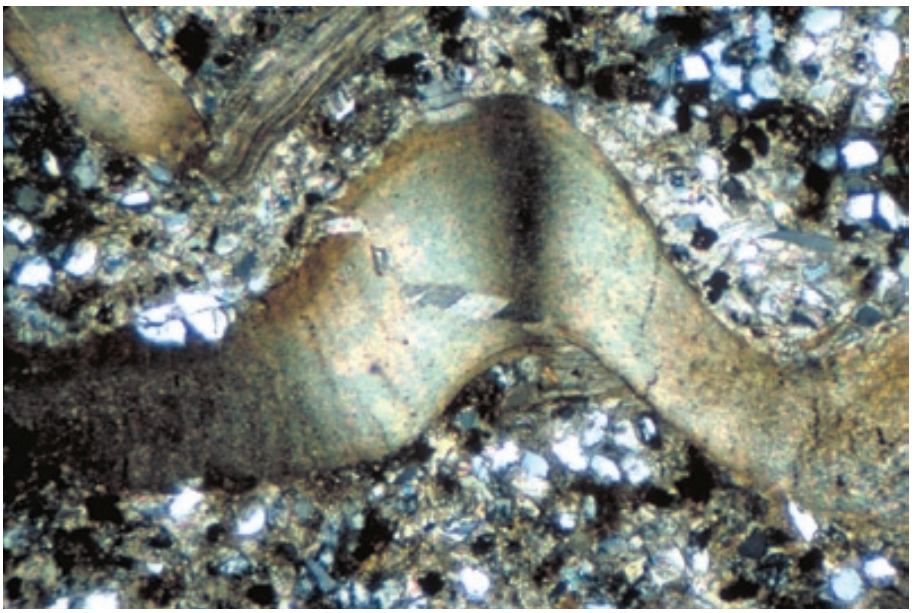

Mid. Ordovician Reedsville Fm., Mifflin Co., Pennsylvania

Same view as above but under cross-polarized light. Note the characteristic dark extinction bands at the center and left of the grain (the parts of the grain where the shell margins are perpendicular/parallel to the microscope cross hairs (not shown). This extinction pattern reflects the orientation of tiny prismatic crystals perpendicular to the carapace wall. As the grain is rotated under cross-polarized light, the extinction bands sweep through the entire grain.

XPL, HA = 3.5 mm

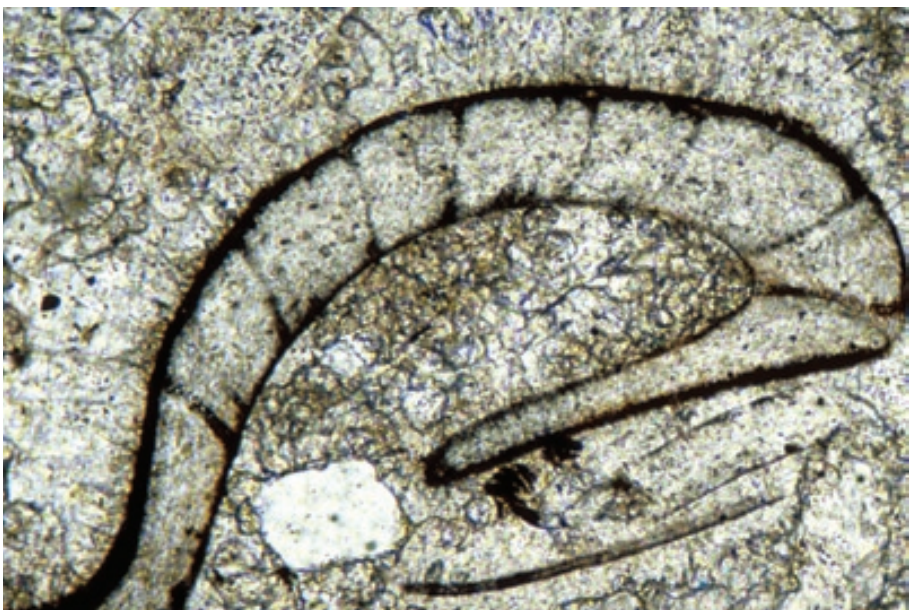

Mid. Ordovician Simpson Gp., Oil Creek Fm., Murray Co., Oklahoma

A curved trilobite fragment with a characteristic shepherd's crook shape. Note variations in carapace thickness along the length of the grain. Micritic encrustations on the surface of the grain extend into the exterior portions of carapace pores (canaliculi), enhancing their visibility relative to areas filled with later, clear calcite cement.

PPL, HA = 1.2 mm

Mid. Ordovician Reedsville Fm., Mifflin Co., Pennsylvania

A curved trilobite fragment with large and well-defined pores (caniculi) that pass through the entire carapace in an orientation roughly perpendicular to the shell surface. These features are characteristic of trilobites, but can be mistaken for the punctae found in some brachiopod shells. The homogeneous prismatic structure of trilobite carapaces, however, allows for reliable differentiation from the more complex structure of brachiopod shells.

PPL, HA = 0.62 mm

Mid. Ordovician Simpson Gp., Oil Creek Fm., Murray Co., Oklahoma

A curved trilobite fragment with well-defined pores (canaliculi) here cut oblique to their long axis. These features are quite clearly visible, especially where filled with organic matter, glauconite or other materials that contrast with the calcite of the shell itself. The slightly ferroan composition of the shell (shown by the purple stain) is common in many Cambro-Ordovician trilobites.

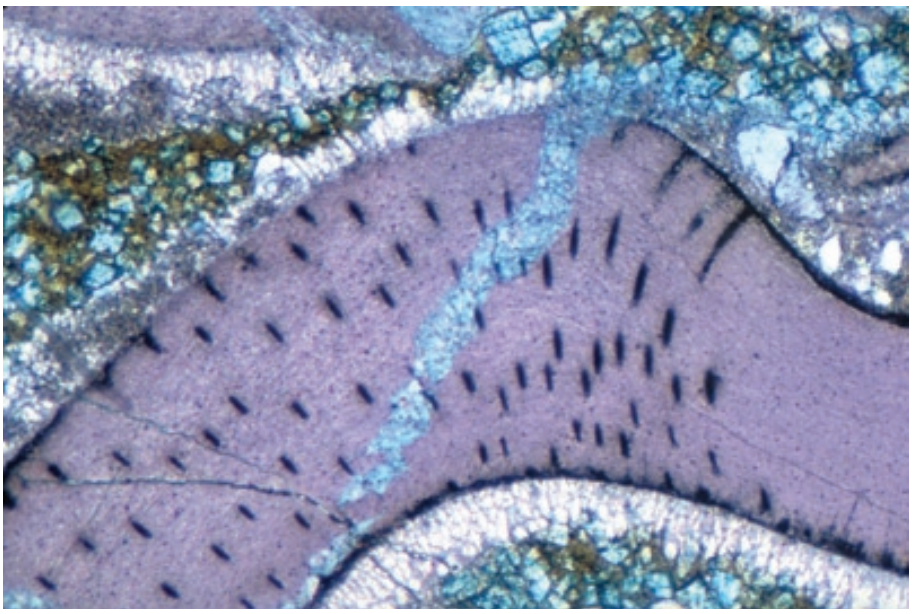

PPL, AFeS, HA = 1.9 mm

Mid. Ordovician Reedsville Fm., Mifflin Co., Pennsylvania

An example of a trilobite-rich sediment with numerous broken fragments of trilobite material set in a matrix of terrigenous sand and comminuted carbonate skeletal grains. The multiple extinction bands that reflect the oriented prismatic crystal structure in trilobite carapaces also are visible.

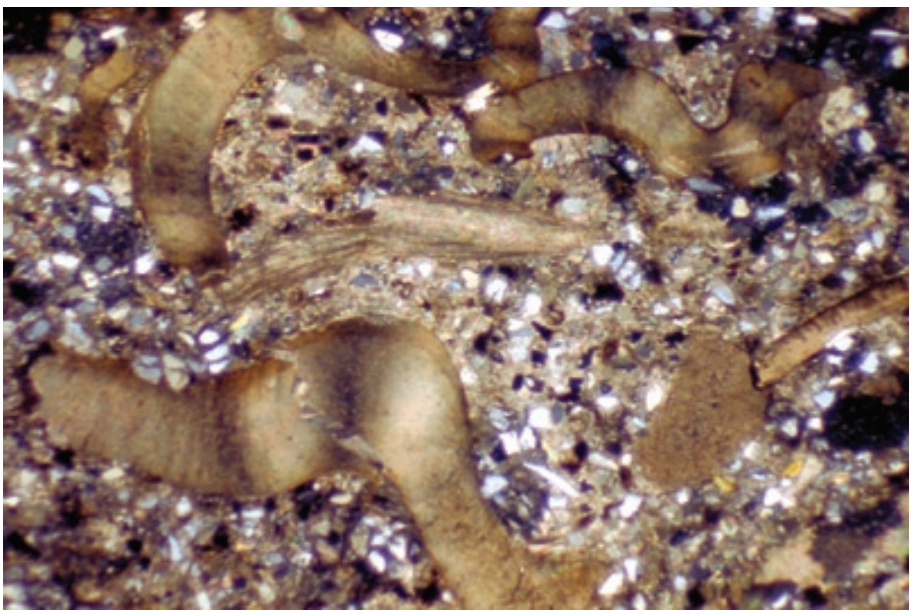

XPL, HA = 3.6 mm

OSTRACODES

Taxonomy and Age Range:

Phylum Arthropoda
Superclass Crustacea
Class Ostracoda — Early Cambrian-Recent

Divided into five orders, of which the Archaeocopida, Leperditicopida and Paleocopida became extinct in the Paleozoic.

Ostracode genera commonly have short stratigraphic ranges and wide geographic distribution making them valuable for stratigraphic studies, especially in brackish-water and non-marine settings.

Environmental Implications:

Ostracodes (also termed ostracods) are aquatic organisms with benthic, or more rarely planktic/nektic, lifestyles. Many burrow into muddy sediment and most are omnivorous scavengers.

Ostracodes are distributed from arctic to tropical latitudes. They are common in fresh, brackish and marine waters and extend into hypersaline settings as well. They rarely are major sediment formers, however, except in stressed (especially brackish, hypersaline, or freshwater) environments.

Skeletal Mineralogy:

Ostracode carapaces are composed of chitin and calcite; some are entirely composed of chitin. The calcite typically ranges from low- to high-Mg concentration (1-5 mole% Mg) but Mg contents as high as 10 mole% have been reported.

Morphologic Features:

Ostracodes have carapaces consisting of pairs of generally unequal valves that are shed during molting cycles. Molting results in an unusual abundance of disarticulated valves in sediments.

Ostracode valves commonly are ovoid in shape and their surfaces may be smooth or ornamented with grooves, ridges, nodes or other features. The carapaces recurve at the margins (duplicature).

Most adult ostracodes are less than 1 to 2 mm in length; marine forms of 20-40 mm size are known, however.

Keys to Petrographic Recognition:

1. **Ostracodes have small, generally thin, curved carapaces that can look like molluscan bivalves but typically are smaller than most bivalve shells.**
2. **Ostracodes molt and grow new carapaces, so their valves do not have growth lines as do molluscan bivalve shells — this helps distinguish large ostracodes from bivalves.**
3. **Ostracode valves typically have an outer calcareous and an inner chitinous layer; various genera exhibit between 2 and 9 layers in their shells; some are known with phosphatic layers.**
4. **Ostracode walls may be perforated by numerous very small, tubular canals. Such pores are rarely petrographically visible in fossil occurrences, probably because of filling with cements.**
5. **Ostracode valves, unlike bivalve shells, have recurved (fish-hook-like) edges and one valve commonly overlaps the other along one or more margins.**
6. **The calcitic layers of ostracode valves are normally well preserved; they have homogeneous prismatic and finely prismatic microstructures with crystal orientation perpendicular to carapace margins. Thus, they show sweeping extinction patterns (extinction bands moving along the length of the shell as the section is rotated under cross-polarized light). This too differentiates them from most (but not all) bivalve shells.**
7. **Ostracode shells may show a localized thickening at the central (sulcus) area.**

Typical ostracode carapace morphology and structure

This diagrammatic view of a typical ostracode depicts some of the characteristic features of the overlapping carapace valves and multilayered shell walls as well as the extinction banding visible under cross-polarized light.

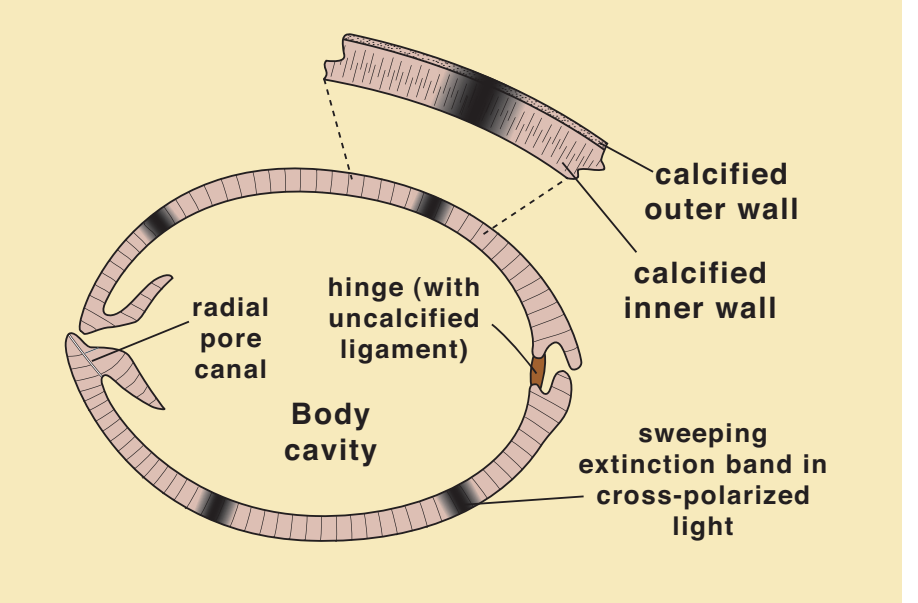

Recent, Belize

An SEM image of the surface of an ostracode, probably of the genus *Cativella*, showing an irregular carapace decorated with small perforations and spiny protrusions.

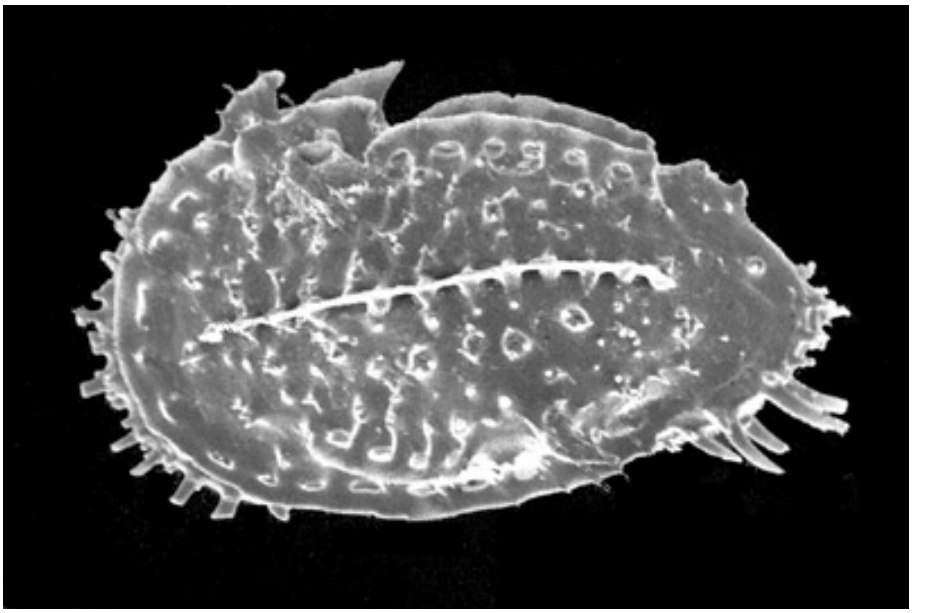

SEM, HA = 1.2 mm

Pliocene, U.S.A.

An SEM image of a smooth-surfaced, calcareous ostracode carapace (probably of the genus *Candona*). Note the overlap of the two valves and the central depression on the one valve (known as a sulcus). Photograph courtesy of Walter E. Dean (photograph taken by Richard M. Forester).

SEM, HA = 0.75 mm

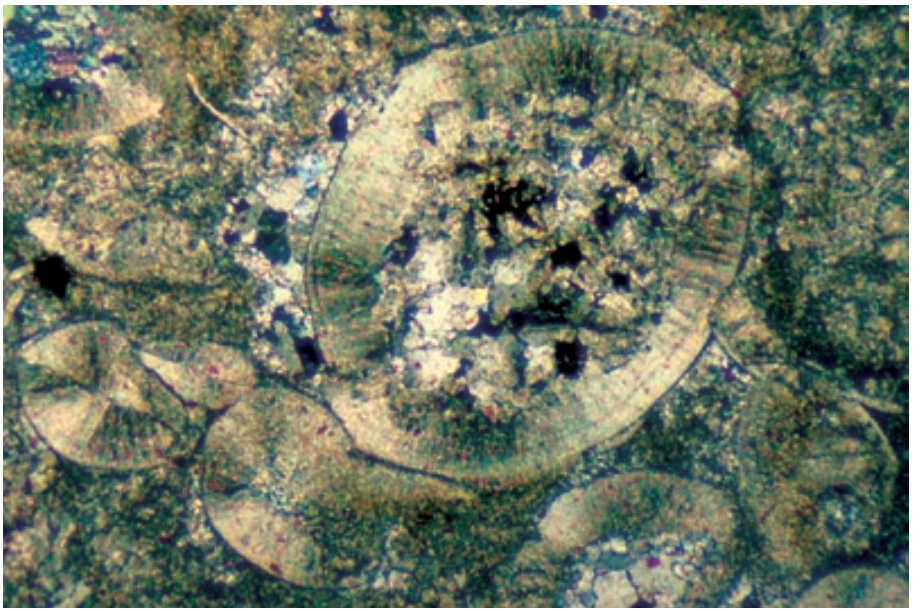

Up. Mississippian Arroyo Peñasco Gp., Terrero Fm., near Montezuma, New Mexico

Large, relatively thick-walled, articulate ostracode shells. Note multiple shell layers and thick cements in internal cavities. The cements have grown in optical continuity with the finely prismatic crystals of the carapace (oriented perpendicular to the carapace margin). Sweeping extinction bands in shells and cement mark this crystal orientation when the stage is rotated.

XPL, HA = 0.9 mm

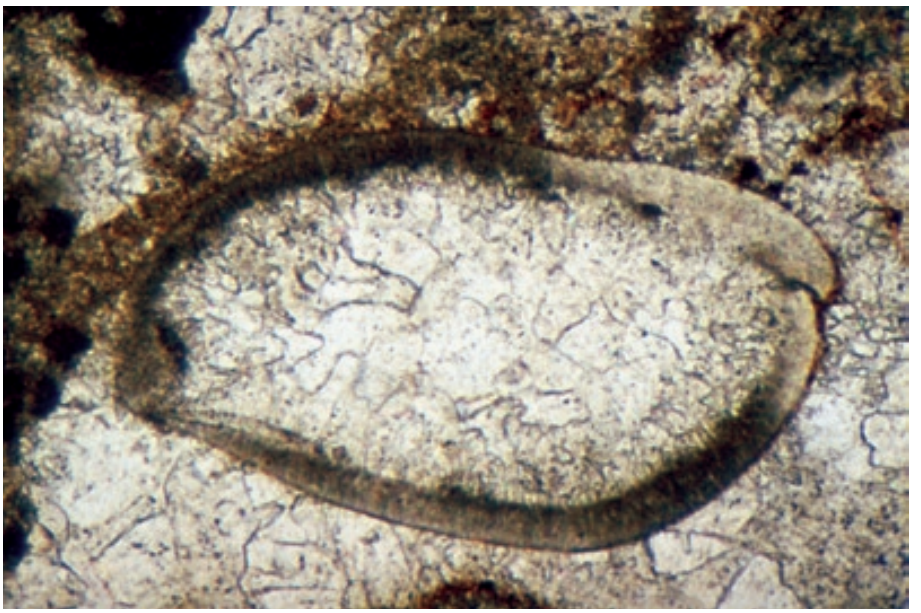

Up. Devonian (Frasnian) Pillara Ls., Canning Basin, Western Australia

A whole ostracode carapace. The shell shows the homogeneous to radial-fibrous shell structure characteristic of this group which also affected the precipitation of early-stage "syntaxial" cements in the carapace interior. Note also the overlap of the two valves.

PPL, HA =1.6 mm

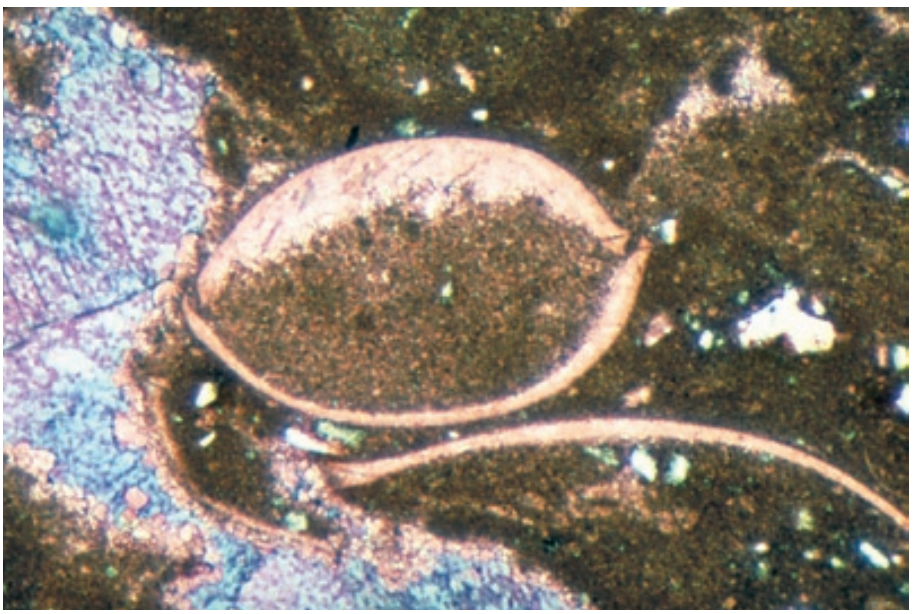

Up. Permian Zechstein Z1, Bolechowice, Poland

Ostracode carapaces from a marginal marine setting. The complete ostracode shows overlap of valves and a geopetal internal sediment fill.

PPL, AFeS, HA = 1.6 mm

Lo. Miocene Lower Otekaike Ls., northern Otago, New Zealand

A fish-hook-like termination of a single ostracode valve. These terminations are distinctive and, in combination with carapace size, structure, and wall morphology, help to reliably identify ostracode remains.

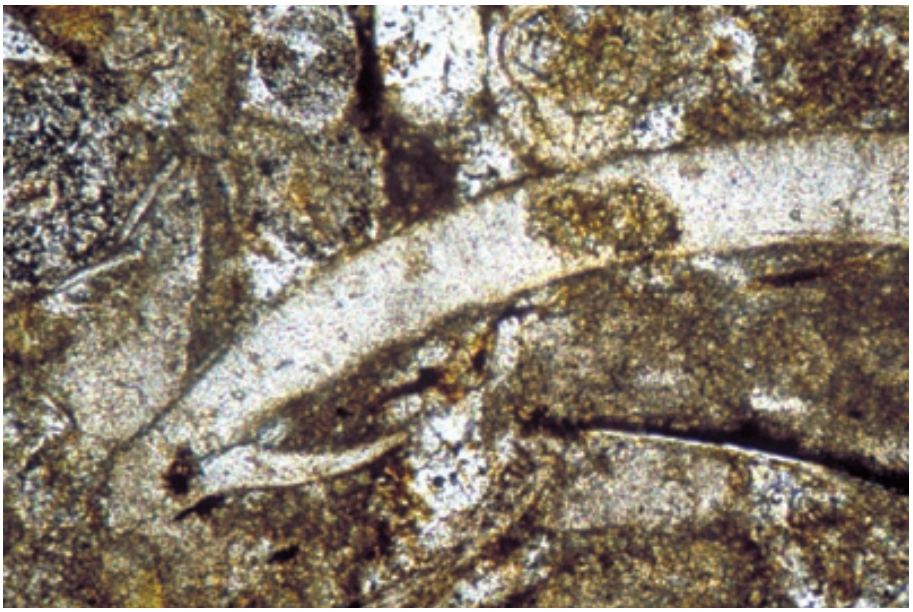

PPL, HA = 0.25 mm

Oligocene Top Globigerina Limestone Fm., Gozo, Malta

A pair of fish-hook-like terminations (recurved margins) of the two valves of an ostracode carapace. The presence of such overlapping margins and the absence of interlocked hinged terminations help distinguish ostracodes from small bivalves.

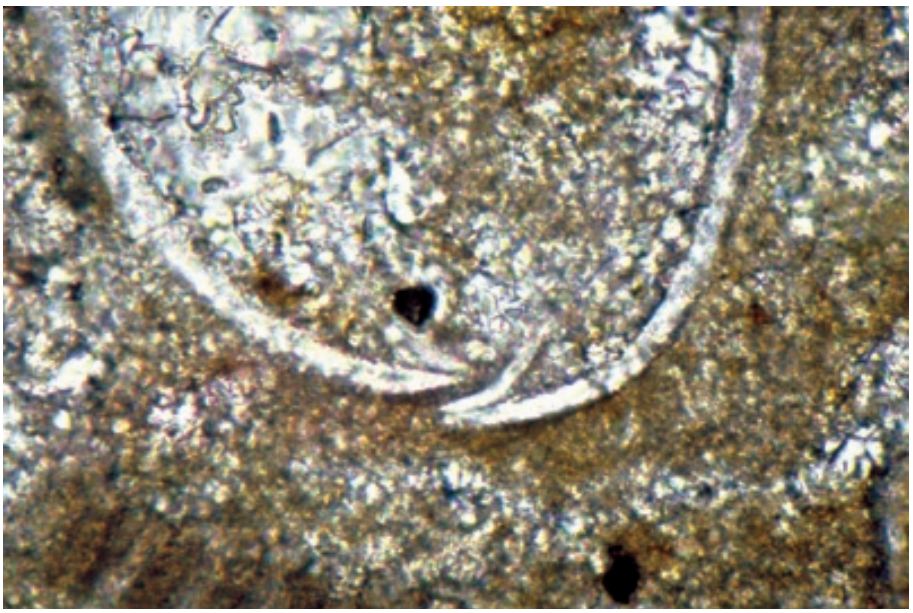

PPL, HA =0.25 mm

Mid. Ordovician limestone, Kingston, Ontario, Canada

Large Leperditid ostracodes with a straight segment of a trilobite shell for comparison. A good example of a limestone in which ostracodes make up a significant portion of the total deposit.

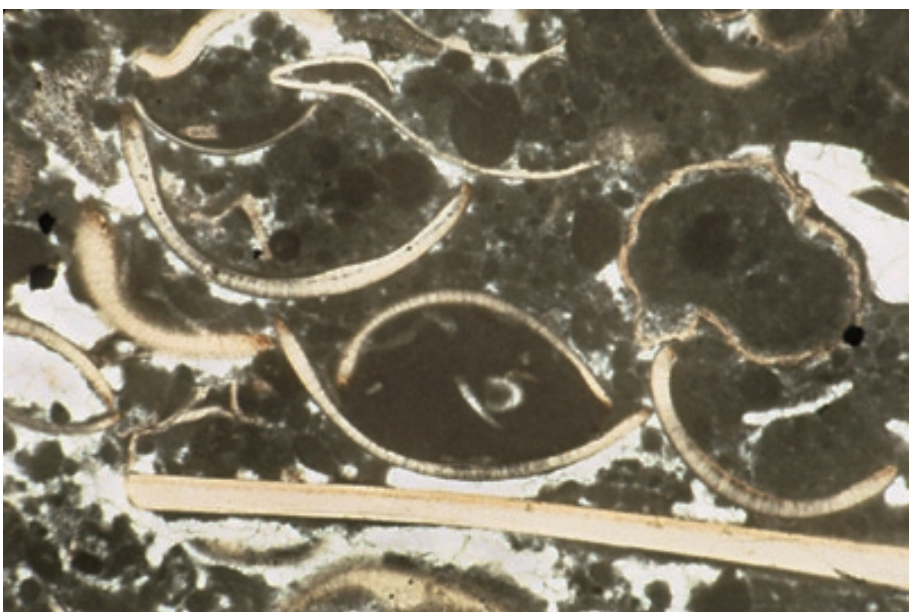

PPL, HA = 4 mm

BARNACLES

Taxonomy and Age Range:

Phylum Arthropoda
Superclass Crustacea
Class Cirripedia — Silurian-Recent

Members of the Suborder Balanomorpha are the most heavily calcified barnacles.

Barnacles have a long geologic record, but they are significant sediment formers only in local areas of Cretaceous and Cenozoic (especially Pliocene to Holocene) deposition.

Environmental Implications:

Barnacles are entirely marine organisms requiring hard substrates for attachment — thus, they thrive in some high-energy environments. They are commonly found attached to rocks or other hard substrates in shallow-marine to intertidal settings, but are also present in neritic settings. Rock boring forms also are common.

Barnacles are a significant component of shallow marine, temperate- and high-latitude carbonate deposits; they are far less common in warmer-water settings.

Skeletal Mineralogy:

Barnacle plates are composed of low-Mg calcite (typically less than 1 mole% Mg) although the basal attachment disc may be aragonitic. Aragonitic attachment plates are more common in warm- rather than cold-water areas as they tend to dissolve in colder waters.

Morphologic Features:

Barnacles have a motile larval stage that posesses a carapace similar to a smooth-shelled ostracode. Adult forms are sessile and secrete a series of calcitized plates. Most barnacles have a discoidal attachment plate that is cemented to hard substrates. Immovable, compartmentalized, calcitic wall plates (usually 6 to 8 in number) are attached to the basal plate and house the organism with its many delicate feeding appendages. Moveable opercular plates are used to seal off the living chamber during times of stress (e.g., low tide exposure).

Whole barnacles are of mm to cm size; fragments usually are in the mm size range.

Keys to Petrographic Recognition:

1. **The low-Mg calcite composition of most barnacle hard parts means that plate structure typically is well preserved.**
2. **Barnacles live primarily in high-energy coastal or shallow shelf environments and shed their plates during molting. Thus, most barnacle fragments are strongly abraded (rounded), although they still tend to have triangular shapes. Barnacle plates and fragments normally are in the mm size range.**
3. **The ribbed and furrowed, partially hollow nature of barnacle wall plates produces characteristic plicated (molar-like) structure in the laminated plates.**
4. **The longitudinal tubules that run through the plates produce a vesicular fabric and can give plates a hollow appearance.**
5. **Skeletal fragments have homogeneous (granular) or foliated microstructure.**
6. **Largely intact barnacles sometimes can be found as encrusters on other organisms or on lithified surfaces (hardgrounds).**

Characteristic features of a representative barnacle

A diagram (modified in part from Moore et al, 1952) that illustrates the main features of modern balanomorph barnacles. Upper left: view of a whole barnacle with cover plates largely closed. Upper right: cross section of a whole barnacle showing orientation of plates and organism. Lower left: view of a single plicated plate. Lower right: cross section of a single plate showing tubular internal structure.

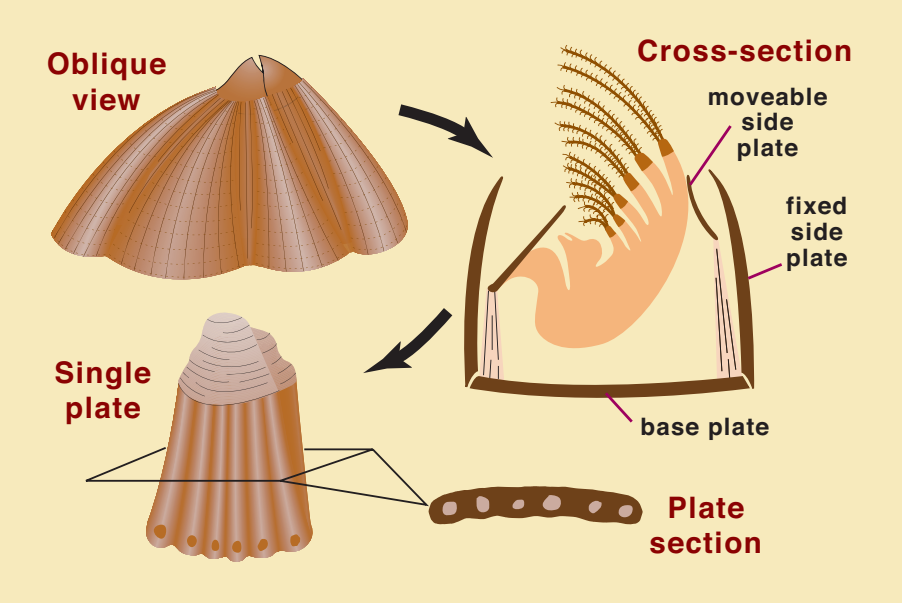

Pleistocene Caloosahatchee Fm., Hendry Co., Florida

A barnacle encrusting an oyster shell. The short white lines mark the approximate contact of the barnacle wall plates and base plate with the underlying vesicular oyster shell. The barnacle shows "tubular" structure in the base plate and complex structure in its side wall plates.

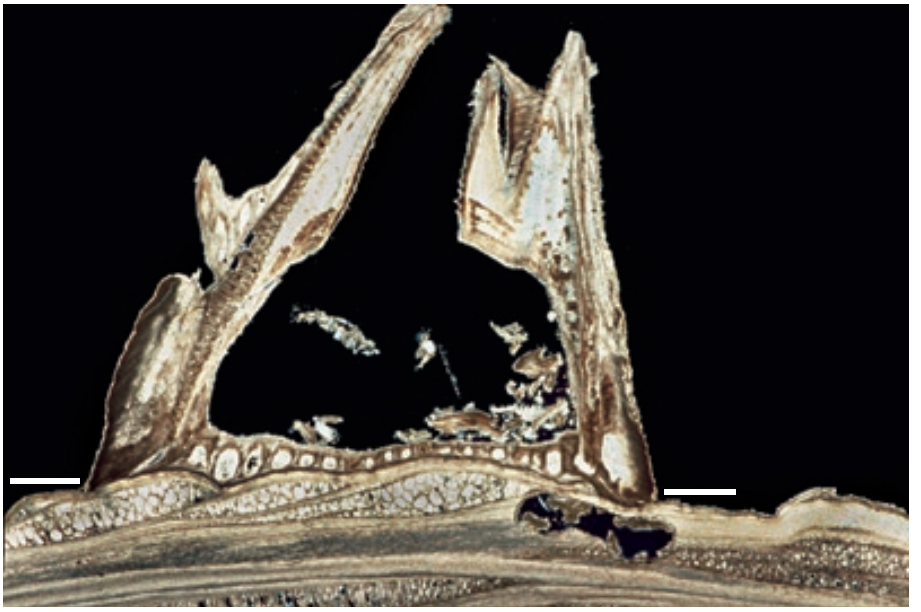

XPL, HA = 10 mm

Pleistocene Caloosahatchee Fm., Hendry Co., Florida

A different cut through a barnacle encrusting an oyster shell. The barnacle shows characteristic plicated fabric giving irregular light and dark banding (sometimes described as a molar-like structure).

XPL, HA =12.5 mm

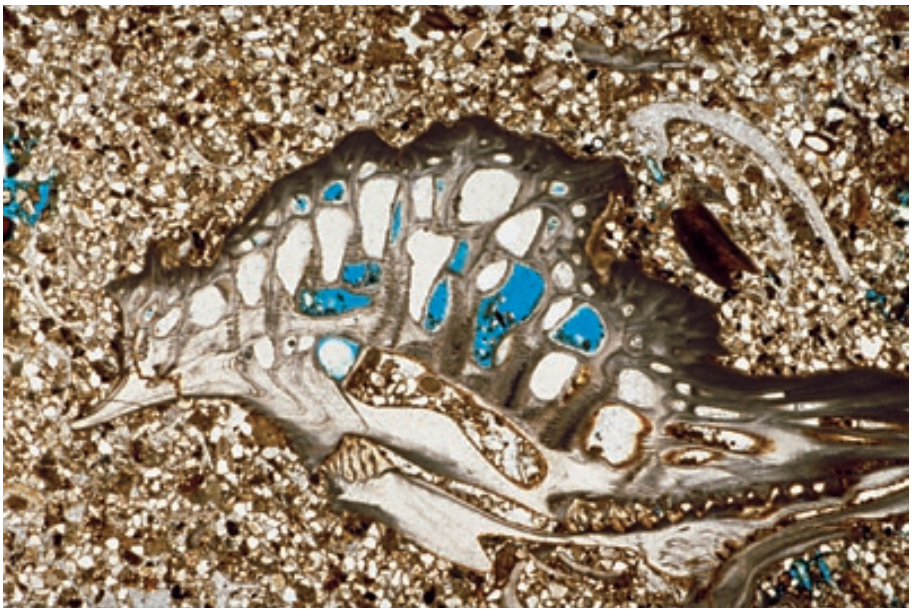

Up. Pliocene Pukenui Ls., Mbr. B, Wairarapa District, New Zealand

A barnacle fragment in a sandy limestone. Note the complex vesicular (porous tubular) structure similar to that seen in some rudistid bivalves.

PPL, BSE, HA =12.5 mm

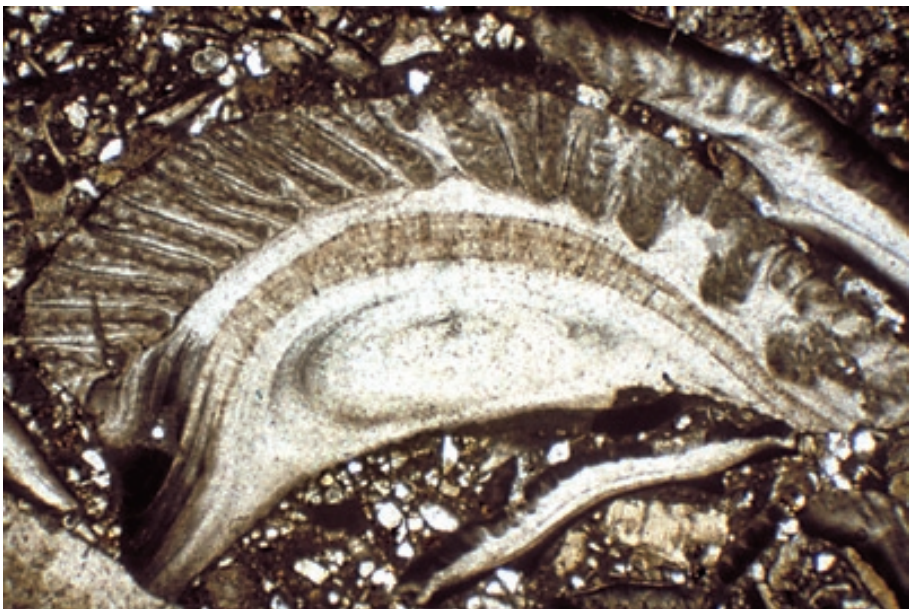

Oligocene Otekaike Ls., Canterbury, New Zealand

A barnacle plate showing a variety of internal structures. Most recognizable is the outer edge that displays deep plications giving the grain a texture similar to a molar tooth.

PPL, HA =5 mm

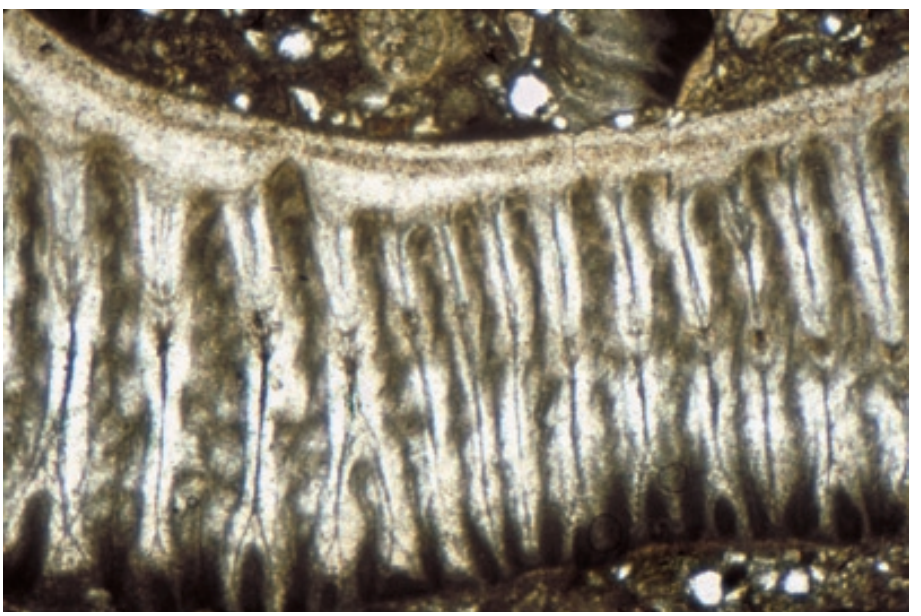

Oligocene Otekaike Ls., Canterbury, New Zealand

Close-up view of a barnacle plate with characteristic plicated (molar-like) internal structure. Most cuts through barnacle plates will show such plications.

PPL, HA = 2.4 mm

Oligocene Otekaike Ls., Canterbury, New Zealand

Plicated, tooth-like barnacle fragments form the dominant element in this sandy, shallow-water limestone from a temperate- to cold-water depositional setting. Two echinoid spines are also visible as the flower-like grains at upper right and upper left.

PPL, BSE, HA =12.5 mm

Eocene-Oligocene? Hanmer Marble, Canterbury, New Zealand

A barnacle- and bryozoan-rich limestone. This is a common association in Cenozoic shallow shelf, temperate to cold-water depositional settings. Echinoids, red algae, foraminifers, oysters and other mollusks are additional common components of this non-tropical assemblage.

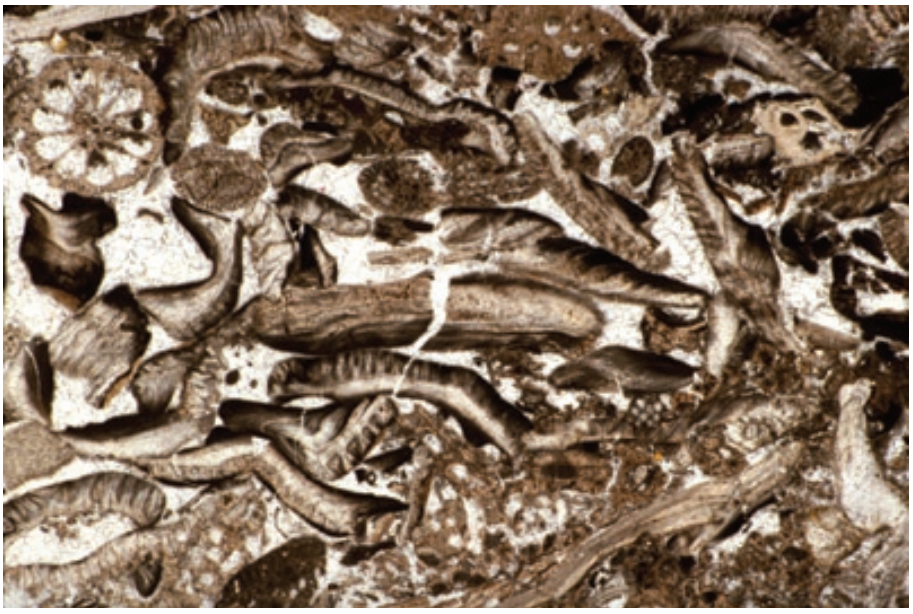

PPL, HA =10 mm

Cited References and Additional Information Sources

Bate, R. H., and B. A. East, 1972, The structure of the ostracod carapace: Lethaia, v. 5, p. 177-194.

Bate, R. H., E. Robinson, L. M. Sheppard, and D. T. Donovan, 1982, Fossil and Recent Ostracods: Chichester, UK, Ellis Horwood, 492 p.

Bourget, E., and F. G. Stehli, 1980, Barnacle shell growth and its relationship to environmental factors, *in* C. C. Rhoads, and R. A. Lutz, eds., Skeletal Growth of Aquatic Organisms; biological records of environmental change: New York, NY, Plenum Press, p. 469-491.

Cohen, A. S., and C. Nielsen, 1986, Ostracodes as indicators of paleohydrochemistry in lakes: a late Quaternary example from Lake Elmenteita, Kenya: Palaios, v. 1, p. 601-609.

Dalingwater, J. E., 1973, Trilobite cuticle microstructure and composition: Palaeontology, v. 16, p. 827-839.

Dudich, F., 1931, Systematische und biologische Untersuchungen über die Kalkeinlagerungen des Crustaceenpanzers im polarisierten Licht: Zoologica, v. 30/80, p. 1-154

Empson, T. R., 1982, Holographic microscopy of fossil ostracods, *in* R. H. Bate, E. Robinson, L. M. Sheppard, and D. T. Donovan, Fossil and Recent Ostracods: Chichester, UK, Ellis Horwood, p. 123-146.

Fischer, A. G., 1946, A carapace of the Ordovician trilobite *Telephus*: Journal of Paleontology, v. 20, p. 566-569.

Fortey, R.A., 2000, Trilobite! Eyewitness to evolution: New York, NY, Alfred A. Knopf, 284 p.

Fortey, R. A., 2001, Trilobite systematics; the last 75 years: Journal of Paleontology, v. 75, no. 6, p. 1141-1151.

Harrington, H. J., 1959, General description of Trilobita, *in* R. C. Moore, ed., Treatise on Invertebrate Paleontology, Part O, Arthropoda 1: Geological Society of America and University of Kansas Press, p. O38-O117.

Harris, A. G., 1979, Conodont color alteration, an organo-mineral metamorphic index and its application to Appalachian Basin geology, *in* P. A. Scholle, and P. R. Schluger, eds., Aspects of Diagenesis: Tulsa, OK, SEPM Special Publication No. 26, p. 3-16.

Hoskin, C. M., 1980, Flux of barnacle plate fragments and fecal pellets measured by sediment traps: Journal of Sedimentary Petrology, v. 50, p. 1213-1218.

Kamp, P. J. J., F. J. Harmsen, C. S. Nelson, and S. F. Boyle, 1988, Barnacle-dominated limestone with giant cross-beds in a non-tropical, tide-swept, Pliocene forearc seaway, Hawke's Bay, New Zealand: Sedimentary Geology, v. 60, p. 173-196.

Kesling, R. V., 1957, A peel technique for ostracod carapaces, and structures revealed therewith in *Hibbardia lacrimosa* (Swartz and Oriel): Contributions from the Museum of Paleontology University of Michigan, v. 14, p. 27-40.

Langer, W., 1971, Rasterelektronenmikroskopische Beobachtungen über den Feinbau von Ostracod-Schalen: Paläontologische Zeitschrift, v. 45, p. 181-186.

Langer, W., 1973, Zur Ultrastruktur, Mikromorphologie und Taphonomie des Ostracoda-Carapax: Palaeontographica, Abt. A, v. 144, 54 p.

Levinson, S. A., 1951, Thin sections of Paleozoic Ostracoda and their bearing on taxonomy and morphology: Journal of Paleontology, v. 25: p. 553-560.

Levinson, S. A., 1961, Identification of fossil ostracods in thin-section, *in* R. C. Moore ed. Treatise on Invertebrate Paleontology, Part Q. Arthropoda 3: Lawrence, KS, University of Kansas Press, p. Q70-Q73.

Majewske, O. P., 1969, Recognition of Invertebrate Fossil Fragments in Rocks and Thin Sections [Internat. Sed. Petrog. Series v. 13]: Leiden, E. J. Brill, 101 p.

Mutvei, H., 1981, Exoskeletal structure in the Ordovician trilobite *Flexicalymene*: Lethaia, v. 14, p. 225-234.

Orr, P. J., and D. E. G. Briggs, 1999, Exceptionally preserved conchostracans and other crustaceans from the Upper Carboniferous of Ireland: London, Palaeontological Association, 68 p.

Pokorny, V., 1978, Ostracodes, *in* B.U. Haq and A. Boersma, eds., Introduction to Marine Micropaleontology: New York, Elsevier, p. 109-150.

Robison, R. A., and R. L. Kaesler, 1987, Phylum Arthropoda, *in* R. S. Boardman, A. H. Cheetham and A. J. Rowell, eds., Fossil Invertebrates: Palo Alto, CA, Blackwell Scientific Publications, p. 205-269.

Ross, A., 1964, Cirripedia from the Yorktown Formation (Miocene) of Virginia: Journal of Paleontology, v. 38, p. 483-491.

Swierczewska-Gladysz, E., 1994, Some balanid cirripedes from the Korytnica Basin (middle Miocene; Holy Cross Mountains, central Poland): Acta Geologica Polonica, v. 44, p. 97-115.

Taylor, R. S., 1969, Transmission electron microscope study of ostracode carapace ultrastructure: The Journal of the Alabama Academy of Science, v. 40, p. 238-241.

Teigler, D. J., and K. M. Towe, 1975, Microstructure and composition of the trilobite exoskeleton: Fossils and Strata, no. 4, p. 137-149.

Willgallis, A., 1969, Untersuchung des chemischen Aufbaus von mittelkambrischen Ostracodenschalen: Lethaia, v. 2, p. 181-183.

Wilmot, N. V., and A. E. Fallick, 1989, Original mineralogy of trilobite exoskeletons: Palaeontology, v. 32, no. 2, p. 297-304.

Facing Page: Diagrammatic reconstruction of a typical *Palaeoaplysina*, a problematic Pennsylvanian to Permian bioherm-building organism. Adapted from Beauchamp et al. (1988).

GRAINS: Skeletal Fragments

PROBLEMATICA

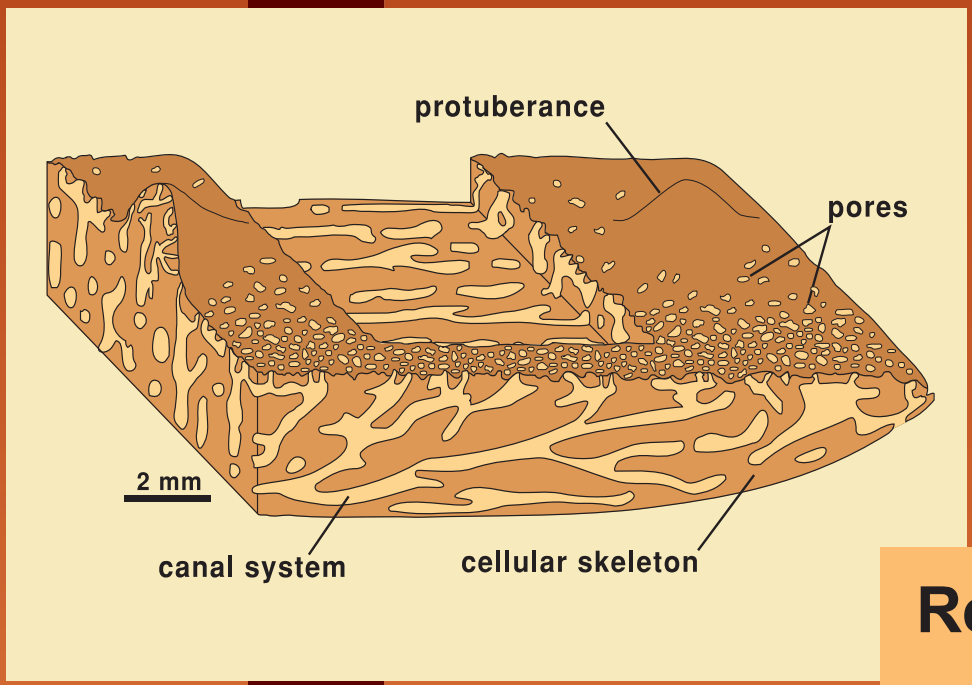

CHAPTER 12

Receptaculitids

Nuia

Palaeoaplysina

Tubiphytes

Lithocodium

Hensonella

PROBLEMATICA

There are thousands of problematic organisms — organisms unassigned to a specific phyletic group, or ones that were assigned to different groups by different workers. We have simply picked a few that are particularly distinctive and/or that are important in rocks of hydrocarbon exploration interest. We list prior phyletic assignments and age ranges below and provide descriptions and keys to recognition in the figure captions.

Prior Taxonomic Assignments and Age Ranges:

Receptaculitids - grouped with sponges, corals, dasycladacean green algae, or problematica — common from Early Ordovician to Late Devonian, with smaller, more globular forms extending into the Permian

***Nuia* - grouped with problematic codiacean algae or as an unassigned organism — Late Cambrian-Ordovician**

***Palaeoaplysina* - grouped with sponges, phylloid algae, or hydrozoans — Mid. Pennsylvanian-Early Permian**

***Tubiphytes* - variously grouped with cyanobacteria/blue-green algae, red algae, calcareous sponges, foraminifers, hydrozoans — at least Late Carboniferous to Late Jurassic**

***Lithocodium* - grouped as codiacean algae or loftusiid foraminifers — Late Triassic to Early Cretaceous (Albian)**

***Hensonella* - grouped as mollusks (scaphopods), coralline red algae, or dasycladacean green algae — Cretaceous (Hauterivian-Albian)**

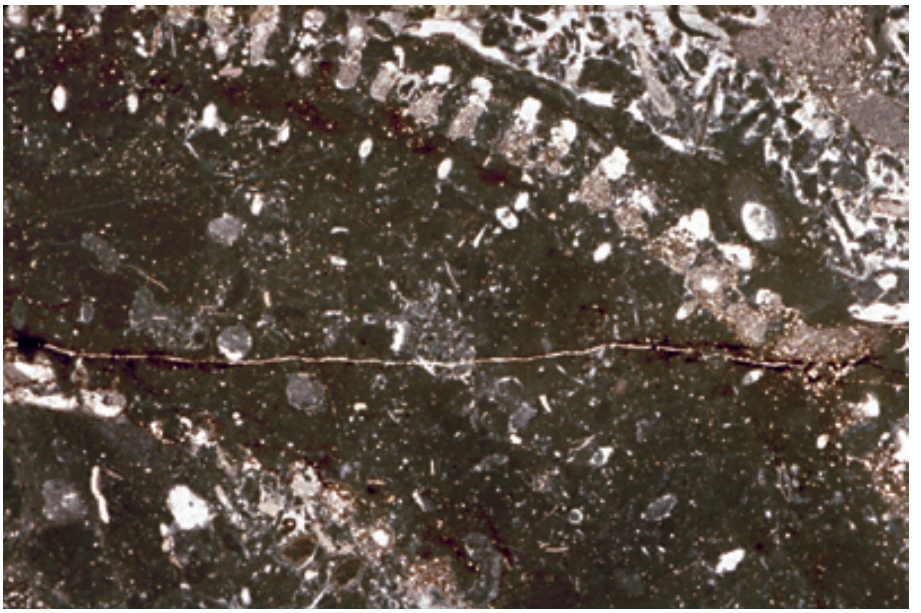

Lo. Ordovician (Canadian) Up. El Paso Gp., El Paso Co., Texas

A cross section of the wall structure of *Calathium* sp., with its central cavity and moderately well-preserved radiating wall structure. Calathids are the earliest receptaculitids — they had ovoid or tubular skeletons that strongly resemble sponges (one of the groups in which receptaculitids commonly are classed). The sparry calcite-filled areas (and micrite-filled circles) are recrystallized, originally aragonitic, elongate pillars that constituted the skeletal wall (see Nitecki et al., 1999); the rest of the micritic sediment has filled areas of former void spaces or sites of later-decomposed organic tissues.

PPL, HA = 14.5 mm

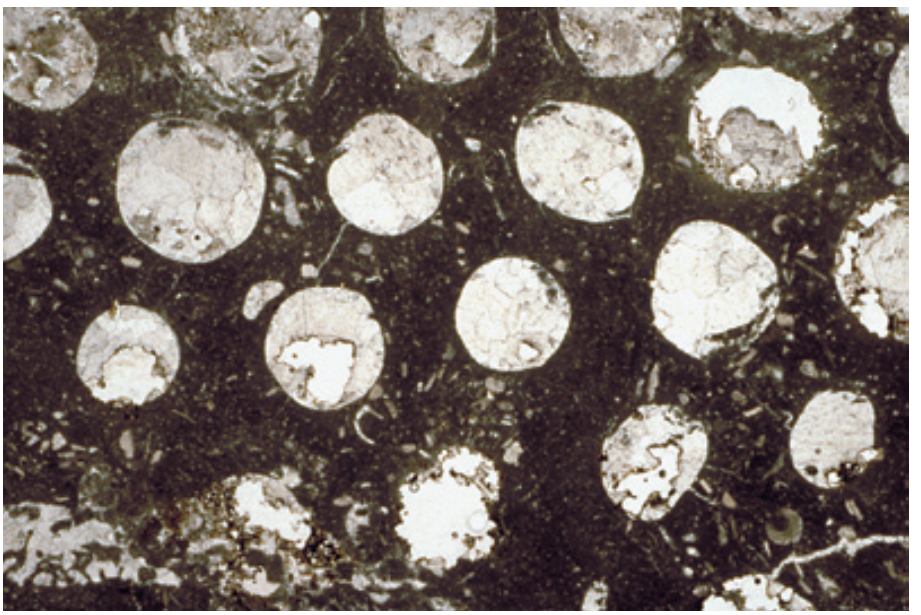

Mid. Ordovician Trenton Ls., Ste. Genevieve Co., Missouri

Receptaculitid colonies usually are globular to platter shaped, hollow structures, and typically range from a few cm to 30 cm in diameter. This transverse section shows the simple wall structure of *Receptaculites oweni* (now renamed *Fischerites oweni*). It consists of a series of thick, regularly arrayed, vertical carbonate pillars (spar-filled circular areas in this image). The pillars flare and merge near the outer margin of the colony to form a surface of rhombohedral or hexagonal facets or plates. Receptaculitids are widespread in shallow shelf sections, especially in lower Paleozoic strata (see Nitecki and Toomey, 1979).

PPL, HA = 12 mm

Lo. Ordovician (Canadian) Up. El Paso Gp., El Paso Co., Texas

Numerous grains of *Nuia sibirica* Maslov (the grains with radial fabric) in a shallow-water shelf carbonate. Although the affinities of this group remain uncertain, it is common in Ordovician rocks in the southwestern United States, often in conjunction with receptaculitids (see Toomey and Klement, 1966; Toomey, 1967). These spherical to elliptical grains can be mistaken for radial-fabric ooids if not examined closely.

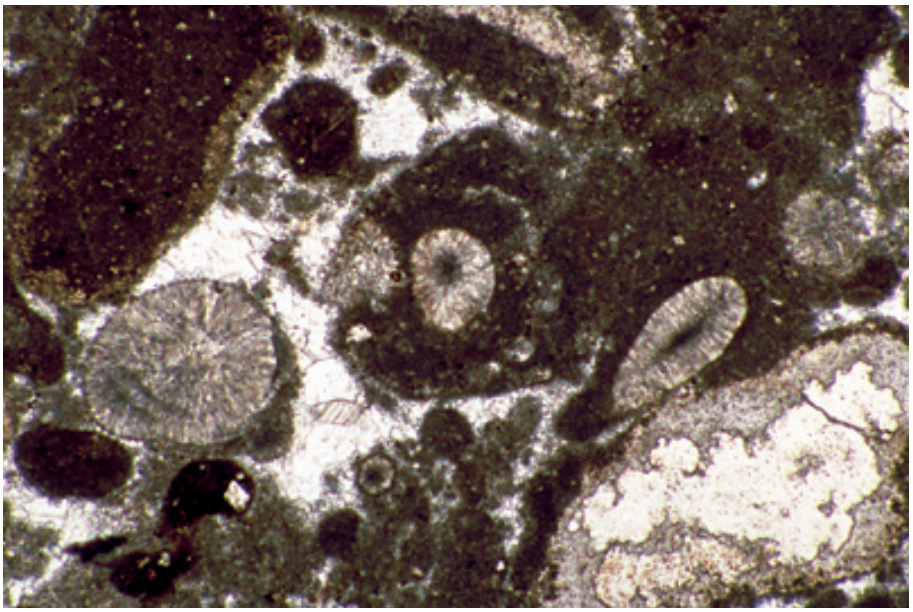

PPL, HA = 3.0 mm

Lo. Ordovician (Canadian) Up. El Paso Gp., El Paso Co., Texas

A close-up view of *Nuia sibirica*. The dark central canal is surrounded by small calcareous tubules, and the walls are composed of radially-oriented calcite prisms, a structure similar in many ways to that of *Microcodium* (see chapter on vadose diagenesis). The consistent preservation of these grains implies that calcite was the primary mineralogy.

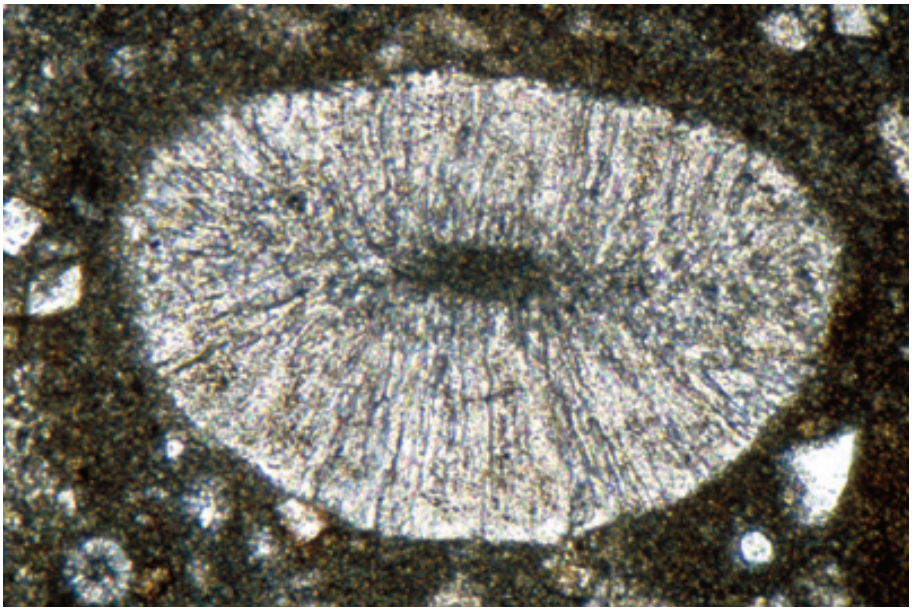

PPL, HA = 0.65 mm

Schematic reconstruction of *Palaeoaplysina*

Palaeoaplysina is made of sheet-like plates that typically are less the 0.5 cm thick, but can be up to 1 m long. The top surface has prominent mamelon-like protuberances and numerous pores that emerge on the surface; tubules and remnants of a cellular fabric sometimes remain visible in the plate interior where the fabric has not been destroyed by neomorphism. The plates are thought to have been originally aragonitic; nevertheless, remnants of internal structure commonly are preserved through sediment infill of the pores, microbial encrustation, or early cementation. Adapted from Beauchamp (1988).

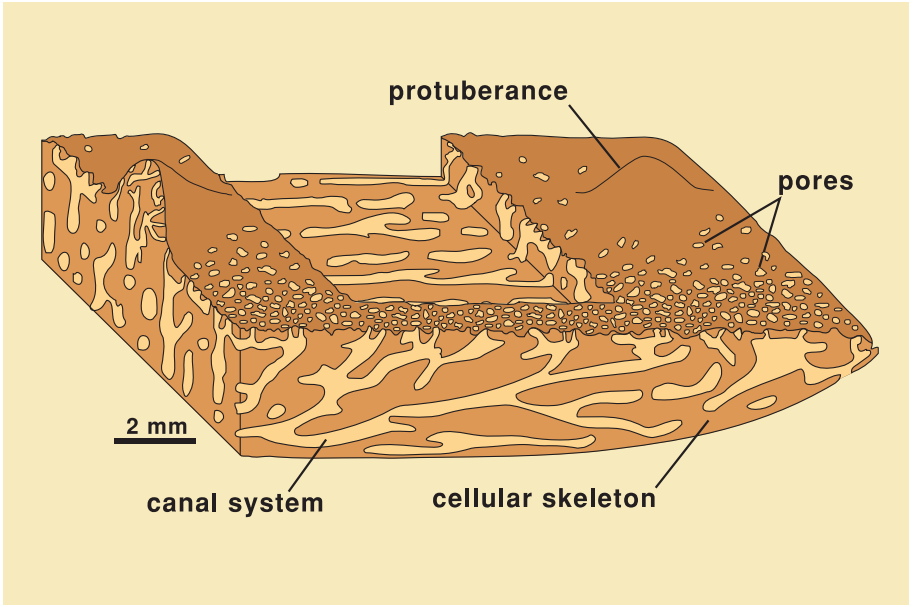

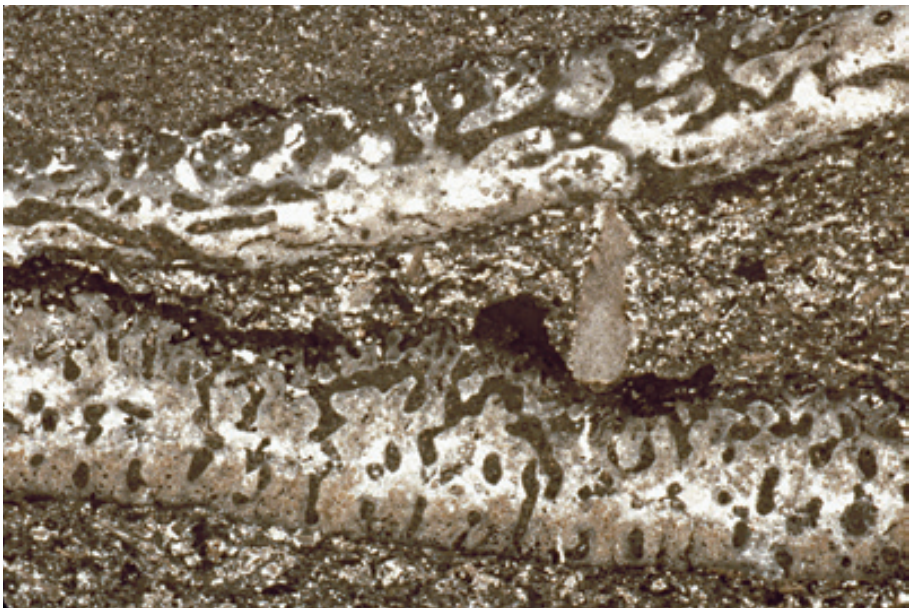

Lo. Permian (lo. Asselian) Kholodnolozhsky Horizon, Gubakha, Perm Region, Russia

Well-preserved skeletal structure in a pair of *Palaeoaplysina* plates. The asymmetry of the plates, with one surface bearing mamelons and pores, probably indicates that they lay flat on the seafloor. Mamelon-like protuberances, tubules and even hints of latticework fabric in the darker marginal zones are visible in these examples.

PPL, HA = 14.5 mm

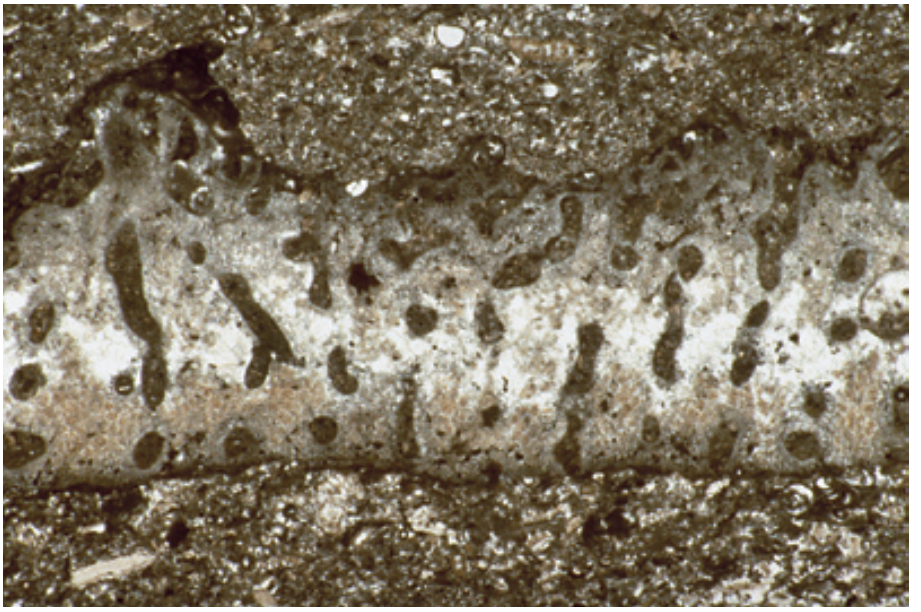

Lo. Permian (lo. Asselian) Kholodnolozhsky Horizon, Gubakha, Perm Region, Russia

An enlarged view of well preserved structure in a *Palaeoaplysina* plate. These problematic organisms have been classed by some workers as phylloid algae, and it is with phylloid algal plates that they are most easily confused. The surface protuberances and the coarse tubular structure are characteristic of *Palaeoaplysina*. The reticulate or latticework fabric (seen well along the lower margin) is reminiscent of some phylloid algae, however.

PPL, HA = 8.0 mm

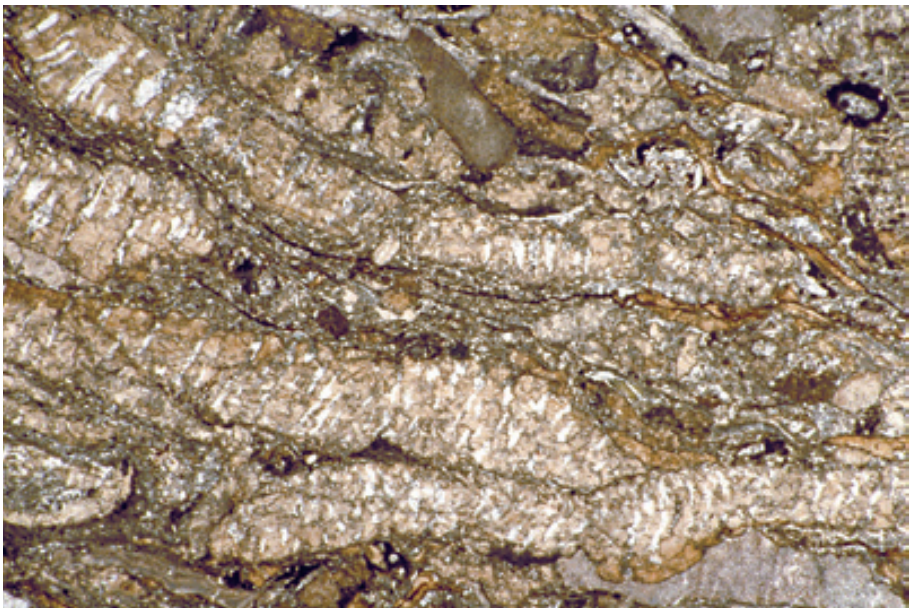

Pennsylvanian (Desmoinesian) Minturn Fm., Robinson Mbr., Eagle Co., Colorado

Poorly preserved probable *Palaeoaplysina* plates. An originally aragonitic organism, *Palaeoaplysina* is commonly leached or otherwise neomorphosed. Only through infill of pores, biological encrustation, or early cementation is any wall structure preserved. Here, filled tubules and possible surface mamelons are still distinguishable but other structures were diagenetically destroyed.

PPL, HA = 6.5 mm

Lo. Permian (up. Artinskian) Sylvinskaya Suite, Kungur, Perm region, Russia

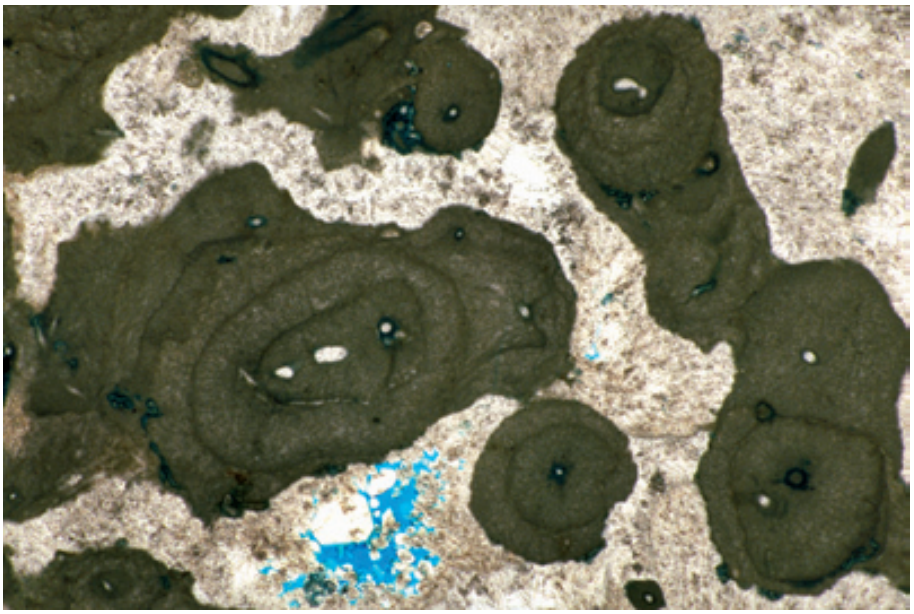

These densely microcrystalline, irregularly lobate structures form parts of a branching colony of *Tubiphytes* sp. This is a problematic organism that forms small framework shrubs (superficially similar to modern stick-like growth forms of the red alga, *Goniolithon*). *Tubiphytes* also is found commonly as an encruster of other organisms. *Tubiphytes* is especially prevalent in Permian reefs, where it occurs in framework-encruster consortia along with calcareous sponges, phylloid algae, *Archaeolithoporella*, and marine cements.

PPL, BSE, HA = 7.0 mm

Up. Permian Middle reef complex, Djebel Tebaga, Tunisia

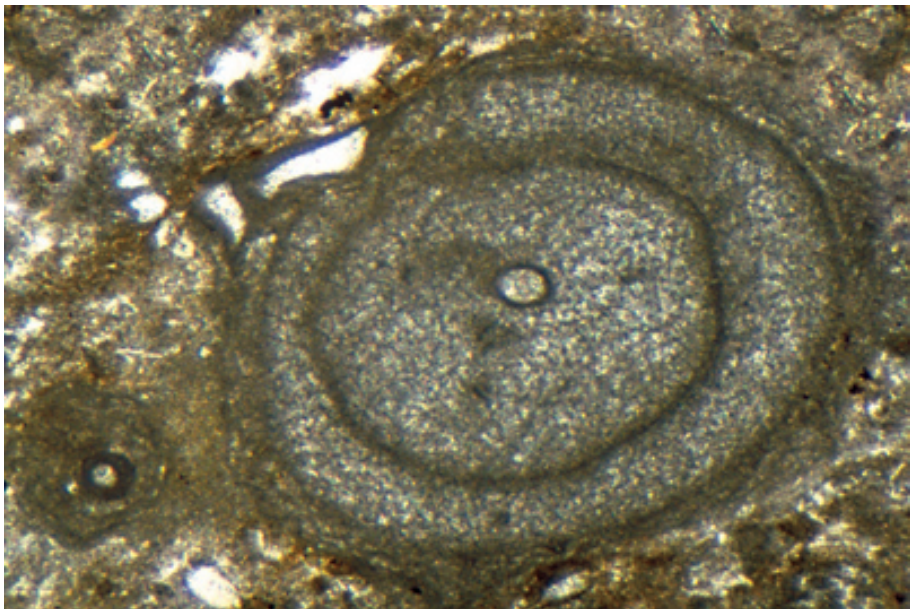

An enlargement showing the internal structure (in transverse section) of *Tubiphytes* sp. This problematic organism has very finely microcrystalline structure, yielding grains that appear almost pure white in reflected light or on outcrop. The skeletal remains show successive irregular, concentric to lobate encrustations and a mesh- or web-like internal fabric that are well illustrated in this example.

PPL, HA = 2.0 mm

Up. Permian (up. Guadalupian) Capitan Fm., Eddy Co., New Mexico

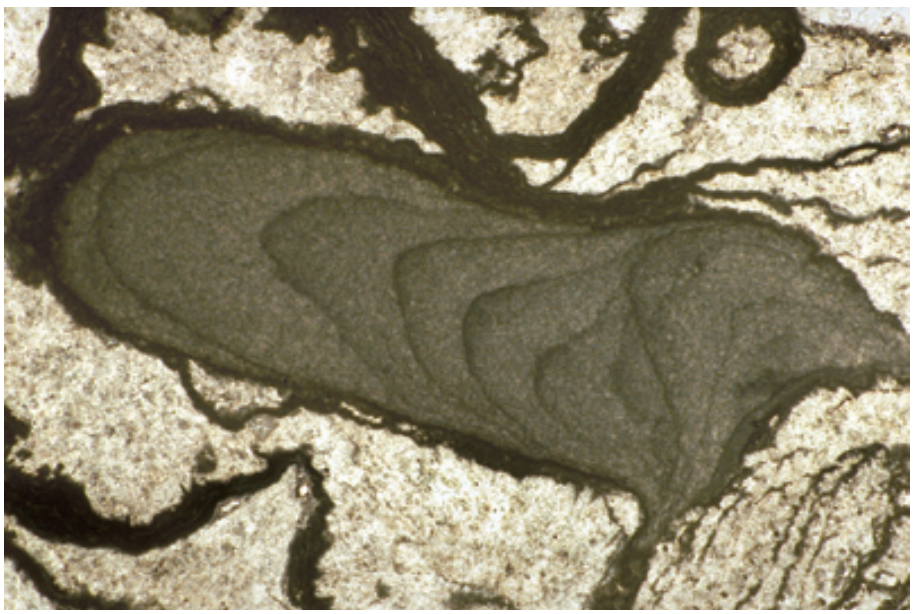

A typical *Tubiphytes* encrustation (in oblique longitudinal section) — here associated with *Archaeolithoporella* and marine cement in a sponge-cement reef. *Tubiphytes* appears to grow extensively on seafloor surfaces, but it may also have been a contributor to cryptic reef communities, growing in dimly lit recesses and cavities in reef and fore-reef settings.

PPL, HA = 9.0 mm

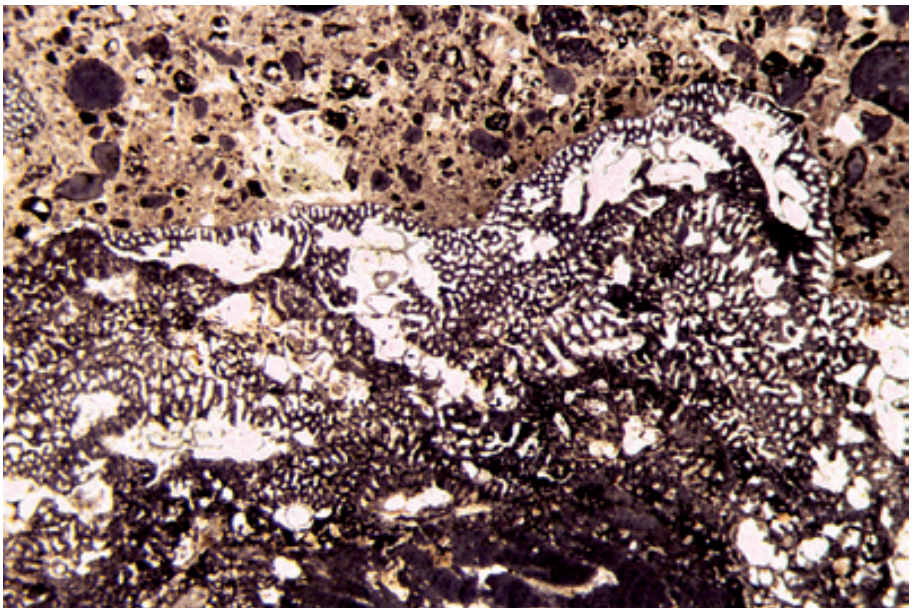

Up. Jurassic (Tithonian) Arranhó Fm., São Tiago dos Velhos, Portugal

Lithocodium aggregatum, shown here in a multilayered example, is common in Mesozoic shelf carbonates where it encrusts reefs and forms oncoids. Interpreted by many earlier workers as a codiacean green alga, recent work has shown that this organism is an encrusting foraminifer (Schmid and Leinfelder, 1996). It lived in association with algal symbionts and another foraminifer, *Troglotella incrustans,* that grew into the alveoli of *Lithocodium*. It also is commonly associated with *Bacinella*, another problematic encruster. Photograph courtesy of Reinhold R. Leinfelder and Dieter Schmid.

PPL, HA = ~12 mm

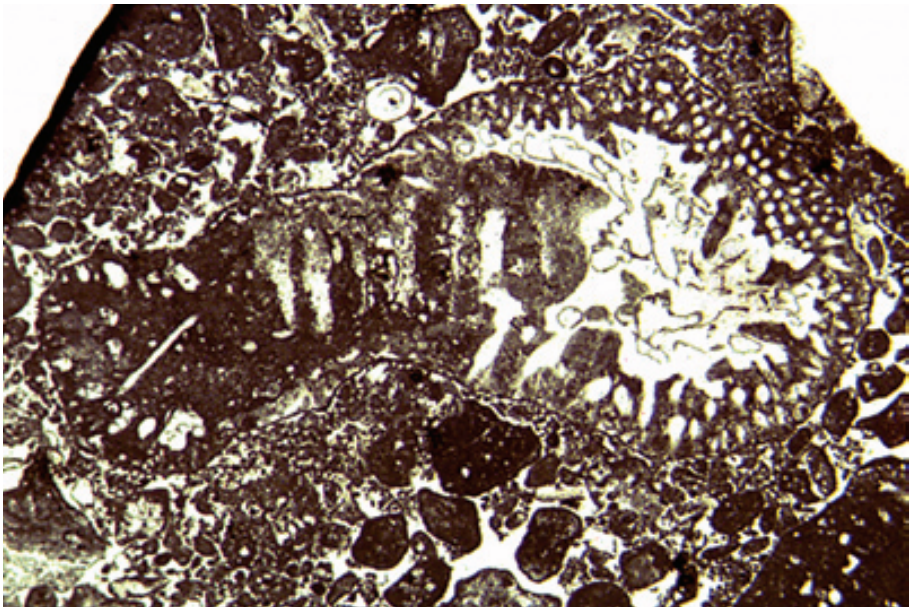

Up. Jurassic (Kimmeridgian) Ota Ls., Alenquer, Portugal

The complex, alveolar (but imperforate) microgranular wall structure of *Lithocodium aggregatum* is seen here. The form is identical to that of other loftusiid foraminifers, although *Lithocodium* is unique within that group in having an encrusting lifestyle. *Lithocodium* is coiled during juvenile growth stages, but its irregular encrusting growth form develops in later stages of life. Photograph courtesy of Reinhold R. Leinfelder and Dieter Schmid.

PPL, HA = ~8 mm

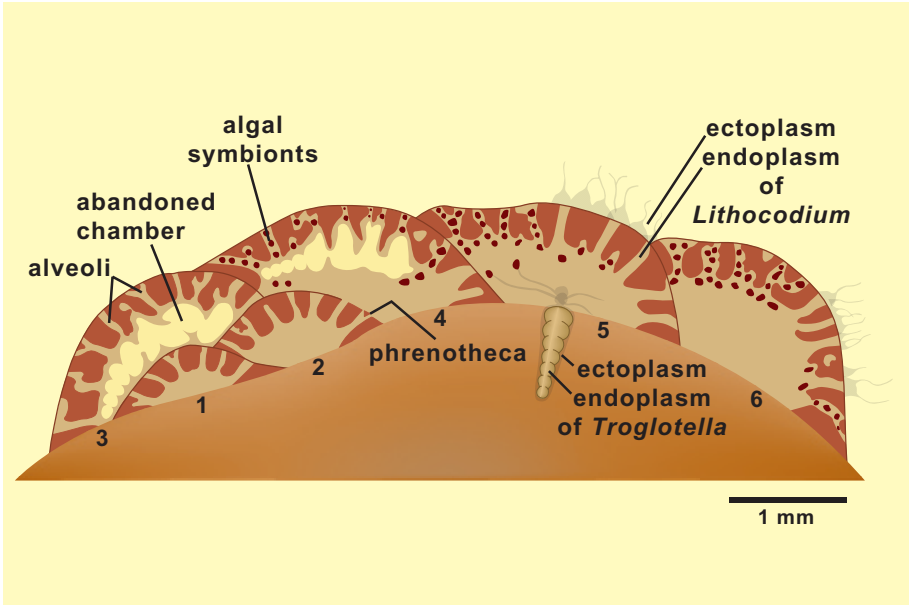

Diagrammatic reconstruction of *Lithocodium aggregatum*

An interpreted reconstruction of *Lithocodium aggregatum* in consortium with *Troglotella* (axial section with algal symbionts not to scale). The numerals indicate the succession of living chambers of *Lithocodium*. The phrenotheca-like structures were interpreted to have served, in part, to shut off chambers that had been deserted by the living *Lithocodium*. Redrawn from Schmid and Leinfelder (1996); used courtesy of Reinhold R. Leinfelder and Dieter Schmid.

Lo. Cretaceous (Barremian)
Kharaib Fm., offshore Qatar

A large intraclastic fragment (center) showing a foraminiferal-microbial community including *Lithocodium* and other encrusters. This sediment is part of a broad, open, shallow-shelf sequence with scattered small bioherms and mounds that include *Lithocodium* as an important encrusting faunal component.

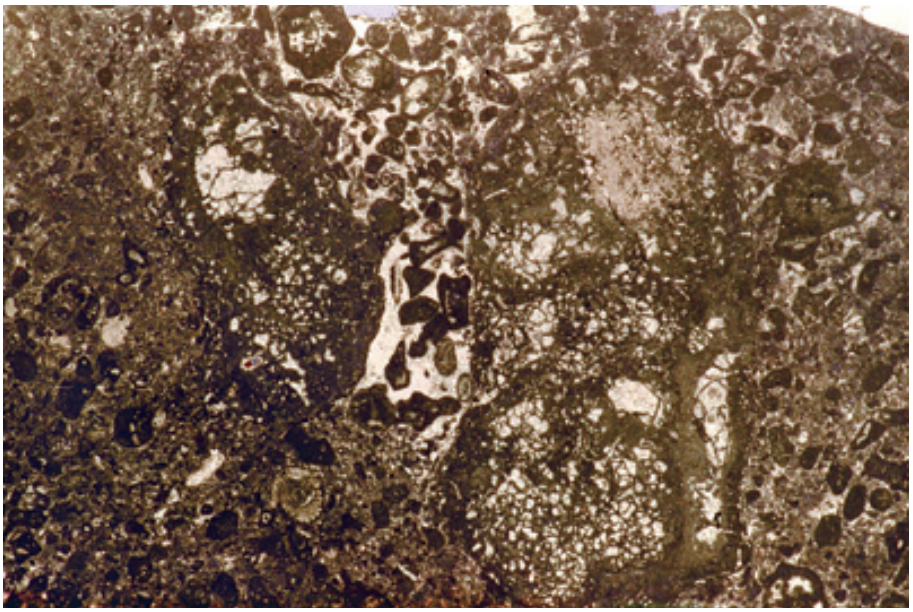

PPL, HA = 10 mm

Lo. Cretaceous (Barremian)
Kharaib Fm., offshore Qatar

A longitudinal cut through a single specimen of *Hensonella dinarica* (?), an Hauterivian-Albian problematic organism. The conical shape and possible two-layer wall are visible — the wall has an inner granular or microcrystalline layer and an outer prismatic calcite layer, with prisms oriented perpendicular to the wall surface. Despite the conical form, this organism is now grouped most commonly with the green algae (see Elliott, 1960).

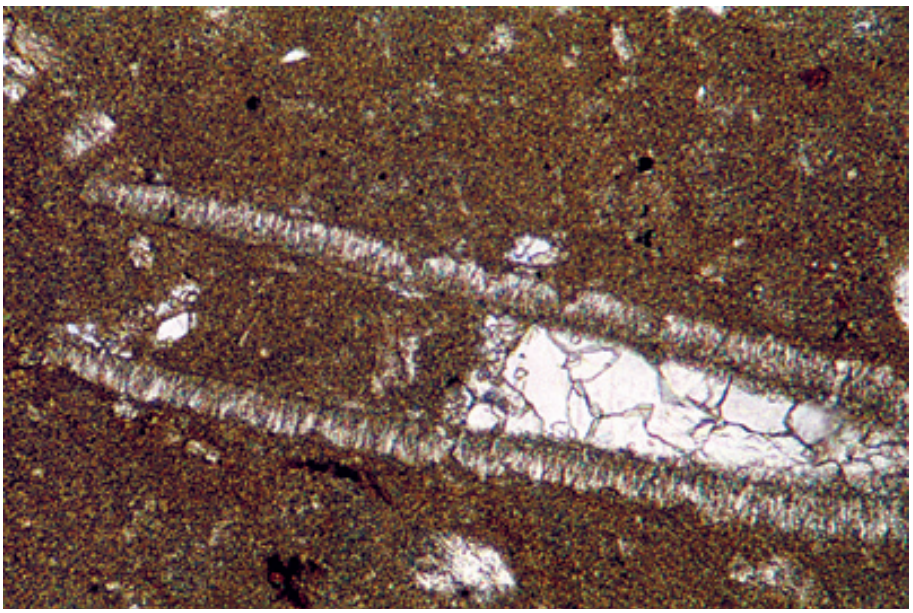

PPL, HA = 1.1 mm

Lo. Cretaceous (Barremian)
Kharaib Fm., offshore Qatar

A transverse cross-section through a single specimen of *Hensonella dinarica* (?). The circular to ovoid shape corresponds to the short-axis section of a slender, tapering cone. The inner microgranular and outer radial prismatic wall layers are clearly visible, along with the somewhat uneven external morphology. This organism is a common contributor to open shelf carbonate deposits in the Lower Cretaceous of the Middle East.

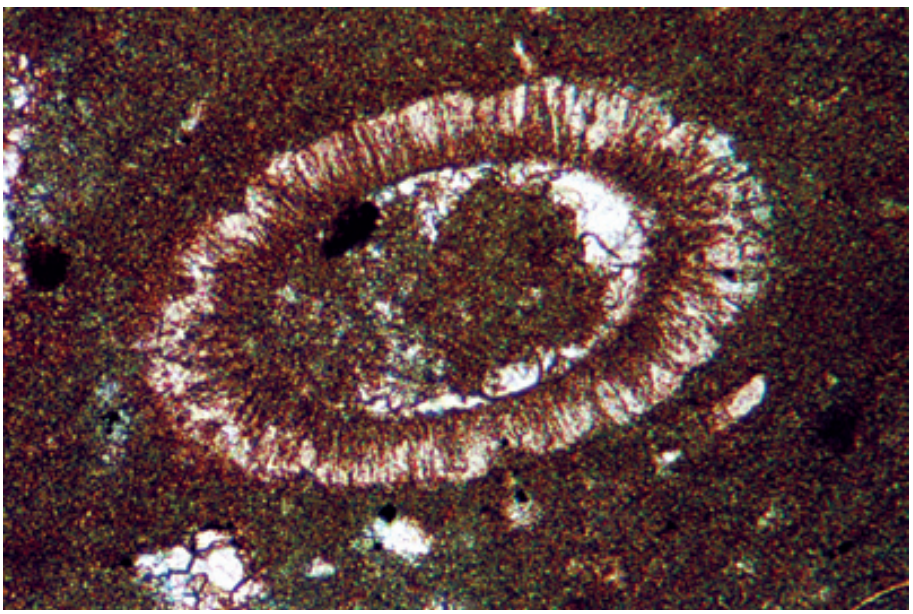

PPL, AFeS, HA = 0.5 mm

Cited References and Additional Information Sources

Babcock, J. A., 1986, The puzzle of alga-like problematica, or rummaging around in the algal wastebasket, *in* A. Hoffman, and M. H. Nitecki, eds., Problematic Fossil Taxa: New York, Oxford University Press, p. 12-26.

Beauchamp, B., 1988, Upper Carboniferous to Lower Permian *Palaeoaplysina*-phylloid algal buildups, Canadian Arctic Archipelago, *in* H. H. J. Geldsetzer, N. P. James, and G. E. Tebbutt, eds., Reefs, Canada and Adjacent Areas: Calgary, Canada, Canadian Society of Petroleum Geologists Memoir 13, p. 590-599.

Breuninger, R. H., 1976, *Palaeoaplysina* (Hydrozoan?) carbonate buildups from Upper Paleozoic of Idaho: American Association of Petroleum Geologists Bulletin, v. 60, p. 584-607.

Chuvashov, B. I., 1973, Morfologiya, ekologiya i systematicheskoe polzhenye roda *Palaeoaplysina*: Paleontol. Zhumal, v. 1973, p. 3-8.

Davies, G. R., and W. W. Nassichuk, 1973, The hydrozoan? *Palaeoaplysina* from the upper Paleozoic of Ellesmere Island, Arctic Canada: Journal of Paleontology, v. 47, p. 251-265.

Dullo, W.-C., E. Flügel, R. Lein, P. Riedel, and B. Senowbari-Darayan, 1987, Algen, Kalkschwämme und Mikroproblematika aus unterkarnischen Riffkalken des Bosruck-Gipfels (Nördliche Kalkalpen, Österreich): Jahrbuch der Geologischen Bundesanstalt (Wien), v. 129, p. 525-543.

Dupraz, C., and A. Strasser, 1999, Microbialites and micro-encrusters in shallow coral bioherms (Middle to Late Oxfordian, Swiss Jura Mountains): Facies, v. 40, p. 101-130.

Elliott, G. F., 1958, Fossil microproblematica from the Middle East: Micropaleontology, v. 4, p. 419-428.

Elliott, G. F., 1960, Fossil calcareous algal floras of the Middle East with a note on a Cretaceous problematicum, *Hensonella cylindrica* gen. et sp. nov.: Quarterly Journal of the Geological Society London, v. 115, p. 217-232.

Elliott, G. F., 1962, More microproblematica from the Middle East: Micropaleontology, v. 8, p. 29-44.

Finney, S. C., and M. H. Nitecki, 1979, *Fisherites* n. gen. *reticulatus* (Owen, 1844), a new name for *Receptaculites oweni* Hall, 1861: Journal of Paleontology, v. 53, p. 750-753.

Flügel, E., 1981, Lower Permian *Tubiphytes*/*Archaeolithoporella* buildups in the southern Alps (Austria and Italy), *in* D. F. Toomey, ed., European Fossil Reef Models: Tulsa, OK, SEPM Special Publication No. 30, p. 143-160.

Hoffman, A., and M. H. Nitecki, eds., 1986, Problematic Fossil Taxa: New York, Oxford University Press [Oxford Monographs on Geology and Geophysics 5], 267 p.

Mazzullo, S. J., and J. M. Cys, 1978, *Archaeolithoporella* boundstones and marine aragonite cements, Permian Capitan reef, New Mexico and Texas, USA: Neues Jahrbuch für Geologie und Paläontologie, Monatshefte, v. 1978, p. 600-611.

Nitecki, M. H., H. Mutvei, D. V. Nitecki, 1999, Receptaculitids: A Phylogenetic Debate on a Problematic Fossil Taxon: New York, Kluwer Academic/Plenum Publishers, 241 p.

Nitecki, M. H., and D. F. Toomey, 1979, Nature and classification of Receptaculitids: Bulletin des Centres de Recherches Exploration-Production Elf-Aquitaine, v. 3, p. 725-732.

Pratt, B. R., and J. A. W. Weissenberger, 1988, Fore-slope receptaculitid mounds from the Frasnian of the Rocky Mountains, Alberta, *in* H. H. J. Geldsetzer, N. P. James, and G. E. Tebbutt, eds., Reefs, Canada and Adjacent Areas: Calgary, Alberta, Canadian Society of Petroleum Geologists Memoir 13, p. 510-513.

Razgallah, S., and D. Vachard, 1991, Systematique et biosédimentologie des algues constructrices permiennes *Tubiphytes* et *Archaeolithoporella* suivant l'example du Jebel Tebaga (Murghabien de Tunisia): Palaeontographica, v. 221, p. 171-205.

Rietschel, S., 1969, Beiträge zur Kenntnis der Receptaculiten; 1, Die Receptaculiten, eine Studie zur Morphologie, Organisation, Ökologie und Überlieferung einer problematischen Fossil-Gruppe und die Deutung ihrer Stellung im System: Senckenbergiana Lethaea, v. 50, p. 465-509.

Riding, R., 1993, *Shamovella obscura*: the correct name for *Tubiphytes obscurus*: Taxon, v. 42, p. 71-72.

Riding, R., and L. Guo, (1992): Affinity of *Tubiphytes*: Palaeontology, v. 35, p. 37-49.

Ross, R. J., Jr., J. E. Valusek, and N. P. James, 1988, *Nuia* and its environmental significance, *in* D. L. Wolberg, ed., Contributions to Paleozoic paleontology and stratigraphy in honor of Rousseau H. Flower: Socorro, NM, New Mexico Bureau of Mines and Mineral Resources Memoir 44, p. 115-121.

Schmid, D. U., 1995, "*Tubiphytes" morronensis* — eine fakultativ inkrustierende Foraminifere mit endosymbiontischen Algen ["*Tubiphytes" morronensis* — a facultatively encrusting foraminifer with endosymbiotic algae]: Profil, v. 8, p. 305-317.

Schmid, D., and R. Leinfelder, R., 1995, *Lithocodium aggregatum* Elliot n'est pas une algue mais un foraminifère encroûtant, commensalisé par le foraminifère *Troglotella incrustans* Wernli et Fookes: Comptes rendus des séances de l'Académie des Sciences (Paris), v. 320, série IIa, p. 531-538.

Schmid, D. U., and R. R. Leinfelder, 1996, The Jurassic *Lithocodium aggregatum* - *Troglotella incrustans* foraminiferal consortium: Palaeontology, v. 39, p. 21-52.

Senowbari-Daryan, B., and E. Flügel, 1994, *Tubiphytes* Maslov, an enigmatic fossil: classification, fossil record and significance through time. Part 1: discussion of Late Paleozoic material: Bolletino della Società Paleontologica Italiana, v. 1, p. 353-382.

Simmons, M.D., D. Emery, and N.A.H. Pickard, 1991. *Hensonella dinarica*, an originally calcitic Early Cretaceous dasycladacean alga: Palaeontology, v. 34, p. 955-961.

Toomey, D. F., 1967, Additional occurrences and extension of stratigraphic range of the problematic micro-organism *Nuia*: Journal of Paleontology, v. 41, p. 1457-1460.

Toomey, D. F., and K. W. Klement, 1966, A problematical micro-organism from the El Paso Group (Lower Ordovician) rocks of west Texas and southern Oklahoma: Journal of Paleontology, v. 40, p. 1304-1311.

Wang S. H., J. S. Fan and J. K. Rigby, 1994, *Archaeolithoporella* and *Tubiphytes* - Affinities and Paleoecology in Permian Reefs of South China: Science in China - Series B, Chemistry, Life Sciences & Earth Sciences, v. 37, p. 723-743.

Watkins, R., and E. C. Wilson, 1989, Paleoecologic and biogeographic significance of the biostromal organism *Palaeoaplysina* in the Lower Permian McCloud Limestone, eastern Klamath Mountains, California: Palaios, v. 4, p. 181-192.

Zhuravlev, A. Y., and M. N. Nitecki, 1985, On the comparative morphology of the archaeocyathids and receptaculitids: Paleontological Journal, v. 19, p. 134-136.

Facing Page: Macrophotograph of a cut and polished section through a piece of silicified wood from the Cretaceous(?) of New Zealand. Photograph courtesy of Douglas W. Lewis.

GRAINS: Skeletal Fragments

VERTEBRATE AND PLANT REMAINS

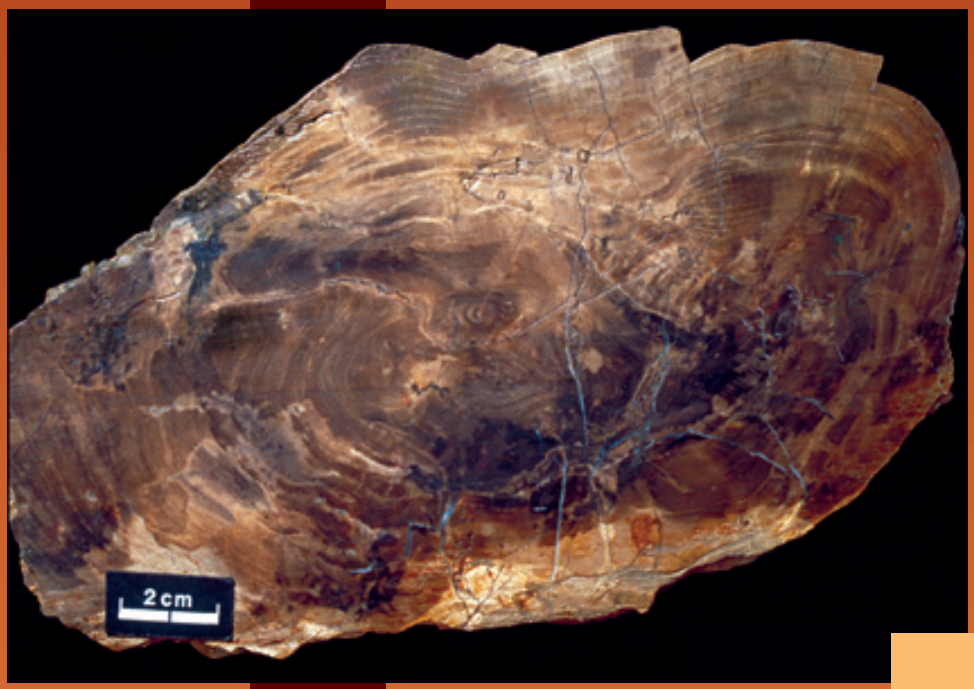

CHAPTER 13

Bones and teeth

Conodonts

Plant fragments

Spores, pollen, and organic matter

VERTEBRATE BONES, TEETH AND SCALES

Taxonomy and Age Range:

Phylum Chordata, subphylum Vertebrata

Vertebrates range from Cambrian to Recent (initially as jawless fish)

- **Jawed vertebrates — Early Silurian-Recent**
- **Terrestrial vertebrates — (Late Devonian) Carboniferous-Recent**
- **Reptiles — Carboniferous-Recent**

Environmental Implications:

Early vertebrate remains (Cambrian-Silurian) are confined to marine settings; subsequent diversification led to expansion into virtually all environments from polar to tropical and from terrestrial to abyssal marine. Most vertebrate remains in carbonate rocks are fish scales and teeth from lacustrine or marine settings; bone and tooth material from other groups, however, also can be found on occasion.

Vertebrate remains are rare but can sometimes be found concentrated by wave or current action or by nonsedimentation of other materials at hiatus surfaces.

Skeletal Mineralogy:

Bones and teeth are largely composed of organic proteins (mainly collagen) and calcium phosphate (carbonate-hydroxylapatite, sometimes termed collophane when it is microcrystalline). The interior parts of bones (the cancellous portions) have a spongy texture that commonly is filled with precipitated cement (most commonly carbonate, silica or phosphate) during diagenesis.

Morphologic Features:

Vertebrate organisms have an enormous range of external morphologies, but all have a vertebral column and other hard parts (other bones, teeth, or scales) that typically disarticulate upon death and can become scattered into carbonate and noncarbonate sedimentary deposits.

Vertebrate debris can range in size from less than a mm to well over 1 m, but is typically in the mm to cm size range.

Most bones share common features: a dense, smooth, outer or cortical part, and an interior composed of multiple layers of porous or spongy, cancellous material (in life, the porous areas are occupied by marrow).

Teeth are constructed of three layers: a pulpy cavity, a covering of dentine, and where the tooth is exposed, an additional covering of enamel.

Dentine is relatively hard and dense and has a mineral content of about 75%; enamel is even denser and is almost 98% hydroxylapatite.

Keys to Petrographic Recognition:

1. **Bone/tooth material is phosphatic and thus is colorless to dark brown in plane-polarized light and has extremely low birefringence (light gray to black) and slightly undulose extinction in cross-polarized light.**
2. **Bone fragments and tooth material have a distinctive, dense exterior and a spongy interior.**
3. **Bone fragments have irregular shapes and a distinctive vesicular fabric with branching, tubular cavities (haversian canals) and concentric, laminar phosphatic structures surrounding the canals. At higher magnifications, tiny holes (caniculi) representing individual bone cells are visible.**
4. **Fish scales or dermal plates have concentrically laminated wall structures and some have a rind of enamel (similar to vertebrate teeth).**
5. **Enamel layers typically appear as a bright exterior to grains and can have a radial prismatic structure.**

PHOTO SCALES AND ABBREVIATIONS ARE EXPLAINED IN THE BOOK'S INTRODUCTION

Up. Cretaceous, Canterbury, New Zealand

A macroscopic view of a sectioned cervical vertebra of an elasmosaur (a marine reptile). Note the originally spongy fabric of the bone material (with most of the pores filled with diagenetic precipitates). Photograph courtesy of D. W. Lewis.

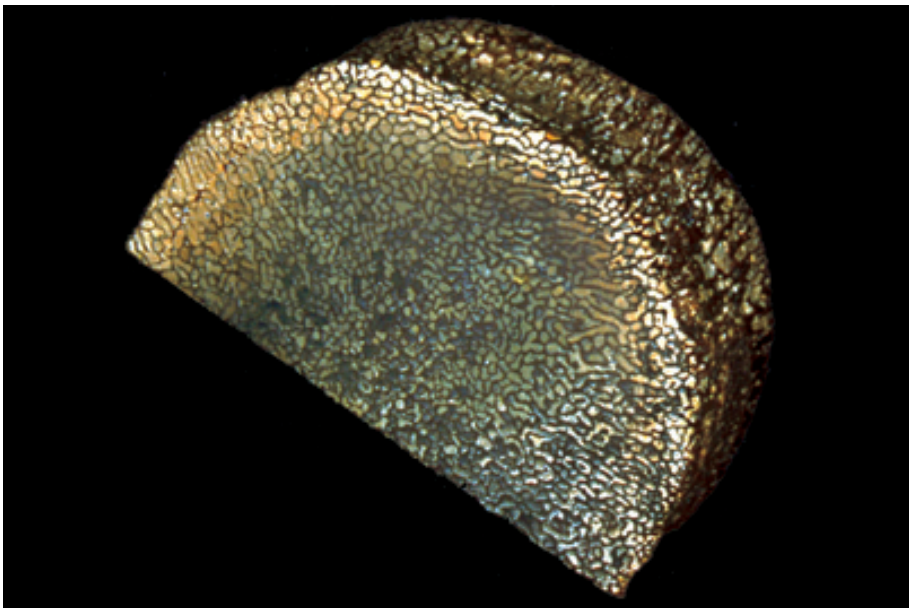

Mac, HA = 12 cm

Eocene Green River Fm., Lincoln Co., Wyoming

A group of partly crushed, porous fish bones and scales (yellowish-brown) in a laminated calcareous shale. Note compactional drape of the soft sediment around the harder skeletal material. The cross-polarized light view shows the typical low birefringence of the collophane (carbonate hydroxylapatite).

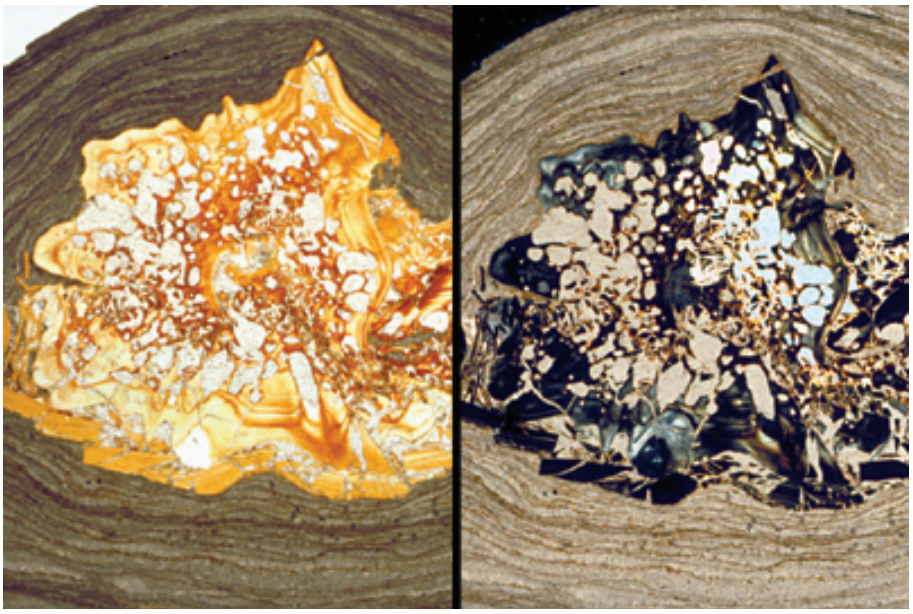

PPL/XPL, HA = 7.2 mm each

Up. Cretaceous, Drumheller, Alberta, Canada

A cross section through a single terrestrial dinosaur bone. The large pores, termed haversian canals, are elongate tubes that extend at right angles to the plane of this thin section. The canals are surrounded by concentrically laminated phosphatic material (collophane), a structure that is especially visible in cross-polarized light (right) and is diagnostic of bone material. The small dots barely visible at this magnification are holes (caniculi) representing individual bone cells. Photograph courtesy of Albert V. Carozzi.

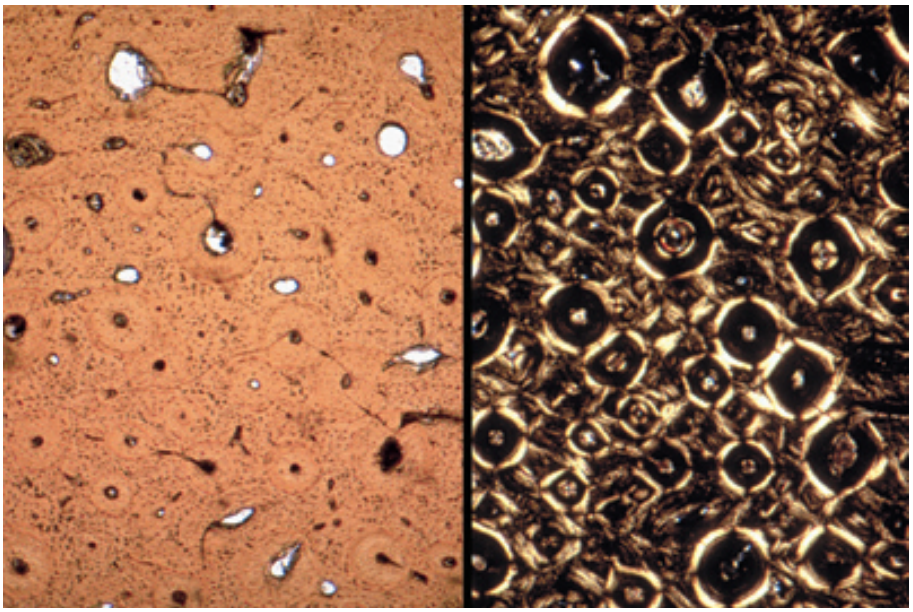

PPL/XPL, HA = 1.5 mm each

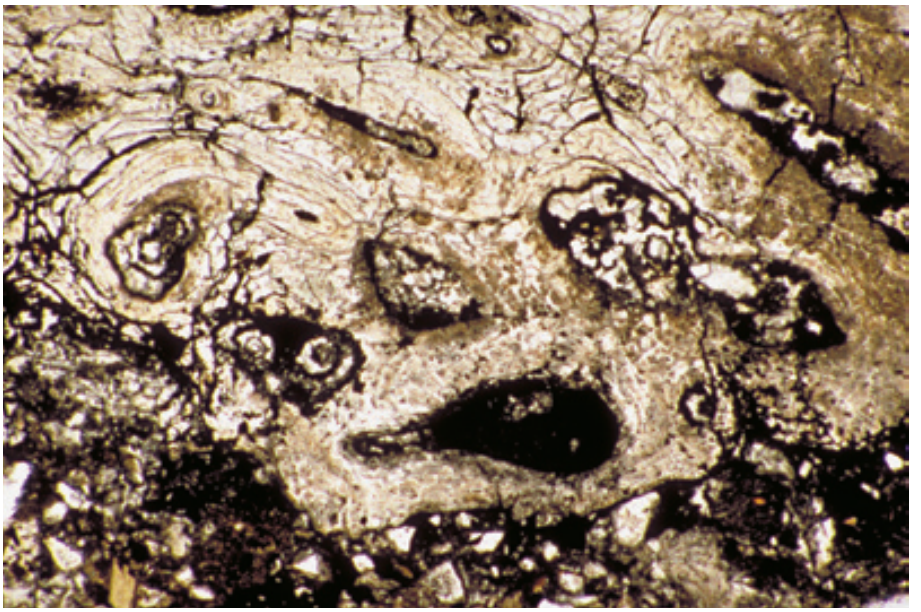

Tertiary Vieja Gp., Presidio Co., Texas

This Titanothere (mammalian) bone shows a structure comparable to that seen in the previous photographs of reptilian bone. It has large haversian canals, concentric structure in the surrounding phosphatic material, and barely visible traces of caniculi.

PPL, HA = 3.0 mm

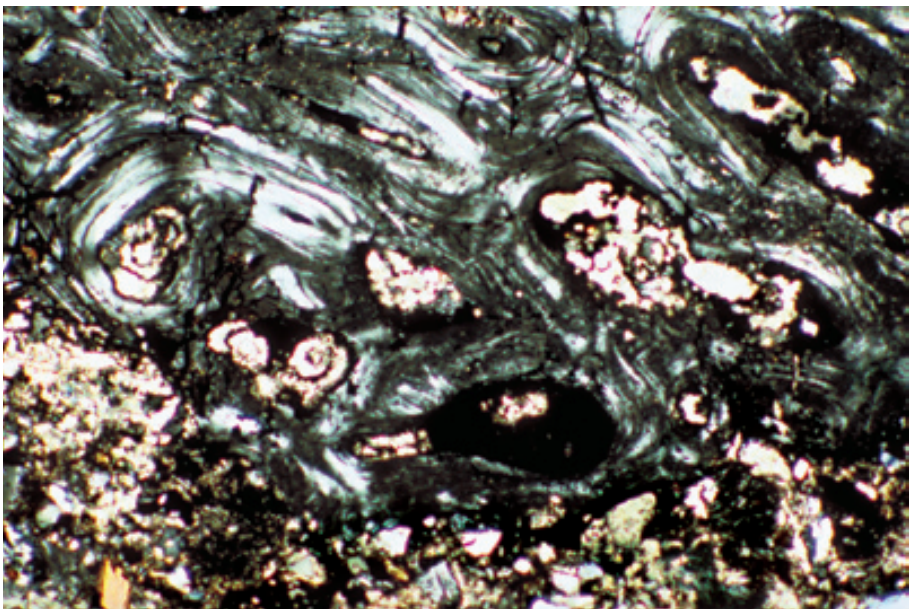

Tertiary Vieja Gp., Presidio Co., Texas

The large pores and concentrically laminated phosphatic structure of the Titanothere bone shown above are accentuated here in cross-polarized light. Note the "streaky" birefringence patterns common to many phosphatic bone fragments.

XPL, HA = 3.0 mm

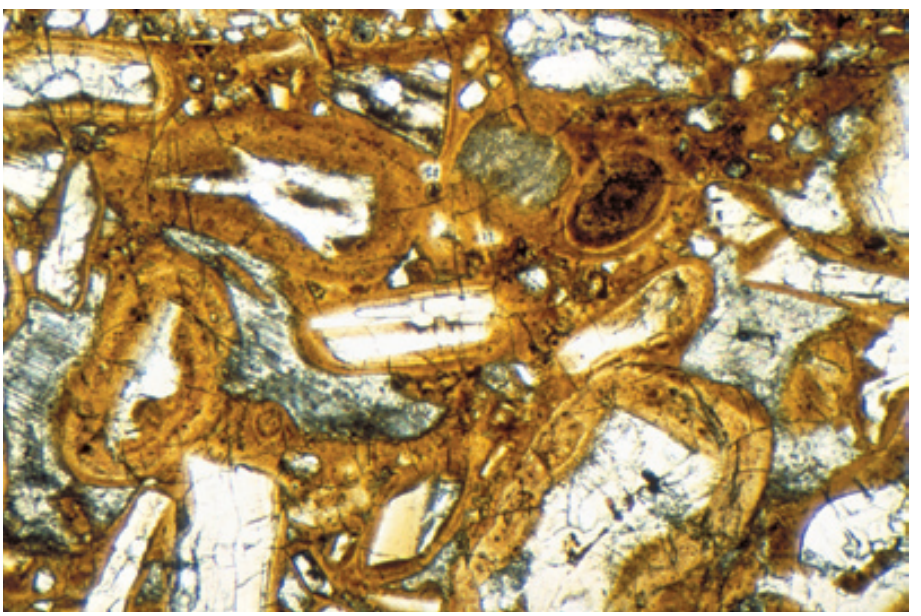

Permian (Leonardian-Guadalupian) Phosphoria Fm., Caribou Co., Idaho

This view of one of the world's great phosphate deposits shows a phosphatic oolite in which phosphatic (collophane) shell and bone fragments act as cores (nuclei) of many of the ooids. The skeletal debris is relatively clear (white to pale yellow); the precipitated phosphatic coatings of the ooids are yellowish brown in this example.

PPL, HA = 2.4 mm

Conodonts

Taxonomy and Age Range:

Long considered as problematic remains, conodonts have been assigned variously to fishes, worms, mollusks, and arthropods. Recent discoveries make it very likely that these are support structures or sieving/screening features embedded in the soft tissues of primitive jawless fish (possibly similar to modern hagfish).

Phylum Conodonta — Late Proterozoic-Late Triassic

Class Paraconodontida — Late Proterozoic-Mid. Ordovician

Class Conodontophorida — Cambrian-Late Triassic

Environmental Implications:

Conodonts occur worldwide and were fully marine with a range from normal salinity to very slightly hypersaline settings. Both pelagic and benthic forms may have existed. Although most common in shallow shelf settings, conodonts are more rarely found in deeper-water environments, primarily in areas of strong upwelling.

Rarely a dominant faunal element (except in minor concentrations or "bone beds") but still common in carbonate rocks; especially prominent in insoluble residues. They are extremely important for biostratigraphic determinations.

Skeletal Mineralogy:

Conodont hard parts ("elements") are composed of calcium phosphate (carbonate-hydroxylapatite, sometimes termed collophane) with included organic matter.

Morphologic Features:

Most are uncalcified and the remainder have largely "nonskeletal" or "extraskeletal" calcification. Conodont elements have varied tooth- or blade-like shapes with three common long-section morphologies — coniform (cone-shaped structures with a base and cusp); ramiform (a main cusp with flanking ridges bearing smaller denticles); and pectiniform (elongate platforms with multiple small denticles). Most are circular to polygonal in short-axis cross section.

Conodont elements range from about 0.2 millimeters to 6 millimeters in length.

Keys to Petrographic Recognition:

1. Individual elements typically are in the mm size range.
2. They have minute calcium phosphate crystals with large amounts of associated organic matter. Grains range from nearly clear to opaque with pale yellow to brown or even black color in plane light, depending on the degree of thermal alteration of the incorporated organic matter; this is widely used as indicator of the paleo-burial history of associated rocks in the form of a conodont alteration index, commonly abbreviated as CAI (Epstein et al., 1977).
3. Conodont elements are isotropic or have very low-order birefringence (gray to white) in cross-polarized light.
4. Conodont elements have characteristic tooth- to blade-shapes that serve to distinguish them from most vertebrate fossil fragments.
5. Most easily mistaken for phosphatic inarticulate brachiopod fragments and fish scales. Conodonts, however, have more irregular (crenulate) internal structure.
6. The wall structure of conodont elements is extremely finely crystalline and typically is finely laminated, sometimes with a crenulate fabric like nested cones associated with the individual denticles. Three layers can sometimes be distinguished: a laminar layer, a non-laminated one (termed "white matter"), and a "basal filling" layer with extremely fine lamination.

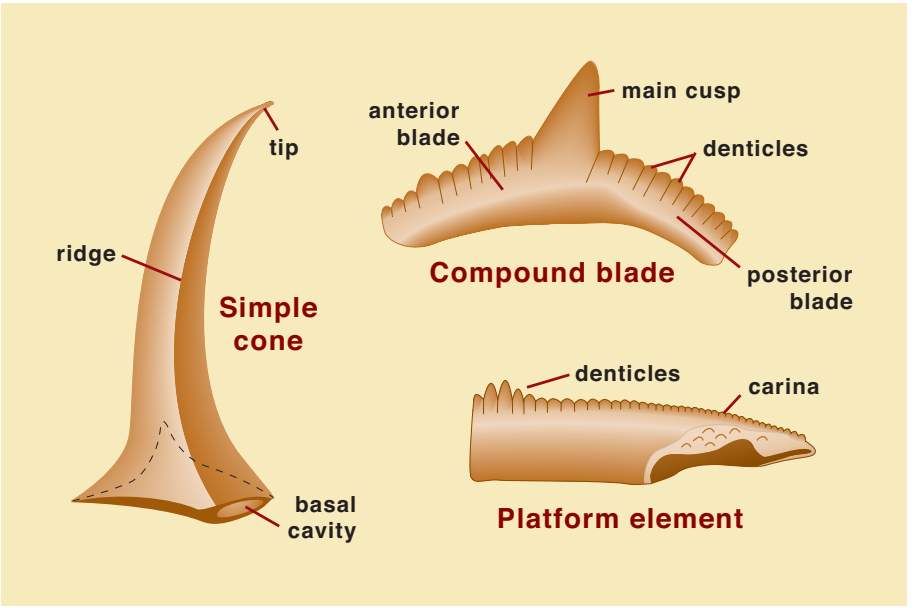

Diagram showing generalized conodont structures

The morphologies and terminology applied to some of the main types of conodont elements (adapted from Brasier, 1980, and original sources cited therein). Although these elements appear tooth-like (hence the name, conodont, which means "cone-tooth"), it is not certain whether they functioned as teeth (because they rarely show wear and apparently were embedded in soft tissue). Although their actual function is not fully known, they may have been teeth, support structures, or may have played a role in grasping or sieving material. Despite uncertainties of origin, conodonts are extremely useful biostratigraphic markers in both carbonate and non-carbonate rocks.

Mississippian Lodgepole Ls., Montana

A macrophotograph of an etched limestone surface showing a concentration of large phosphatic conodonts still partially embedded in carbonate matrix. Note the considerable variety of shapes and sizes of the conodonts.

Mac, HA = 3 cm

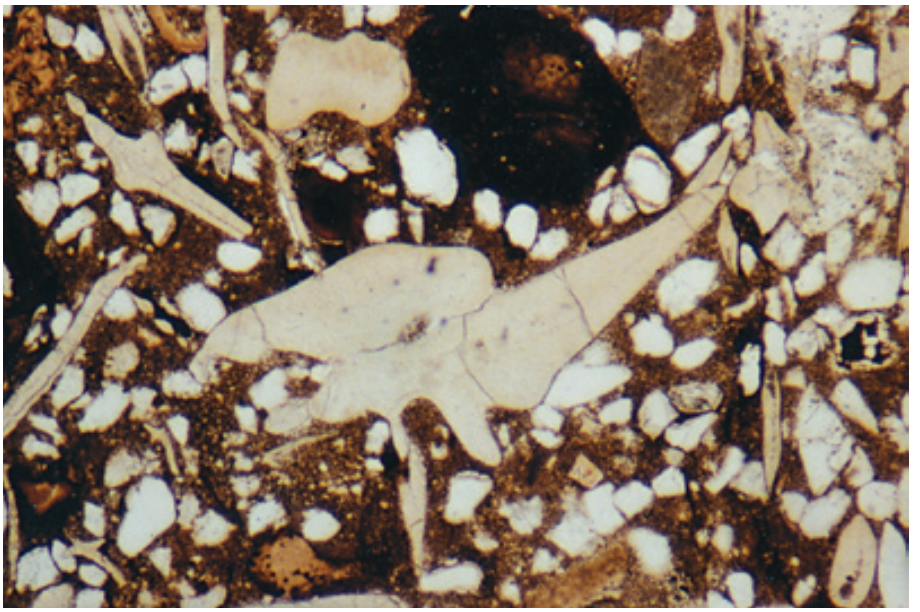

Lo. Mississippian Lodgepole Ls., Cottonwood Canyon Mbr., Montana

Several conodonts, mainly from the genus *Siphonodella*, are visible in a thin section. Note the elongate, tooth-like character and diversity of shapes of these grains. Just as with human teeth, a single organism had a variety of conodont elements with different shapes — thus, conodont workers refer to "associations" of related elements.

PPL, HA = 3.4 mm

Lo. Mississippian Lodgepole Ls., Cottonwood Canyon Mbr., Montana

A natural concentration of conodont elements (in a sandstone intercalation within a carbonate unit). Note the typical extinction behavior under cross-polarized light: the low birefringence of calcium phosphate and the pronounced appearance of "white matter" give a distinctive saw-toothed appearance to the extinction pattern.

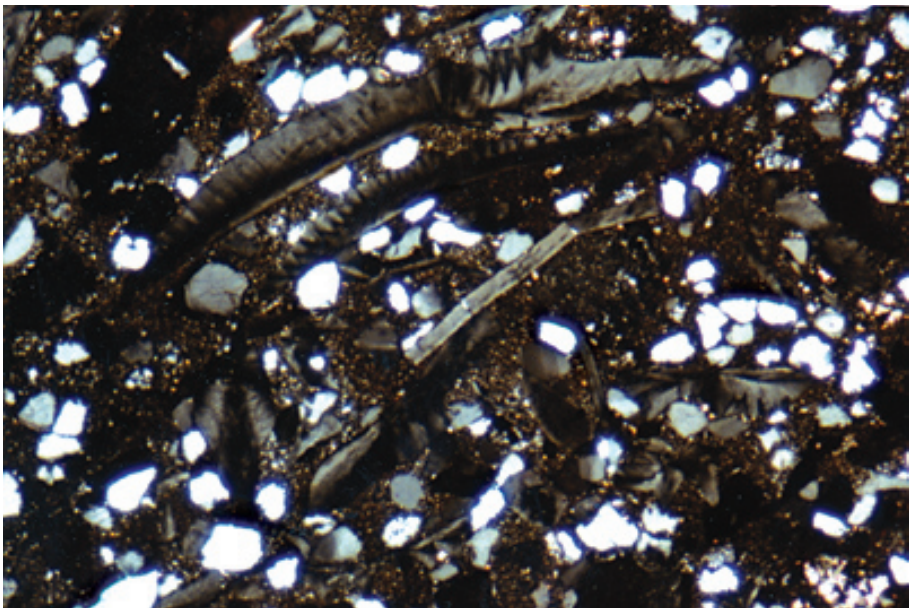

XPL, HA = 3.4 mm

Lo. Mississippian (Kinderhookian) beds near Ada, Oklahoma

Although conodonts can be studied in thin sections, they are much more easily examined in washed, acid concentrates. This is an example of an extracted conodont element (an angulate pectiniform element), termed *Solenognathus* by Hass (1941). The internal structure represents nested, cone-like concentric growth lamellae. The color of these conodonts has been used as an index of the temperatures to which the rock section has been exposed — darker colors generally correspond with higher temperatures and this sample has light colors typical of heating to only 50-90°C. Photograph courtesy of John E. Repetski.

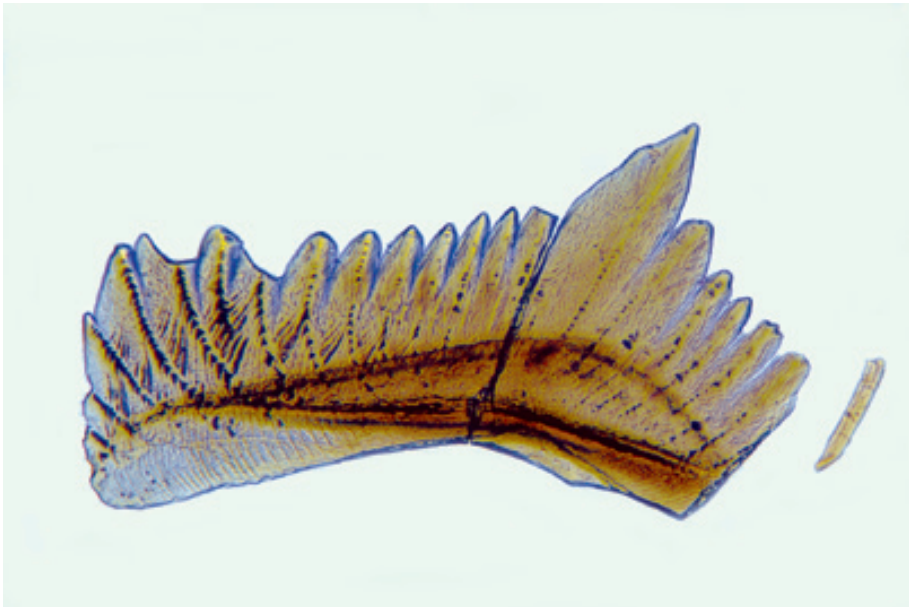

PPL, HA = 1.2 mm

Up. Devonian Saverton Shale, Pike County, Illinois

A view of an extracted conodont assemblage. Note the characteristic marginal denticles that give these grains their tooth-like appearance and the so-called "white matter" in the internal parts of the elements. The white matter consists of zones of phosphate that are especially rich in small air- or water-filled inclusions and actually appear as darker colored bands in this photomicrograph. Photograph courtesy of Albert V. Carozzi.

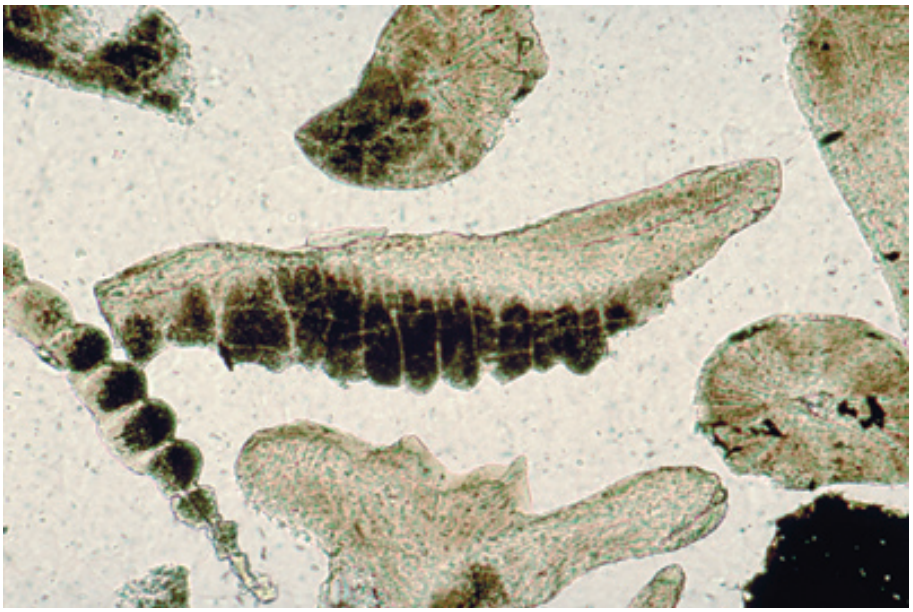

PPL, HA = 3.0 mm

WOODY PLANT REMAINS

Taxonomy and Age Range:

Kingdom Plantae: includes all land plants — mosses, ferns, conifers, flowering plants.

The plants first appeared in the Ordovician and took on modern forms by Late Silurian. By Late Devonian a varied flora with diverse shapes and sizes existed.

Environmental Implications:

Photosynthetic and thus require light for growth.

Found in terrestrial (including lacustrine) and shallow marine environments over an extremely wide climatic range from arctic to tropical.

The fact that most plant material can float (at least before becoming waterlogged) means that it can be widely dispersed beyond its already wide range — thus, terrestrial plant debris is very common in deep-marine sediments.

Skeletal Mineralogy:

Plant material consisted entirely of organic tissue in life and can be either preserved as such or woody material can be diagenetically encased, infilled, or replaced by inorganic minerals (most commonly carbonate or silica).

Morphologic Features:

Many types of plant material can be found. Woody plant material typically is found as leaves, stems or branches with a size range from millimeters to 1 m or more.

Keys to Petrographic Recognition:

1. **Woody tissue has organic composition that may have been infilled or replaced by silica, carbonate or other minerals.**
2. **Plant materials are characterized by distinctly cellular structures, often with prominent radiating rays and/or concentric growth banding (variations in cell size and shape). Specific patterns are dependent on the age, type of plant, and part of the plant being examined.**
3. **Color of woody material can vary from yellow to reddish-brown to dark brown or even black depending on the degree of maturation (coalification) of the organic matter.**

Pennsylvanian Francis Creek Shale, Mazon Creek, Illinois

A photomicrograph of an acetate peel showing a plant fragment from a sideritic concretion. Note the excellent preservation of replaced cellular material along with ray structure and concentric growth banding in this member of the extinct order, Lepidodendrales.

PPL, HA = 12.5 mm

Eocene Green River Fm., Laney Mbr., Fremont Co., Wyoming

A section of a small part of a fossil tree trunk that washed into the Green River lake. Note the reddish-brown color typical of relatively low-maturity organic matter and the coarsely cellular structure with complex patterns that characterize many remains of woody material.

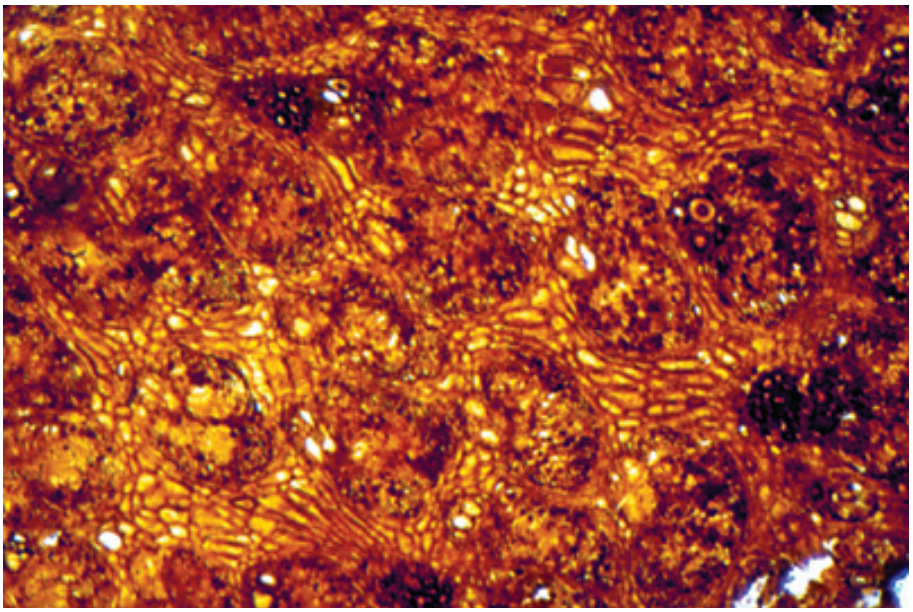

PPL, HA = 1.6 mm

Paleocene Trinidad Fm., Fremont Co., Colorado

A cross section of fossilized wood showing very well-preserved cellular fabric and growth banding (probably annual growth rings of varied thickness). Photograph courtesy of Lee Gerhard.

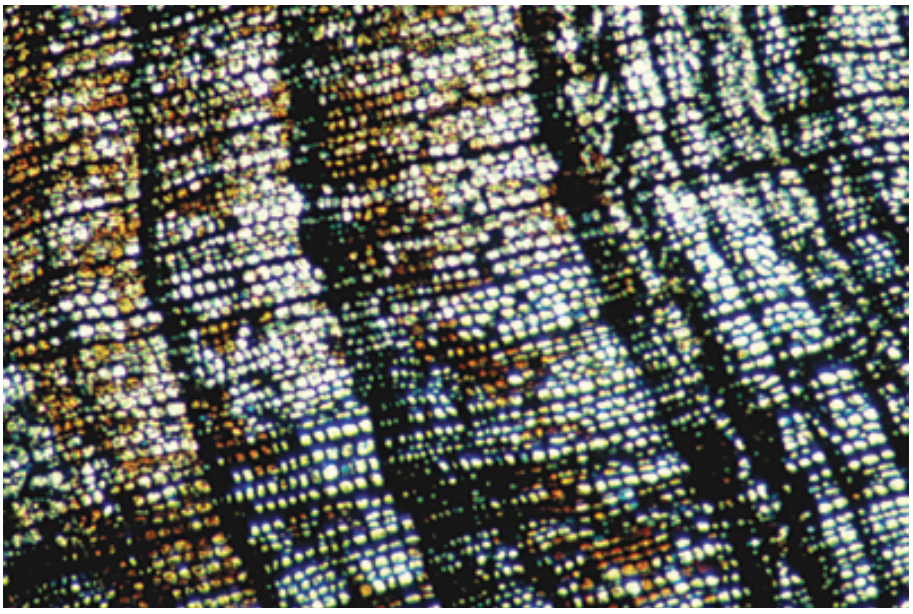

PXPL, HA = ~10 mm

Holocene-Pleistocene soil crust, Sugarloaf Key, Monroe Co., Florida

This sub-recent soil contains numerous fragments of plant remains that appear blackened and cracked by desiccation and shrinkage, yet also still show plant cellular structure. These probably are pieces of burned wood that have been converted to charcoal which then was preserved in the cemented soil crust. This is a good example to show that the color of isolated woody fragments does not always correspond with the thermal maturity of the surrounding sediment.

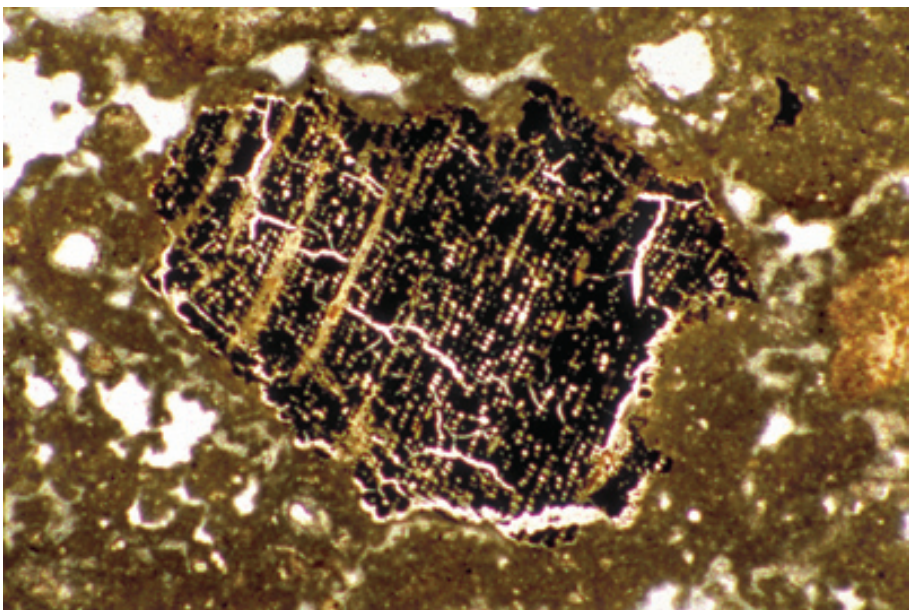

PPL, HA = 3.0 mm

SPORES, POLLEN, AND UNDIFFERENTIATED ORGANIC MATTER

Taxonomy and Age Range:

Spores are reproductive bodies produced by algae, fungi, mosses, and ferns. The earliest unequivocal triradiate spores are Silurian in age and they extend to the Recent.

Pollen are male reproductive structures of angiosperms (flowering plants) and gymnosperms (conifers and others).

Coniferous pollen — Pennsylvanian to Recent.

Angiosperm pollen — Early Cretaceous to Recent.

Environmental Implications:

Spores produced by algae, fungi, and bacteria, are rarely preserved, but terrestrial forms have wall compositions that are highly resistant to decomposition. Thus, spores and pollen in marine carbonates are essentially always transported and thus are not directly related to their environment of deposition. They are easily moved by both wind and water and transport distances of up to 150 km are common.

Spores and pollen, however, are common in carbonate rocks, and are important for biostratigraphic determinations.

They are found in both marine and nonmarine strata from a wide range of climatic zones. They are most common in lacustrine or nearshore marine carbonate deposits.

Skeletal Mineralogy:

Spores and pollen have a tough, dissolution-resistant, multi-layered wall composed of a complex of organic compounds, including sporopollenin.

Morphologic Features:

Most pollen grains are between 20 µm and 80 µm in size (exceptional ones are as small as 10 µm or larger than 200 µm). Late Cenozoic spores have similar sizes; older ones may be as large as 2 mm.

Pollen grains have a wide variety of smooth or spinose, globular, generally radially symmetrical shapes. Some have a central body with peripheral sacs or wings. Pollen also have a variety of apertures that are a major criterion for species-level identification.

Spores typically are spherical elongate or tetrahedral and have surface scares or sutures — monolete forms have a single suture; trilete forms have a triradiate suture.

Keys to Petrographic Recognition:

1. **Organic composition, yellowish to brownish color; rarely identifiable in thin section; best viewed in separates under a standard microscope or SEM.**
2. **Characteristics as noted above under "Morphologic Features".**

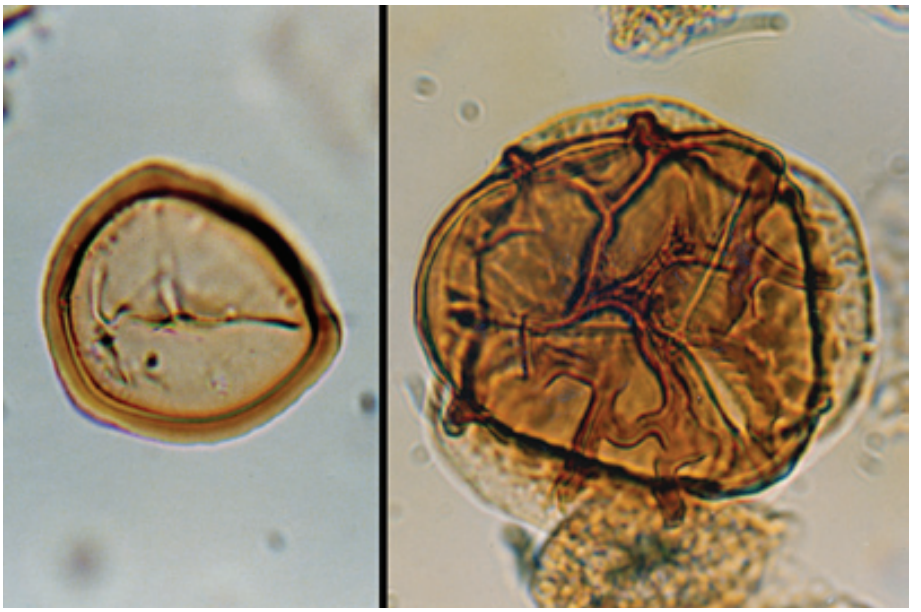

Up. Cretaceous Red Bank Fm., coastal plain, New Jersey

Spores and pollen are seen in thin sections but cannot be accurately identified unless extracted through dissolution and concentration techniques. Here are two stained palynological preparations of separated spores.
Left: a single monolete spore of *Sphagnum* (a moss).
Right: A trilete spore of uncertain affinity.

PPL, OS, L:HA=0.07mm; R: HA=0.1mm

Lo. Cretaceous Dakota Gp., Colorado

An SEM image of a simple trilete spore, *Cyathidites* sp., that is partially collapsed. The three radiating tetrad scars are clearly visible.

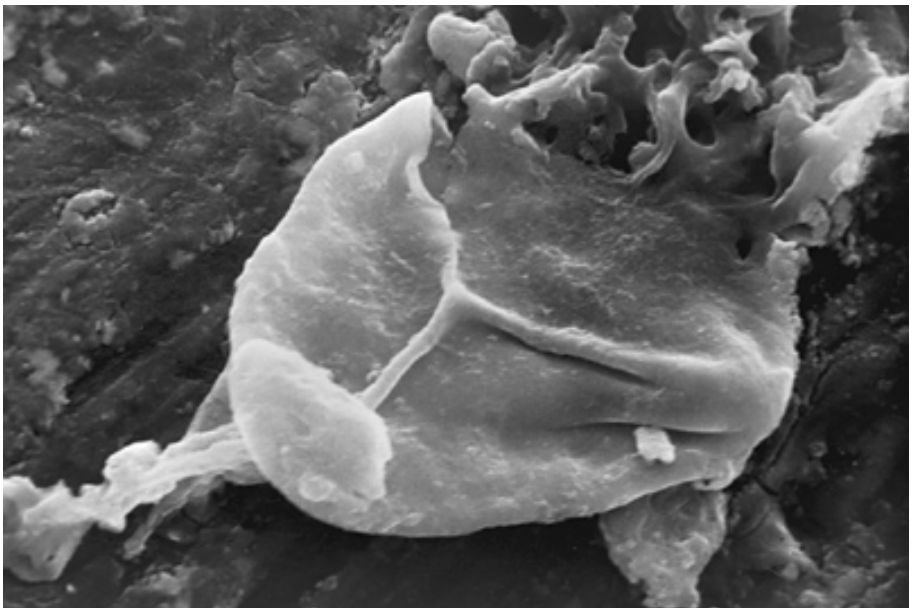

SEM, HA = 55 µm

Up. Cretaceous Mount Laurel Fm., coastal plain, New Jersey

A photomicrograph of a stained palynological preparation showing a single pollen grain of *Pinus*. This is a typical bisaccate form.

PPL, OS, HA = 0.014 mm

Lo. Cretaceous Dakota Gp.(?), Colorado

An SEM image of two tricolpate angiosperm pollen grains, *Tricoplites* sp., with apertures visible.

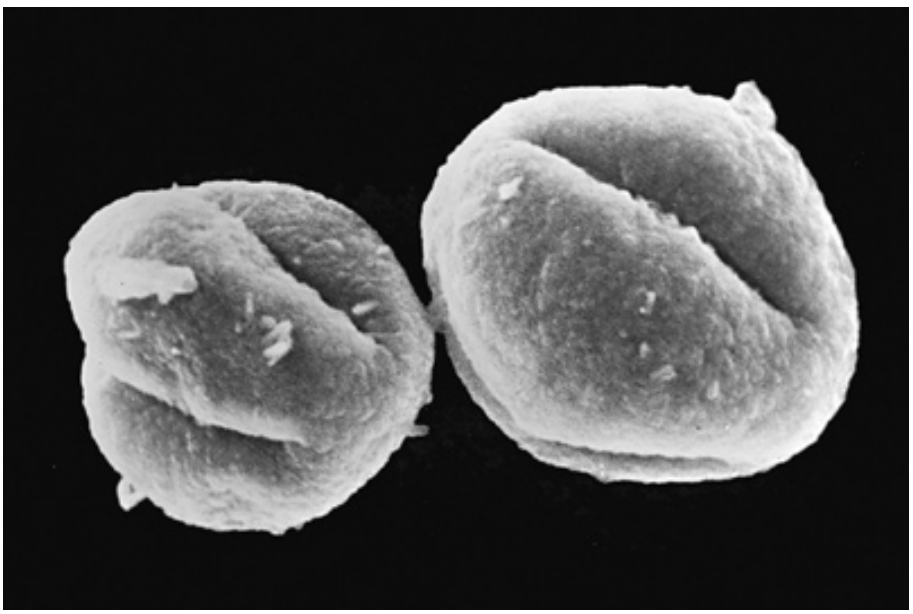

SEM, HA = 112 µm

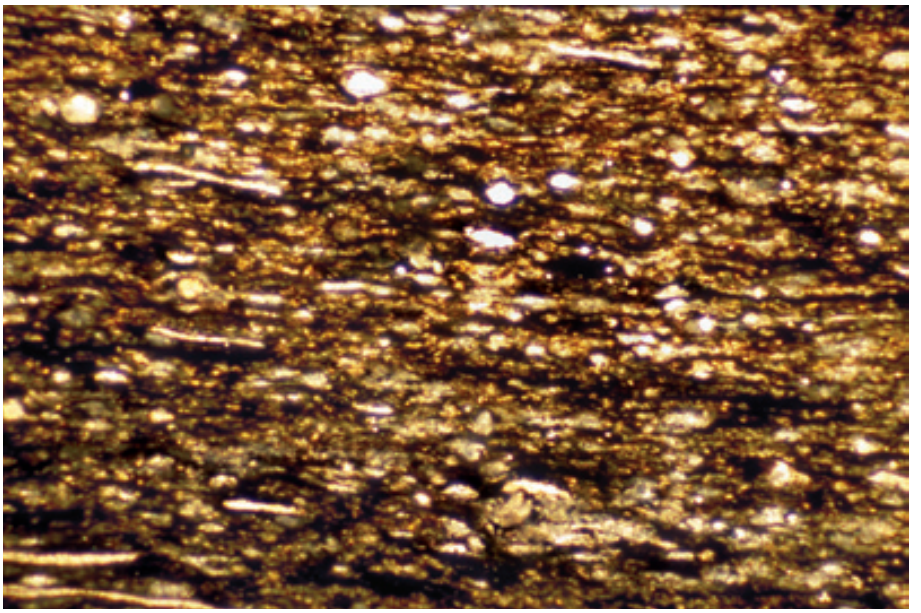

Mid. Triassic (Ladinian) Livinallongo Fm., western Dolomites, Italy

A fine-grained basinal packstone, rich in radiolarians (the spherical, white bodies) and kerogen. Many carbonate rocks have a variety of organic matter of indeterminate origin (visible here as dark brown streaks). Because of the importance of some types of organic matter for generation of hydrocarbons, extensive work has been done on methods for concentration and analysis, both microscopic and geochemical, to determine the origin of such organic detritus. Photograph courtesy of Marco Stefani.

PPL, HA = ~4.0 mm

Cited References and Additional Information Sources

Barron, J.A., 1993, Diatoms, *in* J. H. Lipps, ed., Fossil Prokaryotes and Protists: Oxford, Blackwell Scientific Publ., p. 155-168.

Bertrand, P., J.-L. Pittion, and C. Bernaud, 1986, Fluorescence of sedimentary organic matter in relation to its chemical composition: Organic Geochemistry, v. 10, p. 641-647.

Burckle, L.H., 1978, Marine diatoms, *in* B. U. Haq, and A. Boersma, eds., Introduction to Marine Micropaleontology: New York, Elsevier, p. 245-266.

Carlström, D., 1963, A crystallographic study of vertebrate otoliths: Biol. Bull., v. 125, p. 441-463

Clark, D. L., 1987, Phylum Conodonta, *in* R. S. Boardman, A. H. Cheetham, and A. J. Rowell, eds., Fossil Invertebrates: Palo Alto, CA, Blackwell Scientific Publications, p. 636-662.

Cook, S. F., S. T. Brooks, and H. E. Ezra-Cohn, 1962, Histological studies on fossil bone: Journal of Paleontology, v. 36, p. 483-494.

Donoghue, P. C. J., P. L. Forey and R. J. Aldridge, 2000, Conodont affinity and chordate phylogeny: Biol. Rev. 75: 191-251.

Epstein, A. G., J. B. Epstein, and L. D. Harris, 1977, Conodont color alteration — an index to organic metamorphism: Washington, D.C., U. S. Geological Survey Professional Paper 995, 27 p.

Greguss, P., 1967, Fossil gymnosperm woods in Hungary from the Permian to the Pliocene: Budapest, Akadémiai Kiadó, 136 p.

Haas, W. H., 1941, Morphology of conodonts: Journal of Paleontology, v. 15, p. 71-81.

Haas, W. H., W. Hantzschel, D. W. Fisher, B. F. Howell, F. H. T. Rhodes, K. J. Müller, and R. C. Moore, 1962, Miscellanea, *in* R. C. Moore, ed., Treatise on Invertebrate Paleontology, Part W: Geological Society of America and University of Kansas Press, p. 3-98.

Heusser, L., 1978, Spores and pollen in the marine realm, *in* B. U. Haq, and A. Boersma, eds., Introduction to Marine Micropaleontology: New York, Elsevier, p. 327-340.

Hubert, J. F., and P. T. Panish, 2000, Sedimentology and diagenesis of the dinosaur bones exposed at Dinosaur Ridge along Alameda Parkway in the Morrison Formation (Upper Jurassic), Morrison, Colorado: The Mountain Geologist, v. 37, p. 73-90.

Kozaric, Z., M. Sparica, and Z. Bajraktarevic, 1996, Histological bone structure of Lower Cretaceous dinosaurs from southwest Istria (Croatia): Cretaceous Research, v. 17, p. 741-749.

Lindstrom, M., 1964, Conodonts: Amsterdam, Elsevier Publishing Company, 196 p.

Müller, K.J., 1978, Conodonts and other phosphatic microfossils, *in* B. U. Haq, and A. Boersma, eds., Introduction to Marine Micropaleontology: New York, Elsevier, p. 277-291.

Nicoll, R. S., 1995, Conodont element morphology, apparatus reconstructions and element function; a new interpretation of conodont biology with taxonomic implications, *in* R. Mawson, and J. A. Talent, eds., First Australian Conodont Symposium, v. 182, Senckenbergische Naturforschende Gesellschaft, p. 247-264.

Pietzner, H., et al., 1968, Zur chemischen Zusammensetzung und Mikromorphologie der Conodonten: Palaeontographica, Abt. A, v. 128, p. 115-152.

Rensberger, J. M., and M. Watabe, 2000, Fine structure of bone in dinosaurs, birds and mammals: Nature, v. 406, p. 619-622.

Smoot, E. L., and T. N. Taylor, 1984, The fine structure of fossil plant cell walls: Science, v. 225, p. 621-623.

Stein, C. L., 1982, Silica recrystallization in petrified wood: Journal of Sedimentary Petrology, v. 52, p. 1277-1282.

Stout, S. D., 1978, Histological structure and its preservation in ancient bone: Current Anthropology, v. 19, p. 601-604.

Sweet, W. C., and P. C. J. Donoghue, 2001, Conodonts: past present, future: Journal of Paleontology, v. 75, p. 1174-1184.

Weiner, S., W. Traub, H. Elster, and M. J. DeNiro, 1989, The molecular structure of bone and its relation to diagenesis, *in* H. P. Schwarcz, R. E. M. Hedges, and M. Ivanovich, eds., First international workshop on Fossil bone, v. 4: New York, Pergamon Press, p. 231-232.

Facing Page: Top - Space Shuttle image of the tidal oolite belt at the southern end of the Tongue of the Ocean, Bahamas, in March 1994. Photograph courtesy of NASA, Johnson Space Flight Center.

Bottom - Macrophotograph of modern ooids from Cat Cay, Great Bahama Banks, Bahamas. Photograph courtesy of Clif Jordan.

GRAINS: Non-skeletal Grains

Ooids, pisoids, and other coated grains

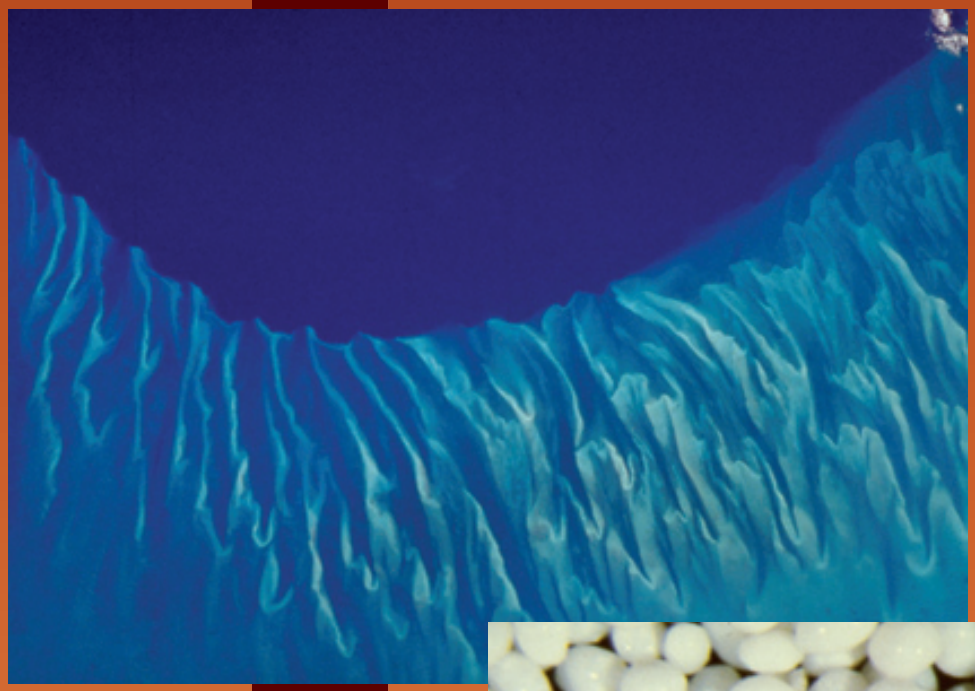

CHAPTER 14

OOIDS, PISOIDS AND OTHER COATED GRAINS

Definitions:

Ooid (oolith) - a spherical to ellipsoidal grain, 0.25 to 2.00 mm in diameter, with a nucleus covered by one or more precipitated concentric coatings (cortical layers) with radial and/or concentric orientation of constituent crystals. Nuclei typically consist of detrital terrigenous grains, skeletal fragments, or pellets and peloids, and coatings can have a variety of compositions. A rock composed dominantly of ooids is termed an "oolite". That term is commonly misused, however, to describe the constituent ooid grains.

Spastolith or deformed ooid - An ooid or other coated grain that has been deformed, generally by shearing the concentric laminations away from each other or from the nucleus. In rarer cases, the deformation is tectonic.

Superficial ooid - An ooid with an incomplete or very thin cortical coating; specifically one in which the thickness of the accretionary coating is less, commonly far less, than the radius of the nucleus.

Pisoid - A small spheroidal particle with concentrically laminated internal structure, larger than 2 mm and (in some usages) less than 10 mm in diameter. A pisolite is a rock containing abundant pisoids.

Oncoid - In North American usage, an oncoid is a coated grain of algal (but not red algal) or microbial origin that is coarser than 2 mm in diameter; a spheroidal form of microbial stromatolite showing a series of concentric (often irregular or scalloped) laminations. These unattached stromatolites are produced by mechanical turning or rolling, exposing new surfaces to microbial/algal growth. Common European usage is less genetic, and in that usage a microbial/algal origin is not a prerequisite. An oncolite is a rock composed of oncoids; the term, however, is often used improperly as a synonym for "oncoid".

Rhodoid (rhodolith) - An irregularly laminated calcareous nodule composed of encrusting coralline algae arranged in more or less concentric layers about a core; spheroidal but knobby surfaced, and up to several centimeters in diameter; form in warm to cool, clear, shallow sea water down to depths of 150-200 m.

Age Range:

Calcareous ooids and pisoids are known from the Late Archean to Recent; specific coated grains, such as *Girvanella* oncoids or red algal nodules (rhodoids) are restricted by the age ranges of the constituent organisms (listed in chapters on organic grains).

Composition:

Modern calcareous ooids are known with aragonite or Mg-calcite compositions (or combinations of both), and there is evidence that these same compositions existed throughout Phanerozoic time, perhaps with specific temporal preferences (e.g., Sandberg, 1983; Wilkinson and Given, 1986). Laminae of organic material are found interlayered in most ooid cortices and help preserve structure during diagenesis.

Calcareous cave and soil pisoids typically have low-Mg calcite compositions. Other ooids/pisoids (covered in later chapters) can have ferruginous (especially hematite or chamosite), siliceous, bauxitic, phosphatic, evaporitic (gypsum, halite) or other coatings.

Environmental Implications:

Ooids and other coated grains require conditions suitable for inorganic or microbial precipitation and for biological encrustation of grains. They also require repeated rotation of grains to allow the formation of concentric coatings. Thus, the best environments for ooid formation are tidal deltas and bars, or beaches (marine or lacustrine) where surficial grains are kept in daily motion. Because reefs or bioherms "compete" with ooids in high-energy settings, biologically stressed areas (with abnormal salinities or temperatures) can favor ooid formation by inhibiting organism growth and enhancing rates of carbonate precipitation. Because of their rounded shape ooids are easily reworked into adjacent environments (especially eolianites).

Other coated grains (superficial ooids, pisoids and oncoids) can be formed in soils and caves (vadoids; cave pearls), in relatively deep-water, current-scoured platform areas (rhodoids), in shelf areas prone to periodic storm action, in partially protected lagoons, and in a wide variety of other settings.

Keys to Petrographic Recognition:

1. **Rounded grains with one or more smoothly concentric to scalloped coatings.**
2. **Size: 0.5 to 2 mm for ooids; >2 mm for pisoids.**
3. **Ooids have concentric or radial primary crystal orientation, typically with a pseudo-uniaxial extinction cross.**
4. **Aragonitic ooids are prone to dissolution — often poorly preserved, forming filled or open moldic porosity.**
5. **Oncoids are characterized by scalloped coatings and (sometimes) by the presence of calcimicrobial fabrics.**

The structural and diagenetic patterns of ooids

A diagrammatic representation of the generalized structure of ooids (left) showing the central nucleus and concentric cortical laminations, composed of calcium carbonate (aragonite or calcite) and organic matter. Four common types of ooid wall structure, primary or secondary also are shown (right) and are explained in subsequent captions. Partially adapted from Tucker (1981).

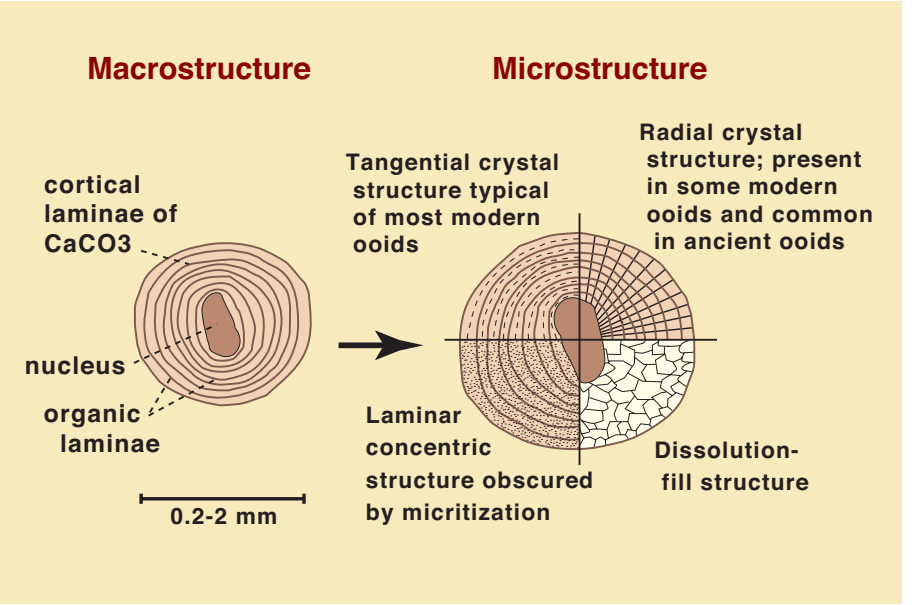

Recent sediment, Joulters Cay, Great Bahama Bank, Bahamas

These modern ooids have peloidal nuclei and numerous concentric cortical coatings of precipitated aragonite. The ooids come from an area where strong tidal currents roll at least the surficial grains every few hours; large storms can move even those grains that are well below the normal sediment-water interface. The brownish color reflects intercrystal microporosity and a high organic content associated with organic films interlayered with the aragonite crystals. Additional organic matter is associated with microbial borings (the small, dark brown patches visible in many grains.

PPL/XPL, HA = 1.0 mm each

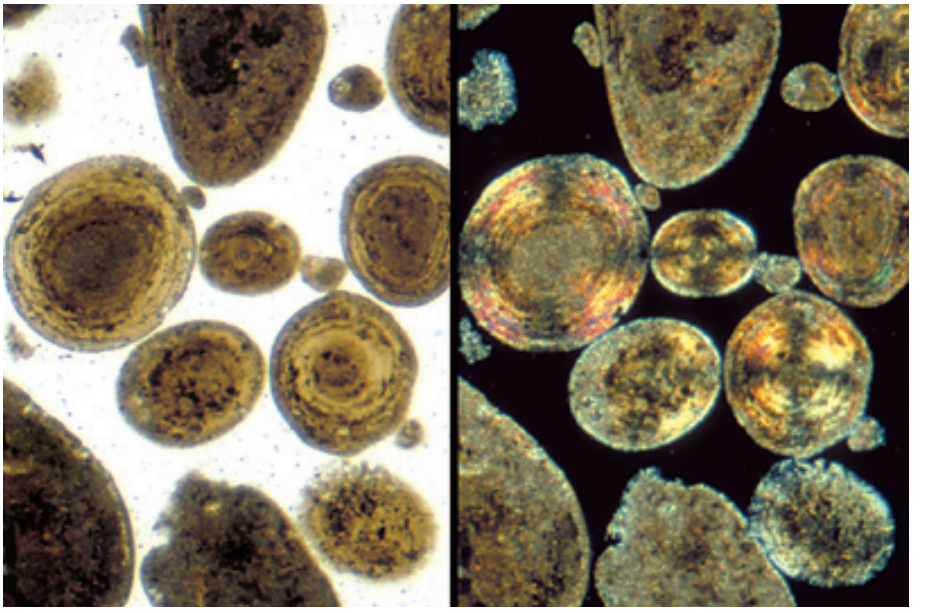

Holocene (<2700 yBP) eolianite, Isla Cancun, Yucatan Peninsula, Mexico

An SEM image of an ooid showing the egg shell-like layering of the precipitated aragonite coatings (cortical layers). Spalling is a result of sample preparation, the presence of organic films that separate individual, thin layers of aragonite crystals, and the partial dissolution of layers that resulted from a short duration of vadose diagenesis. Note also the tubular microbial borings in some parts of the grain. Photograph courtesy of Robert Loucks.

SEM, HA = 250 μm

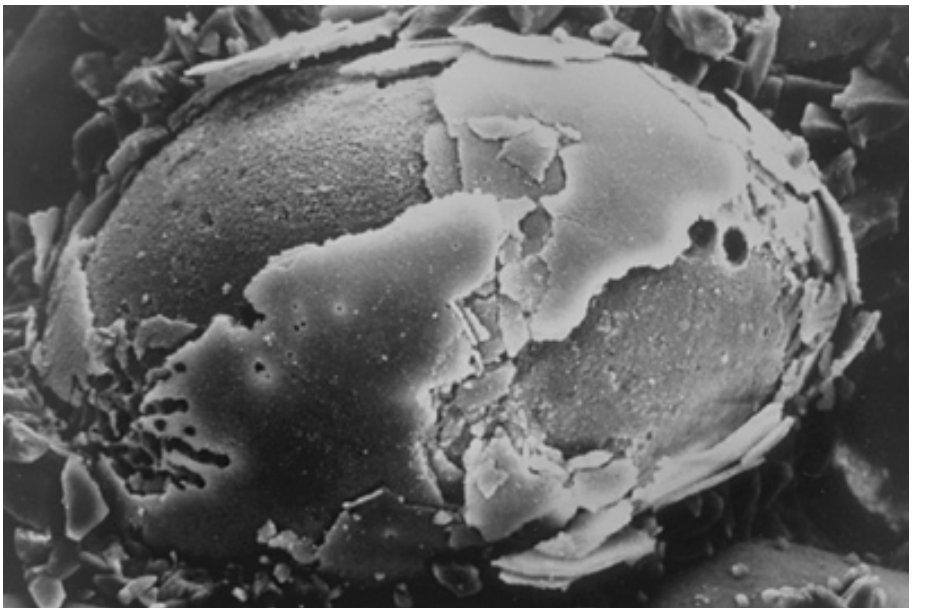

Holocene (<2700 yBP) eolianite, Isla Cancun, Yucatan Peninsula, Mexico

An SEM image of a lightly acid-etched section of a modern aragonitic ooid. The ooid shows alternating layers of tangentially oriented and randomly arranged aragonite needles with high microporosity. The tangentially oriented layers account for the optical behavior of the grains; the randomly oriented layers etch more rapidly, indicating that they may be more susceptible to selective dissolution during diagenesis. Much of the aragonite precipitation has recently been ascribed to nannobacterial activity (Folk and Lynch, 2001). Photograph courtesy of Robert Loucks.

SEM, HA = 4.4 μm

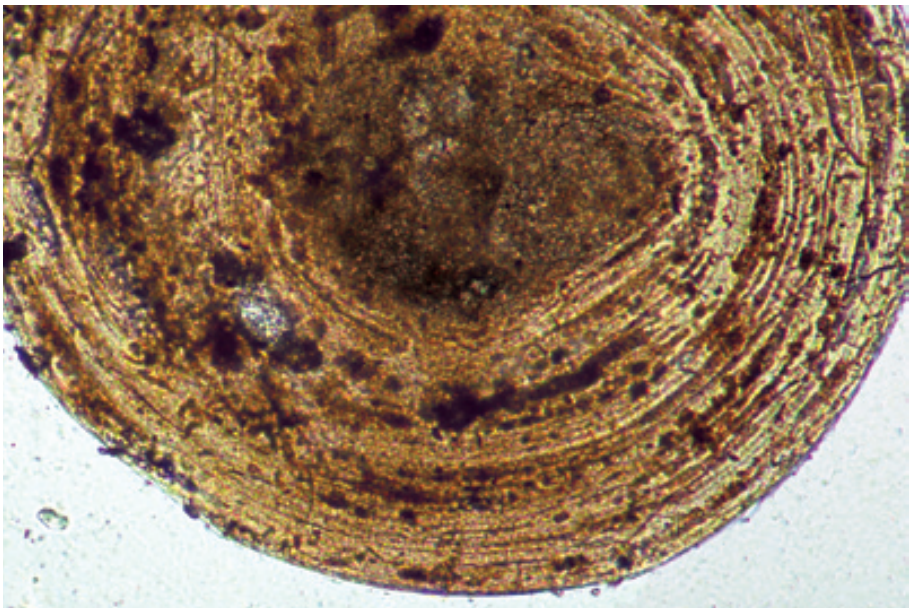

Recent sediment, Bimini area, Great Bahama Bank, Bahamas

A detailed view of a modern concentrically coated ooid showing the peloidal nucleus and multiple concentric layers representing aragonitic coatings of varied thickness. The darker interlayers are rich in organic matter; the small, dark circles and lines represent algal and fungal borings, some filled with micritic cements. These features reflect the battle between constructive and destructive forces in the life of an ooid — construction by precipitation while the grain is in motion at the surface, and destruction by endolithic organisms when it is at rest.

PPL, HA = 0.85 mm

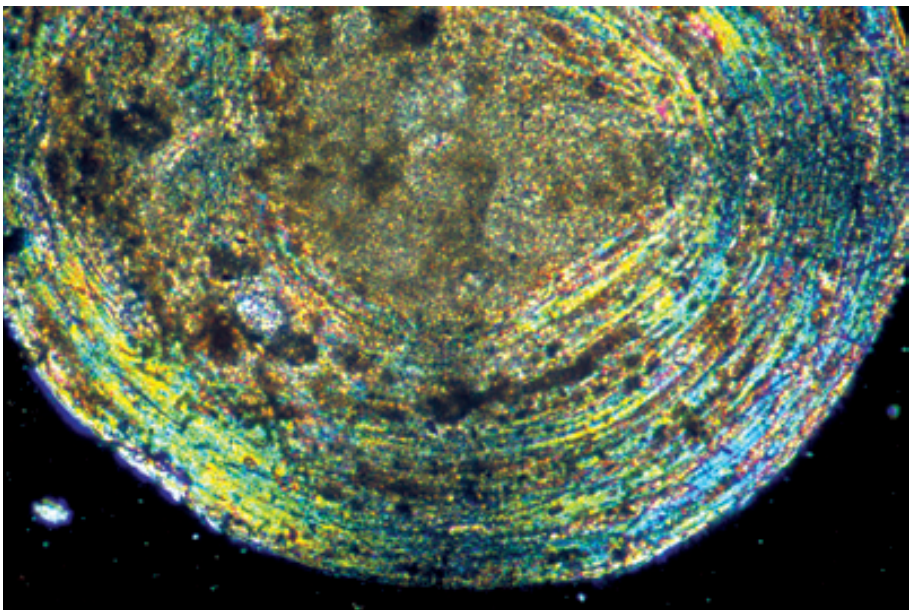

Recent sediment, Bimini area, Great Bahama Bank, Bahamas

The same grain as shown in the previous photograph, here under cross-polarized lighting. The individual layers and borings remain clearly visible and the weak pseudo-uniaxial cross (darker coloration bands at the 0°, 90°, 180°, and 270° positions) reflects the predominantly tangential long-axis (and c-axis) orientations of the aragonite needles that compose the coating layers.

XPL, HA = 0.85 mm

Holocene Cat Cay area, west side of Great Bahama Bank, Bahamas

This thin section of an ooid was de-calcified using hydrochloric acid. Thus, all that remains are the thin layers of organic matter that originally were sandwiched between the layers of (now removed) aragonite crystals; algal borings are also clearly outlined by organic residues. There has been substantial debate over the role of the organic material in facilitating or inhibiting carbonate precipitation and ooid growth (e.g., Mitterer, 1968, 1971; Loreau, 1971). Also note relatively uniform thickness of coating laminae.

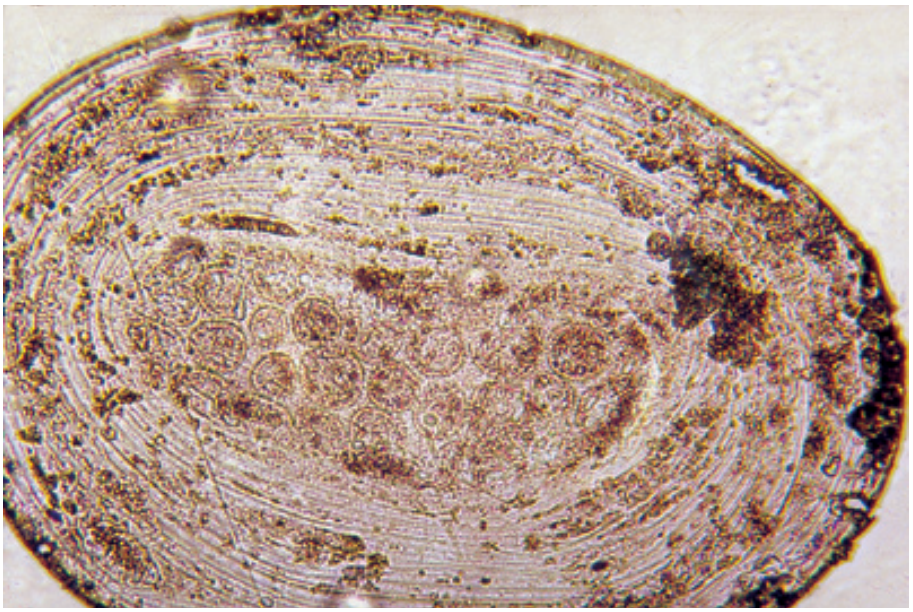

PPL, HA = ~1.2 mm

Holocene, Joulters Cay, Great Bahama Bank, Bahamas

These are sub-Recent and slightly cemented aragonitic ooids that show strong pseudo-uniaxial crosses. SEM studies have demonstrated that this reflects the fact that a majority of the aragonite needles forming the coatings lie randomly in planes tangential to the ooid surface, as one might expect for grains that are being actively abraded by waves and currents. A similar cross can also be produced, however, when crystals are oriented perpendicular to the ooid surface (i.e., radial crystal structure, a fabric that is found in some ooids).

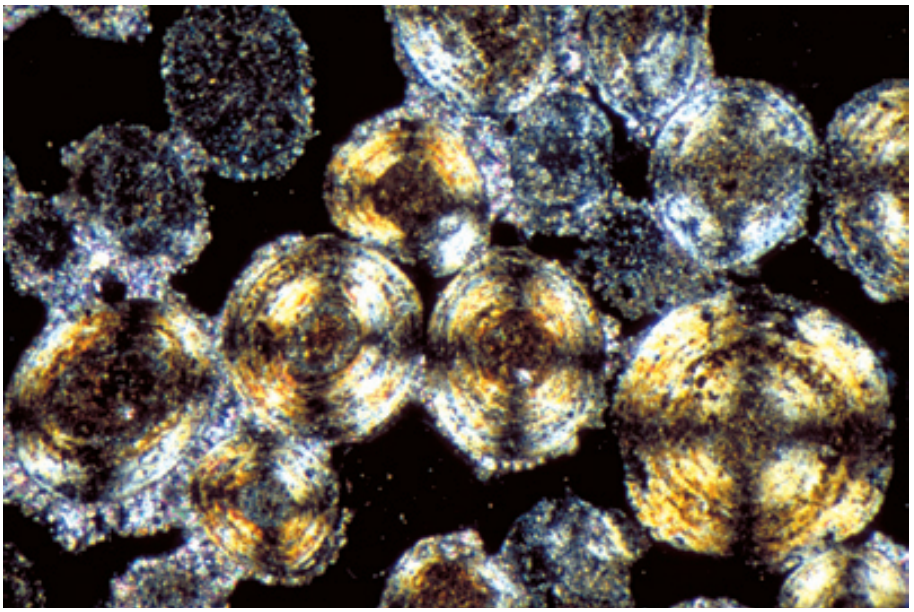

XPL, HA = 2.0 mm

Recent sediment, Joulters Cay, Great Bahama Bank, Bahamas

A modern ooid that has undergone considerable algal and fungal boring (the first of three pictures showing progressive stages of grain alteration). Most of these borings are still unfilled, showing their tubular shape, but some have been filled with Mg-calcite cement and thus appear as diffuse micritic patches. The ultimate recognizability of ooids depends greatly on the degree and nature of syndepositional textural and mineralogical modification.

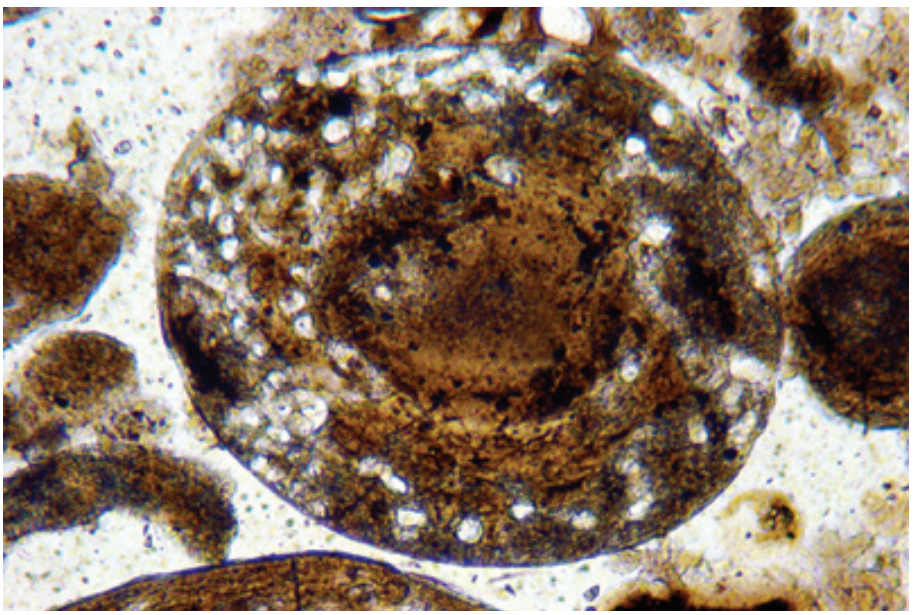

PPL, HA = 0.45 mm

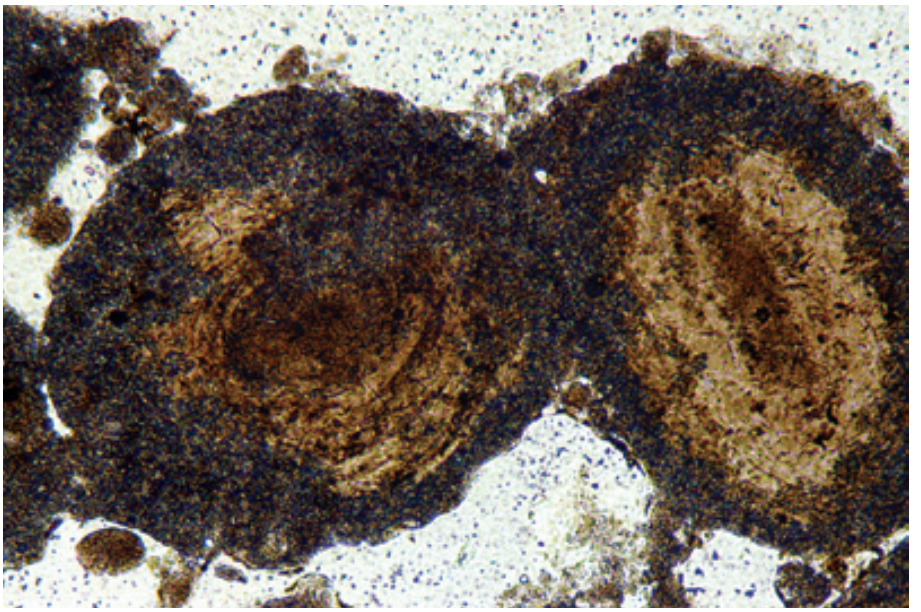

Recent sediment, Joulters Cay, Great Bahama Bank, Bahamas

These ooids have undergone more boring, and even more cementation of those borings, than the ooids in the previous photograph. Although a few individual borings are still visible, most of the grain now has a uniform micritic texture, with some areas of partially unaltered structure in the interior parts of the ooids. This level of grain destruction commonly occurs when ooids are transported from the site of active coating formation in tidal bars to adjacent, more protected settings (washover into grassy subtidal flats, for example).

PPL, HA = 1.0 mm

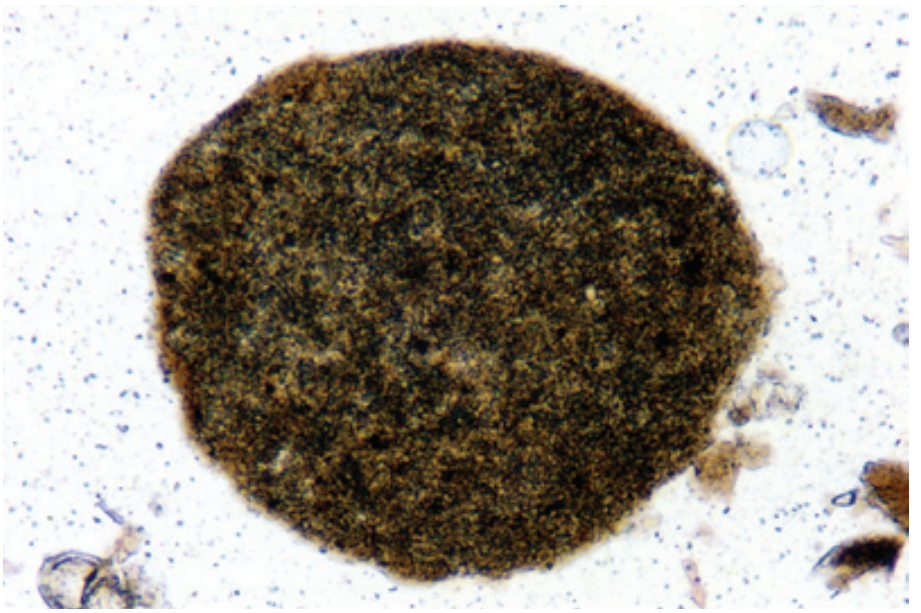

Recent sediment, Joulters Cay, Great Bahama Bank, Bahamas

An example of a probable former ooid that has been completely micritized. Although the section may be somewhat tangential to the ooid center, no remnant structure is visible in this cut, and the grain would have to be classed as a peloid. Other than size and shape, no textural characteristics remain that would allow identification of this grain as an ooid.

PPL, HA = 0.8 mm

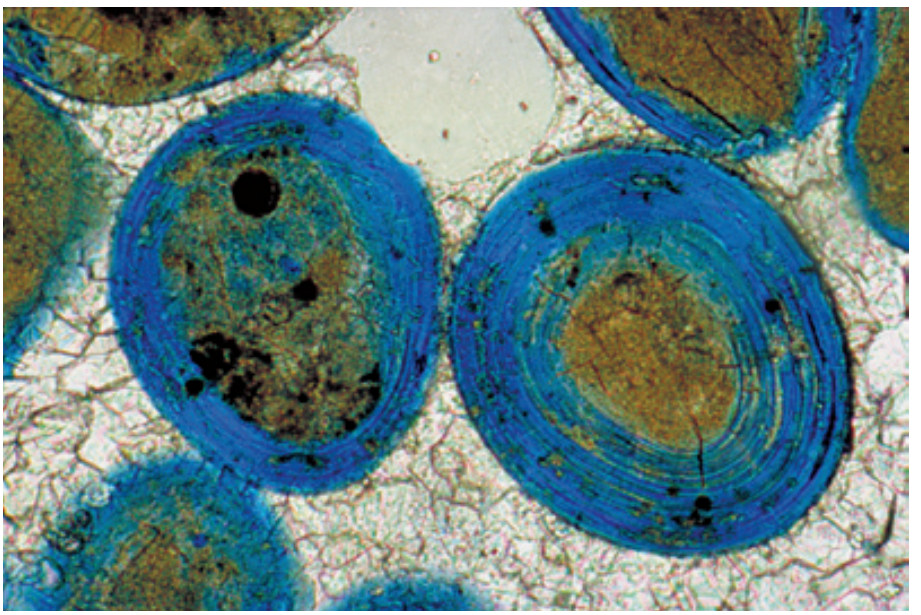

Holocene (<2700 yBP) eolianite, Isla Cancun, Yucatan Peninsula, Mexico

Alteration of ooids also can take place in fresh-water settings, especially where ooids have a primary aragonitic composition. This oolitic eolianite has undergone both vadose and phreatic diagenesis, with cementation of primary porosity and selective ("chalky") dissolution of original ooids. The remarkable lack of collapse of the remaining cores within these grains is largely due to preservation of the organic layers and retention of some minimal framework of primary carbonate material. Photograph courtesy of Robert Loucks.

PPL, BSE, HA = 0.65 mm

Pleistocene (120kyBP) Miami Ls., Dade Co., Florida

This ooid has undergone about 120,000 years of subaerial exposure and meteoric diagenesis. Interparticle porosity was filled with sparry calcite (white) and a substantial part of the original aragonite (some of which is still present in the brownish areas near the center) was dissolved, as in the previous example. Here, however, the secondary pore space created by aragonite dissolution later was filled with low-Mg calcite (the white material in the outer layers). Although the secondary calcite is fairly coarse and blocky, it still preserves elements of the original concentric lamination thanks to the durability of the organic interlayers.

PPL, HA = ~1.0 mm

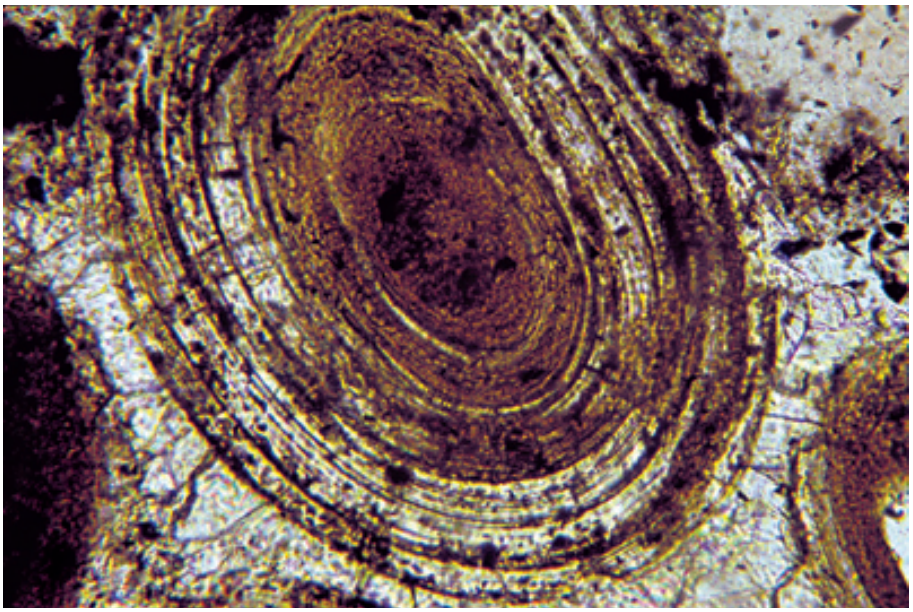

Up. Cambrian Gallatin Ls., Wind River Range, Wyoming

Even the presence of organic interlayers cannot prevent the complete destruction of internal fabric in some cases. This example shows a completely neomorphosed oolite. These grains have probably undergone dissolution of coatings as well as cores and later filling by sparry cement. Although nothing remains to conclusively identify these as ooids, the grain size, the high degree of rounding, and the excellent sorting all make an ooid origin likely. The apparent preferred orientation of elongate ooids may result from deformation during burial.

PPL, HA = 2.8 mm

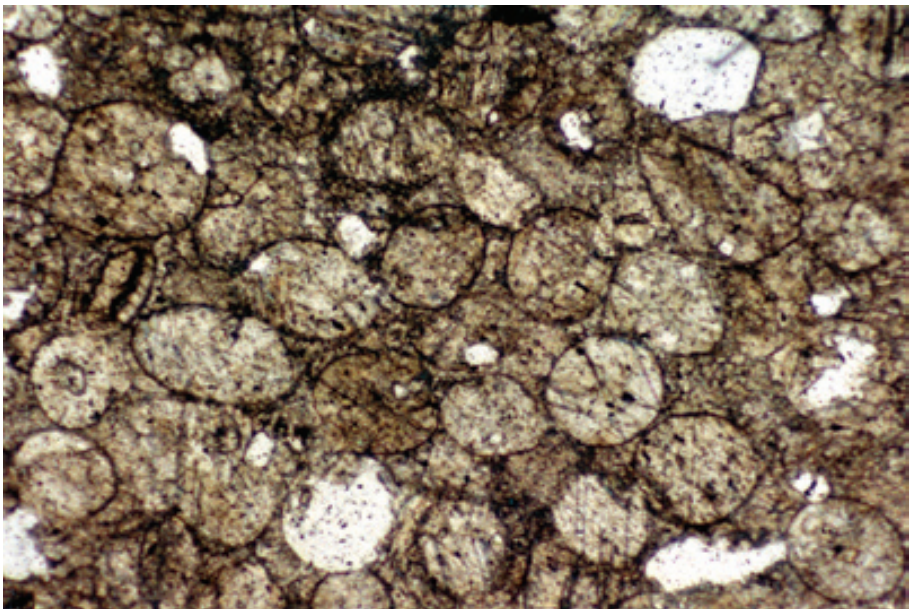

Up. Cambrian Allentown Ls., State College area, Pennsylvania

This is another example of alteration of ooids that originally were at least partially aragonitic. Selective dissolution of the cortical layers left the apparently less soluble (calcitic?) nuclei unsupported. This resulted in gravitational collapse of the undissolved material to the bottoms of the ooid molds, producing a striking geopetal fabric. The collapse was followed at some later date by spar infill of the moldic pores.

PPL, HA = 8 mm

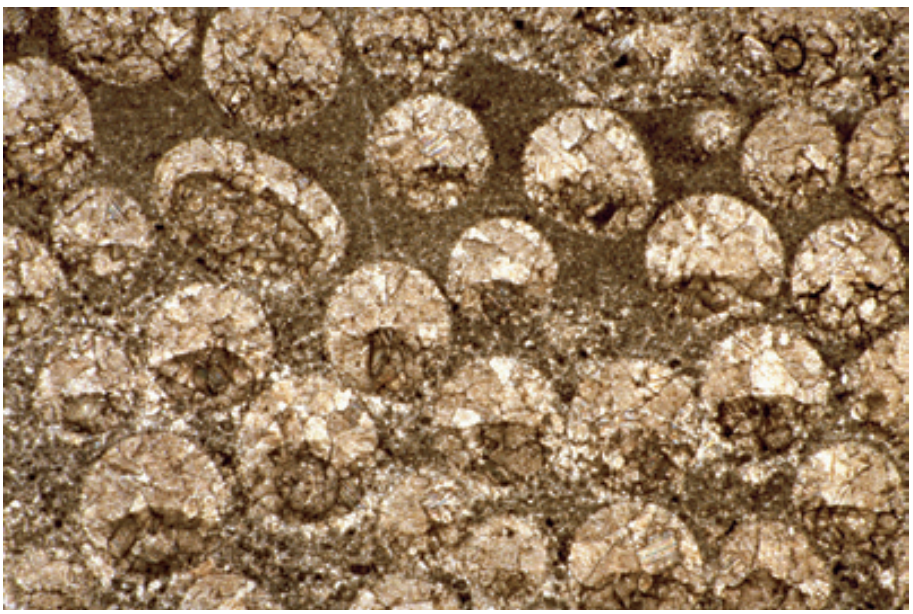

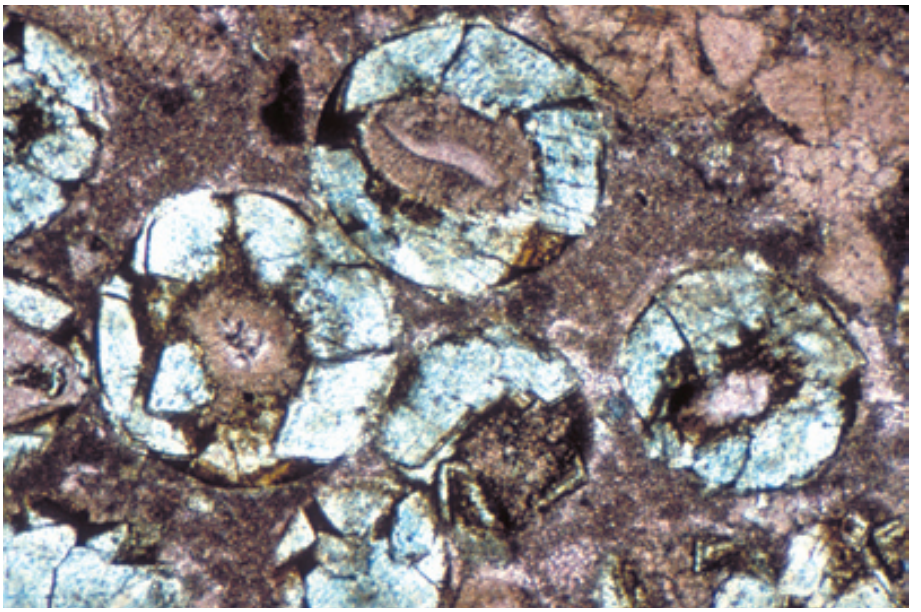

Up. Cambrian Lynx Gp.?, Mountain Park, Alberta, Canada

Destruction of ooid fabrics can also take place during burial diagenesis (no, an ooid can never relax). In this example, the ooid coatings were selectively replaced by saddle (baroque) dolomite — the coarse crystals with curved faces that are stained pale blue in this section. The selective preservation of ooid nuclei and inner cortical coatings, however, makes it easy to identify these grains as ooids despite their late-stage alteration.

PPL, AFeS, HA = 2.4 mm

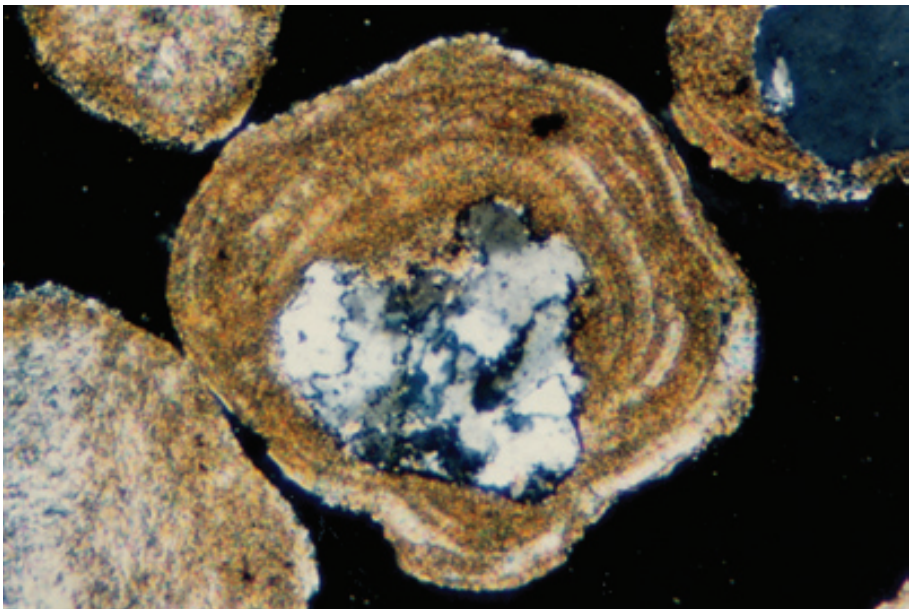

Recent sediment, Point of Rocks, Baffin Bay, Laguna Madre, Texas

Not all modern or ancient ooids were originally composed of aragonite. In the variable (sometimes quite high) salinity and only episodically high-energy environment of Laguna Madre and Baffin Bay, ooids with generally thin and often incomplete coatings of mixed mineralogy are produced. The cortical coatings consist of interlayers of aphanocrystalline, equant (granular) high-Mg calcite and coarser, radial aragonite (both seen here). The nucleus of the grain in the center of the field of view is a detrital metaquartzite fragment.

XPL, HA = 0.55 mm

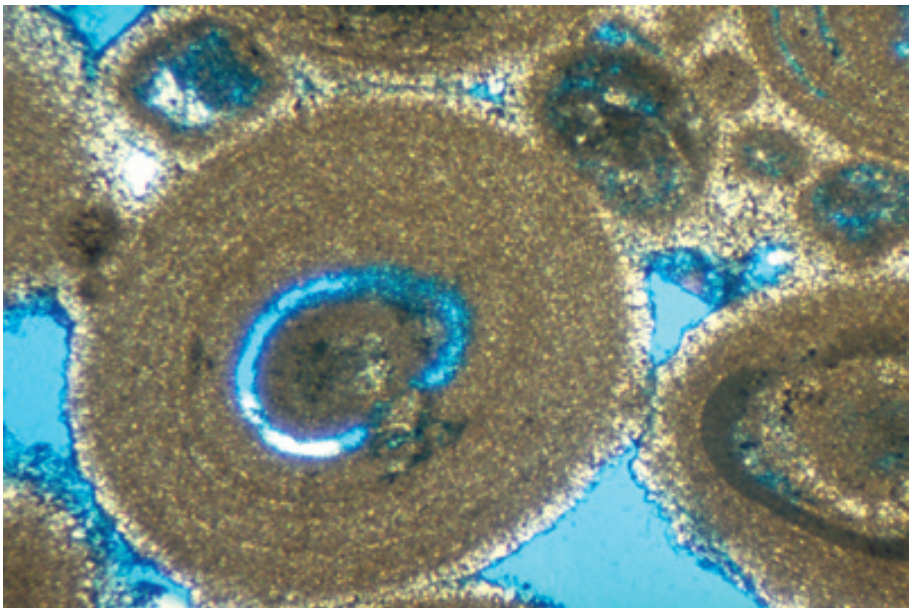

Lo. Permian (up. Kungurian) Irenskaya/Nevolinskaya Suite, Perm Region, Russia

Ancient ooids as well as modern ones can have granular or micritic cortical fabrics — in this case with only traces of preserved concentric structure. These ooids are associated with a strongly evaporitic carbonate section and may have had originally high-Mg calcite compositions.

PPL, BSE, HA = 2.0 mm

Jurassic (Corallian) Lo. Osmington Oolite, Dorset, England, U.K.

Previous pictures have illustrated mainly aragonitic ooids and their extensive alteration or Mg-calcite ooids with granular/micritic fabrics. Calcitic ooids, however, predominated at many times in the past (Sandberg, 1983) and can show diverse and well preserved fabrics. This oosparite, for example, has extremely well preserved ooid fabrics, including concentric layering, brownish color, pseudo-uniaxial crosses, borings and some traces of radial as well as concentric structure.

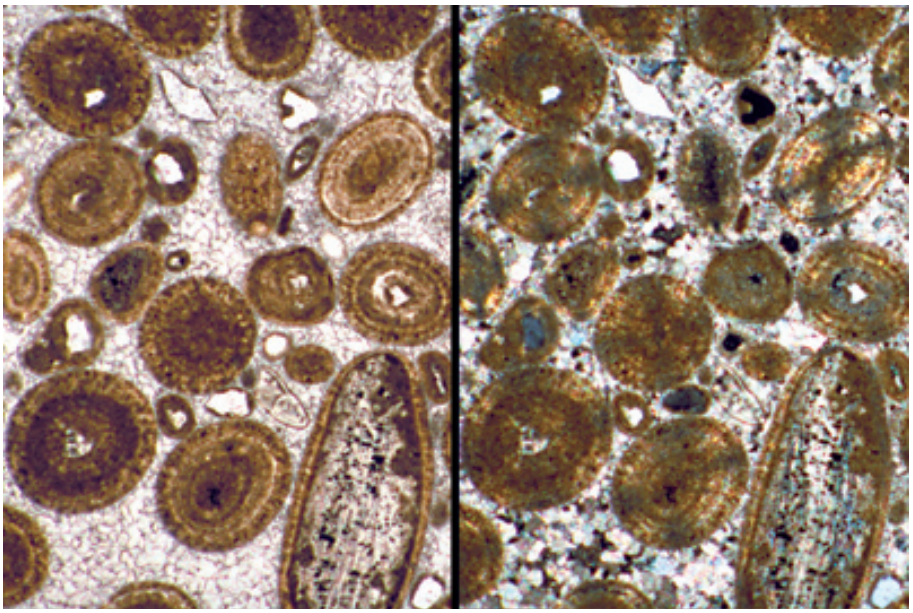

PPL/XPL, HA = 1.6 mm each

Up. Jurassic (Oxfordian) Up. Smackover Fm., 10,216 ft (3,114 m) depth, south Arkansas

This is another example of exceptional fabric preservation in ooids, again of Jurassic age. This ultra-thin section shows superb retention of fine-scale cortical laminae with radial micro-crystal orientation yielding clear pseudo-uniaxial crosses. Note the fact that the marine cement that surrounds the ooids has formed in optical continuity with the radial ooid crystal structure. Photograph courtesy of Clyde H. Moore.

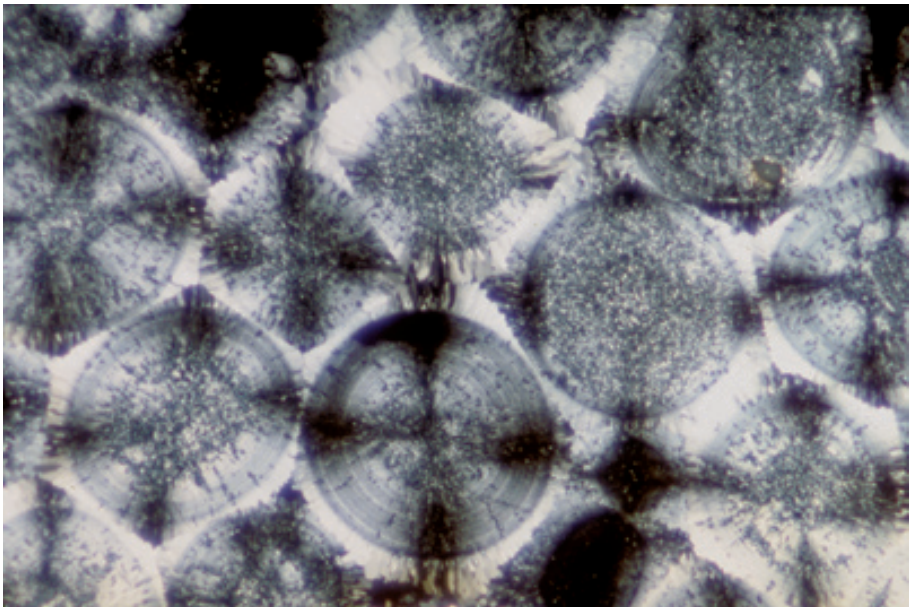

XPL, HA = ~1.2 mm

Recent sediment, Promontory Point, Great Salt Lake, Utah

Radial crystal structure is also found in modern ooids, especially, but by no means exclusively, in lacustrine settings. These ooids have coarse, radiating crystals of bladed to fibrous aragonite interspersed with layers of tangential, very finely crystalline aragonite. Coarsely radial ooid deposits commonly have very high percentages of grains that have broken along the planes of the crystal fabric.

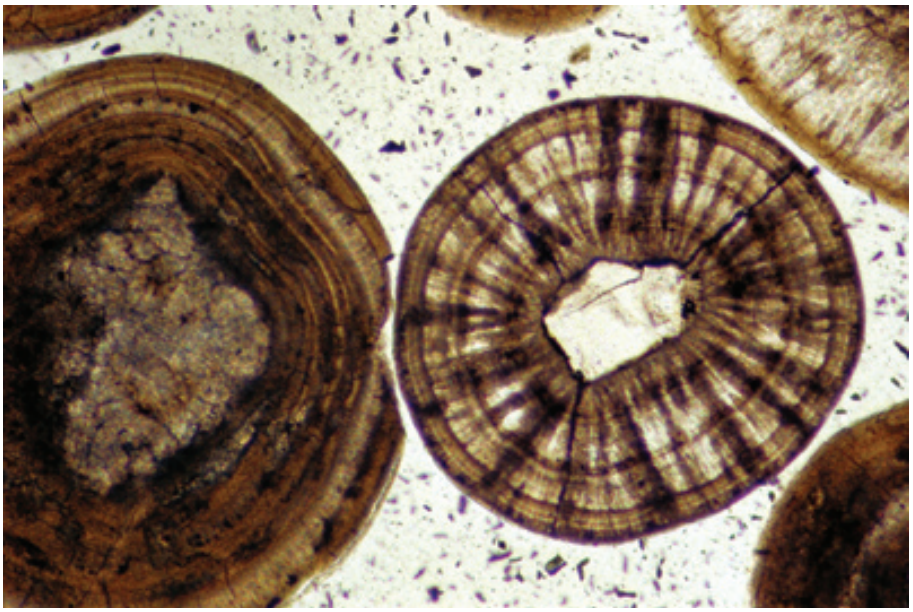

PPL, HA = 0.9 mm

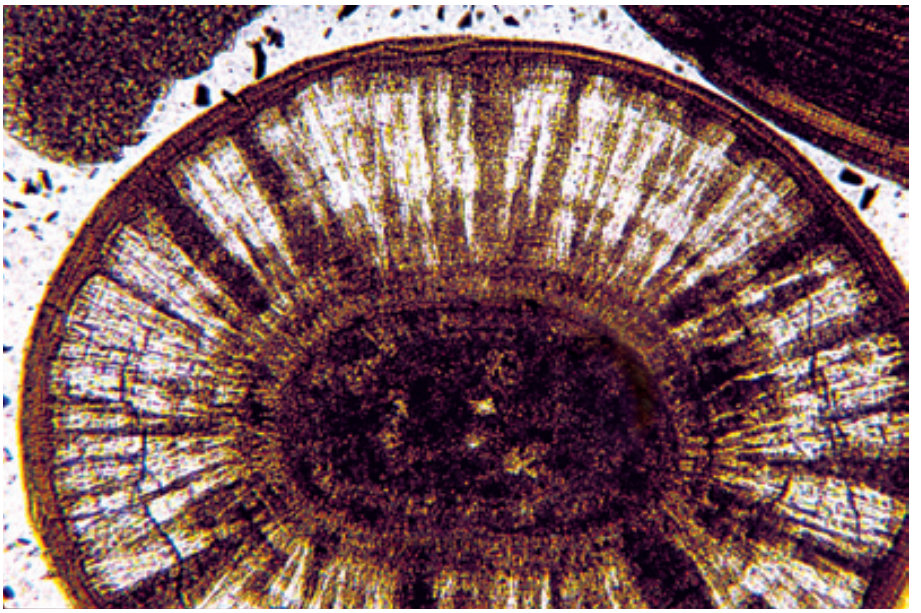

Recent sediment, Great Salt Lake, Utah

A magnified view of a modern ooid with a well defined radial aragonitic structure, as well as strong traces of concentric lamination. Although the coarse, radial aragonite rays appear to cross-cut fabric (and have thus been interpreted by some as a product of recrystallization), they are primary features in these modern grains.

PPL, HA = ~1.2 mm

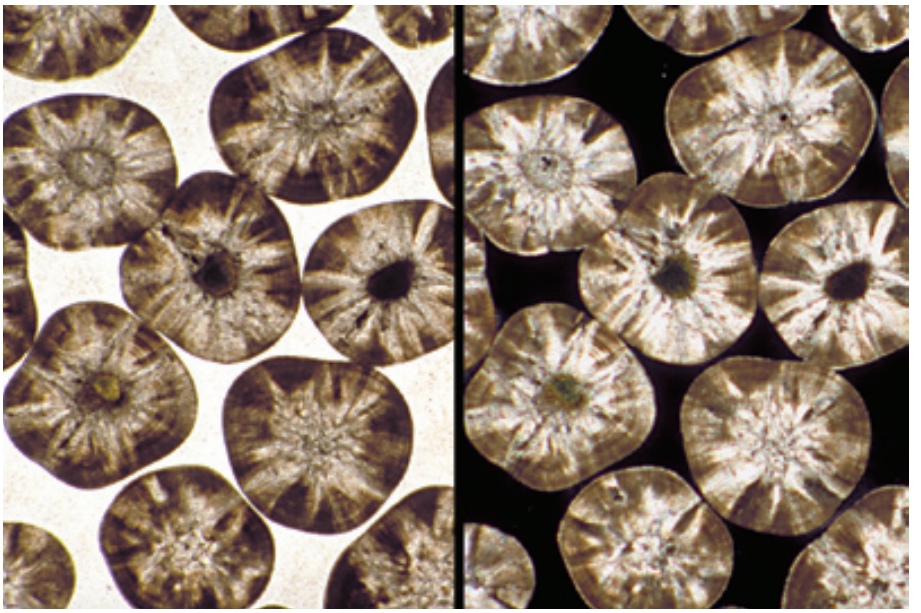

Recent sediment, Florida City, Dade Co., Florida

An example of radial ooids from the boilers of a thermal water-desalinization plant. The calcitic precipitates have formed around quartz, glauconite, and other grains that passed through the plant's intake filters. Radial structure clearly can be a primary fabric, as in this case, but it can also form diagenetically in other cases.

PPL/XPL, HA = 2.0 mm each

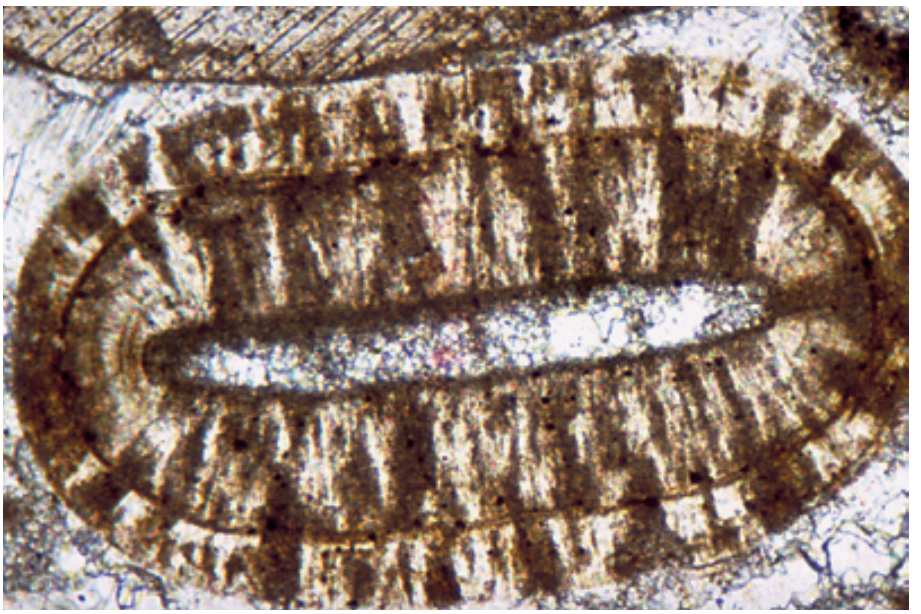

Mid. Jurassic (Bajocian) limestone, Central High Atlas region, Morocco

An example of an ancient ooid with coarse, radial crystal structure and concentric lamination. This appears to be a predominantly primary fabric in an originally calcitic ooid. Determining the original mineralogy of ancient ooids can be difficult unless they still have aragonite or high-Mg calcite compositions. Determination typically involves looking for micro-inclusions of original material or examining trace-element compositions: originally aragonitic ooids *may* have high Sr concentrations and originally high-Mg calcite ooids *may* have high Mg concentrations or micro-dolomite inclusions.

PPL, HA = 0.65 mm

Lo. Ordovician Arbuckle Gp., Cool Creek Ls., Murray Co., Oklahoma

An older oolite with radial crystal structure and concentric lamination in its constituent ooids. In this case, the radial fabric completely cross-cuts other fabric and may be, at least partially, a diagenetic feature.

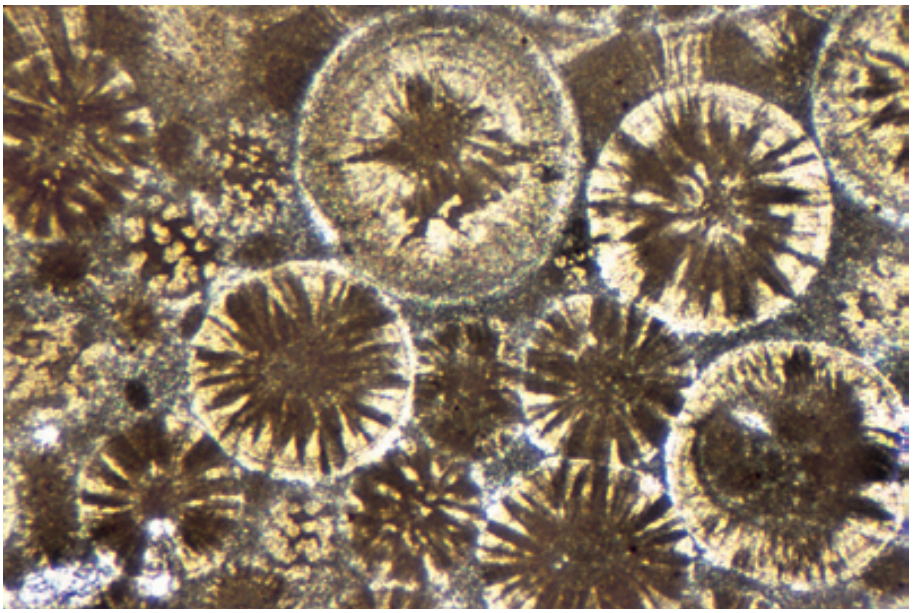

PPL, HA = 2.0 mm

Up. Cambrian Lynx Gp.?, Mountain Park, Alberta, Canada

An example of a 500-m.y.-old oolite in which the ooids have radial fabrics that yield strong pseudo-uniaxial extinction crosses. Upon closer examination, however, it is clear that substantial diagenetic alteration has occurred in this deposit. The original, radiating fibrous crystals in the central parts of the ooids have been incorporated into large single crystals containing subsectors with divergent c-axis orientations.

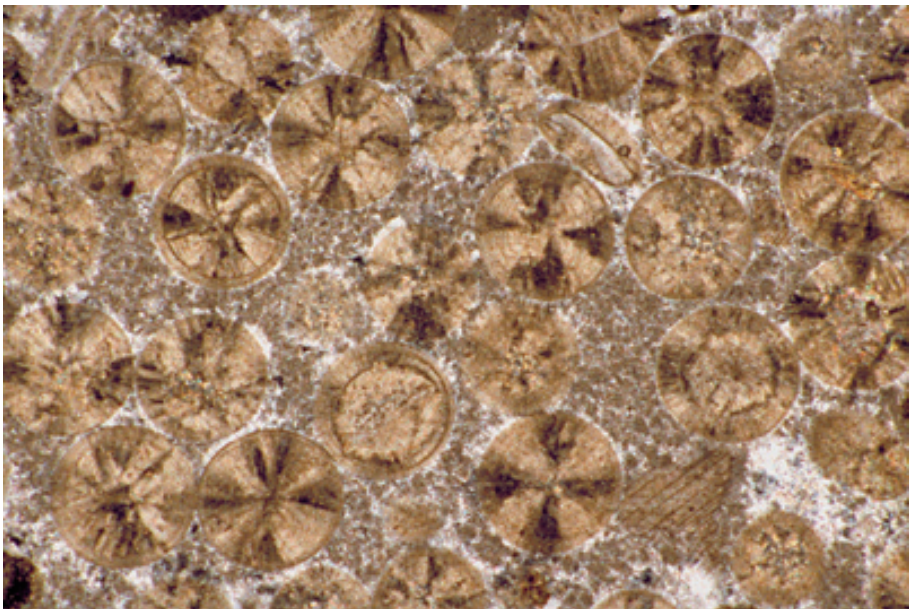

XPL, AS, HA = 5.0 mm

Up. Jurassic (Oxfordian) Up. Smackover Fm., U.S. Gulf Coast

Fabric preservation (or lack thereof) can yield evidence of mixed mineralogy ooids. Some of these ooids have a relatively well preserved, laminated, granular wall fabric that probably was originally calcitic. Other parts, presumably originally composed of more soluble aragonite, were completely leached. In some cases, leaching led to collapse of undissolved cores and residues of cortical layers into geopetal heaps on the cavity floors. Dolomite has partially replaced the primary calcite and the leached (secondary) pores were later filled with blocky calcite. Photograph courtesy of Clyde H. Moore.

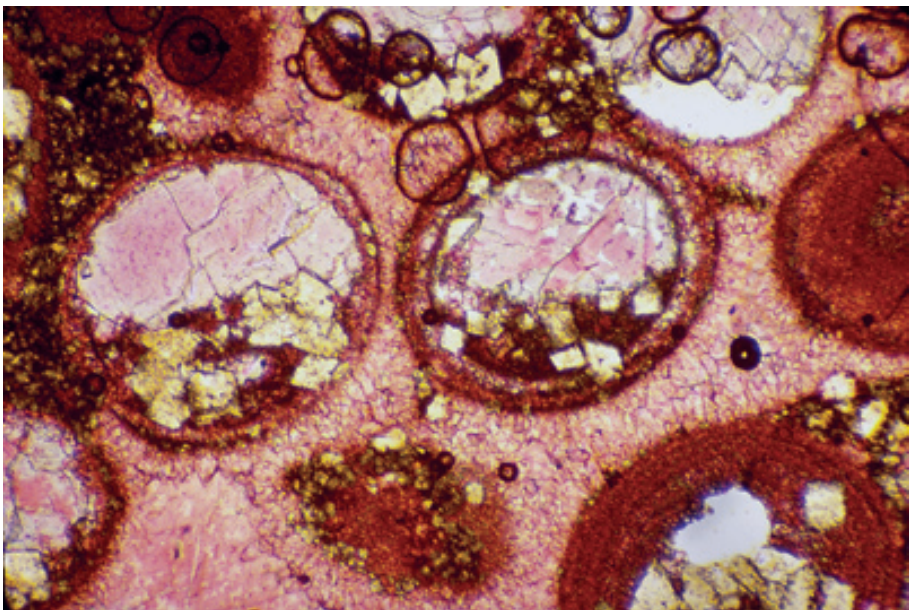

PPL, AS, HA = 1.2 mm

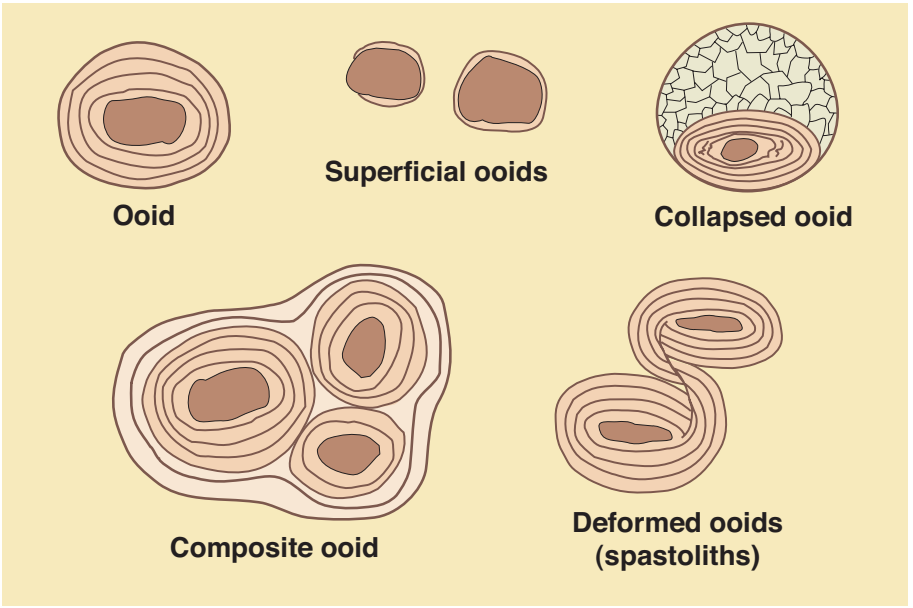

Some common types of ooids

A diagrammatic sketch of some of the common variants of normal ooids. Superficial ooids have only a few thin coatings; collapsed ooids have undergone partial dissolution and internal collapse of remaining undissolved materials to the bottom of the mold; composite ooids represent the coalescence of two or more ooids, with concentric layers covering all the incorporated particles; and deformed ooids reflect compaction or tectonic compression or shearing, commonly with some separation of cortical layers from their nuclei. Partially adapted from Tucker (1981).

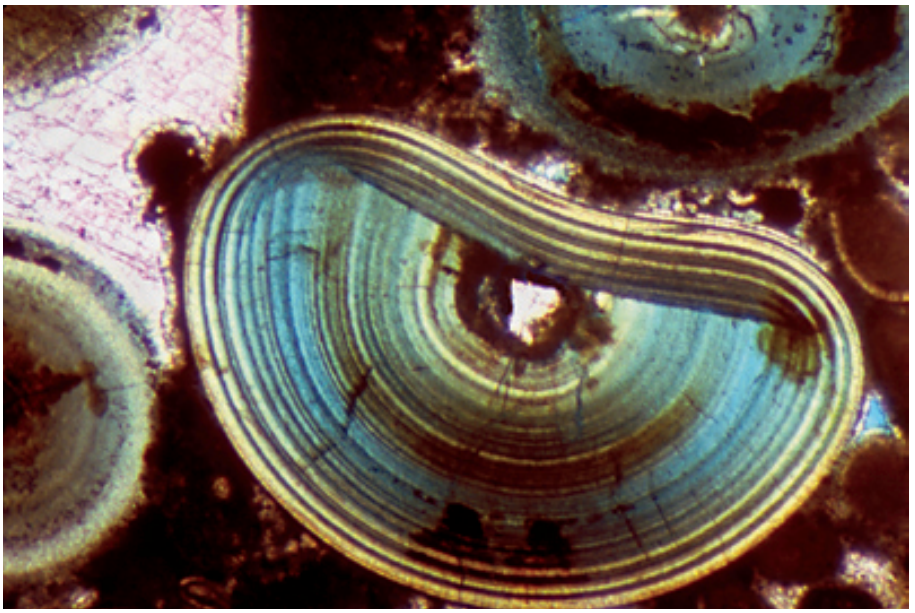

Up. Permian (Ufimian) Solikamsky Horizon, Perm Region, Russia

These beautifully laminated ooids are from a high-energy, hypersaline coastal deposit. This view shows a broken and overgrown ooid (with internal microporosity filled with blue-dyed epoxy). It is common in high-energy settings for ooids to fracture and for the fragments to become nuclei for further ooids. This occurs most frequently in ooids with radial crystal structure but can also occur, as here, in ooids with tangential structure.

PPL, AFeS, BSE, HA = 1.6 mm

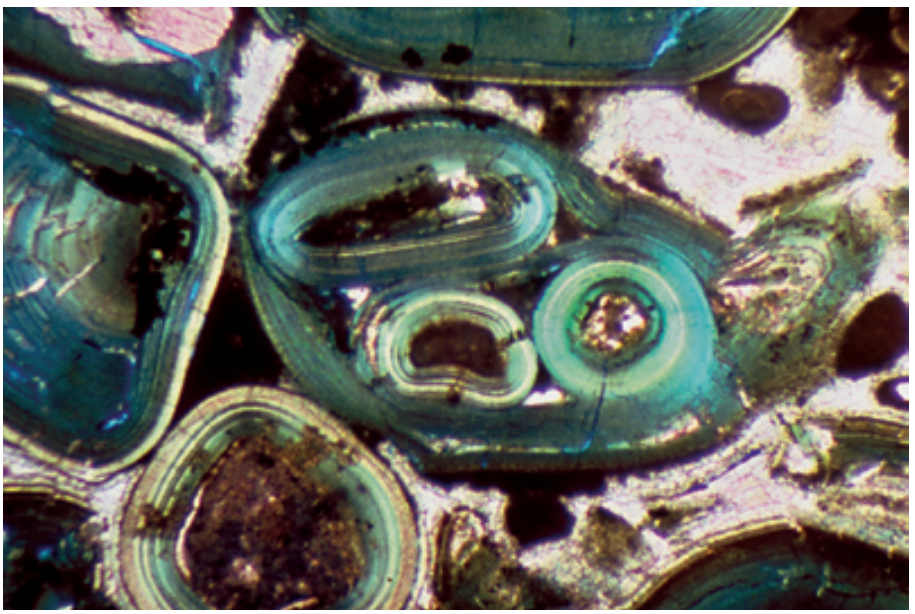

Up. Permian (Ufimian) Solikamsky Horizon, Perm Region, Russia

This is an example of a composite (or compound) ooid, again with internal microporosity filled with blue-dyed epoxy. Note the thick cortical coatings that surround the composited smaller ooids.

PPL, AFeS, BSE, HA = 2.4 mm

Recent sediment, Isla Cancun, Quintana Roo, Mexico

Superficial ooids have thin, sometimes incomplete oolitic cortical coatings. This example shows grains with large nuclei and only one or two thin, birefringent, aragonite coatings. The ooid in the lower center was broken after the formation of its coatings.

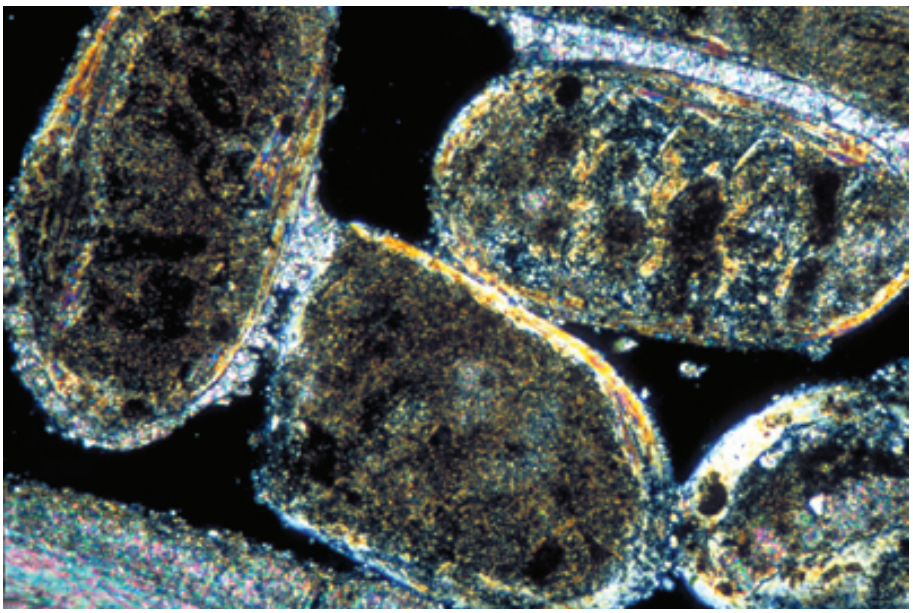

XPL, HA = 0.6 mm

Recent sediment, Point of Rocks, Laguna Madre, Texas

This illustrates an incomplete or eccentric cortical coating on an ooid. These occur most commonly on grains from low energy (or only intermittently high energy) ooid-forming areas. The Mg-calcite and aragonitic coatings are quite thick, but only cover a portion of the grain. The rest of the grain was probably resting on the bottom sediment and agitation was insufficient to cause grain rotation.

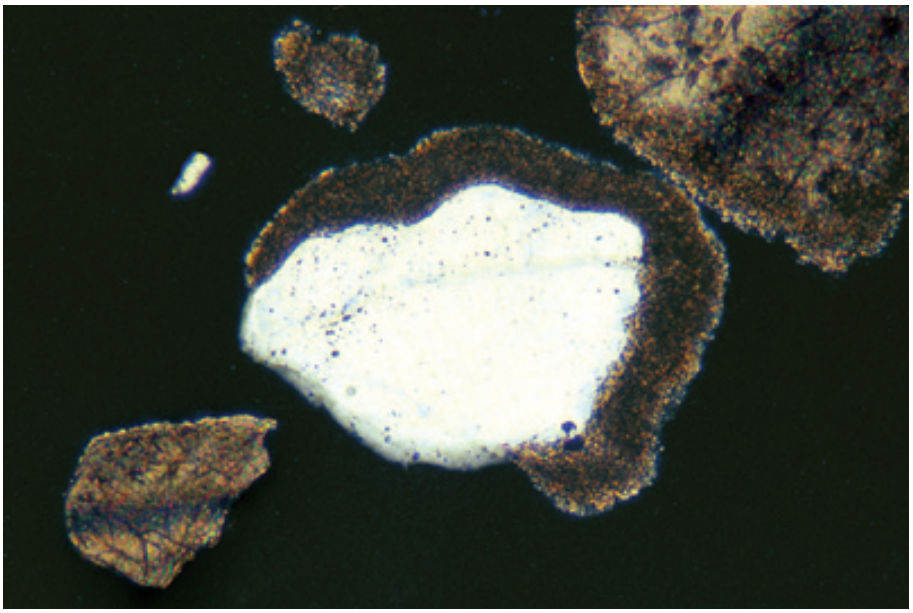

XPL, HA = 0.8 mm

Recent sediment, Isla Cancun, Quintana Roo, Mexico

Superficial ooids and eccentric ooids are common in both modern and ancient deposits. Superficial or eccentric cortical coatings are generally formed on irregularly shaped grains. Here, thin and irregular oolitic coatings thin substantially in some places and thicken in others, especially where they fill indentations in the grain. This infilling process allows many ooids to have a more spherical shape than their nuclei.

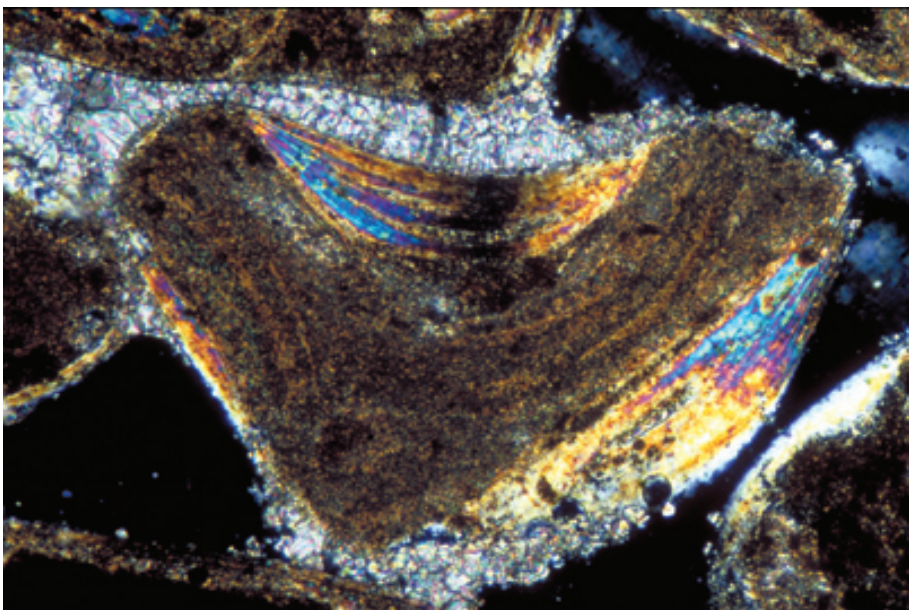

XPL, HA = 0.6 mm

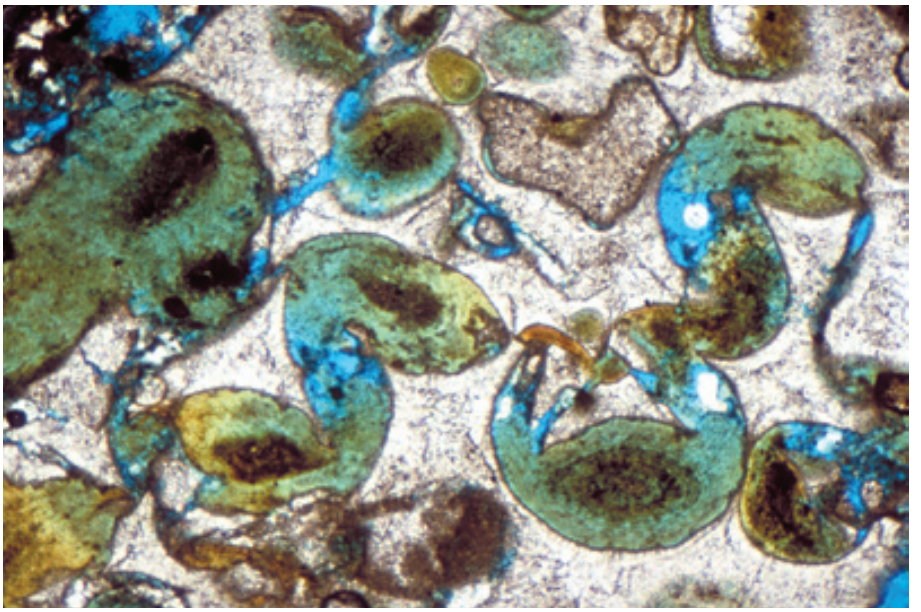

Pennsylvanian (Missourian) Dennis Fm., Winterset Ls., Jackson Co., Missouri

Partially dissolved and/or deformed ooids (spastoliths) that are surrounded by both pre- and post-deformational calcite cement. Unless ooids are surrounded by massive early calcite cement before or during the time of their dissolution, overburden loading or tectonic shearing can easily deform the grains producing these oddly joined fabrics that R. L. Folk has likened to "an elephant parade", where each pachyderm holds the tail of the previous one in its trunk. In this example, some sparry calcite cement has collapsed into the cavities, indicating that some spar predated compaction.

PPL, BSE, HA = 2.4 mm

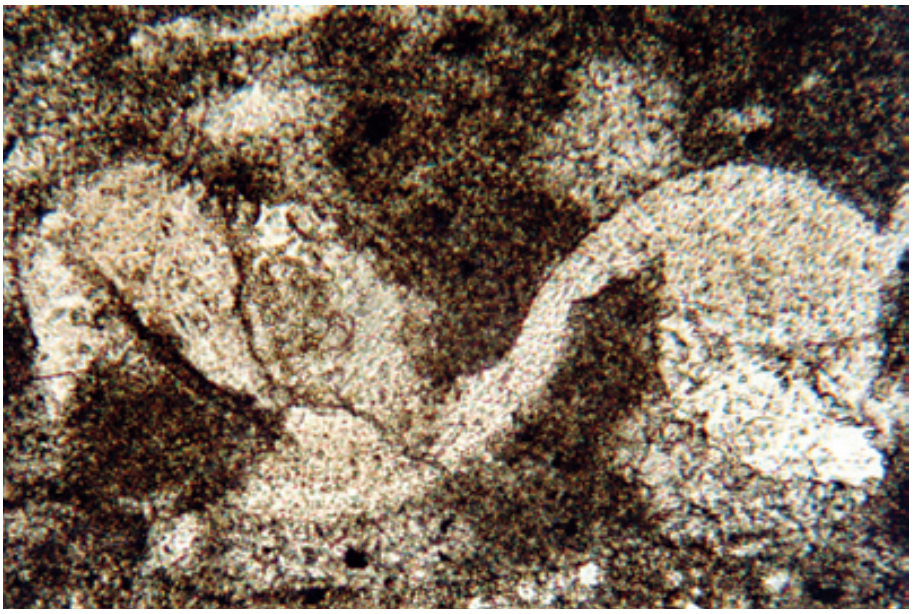

Lo.-Mid. Pennsylvanian Bloyd Fm., Mayes Co., Oklahoma

These deformed ooids have undergone a complex sequence of alteration. They were completely dissolved during the alteration from aragonite to calcite and also have been compacted or sheared, yielding a spastolith texture. The outer cortical layers have been sheared off to produce what looks like a series of linked grains with no remaining internal fabric.

PPL, HA = 0.36 mm

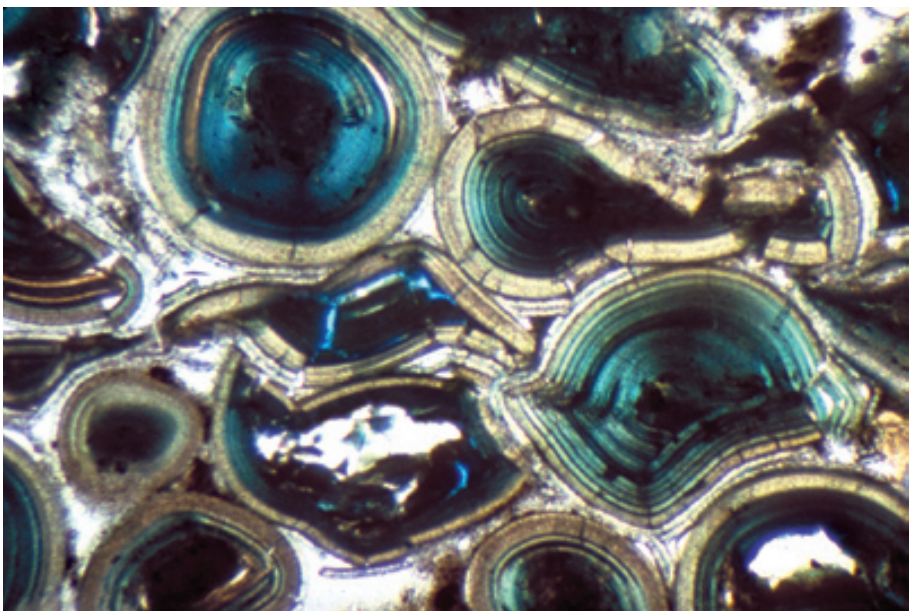

Up. Permian (Ufimian) Solikamsky Horizon, Perm Region, Russia

In these ooids, the presence of soft cores or the selective dissolution of hard cores, coupled with partial dissolution of cortical layers, led to compactional crushing and fitting together of the ooids.

PPL, BSE, HA = 2.4 mm

Late Tertiary-Quaternary caliche, Midland Co., west Texas

Pisoids are coated grains larger than 2 mm in diameter. This is an example of a mature caliche containing soil pisoids (vadoids). Note the irregular, asymmetrically coated grains with abundant inclusions of detrital terrigenous silt and sand. Caliche pisoids grow with preferential downward elongation but the pisoids typically are rotated into a variety of positions. Thus, one can see different directions of elongation between grains and even at different stages of growth within a single grain.

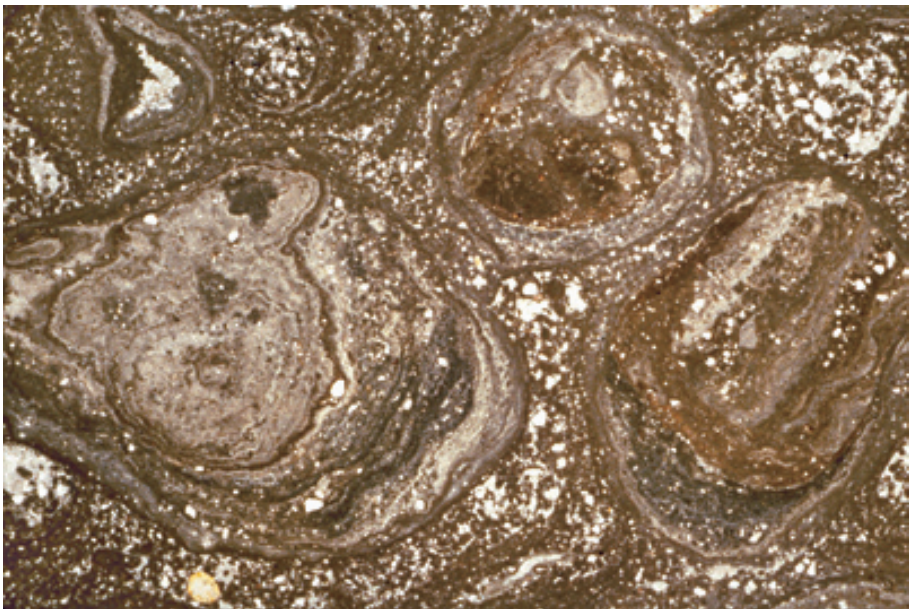

PPL, HA = 16 mm

Tertiary Arkansas Bauxite, near Little Rock, Arkansas

These too are soil-related pisoids, but not of carbonate composition — they are ferruginous pisoids in a commercial bauxite deposit. Note the coated grains containing a variety of aluminous clays and other minerals. This rock is the product of long-term weathering and lateritic/bauxitic "soil" formation.

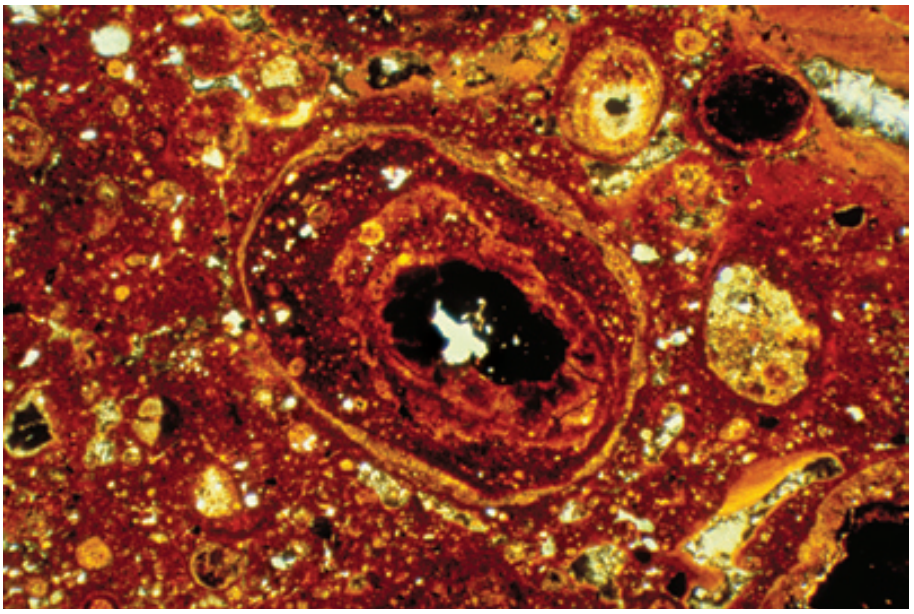

PPL, HA = 5.1 mm

Up. Permian (Guadalupian) Park City Fm., Ervay Mbr., Big Horn Co., Wyoming

These dolomitized pisoids are from an evaporitic coastal environment (probably a shallow, hypersaline lagoon to tidal flat setting). These pisoids are of uncertain origin (caliche, algal/microbial, marine seepage spring, or other). They are, however, interbedded with fenestral, microbially-laminated material. Such deposits are especially common in Permo-Triassic strata in many areas of the world and are usually found in peritidal settings. The fenestrae here are partially filled by dolomite (clear) and calcite cements (stained red).

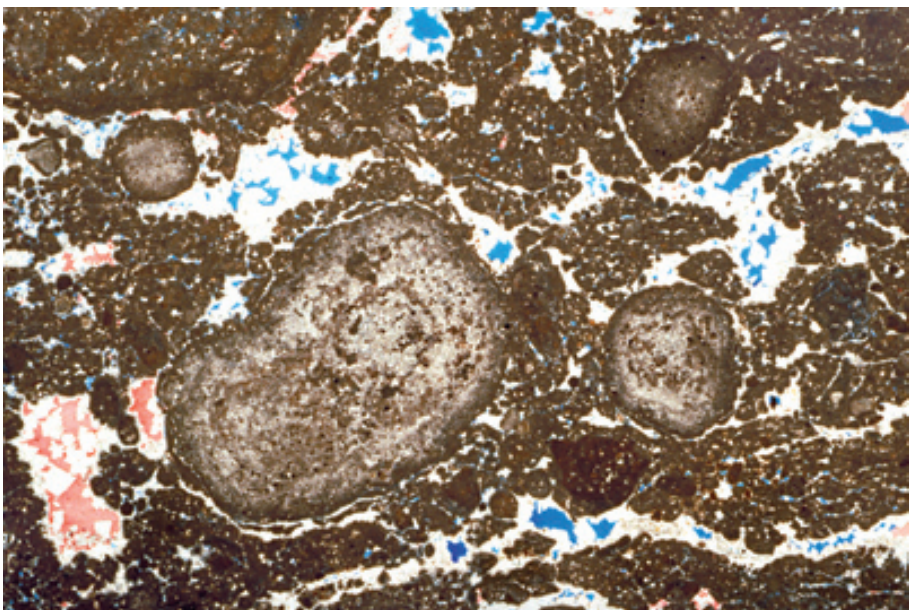

PPL, AFeS, BSE, HA = 16 mm

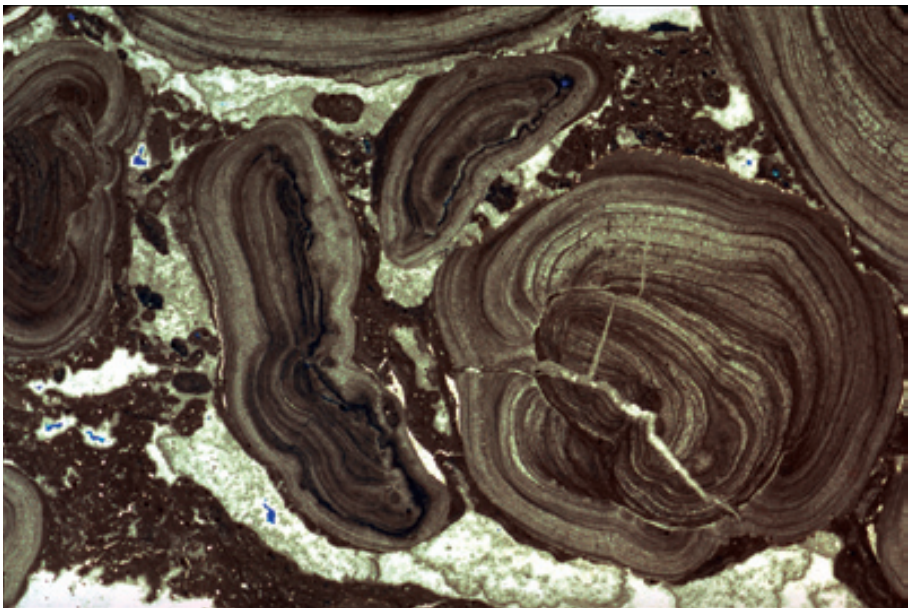

Up. Permian (Guadalupian) Yates Fm., subsurface, Eddy Co., New Mexico

These too are dolomitized pisoids of uncertain origin. These have been interpreted by various authors as the product of microbial growth, coastal caliche formation, back-barrier spring seepage, wave agitation in a coastal setting, and other causes. Marine cements bind the grains together and indeed, marine cementation and pisoid formation are virtually continuous in many samples. Note the frequency of broken older pisoids as cores, the lumpy coatings indicating infrequent rotation of the grains, and the remarkable structural preservation in this aphanocrystalline replacement dolomite.

PPL, BSE, HA = 16 mm

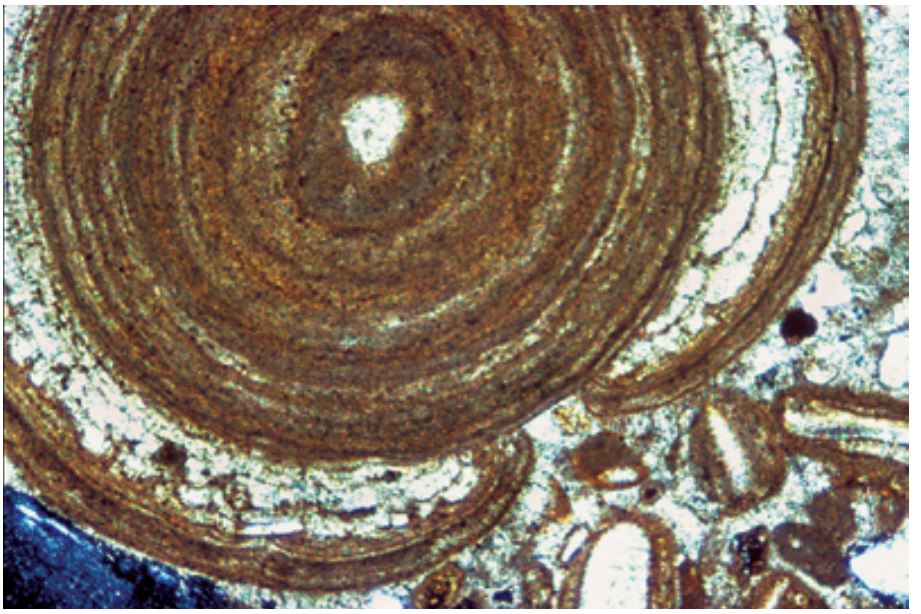

Pleistocene-Holocene sediment, Abu Dhabi, United Arab Emirates

A modern example of a lumpy, incompletely coated grain (pisoid) of probable inorganic origin produced in a coastal caliche along an evaporitic coastline. These are spray zone caliche deposits in which aragonite and high-Mg calcite precipitate in a vadose setting frequently wetted by sea water (Scholle and Kinsman, 1974).

XPL, HA = ~2.4 mm

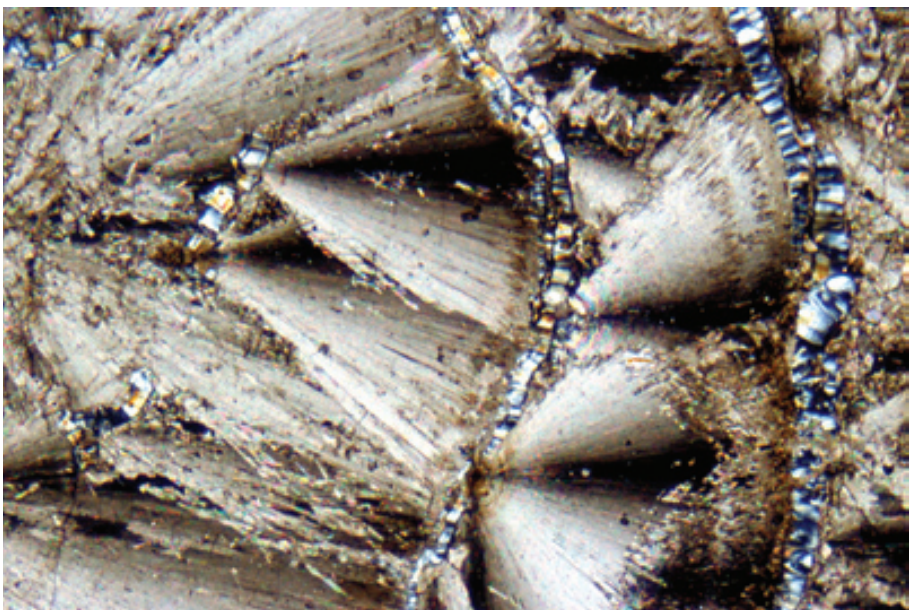

Holocene precipitate, Carlsbad Cavern, Eddy Co., New Mexico

An example of a "cave pearl", an inorganically formed pisoid (vadoid) found on cave floors. It shows coarse, fibrous, low-Mg calcite crystals grown in radially oriented fan-shaped clusters interspersed (in this exceptional case) with thin rinds of gypsum.

XPL, HA = 2.3 mm

Up. Pennsylvanian (Virgilian) Holder Fm., Otero Co., New Mexico

An oncoid with lumpy, layered encrustations around a bivalve shell. Proving a microbial/algal origin (necessary in some definitions of oncoids) can be difficult for many such grains. In this case, filamentous cyanobacterial structure can be seen at very high magnifications (see photographs of *Girvanella* in the chapter on Calcimicrobes and Calcareous Algae).

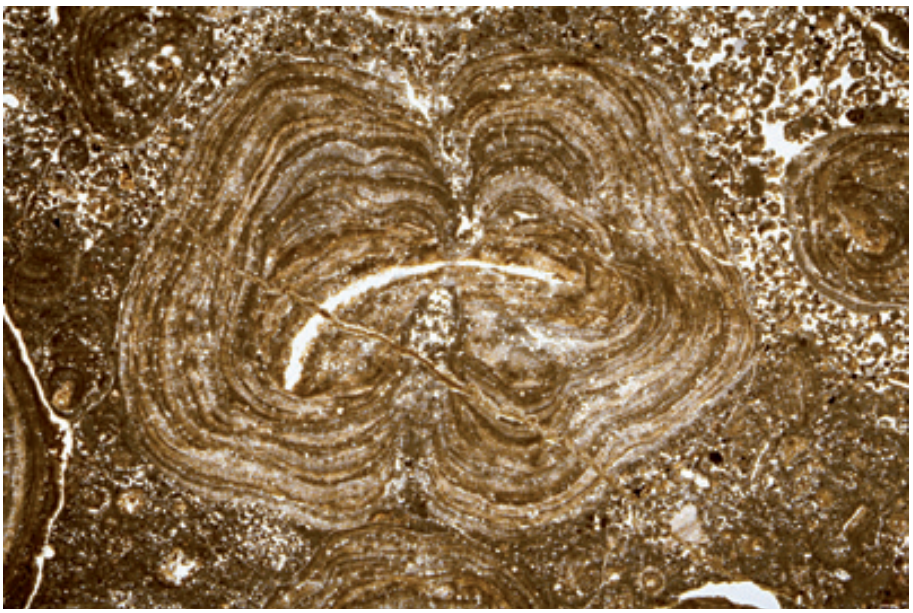

PPL, HA = 20 mm

Mid. Triassic Muschelkalk, Gminny, central Poland

A micritic oncoid with weakly layered, fenestral encrustations around a shell fragment — these are common features of microbial oncoids and they can be found quite typically in shallow- to outer-shelf settings.

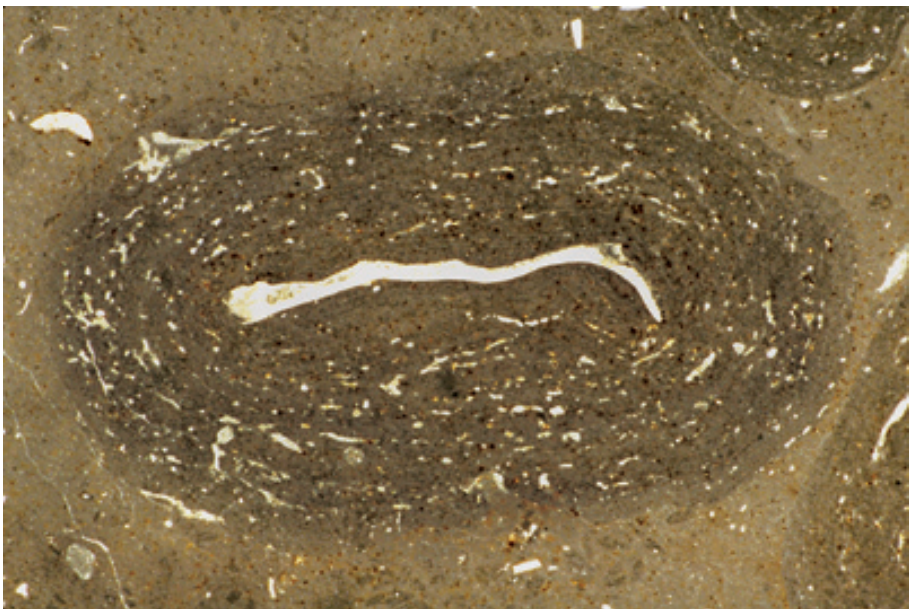

PPL, HA = 10 mm

Eocene Totara Fm., Up. Rhodolith Ls., Oamaru, northern Otago, New Zealand

Rhodoids, such as the one shown here, are a special class of coated grains that were demonstrably formed by red algae. In this example, the irregular strips of apparently dense micrite are coralline red algal encrustations (as shown by the fine-scale cellular structure visible at higher magnifications). Also present in this rhodoid are encrusting foraminifers and a wide range of borings.

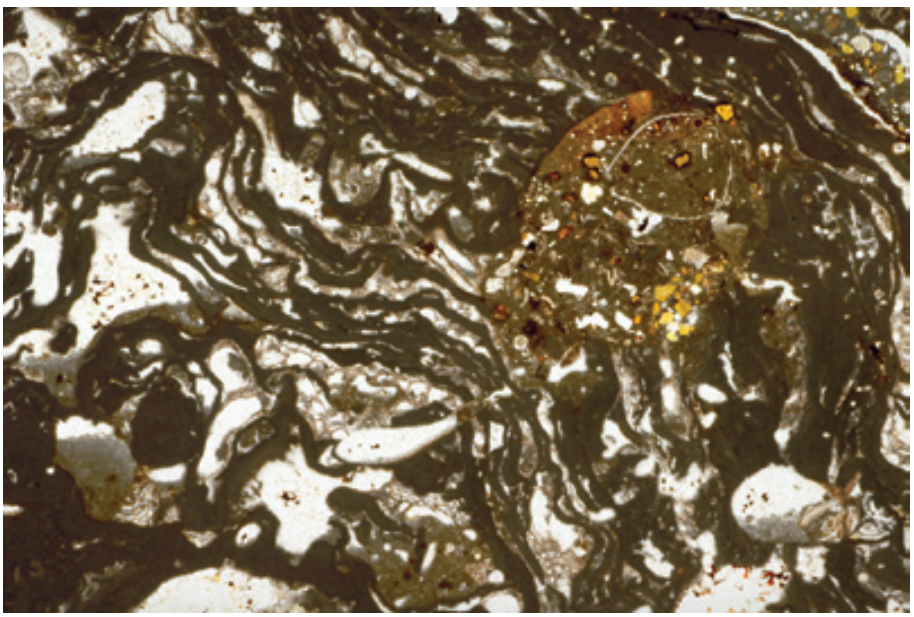

PPL, HA = 14.5 mm

Cited References and Additional Information Sources

Ball, M. M., 1967, Carbonate sand bodies of Florida and the Bahamas: Journal of Sedimentary Petrology, v. 37, p. 556-591.

Bathurst, R. G. C., 1968, Precipitation of ooids and other aragonitic fabrics in warm seas, *in* G. Müller, and G. M. Friedman, eds., Recent Developments in Carbonate Sedimentology in Central Europe: New York, Springer-Verlag, p. 1-10.

Bhattacharyya, D. P., and P. K. Kakimoto, 1982, Origin of ferriferous ooids: an SEM study of ironstone ooids and bauxite pisoids: Journal of Sedimentary Petrology, v. 52, p. 849-857.

Bosence, D. W. J., 1983, Description and classification of rhodoliths (rhodoids, rhodolites), *in* T. M. Peryt, ed., Coated Grains: New York, Springer-Verlag, p. 217-224.

Bosence, D. W. J., 1983, The occurrence and ecology of Recent rhodoliths — a review, *in* T. M. Peryt, ed., Coated Grains: New York, Springer-Verlag, p. 225-242.

Chafetz, H. S., and J. C. Butler, 1980, Petrology of recent caliche pisolites, spherulites and speleothem deposits from central Texas: Sedimentology, v. 27, p. 497-518.

Conley, C. D., 1977, Origin of distorted ooliths and pisoliths: Journal of Sedimentary Petrology, v. 47, p. 554-564.

Davies, P. J., B. Bubela, and J. Ferguson, 1978, The formation of oöids: Sedimentology, v. 25, p. 703-731.

Donahue, J., 1969, Genesis of oolite and pisolite grains: an energy index: Journal of Sedimentary Petrology, v. 39, p. 1399-1411.

Dunham, R. J., 1969, Vadose pisolite in the Capitan reef (Permian), New Mexico and Texas, *in* G. M. Friedman, ed., Depositional Environments in Carbonate Rocks: Tulsa, OK, SEPM Special Publication 14, p. 182-191.

Esteban, M., 1976, Vadose pisolite and caliche: American Association of Petroleum Geologists Bulletin, v. 60, p. 2048-2057.

Fabricius, F. H., 1977, Origin of marine ooids and grapestones: Contributions to Sedimentology, v. 7, p. 1-113.

Fabricius, F. H., and H. Klingele, 1970, Ultrastrukturen von Ooiden und Oolithen: Zur Genese und Diagenese quärtarer Flachwasserkarbonate des Mittelmeeres: Verhandlungen der Geologischen Bundesanstalt (Wien), v. 1970, p. 594-617.

Folk, R. L., and F. L. Lynch, 2001, Organic matter, putative nannobacteria and the formation of ooids and hardgrounds: Sedimentology, v. 48, p. 215-229.

Freeman, T., 1962, Quiet water oolites from Laguna Madre, Texas: Journal of Sedimentary Petrology, v. 32, p. 475-483.

Gasiewicz, A., 1984, Eccentric ooids: Neues Jahrbuch für Geologie und Paläontologie, Monatshefte, v. 1984, p. 204-211.

Halley, R. B., 1977, Ooid fabric and fracture in the Great Salt Lake and the geologic record: Journal of Sedimentary Petrology, v. 47, p. 1099-1120.

Handford, C. R., A. C. Kendall, D. R. Prezbindowski, J. B. Dunham, and B. W. Logan, 1984, Salina-margin tepees, pisoliths, and aragonite cements, Lake MacLeod, Western Australia: their significance in interpreting ancient analogs: Geology, v. 12, p. 523-527.

Harris, P. M., 1979, Facies anatomy and diagenesis of a Bahamian ooid shoal: Sedimenta (University of Miami, Comparative Sedimentology Laboratory), v. 7, p. 1-163.

Harris, P. M., R. B. Halley, and K. J. Lukas, 1979, Endolith microborings and their preservation in Holocene-Pleistocene (Bahama-Florida) ooids: Geology, v. 7, p. 216-220.

Hill, C. A., 1992, Cave pearls and pisoliths: a sedimentological comparison: West Texas Geological Society Bulletin, v. 31, no. 6, p. 4-10.

Kahle, C. F., 1974, Ooids from Great Salt Lake, Utah, as an analogue for the genesis and diagenesis of ooids in marine limestones: Journal of Sedimentary Petrology, v. 44, p. 30-39.

Loreau, J.-P., 1970, Ultrastructure de la phase carbonatée des oolithes marines actuelles: Comptes rendus des séances de l'Académie des Sciences (Paris), Série D, v. 271, p. 816-819.

Loreau, J.-P., and B. H. Purser, 1973, Distribution and ultrastructure of Holocene ooids in the Persian Gulf, *in* B. H. Purser, ed., The Persian Gulf: New York, Springer-Verlag, p. 279-328.

Marshall, J. F., and P. J. Davies, 1975, High-magnesium calcite ooids from the Great Barrier Reef: Journal of Sedimentary Petrology, v. 45, p. 285-291.

Mitterer, R. M., 1968, Amino acid composition of organic matrix in calcareous oolites: Science, v. 162, p. 1498-1499.

Mitterer, R. M., 1971, Influence of natural organic matter on $CaCO_3$ precipitation, *in* O. P. Bricker, ed., Carbonate Cements: Baltimore, MD, Johns Hopkins Press, p. 252-258.

Monty, C. L., 1981, Spongiostromate vs. porostromate stromatolites and oncolites, *in* C. L. Monty, ed., Phanerozoic Stromatolites: New York, Springer-Verlag, p. 1-4.

Opdyke, B. N., and B. H. Wilkinson, 1990, Paleolatitude distribution of Phanerozoic marine ooids and cements: Palaeogeography, Palaeoclimatology, Palaeoecology, v. 78, p. 135-148.

Peryt, T. M., 1981, Phanerozoic oncoids — an overview: Facies, v. 4, p. 197-214.

Peryt, T. M., ed., 1983, Coated Grains: New York, Springer-Verlag, 655 p.

Peryt, T. M., 1983, Classification of coated grains, *in* T. M. Peryt, ed., Coated Grains: New York, Springer-Verlag, p. 3-6.

Richter, D. K., 1983, Calcareous ooids: a synopsis, *in* T. M. Peryt, ed., Coated Grains: New York, Springer-Verlag, p. 71-99.

Sandberg, P. A., 1983, An oscillating trend in Phanerozoic non-skeletal carbonate mineralogy: Nature, v. 305, p. 19-22.

Scholle, P. A., and D. J. J. Kinsman, 1974, Aragonitic and high-Mg calcite caliche from the Persian Gulf — a modern analog for the Permian of Texas and New Mexico: Journal of Sedimentary Petrology, v. 44, p. 904-916.

Simone, L., 1981, Oöids: a review: Earth-Science Reviews, v. 16, p. 319-355.

Sellwood, B. W., and D. Beckett, 1991, Ooid microfabrics: the origin and distribution of high intra-ooid porosity; Mid-Jurassic reservoirs, S. England: Sedimentary Geology, v. 71, p. 189-193.

Shearman, D. J., J. Twyman, and M. Z. Karimi, 1970, The genesis and diagenesis of oolites: Proceedings of the Geologists' Association (London), v. 81, p. 561-575.

Teichert, C., 1970, Oolite, oolith, ooid: discussion: American Association Petroleum Geologists Bulletin, v. 54, p. 1748-1749.

Tucker, M. E., 1981, Sedimentary Petrology: An Introduction: New York, John Wiley & Sons (Halsted Press), 252 p.

Tucker, M. E., 1984, Calcitic, aragonitic and mixed calcitic-aragonitic ooids from the mid-Proterozoic Belt Supergroup, Montana: Sedimentology, v. 31, p. 627-644.

Van Houten, F. B., and D. P. Bhattacharyya, 1982, Phanerozoic oolitic ironstones — geologic record and facies model: Annual Review of Earth and Planetary Sciences, v. 10, p. 441-457.

Wilkinson, B. H., and R. K. Given, 1986, Secular variation in abiotic marine carbonates: constraints on Paleozoic atmospheric carbon dioxide contents and oceanic Mg/Ca ratios: Journal of Geology, v. 94, p. 321-333.

Wilkinson, B. H., and E. Landing, 1978, "Eggshell diagenesis" and primary radial fabric in calcite ooids: Journal of Sedimentary Petrology, v. 48, p. 1129-1138.

Facing Page: Top - Dried and mud-cracked sediment (mainly carbonate mud) deposited in an island-interior pond/microbial flat environment during flooding associated with Hurricane Betsy (1968). Cluett Key, Florida Bay, Florida. Photograph by Ron Perkins, courtesy of E. A. Shinn.

Bottom - Photograph of sediment surface in island-interior pond/algal flat setting showing large intraclasts of torn-up, partially lithified carbonate mud from desiccation polygons. Material was redeposited during Hurricane Donna in 1960. Cluett Key, Florida Bay, Florida. Photograph courtesy of E. A. Shinn.

GRAINS: Non-skeletal Grains

Intraclasts and Extraclasts

CHAPTER 15

INTRACLASTS AND EXTRACLASTS

Definitions:

Intraclast - A fragment of penecontemporaneous, commonly weakly consolidated, carbonate sediment that has been eroded and redeposited, generally nearby, within the same depositional sequence in which it formed (Folk, 1959 and 1962).

Lumps - In modern sediments, irregular composite aggregates of silt- or sand-sized carbonate particles that are cemented together at points of contact: in ancient carbonates, similar-appearing lobate grains that are composed of carbonate mud (micrite). After Illing (1954); no longer widely used.

Grapestone - Sometimes used to describe aggregates of silt-sized carbonate crystals (or grains), but more properly applied to grape-like clusters of such aggregates bound together by cements or organic encrustations.

Extraclast - A detrital grain of lithified carbonate sediment (lithoclast) derived from outside the depositional area of current sedimentation (Folk, 1959).

Calclithite - A rock formed chiefly of carbonate clasts (extraclasts) derived from older, lithified limestone, generally external to the contemporaneous depositional system. Commonly located in arid settings, along downthrown sides of fault scarps. Term coined by Folk (1959).

Age Range:

Intraclasts and extraclasts are found in deposits of any age from Archean to Recent. Intraclasts are especially common in Precambrian to Mid. Ordovician strata, where they form widespread flat-pebble conglomerates. Such deposits probably reflect the abundance of microbial deposits and the scarcity or absence of macrofaunal grazers and burrowers during that time period (e.g., Garrett, 1970).

Mineralogy:

Because intraclasts and extraclasts represent fragments of preexisting carbonate sediment or rock, they can have essentially any mineralogy. Intraclasts normally are aragonitic, calcitic, or dolomitic when formed; those associated with hardgrounds may contain significant phosphate or glauconite.

Environmental Implications:

Intraclasts can form in many environments, but most typically are produced in settings with intermittently high-energy conditions. In such settings, sediments can be weakly cemented or organically bound during times of relatively low-energy conditions and then be torn up into clasts during major storms or other high-energy conditions (including earthquakes and/or tsunami events). The most common sites of intraclast formation are at marine hiatus surfaces (firm- or hardgrounds); in reefs, fore-reef slopes, or carbonate beaches where biological and chemical processes lead to rapid cementation; or on tidal flats where desiccation, cementation, and/or dolomitization may speed lithification.

Extraclasts are typically found in close proximity to exposed sources of older carbonates because carbonate clasts are rapidly abraded or dissolved during transport. Thus, most extraclast-rich deposits are formed where rapid sedimentation occurs in proximity to a source area and/or in relatively cold or arid climates with limited chemical weathering; such settings include arid-region fault-scarp fans, marine environments adjacent to coastal cliffs, or toe-of-slope aprons along eroding submarine escarpments (in debris flows and turbidites).

Keys to Petrographic Recognition:

1. **Intraclasts are typically large grains (several mm to several cm or more) with moderate to good rounding, and with multi-grained internal fabrics derived from a precursor deposit. Intraclasts formed by binding of multiple allochems may be more equant and botryoidal (commonly termed "lumps" or "grapestones"). Intraclasts are usually monomict (that is, they were all derived from a common nearby environment and thus have similar composition and texture). Intraclasts may show signs of early cementation (marine cements or aphanocrystalline dolomite) or of binding by organisms (encrusting algae, foraminifers, or others).**
2. **Extraclasts are large, sub-rounded to well rounded grains (unlike angular grains in collapse breccias) and tend to occur as polymict assemblages (i.e., grains with a variety of textures and compositions, sometimes including cemented fractures). Indeed, because they are detrital grains derived from an older, sedimentary source terrain, they may be mixed with non-carbonate sedimentary rock fragments, especially chert. They may contain fossils older than those in their host deposits and may have distinct weathering rinds.**

Recent sediment, north of Bimini, Bahamas

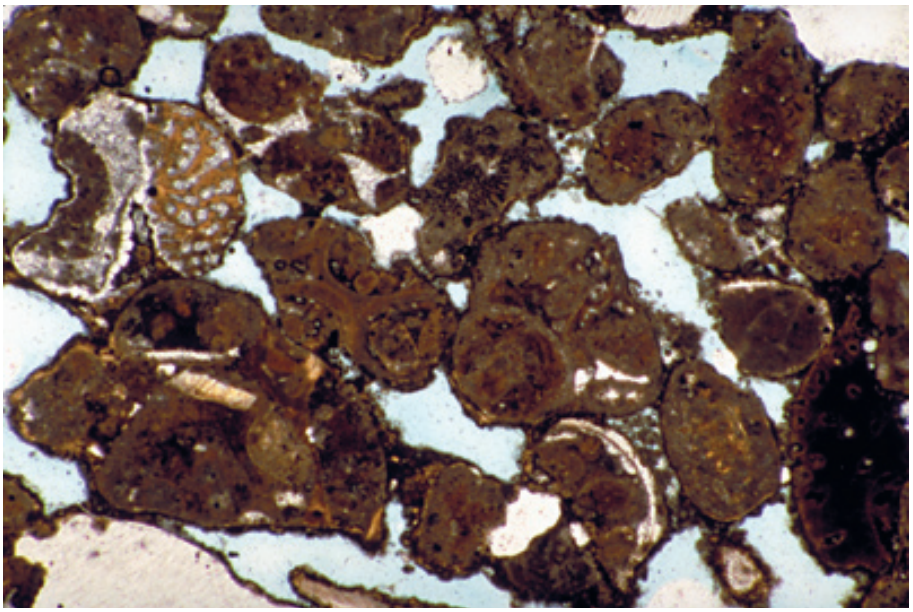

These are grapestone intraclasts that were formed on an open shelf with a low sedimentation rate. The extensively micritized peloidal grains (mainly altered superficial ooids and skeletal fragments) are bound together by inorganic cements as well as microbial coatings and encrusting organisms. The lumpy clasts look a bit like bunches of grapes — hence the terms "lumps" and "grapestone" that are applied to such grains. Occasional hurricanes that sweep across the platform interrupt the cementation process and contribute to the generation of intraclastic fragments rather than a continuous hardground.

PPL, BSE, HA = 3.2 mm

Recent sediment, northwestern Little Bahama Bank, Bahamas

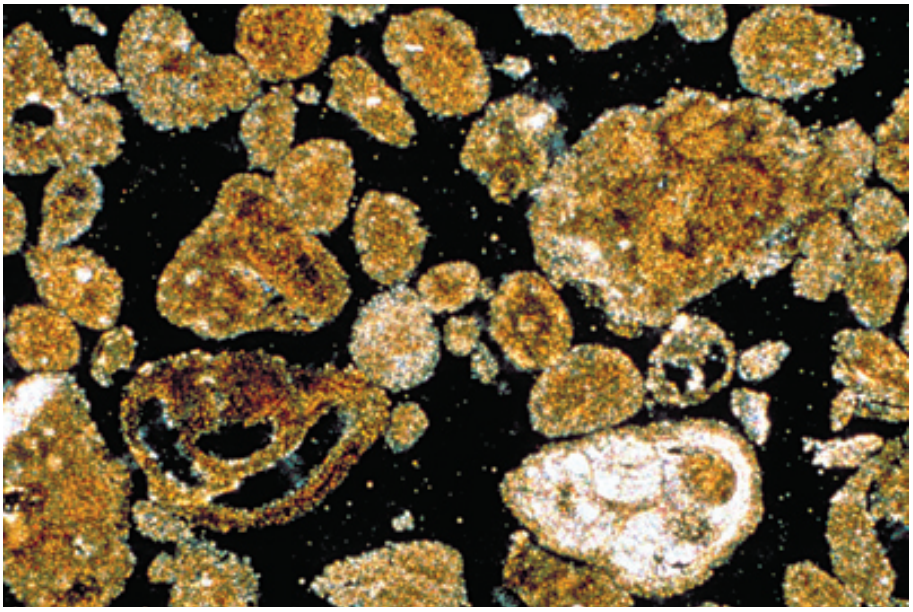

A grapestone sediment from another shelf area of intermittently active transport. The cross-polarized lighting enhances recognition of the constituents of the grapestone grains: ooids, gastropods and other skeletal fragments, and large amounts of synsedimentary fibrous aragonite cement. Photograph courtesy of Albert C. Hine; taken by R. Jude Wilber.

XPL, HA = ~3.0 mm

Recent sediment, Berry Islands, Bahamas

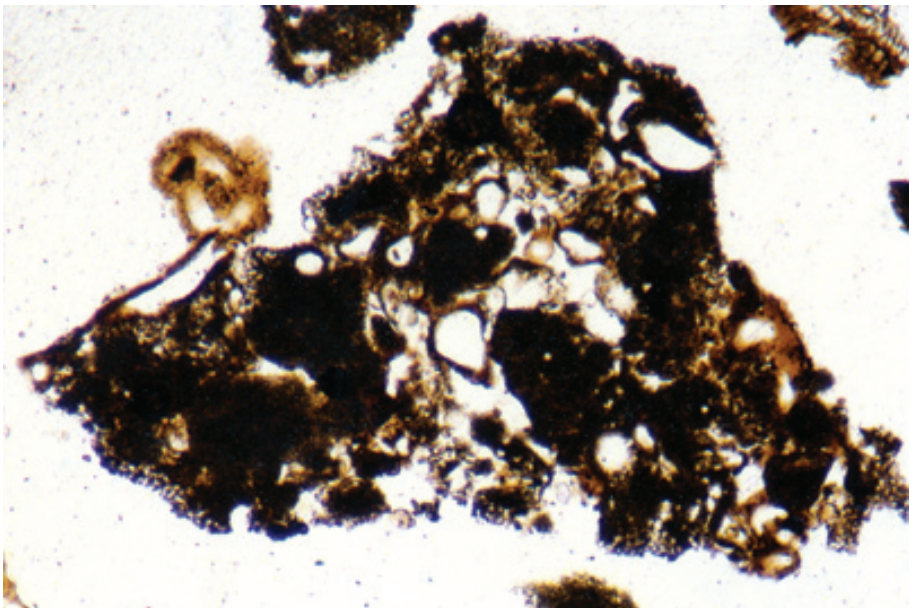

A higher-magnification view of a modern "grapestone" intraclast. This cluster or aggregate of other grains (mostly peloids) are held together by micritic high-Mg calcite cement along with microbial, foraminiferal, and other encrustations. This grapestone, as in the previous examples, formed in an area of intermittent storm agitation — a setting that allowed cementation and encrustation to take place, but where episodic reworking prevented formation of thick and continuous cemented crusts (hardgrounds).

PPL, HA = 2.0 mm

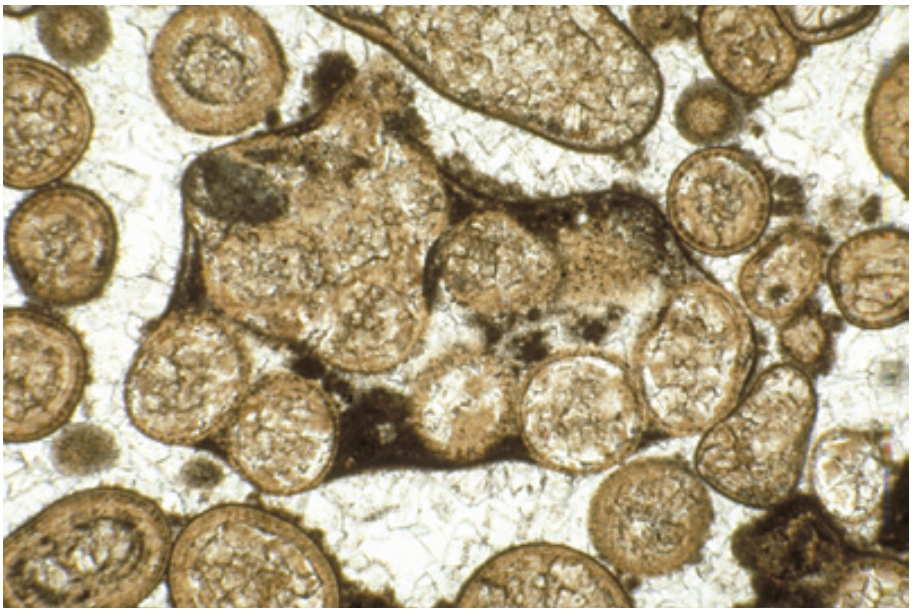

Lo. Paleozoic limestone, Canada

A Paleozoic example of compound grapestone intraclasts containing ooids with thin coatings. Micritic, possibly microbial, precipitates appear to be the main binding material within these intraclasts. Sample from Noel P. James.

PPL, HA = 3.0 mm

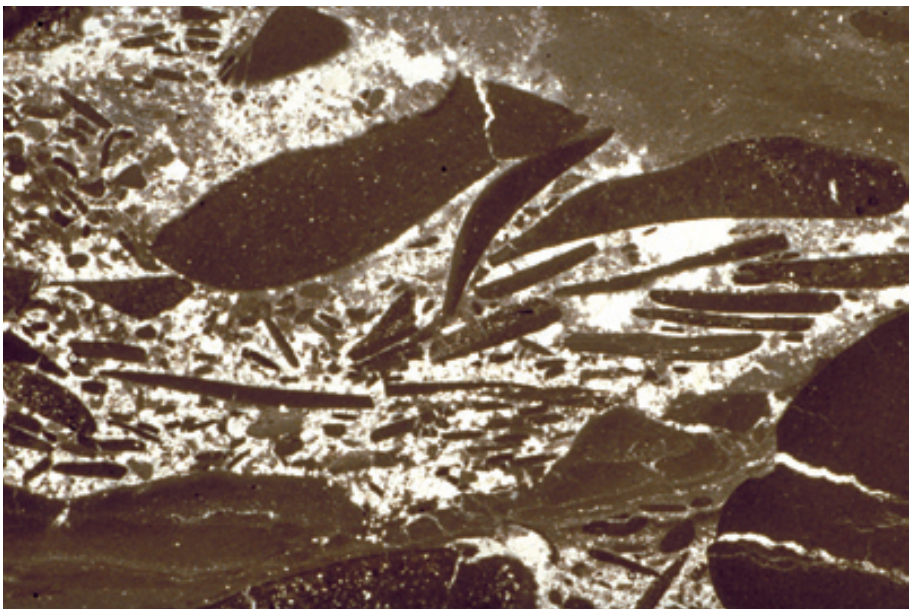

Mid. Triassic Gipsdalen Fm., Jameson Land, East Greenland

These irregular, elongate intraclasts of micritic carbonate are associated with storm-influenced, stromatolitic, tidal flat ares. They are termed "flat-pebble conglomerates" because of the shape of their clasts — the planar shape is controlled by the fine-scale horizontal interlamination of carbonate mud and microbial crusts found in typical carbonate tidal flat deposits. The intraclasts commonly accumulate in tidal channels, beach ridges, or offshore shelf deposits.

PPL, HA = 12.5 mm

Up. Cambrian Gallatin Ls., Hot Springs Co., Wyoming

A coarse-grained flat-pebble conglomerate from a time period when such deposits were extremely widespread. These silty and micritic intraclasts represent rip-up of thinly laminated sediments, but during this time period, prior to complete dominance of grazing and burrowing organisms, laminated microbial deposits may have been common in subtidal as well as intertidal areas. In any case, strong storm action was required to generate these rounded rip-up clasts.

PPL, HA = 20 mm

Mid. Ordovician Black River Gp., Kingston area, Ontario, Canada

A large compound intraclast among dominantly fine-grained ooids and peloids. A compound intraclast is a reworked sediment fragment that includes other intraclasts (from an earlier generation of reworking). Because sediment formation and destruction can be episodic and oft-repeated in storm-influenced coastal and shallow shelf settings, compound intraclasts are common in such deposits. Sample from Noel P. James.

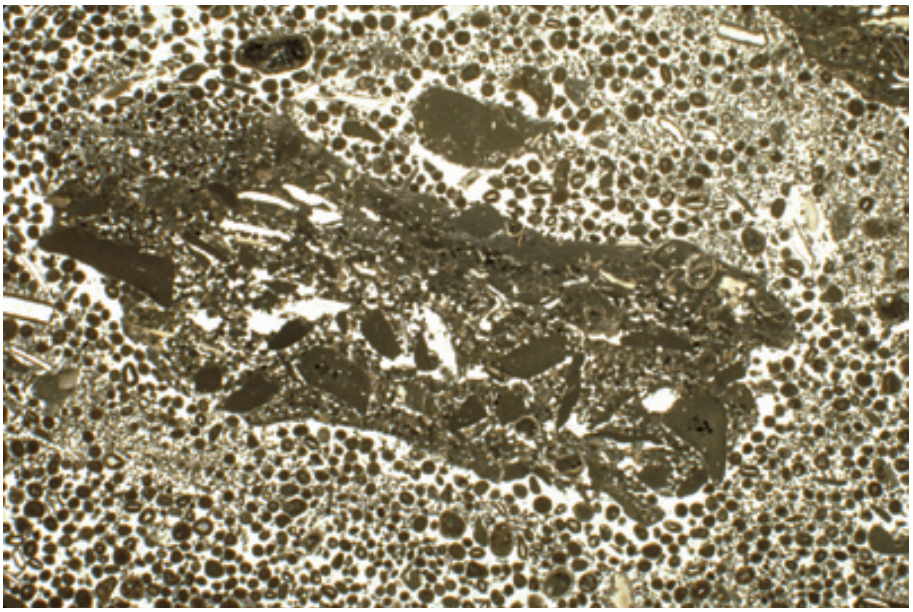

PPL, HA = ~8.0 mm

Up. Cretaceous (Maastrichtian?) limestone, Paxos, Ionian Islands, Greece

Intraclasts also are common in shelf-margin and slope limestones. These reworked grains include marine-cemented rudistid reef material as well as finer-grained back-reef and/or upper slope carbonate fragments. All have been reworked into basinal deposits by turbidity currents and debris flows. Intraclastic slope deposits (and slope-derived basinal limestones) commonly have a more diverse or polymict assemblage of grain lithologies than do most coastal or open shelf deposits.

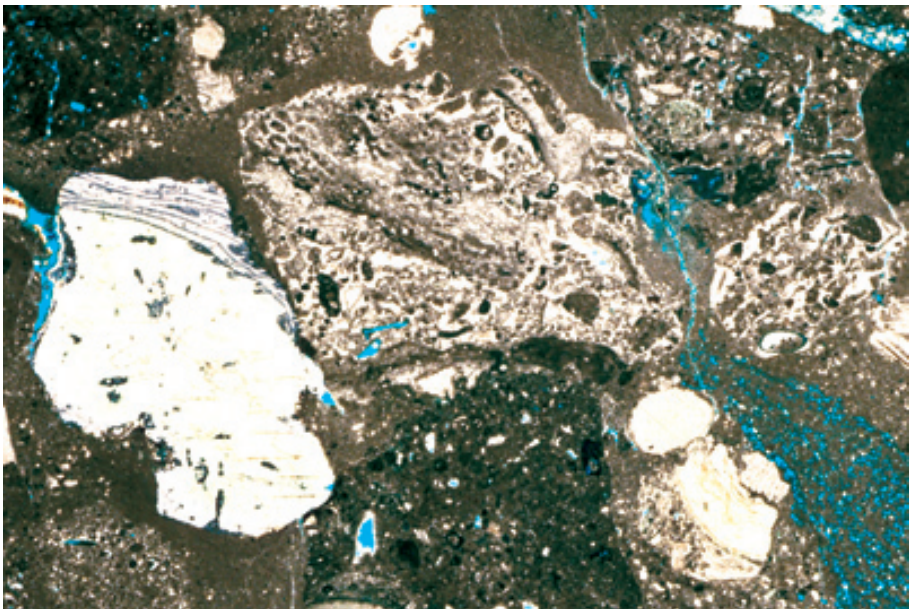

PPL, BSE, HA = 16 mm

Up. Cretaceous (Maastrichtian?) limestone, Paxos, Ionian Islands, Greece

A higher magnification view of an intraclast in a deep-water debris flow. It contains shelf-margin rudistid biosparite with complete occlusion of porosity by extremely early marine cements. Both the rudistid fragments and marine cements were truncated during the formation of this clast. Examination of such deeper water intraclasts can provide considerable information about nearby platforms and their early diagenetic history — information commonly of great value to explorationists.

PPL, BSE, HA = 11 mm

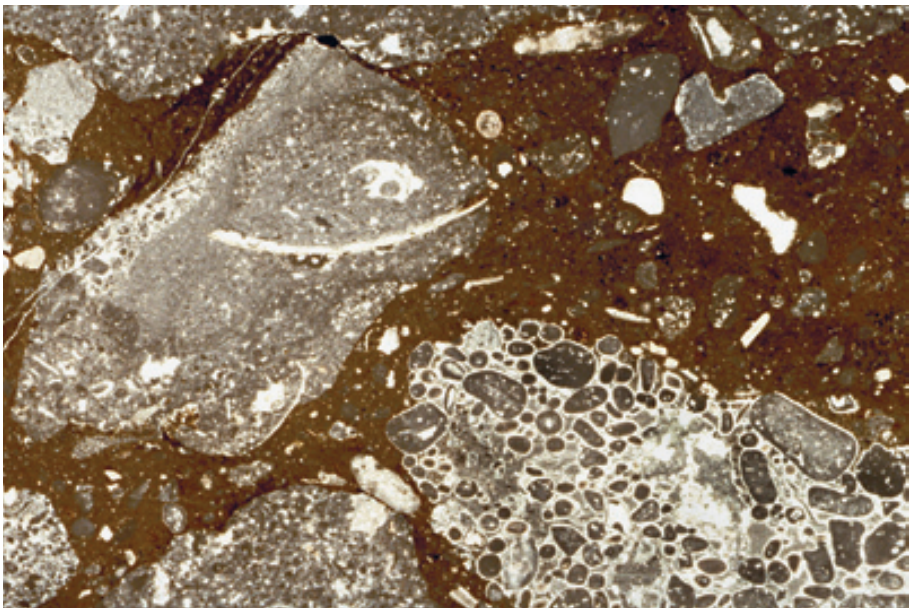

Lo. Jurassic (Liassic) limestone, Central High Atlas region, Morocco

Several different intraclast compositions (oolitic, micritic, biomicritic) are found in this typically poorly sorted debris flow deposit from a lower slope setting. Despite the fact that some clasts were fully cemented prior to transport, these are still considered as penecontemporaneously reworked materials within the same basin of deposition; the grains therefore fit the definition of intraclasts. Circumgranular marine cements are clearly visible in the large grain in the lower right corner.

PPL, HA = 16 mm

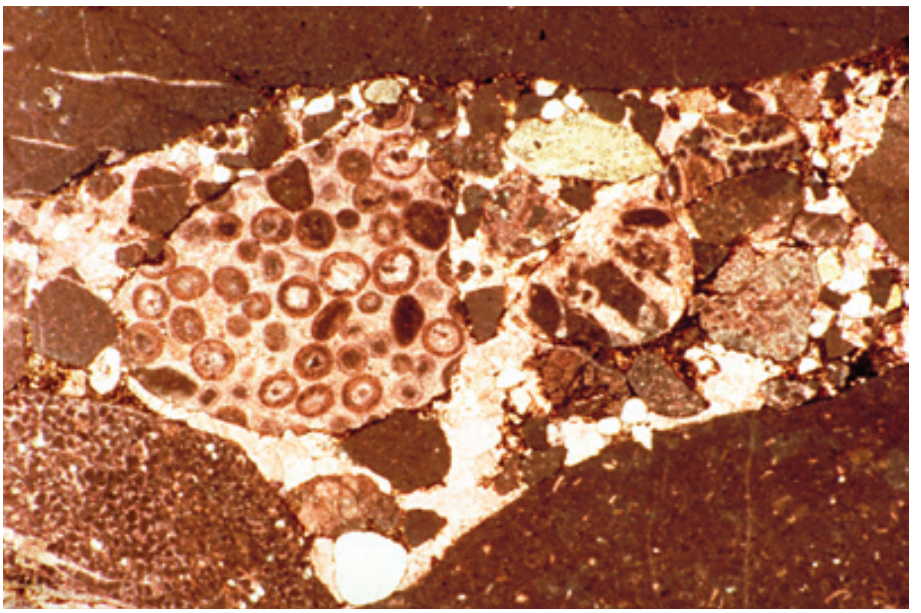

Up. Pennsylvanian (Virgilian) Collings Ranch Cgl., Murray Co., Oklahoma

Distinguishing intraclasts from extraclasts can be difficult. This calclithite deposit formed in a small, fault-bounded basin during a regional tectonic event, and the clasts represent limestone and chert eroded from a thick, uplifted section of primarily Ordovician carbonates. These were clearly not penecontemporaneous with Pennsylvanian deposition, but examination of regional relationships or the fossils contained in the clasts are required to determine that these are extraclasts rather than intraclasts.

PPL, AFeS, HA = 7.5 mm

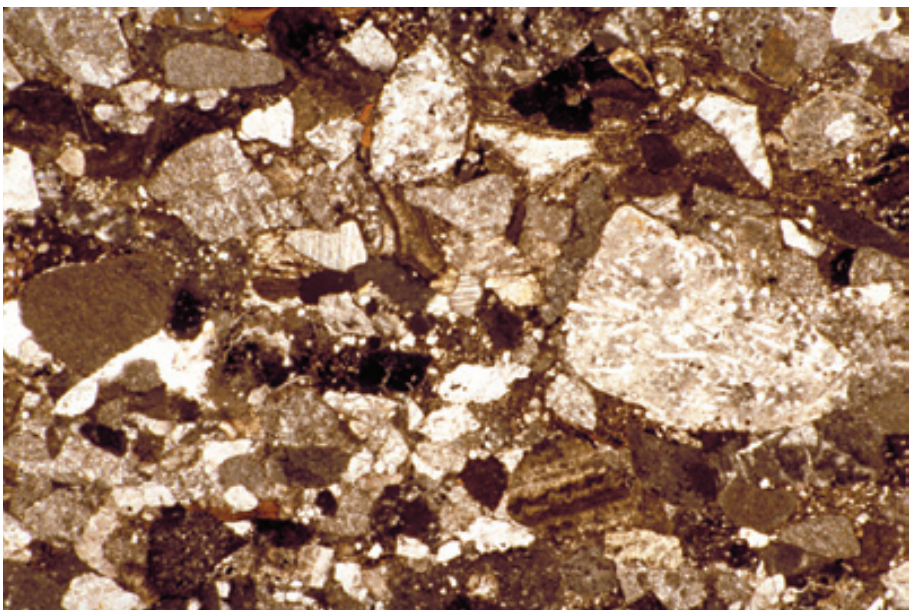

Up. Eocene Oberaudorf Schichten, Northern Calcareous Alps, Austria

Numerous extraclasts in a calclithite. These fragments include shallow-water carbonates and deep-water cherts from strata as old as Jurassic. The deposit was derived by erosion of older strata from advancing thrust sheets during the Alpine orogeny. The diversity of rock types, and especially the inclusion of chert fragments, are clues that these are extraclasts.

PPL, HA = 8.0 mm

Up. Permian (Ufimian) Top Solikamskaya Suite, Perm Region, Russia

Another view of extraclasts in a calclithite. The highly polymict nature of the clasts and the significant rounding of even the very hard chert fragments both are clues to an extraclastic origin of grains. Detailed lithologic and paleontologic examination of such clasts relative to any associated non-reworked material generally is required to prove that hypothesis.

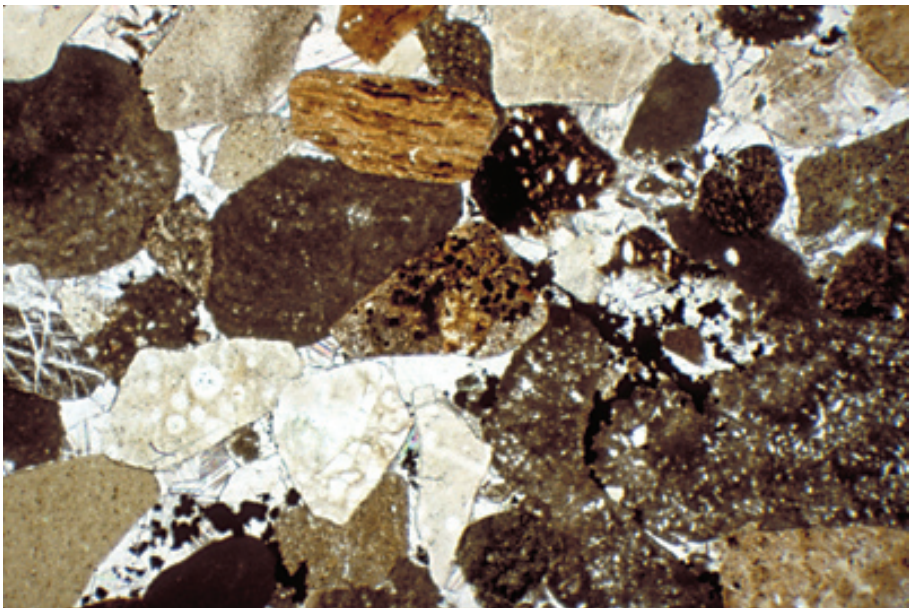

PPL, HA = 5.1 mm

Up. Silurian hiatus surface on Fusselman Fm., El Paso Co., Texas

Solution-collapse and tectonic breccias can appear very similar to intraclast or extraclast-rich rocks. These clasts are part of an exposure-related solution breccia. Note the angularity and size variation (lack of sorting) of these rock fragments, the uniformity of lithology, and the ferruginous terra rossa matrix. All of those are clues to the origin of this deposit, but none is completely diagnostic.

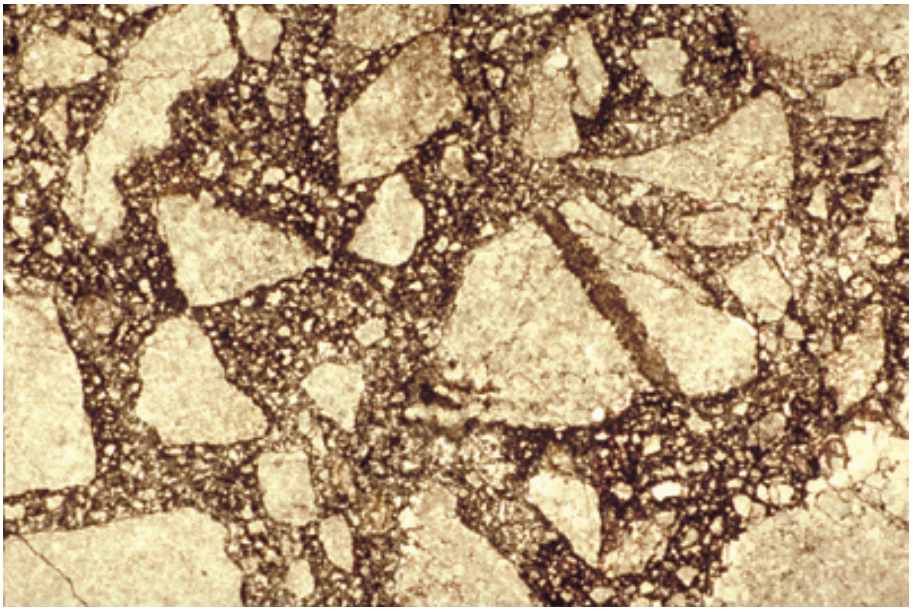

PPL, HA = 11 mm

Neogene breccia, near Lamia, central Greece

An example of a carbonate-rich fault breccia with hematitic terra rossa matrix. This sample came from within the fault zone and has undergone essentially no sedimentary transport. However, the solubility and softness of carbonate clasts makes even moderate-distance fluvial transport of carbonate clasts unlikely, especially in humid climatic settings. Thus, most tectonic calclithites represent deposition in close proximity to active block faults (meters to just a few kilometers).

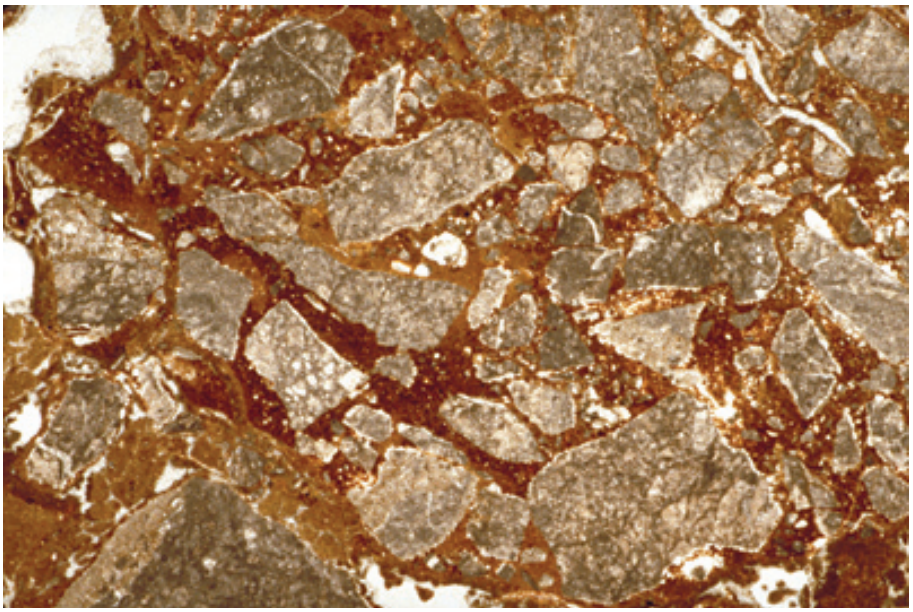

PPL, HA = 13.5 mm

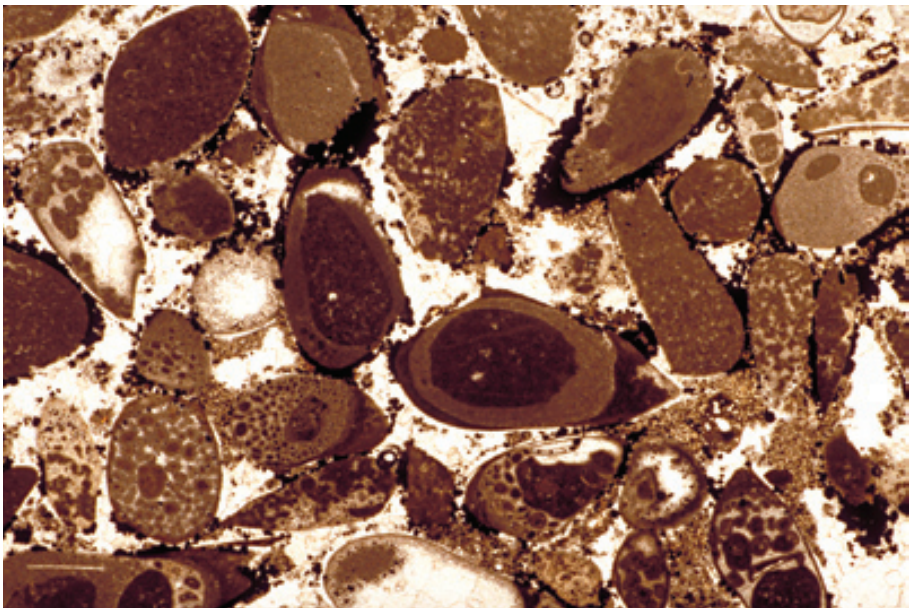

Lo. Cretaceous (Albian) Glen Rose Ls., near Johnson City, Texas

Some grains that look very much like intraclasts may, in reality, have very different origins. These are steinkerns (internal body cavity fillings) of articulate *Corbula* bivalves. The sediment fillings of the bivalves must have undergone very early lithification, for some grains preserve multiple generations of geopetal structures and in-situ fibrous rim-cements. Subsequently, the aragonitic shells were completely dissolved, leaving only the lithified internal cavity fills. These grains can be differentiated from true intraclasts by their consistent "teardrop" shape and their unusual internal fabrics.

PPL, HA = 11 mm

Cited References and Additional Information Sources

Ainardi, R., and Y. Champetier, 1976, Processus de formation d'intraclastes par dessiccation en milieu margino-littoral: exemple dans le "Purbeckien" du Jura: Bulletin de la Société Géologique de France, v. 18, p. 159-164.

Banks, J. E., 1959, Limestone conglomerates (Recent and Cretaceous) in southern Florida: American Association of Petroleum Geologists Bulletin, v. 43, p. 2237-2243.

Bosellini, A., 1966, Protointraclasts: texture of some Werfenian (Lower Triassic) limestones of the Dolomites (northeastern Italy): Sedimentology, v. 6, p. 333-337.

Cros, P. G., 1979, Genèse d'oolithes et de grapestones, plate-forme des Bahamas (Joulters Cays, Grand Banc): Bulletin des Centres de Recherches Exploration-Production Elf-Aquitaine, v. 3, p. 63-139.

Deelman, J. C., 1978, Experimental ooids and grapestones: carbonate aggregates and their origin: Journal of Sedimentary Petrology, v. 48, p. 503-512.

Denison, F. E., J. M. Saenz, and A. E. Fritsche, 1998, Formation of an intraclast megabreccia by sliding on a sand bed, Miocene Modelo Formation, Sherman Oaks, California: AAPG Bulletin, v. 82, p. 845.

Fabricius, F. H., 1977, Origin of marine ooids and grapestones: Contributions to Sedimentology, v. 7, p. 1-113.

Folk, R. L., 1959, Practical petrographic classification of limestones: American Association of Petroleum Geologists Bulletin, v. 43, p. 1-38.

Fontana, D., 1991, Detrital carbonate grains as provenance indicators in the Upper Cretaceous Pietraforte Formation (northern Apennines): Sedimentology, v. 38, p. 1085-1096.

Garrett, P., 1970, Phanerozoic stromatolites: non-competitive ecologic restriction by grazing and burrowing animals: Science, v. 169, p. 171-173.

Jones, B., and K.-C. Ng, 1988, Anatomy and diagenesis of a Pleistocene carbonate breccia formed by the collapse of a seacliff, Cayman Brac, British West Indies: Bulletin of Canadian Petroleum Geology, v. 36, p. 9-24.

Kim, J. C., and Y. I. Lee, 1995, Flat-pebble conglomerate; a characteristic lithology of Upper Cambrian and Lower Ordovician shallow-water carbonate sequences, *in* J. D. Cooper, M. L. Droser, and S. C. Finney, eds., Seventh International Symposium on the Ordovician System, Society of Economic Paleontologists and Mineralogists Pacific Section, v. 77, p. 371-374.

Lindholm, R. C., 1980, Intraclast orientation in Cambro-Ordovician limestones in western Maryland: Journal of Sedimentary Petrology, v. 50, p. 1205-1212.

Mount, J. F., and D. Kidder, 1993, Combined flow origin of edgewise intraclast conglomerates: Sellick Hill Formation (Lower Cambrian), South Australia: Sedimentology, v. 40, p. 315-329.

Roberts, H. H., and C. H. Moore, Jr., 1971, Recently cemented aggregates (grapestones), Grand Cayman Island, B.W.I., *in* O. P. Bricker, ed., Carbonate Cements: Baltimore, MD, The Johns Hopkins Press, p. 88-90.

Sarkar, S., P. P. Chakraborty, and P. K. Bose, 1994, Multi-mode generation of carbonate tabular intraclast deposits: unnamed Proterozoic formation, Maharashtra: Journal of the Geological Society of India, v. 43, p. 415-423.

Sepkoski, J. J., Jr., 1982, Flat-pebble conglomerates, storm deposits, and the Cambrian bottom fauna, *in* G. Einsele, and A. Seilacher, eds., Cyclic and Event Stratification; symposium: Berlin, Springer-Verlag, p. 371-385.

Spalletta, C., and G. B. Vai, 1984, Upper Devonian intraclast parabreccias interpreted as seismites: Marine Geology, v. 55, p. 133-144.

Whisonant, R. C., 1987, Paleocurrent and petrographic analysis of imbricate intraclasts in shallow-marine carbonates, Upper Cambrian, southwestern Virginia: Journal of Sedimentary Petrology, v. 57, p. 983-994.

Whisonant, R. C., 1988, Multiple event stratification in carbonate intraclast conglomerates in the Cambrian of southwestern Virginia: Southeastern Geology, v. 28, p. 181-190.

Wignall, P. B., and R. J. Twitchett, 1999, Unusual intraclastic limestones in Lower Triassic carbonates and their bearing on the aftermath of the end-Permian mass extinction: Sedimentology, v. 46, p. 303-316.

Wilson, M. D., 1985, Origin of Upper Cambrian flat pebble conglomerates in the northern Powder River basin, Wyoming, *in* M. W. Longman, K. W. Shanley, R. F. Lindsay, and D. E. Eby, eds., Rocky Mountain Carbonate Reservoirs — A Core Workshop [Golden, CO, August 10-11, 1985]: Tulsa, OK, SEPM Core Workshop No. 7, p. 1-50.

Winland, H. D., and R. K. Matthews, 1974, Origin and significance of grapestone, Bahama Islands: Journal of Sedimentary Petrology, v. 44, p. 921-927.

Facing Page: Top - View of tidal flat with numerous pellet-covered mounds of the burrowing shrimp, *Callianassa*, exposed at extreme low tide in the Pigeon Creek area of San Salvador Island, Bahamas.

Bottom - Close-up view of one of the mounds shown above. Note the abundance of large, rod-shaped, crustacean fecal pellets.

GRAINS: Non-skeletal Grains

Pellets and peloids

CHAPTER 16

PELLETS AND PELOIDS

Definitions:

Pellets - Small (typically 0.03 to 0.3 mm long), spherical to ovoid or rod- shaped grains composed of carbonate mud (micrite). Most pellets lack internal structure and are uniform in size and shape in any single sample; in the strict sense, pellets are the fecal products of invertebrate organisms (see Folk, 1959).

Peloids - Allochems formed of cryptocrystalline or microcrystalline calcium carbonate with no restrictions on the size or origin of the grains (McKee and Gutschick, 1969). This term allows reference to grains composed of micritic material without the need to imply any particular mode of origin — it is therefore a useful "term of ignorance" covering possible pellets, indistinct intraclasts, micritized ooids or fossil fragments and even some microbial or inorganic precipitates that are not necessarily even "grains" in the sense of primary constituents as opposed to interstitial early diagenetic "cements".

Age range:

Pellets and peloids occur in Precambrian through Phanerozoic strata; pellets are important sediment constituents mainly in Phanerozoic strata. Structured crustacean pellets are especially prominent in Jurassic and Cretaceous rocks (although they are known from middle Paleozoic to Recent strata).

Composition:

Pellets and peloids are composed of aggregated carbonate mud and/or precipitated calcium carbonate. Thus, their original composition is (or was) aragonite or calcite (of any Mg level) or a mixture of both. Pelletal glauconites and phosphorites also are common.

Environmental Implications:

Fecal pellets are produced wherever worms, crustaceans, holothurians and other grazing, burrowing, or swimming invertebrates (or vertebrates) exist, but most pellets are destroyed prior to burial. Rapid cementation, usually bacterially mediated, aids preservation, as does rapid sedimentation in low-energy settings. Thus, lagoons (especially hypersaline ones), low-energy tidal flats, and sheltered or relatively deep-water platforms are common sites of pellet preservation. Fecal pellets of pelagic zooplankton, especially copepods, are common in Cretaceous to Recent deep-sea deposits.

Fecal pellets must be distinguished from microbial peloids or inorganic, peloidal marine cements, especially those composed of high-Mg calcite. Such precipitates are especially common in reef cavities, subtidal to intertidal stromatolites, hot springs or other travertine deposits, and submarine vent areas.

Peloids have varied origins and environmental associations. Algal or fungal boring and micritization of grains are common in a variety of open marine to restricted or coastal settings with relatively slow or intermittent sedimentation rates. In particular, areas subject to occasional storms that move grains from active areas of formation to quiet sites of destruction are especially prone to peloid formation. Such sites include back-barrier or back-bar grass flats, lagoons, and protected deeper shelf settings.

Keys to Petrographic Recognition:

1. **Carbonate fecal pellets of invertebrate organisms are typically micritic and have no internal fabric. Some crustaceans produce pellets that have regularly spaced holes (normally filled with sparry calcite).**
2. **Most fecal pellets are relatively small (typically 0.03 to 0.3 mm long, although some can exceed 1-2 cm) and are rod-shaped or ovoid. Because most pellets in any single sediment sample will have been produced by just one or two types of organisms, they are generally very uniform in both shape and size.**
3. **Because pellets are soft when formed, they can be embayed or partially flattened by compation during burial wherever early cementation has not thoroughly lithified them.**
4. **Pellets commonly occur in clusters, particularly where they have been packed into burrows or have accumulated at or near the surface openings of burrows.**
5. **Peloids formed by the biological degradation or "micritization" of other carbonate grains (mainly ooids or bioclasts) may retain slight vestiges of their original internal structure, albeit not enough to identify those origins. A wide range of borings (algal, fungal and other) also may be visible within peloids.**
6. **Peloidal grains (allochems) can sometimes be distinguished from peloidal cements or biologically-mediated precipitates by their distribution. Precipitates can completely line cavities, whereas allochems are gravitationally confined to cavity floors.**

Recent sediment, Cancun Lagoon, Quintana Roo, Mexico

Two pellets from a modern lagoonal setting. These apparently are true fecal pellets as they show the common rounded, rod-shaped outline of such material. In this sediment, the uniformity of size and shape of pellets aids in their identification as being of fecal origin. Such fecal pellets are common and it has been estimated that all modern muddy carbonate sediment passes through the gut of one or more organisms during its time at or near the seafloor.

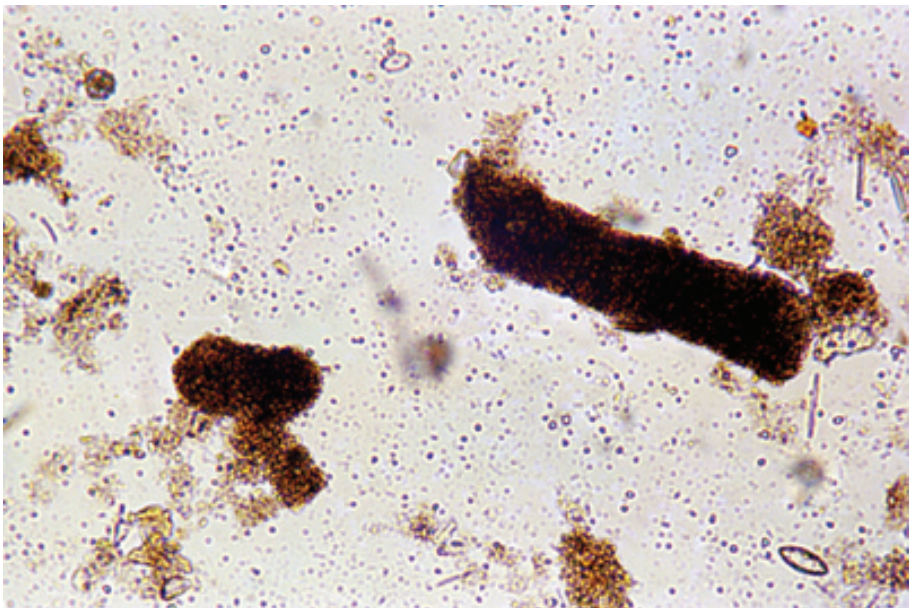

PPL, HA = 0.8 mm

Recent sediment, Coorong Lagoon, South Australia

An example of modern (crustacean?) fecal pellets from a variable salinity (hypersaline to subsaline) carbonate lagoon. The pellets are rod-shaped in longitudinal section and round in transverse section and have relatively large and uniform sizes. Forming pellets is relatively easy, but hardening them, and thus making them preservable, is more difficult. In hypersaline lagoons, high rates of carbonate precipitation, coupled with microbial activity in the pellets, can lead to rapid lithification of pellets and thus can substantially increase the probability of their preservation. Sample from University of Canterbury (NZ) collection.

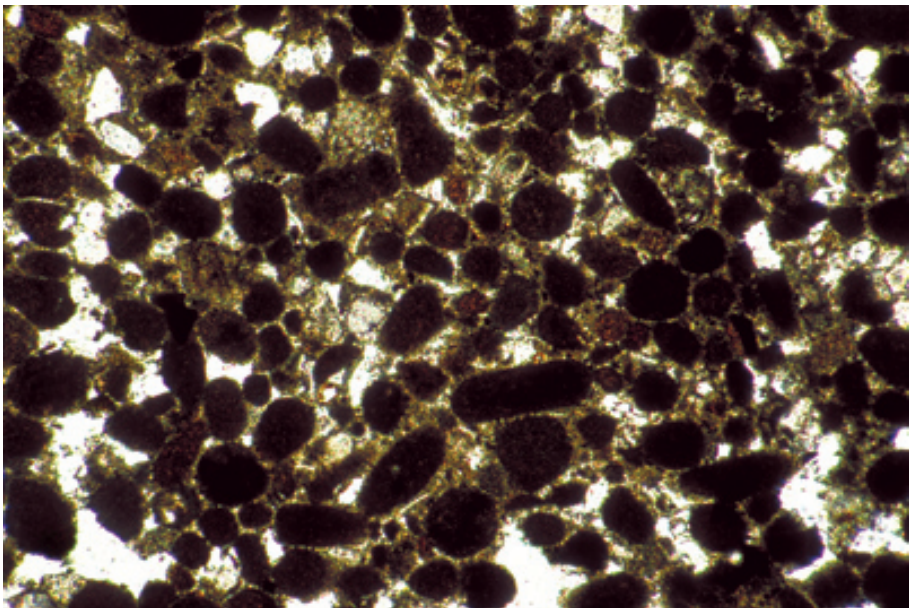

PPL, HA = 3.2 mm

Lo.-Mid. Ordovician Deepkill Shale, Rensselaer Co., New York

An ancient pelsparite containing abundant pellets of unknown, but possibly fecal, origin. Note the uniformly small particle size and consistent shape of these grains (much smaller than the Coorong pellets, but about average for pellets as defined by Folk, 1959). A brown color in reflected light (or "white-card" illumination) also favors a fecal origin, as it indicates a high content of organic matter. Substantial synsedimentary lithification of these pellets must have been followed by relatively early sparry calcite cementation of the rock in order to prevent compaction of these grains.

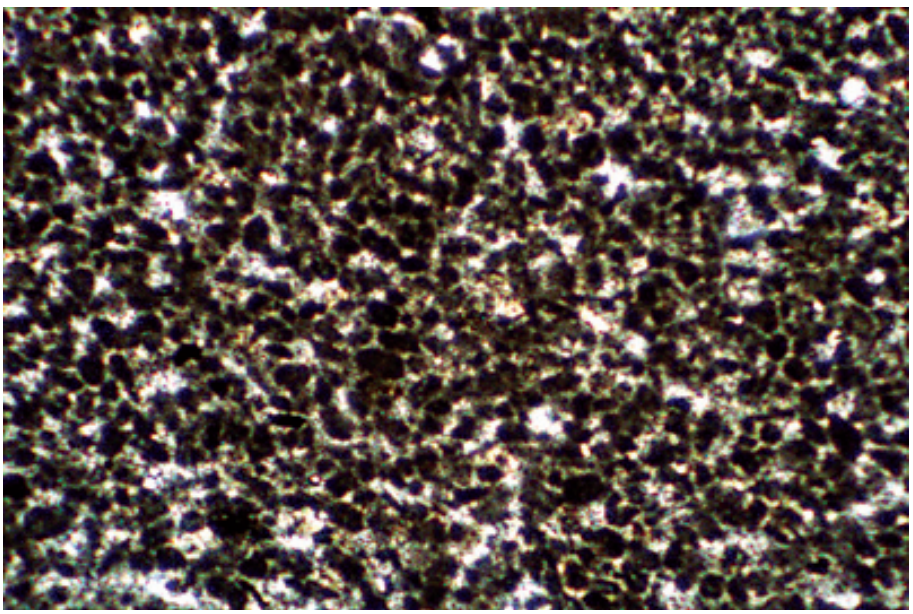

PPL, HA = 3.4 mm

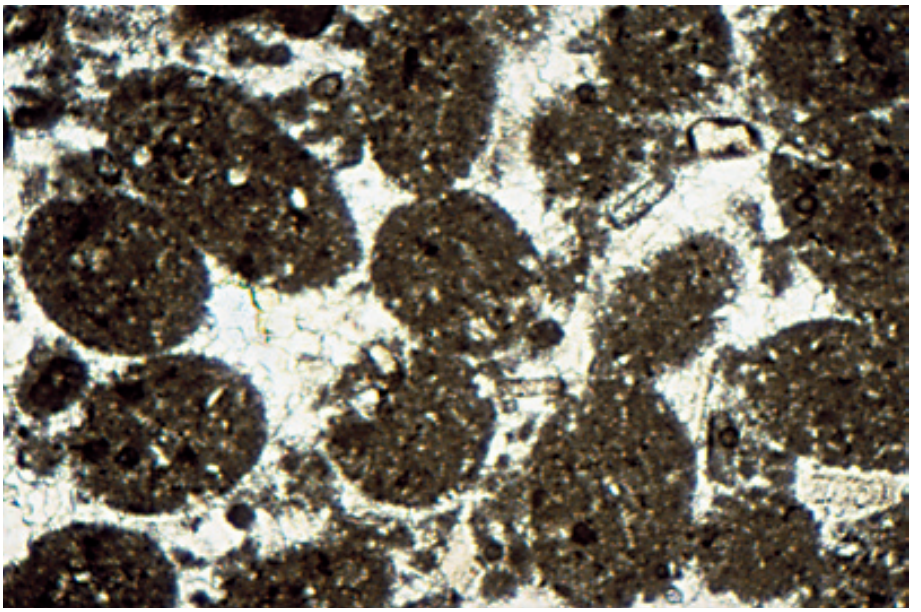

Mississippian (Meramecian) Ste. Genevieve Ls., Milltown, Indiana

These rounded grains are inferred, from their uniform size, ovoid shape, and consistent composition, to be fecal pellets (possibly crustacean pellets). Note the inclusion of silt-sized carbonate and terrigenous particles throughout the grains — this differentiates them from micritized ooids and the randomness of distribution of the included particles rules out tests of arenaceous foraminifers. Finally, the consistent size and rounding of the grains makes it very unlikely that they could be intraclasts.

PPL, HA = 2.4 mm

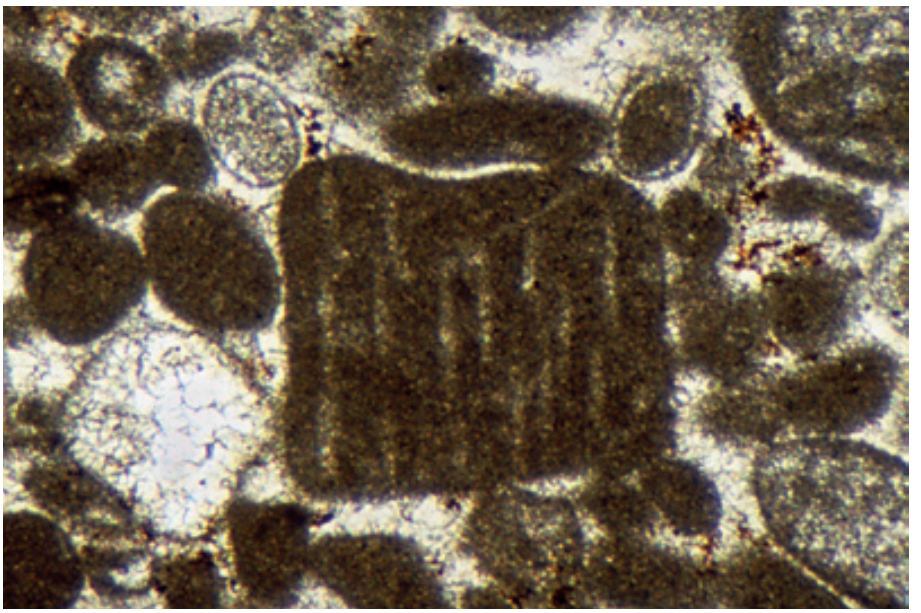

Lo. Jurassic (Liassic) limestone, Central High Atlas region, Morocco

The grain in the center of this image is a micro-coprolite (pellet), of an anomuran decapod crustacean. This pellet probably belongs to the ichnogenus *Favreina*, and the diagnostic internal tubular structures that parallel the long axis of the pellet are the key to the recognition of these grains. The tubular fabric is produced by elongate, sometimes string-like, flaps in the organism's digestive tract.

PPL, HA = 1.6 mm

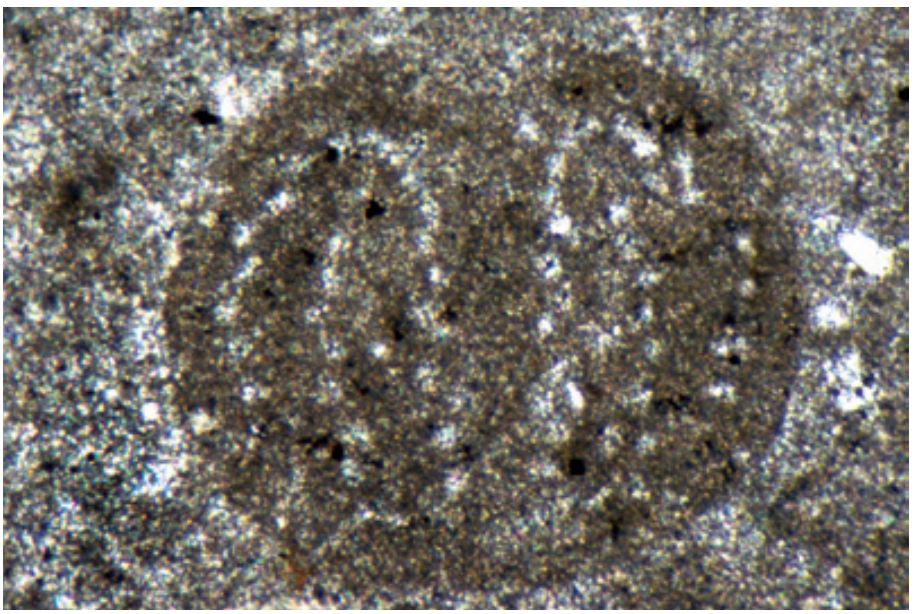

Up. Jurassic (Oxfordian) Smackover Fm., subsurface, Choctaw Co., Alabama

A transverse section through a *Favreina* crustacean pellet with internal tubular structure. Note the circular outline and very distinctive pattern of internal spar-filled pores that characterize these readily recognizable pellets.

PPL, HA = 0.6 mm

Pleistocene Ironshore Fm., Grand Cayman, Cayman Islands, B.W.I.

Grains that have micritic internal structure like pellets, but that have diverse and irregular shapes and sizes, or vague remnants of internal fabric are generally termed peloids. This is a convenient "term of ignorance" for grains for which a definite origin cannot be determined. This sediment shows a variety of micritized grains — in many of them no definitive fabric remains, and thus, those grains would best be termed "peloids".

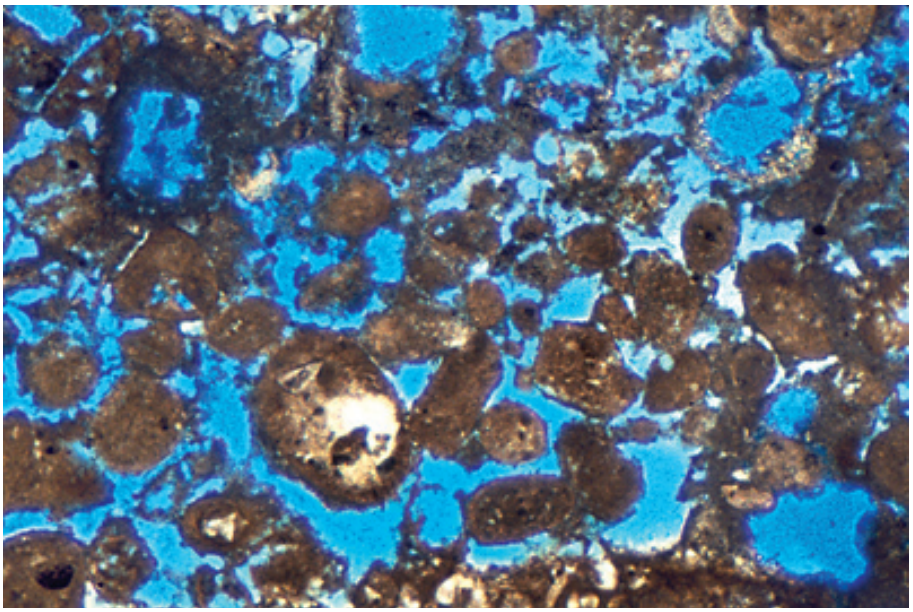

PPL, BSE, HA = 2.4 mm

Recent sediment, coastal Abu Dhabi, United Arab Emirates

Although the general process of grain micritization was illustrated in the section on ooids and pisoids, another example is provided here in the context of peloid formation. This photograph shows an advanced stage of micritization affecting a peneroplid foraminifer. Micro-boring of grains on the seafloor and filling of those pores (and primary intraparticle pores) with aphanocrystalline cement is the main cause of such alteration. Although this grain is still recognizable as a foraminifer, continued alteration will produce an unidentifiable micritic grain — a peloid. Photograph courtesy of Bruce H. Purser.

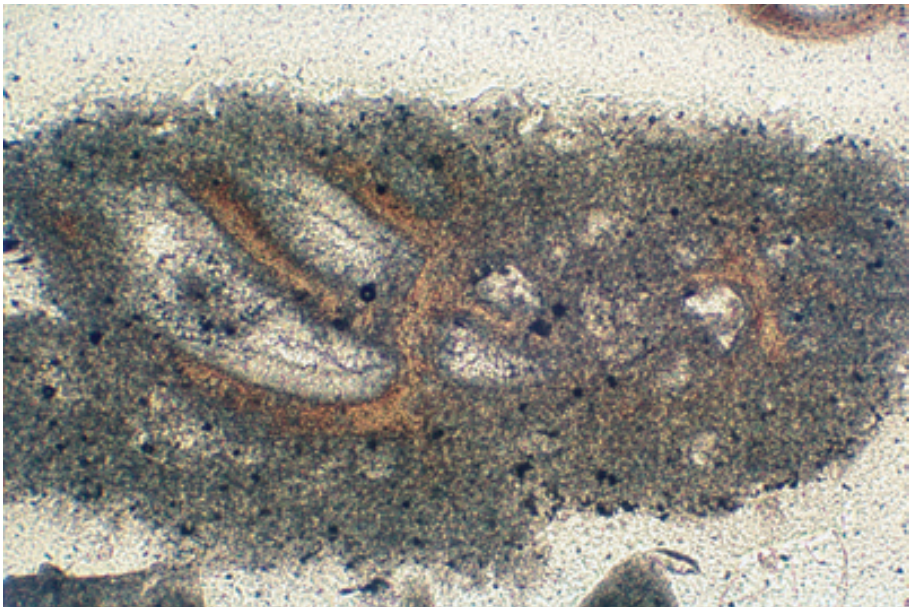

PPL, HA = ~1.0 mm

Oligocene Deborah Volcanic Fm., Oamaru, Otago, New Zealand

Small, rounded micritic grains can also be produced by carbonate precipitation around a variety of microbes. This example shows microbial shrubs that grew in the protected interstices between basaltic pillow lavas on the ocean floor. The shrubs were preserved as a result of rapid cementation by sparry calcite. Many of the shrubs disaggregated prior to spar formation, however, and the constituent small micritic peloids formed layers of internal sediment within this cavity. The formation of internal microbial crusts is, in a sense, a cementation process, but it blurs the line between what is a cement and what is a grain.

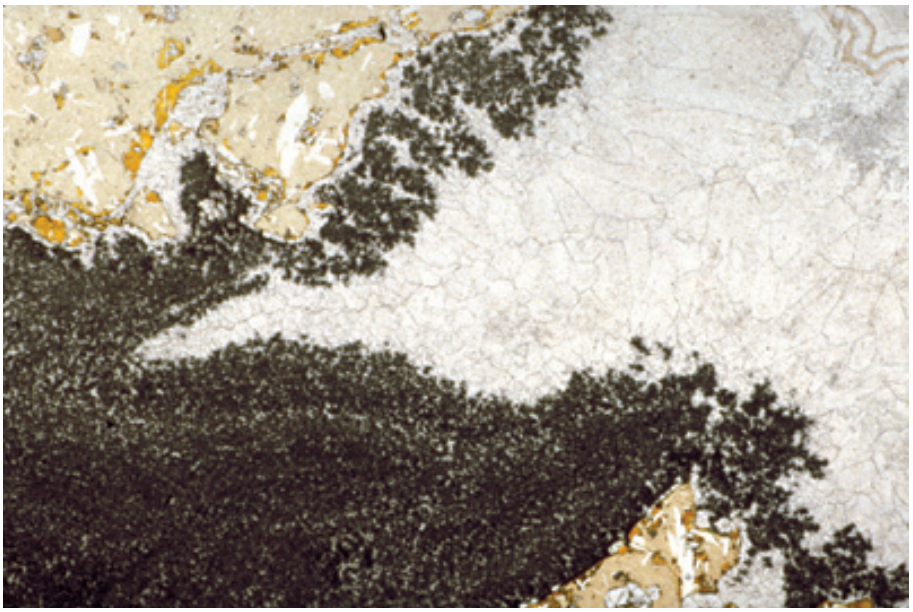

PPL, HA = 14.5 mm

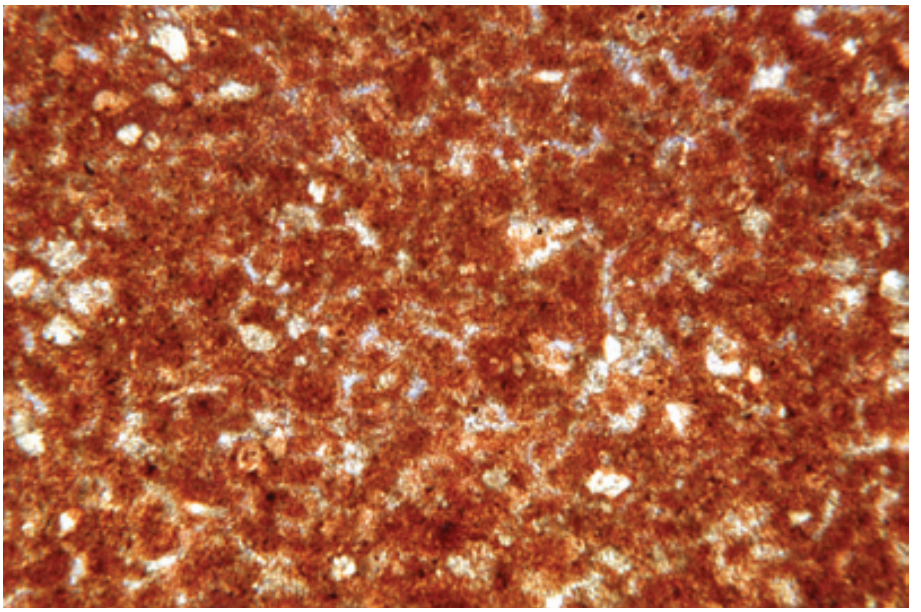

Holocene sediment, Tobacco Cay, Belize

A detail of a large area of cemented internal sediment consisting of fine-silt-sized, peloidal, high-Mg calcite that has been stained red with Clayton Yellow. These peloidal particles act as grains in this cemented internal sediment, but may, in fact, be microbially-influenced precipitates. This blurring of the distinction between small peloidal grains and cement has provoked much discussion in the past decade and most likely will continue to pose problems for petrographers well into the future. Photograph courtesy of Robert N. Ginsburg.

PPL, CYS, HA = 0.8 mm

Cited References and Additional Information Sources

Brown, P. R., 1964, Petrography and origin of some upper Jurassic beds from Dorset, England: Journal of Sedimentary Petrology, v. 34, p. 254-269.

Chafetz, H. S., 1986, Marine peloids: a product of bacterially induced precipitation of calcite: Journal of Sedimentary Petrology, v. 56, p. 812-817.

Eardley, A. J., 1938, Sediments of the Great Salt Lake, Utah: American Association of Petroleum Geologists Bulletin, v. 22, p. 1305-1411.

Fåhrœus, L. E., R. M. Slatt, and G. S. Nowlan, 1974, Origin of carbonate pseudopellets: Journal of Sedimentary Petrology, v. 44, p. 27-29.

Folk, R. L., 1959, Practical petrographic classification of limestones: American Association of Petroleum Geologists Bulletin, v. 43, p. 1-38.

Friedman, G. M., 1985, The term *micrite* or *micritic cement* is a contradiction — discussion of micritic cement in microborings is not necessarily a shallow-water indicator: Journal of Sedimentary Petrology, v. 55, p. 777.

Hattin, D. E., 1975, Petrology and origin of fecal pellets in Upper Cretaceous strata of Kansas and Saskatchewan: Journal of Sedimentary Petrology, v. 45, p. 686-696.

Honjo, S., and M. R. Roman, 1978, Marine copepod fecal pellets: production, preservation and sedimentation: Journal of Marine Research, v. 36, p. 45-57.

Kornicker, L. S., and E. G. Purdy, 1957, A Bahamian fecal-pellet sediment: Journal of Sedimentary Petrology, v. 27, p. 126-128.

Macintyre, I. G., 1985, Submarine cements — the peloidal question, *in* N. Schneidermann, and P. M. Harris, eds., Carbonate Cements: Tulsa, OK, SEPM Special Publication No. 36, p. 109-116.

McKee, E. D., and R. C. Gutschick, 1969, History of the Redwall Limestone of northern Arizona: Boulder, CO, Geological Society of America Memoir 114, 726 p.

Moore, H. B., 1932, The faecal pellets of the *Anomura*: Proceedings of the Royal Society of Edinburgh, v. 52, p. 296-308.

Purdy, E. G., 1963, Recent calcium carbonate facies of the Great Bahama Bank. 1. Petrography and reaction groups: Journal of Geology, v. 71, p. 334-355.

Reid, R. P., and I. G. Macintyre, 1998, Carbonate recrystallization in shallow marine environments: a widespread diagenetic process forming micritized grains: Journal of Sedimentary Research, Section A: Sedimentary Petrology and Processes, v. 68, p. 928-946.

Reid, R. P., and I. G. Macintyre, 2000, Microboring versus recrystallization: further insight into the micritization process: Journal of Sedimentary Research, Section A: Sedimentary Petrology and Processes, v. 70, p. 24-28.

Roth, P. H., M. M. Mullin, and W. H. Berger, 1975, Coccolith sedimentation by fecal pellets: laboratory experiments and field observations: Geological Society of America Bulletin, v. 86, p. 1079-1084.

Scoffin, T. P., 1976, Crustacean faecal pellets, *Favreina* from the Middle Jurassic of Eigg, Inner Hebrides: Scottish Journal of Geology, v. 9, p. 145-146.

Taghon, G. L., A. R. M. Nowell, and P. A. Jumars, 1984, Transport and breakdown of fecal pellets: biological and sedimentological consequences: Limnology and Oceanography, v. 29, p. 64-72.

Triplehorn, D. M., 1966, Morphology, internal structure, and origin of glauconite pellets: Sedimentology, v. 6, p. 247-266.

Facing Page: Thin-section photomicrographs (plane- and cross-polarized light) showing phosphatic ooids with phosphatic shell and bone cores in a shelfal phosphate-carbonate unit. Permian (Leonardian-Guadalupian) Phosphoria Fm., Caribou Co., Idaho. HA = 1.2 mm each.

GRAINS: Non-skeletal Grains

Non-carbonate Grains

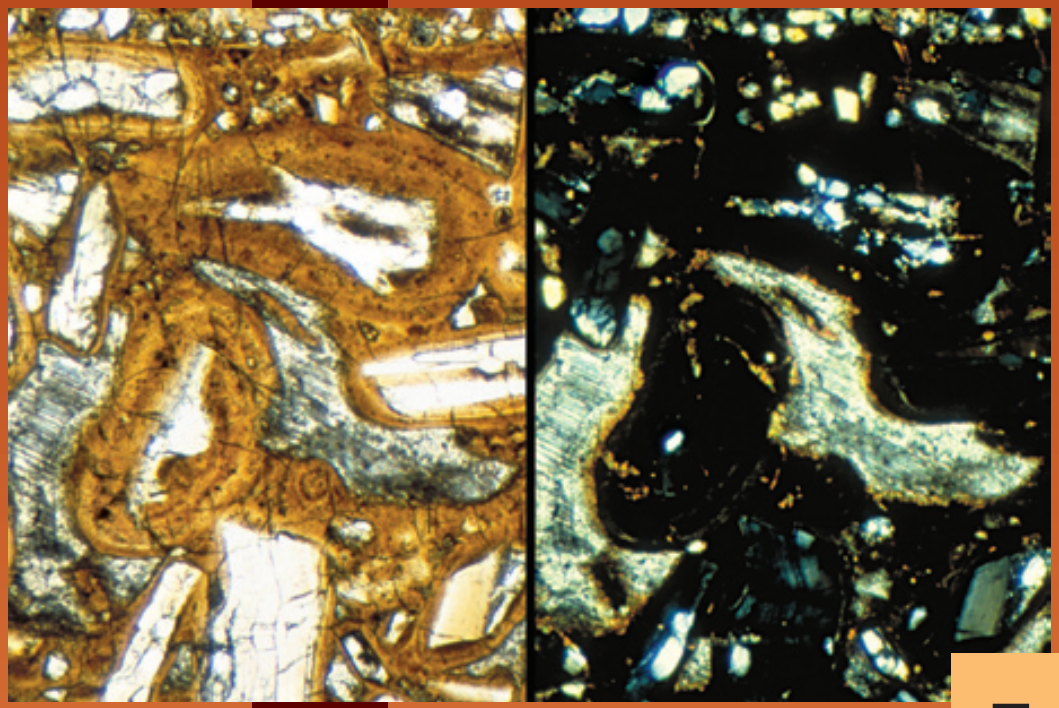

CHAPTER 17

Terrigenous material

Glauconite

Phosphatic detritus

Ferruginous grains

OTHER (NON-CARBONATE) GRAINS

Introduction:

A wide variety of non-carbonate grains can be found as constituents of carbonate rocks. In some cases, these grains are isolated and very subordinate particles; in other examples, they can be important rock-forming elements. Most of these minerals can also be found as diagenetic precipitates in carbonate rocks, but in this section only examples of true grains are illustrated (although some were synsedimentary diagenetic materials that effectively acted as sediment grains).

It is beyond the scope of this book to examine these non-carbonate grains in detail, but a few of the more important types — clastic terrigenous grains, glauconite "pellets", and ferruginous and phosphatic ooids —will be discussed briefly. The criteria for their recognition and the compositional characteristics of these grains are given in the individual figure captions.

The recognition of non-carbonate grains in carbonate rocks is important for the interpretation of depositional environments and for the proper classification of mixed-composition rocks. Most specialized classifications of carbonate rocks simply use adjectives such as "quartzose", "very quartzose", "feldspathic" or "glauconitic" to note the presence and relative abundance of non-carbonate grains (the term "silicified" is appropriately used where a significant amount of silica replacement has affected the deposit).

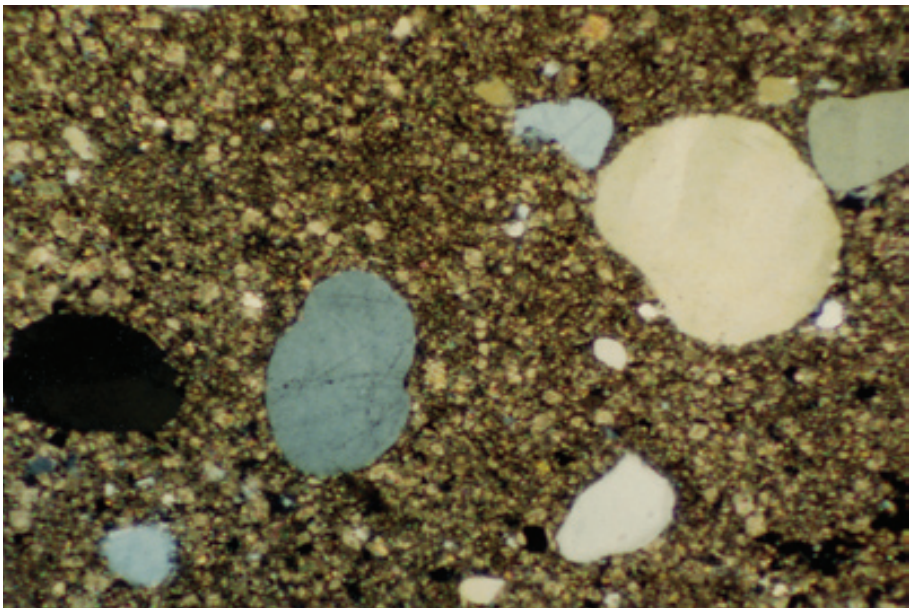

Up. Cambrian Copper Ridge Dol./ Conococheague Ls., Giles Co., Virginia

Well-rounded detrital quartz sand grains are scattered throughout this dolomitized carbonate mudstone. The quartz grains are at various stages of extinction, but none show birefringence colors higher than first order. Such excellent rounding typically indicates a precursor sedimentary source or long-term abrasion in a high-energy setting.

XPL, HA = 2.7 mm

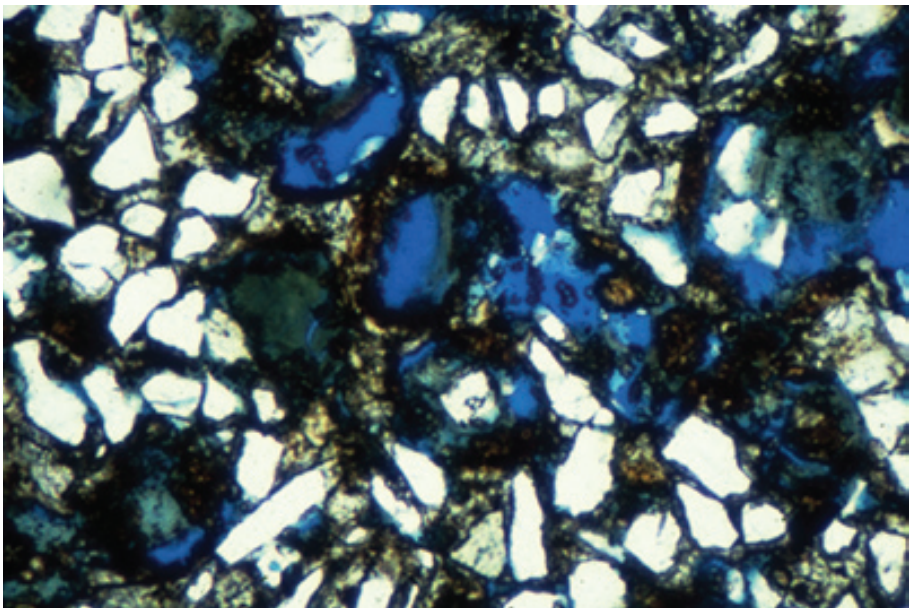

Lo. Cretaceous (Albian) Nahr Umr Fm., offshore Qatar

Abundant angular to subangular, detrital quartz grains (and subordinate feldspar) in a sideritic carbonate. Such angular grains are more common as terrigenous contributions to carbonate sediments than the very well rounded grains of the previous example. The siderite crystals are clear to brownish and have high relief.

PPL, BSE, HA = 1.6 mm

Up. Cretaceous Navesink Fm., Monmouth Co., New Jersey

Large, ovoid, pelletal glauconite grains in a glauconitic marl. The light green color in plane-polarized light and speckled, dark green appearance under cross-polarized illumination are characteristic for glauconite. Although "glauconite" basically is an iron- and magnesium-rich illite-type mineral, the term really refers to a family of related minerals ("glaucony" is sometimes used as a generic term for such materials when detailed mineralogical data is lacking). Glauconite grains can have varying degrees of mineral ordering, as well as a complex range of interlayered clay minerals (especially smectite).

XPL, HA = 2.9 mm

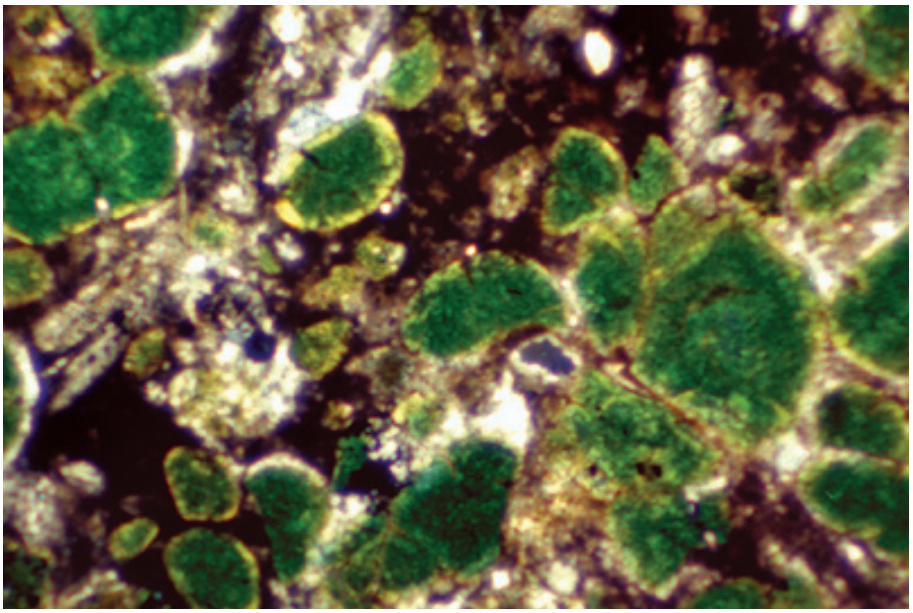

Lo. Miocene Otekaike Ls., Otago, New Zealand

These are pelletal/peloidal glauconite grains from a calcareous greensand (a "glaucony facies"). These glauconite grains have a characteristic pale green to yellowish color; some are internally featureless, whereas others show lobate or cerebroid structures. Glauconite is a seafloor diagenetic product formed primarily in mid- to outer-shelf settings, especially during intervals of slow sedimentation and mildly reducing conditions. Fecal pellets of a variety of organisms provide an excellent site for neoformation of glauconite due to the localized reducing environment that exists in the presence of residual fecal organic matter.

PPL, HA = 2.0 mm

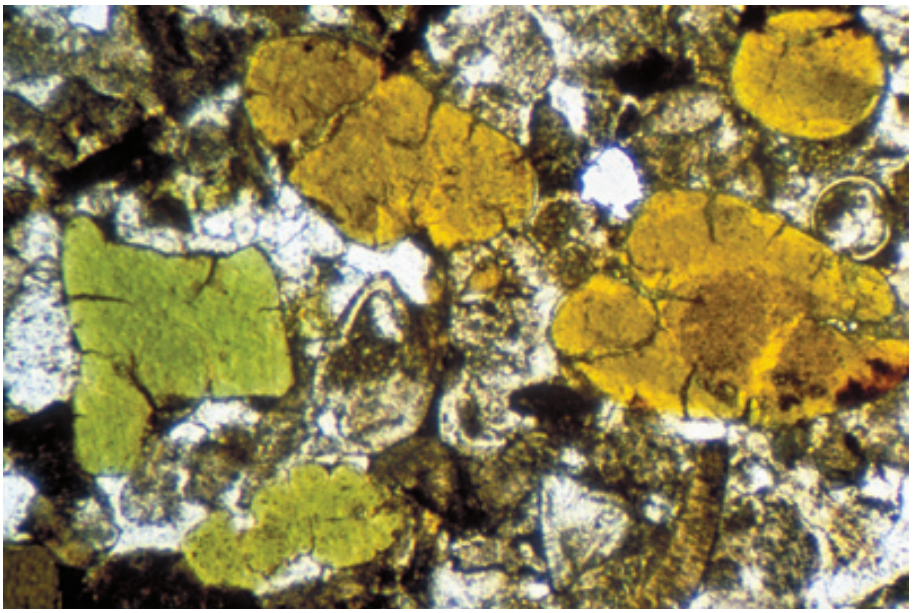

Up. Oligocene-Lo. Miocene Otekaike Ls., Canterbury, New Zealand

A variety of glauconite grains in a greensand. All show characteristic pale green color; most are internally featureless pellet-like grains, but a few have a foliated or vermicular structure. The foliated grains most likely represent synsedimentary (seafloor) glauconitization of detrital biotites, a slow process that takes place under reducing conditions and requires low rates of sediment accumulation to allow long-term contact of the detrital grains with seawater.

PPL, BSE, HA = 0.6 mm

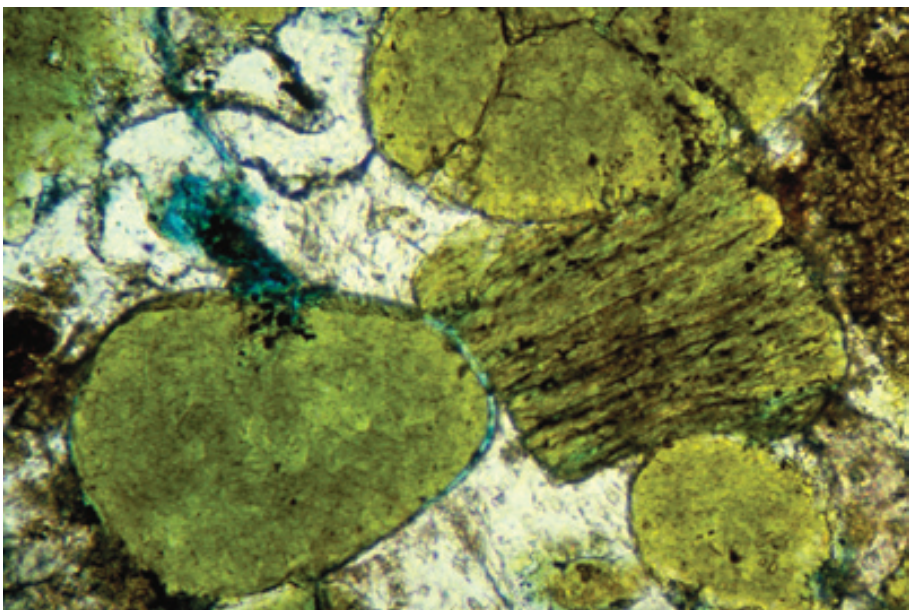

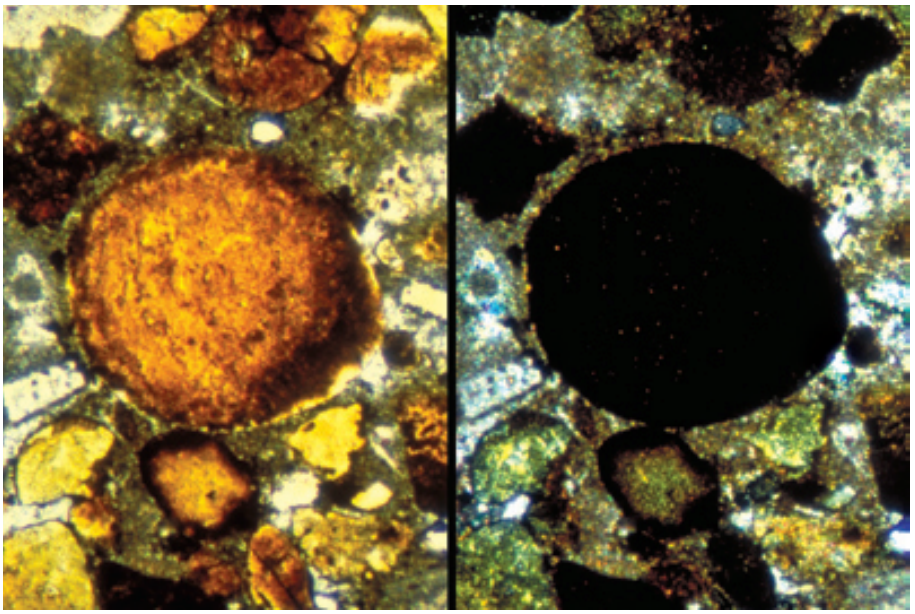

Lo. Oligocene McDonald Ls., Oamaru, Otago, New Zealand

Phosphatic nodules in a hardground section. The yellow-brown color and nearly isotropic extinction behavior are characteristic of phosphatic material. These are effectively intraclasts (albeit not of carbonate composition) as they represent tear-up clasts from a mineralized and lithified, synsedimentary cementation horizon (hardground) associated with a widespread hiatal surface. Recognition of such clasts, and their associated hiatus surfaces, is an important component of modern sequence stratigraphy.

PPL/XPL, HA = 0.8 mm each

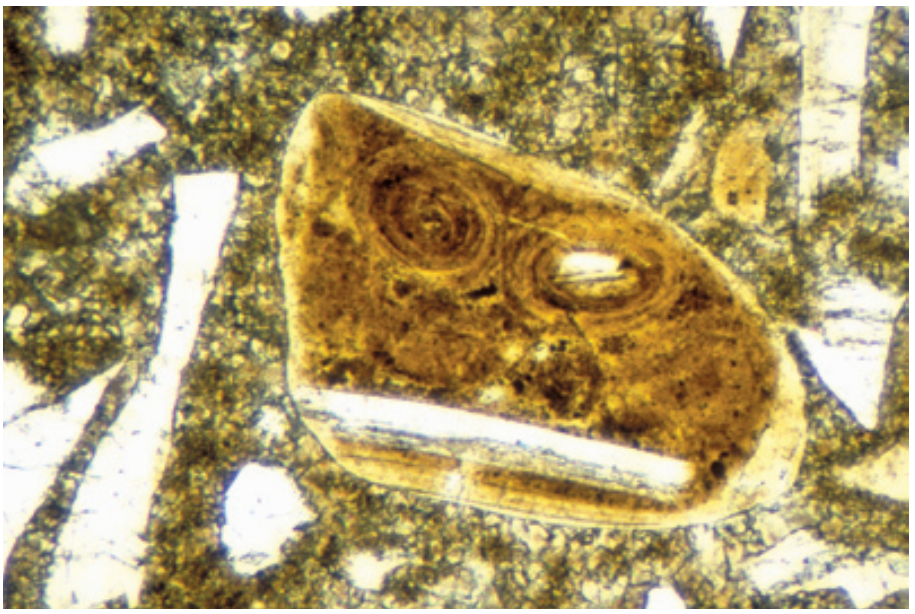

Permian (Leonardian-Guadalupian) Park City Fm., up. Grandeur Mbr., Bonneville Co., Idaho

An intraclast containing ooids and fragmented shell and bone material — all are composed of phosphate and are part of one of the world's largest phosphate deposits. The clear to yellowish brown color of the phosphate is typical for this mineral. A thin, second generation of pale-yellow phosphate coats the exterior of the large intraclastic grain.

PPL, HA = 1.6 mm

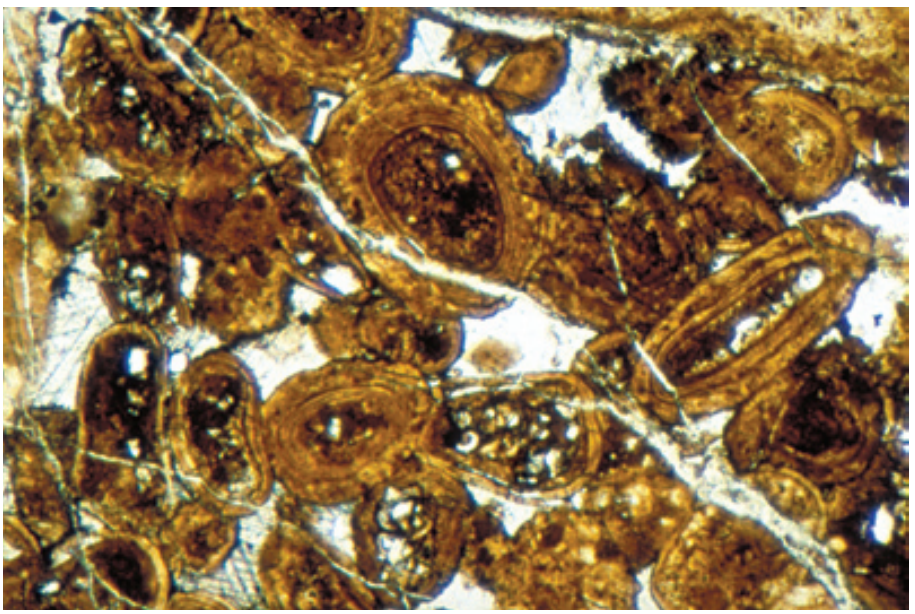

Permian (Leonardian-Guadalupian) Phosphoria Fm., Meade Peak Mbr., Bear Lake Co., Idaho

Well formed phosphatic ooids with phosphatic shell and bone cores. Sedimentation of this unit took place on a cool-water ramp during transgressive cycles across broad carbonate banks. The intraclasts (above) and heavily coated ooids of primary phosphate, both indicators of strong wave or current action, imply a very shallow water environment of phosphate formation.

PPL, HA = 2.6 mm

Pliocene Bone Valley Fm., Polk Co., Florida

Rounded phosphatic grains associated with a major pebble-phosphate deposit. In this example, phosphate accumulated (mainly in the form of vertebrate bones, teeth and scales) in a shallow, coastal shelf setting. The phosphate was then concentrated and reworked into granules and pebbles by later subaerial exposure and weathering. Note the clear color of the pebble phosphates in plane-polarized light and virtual isotropism under cross-polarized light.

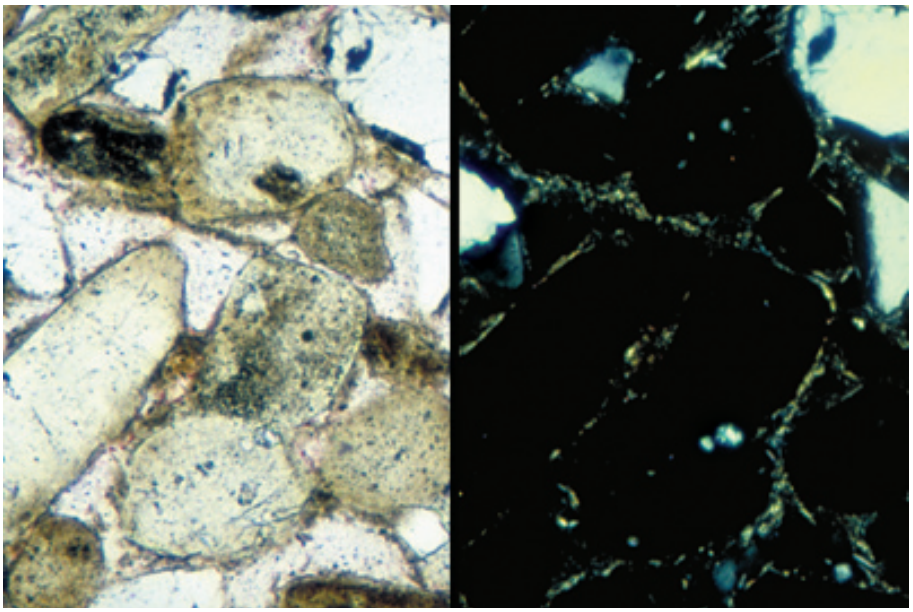

PPL/XPL, HA = 0.8 mm each

Jurassic Eisenoolith, western Bavaria, Germany

Hematite ooids illuminated with the conoscopic condenser in place — this produces a very intense transmitted light beam that shows the reddish-yellow color of this slightly weathered hematite (nearly opaque under normal illumination). These are inferred to have been originally carbonate ooids that were replaced by various iron minerals. Two major periods of oolitic ironstone formation are recognized: Early Ordovician to Devonian and Early Jurassic to mid-Cenozoic (Van Houten and Bhattacharyya, 1982). These were generally times of high sea-level stands with reduced terrigenous sediment influx.

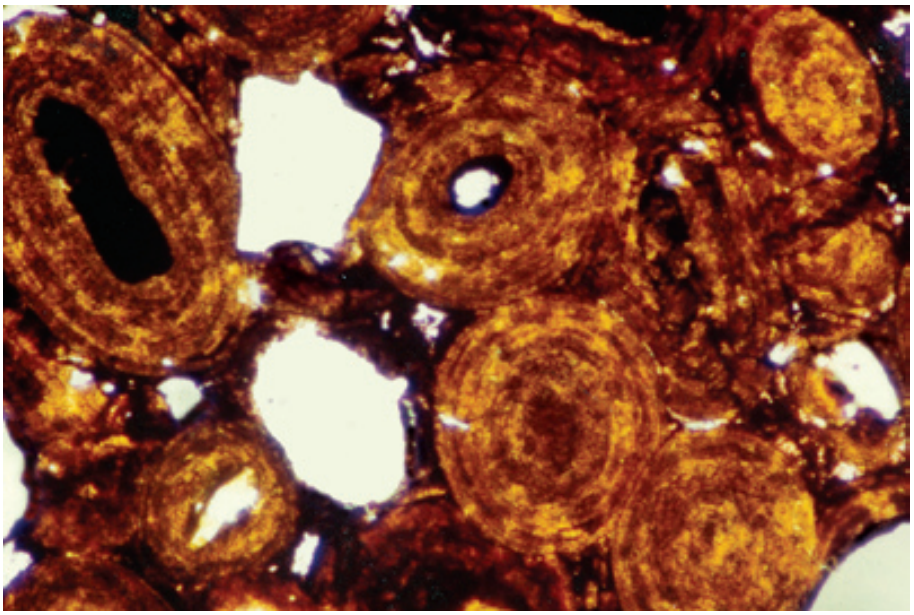

PPL, HA = 2.1 mm

Lo. Cretaceous (Albian) Nahr Umr Fm., offshore Qatar

Chamosite ooids in a glauconitic and sideritic sandstone interval within a shallow-shelf carbonate section. Chamosite (an iron-rich chlorite mineral) is most commonly formed in inner shelf environments during times of relatively slow sedimentation, some wave or current activity, and mildly reducing conditions (especially during transgressive events; Van Houten and Purucker, 1984). Some chamosite ooids may be replacements of carbonate precursors, but most probably are directly precipitated on the seafloor.

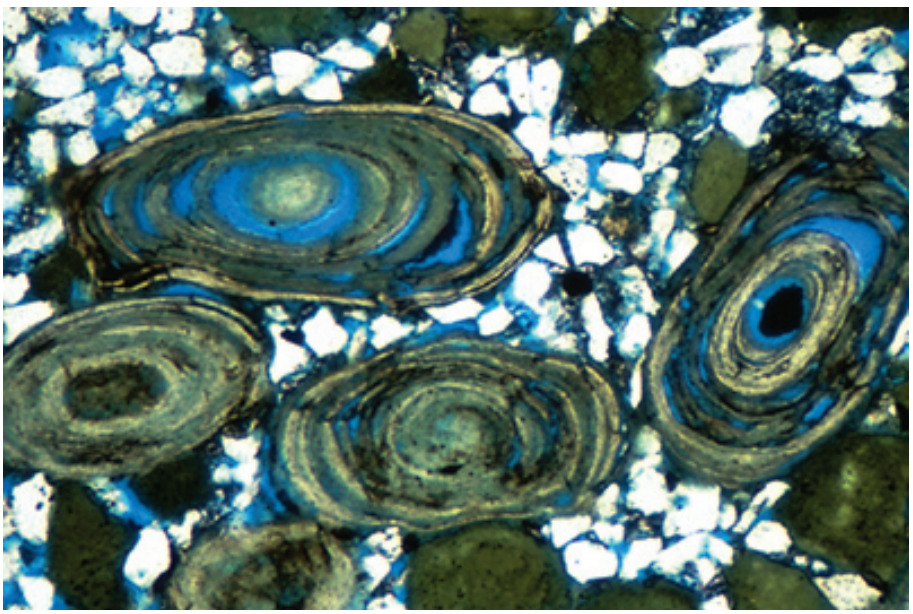

PPL, BSE, HA = 1.6 mm

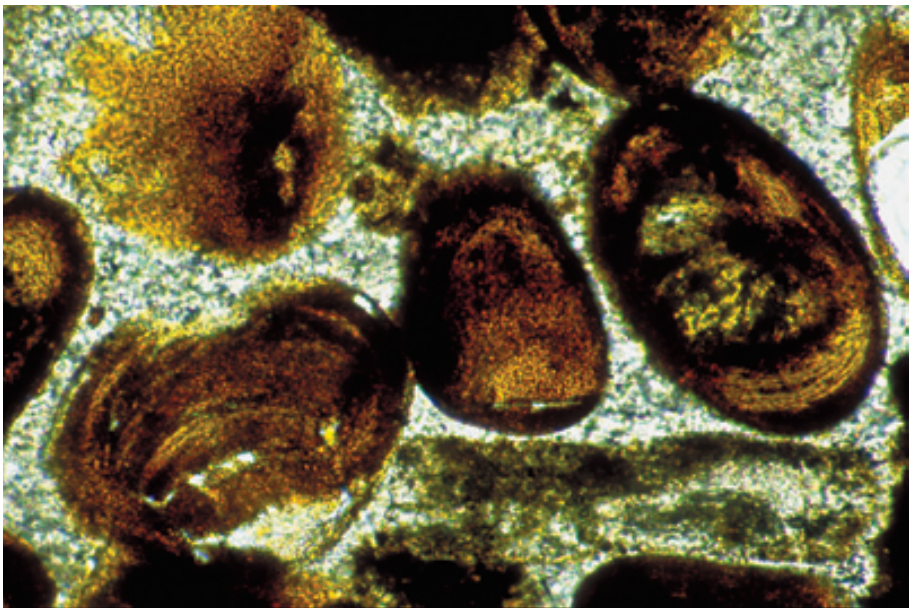

Jurassic ironstone, Midlands, England, U.K.

An enlarged view of chamosite ooids from an oolitic ironstone formation (an economic iron ore). The oolitic coatings here are not as clearly developed as in the previous sample. The bean-like shape of the ooids in this and the previous sample is a common feature in chamosite ooids. Sample from University of Canterbury collection.

PPL, HA = 1.0 mm

Cited References and Additional Information Sources

Amouric, M., and C. Parron, 1985, Structure and growth mechanism of glauconite as seen by high resolution transmission electron microscopy: Clays and Clay Minerals, v. 33, p. 473-482.

Baturin, G. N., 1982, Phosphorites on the Sea Floor. Origin, Composition, and Distribution: New York, Elsevier, 343 p.

Bentor, Y. K., and M. Kastner, 1965, Notes on mineralogy and origin of glauconite: Journal of Sedimentary Petrology, v. 35, p. 155-166.

Bhattacharyya, D. P., and P. K. Kakimoto, 1982, Origin of ferriferous ooids: an SEM study of ironstone ooids and bauxite pisoids: Journal of Sedimentary Petrology, v. 52, p. 849-857.

Braithwaite, C. J. R., 1980, The petrology of oolitic phosphorites from Esprit (Aldabra), Western Indian Ocean: Philosophical Transactions of the Royal Society of London, Series B, v. 288, p. 511-543.

Bromley, R. G., 1967, Marine phosphorites as depth indicators: Marine Geology, v. 5, p. 503-509.

Burst, J. F., 1958, "Glauconite" pellets: their mineral nature and application to stratigraphic interpretation: American Association of Petroleum Geologists Bulletin, v. 42, p. 310-327.

Carson, G. A., and S. F. Crowley, 1993, The glauconite-phosphate association in hardgrounds: examples from the Cenomanian of Devon, southwest England: Cretaceous Research, v. 14, p. 69-89.

Cook, P. J., 1976, Sedimentary phosphate deposits, *in* K. H. Wolf, ed., Handbook of Strata-Bound and Stratiform Ore Deposits: Amsterdam, Elsevier Scientific Publishing Co, p. 505-535.

Kimberley, M. M., 1979, Origin of oolitic iron formations: Journal of Sedimentary Petrology, v. 49, p. 111-132.

Knox, R. W. O. B., 1970, Chamosite ooliths from the Winter Gill ironstone (Jurassic) of Yorkshire, England: Journal of Sedimentary Petrology, v. 40, p. 1216-1225.

Lamboy, M., 1990, Microbial mediation of phosphatogenesis: new data from the Cretaceous phosphatic chalks of northern France, *in* A. J. G. Notholt, and I. Jarvis, eds., Phosphorite Research and Development: London, Geological Society Special Publication 52, p. 1157-1167.

Manheim, F. T., and R. A. Gulbrandsen, 1979, Marine phosphorites, *in* R. G. Burns, ed., Marine Minerals: Washington, D.C., Mineralogical Society of America Short Course Notes, v. 6, p. 151-173.

Martindale, S. G., 1986, Depositional environments and phosphatization of the Meade Peak Phosphatic Shale Tongue of the Phosphoria Formation, Leach Mountains, Nevada: University of Wyoming, Contributions to Geology, v. 24 (2), p. 143-156

McConchie, D. M., and D. W. Lewis, 1980, Varieties of glauconite in late Cretaceous and early Tertiary rocks of the South Island of New Zealand, and new proposals for classification: New Zealand Journal of Geology and Geophysics, v. 23, p. 413-437.

McRae, S. G., 1972, Glauconite: Earth-Science Reviews, v. 8, p. 397-440.

Odin, G. S., 1972, Observations on the structure of the glauconite vermicular pellets: a description of the genesis of these granules by neoformation: Sedimentology, v. 19, p. 285-294.

Odin, G. S., 1988, Green Marine Clays [Developments in Sedimentology 45]: New York, Elsevier, 445 p.

Pacey, N. R., 1985, The mineralogy, geochemistry and origin of pelletal phosphates in the English Chalk: Chemical Geology, v. 48, p. 243-256.

Porrenga, D. H., 1967, Glauconite and chamosite as depth indicators in the marine environment: Marine Geology, v. 5, p. 495-501.

Riggs, S. R., 1979, Petrology of the Tertiary phosphorite system of Florida: Economic Geology, v. 74, p. 195-220.

Sheldon, R. P., 1981, Ancient marine phosphorites: Annual Review of Earth and Planetary Sciences, v. 9, p. 251-284.

Soudry, D., and P. N. Southgate, 1989, Ultrastructure of a Middle Cambrian primary nonpelletal phosphorite and its early transformation into phosphate vadoids: Georgina Basin, Australia: Journal of Sedimentary Petrology, v. 59, p. 53-64.

Swett, K., and R. K. Crowder, 1982, Primary phosphatic oolites from the Lower Cambrian of Spitsbergen: Journal of Sedimentary Petrology, v. 52, p. 587-593.

Triplehorn, D. M., 1966, Morphology, internal structure, and origin of glauconite pellets: Sedimentology, v. 6, p. 247-266.

Van Houten, F. B., and D. P. Bhattacharyya, 1982, Phanerozoic oolitic ironstones — geologic record and facies model: Annual Review of Earth and Planetary Sciences, v. 10, p. 441-457.

Van Houten, F. B., and R. M. Karasek, 1981, Sedimentologic framework of late Devonian oolitic iron formation, Shatti Valley, west-central Libya: Journal of Sedimentary Petrology, v. 51, p. 415-427.

Van Houten, F. B., and M. E. Purucker, 1984, Glauconitic peloids and chamositic ooids — favorable factors, constraints, and problems: Earth-Science Reviews, v. 20, p. 211-243.

Facing Page: Top - Alfred G. Fischer showing students how it feels to be a grain surrounded by carbonate matrix; Everglades coast of Florida Bay, south Florida.

Bottom - Photomicrograph of a molluscan umbrella or shelter void with a geopetal fill of peloidal matrix. Lo. Permian Bone Spring Ls, Culberson Co. Texas. HA = 4.5 mm.

Carbonate Matrix

Carbonate mud, micrite and microspar

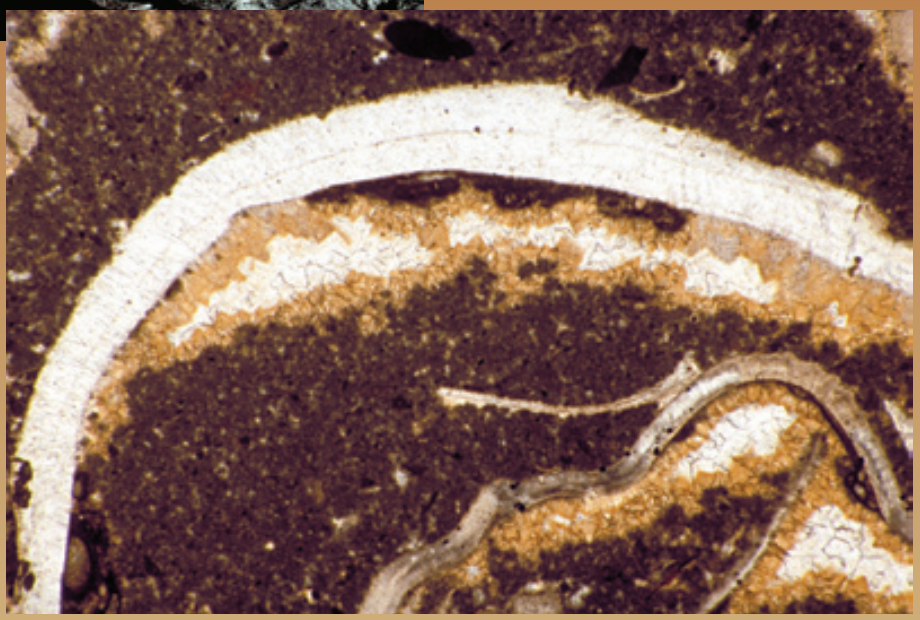

CHAPTER 18

CARBONATE MATRIX

Introduction:

Carbonate mud is the equivalent of clay in terrigenous rocks and can form pure deposits (variously termed micrites, carbonate mudstones, lime mudstones, or calcimudstones on the carbonate side, and claystones or shales on the clastic terrigenous side). Clay-sized particles also act as matrix material that supports larger grains or are lodged interstitially between a self-supporting framework of larger grains. Decades ago, when both life and muds seemed pure and simple, both clays and carbonate muds were viewed as miniature versions of larger grains, acting primarily as reworked particles. It is now known that some clays are detrital, some are altered or neoformed on the seafloor, and some are precipitated during the long diagenetic history that accompanies burial, adding considerable complexity to the interpretation of terrigenous shaly deposits. The same is true on the carbonate side. Carbonate muds can be part of the spectrum of disintegration products of carbonate organisms, some can be formed by direct inorganic precipitation, and some may be formed in association with microbial metabolism. Furthermore, some may be primary sediment that responded to hydrodynamic forces during sediment formation and some may be precipitated interstitially, at or near the seafloor (through organic or inorganic processes), or during later diagenesis. It is even possible for grains to break down into smaller carbonate particles during diagenesis, or for diagenetic conversion of former carbonate mud to a mosaic of coarser calcite crystals (microspar). Although we have learned much over the past decades about mud-sized materials, we are far from having a full understanding of them. We also have not yet developed reliable criteria for the consistent distinction between organically produced and inorganically precipitated materials, or even between detrital particles and authigenic precipitates.

Definitions:

Micrite - An abbreviation of "microcrystalline calcite". The term is used both as a synonym for carbonate mud (or "ooze") and for a rock composed of carbonate mud (calcilutite). Micrite consists of 1 to 4 µm-diameter crystals and forms as an inorganic precipitate or through breakdown of coarser carbonate grains. Micrite is produced within the basin of deposition and shows little or no evidence of significant transport (Folk, 1959).

Microspar - Generally 5- to 20-µm-sized calcite produced by recrystallization (neomorphism) of micrite; can be as coarse as 30 µm (Folk, 1965). Restricted to recrystallization products, not primary precipitates.

Pseudospar - A neomorphic (recrystallization) calcite fabric with average crystal size larger than 30-50 µm (Folk, 1965).

Mineralogy:

Modern marine shelfal carbonate mud is mainly aragonite (with some high-Mg calcite); deep-sea chalk oozes are low-Mg calcite as are most lacustrine calcareous muds. The composition of carbonate muds produced from breakdown of skeletal material are clearly controlled by the mineralogy of those organisms. Paleozoic shells were generally more calcitic than the aragonite-dominated shelled fauna of the modern world. Furthermore, even the mineralogy of "inorganic" marine precipitates (muds as well as cements) is now known to have varied throughout geologic time (Lasemi and Sandberg, 1984, 1993).

Keys to Petrographic Recognition:

1. Modern carbonate mud consists largely of the breakdown products of organisms (due to decomposition of organic binding materials and abrasion or maceration of shells). Macroscopic algae (especially green algae) are major contributors of needle-shaped, mud-sized, aragonitic particles in tropical platform and platform margin settings. Modern inorganic aragonitic precipitates, in the water column or on the seafloor, also are needle-like (with individual crystals typically 3-5 µm in length) and may contribute to carbonate muds.
2. The calcitic micrite of older carbonate rocks was neomorphically formed from mixed mineralogy precursors to form an equant mosaic of 1- to 4-µm crystals. The precursor material acted as detrital particles and so may show geopetal fabrics, scattered coarser particles, and other indications of mechanical sedimentation. Inclusions or molds of precursor minerals may be seen within micritic calcites (especially using SEM).
3. Neoformed microcrystalline cement and microbial precipitates may show clotted or peloidal fabrics and can grow in any position within interparticle pores or larger cavities (non-geopetal fabrics).
4. Microspar and pseudospar typically have patchy distributions grading into normal micrite; crystal outlines tend to be elongate (loaf-shaped) or have irregular, sutured boundaries).

Recent sediment, Belize

An SEM image of a *Halimeda* plate showing the loosely arranged inorganic aragonite needles from the calcified portion of this green algal grain. Needles such as these are found in many species of green algae including *Penicillus*, *Udotea*, and others. When the algae decompose, the needles (and shorter, more rounded, nannobacterial crystals) may be scattered, and can add significantly to the local production of clay-sized calcareous particles. Indeed, a modern platform carbonate mud can look much like the material shown in this image.

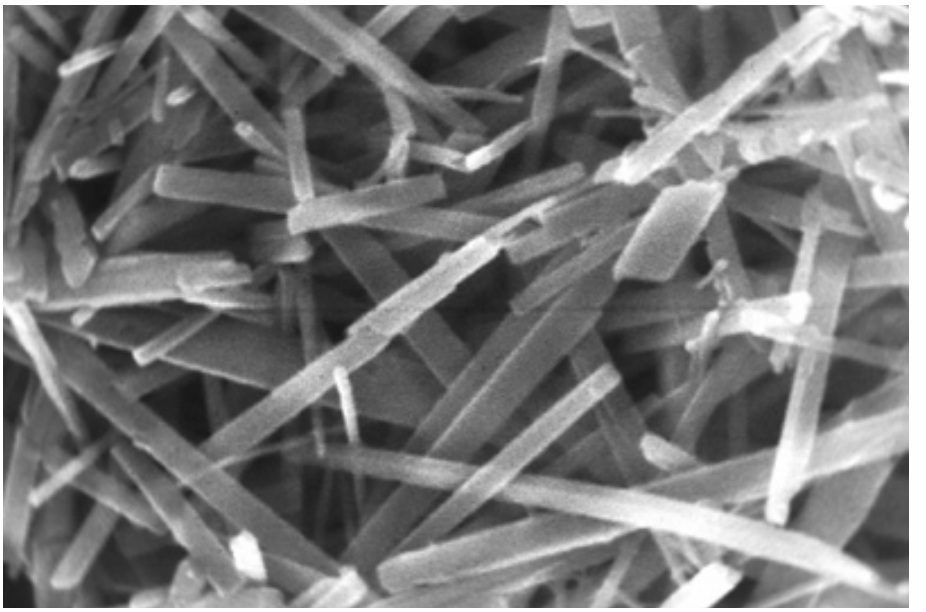

SEM, HA = 11 μm

Up. Jurassic Solnhofen Ls., Kelheim, Bavaria, Germany

This ancient micritic limestone is also known as a lithographic limestone, and is so named because it is pure and fine-grained enough to be used for high-quality lithographic printing plates. Note the interlocking mosaic of micron-sized, equant calcite crystals that is typical for micrite. Inorganic precipitates of this age were predominantly low-Mg calcite (see diagram below), but some aragonitic skeletal-breakdown material may also have contributed to this deposit. Whatever variations were present in the precursor material were homogenized in the neomorphic processes that produced this crystal mosaic.

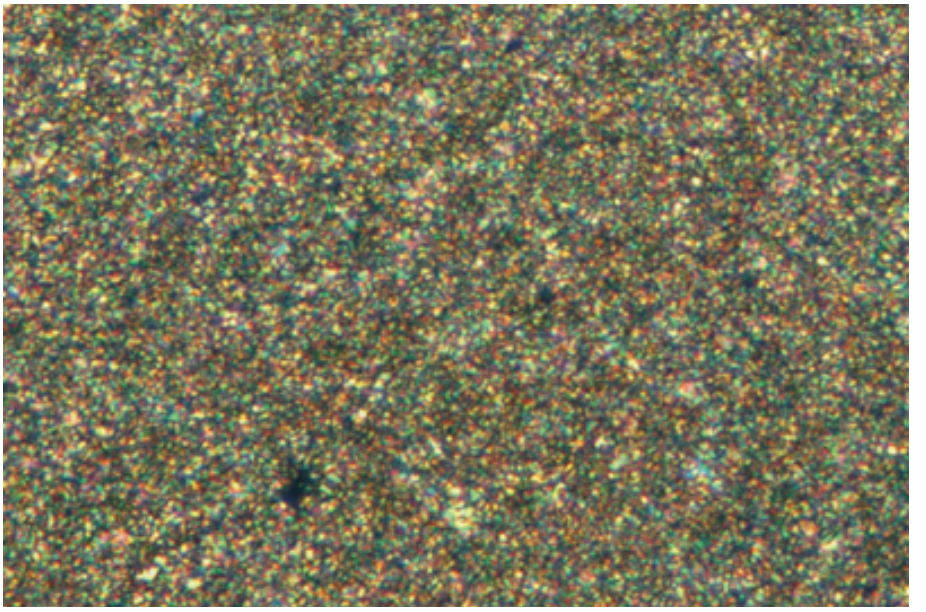

XPL, HA = 1.5 mm

Temporal variability of inorganic carbonate mineralogy

A diagram showing the variability of inorganic carbonate mineralogy through time in comparison to inferred secular changes in climate, sea level and granite emplacement rates. This compilation, by Sandberg (1983), is based on studies of marine cements, ooids and carbonate muds. Based on this work, and a number of confirming studies, one can expect significant temporal variations in the starting mineralogy, and thus the "diagenetic potential", of carbonate matrix materials.

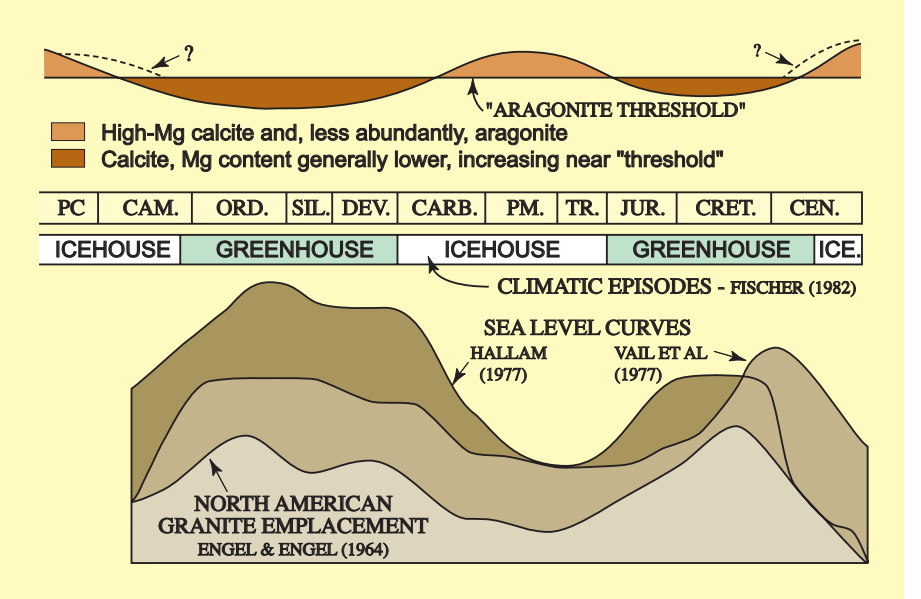

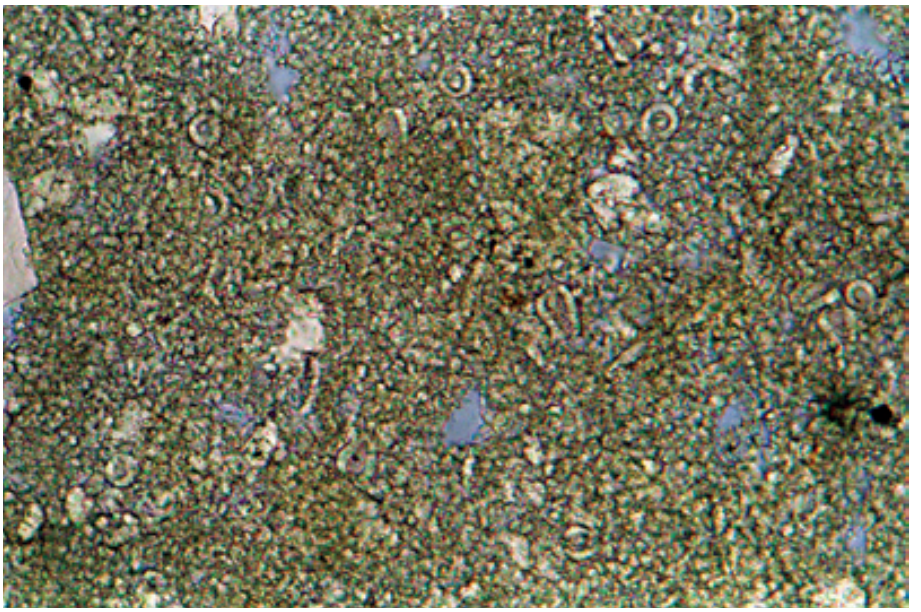

Lo. Cretaceous (Aptian) Shuaiba Fm., offshore Qatar

From the Jurassic onward, nannofossils have formed a significant component of micritic sediment, especially (but not exclusively) in outer shelf and deeper-water deposits. This example is from a shallow shelf limestone and shows abundant circular sections through cup-shaped nannoconids. The individual plates of most such nannofossils are less than 1 μm long, but diagenetic overgrowth can increase that size. As originally calcitic organisms, such microfossils produce matrix material that is far more stable than the typical aragonite muds of modern tropical shelf carbonates.

PPL, BSE, HA = 0.2 mm

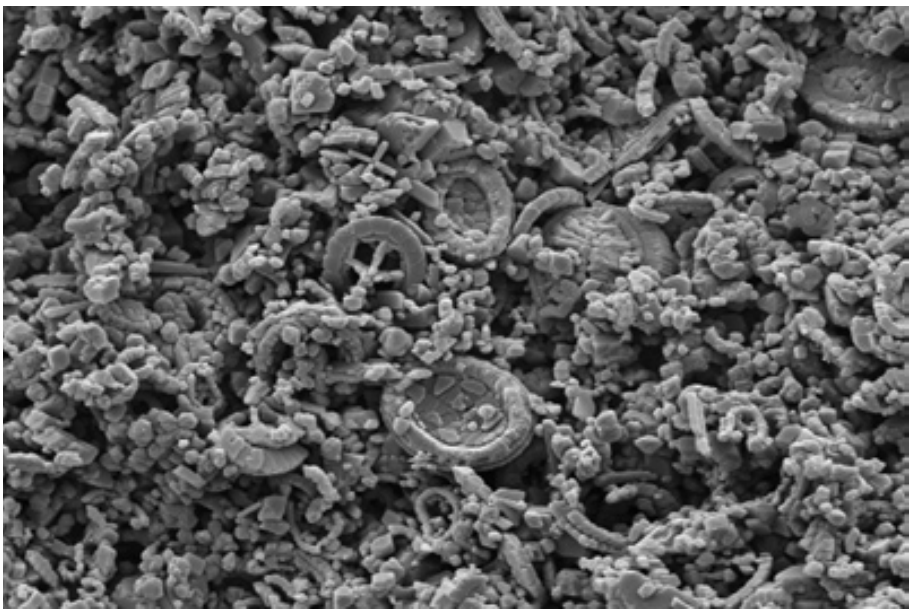

Up. Cretaceous (up. Maastrichtian) Tor Fm., Danish North Sea

An example of a classic shelf chalk in which coccoliths are virtually the only constituents. Although a few larger coccoliths remain intact, most of this deposit consists of the 1-2 μm crystals from disaggregated coccoliths. With normal light microscopy, this would appear as a pure micrite with very uniform crystal size. The remarkably high (45%) porosity in this moderately deeply buried, 65 million year-old limestone is largely due to the lack of diagenetically reactive aragonite in the original sediment.

SEM, HA = 68 μm

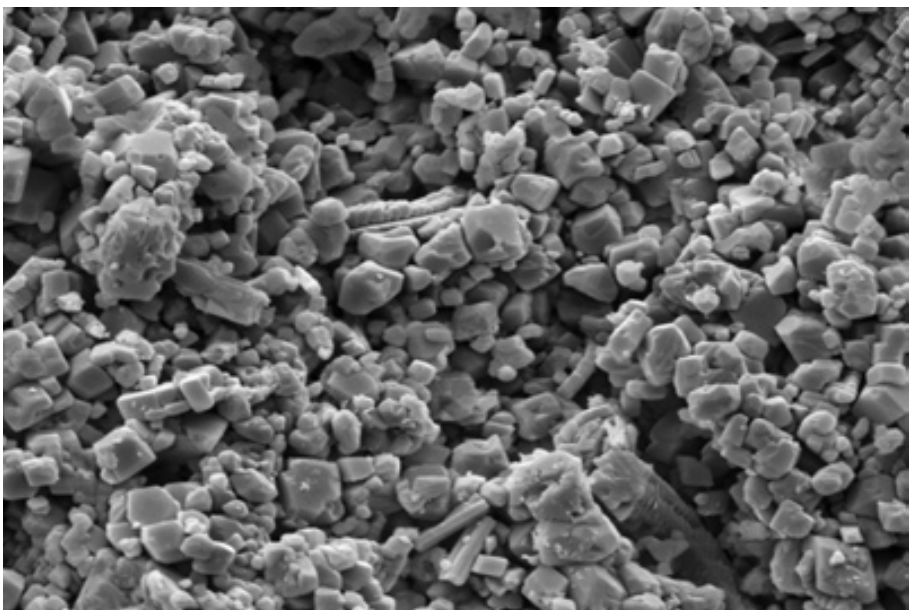

Up. Cretaceous (up. Maastrichtian) Tor Fm., Danish North Sea

A magnified view of a slightly more altered chalk. Porosity here has been reduced to 25-30%, mainly through micro-scale syntaxial overgrowth of individual coccolith crystals. Note the rather uniform crystal size and shape with preservation of only a few recognizable nannofossil fragments. Such nearly complete disaggregation of nannofossil detritus was probably facilitated by repeated ingestion and excretion of these grains on the seafloor and in the water column.

SEM, HA = 34 μm

Lo. Cretaceous, Aptian, Shuaiba Fm., offshore Qatar

This sparsely fossiliferous micrite consists of a mix of nannoconids and other micritic material, including other finely comminuted skeletal particles. Some of those skeletal fragments are in the micrite- (clay)-size range, but others are silt-sized, a common feature in fragmental micrite.

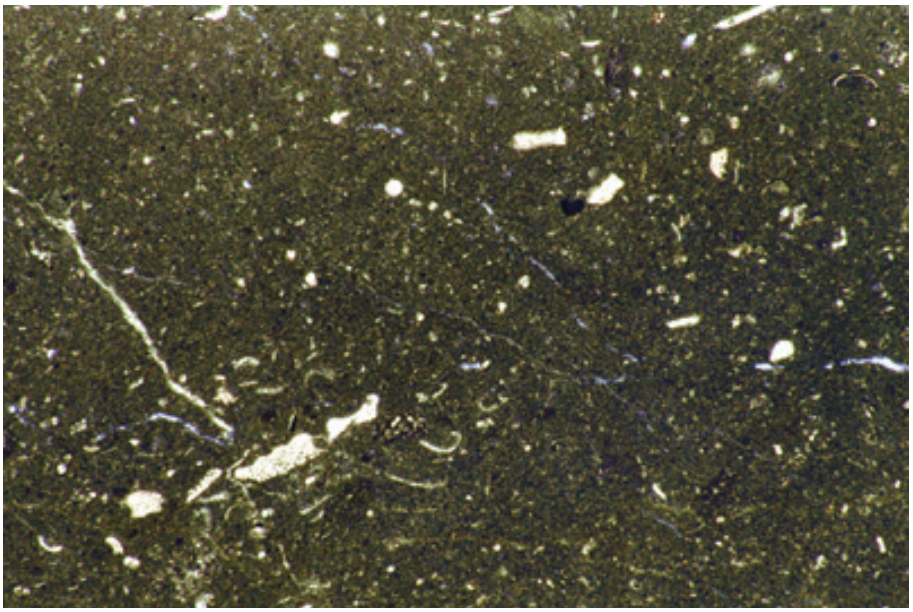

PPL, BSE, HA = 0.2 mm

Lo. Jurassic (mid. Liassic) limestone, Central High Atlas region, Morocco

This "clotted" fabric represents probable microbial crusts in a sponge reef. The darker-colored, slightly more peloidal, microbial material contrasts here with the lighter colored "true" micrite. In the absence of that color contrast, however, recognition that the major part of this microcrystalline carbonate was framework/cement rather than matrix would be difficult at best.

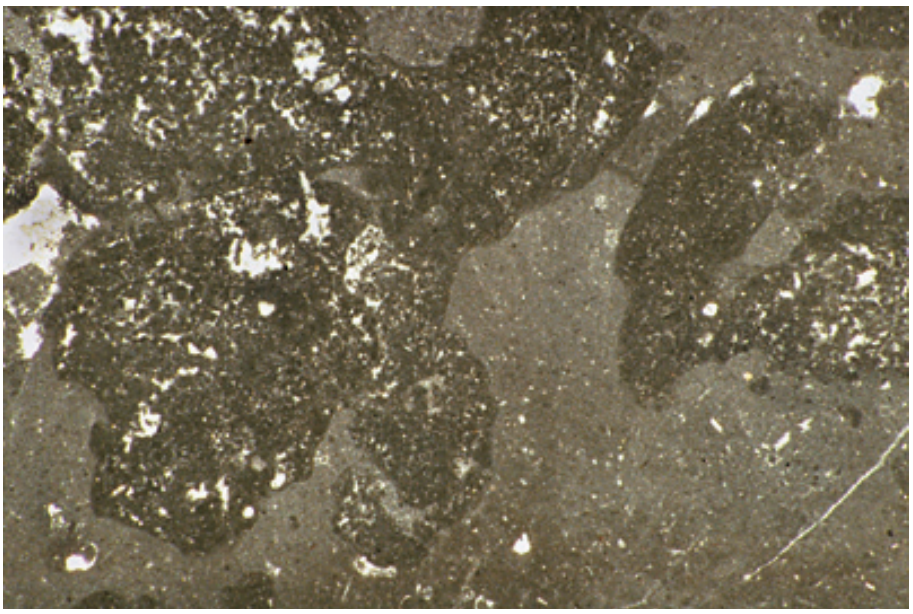

PPL, HA = 6.0 mm

Mid. Jurassic (Bajocian) limestone, Central High Atlas region, Morocco

This poorly-washed biosparite containing echinoid spines, corals, bivalves, and other grains also has patchy microcrystalline calcite matrix. Careful examination of the distribution and fabric of the "micrite", however, shows that it may not really be matrix. It bridges cavities in places, has no consistent geopetal relationships, has a clotted or peloidal texture, and is darker colored than the few patches of uniformly micritic sediment (within part of the coral skeleton, for example). Thus, much of this peloidal "matrix" represents microbially-induced precipitates and should be considered as framework or cement rather than matrix.

PPL, AFeS, HA = 14.5 mm

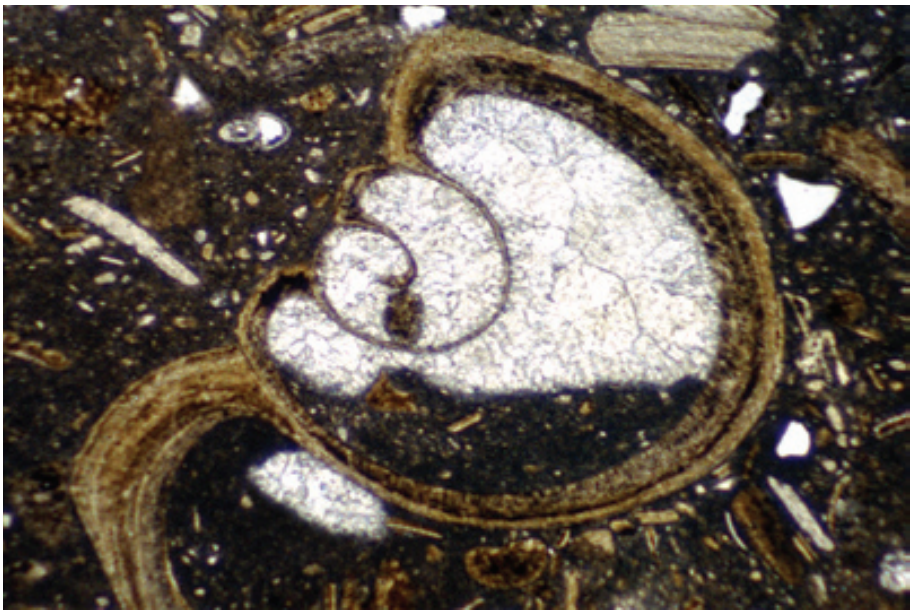

Plio-Pleistocene Caloosahatchee Fm., Hendry Co., Florida

This example of true micritic matrix shows a mix of various sizes of skeletal material (through sand and silt grades), and microcrystalline material both external to the grains and as a geopetal filling within a gastropod chamber. Carbonate mud (micrite) fills the lower part of the cavity while sparry calcite fills the upper part — the contact indicates an approximately level surface at the time of deposition. Such structures are very useful in determining original dip of strata and in confirming at least slight transport of matrix.

PPL, HA = 3.1 mm

Lo. Permian (Leonardian) Bone Spring Ls., Culberson Co., Texas

A rock with numerous umbrella voids (shelter pores) beneath bivalve shells. The geopetal matrix is substantially clotted or peloidal and, in some cases, does not show planar contacts between microcrystalline material and later spar. Is this true matrix? Or is this again microbial material — decomposed peloidal shrubs or peloidal cements? The answer will vary with the petrographer because there are no absolute criteria for the distinction of these fabrics in thin section. The answer is of importance though, for it changes the interpretations of depositional conditions for this rock.

PPL, BSE, HA = 12.5 mm

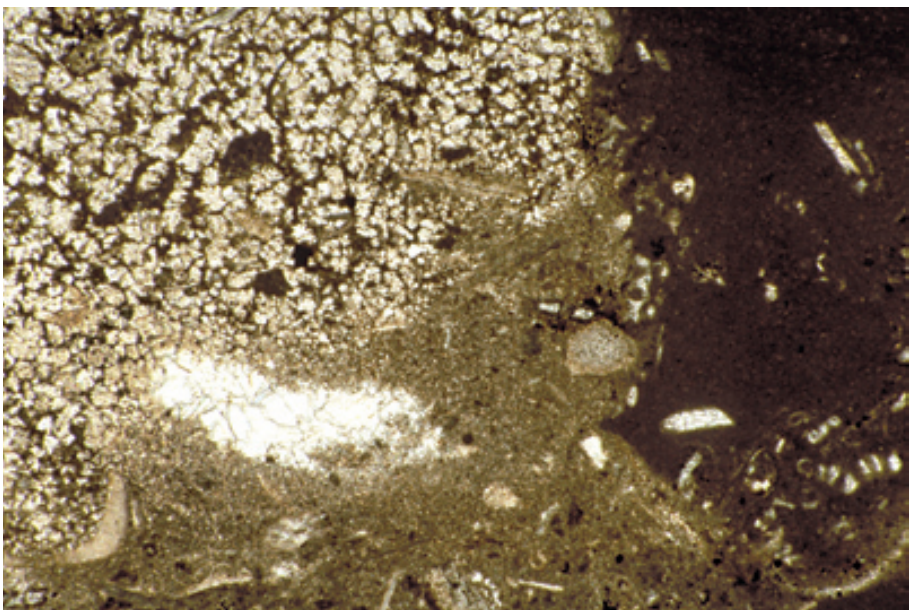

Mid. Ordovician Chazy-Black River Fms., Mifflin Co., Pennsylvania

Micritic materials can be formed within carbonate rocks (as shown in earlier slides), but they can also be destroyed or transformed. This example shows a transition from micrite (right) to microspar (lower center) to pseudospar (upper left). Note the bladed or "loaf-shaped" shape of the pseudospar crystals and the remnants of matrix between those crystals. The causes of microspar and pseudospar recrystallization are not well defined, but early meteoric exposure and tectonic stresses have been implicated in some cases.

PPL, HA = 5.2 mm

Up. Pennsylvanian (Virgilian) Holder Fm., Otero Co., New Mexico

A view of the transitions from micrite to microspar and pseudospar. Note the bladed shape of the pseudospar crystals and the remnants of original matrix between those crystals. This is an example of a unit that underwent early flushing by meteoric pore fluids (a possible cause of such alteration) as a result of large-scale, syndepositional, glacioeustatic sea-level fluctuations.

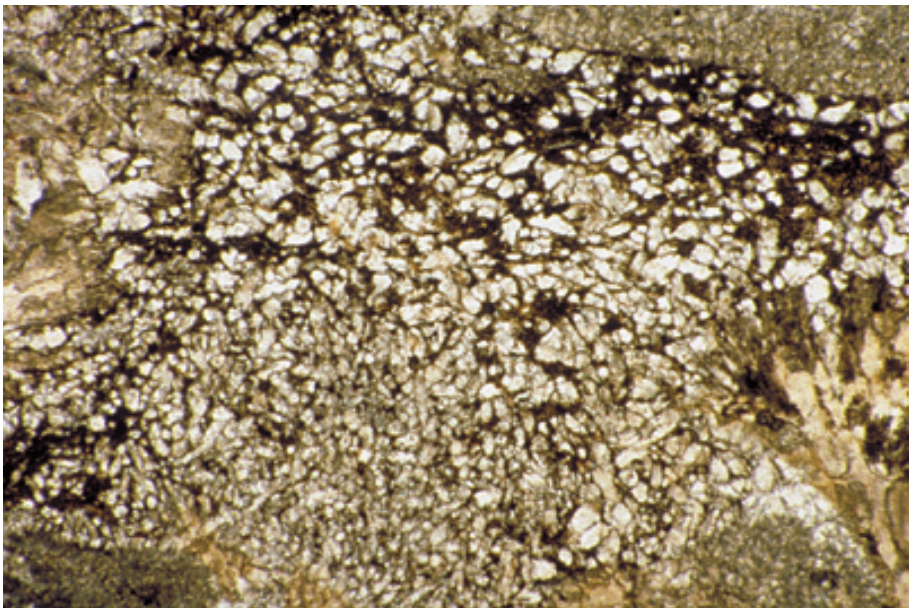

PPL, HA = 4.0 mm

Mid. Jurassic (Bajocian) limestone, Central High Atlas region, Morocco

A high-magnification view of adjacent areas of true precipitated spar (the clear, coarse spar) and microspar formed by neomorphism of micritic matrix. Note the darker color, the smaller crystal size, and the "loaf-like" shape of the microspar crystals.

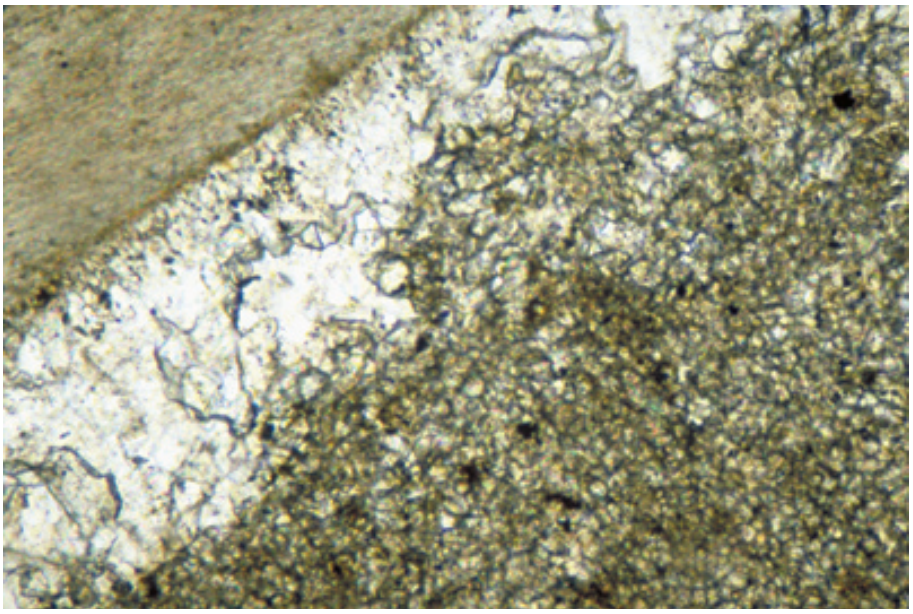

PPL, HA = 0.65 mm

Early Ordovician (Canadian) Arbuckle Gp., West Spring Creek Ls., Murray Co., Oklahoma

Micrite can also be destroyed through replacement by normal spar crystals, a process that generally is difficult to prove. Here replacive calcite spar has embayed the originally smooth margins of a reworked (and thus substantially lithified) micritic intraclast. In many other circumstances, where one cannot show that the micrite was lithified prior to growth of the spar, it is difficult or impossible to prove that the spar did not simply displace (rather than replace) the micrite or that micritic internal sediment was not deposited atop early spar.

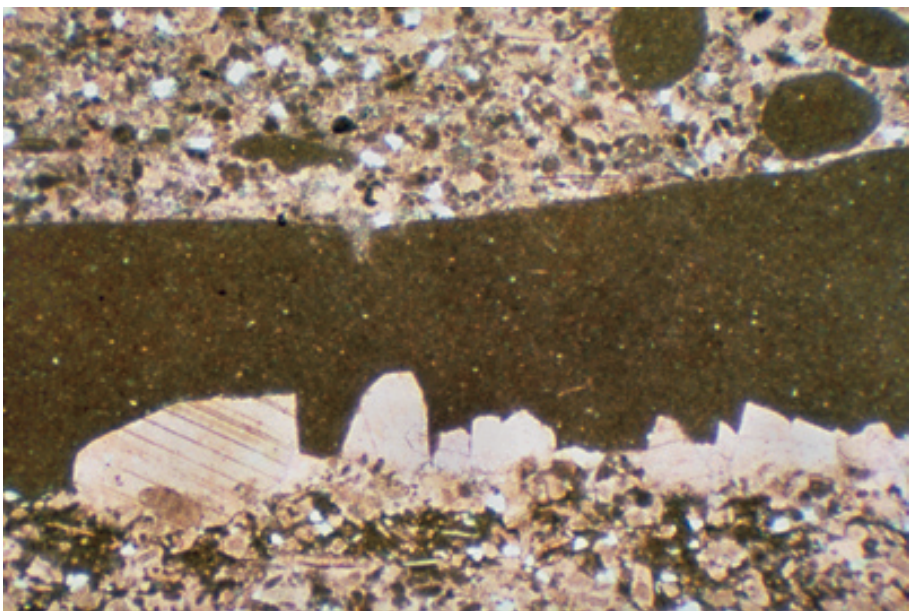

PPL, AFeS, HA = 4.1 mm

Cited References and Additional Information Sources

Andrews, J. E., S. Christidis, and P. F. Dennis, 1997, Assessing mineralogical and geochemical heterogeneity in the sub 63-micron size fraction of Holocene lime muds: Journal of Sedimentary Research, Section A: Sedimentary Petrology and Processes, v. 67, p. 531-535.

Blom, W. M., and D. B. Alsop, 1988, Carbonate mud sedimentation on a temperate shelf: Bass Basin, southeastern Australia: Sedimentary Geology, v. 60, p. 269-280.

Broecker, W. S., and T. Takahashi, 1966, Calcium carbonate precipitation on the Bahama Banks: Journal of Geophysical Research, v. 71, p. 1575-1602.

Debenay, J. P., J. P. Andre, and M. Lesourd, 1999, Production of lime mud by breakdown of foraminiferal tests: Marine Geology, v. 157, p. 159-170.

Drew, G. H., 1911, The action of some denitrifying bacteria in tropical and temperate seas, and the bacterial precipitation of calcium carbonate in the sea: Journal of the Marine Biological Association of the United Kingdom, v. 9, p. 142-155.

Drew, G. H., 1914, On the precipitation of calcium carbonate in the sea by marine bacteria and on the action of denitrifying bacteria in tropical and temperate seas: Carnegie Institute of Washington, Publication 182, Papers from the Tortugas Laboratory, v. 5, p. 7-45.

Ellis, J. P., and J. D. Milliman, 1985, Calcium carbonate suspended in Arabian Gulf and Red Sea waters: biogenic and detrital, not "chemogenic": Journal of Sedimentary Petrology, v. 55, p. 805-808.

Farrow, G. E., and J. A. Fyfe, 1988, Bioerosion and carbonate mud production on high-latitude shelves: Sedimentary Geology, v. 60, p. 281-297.

Flügel, E., H. E. Franz, and W. F. Ott, 1968, Review on electron microscope studies of limestones, *in* G. Müller, and G. M. Friedman, eds., Recent Developments in Carbonate Sedimentology in Central Europe: New York, Springer-Verlag, p. 85-97.

Folk, R. L., 1965, Some aspects of recrystallization in ancient limestones, *in* L. C. Pray, and R. S. Murray, eds., Dolomitization and Limestone Diagenesis: Tulsa, OK, SEPM Special Publication No. 13, p. 14-48.

Folk, R. L., 1971, Unusual neomorphism of micrite, *in* O. P. Bricker, ed., Carbonate Cements: Baltimore, MD, The Johns Hopkins Press, p. 163-166.

Friedman, G. M., 1985, The term micrite or micritic cement is a contradiction — discussion of micritic cement in microborings is not necessarily a shallow-water indicator: Journal of Sedimentary Petrology, v. 55, p. 777.

Fütterer, D. K., 1974, Significance of the boring sponge *Cliona* for the origin of fine grained material of carbonate sediments: Journal of Sedimentary Petrology, v. 44, p. 79-84.

Hay, W. W., S. W. Wise, Jr., and R. D. Stieglitz, 1970, Scanning electron microscope study of fine grain size biogenic carbonate particles: Transactions of the Gulf Coast Association of Geological Societies, v. 20, p. 287-302.

Honjo, S., 1970, Study of fine grained carbonate matrix: sedimentation and diagenesis of "micrite", *in* T. Matsumoto, ed., Litho- and Biofacies of Carbonate Sedimentary Rocks: Tokyo, Japan, Paleontological Society of Japan Special Paper 14, p. 67-82.

Land, L. S., 1970, Carbonate mud: production by epibiont growth on *Thalassia testudinum*: Journal of Sedimentary Petrology, v. 40, p. 1361-1363.

Lasemi, Z., and P. A. Sandberg, 1984, Transformation of aragonite-dominated lime muds to microcrystalline limestones: Geology, v. 12, p. 420-423.

Lasemi, Z., and P. A. Sandberg, 1993, Microfabric and compositional clues to dominant mud mineralogy of micrite precursors, *in* R. Rezak, and D. L. Lavoie, eds., Carbonate Microfabrics: New York, Springer-Verlag, p. 173-185.

Lloyd, R. M., 1971, Some observations on recent sediment alteration ("micritization") and the possible role of algae in submarine cementation, *in* O. P. Bricker, ed., Carbonate Cements: Baltimore, MD, The Johns Hopkins Press, p. 72-79.

Macintyre, I. G., 1985, Submarine cements — the peloidal question, *in* N. Schneidermann, and P. M. Harris, eds., Carbonate Cements: Tulsa, OK, SEPM Special Publication No. 36, p. 109-116.

Matthews, R. K., 1966, Genesis of Recent lime mud in southern British Honduras: Journal of Sedimentary Petrology, v. 36, p. 428-454.

Maurin, A. F., and D. Noël, 1977, A possible bacterial origin for Famennian micrites, *in* E. Flügel, ed., Fossil Algae: Recent Results and Developments: New York, Springer-Verlag, p. 136-142.

Munnecke, A., H. Westphal, J. J. G. Reijmer, and C. Samtleben, 1997, Microspar development during early marine burial diagenesis: a comparison of Pliocene carbonates from the Bahamas with Silurian limestones from Gotland (Sweden): Sedimentology, v. 44, p. 977-990.

Mutti, M., 2000, Microbial origin of microcrystalline carbonate sediment and cements filling fractures in basalts recovered at Site 1001, Caribbean Sea: Proceedings of the Ocean Drilling Program, v. 165, p. 227-232.

Neuweiler, F., P. Gautret, V. Thiel, R. Lange, W. Michaelis, and J. Reitner, 1999, Petrology of Lower Cretaceous carbonate mud mounds (Albian, N. Spain): insights into organomineralic deposits of the geological record: Sedimentology, v. 46, p. 837-860.

Patriquin, D. G., 1972, Carbonate mud production by epibionts on *Thalassia*: an estimate based on leaf growth rate data: Journal of Sedimentary Petrology, v. 42, p. 687-689.

Reid, R. P., I. G. Macintyre, and N. P. James, 1990, Internal precipitation of microcrystalline carbonate: a fundamental problem for sedimentologists: Sedimentary Geology, v. 68, p. 163-170.

Reitner, J., F. Neuweiler, and P. Gautret, 1995, Modern and fossil automicrites: implications for mud mound genesis, *in* J. Reitner, and F. Neuweiler, eds., Mud Mounds: a Polygenic Spectrum of Fine-Grained Carbonate Buildups, v. 32, Facies, p. 1-70.

Riding, R., 2000, Microbial carbonates: the geological record of calcified bacterial-algal mats and biofilms: Sedimentology, v. 47, p. 179-214.

Sandberg, P. A., 1983, An oscillating trend in Phanerozoic non-skeletal carbonate mineralogy: Nature, v. 305, p. 19-22.

Scoffin, T. P., 1993, Microfabrics of carbonate muds in reefs, *in* R. Rezak, and D. L. Lavoie, eds., Carbonate Microfabrics: New York, Springer-Verlag, p. 65-74.

Shinn, E. A., R. P. Steinen, B. H. Lidz, and P. K. Swart, 1989, Whitings, a sedimentologic dilemma: Journal of Sedimentary Petrology, v. 59, p. 147-161.

Stieglitz, R. D., 1972, Scanning electron microscopy of the fine fraction of Recent carbonate sediments from Bimini, Bahamas: Journal of Sedimentary Petrology, v. 42, p. 211-226.

Stieglitz, R. D., 1973, Carbonate needles: additional organic sources: Geological Society of America Bulletin, v. 84, p. 927-930.

Stockman, K. W., R. N. Ginsburg, and E. A. Shinn, 1967, The production of lime mud by algae in south Florida: Journal of Sedimentary Petrology, v. 37, p. 633-648.

Tsien, H. H., 1985, Algal-bacterial origin of micrites in mud mounds, *in* D. F. Toomey, and M. H. Nitecki, eds., Paleoalgology: Contemporary Research and Applications: New York, Springer-Verlag, p. 290-296.

Wefer, G., L. Böhm, R. Dawson, G. Liebezeit, and M. Meyer, 1980, Carbonate production by algae *Halimeda*, *Penicillus* and *Padina*: Nature, v. 285, p. 323-324.

Wolf, K. H., 1965, Grain-diminution of algal colonies to micrite: Journal of Sedimentary Petrology, v. 35, p. 420-427.

Facing Page: Broken modern coral block infested with several species of boring clionid sponges (red and orange colors). These sponges bore living chambers into their rock or coral substrate, by etching out small rock fragments using acid-tipped pseudopods. Block about 10 cm long. Photograph courtesy of Clyde H. Moore.

PRIMARY SEDIMENTARY STRUCTURES

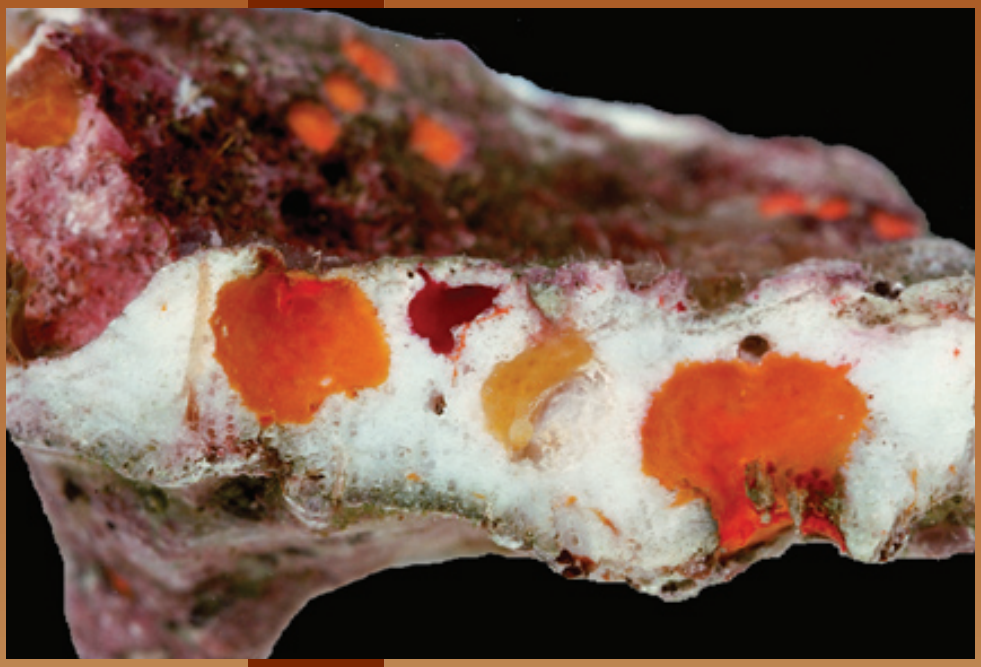

CHAPTER 19

Burrows

Borings

Geopetal fabrics

Fenestral fabrics

Lamination

PRIMARY SEDIMENTARY STRUCTURES

Introduction:

Primary sedimentary structures are physical and/or biological features formed during the process of sediment deposition. Generally such structures are best seen in outcrop, core, or polished hand sample, but smaller features such as borings or fenestral fabrics are both readily apparent in thin section and important to recognize. Their identification can improve interpretations of depositional environments and can also help to decipher patterns and timing of diagenesis. The characteristic features for the recognition and interpretation of primary sedimentary structures are provided in the figure captions. Diagenetic sedimentary structures, such as hardgrounds, soil crusts, or stylolites, are covered in the appropriate diagenetic chapters.

Definitions:

Borings - Openings created in relatively rigid rock, shell, or other material by boring organisms. The rigid host substrate is the feature that distinguishes borings from soft-sediment burrows.

Burrow porosity - Feature created by organic burrowing in relatively unconsolidated sediment, in contrast to borings. Most burrows collapse, become filled with sediment, or are back-filled by the burrow-forming organism itself.

Fenestrae (fenestral fabric) - Primary or penecontemporaneous gaps in rock framework larger than grain-supported interstices. Such features may be open pores or may have been partially or completely filled with internal sediment and/or sparry cement. Fenestrae occur as somewhat rounded features of spherical, lenticular, or more irregular shapes; their large size in comparison to normal interparticle openings and their multigranular roofs, floors, and other margins are key characteristics. Fenestrae are commonly somewhat flattened parallel with the laminae. They may, however, be round or very irregular, and some are elongate in a vertical dimension. Although isolated fenestrae occur in sedimentary carbonates, it is more common to find many in close association. Fenestrae are generally associated with microbial mats and result from shrinkage, gas formation, organic decay, trapping of air through swash-zone wave action, or other synsedimentary processes (Choquette & Pray, 1970).

Geopetal structure - Any internal structure or organization of a rock indicating original orientation such as top and bottom of strata. Common examples are internal sediment accumulating on the floor of a cavity which it partly fills, or solution-collapse residue that has fallen to the bottom of a vug or cave.

Stromatactis - A cavity structure common in muddy carbonate sediments, typically 3 to 10 cm in diameter, characterized by a flat floor and an irregular roof. The floor of this former cavity typically is overlain by peloidal internal sediment; the remaining void is filled with marine cement or later sparry cement. These poorly understood vugs have been attributed to the decay of unknown soft-bodied organisms, to gas formation in impermeable sediments, to gravity sliding and shear, to the alteration of sponges and sponge holdfasts, and to several other causes.

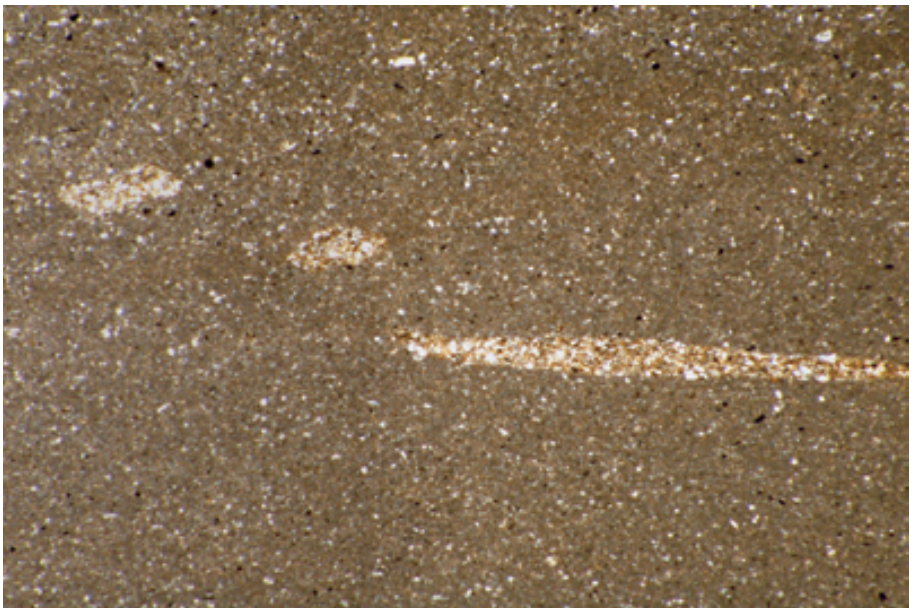

Up. Cretaceous (Campanian-Maastrichtian) Monte Antola Fm., Liguria, Italy

Small, partially flattened burrows at the upper contact of a deep-marine carbonate turbidite. Burrows are recognizable in many instances because of the textural contrast between the burrow fill and surrounding sediment. Organisms sometimes backfill their burrows with sediment or sediment infiltrates downward into open burrows. Lenticular-shaped burrows are common in muddy carbonate units that did not undergo early marine or subaerial lithification.

PPL, HA = 3.6 mm

Lo. Cretaceous (Aptian) Shuaiba Fm., offshore Qatar

This burrow is recognizable not because of a substantial difference in composition between it and the surrounding sediment, but because the burrow fill has a higher porosity than the otherwise comparable surrounding material (shown by the more bluish color caused by more epoxy-filled pores). The porosity variation may be a function of differential packing, but more likely relates to differing diagenesis inside and outside the burrow. Note also the diagenetic pyrite core to the burrow, a fairly common feature in burrows in fine-grained carbonate strata.

PPL, BSE, HA = 4.0 mm

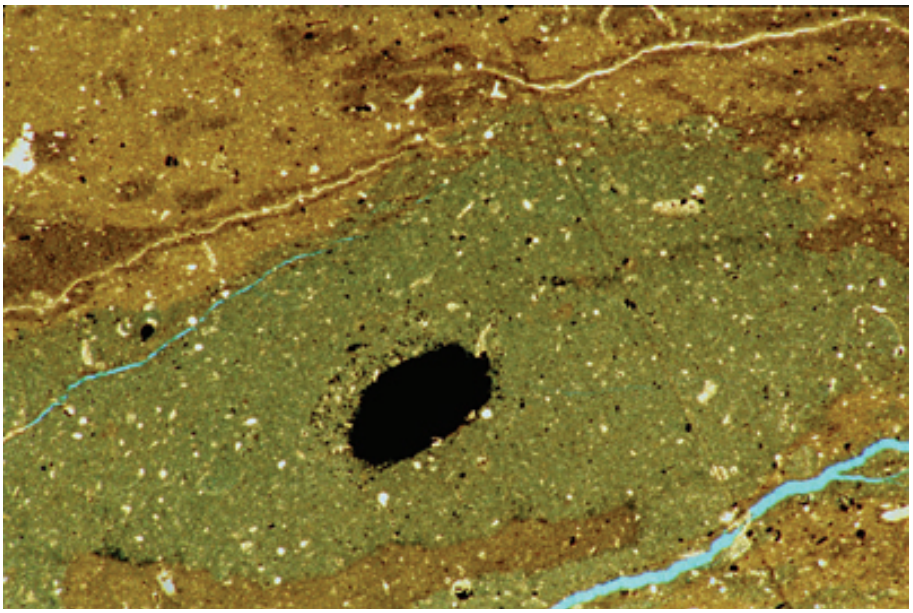

Lo. Cretaceous (Aptian) Shuaiba Fm., offshore Qatar

Although many burrows are backfilled by organisms or are filled by sediment infiltration, other burrows remain open and undeformed, especially in firm substrates. This tangential cut through a sinuous burrow shows a structure that remained open until filled with pyrite and sparry calcite cement. Open burrows or loosely packed burrows can act as significant conduits for diagenetic fluid flow.

XPL, BSE, HA = 8.0 mm

Lo. Ordovician St. George Gp., western Newfoundland, Canada

Partially dolomitized strata commonly show burrow-associated patterns of selective replacement (sometimes with preferential dolomitization of burrows; sometimes with selective replacement of unburrowed host rock). This example shows dolomitized burrow fills, undolomitized host rock, and microspar rims around burrow walls. Selectively dolomitized, burrow mottled carbonate rocks are common in Ordovician strata throughout North America. Photograph courtesy of Noel P. James.

PPL, AFeS, HA = 10 mm

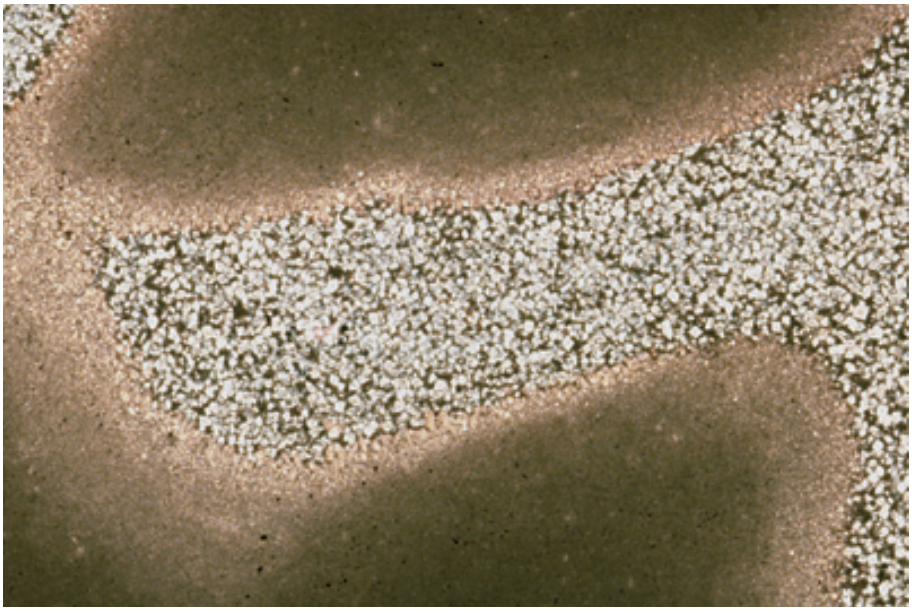

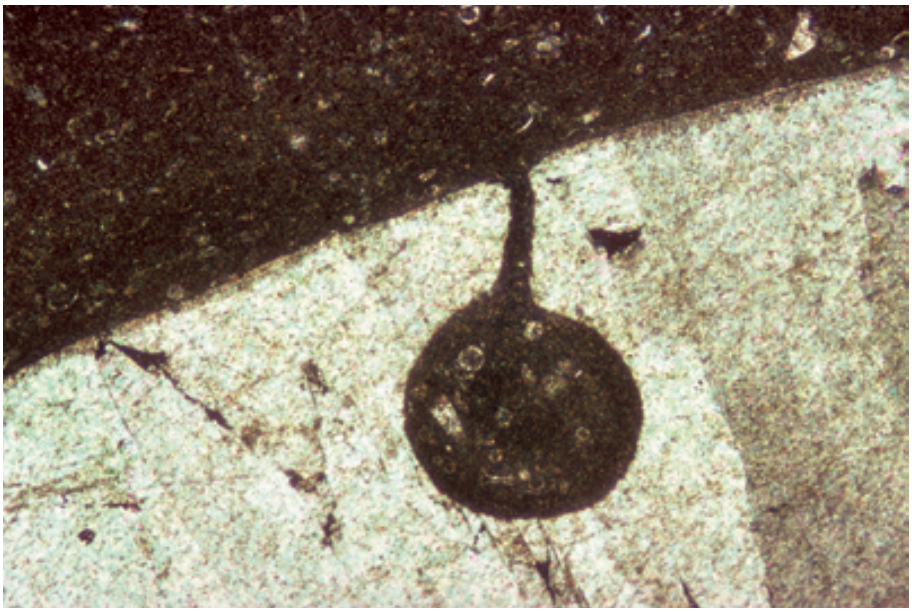

Up. Cretaceous White Ls., Co. Antrim, Northern Ireland

Many different organisms can bore into hard substrates (rasping, dissolving, or chipping their way into hardgrounds, shells, or other lithified materials). In this example, a massive calcite belemnite rostrum was penetrated by a sponge boring (see photograph of modern boring sponges on title page of this section). This is identifiable as a sponge boring because of the large, excavated living chamber and the narrow connecting tube to the grain surface.

XPL, HA = ~2.0 mm

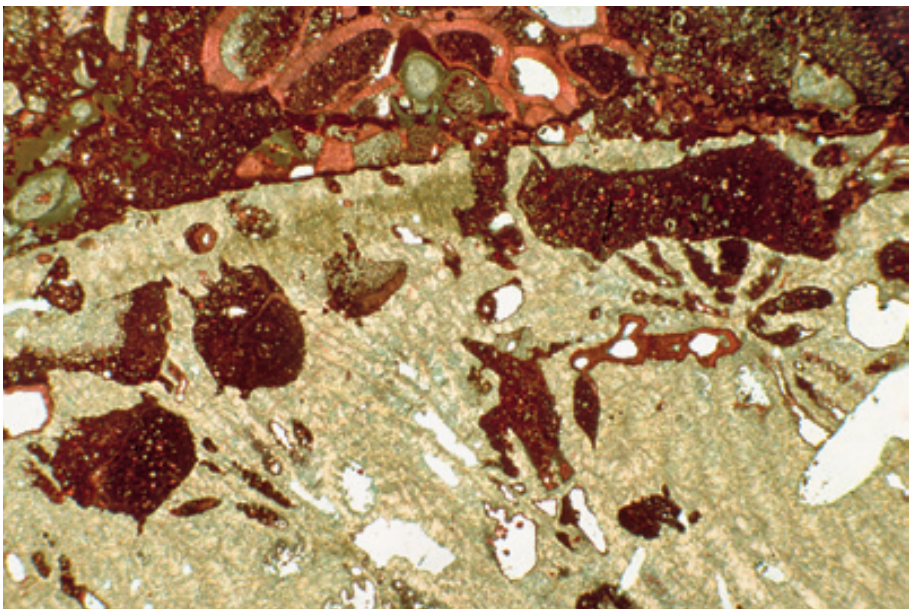

Recent sediment, Belize

This section shows the top of a coral that has been bored by the sponge *Cliona*. The excavated cavities (and their small connecting tubes) were subsequently filled with cemented fine-grained carbonate sediment. The grains are cemented by Mg-calcite (shown by the red staining). Clionids and other boring sponges are major weakeners or destroyers of reef framework; at the same time, they are substantial producers of silt-sized carbonate sediment created during the excavation process (see subsequent images). Photograph courtesy of Noel P. James.

PPL, CYS, HA = 10 mm

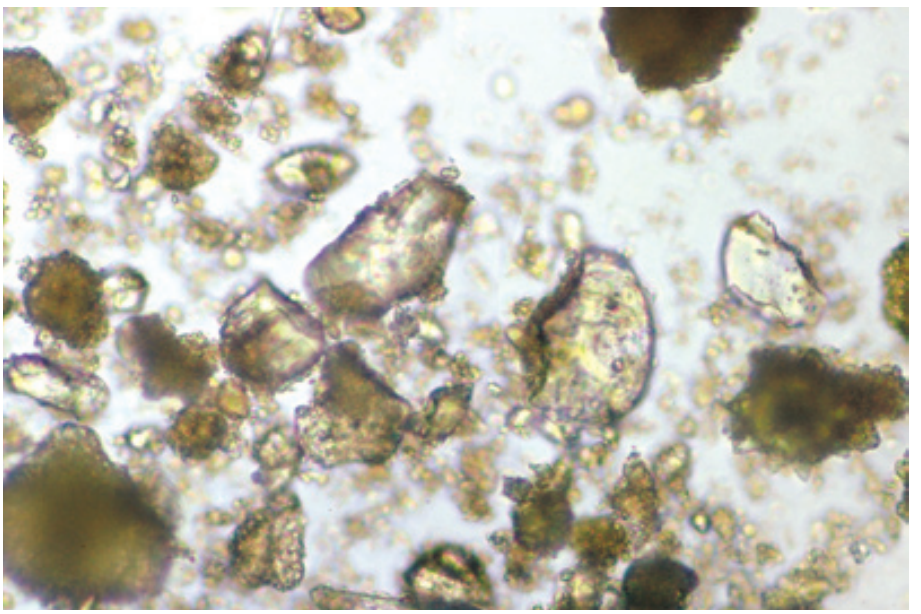

Recent sediment, St. Croix, U.S. Virgin Islands

Clionid sponges bore living chambers into their rock or coral substrate by etching out small rock fragments using acid-tipped pseudopods. They thereby create large, protected cavities within the rock in which they reside. These are silt-sized clionid-produced carbonate chips taken from suspended sediment at 55-m (180-ft) depth on a fore-reef slope. Photograph courtesy of Clyde H. Moore.

PPL, HA = ~0.35 mm

Recent sediment, St. Croix, U.S. Virgin Islands

This SEM image shows the characteristic scalloped shape of a clionid sponge boring chip. The composition, and thus the preservability, of these distinctive grains, depends on the composition of the substrate being bored. Photograph courtesy of Clyde H. Moore.

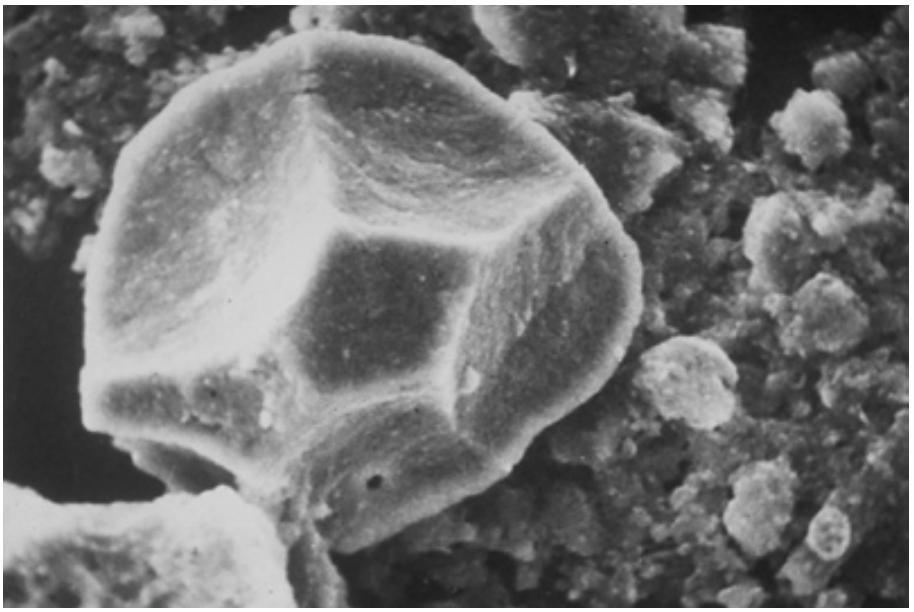

SEM, HA = 95 μm

Recent sediment, Joulters Cay, Bahamas

Although sponges produce large and distinctive borings, many other boring organisms also infest hard substrates. This modern ooid, for example, has undergone considerable algal and fungal boring. Most of the borings are still unfilled, showing their tubular shape, but some were filled with Mg-calcite cement and thus appear as diffuse micritic patches. The algal borings are the large tubular openings; the fungal boring appear as long, thin, straight, dark-colored lines.

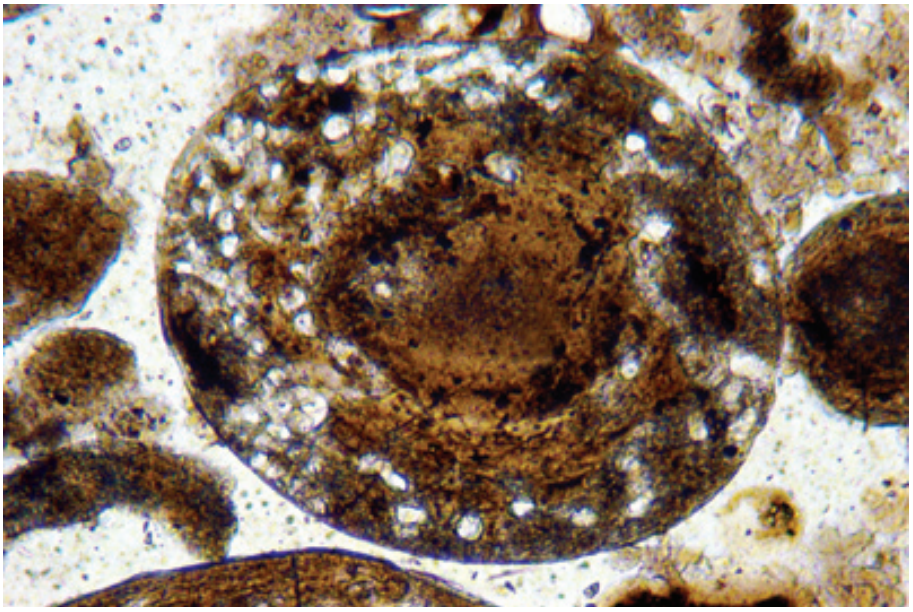

PPL, HA = 0.45 mm

Recent sediment, Bimini Lagoon, Bahamas

A strongly bored mollusk fragment. Numerous small, dark algal and fungal tubes have cut the crossed-lamellar structure of this grain. Recognition of algal borings is important in that it is evidence that the grain was derived from the photic zone. The borings (or portions of borings) of clionid sponges, acrothoracian barnacles, and ctenostome bryozoans could all be mistaken for algal borings unless carefully examined.

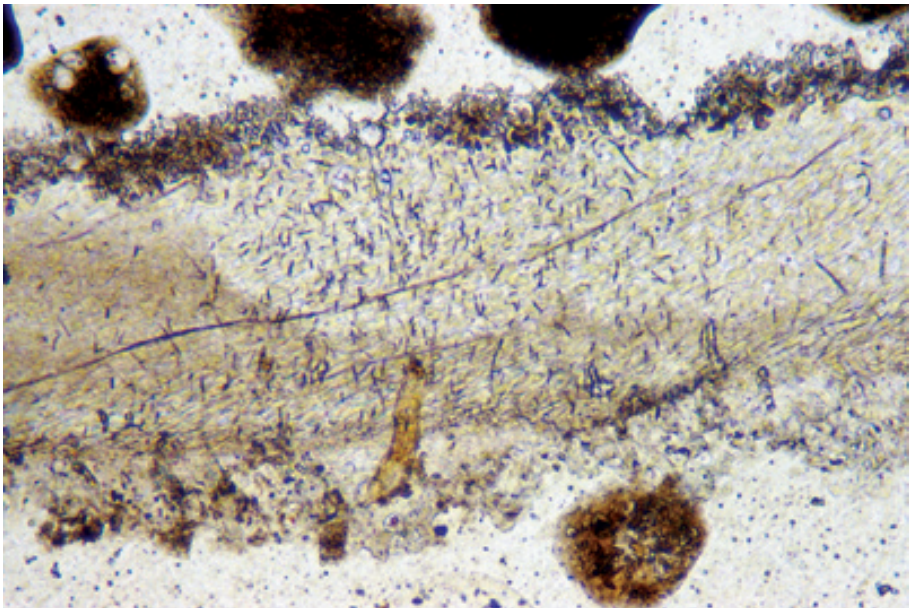

PPL, HA = 0.8 mm

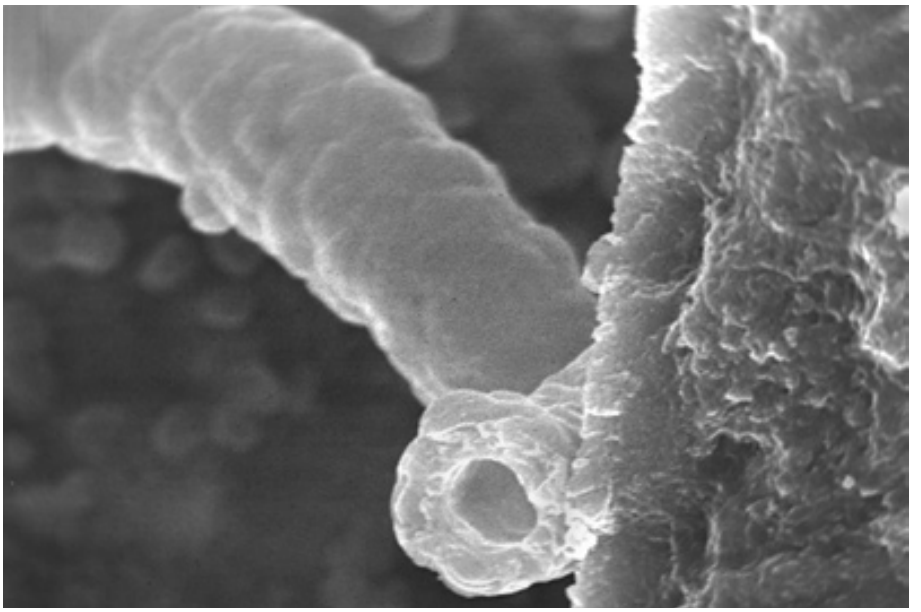

Recent sediment, Belize

An SEM image of an algal tubule within a coral skeleton. Algal photosynthetic activities can lead to the precipitation of a sheath of carbonate (generally aragonite or high-Mg calcite) around the filaments; these are common in SEM views of modern sediments. Again, recognition of algal tubules allows determination of a depositional environment within the photic zone. Algal tubules can be free-standing, but the dissolution of aragonitic grains also can expose Mg-calcite-filled tubules that formed as endolithic borings.

SEM, HA = 37 μm

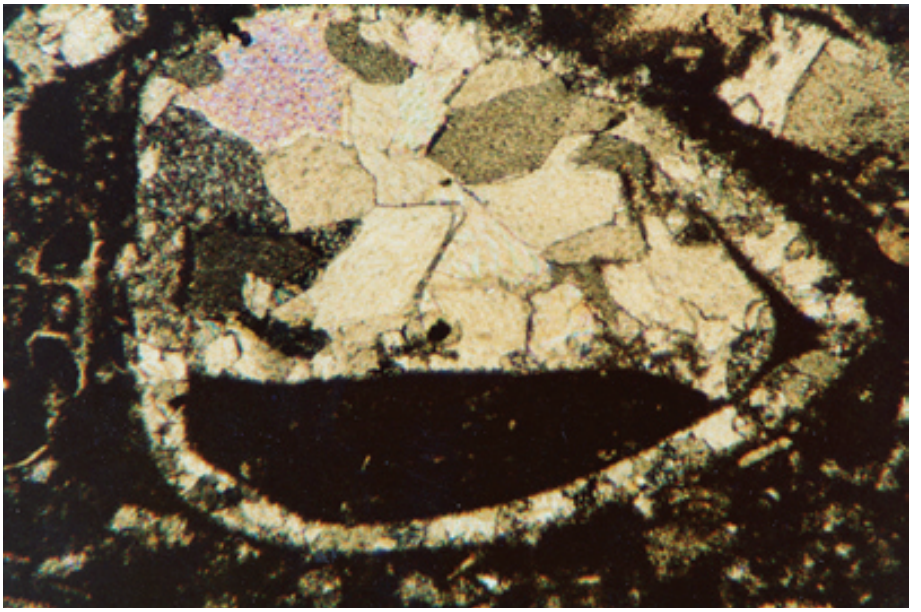

Late Mississippian Hindsville Ls. Mayes Co., Oklahoma,

Geopetal structures are indicators of original horizontal surfaces in sedimentary rocks. Partial mud fills within the protected chambers of organisms, such as this sediment infill of a bivalve shell, are especially reliable geopetal structures. Note the alteration of the shell wall without the downward displacement of the sediment filling. This may indicate inversion rather than complete dissolution and subsequent void fill. Not all geopetal fills are precisely horizontal, so a statistical sampling should be used. When properly applied, studies of geopetal features can aid in determining pre-tectonic depositional slopes.

XPL, HA = 1.6 mm

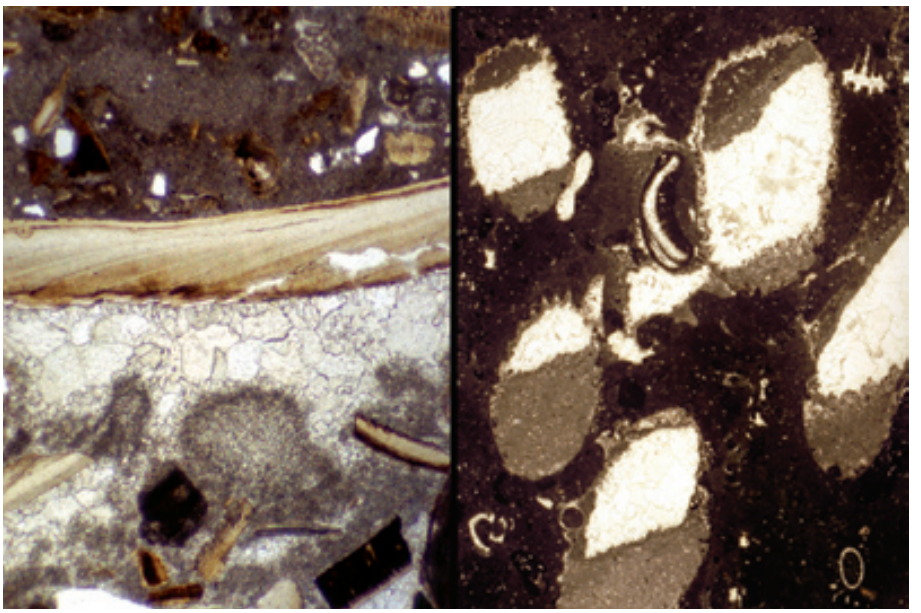

Plio-Pleistocene Caloosahatchee Fm., Hendry Co., Florida (left)

A geopetal "umbrella" void formed where a large bivalve fragment prevented infiltration of micrite and maintained an open cavity filled by later bladed and equant spar.

PPL, HA = 2.25 mm

Lo. Jurassic, Central High Atlas region, Morocco (right)

Two generations of geopetal micrite fillings within some, but not all, of the leached scleractinian corallites from a slope limestone. This presumably reflects penecontemporaneous erosion and rotation of a reef talus block with repeated infill and lithification of matrix.

PPL, HA = 10.7 mm

Lo. Permian (up. Leonardian) Bone Spring Ls., Culberson Co., Texas

Umbrella void in a bivalve limestone. The peloidal nature of the fill, the presence of some microcrystalline material on the roof of the cavities, and the irregular tops of the cavity sediment fills all indicate that these may be, at least in part, microbial precipitates rather than purely mechanically transported matrix fills. This can give misleading results if not properly evaluated. Two generations of calcite cement, one cloudy and one clear, filled the remaining geopetal pore space.

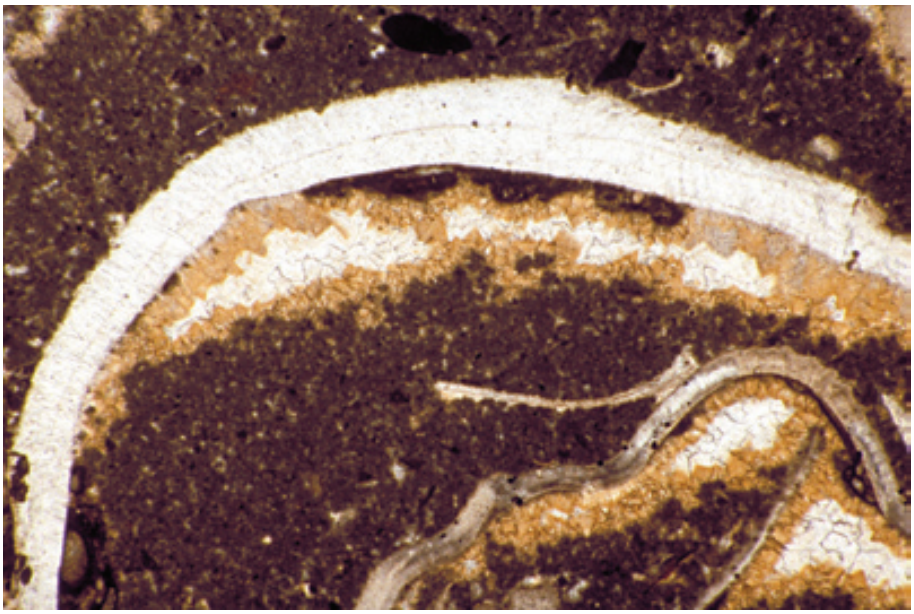

PPL, HA = 4.5 mm

Up. Permian (Guadalupian) Yates Fm., subsurface well, Eddy Co., New Mexico

Fenestral fabrics generally consist of a series of regular (lamination-parallel) or irregular cavities (vugs) that are larger than the grains that constitute the sediment. In this example, elongate anhydrite-filled pores parallel the laminae in a stromatolitic dolomite. The allochems trapped within this stromatolite are mainly pellets (peloids) or small pisoids. Fenestral fabrics are of particular importance to sedimentologists because they commonly denote peritidal deposition — sedimentation essentially at sea level.

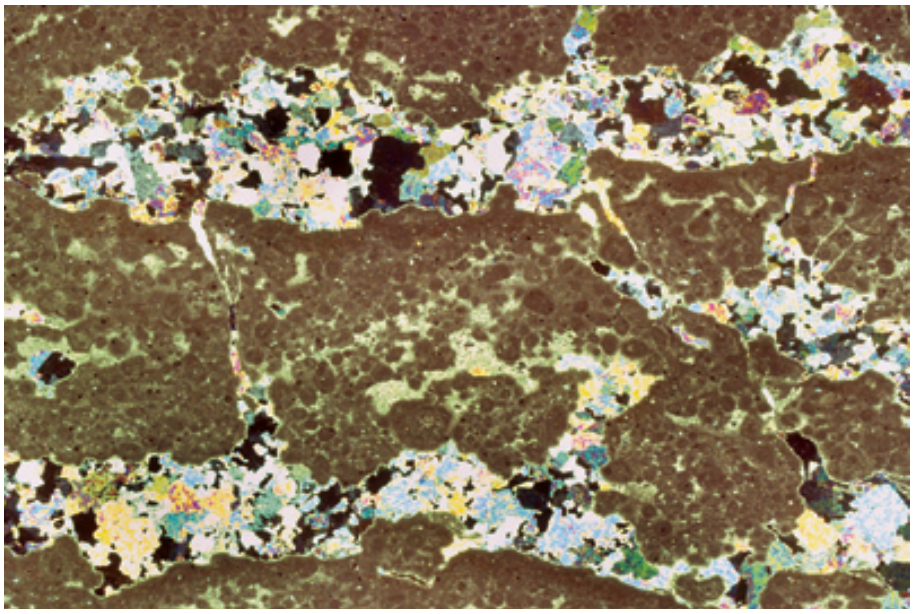

XPL, HA = 16 mm

Up. Permian (Guadalupian) Park City Fm., Ervay Mbr., Big Horn Co., Wyoming

An example of somewhat more irregular fenestrae that still maintain a preferred, lamination-parallel orientation. These fenestrae are filled with blocky calcite and dolomite cements that completely occluded porosity in this peloidal and pisolitic peritidal deposit.

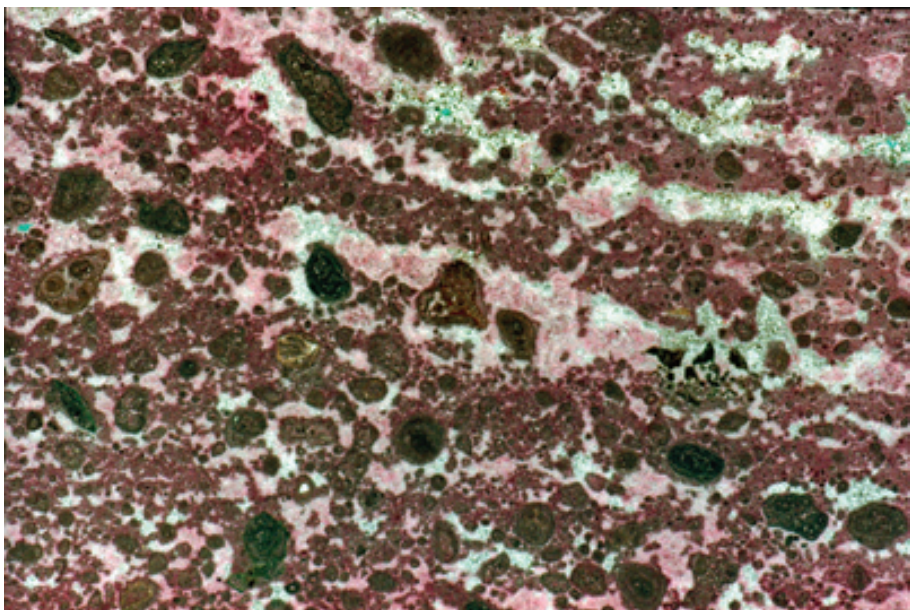

PPL, AFeS, HA = 0.8 mm

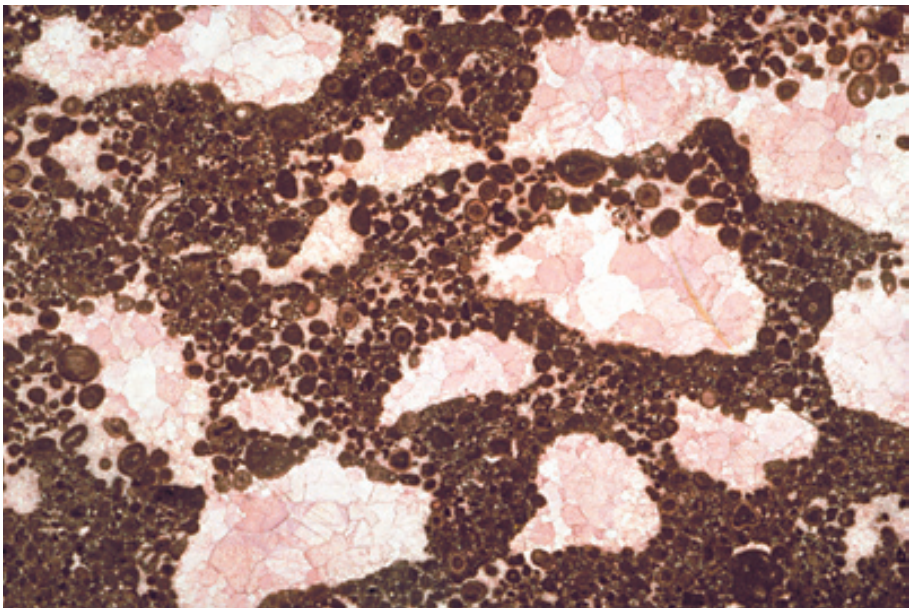

Up. Devonian (Frasnian) Pillara Ls., Canning Basin, Western Australia

Fenestral fabric with very irregular fenestrae in a relatively coarse-grained rock — an oolitic limestone. Fenestral fabric may result from gas bubbles, grain bridging ("keystone vugs"), bioturbation, decomposition of organic material and other causes; all of these are processes commonly (but not exclusively) associated with peritidal sediments.

PPL, AFeS, HA = 16 mm

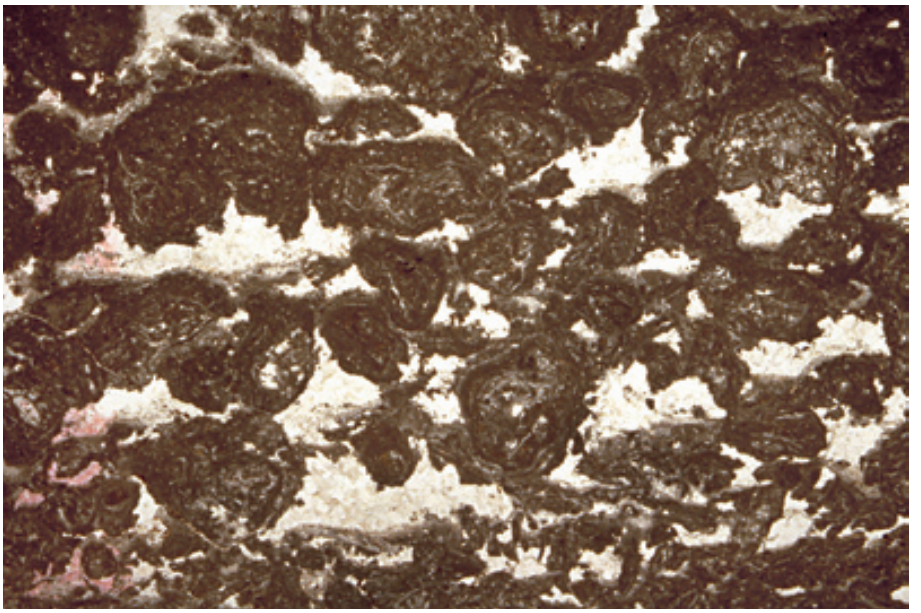

Up. Permian (Guadalupian) Tansill Fm., Eddy Co., New Mexico

Fenestral fabrics often also have included geopetal fabrics. These irregular fenestrae in a pisolitic dolostone have "internal sediment" floors with relatively level tops that are overlain by blocky calcite cements.

PPL, AFeS (at left only), HA = 25 mm

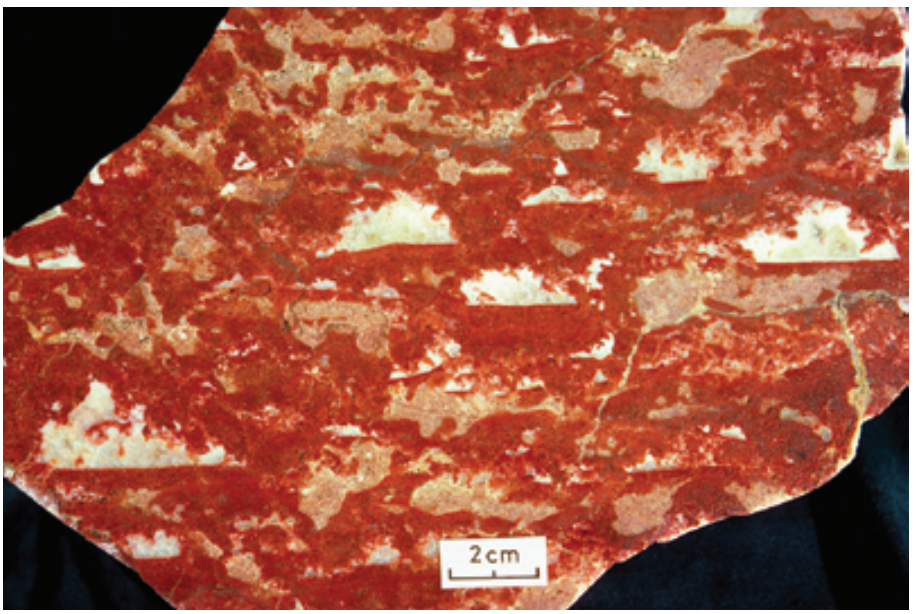

Up. Devonian (Famennian) Napier Fm., Canning Basin, Western Australia

A slope-facies "stromatactis" limestone. Stromatactis cavities, like many other fenestral cavities, are vugs that are larger than surrounding grains. They have flat floors (generally covered with internal sediment) and irregular cavity tops. These particular stromatactis cavities are believed to have formed through the decay of sponges. Photograph courtesy of Phillip E. Playford.

Mac, HA = 20.5 cm

Carboniferous (Waulsortian, phase "A") limestone, Dinant, Belgium

A reticulate biomicrite framework with "stromatactis" cavities floored with geopetal internal sediment. The cavity tops are irregular and the majority of the cavity is filled with fibrous to bladed, marine or later calcite cements. Stromatactis has been attributed to the decay of various soft-bodied organisms, to gas formation in impermeable sediments, to gravity sliding and shear, to the alteration of sponges and sponge holdfasts, and to other causes. Photograph courtesy of Brian R. Pratt.

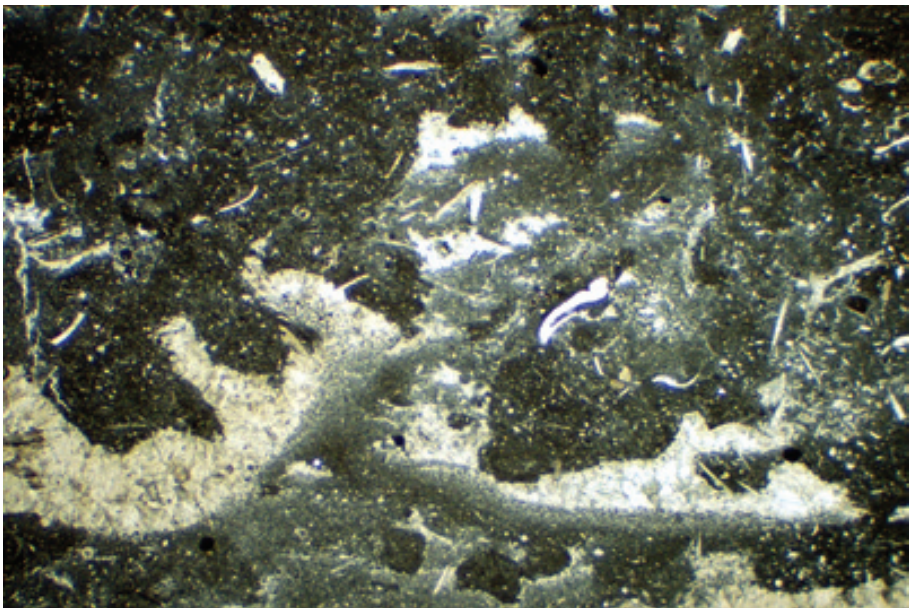

PPL, HA = 3.5 mm

Up. Permian (Kazanian?) Zechstein Ca2, Poznan area, Poland

An example of a finely-laminated, shaly carbonate from a small, but deep, basin setting surrounded by continental shelves and land masses. As this sediment predates the advent of most calcareous pelagic microorganisms, the carbonate must represent either direct precipitation from seawater or the reworking of carbonate muds from shelf areas into the basin.

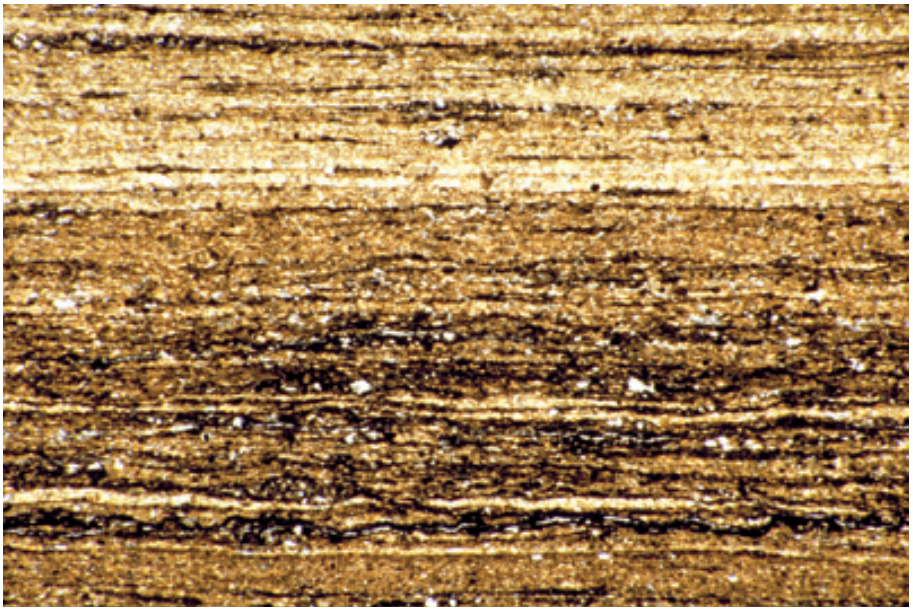

PPL, HA = 4.5 mm

Mid. Ordovician dolostone, Ontario, Canada

Traces of lamination can remain visible in thin section even after substantial diagenesis, largely because compositional and grain-size differences between adjacent laminae may control the nature and intensity of diagenetic alteration. Here original lamination is preserved in a synsedimentary, finely-crystalline dolomite. Sample from Noel P. James.

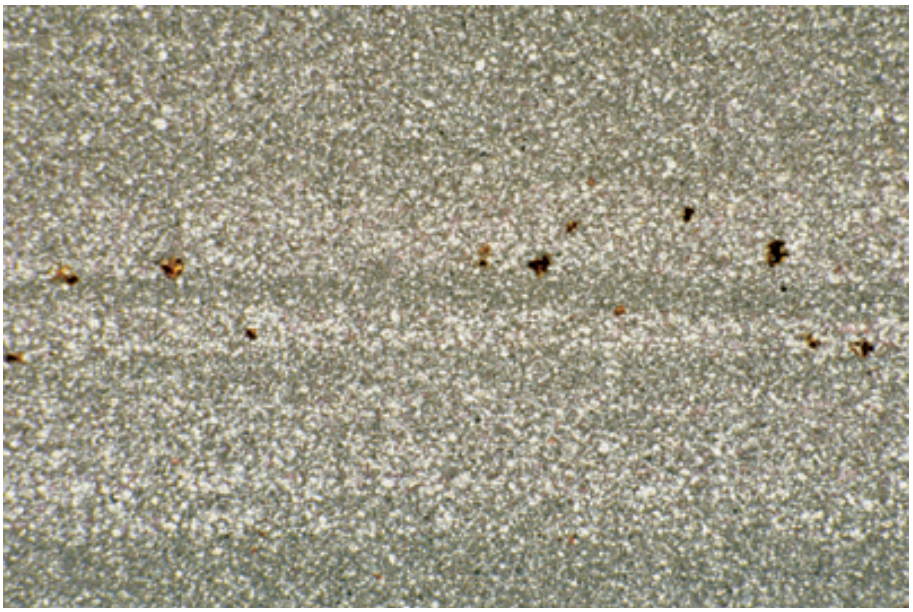

PPL, AS, HA = 3.0 mm

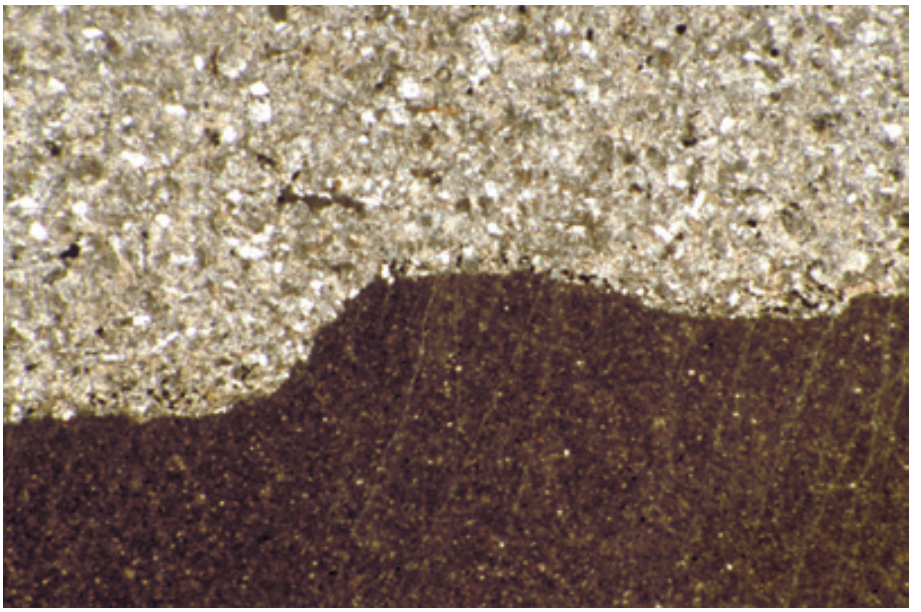

Up. Cretaceous (Campanian-Maastrichtian) Monte Antola Fm., Liguria, Italy

Other types of internal sedimentary interfaces can sometimes be seen in thin section, although they are generally better seen in hand specimen or outcrop. This sharp and irregularly eroded surface represents the contact between a fine-grained pelagic carbonate and an overlying sandy carbonate turbidite in abyssal water depths.

PPL, HA = 3.6 mm

Cited References and Additional Information Sources

Bathurst, R. G. C., 1959, The cavernous structure of some Mississippian Stromatactis reefs in Lancashire, England: Journal of Geology, v. 67, p. 506-521.

Bathurst, R. G. C., 1966, Boring algae, micrite envelopes and lithification of molluscan biosparites: Geological Journal, v. 5, p. 15-32.

Bathurst, R. G. C., 1982, Genesis of stromatactis cavities between submarine crusts in Paleozoic carbonate mud buildups: Journal of the Geological Society of London, v. 139, p. 165-181.

Bourque, P.-A., and H. Gignac, 1983, Sponge-constructed stromatactis mud mounds, Silurian of Gaspé, Québec: Journal of Sedimentary Petrology, v. 53, p. 521-532.

Boyd, D. W., 1975, Fenestral fabric in Permian carbonates of the Bighorn Basin, Wyoming, *in* F. A. Exum, and G. R. George, eds., Geology and Mineral Resources of the Bighorn Basin: 27th Annual Field Conference Guidebook: Casper, WY, Wyoming Geological Association, p. 101-106.

Choquette, P. W., and L. C. Pray, 1970, Geologic nomenclature and classification of porosity in sedimentary carbonates: American Association of Petroleum Geologists Bulletin, v. 54, p. 207-250.

Dunham, R. J., 1970, Keystone vugs in carbonate beach deposits [abs.]: American Association of Petroleum Geologists Bulletin, v. 54, p. 845.

Ekdale, A. A., R. G. Bromley, and S. G. Pemberton, 1984, Ichnology: Trace Fossils in Sedimentology and Stratigraphy: Tulsa, OK, SEPM Short Course No. 15, 316 p.

Golubic, S., R. D. Perkins, and K. J. Lukas, 1975, Boring microorganisms and microborings in carbonate substrates, *in* R. W. Frey, ed., The Study of Trace Fossils: New York, Springer-Verlag, p. 229-259.

Goreau, T. F., and W. D. Hartman, 1963, Boring sponges as controlling factors in the formation and maintenance of coral reefs, *in* R. F. Sognnaes, ed., Mechanisms of Hard Tissue Destruction: Washington, D.C., American Association for the Advancement of Science, Publication 75, p. 24-54.

Grover, G., Jr., 1978, Fenestral and associated vadose diagenetic fabrics of tidal flat carbonates, Middle Ordovician New Market Limestone, southwestern Virginia: Journal of Sedimentary Petrology, v. 48, p. 453-473.

Kennedy, W. J., 1975, Trace fossils in carbonate rock, *in* R. W. Frey, ed., The Study of Trace Fossils: New York, Springer-Verlag, p. 377-398.

Kobluk, D. R., and D. F. Kahle, 1978, Geologic significance of boring and cavity-dwelling marine algae: Bulletin of Canadian Petroleum Geology, v. 26, p. 362-379.

Lees, A., 1964, The structure and origin of the Waulsortian (Lower Carboniferous) "reefs" of west-central Eire: Philosophical Transactions of the Royal Society of London, Series B, v. 247 (no. 740), p. 483-531.

Mazzullo, S. J., and B. A. Birdwell, 1989, Syngenetic formation of grainstones and pisolites from fenestral carbonates in peritidal settings: Journal of Sedimentary Petrology, v. 59, p. 605-611.

Monty, C. L. V., D. W. J. Bosence, P. H. Bridges, and B. R. Pratt, eds., 1995, Carbonate Mud Mounds: Oxford, England, International Association of Sedimentologists Special Publication No. 23, 544 p.

Osgood, R. G., Jr., 1987, Trace fossils, *in* R. S. Boardman, A. H. Cheetham, and A. J. Rowell, eds., Fossil Invertebrates: Palo Alto, CA, Blackwell Scientific Publications, p. 663-674.

Pratt, B. R., 1982, Stromatolitic framework of carbonate mud mounds: Journal of Sedimentary Petrology, v. 52, p. 1203-1227.

Risk, M. J., and R. B. Szczuczko, 1977, A method for staining trace fossils: Journal of Sedimentary Petrology, v. 47, p. 855-859.

Roehl, P. O., 1967, Stony Mountain (Ordovician) and Interlake (Silurian) facies analogs of Recent low-energy marine and sub-aerial carbonates, Bahamas: American Association of Petroleum Geologists Bulletin, v. 51, p. 1979-2032.

Rützler, K., 1975, The role of boring sponges in bioerosion: Oecologia, v. 19, p. 203-216.

Sander, B. K., 1951, Contributions to the Study of Depositional Fabrics — rhythmically deposited Triassic limestones and dolomites [translated from 1936 original by E. B. Knopf]: Tulsa, OK, American Association of Petroleum Geologists, 207 p.

Sander, B. K., 1970, An Introduction to the Study of Fabrics of Geological Bodies [translated by F. C. Phillips & G. Windsor]: New York, Pergamon Press, 641 p.

Shrock, R. R., 1948, Sequence in Layered Rocks: New York, McGraw-Hill, 507 p.

Warme, J. E., 1975, Borings as trace fossils, and the processes of marine bioerosion, *in* R. W. Frey, ed., The Study of Trace Fossils: New York, Springer-Verlag, p. 181-227.

Wieczorek, J., 1979, Geopetal structures as indicators of top and bottom: Annales Societatis Geologorum Poloniae, v. 49, p. 215-221.

Facing Page: Fundamental to understanding sedimentary rocks is the distinction of three basic components: GRAINS (termed allochems by Folk), MATRIX (carbonate mud), and porosity or porosity-filling CEMENT. Typical carbonate rocks are plotted here on a ternary diagram using those three end members (redrawn from Folk, 1962).

CARBONATE CLASSIFICA-
ROCKS AND SEDIMENTS

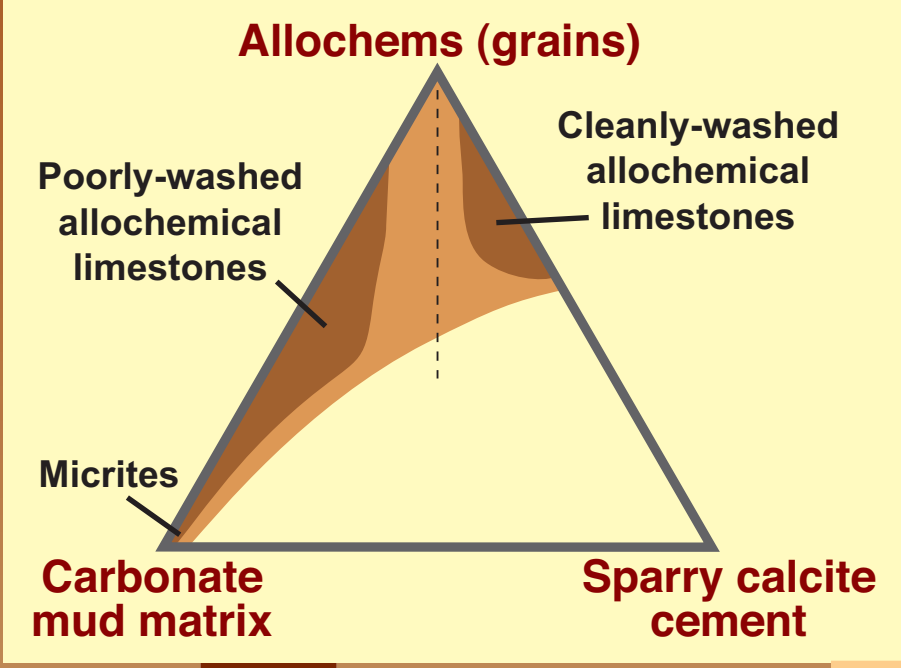

CHAPTER 20

Folk (1959/1962)

Dunham (1962)

Embry & Klovan (1971)

Wright (1992)

INTRODUCTION TO LIMESTONE CLASSIFICATIONS

Consistent classification and concise naming of rocks and sediments are essential for effective communication throughout the international scientific community. An ideal classification scheme combines objective, quantifiable description of readily observable features that are grouped into named categories. At the same time, it is desirable to have groupings that incorporate a maximum level of genetic or interpretive significance (groupings that reflect mechanisms of formation, environments of deposition, and the like). Although many classifications have been proposed for carbonate rocks and sediments, only two — the Folk (1959/62) and Dunham (1962) classifications — have successfully met the test of time (along with two others that are variants of the Dunham scheme). All four schemes are based on the distinction of three fundamental components: grains (skeletal fragments, ooids, pellets/peloids, intraclasts, and non-carbonate detritus), matrix or carbonate mud, and open pores or sparry-calcite-filled primary interparticle porosity (see diagram on previous page). The differences between the classifications are mainly that Folk uses the relative percentages of grains and matrix, Dunham as well as Embry and Klovan use mud- versus grain-supported fabrics, and Wright uses a more genetic division into biological, diagenetic, and depositional fabrics. This chapter summarizes the features of each classification and provides petrographic examples of carbonate rocks with their Folk and Dunham names; dolostone classifications and examples are covered in the chapter on dolomites.

FOLK (1959 AND 1962) CLASSIFICATIONS

Methodology:

The Folk classification uses multiple descriptive terms. The fundamental name is based on the four grain types and the relative abundances of grains (allochems), matrix, and cement or pore space. Eleven basic terms are generated (top diagram on facing page), including ones for pure mud rocks (micrites), muddy rocks with spar patches (dismicrites) and organically-bound rocks (biolithites). Because of their special environmental significance, intraclasts and ooids are favored in the naming process (see top diagram caption).

To describe the features of carbonate rocks that reflect the degree of sorting and rounding, Folk's terminology includes textural modifiers (middle diagram on facing page). In general, deposits classed on the left side of the diagram were formed in "low-energy" settings; rock types farther to the right represent deposition in increasingly high-energy depositional settings.

A third component of a full Folk name relates to the average grain or crystal size of the rock. That terminology is summarized in the bottom diagram on the facing page.

A carbonate rock named under the Folk classification can include any or all of the terms generated in these three categories, plus any additional descriptive terms the user desires. Thus, for example, the same rock could be termed a "biosparite" or a "rounded biosparite" or a "coarse calcarenite: rounded biosparite" or a "coarse calcarenite: rounded rudist-coral biosparite" or a "slightly dolomitized coarse calcarenite: rounded rudist-coral biosparite", depending on the level of detail desired.

Advantages:

1. **Quantifiable, descriptive (objective) terminology.**
2. **Although primarily descriptive, rock terms convey considerable genetic (environmental) information.**
3. **Multiple optional terms — for grain size, faunal composition, alteration, non-carbonate constituents, and other features — allow informative names at any desired level of detail.**
4. **Used worldwide, especially by petrographers in academic settings.**

Drawbacks:

1. **Microscope work needed for accurate naming — especially to identify pellets and other small grains or to determine exact percentages of grains, matrix and cement.**
2. **Somewhat awkward to use with modern sediments (e.g., calling sediment lacking cement a "sparite").**
3. **Does not describe the varied fabrics of reefal carbonates as well as other classifications.**
4. **Not widely used in industrial settings, probably because it is not as easy to use for general core descriptions as the Dunham classification.**
5. **Can be very difficult to distinguish true micritic matrix from microbial or inorganic in-situ microcrystalline precipitates, a problem for all classifications.**

Graphic classification table of limestones (Folk, 1962)

The Folk limestone nomenclature is based on 1) the nature of the constituent grains and 2) the relative abundance of micritic matrix versus open pore space (or sparry calcite cement filling such pores). All grains are not treated equally, however. If intraclasts are >25% of the grains, the rock is an intraclastic limestone; if intraclasts are <25% and ooids are >25%, the rock is an oolitic limestone; if intraclasts and ooids are <25% each, then the rock is a biogenic or pelletal limestone, depending on the relative percentages of those grains. Terms can be combined if desired (e.g. a biopelsparite). A dismicrite is a micrite with spar-filled blebs (generally burrows) and a biolithite is a biologically bound rock.

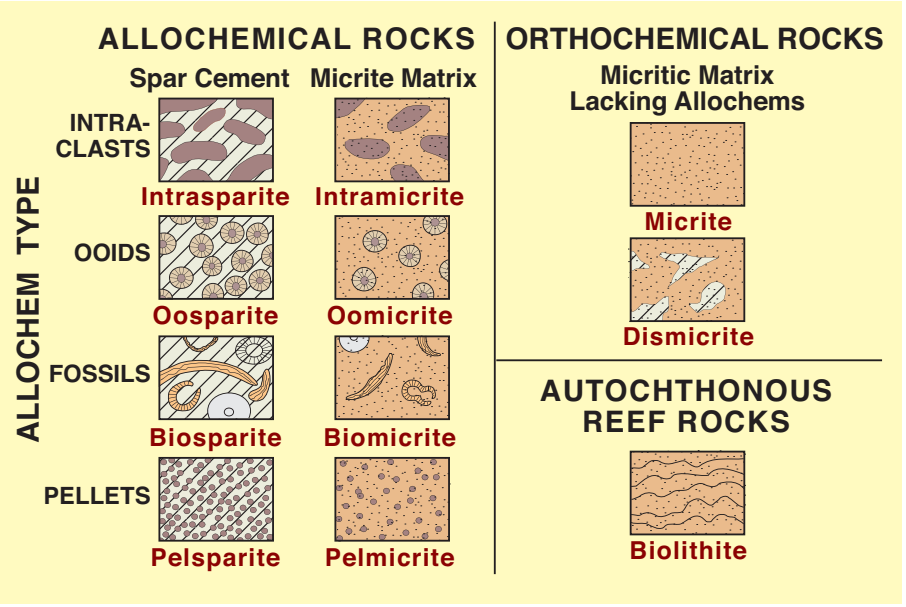

A textural spectrum for carbonate deposits (Folk, 1962)

These eight stages of sorting and rounding reflect, in general, deposition of sediments in a spectrum from low-energy settings (left) to high-energy settings (right). In very low-energy environments, pure or nearly pure carbonate muds typically accumulate; in intermediate-energy environments, muds with higher grain concentrations or partially winnowed grain and mud accumulations are formed; in high-energy settings, sorting and rounding of grains occur and virtually all mud matrix is removed. Textural inversions occur where unusual or episodic events (tsunamis or hurricanes) mix sediment from different environments or introduce short-term, high-energy conditions into a normally low-energy area.

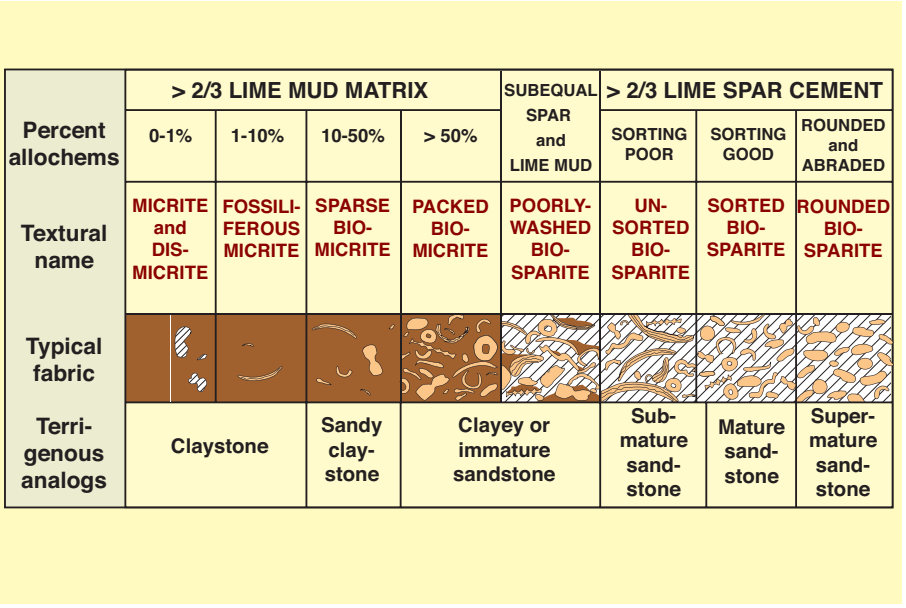

A grain- and crystal-size scale for carbonate rocks (Folk, 1962)

The left-center column provides standardized terms for various sizes of transported materials (fossil fragments, ooids, intraclasts, pellets, and other grains); the right-center column provides comparable terminology for authigenic precipitates, as well as the products of recrystallization or replacement (dolomite or marble, for example). The Folk classification includes terms (not shown in any of these diagrams) for dolomites of various crystal sizes, with and without preserved primary fabrics.

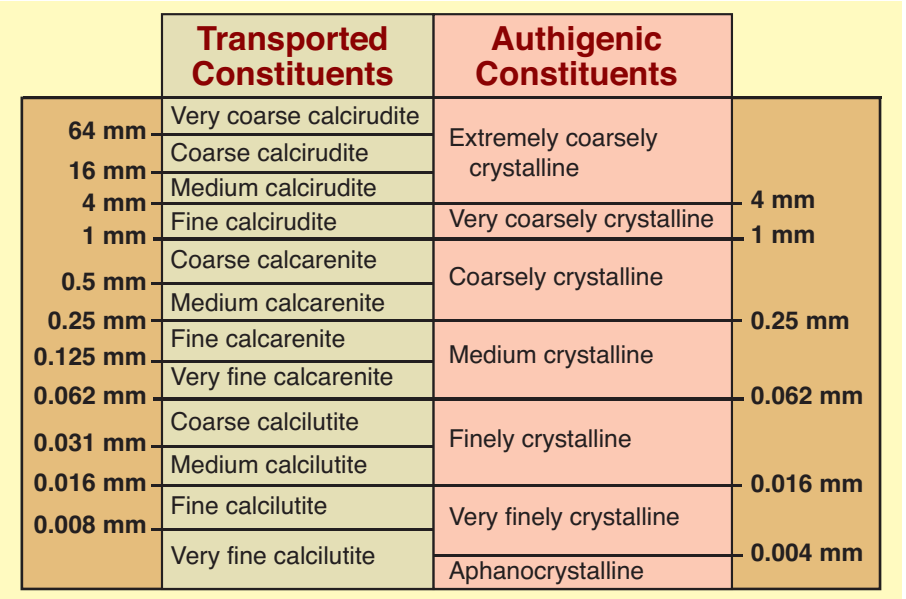

DUNHAM (1962) CLASSIFICATION WITH EMBRY & KLOVAN (1971) AND WRIGHT (1992) MODIFICATIONS

Methodology:

The Dunham classification is based on the characterization of the support framework of the rock or sediment. If the grains generally touch each other and support the overall framework, the rock is grain-supported; if grains are "floating" in mud, the rock is mud-supported (Dunham defined mud as material of less than 20 μm size as contrasted to Folk's definition of less than 4 μm). The relative percentages of grains and mud are then used to generate the four main names — mudstone, wackestone, packstone and grainstone (top diagram, facing page). Additional terms are provided for organically lithified strata (e.g., reefs, stromatolites) and recrystallized carbonates. Further modifiers can be applied to describe grain types, dominant organisms, and diagenesis, although these are not all explicitly codified by Dunham.

The Embry & Klovan (1971) classification modified the Dunham scheme by further subdividing coarse-grained skeletal deposits and organically formed or organically bound carbonate rocks. The five new terms (see center diagram, facing page) add to the descriptive capability of the Dunham classification in the area of biogenic deposits, especially reefs and bioherms.

The classification of Wright (1992) is a further, more fundamental modification of the Dunham and Embry & Klovan terminologies. It is based on the premise that limestone textures result from an "interplay of three factors: depositional regime, biological activity and diagenesis" (see bottom diagram, facing page). Depositional components were emphasized in the Dunham classification; biological activity was emphasized in the Embry and Klovan terminology, and the diagenetic components are expanded upon in the Wright classification. Several new terms were developed in the Wright classification: the Dunham term "mudstone" was changed to "calcimudstone" for increased clarity, and five new terms were added to cover diagenetic textures that may or may not have obliterated earlier fabrics.

Dunham/Embry & Klovan classification advantages:

1. Partially quantifiable, descriptive (objective) terminology.
2. Terms reflect environmental "energy" and thus convey genetic information.
3. Relatively easy to use in the field or when looking at core; usable without microscopic examination.
4. Sensible names for use in modern sediments lacking cement.
5. Used worldwide, especially in the petroleum industry.

Dunham/Embry & Klovan classification drawbacks:

1. Generally not as detailed as the Folk classification (although Folkian modifiers can be used).
2. Often difficult to decide whether a rock is grain- or mud-supported, especially in rocks with very large or irregularly-shaped grains (e.g., fenestrate bryozoans). This determination is also complicated because thin sections are two-dimensional cuts through a three-dimensional fabric, and grains that apparently "float" in matrix may actually touch outside the plane of the thin section.
3. Offers little flexibility in classifying diagenetically altered rocks.
4. Less widely used in academic settings.

Wright classification advantages:

1. Has all the positive features of the Dunham and Embry & Klovan classifications.
2. Provides balance in terminology between primary (sedimentologic-biologic) and secondary (diagenetic) features of limestones.
3. This scheme tempers the sometimes simplistic assumptions on which previous classifications were based (i.e., it takes advantage of increased knowledge of microbial and diagenetic process gained in the three decades from 1962 to 1992).

Wright classification drawbacks:

1. Has same drawbacks as Dunham and Embry & Klovan classifications.
2. Recognizes complex depositional and diagenetic origins of micrite matrix, but does not fully integrate such realities in its terminology.
3. Relatively new and not yet very widely used.

Classification table of carbonate rocks (Dunham, 1962)

A diagram showing the Dunham classification of carbonate rocks according to their depositional textures. The distinction as to whether a rock is supported by matrix (mud) or framework (grains) is fundamental to this scheme. The four basic terms for normal (non-crystalline) limestones can be further modified with terms describing constituent grains or other features. The most difficult aspect of this classification, in many case, is in deciding whether a rock with large and irregular (skeletal or intraclastic) grains, or one that has undergone substantial post-depositional compaction, was originally mud- or grain-supported.

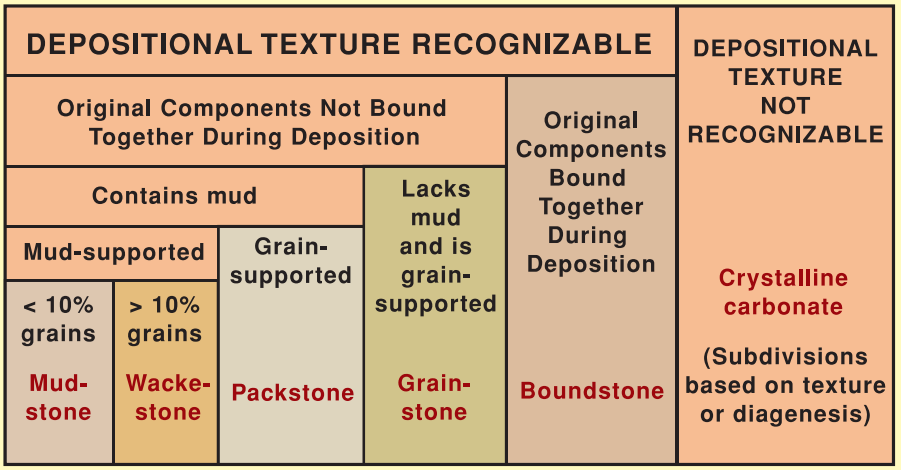

Classification table of skeletal limestones (Embry & Klovan, 1971)

A diagrammatic summary of the major modifications provided by the Embry and Klovan (1971) scheme to the Dunham (1962) classification. For biogenic limestones, the term "floatstone" replaces Dunham's "packstone". For coarser, grain-supported biogenic limestones, the term "rudstone" was coined. In addition, an organically bound rock can be termed a "bafflestone", a "bindstone", or a "framestone", depending on the nature of the organic structures. These last three terms, in particular, have been widely adopted by those working on reefs, bioherms, and other biogenic carbonates.

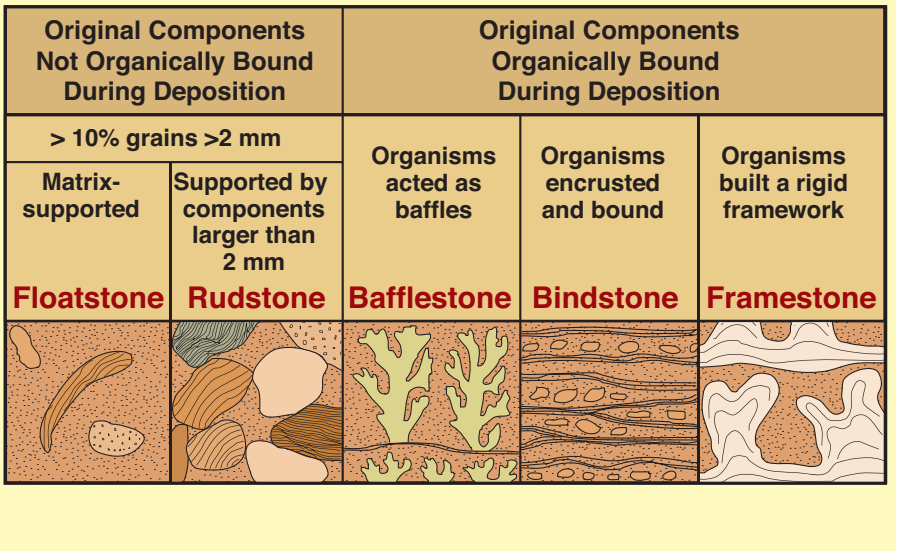

Classification table of limestones (Wright, 1992)

This summary diagram, showing the essential components of the Wright classification, emphasizes the distinction between carbonate strata influenced by depositional processes (physical), biological processes, or diagenetic processes (both synsedimentary and post-depositional). Although the names are mainly derived from the Dunham or Embry-Klovan classifications, several useful new terms were coined, including "cementstone", "condensed grainstone", and "fitted grainstone" for cement-rich or chemically compacted limestones.

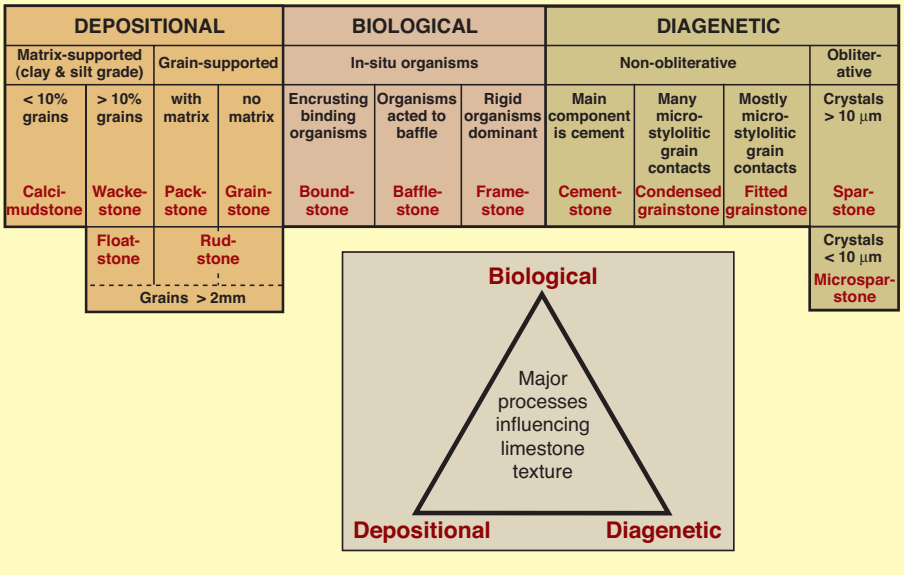

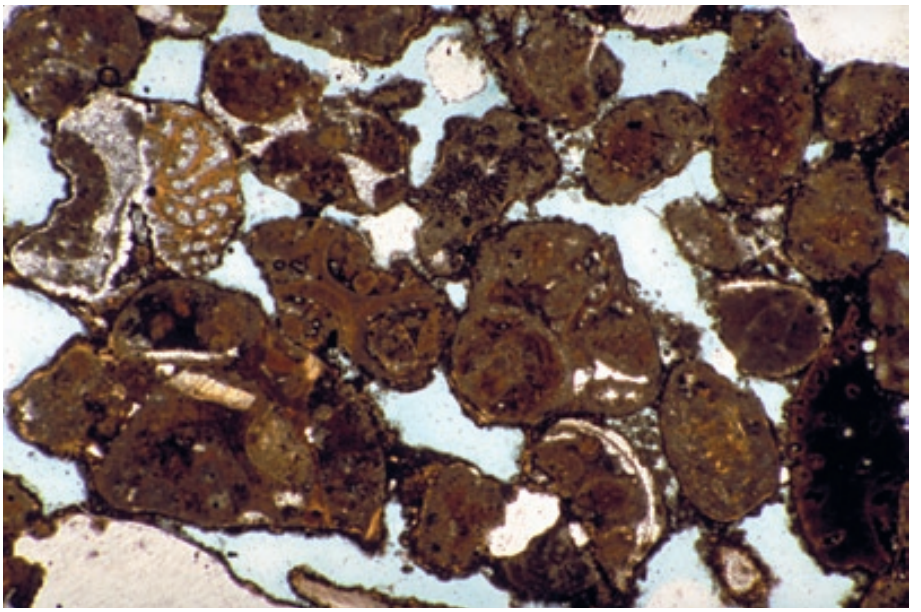

Recent sediment, Bimini, Bahamas

A modern sediment composed of grapestone intraclasts and peloidal grains. The micritized peloidal grains are bound together with thin, high-Mg calcite cements as well as organic coatings and encrustations Folk name: **poorly-sorted intrasparite**. Dunham name: **lithoclast grainstone**.

PPL, BSE, HA = 3.2 mm

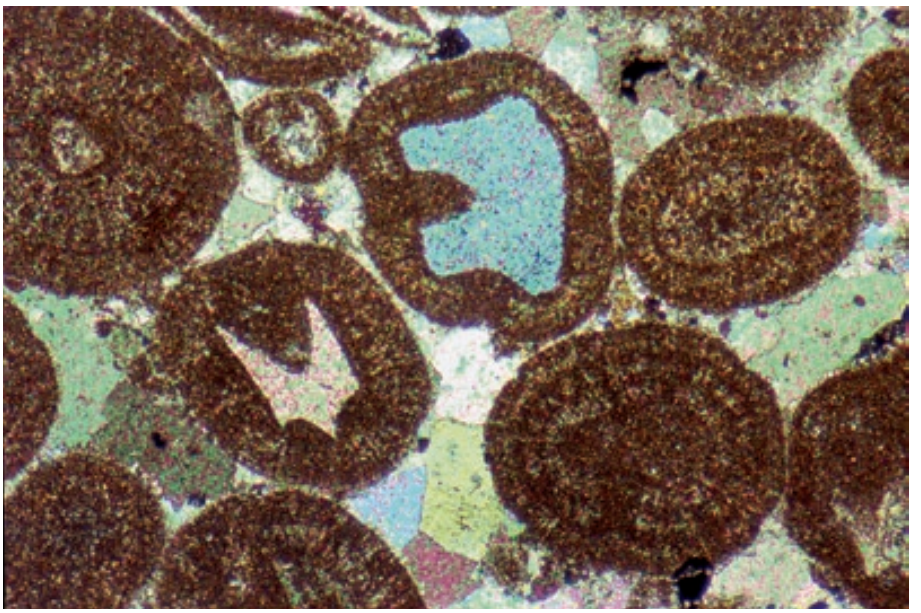

Paleozoic limestone, midcontinent, U.S.A.

An oolitic limestone with coated fossil fragments. Folk name: **rounded oosparite**. Dunham name: **oolitic grainstone**.

XPL, HA = 2.7 mm

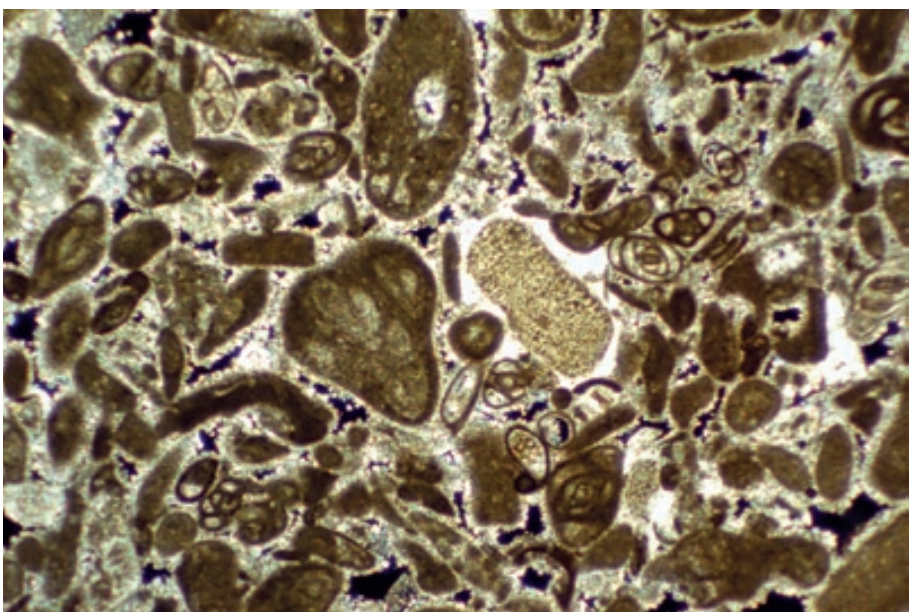

Up. Oligocene Suwanee Ls., Citrus Co., Florida

A bioclastic limestone containing echinoderms, miliolid foraminifers, mollusks, and other grains with a wide variety of shapes and sizes. Folk name: **unsorted biosparite**. Dunham name: **mixed-fossil grainstone**.

XPL, HA = 3.4 mm

Mississippian (Meramecian) Arroyo Peñasco Gp., San Miguel Co., New Mexico

A pellet-rich limestone with possible early cements and little or no matrix. The pellets are inferred, from their small and uniform size, to be of fecal origin. Folk name: **sorted pelsparite**. Dunham name: **pelletal grainstone**.

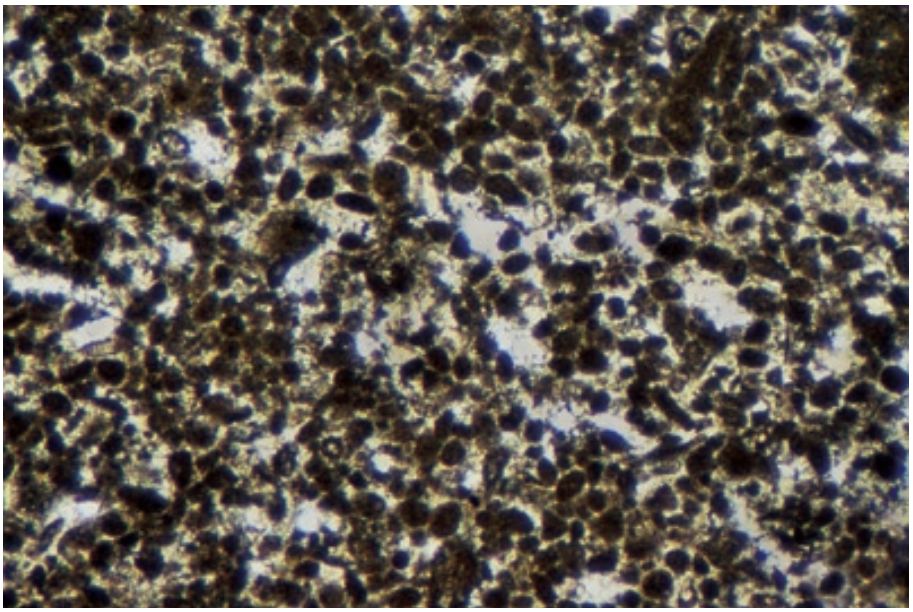

PPL, HA = 2.0 mm

Up. Permian (up. Guadalupian) Capitan Fm., Eddy Co., New Mexico

A compacted intraclast-rich limestone with extensive carbonate mud matrix. Several different types of reef and slope limestone fragments are found in this slope debris flow deposit. Despite the fact that some clasts were fully cemented prior to transport, these are still considered as penecontemporaneously reworked materials within the same basin of deposition and thus qualify as intraclasts. Folk name: **packed intramicrite**. Dunham name: **lithoclastic wackestone**. Embry and Klovan name: **lithoclastic floatstone or rudstone** (depending on whether one considers this to be a grain- or mud-supported fabric).

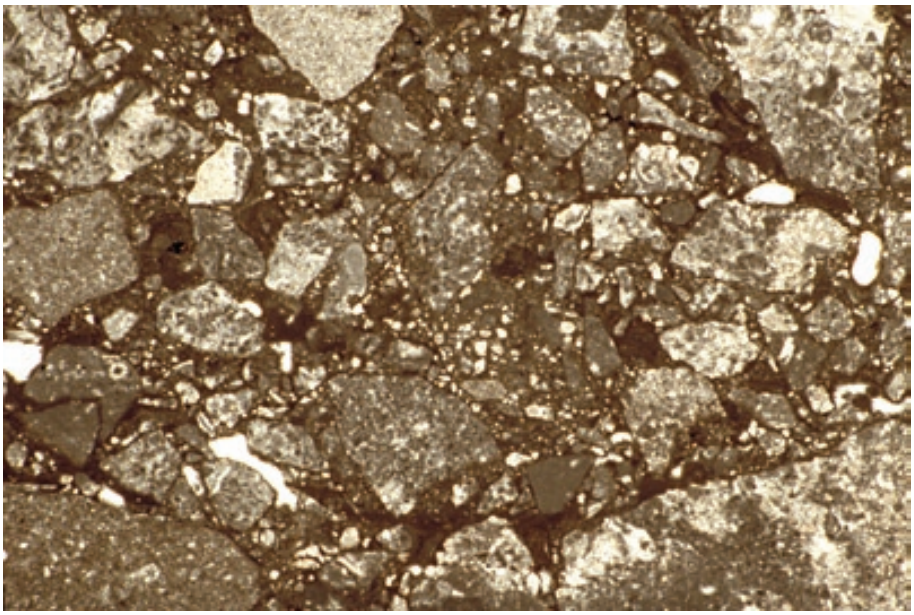

PPL, HA = 10 mm

Up. Cambrian Beekmantown Ls., Washington Co., Maryland

Tectonically deformed ooids in a carbonate mud matrix (Cloos, 1947). An unusual rock type because ooids typically reflect high energy settings of formation but the micrite matrix implies a low-energy depositional environment. This "textural inversion" may have resulted from bioturbation or storm reworking of ooids into a nearby lagoon or other protected environment. Folk name: **packed oomicrite**. Dunham name: **oolith lime packstone or oolith lime wackestone** (depends on whether you see this as grain- or mud-supported; a major difficulty with the Dunham classification).

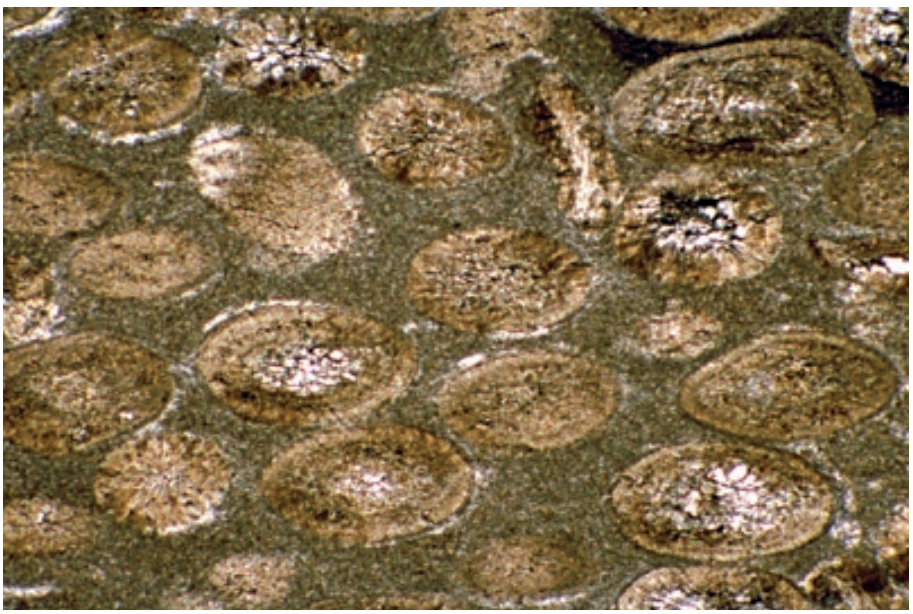

PPL, HA = 3.1 mm

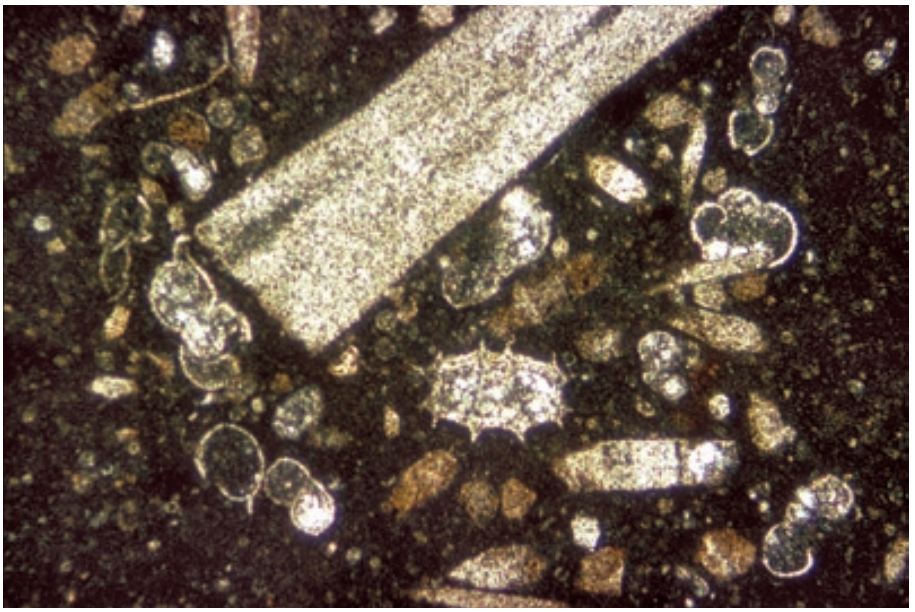

Up. Cretaceous Chalk, Kent, England, U.K.

A variety of skeletal constituents in a shelf chalk. The largest grain is an echinoid fragment; numerous inoceramid prisms, foraminifers, and calcispheres are also visible. Folk name: **packed biomicrite**. Dunham name: **mixed-fossil lime wackestone**.

PPL, HA = ~1.0 mm

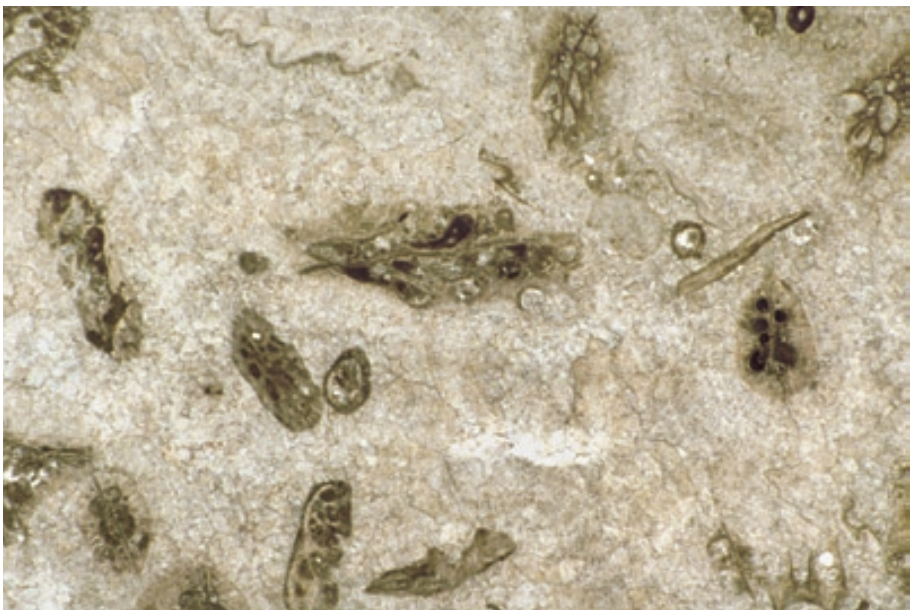

Up. Permian (Kazanian?) Wegener Halvø Fm., Jameson Land, East Greenland

A rock that originally consisted mainly of fallen fronds of fenestrate bryozoans. Cloudy, bladed, marine cement filled the 80-90% pore space prior to burial, preventing compaction. Clearly, given the absence of matrix, this must have been a grain-supported deposit; but if carbonate mud had infiltrated into the porous sediment, it would now be difficult to determine that this once was a grain-supported fabric. Folk name: **unsorted bryozoan biosparite**. Dunham name: **bryozoan grainstone**. Embry/Klovan name: **bryozoan bafflestone**. Wright name: **bryozoan cementstone**.

PPL, HA = 8.0 mm

Up. Jurassic Solnhofen Ls., Kelheim, Bavaria, Germany

A lithified, pure carbonate mud (here micrite is not just matrix, but essentially is the only rock constituent. Folk name: **micrite**. Dunham name: **lime mudstone**.

XPL, HA = 3.4 mm

Up. Miocene (Tortonian-Messinian) Up. Coralline Limestone Fm., Malta

A sediment formed of intergrown red algal and foraminiferal encrustations and small amounts of other trapped skeletal and peloidal grains. Folk name: **red algal biolithite**. Dunham (and Wright) name: **red algal boundstone**. Embry/Klovan name: **red algal bindstone**.

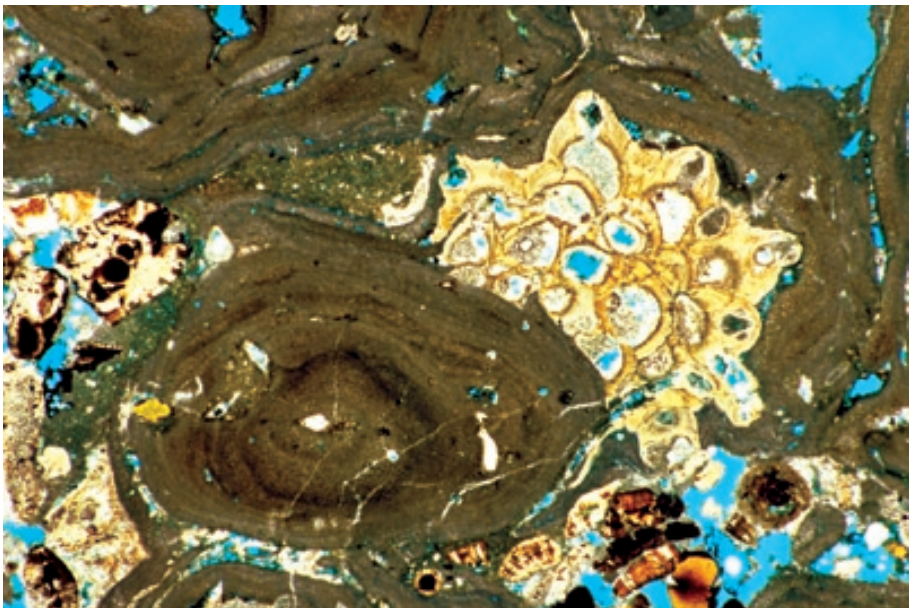

PPL, BSE, HA = 5.5 mm

Paleozoic limestone, unknown location

A rock with both large, irregularly shaped, calcite-filled cavities and ooids scattered in a micrite matrix — a very unusual carbonate sediment fabric. Folk name: **oolitic dismicrite**. Dunham name: **oolitic wackestone**. Sample from Noel P. James.

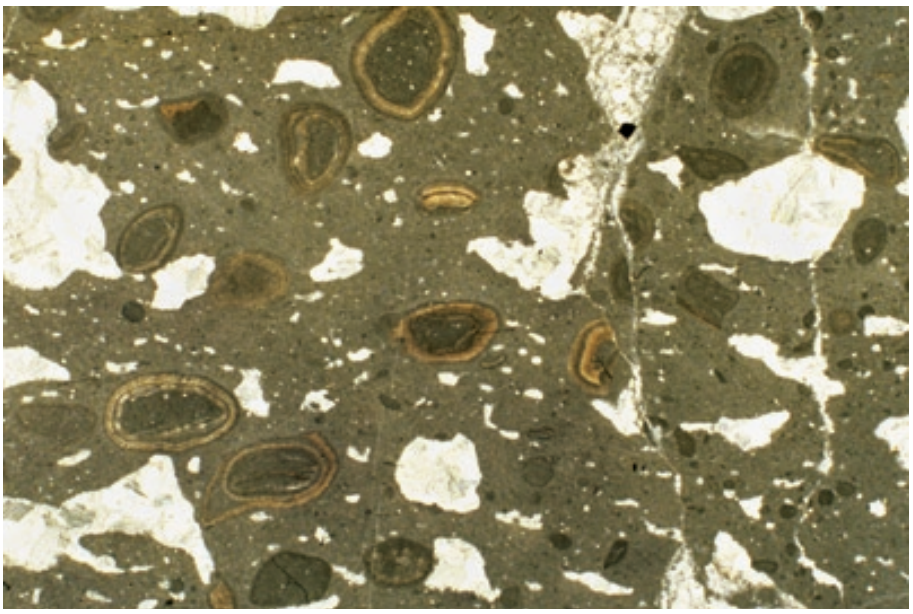

PPL, HA = 13.5 mm

Lo. Cretaceous dolostone, Cephalonia, Ionian Islands, Greece

A coarsely crystalline, subhedral, zoned, nonferroan replacement dolomite. The rhombs have cloudy cores and clear rims (a common feature in replacement dolomites) and completely obliterated primary fabrics. Folk name: **coarsely crystalline dolomite**. Dunham name: **crystalline dolomite**. Wright name: **dolomitic sparstone**.

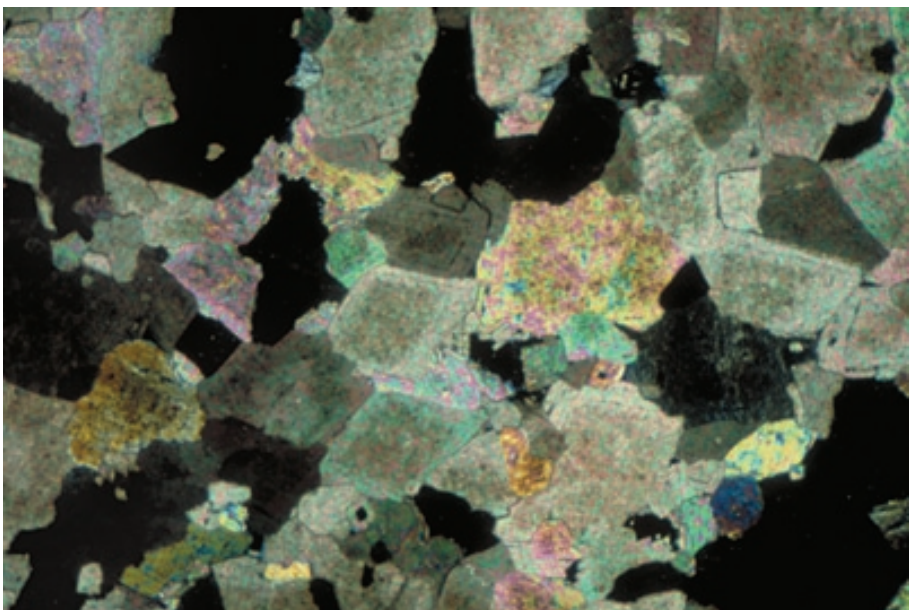

XPL, AFeS, HA = 2.4 mm

Cited References and Additional Information Sources

Archie, G. E., 1952, Classification of carbonate reservoir rocks and petrophysical considerations: AAPG Bulletin, v. 36, p. 278-298.

Baisert, H., 1967, Analyse der Nomenklaturen sedimentärer Karbonatgesteine: Zeitschrift für Angewandte Geologie, v. 13, p. 642-650.

Bissell, H. J., and G. V. Chilingar, 1967, Classification of sedimentary carbonate rocks, *in* G. V. Chilingar, H. J. Bissell, and R. W. Fairbridge, eds., Carbonate Rocks: Origin, Occurrence and Classification: Developments in Sedimentology 9A: New York, Elsevier Publ. Co., p. 87-168.

Bosellini, A., 1964, Sul significato genetico e ambientale di alcuni tipi de rocce calcaree in base alle più recenti classificazioni: Memorie del Museo di storia naturale della Venezia tridentina (Trento), v. 15, p. 1-58.

Catalov, G. A., 1971, Structural classification of the limestones [in Bulgarian with English summary]: Bulletin of the Geological Institute, Bulgarian Academy of Sciences (Sofia), Series Strat. Lithology, v. 20, p. 133-156.

Chilingar, G. V., 1957, Classification of limestones and dolomites on the basis of Ca/Mg ratio: Journal of Sedimentary Petrology, v. 27, p. 187-189.

Chilingar, G. V., 1960, Notes on classification of carbonate rocks on the basis of chemical composition: Journal of Sedimentary Petrology, v. 30, p. 157-158.

Chilingar, G. V., H. J. Bissell, and R. W. Fairbridge, eds., 1967, Carbonate Rocks: Origin, Occurrence and Classification: New York, Elsevier Publishing Co., 471 p.

Cloos, E., 1947, Oolite deformation in the South Mountain fold, Maryland: Geological Society of America Bulletin, v. 58, p. 843-918.

Cuffey, R. J., 1985, Expanded reef-rock textural classification and the geologic history of bryozoan reefs: Geology, v. 13, p. 307-310.

Dunham, R. J., 1962, Classification of carbonate rocks according to their depositional texture, *in* W. E. Ham, ed., Classification of Carbonate Rocks—a symposium: Tulsa, OK, American Association of Petroleum Geologists Memoir 1, p. 108-121.

Embry, A. F., and J. E. Klovan, 1971, A Late Devonian reef tract on northeastern Banks Island, N.W.T.: Bulletin of Canadian Petroleum Geology, v. 19, p. 730-781.

Feray, D. E., Jr., E. Heuer, and W. G. Hewatt, 1962, Biological, genetic, and utilitarian aspects of limestone classification, *in* W. E. Ham, ed., Classification of Carbonate Rocks—a symposium: Tulsa, OK, American Association of Petroleum Geologists Memoir 1, p. 20-32.

Folk, R. L., 1959, Practical petrographic classification of limestones: AAPG Bulletin, v. 43, p. 1-38.

Folk, R. L., 1962, Spectral subdivision of limestone types, *in* W. E. Ham, ed., Classification of Carbonate Rocks—a symposium: Tulsa, OK, American Association of Petroleum Geologists Memoir 1, p. 62-84.

Friedman, G. M., 1965, Terminology of crystallization textures and fabrics in sedimentary rocks: Journal of Sedimentary Petrology, v. 35, p. 643-655.

Friedman, G. M., 1985, The problem of submarine cement in classifying reefrock: an experience in frustration, *in* N. Schneidermann, and P. M. Harris, eds., Carbonate Cements: Tulsa, OK, SEPM Special Publication 36, p. 117-121.

Friedman, G. M., 1985, The term *micrite* or *micritic cement* is a contradiction—discussion of micritic cement in microborings is not necessarily a shallow-water indicator: Journal of Sedimentary Petrology, v. 55, p. 777.

Grabau, A. W., 1904, On the classification of sedimentary rocks: American Geologist, v. 33, p. 228-247.

Ham, W. E., and L. C. Pray, 1962, Modern concepts and classifications of carbonate rocks, *in* W. E. Ham, ed., Classification of Carbonate Rocks—a symposium: Tulsa, OK, American Association of Petroleum Geologists Memoir 1, p. 2-19.

Imbrie, J., and E. G. Purdy, 1962, Classification of modern Bahamian carbonate, *in* W. E. Ham, ed., Classification of Carbonate Rocks—a symposium: Tulsa, OK, American Association of Petroleum Geologists Memoir 1, p. 253-272.

Klement, K. W., 1967, Practical classification of reefs and banks, bioherms and biostromes: AAPG Bulletin, v. 51, p. 167-168.

Leighton, M. W., and C. Pendexter, 1962, Carbonate rock types, *in* W. E. Ham, ed., Classification of Carbonate Rocks, a symposium: Tulsa, OK, American Association of Petroleum Geologists Memoir 1, p. 33-61.

Monty, C., 1963, Bases d'une nomenclature des roches calcaires marines: Annales de la Société Géologique de Belgique, v. 86, p. B87-B122.

Morrow, D. W., 1982, Descriptive field classification of sedimentary and diagenetic breccia fabrics in carbonate rocks: Bulletin of Canadian Petroleum Geology, v. 30, p. 227-229.

Munoz, N. G., 1988, Dunham's carbonate rock classification: a Spanish terminology: Carbonates and Evaporites, v. 3, p. 65-66.

Nelson, H. F., C. W. Brown, and J. H. Brineman, 1962, Skeletal limestone classification, *in* W. E. Ham, ed., Classification of Carbonate Rocks, a Symposium: Tulsa, OK, American Association of Petroleum Geologists Memoir 1, p. 224-252.

Peryt, T. M., 1983, Classification of coated grains, *in* T. M. Peryt, ed., Coated Grains: New York, Springer-Verlag, p. 3-6.

Plumley, W. J., G. A. Risley, R. W. Graves, Jr., and M. E. Kaley, 1962, Energy index for limestone interpretation and classification, *in* W. E. Ham, ed., Classification of Carbonate Rocks—a symposium: Tulsa, OK, American Association of Petroleum Geologists Memoir 1, p. 85-107.

Powers, R. W., 1962, Arabian Upper Jurassic carbonate reservoir rocks, *in* W. E. Ham, ed., Classification of Carbonate Rocks—a symposium: Tulsa, OK, American Association of Petroleum Geologists Memoir 1, p. 122-192.

Riding, R., 1991, Classification of microbial carbonates, *in* R. Riding, ed., Calcareous Algae and Stromatolites: Berlin, Springer-Verlag, p. 21-51.

Sander, N. J., 1967, Classification of carbonate rocks of marine origin: American Association of Petroleum Geologists Bulletin, v. 51, p. 325-336.

Shvetzov, M. S., 1958, Main types of limestones and their classification: Eclogae geologicae Helvetiae, v. 51, p. 737-742.

Sibley, D. F., and J. M. Gregg, 1987, Classification of dolomite rock textures: Journal of Sedimentary Petrology, v. 57, p. 967-975.

Strohmenger, C., and G. Wirsing, 1991, A proposed extension of Folk's (1959, 1962) textural classification of carbonate rocks: Carbonates and Evaporites, v. 6, p. 23-28.

Thomas, G. E., 1962, Grouping of carbonate rocks into textural and porosity units for mapping purposes, *in* W. E. Ham, ed., Classification of Carbonate Rocks—a Symposium: Tulsa, OK, American Association of Petroleum Geologists Memoir 1, p. 193-223.

Todd, T. W., 1966, Petrogenetic classification of carbonate rocks: Journal of Sedimentary Petrology, v. 36, p. 317-334.

Wilson, R. C. L., 1967, Particle nomenclature in carbonate sediments: Neues Jahrbuch für Geologie und Paläontologie, Monatshefte, v. 1967/68, p. 498-510.

Wolf, K. H., 1960, Simplified limestone classification: AAPG Bulletin, v. 44, p. 1414-1416.

Wolf, K. H., 1961, An introduction to the classification of limestones: Neues Jahrbuch für Geologie und Paläontologie, Monatshefte, v. 1961, p. 236-250.

Wright, V. P., 1992, A revised classification of limestones: Sedimentary Geology, v. 76, p. 177-185.

Yang, C., and A. V. Carozzi, 1987, Practical Classification and Microfacies Analysis of Carbonate Rocks: Beijing, Peking University Press, 295 p.

Facing Page: Top - The world as viewed from a macropore. Entrance to Carlsbad Cavern, Eddy Co., New Mexico.
Bottom - Thin-section view of slightly reduced primary interparticle porosity coupled with leached and then slightly reduced secondary porosity within ooids. Eocene Green River Fm., Laney Mbr., Fremont Co., Wyoming. PPL, BSE, HA = 2.4 mm.

CARBONATE CLASSIFICA-
POROSITY

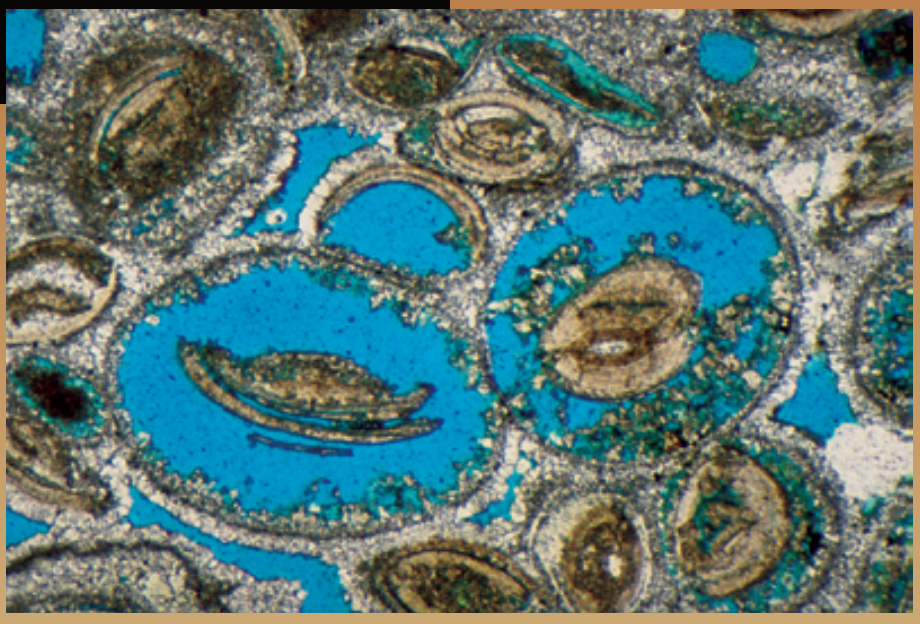

CHAPTER 21

POROSITY

Introduction:

Although most of this book focuses on the identification of grains and cements, what is often of prime interest to hydrocarbon explorationists is understanding the absence of those materials — in other words, the origin and history of open primary or secondary pore space. This chapter, therefore, will deal with recognition of different types of porosity; the chapters on diagenesis will cover the mechanisms and relative timing of porosity creation, retention, reduction, or destruction.

Classification:

A number of classifications of porosity in carbonate rocks have been proposed (see citations at end of section), but only the Choquette and Pray (1970) scheme has met with widespread acceptance. Thus, it will be the only one described and applied in this book. This classification combines terms that encompass four separate categories of observations. The main term (called the "basic porosity type") codifies the location and type of pore space. That term is prefaced with a genetic modifier or modifiers that relate to the process, direction or stage (enlarged, reduced or filled) of porosity evolution, and the time of pore formation; an additional term describing pore sizes can also be added. Finally, an abundance term can be appended at the end of the name to describe the percentage of pore space. In practice, most geologists simply specify the basic porosity type along with the one or two modifiers that are best suited to their needs.

The basic porosity types are illustrated in two diagrams (below and at the top of the next page). The basic porosity types are organized according to whether they are fabric selective, not fabric selective, or either fabric selective or not. The modifying terms are shown in the middle diagram (next page). Examples of the major porosity types (and some more minor ones) are given in subsequent illustrations.

A final note: the proper classification of porosity requires accurate observation of the amount and nature of pore spaces. Some porosity is either too large or too small to be recognizable in thin section (see upper photograph on the title page of this chapter), but most is visible at thin-section scales. To recognize and measure porosity properly under the microscope, one MUST use thin sections prepared from rock chips that were pressure-impregnated with color-dyed epoxy. Grains or crystals commonly are plucked out of sections during cutting and grinding; only with colored impregnation media can one distinguish pre-sectioning "real" pores from ones created during section preparation. Intensely dyed epoxy also lends emphasis to porosity and helps to reveal micropores that could otherwise be overlooked. To do quantitative or semiquantitative measurements of porosity using microscopy, one must mathematically correct the observations made in two-dimensional space (see, for example, Halley, 1978); modern digital image analysis methodologies can also be applied to this process (e.g., Anselmetti et al., 1998).

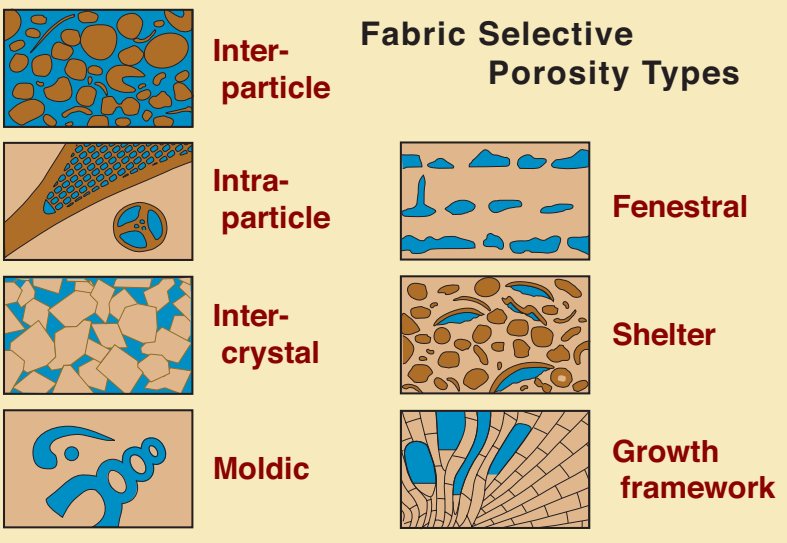

Choquette & Pray (1970) basic fabric-selective porosity types

A diagrammatic representation of the basic fabric-selective porosity types used in the Choquette and Pray (1970) carbonate porosity classification. What is meant by fabric selectivity is that the porosity is controlled by the grains, crystals, or other physical structures in the rock and the pores themselves do not cross those primary boundaries.

Choquette & Pray (1970) basic non-fabric-selective or variable porosity types

A diagrammatic representation of the basic non-fabric-selective or variably fabric-selective porosity types used in the Choquette and Pray (1970) carbonate porosity classification. These are all porosity patterns that actually or potentially can cross-cut primary grains and depositional fabrics. They also include porosity types that potentially can be much larger than any single primary framework element.

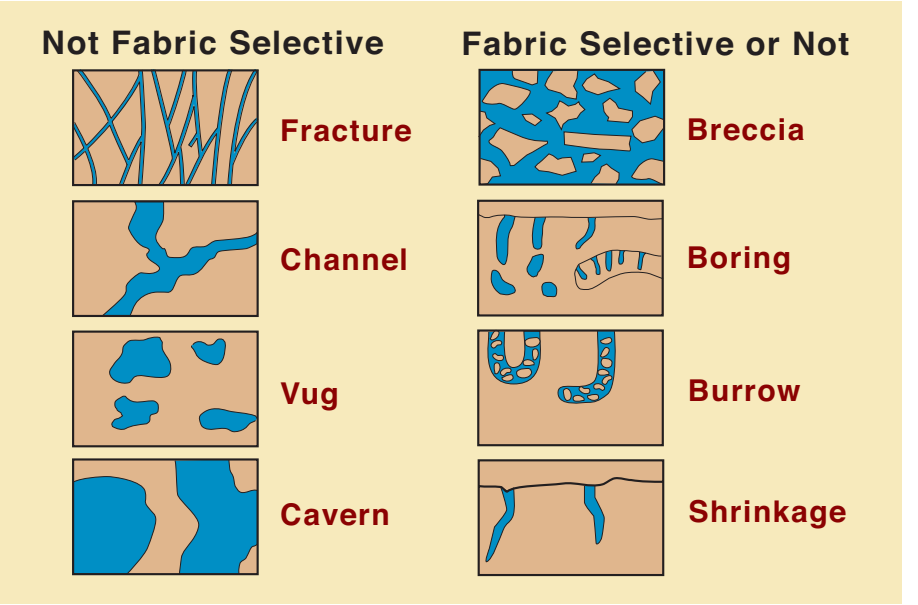

Choquette & Pray (1970) genetic, size, and abundance modifiers

The list of genetic modifiers that can be used to describe the process, direction or stage, and time of formation of porosity (if known or needed). As shown in the example at the bottom of the genetic column, multiple terms can be combined. Pore-size and abundance modifiers can also be added to the name if desired. This "modular" nomenclature allows considerable flexibility of naming, based on the user's needs, while still allowing a universally comprehensible terminology. Definitions of the main terms in this classification are provided in the glossary near the end of the book and complete discussions are found in Choquette and Pray (1970).

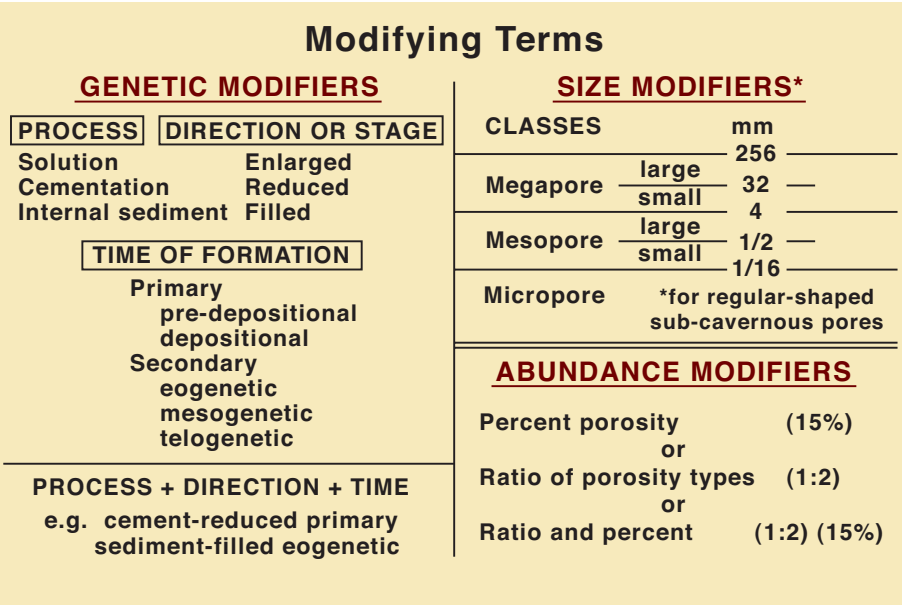

Recent sediment, Grand Cayman, Cayman Islands, B.W.I.

A modern calcarenite; a mixed algal-foraminiferal-molluscan limestone that has two types of initial porosity (shown in blue) — interparticle pore spaces (openings between framework grains) and intraparticle pore space (consisting of voids within the constituent grains). Intraparticle porosity is relatively minor in most of the grains, but is clearly visible in the *Halimeda* green algal plates and peneroplid foraminiferal tests.

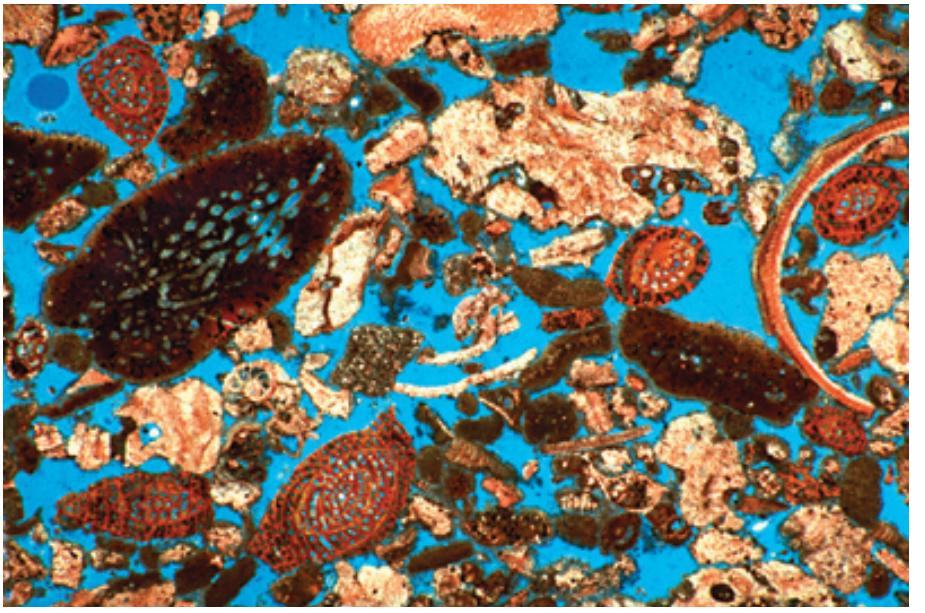

PPL, BSE, AFeS, HA = 6.0 mm

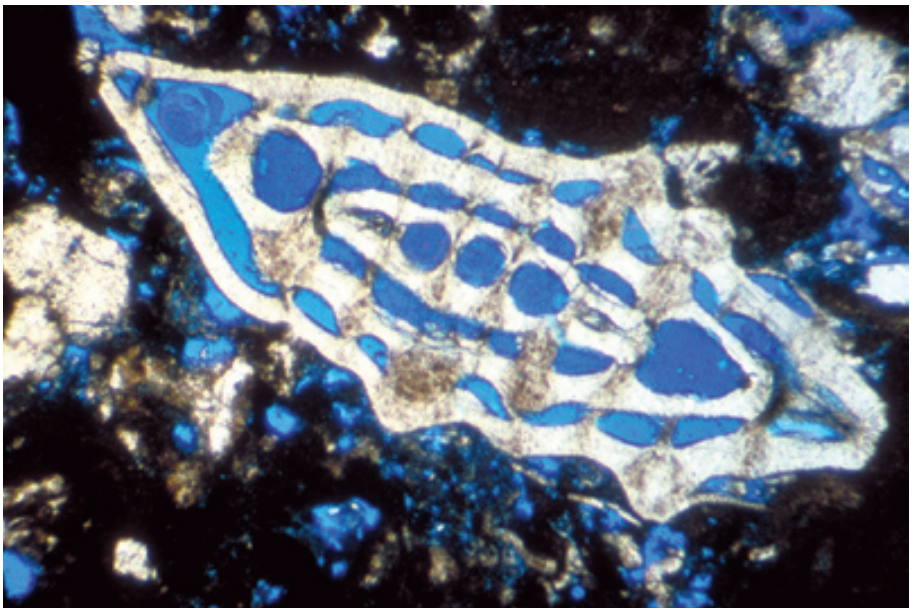

Eocene limestone, Zakinthos, Ionian Islands, Greece

Substantial unfilled primary intraparticle porosity within a nummulite benthic foraminifer. Substantial interparticle porosity is also present outside the foraminiferal test.

PPL, BSE, HA = 2.4 mm

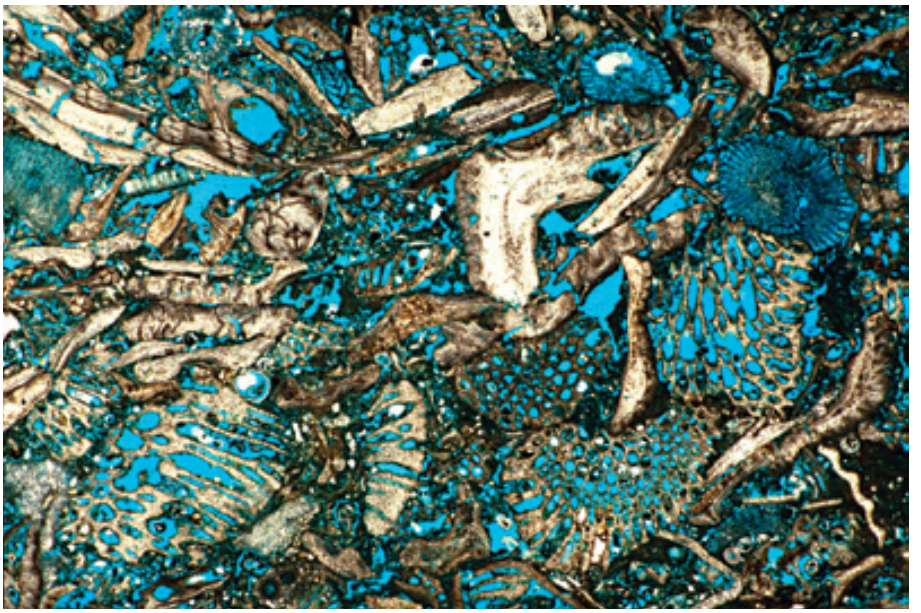

Mid. Pliocene Up. Haurangi Ls., Wairarapa District, New Zealand

This porous, bryozoan-rich, temperate-water limestone contains both intraparticle and interparticle porosity. Mechanical compactional crushing has reduced interparticle pore space, but in the absence of cementation, the volume of intraparticle porosity has remained high. In general, interparticle porosity is better connected and is thus associated with higher permeabilities, than intraparticle porosity. Barnacle fragments and echinoid spines are also visible in this section.

PPL, BSE, HA = 8.0 mm

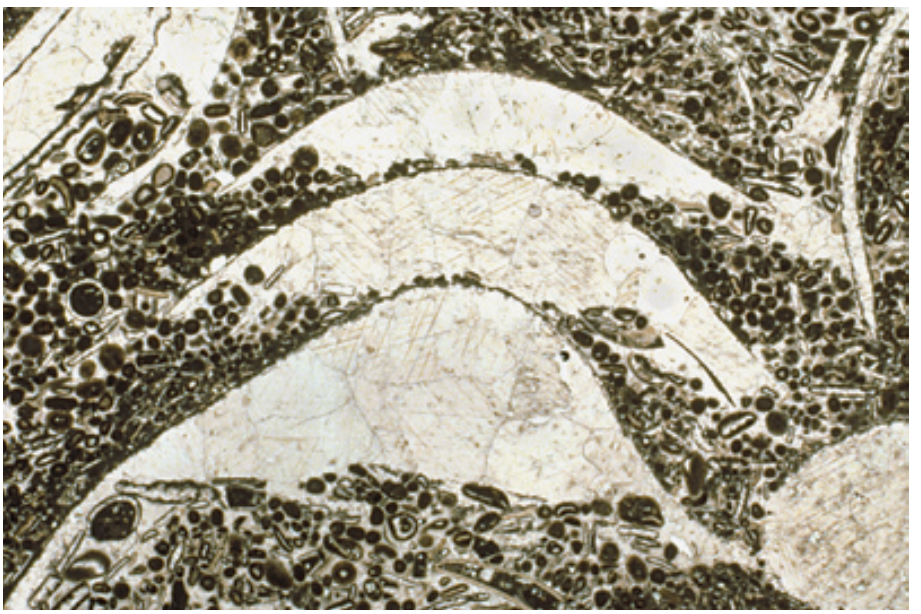

Mid. Ordovician Black River Gp., Kingston area, Ontario, Canada

Neomorphosed, originally aragonitic bivalve shells with underlying "umbrella" voids. This is an example of cement-reduced primary shelter porosity. Sample from Noel P. James.

PPL, HA = 11 mm

Permian (Guadalupian?) Park City Fm., Ervay Mbr., Washakie Co., Wyoming

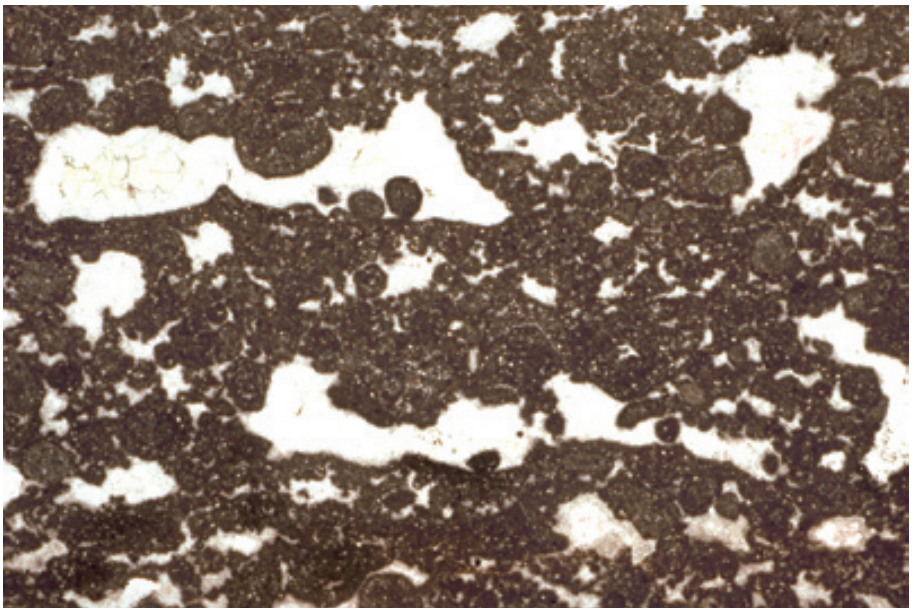

An example of "fenestral fabric", with elongate, spar-filled pores in micritic sediment. Fenestral fabric (sometimes called birdseye porosity) may result from grain bridging, bioturbation, gas bubble formation associated with decomposition of organic material, and other causes. It is most commonly associated with tidal flat deposits and other peritidal sediments. In the Choquette and Pray scheme, this rock would be classified as having cement-reduced primary fenestral porosity.

PPL, HA = 15 mm

Lo. Cretaceous (Aptian-Albian) limestone, Cephalonia, Ionian Islands, Greece

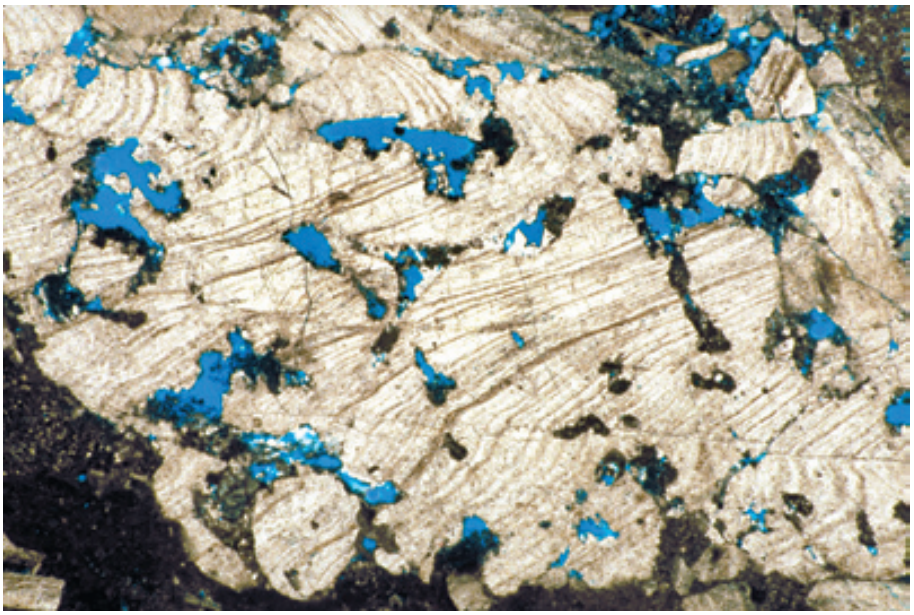

Solution-enlarged boring porosity is visible here within a massive rudistid bivalve fragment. The primary boring porosity was reduced by micrite infill or microcrystalline calcite cementation. Although individual grains can be extensively bored, boring porosity rarely is a major contributor to reservoir productivity.

PPL, BSE, HA = 8.0 mm

Up. Permian Wegener Halvø Fm., Jameson Land, East Greenland

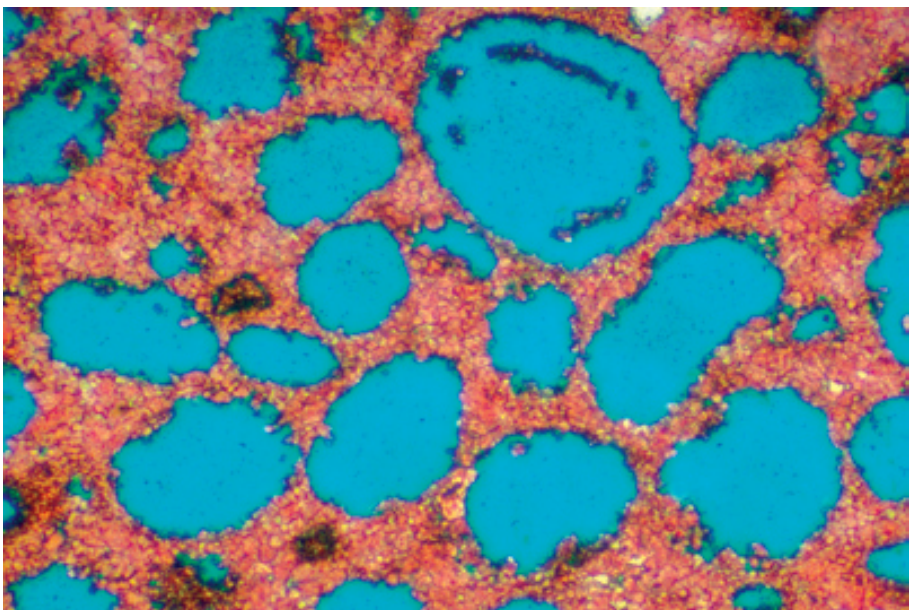

This sample shows extensive development of secondary porosity through leaching of ooids from a grainstone, The sample comes from just below a Permian subaerial exposure surface (a third-order sequence boundary). Vadose diagenesis led to complete filling of primary interparticle pores by blocky calcite cement and near-complete leaching of ooids, generating oomoldic secondary porosity. Although porosity remained high, permeability was substantially reduced because the moldic pores are poorly connected (mainly at point contacts or through intercrystal gaps).

PPL, BSE, AFeS, HA = 3.2 mm

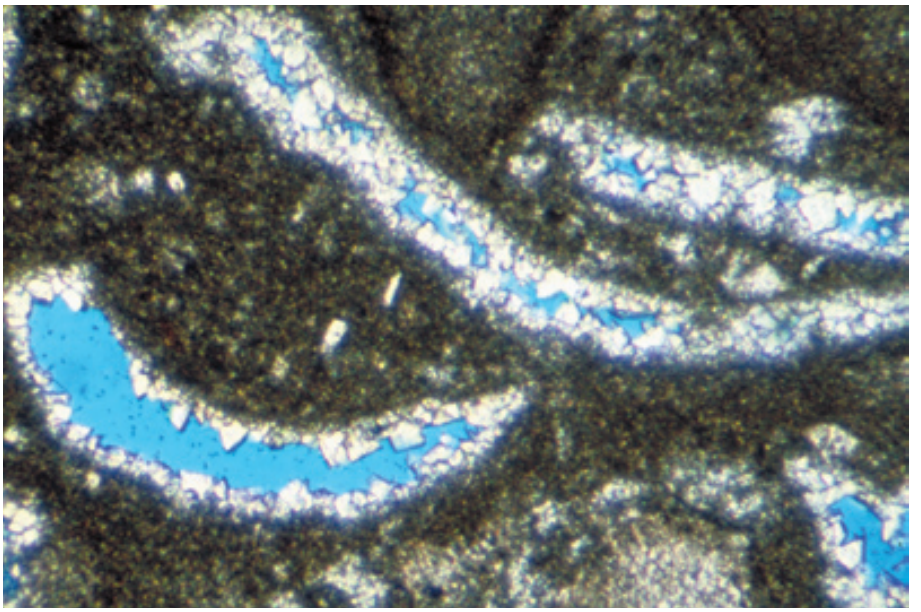

Oligocene Bluff Fm., Grand Cayman, Cayman Islands, B.W.I.

Meteorically leached bivalve shells have added some biomoldic porosity to this marine limestone. The moldic secondary porosity has been partially reduced through cementation with blocky, probably also meteoric, calcite cement.

PPL, BSE, HA = 1.6 mm

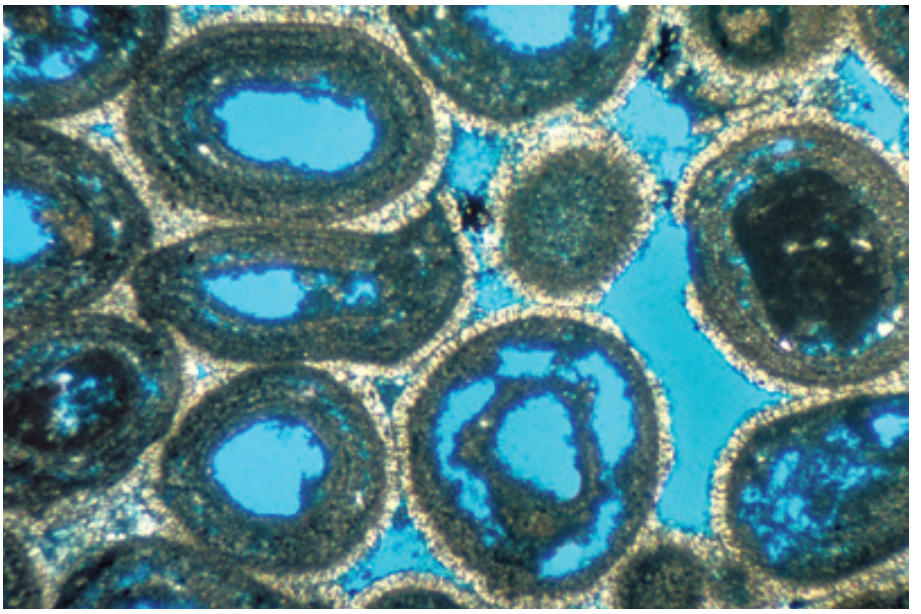

Lo. Permian (up. Kungurian) Irenskaya/Nevolinskaya Suite, Perm Region, Russia

In this rock, slightly reduced primary interparticle porosity is coupled with leached secondary (moldic) porosity within the ooids. The leached ooid nuclei may have had a different mineralogy from at least some of the coatings. Note the compactional crushing of some of the partially leached ooids and their cement coatings, a process that reduces total porosity, but helps to establish the relative timing of cementation and compaction.

PPL, BSE, HA = 2.4 mm

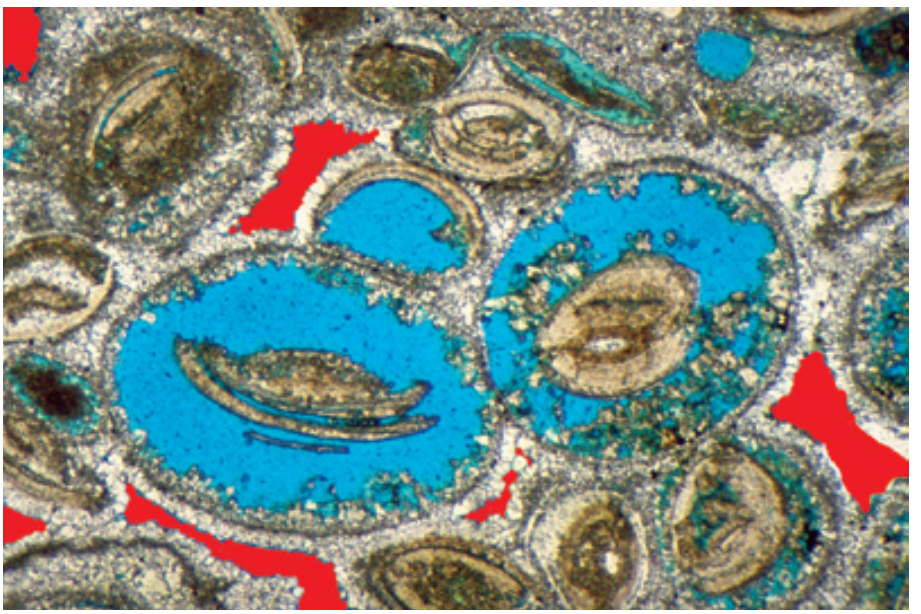

Eocene Green River Fm., Laney Mbr., Fremont Co., Wyoming

Cementation reduced the primary interparticle porosity (colored red using computer processing) in this lacustrine limestone. That was followed by selective leaching of oolitic coatings forming secondary moldic porosity (marked by blue epoxy impregnation). The moldic porosity, in turn, was reduced by further calcite cementation. Computer colorization can help to make the relative volumes of various types of porosity easier to estimate or to measure quantitatively using image analysis programs.

PPL, BSE+, HA = 2.4 mm

Jurassic Ronda unit (Subbetic), near Ronda, Spain

Crystal-moldic porosity produced by selective leaching of dolomite crystals. This is probably a telogenetic (uplift stage) process that is enhanced by the presence of evaporite (sulfate) minerals in the section. Crystal-moldic porosity commonly also results from dissolution of gypsum, anhydrite, halite, and other very soluble minerals.

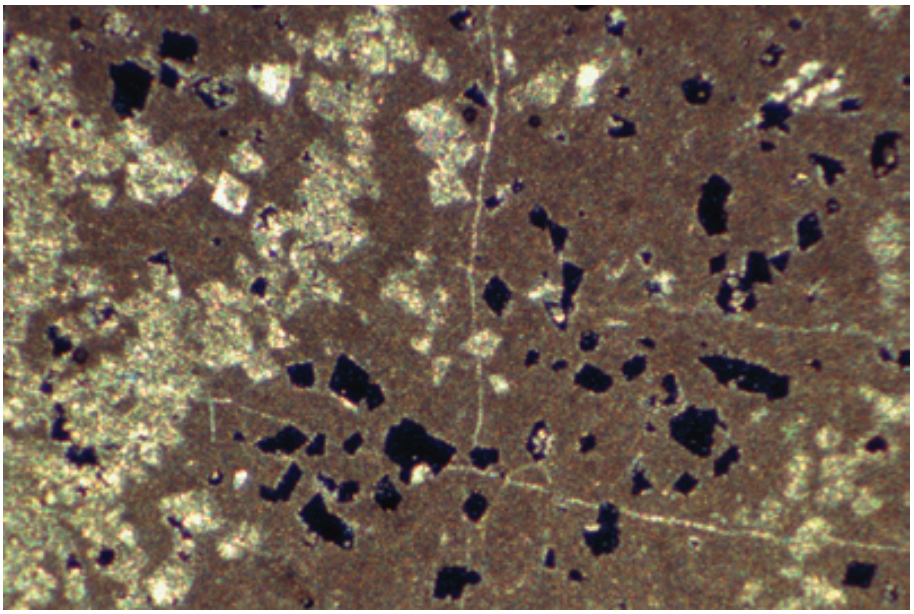

XPL, HA = 3.4 mm

Lo. Permian (Leonardian) Skinner Ranch Fm., Brewster Co., Texas

Intercrystal porosity in a medium to coarsely crystalline replacement dolomite. In a sense, this too is moldic porosity (or enlarged intercrystal porosity) as it involved replacement of a precursor limestone followed by probable dissolution of undolomitized limestone remnants.

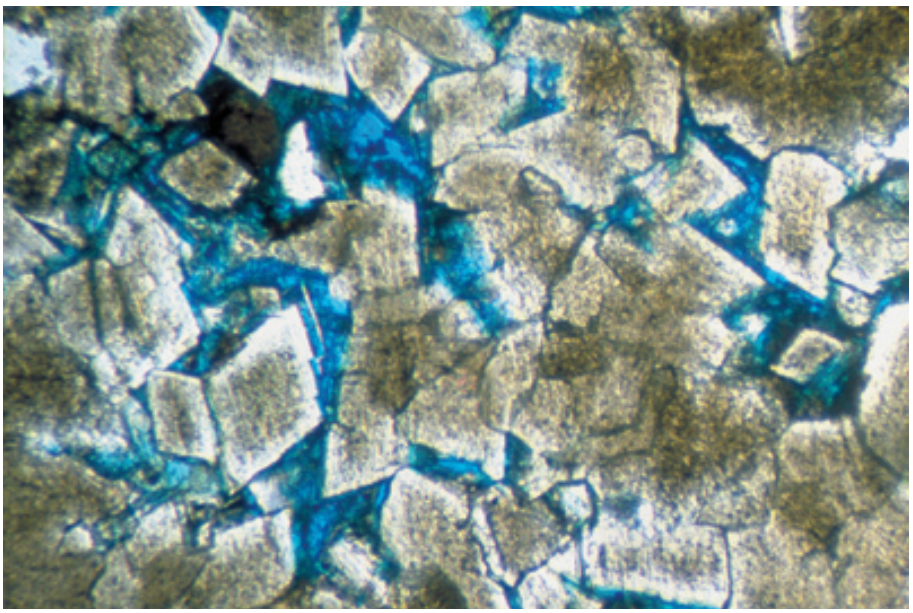

PPL, BSE, HA = 2.0 mm

Lo. Cretaceous (Aptian) Shuaiba Fm., offshore Qatar

Solution-enlarged intercrystal porosity in a medium-crystalline replacement dolomite. The enormous volume of porosity, coupled with the large and irregular shapes of the intercrystal pores relative to the size of the dolomite rhombs, clearly indicates extensive post-dolomite dissolution of calcite matrix.

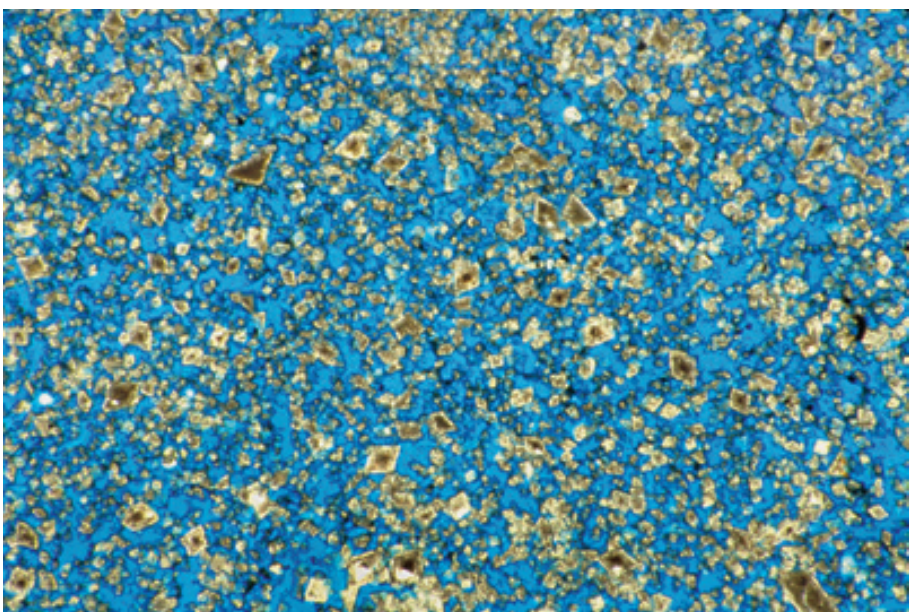

PPL, BSE, AFeS, HA = 5.2 mm

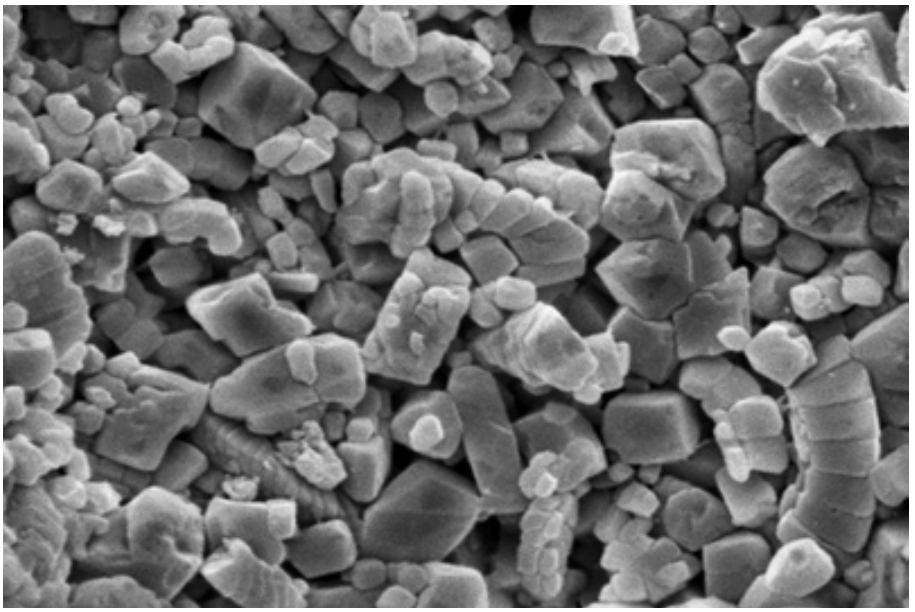

Up. Cretaceous (lo. Maastrichtian) Tor Fm. chalk, Danish North Sea

Substantial intercrystal porosity can be of a size so small that it is impossible to observe with standard light microscopy. This SEM image illustrates chalk microporosity (roughly 25% porosity and 0.5 md permeability) — most individual intercrystal pores are less than 1 μm across and some are smaller than 0.1 μm. Impregnation and pore casting (using ultra-low viscosity impregnation media and vacuum/high pressure techniques) allow 3-D imaging of microporosity networks with an electron microscope.

SEM, HA = 15 μm

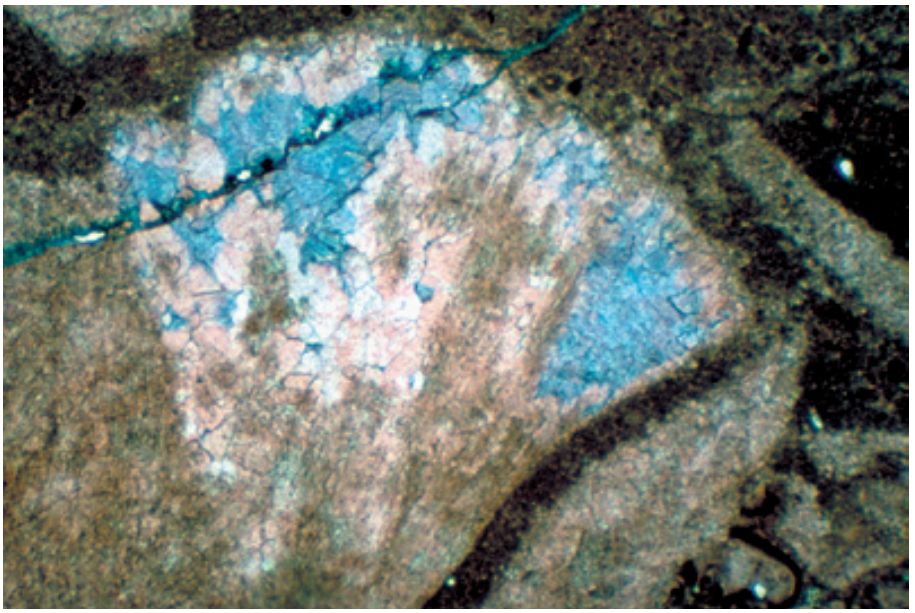

Up. Permian (Kazanian?) Wegener Halvø Fm., Jameson Land, East Greenland

This stained section reveals a complex history of porosity variations. A large void in a bioherm was completely filled with a botryoid of aragonitic marine cement botryoid (still partially visible as cloudy, divergent rays). Subaerial exposure led to partial meteoric leaching of the aragonite cement and partial conversion of it to non-ferroan calcite. The secondary porosity generated by leaching was filled by burial-stage ferroan calcite (stained blue).

PPL, AFeS, HA = 4.1 mm

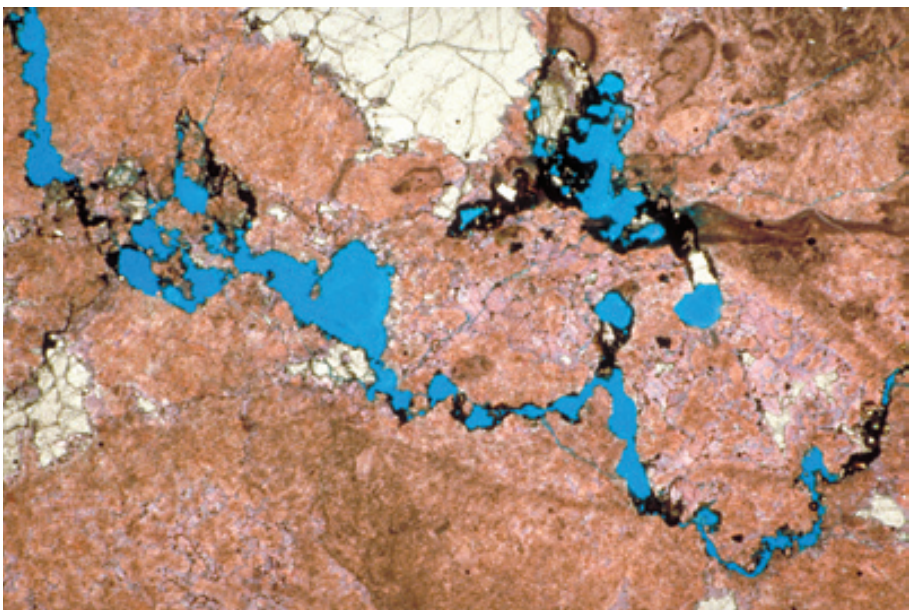

Up. Permian (Kazanian?) Wegener Halvø Fm., Jameson Land, East Greenland

An oblique cut through stylolite-associated porosity. Uplift and load release commonly lead to separation of the rock fabric along weak, sometimes clay-rich stylolites, generating elongate, often unconnected, secondary porosity zones. Hydrocarbon residues are seen throughout these stylolitic pore spaces.

PPL, BSE, AFeS, HA = 10 mm

Up. Permian (Guadalupian) Road Canyon Fm., Brewster Co., Texas

Multiple generations of cement-reduced fracture porosity in a shelf limestone. Note offset of an earlier generation of completely filled fractures by later, partially filled ones. Fracture porosity commonly constitutes only a few percent of total porosity in carbonate rocks; however, it can have a disproportionate importance to permeability and hydrocarbon production because it connects pores that may otherwise be largely isolated.

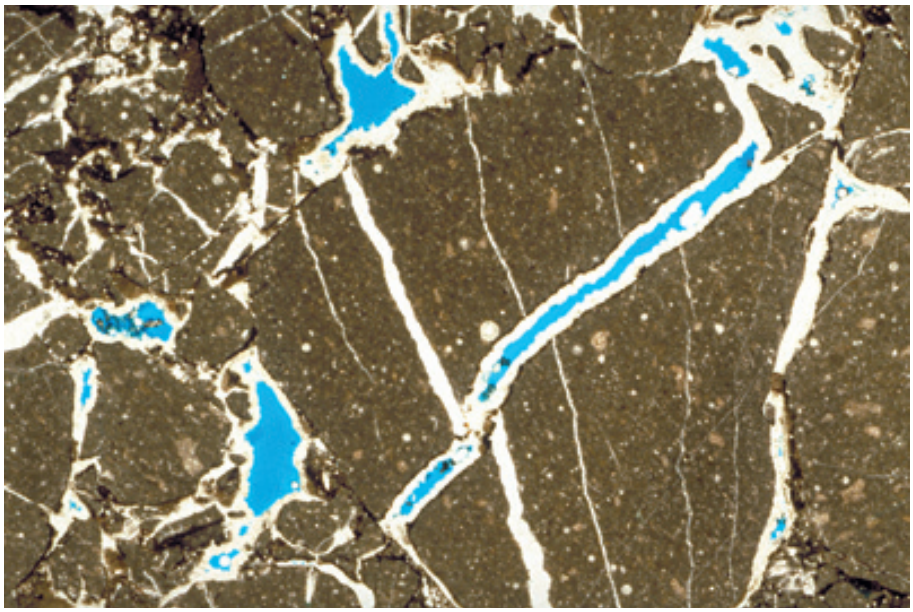

PPL, BSE, HA = 16 mm

Up. Cretaceous limestone, Zakinthos, Ionian Islands, Greece

The irregular shape of this large, porous fracture indicates that some solution-enlargement occurred along the fracture, thus creating what is termed channel porosity in the Choquette and Pray classification.

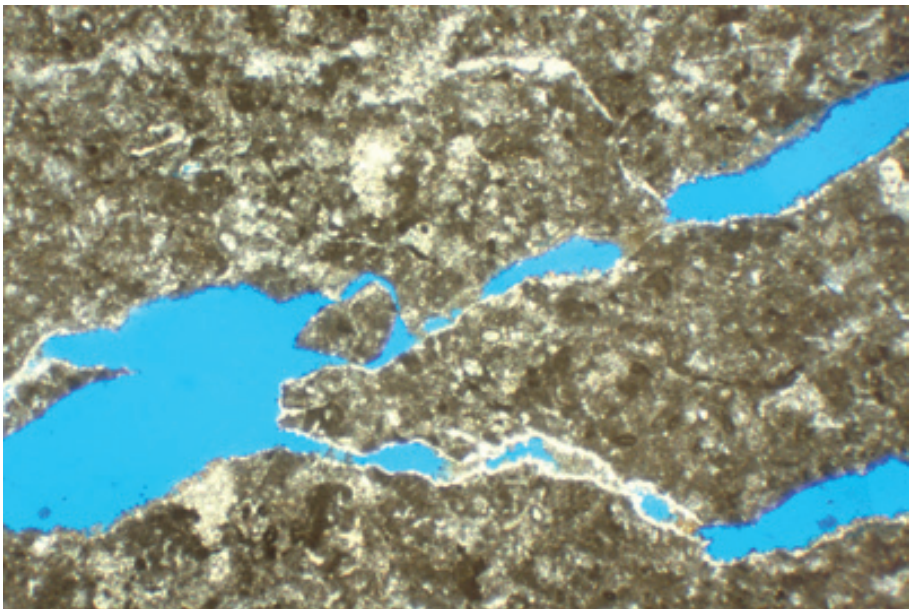

PPL, BSE, HA = 5.1 mm

Pleistocene (120 ky) Coral Rock Fm., St. James Parish, Barbados

An example of vuggy porosity created by roughly 100,000 years of meteoric dissolution. The fact that the size of the pores greatly exceeds the size of surrounding grains is a characteristic feature of vugs.

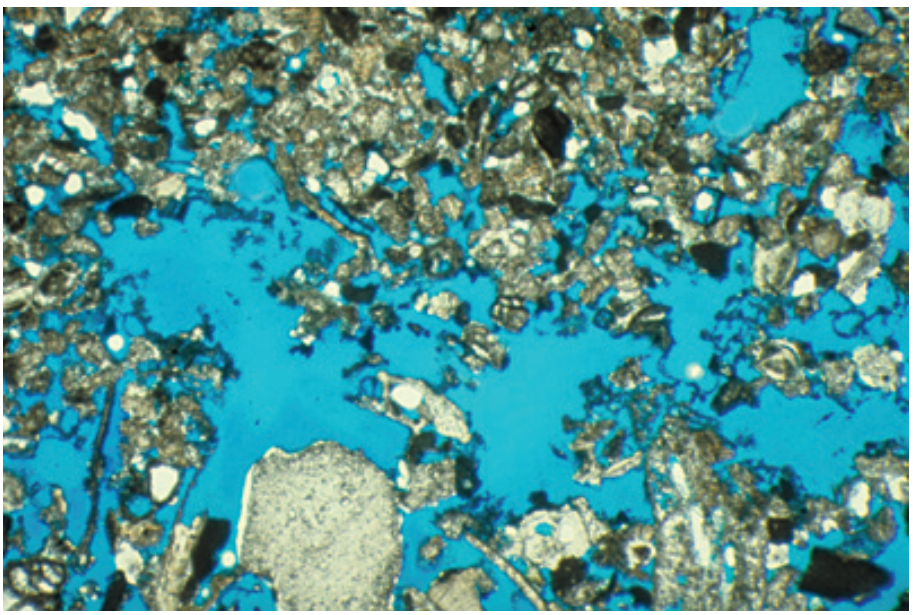

PPL, BSE, HA = 5.1 mm

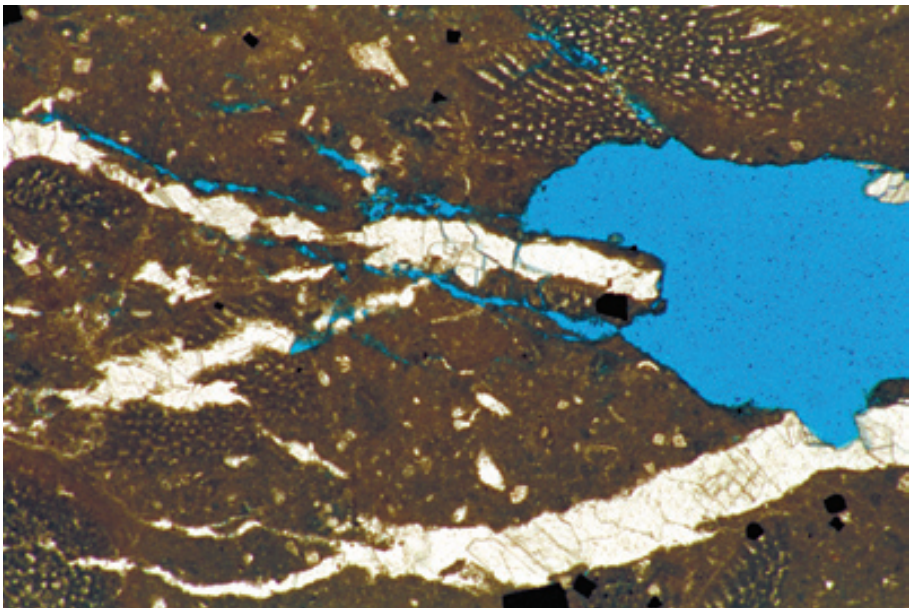

Lo. Cretaceous (Aptian) Shuaiba Fm., offshore Qatar

A large vug resulting from late-stage leaching in a partially dolomitized orbitolinid wackestone. Note the corrosion around earlier calcite-filled fractures indicating that dissolution occurred late in the diagenetic history of this rock. Petrographic observations such as these are essential for the proper understanding of the origin and timing of porosity development or retention in carbonate reservoir rocks.

PPL, BSE, AFeS, HA = 4.0 mm

Cited References and Additional Information Sources

Anselmetti, F. S., S. Luthi, and G. P. Eberli, 1998, Quantitative characterization of carbonate pore systems by digital image analysis: AAPG Bulletin, v. 82, p. 1815-1836.

Choquette, P. W., and L. C. Pray, 1970, Geologic nomenclature and classification of porosity in sedimentary carbonates: American Association of Petroleum Geologists Bulletin, v. 54, p. 207-250.

Ehrlich, R., S. J. Crabtree, K. O. Horkowitz, and J. P. Horkowitz, 1991, Petrography and reservoir physics, I: Objective classification of reservoir porosity: American Association of Petroleum Geologists Bulletin, v. 75, p. 1547-1562.

Enos, P., and L. H. Sawatsky, 1981, Pore networks in Holocene carbonate sediments: Journal of Sedimentary Petrology, v. 51, p. 961-986.

Etrus, E. L., D. S. Brumfield, R. Ehrlich, and S. J. Crabtree, Jr., 1988, Relations between pores, throats, and permeability: a petrographic/physical analysis of some carbonate grainstones and packstones: Carbonates and Evaporites, v. 3, p. 17-32.

Halley, R. B., 1978, Estimating pore and cement volumes in thin section: Journal of Sedimentary Petrology, v. 48, p. 641-650.

Harris, J. F., 1968, Carbonate rock characteristics and effect on oil accumulation in Mid-Continent area: American Association of Petroleum Geologists Bulletin, v. 52, p. 1662-1669.

Heling, D., 1968, Microporosity of carbonate rocks, *in* G. Müller, and G. M. Friedman, eds., Recent Developments in Carbonate Sedimentology in Central Europe: New York, Springer-Verlag, p. 98-105.

Jodry, R. L., 1972, Pore geometry of carbonate rocks — basic geologic concepts, *in* G. V. Chilingar, R. W. Mannon, and H. H. Rieke, eds., Oil and Gas Production from Carbonate Rocks: New York, Elsevier, p. 35-82.

Kopaska-Merkel, D. C., and S. D. Mann, 1993, Classification of lithified carbonates using ternary plots of pore facies: examples from the Jurassic Smackover Formation, *in* R. Rezak, and D. L. Lavoie, eds., Carbonate Microfabrics: New York, Springer-Verlag, p. 265-277.

Lucia, F. J., 1983, Petrophysical parameters estimated from visual descriptions of carbonate rocks: a field classification of carbonate pore space: Journal of Petroleum Technology, v. 35, p. 629-637.

Lucia, F. J., 1995, Rock-fabric/petrophysical classification of carbonate pore space for reservoir characterization: American Association of Petroleum Geologists Bulletin, v. 79, p. 1275-1300.

Lucia, F. J., 1999, Carbonate Reservoir Characterization: New York, NY, Springer-Verlag, 226 p.

Mazzullo, L. J., and P. M. Harris, 1991, An overview of dissolution porosity development in the deep-burial environment, with examples from carbonate reservoirs in the Permian Basin, *in* M. P. Candellaria, ed., Permian Basin Plays — Tomorrow's Technology Today: Midland, TX, West Texas Geological Society Publication No. 91-89, p. 125-138.

Moore, C. H., 1989, Carbonate Diagenesis and Porosity: New York, Elsevier, 338 p.

Moshier, S. O., 1989, Microporosity in micritic limestones: a review: Sedimentary Geology, v. 63, p. 191-216.

Murray, R. C., 1960, Origin of porosity in carbonate rocks: Journal of Sedimentary Petrology, v. 30, p. 59-84.

Pittman, E. D., 1971, Microporosity in carbonate rocks: American Association of Petroleum Geologists Bulletin, v. 55, p. 1873-1881.

Pittman, E. D., and R. W. Duschatko, 1970, Use of pore casts and scanning electron microscopy to study pore geometry: Journal of Sedimentary Petrology, v. 40, p. 1153-1157.

Purser, B. H., A. Brown, and D. M. Aissaoui, 1994, Nature, origins and evolution of porosity in dolomites, *in* B. H. Purser, M. E. Tucker, and D. H. Zenger, eds., Dolomites - A Volume in Honour of Dolomieu: International Association of Sedimentologists Special Publication No. 21: Cambridge, Blackwell Scientific Publications, p. 283-308.

Stout, J. L., 1964, Pore geometry as related to carbonate stratigraphic traps: American Association of Petroleum Geologists Bulletin, v. 48, p. 329-337.

Thomas, G. E., 1962, Grouping of carbonate rocks into textural and porosity units for mapping purposes, *in* W. E. Ham, ed., Classification of Carbonate Rocks—a Symposium: Tulsa, OK, American Association of Petroleum Geologists Memoir 1, p. 193-223.

Waldschmidt, W. A., P. E. Fitzgerald, and C. L. Lunsford, 1956, Classification of porosity and fractures in reservoir rocks: American Association of Petroleum Geologists Bulletin, v. 40, p. 953-974.

Wardlaw, N. C., 1976, Pore geometry of carbonate rocks as revealed by pore casts and capillary pressure: American Association of Petroleum Geologists Bulletin, v. 60, p. 245-257.

Facing Page: Top: Petrographic studies can be "handy" in unraveling complex diagenetic histories. Up. Permian Wegener Halvø Fm., Jameson Land, East Greenland. PPL, AFeS, HA = 2.0 mm.

Bottom: An euhedral authigenic quartz crystal replacing limestone (note abundant carbonate inclusions). Lower Jurassic turbidite limestone, Central High Atlas region, Morocco. PPL, AFeS, HA = 0.65 mm.

CARBONATE DIAGENESIS

PROCESSES AND TERMINOLOGY

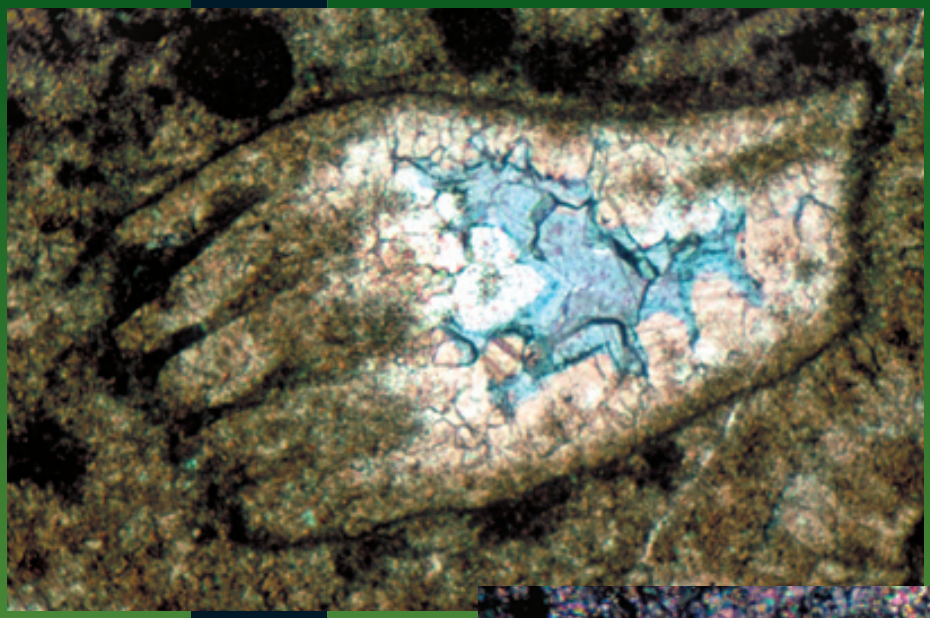

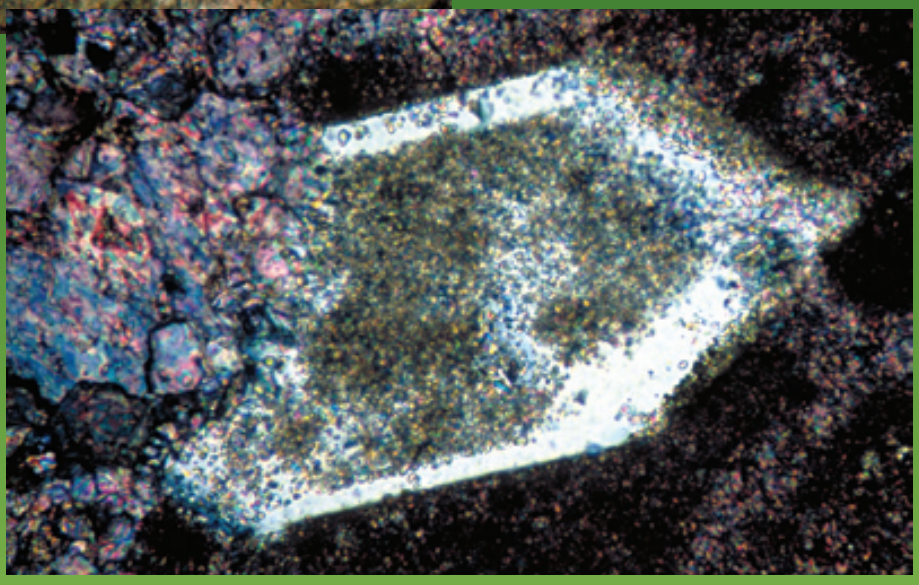

CHAPTER 22

DIAGENETIC PROCESSES AND TERMINOLOGY

Introduction:

Diagenesis encompasses any physical or chemical changes in sediments or sedimentary rocks that occur after deposition (excluding processes involving high enough temperatures and pressures to be called metamorphism). Diagenesis, thus, can begin at the sea floor (syngenetic or eogenetic alteration), continue through deep burial (mesogenetic alteration), and extend to subsequent uplift (telogenetic alteration). Diagenesis can obscure information about primary features, but diagenesis also can leave behind substantial information about the history of post-depositional settings, pore water compositions, and temperatures.

Diagenesis can reduce porosity and permeability, or it can increase them. In general, though, the trend is toward progressive loss of porosity and permeability with increased time and depth of burial, and that shift is commonly quite substantial. The top diagram (opposite page) shows the highly generalized average porosities of modern carbonate sediments, typical ancient carbonates, and the "exceptionally porous" rocks that constitute hydrocarbon reservoirs. Modern sediment porosities range from 35-45% for grainstones to 70% or more for mudstones or chalks. Typical ancient carbonates have less than 5% porosity, and even reservoir rocks average far less than half the porosity of their modern carbonate equivalents. Thus, understanding diagenetic processes, the factors that inhibit porosity loss, and the relative timing of oil migration versus porosity evolution are critical to exploration for hydrocarbons and carbonate-hosted mineral deposits.

Diagenesis typically involves a variety of physical and chemical processes — the most common of these are:

1. Cementation (the filling of open pore space, of primary or secondary origin, with newly precipitated materials)
2. Dissolution (the leaching of unstable minerals forming secondary pores, vugs, or caverns)
3. Replacement of one mineral by another (or "inversion", the replacement of one polymorph of a mineral by another)
4. Recrystallization or strain recrystallization (changes in crystal size, strain state, or geometry without change in mineralogy)
5. Physical or mechanical compaction (including dewatering and deformation or reorientation of grains)
6. Chemical compaction (dissolution mainly along surfaces such as stylolites or solution seams)
7. Fracturing

The terminology applied to such a complex range of carbonate diagenetic processes and products is understandably also complex and is generally applied with disconcerting inconsistency. Folk (1965) provided what is still the most concise, yet inclusive, terminology for diagenetic fabrics. Pore-filling cements are described based on their mode of formation (passive or displacive precipitation), crystal morphology (based on length-width ratios as shown in the middle diagram, facing page), crystal size (see table in limestone classification chapter), and relationship to foundation (overgrowth, crust, or spherulitic growth without obvious nucleus).

The Folk (1965) terminology for the complex group of processes loosely termed "recrystallization" is shown and explained on the bottom diagram (facing page). Of particular note are two useful terms: "solution and cavity fill" which describes the common two-stage diagenetic process of dissolution of one mineral forming a void that is filled by later (sometimes much later) precipitation of a different mineral; the second term, "neomorphism", is a "term of ignorance" for all diagenetic transformations between one mineral and itself or a polymorph, whether the new crystals are larger or smaller, simply differ in shape from the previous ones, or represent a new mineral species. This is an essential term when there is uncertainty about the precursor mineral(s).

This chapter illustrates some of the main types of diagenesis to clarify their nomenclature. However, because the purpose of most diagenetic studies is to interpret the origin and timing of alteration, the details of diagenesis will be presented by environment: synsedimentary marine processes, subaerial (meteoric and shallow phreatic) alteration, and burial diagenesis. This mixes different processes (dissolution, precipitation, recrystallization) together, but it allows the presentation of a more unified picture of the fabrics indicative of different stages and environments of alteration. Alteration by non-calcium carbonate minerals (dolomite, siderite, silica, evaporites, and others) is dealt with in separate chapters.

Although the diagenetic products of different environments are presented separately in this book, most ancient limestones contain a mix of features generated in different settings. Often, the most useful part of petrographic studies is the determination of the sequencing (termed paragenesis) of diagenetic events relative to each other and to external marker events (uplift, hydrocarbon generation, and others).

A comparison of porosities in modern and ancient carbonate deposits

A generalized plot showing the remarkable difference in porosities among typical modern carbonate sediments, ancient carbonate strata, and typical carbonate hydrocarbon-reservoir rocks. The porosity loss is related to a variety of marine, meteoric, and burial diagenetic processes that act throughout the syn- and post-depositional history of these strata. Redrawn from a 1966 slide by Lloyd Pray and Phillip Choquette.

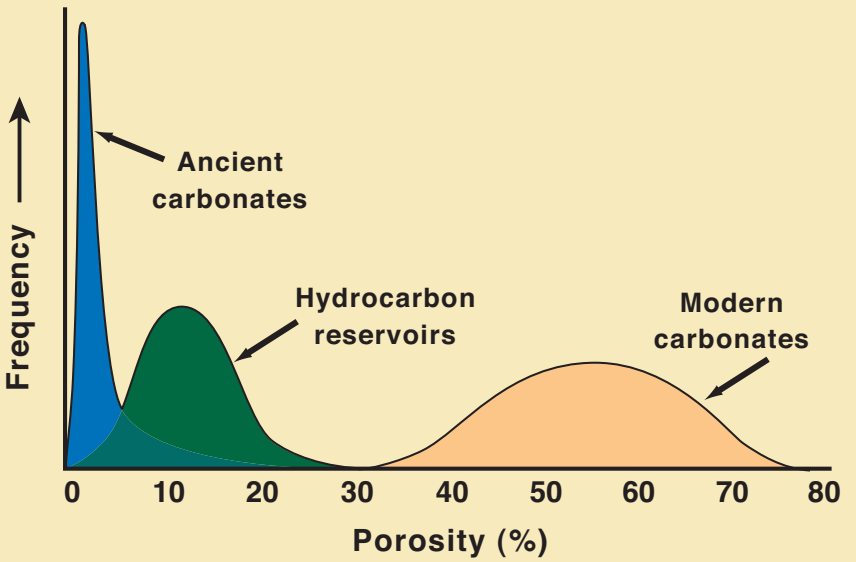

Folk (1965) terminology for carbonate crystal shapes

Carbonate crystal shapes are classified based on their relative length to width ratios. Highly elongate (fibrous) crystals have length to width ratios greater than 6 to 1. Equant crystals have length to width ratios of less than 1.5 to 1. Bladed crystals have length to width ratios intermediate between those of fibrous and equant crystals. The Folk classification also includes crystal size terms and terms describing the relationship between cement and substrate (crust, overgrowth, or spherulite).

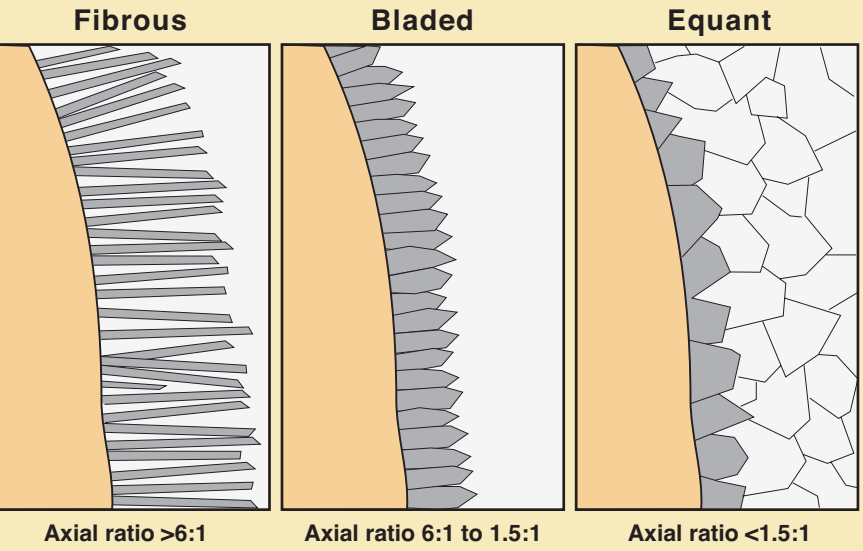

Folk (1965) terminology for diagenetic mineral alteration processes

This classification of carbonate diagenetic phenomena is based on a determination of the operative alteration processes as interpreted from the compositional and textural relationships between precursor and successor minerals. This table describes those process and gives examples of the types of transformations involved in each case.

PROCESS	EXAMPLE	FOLK (1965) TERMINOLOGY Loose usage / Strict usage
One mineral replaces another of different composition	Calcite → dolomite, pyrite, etc.	REPLACEMENT
A mineral is replaced by its polymorph	Aragonite mud or shell → calcite mosaic	REPLACEMENT (LOOSELY) / RECRYSTALLIZATION / INVERSION / NEOMORPHISM
Deformed mineral changes to a mosaic of undeformed crystals of same mineral	Strained calcite → unstrained calcite	REPLACEMENT (LOOSELY) / RECRYSTALLIZATION / STRAIN RECRYSTALLIZATION / NEOMORPHISM
An undeformed mineral changes its form, grain size or orientation	Calcite mud or fibers → calcite mosaic, etc.	REPLACEMENT (LOOSELY) / RECRYSTALLIZATION (AND DEGRADING RECRYSTALLIZATION) / NEOMORPHISM
A mineral dissolves leaving a cavity; cavity is filled later	Allochem → cavity → calcite	SOLUTION-CAVITY FILL

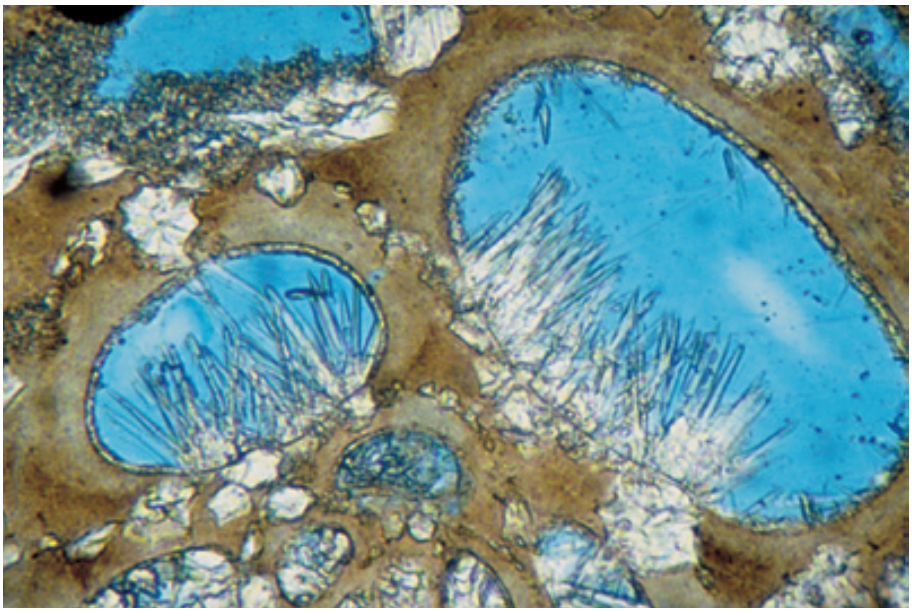

Recent beachrock, Grand Cayman, Cayman Islands, B.W.I.

Cementation: fibrous (also called acicular), marine cement here partially fills foraminiferal chambers. The relationship of this fibrous aragonite cement to its substrate would be termed a "crust" in the Folk (1965) terminology (as opposed to an "overgrowth" or a "spherulitic growth"). Most modern marine aragonite cement has a fibrous, encrusting habit.

PPL, BSE, HA = 0.42 mm

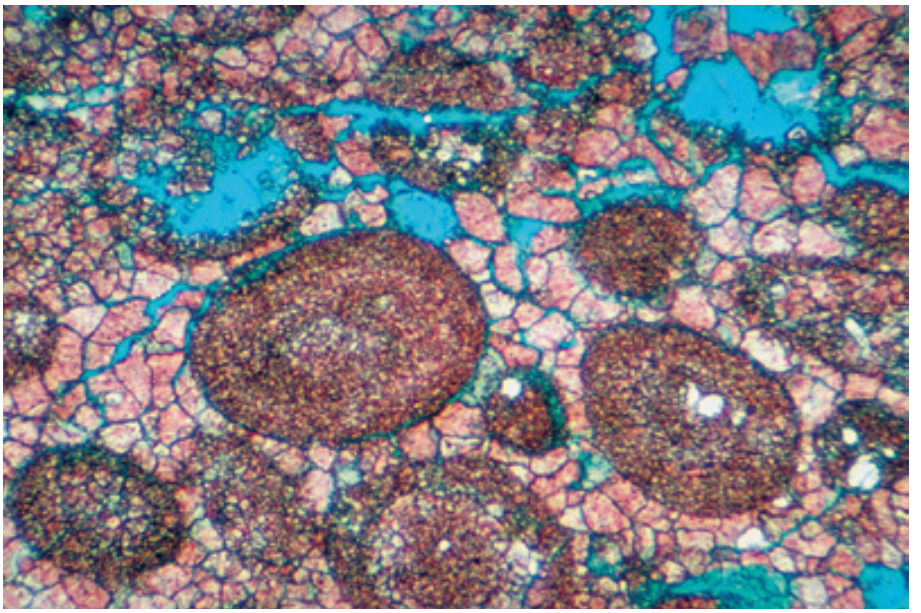

Up. Permian (Kazanian?) Wegener Halvø Fm., Jameson Land, East Greenland

Cementation: equant or blocky calcite spar cementing a meteorically altered oolitic limestone. Cement infill of primary porosity probably was temporally associated with the leaching of originally aragonitic grains.

PPL, BSE, AFeS, HA = 2.0 mm

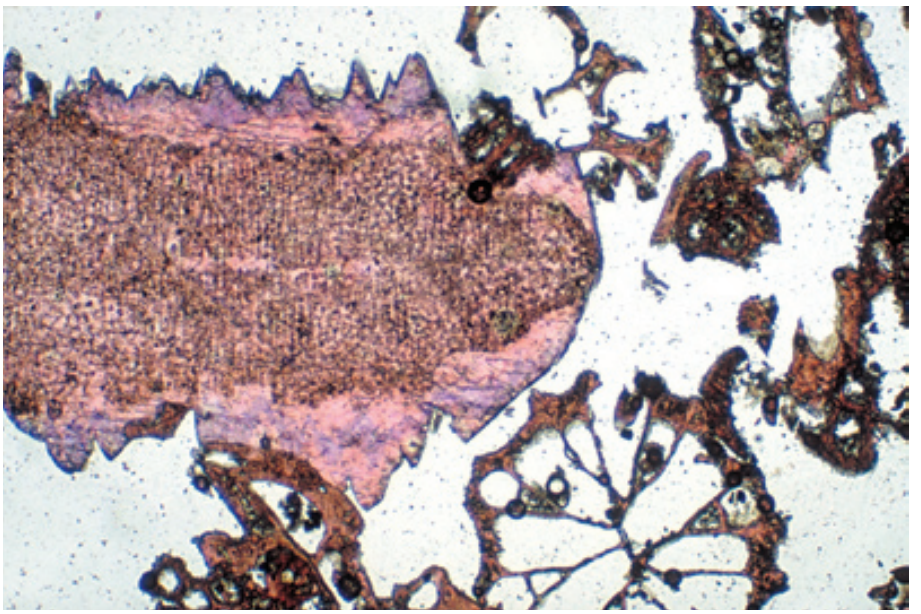

Oligocene Gambier Fm., South Australia

Cementation: a skeletal grainstone composed of bryozoans with no cement and an echinoid fragment with zoned syntaxial overgrowth cement — the early non-ferroan, intermediate ferroan, and late non-ferroan stages have been revealed by staining. Such syntaxial cements form as overgrowths in optical continuity with their substrate. In the case of large echinoderm overgrowths, such cements may form over long periods of time, from the earliest stages of marine diagenesis through extensive burial. Photograph courtesy of Noel P. James.

PPL, AFeS, HA = 1.0 mm

Cretaceous White Ls., Co. Antrim, Northern Ireland

Cementation: an SEM image showing that the process of overgrowth cementation also occurs during burial diagenesis of microcrystalline grains. This single coccolith shield isolated inside a foraminiferal chamber has had differential overgrowth of its individual radial calcite elements, each of which was originally the same length. Even the large, pore filling calcite crystals are in crystallographic continuity with one of the coccolith elements. Such overgrowth crystals are much more difficult to identify, however, when they occur in the jumbled matrix of a chalk.

SEM, HA = ~18 μm

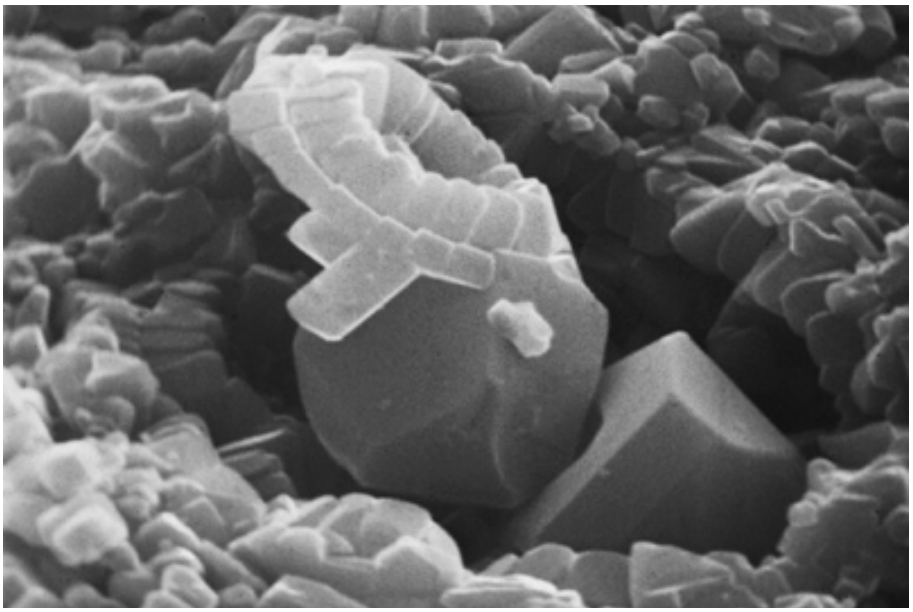

Holocene sediment, Dead Sea, Israel and Jordan

Cementation: spherulitic growth of fibrous calcite. An SEM image of bundles of aragonite from a core retrieved from the northern basin of the Dead Sea. Although these may be primary precipitates rather than diagenetic products, they do illustrate the Folk (1965) concept of spherulitic growth with no obvious nucleus. Primary spherules may undergo diagenetic overgrowth that preserves and enlarges the radiating fabric. Photograph courtesy of Raymond A. Garber.

SEM, HA = ~95 μm

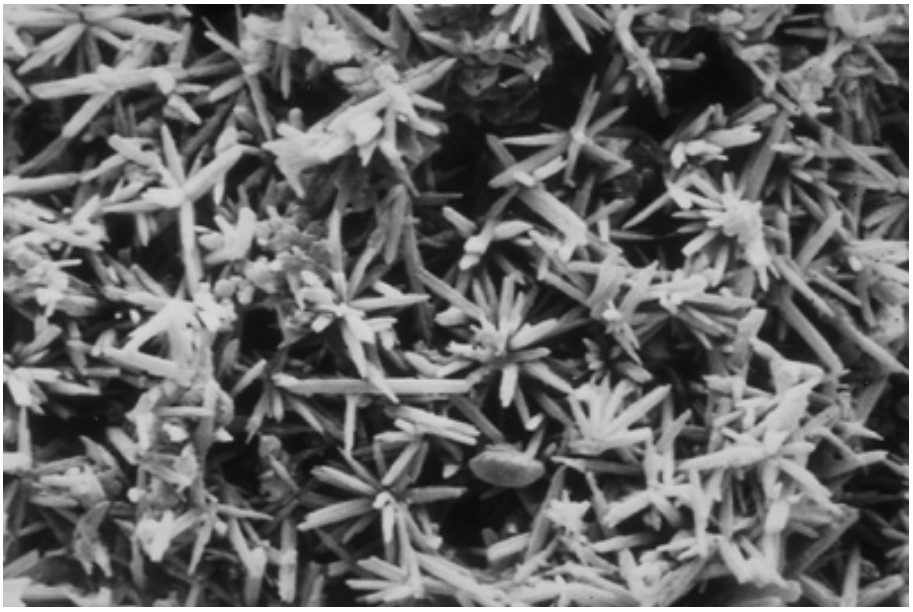

Up. Permian reefal ls., Guangxi Province, People's Republic of China

Cementation: radiaxial-fibrous calcite cements growing as a crust on an *Archaeolithoporella* reefal boundstone (left). Radiaxial-fibrous calcite (RFC) mosaics consist of fibrous crystals (and subcrystals) radiating away from the initial growth surface and allied to optic axes that converge away from the pore wall. RFC is characterized by curved cleavages (well shown in this example), undulose extinction, and irregular intergranular boundaries which distinguish this fabric from simple radial-fibrous calcite.

PPL, HA = 8.0 mm

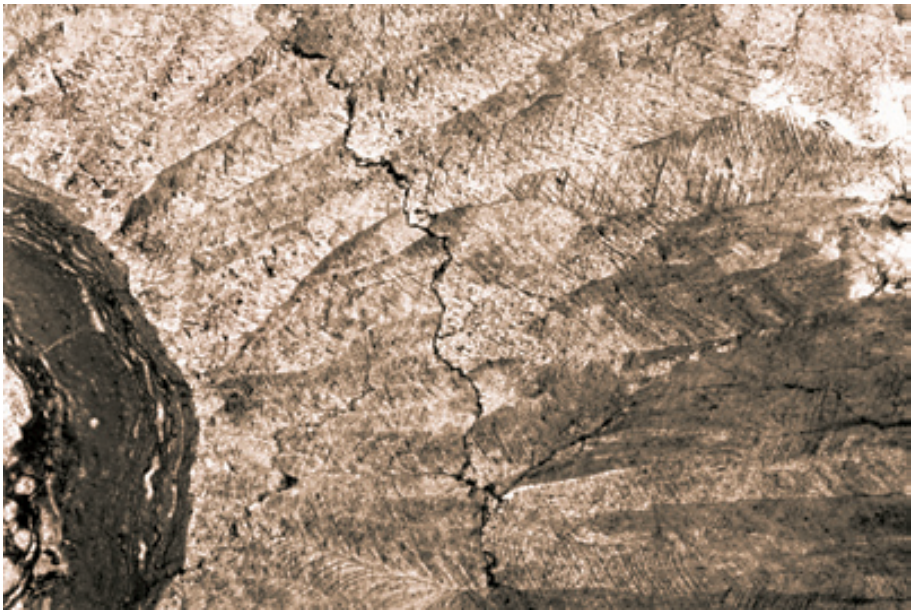

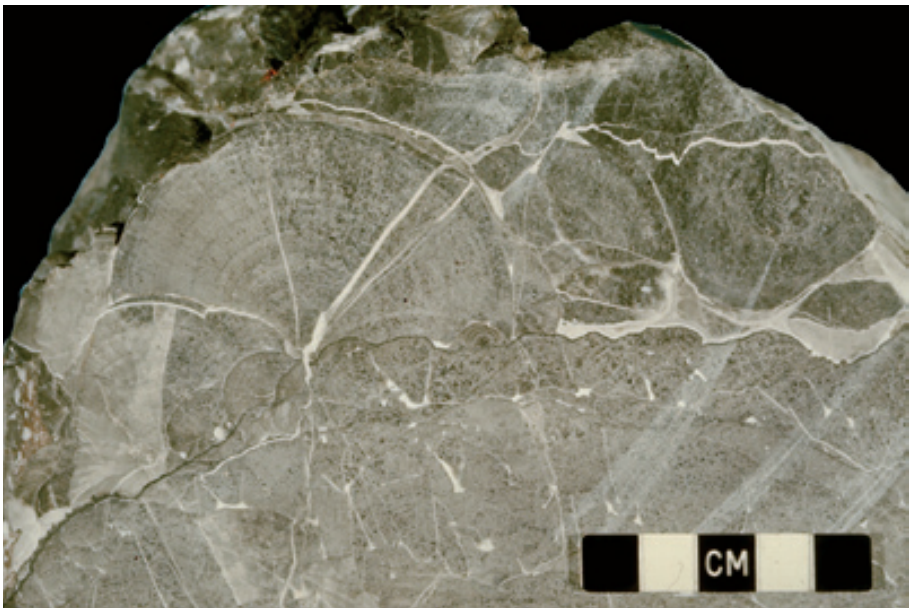

Lo. Permian? Nansen Fm., Ellesmere Island, Arctic Archipelago, Canada

Cementation: botryoidal cements. These large botryoids of radial-array calcite (after submarine botryoidal aragonite) are cut by fractures lined by radial-fibrous calcite (after Mg calcite submarine cement). Botryoidal growth forms are hemispherical arrays of fibrous crystals that commonly have formed as seafloor growths or as growths within large reefal cavities. Microprobe and chemical analyses show preservation of up to 8,000 ppm Sr in this replacement calcite after aragonite. Photograph courtesy of Graham R. Davies.

Mac, HA = 16 cm

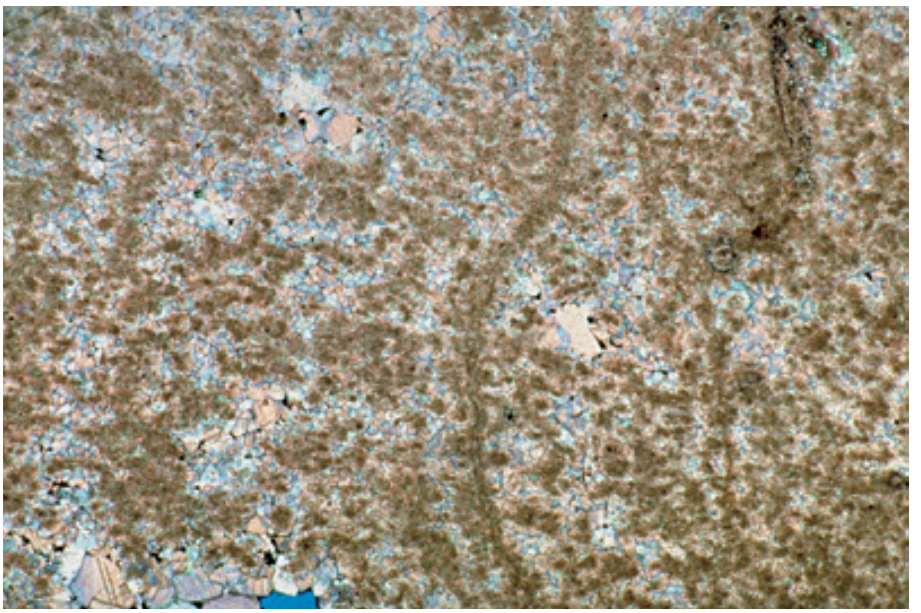

Up. Permian (Kazanian?) Wegener Halvø Fm., Jameson Land, East Greenland

Cementation: a detailed view of a small portion of a large botryoid of marine cement. This cement, from a bryozoan bioherm, has an organized peloidal fabric. Such (originally high-Mg calcite?) peloids may be inorganic or, more likely, represent bacterially-induced precipitates that were intergrown with inorganic fibrous aragonite. The aragonite was subsequently dissolved and the voids filled with non-ferroan to slightly ferroan calcite (pink to blue stained). This is an example of the complex diagenetic history to which even cements are subject.

PPL, BSE, AFeS, HA = 11 mm

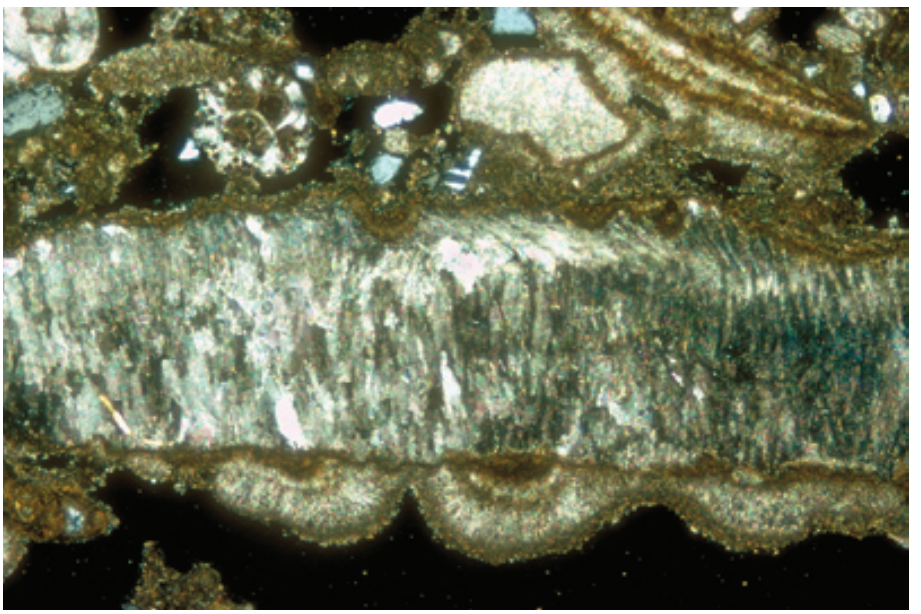

Holocene limestone, Abu Dhabi, United Arab Emirates

Cementation: the spatial distribution and composition of cements are important factors in the interpretation of their origin. These coastal spray-zone cements show a pendant (gravitational or microstalactitic) morphology beneath a bivalve shell. That is, the small cement botryoids are found only on the undersides of the grain, where water droplets hang in a vadose setting. The mineralogy (banded fibrous aragonite and microcrystalline high-Mg calcite), however, indicates a marine source of water. This combination of vadose conditions and saline fluids occurs primarily, but not exclusively, in marine coastal settings.

XPL, HA = ~12.5 mm

Lo. Cretaceous (Albian) Up. Folkestone Beds, Kent, England, U.K.

Cementation: a poikilitic calcite cement in a calcareous sandstone. Poikilitic (or poikilotopic) cements have small granular crystals or grains (here clastic terrigenous sand grains) that are irregularly scattered without common orientation in a larger crystal of another mineral (generally, calcite or gypsum). Poikilitic calcite cements can have an overgrowth relationship to a carbonate grain, such as an echinoderm fragment, that may or may not be visible in the plane of section.

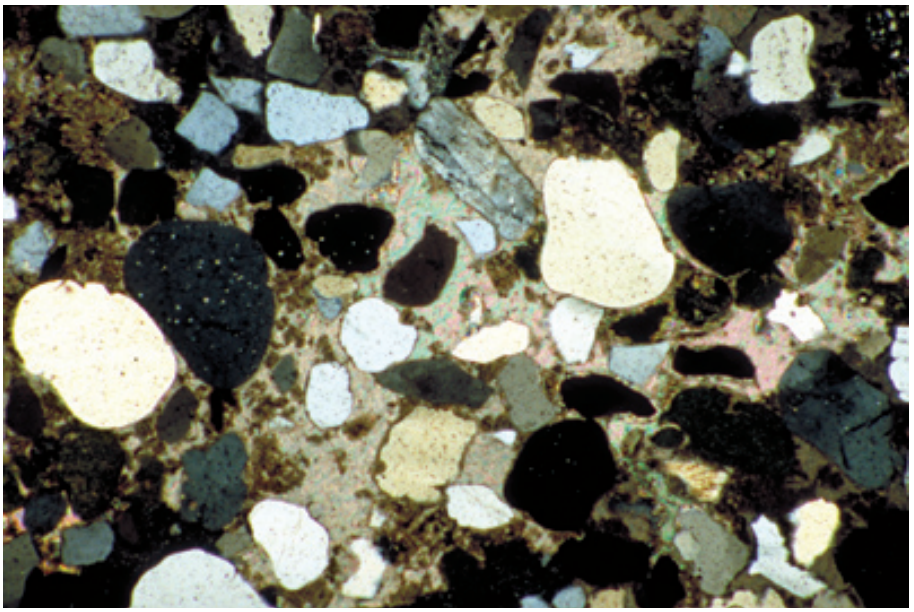

XPL, HA = 3.5 mm

Mid-Cretaceous Tamabra Ls., San Luis Potosí, Mexico

Cementation and infiltration: this combination of marine cements coupled with layered internal sediment reflects a diagenetic history that is apparently completely marine. A thick band of radiaxial-fibrous calcite cement lines all former pores. The marine cement is overlain by vaguely layered, peloidal internal sediment containing sparse planktonic fossils. A second thin layer of marine cement and another deposit of micritic sediment with planktonic fossils is visible near the top of the image. Such multigenerational interlayers of cement and sediment are common in reefal and biohermal limestones. Photograph courtesy of Paul Enos.

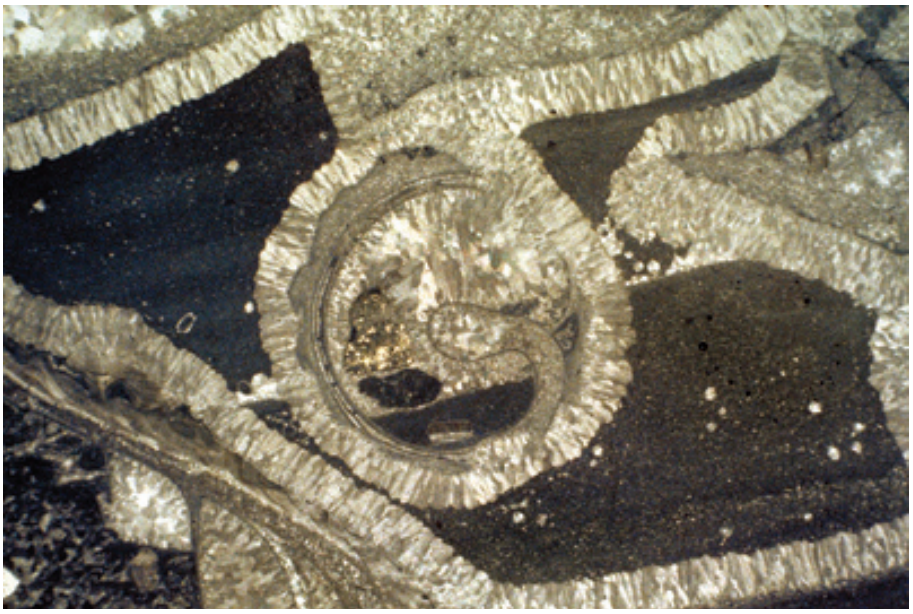

PPL, HA = 35 mm

Holocene (<2700 yBP) eolianite, Isla Cancun, Quintana Roo, Mexico

Dissolution (leaching): an oolitic eolianite with substantial leaching of originally aragonitic ooids as a result of meteoric exposure. Accompanying cementation by equant calcite has completely occluded primary interparticle porosity. Photograph courtesy of Robert G. Loucks.

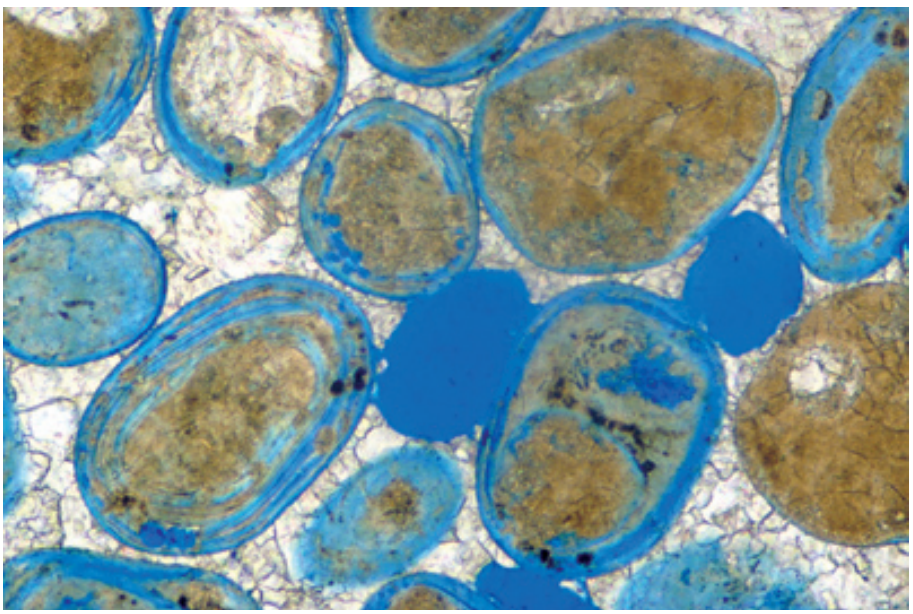

PPL, BSE, HA = 0.83 mm

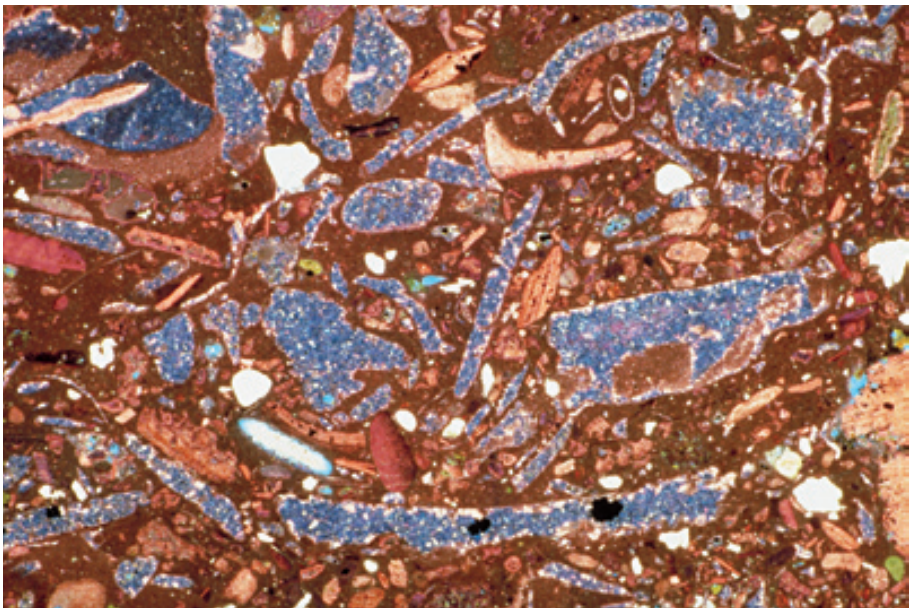

Oligocene Nile Gp., Karamea, Westland, New Zealand

Aragonite inversion (solution-fill): secondary (leached bivalve) porosity was selectively filled, first with a thin coating of non-ferroan cement (pale pink), and later by ferroan calcite cement (stained purple-blue). These relations, coupled with collapsed fills of shell borings, indicate a void phase (and a temporal gap) between dissolution and cementation.

PPL, BSE, AFeS, HA = 12.5 mm

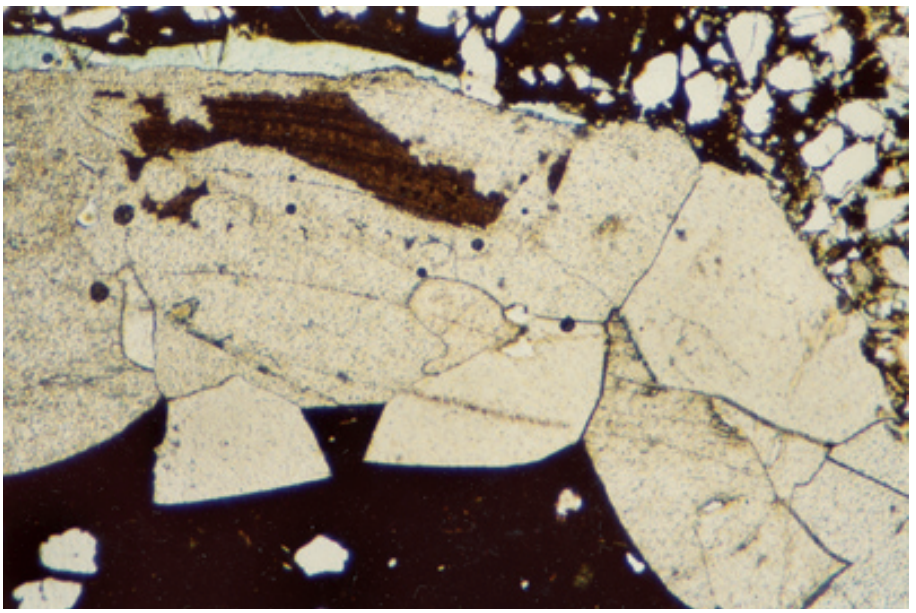

Plio-Pleistocene Caloosahatchee Fm., Glades Co., Florida

Inversion: an example of partial inversion of a vermetid gastropod shell. The patchy brown inclusions are unaltered remnants of the primary aragonitic shell while the rest of the shell has been converted to coarsely crystalline sparry calcite. Virtually no relict textures are visible in inverted areas, yet it is unlikely that a void space was ever present because there has been no collapse of the small remnants of primary shell. Also note the extension of calcite crystals into the cavity-filling micrite through displacement or replacement.

PPL, BSE, HA = 5.7 mm

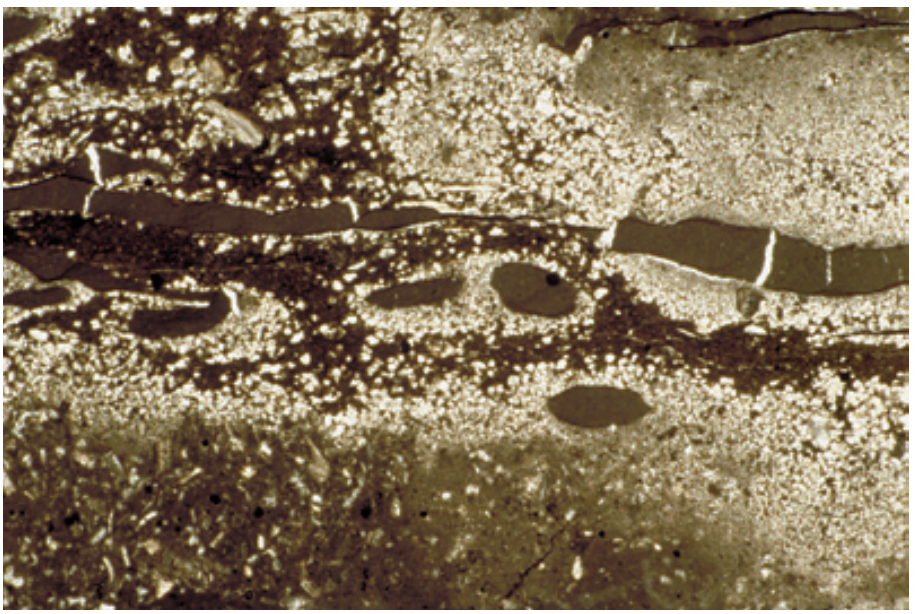

Mid. Ordovician Chazy-Black River Fms., Mifflin Co., Pennsylvania

Recrystallization (or aggrading neomorphism): a transition from micrite to microspar and pseudospar (a case of probably unstrained micrite crystals undergoing a process of growth or coalescence, to form larger crystals. Note the characteristic bladed shapes of the pseudospar crystals and the remnants of unaltered matrix between those crystals (also see "Matrix" chapter). If the precursor micrite was calcitic, then "recrystallization" is the proper term for this diagenetic alteration. If one does not know the precursor mineral composition, then "aggrading neomorphism" would be the better term to use.

PPL, HA = 10 mm

Up. Cambrian Riley Fm., Lion Mountain Ss. Mbr., Burnet Co., Texas

Replacement: euhedral, ferroan dolomite replacement crystals in a limestone. The critical part of the definition of replacement is that the host mineral and its successor have different compositions (that is, that they are not polymorphs of each other). In this case, although both minerals are carbonates, they are compositionally quite distinct and clearly qualify as different minerals.

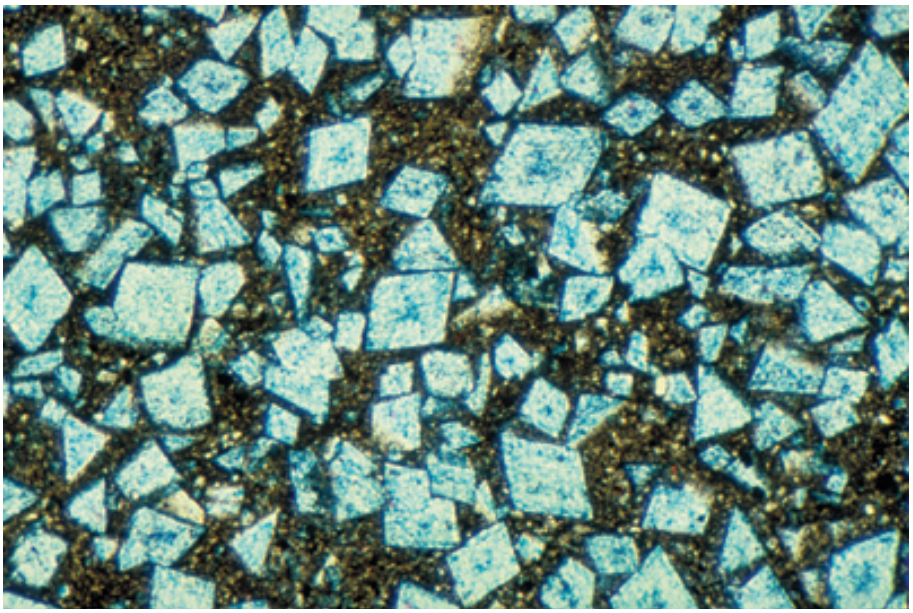

PPL, AFeS, HA = 2.4 mm

Up. Cambrian Beekmantown Gp., Mines Dolomite, Centre Co., Pennsylvania

Replacement: a silicified oolitic limestone. Chert and megaquartz are the main forms of replacement silica in this sample and both show characteristic low birefringence. The original carbonate fabric is well preserved due to the incorporation of small mineral and fluid inclusions in the silica.

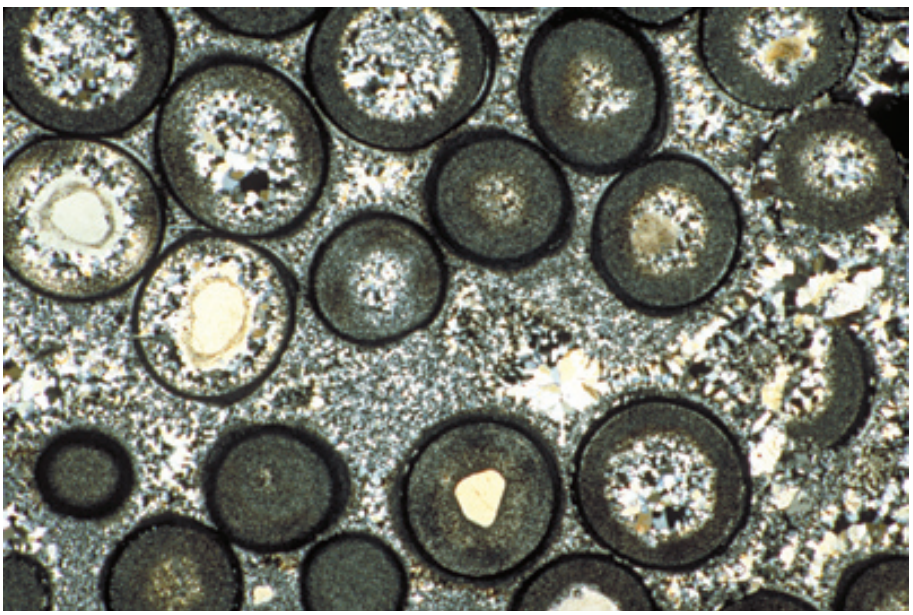

XPL, HA = 6.0 mm

Lo. Cretaceous Paw Paw Fm., Quarry Ls., Grayson Co., Texas

Mechanical compaction: fracturing of bivalve shells followed by late-stage ferroan calcite cementation. The shattering of relatively strong shells occurs mainly in grainstones that underwent little or no cementation prior to burial and overburden loading. Mechanical compaction includes dewatering, grain reorientation, and brittle or plastic grain deformation and it accounts for substantial porosity loss in many carbonate deposits, especially fine grained ones.

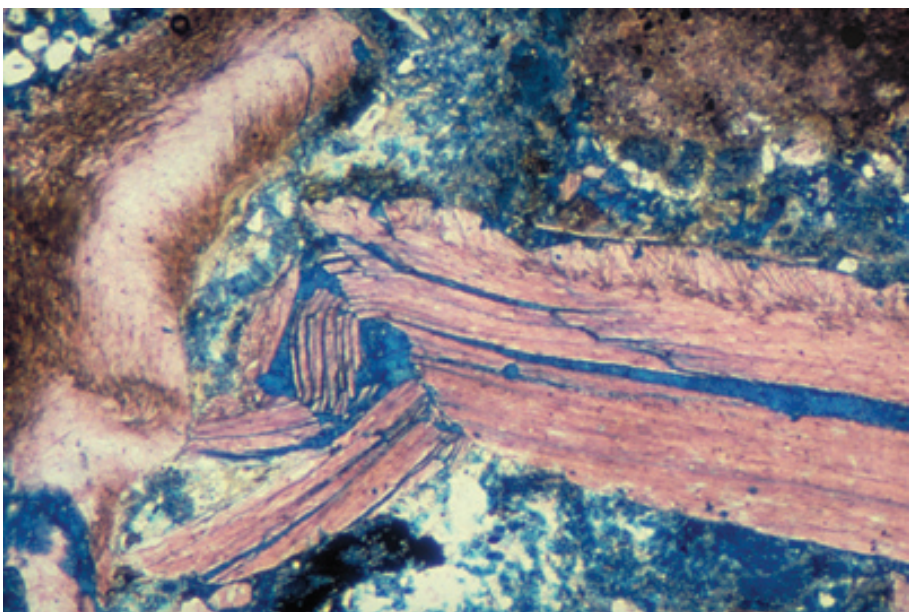

PPL, AFeS, HA = 1.6 mm

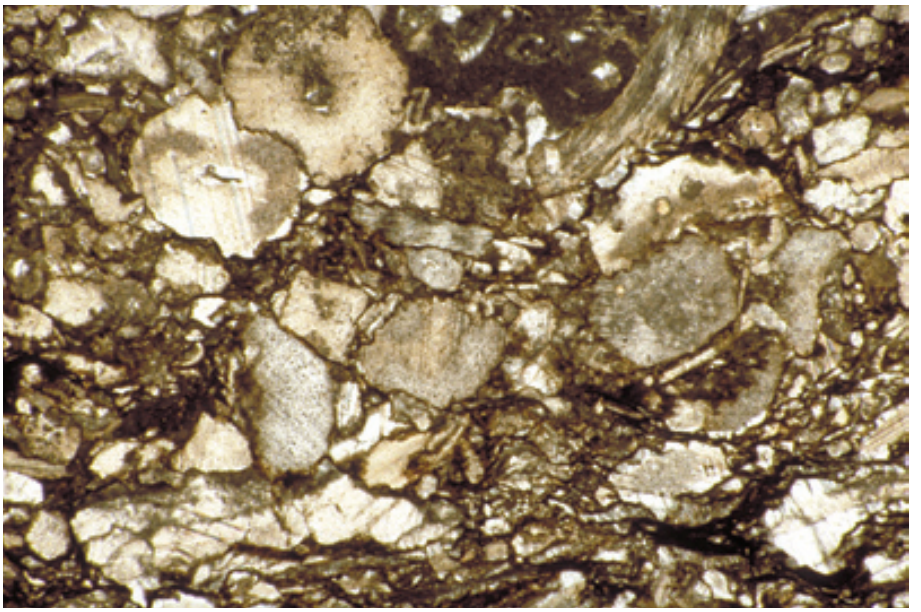

Up. Silurian Tonoloway-Keyser Ls., Mifflin Co., Pennsylvania

Chemical compaction: a crinoidal limestone (encrinite) with sutured contacts and solution seams (irregular brown zones) between most adjacent grains. These features indicate extensive chemical compaction (pressure solution) during burial of the limestone. The compaction here postdates syntaxial overgrowths on some of the crinoids.

PPL, HA = 5.7 mm

Cited References and Additional Information Sources

Banner, F. T., and G. V. Wood, 1964, Recrystallization in microfossiliferous limestone: Geological Journal, v. 4, p. 21-34.

Bathurst, R. G. C., 1958, Diagenetic fabrics in some British Dinantian limestones: Liverpool and Manchester Geological Journal, v. 2, p. 11-36.

Bathurst, R. G. C., 1975, Carbonate Sediments and their Diagenesis: New York, Elsevier Science Publ. Co., 658 p.

Bathurst, R. G. C., 1979, Diagenesis in carbonate sediments: a review: Geologische Rundschau, v. 68, p. 848-855.

Bathurst, R. G. C., 1993, Microfabrics in carbonate diagenesis: a critical look at forty years in research, *in* R. Rezak, and D. L. Lavoie, eds., Carbonate Microfabrics: New York, Springer-Verlag, p. 3-14.

Chanda, S. K., 1967, Selective recrystallization in limestones: Sedimentology, v. 8, p. 73-76.

Chilingar, G. V., D. H. Zenger, H. J. Bissell, and K. H. Wolf, 1979, Diagenesis of carbonate sediments and epigenesis (or catagenesis) of limestones, *in* G. Larsen, and G. V. Chilingar, eds., Diagenesis in Sediments and Sedimentary Rocks: Developments in Sedimentology 25A: New York, Elsevier Scientific Publishing Co., p. 249-424.

Dickson, J. A. D., 1993, Crystal growth diagrams as an aid to interpreting the fabrics of calcite aggregates: Journal of Sedimentary Petrology, v. 63, p. 1-17.

Folk, R. L., 1965, Some aspects of recrystallization in ancient limestones, *in* L. C. Pray, and R. S. Murray, eds., Dolomitization and Limestone Diagenesis: Tulsa, OK, SEPM Special Publication No. 13, p. 14-48.

Folk, R. L., 1971, Unusual neomorphism of micrite, *in* O. P. Bricker, ed., Carbonate Cements: Baltimore, MD, The Johns Hopkins Press, p. 163-166.

Griggs, D. T., M. S. Patterson, H. C. Heard, and F. J. Turner, 1960, Annealing recrystallization in calcite crystals and aggregates, *in* D. T. Griggs, and J. Handin, eds., Rock Deformation, A Symposium: New York, Geological Society of America Memoir 79, p. 21-37.

Hugman, R. H. H., and M. Friedman, 1979, Annealing recrystallization in calcite crystals and aggregates: American Association of Petroleum Geologists Bulletin, v. 63, p. 1478-1489.

James, N. P., and P. W. Choquette, 1983, Diagenesis 5. Limestones: Introduction: Geoscience Canada, v. 10, p. 159-161.

Kennedy, L. A., and J. C. White, 2001, Low-temperature recrystallization in calcite: Mechanisms and consequences: Geology, v. 29, p. 1027-1030.

Larsen, G., and G. V. Chilingar, eds., 1979, Diagenesis in Sediments and Sedimentary Rocks, v. 1: New York, Elsevier, 579 p.

Larsen, G., and G. V. Chilingar, eds., 1983, Diagenesis in Sediments and Sedimentary Rocks, v. 2: New York, Elsevier, 572 p.

Machel, H. G., 1997, Recrystallization versus neomorphism, and the concept of "significant recrystallization" in dolomite research: Sedimentary Geology, v. 113, p. 161-168.

Maliva, R. G., and J. A. D. Dickson, 1992, The mechanism of skeletal aragonite neomorphism: evidence from neomorphosed mollusks from the Purbeck Formation (Late Jurassic-Early Cretaceous), southern England: Sedimentary Geology, v. 76, p. 221-232.

Martin, G. D., B. H. Wilkinson, and K. C. Lohmann, 1986, The role of skeletal porosity in aragonite neomorphism — *Strombus* and *Montastrea* from the Pleistocene Key Largo Limestone, Florida: Journal of Sedimentary Petrology, v. 56, p. 194-203.

Misik, M., ed., 1968, Some aspects of diagenetic recrystallization in limestones: Prague, International Geological Congress, Report of 23rd Session (Prague), Proceedings of Section 8 - Genesis and Classification of Sedimentary Rocks, 129-136 p.

Moore, C. H., 1989, Carbonate Diagenesis and Porosity [Developments in Sedimentology, 46]: New York, Elsevier, 338 p.

Moore, C. H., 2001, Porosity Evolution and Diagenesis in a Sequence Stratigraphic Framework [Developments in Sedimentology, 55]: New York, Elsevier, 460 p.

Reid, R. P., and I. G. Macintyre, 1998, Carbonate recrystallization in shallow marine environments: a widespread diagenetic process forming micritized grains: Journal of Sedimentary Research, v. 68, p. 928-946.

Reid, R. P., and I. G. Macintyre, 2000, Microboring versus recrystallization: further insight into the micritization process: Journal of Sedimentary Research, v. 70, p. 24-28.

Saller, A. H., 1992, Calcitization of aragonite in Pleistocene limestones of Enewetak Atoll, Bahamas, and Yucatan — an alternative to thin-film neomorphism: Carbonates and Evaporites, v. 7, p. 56-73.

Tucker, M. E., 1991, Carbonate Petrology: An Introduction [2nd edition]: Oxford, Blackwell Scientific Publications, 272 p.

Facing Page: Top - Submarine-cemented hardground exposed by tidal or storm scour. Open shelf just south of Tongue of the Ocean, Great Bahama Bank, Bahamas. Photograph courtesy of E. A. Shinn.

Bottom - Macrophotograph of botryoidal aragonite cement in a vug in reef wall limestone. Holocene, Belize. HA = 15.5 cm. Photograph courtesy of Noel P. James.

CARBONATE DIAGENESIS

SYNGENETIC/EOGENETIC MARINE DIAGENESIS

CHAPTER 23

MARINE DIAGENESIS

Introduction:

Synsedimentary diagenesis in the marine realm is relatively uncomplicated (by comparison with meteoric and burial diagenesis) because it generally operates over short time spans (only years to thousands of years, in most cases) and involves a restricted range of pore fluid chemistries. Nevertheless, through a combination of physical, chemical and biological processes, coupled with access to a nearly unlimited supply of dissolved materials in seawater, marine diagenesis can often bring about remarkable change in carbonate sediments and produce some very complex fabrics. Furthermore, the subsequent overlay of meteoric or burial diagenetic alterations can greatly complicate the recognition of marine diagenetic fabrics in ancient carbonate rocks. That is especially true because the aragonitic or Mg-calcitic cements that result from marine diagenesis are essentially just as unstable in meteoric or burial-stage pore fluids as primary grains of those compositions.

The intensity or extent of marine cementation is a function of the supply of solutes from seawater. Solute supply, in turn, depends on sedimentation rates and the effectiveness of water transport from the surface into the interior of a sediment pile. Mechanisms of water movement include, among others, wave forcing, tidal pumping, thermal convection, and diffusive transport. Areas of very slow sedimentation (e.g., hiatus surfaces, low-sedimentation-rate platform interiors, or low-productivity deep sea settings) can have substantial marine cementation (including hardgrounds) because they all have long times of contact between seawater and a thin package of sediment, even with no special mechanism for water pumping. In high-sedimentation rate areas, on the other hand, substantial marine cementation occurs mainly in reef front or coastal settings where wave or tidal action can force seawater through the sediments to a considerable depth. Likewise, atoll margins and steep carbonate platform flanks are sites of extensive marine cementation because of convective water input coupled, in some cases, with low sediment accumulation rates. Hot or cold seeps on the sea floor also represent sites of exceptional water throughput and extensive cementation.

Grain and matrix dissolution are widespread in certain marine environments, particularly in cold- and deep-water areas. Modern oceanic waters have an aragonite compensation depth or ACD at roughly 1,500 m (the ACD is the depth below which aragonite does not accumulate because the rate of dissolution exceeds the rate of aragonite supply). Aragonite also is extensively dissolved in cool and cold-water shelf areas. The modern calcite compensation depth (CCD) lies at roughly 4,500 m (but that depth, as well as that of the ACD, varies with latitude, productivity, and other factors, and undoubtedly has varied significantly with geologic time).

Major diagenetic fabrics:

Bored (biodegraded) grains with cement infill of borings and generation of micrite envelopes (also discussed in the sections on pellets/peloids and sedimentary structures-borings).

Isopachous crusts of fibrous to bladed, peloidal, or aphanocrystalline high-Mg calcite cement. The aphanocrystalline crusts consist of equant, less than 4 μm-sized rhombs that look much like micrite.

Isopachous crusts of fibrous aragonite cement within grain cavities and as intergranular cements (predominantly found in warm-water, slightly hypersaline settings and tropical beachrock deposits).

Marine-cemented hardground formation in selected areas (see above) — associated, in many cases, with phosphate and glauconite cementation, boring and faunal encrustation, and intraclast formation.

Large botryoids of cavity-filling aragonite and high-Mg calcite cement.

Internal sediment fills of primary cavities or neptunian dikes in framework-supported sediments.

Coastal beachrock and spray-zone cements.

Microbe/cement associations in marine methane and thermal seeps.

Mineralogy:

Modern marine cements in warm-water settings consist mainly of high-Mg calcite (~12-18 mol% Mg), but with extensive aragonite as well. In colder-water areas (temperate, polar and deep marine), high-Mg calcite cements predominate, but become scarcer and less Mg-rich at higher latitudes. Many ancient carbonate deposits certainly had aragonite and high-Mg calcite cements, perhaps with secular variations in their abundance (e.g., Wilkinson and Given, 1986), but low-Mg calcite marine cements may also have formed at some times. In older limestones, original aragonite and high-Mg calcite cements generally have been converted diagenetically to low-Mg calcite and must be recognized by micro-inclusions, geochemical analysis (especially Mg and Sr contents), relict morphologies or crystal outlines, or, as a last resort, characteristic patterns of preservation or alteration (former aragonitic cements, for example, typically have poor primary fabric preservation.)

Characteristic morphologies of marine cements

A diagrammatic depiction of some common types of modern marine high-Mg calcite and aragonite cements. Most of these morphologies will be illustrated in this section. Adapted from James and Choquette (1983).

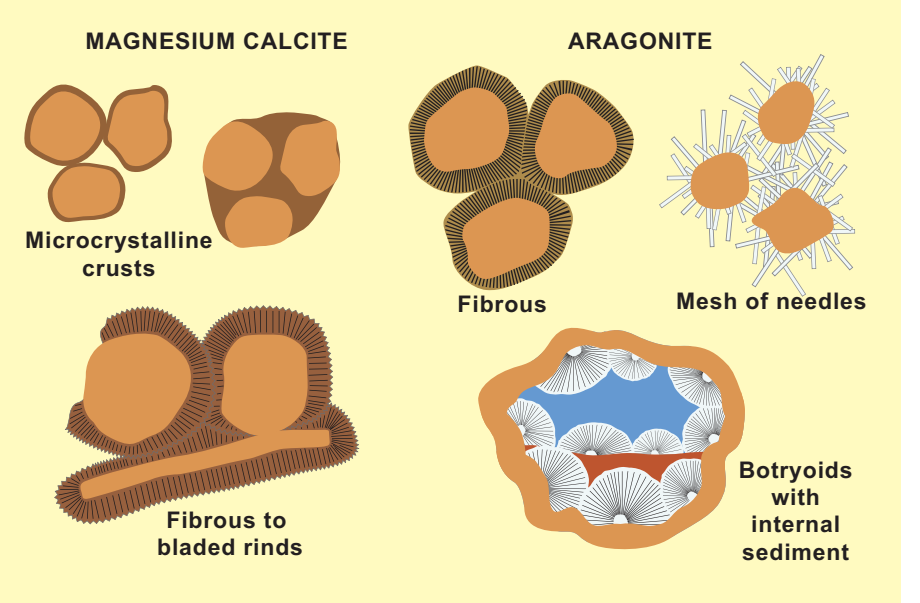

Recent sediment, Grand Cayman, Cayman Islands, B.W.I.

Biodegradation of grains was discussed in several previous chapters and, therefore, will be mentioned only briefly here. These aragonitic gastropod shells show early stages of microboring and aphanocrystalline high-Mg calcite cementation of the outer grain surfaces. This process leads to the creation of grain rims (termed "micrite envelopes") that may be more resistant to dissolution than the grains themselves.

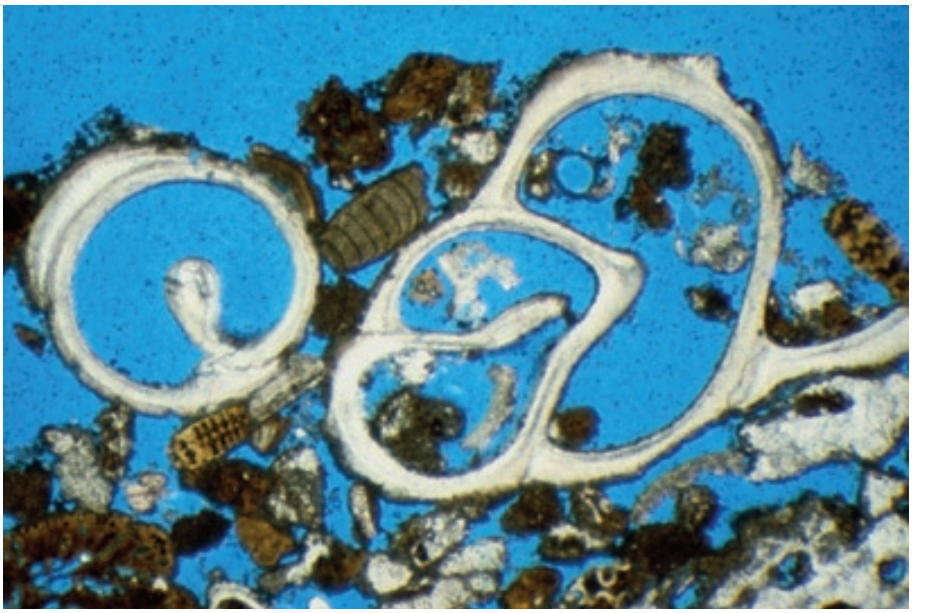

PPL, BSE, HA = 4.1 mm

Holocene sediment, Abu Dhabi, United Arab Emirates

A marine-cemented limestone with thick high-Mg calcite micrite envelopes surrounding most grains. These irregular envelopes, like the thinner versions in the previous illustration, consist of filled borings along the grain margins coupled with aphanocrystalline high-Mg calcite cement coatings surrounding the grains. The rest of the pore space in this sediment is filled with acicular (fibrous) marine aragonite that was precipitated from hypersaline lagoonal waters.

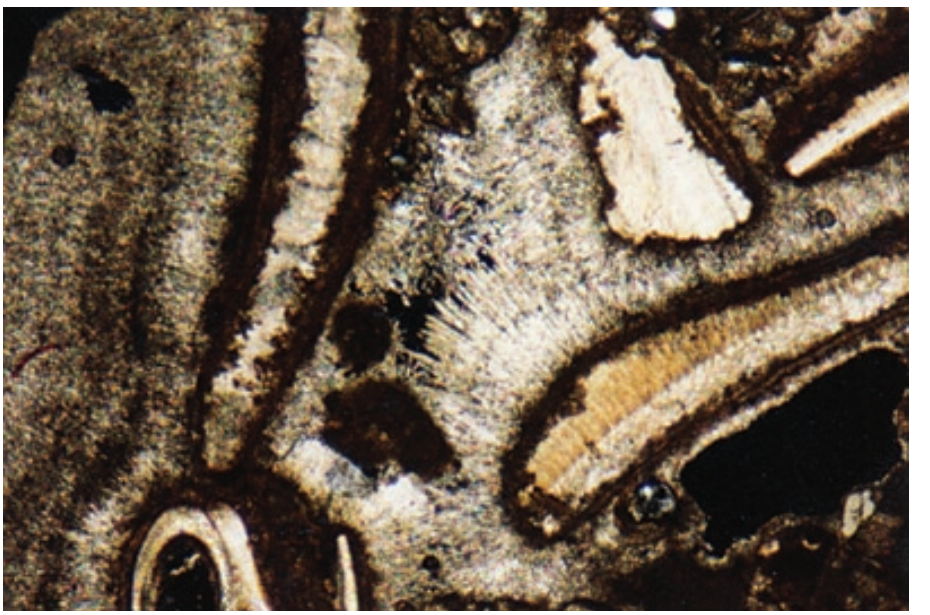

XPL, HA = 2.25 mm

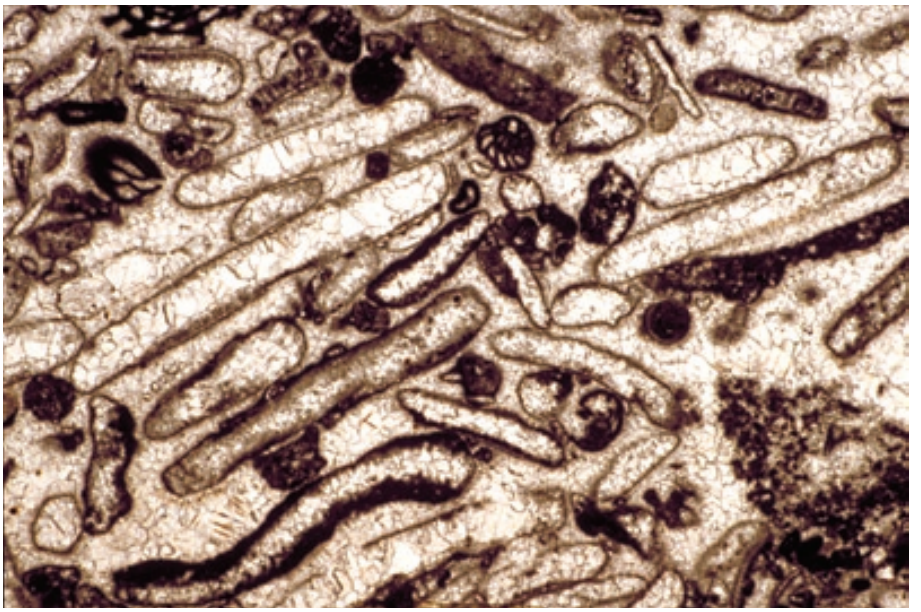

Lo. Permian (Wolfcampian) Hueco Ls., Hudspeth Co., Texas

This ancient limestone originally consisted largely of aragonitic grains (bivalves and possible phylloid algae). It underwent marine diagenesis, followed by extensive meteoric and burial alteration. The aragonitic grains were completely leached, and both intraparticle and interparticle porosity was later filled with sparry calcite. The only traces of the original nature of this sediment result from the preservation of the stable micrite envelopes and encrustations formed during synsedimentary marine alteration. Sample from Robert Laury.

PPL, HA = 10 mm

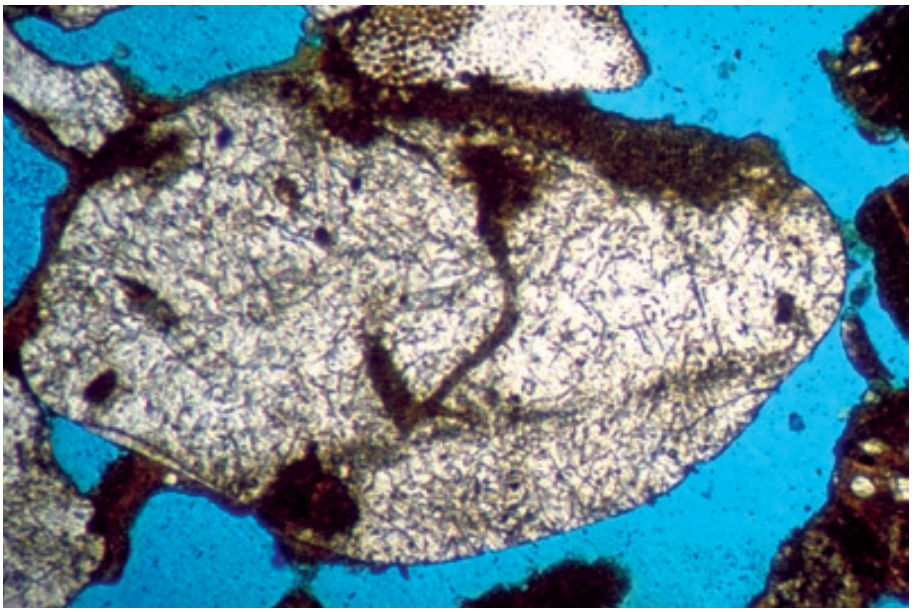

Recent sediment, St. Peter's Parish, Barbados

Although infilled borings along grain margins can improve the long-term recognizability of aragonitic grains, more extensive borings can ultimately lead to conversion of a skeletal fragment to an unclassifiable peloid. This example shows an intermediate stage of grain destruction in which numerous large and small borings have riddled a molluscan shell fragment. The "peloidization" of grains is a common process in marine diagenesis, especially in settings in which grains are only rarely moved (grass flats, deeper platform settings, and the like).

PPL, BSE, HA = 1.6 mm

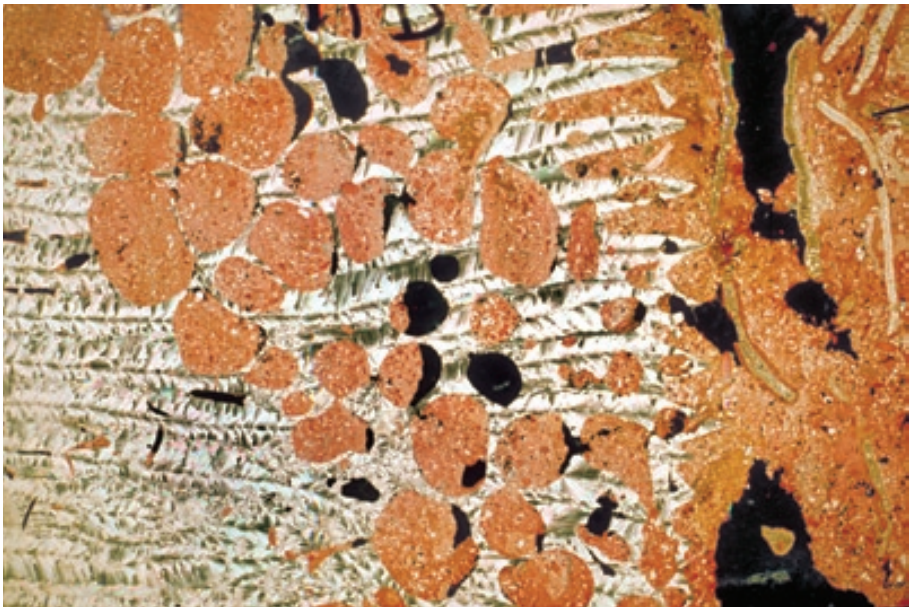

Holocene reef wall limestone, Belize

Another example of extensive marine diagenetic grain destruction through boring — in this case, a coral bored by sponges. The sponge galleries, however, are filled with fine-grained high-Mg calcite sediment and cement. This demonstrates the continuing "battle" between destructive and constructive processes during marine diagenesis. Photograph courtesy of Noel P. James.

XPL, CYS, HA = 10 mm

Recent sediment, Schooner Cays, Bahamas

The line between deposition and diagenesis commonly is hard to define in marine sediments. Here, a hardground with aragonite ooids has been lithified by calcified algal filaments surrounded by high-Mg calcite micrite cement (selectively stained red). The ooids are primary sediment; the calcified filaments that lithify the sediment can be viewed as marine diagenetic products. Photograph courtesy of Noel P. James.

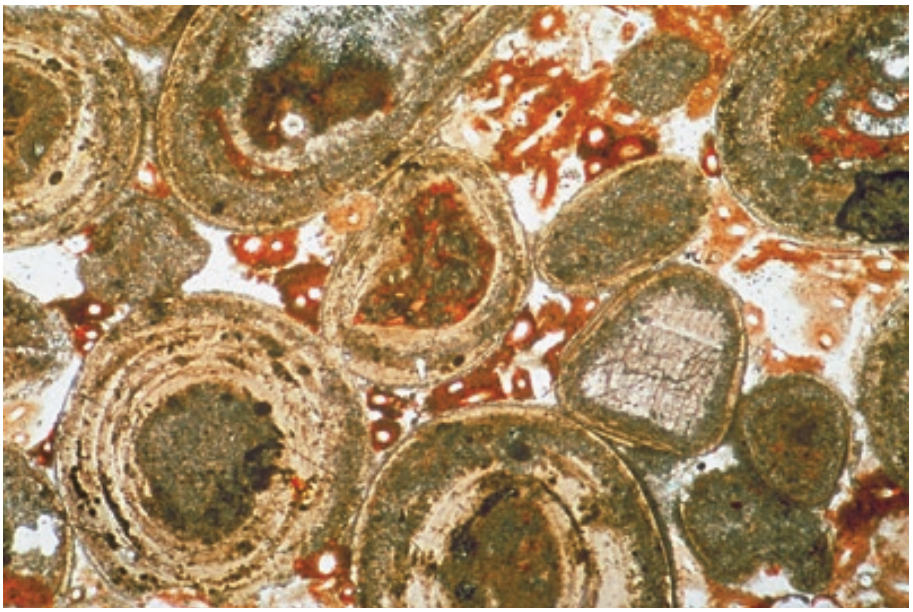

PPL, CYS, HA = 1.5 mm

Holocene reef wall limestone, Belize

Marine cementation is widespread in modern carbonate deposits, especially in tropical regions. This *Halimeda* grainstone, for example, was cemented with isopachous rinds of fibrous to bladed high-Mg calcite. High-Mg calcite is the predominant marine cement in most settings other than very warm, slightly hypersaline platform and coastal areas. Staining (or geochemical analysis) is essential for proper identification of modern marine high-Mg calcite cements. Photograph courtesy of Noel P. James.

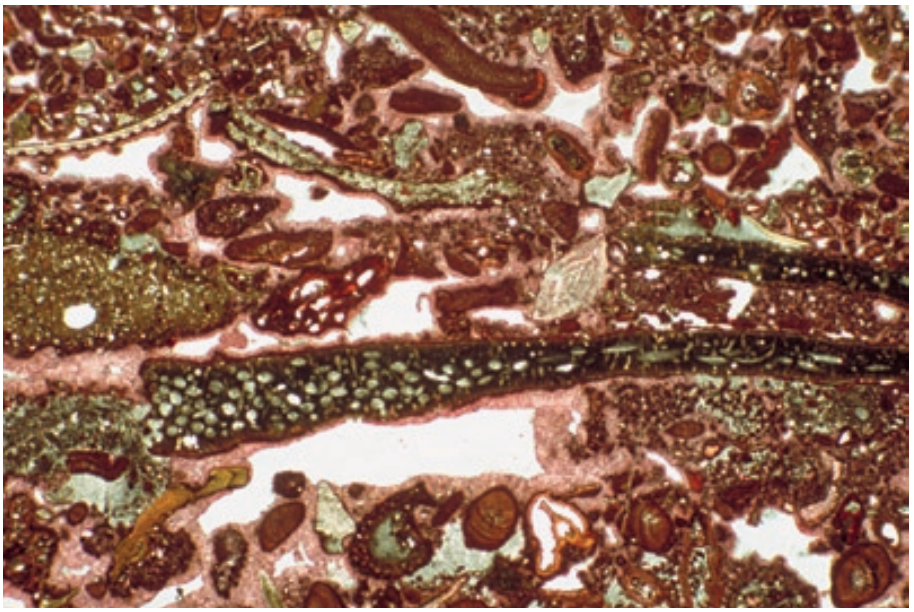

PPL, CYS, HA = 2.0 mm

Up. Jurassic (Oxfordian) Buckner Fm., subsurface Arkansas

Fibrous to bladed marine high-Mg calcite cements are commonly found in ancient rocks as well as modern sediments. This ultra-thin section shows well defined, bladed, marine cements that have grown in optical continuity with ooids exhibiting primary radial architecture. Such well preserved fabric in such old rocks virtually requires a primary calcitic mineralogy for both ooids and cements. SEM or microprobe analysis can be used to detect micro-dolomite inclusions or elevated Mg trace element concentrations in order to confirm an original high-Mg calcite composition. Photograph courtesy of Clyde H. Moore.

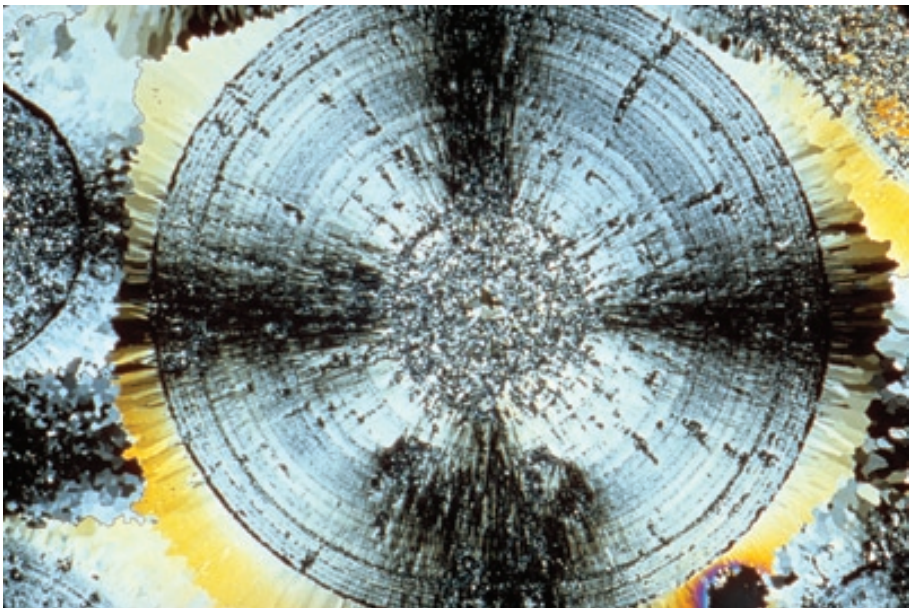

XPL, HA = ~0.5 mm

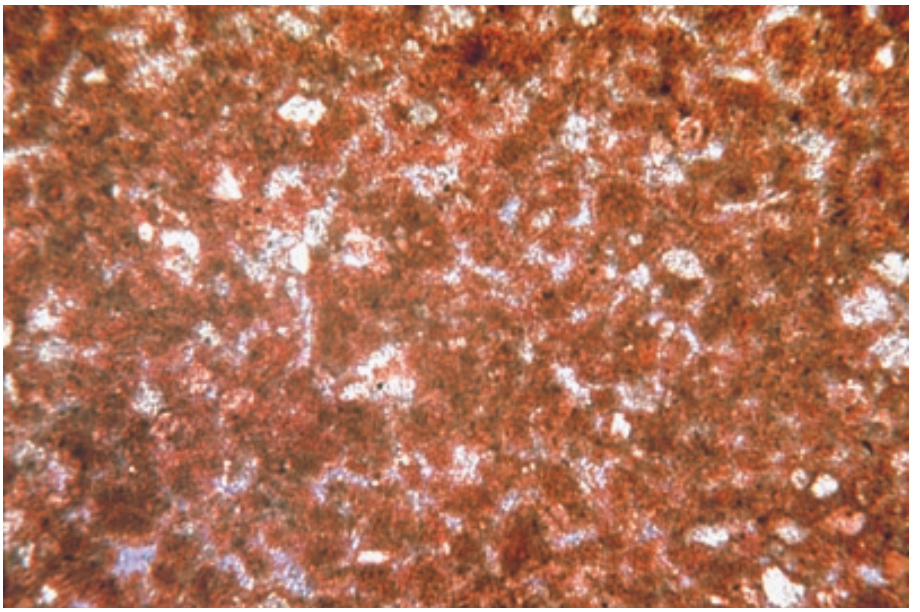

Holocene limestone, Tobacco Cay, Belize

Micropeloidal high-Mg calcite cement (selectively stained red) in reef flat limestone. The precipitation of micropeloidal cements most likely is microbially mediated, and it often is very difficult to distinguish micropeloidal cements from transported micropeloidal internal sediment. Photograph courtesy of Noel P. James.

PPL, CYS, HA = ~0.8 mm

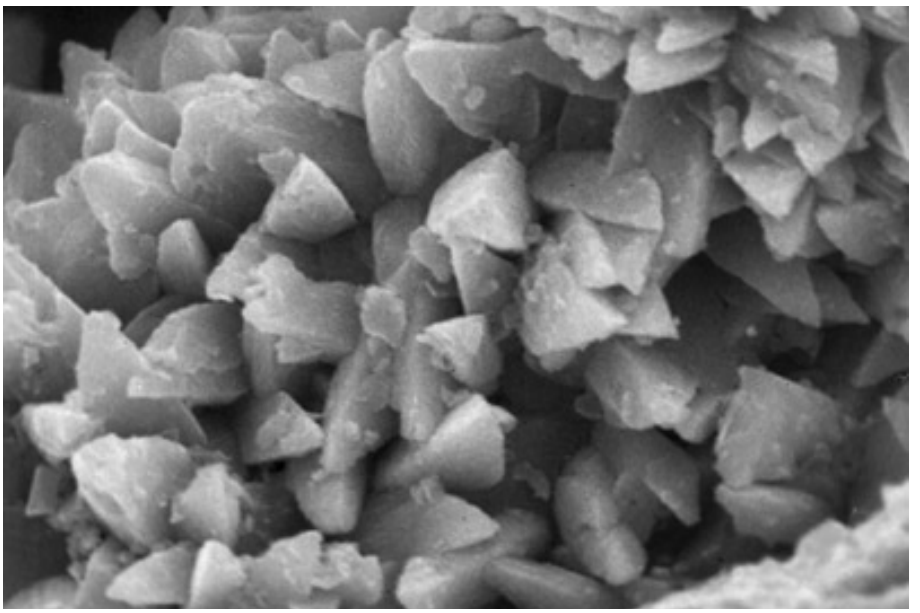

Holocene reef sediment, St. Johns, Virgin Islands

An SEM image of a high-Mg calcite cement rind on a skeletal grain (the substrate grain is not visible in this photograph). In thin section, these small, equant crystals appear very similar to a micritic (microcrystalline) or peloidal grain coating. Only through scanning electron microscopy can one observe the details of crystal shapes. This cement is from a shallow marine setting.

SEM, HA = 37 μm

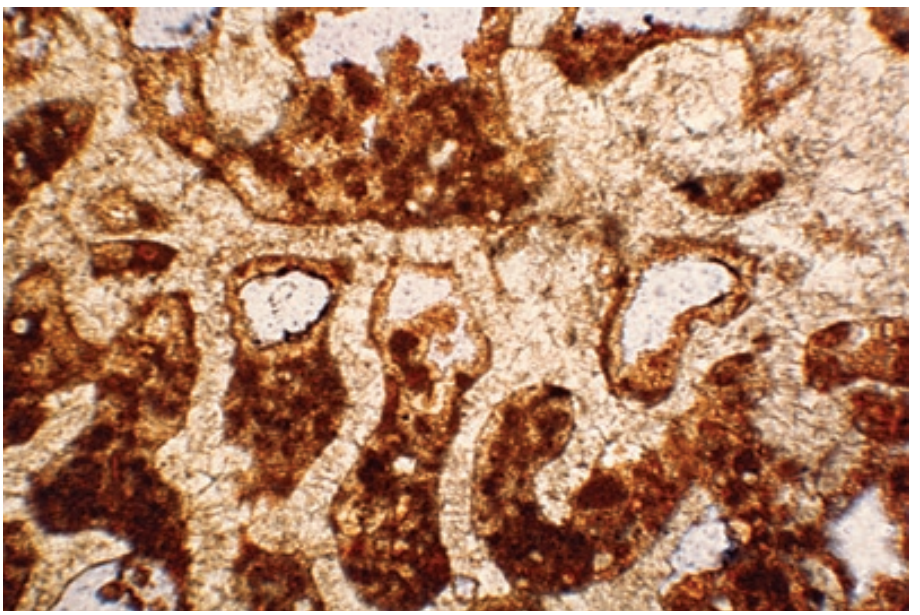

Holocene sediment, Tobacco Cay, Belize

Cement and peloidal internal sediment, some of it with geopetal fabric, within voids in a coral skeleton from sediment that is less than 500 years old. The distinction between sediment and cement is difficult to impossible to draw in the case of such peloids. The high-Mg calcite in this sample is stained red with Clayton Yellow. Photograph courtesy of Robert N. Ginsburg.

PPL, CYS, HA = 1.5 mm

Recent sediment, Grand Cayman, Cayman Islands, B.W.I.

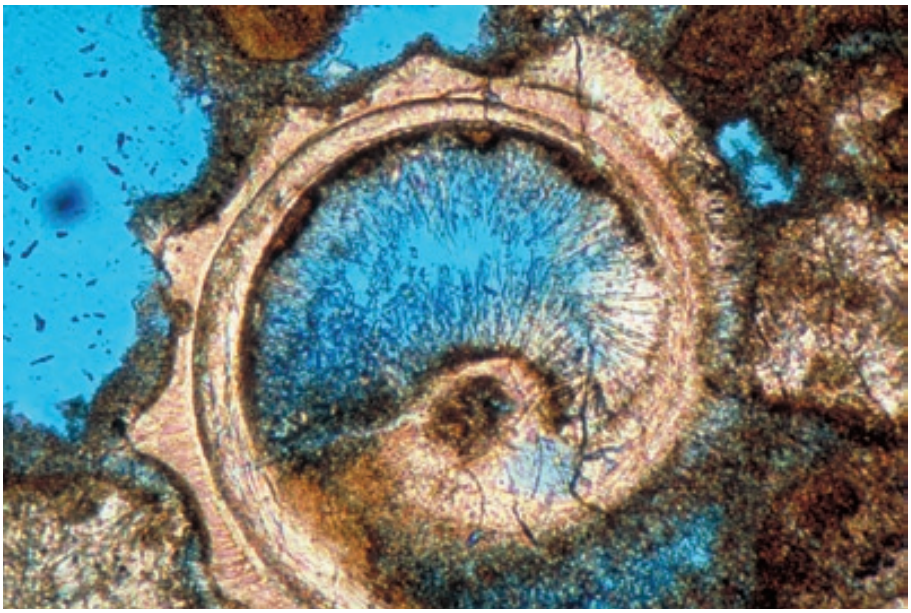

The most easily recognizable marine cements in modern sediments are composed of acicular (fibrous or needle-like) aragonite. In this case, such cements partially fill the intraparticle porosity within a gastropod. The exterior of the grain, in contrast, is cemented by microcrystalline high-Mg calcite cement. Holocene fibrous aragonite cements are most commonly formed in warm, shallow, slightly hypersaline waters in tropical shallow-shelf and coastal areas. The aragonite needles typically are longer and thinner than the crystals found in typical high-Mg calcite cements.

PPL, BSE, AFeS, HA = 0.65 mm

Quaternary sediment, Isla Mujeres, Quintana Roo, Mexico

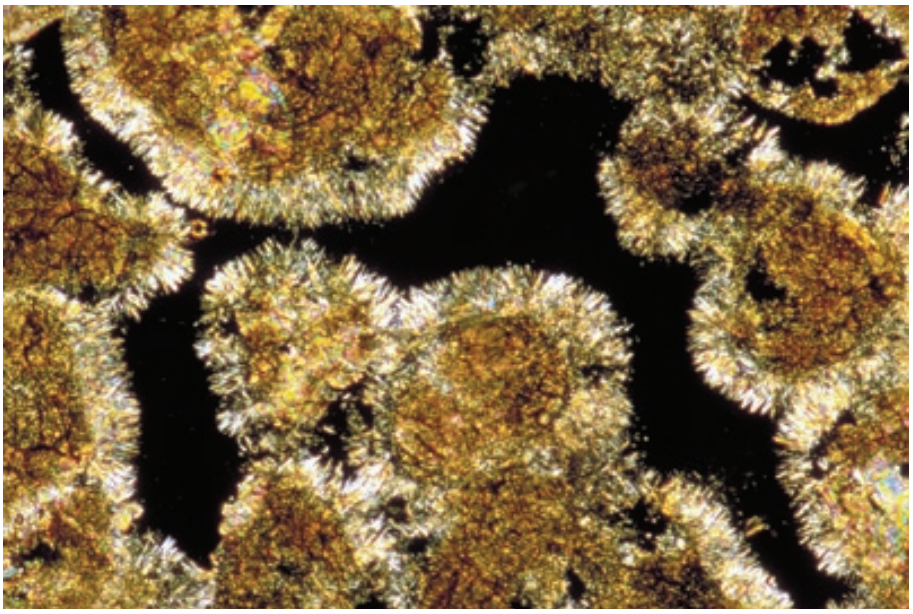

A view of Holocene fibrous aragonite cements lining the pores of a weakly lithified Pleistocene eolianite that currently is submerged in the intertidal zone. Note the uniform thickness of the aragonite crust (commonly termed an "isopachous" coating) and the predominant orientation of aragonite crystals perpendicular to the surface of the substrate grains. Photograph courtesy of William C. Ward.

XPL, HA = 6.8 mm

Recent sediment (beachrock), Salt Cay, Bahamas

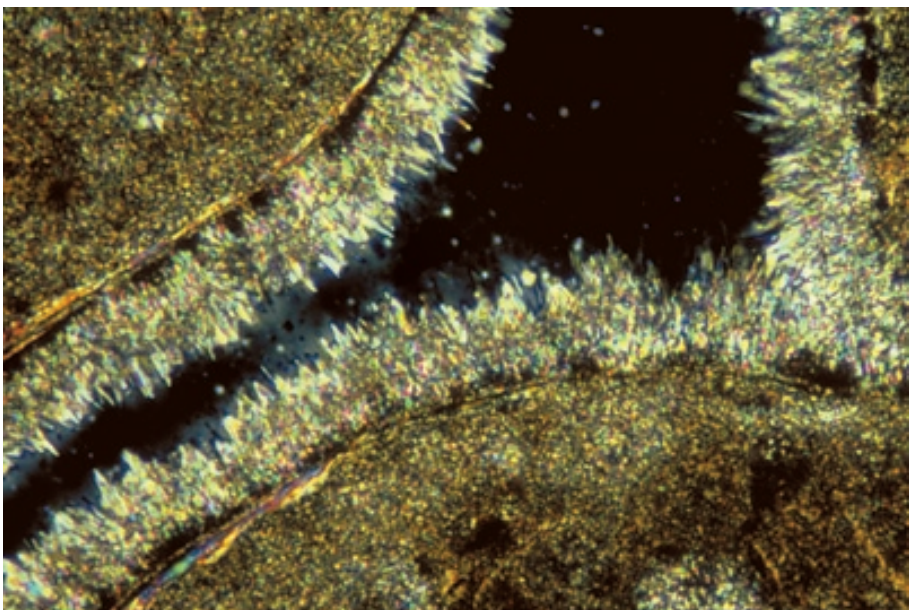

Acicular aragonite cement forming isopachous grain coatings in a beachrock. Beachrock is a friable to well-cemented rock consisting of calcareous sand cemented by aragonite or high-Mg calcite crusts precipitated in the intertidal zone. It generally occurs as thin beds dipping seaward at less than 15 degrees and, as in this example, can form in as little as a few years. Although most commonly found in tropical areas, beachrocks also form, albeit less commonly, in cool-water settings. The intertidal environment allows wave pumping of ocean water through the sediment, and also allows mixing of marine and meteoric fluids in at least some cases.

XPL, HA = 0.42 mm

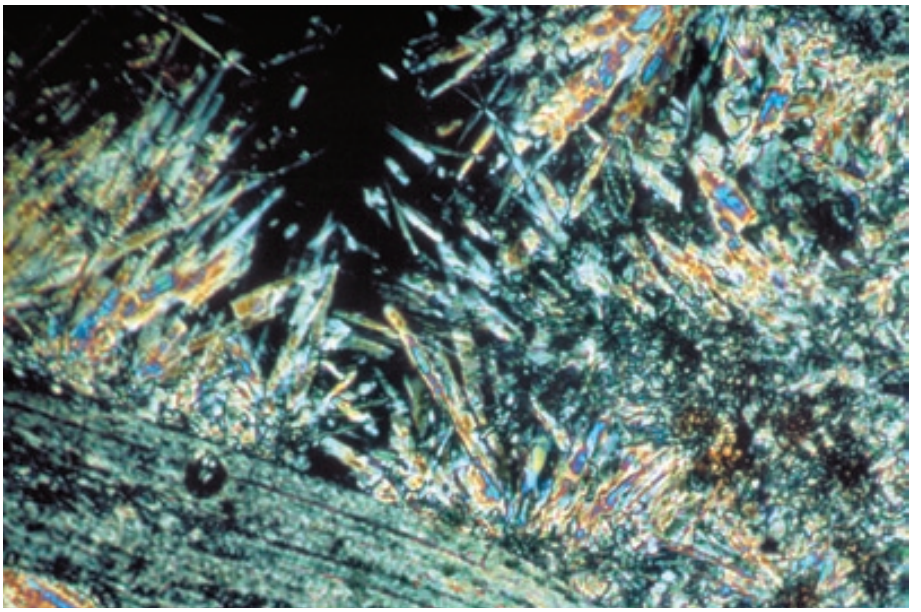

Recent sediment, Schooner Cays, Bahamas

A high-magnification photomicrograph showing another example of an acicular aragonitic marine cement. In this subtidal example, however, there is much less consistent orientation of aragonite crystals, in part because some of the needle-like crystals radiate outward from isolated growth centers. Photograph courtesy of Noel P. James.

XPL, HA = 0.1 mm

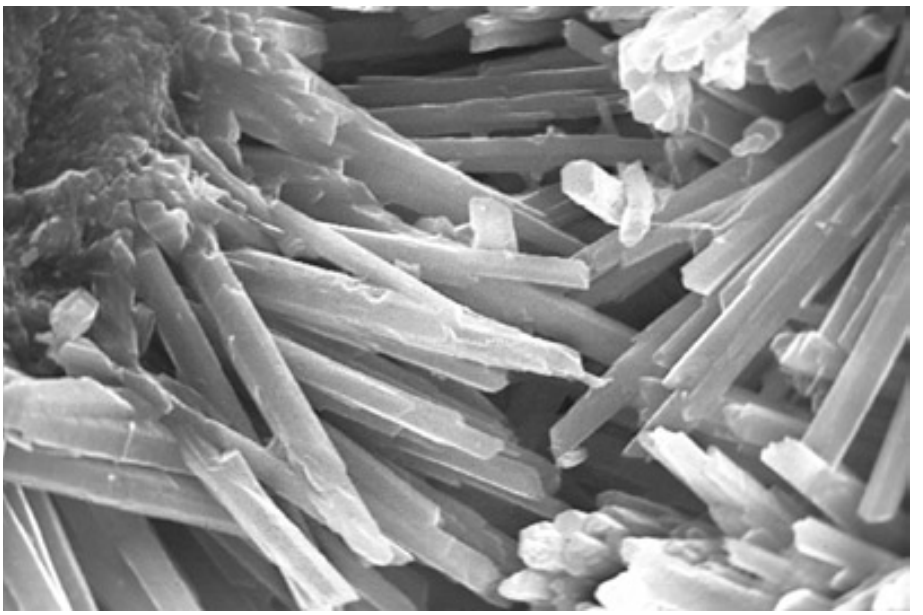

Recent sediment, Belize

An SEM image of submarine aragonite-needle cement forming isopachous linings of intraparticle voids in a coral skeleton. Note the irregular, but basically substrate-normal, arrangement of the fibrous crystals. Individual crystals reach 20-μm length in this sample.

SEM, HA = 37 μm

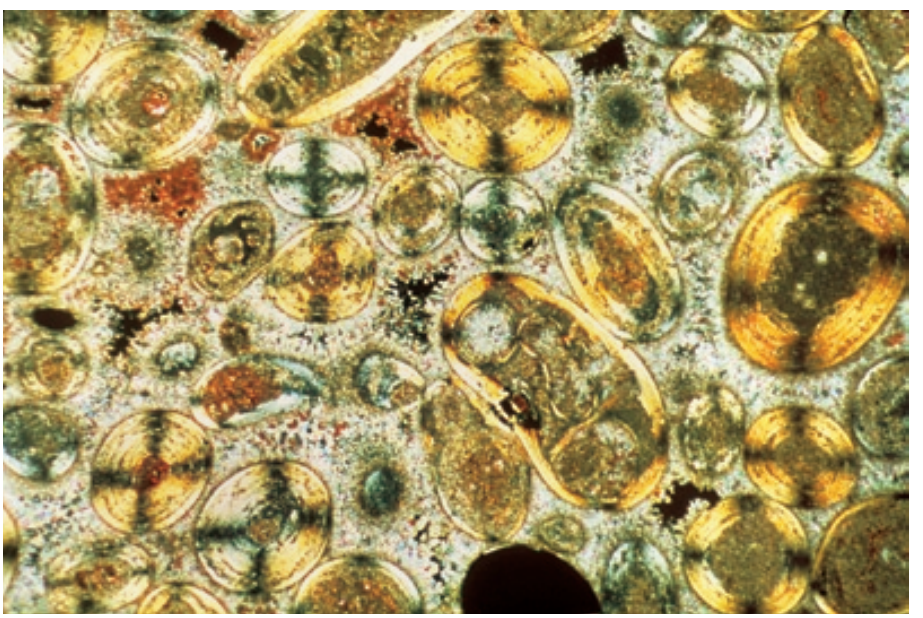

Holocene sediment, Schooner Cays, Bahamas

Synsedimentary aragonite cementation of hardgrounds and beachrocks can be both extensive and rapid (in many cases, forming lithified rock within just a few years). This modern open-shelf hardground shows aragonite ooids fully encased within aragonite cement. Photograph courtesy of Noel P. James.

XPL, HA = 3.0 mm

Holocene hardground, Great Bahama Bank, Bahamas

A completely marine-cemented sample from a modern oolitic hardground. The ooids are completely surrounded by fibrous, isopachous aragonite crusts. Uniform growth of aragonite needles from spherical substrates has led to hexagonal compromise boundaries marked by lines of inclusions where cements from opposite sides of a pore have met. These inclusion-rich boundaries can be preserved even in ancient limestones. Photograph courtesy of E. A. Shinn.

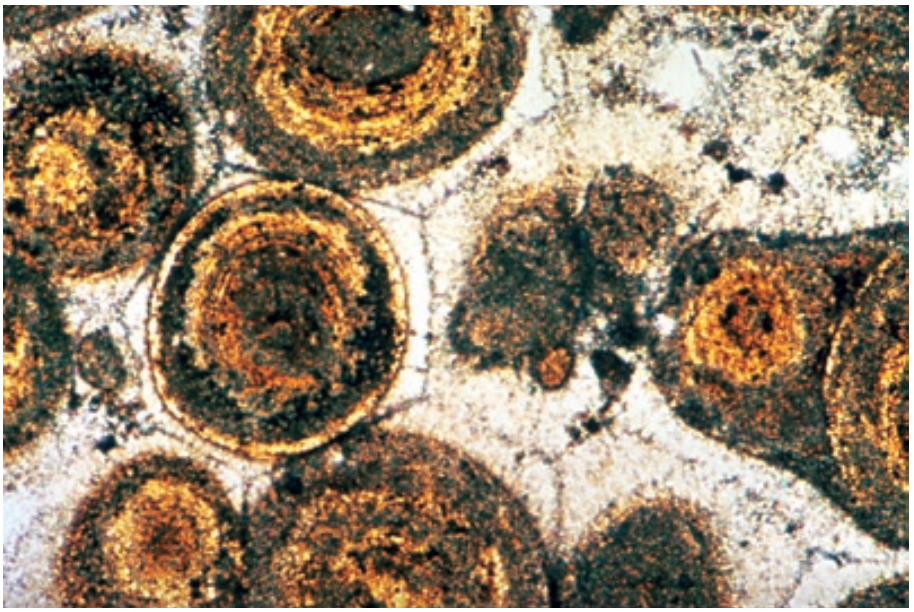

PPL, HA = ~2.0 mm

Up. Pennsylvanian (Missourian) Westerville Ls., Jackson Co., Missouri

A preserved fabric of acicular marine cement in an ancient oolitic grainstone. The original cement was probably fibrous aragonite, now neomorphosed to bladed calcite. To confirm the hypothesis of original calcite mineralogy, one would need to look for primary or secondary mineral inclusions (relict aragonite or micro-dolomite after high-Mg calcite) or examine the trace element geochemistry of the cements (neomorphic products of former aragonite can have high Sr contents; replacements of high-Mg calcite may contain elevated levels of Mg).

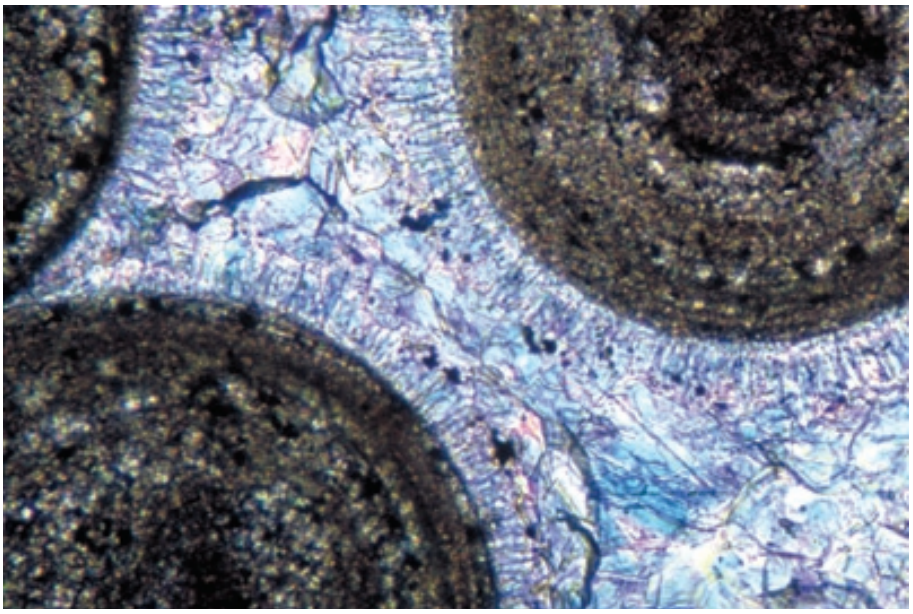

PPL, AFeS, HA = 0.5 mm

Up. Permian (up. Guadalupian), Tansill Fm., Eddy Co., New Mexico

A green-algal grainstone, consisting mainly of *Mizzia* sp., with grains encased in typically cloudy (inclusion-rich), penecontemporaneous, isopachous marine cements. These cements were probably precipitated as aragonite, but then were subsequently neomorphosed to calcite. Remnants of their primary radial-fibrous fabric are still visible. Most marine cements form rapidly and consequently are rich in inclusions. The inclusions, which are mainly water filled, yield a characteristic brownish color in thin section.

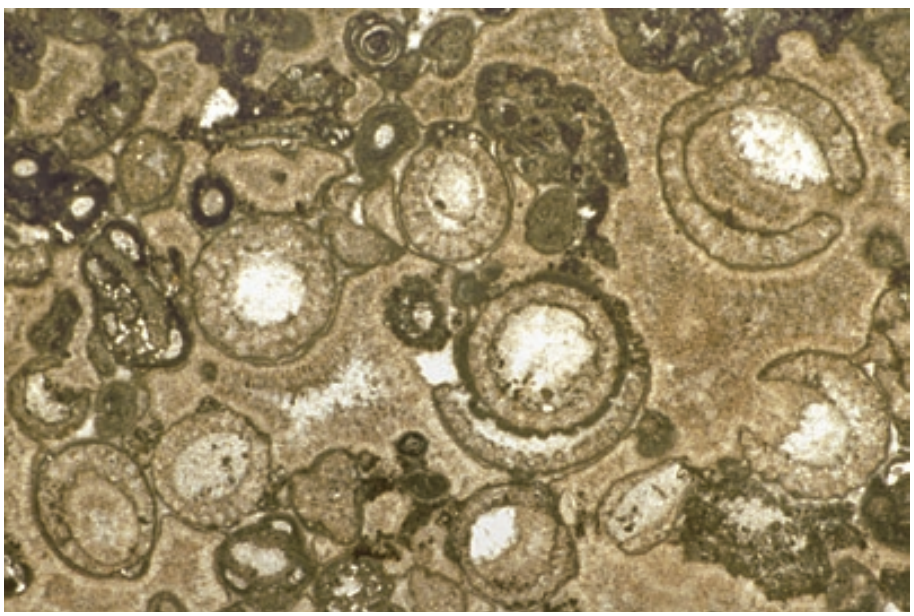

PPL, HA = 10 mm

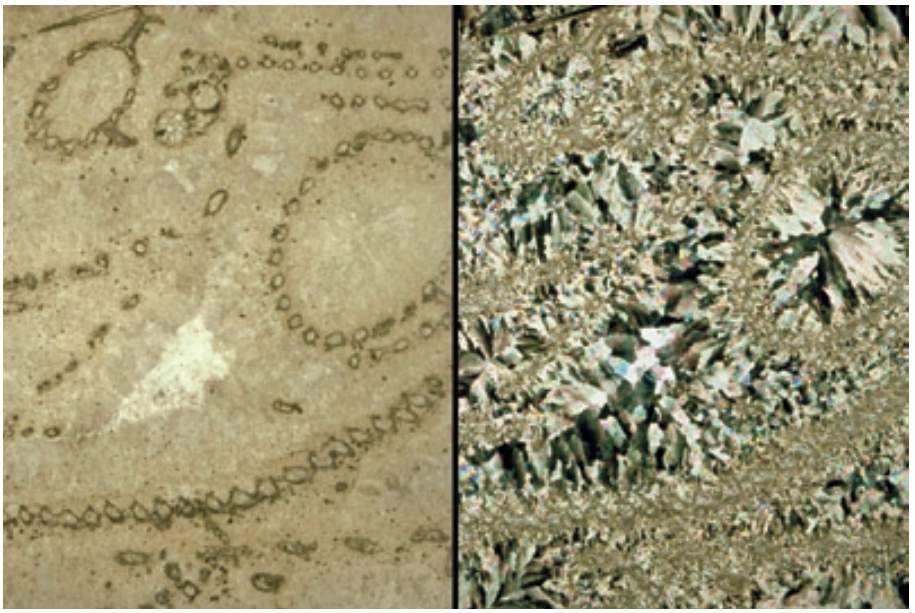

Lo. Carboniferous (Tournaisian-lo. Visean) Waulsortian limestone, Co. Dublin, Ireland

An example of a fenestrate bryozoan grainstone in which all porosity was occluded by syndepositional fibrous marine cements. Each fenestrate bryozoan is surrounded by cloudy (brownish, again due to inclusions), radial-fibrous to bladed cement crusts. The complete lack of compaction in this pile of otherwise unsupported, very delicate grains with nearly 85% initial porosity is a strong indication that this cement was of syndepositional origin.

PPL/XPL, HA = 10 mm each

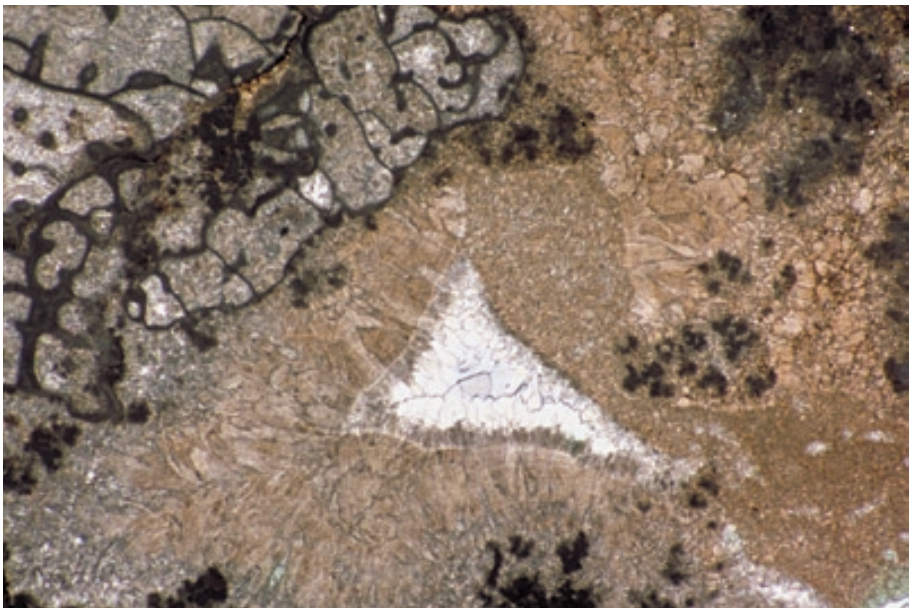

Lo. Cambrian Forteau Fm., southern Labrador, Canada

Cloudy marine cements extend far back in the geologic record (well into the Precambrian). This view shows a growth cavity within a Cambrian archaeocyath-*Renalcis* reef limestone that is filled with inclusion-rich, fibrous calcite cement. The remnant void was occluded by clear non-ferroan and ferroan blocky calcite cement. Photograph courtesy of Noel P. James.

PPL, AFeS, HA = ~10 mm

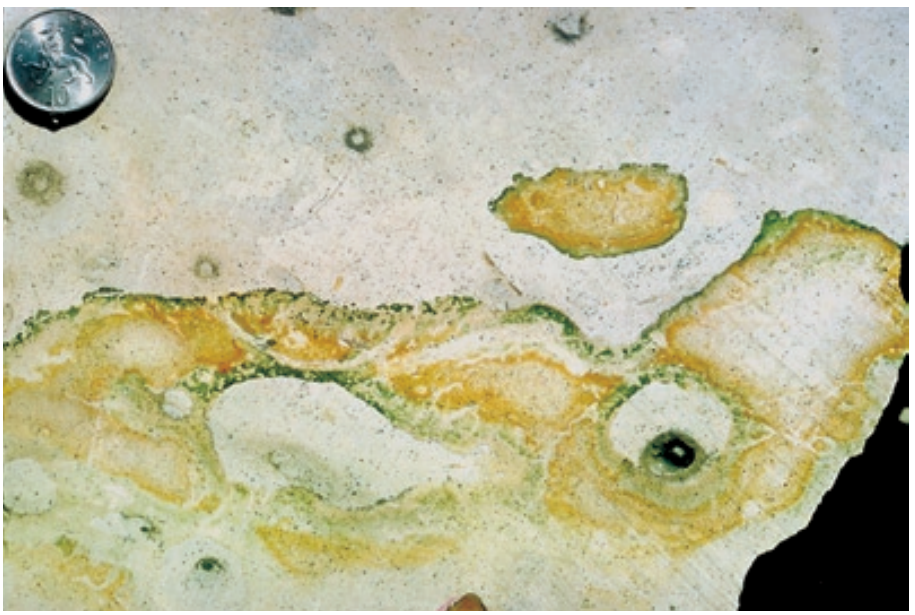

Up. Cretaceous (Turonian) Chalk Rock, Bedfordshire, England, U.K.

Marine lithification is widespread even in fine-grained, deep shelf to oceanic sediments, primarily at hiatus surfaces. This rock slab shows one of several stacked hardgrounds in a shelf chalk. The hardgrounds consist of irregular, Mg-calcite-cemented intervals, roughly 5-15 cm thick with associated phosphatized (yellowish) and glauconitized (greenish) areas. Note the large pre-lithification burrows, smaller post-lithification borings, and the reworked pebble of hardground material. As pelagic ooze is a very soft, even soupy material, encrustation, reworking and boring demonstrate synsedimentary lithification.

Mac, HA = 21.5 cm

Lo. Jurassic (up. Pliensbachian) limestone, Central High Atlas region, Morocco

Hardgrounds can form much more rapidly in shallow-water marine settings with warm, carbonate-supersaturated waters than in deeper, colder-water settings. The same kinds of criteria are used for their recognition, however, Here, a lithiotid bivalve was truncated at a marine hardground surface overlain by oolitic sediment. The sediment must have been lithified at the sea-floor for such truncation to occur. Borings, attached fauna, and reworked hardened pebbles are other indications of hardground lithification.

PPL, HA = 12.5 mm

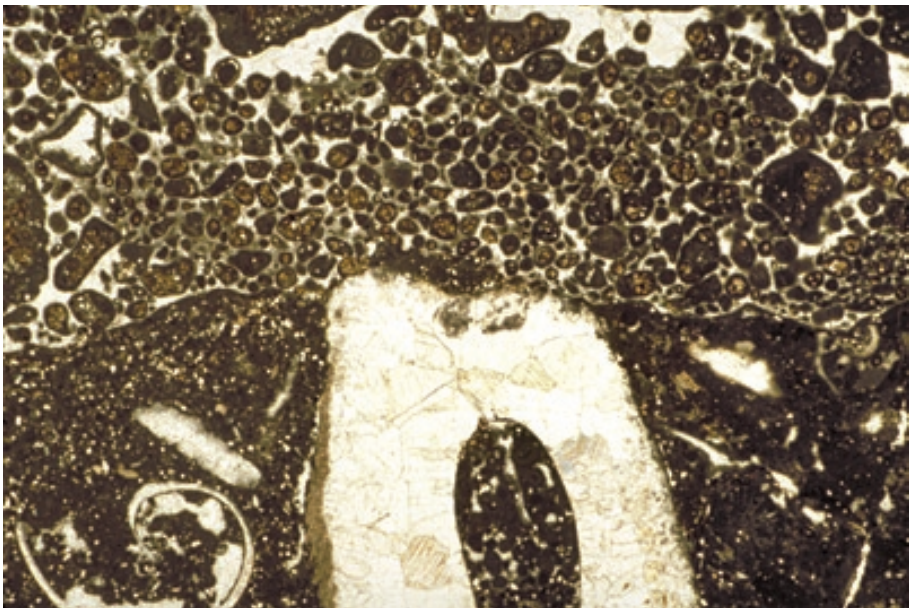

Recent sediment, 122 meter (400 ft) depth, Tongue of the Ocean, Bahamas

A sample from the surface of a modern cemented platform-margin slope showing evidence of post-lithification boring in a hardground surface. Cementation in this facies is primarily by high-Mg calcite. Note how the boring (center) has cut across two ooids and a large peloid (reworked downslope from the platform top) and how renewed cementation has begun within the boring. Photograph courtesy of G. Michael Grammer.

PPL, BSE, HA = 3.0 mm

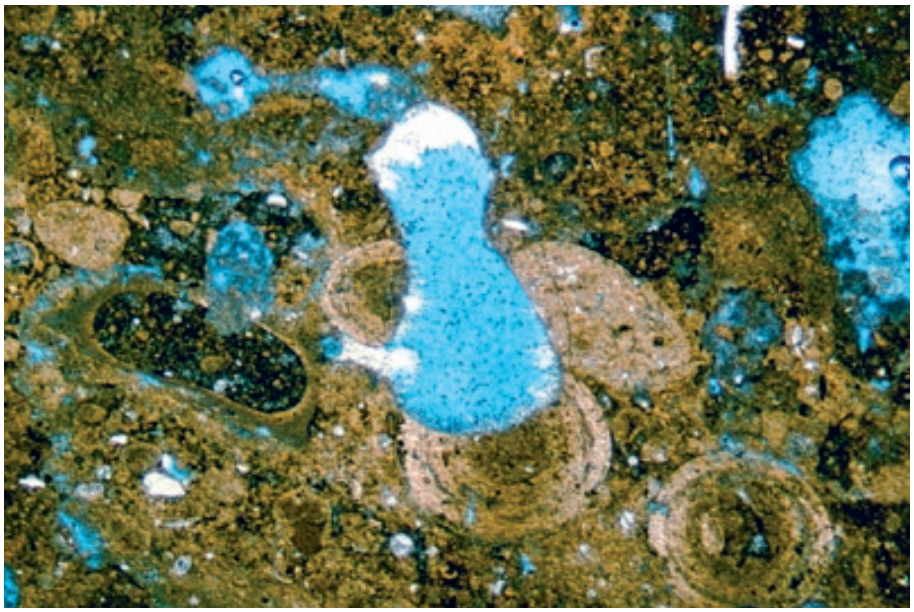

Mid-Cretaceous El Abra Ls., Querétaro, Mexico

Synsedimentary marine cements that form within cavities in coarse grainstone or boundstone deposits are commonly associated with geopetal internal sediment. This example shows caprinid (rudistid) bivalves cemented by isopachous, radiaxial-fibrous marine cement interlayered with substantial micritic internal sediment. Additional marine cement post-dates the sediment, confirming the essential synchronicity of cementation and sedimentation. Photograph courtesy of Paul Enos.

PPL, HA = 38 mm

Up. Devonian (Frasnian) Sadler Fm.(?), Canning Basin, Western Australia

Sediments with extensive marine cementation are brittle and subject to early fracturing and faulting, especially where they occur near steep platform margins. This sample shows a limestone composed of alternating sea-floor cement crusts and carbonate sediment, including sheet-like stromatoporoids (the layers with regularly arranged but irregularly shaped white spar blebs). The marine-lithified sediment was cut by fractures lined with additional marine cement, followed by infiltrated, layered sediment. This downward movement of internal sediment constitutes a neptunian dike.

PPL, HA = 23 mm

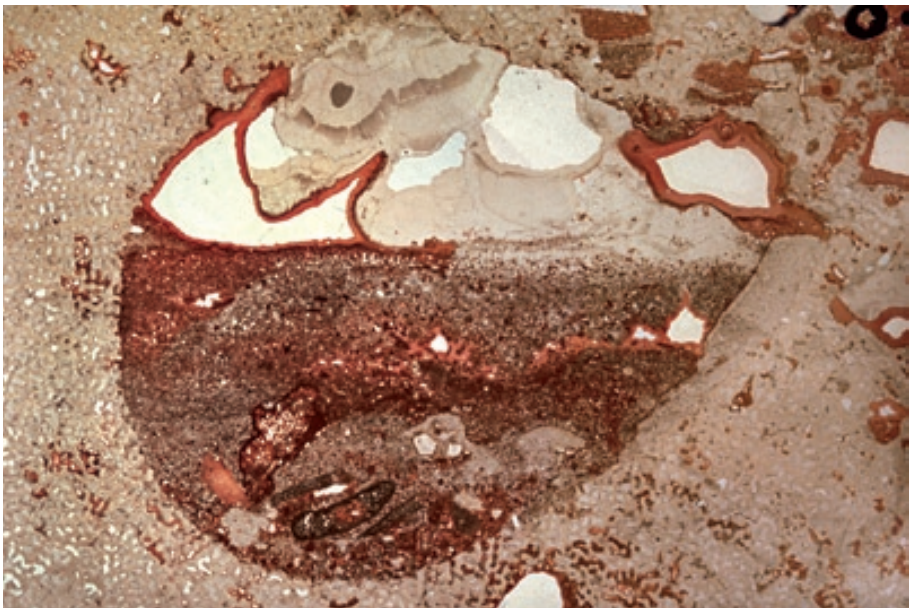

Holocene reef wall limestone, Belize

Internal sediment commonly is interspersed with marine cements within a variety of sediment cavities. In this example, a bivalve boring in a coral skeleton (*Porites* sp.) is filled with geopetal sediment cemented by Mg-calcite and aragonite and roofed by botryoidal aragonite cement. The tiny remaining cavity was lined with a final stage of high-Mg calcite fibrous cement (stained red). Photograph courtesy of Noel P. James.

PPL, CYS, HA = 30 mm

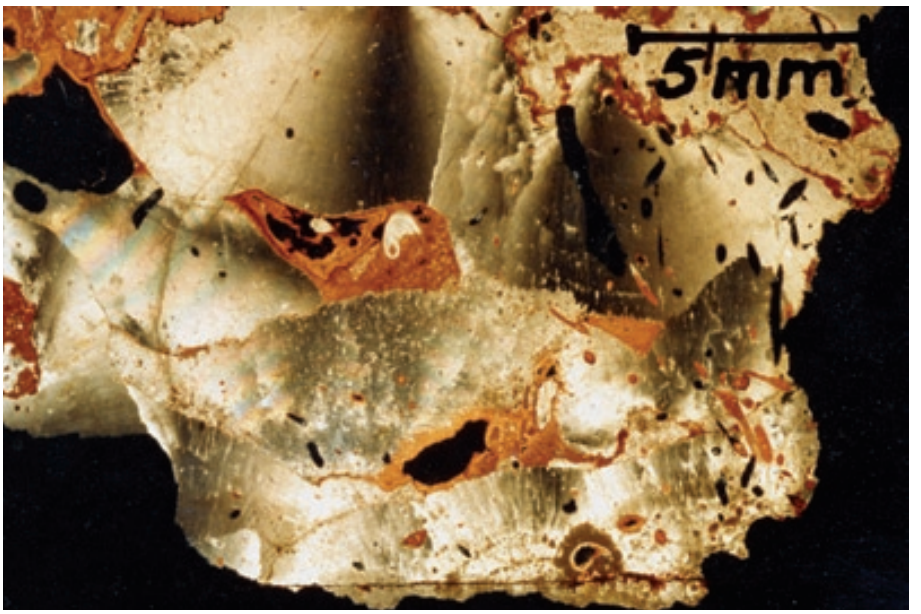

Holocene reef wall limestone, Belize

Marine cementation of large voids, especially in reefs (modern and ancient), commonly takes the form of large, dense botryoids composed of aragonite with, at least in modern examples, very subordinate high-Mg calcite (stained red). Note the unfilled circular to elliptical borings that cut the cement, excellent evidence of its formation in cavities with sufficient contact with the surface to allow colonization by boring organisms. This rock is less than 12,000 years old and the cements are thought to be mid-Holocene. Photograph courtesy of Robert N. Ginsburg.

XPL, CYS, HA = 18 mm

Holocene reef wall limestone, Belize

Another example of aragonitic botryoidal cements in a vug in forereef sediments. The densely packed, radiating splay of fibrous crystals is clearly shown in this example. Sample from Noel P. James.

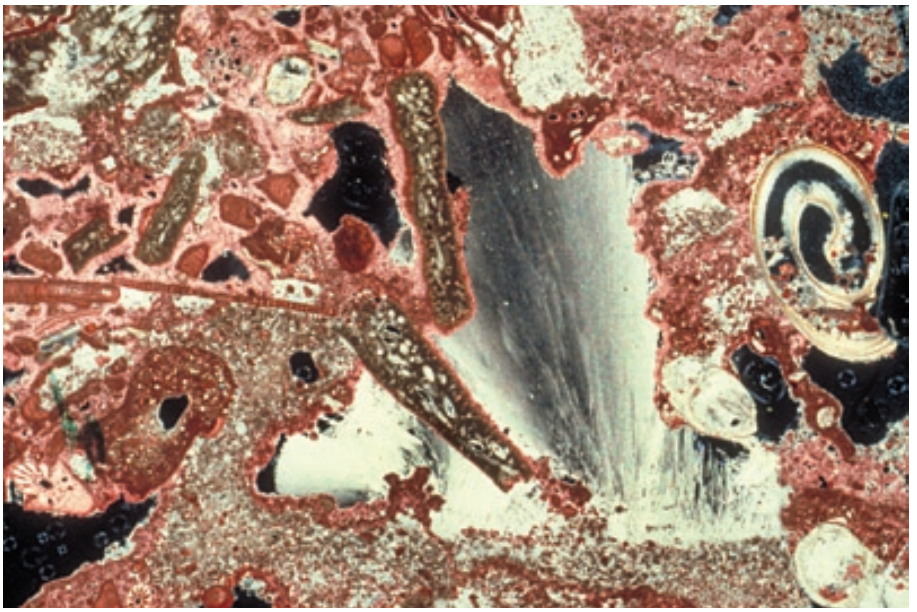

XPL, CYS, HA = 10 mm

Up. Pennsylvanian (Virgilian) Holder Fm., Otero Co., New Mexico

This ancient example of a marine cement botryoid grew in interstices within a foraminiferal-microbial bioherm. The neomorphosed cement retains abundant, but very small, inclusions of original fibrous aragonite. Those, and other inclusions, help to give the cement its brownish color.

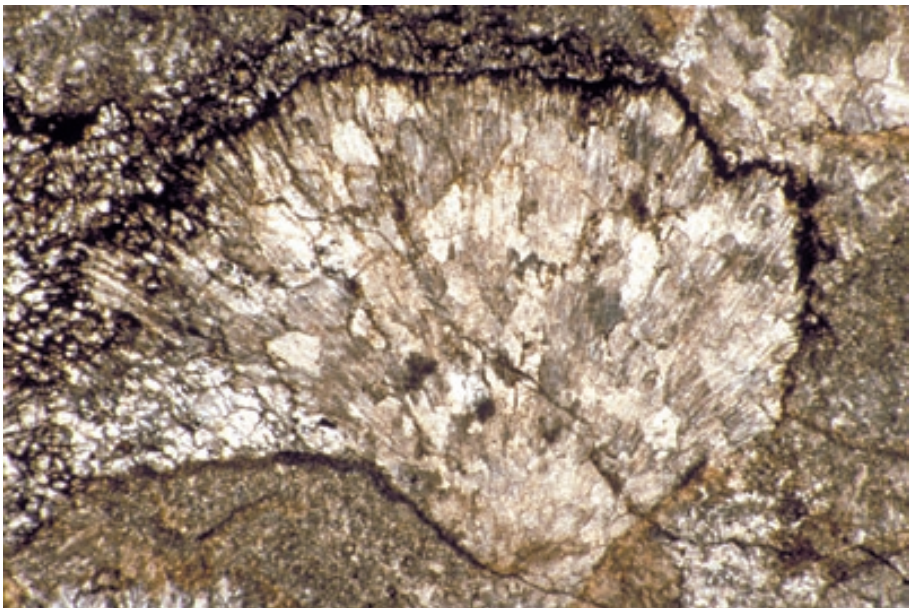

PPL, HA = 4.1 mm

Up. Permian (Guadalupian) Capitan Fm., Eddy Co., New Mexico

A large marine cement botryoid in a reefal limestone that consists of up to 70% cement. The neomorphosed cement retains its original fibrous character and abundant inclusions. In this example, marine cement is volumetrically more abundant than any single framework organisms and the rock could realistically be considered a "cementstone" (as used in the Wright 1992 classification).

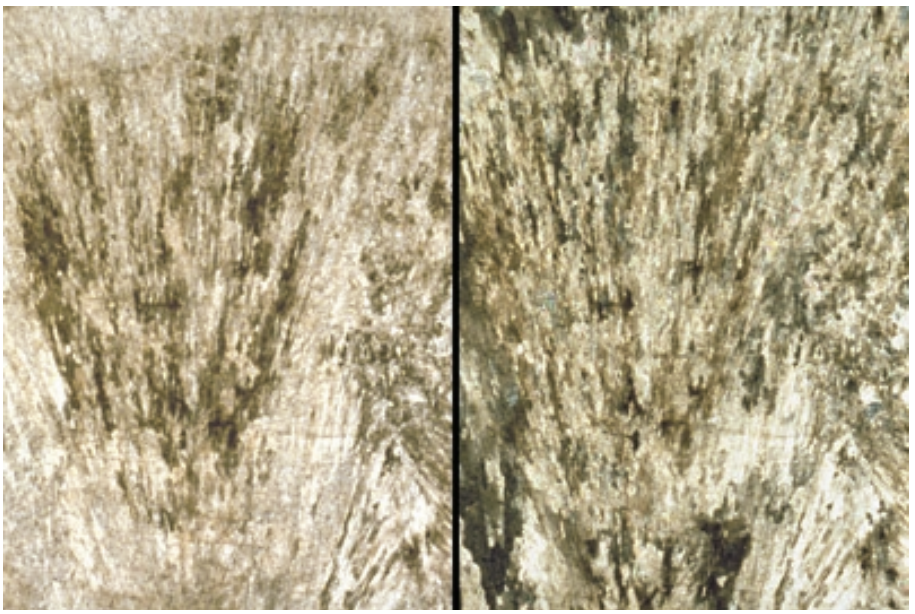

PPL/XPL, HA = 8.0 mm each

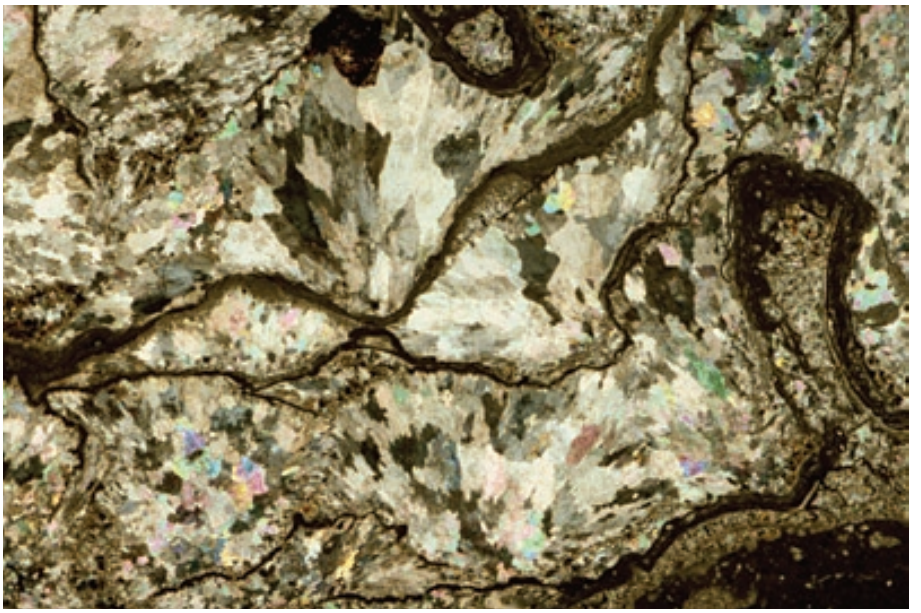

Up. Permian reef limestone, Djebel Tebaga, southern Tunisia

Early marine cement in a reefal limestone. These coarsely bladed marine cement botryoids are intergrown with *Archaeolithoporella*, a problematic algal/cyanobacterial organism. The intergrowth of multiple generations of cement with marine organisms helps to establish a synsedimentary marine origin for these precipitates, despite the poor fabric preservation.

XPL, HA = 14.5 mm

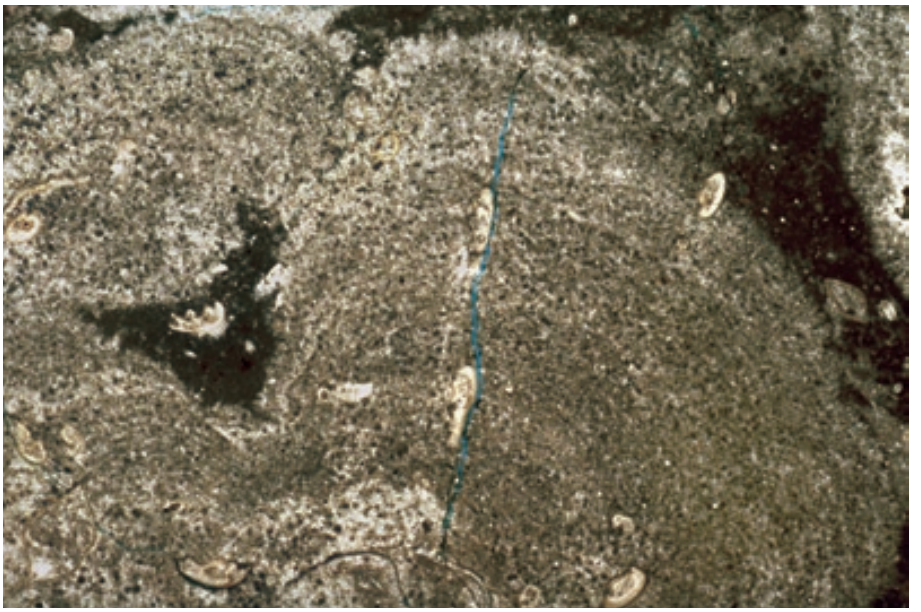

Up. Permian (Kazanian?) Wegener Halvø Fm., Jameson Land, East Greenland

Botryoidal marine cements can also form with a regularly-arranged peloidal fabric — in this case as massive cements within a bryozoan bioherm. Such (originally high-Mg calcite?) peloidal cements may be inorganic or may represent, at least in part, bacterially-induced precipitates.

PPL, BSE, HA = 16 mm

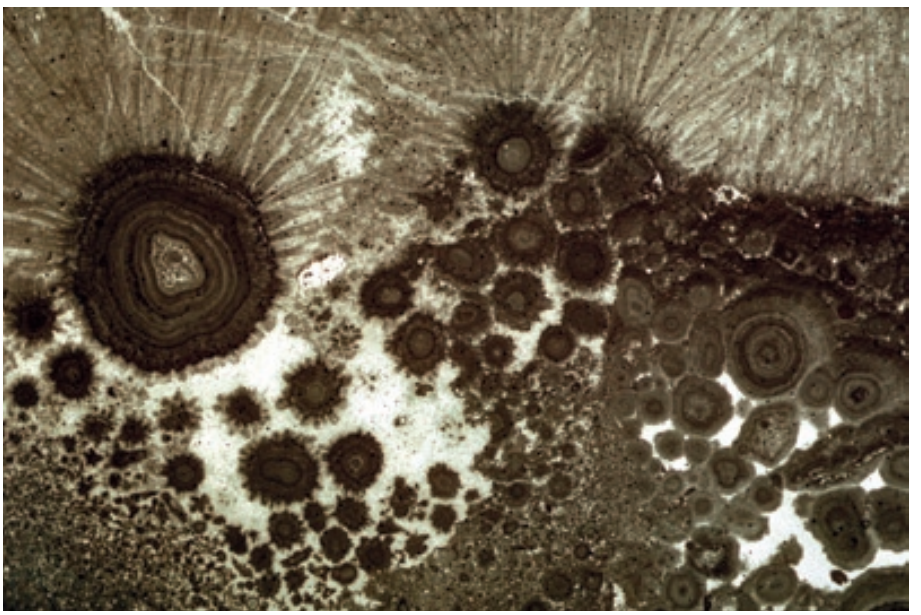

Up. Permian (Guadalupian) Seven Rivers-Yates Fm., Eddy Co., New Mexico

Some radiating cement splays or botryoidal cements grew directly on the sea floor. These formerly aragonitic, bladed cements (now completely dolomitized) grew in conjunction with, and sometimes directly atop, pisoids. The interpretation of these deposits is uncertain, but it clearly involved marine fluids or evaporatively concentrated marine fluids, perhaps on a shallow shoal or as seepage-spring deposits.

PPL, HA = 16 mm

Up. Permian (Guadalupian) Seven Rivers-Yates Fm., Eddy Co., New Mexico

A magnified view of pisolite-associated marine cements similar to the ones shown in the previous photograph. These spectacular bladed cement crystals (now extensively replaced by dolomite) have "square-tipped rays". Such crystal terminations have been used to infer an original aragonite composition for the cements (Loucks and Folk, 1976). The microcrystalline coatings that outline the rays, however, most likely were originally aphanocrystalline high-Mg calcite cements, and perhaps also draped sediment that partially covered the crystals.

PPL, HA = 5.7 mm

Different types of fibrous calcite cements

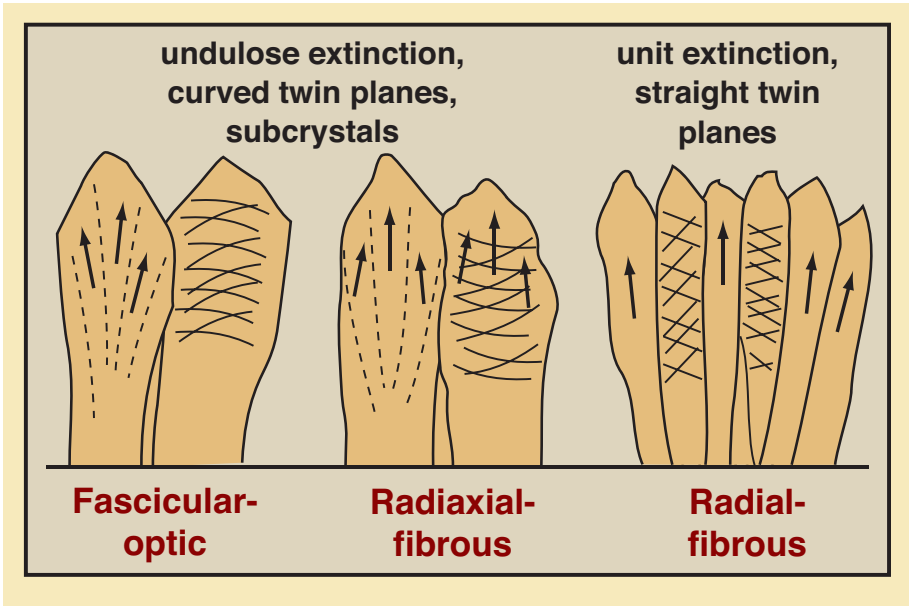

A diagrammatic depiction of the morphologies and crystal-orientations of the three major types of fibrous calcite cement. Arrows represent fast vibration directions (distally divergent in fascicular-optic calcite; distally convergent in radiaxial-fibrous calcite; and uniform in radial-fibrous calcite). Dashed lines represent sub-crystal boundaries and solid crossing lines represent twin planes. All three types of cement have been interpreted either as primary marine cements or as replacements of marine cements (Kendall and Tucker, 1971; Kendall, 1985; Wilson and Dickson, 1996).

Up. Permian limestone, Guangxi Province, People's Republic of China

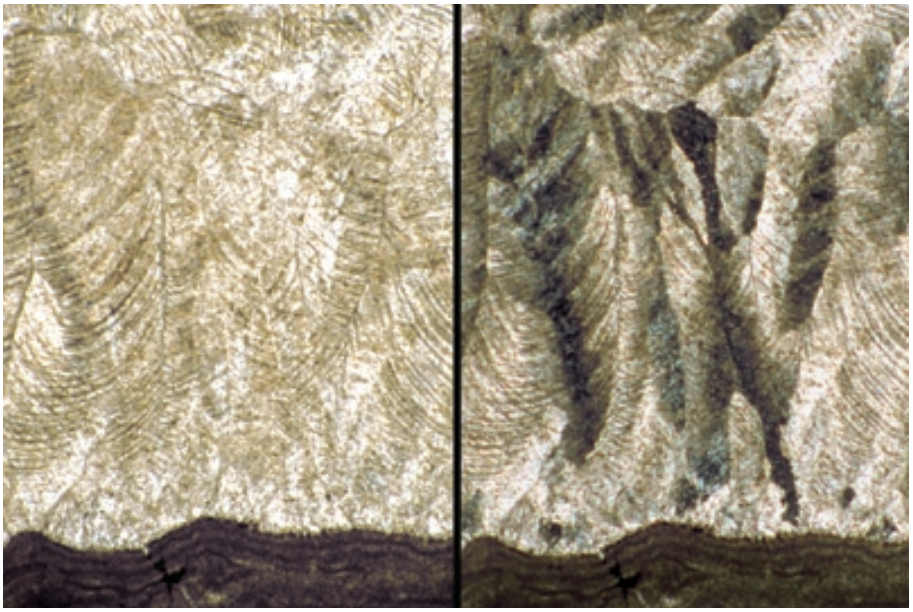

An example of radiaxial-fibrous calcite cements growing atop *Archaeolithoporella* encrustations in a reefal boundstone. Note the cloudy fabric, strongly curved cleavage planes (with distal convergence of optic axes), and undulose extinction of radiaxial-fibrous cements. In this example, the cements were interpreted to have formed from marine waters over a long period of burial along a steep atoll margin that remained in contact with marine waters for tens of millions of years (Halley and Scholle, 1985).

PPL/XPL, HA = 2.1 mm each

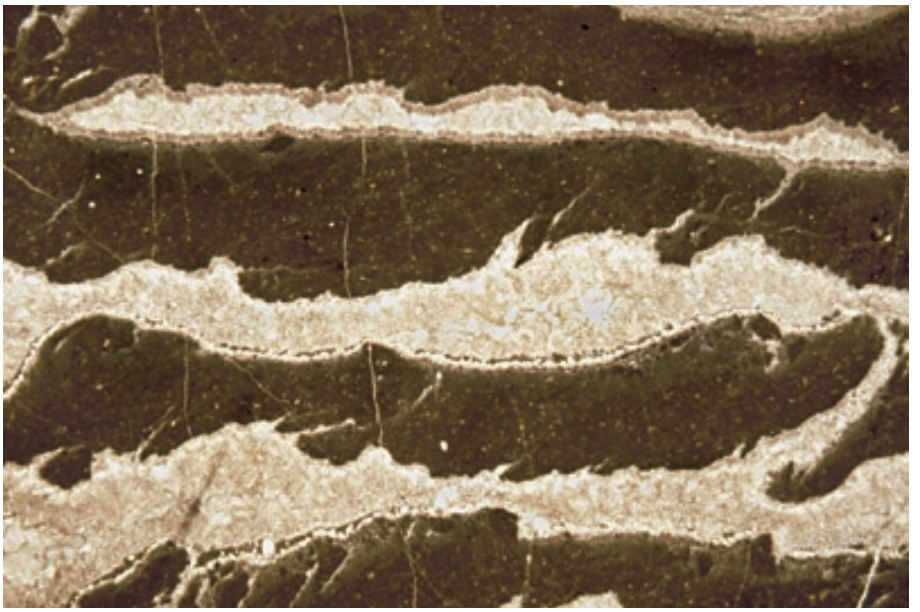

Devonian (Frasnian) limestone, Kielce, Holy Cross Mountains, Poland

A so-called zebra limestone with bands of synsedimentary, slightly cloudy marine cement (with very thin internal sediment) alternating with seafloor micritic sediment. The origin of zebra limestones remains controversial and perhaps has a variety of origins similar to those described for stromatactis cavities in the section on sedimentary structures (decay of various soft-bodied organisms, to gas formation in impermeable sediments, to shear accompanying gravity sliding, and others). Like stromatactis cavities, these more elongate cavities have relatively flat floors and more irregular tops.

PPL, AFeS, HA = 20 mm

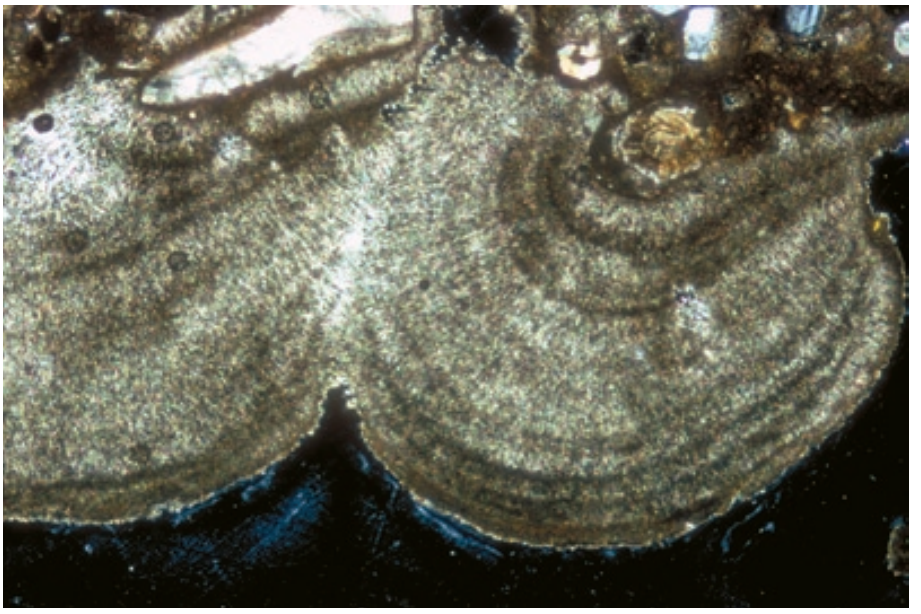

Holocene sediment, Abu Dhabi, United Arab Emirates

Marine diagenesis, or at least the influence of marine fluids, can extend into the upper intertidal zone and beyond. This photograph shows an example of coastal subaerial (spray zone) diagenesis. The pendant or microstalactitic cement morphology reflects vadose conditions; the cement, however, is composed of fibrous aragonite and microcrystalline high-Mg calcite (typically marine mineralogies). The combination reflects the blend of marine waters and vadose conditions in this transitional environment.

XPL, HA = ~2.0 mm

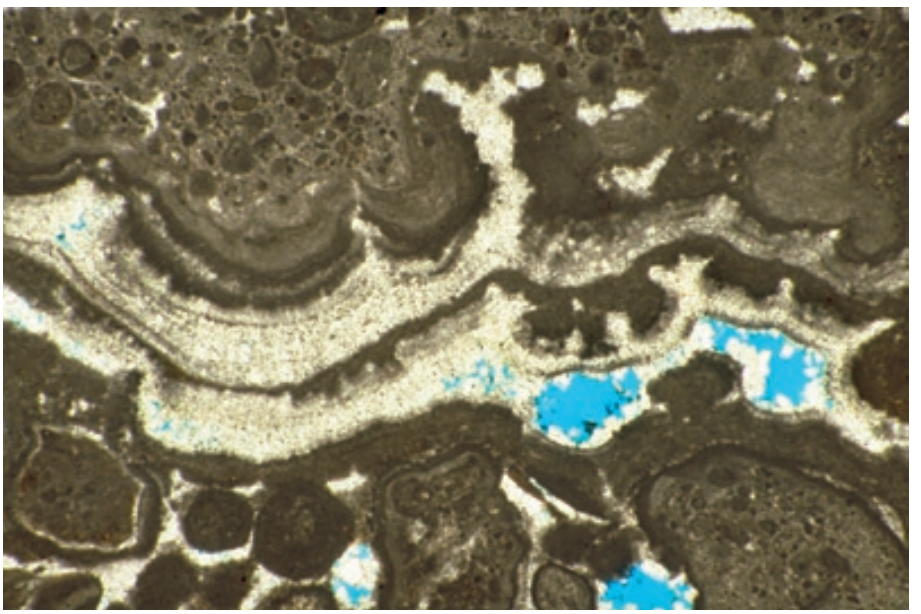

Permian (Guadalupian?) Park City Fm., Ervay equivalent, Big Horn Co., Wyoming

Fabrics reflective of the marine influenced coastal zone can be found in ancient limestones as well. This sample depicts synsedimentary fibrous (probably originally aragonite) and microcrystalline (probably originally high-Mg calcite) cements hanging as pendants from the roof of a large fenestral pore in a pisolitic peritidal unit. All of these marine cements were later neomorphosed to low-Mg calcite.

PPL, BSE, HA = 5.0 mm

Permian (Guadalupian?) Park City Fm., Ervay equivalent, Washakie Co., Wyoming

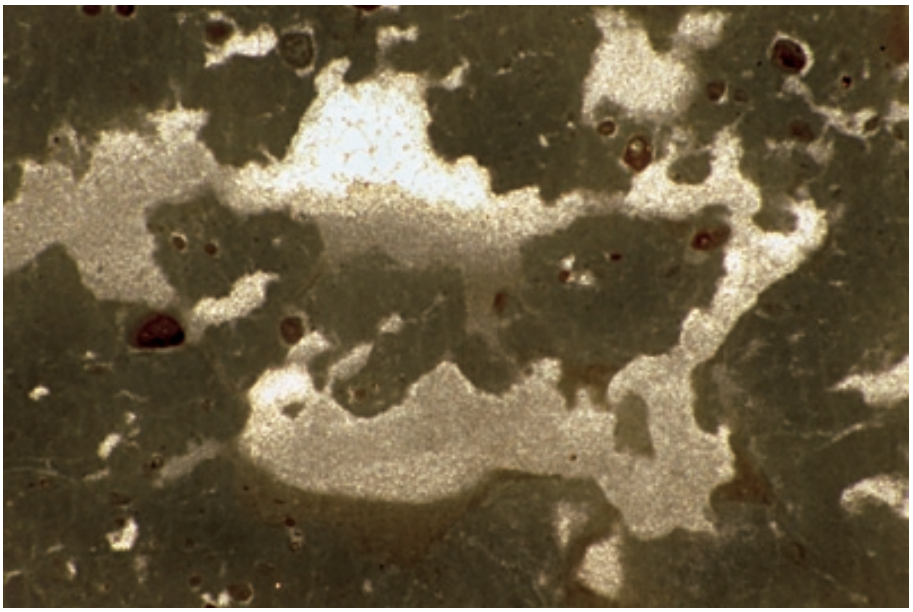

Another example of coastal diagenesis, here showing crystal silt as internal sediment in birds-eye (or fenestral) vugs in peritidal carbonates. Such crystal silt has been interpreted as an indicator of subaerial exposure by Dunham (1969), but in this deposit it is associated with cements with typically "marine" mineralogies (see previous photograph) reflective of hypersaline coastal pore waters. Remnant pore spaces within the fenestrae were filled with sparry calcite. See subsequent chapter on "Meteoric Diagenesis" for additional explanation of these fabrics.

PPL, HA = 5.0 mm

Up. Cretaceous (Campanian-Maastrichtian) Pierre Shale, Pueblo Co., Colorado

These complex, layered, synsedimentary, fibrous crusts of marine calcite cement were precipitated in an inferred submarine methane vent zone. Methane seeps support rich microbial communities and cements associated with such vents are especially rich in inclusions of organic (bacterial?) material.

PPL, AS, HA = ~6.0 mm

Up. Cretaceous (Campanian-Maastrichtian) Pierre Shale, Pueblo Co., Colorado

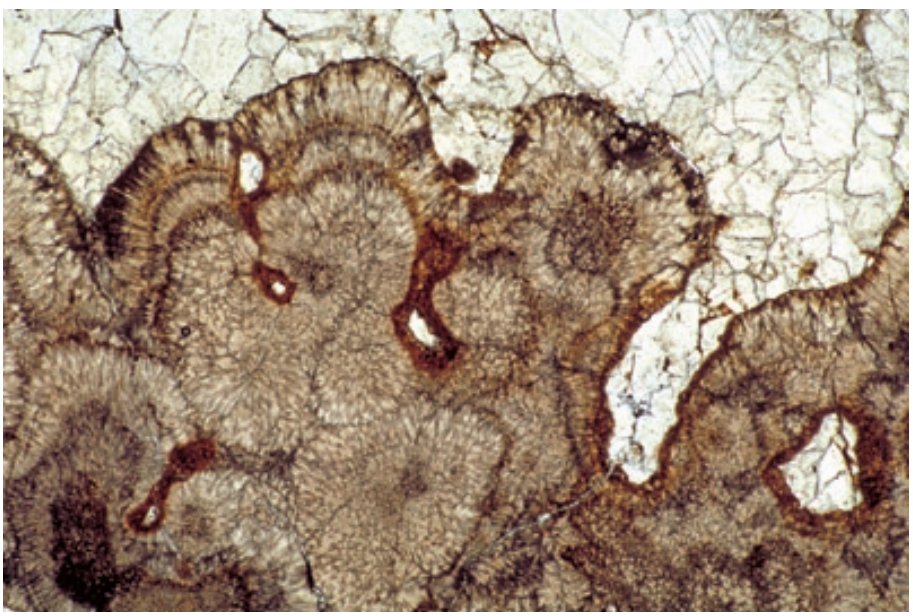

Another example of synsedimentary crusts of marine, fibrous calcite cement and ferruginous material from an inferred submarine methane vent zone. The complex, embayed morphologies of these cement crusts and fans are common in vent cements.

PPL, HA = ~10 mm

Cited References and Additional Information Sources

Alexandersson, T., 1972, Intragranular growth of marine aragonite and Mg-calcite: evidence of precipitation from supersaturated seawater: Journal of Sedimentary Petrology, v. 42, p. 441-460.

Bathurst, R. G. C., 1966, Boring algae, micrite envelopes and lithification of molluscan biosparites: Geological Journal, v. 5, p. 15-32.

Bathurst, R. G. C., 1971, Radiaxial fibrous mosaic, *in* O. P. Bricker, ed., Carbonate Cements: Studies in Geology No. 19: Baltimore, MD, The Johns Hopkins Press, p. 294-295.

Davies, G. R., and W. W. Nassichuk, 1990, Submarine cements and fabrics in Carboniferous to Lower Permian, reefal, shelf margin, and slope carbonates, northwestern Ellesmere Island, Canadian Arctic Archipelago: Ottawa, Geological Survey of Canada Bulletin 399, 77 p.

Friedman, G. M., 1998, Rapidity of marine carbonate cementation — implications for carbonate diagenesis and sequence stratigraphy: perspective: Sedimentary Geology, v. 119, p. 1-4.

Friedman, G. M., and A. J. Amiel, 1974, Submarine cementation in reefs: example from the Red Sea: Journal of Sedimentary Petrology, v. 44, p. 816-825.

Grammer, G. M., C. M. Crescini, D. F. McNeill, and L. H. Taylor, 1999, Quantifying rates of syndepositional marine cementation in deeper platform environments-new insight into a fundamental process: Journal of Sedimentary Research, v. 69, p. 202-207.

Grammer, G. M., R. N. Ginsburg, P. K. Swart, D. F. McNeill, A. J. T. Jull, and D. R. Prezbindowski, 1993, Rapid growth rates of syndepositional marine aragonite cements in steep marginal slope deposits, Bahamas and Belize: Journal of Sedimentary Petrology, v. 63, p. 983-989.

Halley, R. B., and P. A. Scholle, 1985, Radiaxial fibrous calcite as early-burial, open-system cement: isotopic evidence from Permian of China [abs.]: American Association of Petroleum Geologists Bulletin, v. 69, p. 261.

Hanor, J. S., 1978, Precipitation of beachrock cements: mixing of marine and meteoric waters vs. CO_2-degassing: Journal of Sedimentary Petrology, v. 48, p. 489-501.

Hood, S. D., and C. S. Nelson, 1996, Cementation scenarios for New Zealand Cenozoic nontropical limestones: New Zealand Journal of Geology and Geophysics, v. 39, p. 109-122.

James, N. P., and P. W. Choquette, 1983, Diagenesis 6. Limestones — The sea floor diagenetic environment: Geoscience Canada, v. 10, p. 162-179.

Jørgensen, N. O., 1976, Recent high magnesian calcite/aragonite cementation of beach and submarine sediments from Denmark: Journal of Sedimentary Petrology, v. 46, p. 940-951.

Kendall, A. C., 1985, Radiaxial fibrous calcite: a reappraisal, *in* N. Schneidermann, and P. M. Harris, eds., Carbonate Cements: Tulsa, OK, SEPM Special Publication No. 36, p. 59-77.

Kendall, A. C., and M. E. Tucker, 1971, Radiaxial fibrous calcite as a replacement after syn-sedimentary cement: Nature (Physical Science), v. 232, p. 62-63.

Kendall, C. G. St. C., J. L. Sadd, and A. S. Alsharhan, 1994, Holocene marine cement coatings on beachrocks of the Abu Dhabi coastline (U.A.E.), an analog for cement fabrics in ancient limestone: Carbonates and Evaporites, v. 9, p. 119-131.

Kennedy, W. J., and R. E. Garrison, 1975, Morphology and genesis of nodular chalks and hardgrounds in the Upper Cretaceous of southern England: Sedimentology, v. 22, p. 311-386.

Lohmann, K. C., and J. C. G. Walker, 1989, The $\delta^{18}O$ record of Phanerozoic abiotic marine calcite cements: Geophysical Research Letters, v. 16, p. 319-322.

Loucks, R. G., and R. L. Folk, 1976, Fanlike rays of former aragonite in Permian Capitan reef pisolite: Journal of Sedimentary Petrology, v. 46, p. 483-485.

Macintyre, I. G., 1985, Submarine cements — the peloidal question, *in* N. Schneidermann, and P. M. Harris, eds., Carbonate Cements: Tulsa, OK, SEPM Special Publication No. 36, p. 109-116.

Mazzullo, S. J., 1980, Calcite pseudospar replacive of marine acicular aragonite, and implications for aragonite cement diagenesis: Journal of Sedimentary Petrology, v. 50, p. 409-422.

Mazzullo, S. J., and J. M. Cys, 1978, *Archaeolithoporella*-boundstones and marine aragonite cements, Permian Capitan reef, New Mexico and Texas, USA: Neues Jahrbuch für Geologie und Paläontologie, Monatshefte, v. 1978, p. 600-611.

Mazzullo, S. J., and J. M. Cys, 1979, Marine aragonite sea-floor growths and cements in Permian phylloid algal mounds, Sacramento Mountains, New Mexico: Journal of Sedimentary Petrology, v. 49, p. 917-936.

Melim, L. A., P. K. Swart, and R. G. Maliva, 1995, Meteoric-like fabrics forming in marine waters: Implications for the use of petrography to identify diagenetic environments: Geology, v. 23, p. 755-758.

Moore, C. H., Jr., 1973, Intertidal carbonate cementation, Grand Cayman, West Indies: Journal of Sedimentary Petrology, v. 43, p. 591-602.

Pingitore, N. E., Jr., 1971, Submarine precipitation of void-filling needles in Pleistocene coral, *in* O. P. Bricker, ed., Carbonate Cements: Baltimore, MD, The Johns Hopkins Press, p. 68-71.

Savard, M. M., B. Beauchamp, and J. Veizer, 1996, Significance of aragonite cements around Cretaceous marine methane seeps: Journal of Sedimentary Research, v. 66, p. 430-438.

Shinn, E. A., 1971, Holocene submarine cementation in the Persian Gulf, *in* O. P. Bricker, ed., Carbonate Cements: Baltimore, MD, Johns Hopkins Press, p. 63-65.

Sumner, D. Y., and J. P. Grotzinger, 2000, Late Archean aragonite precipitation: petrography, facies associations, and environmental significance, *in* J. P. Grotzinger, and N. P. James, eds., Carbonate Sedimentation and Diagenesis in the Evolving Precambrian World: Tulsa, OK, Society for Sedimentary Geology (SEPM) Special Publication No. 67, p. 123-144.

Tobin, K. J., and K. R. Walker, 1996, Ordovician low- to intermediate- Mg calcite marine cements from Sweden: marine alteration and implications for oxygen isotopes in Ordovician seawater: Sedimentology, v. 43, p. 719-735.

Walker, K. R., D. G. Jernigan, and L. J. Weber, 1990, Petrographic criteria for the recognition of marine, syntaxial overgrowths, and their distribution in geologic time: Carbonates and Evaporites, v. 5, p. 141-152.

Whittle, G. L., C. G. St. C. Kendall, R. Dill, and L. Rouch, 1993, Carbonate cement fabrics displayed: a traverse across the margin of the Bahamas Platform near Lee Stocking Island in the Exuma Cays: Marine Geology, v. 110, p. 213-243.

Wilber, R. J., and A. C. Neumann, 1993, Effects of submarine cementation on microfabrics and physical properties of carbonate slope deposits, northern Bahamas, *in* R. Rezak, and D. L. Lavoie, eds., Carbonate Microfabrics: New York, Springer-Verlag, p. 79-94.

Wilkinson, B. H., and R. K. Given, 1986, Secular variation in abiotic marine carbonates: constraints on Paleozoic atmospheric carbon dioxide contents and oceanic Mg/Ca ratios: Journal of Geology, v. 94, p. 321-333.

Wilson, P. A., and J. A. D. Dickson, 1996, Radiaxial calcite: Alteration product of and petrographic proxy for magnesian calcite marine cement: Geology, v. 24, p. 945-948.

Winland, H. D., 1971, Nonskeletal deposition of high-Mg calcite in the marine environment and its role in the retention of textures, *in* O. P. Bricker, ed., Carbonate Cements: Baltimore, MD, The Johns Hopkins Press, p. 278-284.

Facing Page: Top - Holocene (ca. 6,000 yBP) eolianite, San Salvador Island, Bahamas. Note selective lithification of the upper surface of the dune as a result of meteoric cementation,
Bottom - Polished slab of a laminated calcrete crust overlying an irregular erosion surface on a marine Pennsylvanian limestone (Bethany Falls Ls., Linn County, Kansas). Photograph courtesy of Robert H. Goldstein.

CARBONATE DIAGENESIS

EOGENETIC METEORIC DIAGENESIS

CHAPTER 24

METEORIC DIAGENESIS

Introduction:

Meteoric diagenesis represents alteration that occurs at or near the earth's surface in strata influenced or pervaded by waters of recent atmospheric origin. The meteoric environment is typically divided into unsaturated (vadose) and saturated (phreatic) zones divided by a water table (see top diagram, facing page). The interfaces between surficial meteoric fluids and strata filled with other pore fluids (seawater or basinal waters) are "mixing zones" that can have special diagenetic characteristics.

Many, perhaps most, shallow marine carbonate deposits undergo meteoric diagenesis, either as a consequence of buildup of sediments above sea level, or through drops in sea level that expose platform carbonates. In addition, meteoric water can circulate well below the land surface to alter carbonate deposits far older than the exposure interval. Meteoric processes commonly act over time periods of hundreds to millions of years.

Meteoric diagenetic patterns typically are complex and variable for the following reasons: 1. regional and temporal variations in starting material; 2. variations in rainfall and water throughput rates (in part, related to permeability variations); 3. variations in water chemistry (from locality to locality or vertically through the water column at any one site, especially at mixing interfaces); 4. variations in the duration of exposure or alteration during multiple episodes of exposure; and 5. the effects of plants and plant-derived acids that vary regionally and also changed through geologic time as a consequence of evolution of different plant groups.

Major diagenetic fabrics:

The vadose zone is characterized by extensive dissolution of unstable carbonate minerals (aragonite and high-Mg calcite), often with reprecipitation of more stable carbonate (low-Mg calcite). As a consequence, primary porosity commonly is filled during meteoric diagenesis, and secondary porosity is created.

Unless there is a thinning or collapse of the rock section, meteoric diagenesis is relatively porosity neutral, at least at the scale of grains, with dissolution at one site supplying solutes for reprecipitation elsewhere. Meteoric diagenesis does, however, have a strong effect on permeability (e.g., permeability reductions through cementation of interconnected primary pores or permeability increases through solution enlargement of fractures).

Many vadose cements have fabrics reflecting the selective distribution of water in that environment — pendant (microstalactitic or gravitational) cements hanging from undersides of grains and meniscus cements concentrated at grain contacts. Whisker crystals (also termed needle-fiber cements), calcified filaments, blackened pebbles, root structures (rhizoliths), microspar, and *Microcodium* also are common features.

Phreatic zone cements are typically isopachous rims or complete pore fillings of equant calcite.

Freshwater meteoric calcites are depleted in Sr^{2+}, Mg^{2+}, $\delta^{18}O$, and $\delta^{13}C$, relative to their marine precursors. Most, but not all, meteoric settings are oxidizing, resulting in typically low Fe^{2+} and Mn^{2+} contents in meteoric cements (reflected in non-ferroan staining and no cathodoluminescence response).

Freshwater meteoric areas commonly have extensive dissolution features — e.g., solution-enlarged fractures, sinkholes, caves, or collapse breccias (karstic features). Such dissolution is especially common in the vadose zone, at the vadose-phreatic mixing zone (the water table), and perhaps in marine- to freshwater mixing zones. Selective dissolution affecting primarily aragonitic constituents is widespread, and thus geologic time periods with highly aragonitic sediments have enhanced meteoric diagenetic potential. Alteration rates vary widely and are a function of rainfall, sediment permeability, and other factors affecting water throughput rates.

Various types of surficial deposits occur in areas of meteoric exposure, including residual soils with carbonate rhizocretions or nodules, soil crusts, calcretes and caliches, or spring-fed travertines.

Vadose alteration leads to diagenetic stabilization of unstable marine limestones; in the absence of meteoric alteration, however, similar processes of aragonite and Mg-calcite dissolution and low-Mg calcite precipitation eventually take place during burial. Recent studies have shown that very similar products are produced during meteoric phreatic and burial-stage transformations (e.g., Melim et al., 2002) and geochemical studies may be required to help determine the diagenetic setting in which such transformations took place.

Mineralogy:

Freshwater meteoric cements (vadose and phreatic) consist mainly of low-Mg calcite. In arid regions with saline groundwater, aragonite, high-Mg calcite, low-Mg calcite, calcian dolomite, gypsum, anhydrite, and other evaporite minerals are common precipitates. Dolomite also is formed in fresh- to marine-water mixing zones. In surficial weathering crusts, calcite, dolomite, silica, phosphate, iron and aluminum oxides, clays, and other minerals can accumulate and/or precipitate.

The major subdivisions of a coastal meteoric diagenetic zone

There are two primary subdivisions of the environment of meteoric alteration. The vadose zone (also termed the undersaturated zone) lies closest to the surface and is divided into an upper zone of infiltration and a lower area of gravity percolation. The vadose zone overlies the shallow phreatic zone (also termed the saturated zone). The dividing line between the vadose and phreatic environments is termed the water table. A brackish-water transition zone occurs between meteoric and marine waters and is termed the mixing zone. Redrawn from James and Choquette (1984).

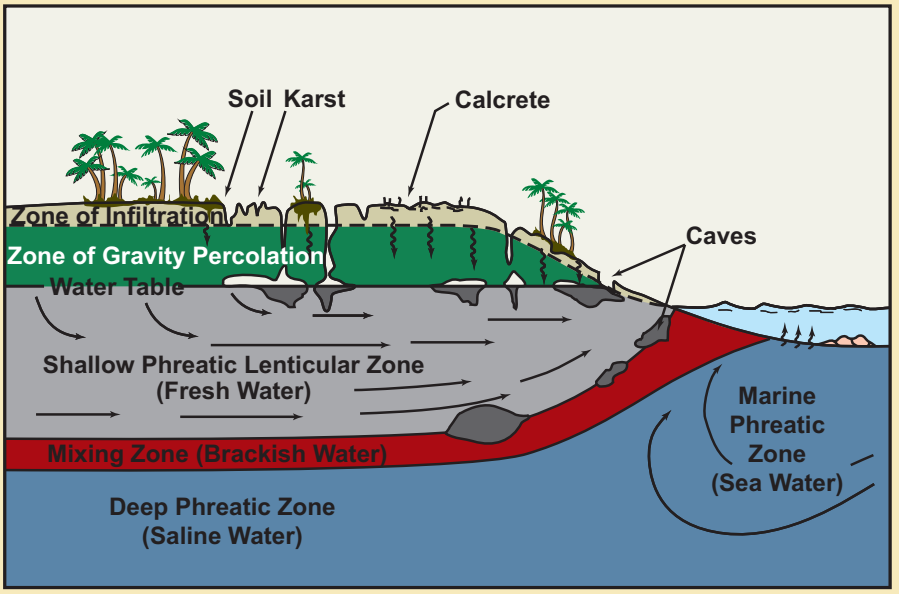

Morphologies of major types of meteoric cements

A diagrammatic depiction of the morphologies of some major types of cements commonly precipitated during meteoric diagenesis — vadose zone fabrics are shown on the left side; phreatic zone fabrics are shown on the right side. Syntaxial (also termed epitaxial) overgrowths can form in both environments but will be covered under burial diagenesis in this book. Vadose fabrics are influenced by the localized distribution of water at grain contacts and as droplets hanging from the undersides of grains. Phreatic cements are more uniformly distributed, reflecting the complete saturation of pores with water in that environment. Adapted from James and Choquette (1984).

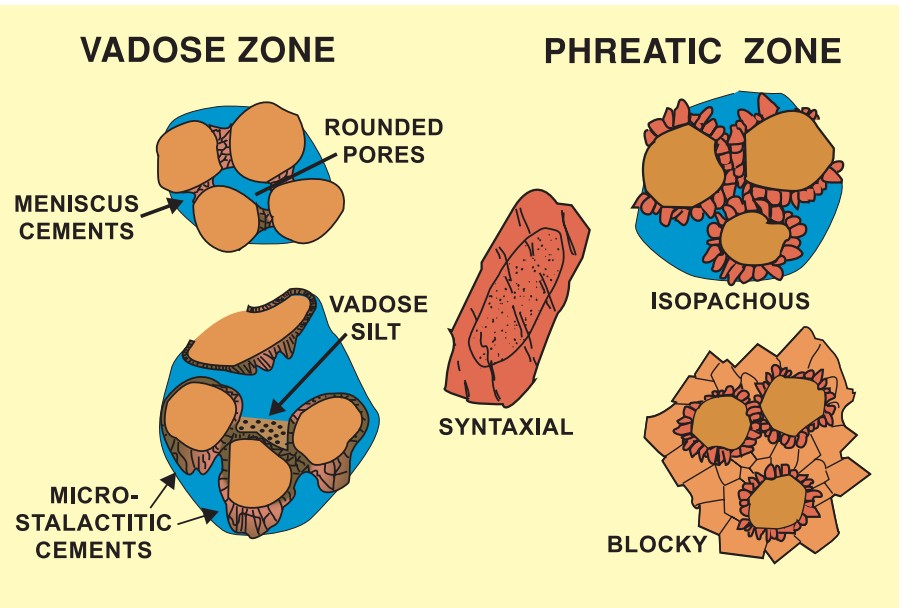

Stages of meteoric diagenesis

Meteoric diagenesis generally is a cannibalistic process, with dissolution of unstable materials at one site supplying material for precipitation at another. In this diagram, early stages of phreatic cementation are matched by initial dissolution of unstable materials, although some or most of that dissolution may occur in vadose settings and much of the cementation may occur in the phreatic zone. With extended meteoric diagenesis this process can lead to complete fabric inversion — former grains become secondary pores; former (primary) pores become cement filled. If the process is continued with an external supply of solutes, even the secondary porosity can be filled with cements (a stage not shown here).

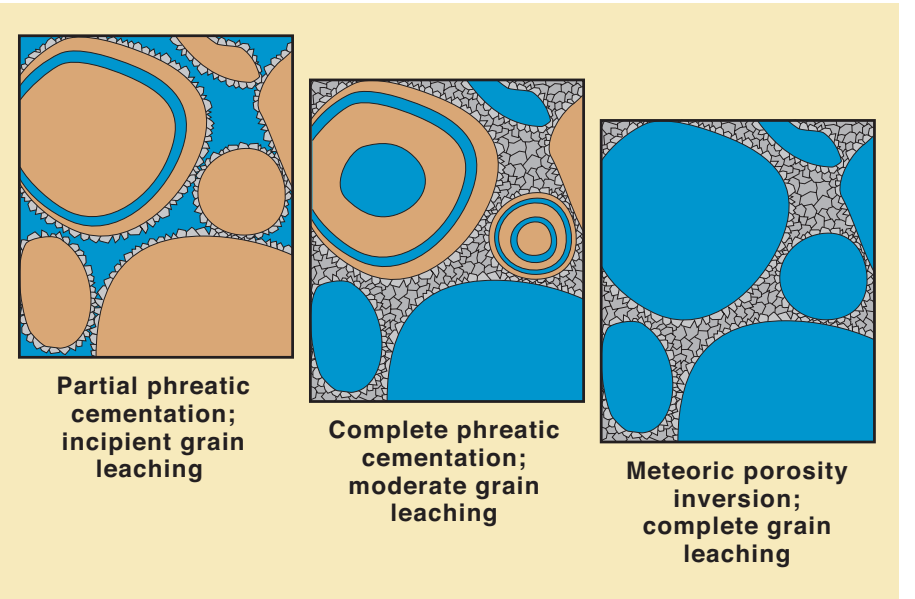

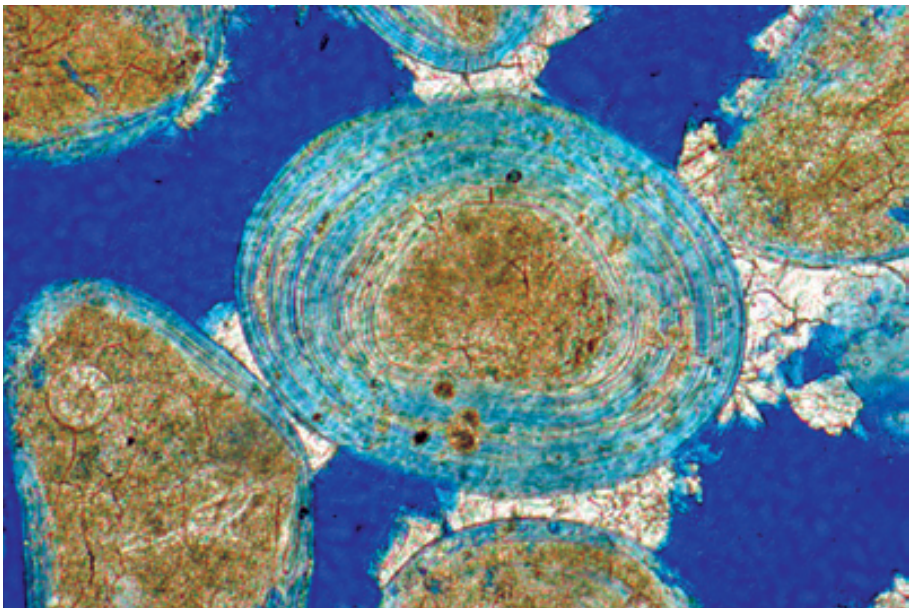

Holocene (<2700 yBP) eolianite, Isla Cancun, Quintana Roo, Mexico

An oolitic eolianite at an early stage of freshwater vadose diagenesis. The alteration consists of selective ("chalky") dissolution of original aragonitic ooids, combined with partial filling of primary porosity by meniscus calcite cement. The meniscus fabric is characterized by a marked concentration of crystals at or near grain contacts (sites where capillary water films with curved meniscus boundaries would be concentrated). Photograph courtesy of Robert G. Loucks.

PPL, BSE, HA = ~ 0.7 mm

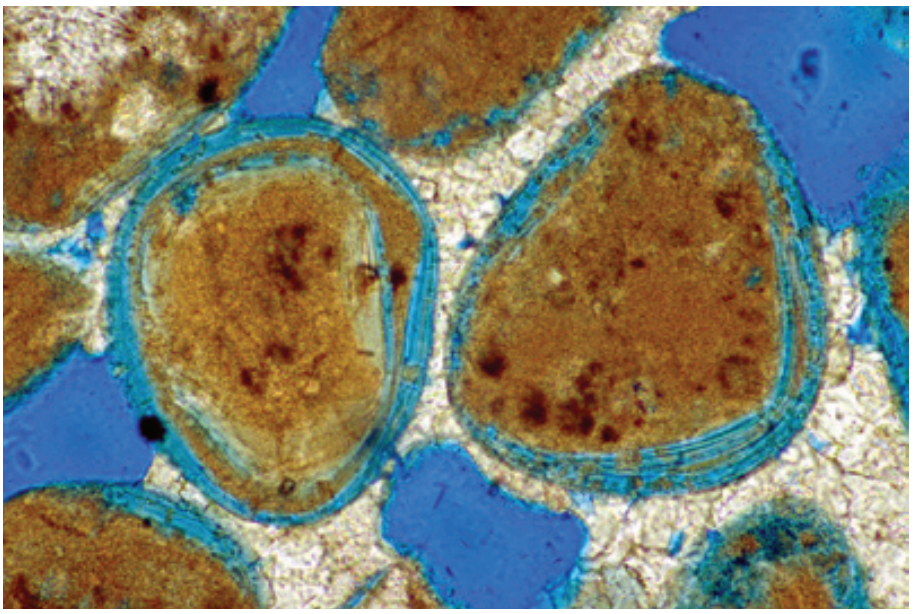

Holocene eolianite, Isla Cancun, Quintana Roo, Mexico

An example of somewhat more extensive vadose diagenesis in a Holocene eolianite. The thin (superficial) aragonitic ooid cortices are extensively dissolved and the sediment has been substantially cemented with coarse meniscus calcite. Note the blocky, equant nature of the low-Mg calcite cement and the production of highly rounded pores conforming to the meniscus surfaces of water held at grain contacts. Photograph courtesy of Robert G. Loucks.

PPL, BSE, HA = 0.6 mm

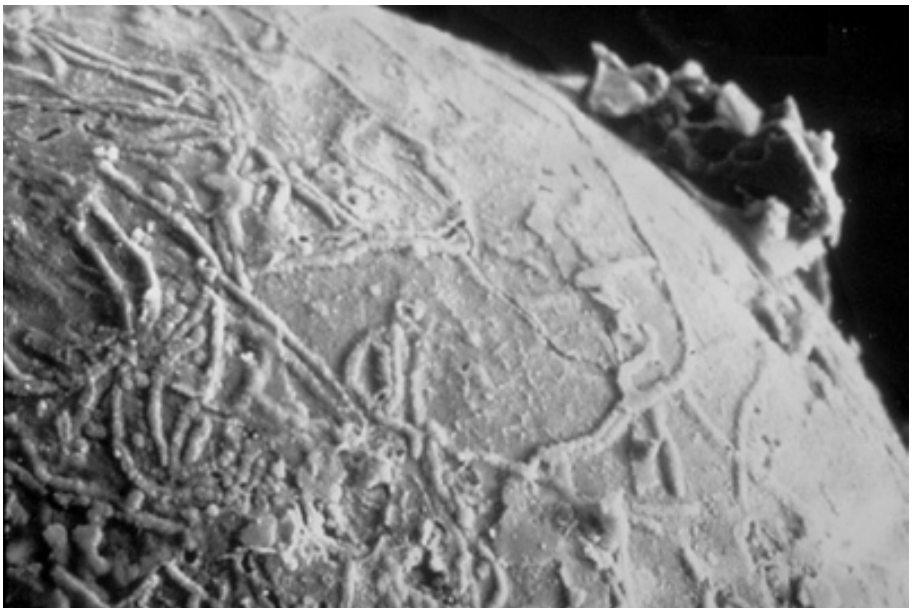

Holocene sediment, Joulters Cay, Great Bahama Banks, Bahamas

An SEM image of a 1000-year-old ooid that has undergone dissolution of its aragonitic outer cortical layer, exposing the high-Mg calcite-filled endolithic microbial borings that were once enclosed in the aragonite. This dissolution has taken place in the vadose zone associated with the small freshwater lens that underlies this island. Although rates of aragonite dissolution are highly variable, porous grainstones in high rainfall areas can be extensively altered on time scales of thousands to tens of thousands of years. Photograph courtesy of Robert B. Halley.

SEM, HA = 160 μm

Holocene eolianite, Isla Cancun, Quintana Roo, Mexico

Although aragonite dissolution is the norm in freshwater vadose settings, calcite cementation can occur, at least locally, without extensive aragonite removal. These superficial ooids were cemented by low-Mg calcite with a meniscus fabric that has formed rounded pores. This "spot welding" produces a structurally strong fabric that can preserve porosity through extensive burial. Continued cementation will both obscure the meniscus fabrics and set up the potential for producing moldic porosity through the removal of the unstable aragonitic grains from a framework of stable calcite cement.

XPL, HA = 0.65 mm

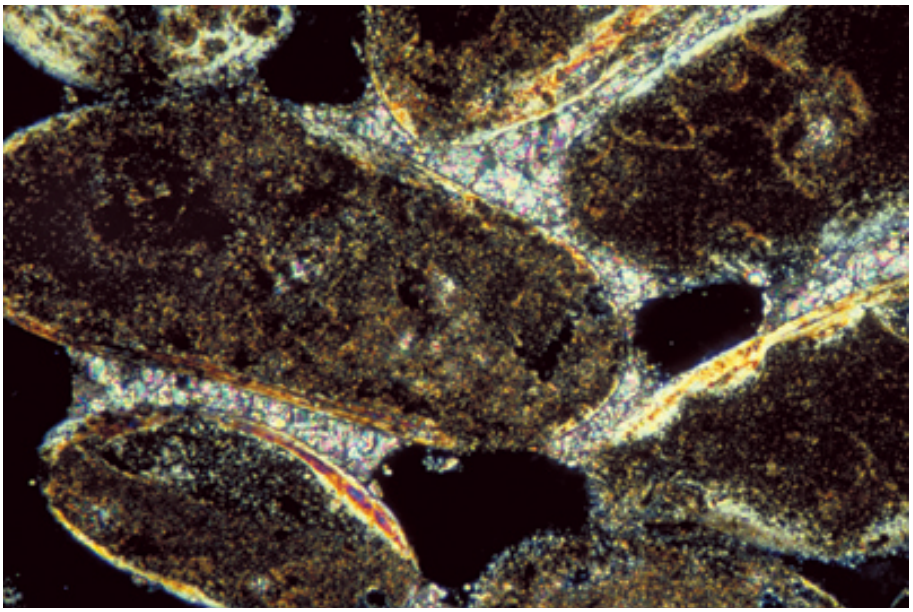

Holocene sediment, Joulters Cay, Great Bahama Banks, Bahamas

An SEM image of meniscus-cemented ooids. The meniscus fabric is characterized by thickened cements near grain contacts and resultant smoothly ovoid to circular remnant pores (a meniscus shape). This view shows the smoothly curved surface of the calcite cement between two aragonitic ooids. In some vadose settings, however, grain contacts are the sites of preferential dissolution which can yield fabrics that appear "overcompacted" (Knox, 1977). Photograph courtesy of Robert B. Halley.

SEM, HA = 160 μm

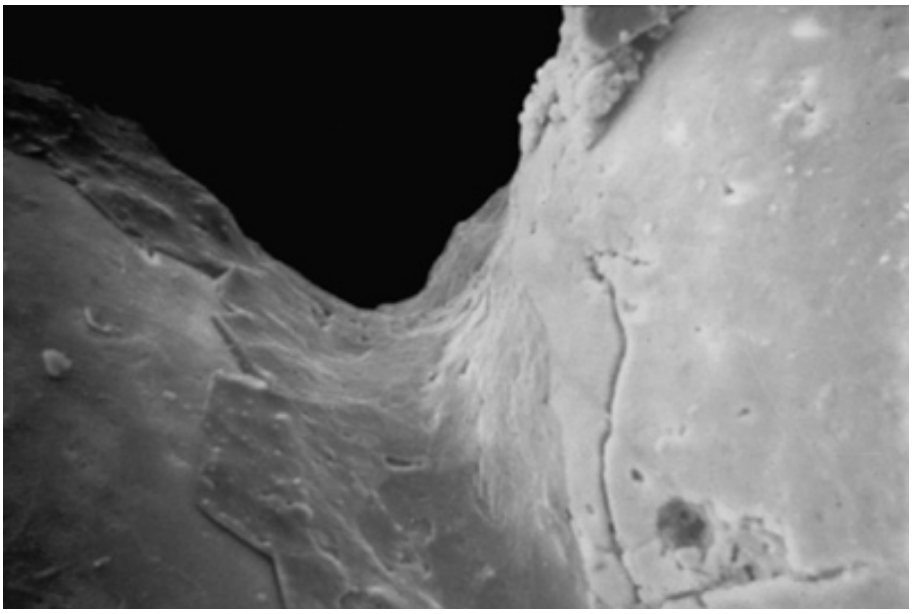

Lo. Holocene (ca. 6000 yBP) eolianite, San Salvador Island, Bahamas

Meteoric cements are selectively precipitated in places where capillary water is held and can gradually evaporate. In this example, blocky calcite cements are concentrated only in the finer-grained avalanche layers of carbonate dune sands; the coarser layers are virtually uncemented. The selective cementation of the finer-grained layers demonstrates how small-scale primary porosity and permeability variations can be accentuated by diagenetic processes.

PXPL, BSE, HA = 14.5 mm

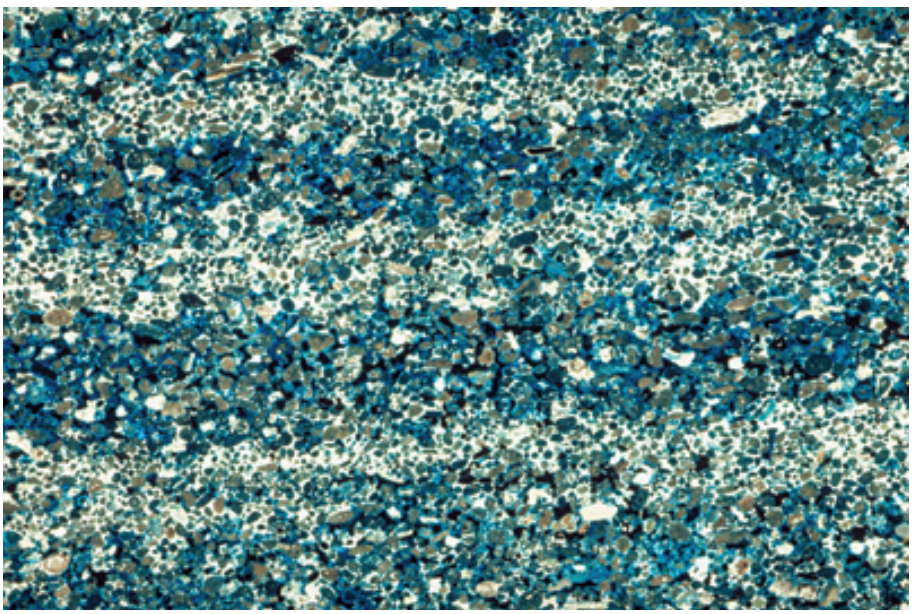

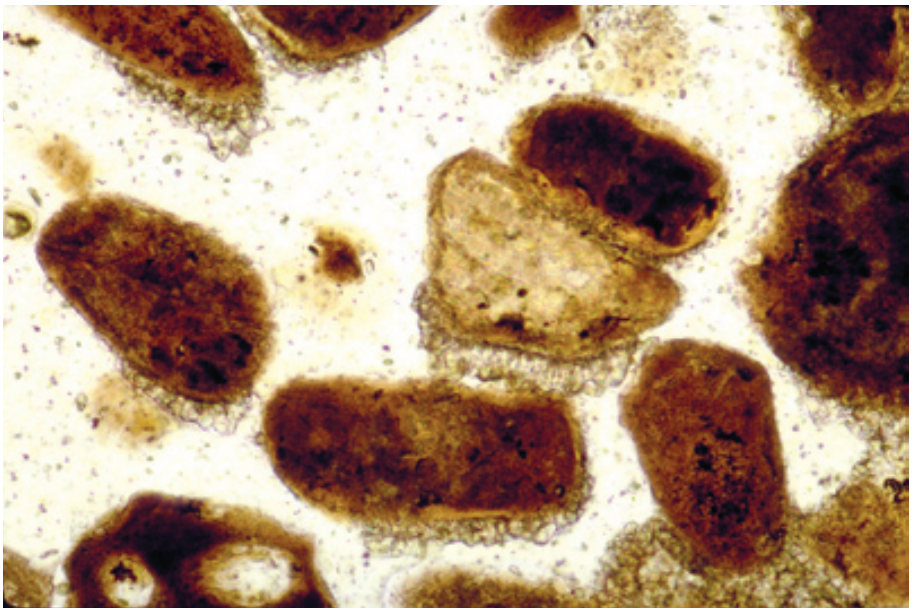

Holocene eolianite, Isla Blanca, Quintana Roo, Mexico

Another vadose meteoric cement morphology that reflects partial water saturation in that setting is pendant or microstalactitic cement (also termed gravitational cement). As the names imply, these cements form pendants that hang from the bottoms of grains, in exactly the same positions that water droplets would occupy. Although not seen in this example, the tops of grains in pendant-cemented strata are commonly corroded. Pendant cements are composed of low-Mg calcite in freshwater areas but are aragonite and high-Mg calcite in coastal spray zone deposits. Photograph courtesy of William C. Ward.

PPL, HA = 0.8 mm

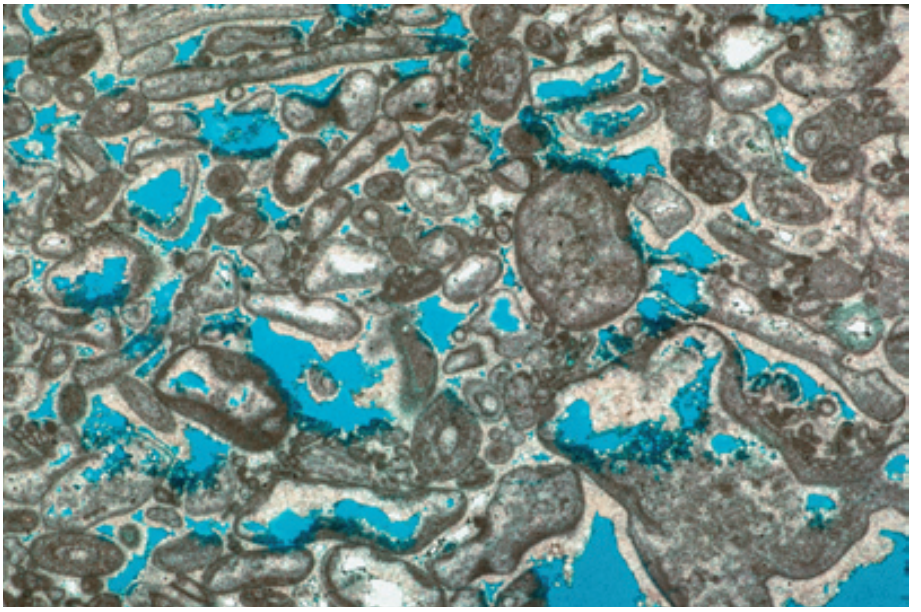

Up. Permian (Kazanian?) Wegener Halvø Fm., Jameson Land, East Greenland

Continued cementation during meteoric and burial diagenesis commonly obscures early vadose cement fabrics. In this example, however, a partially-cemented skeletal grainstone from just below a major sequence boundary preserves distinctive calcitic vadose cements. Note the pendants of cement hanging from the bottoms of many grains and filling primary porosity. In addition, pendant cements also hang downward within moldic pores surrounded by micrite envelopes, molds presumably also produced during vadose exposure.

PPL, AFeS, BSE, HA = 13.5 mm

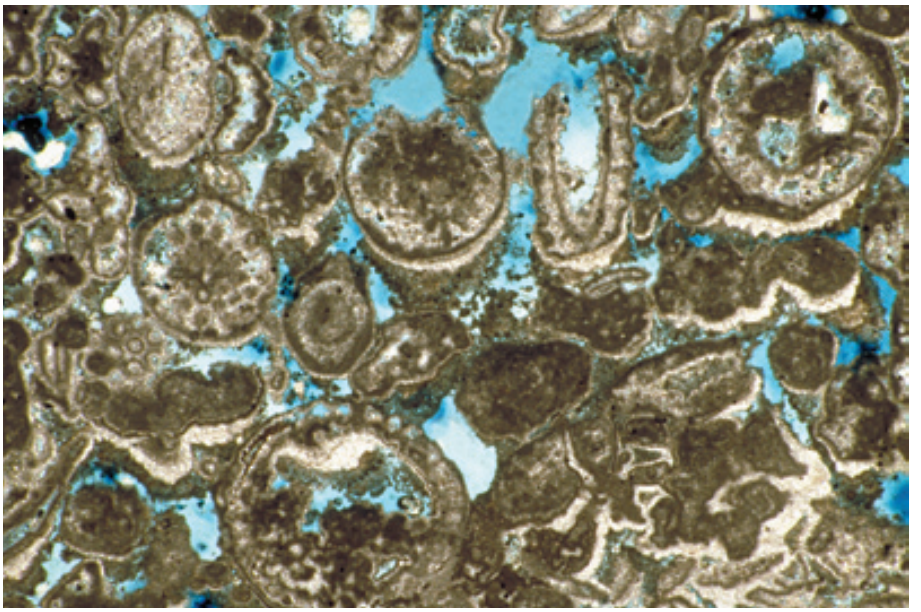

Up. Permian (Guadalupian) Tansill Fm., Eddy Co., New Mexico

Another example of preserved vadose cements in an ancient limestone. These microstalactitic or pendant fabrics were precipitated from water droplets hanging from intra- and intergranular surfaces in the sediment. Note also the dissolution of the tops of many of these *Mizzia* green-algal grains by undersaturated meteoric waters percolating downward through the sediment. Pendant cements in this area are very localized and are apparently associated with small islands that built up above sea level during sedimentation.

PPL, BSE, HA = 7.0 mm

Pleistocene Key Largo Ls., Florida Keys, Monroe Co., Florida

A partially leached void filled with low-Mg calcite "needle-fiber" or "whisker crystal" cement. These are thin, randomly oriented crystals that are commonly found in meteorically altered limestones. They probably are precipitated mainly in the vadose zone and can be difficult to recognize in older rocks when obscured by later sparry calcite cements.

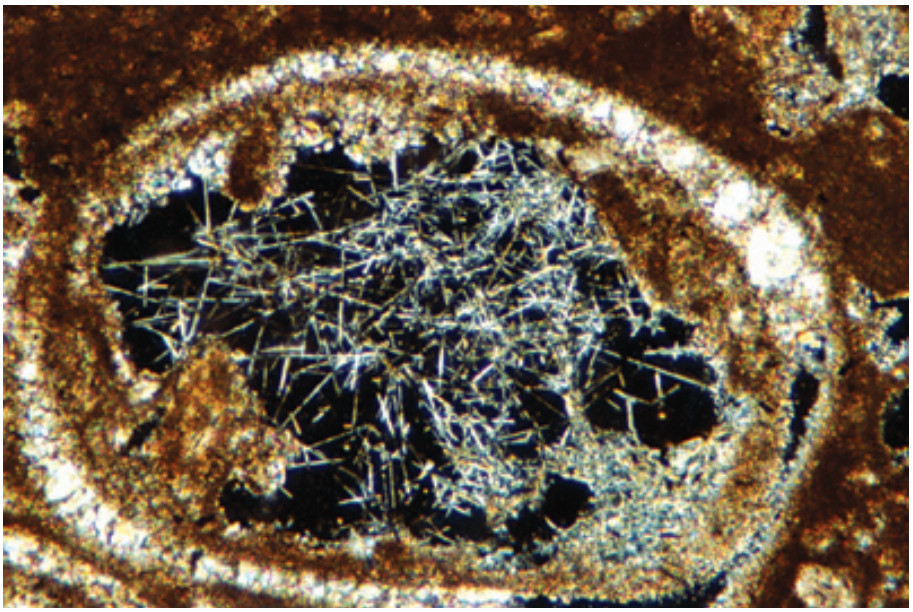

XPL, HA = 3.4 mm

Pleistocene eolianite, Isla Mujeres, Quintana Roo, Mexico

Another example of needle-fiber or whisker crystal calcite cement from the vadose zone. Here much more of the porosity was occluded by a coarse meshwork of crystal laths. Photograph courtesy of William C. Ward.

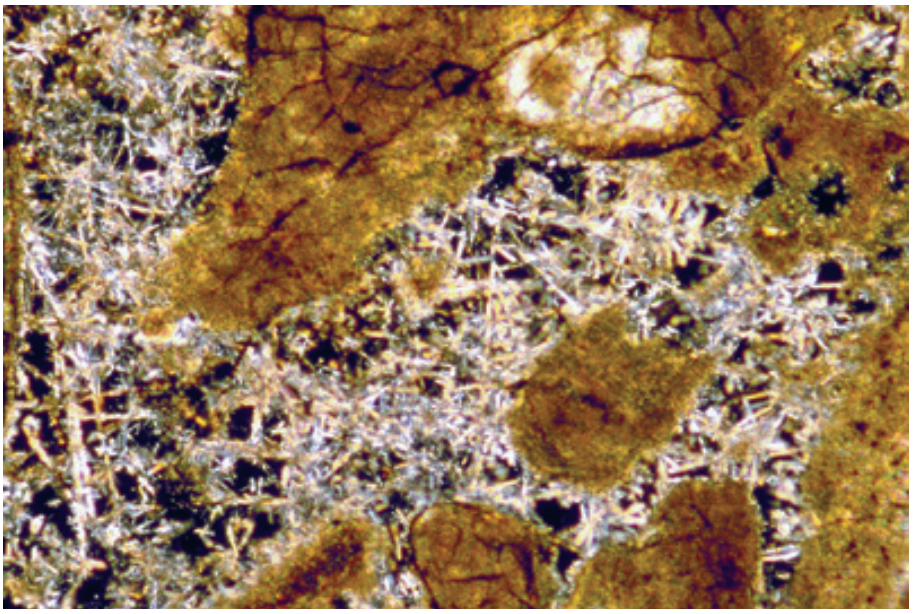

XPL, HA = 0.7 mm

Up. Pennsylvanian (Virgilian) Holder Fm., Otero Co., New Mexico

Recognition of needle fiber or whisker crystal cements in ancient limestones is relatively uncommon, but is possible with careful observation. In this example, random needle fibers of calcite are readily visible because they are highlighted as inclusions within a single crystal of later calcite cement that is at optical extinction in this image. Photograph courtesy of Robert H. Goldstein.

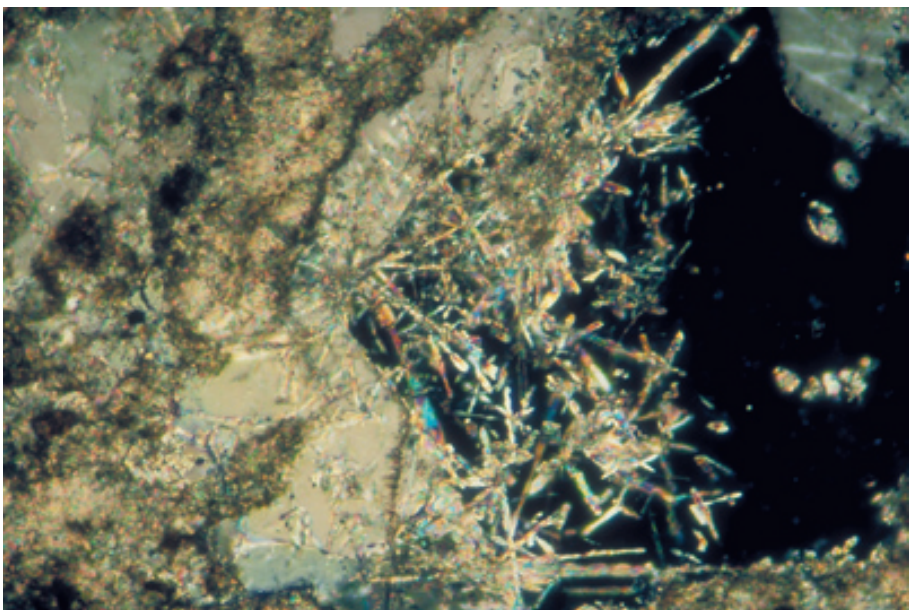

XPL, HA = 0.65 mm

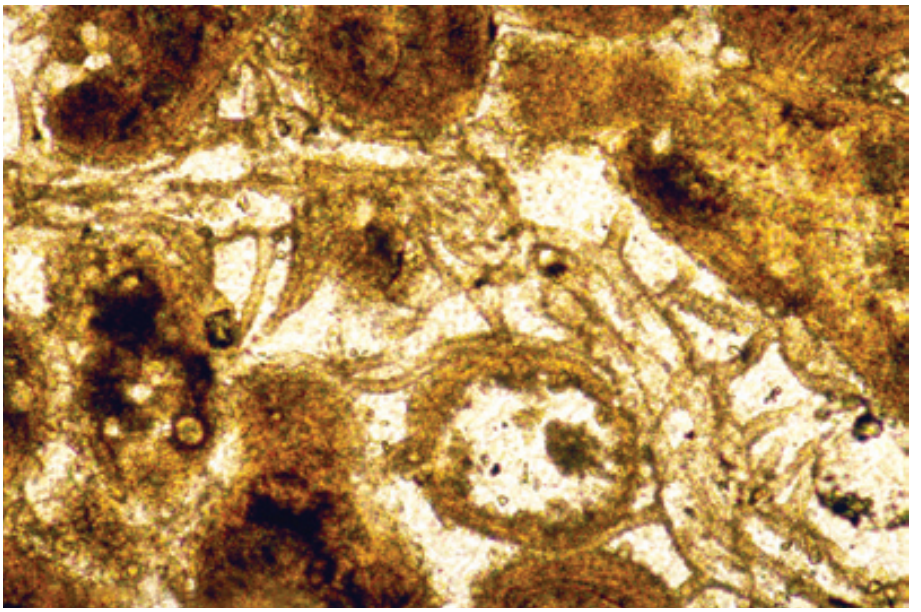

Pleistocene eolianite, Isla Cancun, Quintana Roo, Mexico

Calcified plant remains or plant root structures are characteristic features for the recognition of paleosols and calcrete horizons. This view shows calcified root-hair sheaths (nonseptate tubules) extending from a calcified rootlet (the larger multicellular tube). Photograph courtesy of William C. Ward.

PPL, HA = 0.76 mm

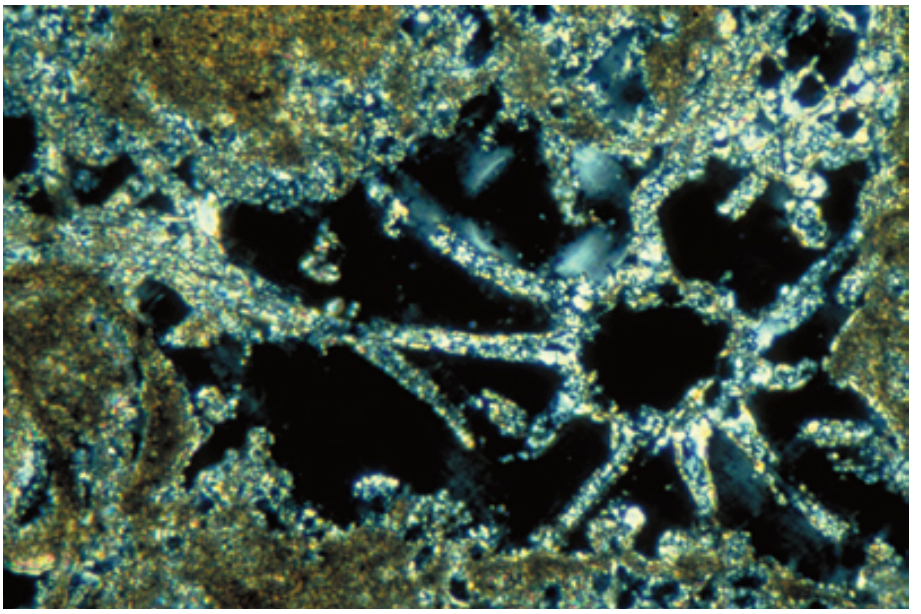

Pleistocene Key Largo Ls., Florida Keys, Monroe Co., Florida

The early calcification of rootlets and root-hair sheaths is visible in this cross-polarized light view. These meteoric precipitates have formed in a reefal limestone that has been exposed to approximately 120,000 years of meteoric alteration. The water uptake and CO_2 exchange between water and plants make rootlets especially prone to calcification and a common feature in Devonian and younger paleosols.

XPL, HA = 0.52 mm

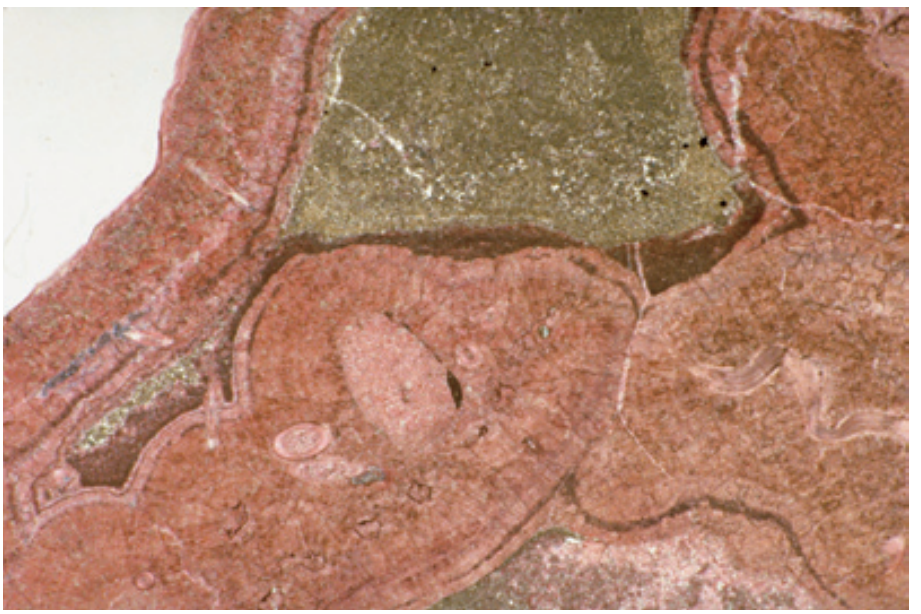

Up. Permian (Kazanian?) Wegener Halvø Fm., Jameson Land, East Greenland

Another feature commonly found in carbonate deposits exposed to meteoric alteration is "vadose silt". Here botryoids of marine cement were partially leached (note the irregular truncation surface on some of the botryoids). The dissolution surface is overlain by a dark brown microcrystalline crust that predates infill of the remaining cavity by lighter-colored crystal silt. Such silt may, in part, be precipitated, but it likely also includes substantial dissolution residue, including perhaps residues of collapsed early meteoric cements.

PPL, AFeS, HA = 9.0 mm

Up. Cretaceous limestone, Cephalonia, Ionian Islands, Greece

Geopetal crystal silt is visible here as partial fillings of leached coral skeletons. Such crystal silt has been interpreted as an indicator of subaerial exposure and vadose diagenesis by Dunham (1969) and other authors, and that interpretation is especially likely in cases such as this where the voids themselves are formed by leaching. The crystal silt in the coral molds is lighter colored and coarser grained than the micrite fraction of the surrounding, darker-colored sediment.

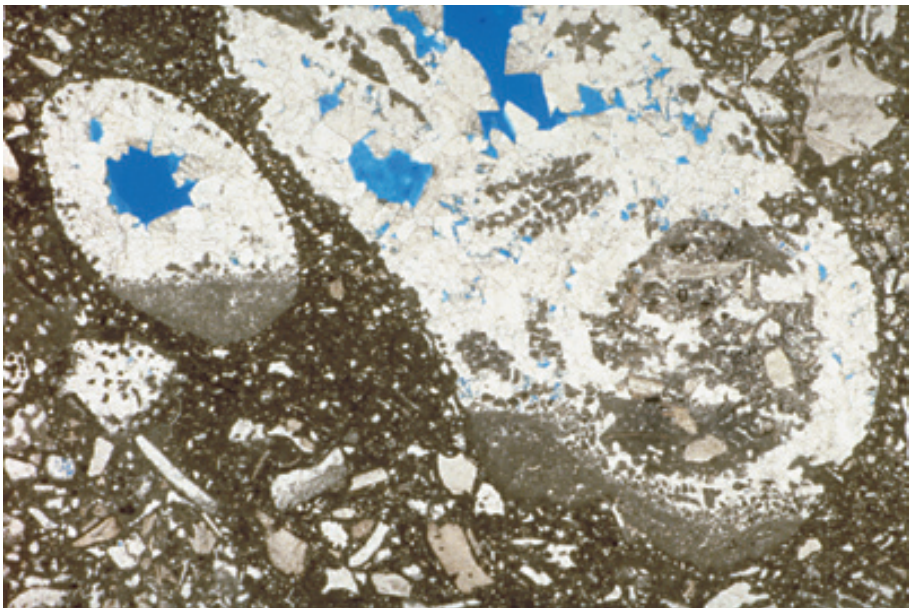

PPL, BSE, HA = 12.5 mm

Holocene sediment, Joulters Cay, Great Bahama Bank, Bahamas

Phreatic cements, by definition precipitated in a fully water-saturated sediment, do not show differential cement crystal distributions and have instead, relatively isopachous (uniform thickness) fabrics. This SEM image shows incipient phreatic cementation of ooids. Note the isolated, equant rhombs of low-Mg calcite cement scattered on the smooth surface of the ooids. Photograph courtesy of Robert B. Halley.

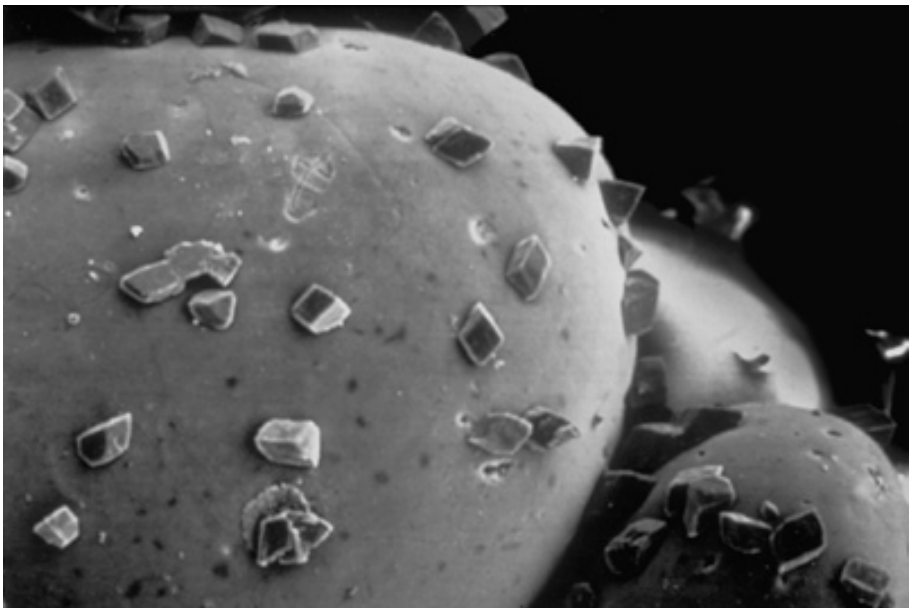

SEM, HA = 0.48 mm

Holocene sediment, Joulters Cay, Great Bahama Bank, Bahamas

An SEM image of extensive phreatic cementation of ooids. Note the continuous, relatively uniform-thickness coating of equant, rhombic, low-Mg calcite cement crystals that cover the once-smooth surface of the ooids. Photograph courtesy of Robert B. Halley.

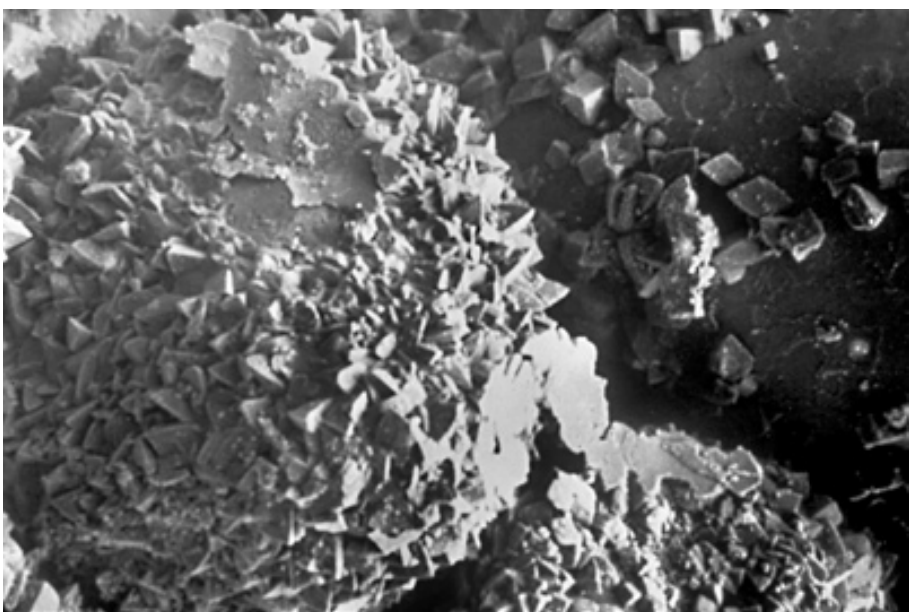

SEM, HA = 0.9 mm

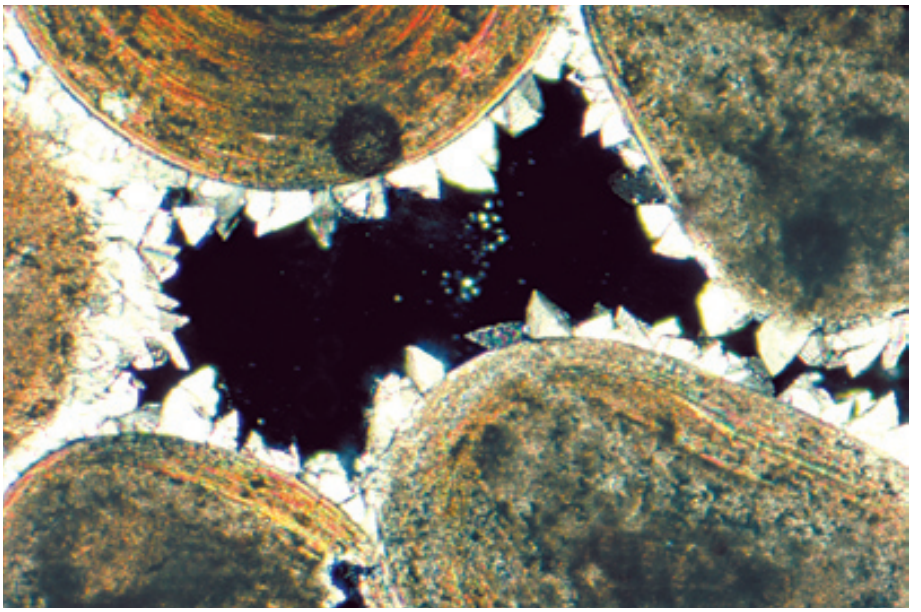

Holocene sediment, Joulters Cay, Great Bahama Bank, Bahamas

An ooid grainstone from an eolianite (carbonate dune) ridge with cements formed below the water table in the freshwater phreatic zone. These low-Mg calcite cements occur as slightly uneven, but still generally isopachous, coatings of equant to bladed crystals around the ooids. Photograph courtesy of Paul M. Harris.

XPL, HA = ~1.0 mm

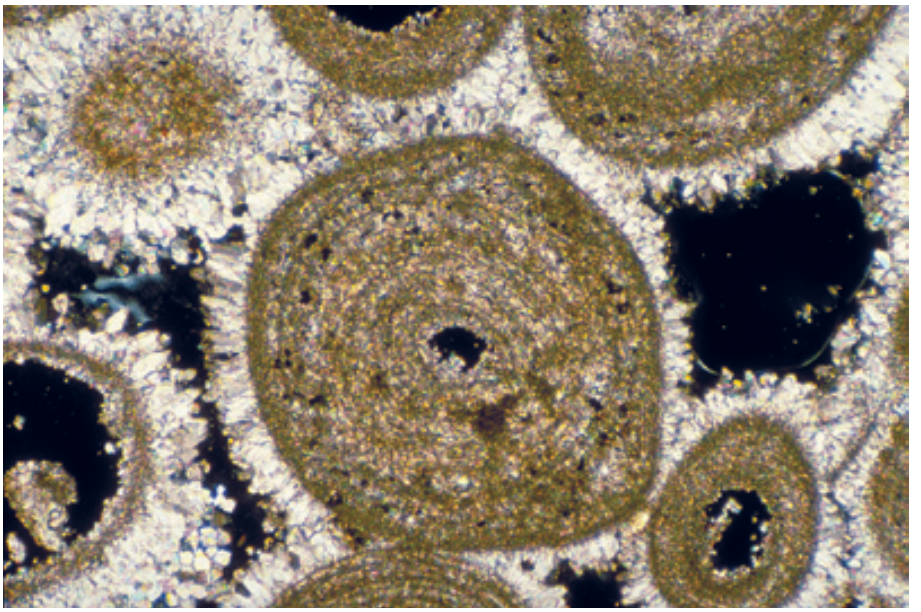

Up. Jurassic (Oxfordian) Up. Smackover Fm., 7,762 ft (2,366 m) depth, southern Arkansas

An ancient example of probable meteoric phreatic calcite cement developed in a Smackover ooid grainstone reservoir. Some leaching has occurred in the grains, in addition to the formation of isopachous crusts of bladed, calcite. Geochemical studies, especially of stable carbon and oxygen isotopic compositions, should be coupled with petrography to prove that these crusts are of meteoric, rather than marine, origin. Photograph courtesy of Clyde H. Moore.

XPL, HA = ~0.6 mm

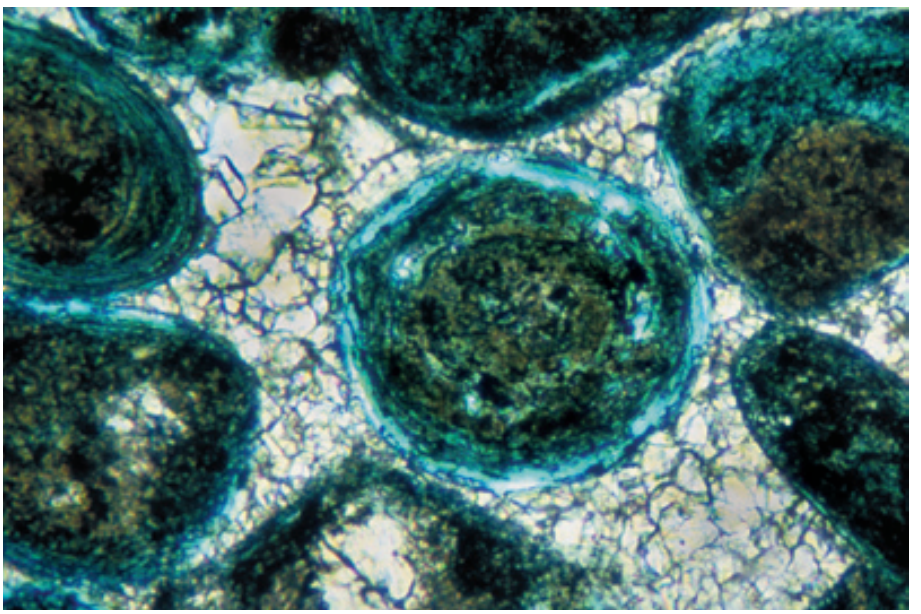

Lo. Holocene (ca. 6000 yBP) eolianite, San Salvador Island, Bahamas

Dissolution of unstable grains, as noted earlier, is a major component of meteoric diagenesis and the main source of materials for most meteoric cements. The two processes are, however, not always locally balanced. Here, aragonitic ooids are largely preserved in a sediment fully cemented by blocky, meteoric calcite spar. Note incipient dissolution/corrosion of some of the ooids with the formation of minor secondary porosity (filled with blue-green-stained epoxy).

PPL, BSE, HA = 0.4 mm

Holocene (<2700 yBP) eolianite, Isla Cancun, Quintana Roo, Mexico

A phreatic calcite-cemented eolianite with complete filling of primary porosity and much more substantial selective dissolution of original ooids than in the previous example. The presence of organic layers, coupled with a remaining meshwork of incompletely dissolved constituent needles, keeps these ooids from collapsing. Compare with views of vadose alteration of this same unit (page 334). Photograph courtesy of Robert G. Loucks.

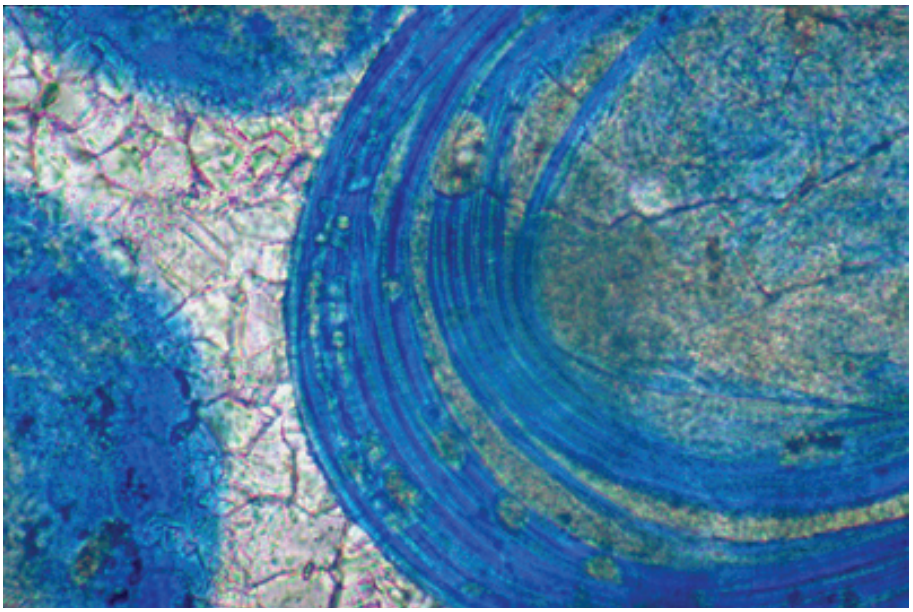

PPL, BSE, HA = 0.23 mm

Up. Jurassic (Oxfordian) Up. Smackover Fm., Gulf Coast, U.S.A.

An example of an oolitic grainstone in which dissolution led to collapse of remnant ooid components, The timing of dissolution-collapse structures such these is commonly difficult to determine with petrography alone. The association, in this case, with equant to bladed calcite spar crusts outside the ooids (followed by later blocky calcite cement), however, makes meteoric exposure a possible cause of the dissolution. The small, irregularly circular features, mainly along the top edge, are air bubbles in the slide and the light-colored, rhombic crystals are dolomite. Photograph courtesy of Clyde H. Moore.

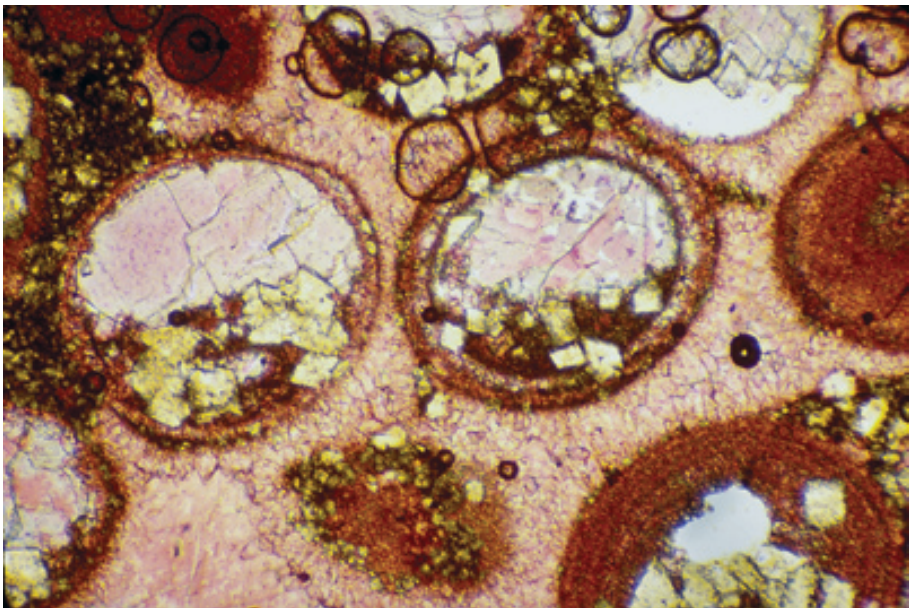

PPL, AS, HA = ~1.2 mm

Up. Permian (Kazanian?) Wegener Halvø Fm., Jameson Land, East Greenland

An example of an oolitic grainstone that has undergone essentially complete porosity inversion during meteoric diagenesis. The nearly complete cementation of primary porosity by non-ferroan, blocky calcite cement is matched by nearly complete leaching of original ooids (identifiable only vaguely by shape and the preservation of a few possible cortical coatings. The sample comes from just below a major Permian sequence boundary.

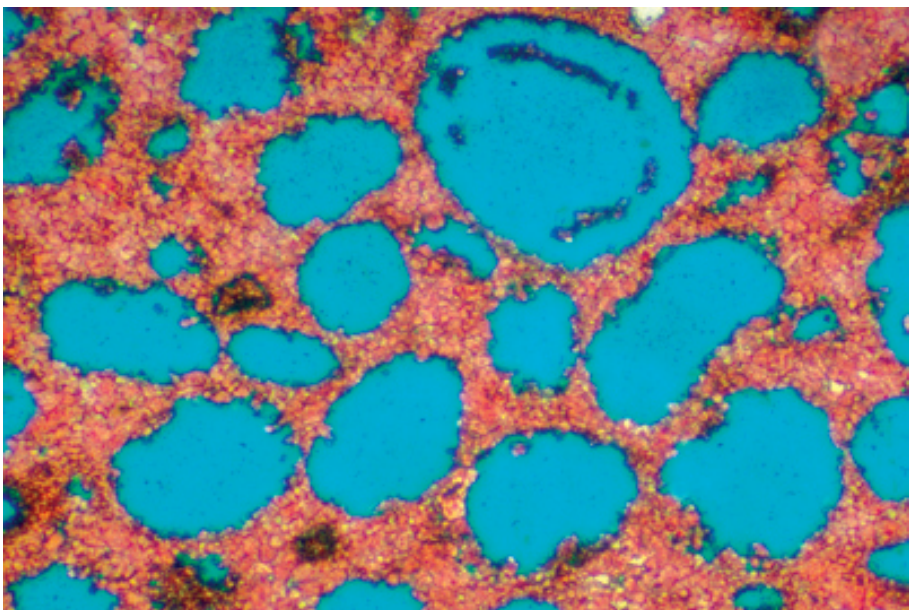

PPL, AFeS, BSE, HA = 3.2 mm

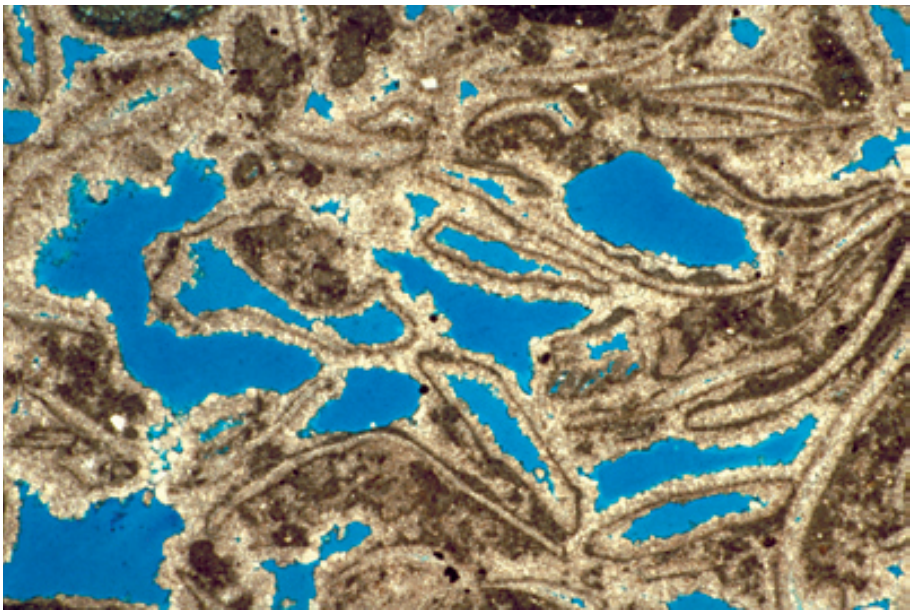

Up. Permian Zechstein Ca1 unit, 2,429 m depth, W of Gdansk, Poland

The micrite envelopes that form around skeletal and other grains in the marine environment (discussed in the section on marine diagenesis) play a substantial role in fabric preservation during meteoric or early burial alteration. Here, micrite envelopes (probably originally high-Mg calcite) mark the locations of leached aragonitic grains. Most envelopes have a thin coating of probable phreatic calcite cement on their exterior (primary interparticle pore) surfaces and on their interior (secondary porosity) surfaces.

PPL, BSE, HA = 9.0 mm

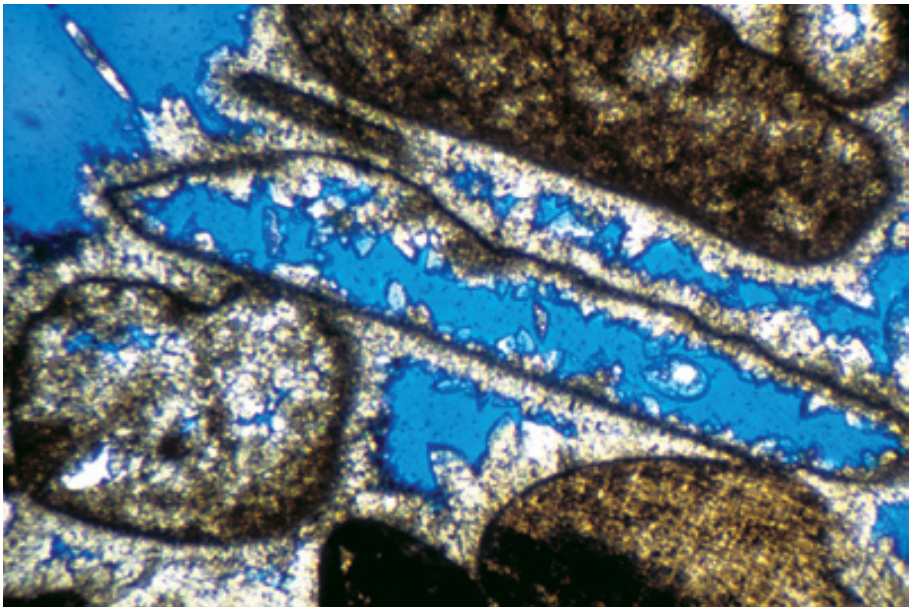

Up. Cretaceous limestone, Zakinthos, Ionian Islands, Greece

A magnified view of a micrite envelope surrounding a leached aragonitic bioclast. Complete bladed calcite cement crusts surround the envelopes on their exterior surface and fewer and more isolated crystals are present on the inside surfaces. Although this may well reflect meteoric diagenetic processes, it could also be the product of shallow burial diagenesis (e.g., Melim et al., 2002).

PPL, BSE, HA = 2.0 mm

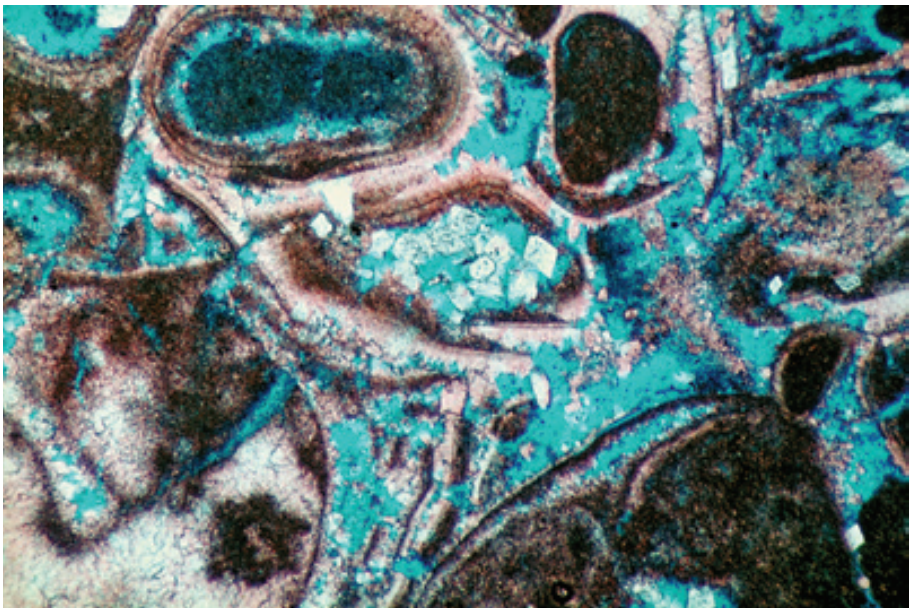

Up. Jurassic (Portlandian?) Arab D Carbonate, Dukhan field, Qatar

Some of the world's greatest carbonate hydrocarbon reservoirs were stabilized and enhanced through meteoric diagenesis. This oolitic-bioclastic-grainstone was exposed soon after deposition, resulting in development of oomoldic and biomoldic porosity. Leaching was followed by the growth of a thin rim of phreatic(?) calcite cement that lines both the primary and secondary pores. Finally, the grainstone underwent mechanical compaction during deeper burial, causing some of the leached grains to collapse. The rock, however, still retains remarkable porosity. Photograph courtesy of David N. Clark.

PPL, AS, BSE, HA = 1.6 mm

Up. Jurassic (Portlandian?) Arab D Carbonate, Dukhan field, Qatar

Another example of a meteorically leached, but more extensively cemented, bioclastic-peloidal grainstone from a classic hydrocarbon reservoir. The bioclasts consist mostly of rounded, micritized and subsequently leached peloids and bivalve fragments. Early meteoric leaching resulted in the widespread development of intragranular (moldic) pores and was followed by the phreatic or early burial-stage growth of calcite cement (stained red). This stabilized rock framework survived 2 km of overburden loading during subsequent burial. Photograph courtesy of David N. Clark.

PPL, AS, BSE, HA = 4.0 mm

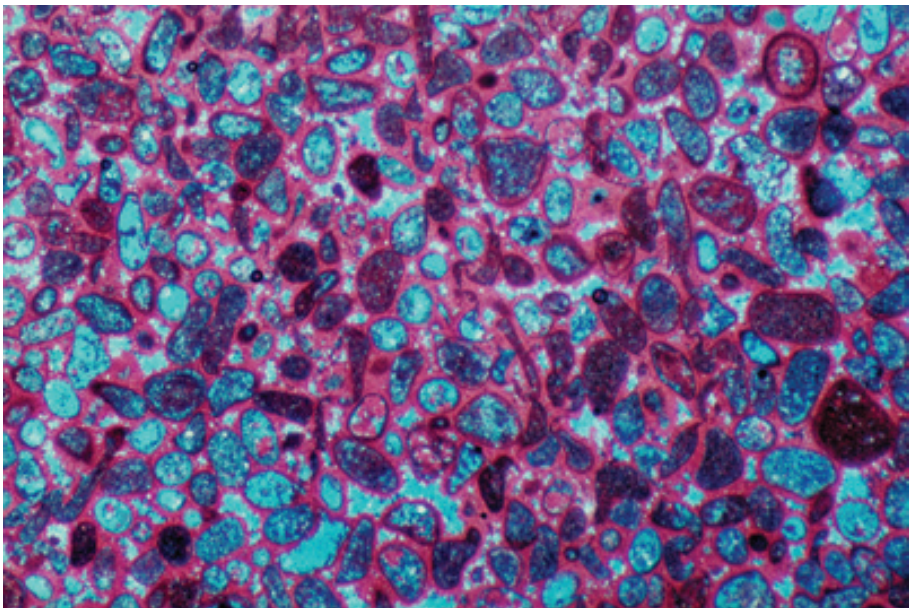

Mid-Late Ordovician Simpson Gp., Oil Creek Fm., Johnston Co., Oklahoma

Calcitic syntaxial overgrowth cement on crinoid fragments. The porosity in this encrinite was obliterated by such cementation except for blue-stained areas which represent later ferroan calcite cements. The timing of such cementation is very difficult to determine and may, in fact, extend through a long period of time. Incipient syntaxial overgrowths are inferred from marine environments, but such overgrowths form primarily in meteoric and burial diagenetic settings. Fluid inclusion and isotopic geochemical studies may help in determining environments of formation.

PPL, AFeS, HA = 3.7 mm

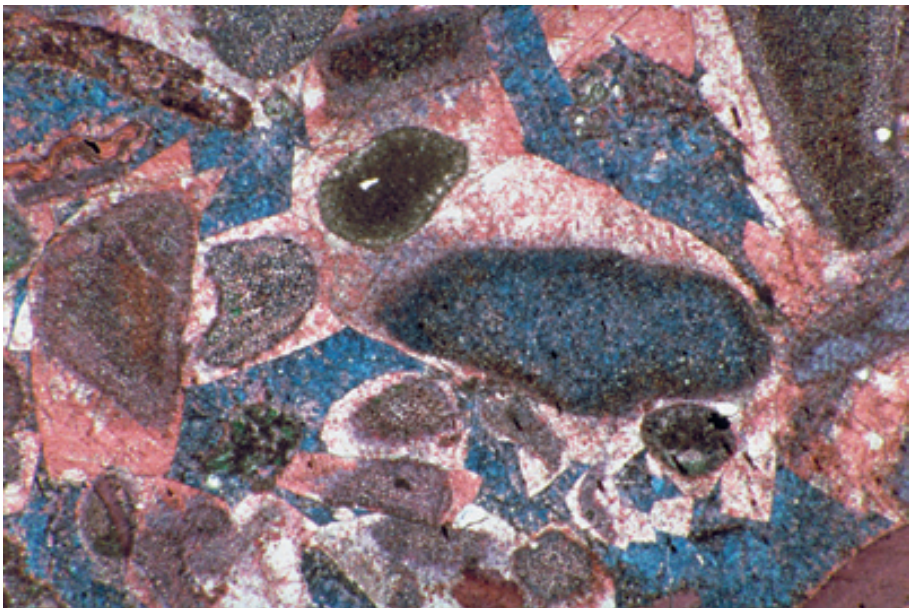

Pliocene-Pleistocene calcrete, Boca Grandi, Aruba

A dense, irregularly laminated, microcrystalline soil crust (pedogenic carbonate) developed as a weathering rind on a coral limestone. Surficial laminated crusts and hardpans are very common features that form at, or near, the top of the zone of infiltration, especially in sub-humid to arid settings. Rhizoliths, manganese-blackened pebbles, glaebules, and pisoids (pisoliths) commonly accompany such crusts. Recognition of these rather subtle features is important because they commonly mark substantial hiatal surfaces. An ancient example of such a crust is shown on the lower picture on the title page of this section.

PPL, BSE, HA = 12.5 mm

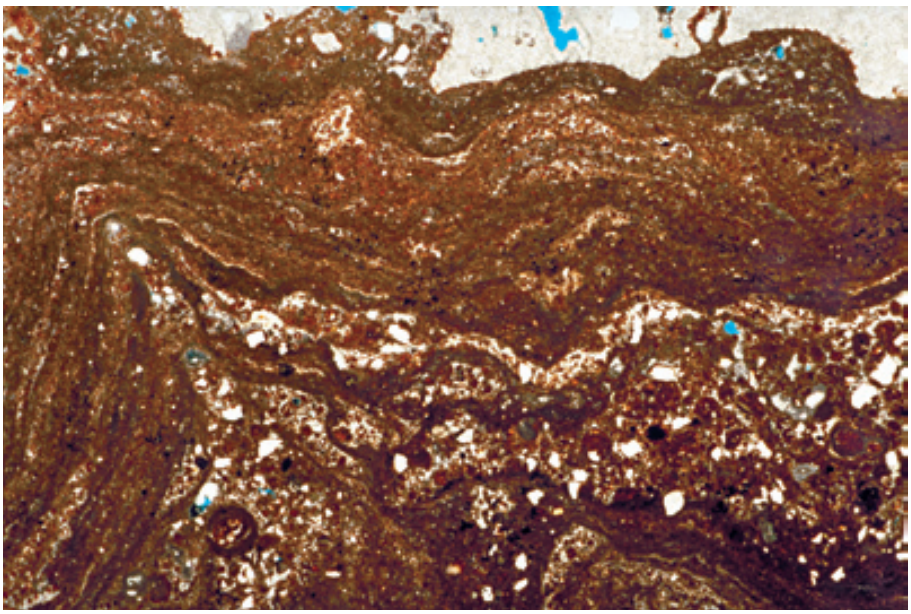

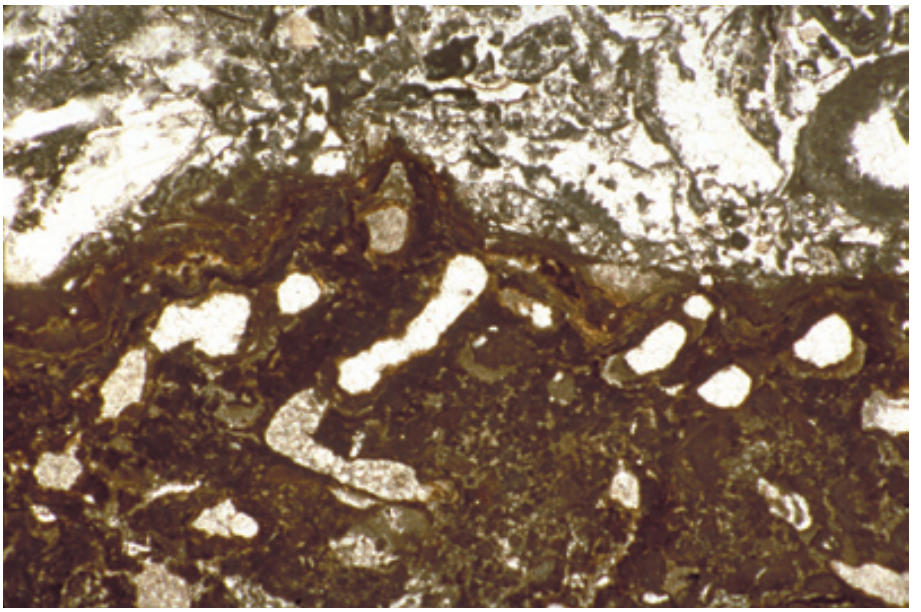

Up. Pennsylvanian (Virgilian) Holder Fm., Otero Co., New Mexico

A microscopic view of an ancient lithified paleosol or calcrete deposit. Note the sharply bounded, irregular surface underlain by a laminar, somewhat contorted microcrystalline crust. The abundant circular to elliptical tubes with dark rinds are calcified root structures (rhizoliths). This Pennsylvanian example is related to a major glacioeustatic drop in sea level with resulting exposure of shelf limestones (Goldstein, 1988a and b). Calcretes with extensive evidence of biological activity, such as this one, are termed "beta calcretes" by Wright (1991).

PPL, HA = 5.8 mm

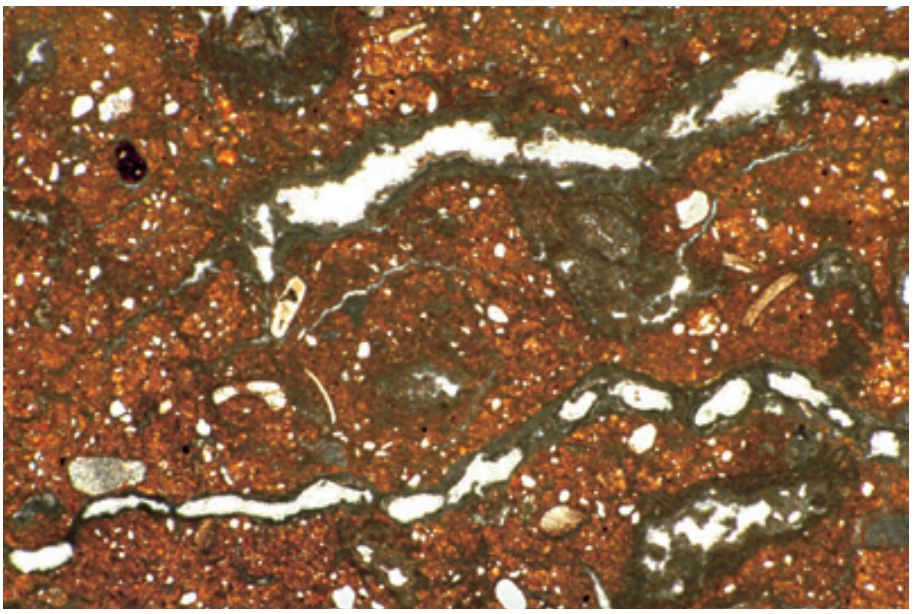

Quaternary calcrete, Marfa Point, Malta

An example of a near-Recent laminated, microcrystalline soil crust (calcrete) in which micrite-sized pedogenic carbonate has engulfed carbonate and terrigenous clastic detritus. Note the vague laminations and well developed, carbonate-lined root tubules of different sizes (rhizoliths). The dark-brown patchy areas are somewhat more heavily calcified, incipient nodules (glaebules). Note also the remarkable similarity of size and shape of structures, and even the degree of fabric preservation, between this and the previous (roughly 300 m.y.-old) example.

PPL, HA = 5.5 mm

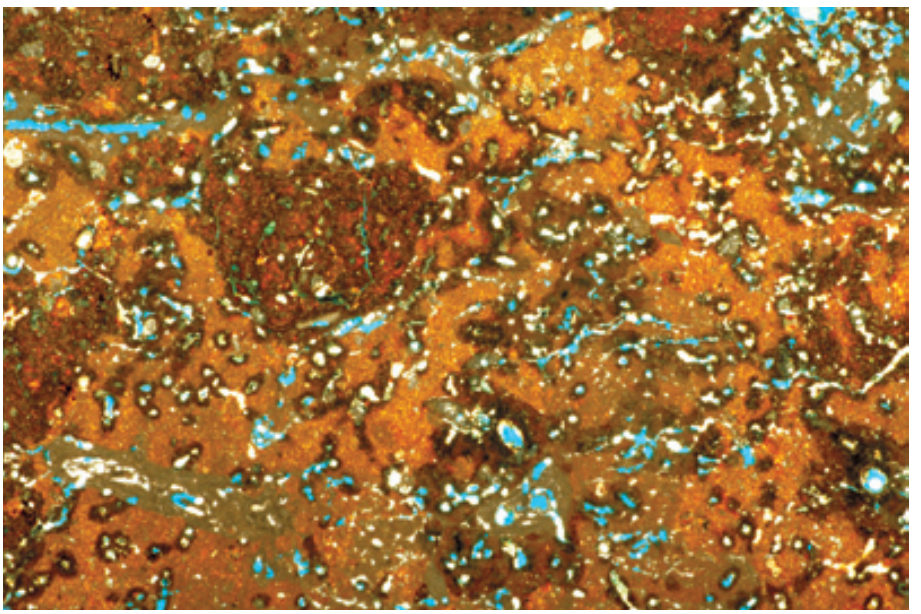

Pleistocene, (>700,000 yBP) Owl's Hole Fm., San Salvador Island, Bahamas

A soil crust associated with one of many Pleistocene sea-level lowstands, each of which resulted in tens of thousands of years of meteoric alteration of reef and back-reef limestones. Note the formation of glaebules (nodular features) and a complex network of small rhizoliths.

PPL, AFeS, BSE, HA = 11 mm

Up. Pennsylvanian (Virgilian) Holder Fm., Otero Co., New Mexico

An ancient example of a calichified crust (calcrete). There are many characteristic features — the best-developed ones in this example are incipient nodules (glaebules) with spar-filled circumgranular shrinkage cracks. The very complex fractures of different sizes and orientations, in many cases outlining the circumferences of nodules are quite diagnostic of subaerial exposure horizons. Repeated fracturing allows rotation of grains and formation of precipitated pisolitic coatings, a process just in the early stages of development in this example.

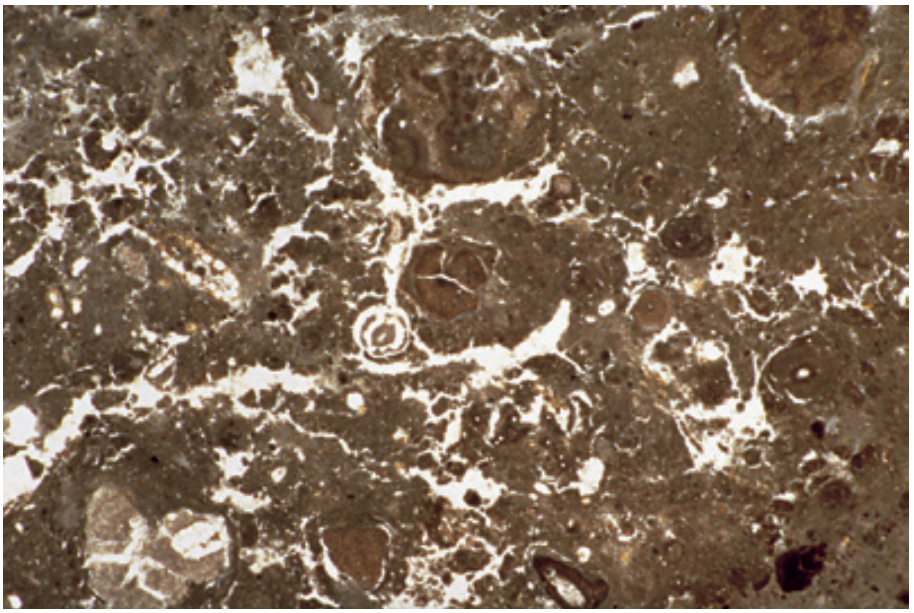

PPL, HA = 9.0 mm

Pleistocene, West Tanfield, Yorkshire, United Kingdom

Fungal structures, especially ones related to plant root activities, are common in calcretes (beta calcretes of Wright, 1991) and can be used to help identify exposure horizons. This SEM image shows an alveolar septal structure (with needle-fiber calcite) that is bridging a pore. This structure consists of narrow, curved septa composed of bundles of parallel-oriented calcite needles and represents the site of fungal mycelial bundles. Interestingly, this calcrete was developed in a late Pleistocene esker gravel composed of limestone clasts and has formed under a temperate climate. Photograph courtesy of V. Paul Wright.

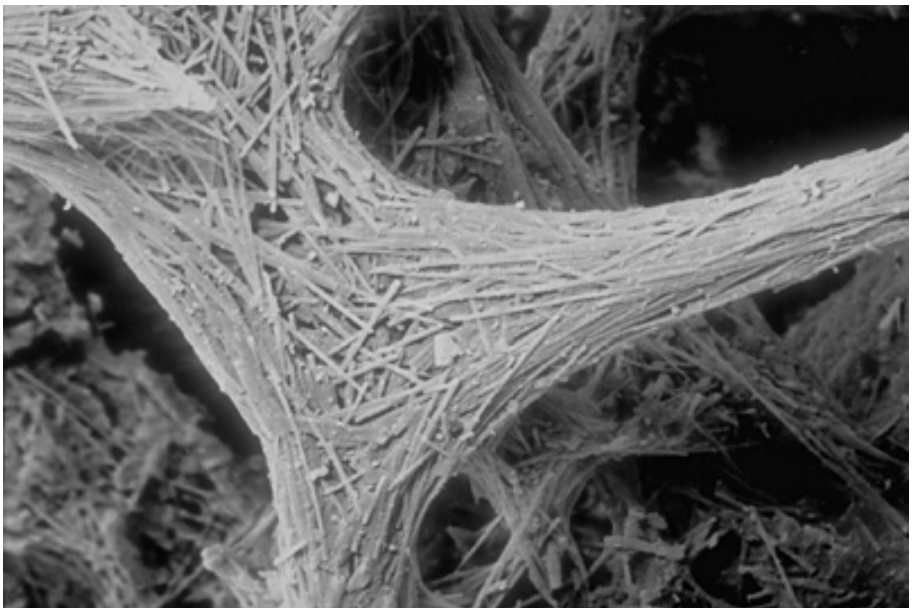

SEM, HA = 100 μm

Jurassic-Paleogene calcrete, Ordal, Barcelona, NE Spain

The tubular fabric of *Microcodium* in a Paleogene shallow vadose karst zone in Jurassic dolomite. *Microcodium* fabrics apparently are related to calcified root communities (calcified root cells?) and may penetrate several tens of meters beneath the soil surface. *Microcodium* has been described from Upper Jurassic to Recent strata. Photograph courtesy of Mateu Esteban (from Esteban and Klappa, 1983).

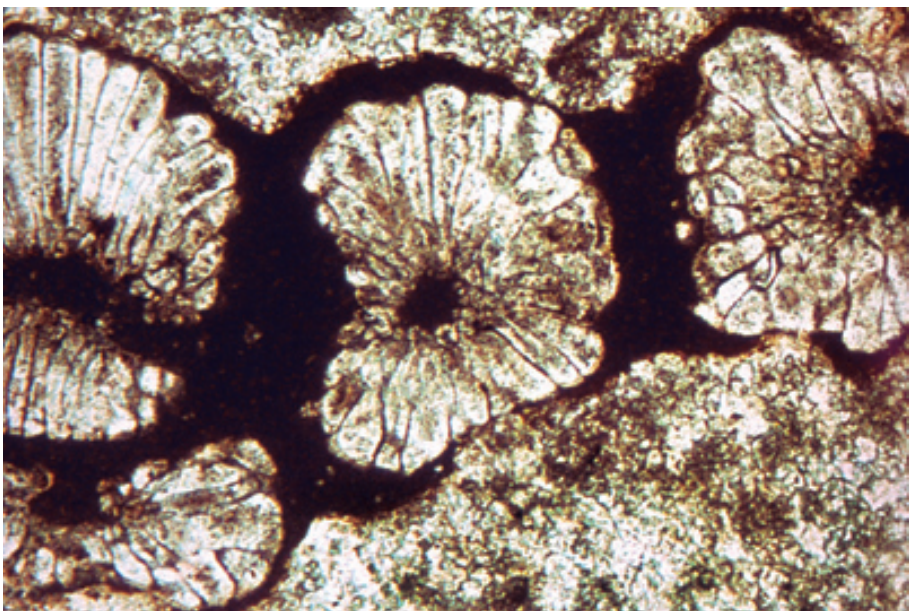

PPL, HA = 3.0 mm

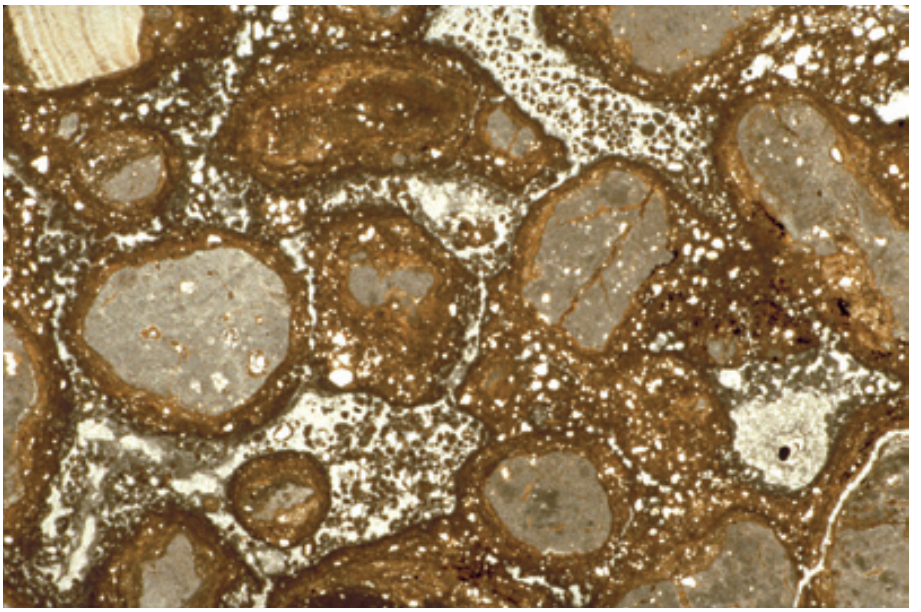

Up. Tertiary-Quaternary caliche, Jim Wells Co., west Texas

A mature "High Plains" caliche. Note the irregularly shaped coated grains (termed soil pisoids or pisoliths) and abundant inclusions of detrital terrigenous silt and sand that are engulfed by pedogenic carbonate. The insoluble terrigenous components are concentrated during the dissolution process that characterizes such long-term exposure surfaces. Circumgranular cracking also is visible in this example. Calcrete with little or no evidence of biological activity, such as this one, is termed an "alpha calcrete" by Wright (1991).

PPL, HA = 12 mm

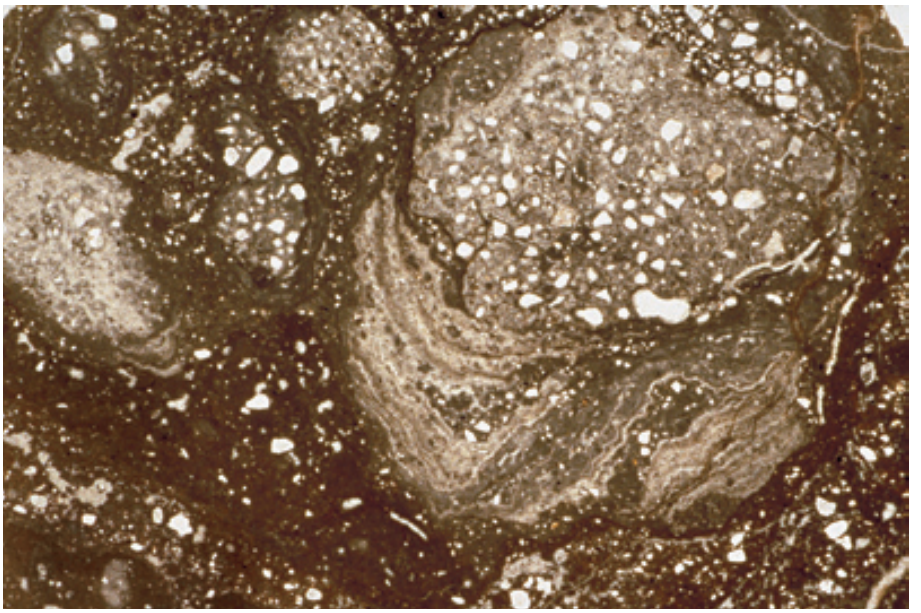

Up. Tertiary-Quaternary caliche, Midland Co., west Texas

Another view of the same mature "High Plains" caliche. Note the irregular, highly asymmetrical coated grains (pisoids/pisoliths) and abundant inclusions of detrital terrigenous silt and sand. Caliche pisoids grow with preferential downward elongation, but typically are rotated into a variety of positions during the long periods (commonly hundreds of thousands to millions of years) of exposure and displacive crystal growth represented by such deposits.

PPL, HA = 14.5 mm

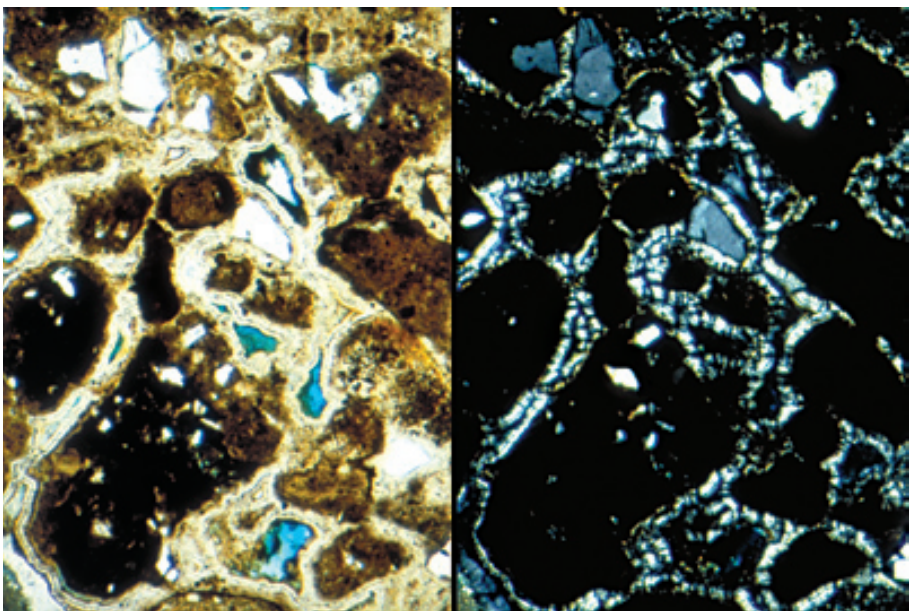

Pliocene-Pleistocene silcrete, Colorado Point, Aruba

Not all exposure surfaces are marked by calcareous crusts (calcretes, petrocalcic horizons, or caliches). Siliceous, phosphatic, ferruginous, and bauxitic crusts or deposits are also quite common. This example shows a siliceous crust (a silcrete) developed on a coral limestone. Note the fragments of silicified and iron-stained limestone that are surrounded by various forms of silica cement.

PPL/XPL, BSE, HA = 1.2 mm each

Tertiary Arkansas Bauxite, near Little Rock, Arkansas

This ferruginous, pisolitic bauxite is an example of long-term weathering and "soil" formation in a high rainfall setting. Note the abundant irregular pisoids and circumgranular cracking of finer-grained matrix. Intense chemical weathering has left behind only the most insoluble chemical components.

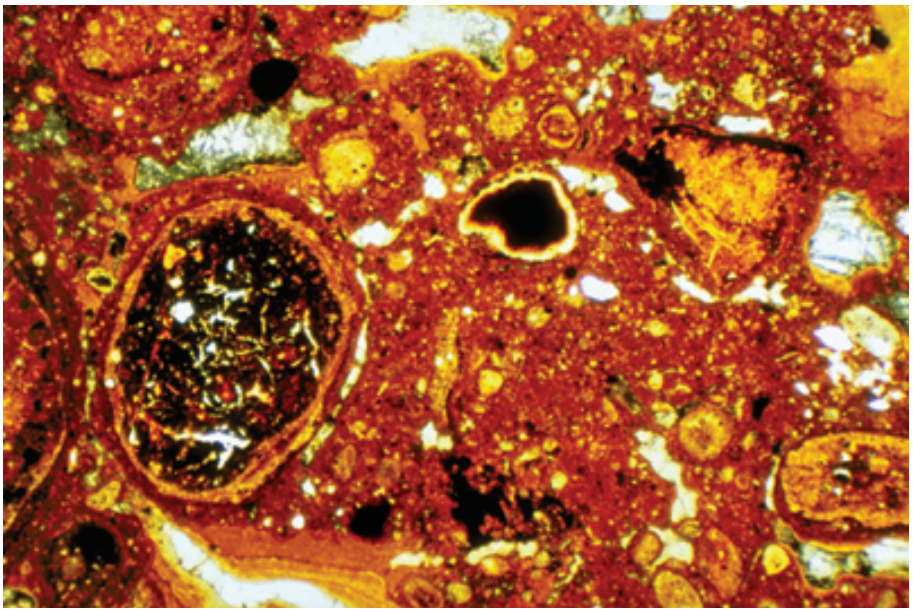

PPL, HA = 4.1 mm

Mesozoic-Miocene, offshore well, NE Spain

A number of other features can be used to recognize exposure zones. This terra rossa is associated with a major paleokarst zone. Like many such deposits, it is a fully lithified, moderately fine-grained, extensively recrystallized carbonate — a uniform microspar. Although this may not be the only way microspar is formed, there is a common association of microspars with meteorically altered micrites. Photograph courtesy of Mateu Esteban.

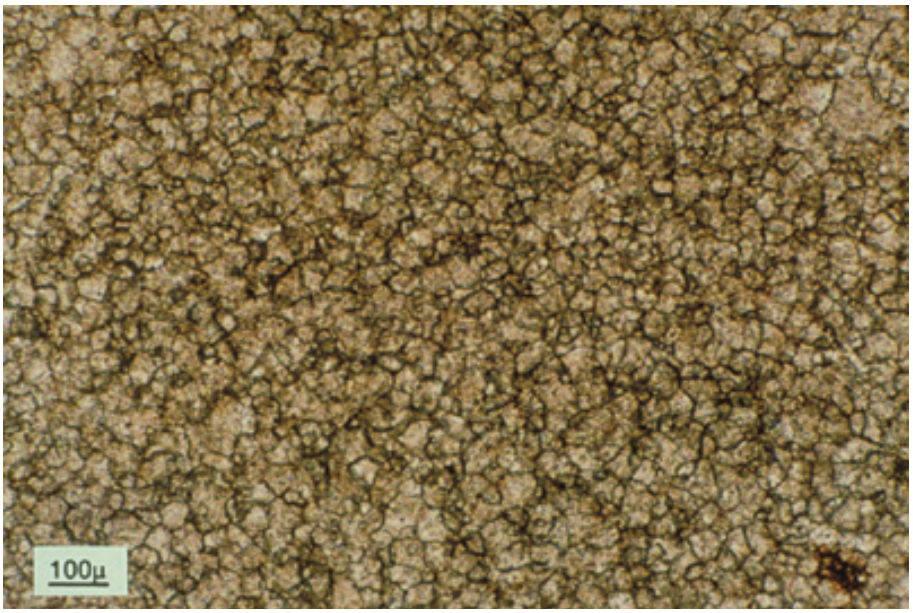

PPL, HA = 1.46 mm

Oligocene Bluff Fm., Grand Cayman Island, Cayman Islands, B.W.I.

This cave-fill breccia is associated with a nearby subaerial exposure surface (a paleokarst zone). Such features generally are very coarse-grained and thus are best recognized in outcrop. They can occasionally be identified in thin section as well, however. Note the angular fragments produced by rock collapse. They are set in reddish (terra rossa) micritic matrix that has infiltrated though a solution-enlarged fracture network and fills vugs and caves with banded internal sediment that is locally termed "caymanite".

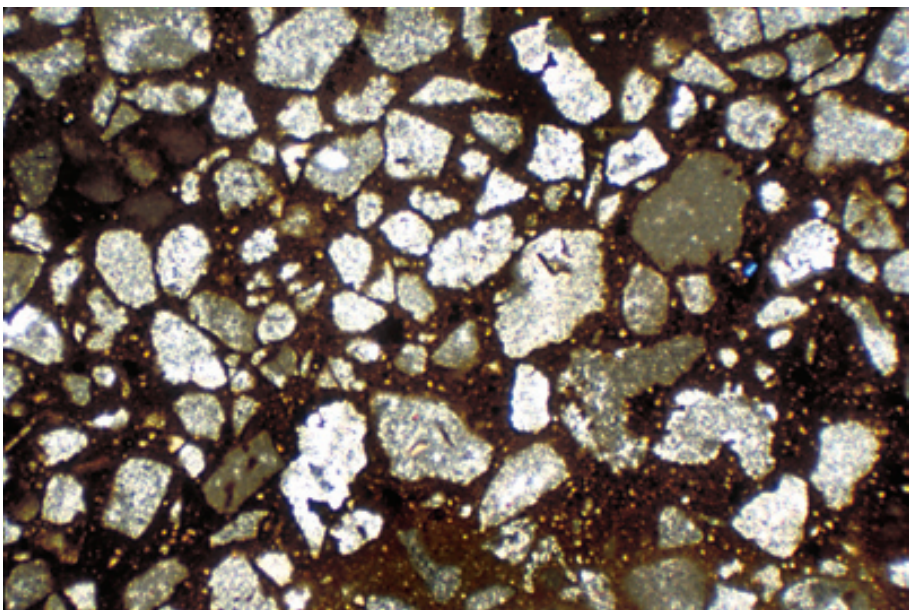

PPL, HA = 4.1 mm

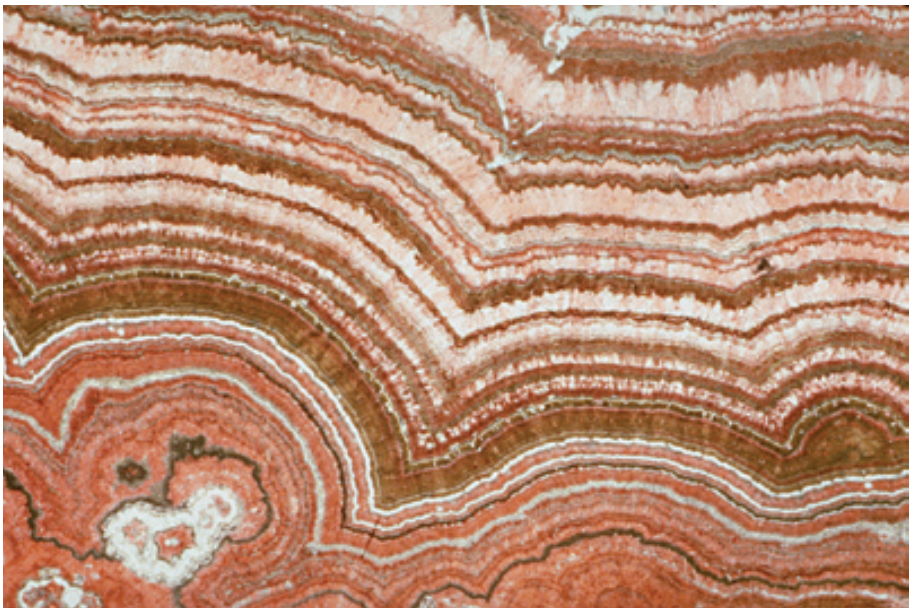

Cave fill in Up. Permian limestone, Djebel Tebaga, southern Tunisia

Paleokarst zones sometimes can be recognized by depositional as well as dissolutional features. These cave-lining cements are associated with a cave that extends well below a regional subaerial exposure surface. The regular banding of light and dark cement layers is very typical and reflects repeated variations in aqueous geochemical conditions within the cave system.

PPL, AFeS, HA = 14.5 mm

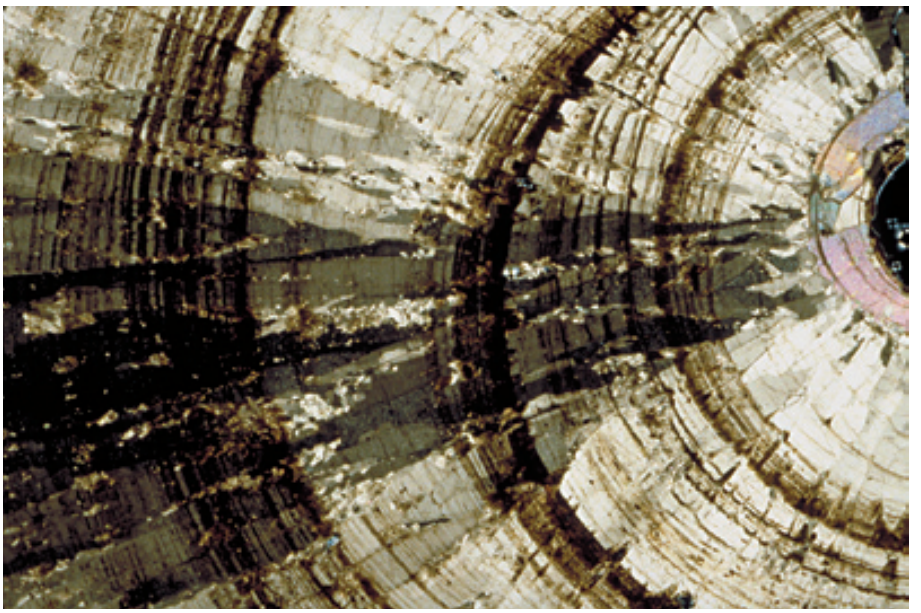

Tertiary-Quaternary cave fill, Mifflin Co., Pennsylvania

A stalactite from a Cenozoic cave cut into mid-Ordovician limestone. Note the coarsely crystalline, radially-oriented, low-Mg calcite crystals that transect numerous dark growth bands. This fabric is reminiscent of the structure of belemnite rostra, but the two should be easily distinguishable by differences in size and context.

XPL, HA = 16 mm

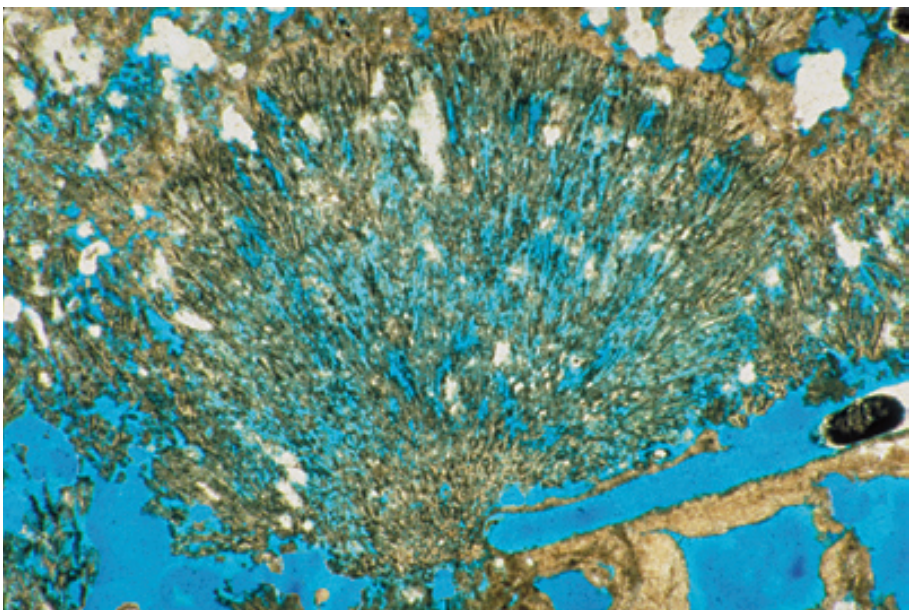

Holocene travertine, Culberson Co., Texas

A variety of other kinds of fabrics can be found in localized, sometimes quite isolated and unusual subaerial settings. This example shows a stream-bed tufa or travertine. This cold- and freshwater deposit consists of precipitated microcrystalline carbonate (low-Mg calcite) covering plant fragments (mainly reeds and grasses). Decomposition of the organic plant fragments leaves a very porous structure; here blue epoxy highlights the porosity. Travertine or tufa deposits many tens of meters thick, and composed either of calcite or silica, can form in subaerial settings associated with springs.

PPL, BSE, HA = 5.0 mm

Quaternary travertine, Bonneville Co., Idaho

Probable bacterial shrubs in a hot-spring travertine deposit. The travertine deposits are strongly laminated, consist of branching clusters of peloidal micrite, commonly contain abundant plant fragments, and generally have high porosity associated with the decomposition of incorporated organic matter.

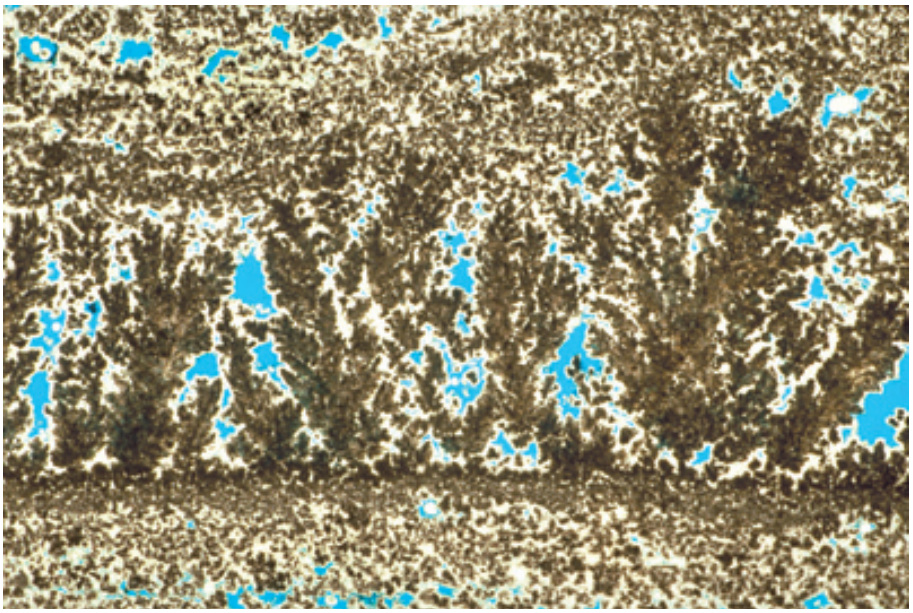

PPL, BSE, HA = 12.5 mm

Recent spring deposit, Yorke Peninsula, South Australia

An example of "floe aragonite" from a marine seepage spring in a coastal hypersaline lake that lies below sea level. As marine water percolates through a permeable barrier, emerges into the lake via underwater springs, and then circulates to the surface, aragonite precipitates. The aragonite crystals form rafts held at the air-water contact by surface tension. Continued growth eventually makes the rafts so heavy that they sink to the lake floor where they are cemented into a breccia-like deposit. This is an example of terrestrial spring deposition where mixing with marine waters produces a typically marine mineralogy.

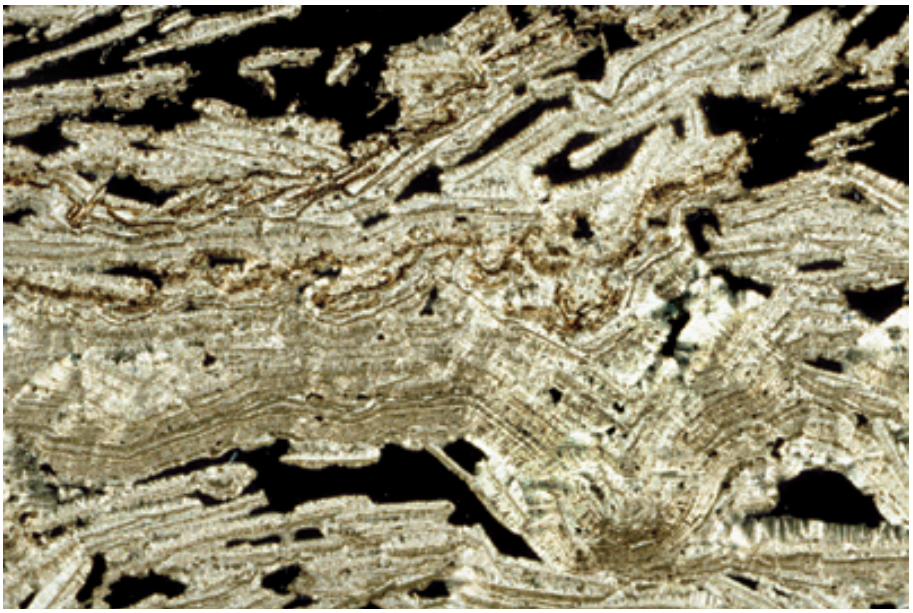

XPL, HA = 16 mm

Recent spring deposit, Lake MacLeod, Carnarvon area, Western Australia

A photomicrograph of a botryoidal aragonite crust formed beneath a coastal "tepee structure". This is another example of marine seepage springs in which marine water percolated through coastal dune barriers into a playa basin that lies below sea level. Cement crusts and pisoids with "marine" mineralogies and fabrics thus precipitate from hypersaline marine fluids in this subaerially exposed, non-marine setting. Photograph courtesy of C. Robertson Handford (see Handford et al., 1984).

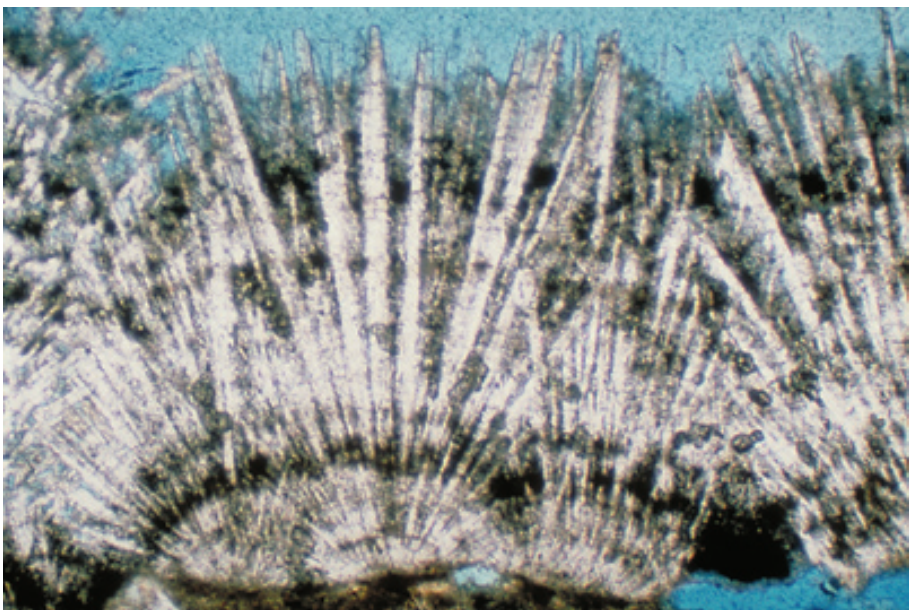

PPL, BSE, HA = ~2.0 mm

Cited References and Additional Information Sources

Aristarain, L. F., 1971, Characteristics and genesis of caliche deposits: Boletin de la Sociedad Geológica Mexicana, v. 32, p. 117-141.

Bain, R. J., and A. M. Foos, 1993, Carbonate microfabrics related to subaerial exposure and paleosol formation, *in* R. Rezak, and D. L. Lavoie, eds., Carbonate Microfabrics: New York, Springer-Verlag, p. 29-39.

Bathurst, R. G. C., 1983, Early diagenesis of carbonate sediments, *in* A. Parker, and B. W. Sellwood, eds., Sediment Diagenesis: Proceedings, NATO Advanced Study Institute, Series C, v. 115: Dordrecht (Netherlands), D. Reidel Publishing Co., p. 349-378.

Bernoulli, D., and C. W. Wagner, 1971, Subaerial diagenesis and fossil caliche deposits in the Calcare Massiccio Formation (Lower Jurassic, central Apennines, Italy): Neues Jahrbuch für Geologie und Paläontologie, Abhandlungen, v. 138, p. 135-149.

Bögli, A., 1980, Karst Hydrology and Physical Speleology: Berlin, Springer-Verlag, 284 p.

Bricker, O. P., ed., 1971, Carbonate Cements: Baltimore, MD, Johns Hopkins University Studies in Geology No. 19, 376 p.

Chafetz, H. S., A. G. McIntosh, and P. F. Rush, 1988, Freshwater phreatic diagenesis in the marine realm of Recent Arabian Gulf carbonates: Journal of Sedimentary Petrology, v. 58, p. 433-440.

Dunham, R. J., 1969, Early vadose silt in Townsend mound (reef) New Mexico, *in* G. M. Friedman, ed., Depositional Environments in Carbonate Rocks: Tulsa, OK, SEPM Special Publication 14, p. 139-181.

Esteban Cerdà, M., 1974, Caliche textures and "*Microcodium*": Bolletino della Società Geologica Italiana, v. 92, p. 105-125.

Esteban, M., 1976, Vadose pisolite and caliche: AAPG Bulletin, v. 60, p. 2048-2057.

Esteban, M., and C. F. Klappa, 1983, Subaerial exposure environment, *in* P. A. Scholle, D. G. Bebout, and C. H. Moore, eds., Carbonate Depositional Environments: Tulsa, OK, American Association of Petroleum Geologists Memoir 33, p. 1-54.

Frank, T. D., and K. C. Lohmann, 1995, Early cementation during marine-meteoric fluid mixing: Mississippian Lake Valley Formation, New Mexico: Journal of Sedimentary Research, v. A65, p. 263-273.

Goldstein, R. H., 1988a, Cement stratigraphy of Pennsylvanian Holder Formation, Sacramento Mountains, New Mexico: AAPG Bulletin, v. 72, p. 425-438.

Goldstein, R. H., 1988b, Paleosols of Late Pennsylvanian cyclic strata, New Mexico: Sedimentology, v. 35, p. 777-804.

Handford, C. R., A. C. Kendall, D. R. Prezbindowski, J. B. Dunham, and B. W. Logan, 1984, Salina-margin tepees, pisoliths, and aragonite cements, Lake MacLeod, Western Australia: their significance in interpreting ancient analogs: Geology, v. 12, p. 523-527.

Harris, W. H., and R. K. Matthews, 1968, Subaerial diagenesis of carbonate sediments: efficiency of the solution-reprecipitation process: Science, v. 160, p. 77-79.

Harrison, R. S., and R. P. Steinen, 1978, Subaerial crusts, caliche profiles and breccia horizons: Comparison of some Holocene and Mississippian exposure surfaces, Barbados and Kentucky: Geological Society of America Bulletin, v. 89, p. 385-396.

Horbury, A. D., and A. E. Adams, 1989, Meteoric phreatic diagenesis in cyclic late Dinantian carbonates, northwest England: Sedimentary Geology, v. 65, p. 319-344.

Humphrey, J. D., K. L. Ransom, and R. K. Matthews, 1986, Early meteoric diagenetic control of Upper Smackover production, Oaks Field, Louisiana: AAPG Bulletin, v. 70, p. 70-85.

James, N. P., 1972, Holocene and Pleistocene calcareous crust (caliche) profiles: criteria for subaerial exposure: Journal of Sedimentary Petrology, v. 42, p. 817-836.

James, N. P., 1974, Diagenesis of scleractinian corals in the subaerial vadose environment: Journal of Paleontology, v. 48, p. 785-799.

James, N. P., and Y. Bone, 1989, Petrogenesis of Cenozoic, temperate water calcarenites, South Australia: a model for meteoric/shallow burial diagenesis of shallow water calcite sediments: Journal of Sedimentary Petrology, v. 59, p. 191-203.

James, N. P., and P. W. Choquette, 1984, Diagenesis 9. Limestones — the meteoric diagenetic environment: Geoscience Canada, v. 11, p. 161-194.

James, N. P., and P. W. Choquette, eds., 1988, Paleokarst: New York, Springer-Verlag, 416 p.

Jones, B., E. B. Lockart, and C. Squair, 1984, Phreatic and vadose cements in the Tertiary Bluff Formation of Grand Cayman Island, British West Indies: Bulletin of Canadian Petroleum Geology, v. 32, p. 382-397.

Kahle, C. F., 1977, Origin of subaerial Holocene calcareous crusts: role of algae, fungi and sparmicritization: Sedimentology, v. 24, p. 413-435.

Klappa, C. F., 1979, Calcified filaments in Quaternary calcretes: organo-mineral interactions in the subaerial vadose environment: Journal of Sedimentary Petrology, v. 49, p. 955-968.

Knox, G. J., 1977, Caliche profile formation, Saldanha Bay (South Africa): Sedimentology, v. 24, p. 657-674.

Land, L. S., 1970, Phreatic versus vadose meteoric diagenesis of limestones: evidence from a fossil water table: Sedimentology, v. 14, p. 175-185.

Mazzullo, S. J., and W. D. Bischoff, 1992, Meteoric calcitization and incipient lithification of recent high-magnesium calcite muds, Belize: Journal of Sedimentary Petrology, v. 62, p. 196-207.

Melim, L. A., H. Westphal, P. K. Swart, G. P. Eberli, and A. Munnecke, 2002, Questioning carbonate diagenetic paradigms: evidence from the Neogene of the Bahamas: Marine Geology, v. 185, p. 27-53.

Multer, H. G., and J. E. Hoffmeister, 1968, Subaerial laminated crusts of the Florida Keys: Geological Society of America Bulletin, v. 79, p. 183-192.

Müller, G., 1971, Gravitational cement: an indicator for the vadose zone of the subaerial diagenetic environment, *in* O. P. Bricker, ed., Carbonate Cements: Baltimore, MD, Johns Hopkins Press, p. 301-302.

Pingitore, N. E., Jr., 1976, Vadose and phreatic diagenesis: processes, products and their recognition in corals: Journal of Sedimentary Petrology, v. 46, p. 985-1006.

Reeves, C. C., Jr., 1976, Caliche: Origin, Classification, Morphology and Uses: Lubbock, TX, Estacado Books, 233 p.

Saller, A. H., and C. H. Moore, Jr., 1989, Meteoric diagenesis, marine diagenesis, and microporosity in Pleistocene and Oligocene limestones, Enewetak Atoll, Marshall Islands: Sedimentary Geology, v. 63, p. 253-272.

Steinen, R. P., 1974, Phreatic and vadose diagenetic modification of Pleistocene limestone: petrographic observations from subsurface of Barbados, West Indies: AAPG Bulletin, v. 58, p. 1008-1024.

Thorstenson, D. C., F. T. MacKenzie, and B. L. Ristvet, 1972, Experimental vadose and phreatic cementation of skeletal carbonate sand: Journal of Sedimentary Petrology, v. 42, p. 162-167.

Thrailkill, J., 1968, Chemical and hydrologic factors in the excavation of limestone caves: Geological Society of America Bulletin, v. 79, p. 19-46.

Vacher, H. L., T. O. Bengtsson, and L. N. Plummer, 1990, Hydrology of meteoric diagenesis: residence time of meteoric ground water in island fresh-water lenses with application to aragonite-calcite stabilization rate in Bermuda: Geological Society of America Bulletin, v. 102, p. 223-232.

Wright, V. P., 1991, Paleokarst: types, recognition, controls and associations, *in* V. P. Wright, M. Esteban, and P. L. Smart, eds., Paleokarsts and Paleokarstic Reservoirs: P.R.I.S. Occasional Publication Series No. 2: Reading, University of Reading, p. 56-88.

Wright, V. P., and M. E. Tucker, eds., 1991, Calcretes: Oxford, International Association of Sedimentologists, Reprint Series 2, 360 p.

Facing Page: Top: Internal sediment and two generations of cement inside a brachiopod shell. The highly ferroan burial cements are stained deep blue. Up. Permian Wegener Halvø Fm., Jameson Land, East Greenland, PPL, AFeS, HA = 4.1 mm.
Bottom: Stylolites following bedding of the fore-reef deposits. HA = ~7 cm. Up. Devonian Napier Fm., Canning Basin, Western Australia. Photograph courtesy of Phillip Playford.

CARBONATE DIAGENESIS

MESO- AND TELOGENETIC BURIAL DIAGENESIS

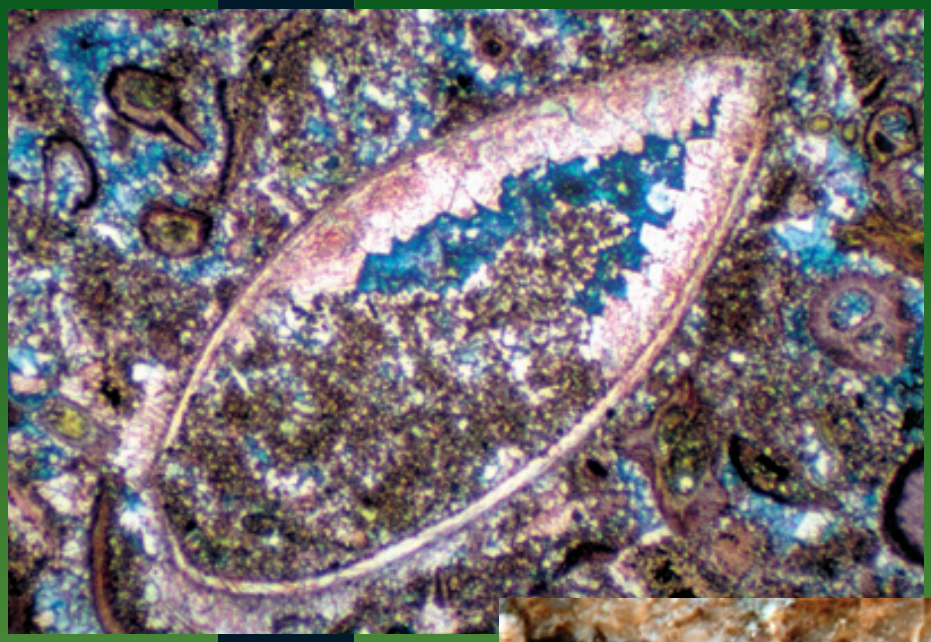

CHAPTER 25

BURIAL DIAGENESIS

Introduction:

This chapter deals only with the diagenesis of calcitic components of limestones — the formation of dolomite, silica and other minerals is covered in subsequent chapters.

Burial diagenesis represents alteration that occurs below the zone of near-surface water circulation (i.e., below the meteoric phreatic mixing zone or below the zone of active seawater circulation). Burial diagenesis plays a major, often THE major role, in the diagenesis of sediments from the point of view of length of time spent in that environment (commonly millions to hundreds of millions of years) and in terms of porosity changes.

Burial diagenetic features are among the most difficult to identify with assurance for a variety of reasons: 1. the transition between surficial (meteoric or marine) pore fluids and burial realm fluids is ill-defined, variable, indistinct, and rarely well understood (so often it is not clear where surficial diagenesis ends and burial diagenesis begins); 2. the burial realm is "out of sight and out of mind", which means that the processes and products formed there can only be remotely and incompletely observed; 3. deposits found in the burial diagenetic zone must have passed through marine or meteoric diagenesis zones (or both), making it difficult to determine precisely whether a particular fabric is exclusively a product of burial diagenesis.

Several factors mitigate for and against extensive burial diagenesis. Burial diagenesis is hindered by water circulation rates that typically are lower in subsurface settings than in near-surface environments (because of slower circulation mechanisms as well as reduced permeabilites). Higher temperatures and increased pressures at depth, however, tend to accelerate many diagenetic processes. Elevated pore-fluid pressures (reducing grain-to-grain stress) and early hydrocarbon input retard mechanical and chemical burial diagenesis.

Statistical evidence (top diagram, facing page) indicates that burial diagenesis is very important in porosity reduction. Most rocks, especially limestones, show a consistent loss of porosity with progressive burial.

Major diagenetic fabrics:

The burial-diagenetic zone is characterized by a mix of physical and chemical diagenetic processes, most leading to porosity destruction, but in some cases yielding net porosity increases.

Burial-related mechanical compaction features include dewatering structures, compactional drape around shells and nodules, plastic or brittle grain deformation, and fractures.

Embayed grain contacts, fitted fabrics, solution seams, and stylolites are common chemical compaction features that form mainly in burial settings.

Burial-stage calcite cements are low-Mg calcite. Most crystals grew slowly, and thus are relatively imperfection-free, clear (limpid) crystals as compared with marine and even meteoric precipitates. Morphologies include bladed, prismatic overgrowths of earlier cement crusts; equant calcite mosaics; drusy calcite mosaics with crystal sizes increasing toward pore centers; very coarse to poikilotopic blocky calcite spar; and outer, inclusion-poor stages of syntaxial overgrowths. Although these fabrics are common in mesogenetic precipitates, none is unequivocally or exclusively formed during burial diagenesis. Bathurst (1971 and 1975) and Dickson (1983) provide more detailed discussion of geometric criteria for recognition of burial cements.

Many burial-stage cements are formed from relatively reducing pore fluids and, thus, may have elevated Mn^{2+} and Fe^{2+} contents. The iron is easily detected with staining techniques; the manganese/iron ratio is qualitatively identifiable with cathodoluminescence (CL). The typical CL pattern found in burial stage calcite cements is a transition from nonluminescent to brightly luminescent to dully luminescent response. This is generally interpreted as a transition from oxidizing (pre-burial or early burial) conditions with little or no Mn^{2+} or Fe^{2+} incorporation into the calcite lattice, to reducing conditions with Mn^{2+} and Fe^{2+} incorporation, and finally to reducing conditions in which Fe^{2+} availability and incorporation exceed Mn^{2+} availability and incorporation. More complex CL stratigraphies, however, are common.

The most reliable method for recognition of burial cements is the determination of paragenetic relations (the relative timing of features). Thus, cements that postdate earlier cements, or are coeval with or postdate stylolites, compaction features, tectonic fractures, oil emplacement, hydrothermal mineralization, saddle dolomite, silica cements, or similar features, are probable burial-stage (mesogenetic) or uplift-stage (telogenetic) cements.

The integration of petrography with advanced analytical techniques (fluid-inclusion geothermometry, epi-fluorescence microscopy, carbon and oxygen isotope and/or strontium isotope analysis, and trace-element geochemical analysis) is a virtual necessity for the study of burial-stage cementation (see Techniques chapter).

Secondary porosity is known to form, in at least some cases, in the burial setting — mainly in association with acidic waters developed through sulfate reduction, organic maturation and other diagenetic processes.

Porosity-depth data for south Florida carbonate rocks

These diagrams show porosity-depth data derived from electric logs and bore-hole gravity measurements for Cretaceous to Cenozoic carbonate rocks in 15 wells from south Florida. The least-squares exponential curve fitted to the data emphasizes the consistent porosity loss with increasing depth of burial. Near-surface strata in this section underwent both marine and meteoric diagenesis and yet retained 35-50% porosity. Most porosity loss, down to the typical average of <5% for ancient carbonate rocks, occurred during burial. The curves on the right show that dolomites have lower porosity than limestones at the surface, but lose porosity more gradually during burial. From Schmoker and Halley (1982).

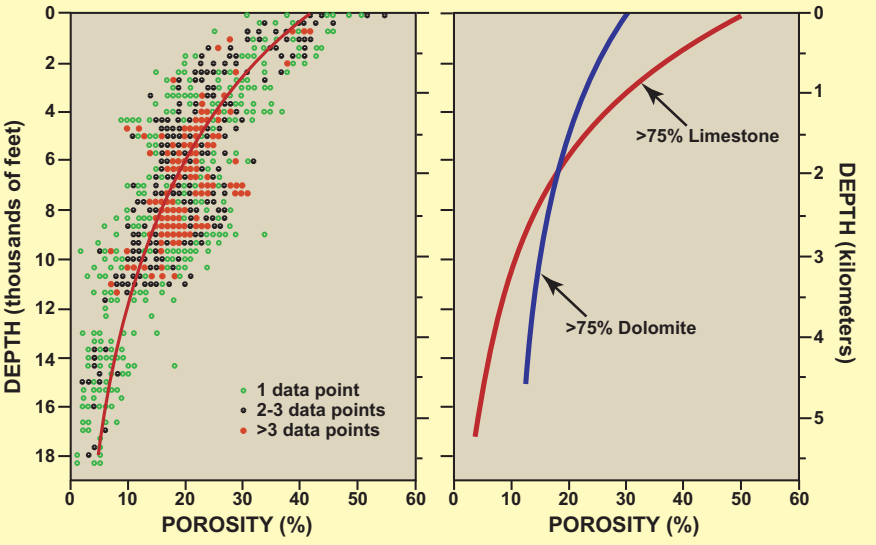

Mechanical and chemical compaction features

Much of burial diagenesis, and thus much of the porosity loss seen in the diagram above, results from physical (mechanical) and chemical compaction of carbonate sediments and rocks. Some of the many features used to identify compaction are shown in this diagram. The chemical compaction features are particularly significant because they lead to local rock compaction and, in addition, put calcium carbonate into solution for precipitation as cements at other sites.

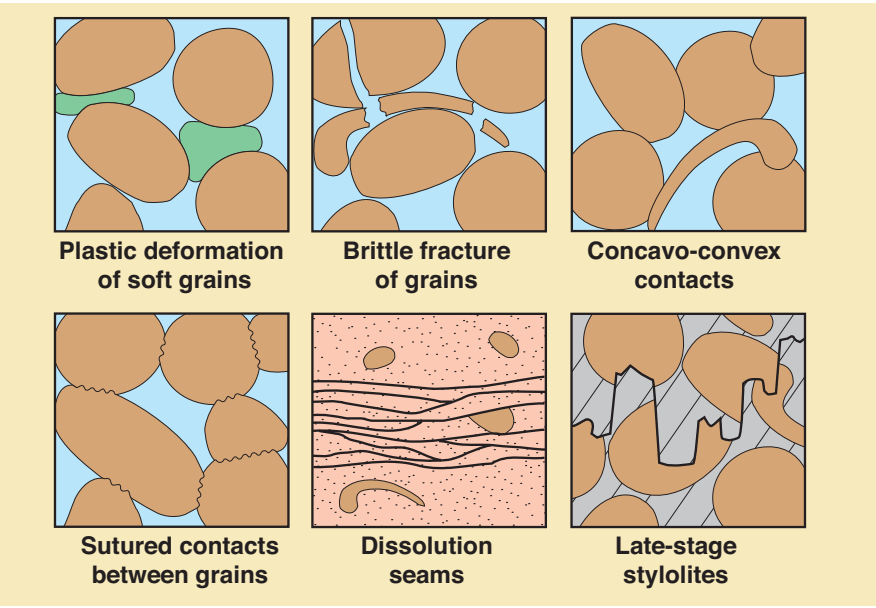

Common burial-stage cement fabrics

Four common morphologies found in burial-stage cements. Unfortunately, none are completely diagnostic of burial cementation — prismatic spar, for example, could be a product of marine cementation (or of the alteration of marine cements); drusy mosaics can also be formed in meteoric environments; and syntaxial overgrowths have been reported from marine, meteoric, and burial diagenetic settings — and indeed, single overgrowths may grow through all three stages of diagenesis.

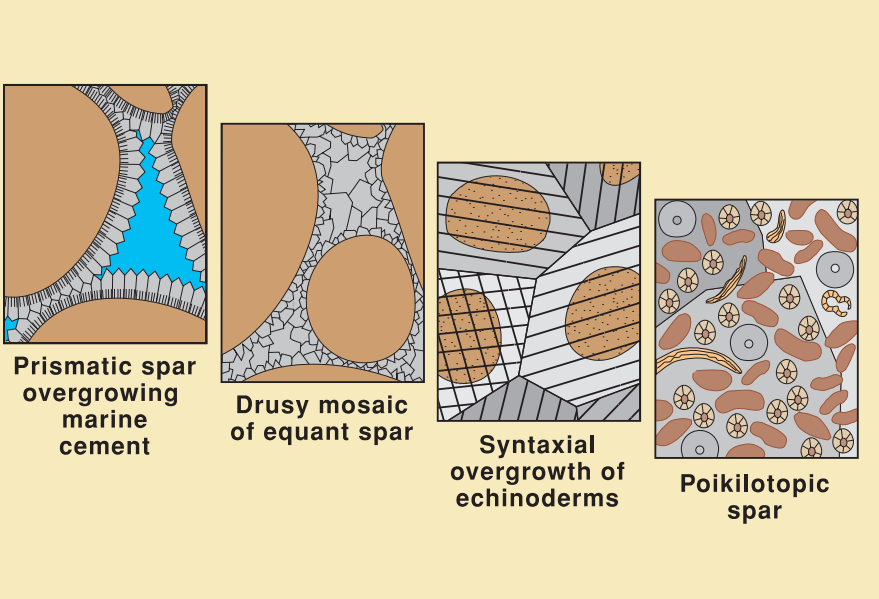

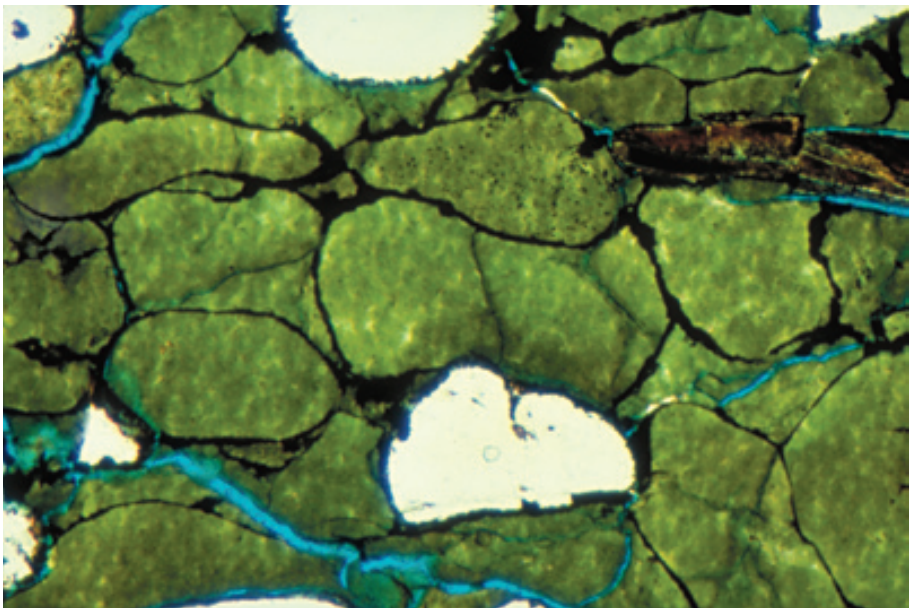

Mid.-Up. Cambrian Riley Fm., Lion Mountain Ss. Mbr., Burnet Co., Texas

Physical (mechanical) compaction features, especially dewatering structures or grain reorientation, can form even at minor burial depths. More pervasive deformation, however, requires substantial burial. These soft glauconite grains, from a greensand unit, were plastically deformed to produce a fitted fabric with linear (as opposed to point) contacts between grains. Plastic grain deformation begins at shallow depths in glauconites, but is far less common in limestones because most carbonate grains are at least partially lithified and thus resist such deformation.

PPL, BSE, HA = 1.6 mm

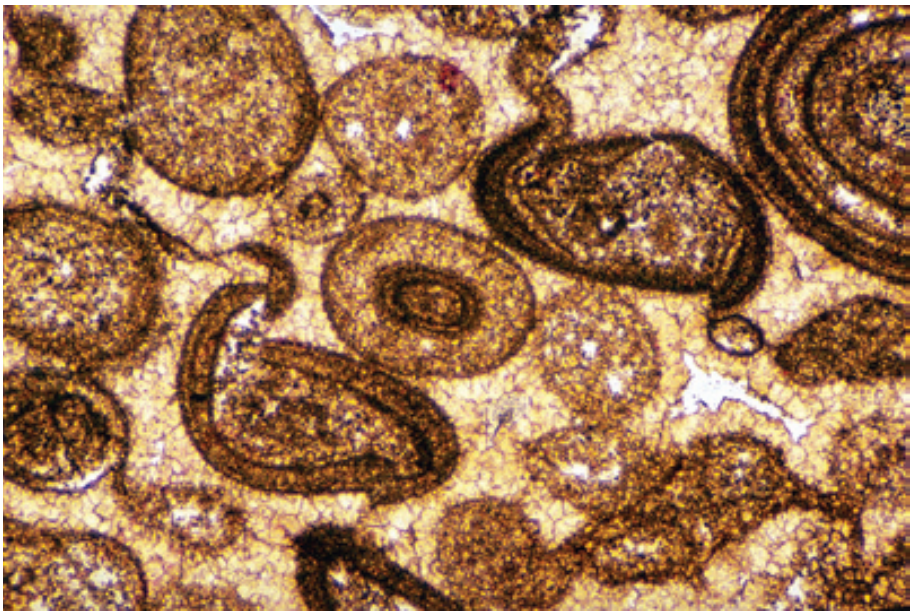

Up. Jurassic (Oxfordian) Up. Smackover Fm., 7,878 ft (2,401 m) depth, Arkansas

These ooids have been deformed by early-burial physical compaction despite the dense structure of ooids. Most likely meteoric leaching of parts of the ooids (as shown in the meteoric diagenesis section) weakened the ooids and allowed collapse of such grains during overburden loading. While some collapse of this type can occur in near-surface areas, this deformation and subsequent cementation probably occurred somewhere in the deep phreatic to shallow burial zone. Photograph courtesy of Clyde H. Moore.

PPL, AS, HA = ~1.2 mm

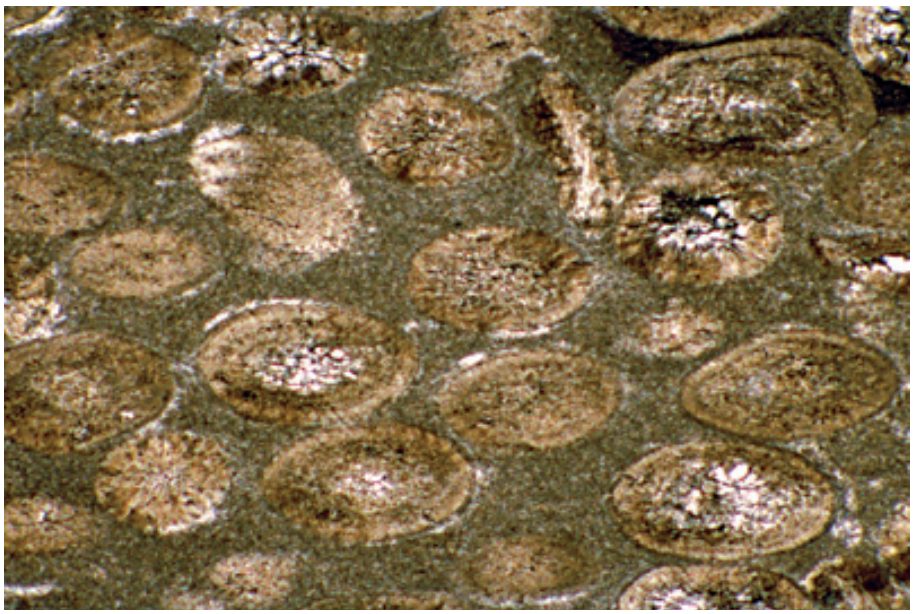

Up. Cambrian Beekmantown Gp., Washington Co., Maryland

An example of pervasive grain deformation of rigid carbonate grains (despite the presence of micritic matrix which normally cushions grains and absorbs most deformation through flowage). In this case, ooid deformation resulted from pervasive tectonic shear after lithification of the entire rock. Because ooids typically have near-circular original outlines, these flattened grains have been used by structural geologists as natural strain ellipsoids for determining the major tectonic stress directions (e.g., Cloos, 1947; cited in the Carbonate Rock/Sediment Classification chapter).

PPL, HA = 3.1 mm

Up. Cambrian Gatesburg Fm., central Pennsylvania

An example of a brittle deformation of an ooid showing outer concentric laminations that are sheared away from the rest of the ooid. Dissolution of thin interlayers within the ooid may have aided this deformation, but substantial overburden stress was also required. Such textures indicate that much of the cementation in this rock postdates compactional deformation.

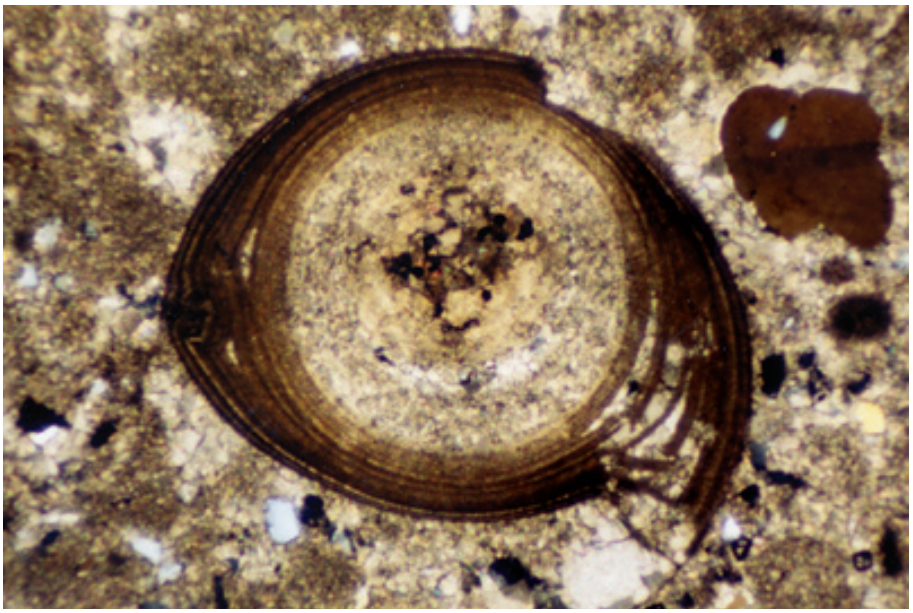

XPL, HA = 2.8 mm

Up. Cretaceous limestone, Zakinthos, Ionian Islands, Greece

Most carbonate grains that survive sedimentation processes in shelf settings are fairly robust. Thus, physical compaction effects are found most commonly in grains that were affected by boring, leaching, or other grain-weakening processes during marine or meteoric diagenesis. In this example, an aragonitic grain was leached leaving only a micrite envelope (strengthened slightly by thin internal and external crusts of probable phreatic meteoric cement). The near absence of later-stage cement allowed compactional crushing of the thin and structurally weak envelope during shallow burial.

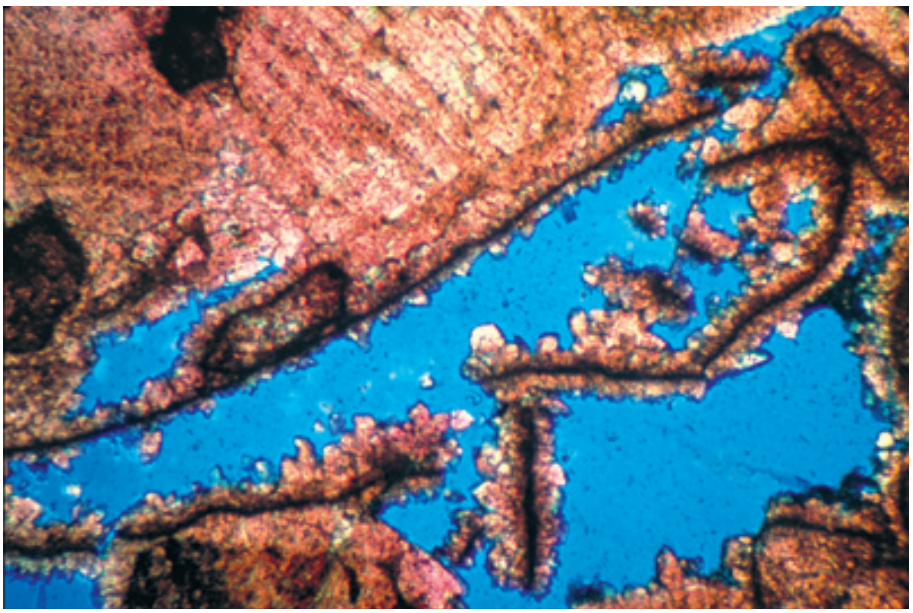

PPL, AFeS, BSE, HA = 2.4 mm

Lo. Cretaceous Sunniland Fm., Sunniland field, south Florida

More extensive crushing of multiple micrite envelopes around leached aragonitic grains. In meteorically leached sections with only incipient cementation, even relatively minor overburden loading can lead to extensive deformation and porosity loss. This remarkably porous sample, however, is from greater than 3 km (10,000 ft) depth and may reflect elevated pore fluid pressures (overpressuring) partially reducing the effects of lithostatic loading. Photograph courtesy of Robert B. Halley.

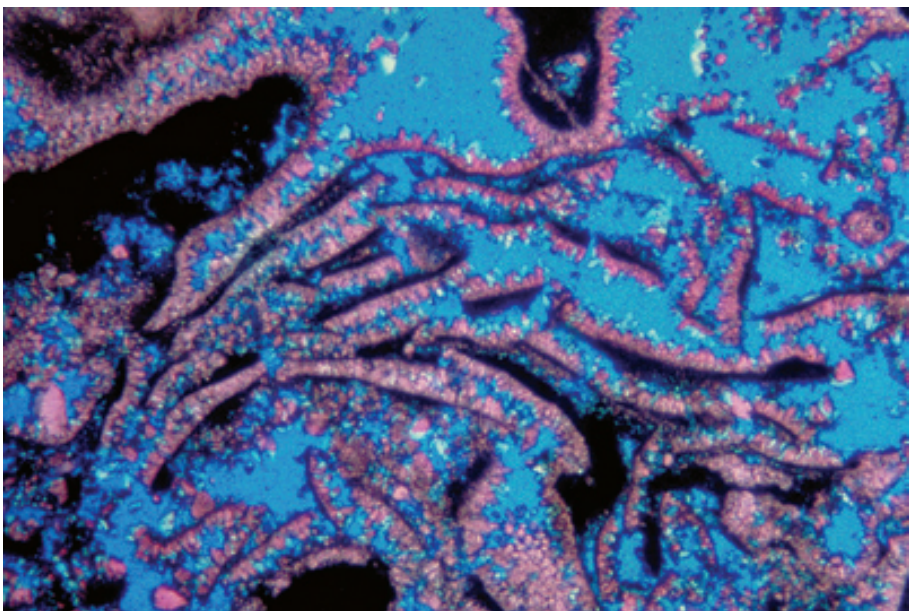

PPL, AS, BSE, HA = ~ 8.0 mm

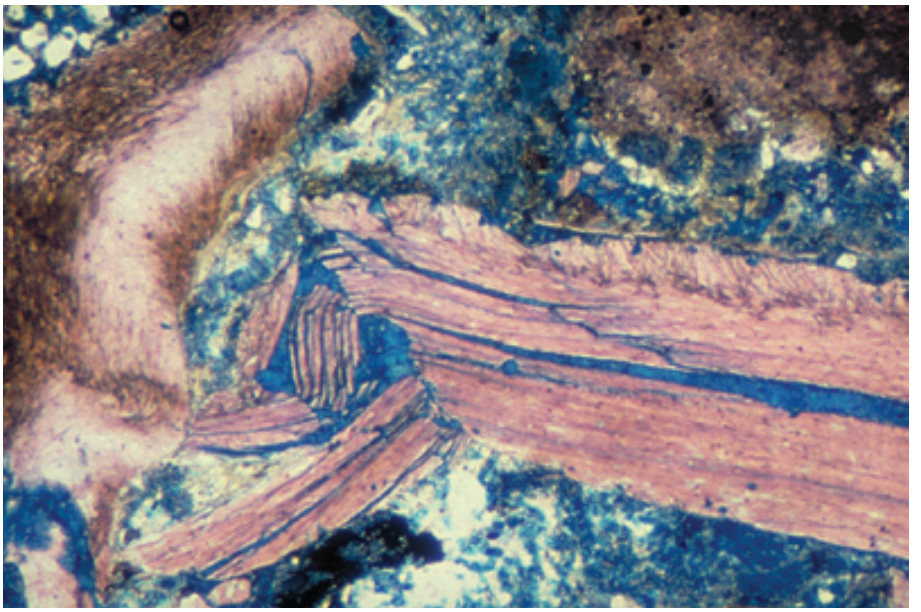

Lo. Cretaceous Paw Paw Fm., Grayson Co., Texas

Compactional fracturing of robust oyster-like bivalve shells followed by late-stage ferroan calcite and minor siderite cementation. Breakage of strong, rigid grains occurs mainly in strata with little or no matrix in which large grains are in direct contact with each other. Each point contact then acts as a fulcrum for physical grain breakage or a high-stress site for chemical dissolution.

PPL, AFeS, BSE, HA = 1.6 mm

Eocene Green River Fm., Laney Mbr., Sweetwater Co., Wyoming

Compactional shattering of thin-walled gastropod shells in a lacustrine limestone. Brittle and thin shells and tests that are not cushioned by micritic matrix are very susceptible to deformation under even moderate overburden loads (e.g., Shinn and Robbin, 1983).

PPL, HA = 7.0 mm

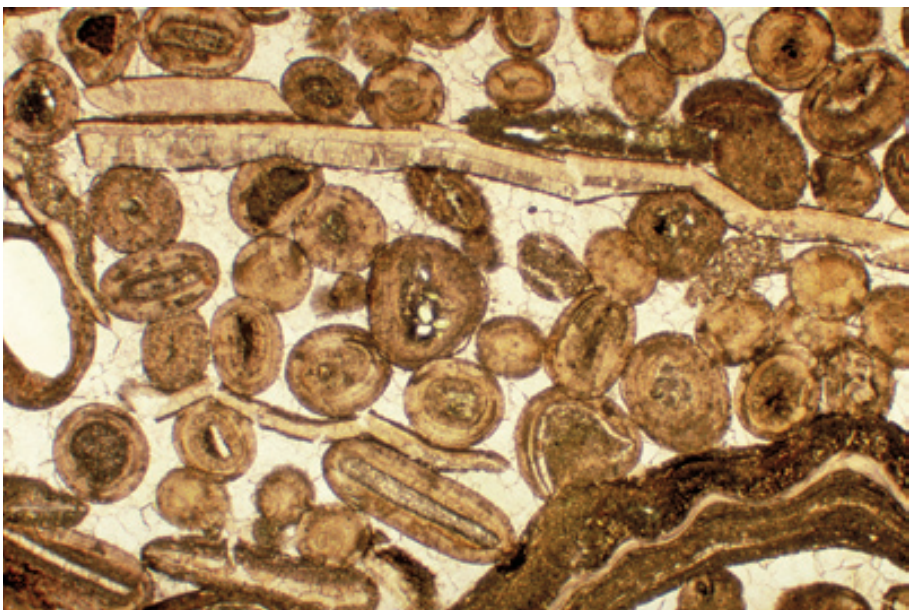

Up. Pennsylvanian (Missourian) Stanton cyclothem, Buffalo, Kansas

This transgressive calcarenite has overpacked (pressure embayed) ooids and brittly fractured bivalve shells. This indicates substantial compaction in the absence of early marine or meteoric cements, followed by cementation in a later burial environment. This diagenetic pattern is common in the lower parts of cyclothems where strata are unlikely to have been substantially cemented prior to burial. Photograph courtesy of Phillip H. Heckel.

PPL, HA = ~5 mm

Lo. Jurassic (Liassic) limestone, Central High Atlas region, Morocco

Mechanical compaction is usually, but not always, inhibited by early cementation. In this oolitic limestone, compaction postdated early-diagenetic formation of thin, isopachous, marine cement crusts. This is demonstrated by the pervasive deformation of adjacent, originally spherical grains, despite the consistent presence of intervening cements.

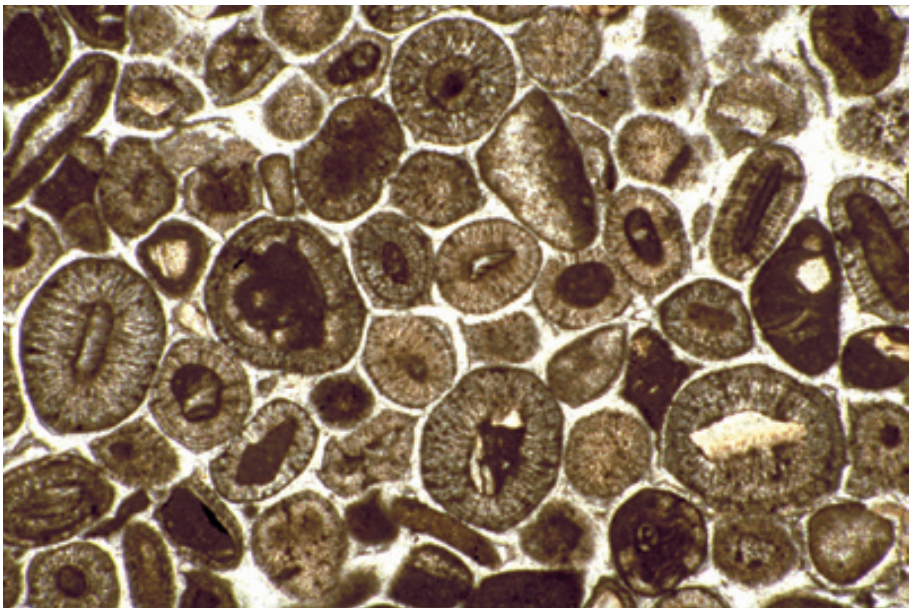

PPL, HA = 4.5 mm

Eocene Green River Fm., Lincoln Co., Wyoming

Physical compaction features in limestones are especially common in fine-grained sediments that escaped cementation in marine or meteoric settings. Seafloor porosities of 70% or more are common in carbonate muds, and mechanical dewatering and grain reorientation are inevitable in such sediments. This example shows compactional drape of laminated, fine-grained, lacustrine carbonate muds around an early-formed phosphatic nodule. Because the nodule itself is a diagenetic feature, and because the compaction requires at least moderate overburden, this extensive compaction can be attributed to the effects of burial.

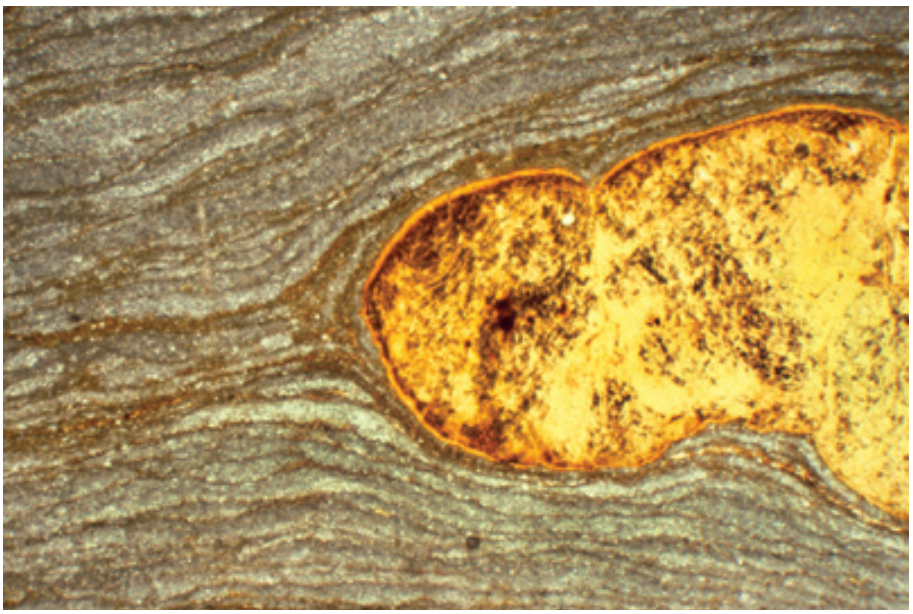

PPL, HA = 5.1 mm

Up. Cretaceous (Coniacian-Santonian) Niobrara Fm., Ft. Hays Ls. Mbr., Fort Collins, Colorado

This foraminiferal chalk shows extensive mechanical compaction in which foraminiferal tests and other grains were completely flattened, forming an intensified bedding-parallel lamination. Such dramatic physical crushing of grains is relatively rare in chalks and generally reflects unusually high rates of loading or rapid loss of overpressuring (another way of achieving very rapid rates of effective loading).

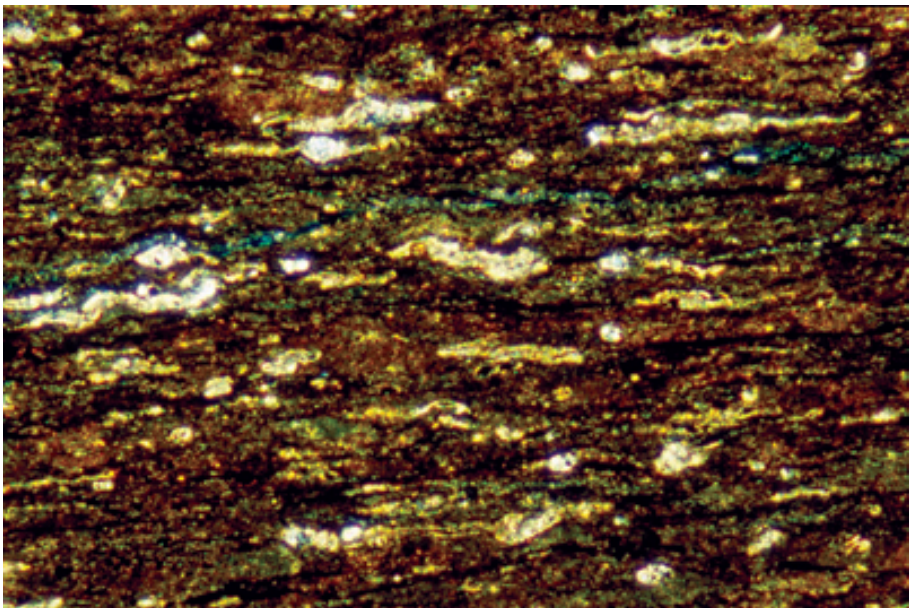

PPL, BSE, HA = ~1.2 mm

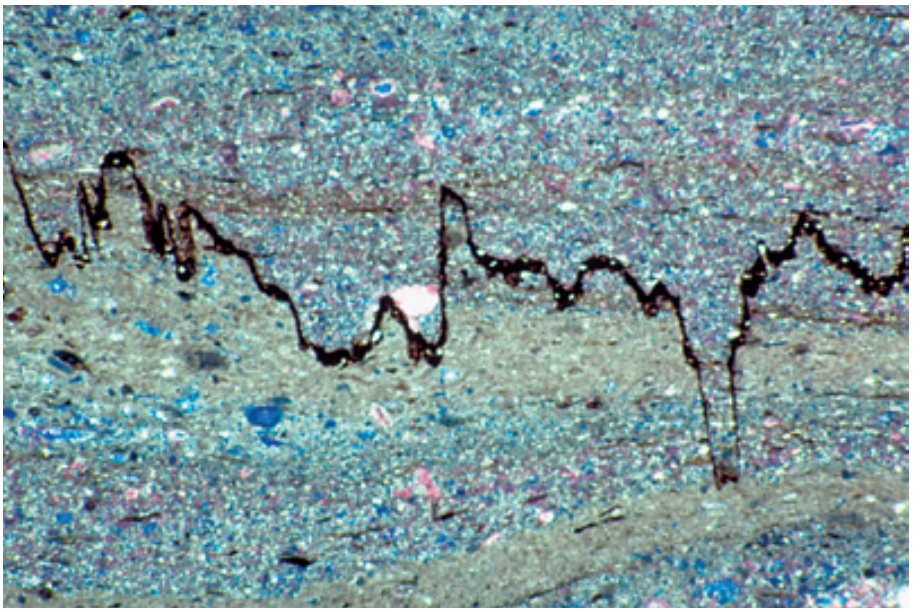

Up. Permian (Guadalupian) Capitan Fm. slope facies, 3,479 ft (1,060 m) depth, Eddy Co., New Mexico

Chemical dissolution takes many forms in carbonate rocks, and stylolites are probably the most readily identifiable of them. This stylolite, from a laminated shaly limestone, is marked by concentration of insoluble materials along its irregular surface. The surface represents a pressure-induced zone of dissolution with differential grain interpenetration depending on the relative solubilities of grains present on each side of the surface. Stylolite formation is associated with thin water films that allow solutes to move away from sites of dissolution (see Weyl, 1959; Bathurst, 1975).

PPL, BSE, AS, HA = 5.0 mm

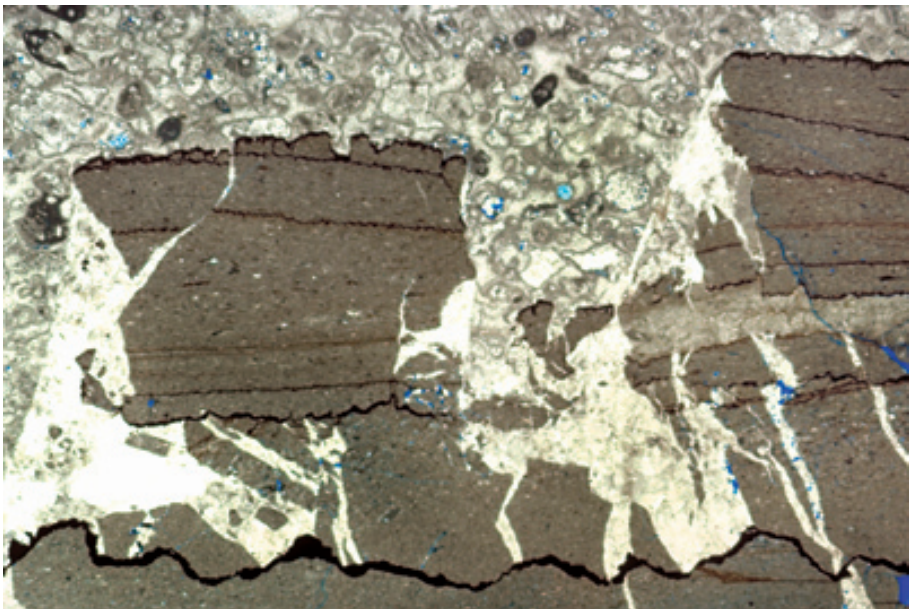

Up. Permian (Guadalupian) Capitan Fm. slope facies, 3,484 ft (1,062 m) depth, Eddy Co., New Mexico

Multiple generations of stylolites cutting a slope limestone. The major, late-stage stylolite was formed by selective dissolution at a surface of fabric and compositional change — a boundary between a turbidite grainstone and an underlying pelagic limestone. Numerous fractures radiate from one of the stylolite "teeth", a common occurrence in stylolitic limestones. Most stylolites parallel bedding, but others form at high angles to primary bedding, especially where influenced by folding or compressional tectonic stresses.

PPL, BSE, HA = 16 mm

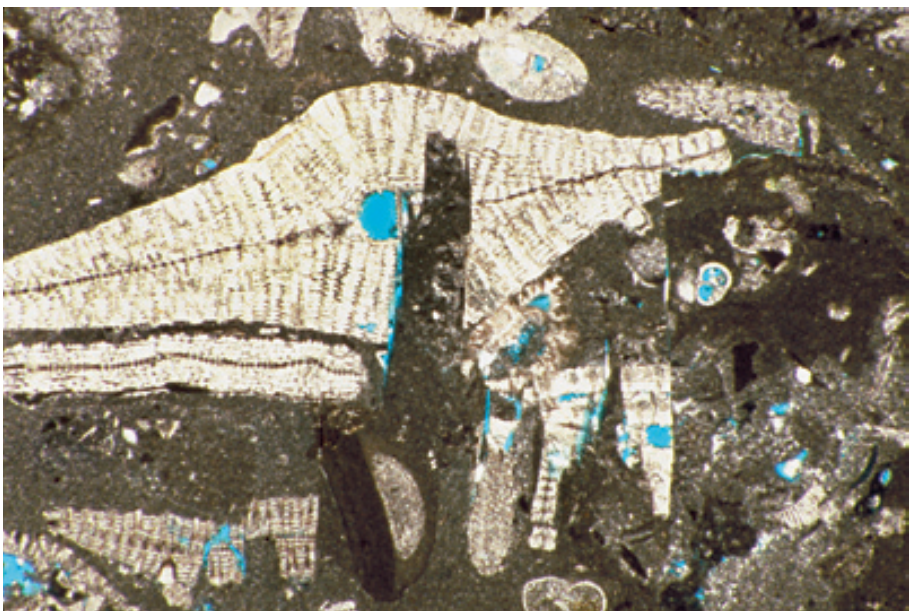

Eocene limestone, Paxos, Ionian Islands, Greece

An example of the remarkable dissolution that can occur along stylolites, in this case a nummulitic slope limestone. The minimum depth of burial needed for the formation of stylolites is rather poorly understood, but substantial stylolites, such as this one, probably require a minimum of at least 300-1000 meters of burial (or equivalent tectonic stresses) for their formation. Thus, stylolites postdate substantial cementation and lithification in many limestones. They also supply solutes for further cementation, either in the vicinity of the stylolites or at some distance removed from them.

PPL, BSE, HA = 5.5 mm

Paleozoic, Canada

A dramatic example of deeply stylolitized ooids. An estimate of the minimum amount of material dissolved can be obtained by looking at the amplitude of the stylolite teeth and the loss of large parts of the affected ooids. Sample from Noel P. James.

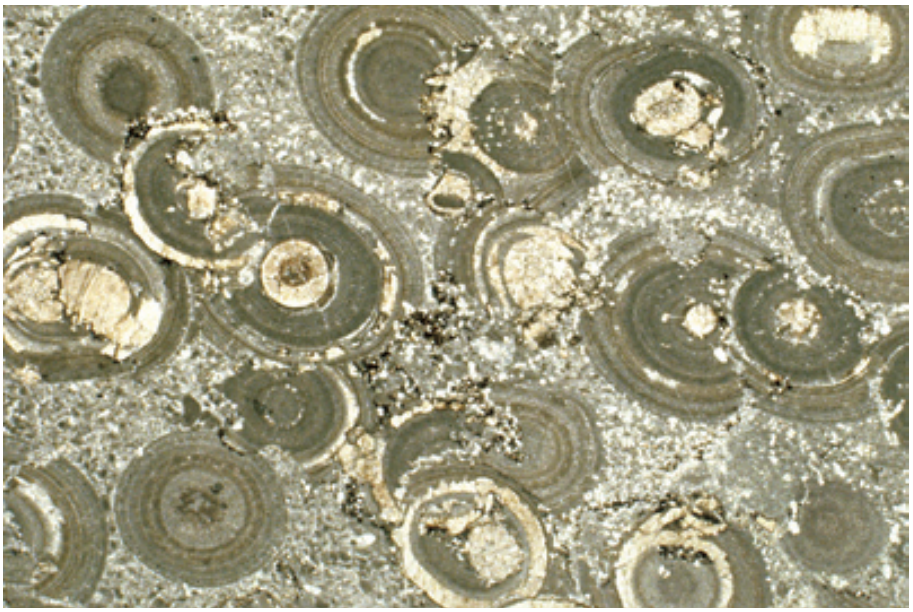

PPL, HA = 11 mm

Lo. Cretaceous (Albian) Glen Rose Ls., Somervell Co., Texas

Isolated pressure-solution (chemical compaction) features can also occur between adjacent individual grains in a limestone. In this example, a bivalve (*Gryphaea*) shell has pressure-dissolved an adjacent bivalve fragment along an irregular contact. The stylolitic contact, in this case, does not extend beyond the contact between the grains. However, even such localized burial-stage dissolution can provide substantial material for cementation of nearby pores.

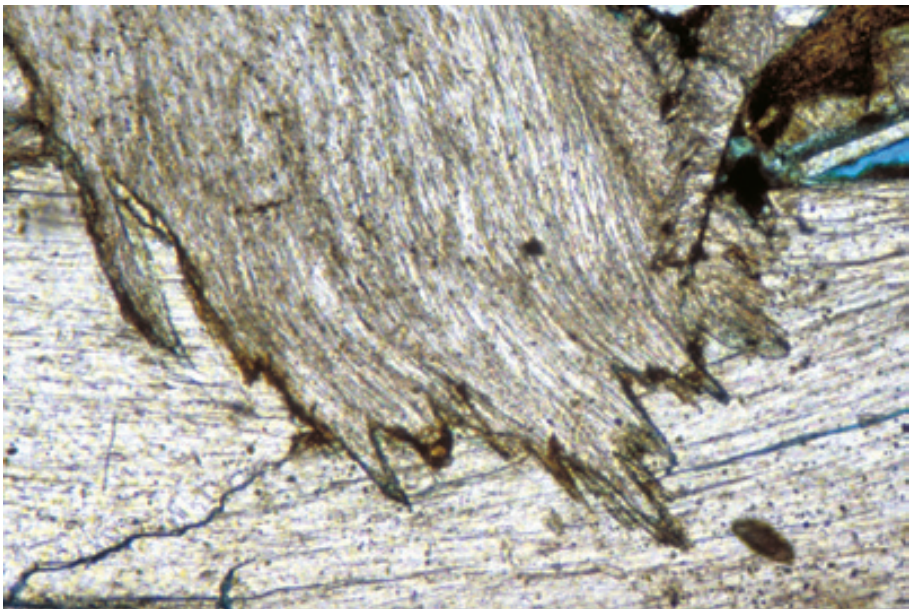

PPL, BSE, HA = 0.65 mm

Up. Jurassic (Oxfordian) Up. Smackover Fm., Gulf Coast, U.S.A.

Another example of grain-to-grain pressure solution, here in an ooid grainstone. Note the irregular or sutured grain contacts, the solution residue between grains, and the development of a "fitted" grain-to-grain fabric with little intervening cement or porosity. Photograph courtesy of Clyde H. Moore.

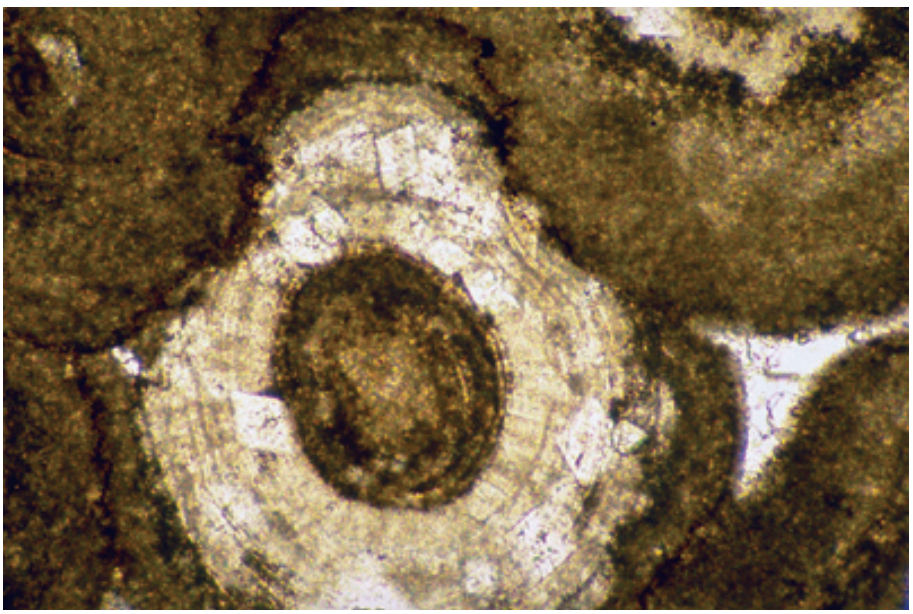

PPL, HA = ~0.65 mm

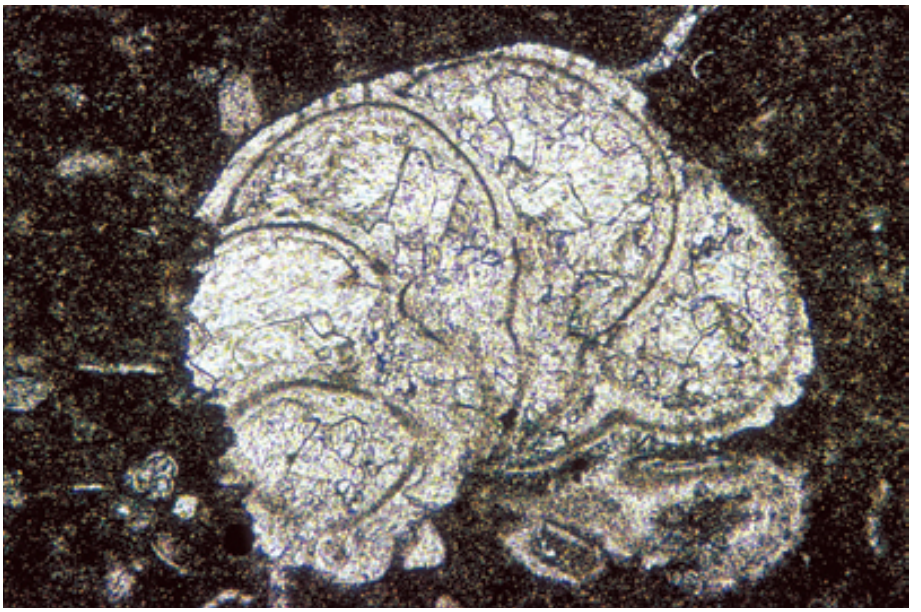

Cretaceous (Senonian) Upper Chalk, Kent, England, U.K.

Dissolved and sutured margins can occasionally be found even on grains surrounded by micritic sediment. Here a foraminiferal test has been truncated on two sides, presumably along a subtle solution seam that is largely concealed in the dense micritic matrix. Seafloor corrosion, of course, also could lead to partially dissolved grains, but would most likely affect more parts of the test (or, in cases where the grains are partially submerged in matrix sediment, only the tops of such grains).

PPL, HA = ~1.0 mm

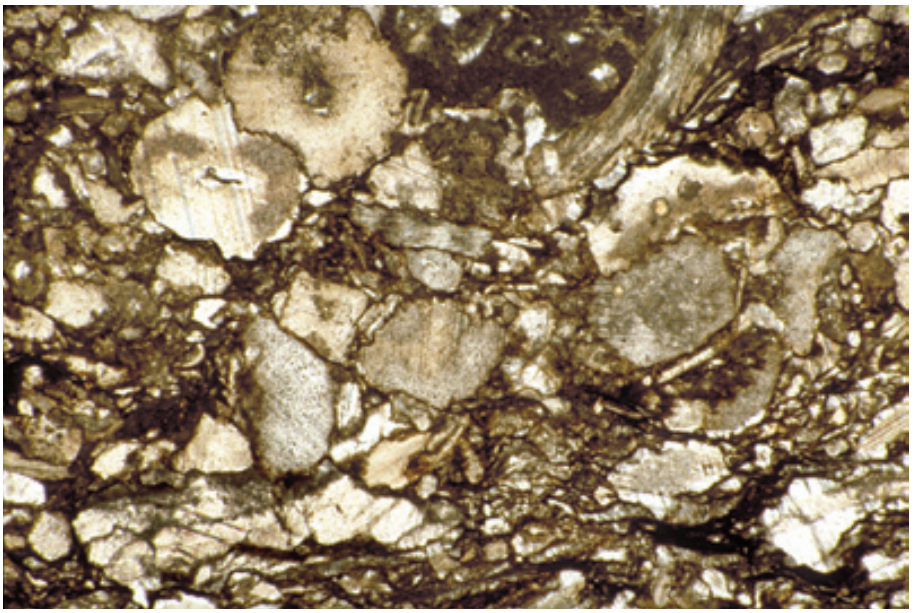

Up. Silurian Tonoloway-Keyser Ls., Mifflin Co., Pennsylvania

A crinoidal limestone (encrinite) with sutured contacts between most adjacent grains, indicating extensive chemical compaction (pressure solution) produced during burial of the limestone. The compaction postdates syntaxial overgrowths on some of the crinoids. Note the dark residues along the numerous solution contacts and the development of irregular solution laminae. Stylolites and solution seams commonly produce pseudo-bedding (also termed stylo-bedding) in limestones.

PPL, HA = 5.7 mm

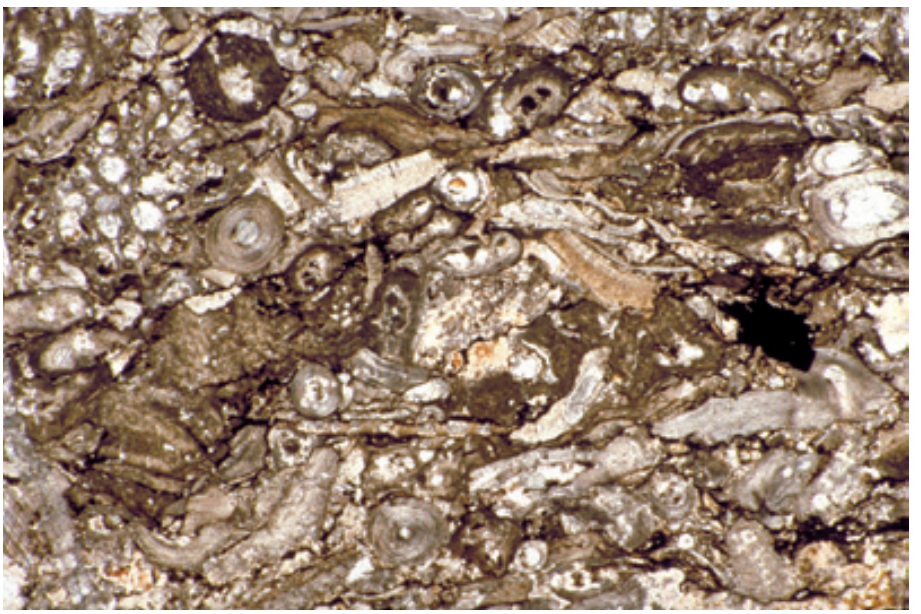

Up. Permian (Kazanian?) Wegener Halvø Fm., Jameson Land, East Greenland

An example of an over-compacted fabric in a skeletal limestone. Adjacent grains show embayment (pressure solution) and the overall fabric has closer grain packing than is normal with such irregularly-shaped allochems. As above, insoluble residues mark some of the sites of most extensive dissolution.

PPL, HA = 6.0 mm

Up. Permian (Guadalupian) Capitan Fm., subsurface, Eddy Co., New Mexico

These dissolution structures resulted from chemical compaction around an early-formed carbonate nodule, probably created by preferential cementation of a crustacean burrow. Compaction here involved formation of numerous solution seams (brownish, irregular streaks) in areas not strongly cemented during early diagenesis. Solution seams are more planar than stylolites, involve less dissolution along any single surface, but occur in such numbers that, in aggregate, they can accomplish extensive alteration; the swarms of surfaces are sometimes called "horsetail seams".

PPL, HA = 16 mm

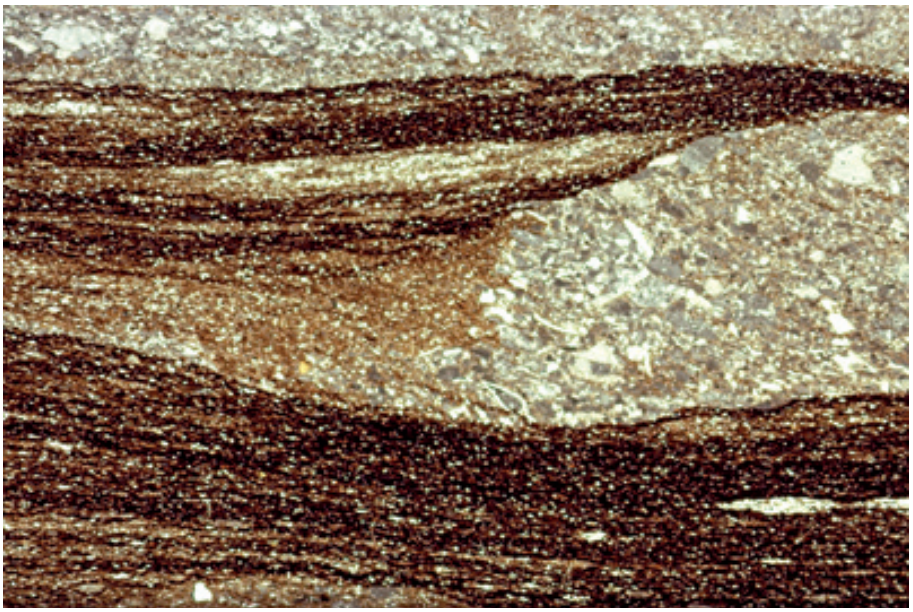

Up. Silurian Tonoloway-Keyser Ls., Mifflin Co., Pennsylvania

A crinoidal biomicrite with abundant but irregular, solution seams or microstylolites — thin, but numerous, zones of pressure dissolution form during early- to intermediate-stage burial diagenesis, especially in micritic limestones.

PPL, HA = 11 mm

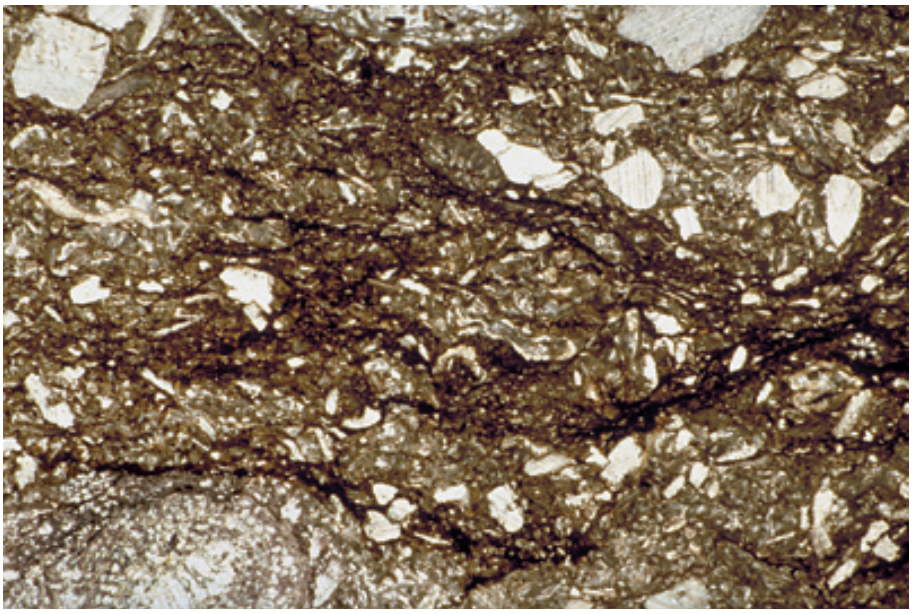

Up. Ordovician Takaka Marble, Nelson, New Zealand

A strongly sheared limestone formed along New Zealand's famous Alpine fault zone. Note the lenticular bodies of recrystallized limestone bounded by finer-grained seams filled with solution residues. These micritic-clayey seams also act as shear planes in this setting. The lenticular sparry areas show extensive development of twin lamellae, another manifestation of shearing in this rock.

XPL, BSE, HA = 2.4 mm

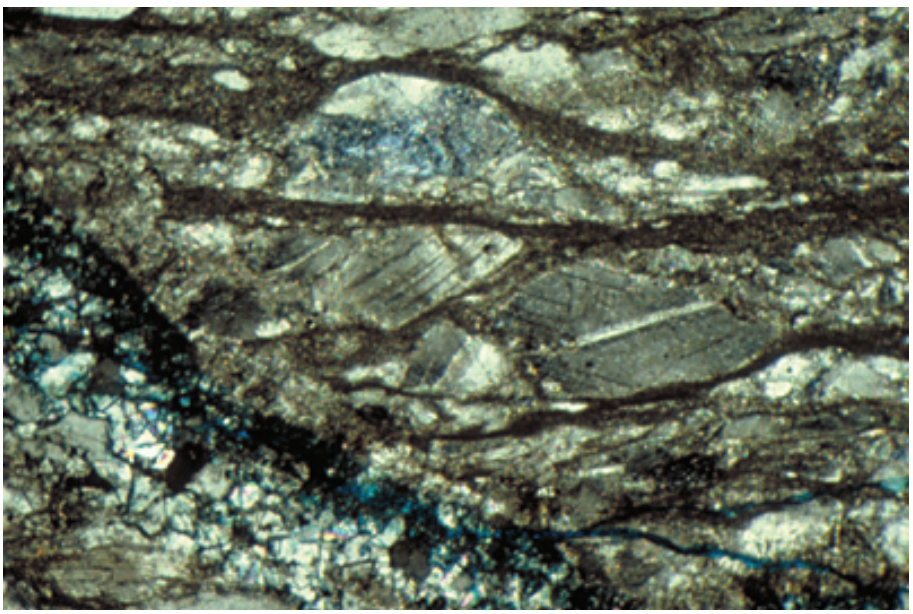

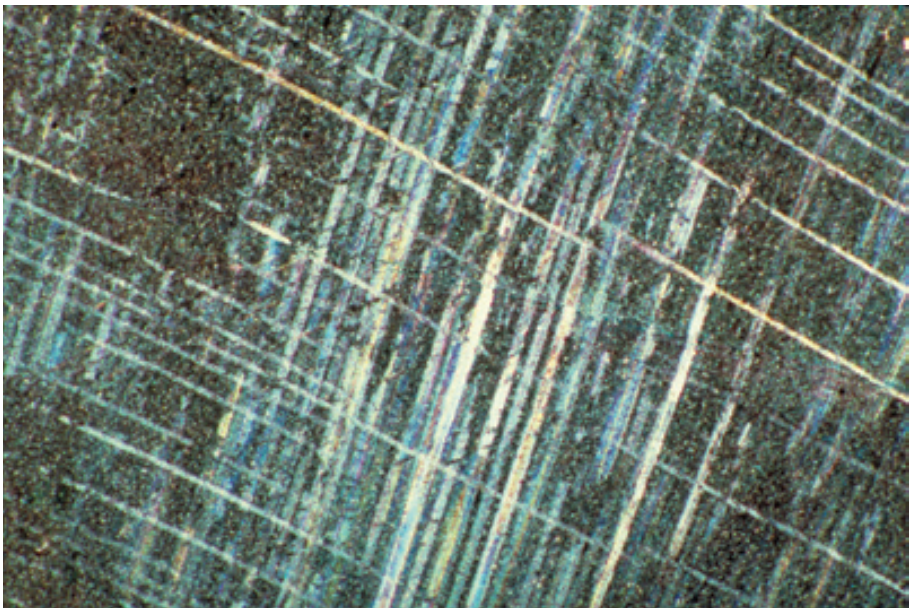

Up. Permian (Kazanian?) Wegener Halvø Fm., Jameson Land, East Greenland

A crystal with strong development of twinning (twin lamellae) in calcite. Intense twinning commonly involves dissolution as well as crystal dislocation and is typically a result of burial loading or tectonic deformation. Twin lamellae are developed far more easily in calcite than in dolomite, and indeed can be a way of differentiating the two minerals in the absence of staining or analytical information.

XPL, HA = 5.0 mm

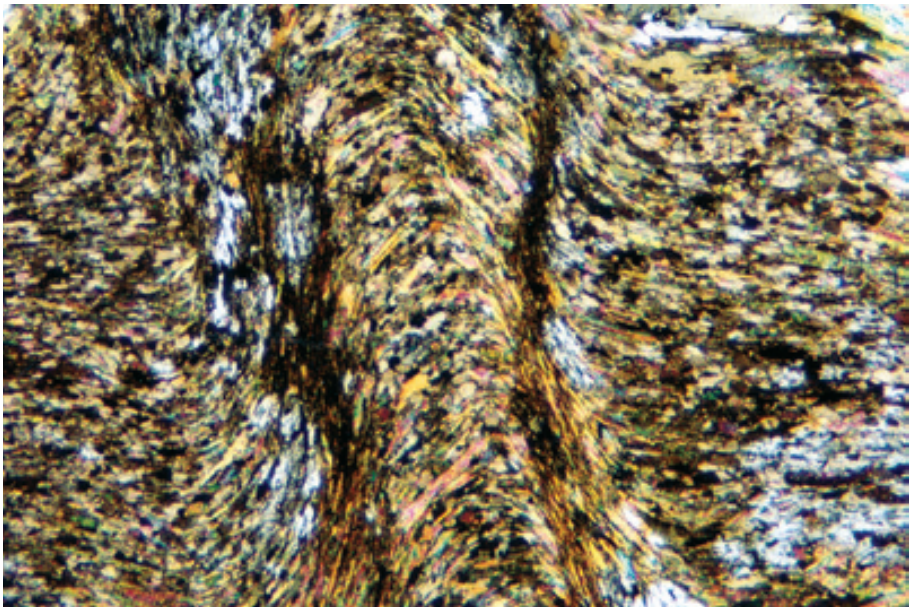

Jurassic Pennine Bündnerschiefer, Switzerland

Extreme deformation and alteration of an impure limestone. Crenulate folding, development of a authigenic micas, and strain recrystallization of calcite are all present. This exceeds the limits of what is defined as burial diagenesis and represents a transition to metamorphism with the formation of marble.

XPL, HA = 5.8 mm

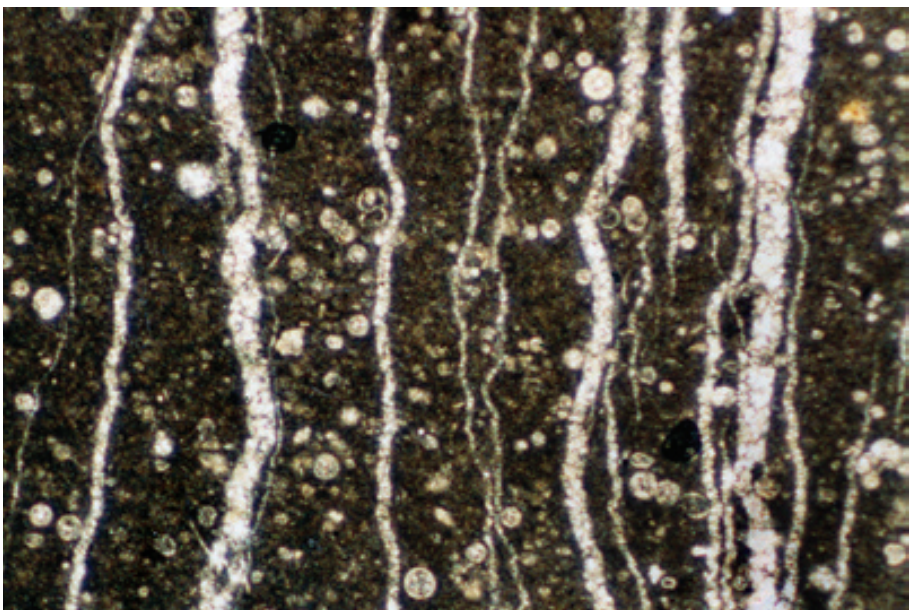

Up. Cretaceous Chalk, Yorkshire, England, U.K.

Calcite-filled fractures cutting a calcisphere- and foraminifer-rich chalk. The presence of fractures (when unhealed by calcite or other minerals) can, and in many cases does, greatly increase the effective permeability of chalks and other carbonate rocks, substantially improving hydrocarbon production. Some fracturing can occur in early-cemented limestones in both marine and meteoric settings. Extensive fracturing, however, is most commonly a burial diagenetic phenomenon and is one of the few burial-related processes that can lead to subsurface porosity increases.

PPL, HA = 3.5 mm

Up. Permian (Kazanian?) Wegener Halvø Fm., Jameson Land, East Greenland

A fracture cross-cutting both a brachiopod shell and its surrounding limestone matrix. In this example, the fracture is filled with late-stage, highly ferroan calcite spar (stained dark blue). The combination of the cross-cutting nature of the fracture and the ferroan calcite fill makes it very likely that this fracture formed, and was cemented, in a burial setting.

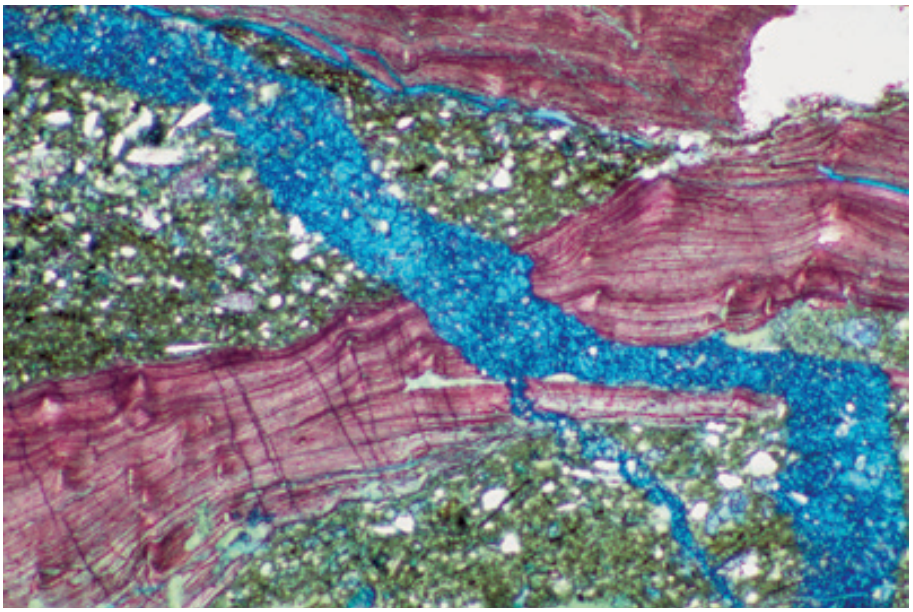

PPL, AFeS, BSE, HA = 3.2 mm

Paleocene-Oligocene Amuri Ls., Marlborough, New Zealand

A limestone with multiple fracture generations. The largest of these fractures was lined with micro-botryoidal silica cement. The remaining pore space in the main fracture, and in the smaller, presumably younger fractures, was filled with coarsely crystalline calcite (stained very pale pink). Both sets of fractures and their fillings are burial-stage diagenetic features in this outer shelf limestone.

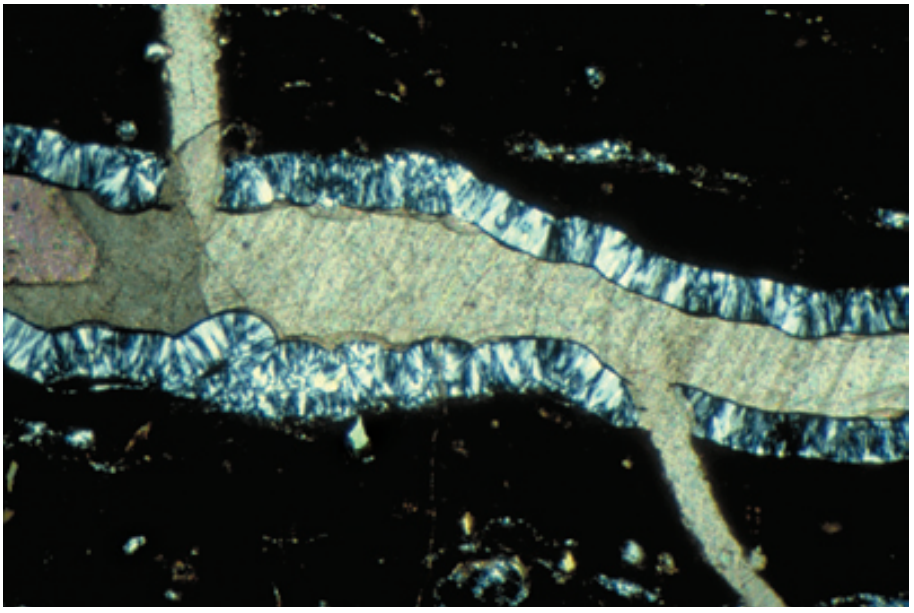

XPL, HA = 2.4 mm

Lo. Cretaceous (Aptian) Shuaiba Fm., offshore Qatar

This example shows a sinuous, rubble-filled fracture dissipating into the micritic matrix of a deep shelf limestone. Fractures like this may represent the early stages of burial in fine-grained sediments. The dewatering of very porous, still semi-fluid carbonate muds and silts can carry fluidized sediment into the fractures, eventually plugging them. Sometimes called "hairline fractures", these structures, even when rubble-filled, may enhance the otherwise extremely low permeability of chalks and other micritic limestones.

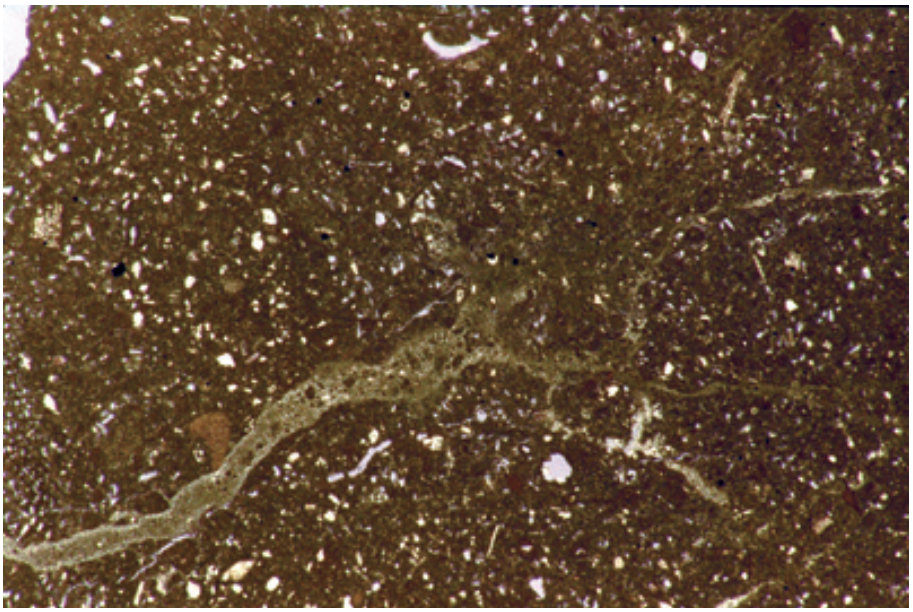

PPL, HA = 4.2 mm

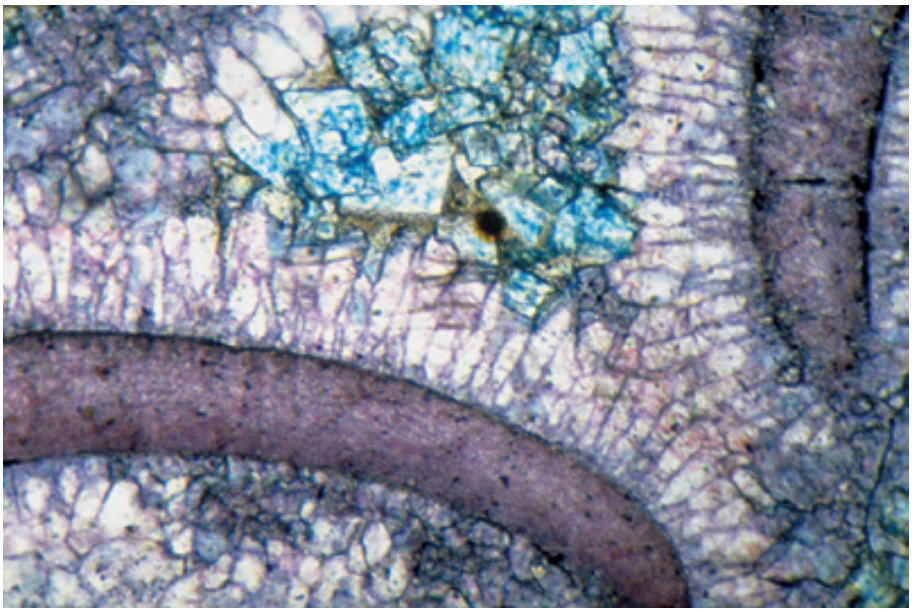

Mid. Ordovician Simpson Gp., Oil Creek Fm., Murray Co., Oklahoma

A trilobite fragment encased in multiple generations of cement. The early, bladed calcite cement is slightly ferroan; later-stage dolomite cements in the center of the pore have higher iron concentrations. The oriented crystallite structure in the trilobite shell wall may have influenced the shell-perpendicular orientation of the bladed calcite cement. The bladed cements are probably an early burial diagenetic product that altered, or formed overgrowths on, marine cement precursors. Using the diagram near the beginning of this section, this cement would be termed "prismatic spar overgrowing marine cement".

PPL, AFeS, HA = 0.65 mm

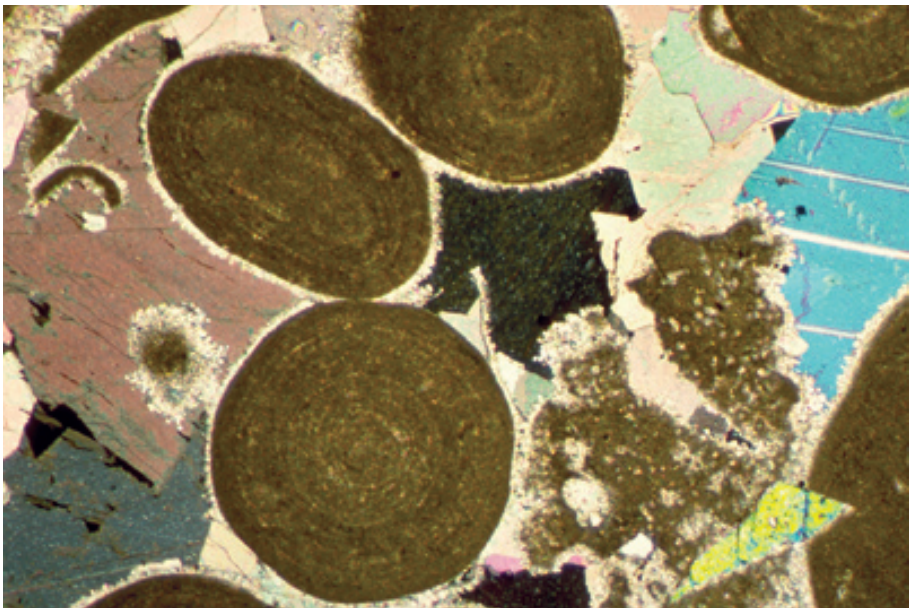

Up. Jurassic (Oxfordian) Up. Smackover Fm., 13,613 ft (4,149 m) depth, Mississippi

An oolitic limestone with thin fringes of pre-burial cement surrounding the ooids, followed by post-compaction burial-stage poikilotopic cement. The very coarse crystal size (in some cases enveloping multiple grains) and the clear, largely inclusion-free character of the crystals are characteristic of burial-stage calcite cement. Photograph courtesy of Clyde H. Moore.

PPL, AFeS, HA = ~1.2 mm

Permian (Leonardian-Guadalupian) Park City Fm., basal Franson Mbr., Daggett Co., Utah

Another example of a limestone cemented mainly by poikilotopic burial-stage calcite cements. The diagenetic history of this rock involved initial isopachous rims of carbonate cement followed by leaching of many of the grains. Single crystals of poikilotopic calcite here filled both primary (intergranular) and secondary (intragranular) porosity. In this case, the poikilotopic calcite may have resulted from dissolution or replacement of a precursor stage of coarse gypsum cements in this evaporitic unit.

XPL, HA = 7.0 mm

Up. Permian (Guadalupian) Capitan Fm., Culberson Co., Texas

A fusulinid-rich slope limestone showing a sequence of three cements. Altered crusts of cloudy, fibrous marine cement directly coat the fusulinid foraminifers and are followed by an extremely thin rind of dolomite (the unstained margin of the cloudy cements). These early cements are followed by late burial or early uplift-stage, coarsely crystalline calcite spar. The spar formed as a solution-fill replacement of anhydrite and gypsum cements that are no longer preserved in this section, but are preserved in subsurface equivalents. Again, the slowly crystallized burial cements are coarse and relatively clear and imperfection-free.

PPL, AS, HA = 4.5 mm

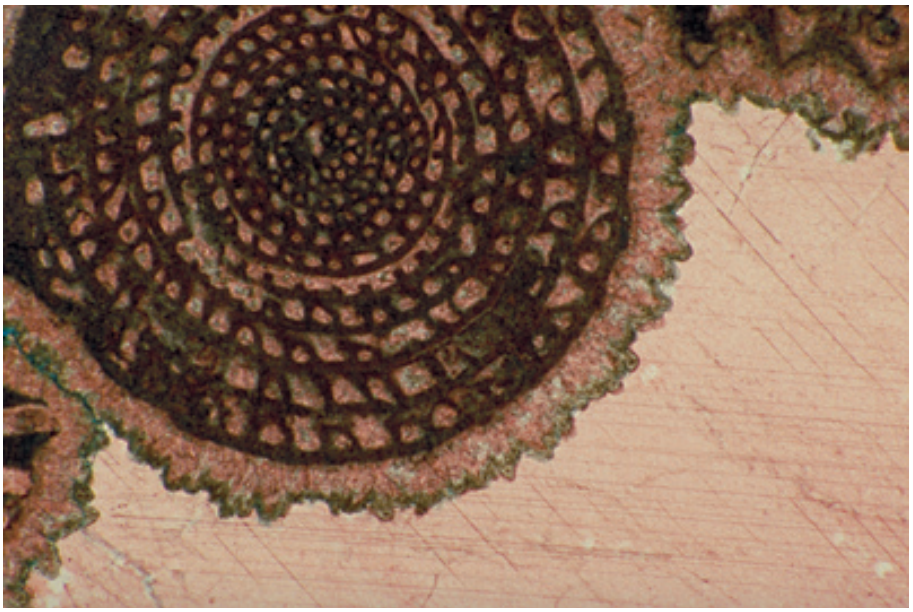

Oligocene Nile Gp., Waitakere Ls., Westland, New Zealand

Staining, especially staining using potassium ferricyanide to distinguish ferroan constituents, is very important for recognition of cement generations. In this case, non-ferroan calcite predates highly ferroan calcite. Because only Fe^{2+} readily substitutes in the calcite lattice, reducing condition are required to precipitate ferroan calcite. Most (but by no means all) near-surface environments are oxidizing and most burial settings tend to be reducing. Thus, strongly ferroan calcites like these are normally considered to be burial-diagenetic precipitates, especially where they are coarse, clear, and form the final pore-filling precipitates.

PPL, AFeS, HA = 0.6 mm

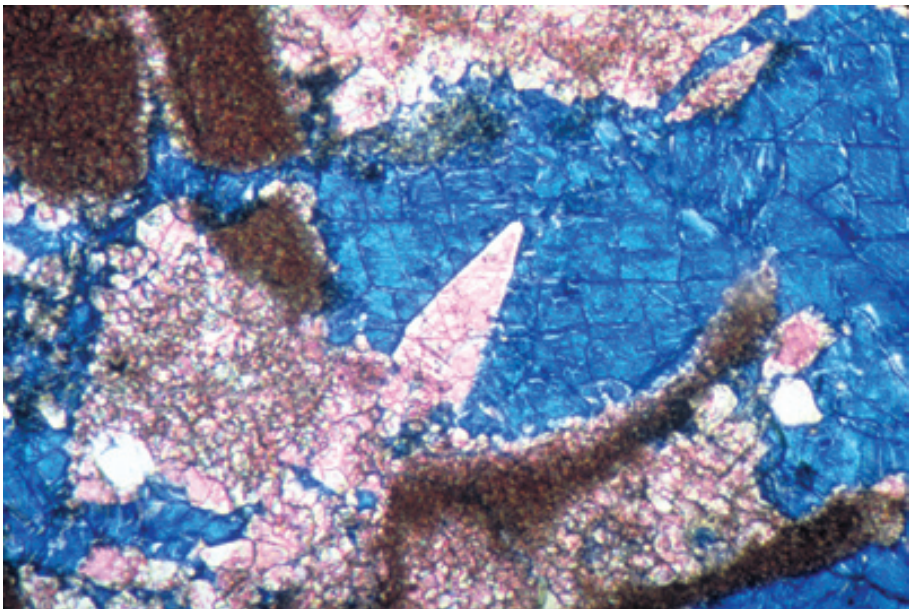

Mid.-Up. Ordovician Simpson Gp., Oil Creek Fm., Johnston Co., Oklahoma

An example of extensive calcitic syntaxial overgrowth cements on crinoid fragments. The porosity in this encrinite has been largely obliterated by such cementation. Note the cloudy interiors of crystals that mark the original crinoid outlines. Such cements may begin in the marine environment, they can certainly precipitate in meteoric settings, but in many cases, they continue to grow in the burial environment as well. Many such overgrowths have very clear, somewhat ferroan outer margins that represent the burial-stage additions.

XPL, HA = 8.0 mm

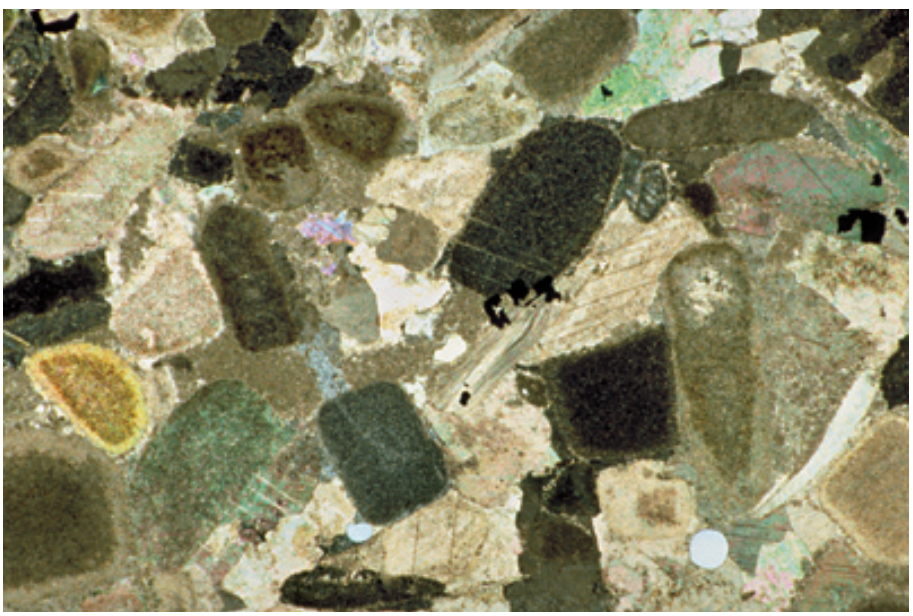

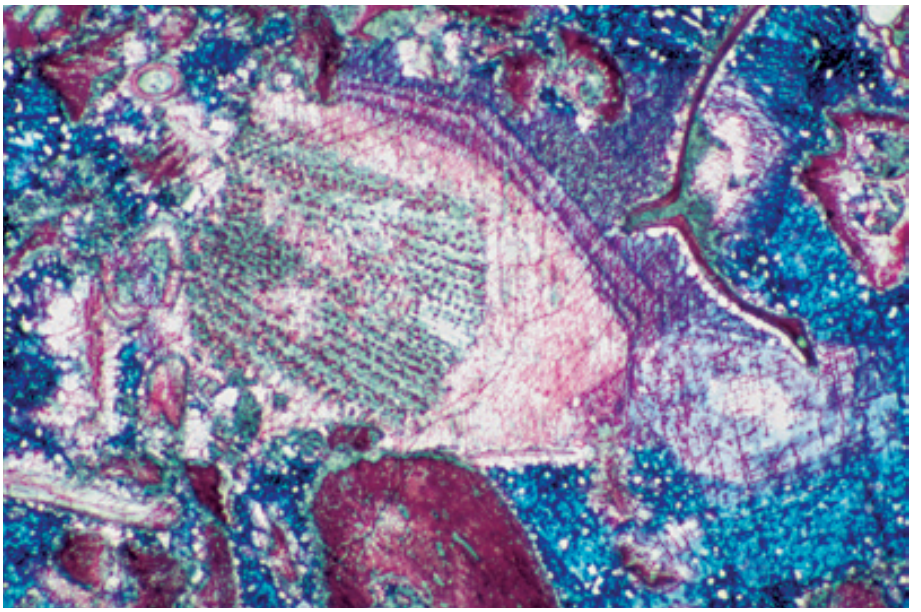

Up. Permian (Kazanian?) Wegener Halvø Fm., Jameson Land, East Greenland

An echinoderm fragment with an extensive syntaxial overgrowth. Staining indicates that overgrowth cementation persisted through a significant time period during which pore fluids became progressively more reducing (thereby incorporating more iron into the calcite lattice). Later, even more ferroan calcite cements postdate the overgrowth. The transition from surficial to burial cementation lies somewhere in the overgrowth, but isotopic, fluid-inclusion, or other geochemical data is required to clarify these relationships.

PPL, AFeS, HA = 3.0 mm

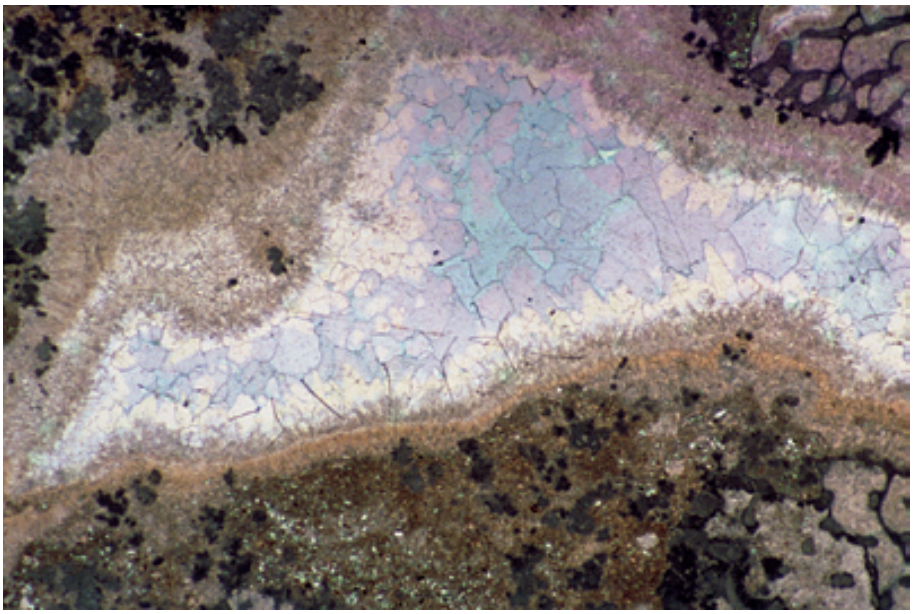

Early Cambrian Forteau Fm. Southern Labrador, Canada

A reef limestone with a growth cavity lined with cloudy, fibrous calcite of probable marine origin. The rest of the cavity is filled with non-ferroan bladed and slightly ferroan blocky calcite, much of which is likely of burial origin. Note the increase in crystal size of the blocky calcites from margin to cavity center, a common feature of pore-filling cements. Photograph courtesy of Noel P. James.

PPL, AFeS, HA = 10 mm

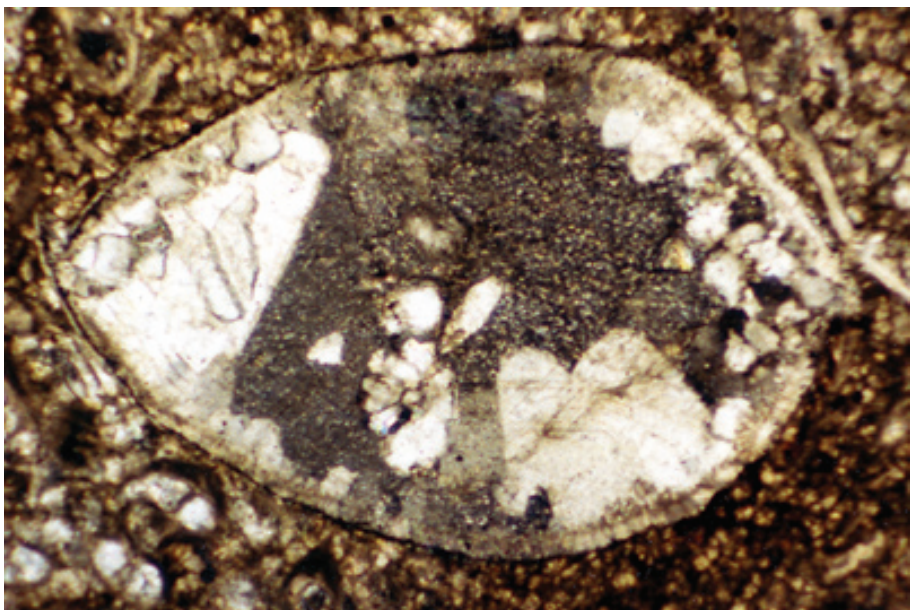

Mississippian Coral Ls., England, U.K.

This intraparticle pore was plugged with coarse, cavity-filling sparry calcite. The fringe of finely-crystalline, meteoric phreatic or early burial cement inside the shell is followed by very coarse spar that is almost certainly of burial diagenetic origin. Crystal sizes again increase toward the center of the cavity (although dominated in this case by just a few very large central crystals and the tips of crystals coming in from outside the plane of this section).

XPL, HA = 3.2 mm

Oligocene Nile Gp., Karamea, Westland, New Zealand

The secondary porosity in this temperate-water limestone (mainly abraded and leached bivalve fragments) was filled primarily with ferroan calcite cement (blue). Careful examination, however, shows thin rinds, or isolated small crystals, of non-ferroan calcite on the edges of the leached pores. Again, staining is crucial in distinguishing these thin, early-stage cements from the volumetrically more important burial-stage precipitates.

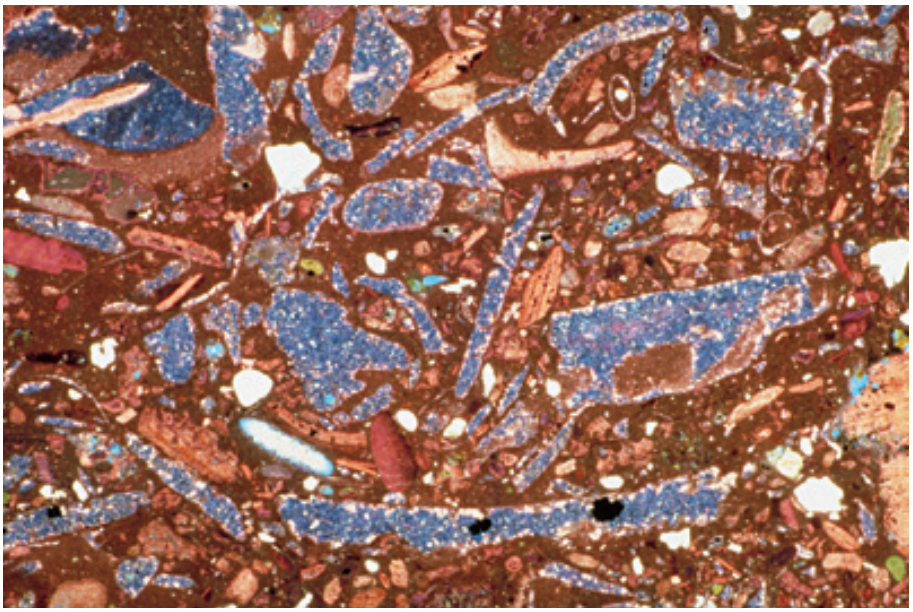

PPL, AFeS, HA = 12.5 mm

Up. Permian (Kazanian?) Wegener Halvø Fm., Jameson Land, East Greenland

Paragenetic relations — the relative sequencing of diagenetic events — can be crucial in proving a burial-stage origin for cements. Here, the early, bladed, non-ferroan cements (stained pink) could have a variety of origins including altered marine, meteoric, or shallow burial precipitates. They were postdated, however, by highly ferroan blocky calcite spar (stained dark blue). The burial diagenetic origin of these cements in supported by the fact that they contain abundant hydrocarbon inclusions (black asphaltic inclusion zones).

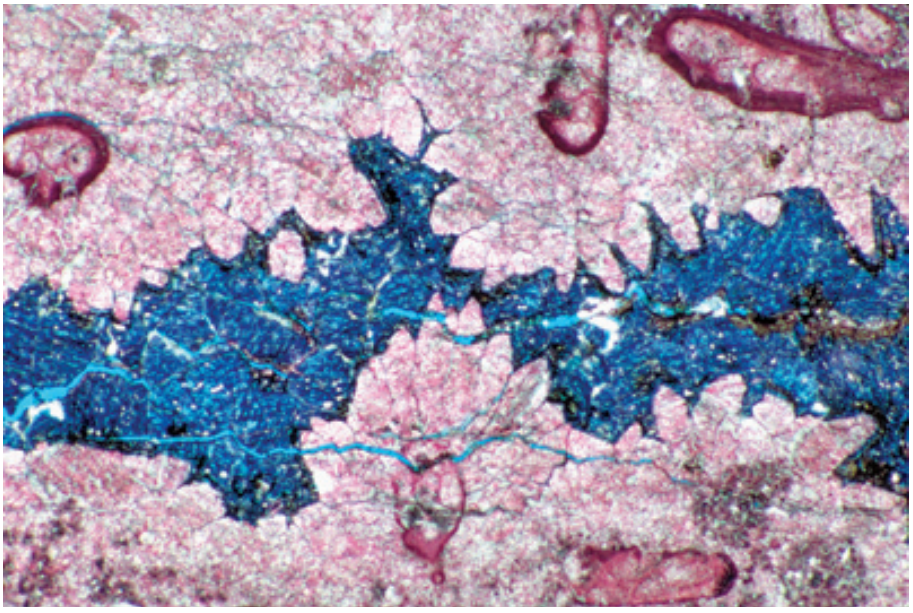

PPL, AFeS, BSE, HA = 4.0 mm

Up. Permian (Kazanian?) Wegener Halvø Fm., Jameson Land, East Greenland

Although most burial-stage cements are uniformly ferroan, reflecting the stability of most subsurface settings, that statement has numerous exceptions. Many burial cements, especially ones associated with highly permeable fracture or vug systems, show repeated geochemical fluctuations. This fracture, for example, is filled with successive bands of ferroan (blue stain) and non-ferroan (pink stain) calcite indicative of major fluctuations in redox conditions of pore fluids during precipitation. The final ferroan calcite cement contains hydrocarbon traces.

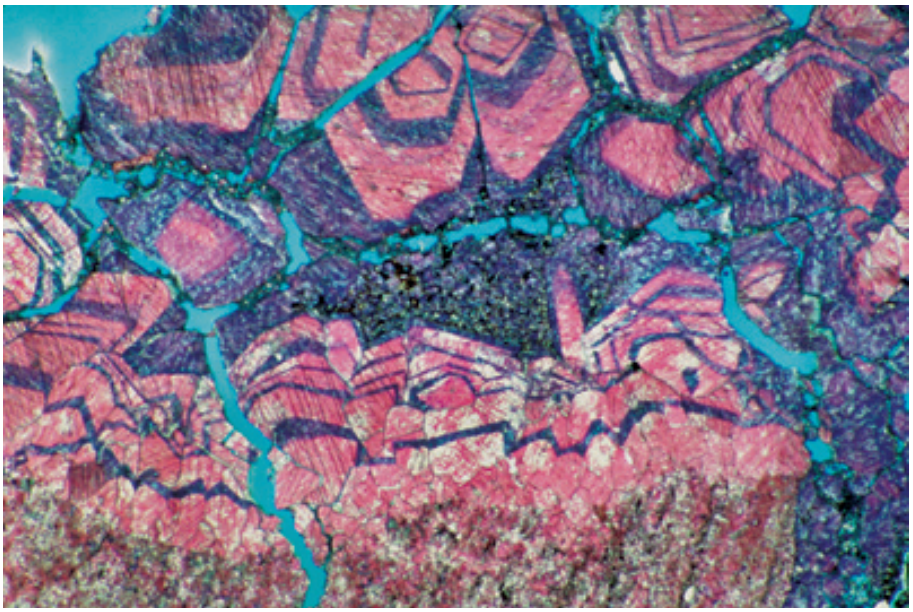

PPL, AFeS, BSE, HA = 4.5 mm

Up. Permian (Kazanian?) Wegener Halvø Fm., Jameson Land, East Greenland

Paragenetic relationships can help to decipher very complex diagenetic histories. This rock was extensively cemented by thick crusts of banded marine cements (probable alternating layers of aragonite and high-Mg calcite). Some layers were selectively leached and the void space was later filled with burial-stage ferroan calcite (stained blue). Finally, barite replacement (white crystals) occurred during hydrothermal alteration. Such petrographic observations are essential in charting temporal successions of diagenetic events including the creation and/or destruction of porosity.

PPL, AFeS, HA = 5.8 mm

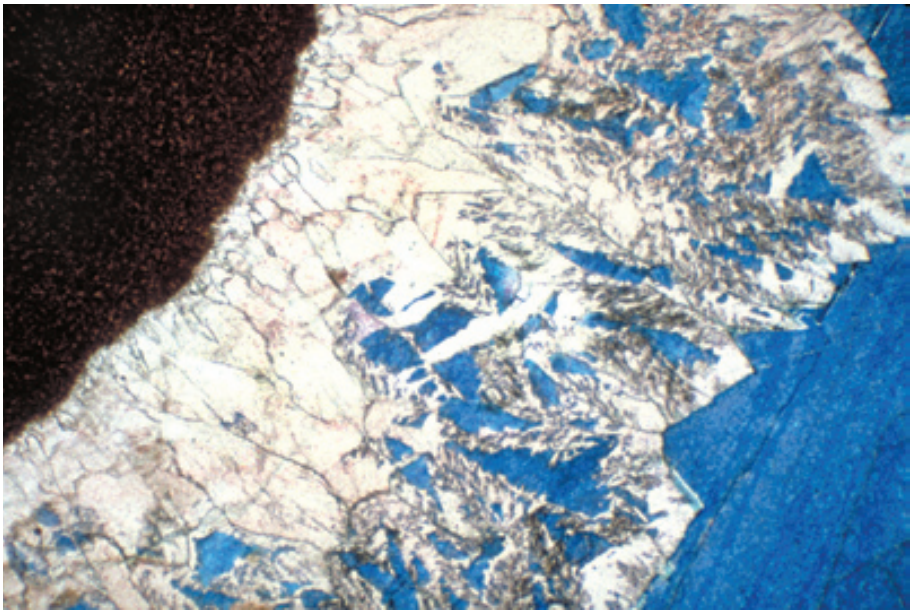

Up. Cretaceous (Turonian) Eagle Ford Shale, Dallas Co., Texas

Concretions are localized carbonate precipitates that commonly span the meteoric to early-burial diagenetic realms. Here, multiple generations of cement are visible in a septarian nodule. Early-stage non-ferroan calcite (white, unstained cement) formed skeletal crystals or crystals that were later corroded. The final stage of cement formed under reducing conditions and incorporated iron into the calcite lattice (blue stain). The ferroan calcite filled both the skeletal voids and other remaining pore space.

PPL, AFeS, HA = 5.1 mm

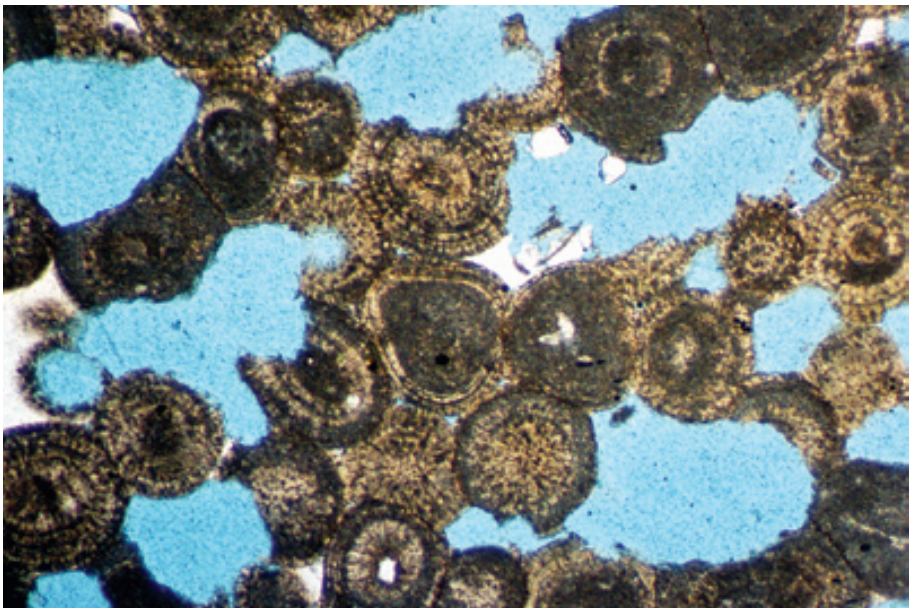

Up. Jurassic (Oxfordian) Up. Smackover Fm., subsurface, Arkansas

Burial-stage secondary porosity is well known in sandstones. The existence of late-stage dissolution and porosity development is more controversial in carbonate rocks, but more and more examples have come to light in recent years. This example shows vugs that cross-cut compacted ooids with interpenetrative contacts. Dissolution clearly postdates very substantial compaction and, therefore, is interpreted as burial-stage leaching, perhaps due to influx of hydrocarbon-associated acidic fluids. Photograph courtesy of Clyde H. Moore (see Moore and Druckman, 1981).

PPL, BSE, HA = ~3.0 mm

Lo. Cambrian Forteau Fm., southern Labrador, Canada

Cavity-filling calcite cements in a reef limestone with cathodoluminescent zoning showing a typical temporal succession of non-luminescence, bright luminescence, and dull luminescence. That succession reflects temporal geochemical changes allowing variations in incorporation of Mn^{2+} (a CL-exciting ion) and Fe^{2+} (a CL-quenching ion). Late-stage burial fluids generally are depleted in Mn and enriched in Fe, producing dull luminescence. CL, isotope geochemistry, and fluid inclusion geothermometry are essential adjuncts to petrography in understanding burial diagenesis. Photograph courtesy of Noel P. James.

CL, HA = 10 mm

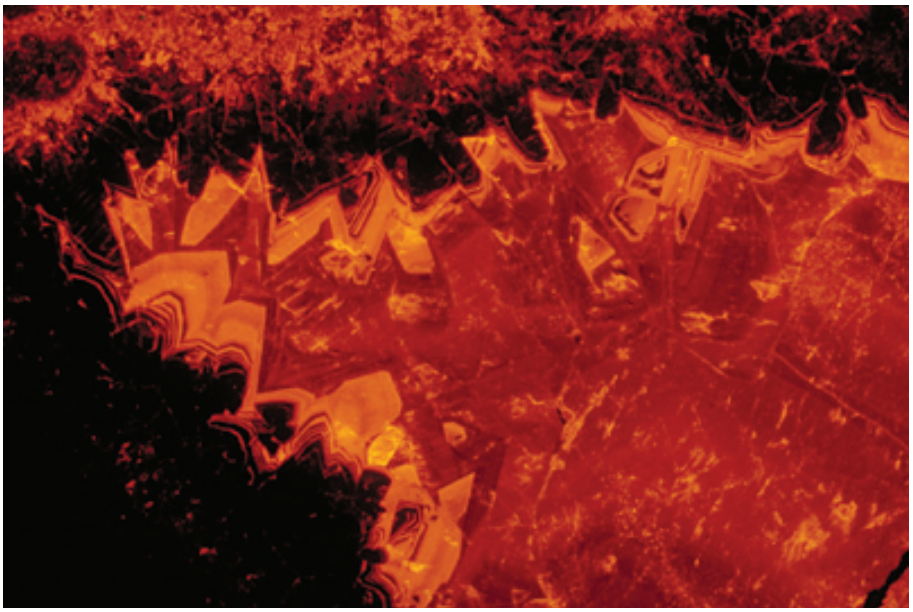

Up. Cretaceous chalk, 1,420 ft (433 m) depth, British North Sea

Burial diagenesis is of great importance in fine-grained carbonate rocks, but is much more difficult to document petrographically because of the small crystal sizes. This SEM image shows a typical shallowly buried chalk (ca. 430 m burial depth). Note the rounded grains, easily recognizable coccolith remains and lack of obvious cements (porosity is in excess of 35%). Compare with the next image.

SEM, HA = ~20 μm

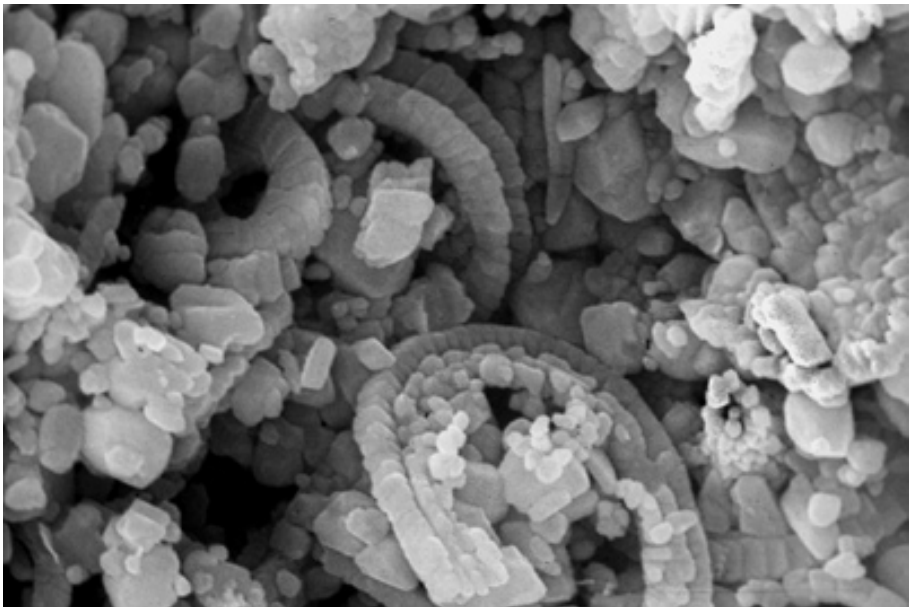

Up. Cretaceous chalk, 11,026 ft (3,361 m) depth, British North Sea

An SEM image showing a typical view of a deeply buried chalk (ca. 2,230 m). Note the extensive development of angular, largely interlocking, crystalline overgrowths on most matrix grains, although some remnants of coccoliths can still be seen. Porosity in this sample has been reduced to approximately 10%. Overburden pressure resulted in local dissolution, compaction and burial-stage precipitation, resulting in the fabric changes between the previous sample and this one. Overpressuring and early oil input can minimize such burial-related porosity changes (Scholle, 1977).

SEM, HA = ~10 μm

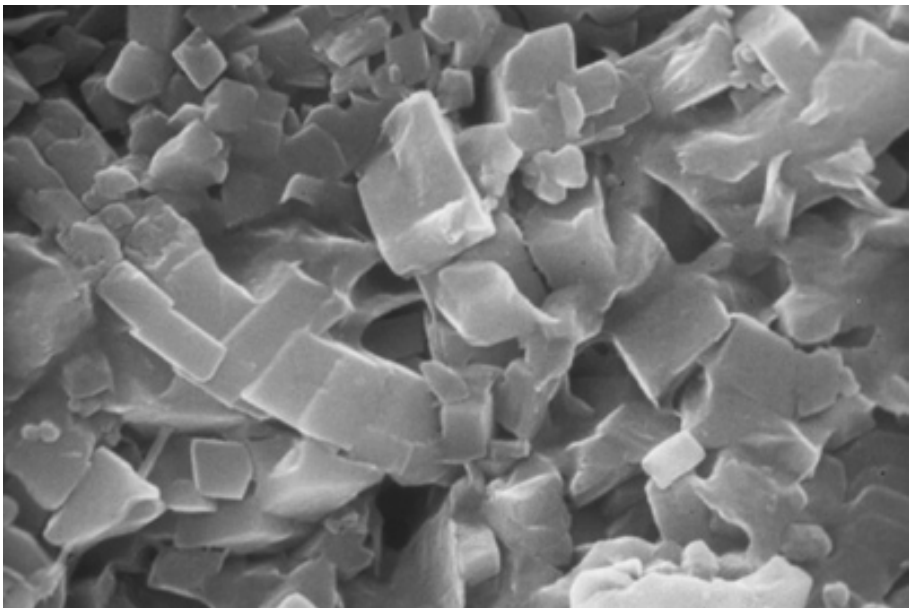

Cited References and Additional Information Sources

Bathurst, R. G. C., 1971, The enfacial junction, in O. P. Bricker, ed., Carbonate Cements: Studies in Geology No. 19: Baltimore, MD, The Johns Hopkins Press, p. 296.

Bathurst, R. G. C., 1975, Carbonate Sediments and their Diagenesis: New York, Elsevier Science Publ. Co., 658 p.

Bathurst, R. G. C., 1980, Deep crustal diagenesis in limestones: Revista del Instituto de Investigaciones Geologicas de la Diputación de Barcelona (Universidad de Barcelona), v. 34, p. 89-100.

Bathurst, R. G. C., 1995, Burial diagenesis of limestones under simple overburden. Stylolites, cementation and feedback: Bulletin de la Société géologique de France, v. 116, p. 181-192.

Buxton, T. M., and D. F. Sibley, 1981, Pressure solution features in a shallow buried limestone: Journal of Sedimentary Petrology, v. 51, p. 19-26.

Cercone, K. R., and K. C. Lohmann, 1987, Late burial diagenesis of Niagaran (Middle Silurian) pinnacle reefs in Michigan basin: AAPG Bulletin, v. 71, p. 156-166.

Choquette, P. W., and N. P. James, 1987, Diagenesis #12. Diagenesis in limestones - 3. The deep burial environment: Geoscience Canada, v. 14, p. 3-35.

Dickson, J. A. D., 1983, Graphical modeling of crystal aggregates and its relevance to cement diagnosis: Philosophical Transactions of the Royal Society of London, Series A, v. 309, p. 465-502.

Dickson, J. A. D., and M. L. Coleman, 1980, Changes in carbon and oxygen isotope composition during limestone diagenesis: Sedimentology, v. 27, p. 107-118.

Dorobek, S. L., 1987, Petrography, geochemistry, and origin of burial diagenetic fabrics, Siluro-Devonian Helderberg Group (carbonate rocks), central Appalachians: American Association of Petroleum Geologists Bulletin, v. 71, p. 492-514.

Druckman, Y., and C. H. Moore, Jr., 1985, Late subsurface secondary porosity in a Jurassic grainstone reservoir, Smackover Formation, Mt. Vernon field, southern Arkansas, *in* P. O. Roehl, and P. W. Choquette, eds., Carbonate petroleum reservoirs: New York, Springer-Verlag, p. 369-384.

Dunnington, H. V., 1967, Aspects of diagenesis and shape change in stylolitic limestone reservoirs, *in* Proceedings of the Seventh World Petroleum Congress (Mexico City, Mexico), v. 2: New York, Elsevier, p. 339-352.

Durney, D. W., 1976, Pressure-solution and crystallization deformation: Philosophical Transactions of the Royal Society of London, Series A, v. 282, p. 229-240.

Emery, D., and J. D. Marshall, 1989, Zoned calcite cements: has analysis outpaced interpretation?: Sedimentary Geology, v. 65, p. 205-210.

Frank, J. R., A. B. Carpenter, and T. W. Oglesby, 1982, Cathodoluminescence and composition of calcite cement in Taum Sauk Limestone (Upper Cambrian), southeast Missouri: Journal of Sedimentary Petrology, v. 52, p. 631-638.

Grover, G., Jr., and J. F. Read, 1983, Paleoaquifer and deep burial related cements defined by regional cathodoluminescent patterns, Middle Ordovician carbonates, Virginia: AAPG Bulletin, v. 67, p. 1275-1303.

Halley, R. B., 1987, Burial diagenesis of carbonate rocks: Colorado School of Mines Quarterly, v. 82, p. 1-15.

Kaufman, J., W. J. Meyers, and G. N. Hanson, 1990, Burial cementation in the Swan Hills Formation (Devonian), Rosevear field, Alberta, Canada: Journal of Sedimentary Petrology, v. 60, p. 918-939.

Klosterman, M. J., 1981, Applications of fluid inclusion techniques to burial diagenesis in carbonate rock sequences: Baton Rouge, LA, Louisiana State University, Applied Carbonate Research Program, Technical Series Contribution No. 7, 101 p.

Machel, H. G., 1990, Burial diagenesis, porosity and permeability development of carbonates, *in* G. R. Bloy, and M. G. Hadley, eds., The Development of Porosity in Carbonate Reservoirs: Calgary, Canadian Society of Petroleum Geologists Continuing Education Short Course Notes, p. 2.1-2.18.

Meyers, W. J., 1974, Carbonate cement stratigraphy of the Lake Valley Formation (Mississippian), Sacramento Mountains, New Mexico: Journal of Sedimentary Petrology, v. 44, p. 837-861.

Meyers, W. J., and B. E. Hill, 1983, Quantitative studies of compaction in Mississippian skeletal limestones, New Mexico: Journal of Sedimentary Petrology, v. 53, p. 231-242.

Moore, C. H., and Y. Druckman, 1981, Burial diagenesis and porosity evolution, Upper Jurassic Smackover, Arkansas and Louisiana: AAPG Bulletin, v. 65, p. 597-628.

Nelson, C. S., G. J. Harris, and H. R. Young, 1988, Burial-dominated cementation in non-tropical carbonates of the Oligocene Te Kuiti Group, New Zealand: Sedimentary Geology, v. 60, p. 233-250.

Oldershaw, A. E., and T. P. Scoffin, 1967, The source of ferroan and non-ferroan calcite cements in the Halkin and Wenlock Limestones: Geological Journal, v. 5, p. 309-320.

Park, W.-C., and E. H. Schot, 1968, Stylolitization in carbonate rocks, *in* G. Müller, and G. M. Friedman, eds., Recent Developments in Carbonate Sedimentology in Central Europe: New York, Springer-Verlag, p. 66-74.

Railsback, L. B., 1993, Lithologic controls on morphology of pressure-dissolution surfaces (stylolites and dissolution seams) in Paleozoic carbonate rocks from the mideastern United States: Journal of Sedimentary Petrology, v. 63, p. 513-522.

Schmoker, J. W., and R. B. Halley, 1982, Carbonate porosity versus depth: a predictable relation for south Florida: AAPG Bulletin, v. 66, p. 2561-2570.

Scholle, P. A., 1977, Chalk diagenesis and its relation to petroleum exploration: oil from chalks, a modern miracle?: AAPG Bulletin, v. 61, p. 982-1009.

Scholle, P. A., and R. B. Halley, 1985, Burial diagenesis: out of sight, out of mind!, *in* N. Schneidermann, and P. M. Harris, eds., Carbonate Cements: Tulsa, OK, SEPM Special Publication No. 36, p. 309-334.

Shinn, E. A., and D. M. Robbin, 1983, Mechanical and chemical compaction in fine-grained shallow-water limestones: Journal of Sedimentary Petrology, v. 53, p. 595-618.

Simonsen, J. M., and G. M. Friedman, 1992, Closely spaced twin lamellae in limestones as an indicator of deep-burial diagenesis: Carbonates and Evaporites, v. 7, p. 38-47.

Walkden, G. M., and J. R. Berry, 1984, Syntaxial overgrowths in muddy crinoidal limestones: cathodoluminescence sheds new light on an old problem: Sedimentology, v. 31, p. 251-267.

Walls, R. A., E. W. Mountjoy, and P. Fritz, 1979, Isotopic composition and diagenetic history of carbonate cements in Devonian Golden Spike reef, Alberta, Canada: Geological Society of America Bulletin, v. 90, p. 963-982.

Wanless, H. R., 1983, Burial diagenesis in limestones, *in* A. Parker, and B. W. Sellwood, eds., Sediment Diagenesis: NATO Advanced Studies Institute, Series C, v. 115: Dordrecht (Netherlands), J. Reidel and Co., p. 379-417.

Weyl, P. K., 1959, Pressure solution and the force of crystallization — a phenomenological theory: Journal of Geophysical Research, v. 64, p. 2001-2025.

Wong, P. K., and A. Oldershaw, 1981, Burial cementation in the Devonian Kaybob reef complex, Alberta, Canada: Journal of Sedimentary Petrology, v. 51, p. 507-520.

Woronick, R. E., and L. S. Land, 1985, Late burial diagenesis, Lower Cretaceous Pearsall and lower Glen Rose Formations, south Texas, *in* N. Schneidermann, and P. M. Harris, eds., Carbonate Cements: Tulsa, OK, SEPM Special Publication No. 36, p. 265-275.

Facing Page: Top: Dolomitic supratidal crusts eroded and redeposited in imbricate fashion along the edge of a nearly abandoned tidal channel on Andros Island (Bahamas). Photograph courtesy of E. A. Shinn.

Bottom: Dolomite crystals (blue) replacing matrix in a trilobite-rich limestone. Simpson Gp., Murray Co., Oklahoma. PPL, AFeS, HA = 0.45 mm.

CARBONATE DIAGENESIS

DOLOMITE AND SIDERITE

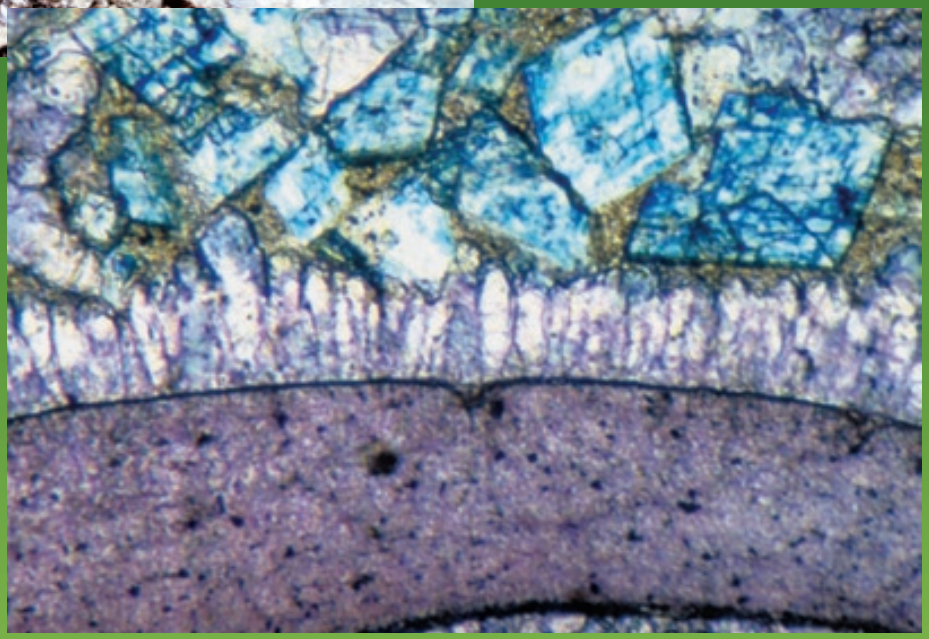

CHAPTER 26

DOLOMITE AND SIDERITE

Introduction:

Dolomite is a rhombohedral mineral, $CaMg(CO_3)_2$; dolostone is the appropriate term for a rock composed of that mineral. Dolomite is best identified through staining, and by its rhombic, often zoned, untwinned habit.

Dolomite is a complex and relatively poorly understood mineral. Thermodynamically, dolomite should be a stable, widespread precipitate from seawater, but kinetic factors (hydration of Mg^{2+} ions in seawater, the high ionic strength of seawater, the relative efficiency of aragonite and high-Mg calcite precipitation, inhibition effects of SO_4^{2-} ions) mitigate against its formation. Modern dolomite therefore is relatively scarce. In addition, ordered dolomite is slow-growing, and thus is difficult to synthesize in the laboratory under earth-surface conditions.

True dolomite (stoichiometric, ordered dolomite; top diagram, facing page) is well ordered, with one cation layer entirely composed of Mg^{2+} and the next entirely composed of Ca^{2+}. If perfectly formed, that also ensures a 50:50 (stoichiometric) balance between Ca^{2+} and Mg^{2+} in the dolomite structure. Most modern dolomites, however, are poorly ordered and Ca-rich (termed "protodolomite" by some workers). Those crystals are relatively unstable and "ripen" or eventually neomorphose to more stable, ordered dolomite crystals.

Many models have been proposed for dolomitization (see excellent summaries in Morrow, 1982b; Land, 1985; Tucker, 1990; and Purser et al., 1994). All center around three basic factors: a source of Mg (generally seawater), a way to move large volumes of that water through the sediment package, and a way to reduce the kinetic inhibitions to dolomite precipitation. Sabkha and brine reflux models call upon evaporative concentration of seawater (with removal of sulfate through bacterial reduction or inorganic sulfate precipitation); marine-fresh water mixing zone and Coorong models rely on dilution of seawater; the burial model uses elevated temperatures, modified pore water compositions, and, in some cases, thermochemical sulfate reduction to reduce inhibitions on dolomite precipitation. Organogenic dolomitization relies on intense bacterial sulfate reduction and methanogenesis in organic-rich sediments in a wide range of settings (Mazzullo, 2000).

Modern dolomite has been found in small volumes in many settings, ranging from hypersaline sabkhas to normal salinity tidal flats, and subsaline lagoonal environments. Modern dolomite is predominantly a replacement product; subsurface dolomites are found as either replacements or as primary pore-filling precipitates. Some authors have speculated that dolomites of other ages (especially the Precambrian) were primary precipitates, but that hypothesis has not been confirmed.

Given one mechanism or another, dolomite can form at virtually any stage of diagenesis. Synsedimentary dolomite forms as replacement of high-Mg calcite or aragonite in hypersaline sabkha sediments and also in other tidal flat deposits; mixing zone dolomite cementation and replacement affect somewhat older sediments in marine-meteoric phreatic mixing zones; and burial dolomitization affects carbonate deposits of any age in the intermediate to deep subsurface. Dolomite, like other carbonate minerals, may exhibit secular variations in abundance, with enhanced dolomite formation "during times of global transgression, elevated atmospheric pCO_2, and lower calcite saturation state in shallow marine settings" (Given and Wilkinson, 1987, p. 1068).

Dissolution and/or calcitization of dolomite (sometimes termed "dedolomitization") is a common phenomenon, especially where gypsum or anhydrite are undergoing dissolution (thereby greatly increasing the Ca/Mg ratios and sulfate concentrations in pore fluids).

Siderite was once thought to form mainly from brackish to non-marine pore fluids. More recent work has shown that siderite can form in fully marine strata during early burial diagenesis from marine pore fluids in association with in-situ decomposition of organic matter (Carpenter et al., 1988; Mozley and Burns, 1993).

Major diagenetic fabrics:

Dolomite fabrics were classified by Sibley and Gregg (1987) as planar (idiotopic) and non-planar (xenotopic) based on the nature of crystal boundaries (middle diagram, facing page). Sibley and Gregg (1987) also divide replacement fabrics by crystal size distributions into unimodal and polymodal, and by degree of preservation of precursor fabrics into mimic (fabric-preserving) and nonmimic (fabric destroying) varieties.

As a general rule, crystal sizes in dolomites are a function of the number of nucleation sites and the rates of crystal growth. Generally, fine-grained precursor sediments offer many potential nucleation sites and thus tend to be replaced by more finely crystalline dolomite, and show better fabric preservation than, coarse-grained sediments. On the basis of crystal growth rates, early-formed dolomites tend to be more finely crystalline than burial-stage dolomites. Dolomites with unimodal size distributions generally represent a single phase of formation with uniformly available nucleation sites. Planar fabrics are favored at lower precipitation temperatures; non-planar (xenotopic) fabrics are favored above a "critical roughening temperature",

suggested to be above 50-100°C (Gregg and Sibley, 1984).

Aragonite and high-Mg calcite are far more susceptible to dolomitization than low-Mg calcite. This can lead to partial dolomitization followed by leaching of undolomitized remnants (forming dolomoldic porosity). Dolomitized high-Mg calcite shells/tests typically are well preserved; aragonitic ones are less well preserved.

Many replacement dolomites have cloudy cores (initial growth phases rich in undigested host-rock mineral inclusions or early, metastable precipitates) and clear exteriors (compare Sibley, 1982; Kyser et al., 2002).

Mixing zone dolomites range from microcrystalline replacements to limpid, zoned replacements and cements. True dolomite cements often are hard to distinguish from dolomitized precursor calcite cements, except through examination using CL.

Baroque or saddle dolomites are readily recognizable because they have curved crystal faces, a cloudy appearance (due to abundant fluid and mineral inclusions), and undulose extinction. They commonly are Ca- and Fe-rich, and most reflect formation at elevated temperatures (~60-150°C) from hydrothermal or hydrocarbon-associated burial fluids of high ionic strength. Paragenetic relations, coupled with isotopic geochemistry, and fluid-inclusion geothermometry, are the best methods for recognizing non-baroque burial stage dolomites.

Calcitized dolomites are best recognized through staining. In the absence of staining, the presence of rhombic crystal outlines filled with multiple anhedral crystals can be a clue to recognition.

The primary characteristics for the recognition of siderite crystals are flattened rhombs (lozenge or American football-shaped crystals) that may have a reddish (ferruginous) alteration stain.

Crystal models three Mg-bearing carbonate minerals

A comparison of the crystal structures of high-Mg calcite, calcian dolomite and stoichiometric dolomite. Naturally occurring calcites have from 0 to about 32 mol% Mg substitution for Ca on a random basis within the calcite lattice. At the other end of the spectrum, well-ordered, stoichiometric dolomite has a 50:50 Ca to Mg ratio, with near perfect ordering of the Mg and Ca in alternate cation layers. Calcian, poorly-ordered dolomite has roughly 55-60 mol% Ca in the lattice with incomplete segregation of Ca and Mg into separate layers. Disordered, calcian dolomites are neomorphosed during diagenesis to the more stable near-stoichiometric, ordered dolomites.

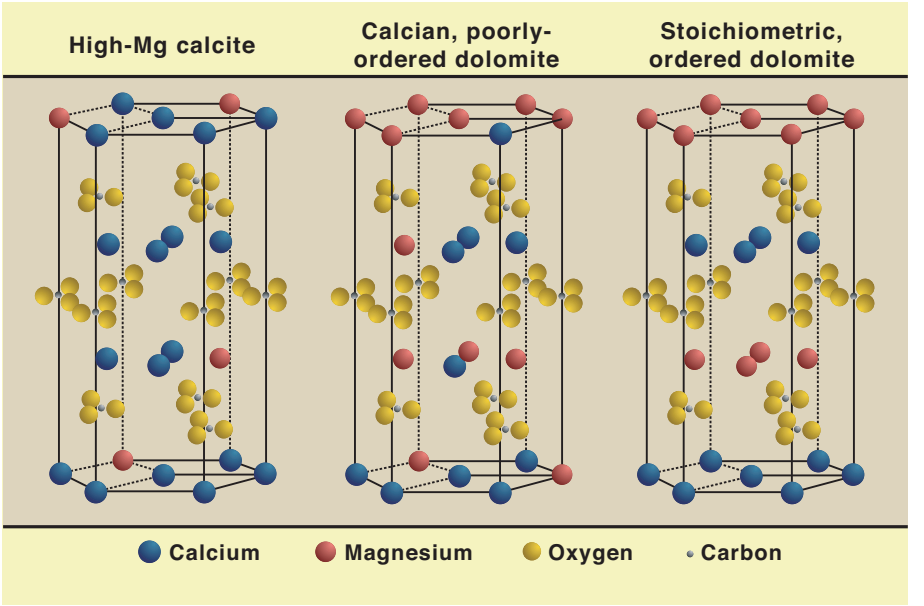

Classification of dolomite crystal fabrics

Illustrations of the three main textural fabrics of dolomites, as defined by Sibley and Gregg (1987). Fabrics with irregular, nonlinear, crystal boundaries between anhedral crystals are termed "nonplanar". Fabrics showing planar crystal boundaries with subhedral or euhedral crystal outlines are termed "planar-s" and "planar-e" respectively. Those terms can be supplemented with descriptors for degree of primary fabric retention (mimic or nonmimic; alternatively, mimetic or nonmimetic), crystal size (see Folk's authigenic constituent terminology in the section on limestone classification), and crystal size variability (unimodal or polymodal).

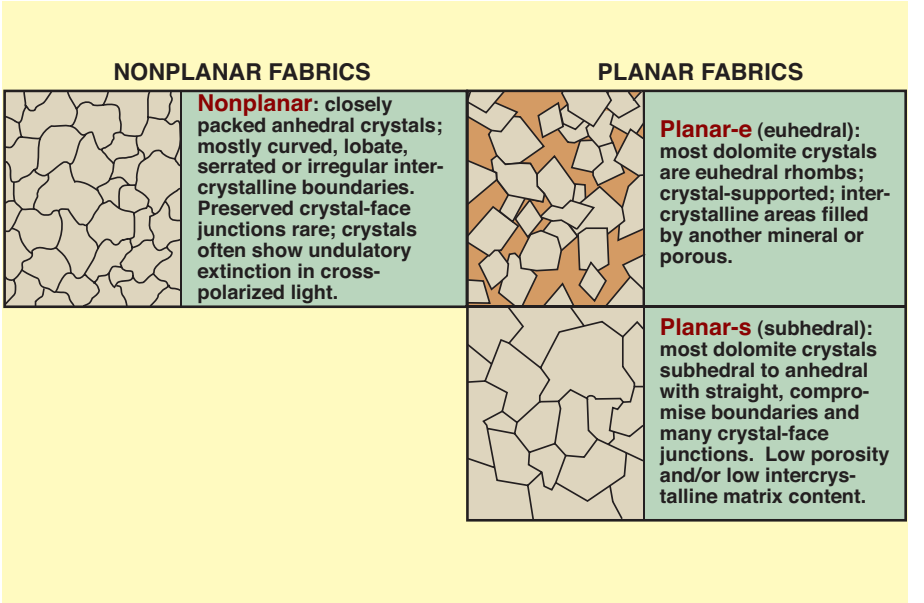

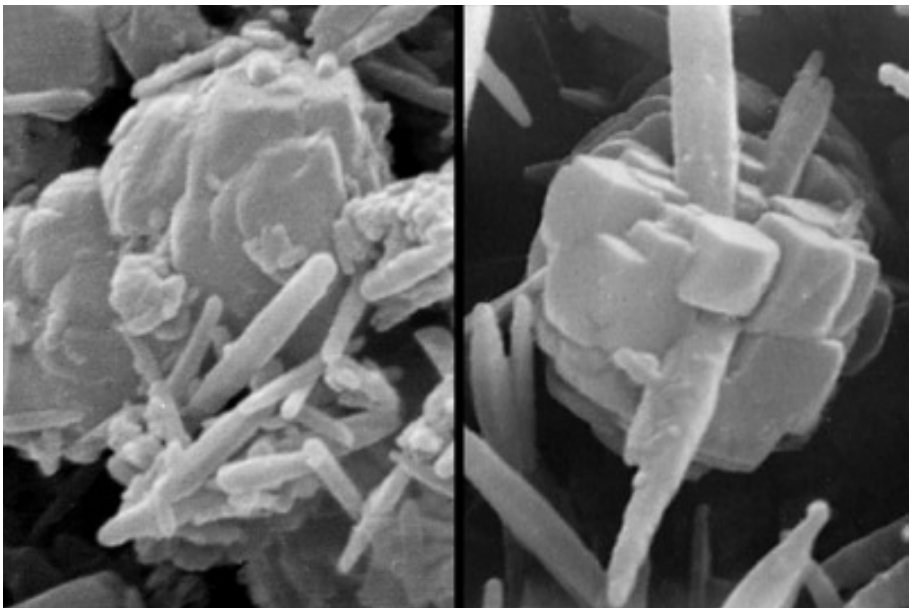

Holocene sediment, Abu Dhabi sabkha, United Arab Emirates

SEM images of partially dolomitized aragonitic carbonate mud from a pit dug beneath the sabkha one kilometer inland from the lagoonal shoreline. The dolomite crystals grow around, and perhaps partially replace, aragonite needles in pore space within a crust buried beneath the sabkha. Dolomite formation here occurred in warm (30-40°C), highly saline pore fluids with elevated Mg/Ca ratios (as a result of prior calcium sulfate precipitation). Bacterial sulfate reduction in organic-rich layers may also aid dolomitization. Photographs courtesy of Judith A. McKenzie (McKenzie, 1981).

SEM, L: HA = ~4.2 μm; R: HA= ~3.4 μm

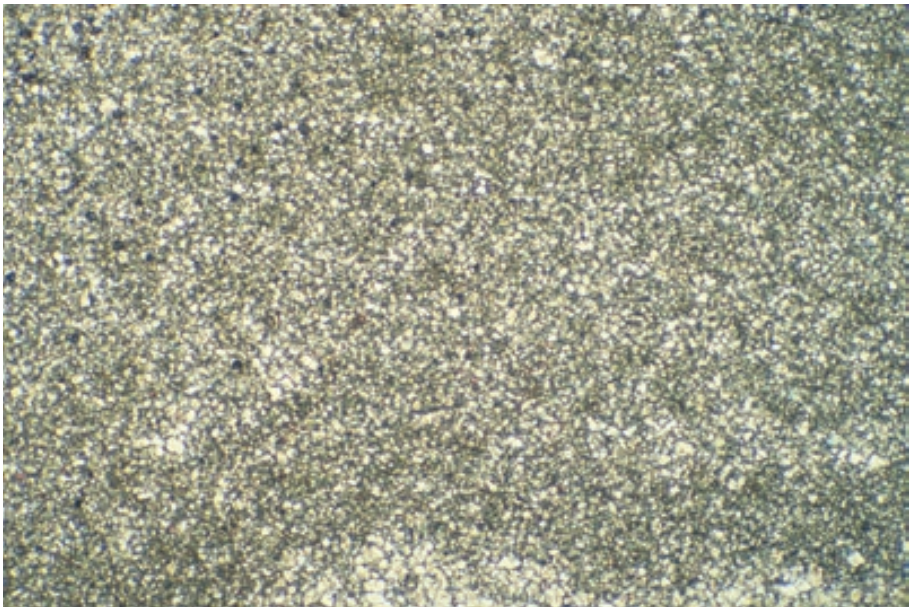

Lo. Ordovician St. George Gp., western Newfoundland, Canada

An ancient example of very finely crystalline dolomite from an interpreted peritidal deposit. This may represent penecontemporaneous sabkha-type dolomite formation, similar to that shown in the modern example above. Photograph courtesy of Noel P. James.

PPL, HA = 4.4 mm

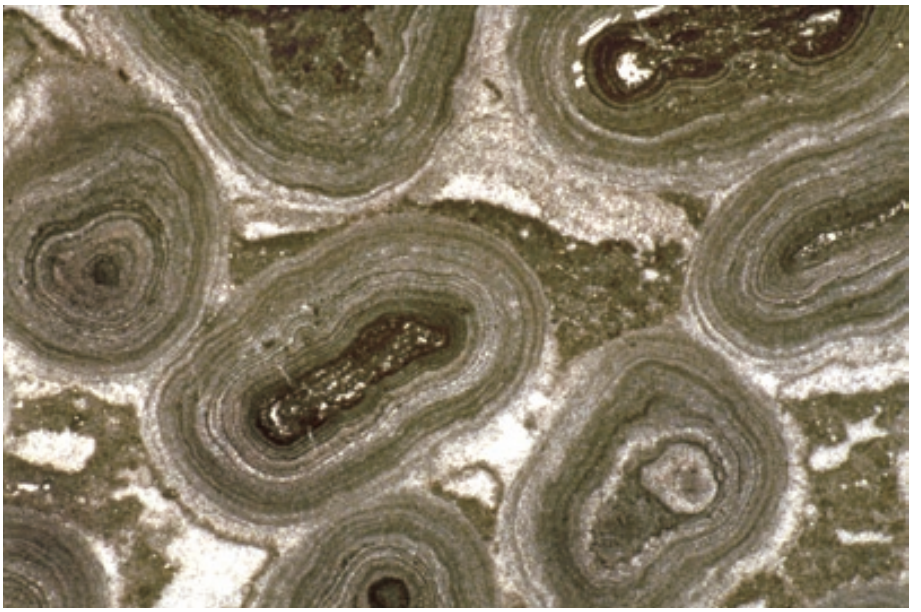

Up. Permian (Guadalupian) Tansill Fm., Eddy Co., New Mexico

These pisoids have been interpreted by various authors as the product of algal growth, coastal caliche formation, seepage spring deposits, wave agitation in a coastal setting, and other causes. Whatever their specific origin, they were formed adjacent to a broad hypersaline lagoon and were penecontemporaneously dolomitized. The aphanocrystalline dolomite has preserved remarkable detail in the pisoids as well as in their early marine cements and internal sediment fabrics. Indeed, in the absence of staining or geochemical data, it would be very difficult to recognize the complete dolomite replacement.

PPL, HA = 10 mm

Miocene dolomite, Abu Shaar, Red Sea area, Egypt

Another example of remarkable mimetic (fabric-preserving) replacement by early dolomite. These periplatform slope deposits were extensively cemented by fibrous precipitates, probably of submarine origin. However, both sediment and cement were subsequently totally dolomitized. The key to mimetic (or mimic) replacement is growth of crystals from numerous nucleation sites. Growth then can occur in optical alignment with former fabrics. Incorporation of inclusions of precursor material also helps to enhance fabric retention. Photograph courtesy of Bruce H. Purser.

PPL, HA = ~2.0 mm

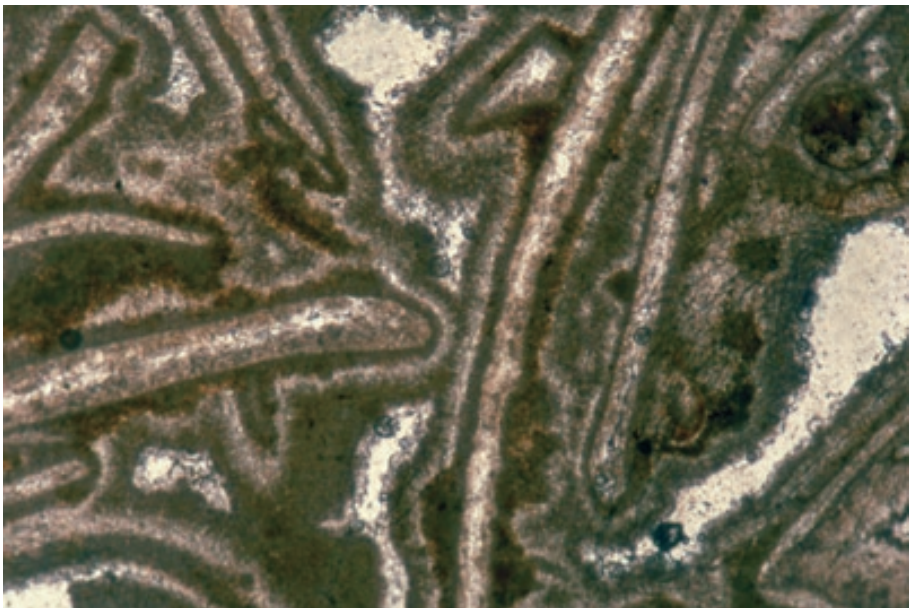

Up. Permian (Guadalupian) Capitan Fm., Culberson Co., Texas

This block of reef-derived material in upper fore-reef talus shows selective replacement of originally micritic clasts by medium crystalline dolomite. The abundant marine cements (generally stained pink) were not dolomitized. Dolomitizing fluids were derived from shelfward and overlying evaporitic settings (Guadalupian or Ochoan in age). Mesosaline (and locally perhaps hypersaline) refluxing fluids flowed through syndepositional fractures in the reef and dispersed through the more permeable units in the fore-reef slope, selectively dolomitizing isolated constituents in their path (Melim and Scholle, 2002).

PPL, AS, HA = 3.0 mm

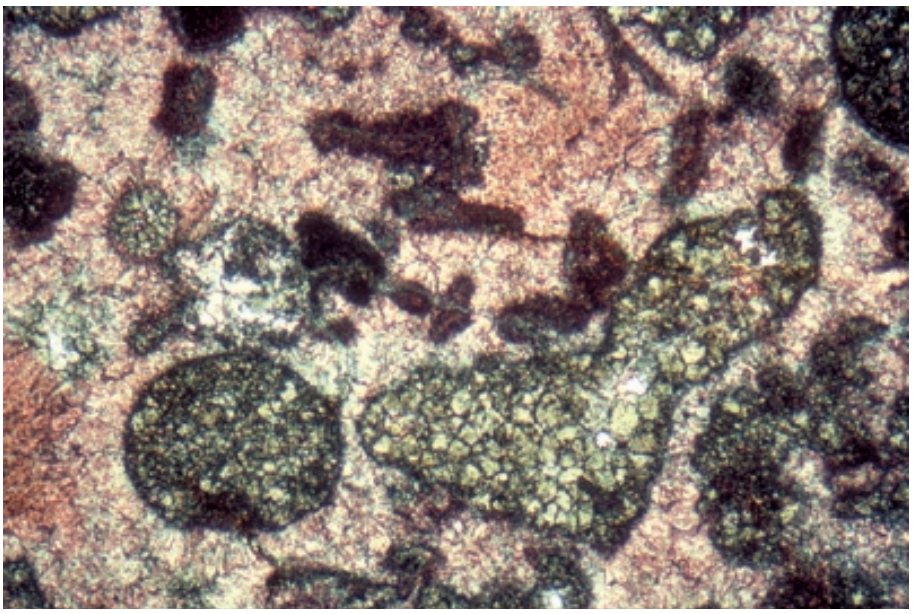

Up. Permian (Guadalupian) Capitan Fm., Culberson Co., Texas

Three generations of cement are visible in this reefal biolithite (boundstone). Cloudy, isopachous crusts of penecontemporaneous marine cement (dark pink) are postdated by a thin rind of dolomite formed by the same refluxing brines noted in the previous example. The dolomite (clear to pale blue) may locally replace earlier cements, but clearly also forms new cement crystals. The dolomite is postdated by coarse, blocky, non-ferroan calcite spar (bright pink), which itself may be a replacement of pore-filling anhydrite and gypsum cements, further evidence of saline pore fluid influx.

PPL, AFeS, BSE, HA = 1.6 mm

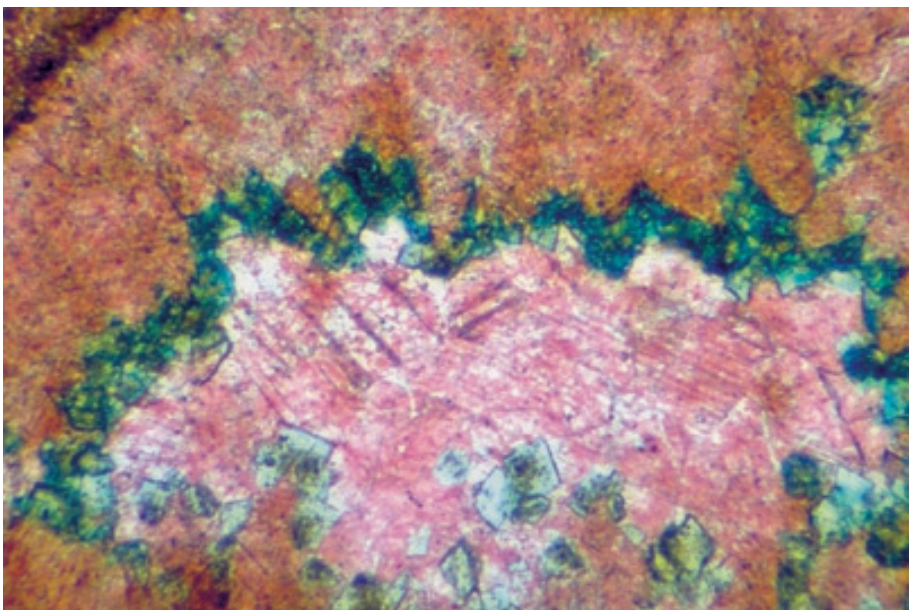

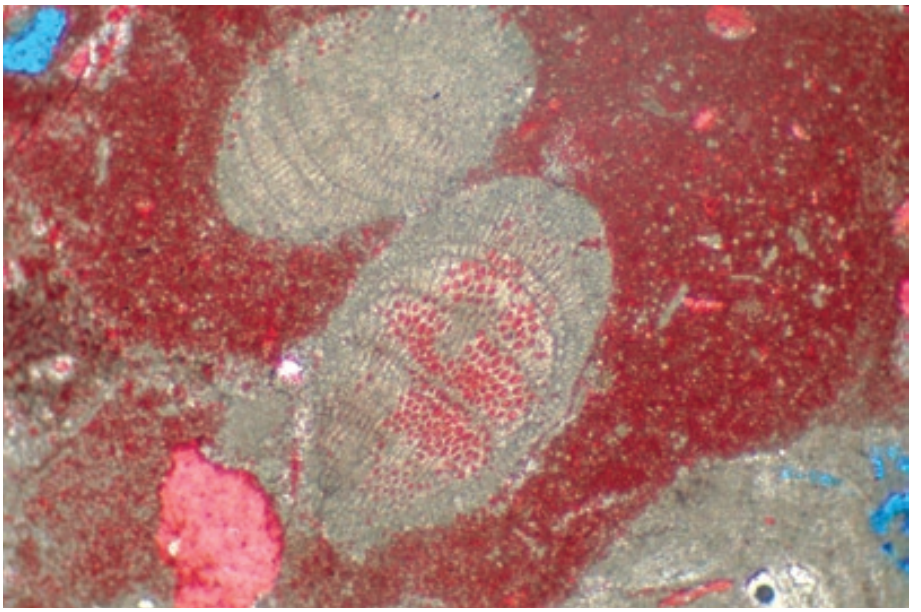

Pleistocene Coral Rock Fm., corehole, Bottom Bay, Barbados

An example of inferred marine-meteoric mixing zone replacement dolomitization (originally termed "Dorag" dolomitization) in Pleistocene fore-reef wackestones. Calcite here is stained red and dolomite is unstained. High-Mg calcite allochems, such as these red algae, tend to be the first components dolomitized and are the ones that most commonly retain primary fabrics. Note also the partial dolomitization of micritic matrix. Photograph courtesy of John D. Humphrey.

PPL, AS, BSE, HA = 1.2 mm

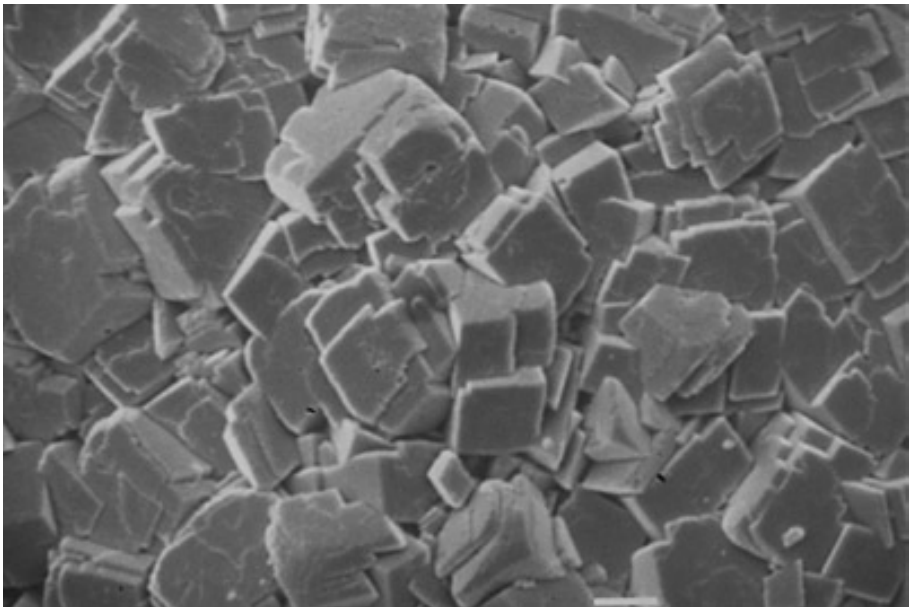

Holocene sediment, Ambergris Cay, Belize

An SEM image of early-stage dolomite that has mimetically replaced high-Mg calcite in a foraminiferal wall. The very finely crystalline nature of the replacement, with a multitude of nucleation sites and competing small crystals, allows preservation of primary high-Mg calcite fabrics with great fidelity. Photograph courtesy of Jay M. Gregg.

SEM, HA = 13.5 μm

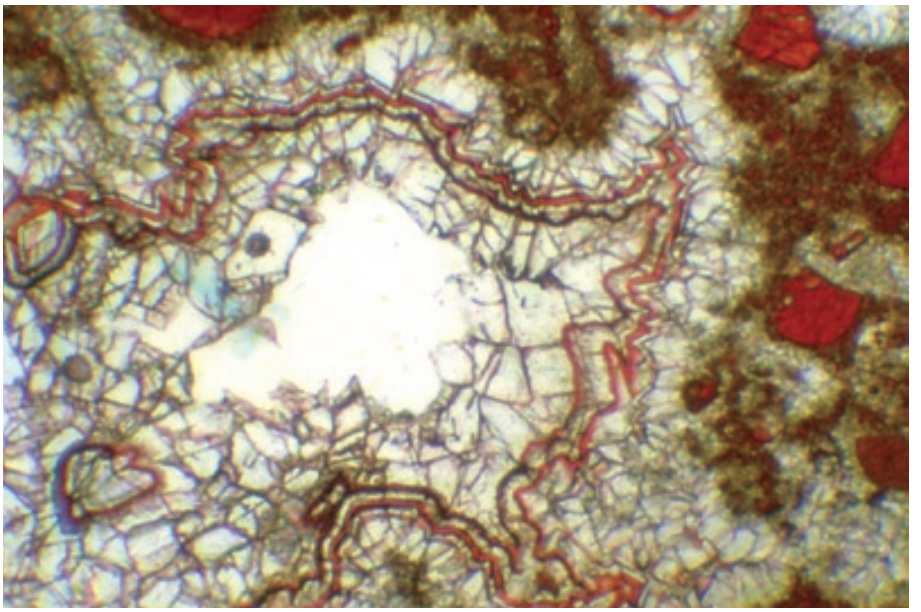

Pleistocene Coral Rock Fm. Golden Grove, Barbados

An example of mixing zone dolomite cements in a Pleistocene wackestone. Calcite is stained red and dolomite remains unstained. Note the limpid (very clear, nearly inclusion-free) character of the cements and the thin, interlayered bands of low-Mg calcite cements growing in continuity with the dolomite. Clear pore space remains at the center of the pore. Photograph courtesy of John D. Humphrey.

PPL, AS, HA = 1.2 mm

Permian (Leonardian-Guadalupian) Park City Fm., Up. Ervay Mbr., Daggett Co., Utah

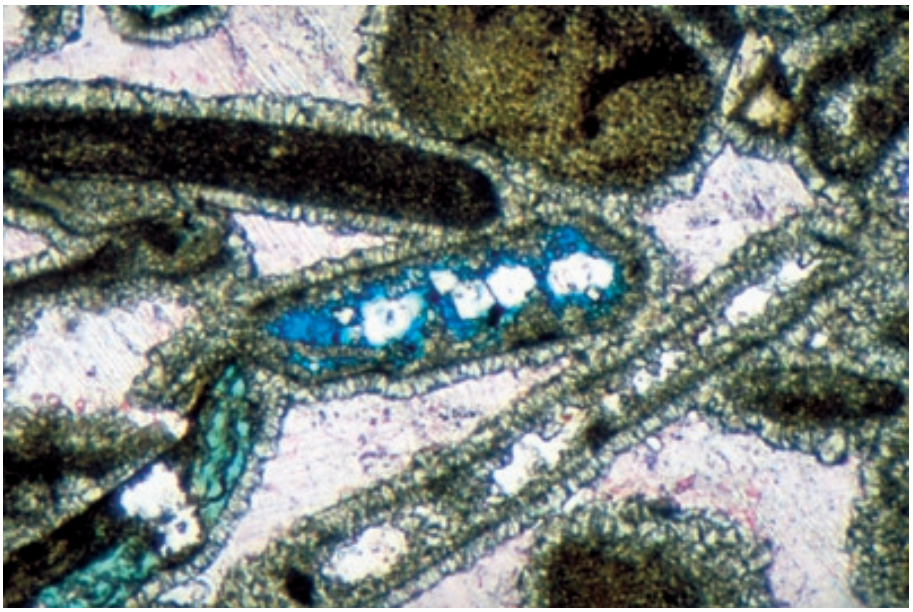

This example shows dolomite cement rims on detrital grains. The dolomite is postdated by coarse, sparry calcite cement (marked by a slight pink stain). Although the dolomite clearly occupies the position of a cement, primary dolomite cement can be very difficult to distinguish from dolomite formed by replacement of a precursor calcium carbonate cement. The bladed character of these dolomite "cements" should raise concerns for the petrographer that this may well represent replacement of precursor marine or vadose phreatic calcite cements.

PPL, AFeS, BSE, HA = 1.6 mm

Mid. Silurian (Wenlockian) Springfield Fm., Green Co., Ohio

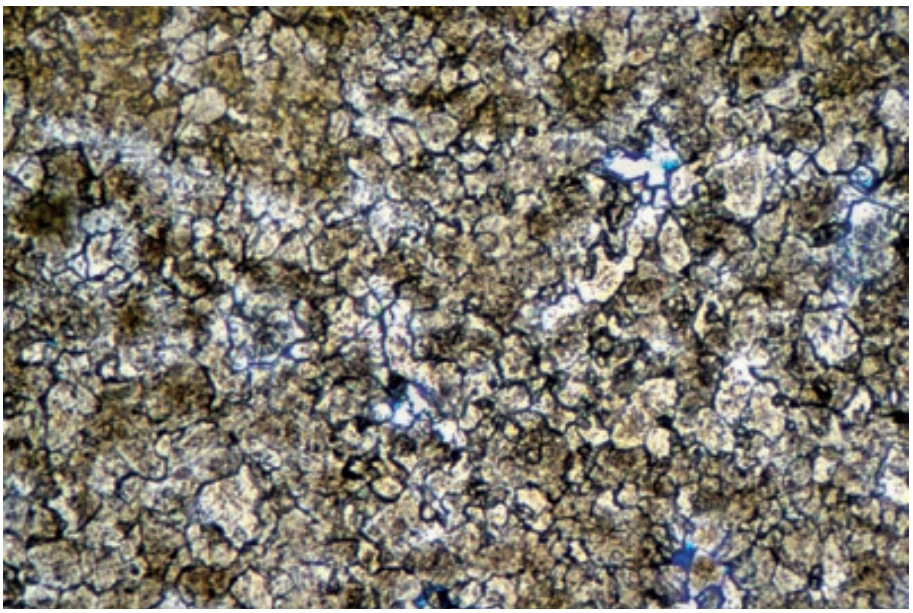

At the opposite end of the spectrum from the high-fidelity replacement shown to this point are rocks with nonmimic (nonmimetic) replacement fabrics. Here anhedral, largely nonplanar dolomite has replaced a probable skeletal limestone. Ghosts of original grains and matrix can still be seen but are almost impossible to identify. Several techniques including "white card" microscopy and cathodoluminescence can be used to accentuate what little fabric is preserved (see techniques section).

PPL, AFeS, BSE, HA = 1.6 mm

Lo. Ordovician Stonehenge Ls., Centre Co., Pennsylvania

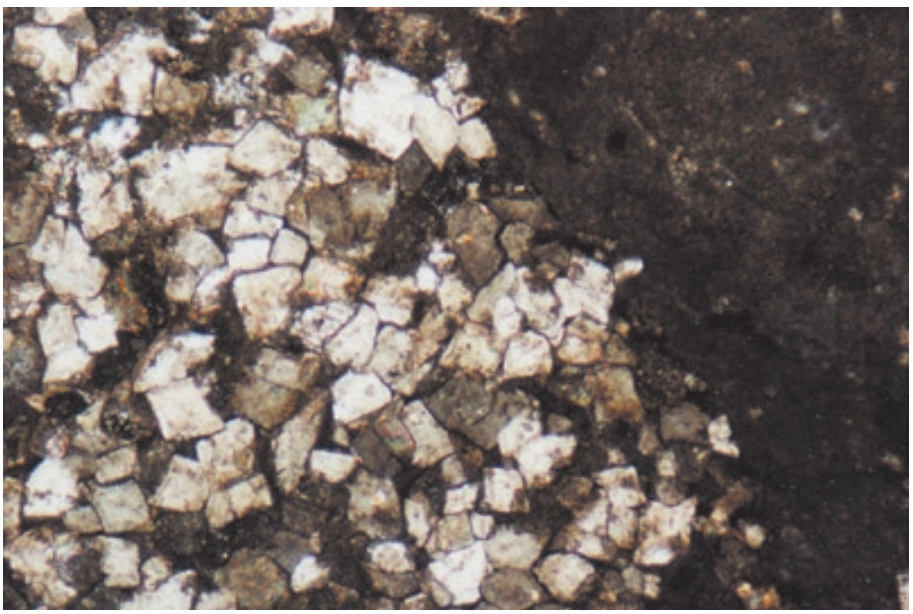

Coarse replacement dolomite in an intramicrite. Large areas of matrix and some grains were preferentially replaced with little or no fabric preservation. Other clasts, such as the intraclast on the right side, however, were apparently less susceptible to dolomitization. The dolomite crystals are subhedral to euhedral, with planar boundaries; therefore, the rock would be classed as nonmimic planar-s to planar-e in the Sibley and Gregg (1987) classification.

XPL, HA = 3.4 mm

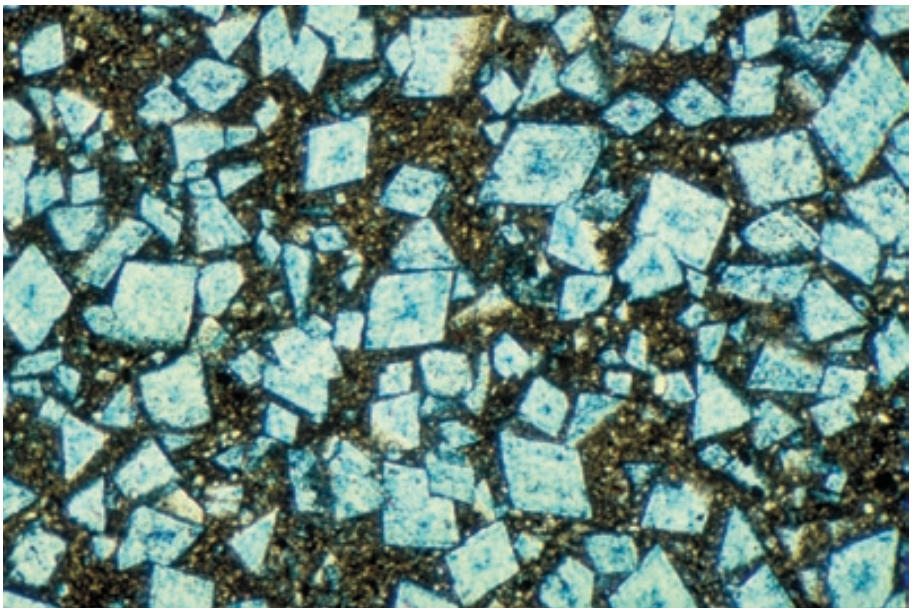

Up. Cambrian Riley Fm., Lion Mountain Ss. Mbr., Burnet Co., Texas

An example of euhedral, ferroan dolomite replacement of a limestone. Note the consistently more ferroan cores (darker stain) and less ferroan rims. There is extensive solid solution along the line from pure dolomite to ferrodolomite (see ternary diagram in the introduction section of this book). Ferroan dolomites and ankerite thus are common precipitates. In this example, the crystals are planar and euhedral. They either grew displacively in carbonate mud or grew in a nonmimic fashion because no precursor structure is visible within the crystals.

PPL, AFeS, HA = 2.4 mm

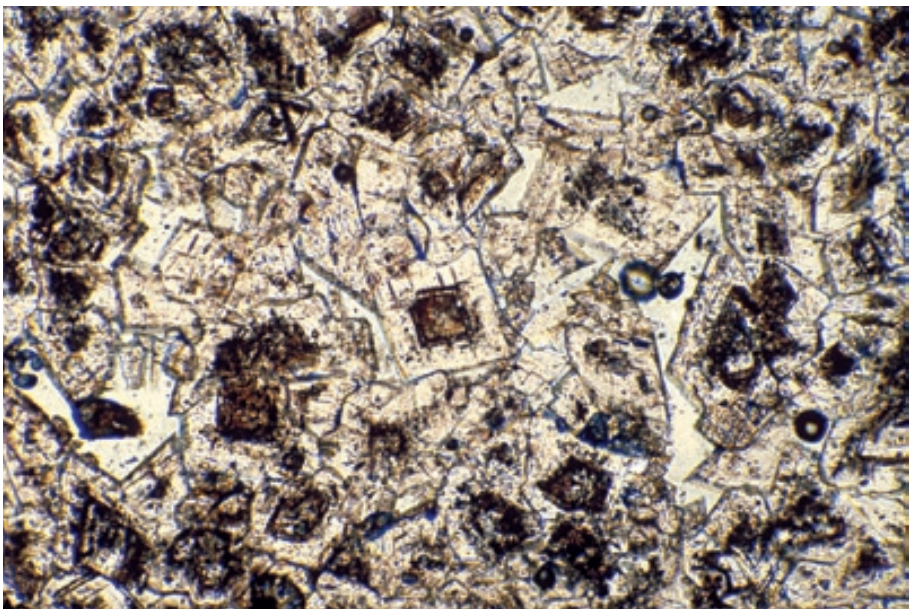

Oligocene Gambier Fm., coastal South Australia

An example of largely euhedral dolomite where the crystals have dark cores and limpid rims. This is an extremely common fabric in dolomites. The cloudy cores have been interpreted to reflect mixing zone conditions in which metastable, inclusion-rich dolomite formed. A shift to more marine conditions led to precipitation of the more inclusion-free, limpid dolomite outer zones that may, in part, be cements (Kyser et al., 2002). The rhombic outlines, zoning, and lack of twinning seen here are characteristics that allow recognition of most dolomites, even without staining. Photograph courtesy of Noel P. James.

PPL, HA = 1.0 mm

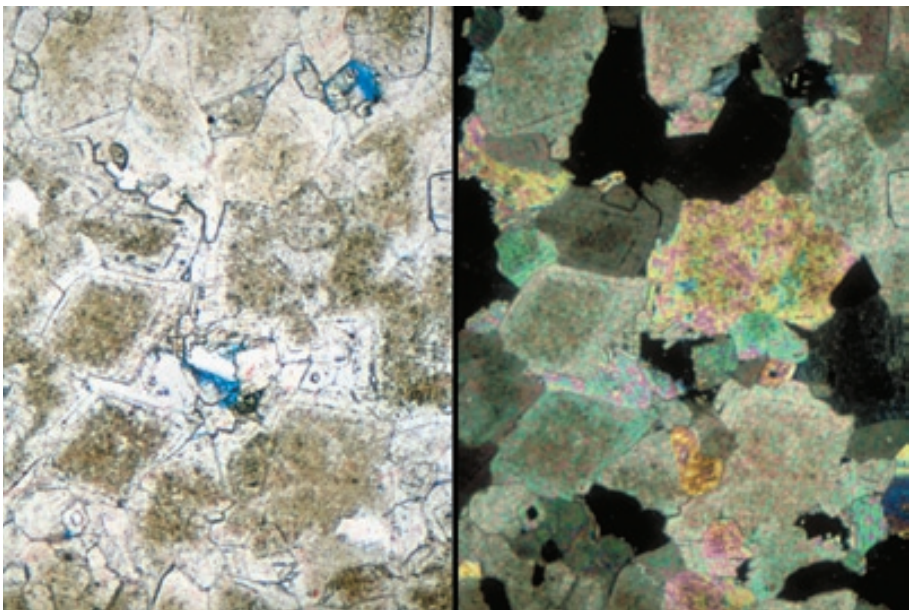

Lo. Cretaceous dolostone, Cephalonia, Ionian Islands, Greece

Another example of coarsely crystalline, subhedral, zoned, nonferroan replacement dolomite. Note the cloudy cores, clear rims or cement overgrowths (a common feature in replacement dolomites), and complete obliteration of primary fabrics. The cross-polarized illumination shows how the final stages of dolomite crystal growth have irregular shapes as they grow into the available intercrystalline pore space.

PPL/XPL, AFeS, BSE, HA = 1.2 mm each

Lo. Ordovician St. George Gp., western Newfoundland, Canada

Compositional and/or inclusion zoning is present in most dolomites. Sometimes, as in the previous example, it is readily visible because of variations in inclusion content. In other examples, such as this euhedral to subhedral dolomite, zoning is not readily visible because it consists mainly of slight elemental variations. In such cases, staining, cathodoluminescence, backscattered electron imaging or other techniques can be used to accentuate zonation. This pair of photographs demonstrates the contrast between normal illumination and cathodoluminescence. Photograph courtesy of Noel P. James; taken by D. Haywick.

PPL/CL, HA = 0.75 mm each

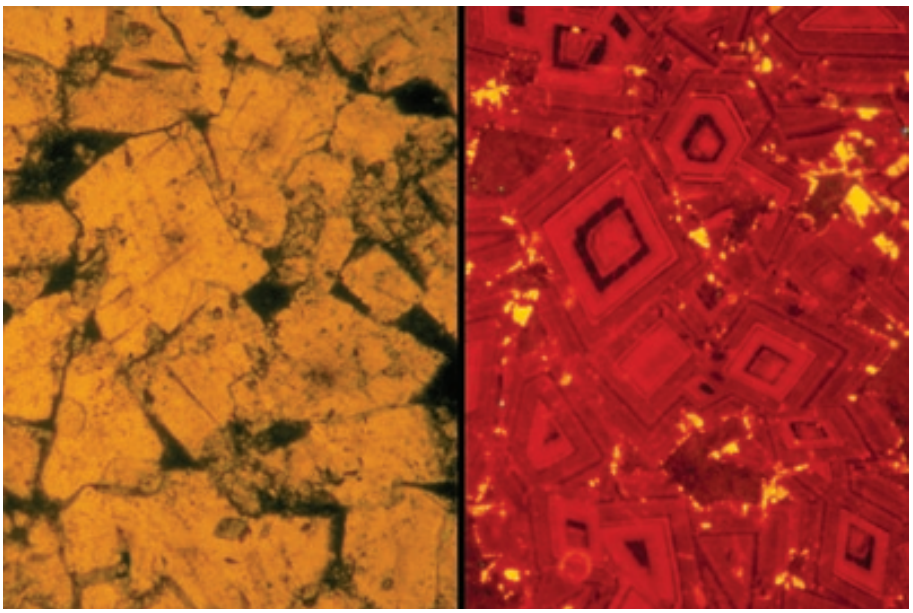

Lo. Cretaceous (Aptian) Shuaiba Fm., 3,131 ft (954 m) depth, offshore Qatar

Replacement dolomite crystals, with cloudy ferroan cores and clear, less ferroan rims, in a wackestone sediment. Although most of the dolomite crystals are euhedral, they have considerable variation in crystal sizes (polymodal). Many of these crystals formed by overgrowth and replacement of fossil fragments (the largest is a replacement of an echinoid fragment).

PPL, AFeS, HA = 4.5 mm

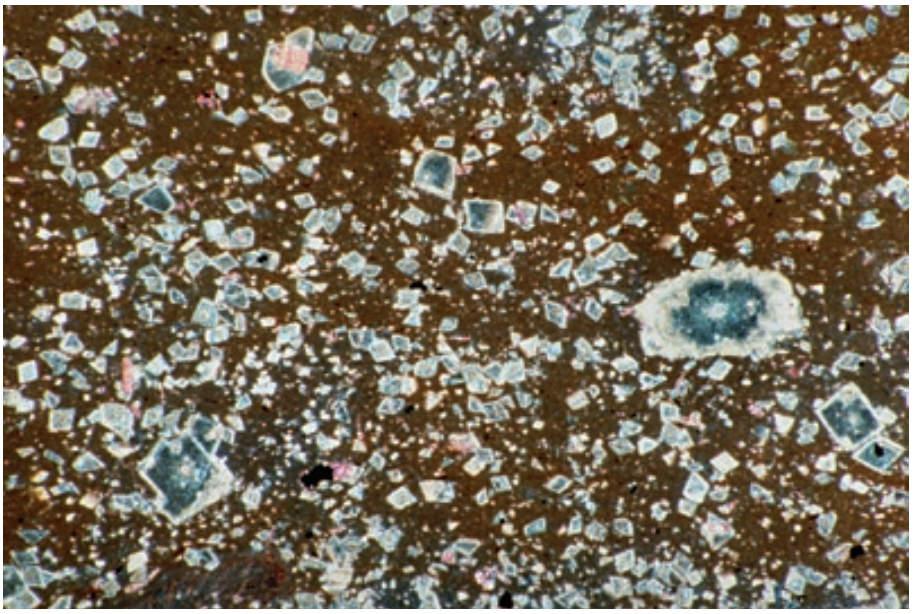

Up. Devonian (Famennian) Wabamun Fm., Alberta, Canada

A dolomitization front in a micritic limestone — dolomitization is complete on the right side and sparse on the left. In this case, the presence of permeable burrows led to highly heterogeneous replacement patterns as dolomitizing fluids moved preferentially through the burrows and altered material within, and directly adjacent to, those fluid conduits.

PPL, HA = 5.0 mm

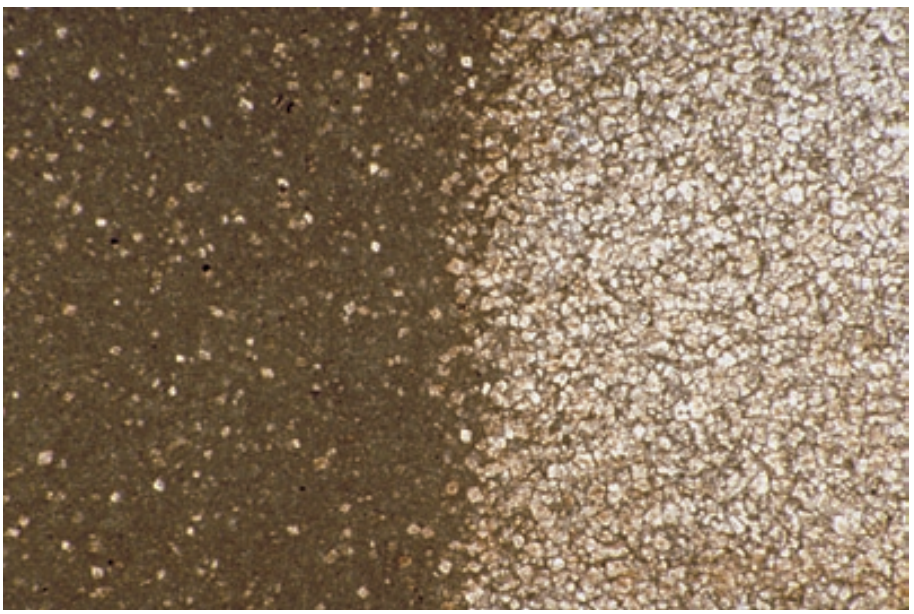

Mid.-Up. Ordovician Red River Fm., "D" Zone, 9,132 ft (2,783 m) depth, Bowman County, North Dakota

A sample of a dolomitic hydrocarbon reservoir. It shows a dolomitized burrow fill (center) in a porous dolomite matrix. Intercrystal porosity is far better developed in the matrix, possibly due to dissolution of undigested limestone after complete dolomitization of burrows and partial dolomitization of surrounding areas. The nature of the porosity is more easily seen in the next slide taken at higher magnification. Photograph courtesy of Mark Longman.

PPL, AS, BSE, HA = 8.2 mm

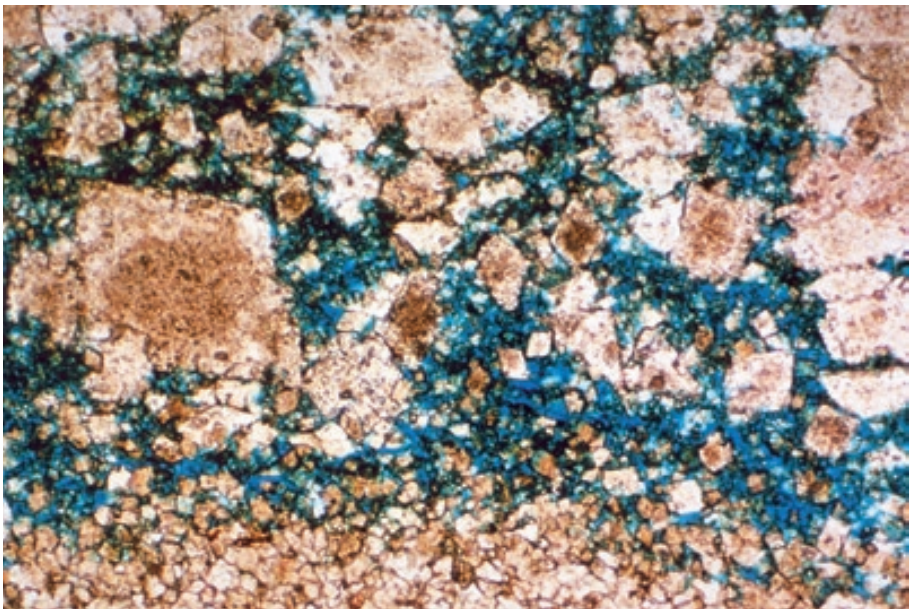

Mid.-Up. Ordovician Red River Fm., "D" Zone, 9,132 ft (2,783 m) depth, Bowman County, North Dakota

A higher-magnification view of the intercrystalline porosity from which this hydrocarbon reservoir produces. Note the variable size of the dolomite crystals, suggesting, perhaps, that several stages of dolomitization occurred and/or that fewer dolomite nucleation sites existed in areas outside the burrows. Photograph courtesy of Mark Longman.

PPL, AS, BSE, HA = 1.8 mm

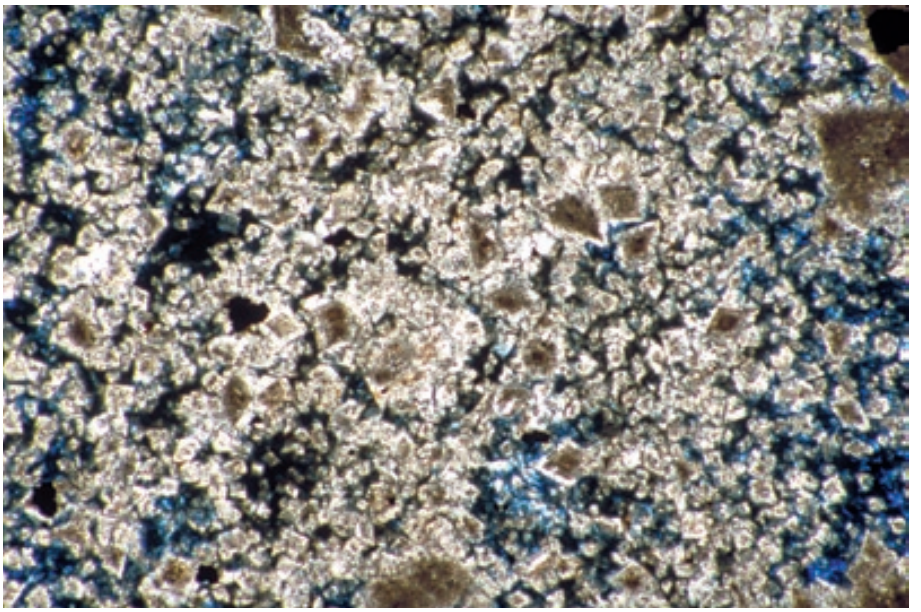

Lo. Cretaceous (Aptian) Shuaiba Fm., 3,131 ft (954 m) depth, offshore Qatar

Another example of a hydrocarbon reservoir in a replacement dolomite with variable crystal sizes. In this case, the dolomite crystals formed in a shallow-shelf skeletal wackestone and are strongly zoned, with cloudy cores and clear rims. Patchy porosity resulting from matrix leaching is distributed throughout this slide and is connected by intercrystalline microporosity.

PPL, AFeS, BSE, HA = 6.0 mm

Mid. Eocene Avon Park Fm., Levy Co., Florida

Dolomoldic porosity is common in partially dolomitized strata, especially where dolomitization was fabric selective. Here, medium crystalline dolomite has replaced the micritic matrix of a former biomicrite. Fossil fragments were not dolomitized and have been subsequently dissolved, leaving moldic porosity. Such reservoir rocks have high porosity, but only moderate permeability, because the large moldic pores are connected to each other only through small intercrystalline conduits.

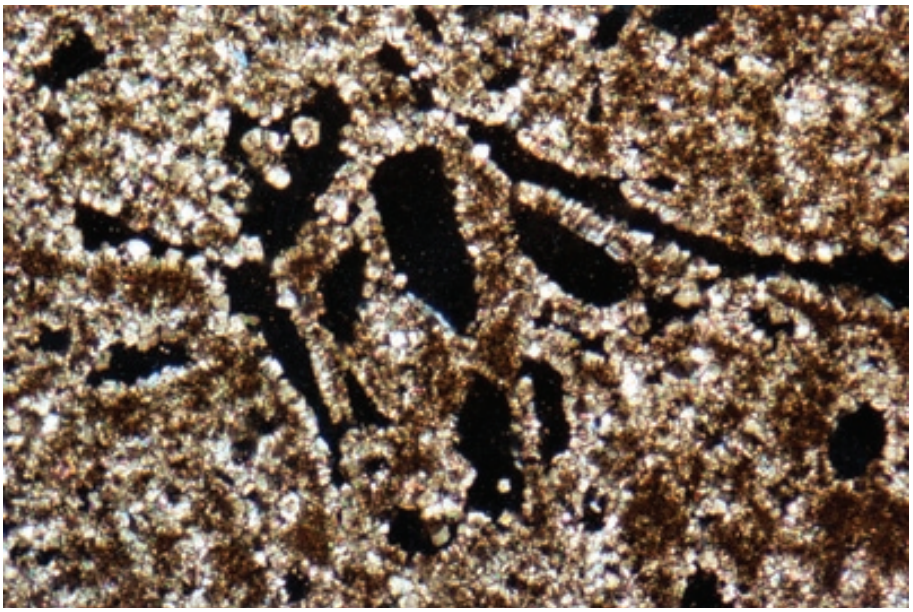

XPL, HA = 3.4 mm

Lo. Cambrian Forteau Fm., southern Labrador, Canada

An example of highly selective dolomite replacement in ooid-peloid grainstone with crinoid fragments. Selected ooid cortical layers and nuclei were replaced by ferroan dolomite (stained blue); others were left completely unaltered and still show concentric and radial fabrics. In modern settings as well, dolomitization is highly selective, with aragonite and very high-Mg calcite being most susceptible to replacement. Low-Mg calcite (and high-Mg calcite with only a few mol% Mg) are more resistant to dolomitization. Photograph courtesy of Noel P. James.

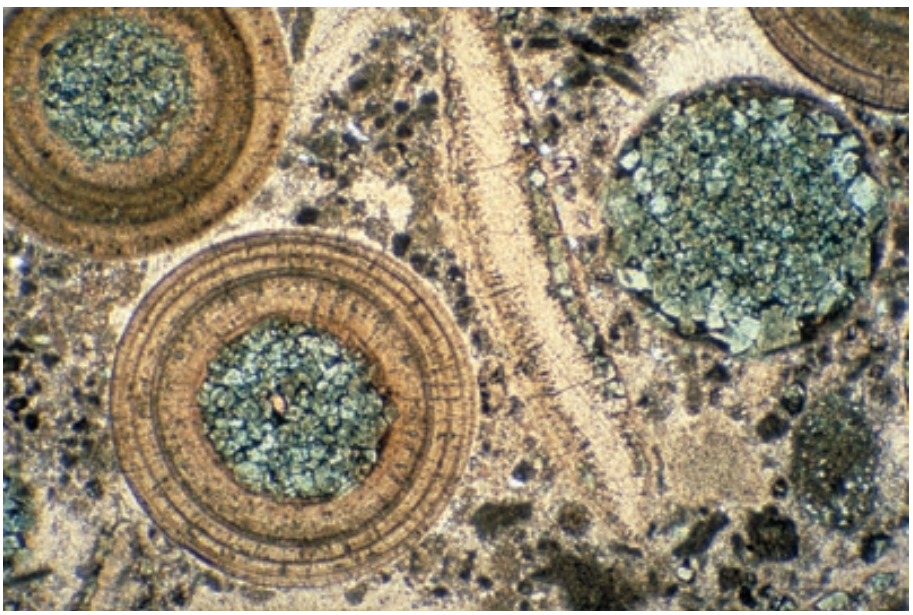

PPL, AFeS, HA = 4.4 mm

Up. Jurassic (Oxfordian) Smackover Fm., subsurface, Van Zandt Co., Texas

The next series of slides shows progressive dolomitization and fabric obliteration in oolitic grainstones. Selective dolomitization of the ooids in this limestone is coarse and not very fabric-retentive, but it also has not proceeded very far and so the ooids are easily identifiable. Note the preferential replacement of individual coatings within some ooids and nearly complete replacement in others. It is rarely possible to determine exactly why some zones are replaced and others not, but primary mineralogic differences and variations in organic content are likely factors.

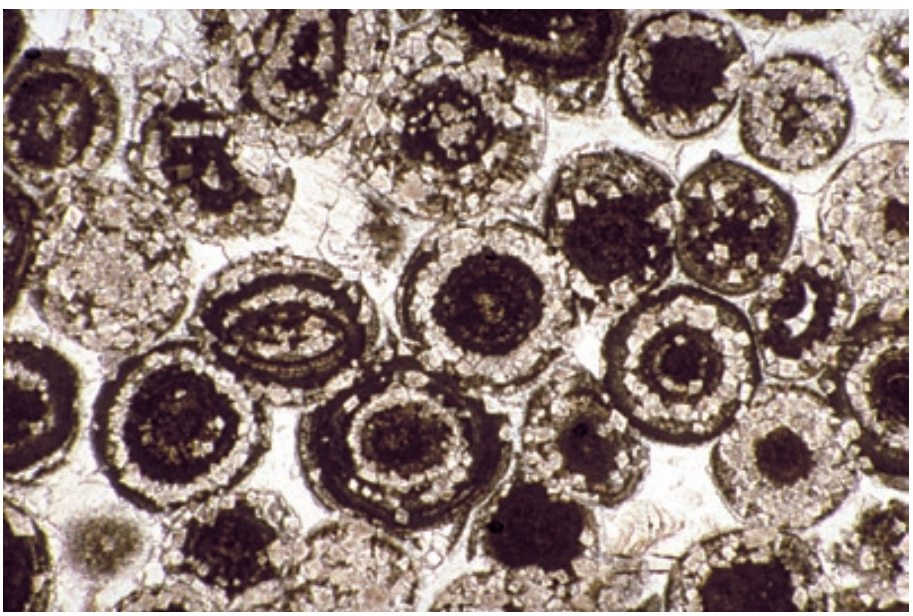

PPL, HA = 4.0 mm

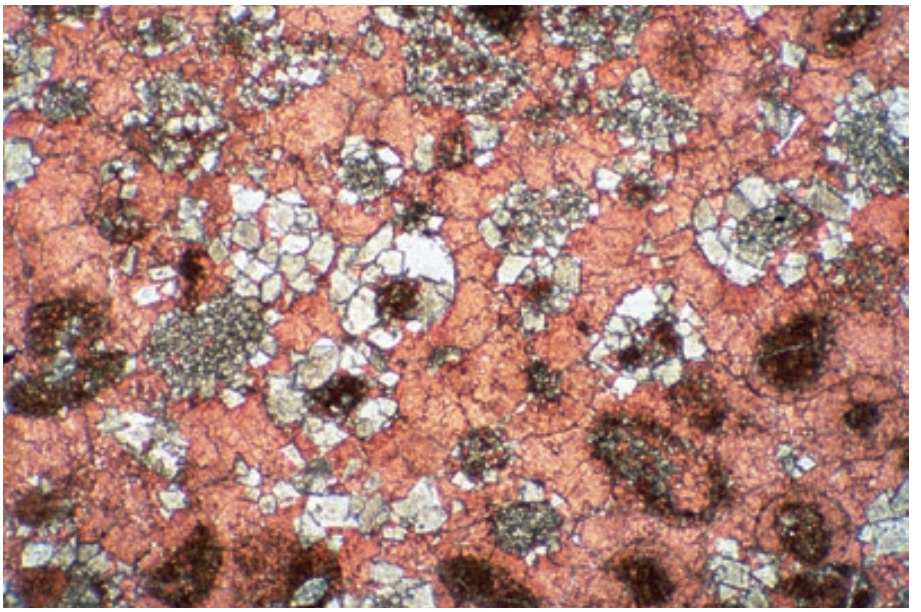

Mid. Cambrian limestone, Utah

In this ooid grainstone, some ooids were replaced by medium crystalline calcite and other ooids were partially replaced by medium crystalline euhedral to subhedral dolomite. Fabric preservation is equally poor in calcitized and dolomitized areas. This likely represents late-stage dolomitization that took place after neomorphism (calcitization) and fabric destruction in unstable ooids. Photograph courtesy of Noel P. James.

PPL, AS, HA = 4.4 mm

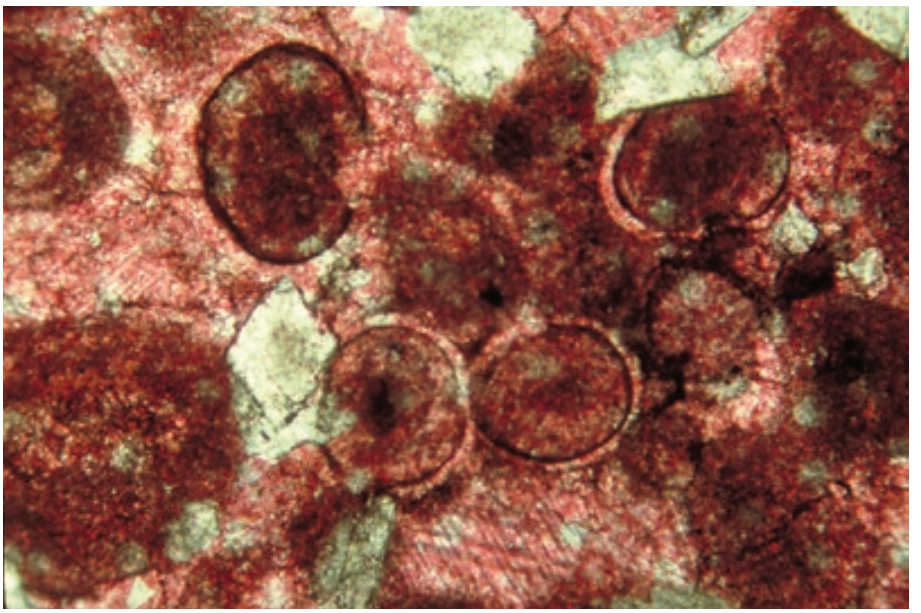

Up. Cambrian Bestogai Fm., Malyi Karatau, southern Kazakhstan

This is an oolitic grainstone clast from a megabreccia debris-flow deposit. Although the ooids are well preserved, this example shows how dolomitization can occur in a very non-selective manner. Individual dolomite crystals (unstained) cut across various grains as well as the adjacent calcite cement. Where such dolomitization is more extensive, primary fabrics can be completely obliterated. Photograph courtesy of Harry E. Cook.

PPL, AS, HA = 2.0 mm

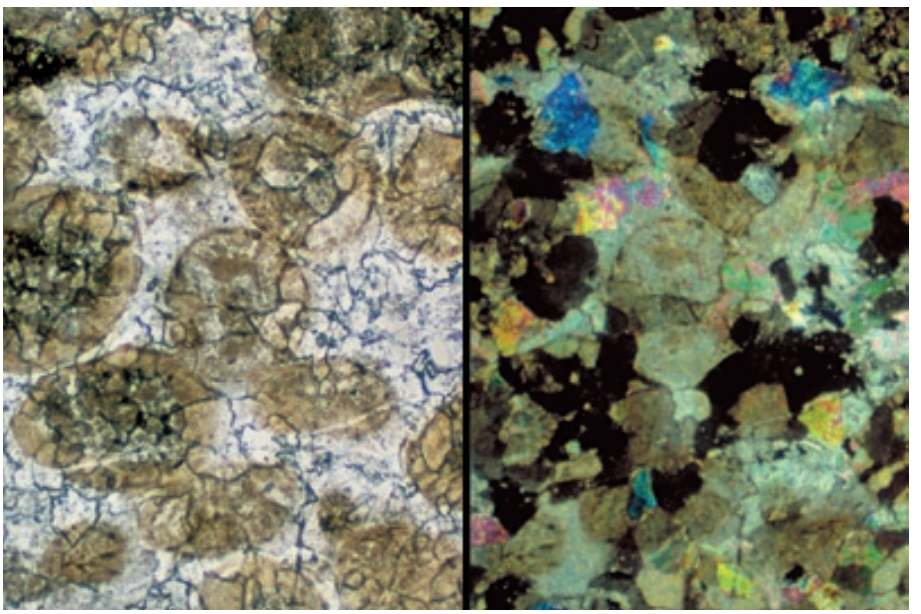

Lo. Ordovician, Lo. El Paso Gp., El Paso Co., Texas

This oolitic grainstone was completely replaced by medium- to coarsely-crystalline dolomite. Note how individual dolomite crystals here, as in the previous case, cross both the internal fabrics within the grains and the grain-cement boundaries. Recognition of original fabrics here is entirely a result of the abundance of inclusions of primary material within the replacement dolomite crystals. Most ooids are laden with organic matter, much of which may be retained during replacement (see section on ooids and other coated grains).

PPL/XPL, HA = 1.8 mm each

Up. Cambrian Kittatiny Fm., northern New Jersey

This oolitic grainstone was completely replaced by medium-crystalline dolomite. Note the fact that recognition of the outlines of the original ooids results mainly from the preservation of organic material (and associated iron oxides, probably after pyrite). Here however, the organic matter and associate iron minerals were substantially disrupted and apparently reside largely in the intercrystal spaces between adjacent dolomite rhombs (see also the photograph of this sample in white-card reflected light in the section on techniques). Sample from F. B. Van Houten.

PPL, HA = 2.4 mm

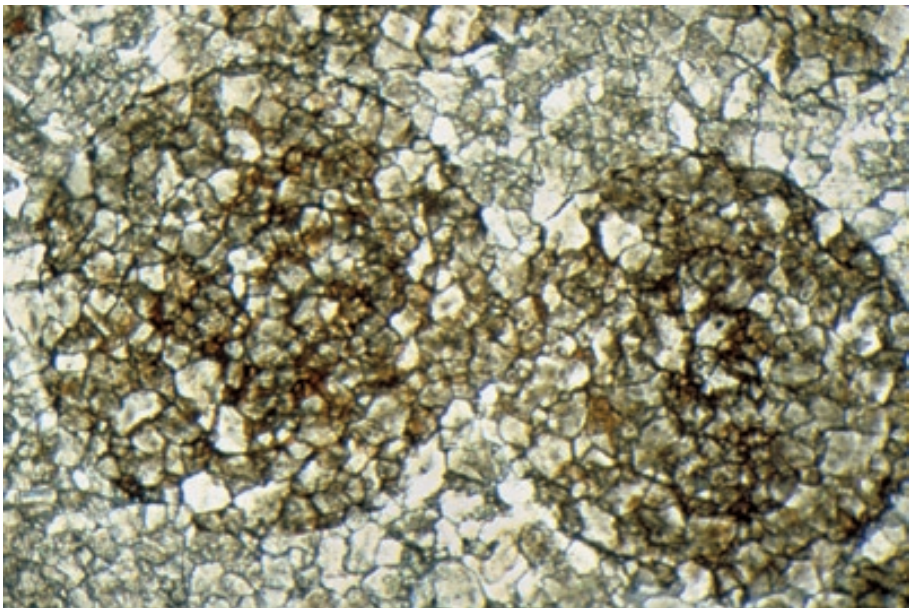

Mid. Eocene Naranjo Fm., Coamo Springs Mbr., Ponce-Coamo area, Puerto Rico

Determining the timing of dolomitization is difficult and, as with other cements and replacements, is based mainly on composition and paragenetic relations. The next series of pictures shows dolomites that have a clear paragenetic context. Here, selective development of replacement dolomite occurred along a fracture in a red algal grain. The rusty appearance of the grains in this weathered sample indicates an original ferroan composition. Thus, dolomitization occurred after fracturing and under somewhat reducing conditions — probably during mesogenetic diagenesis.

PPL, HA = 2.0 mm

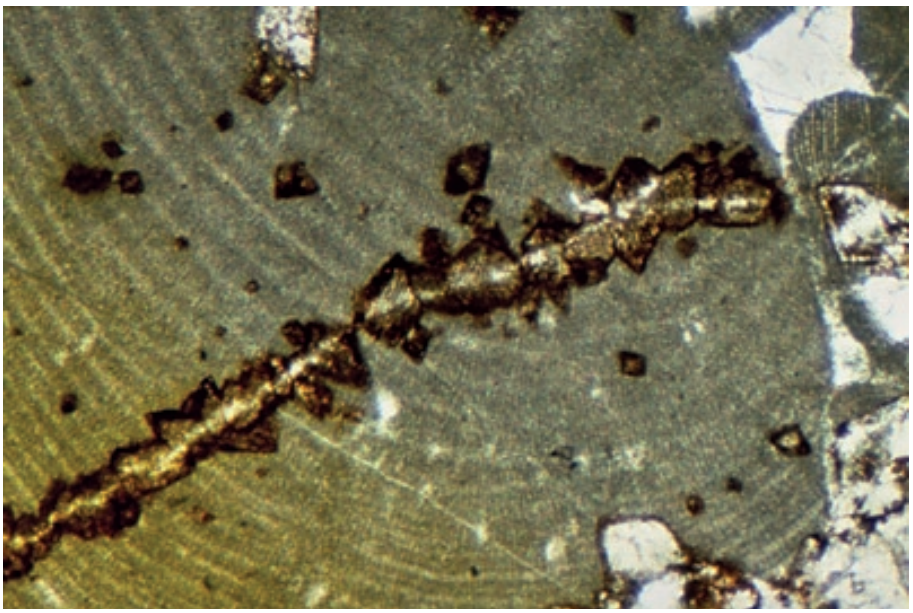

Mid. Ordovician Laval Ls., Quebec, Canada

This pelmatozoan grainstone with syntaxial cements is cut by a stylolite that has associated euhedral, slightly ferroan dolomite. The dolomite apparently formed along the stylolite as the rest of the rock contains little dolomite. Thus the dolomite formation postdates stylolitization. In this era of analytical geochemistry, such paragenetic determinations take on a great importance in making sense of isotopic or elemental data. Conversely, geochemical data can greatly aid the petrographer in limiting the range of possible explanations of textural or paragenetic observations. Photograph courtesy of Noel P. James.

PPL, AFeS, HA = 2.0 mm

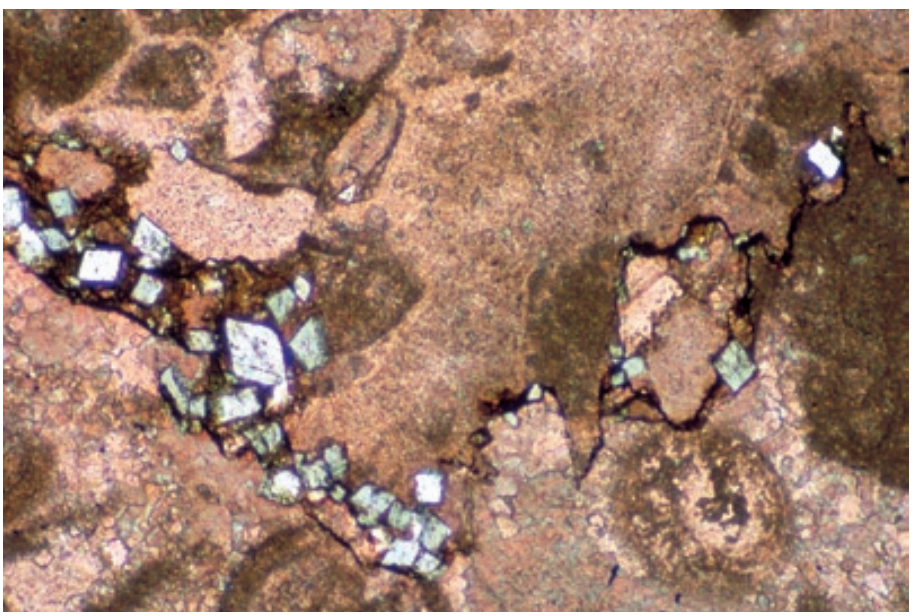

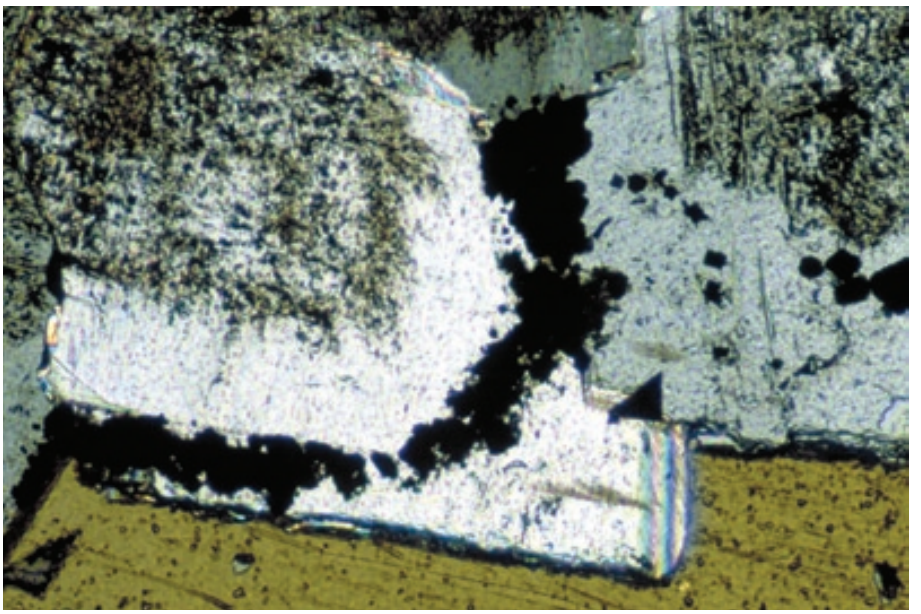

Cambrian Bonneterre Fm., Shannon Co., Missouri

These gangue dolomite crystals are associated with a major MVT ore deposit and contain metallic sulfide inclusions. Thus they were precipitated in association with hydrothermal mineralizing solutions that moved through these rocks. Because the relative timing of mineralization can be tied to well-dated tectonic events, this constrains the time of dolomite formation. Photograph courtesy of Jay M. Gregg (Gregg, 1985).

PXPL, HA = 1.3 mm

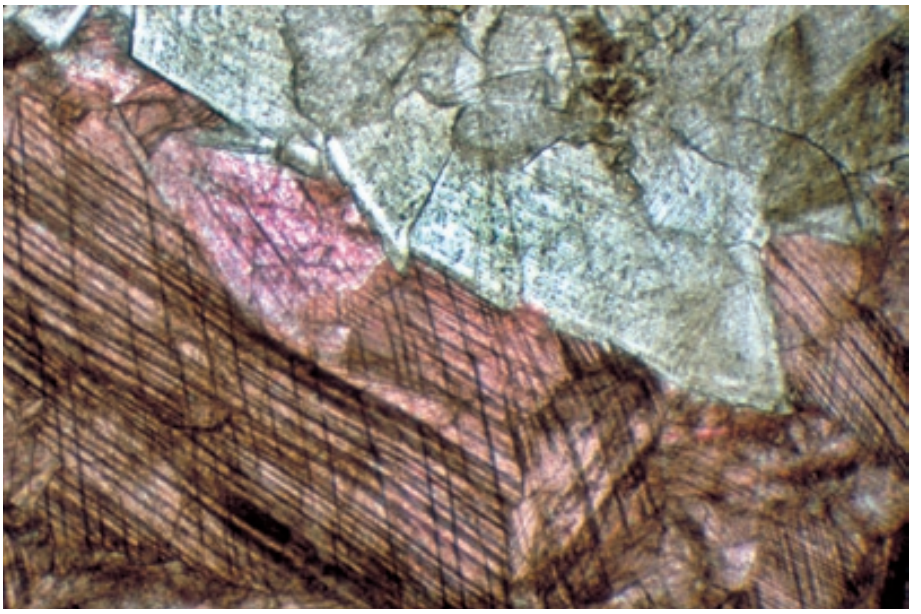

Up. Devonian (Frasnian) Perdrix-Mount Hawk Fms., Alberta, Canada

In this case, dolomitization predates a major deformation event. Note the brittle fracturing of the dolomite relative to the more distributed deformation of the adjacent calcite (stained pink) along twin lamellae. Such intense twinning typically results from tectonic deformation and is developed far more easily in calcite than in dolomite — indeed, that difference can sometimes be used to differentiate the two minerals in the absence of staining or analytical information.

PPL, AFeS, HA = 4.1 mm

Up. Jurassic (Portlandian?) Arab D Carbonate, ~6,500 ft (~1,980 m) depth, Dukhan field, Qatar

Dolomite cements, once considered rare, are now recognized as widespread precipitates. In this world-class oil reservoir, an articulated bivalve shell and adjacent ooids were leached to form biomoldic and oomoldic pores. Leaching was followed by the growth of calcite and dolomite cements in both primary (intra- and interparticle) and secondary (moldic) pores. These cements are especially well developed in the internal cavity of the bivalve which is lined with fibrous calcite (stained red) followed by rhombic dolomite cement (white). Photograph courtesy of David N. Clark.

PPL, AS, BSE, HA = 1.6 mm

Mid. Cretaceous Edwards Fm., Bell Co., Texas

Cathodoluminescence (CL) studies provide an additional tool to aid in the recognition of dolomite cements and the paragenetic relations with their host rocks. This standard light microscope view (that should be compared with the subsequent CL image) shows a finely crystalline dolostone in which syntaxial dolomite cement is prominent, forming 24% of the rock and lining molds in somewhat patchy fashion. The total porosity in this rock is 25% and the brown pore fillings are epoxy impregnation medium that has been "burned" by the electron beam. Photograph courtesy of Philip W. Choquette.

PPL, HA = 1.5 mm

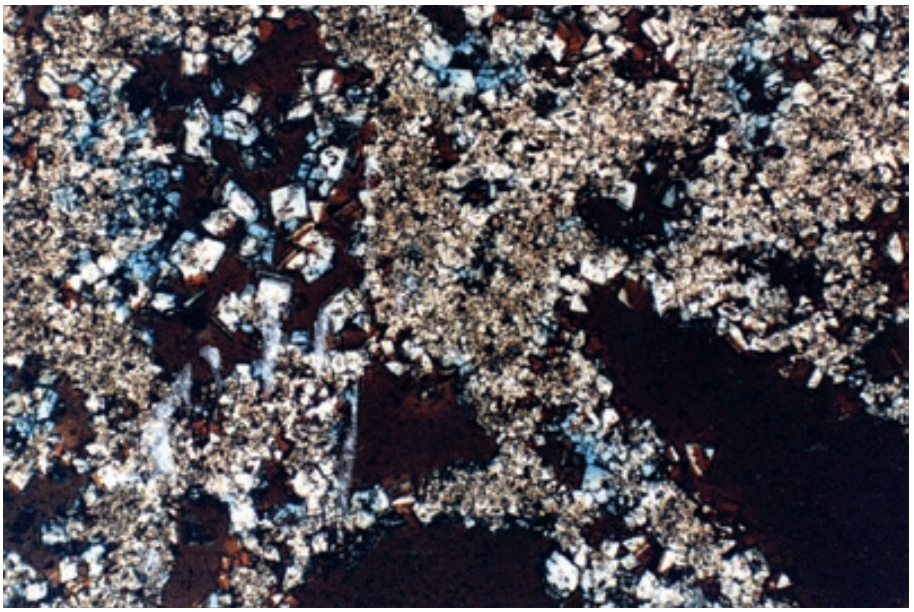

Mid. Cretaceous Edwards Fm., Bell Co., Texas

A CL view of the previous sample. Note the clear distinction of dolomite-overgrowth cements and their patchy distribution as linings of molds. One cement zone has been dissolved during subaerial weathering, perhaps because it contained more Mg than other zones. The Edwards Fm. is an important fresh-water aquifer in central and south Texas and these extensive dolomite cements may have formed early in the geologic history of the aquifer. Photograph courtesy of Philip W. Choquette.

CL, HA = 1.5 mm

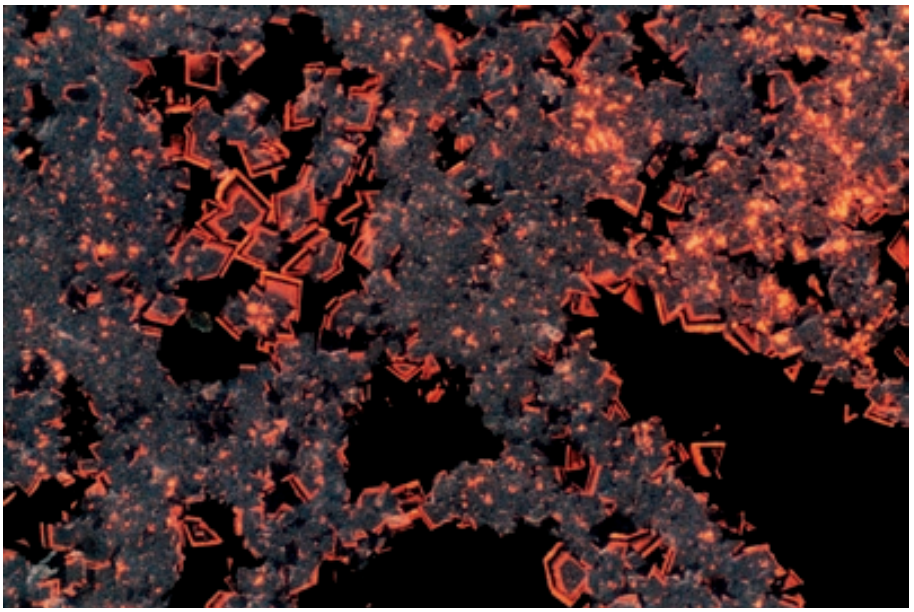

Mid. Eocene Avon Park Fm., south Florida

This coarsely crystalline dolomite shows extensive interlocking of adjacent crystals, but the detailed relationships are difficult to determine under standard microscopy. The next image shows a CL view that better reveals the replacement and cementation relationships in this dolostone. Dolomitization has substantially indurated this rock, leaving only 9% total porosity. Photograph courtesy of Philip W. Choquette.

PPL, HA = 2.5 mm

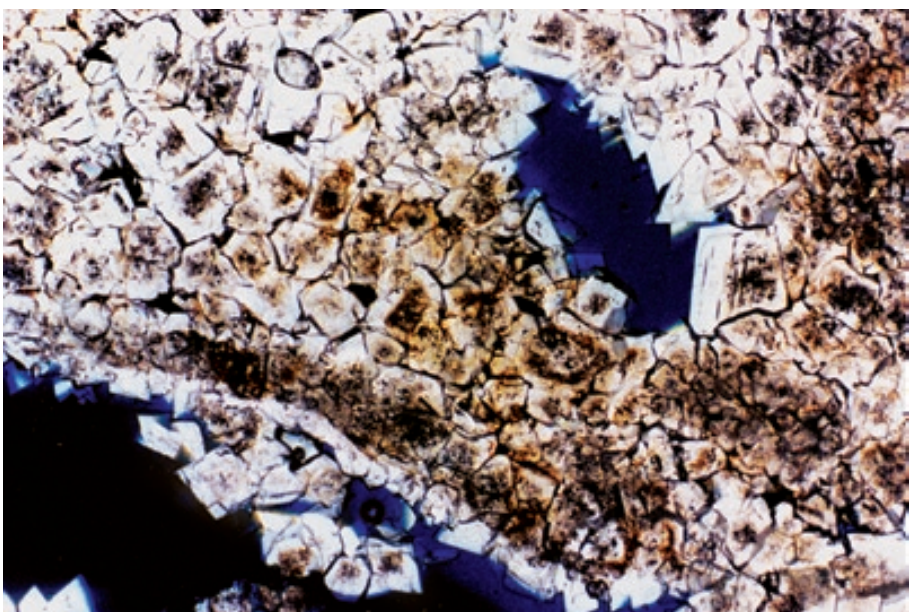

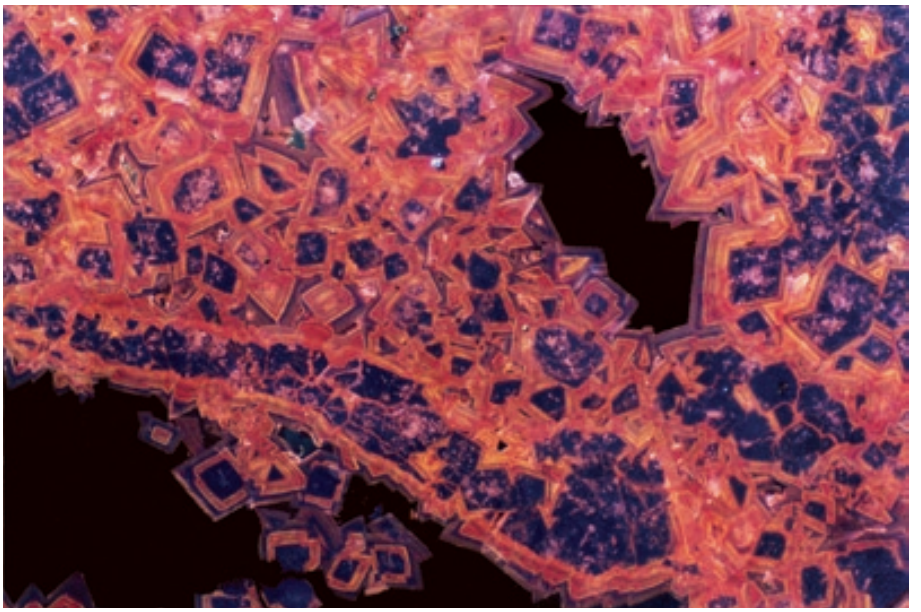

Mid. Eocene Avon Park Fm., south Florida

This CL image of the area shown in the previous photograph reveals one phase of replacement and two phases of overgrowth cementation The dark nuclei have been interpreted as replacement dolomites produced in marine pore waters and the lighter-luminescing overgrowths as products of cement precipitation from mixed marine-meteoric groundwaters (Cander, 1994). The final stage of darker-luminescing dolomite further cements and interlocks the crystals. This linking or welding together of clusters of earlier crystals is a diagnostic feature of pore-filling dolomite cements. Photograph courtesy of Philip W. Choquette.

CL, HA = 2.5 mm

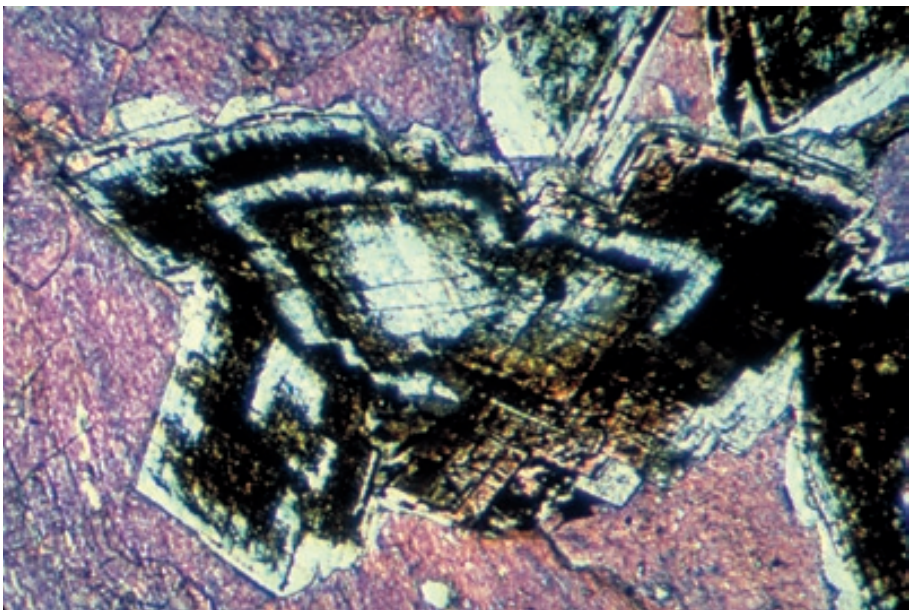

Up. Permian limestone, Djebel Tebaga area, southern Tunisia

This distinctive fabric, termed "saddle" or "baroque" dolomite, characterizes some burial-stage dolomites. Baroque dolomite has curved crystal faces and undulose extinction. Most is precipitated from hydrothermal brines at temperatures above about 60°C (and commonly up to 150°C or higher), commonly in association with metallic sulfide ores, barite, fluorite, and/or hydrocarbons. Deformation of the crystal lattice results from substitution of up to 15 mol% Fe and other cations. This baroque dolomite is partially calcitized (note the pink-stained areas), yet still shows excellent crystal surface curvature.

PPL, AFeS, HA = 2.4 mm

Mississippian (Osagean) Lake Valley Fm., Otero Co., New Mexico

This example of baroque (saddle) dolomite has curved crystal surfaces similar to those shown in the previous sample. In this cross-polarized view, however, it also depicts the strongly undulose or sweeping extinction that is characteristic of these high temperature precipitates.

XPL, AFeS, HA = 2.4 mm

Up. Permian (Guadalupian) Park City Fm., Ervay Mbr., Big Horn Co., Wyoming

Baroque dolomite (the unstained crystals with curved faces) can form either as cement or as replacement of earlier grains and cements. These baroque dolomites are mainly cements (or replacements of earlier calcite cements). They probably resulted from thermochemical sulfate reduction, where sulfates and hydrocarbons react at elevated temperatures to cause dissolution of evaporites, and, sometimes, the precipitation of associated baroque dolomite.

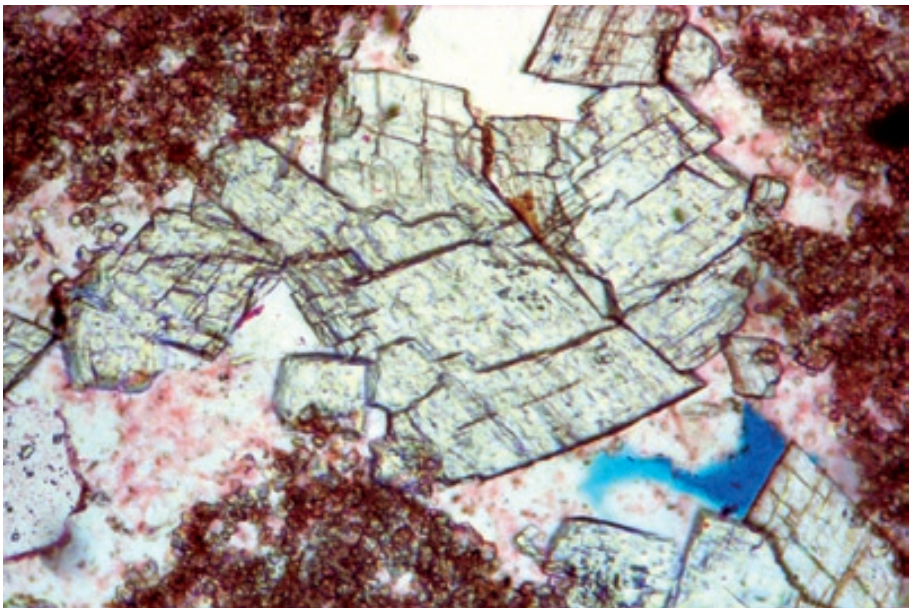

PPL, AS, BSE, HA = 1.3 mm

Up. Jurassic (Oxfordian) Up. Smackover Fm., Gulf Coast, U.S.A.

The late-stage saddle dolomite (unstained crystal with undulose extinction) in this oolitic grainstone clearly occupies the position of a cement and avoids replacement of adjacent grains. Although a cement origin is very likely, it is difficult to prove absolutely that this baroque dolomite was not a selective replacement of a precursor cement. Photograph courtesy of Clyde H. Moore.

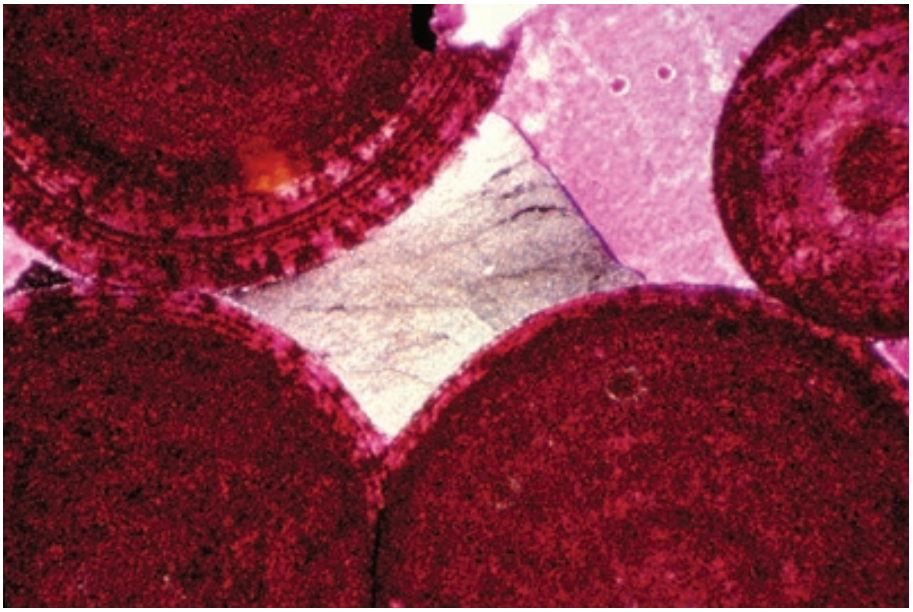

XPL, AS, HA = ~0.6 mm

Lo. Ordovician St. George Gp., western Newfoundland, Canada

This saddle dolomite with sweeping extinction has formed as a replacement of carbonate rock. The evidence for a replacement origin comes from the pattern of inclusions incorporated in the dolomite crystals that show the locations of precursor grains. Photograph courtesy of Noel P. James.

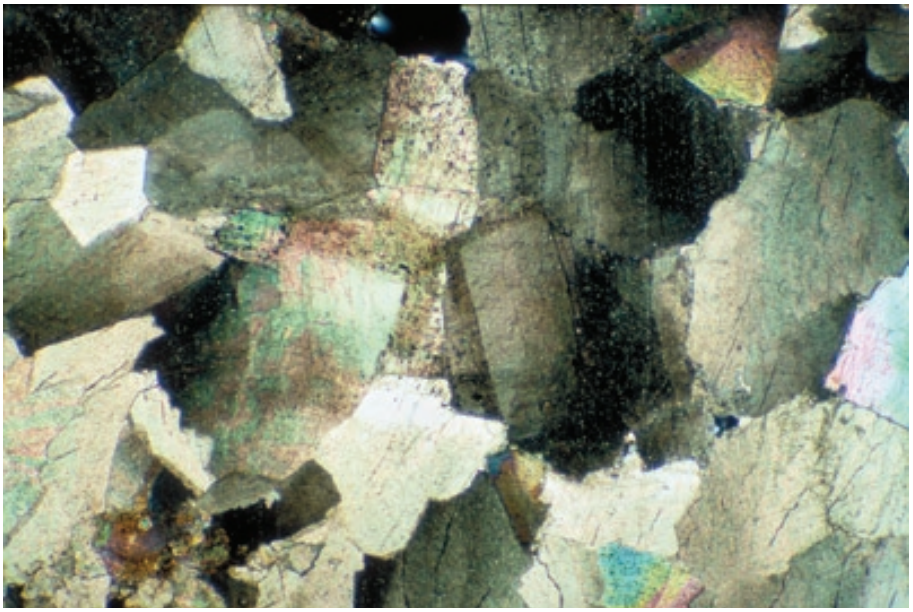

XPL, HA = 4.4 mm

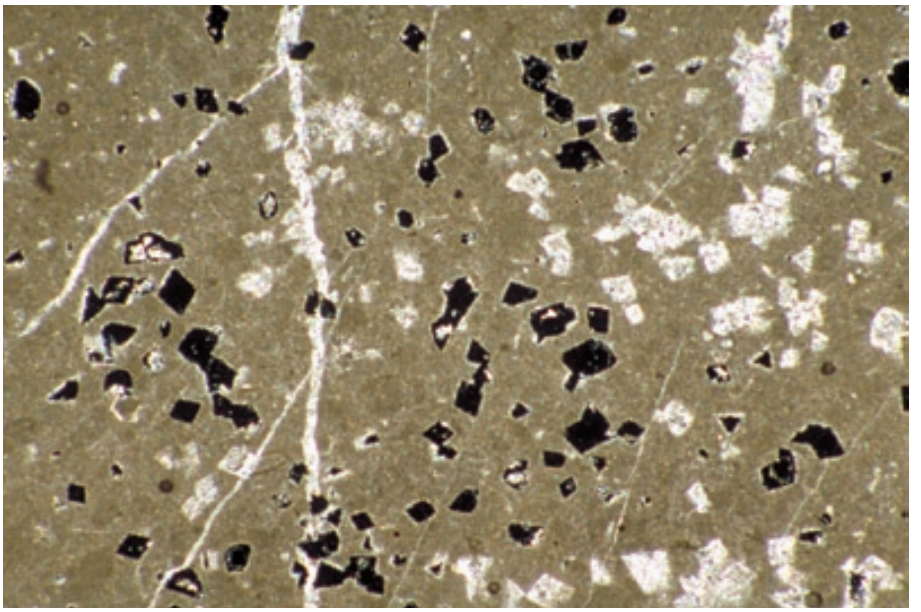

Jurassic Ronda unit (Subbetic), near Ronda, Spain

An example of selective leaching of some dolomite crystals in a partially dolomitized limestone. Dolomite dissolution and/or replacement by calcite is especially common in association with surface or subsurface dissolution of sulfate evaporites. The term "dedolomitization" is often used to describe this process, but it is not a very precise term. Dolomite leaching or dissolution is seen here, but dolomite calcitization is equally common and is also referred to as dedolomitization.

XPL, HA = 3.6 mm

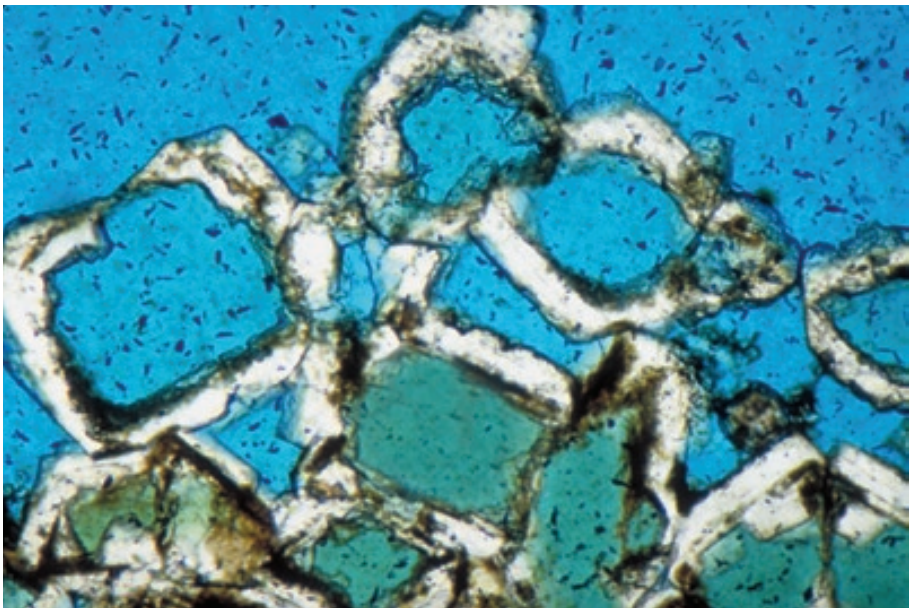

Mid. Silurian (Wenlockian) Lilley Fm., Adams Co., Ohio

Dissolution of dolomites often is highly selective. Here, for example, late-diagenetic, possibly telogenetic (uplift-stage) alteration produced hollow crystals due to selective leaching of the cores of these dolomite crystals. Compositional variations in dolomite crystals commonly are great enough that such selective dissolution is almost the norm in altered dolomites. Inclusion-rich, cloudy dolomite cores are generally more susceptible to leaching than the clear rims.

PPL, BSE, HA = 0.65 mm

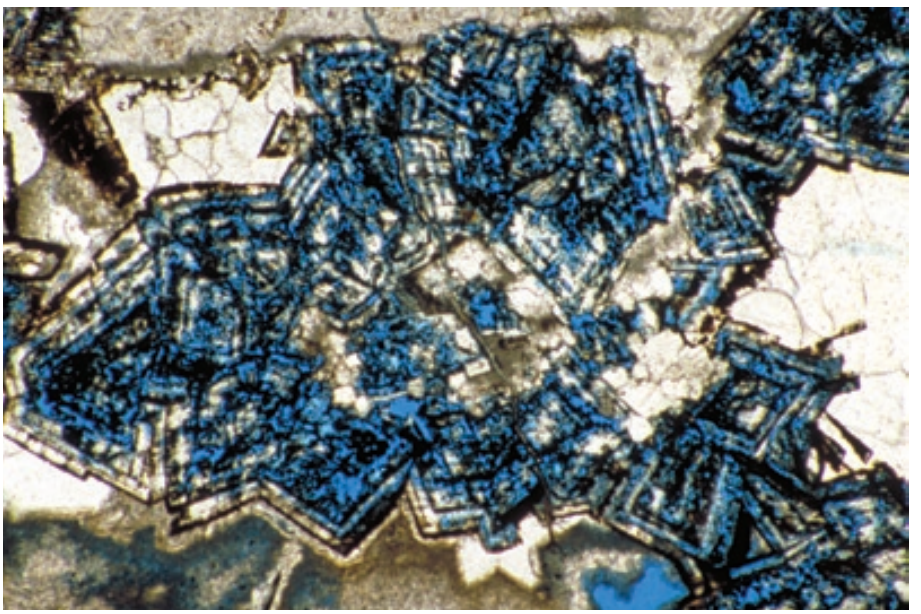

Up. Permian limestone, Djebel Tebaga area, southern Tunisia

Selective leaching of zones within dolomite crystals can leave remarkably delicate and complex structures, as in this example of late-stage dissolution. Such skeletal crystals can collapse to form geopetal structures, or they can be filled with other cements, most commonly calcite. Sample from Lars Stemmerik.

PPL, BSE, HA = 3.0 mm

Mississippian (Visean) Arroyo Peñasco Gp., Terrero Fm., Taos Co., New Mexico

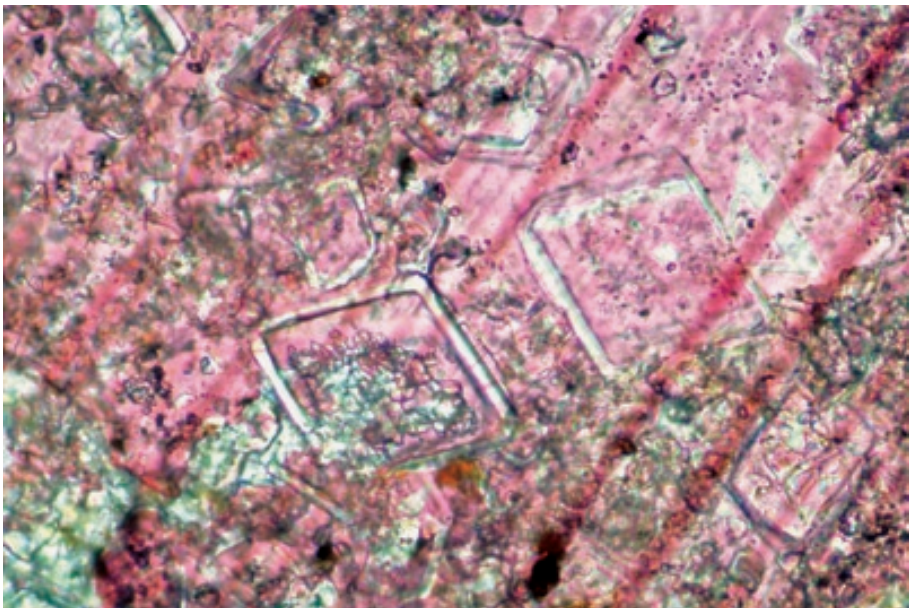

Dedolomitization (calcitization of dolomite) is demonstrated in this example by a combination of staining and observation of internal collapse fabrics. The cores and/or certain zones of the crystals are inferred to have been poorly ordered dolomite that was susceptible to dissolution. The residual zones of less soluble dolomite collapsed and formed geopetal mounds at the bottom of rhombic voids still rimmed by thin dolomite rinds. The void spaces from dolomite dissolution and collapse were cemented by calcite at a later stage.

PPL, AS, HA = ~0.4 mm

Mississippian (Visean) Arroyo Peñasco Gp., Terrero Fm., Taos Co., New Mexico

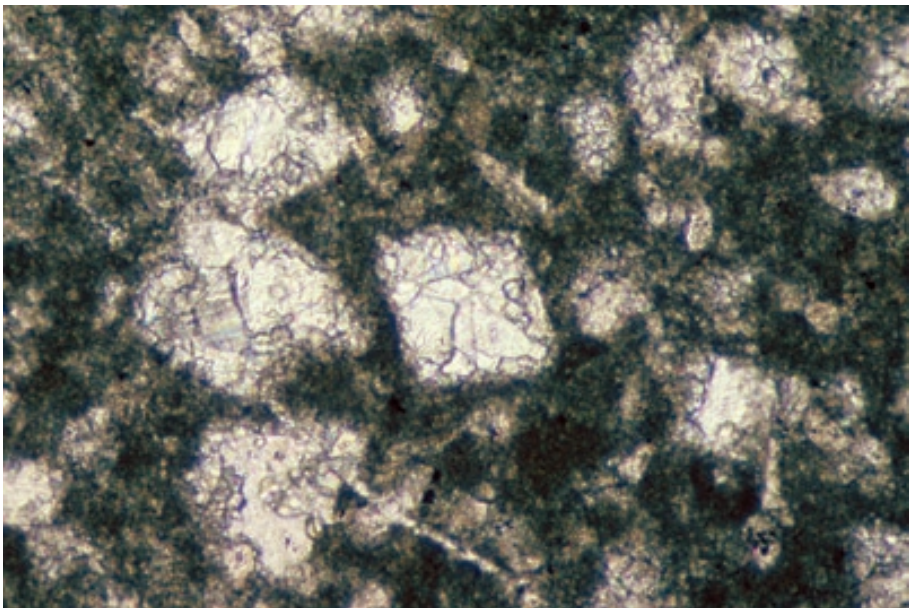

An example of a calcitized dolomite (dedolomite) in an evaporite-associated dolomitic limestone. In the absence of staining, careful examination reveals that the rhombic crystal outlines of the precursor dolomites are now filled with multiple pore-filling calcite crystals. This implies complete leaching of the dolomite crystals, followed by calcite filling of open dolomite molds.

PPL, HA = ~2.0 mm

Oligocene Gambier Fm., coastal South Australia

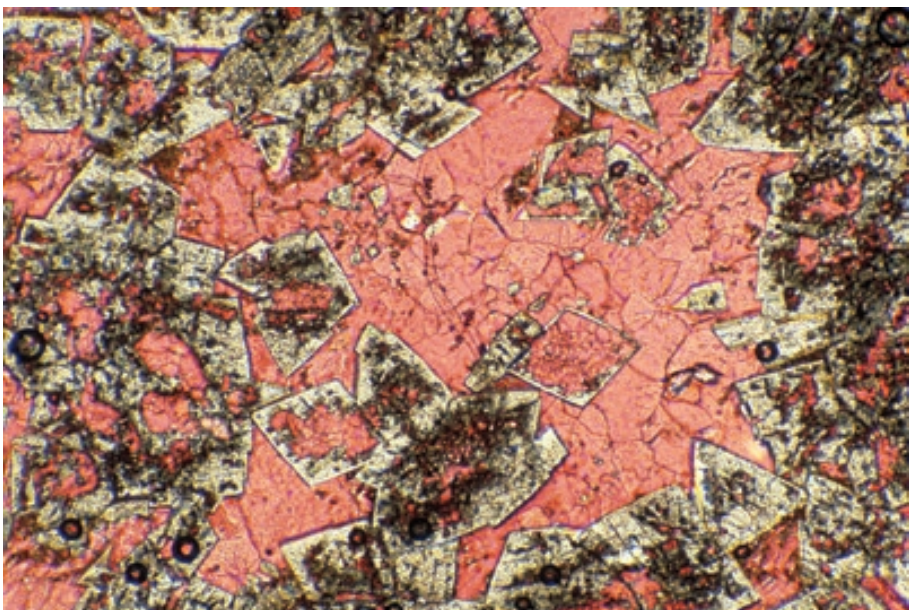

A stained example showing euhedral dolomite crystals in which the cloudy, inclusion-rich cores were dissolved and the resultant pore spaces were filled by calcite cement (red). Note the multicrystalline nature of the calcite fills within many of the rhombic dolomolds. Photograph courtesy of Noel P. James.

PPL, AS, HA = 1.5 mm

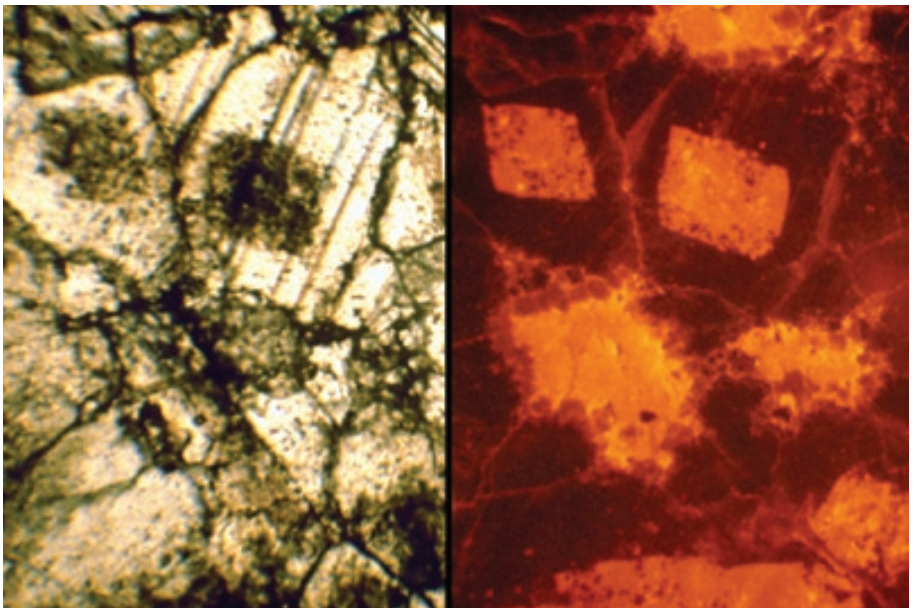

Mississippian (Tournaisian) Arroyo Peñasco Gp., Espiritu Santo Fm., San Miguel Co., New Mexico

An example of calcitized dolomites that show a completely different mode of alteration. Subhedral, rhombic, zoned, dolomite crystal outlines are clearly visible in both the normal and cathodoluminescent views. The entire rock is now calcite, however (as can be seen from the strong twinning that runs through some of the crystals). The preservation of large cloudy cores and clear rims, with no collapse features, implies alteration by a thin-film solution front that allowed dolomite dissolution and calcite precipitation to occur with no substantial void phase.

PPL/CL, HA = 1.8 mm each

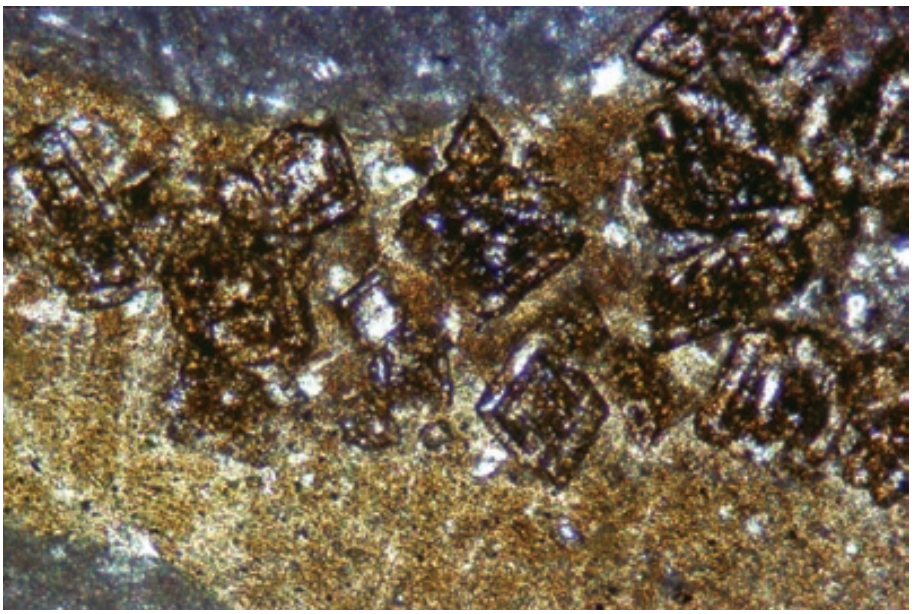

Up. Ordovician Ellenburger Ls., Llano area, Texas

Weathering and dolomite alteration can accentuate zonal variations in the iron contents of dolomites through the formation of hematite or limonite alteration zones. This medium crystalline replacement dolomite has been extensively calcitized, yet shows preservation of iron zoning as ferruginous oxide bands. Note the consistency of zonation from crystal to crystal, indicating that original dolomite crystals formed more or less simultaneously during a period of fluctuating geochemical conditions. It also indicates that, in this case as well, calcitization did not involve a void phase (solution-fill).

PPL, HA = 1.0 mm

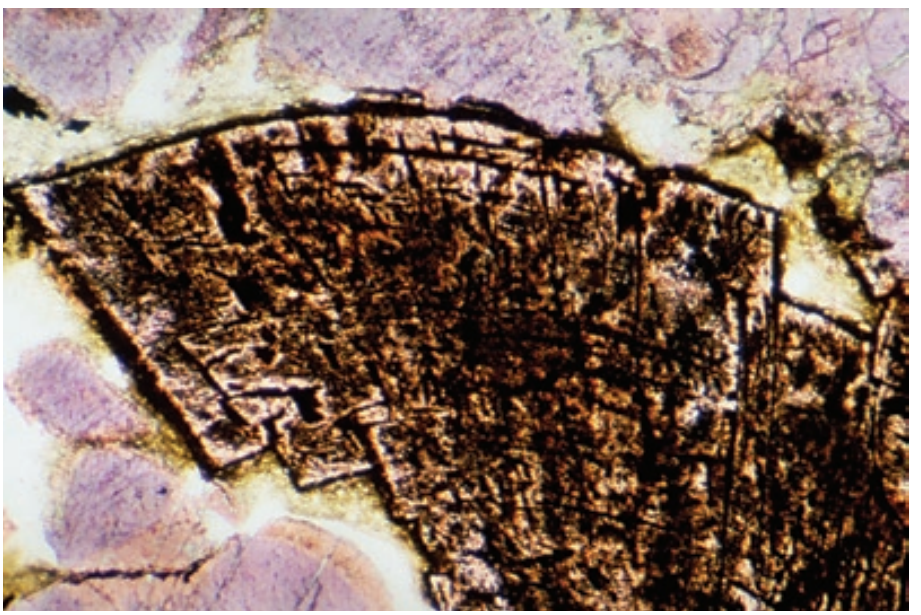

Mississippian (Osagean) Lake Valley Fm., Otero Co., New Mexico

The rusty-appearing material with curved crystal surfaces has the morphology of a typical baroque dolomite and is found cementing late-stage fractures in a biohermal limestone. In this case, however, staining shows that the baroque dolomite itself has been replaced by calcite filled with iron oxide inclusions, probably during late-stage (telogenetic) uplift and influx of meteoric waters. Baroque (saddle) dolomites are quite susceptible to telogenetic meteoric alteration, even in the absence of associated sulfate evaporites.

PPL, AFeS, HA = 2.4 mm

Lo. Cretaceous Paw Paw Fm., Grayson Co., Texas

An example of siderite cements in a shallow-marine limestone. Siderite forms in fine-grained brackish-water deposits, but it is also precipitated in fully marine, organic-rich strata. It is precipitated primarily during early burial in association with microbial decomposition of organic matter, especially in carbonate concretions. Siderite is readily recognized because it forms small, strongly flattened rhombs (discoid or football-shaped crystals). The crystals have high relief and are clear to yellowish-brown — these colors may be associated with weathering and formation of surficial hematite or limonite staining.

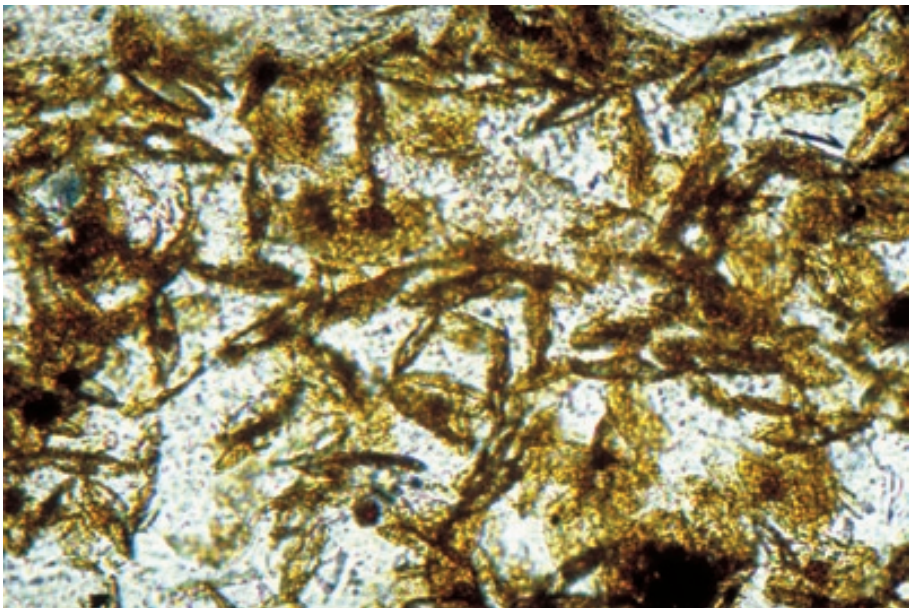

PPL, HA = 0.25 mm

Lo. Cretaceous (Albian) Nahr Umr Fm., 3,119 ft (951 m) depth, offshore Qatar

Another example of siderite cements, here in a shallow-marine sandy limestone with associated glauconite and chamosite. In this case, the siderite crystals are slightly zoned and form somewhat more equant, but still distinctively flattened or lenticular, colorless to brownish rhombs.

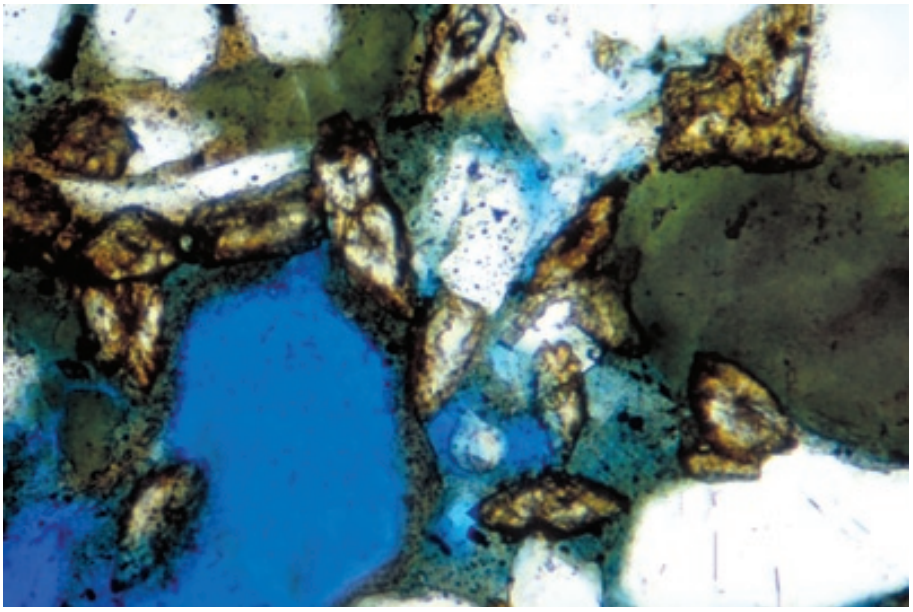

PPL, BSE, HA = 0.52 mm

Unknown unit; unknown locality

This example shows siderite crystals with small cores and large, rounded, nearly anhedral exteriors. The high relief and brownish yellow color are, once again, distinguishing characteristics, but the flattened rhomb crystal outlines seen in the previous examples are not present here. X-ray analysis, microprobe examination, or other analytical work generally is required in order to unequivocally distinguish siderite from ferroan dolomite. Sample from Canterbury University (NZ) collection.

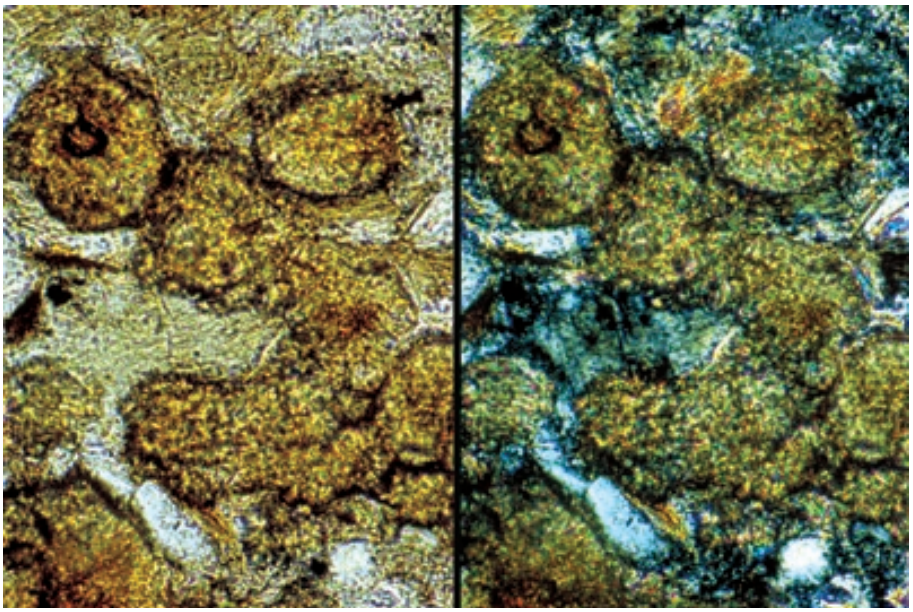

PPL/XPL, HA = 0.5 mm each

Cited References and Additional Information Sources

Allan, J. R., and W. D. Wiggins, 1993, Dolomite reservoirs: geochemical techniques for evaluating origin and distribution: Tulsa, OK, AAPG Short Course Note Series No. 36, 129+ p.

Arvidson, R. S., and F. T. Mackenzie, 1999, The dolomite problem: control of precipitation kinetics by temperature and saturation state: American Journal of Science, v. 299, p. 257-288.

Badiozamani, K., 1973, The Dorag dolomitization model — application to the Middle Ordovician of Wisconsin: Journal of Sedimentary Petrology, v. 43, p. 965-984.

Cander, H. S., 1994, An example of mixing-zone dolomite, middle Eocene Avon Park Formation, Floridan aquifer system: Journal of Sedimentary Research, v. A64, p. 615-629.

Carpenter, S. J., J. M. Erickson, K. C. Lohmann, and M. R. Owen, 1988, Diagenesis of fossiliferous concretions from the Upper Cretaceous Fox Hills Formation, North Dakota: Journal of Sedimentary Petrology, v. 58, p. 706-723.

Chilingar, G. V., D. H. Zenger, H. J. Bissell, and K. H. Wolf, 1979, Dolomites and dolomitization, *in* G. Larsen, and G. V. Chilingar, eds., Diagenesis in Sediments and Sedimentary Rocks: Developments in Sedimentology 25A: New York, Elsevier Scientific Publishing Co., p. 425-536.

Choquette, P. W., and R. P. Steinen, 1980, Mississippian non-supratidal dolomite, Ste. Genevieve Limestone, Illinois Basin: evidence for mixed water dolomitization, *in* D. H. Zenger, J. B. Dunham, and R. L. Ethington, eds., Concepts and Models of Dolomitization: Tulsa, OK, SEPM Special Publication No. 28, p. 163-196.

Curtis, C. D., and M. L. Coleman, 1986, Controls on the precipitation of early diagenetic calcite, dolomite and siderite concretions in complex depositional sequences, *in* D. L. Gautier, ed., Roles of Organic Matter in Sediment Diagenesis: Tulsa, OK, SEPM Special Publication No. 38, p. 23-33.

Evamy, B. D., 1967, Dedolomitization and the development of rhombohedral pores in limestone: Journal of Sedimentary Petrology, v. 37, p. 1204-1215.

Fairchild, I. J., 1980, Stages in a Precambrian dolomitization, Scotland: cementing versus replacement textures: Sedimentology, v. 27, p. 631-650.

Frank, J. R., 1981, Dedolomitization in the Taum Sauk Limestone (Upper Cambrian), southeast Missouri: Journal of Sedimentary Petrology, v. 51, p. 7-18.

Friedman, G. M., 1965, Terminology of crystallization textures and fabrics in sedimentary rocks: Journal of Sedimentary Petrology, v. 35, p. 643-655.

Gawthorpe, R. L., 1987, Burial dolomitization and porosity development in a mixed carbonate-clastic sequence: an example from the Bowland Basin, northern England: Sedimentology, v. 34, p. 533-558.

Given, R. K., and B. H. Wilkinson, 1987, Dolomite abundance and stratigraphic age: constraints on rates and mechanisms of Phanerozoic dolostone formation: Journal of Sedimentary Petrology, v. 57, p. 1068-1078.

Gregg, J. M., 1985, Regional epigenetic dolomitization in the Bonneterre Dolomite (Cambrian), southeastern Missouri: Geology, v. 13, p. 503-506.

Gregg, J. M., and D. F. Sibley, 1984, Epigenetic dolomitization and the origin of xenotopic dolomite texture: Journal of Sedimentary Petrology, v. 54, p. 908-931.

Humphrey, J. D., 1988, Late Pleistocene mixing zone dolomitization, southeastern Barbados, West Indies: Sedimentology, v. 35, p. 327-348.

Kyser, T. K., N. P. James, and Y. Bone, 2002, Shallow burial dolomitization and dedolomitization of Cenozoic cool-water limestones, southern Australia: geochemistry and origin: Journal of Sedimentary Research, v. 72, p. 146-157.

Land, L. S., 1982, Dolomitization: Tulsa, OK, AAPG Short Course Note Series No. 24, 20 p.

Land, L. S., 1985, The origin of massive dolomite: Journal of Geological Education, v. 33, p. 112-125.

Machel, H. G., and E. W. Mountjoy, 1986, Chemistry and environments of dolomitization—a reappraisal: Earth-Science Reviews, v. 23, p. 175-222.

Mazzullo, S. J., 2000, Organogenic dolomitization in peritidal to deep-sea sediments: Journal of Sedimentary Research, v. 70, p. 10-23.

McKenzie, J. A., 1981, Holocene dolomitization of calcium carbonate sediments from the coastal sabkhas of Abu Dhabi, U.A.E.: a stable isotope study: Journal of Geology, v. 89, p. 185-198.

Melim, L. A., and P. A. Scholle, 2002, Dolomitization of the Capitan Formation forereef facies (Permian, west Texas and New Mexico): seepage reflux revisited: Sedimentology, v. 49, p. 1207-1227.

Moore, S. E., R. E. Ferrell, Jr., and P. Aharon, 1992, Diagenetic siderite and other ferroan carbonates in a modern subsiding marsh sequence: Journal of Sedimentary Petrology, v. 62, p. 357-366.

Morrow, D. W., 1982a, Diagenesis 1. Dolomite - Part 1: The chemistry of dolomitization and dolomite precipitation: Geoscience Canada, v. 9, p. 5-13.

Morrow, D. W., 1982b, Diagenesis 2. Dolomite - Part 2: Dolomitization models and ancient dolostones: Geoscience Canada, v. 9, p. 95-107.

Mozley, P. S., and S. J. Burns, 1993, Oxygen and carbon isotopic composition of marine carbonate concretions: an overview: Journal of Sedimentary Petrology, v. 63, p. 73-83.

Mozley, P. S., and P. Wersin, 1992, Isotopic composition of siderite as an indicator of depositional environment: Geology, v. 20, p. 817-820.

Murray, R. C., and F. J. Lucia, 1967, Cause and control of dolomite distribution by rock selectivity: Geological Society of America Bulletin, v. 78, p. 21-36.

Purser, B. H., M. E. Tucker, and D. H. Zenger, eds., 1994, Dolomites - A Volume in Honor of Dolomieu [IAS Special Publication No. 21]: Cambridge, Blackwell, 451 p.

Radke, B. M., and R. L. Mathis, 1980, On the formation and occurrence of saddle dolomite: Journal of Sedimentary Petrology, v. 50, p. 1149-1168.

Shinn, E. A., R. N. Ginsburg, and R. M. Lloyd, 1965, Recent supratidal dolomite from Andros Island, Bahamas, *in* L. C. Pray, and R. C. Murray, eds., Dolomitization and Limestone Diagenesis: Tulsa, OK, SEPM Special Publication No. 13, p. 112-123.

Sibley, D. F., 1982, The origin of common dolomite fabrics: clues from the Pliocene: Journal of Sedimentary Petrology, v. 52, p. 1087-1100.

Sibley, D. F., 1991, Secular changes in the amount and texture of dolomite: Geology, v. 19, p. 151-154.

Sibley, D. F., R. E. Dedoes, and T. R. Bartlett, 1987, Kinetics of dolomitization: Geology, v. 15, p. 1112-1114.

Sibley, D. F., and J. M. Gregg, 1987, Classification of dolomite rock textures: Journal of Sedimentary Petrology, v. 57, p. 967-975.

Sibley, D. F., J. M. Gregg, R. G. Brown, and P. R. Laudon, 1993, Dolomite crystal size distribution, *in* R. Rezak, and D. L. Lavoie, eds., Carbonate Microfabrics: New York, Springer-Verlag, p. 195-204.

Sonnenfeld, P., 1964, Dolomites and dolomitization: a review: Bulletin of Canadian Petroleum Geology, v. 12, p. 101-132.

Sun, S. Q., 1995, Dolomite reservoirs: porosity evolution and reservoir characteristics: AAPG Bulletin, v. 79, p. 186-204.

Tucker, M. E., 1990, Dolomites and dolomitization models, *in* M. E. Tucker, and V. P. Wright, Carbonate Sedimentology: Oxford, Blackwell Scientific Publications, p. 365-400.

Ward, W. C., and R. B. Halley, 1985, Dolomitization in a mixing zone of near-seawater composition, Late Pleistocene, northeastern Yucatan Peninsula: Journal of Sedimentary Petrology, v. 55, p. 407-420.

Wright, D. T., 1997, An organogenic origin for widespread dolomite in the Cambrian Eilean Dubh Formation, northwestern Scotland: Journal of Sedimentary Research, v. 67, p. 54-64.

Zenger, D. H. J. B. Dunham, and R. L. Ethington, eds., 1980, Concepts and Models of Dolomitization: Tulsa, OK, SEPM Special Publication No. 28, 320 p.

Facing Page: Top: Pit wall showing contorted layers of displacive "enterolithic" anhydrite in supratidal Holocene sabkha sands of Abu Dhabi, United Arab Emirates. HA.= ~1.5 m. Bottom: Buckled gypsum layers in modern teepee structures, Bonaire, Netherlands Antilles. Photograph courtesy of C. Robertson Handford.

CARBONATE DIAGENESIS

SULFATE AND CHLORIDE MINERALS

CHAPTER 27

SULFATE AND CHLORIDE MINERALS

Introduction:

Sulfate and chloride minerals occur as cements, displacive and replacive nodules, and interbedded strata in carbonate rocks. They precipitate from evaporatively concentrated waters in arid-region lakes, ponds and lagoons along marine shorelines and, more rarely, in deeper shelf and basinal settings with restricted marine inflow. Evaporite deposits are products of arid environments; however, evaporitic solutions are highly mobile due to their high density. Evaporative brines thus may migrate into adjacent or underlying strata and precipitate diagenetic sulfate or chloride minerals (generally as displacive crystals and nodules, or as carbonate replacements) in units that may otherwise be unrelated to arid settings. Even after deposition and substantial burial, evaporite minerals can be remobilized and reprecipitated in distant, stratigraphically unrelated units. Therefore, careful petrographic analysis is needed to determine both the conditions of primary deposition and the timing of diagenetic events in evaporite-bearing limestones and dolomites.

Barite, celestite and anhydrite also can occur as hydrothermal precipitates in carbonate rocks.

Calcite solution-fill replacement (calcitization) of gypsum and anhydrite results from the dissolution of evaporites by sulfate-poor pore fluids. These pore fluids become saturated to supersaturated with respect to Ca^{2+}; if there is enough bicarbonate in the pore fluids, calcite may precipitate.

Major Diagenetic Fabrics:

Anhydrite crystals have high birefringence (up to third order); in thin section, the other common sulfate and halide minerals have much lower birefringence. Anhydrite's birefringence also can appear to "twinkle" like that of calcite, but the effect is less strongly developed than in calcite. Anhydrite crystals normally are colorless, but may contain inclusions of precursor phases. Anhydrite may form large tabular crystals or felted, fibrous crystal masses (generally as nodules). The larger crystals may exhibit pseudo-cubic cleavages.

Gypsum, celestite and barite can be extremely difficult to differentiate from each other in thin section. They all have low relief and birefringence (gray to white). Gypsum tends to form colorless, elongate, tabular to lenticular crystals or fibrous masses or aggregates of crystals. Gypsum also tends to form poikilotopic cements that encase numerous grains – siliciclastic or carbonate. Gypsum's cleavage is lozenge-shaped; therefore, if cleavage planes are visible, they are diagnostic for gypsum. Gypsum crystals may form rosettes and twins that are called swallow- or fish-tailed selenite. These larger crystals form displacively below the sediment/water interface in unconsolidated sediments; such crystals contain abundant inclusions of the sediment. Selenite crystals also can grow upward from the sediment-water interface into standing saline water bodies.

Celestite ranges from colorless to blue in thin section. Blue crystals of celestite can be pleochroic, which helps to differentiate it from gypsum and barite. Celestite forms fibrous to rounded aggregates of crystals. When it is found in fibrous masses, the crystals are normally more elongate than similar crystals of gypsum. Cleavage, when visible, is pseudo-cubic.

Barite normally is colorless and forms globular concretions, granular to earthy masses, fibrous or bladed crystals. Cleavage, when visible, is pseudo-cubic. Because barite and celestite form a solid solution series, they are extremely difficult to tell apart in thin section. Generally, other chemical techniques must be used to be confirm identifications. Like gypsum, barite also forms crystal rosettes.

Halite is difficult to see in thin section, because it is isotropic and highly soluble. Because halite is isotropic, it can easily be overlooked if the cleavages are not prominent or if it doesn't contain inclusions (i.e., it may be indistinguishable from the glass on which the section is mounted). Impregnating the sample with blue epoxy makes the halite stand out from the porosity. If the thin section is not properly prepared (cut and ground in oil, not water), however, halite is unlikely to be preserved. Halite crystals are normally colorless and exhibit low relief, but they may appear dusty due to the great abundance of solid and liquid inclusions. Halite can occur as a poikilotopic cement in either carbonate or siliciclastic strata.

Mineralogies:

Anhydrite – $CaSO_4$, orthorhombic

Gypsum – $CaSO_4 \cdot 2H_2O$, monoclinic

Celestite – $SrSO_4$, orthorhombic, complete solid solution series exists with barite

Barite – $BaSO_4$, orthorhombic, commonly contains up to 3% lead

Halite – NaCl, isometric (cubic)

Mississippian Up. Debolt Fm., subsurface, Alberta, Canada

An example of gypsum crystals replacing or displacing micritic carbonate sediment. A variety of characteristic crystal outlines are visible as a result of non-uniform crystal orientations. Gypsum has low birefringence, with first-order gray to white colors. It can, therefore, easily be confused with euhedral, authigenic quartz. The presence of cleavage in gypsum crystals, however, can help to distinguish it from quartz.

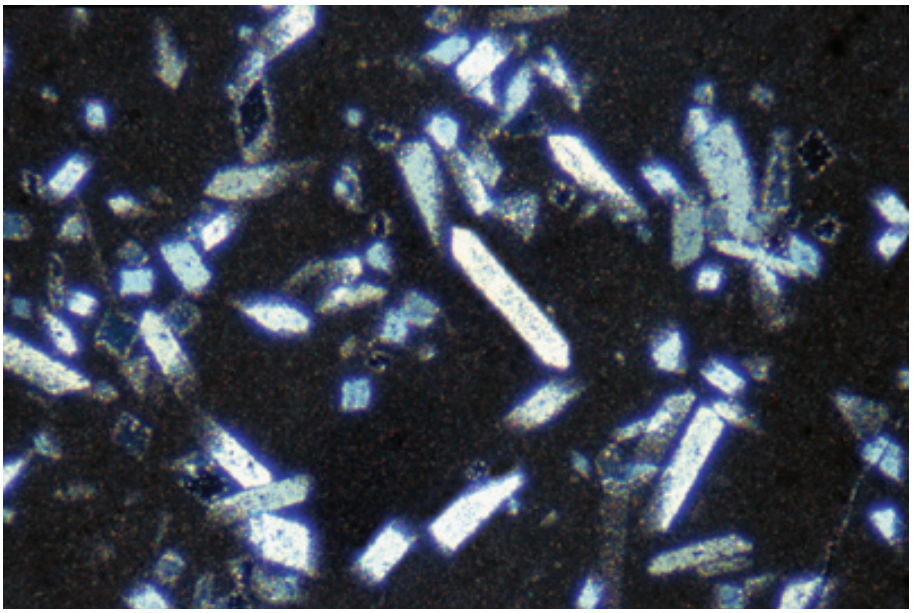

XPL, HA = 2.25 mm

Mid. Pennsylvanian Paradox Fm., San Juan Co., Utah

These gypsum crystals are typical of replacement evaporites; they contain abundant carbonate inclusions of the original matrix. The lenticular- shaped crystal is a cross-section through a discoidal gypsum (selenite) crystal; the other is a oblique longitudinal cut. During thin section preparation, care must be taken not to lose the gypsum through prolonged water-based cutting and grinding.

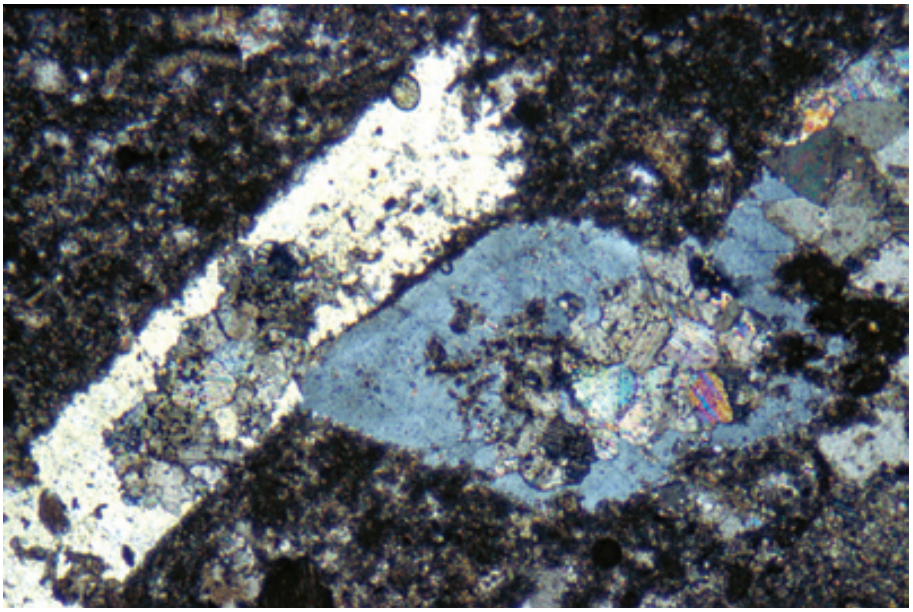

XPL, HA = 2.25 mm

Recent sediment, Shark Bay, Australia

These modern gypsum crystals are from sediments in the Wooramel deltaic-hypersaline tidal complex. The crystals form near the sediment-water interface and poikilotopically encase ooids and skeletal grains. Note that most of the grains appear to be floating in the gypsum crystals, perhaps due to slight displacement of grains during crystal growth. Photograph courtesy of Graham R. Davies.

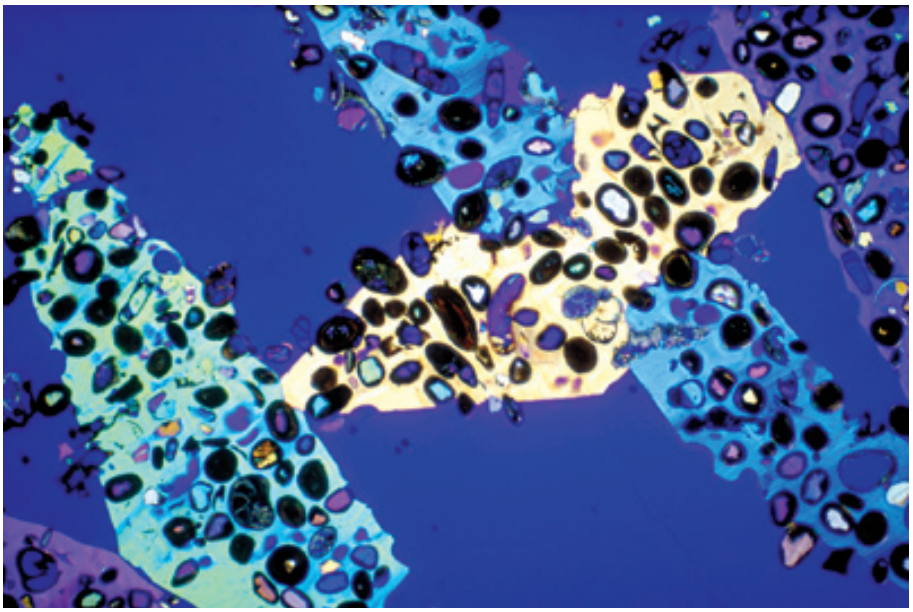

PXPL, BSE, HA = 6.3 mm

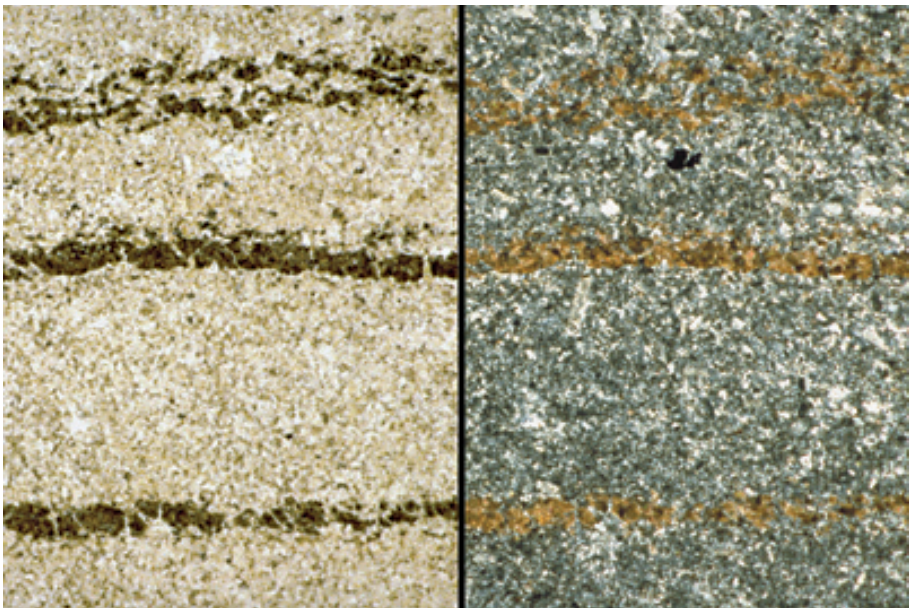

Up. Permian (Ochoan) Castile Fm., Eddy Co., New Mexico

Laminated or varved gypsum deposits, such as this example from the famous Castile Fm., may represent deposition in relatively deep water within a basin with restricted seawater inflow. The thick, light-colored layers (in plane-polarized light) consist of gypsum interpreted to have precipitated during summer seasons from highly evaporative waters; the thin, dark brown layers are composed of calcite and organic matter inferred to have precipitated during cooler winter conditions. The entire Castile deposit contains approximately 260,000 of these varve couplets (Anderson, 1972).

PPL/XPL, HA = 4.9 mm each

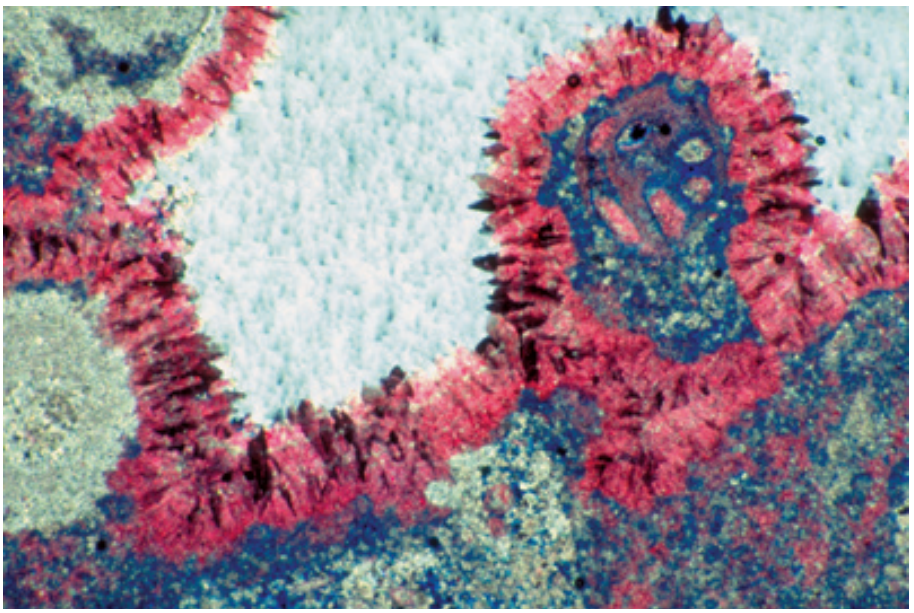

Up. Permian (Guadalupian) Capitan Fm., subsurface, Eddy Co., New Mexico

This partially-dolomitized limestone block, part of the upper fore-reef talus slope-debris of the Capitan reef, was cemented by early marine, fibrous to bladed calcite (stained red). The gypsum cements (grayish white) filling the remnant pore space were precipitated from brines percolating downward from overlying shelfal evaporites. The porosity originally may have been filled by anhydrite, but during late-stage uplift, the anhydrite rehydrated to form gypsum.

XPL, AS, BSE, HA = 4.5 mm

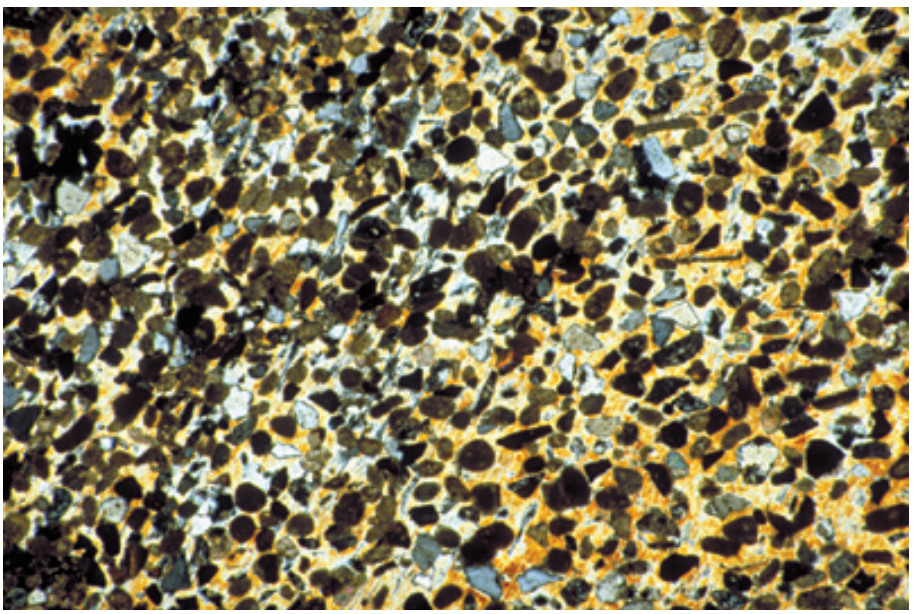

Holocene sediment, Abu Dhabi, United Arab Emirates

Calcareous sandstones on the supratidal sabkha in Abu Dhabi are widely cemented by poikilitic gypsum. In this view, the yellow birefringent cement is a single crystal of gypsum; the birefringence is slightly high due to the greater-than-normal thickness of this thin section. The gypsum cement is derived from groundwater dissolution of synsedimentary diagenetic gypsum and anhydrite nodules and reprecipitation as coarse cements. The original evaporites formed as a result of storm washover and evaporation on the low-relief sabkha flats.

XPL, HA = 4.75 mm

Lo. Cretaceous Ferry Lake Anhydrite (?), subsurface, Henderson Co., Texas

Fine-grained "chicken-wire" anhydrite here has replaced and displaced micritic sediment. As anhydrite nodules grow and coalesce, remnants of the original carbonate material is compressed into thin zones that separate the nodules. The entire fabric looks very similar to chicken wire, hence the name. The original carbonate material in this slide is extensively disrupted because of the growth of the anhydrite nodules. Like halite, anhydrite can easily be lost from thin sections unless they are properly prepared.

XPL, HA = 3.42 mm

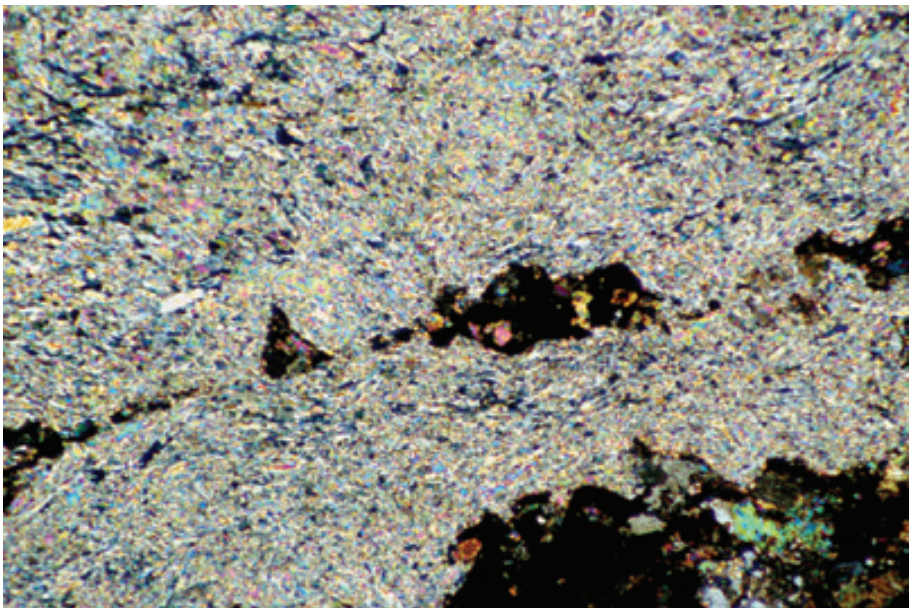

Up. Permian (Guadalupian) Grayburg-Up. San Andres Fms., 3,061 ft (933 m) depth, Crane Co., Texas

These dolomitized shallow-water deposits had most of their porosity occluded by anhydrite. Anhydrite is easy to distinguish from gypsum because its birefringence is high first order; whereas, gypsum's birefringence is low first order (maximum gray-white). Based on the uniformity of shapes and the faint traces of concentric laminations, most of the grains in this deposit are inferred to have been ooids originally, but they now are best termed peloids. Photograph courtesy of Susan Longacre.

XPL, HA = 0.95 mm

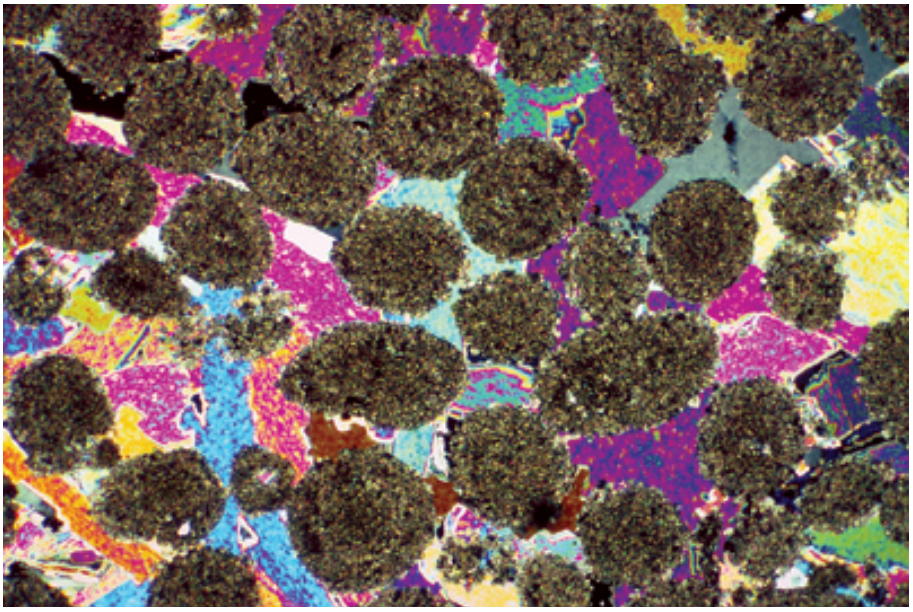

Lo. Cretaceous Ferry Lake Fm., subsurface, Henderson Co., Texas

In addition to cementing carbonate rocks, anhydrite also replaces grains and bioclasts. In this view, large blocky crystals of anhydrite are replacements of serpulid worm tubes, whereas bladed crystals fill the remnant porosity within the interior of the worm tubes.

PPL/XPL, HA = 4 mm each

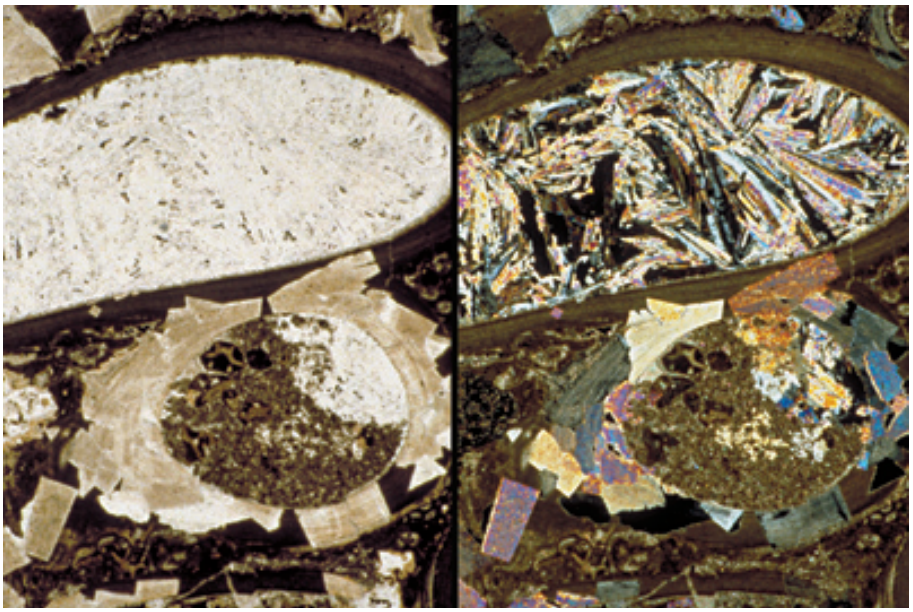

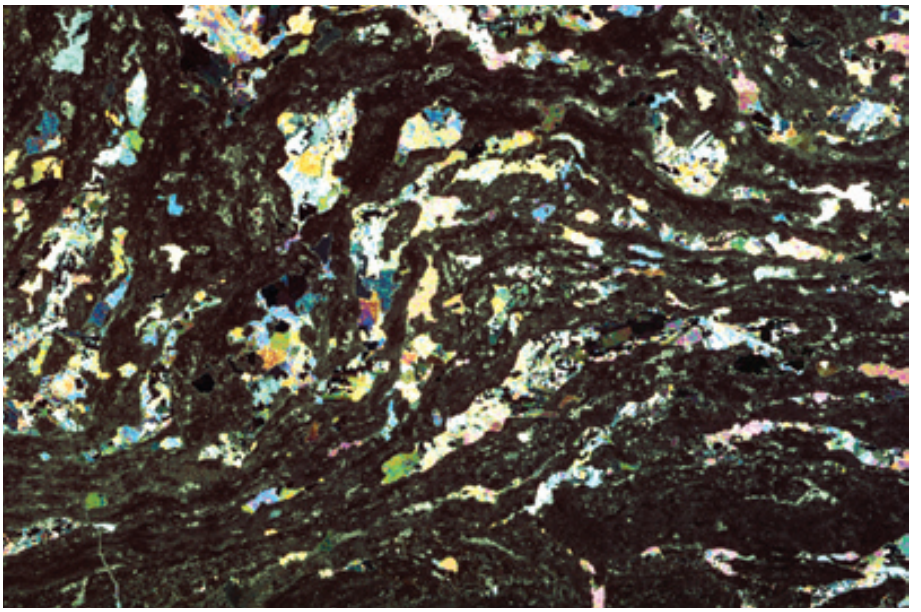

Up. Permian (Guadalupian) Yates-Tansill Fms., subsurface, Eddy Co., New Mexico

This algally laminated, tidal-flat dolomicrite had extensive fenestral porosity that has been completely filled with anhydrite. Anhydrite cements are commonly found as early porosity-filling agents in arid-region, coastal, evaporitic carbonates, so much so that effective exploration commonly is focussed on finding areas where such cements either did not form, or were later leached.

XPL, HA = 16 mm

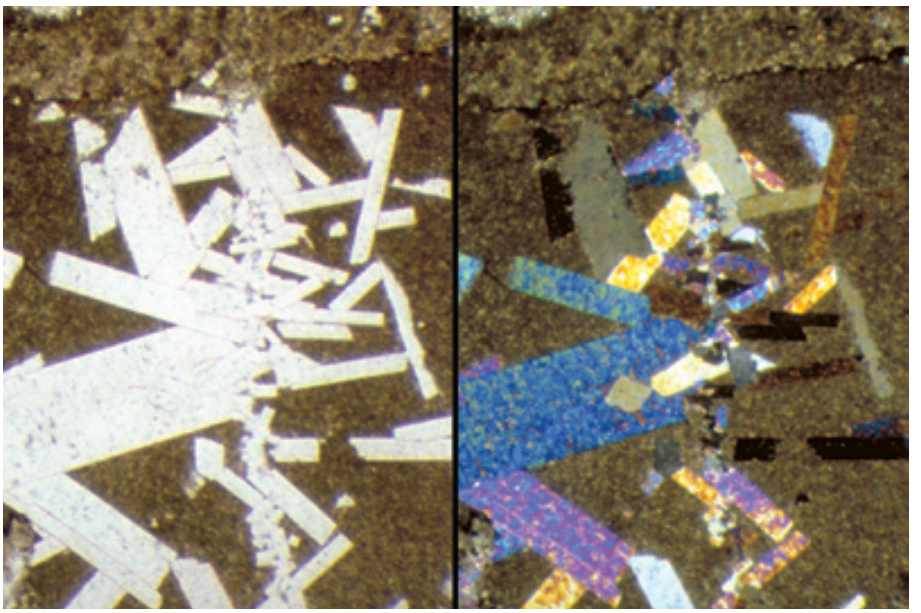

Up. Permian (Kazanian?) Zechstein Ca2, subsurface, Poland

In this example, anhydrite has partially replaced a carbonate intraclast. The calcium sulfate-rich fluids migrated along a small fracture and replaced the surrounding sediment. Note the well-formed tabular to bladed crystals. Despite being replacements, the crystals do not contain obvious inclusions of the precursor sediment.

PPL/XPL, HA = 2 mm each

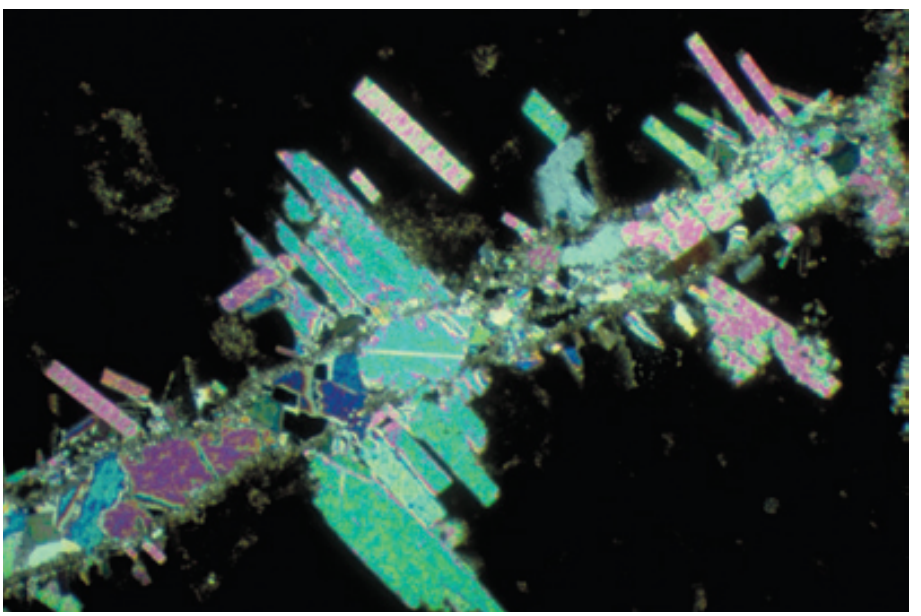

Up. Permian (Kazanian?) Zechstein Ca2, subsurface, Poland

This view, from the same sample as the previous photomicrograph, shows anhydrite crystals that fill a fracture and replace the adjacent micritic carbonate. Prior to the formation of anhydrite, fluids migrating through the open fracture precipitated a lining of dolomite along the fracture wall. This dolomite was more resistant to replacement than the surrounding calcitic micrite.

XPL, HA = 4.1 mm

Up. Jurassic (Oxfordian) Up. Smackover Fm., subsurface, Gulf Coast, USA

An example of late-stage anhydrite replacement of a well-compacted ooid grainstone (stained red). It shows the preservation of some of the original carbonate rock fabric within the large anhydrite crystal (yellow). The preserved fabric remains visible mainly through the presence of undigested remnants of carbonate as inclusions within the anhydrite. Photograph courtesy of Clyde H. Moore.

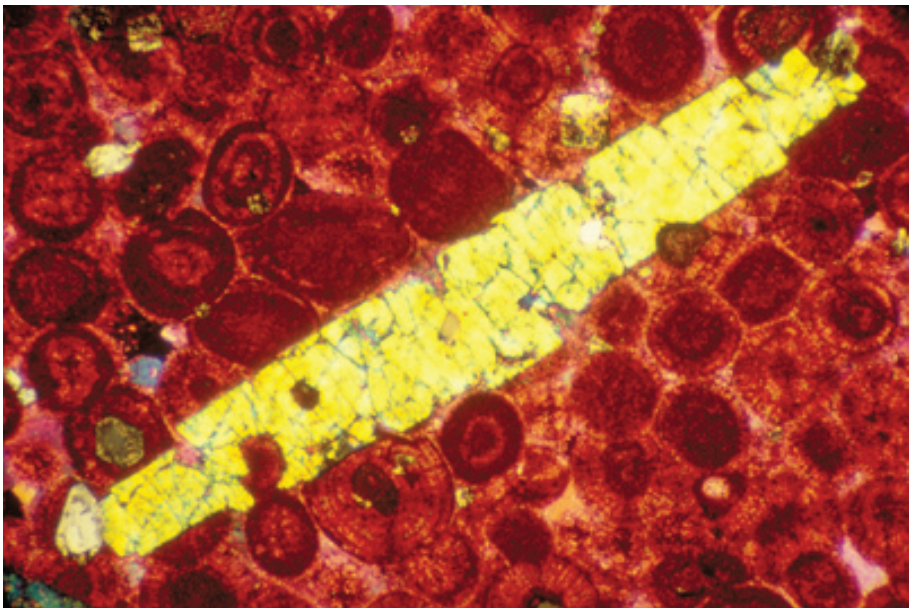

XPL, AS, HA = ~3 mm

Up. Permian (Guadalupian) Grayburg-Up. San Andres Fms, 3,017 ft (920 m) depth, Crane Co., Texas

This complex fabric was produced by early dolomitization of carbonate allochems followed by leaching of the less stable calcitic material. This secondary porosity later was filled by large poikilotopic crystals of anhydrite, probably while still in a near-surface diagenetic setting. Photograph courtesy of Susan Longacre.

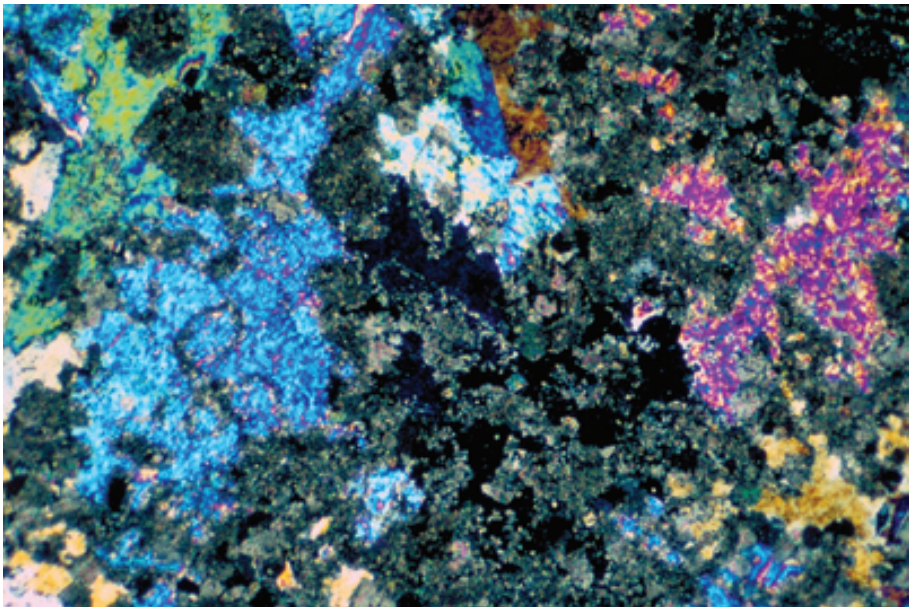

XPL, HA = 0.7 mm

Devonian Keg River-Muskeg Fm., subsurface, Alberta, Canada

Dolomitization and anhydrite replacement often are temporally associated. Both minerals can be precipitated at relatively low temperatures from refluxing hypersaline fluids that formed in evaporative coastal marine settings, or at elevated temperatures from deep-seated brines. Here, dolomite crystals "float" in anhydrite within an early-diagenetic replacement nodule. In cases like this, it can be very difficult to determine unequivocally which mineral precipitated first.

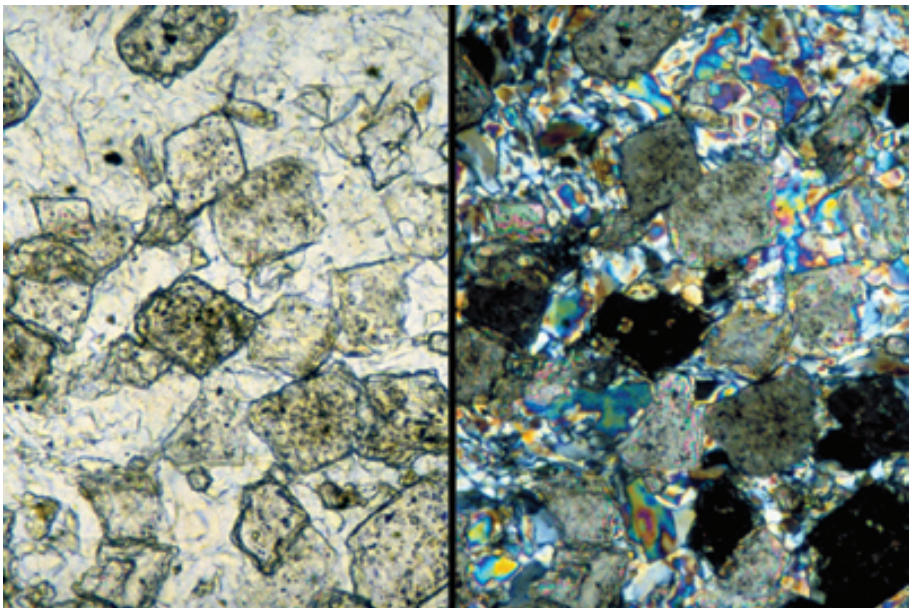

PPL/XPL, HA = 0.32 mm each

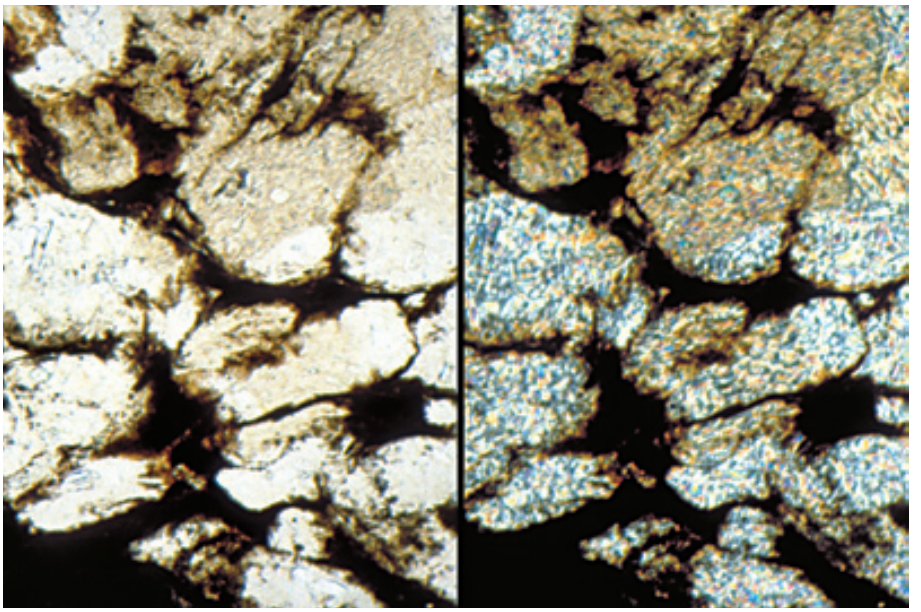

Lo. Permian (Kungurian) Irenskaya/ Nevolinskaya Suite, Perm Region, Russia

During diagenesis, anhydrite and gypsum can transform from one to the other by the gain or loss of bound water. This can occur multiple times during a rock's diagenetic history, through climate cycles and various stages of burial and uplift. Repeated gypsum-anhydrite transitions can even be seen in modern surficial sabkha sediments in the Persian Gulf region. The nodules making up the "chicken-wire" fabric in this view are composed mainly of gypsum, but originally they were probably anhydrite (based on retained anhydrite inclusions).

PPL/XPL, HA = 1.2 mm each

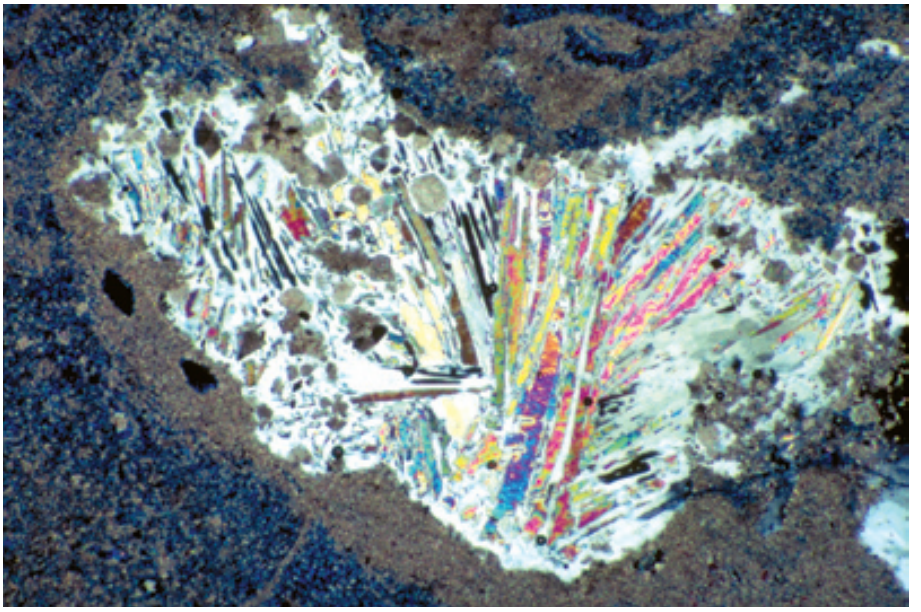

Up. Permian (Guadalupian) Capitan Fm., subsurface Eddy Co., New Mexico

Large, bladed anhydrite fills pores in this dolomitized fore-reef talus from the Capitan reef complex. Hypersaline brines from penecontemporaneous or slightly younger evaporitic shelf settings gravitationally refluxed through the sediments, first dolomitizing and then cementing them with anhydrite. During telogenetic (uplift related) diagenesis, anhydrite (high birefringence) crystals were partially converted to gypsum (low birefringence).

XPL, BSE, HA = 3.9 mm

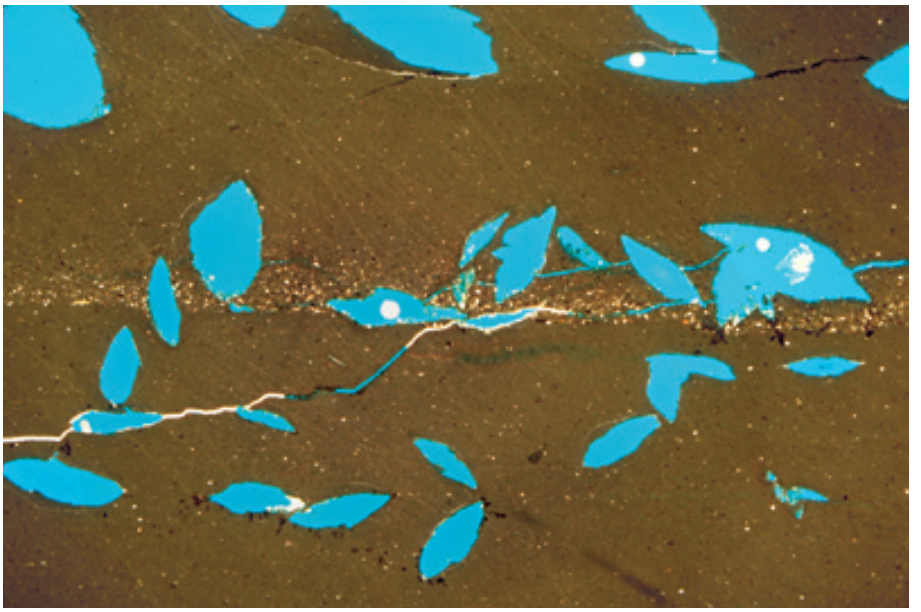

Permian (Ufimian) Up. Solikamskaya Suite, Perm Region, Russia

In this peritidal carbonate deposit, the evaporite minerals have been completely leached to form distinctive moldic porosity. The well formed, lenticular crystal molds indicate that the precursor evaporite mineral was probably gypsum.

PPL, BSE, HA = 20 mm

Up. Permian (Ufimian) Up. Solikamskaya Suite, Perm Region, Russia

This example of evapomoldic porosity shows partially leached evaporite nodules in a dolomitic carbonate rock. The original displacive evaporite nodules (probably anhydrite) were grown syndepositionally in soft carbonate muds. Late-stage uplift and meteoric exposure led to dissolution of anhydrite and development of moldic porosity. The resultant "cellular" dolomite (or rauhwacke) is characteristic of evaporite dissolution.

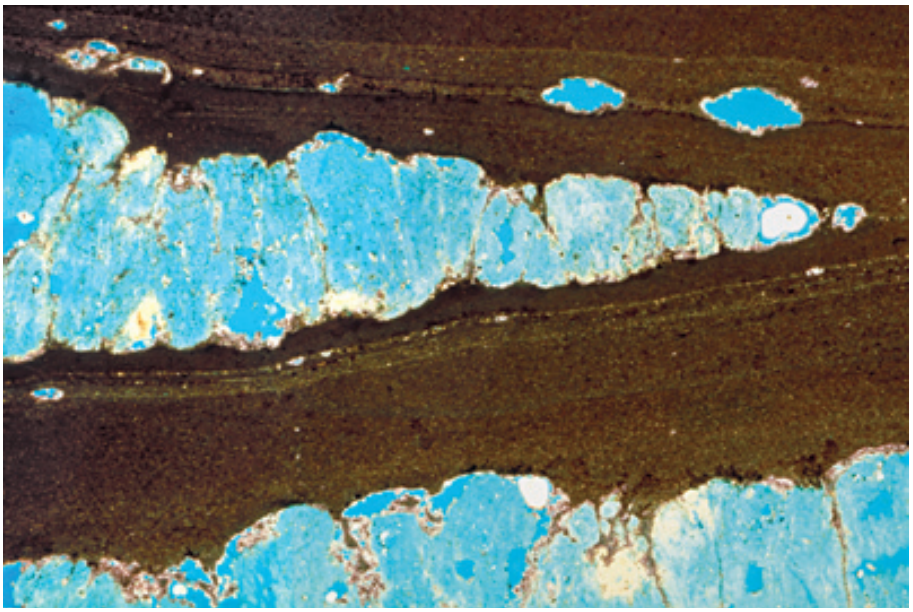

PPL, BSE, HA = 16 mm

Up. Permian (Guadalupian) Park City Fm., Ervay Mbr., Hot Springs Co., Wyoming

Another common diagenetic fabric in carbonate-evaporite sequences is the calcitization of evaporite minerals. Calcitization occurs when diagenetic fluids that are undersaturated in sulfate dissolve the evaporites, causing pore fluids to become saturated with calcium and eventually precipitate calcite. Here, supratidal dolomitic mudstones were partially replaced and/or displaced by enterolithic gypsum (the white, intestinal-looking material). The gypsum was later replaced by calcite. In this example, both the internal and external morphologies are well preserved.

PPL, HA = 1.5 mm

Mississippian (Tournaisian) Arroyo Peñasco Gp., Espiritu Santo Fm., Taos Co., New Mexico

This cluster of former gypsum crystals in dolomitized sabkha sediments was replaced by calcite. The calcite crystals contain abundant inclusions of the carbonate matrix indicating that replacement proceeded as thin-film dissolution/reprecipitation not as a dissolution/void fill. In the latter case, the inclusions would have formed geopetal fills.

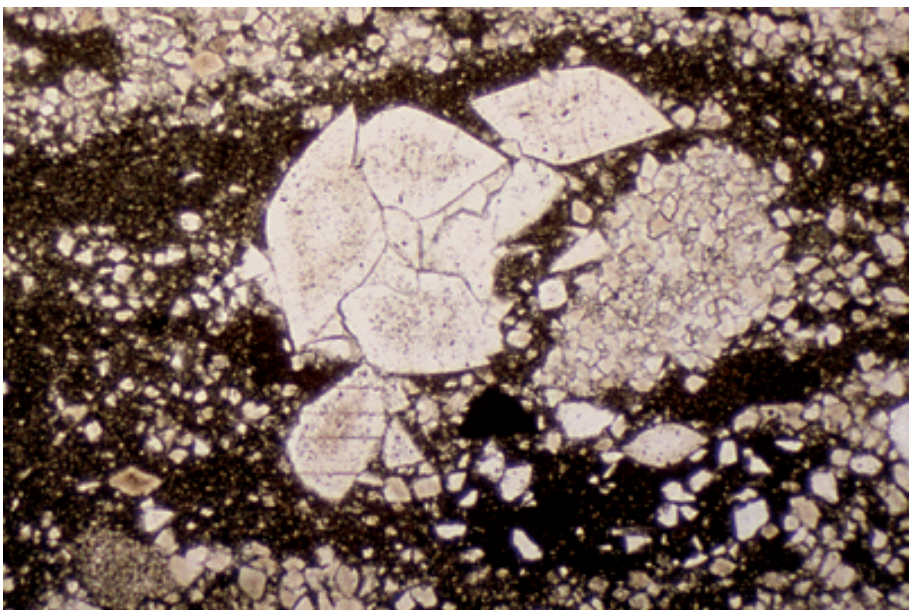

PPL, HA = 1.1 mm

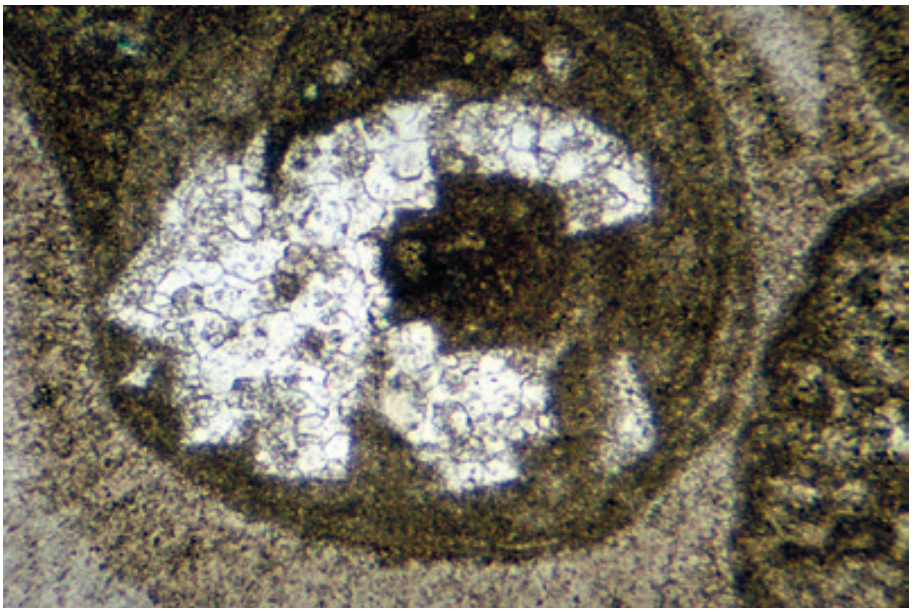

Up. Permian (Guadalupian) Tansill Fm. or Up. Yates Fm., Eddy Co., New Mexico

Early-diagenetic anhydrite replaced an earlier formed pisoid by the seaward movement of saline brines through this near-back-reef limestone. During telogenetic (uplift-related) diagenesis, the influx of meteoric waters resulted in the anhydrite being replaced by calcite. The anhydrite intermediary is recognizable by the crystal outlines and the rare presence of anhydrite inclusions in replacement phases.

PPL, HA = 2.0 mm

Up. Permian (Ufimian) Up. Solikamskaya Suite, Perm Region, Russia

The white crystals present in the coarsely crystalline, cloudy calcite pseudospar are calcitized gypsum crystals. These crystals preserve the lenticular crystal shapes (and possible twins) of the original gypsum. The cloudy calcite pseudospar was also probably produced by evaporite replacement.

PPL, BSE, HA = 5.1 mm

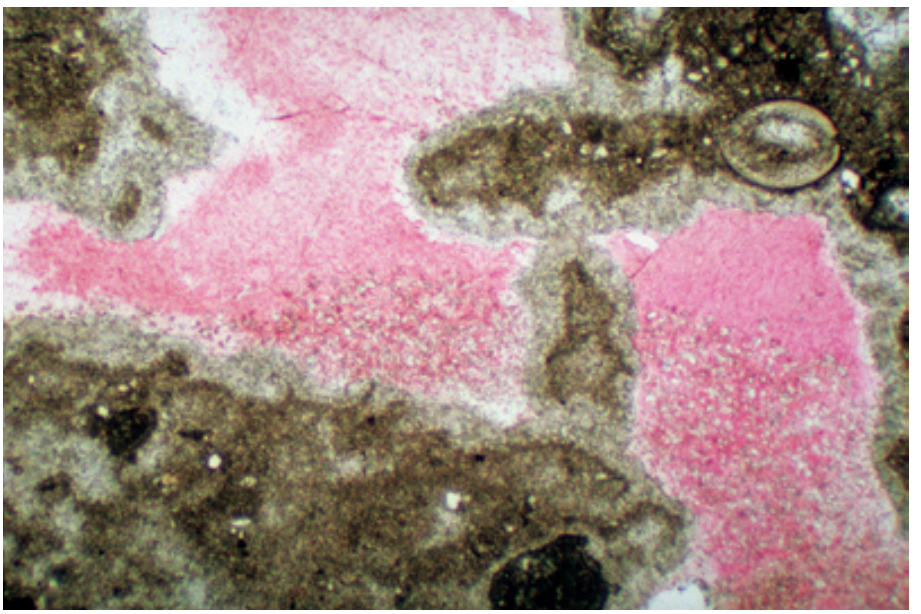

Up. Permian (Guadalupian) Yates Fm., Eddy Co., New Mexico

In this example, an evaporite nodule was "replaced" by calcite. The cloudy, geopetal fabric within the lower half of the calcite cement consists of loosely packed kaolinite (or dickite) "books" that fell to the bottom of a cavity formed by the dissolution of gypsum or anhydrite and then were engulfed by calcite cement. Because of the geopetal fabric and the lack of evaporite inclusions in the calcite, these evaporite nodules clearly went through a period of being open voids prior to calcite infilling. This, therefore, is an example of solution and fill, not direct replacive calcitization of evaporites.

PPL, AFeS, HA = 4.0 mm

Up. Permian (Kazanian?) Wegener Halvø Fm., Jameson Land, East Greenland

Calcitization preserved the primary laminar fabric of these bedded evaporites that were similar to the Castile evaporites shown earlier in this section. The pale pink-stained layers were probably original carbonate interlayers that were stabilized and cemented prior to evaporite dissolution. The evaporite laminae were then dissolved and the voids were later substantially filled, probably during early burial, with zoned, moderately ferroan calcite spar.

PPL, AFeS, BSE, HA = 10 mm

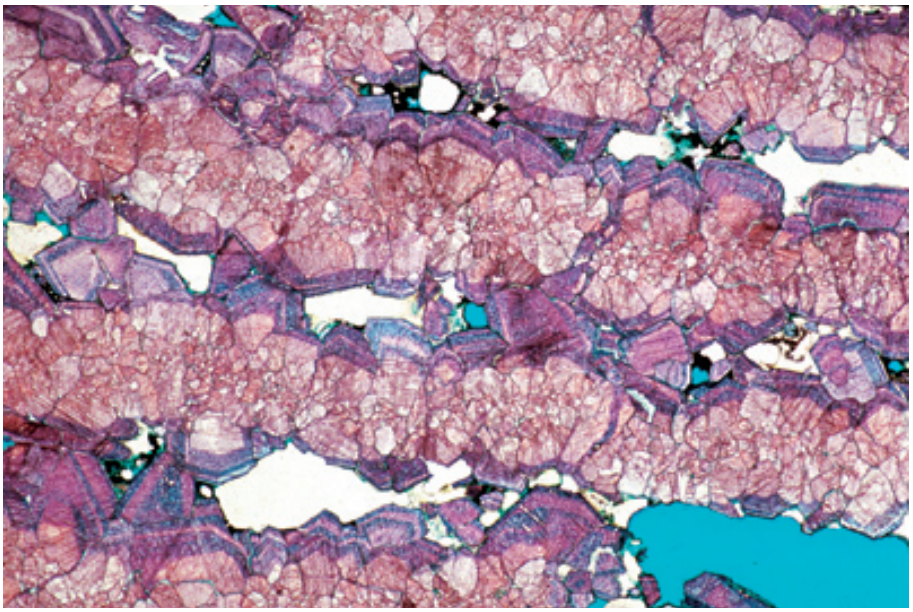

Mississippian (Tournaisian) Arroyo Peñasco Gp., Espiritu Santo Fm., Taos Co., New Mexico

Cathodoluminescence petrography can be an important tool for examining calcitized evaporites. It is especially useful in clarifying how replacement proceeded — through thin-film dissolution/precipitation or dissolution/void fill. In this view, the coarsely crystalline pseudospar, which has no obvious primary fabrics under plane- and crossed-polarized light, shows fine-scale luminescent zoning that pseudomorphs gypsum crystals. This would not be the case if diagenesis had proceeded through wholesale gypsum dissolution with later void fill.

CL, HA = 1.6 mm

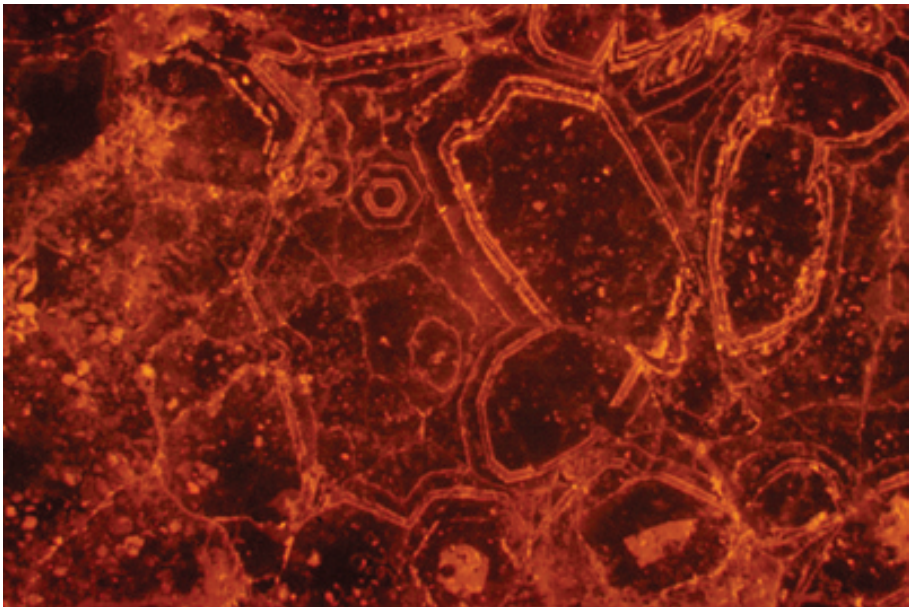

Modern sediment, Salina Ometepec, Baja California, Mexico

It can be difficult to observe halite in thin section, because halite is so soluble that it is commonly destroyed during thin-section preparation. If halite is suspected to be in the sample, the section should be prepared in oil instead of water. In this view, a porous halite chevron is visible. The cubic crystal form and inclusion zoning are clearly visible. Photograph courtesy of Susan Hovorka. Hand sample from C. Robertson Handford.

PXPL, BSE, HA = 4.3 mm

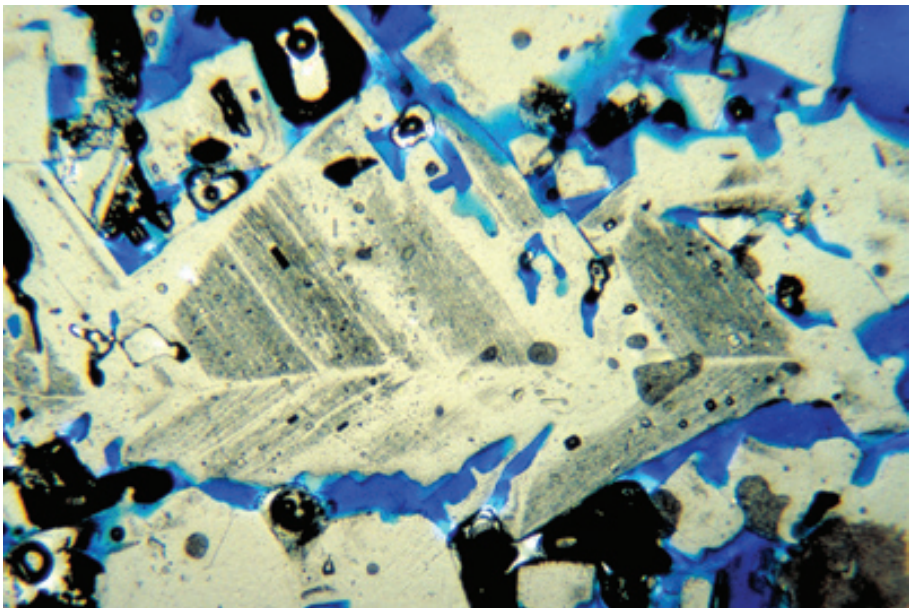

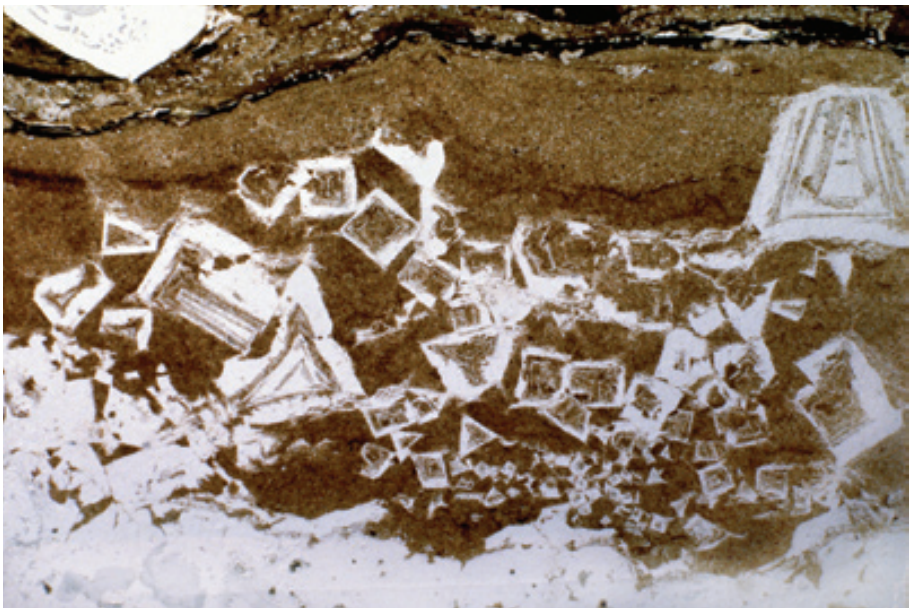

Up. Permian (Guadalupian) San Andres Fm., Randall Co., Texas

In this view, sand-sized halite crystals grew in ponds and were blown out onto the sabkha surface. As the halite crystals were buried, the hoppers continued to grow displacively in the sediment. Along the upper surface, probably related to storm events, the halite hoppers were syndepositionally dissolved. Photograph courtesy of Susan Hovorka.

PPL, HA = 3.5 mm

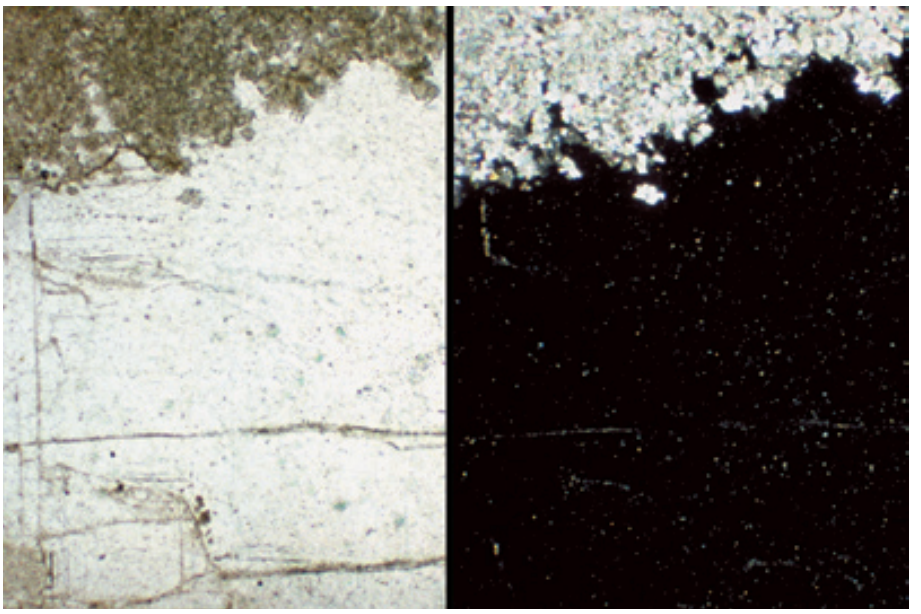

Devonian Keg River Fm. equivalent, subsurface, Alberta, Canada

Here, halite cement fills former porosity in a stromatolitic carbonate rock. Petrographically, halite is isotropic, has cubic cleavage and crystal form, and is colorless to pale gray. Halite can be difficult to see, but it is often recognizable, despite its isotropism, because of prominent cubic cleavage and abundant inclusions, both visible here.

PPL/XPL, HA = 2.1 mm each

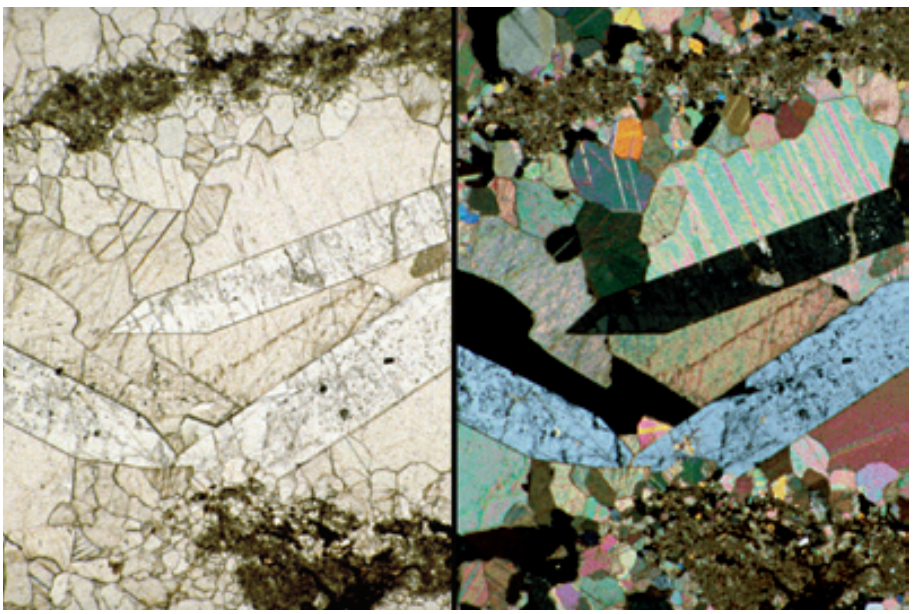

Up. Permian (Kazanian?) Karstryggen Fm., Jameson Land, East Greenland

Celestite and calcite have replaced an evaporite nodule in peritidal carbonates in this deposit. Celestite ($SrSO_4$) is best identified using x-ray diffraction, because it is so similar in birefringence to gypsum, a far more common mineral. The strongly elongate crystal morphology, however, is most common in celestite (and barite).

PPL/XPL, HA = 2.5 mm each

Up. Permian (Kazanian?) Karstryggen Fm., Jameson Land, East Greenland

Another view of a celestite- and calcite-replaced evaporite nodule. Note the abundant calcium sulfate inclusions within the very elongate celestite crystals.

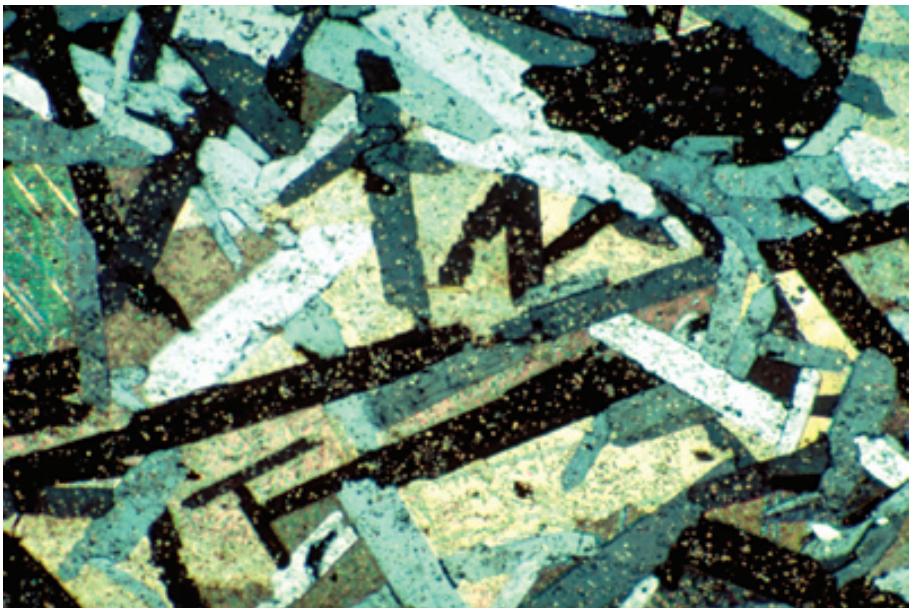

XPL, HA = 3.0 mm

Lo. Cretaceous (Up. Aptian) Marnes Bleues Fm., Vocontien Trough, Haute Provence, France

This early diagenetic nodule from organic-rich basinal shales is composed of a felted mass of barite crystals. Like celestite, barite ($BaSO_4$) can be easily confused with gypsum. Barite is common in anoxic marine sediments, and the occurrence of barite layers may mark changes in salinity and/or interruptions in sedimentation.

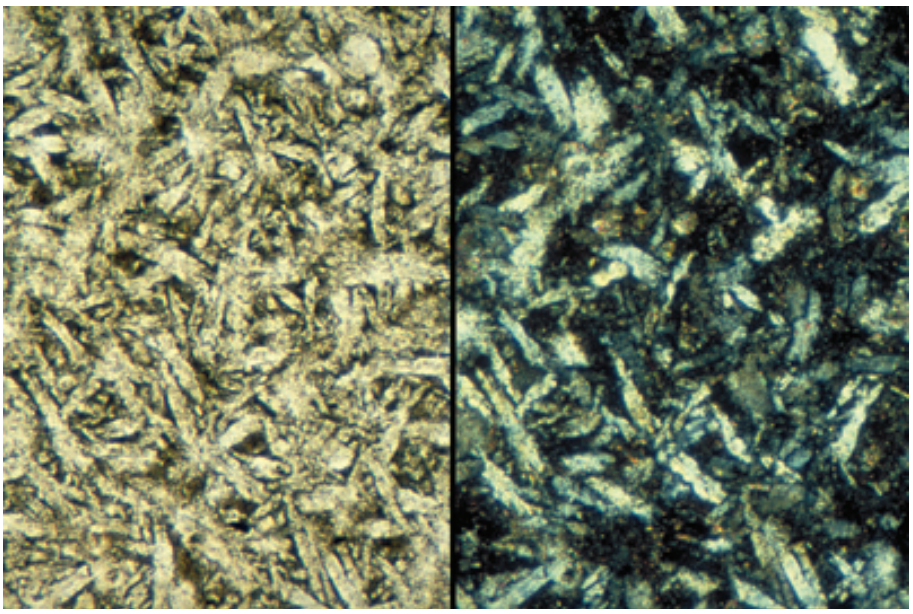

PPL/XPL, HA = 1.0 mm each

Up. Permian (Kazanian?) Wegener Halvø Fm., Jameson Land, East Greenland

Barite also is commonly found as a late-diagenetic precipitate, as in the case of these large, bladed crystals associated with ferroan calcite. Both the barite crystals and the coeval or slightly younger calcites were probably precipitated from hydrothermal pore fluids. Note how similar celestite (top picture, this page) and barite crystals are to each other. Because of the solid solution series that exists between the two minerals, petrographic determination can be difficult without the aid of chemical or x-ray analyses.

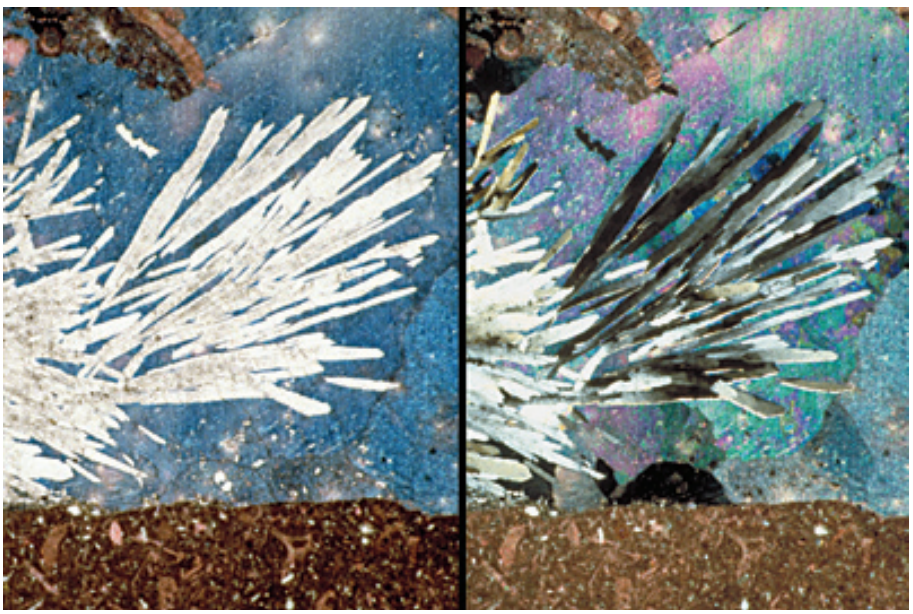

PPL/XPL, AFeS, HA = 4.5 mm each

Cited References and Additional Information Sources

Anderson, R. Y., W. E. Dean, D. W. Kirkland, and H. I. Snider, 1972, Permian Castile varved evaporite sequence, west Texas and New Mexico: Geological Society of America Bulletin, v. 83, p. 59-86.

Baker, P. A., and S. H. Bloomer, 1988, The origin of celestite in deep-sea carbonate sediments: Geochimica et Cosmochimica Acta, v. 52, p. 335-339.

Braithwaite, P., 1971, Textures of calcium sulfate cement in carbonates associated with evaporites, *in* O. P. Bricker, ed., Carbonate Cements: Studies in Geology No. 19: Baltimore, MD, Johns Hopkins Press, p. 352-358.

Brodtkorb, M. K., de, V. Ramos, M. Barbieri, and S. Ametrano, 1982, The evaporitic celestite-barite deposits of Neuquen, Argentina: Mineralium Deposita (Berlin), v. 17, p. 423-436.

Butler, G. P., 1969, Modern evaporite deposition and geochemistry of coexisting brines, the sabkha, Trucial Coast, Arabian Gulf: Journal of Sedimentary Petrology, v. 39, p. 70-89.

Carlson, E. H., 1987, Celestite replacements of evaporites in the Salina Group: Sedimentary Geology, v. 54, p. 93-112.

Church, T. M., 1979, Marine barite, in R. G. Burns, ed., Marine Minerals: Washington, D.C., Mineralogical Society of America Short Course Notes, Vol. 6, p. 175-209.

Clark, D. N., and D. J. Shearman, 1980, Replacement anhydrite in limestones and the recognition of moulds and pseudomorphs: a review: Revista del Instituto de Investigaciones Geologicas de la Diputación de Barcelona (Universidad de Barcelona), v. 34, p. 161-186.

Davies, G. R., 1977, Carbonate-anhydrite facies relationships, Otto Fiord Formation (Mississippian-Pennsylvanian), Canadian Arctic Archipelago: AAPG Bulletin, v. 61, p. 1929-1949.

Decima, A., J. A. McKenzie, and B. C. Schreiber, 1988, The origin of "evaporative" limestones: an example from the Messinian of Sicily (Italy): Journal of Sedimentary Petrology, v. 58, p. 256-272.

Dejonghe, L., 1990, The sedimentary structures of barite: examples from the Chaudfontaine ore deposit, Belgium: Sedimentology, v. 37, p. 303-323.

Dworkin, S. I., and L. S. Land, 1994, Petrographic and geochemical constraints on the formation and diagenesis of anhydrite cements, Smackover sandstones, Gulf of Mexico: Journal of Sedimentary Research, v. A64, p. 339-348.

Evans, G., and D. J. Shearman, 1964, Recent celestite from the sediments of the Trucial Coast of the Persian Gulf: Nature, v. 202, p. 385-386.

Hardie, L. A., T. K. Lowenstein, and R. J. Spencer, 1985, The problem in distinguishing between primary and secondary features in evaporites, *in* B. C. Schreiber, and H. L. Harner, eds., Sixth International Symposium on Salt, v. 1: Alexandria, VA, Salt Institute, p. 11-40.

Harwood, G. M., 1980, Calcitized anhydrite and associated sulphides in the English Zechstein First Cycle Carbonate (EZ1 Ca), *in* H. Füchtbauer, and T. M. Peryt, eds., The Zechstein Basin with Emphasis on Carbonate Sequences: Contributions to Sedimentology 9: Stuttgart, E. Schweizerbart'sche Verlagsbuchhandlung (Nägele u. Obermiller), p. 61-72.

Harwood, G. M., 1983, The application of cathodoluminescence in relative dating of barite mineralization in the Lower Magnesian Limestone (Upper Permian), United Kingdom: Economic Geology, v. 78, p. 1022-1027.

Holliday, D. W., 1970, The petrology of secondary gypsum rocks: a review: Journal of Sedimentary Petrology, v. 40, p. 734-744.

Holser, W. T., 1979, Mineralogy of evaporites, *in* R. G. Burns, ed., Marine Minerals: Washington, D.C., Mineralogical Society of America Short Course Notes, Vol. 6, p. 211-235.

Hovorka, S. D., 1992, Halite pseudomorphs after gypsum in bedded anhydrite — clue to gypsum-anhydrite relationships: Journal of Sedimentary Petrology, v. 62, p. 1098-1111.

Kendall, A. C., 1992, Evaporites, in R. G. Walker, and N. P. James, eds., Facies Models: Response to Sea Level Change: St. John's, Newfoundland, Geological Association of Canada, p. 375-409.

Kirkland, D. W., and R. Evans, eds., 1973, Marine Evaporites, Origin, Diagenesis and Geochemistry: Stroudsburg, PA, Dowden, Hutchinson and Ross, 426 p.

Machel, H. G., 1986, Early lithification, dolomitization, and anhydritization of Upper Devonian Nisku buildups, subsurface of Alberta, Canada, *in* J. H. Schroeder, and B. H. Purser, eds., Reef Diagenesis: New York, Springer-Verlag, p. 336-356.

Machel, H. G., 1993, Anhydrite nodules formed during deep burial: Journal of Sedimentary Petrology, v. 63, p. 659-662.

Murray, R. C., 1964, Origin and diagenesis of gypsum and anhydrite: Journal of Sedimentary Petrology, v. 34, p. 512-523.

Müller, G., and H. Puchelt, 1961, Die bildung von Coelestin ($SrSO_4$) aus Meerwasser: Naturwissenschaften, v. 48, p. 301-302.

North, N. A., 1974, Pressure dependence of $SrSO_4$ solubility: Geochimica et Cosmochimica Acta, v. 38, p. 1075-1081.

Olaussen, S., 1981, Formation of celestite in the Wenlock, Oslo region Norway — evidence for evaporitic depositional environments: Journal of Sedimentary Petrology, v. 51, p. 37-46.

Parfenov, S. I., 1967, Characteristics of gypsification of anhydrites (in Russian): Litologiya i Poleznye Iskopaemye, v. 3, p. 117-127.

Pierre, C., and J. M. Rouchy, 1988, Carbonate replacements after sulfate evaporites in the middle Miocene of Egypt: Journal of Sedimentary Petrology, v. 58, p. 446-456.

Richter-Bernburg, G., 1985, Zechstein Anhydrit — Fazies und Genese: Geologisches Jahrbuch, v. A85, p. 3-82.

Schenk, C. J., and R. W. Richardson, 1985, Recognition of interstitial anhydrite dissolution: a cause of secondary porosity, San Andres Limestone, New Mexico and upper Minnelusa Formation, Wyoming: AAPG Bulletin, v. 69, p. 1064-1076.

Scholle, P. A., L. Stemmerik, and O. Harpøth, 1990, Origin of major karst-associated celestite mineralization in Karstryggen, central East Greenland: Journal of Sedimentary Petrology, v. 60, p. 397-410.

Schreiber, B. C., ed., 1988, Evaporites and Hydrocarbons: New York, Columbia University Press, 475 p.

Schreiber, B. C., and M. El Tabakh, 2000, Deposition and early alteration of evaporites: Sedimentology, v. 47, p. 215-239.

Schreiber, B. C., and G. M. Friedman, 1976, Depositional environments of upper Miocene (Messinian) evaporites of Sicily as determined from analysis of intercalated carbonates: Sedimentology, v. 23, p. 255-270.

Shearman, D. J., 1985, Syndepositional and late diagenetic alteration of primary gypsum to anhydrite, *in* B. C. Schreiber, and H. L. Harner, eds., Sixth International Symposium on Salt, v. 1: Alexandria, VA, Salt Institute, p. 41-50.

Shearman, D. J., and J. G. Fuller, 1969, Anhydrite diagenesis, calcitization, and organic laminites, Winnipegosis Formation, Middle Devonian, Saskatchewan: Bulletin of Canadian Petroleum Geology, v. 17, p. 496-525.

Spencer, R. J., and T. K. Lowenstein, 1990, Evaporites, *in* I. A. McIlreath, and D. W. Morrow, eds., Diagenesis: Geoscience Canada Reprint Series 4: Toronto, Geological Association of Canada, p. 141-163.

Warren, J. K., 1989, Evaporite Sedimentology: Importance in Hydrocarbon Accumulation: Englewood Cliffs, NJ, Prentice Hall Advanced Reference Series, 285 p.

Facing Page: Top - Complex quartz and dolomite cementation in a deep-water hydrocarbon reservoir Mid-Cretaceous Tamabra Ls., subsurface, Poza Rica trend, Veracruz, Mexico. Photograph courtesy of Paul Enos. PPL, GP, HA = 2.4 mm.
Bottom: Botryoidal chalcedonic quartz infilling the central cavity of a calcareous sponge. Up. Permian Cherry Canyon Fm., Culberson Co., Texas. XPL, HA = 5.7 mm.

CARBONATE DIAGENESIS

SILICA CEMENTATION AND REPLACEMENT

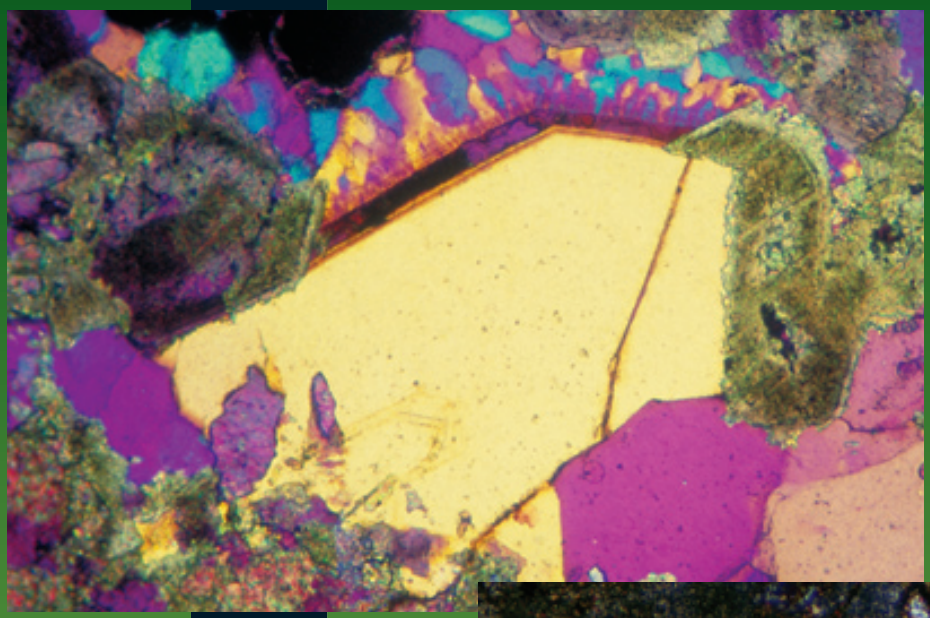

CHAPTER 28

SILICA CEMENTATION AND REPLACEMENT

Introduction:

Silica, a general term used for a variety of crystal forms or morphologies of SiO_2, is a widespread diagenetic mineral in carbonate rocks. Silica may occur as cement or it may be found as a replacement of original or diagenetically altered sediment. Silica typically replaces or infills carbonate minerals, evaporites and organic material (e.g., petrified wood).

The major source of silica for diagenesis is biogenic opal; therefore, silica is especially prevalent in deep-marine sediments from active upwelling zones and shallower-water carbonates from nutrient-rich carbonate shelves. Sponge spicules, diatoms and radiolarians are the most common biogenic contributors and are diagenetically unstable when compared to siliciclastic grains. Other, generally less significant sources of silica in carbonate rocks include volcanic ash, by-products of chemical weathering in soil zones (silcretes), and hydrothermal fluids. Some bedded cherts from saline lakes may be related to hydrous sodium silicate precursors (e.g. Eugster, 1967).

Except for silcrete formation or hydrothermal alteration, silica diagenesis is rarely a very early- or a very late-stage diagenetic event in carbonate rocks. Rather, it is most typically a product of burial diagenesis. This is due to the timing of the conversion of biogenic opal-A, first to opal-CT lepispheres, and then to stable microquartz or megaquartz. These silica reactions are dependent on temperature (and/or burial depth) and time. In pelagic deposits (away from hydrothermal input), opal-A to opal-CT conversion begins at 20-30°C and may take 10 million years to go to completion; opal-A is rarely found in sediments older than 20 Ma (Hesse, 1990). The conversion of opal-CT to quartz most likely starts at temperatures of ~ 50°C and depths of 500 m, but continues to higher temperatures. Opal-CT is not found in sediments older 144 Ma and chert is relatively scarce in young Cenozoic deposits.

Major Diagenetic Fabrics:

Amorphous silica— also known as opal; isotropic; high negative relief; colorless to gray or brown; normally contains irregular cracks or fractures; occurs as cements, nodules or replacements (especially wood).

Equigranular quartz — equant crystals; in polarized light, the maximum birefringence should be first-order white to pale straw-yellow (unless the thin section is thicker than normal); larger individual crystals are normally hexagonal and may be doubly terminated; no cleavage; normally colorless, but may contain inclusions. Fabric is termed cryptocrystalline (chert) when crystals are <5 µm, microcrystalline for crystals 5-20 µm, and megaquartz for crystals >20 µm. Quartz may occur as individual crystals or in large nodular masses replacing or displacing sediment.

Fibrous quartz — elongate fibers of quartz; same birefringence as equigranular quartz (but birefringence decreases with increasing water content); colorless to brown; common banding or zoning (bands may consist of alternating forms of chalcedony); commonly forms cements, small to very large nodules, and may pseudomorphs other grains nodules or minerals.

- Length-fast chalcedony - "normal" chalcedony; crystallographic c-axis (slow axis) perpendicular to the fibers; common as cements and replacements.
- Length-slow chalcedony - also called quartzine; crystallographic c-axis lies parallel to long axis of fibers; occurs in replacements of evaporites, bioclasts and cements; may be associated with increased Mg^{2+} or SO_4^{2-} contents in diagenetic fluids (exact controls are still uncertain).
- Zebraic chalcedony - banded chalcedony; length-fast, but c-axis lies normal to fiber long axis; occurs as cements and as a replacement of evaporites.
- Lutecite - a fibrous form intermediate between length-fast and length-slow chalcedony; c-axis is oriented at a ~30° angle to the long axis of the fibers.
- Microflamboyant chalcedony - a more coarsely crystalline form of chalcedony with undulose extinction.

Mineralogy:

Opal-A — $SiO_2 \cdot nH_2O$; up to 10-12 weight % water, amorphous, high solubility

Opal-CT — forms lepispheres of alternating cristobalite and tridymite (hence the "CT" designation)

Cristobalite — SiO_2; tetragonal; low temperature

Quartz — SiO_2; trigonal

Up. Cretaceous (Campanian) Craie Grise, Limburg, The Netherlands

An SEM image showing abundant silica lepispheres (probably opal-CT) in a marly chalk. The presence of clay minerals commonly retards the transformation of opal-CT to the alpha quartz of chert nodules.

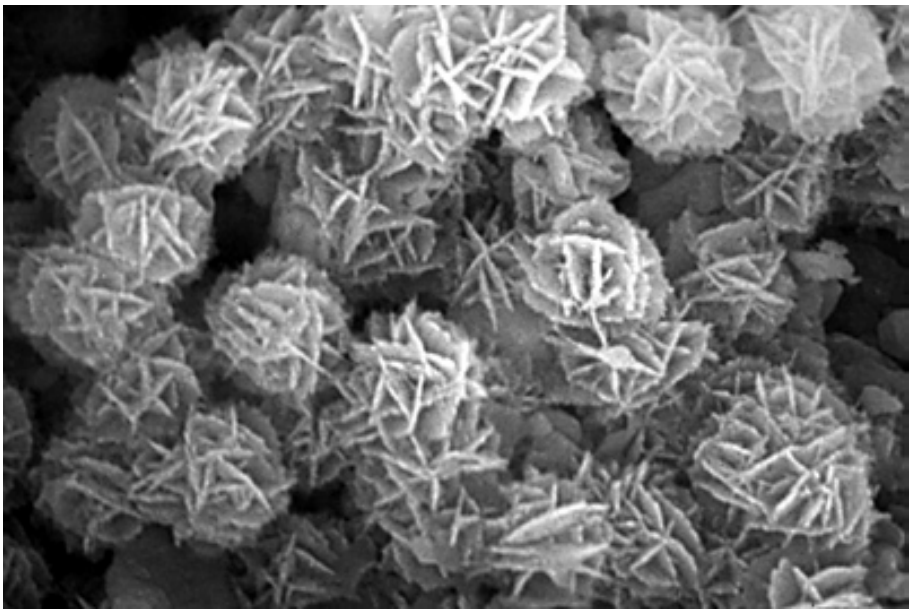

SEM, HA = 18 μm

Up. Eocene Ocala Gp., Citrus Co., Florida

This carbonate grainstone has been partially cemented by silica (microflamboyant chalcedony and megaquartz). The quartz cements fringe all the carbonate grains, including a large nummulite foraminifer.

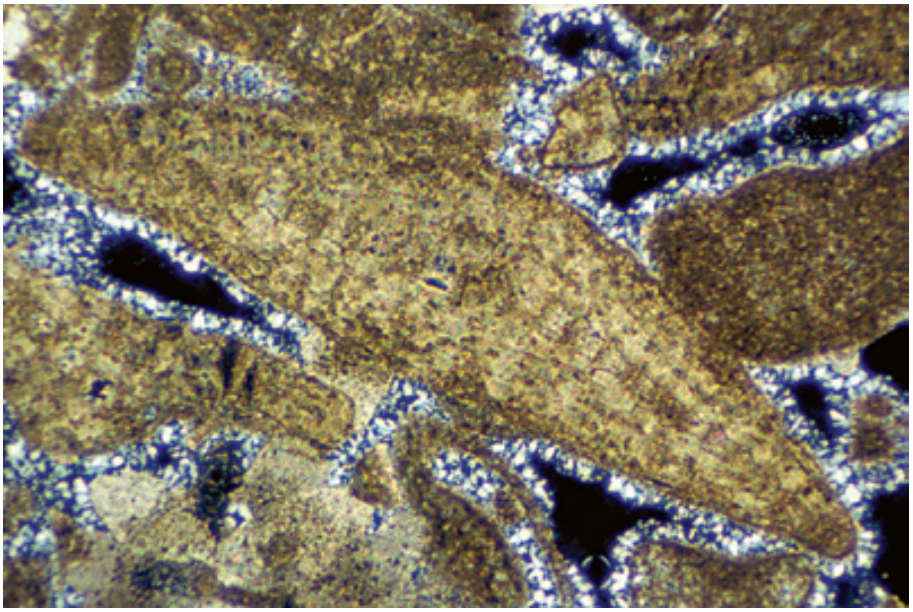

XPL, HA = 2.7 mm

Eocene Green River Fm., Laney Mbr., Sweetwater Co., Wyoming

The large gastropod in this lacustrine carbonate was cemented initially by chert, chalcedony and megaquartz. The remaining intraparticle porosity was occluded by coarsely-crystalline blocky calcite cement. Chalcedony, when viewed under cross-polarized light, exhibits pseudo-uniaxial crosses because of its fibrous crystal form. The geopetal fills within the gastropod (including a smaller gastropod) were also replaced and cemented by silica.

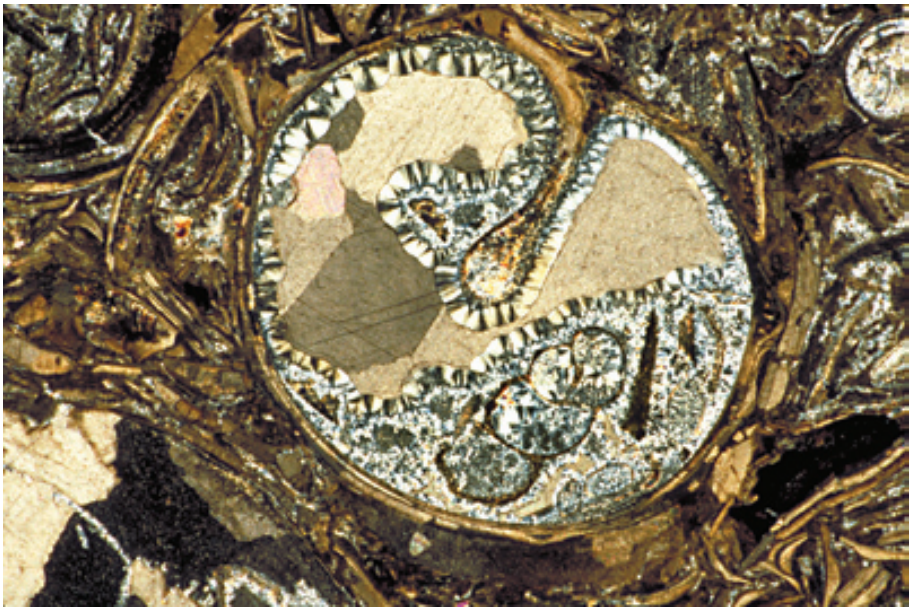

XPL, HA = 9 mm

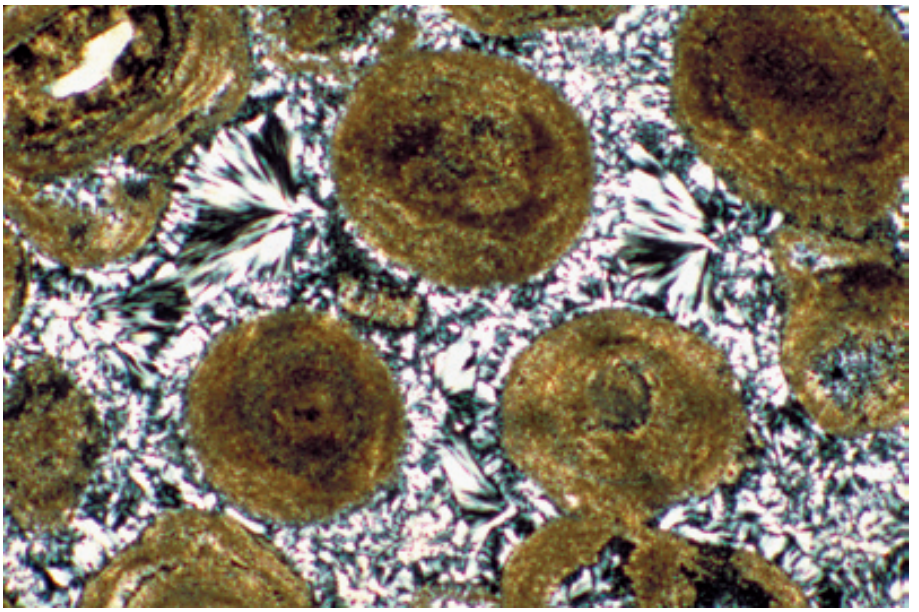

Eocene Green River Fm., Laney Mbr., Sweetwater Co., Wyoming

This lacustrine oolitic grainstone was cemented by several generations of radiating splays of chalcedony. The grains are also partially replaced chalcedony.

XPL, HA = 3.7 mm

Up. Permian (Guadalupian) Cherry Canyon Fm., Culberson Co., Texas

This example shows a chambered calcareous sponge that was partially replaced by silica, and the central cavity was filled with multiple generations of chalcedonic cement. Radiating splays or fans of fibrous crystals, low birefringence and pseudo-uniaxial crosses all are characteristic features of chalcedony. The color banding, visible even in cross-polarized light, is due to variations in concentration of minute aqueous (and possibly also mineral) inclusions.

XPL, HA = 14.5 mm

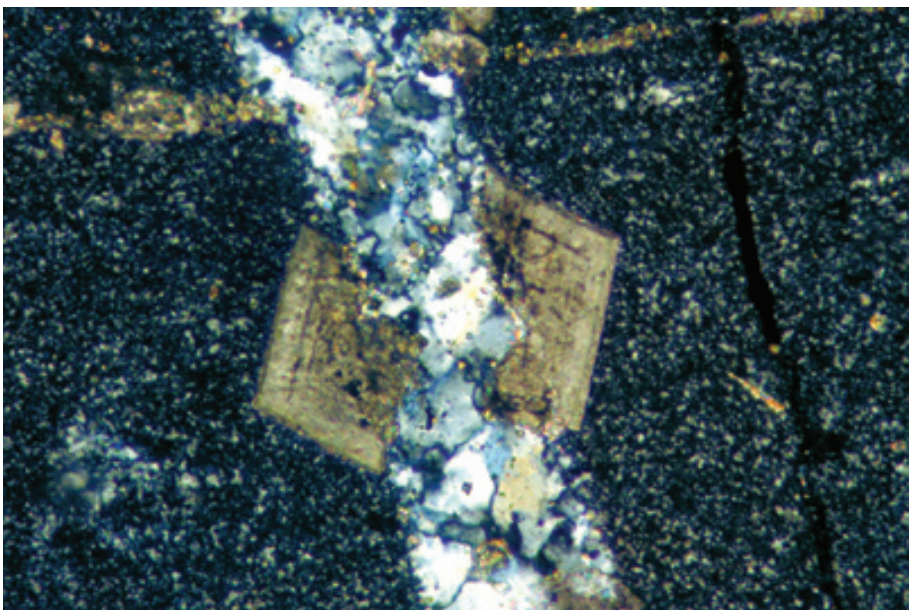

Up. Cambrian Copper Ridge Dol. and Conococheague Ls., Giles Co., Virginia

The gray to black speckled background in this photomicrograph is chert (microcrystalline quartz) that has replaced the original limestone. The euhedral dolomite crystal in the center most likely is a later partial replacement of the chert. Finally, both the dolomite and the chert were cut by fractures that were subsequently filled by megaquartz.

XPL, HA = 0.72 mm

Up. Cambrian Copper Ridge Dol./ Conococheague Ls., Giles Co., Virginia

This dolomitized limestone is cut by a fracture that is filled by quartz and calcite. Due to the euhedral crystal terminations and the lack of any inclusions within the quartz crystals, the megaquartz probably grew into the empty fracture. Later, the fracture was filled by coarsely-crystalline calcite. Determining if the quartz grew into an empty pore or is replacive can be problematic. The relative lack of inclusions in the quartz crystal is probably the best indicator of its origin.

XPL, HA = 0.72 mm

Up. Jurassic Zuloaga Fm., Tamaulipas, Mexico

In this example, authigenic quartz is clearly replacing the limestone. As in the previous photomicrograph, the quartz crystals have euhedral crystal terminations, but unlike the previous example, most of the quartz crystals have cores composed predominately of unreplaced carbonate.

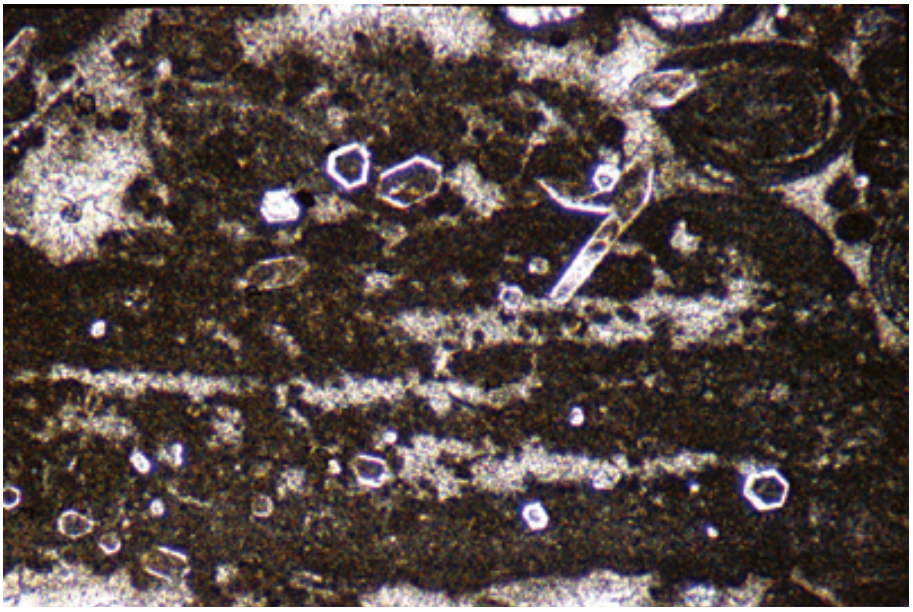

PPL, HA = 2.25 mm

Up. Devonian Cairn Fm., Alberta, Canada

If detrital quartz grains are present in a carbonate rock, those grains can act as a nucleation sites for authigenic quartz. In this example, a shelf limestone contains scattered detrital quartz grains, some of which have euhedral quartz overgrowths. The detrital quartz cores and the surrounding overgrowths are in optical continuity with each other, but only the overgrowths contain undigested carbonate inclusions. The euhedral to subhedral quartz crystal outlines and the carbonate inclusions are the strongest criteria for the recognition of authigenic quartz.

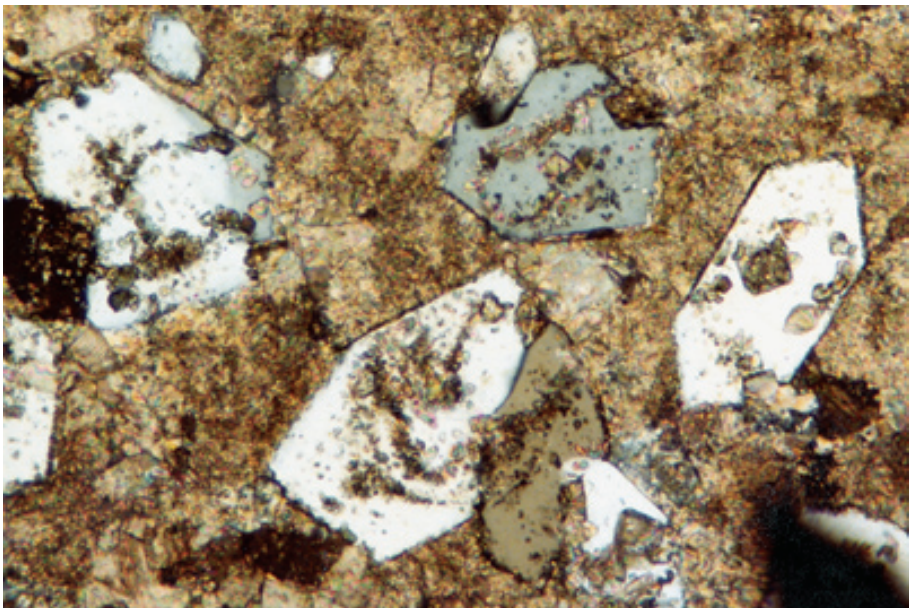

XPL, HA = 2.0 mm

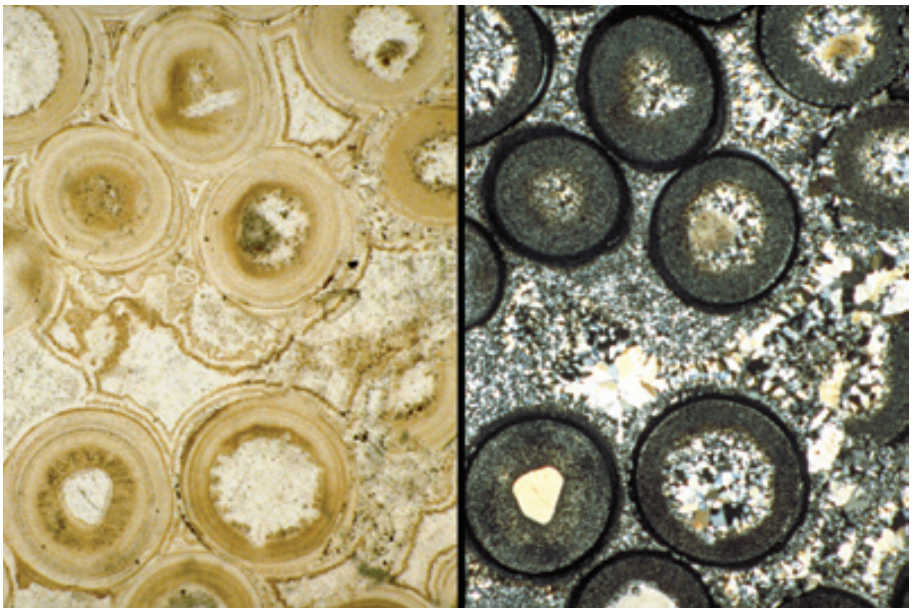

Up. Cambrian Beekmantown Gp., Mines Dolomite, Centre Co., Pennsylvania

An oolitic limestone that was completely replaced by chert and megaquartz. The original fabric of the oolitic limestone is well preserved and individual laminae within the ooids are clearly visible. The excellent fabric preservation is due to the incorporation of mineral and fluid inclusions in the silica. The brownish color in plane polarized light is due mainly to an abundance of aqueous inclusions.

PPL/XPL, HA = 3 mm each

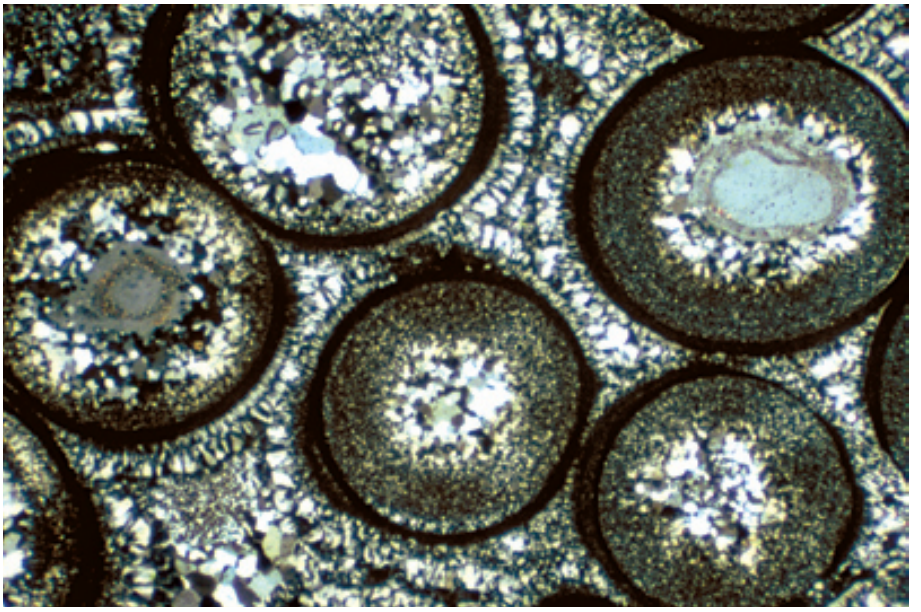

Up. Cambrian Beekmantown Gp., Mines Dolomite, Centre Co., Pennsylvania

Another view of the same unit illustrated above showing the complexity of the silicification history. Some of the ooids have detrital quartz grains as their cores; these grains acted as nucleation sites for syntaxial replacements. Chert and megaquartz replaced the remainder of the ooids. Silica also appears to be cementing the ooids and not replacing a precursor cement. The consistent silica cement stratigraphy present (from chalcedony to megaquartz and finally chert), and the lack of carbonate inclusions, support this interpretation.

XPL, HA = 3.6 mm

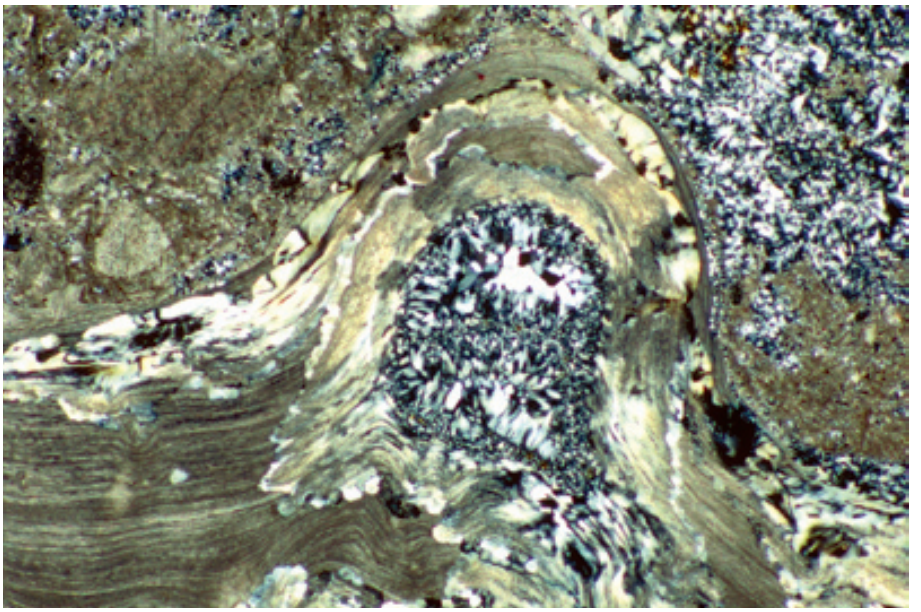

Up. Permian (Kazanian?) Wegener Halvø Fm., Jameson Land, East Greenland

Individual bioclasts also are commonly replaced by quartz. In this example, a brachiopod from the flank facies of a bioherm was partially replaced by chalcedony and megaquartz. The replacement silica was presumably derived from the abundant sponge spicules associated with these slightly deeper-water, bioherm-flanking units.

XPL, HA = 4.1 mm

Up. Silurian Tonoloway-Keyser Ls., Mifflin Co., Pennsylvania

A crinoid columnal that was partially replaced by chert. Echinoderm, brachiopod and bryozoan bioclasts are among the most commonly silicified grains. This may reflect a structural or geochemical susceptibility to silica replacement, or it may simply represent a closer ecological association with the organisms that provide silica for replacement (especially siliceous sponges).

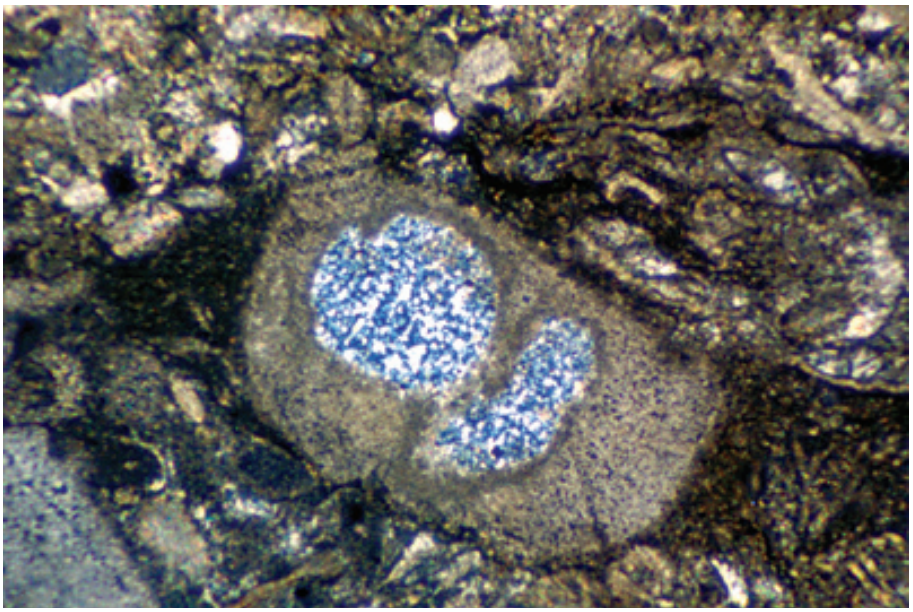

XPL, HA = 2.7 mm

Up. Permian (Guadalupian) Park City Fm., Tosi Chert, Hot Springs Co., Wyoming

In this limestone, the cystoporid bryozoans have been selectively replaced by megaquartz. The replacement quartz is a characteristic brownish gray in plane-polarized light because of the abundant carbonate inclusions preserving the details of the bryozoan wall structure.

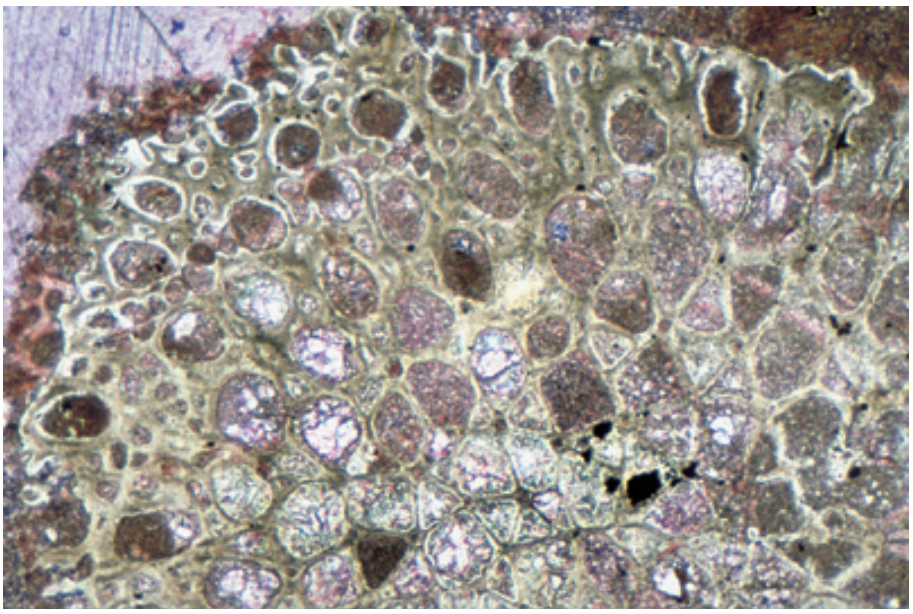

PPL, AFeS, BSE, HA = 5.1 mm

Up. Mississippian (Visean) Arroyo Peñasco Gp., Terrero Fm., San Miguel Co., New Mexico

Silicification of evaporite minerals is a common phenomenon in evaporitic carbonate strata. In this photomicrograph, gypsum crystal rosettes and surrounding carbonate grains were replaced by both length-fast chalcedony and megaquartz (yellowish-brown to white material). The evaporite precursors here are recognizable only by overall crystal outlines as no evaporite mineral inclusions were preserved.

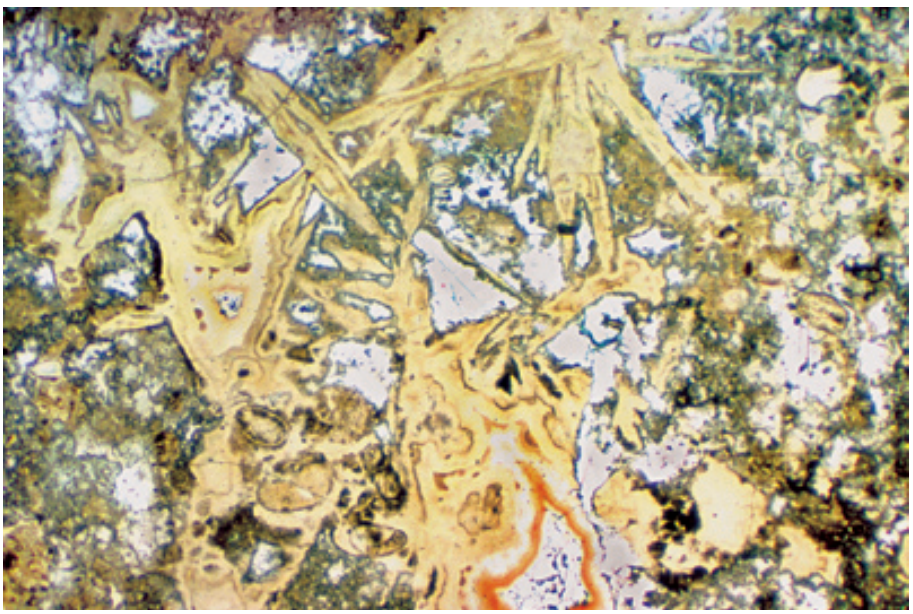

PPL, BSE, HA = 3.6 mm

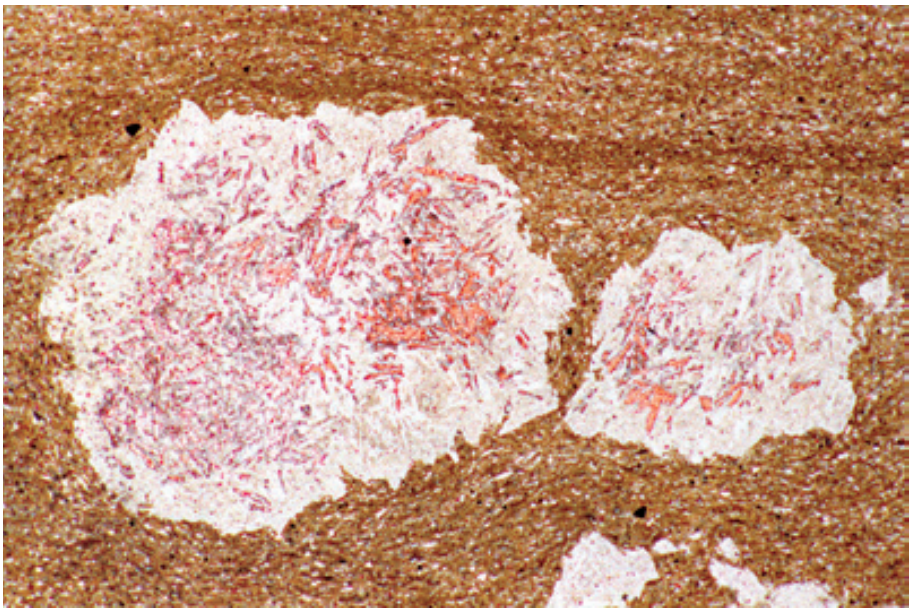

Up. Permian (Guadalupian) Park City Fm., Tosi Chert, Park Co., Wyoming

Evaporite minerals can be found in most carbonate environments. In the Tosi Chert, even relatively deep-water strata contain abundant evaporite nodules where dense sulfate-rich brines descended from evaporitic shelfal areas. The resulting evaporite nodules (probably anhydrite originally) later were replaced by quartz. Remnant anhydrite crystal-lath inclusions were dissolved after silicification, and the leached voids were then filled by calcite (stained red). Note the compactional drape around the nodules due to compaction or nodule growth.

PPL, AFeS, BSE, HA = 5.45 mm

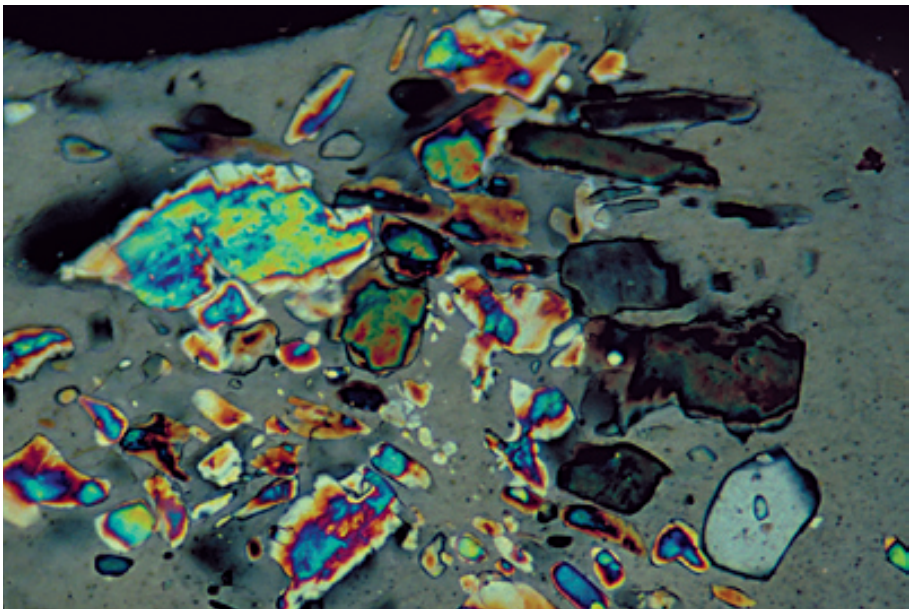

Up. Permian (Guadalupian) Yates Fm., Eddy Co., New Mexico

This anhydrite nodule in a dolomitic carbonate was replaced by megaquartz crystals. Silicification was incomplete, however, and numerous remnants of anhydrite were encased in the silica. The anhydrite crystals are the highly birefringent, blocky inclusions within the quartz. The inclusions with low birefringence may also be anhydrite (showing low birefringence colors due to the thinness of the inclusions or their optic orientation), but they may also be gypsum. The silicification occurred at depth and was related to fluids accompanying hydrocarbon emplacement (Ulmer-Scholle et al., 1993).

XPL, HA = 0.5 mm

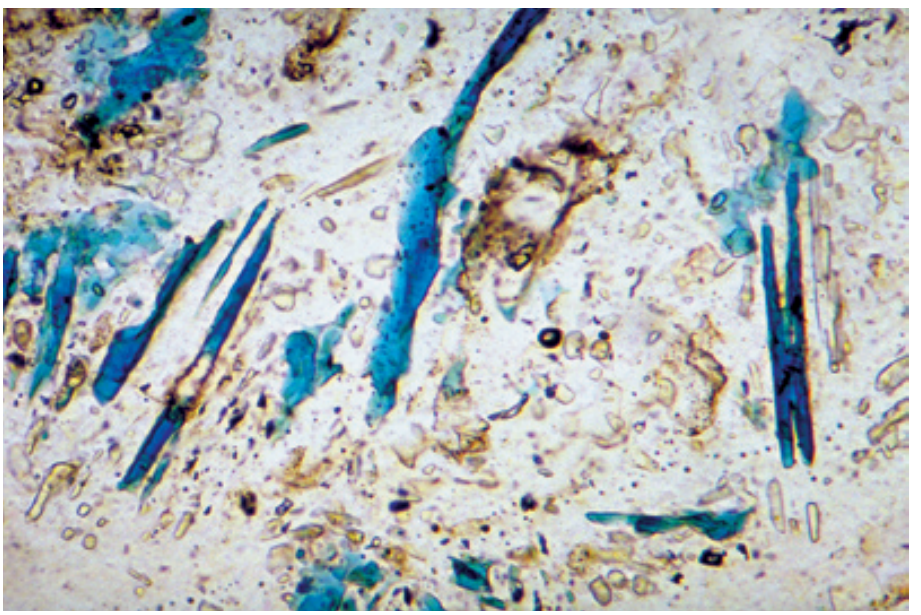

Up. Permian (Guadalupian) Park City Fm., Tosi Chert, Hot Springs Co., Wyoming

An anhydrite nodule in a dolomitized limestone that was replaced by coarsely crystalline megaquartz. The replacement quartz contains anhydrite inclusions and elongate pores (blue) formed by the dissolution of anhydrite. Note the skeletal anhydrite crystal mold that is filled with blue-stained epoxy. It is remarkable that anhydrite can be leached even where encased in low-permeability silica nodules.

PPL, BSE, HA = 0.5 mm

Up. Permian (Guadalupian) Park City Fm., Ervay Mbr., Hot Springs Co., Wyoming

This is a biomoldic pore in a dolomitized limestone that was filled with anhydrite. Later, the anhydrite was partially replaced by euhedral megaquartz. The quartz has characteristic first-order birefringence (gray to white); most of the preserved anhydrite shows higher order (purple and blue) birefringence colors.

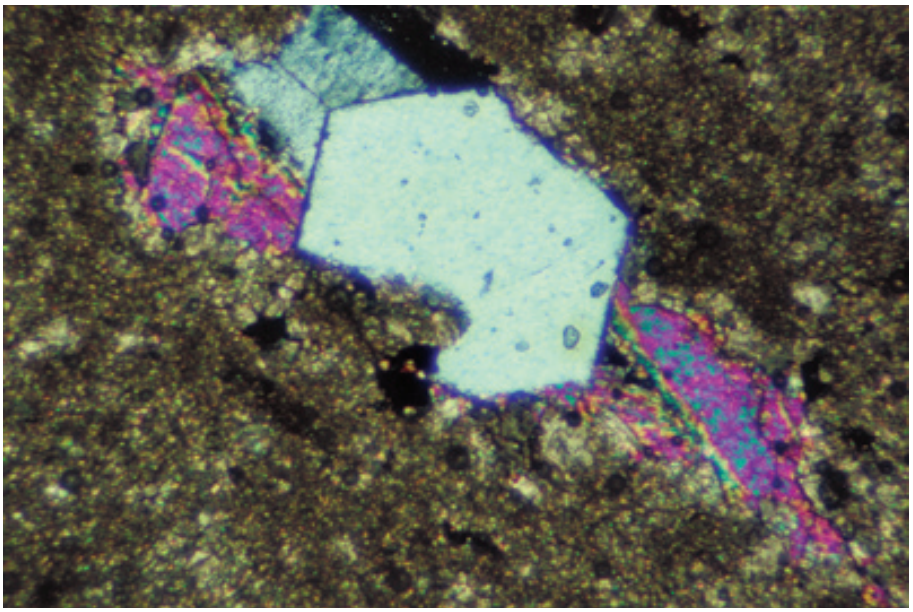

XPL, BSE, HA = 0.25 mm

Up. Mississippian (Visean) Arroyo Peñasco Gp., Terrero Fm., San Miguel Co., New Mexico

Chalcedony normally forms length-fast crystal masses, but length-slow chalcedony also is common. Length-slow chalcedony may be the preferred phase when the fluids have high sulfate concentrations. Inserting a gypsum plate into the microscope allows determination of the fast-vibration direction. In this thin-section photomicrograph, a length-fast gypsum plate was inserted from the SE quadrant. The birefringence colors in the NE and SW quadrants increased, whereas the colors in the NW and SE quadrants decreased, which means that this chalcedony is length-slow.

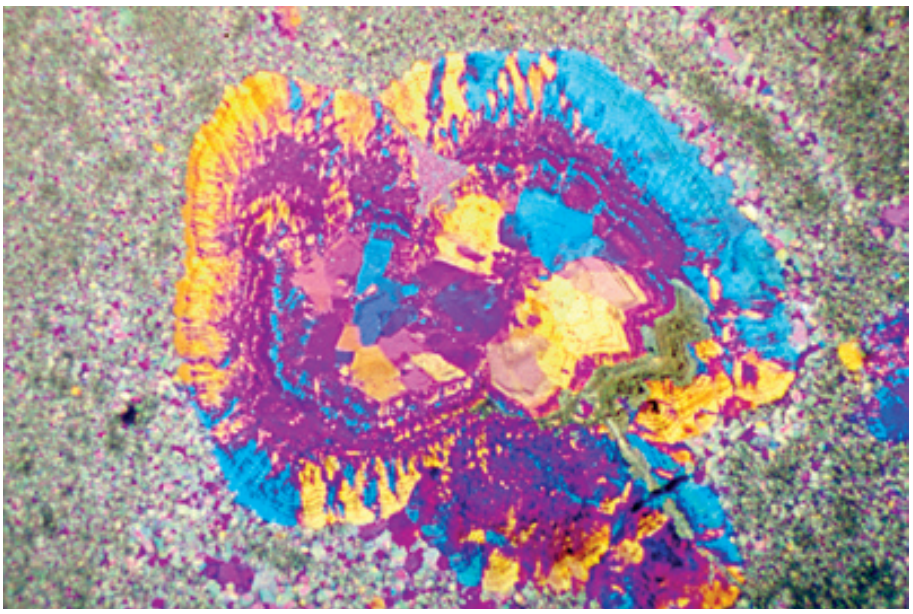

XPL, GP, HA = 1.16 mm

Up. Mississippian (Visean) Arroyo Peñasco Gp., Terrero Fm., San Miguel Co., New Mexico

This chalcedony shows a fabric that has been termed "fortification zoning". Fortification zoning is the cubic-terminated zoning within the authigenic silica. The chalcedony is probably replacing gypsum, but Folk and Pittman (1971) consider this fabric to be indicative of silica replacement of halite.

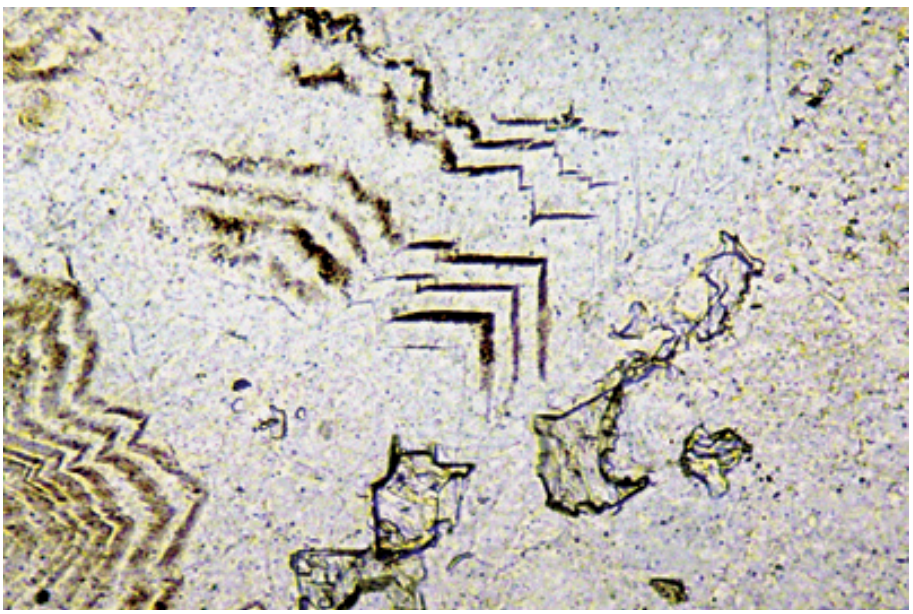

PPL, HA = 0.23 mm

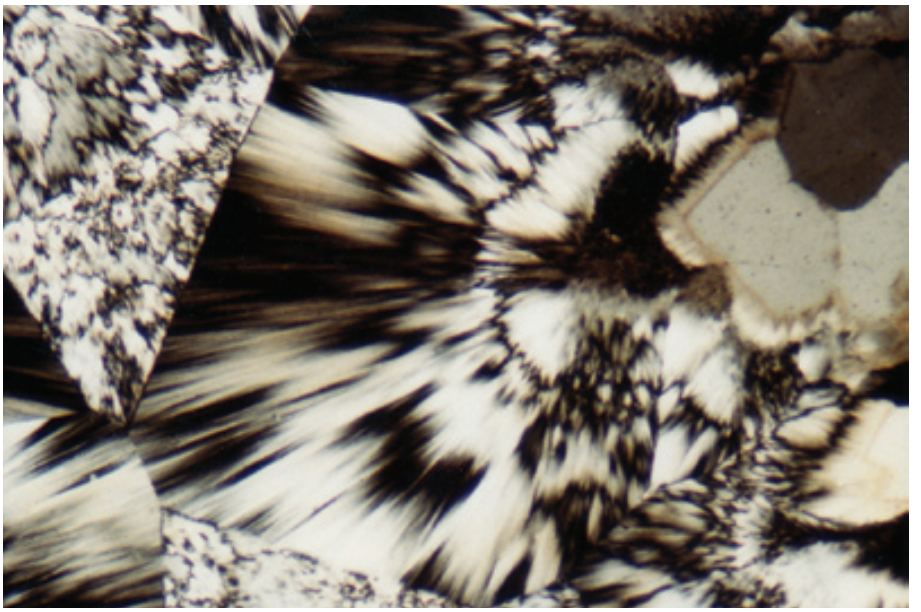

Up. Jurassic Radiolariti, northern Italy

An example of "zebraic" chalcedony forming a fibrous microquartz cavity lining in a bedded chert. The fibers are alternately light and dark when viewed along the fiber elongation direction under cross-polarized light. Some workers (McBride and Folk, 1977) have described an association of zebraic chalcedony with replaced evaporite minerals, but it also occurs, as in this example, in deep marine strata with no known associated evaporites.

XPL, HA = 2.4 mm

Cited References and Additional Information Sources

Arbey, F., 1980, Les formes de la silice et l'identification des évaporites dans les formations silicifiées: Bulletin des Centres de Recherches Exploration-Production Elf-Aquitaine, v. 4, p. 309-365.

Bennett, P. C., M. E. Melcer, D. I. Siegel, and J. P. Hassett, 1988, The dissolution of quartz in dilute aqueous solutions of organic acids at 25°C: Geochimica et Cosmochimica Acta, v. 52, p. 1521-1530.

Buurman, P., and L. Van Der Plas, 1971, The genesis of Belgian and Dutch flint cherts: Geologie en Mijnbouw, v. 50, p. 9-28.

Choquette, P. W., 1955, A petrographic study of the "State College" siliceous oolite: Journal of Geology, v. 63, p. 337-347.

Chowns, T. M., and J. E. Elkins, 1974, The origin of quartz geodes and cauliflower cherts through the silicification of anhydrite nodules: Journal of Sedimentary Petrology, v. 44, p. 885-903.

Dapples, E. C., 1979, Silica as an agent in diagenesis, *in* G. Larsen, and G. V. Chilingar, eds., Diagenesis in Sediments and Sedimentary Rocks: Developments in Sedimentology 25A: New York, Elsevier, p. 99-141.

Eugster, H. P., 1967, Hydrous sodium silicates from Lake Magadi, Kenya: precursors of bedded chert: Science, v. 157, p. 1177-1180.

Folk, R. L., and J. S. Pittman, 1971, Length-slow chalcedony: a new testament for vanished evaporites: Journal of Sedimentary Petrology, v. 41, p. 1045-1058.

Folk, R. L., and C. E. Weaver, 1952, A study of the texture and composition of chert: American Journal of Science, v. 250, p. 498-510.

Greenwood, R., 1973, Cristobalite: its relationship to chert formation in selected samples from the Deep Sea Drilling Project: Journal of Sedimentary Petrology, v. 43, p. 700-708.

Hesse, R., 1989, Silica diagenesis: origin of inorganic and replacement cherts: Earth-Science Reviews, v. 26, p. 253-284.

Ireland, H. A., ed., 1959, Silica in Sediments: Tulsa, OK, SEPM Special Publication No. 7, 185 p.

Kastner, M., and J. M. Gieskes, 1983, Opal-A to opal-CT transformation: a kinetic study, *in* A. Iijima, J. R. Hein, and R. Siever, eds., Siliceous Deposits of the Pacific Region: New York, Elsevier, p. 211-228.

Keene, J. B., 1983, Chalcedonic quartz and occurrence of quartzine (length-slow chalcedony) in pelagic sediments: Sedimentology, v. 30, p. 449-454.

Knauth, L. P., 1979, A model for the origin of chert in limestone: Geology, v. 7, p. 274-277.

Maliva, R. G., 1987, Quartz geodes: early diagenetic silicified anhydrite nodules related to dolomitization: Journal of Sedimentary Petrology, v. 57, p. 1054-1059.

Maliva, R. G., and R. Siever, 1988, Mechanism and controls of silicification of fossils in limestones: Journal of Geology, v. 96, p. 387-398.

McBride, E. F., and R. L. Folk, 1977, The Caballos Novaculite revisited: Part II: chert and shale members and synthesis: Journal of Sedimentary Petrology, v. 47, p. 1261-1286.

Meyers, W. J., 1977, Chertification in the Mississippian Lake Valley Fm., Sacramento Mts., New Mexico: Sedimentology, v. 24, p. 75-105.

Milliken, K. L., 1979, The silicified evaporite syndrome — two aspects of silicification history of former evaporite nodules from southern Kentucky and northern Tennessee: Journal of Sedimentary Petrology, v. 49, p. 245-256.

Noble, J. P. A., and D. R. van Stempvoort, 1989, Early burial quartz authigenesis in Silurian platform carbonates, New Brunswick, Canada: Journal of Sedimentary Petrology, v. 59, p. 65-76.

Oehler, J. H., 1975, Origin and distribution of silica lepispheres in porcelanite from the Monterey Formation of California: Journal of Sedimentary Petrology, v. 45, p. 252-257.

Penela, A. J. M., and G. Barragan, 1995, Silicification of carbonate clasts in a marine environment: Sedimentary Geology, v. 97, p. 21-32.

Renaut, R. W., B. Jones, and J.-J. Tiercelin, 1998, Rapid in situ silicification of microbes at Loburu hot springs, Lake Bogoria, Kenya Rift Valley: Sedimentology, v. 45, p. 1083-1103.

Richter, D. K., 1972, Authigenic quartz preserving skeletal material: Sedimentology, v. 19, p. 211-218.

Siedlecka, A., 1972, Length-slow chalcedony and relicts of sulphates — evidences of evaporitic environments in the Upper Carboniferous and Permian beds of Bear Island, Svalbard: Journal of Sedimentary Petrology, v. 42, p. 812-816.

Summerfield, M. A., 1983, Silcrete, *in* A. S. Goudie, and K. Pye, eds., Chemical Sediments and Geomorphology: Precipitates and Residua in the Near-surface Environment: London, Academic Press, p. 59-92.

Ulmer-Scholle, D. S., P. A. Scholle, and P. V. Brady, 1993, Silicification of evaporites in Permian (Guadalupian) back-reef carbonates of the Delaware Basin, west Texas and New Mexico: Journal of Sedimentary Petrology, v. 63, p. 955-965.

Zijlstra, H. J. P., 1987, Early diagenetic silica precipitation, in relation to redox boundaries and bacterial metabolism, in Late Cretaceous chalk of the Maastrichtian type boundary: Geologie en Mijnbouw, v. 66, p. 343-355.

Facing Page: Polished rock slab showing marine cements with bitumen (dead oil) in residual pore spaces. Up. Permian, Guangxi Province, People's Republic of China. HA = ~8 cm.

CARBONATE DIAGENESIS

OTHER DIAGENETIC MATERIALS

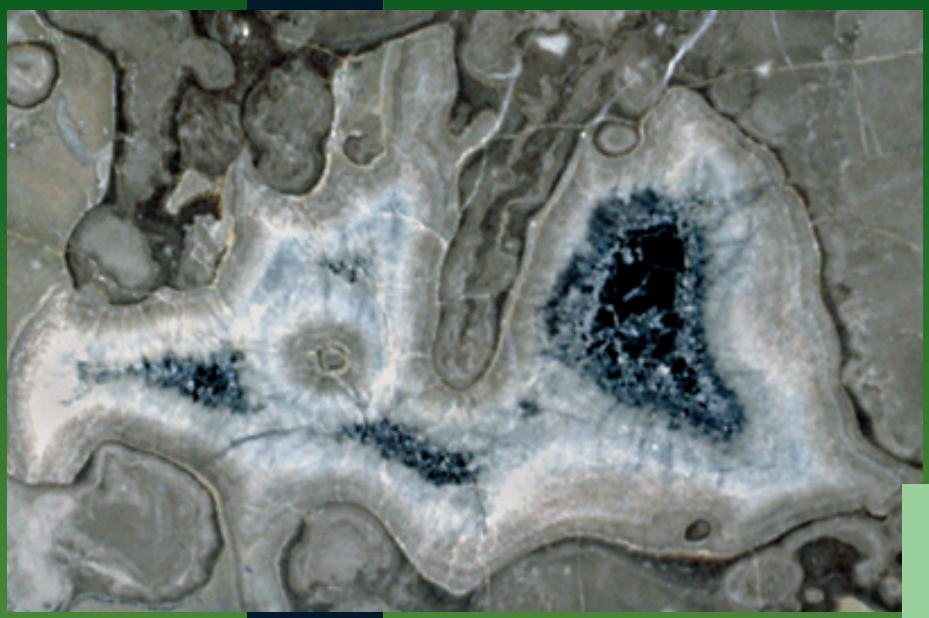

CHAPTER 29

- Sulfides and oxides
- Fluorite
- Phosphate and glauconite
- Authigenic feldspar
- Hydrocarbons

OTHER DIAGENETIC MATERIALS

Iron Sulfides & Oxides:

Pyrite (FeS_2) is the most abundant iron sulfide mineral found in carbonate sediments. Pyrite is an isometric mineral that commonly forms crystals that are cubic, pyritohedral or octahedral, but it may also form anhedral replacement masses. In sediments, pyrite also occurs as framboids or spheres composed of aggregates of minute crystals. Pyrite is opaque in thin section and is readily identified by reflected light microscopy due to its brassy to golden yellow color (simply holding a strong light source above the thin section as it sits on the microscope stage and blocking transmitted light illumination will generally suffice for identification).

Hematite (Fe_2O_3) is normally an opaque mineral. In reflected light, hematite is deep red to rusty red. It rarely forms crystals and occurs typically as amorphous masses. Hematite commonly forms through weathering and oxidation of pyrite or other iron sulfides, and it is not unusual to find pyrite and hematite together.

Goethite (FeO(OH)) is an opaque orthorhombic mineral, whereas limonite ($FeO(OH)\cdot nH_2O$) is a cryptocrystalline or amorphous, hydrated form of this compound. Both minerals are reddish brown to yellowish brown in reflected light, and they can be difficult to tell apart from hematite. They are weathering products of either iron sulfides or hematite.

Sphalerite:

Sphalerite (ZnS) is an isometric mineral that is isotropic in cross-polarized illumination, has a high positive relief, and ranges from colorless to pale yellow or light brown. A slight birefringence may be present when the crystals have been strained. Crystals are usually not well formed, but where present, crystal faces may be curved. Well-developed lamellar twinning is common in sphalerite. Sphalerite is found in Mississippi Valley-type mineralized carbonate rocks and other hydrothermal deposits.

Fluorite:

Fluorite (CaF_2) is an isometric mineral that forms cubic crystals, although anhedral masses are common in carbonate rocks. Fluorite normally is colorless in thin section, but strongly colored samples may be pale purple to green. Halite and fluorite are easily confused since they are both isotropic, form euhedral cubic crystals and have negative relief. Fluorite can be distinguished from halite based on its well-developed octahedral cleavage, lower negative relief, and color spots that are produced by inclusions within the crystals. Most fluorite was precipitated from hydrothermal fluids and may be associated with Mississippi Valley-type mineralization.

Phosphate:

The two most common phosphatic minerals in carbonate rocks are fluorapatite ($Ca_5(PO_4)_3F$) and hydroxylapatite ($Ca_5(PO_4,CO_3,OH)_3(F,OH)_x$). When intergrown, the minerals formed are francolite (crystalline form) and collophane (cryptocrystalline form). Collophane is the more common mineral — it is isotropic to very weakly birefringent with colors that range from yellowish to brownish. Most early diagenetic phosphate is made of collophane. Francolite has a higher relief and low birefringence (gray to low white); it is colorless to pale brown, and may be slightly pleochroic. Diagenetic phosphatic minerals can form amorphous nodular masses, cements or replacements. Diagenetic phosphates form mainly in areas with substantial primary sedimentary phosphate accumulation — areas with low sediment accumulation rates and high nutrient inputs.

Glauconite:

Glauconite $(K,Ca,Na)_{1\text{-}0.56}(Fe^{3+}, Mg, Fe^{2+},Al)_2(Si, Al)_4O_{10}(OH)_2$ is a clay mineral found only in marine deposits. It forms pellets or granules in areas of slow sedimentation. It also precipitates as an early diagenetic mineral replacing clasts or filling porosity in shallow to deep marine settings that have high nutrient levels and low sediment accumulation rates. Glauconite is green to olive green in color and has a greenish birefringence; it can look similar to chlorite, but chlorite is usually more platy and has anomalously low birefringence.

Hydrocarbons:

Hydrocarbons can be found as interstitial material in carbonate rocks or as fluid inclusions within carbonate cements. In some cases, hydrocarbons effectively terminate cementation by blocking the entry of aqueous fluids responsible for diagenesis. Bitumen, asphalt and hydrocarbon-filled inclusions all are products of this complex interplay of hydrocarbon-bearing and aqueous fluids. Evidence of hydrocarbon entry includes residues and inclusions, as well as curved meniscus cements and the preservation of unstable carbonate phases, such as aragonite, in very old rocks.

Up. Cretaceous, subsurface, British North Sea

An SEM image of a pyrite framboid. Framboids are almost perfectly spherical bodies of small, interlocking pyrite crystals. These spherical aggregates typically form discrete bodies, but they are also found as clusters or multiple spheroids. They are authigenic in origin and form in reducing environments or in reducing microenvironments associated with decomposing organic matter.

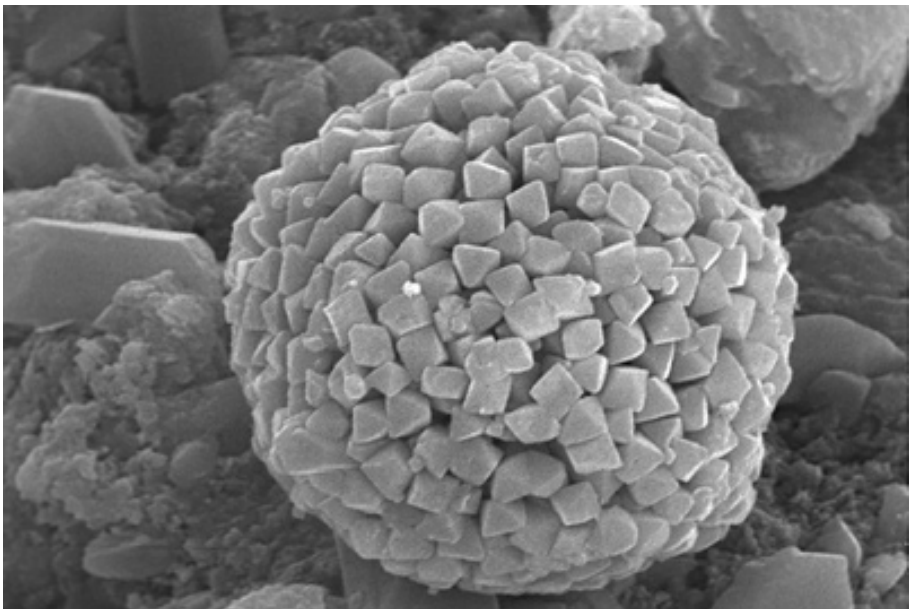

SEM, HA = 27 μm

Up. Cretaceous Monte Antola Fm., Genova region, Liguria, Italy

Because pyrite is an opaque mineral, it can easily be confused with other opaque minerals (such as magnetite, marcasite, or hematite); therefore, reflected light or a combination of reflected and transmitted light should be utilized. In this view, a combination of light sources was used to accentuate the brassy golden reflectance color of the framboidal pyrite filling of this burrow. Pyrite is commonly associated with burrows because of the high organic content of such structures. The surrounding carbonate matrix is stained by an alteration halo of limonite.

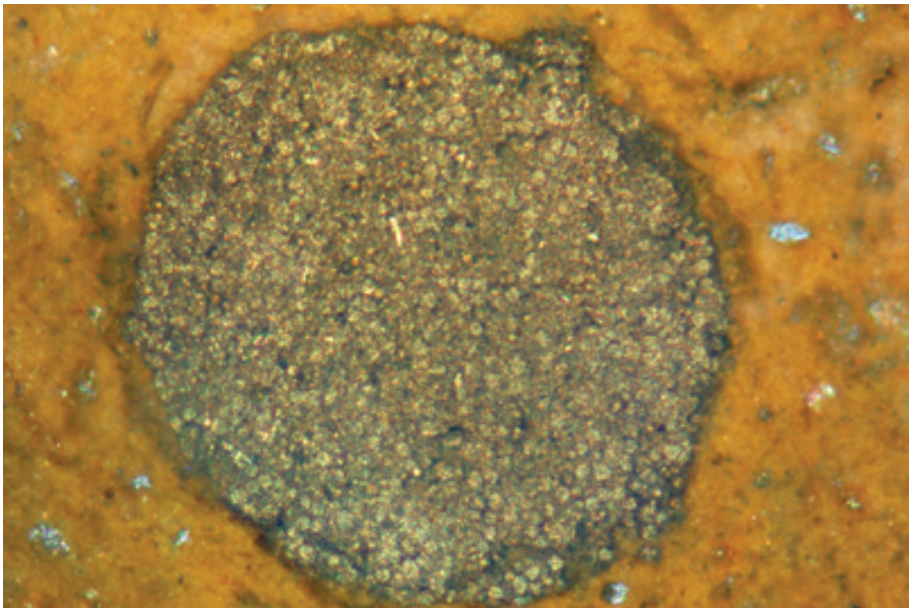

PPL + RL, HA = 0.40 mm

Precambrian Wynd Fm., British Columbia, Canada

Replacement pyrite crystals commonly have a cubic habit. In this view, a large euhedral crystal of pyrite has replaced carbonate matrix. Reflected light should be used to confirm this identification (we did, and it is). Photograph courtesy of Lee Gerhard.

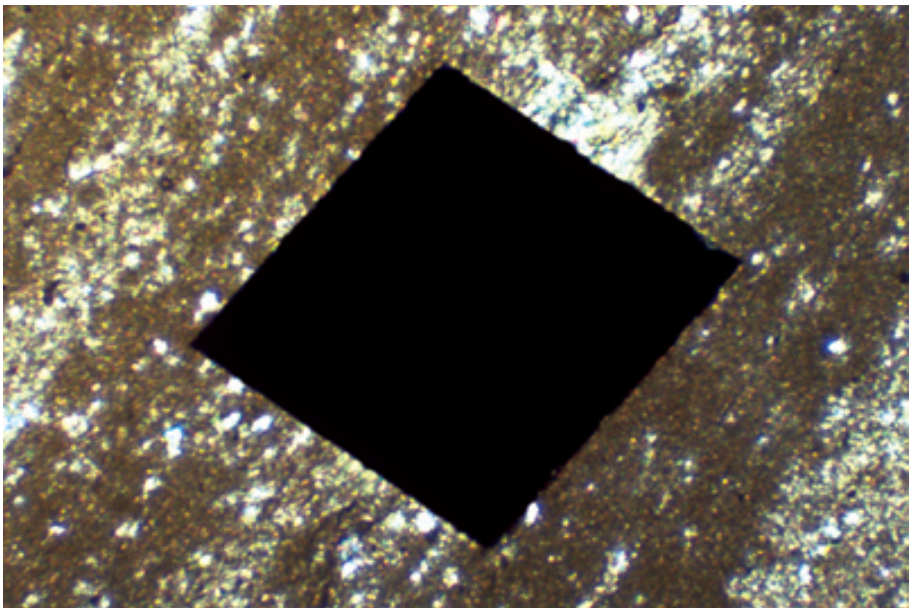

PXPL, HA = 4.0 mm

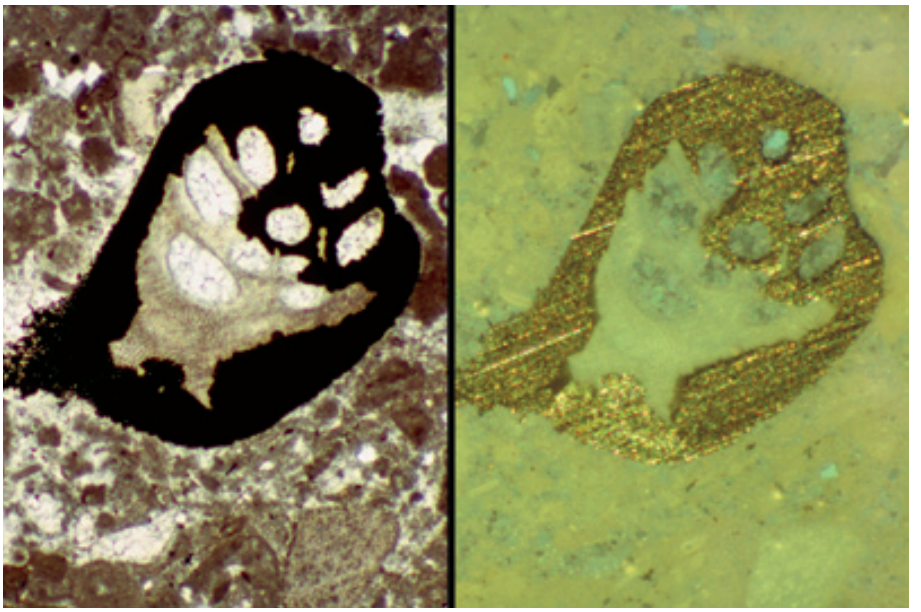

Up. Permian (Guadalupian) Capitan Fm., subsurface, Eddy Co., New Mexico

Pyrite replacement of bioclasts is common because of the organic material incorporated within many skeletal structures. Here, a pair of transmitted and reflected light views show pyrite replacing the outer margins of a bryozoan. Here again, pyrite has a brassy gold reflectance.

PPL/RL, HA = 1.5 mm each

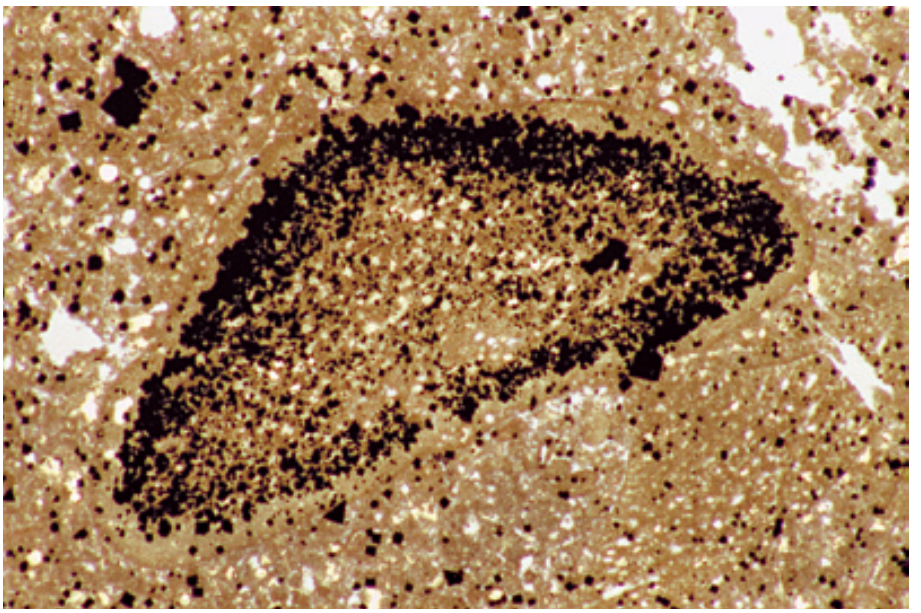

Lo. Cretaceous (Aptian) Shuaiba Fm., offshore Qatar

In this view, an orbitolinid foraminifer has been extensively replaced by euhedral crystals of pyrite. Note some of the trigonal crystal orientations achieved by cutting across the cube's corners, and how the pyrite replacement is most intense in a consistent zone just inside the margin of the foraminiferal test. Extensive moldic to vuggy porosity is visible in the surrounding sediment.

PPL, AFeS, HA = 3.4 mm

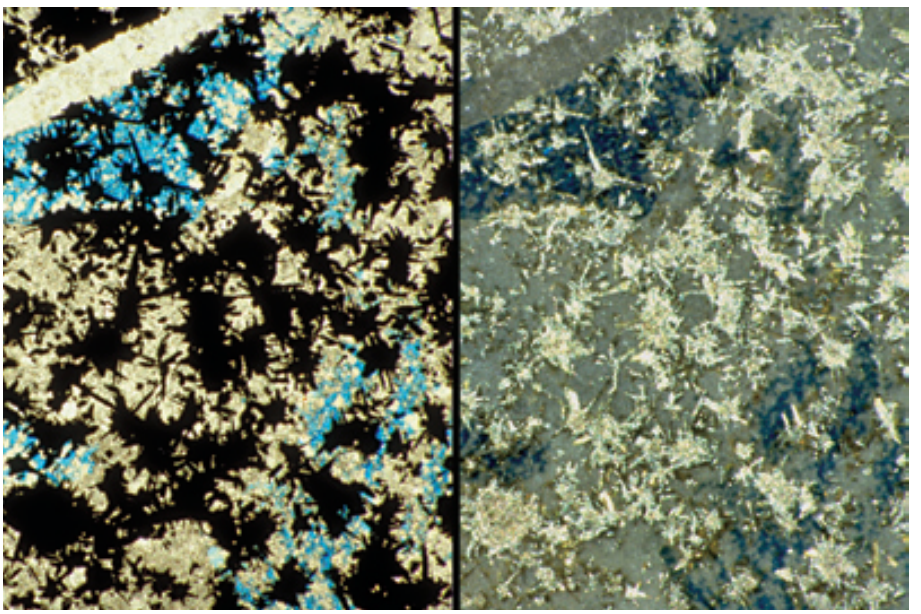

Lo. Cretaceous (Aptian) Shuaiba Fm., subsurface, offshore Qatar

The pyrite replacement shown in these transmitted and reflected light photomicrographs takes the form of rosettes of needle-like crystals. Although this pyrite replacement occurred in the same setting and sediment type as that shown in the previous photograph, the fabrics are quite dissimilar. The previous example showed fabric-selective infill or replacement; the pyrite here does not appear to have any fabric selectivity, despite the presence of the same types of foraminifers (best seen in the reflected light image).

PPL/RL, BSE, HA = 2.5 mm each

Up. Mississippian Arroyo Peñasco Gp., Terrero Fm., San Miguel Co., New Mexico

In this reflected light view, the pyrite replacements have been partially altered to hematite (reddish), probably during outcrop weathering. The surrounding carbonate rock is a dolomitized and silicified limestone.

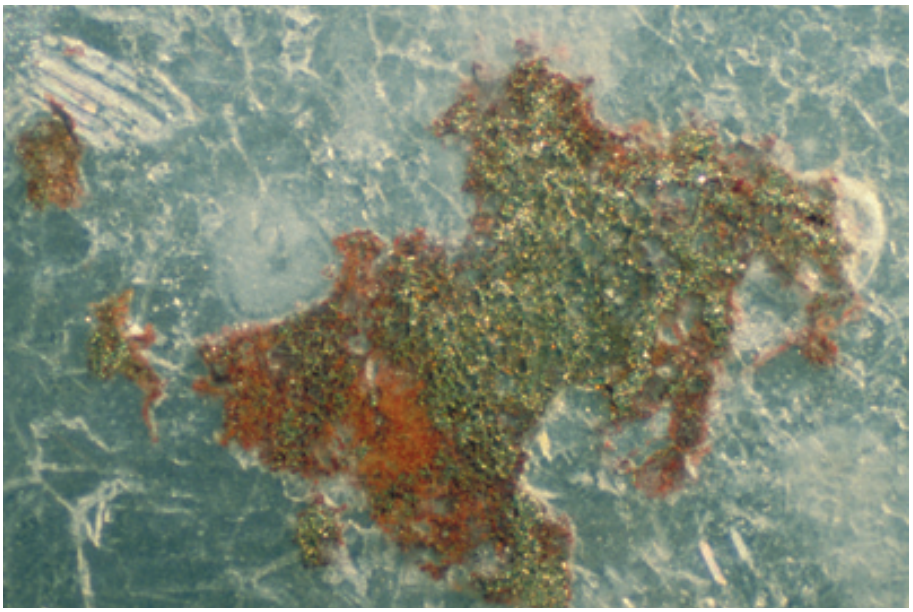

RL, HA = 1.0 mm

Cambrian limestone, Colorado

Hematite is readily visible in these transmitted and reflected light photomicrographs. In transmitted light, hematite is opaque (like pyrite), but in reflected light, hematite is red to brownish red (and thus differs from the brassy gold reflectance of pyrite). Hematite here has replaced a fine-grained carbonate grainstone. Sample courtesy of Robert L. Laury.

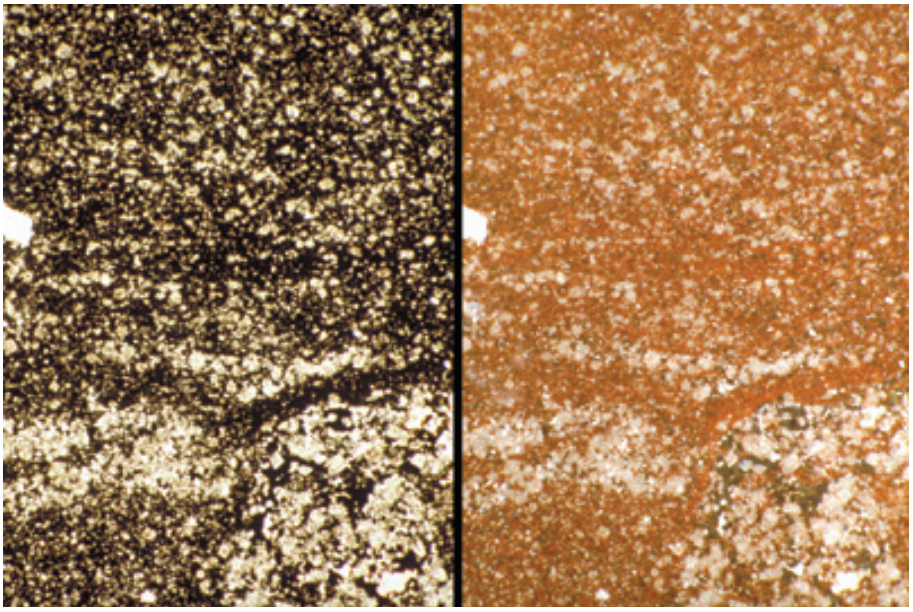

PPL/RL, HA = 2.5 mm each

Mid. Silurian Clinton Fm., Huntingdon Co., Pennsylvania

Hematite cements also are common, especially in carbonate interbeds in terrigenous strata, and even can form economic iron ore deposits. In this sample, the hematite ore encases silt grains and large trilobite fragments.

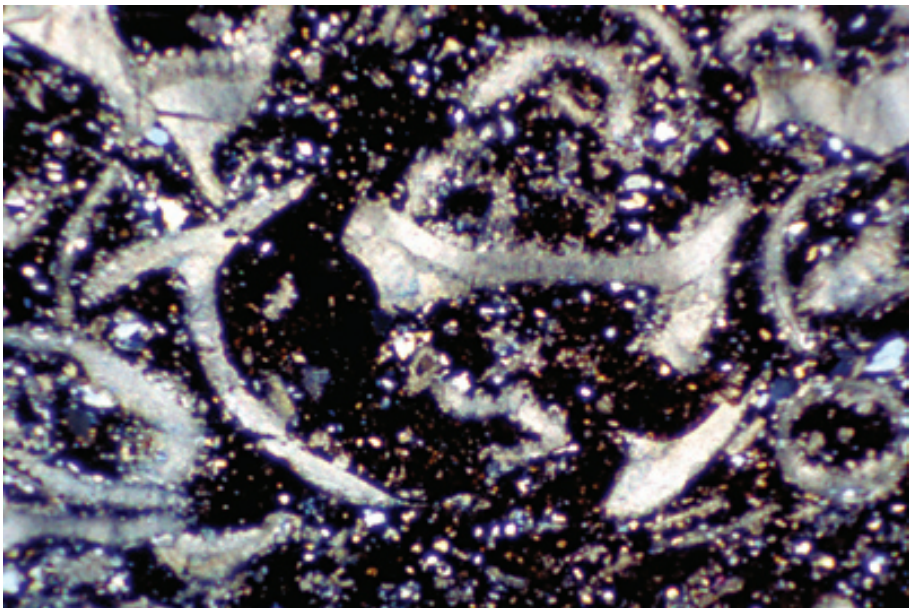

XPL, HA = 3.4 mm

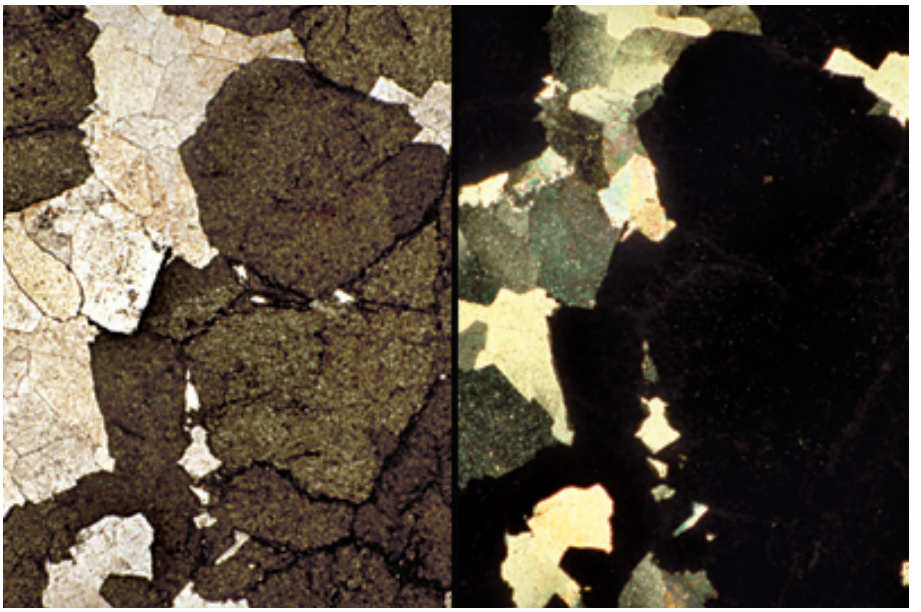

Mid. Ordovician St. George Gp., Newfoundland, Canada

Sphalerite commonly is found in association with baroque (saddle) dolomite because both form in association with hydrothermal fluids. In transmitted light, sphalerite crystals have high relief and are dark colored (normally brownish). In this sample, the dolomite (lighter colored) and sphalerite crystals are intergrown. In cross-polarized light, sphalerite is isotropic, whereas the baroque dolomite has high third-order colors and undulose extinction. Sample from Noel P. James.

PPL/XPL, HA = 3.0 mm each

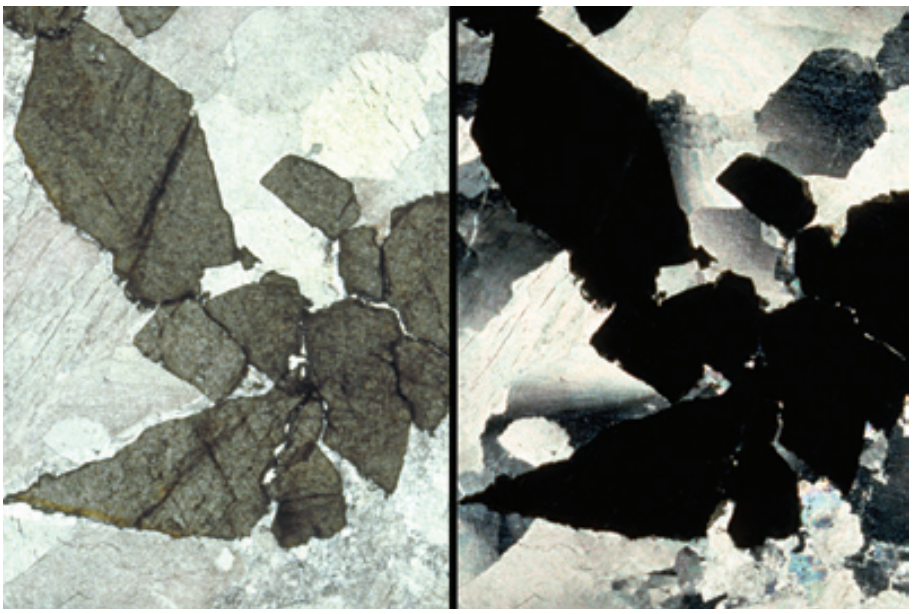

Lo. Ordovician St. George Gp., Newfoundland, Canada

Another example of sphalerite and baroque dolomite formed from hydrothermal fluids. The reflected light view shows large, isotropic crystals of sphalerite surrounded by large baroque (saddle) dolomite crystals with undulose extinction clearly visible. Photograph courtesy of Noel P. James.

PPL/XPL, HA = 3.5 mm each

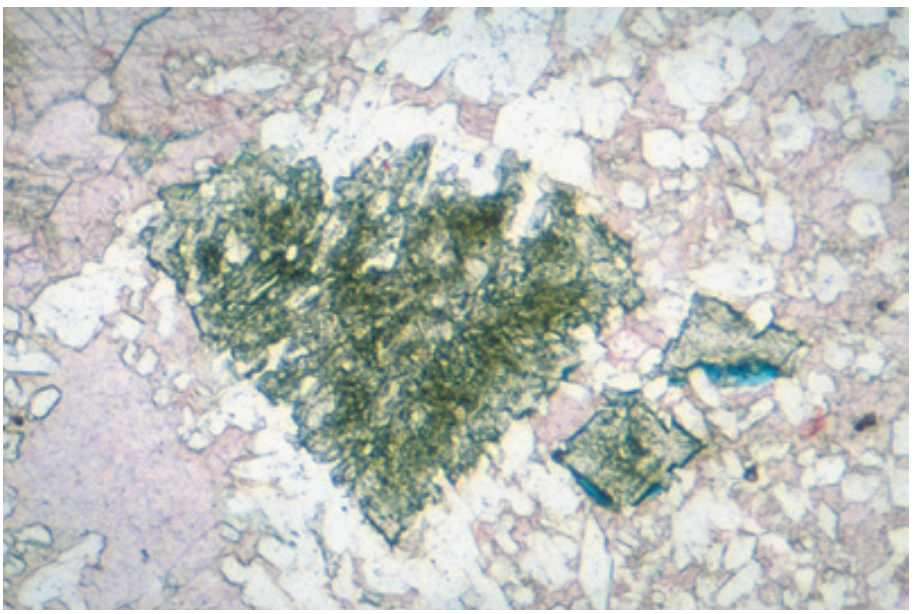

Up. Permian (Leonardian-Guadalupian) Park City Fm., Tosi Chert Mbr., Big Horn Co., Wyoming

Fluorite is a high-relief, isotropic mineral that normally forms cubic crystals. In this sample, chalcedony (clear) and calcite (pink) surround the fluorite crystals. Fluorite forms at elevated temperatures; here, the fluorite, calcite and chalcedony are probably replacements of sulfate minerals associated with thermo-chemical sulfate reduction.

PPL, AFeS, BSE, HA = 0.5 mm

Up. Permian (Kazanian?) Wegener Halvø Fm., Jameson Land, East Greenland

The combined Alizarin Red S-potassium ferricyanide staining of the carbonate constituents in this section makes the unstained fluorite stand out in clear contrast. The fluorite crystals are roughly coeval with blocky ferroan calcite spar that fills the late-stage porosity. Non-ferroan calcite spar predates both. During burial diagenesis, the fluorite and calcite were precipitated from fluids at elevated temperatures and under reducing conditions.

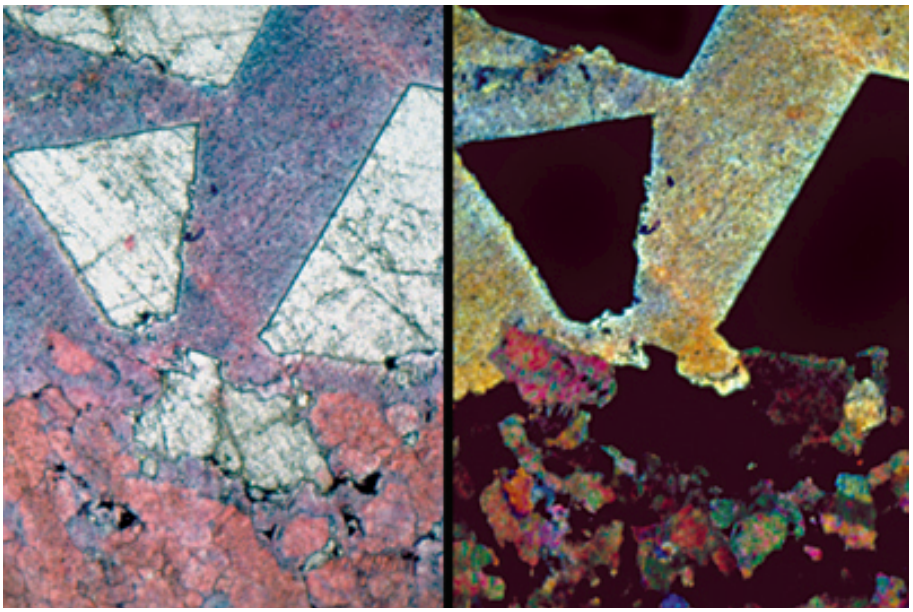

PPL/XPL, AFeS, HA = 1.2 mm each

Miocene (Aquitanian-Burdigalian) Globigerina Limestone Fm., Gozo, Malta

Marine hardgrounds can be sites of erosion, boring and mineralization. This marine hardground has a clearly identifiable, irregular upper surface. The top few millimeters of the hardground are heavily impregnated with phosphate and iron oxides (possibly after pyrite).

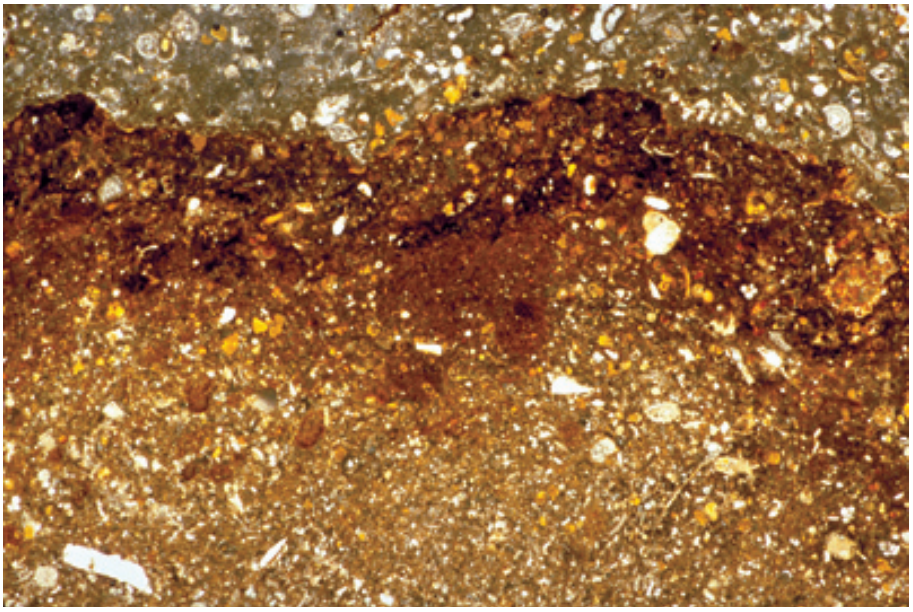

PPL, HA = 10 mm

Oligocene-Miocene above McDonald Ls., northern Otago, New Zealand

This sample shows a digitate microbial crust that has formed on the surface of a marine hardground. The lumpy crusts are largely composed of precipitated phosphate, but they have also been heavily stained by iron oxides. Interstices within the microbialite "fingers" are filled with glauconite grains, another indication of the very low sedimentation rates that existed in this area at the time of formation.

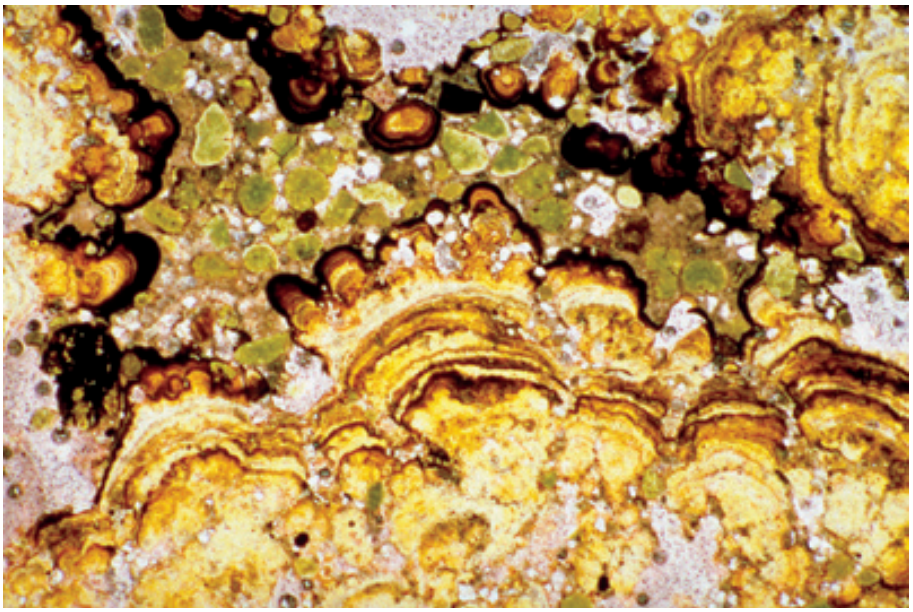

PPL, HA = 5 mm

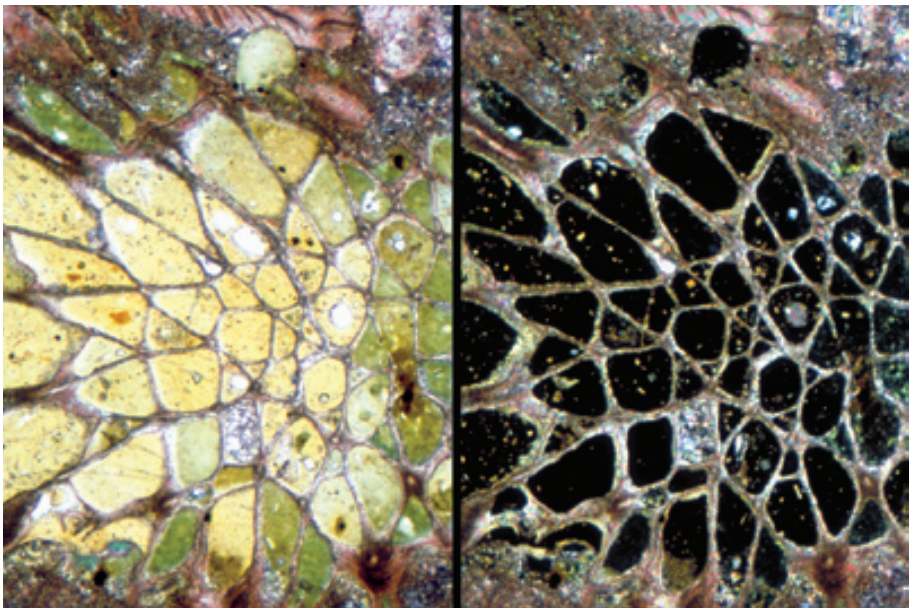

Up. Permian (Leonardian-Guadalupian) Park City Fm., Tosi Chert-Ervay Mbr., Hot Springs Co., Wyoming

Phosphate and glauconite are commonly associated as early diagenetic minerals in shelf and deep-water sediments. For example, the zooecia in this bryozoan fragment were filled with precipitated phosphate (pale yellow) and subordinate glauconite (greenish). The phosphate also pervades most of the glauconitic areas, and the entire precipitate appears isotropic in cross-polarized light.

PPL/XPL, AFeS, HA = 1.2 mm each

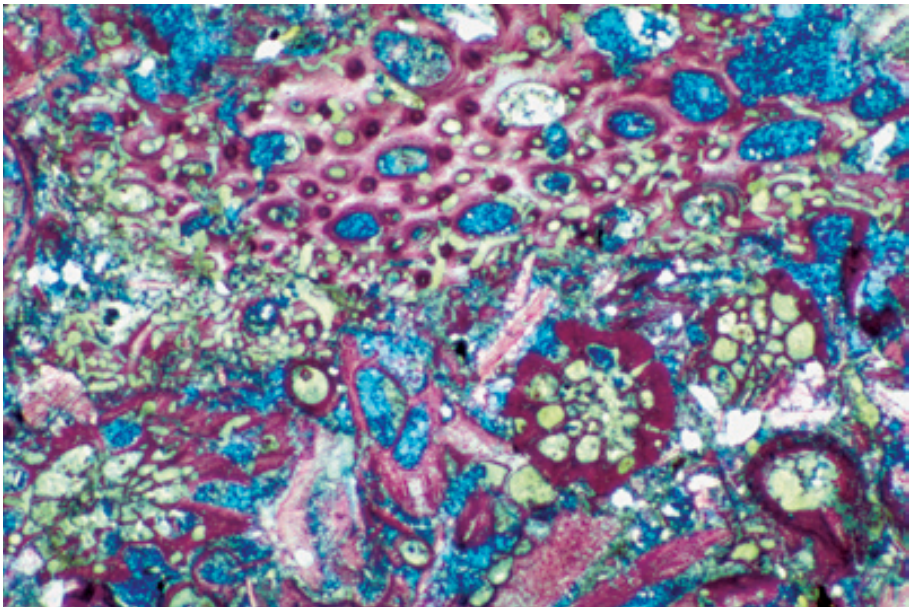

Up. Permian (Kazanian?) Wegener Halvø Fm., Jameson Land, East Greenland

Slowly deposited, cool-water carbonates commonly have glauconite or phosphate filling the porosity within bioclasts or other grains. In this section, pale greenish glauconite cement fills the zooecia, mesopores and borings within these bryozoans.

PPL, AFeS, BSE, HA = 1.65 mm

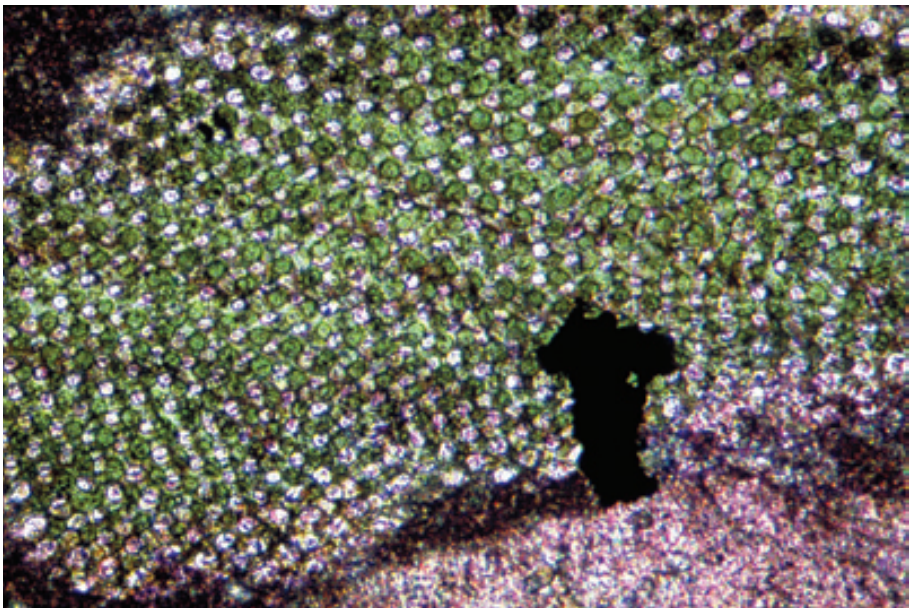

Oligocene Nile Gp., Karamea, Westland, New Zealand

This example shows glauconite filling the regularly-arranged intraparticle pores within a single-crystal echinoid plate. In higher energy deposits, these pores are normally filled with carbonate cement or micrite, but in environments with minimal sedimentation, glauconite can precipitates in the pores.

PPL, AFeS, HA = 0.6 mm

Up. Cretaceous Monte Antola Fm., Genova region, Liguria, Italy

Authigenic feldspars are rarely a significant component in carbonate rocks, but in some diagenetic environments they can be common. Albite is the most frequently encountered replacement feldspar in limestones, although other feldspars are found as well. Feldspar replacements can be easily confused with megaquartz replacements due to their similar birefringence; they can be differentiated based on euhedral crystal shapes, the presence of twinning, or by staining. Since they are replacements, they also commonly contain inclusions of the original carbonate material, as in this example.

XPL, HA = 0.36 mm

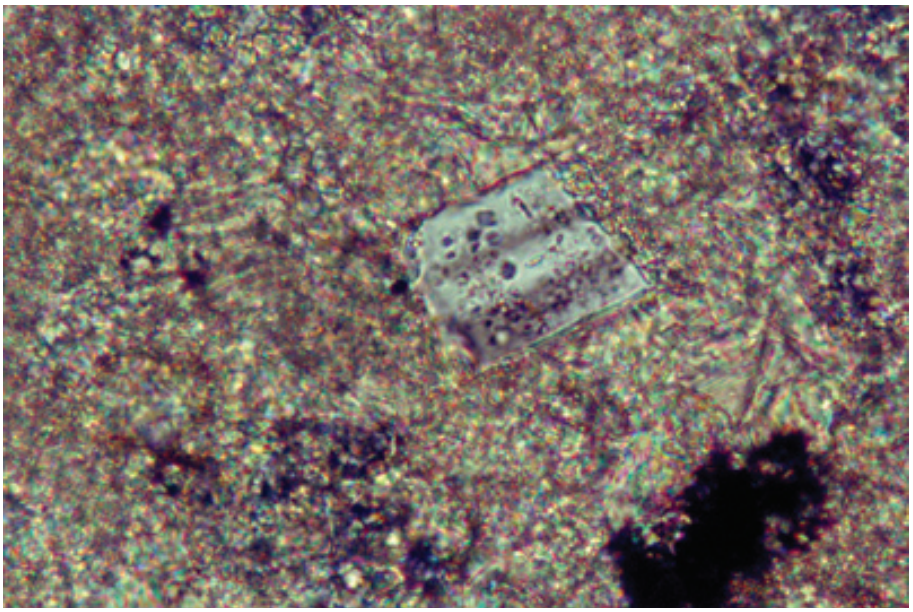

Pennsylvanian Buckhorn Asphalt, Murray Co., Oklahoma

An asphalt-impregnated limestone — the brownish color and pervasive distribution of material between and within grains and crystals are characteristic of hydrocarbon residues. In this case, the early input of oil allowed the preservation of aragonite in a 300 million year-old rock containing algae and mollusks. Here, a possible *Palaeoaplysina* sp. fragment (see section on Problematica) has been superbly preserved due to the early saturation of the rock by hydrocarbons.

PPL, HA = 1.65 mm

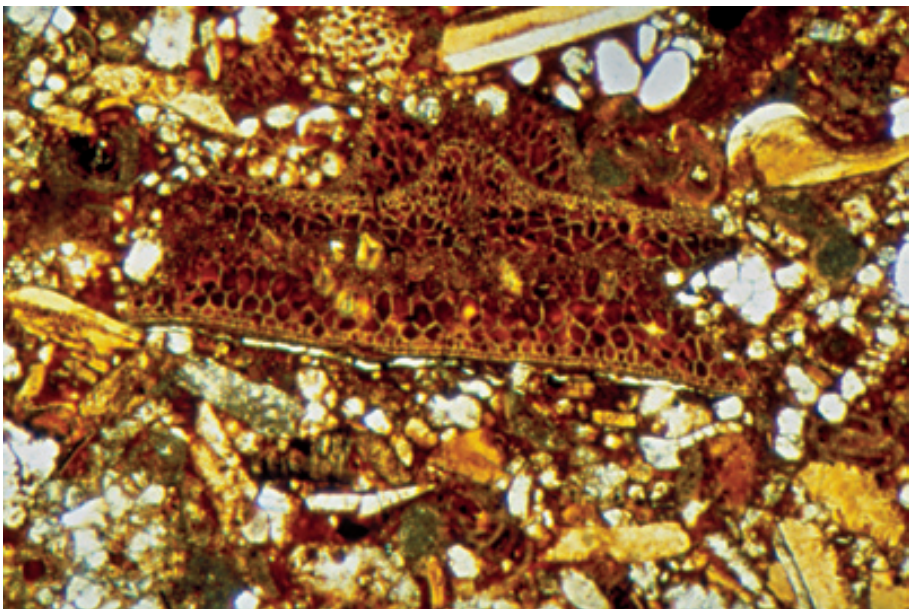

Pennsylvanian Buckhorn Asphalt, Murray Co., Oklahoma

The Buckhorn Asphalt is unusual because of its extensive aragonite preservation. Early entry of hydrocarbons into the unit and high hydrocarbon saturation levels effectively terminated chemical diagenesis in this limestone, because the asphaltic residues prevent aqueous fluids from entering the rock. The asphalt precluded chemical diagenetic alteration, but not compactional crushing — therefore, there is minimal cementation, and the 300 million year-old aragonitic grains (mainly thin-walled cephalopod shells) are extensively fractured.

PPL, HA = 5.0 mm

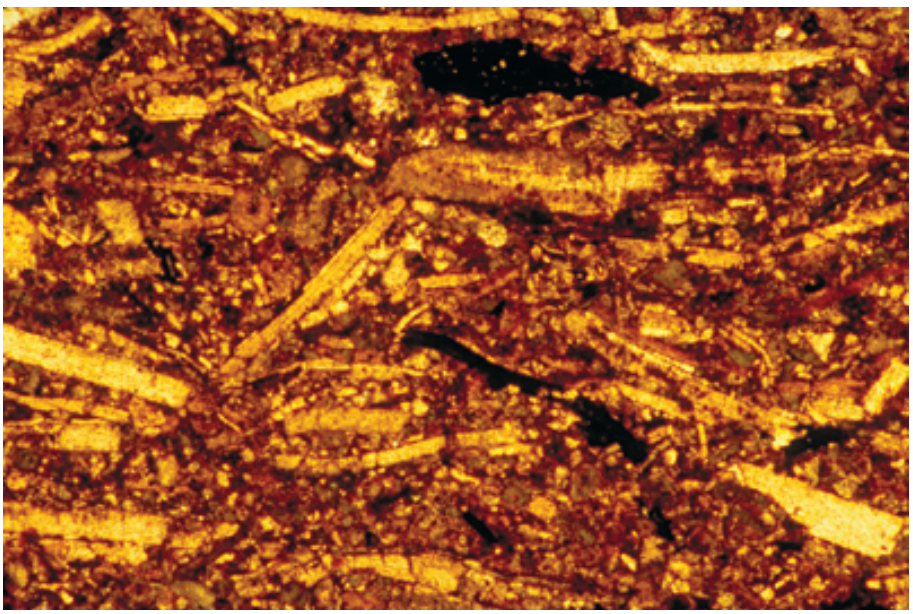

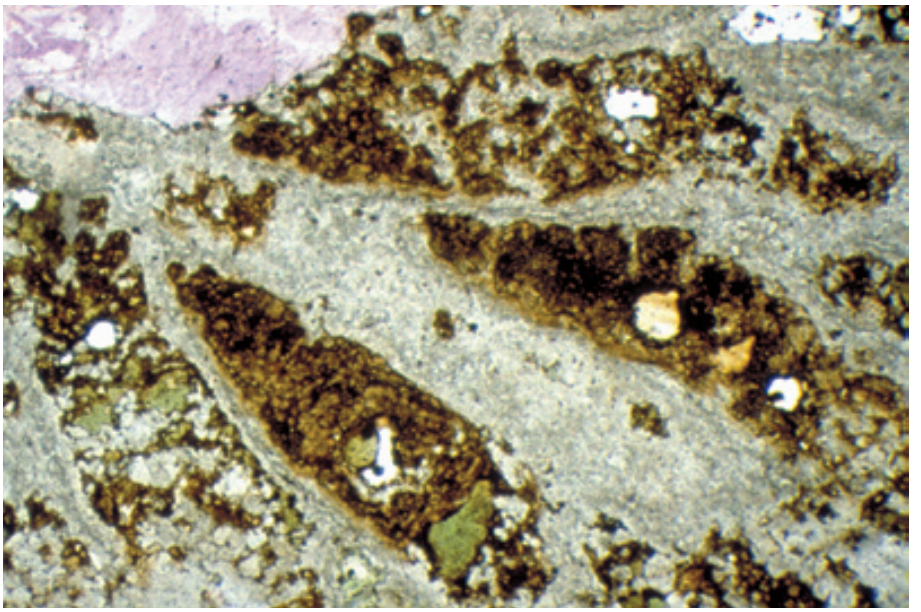

Silurian (Wenlockian) Lilley Fm., Adams Co., Ohio

The hydrocarbon impregnation of this limestone predates the burial-stage ferroan calcite visible in the upper left corner of photomicrograph. The hydrocarbons infiltrated and stained most porosity within or between the grains and crystals, but did not preclude cementation in large, late-stage, vuggy pores.

PPL, AFeS, HA = 5.1 mm

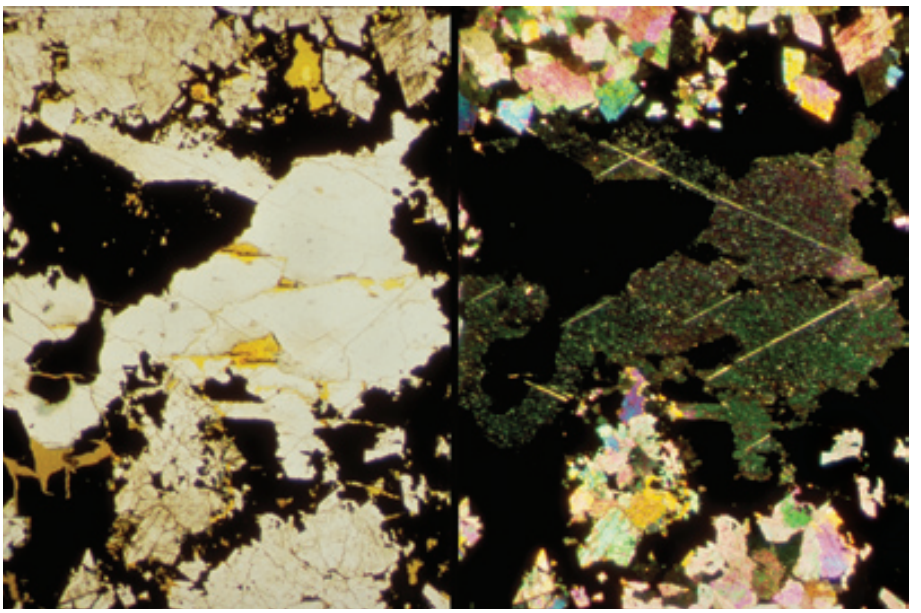

Up. Jurassic (Oxfordian) Up. Smackover Fm., subsurface, Gulf Coast, USA

Even after hydrocarbons saturate a rock, it is still possible to flush the rock and remove enough of the hydrocarbons to allow diagenesis to continue. In this example, the hydrocarbons (black) have either converted to bitumen (dead oil) or have been partially flushed from the rock permitting later calcite cementation. Note the brown staining in the calcite; this is probably due to trapped liquid hydrocarbon inclusions. The host rock here consists of baroque dolomite. Photograph courtesy of Clyde H. Moore.

PPL/XPL, HA = ~2 mm each

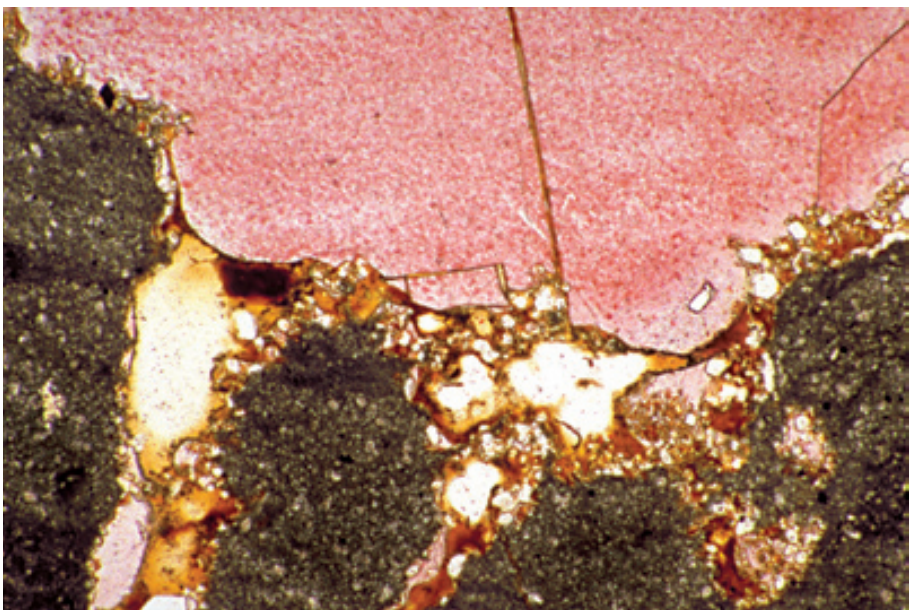

Up. Permian (Guadalupian) Yates Fm., Eddy Co., New Mexico

The hydrocarbons in this sample (now visible as brownish colored residues in lower half of the photograph) once filled this leached evaporite nodule and long predate the precipitation of blocky, non-ferroan, calcite spar (pink). Uplift-stage partial flushing of the trapped oil allowed precipitation of the calcite in contact with hydrocarbon residues. The calcite spar crystals thus have rounded or curved edges formed by contact with a meniscus surface between residual oil and water.

PPL, AFeS, HA = 3.0 mm

Up. Permian (Kazanian?) Wegener Halvø Fm., Jameson Land, East Greenland

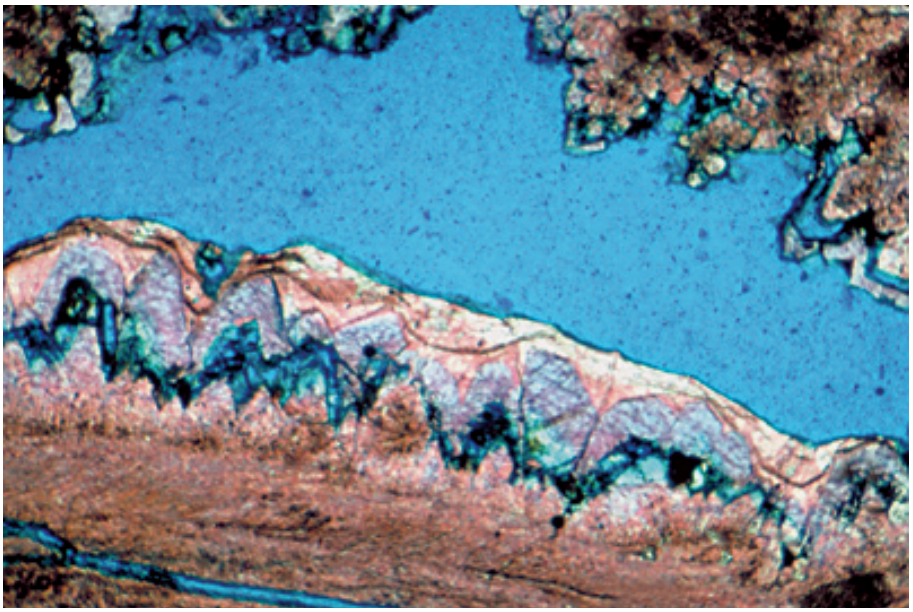

In this view, dead-oil residues cover an early non-ferroan calcite spar cement. After partial flushing of the hydrocarbons, cementation continued with ferroan and then non-ferroan calcite spar. With close examination, it may be noted that the early calcite spars contact the later ferroan and non-ferroan spars at only a few points. Hydrocarbons essentially coated the calcite preventing direct nucleation on the earlier cements. Continued meteoric flushing removed some of the hydrocarbons and resulted in an irregular linear pore (with some asphaltic residues) separating the two cements.

PPL, AFeS, BSE, HA = 2.4 mm

Up. Permian (Kazanian?) Wegener Halvø Fm., Jameson Land, East Greenland

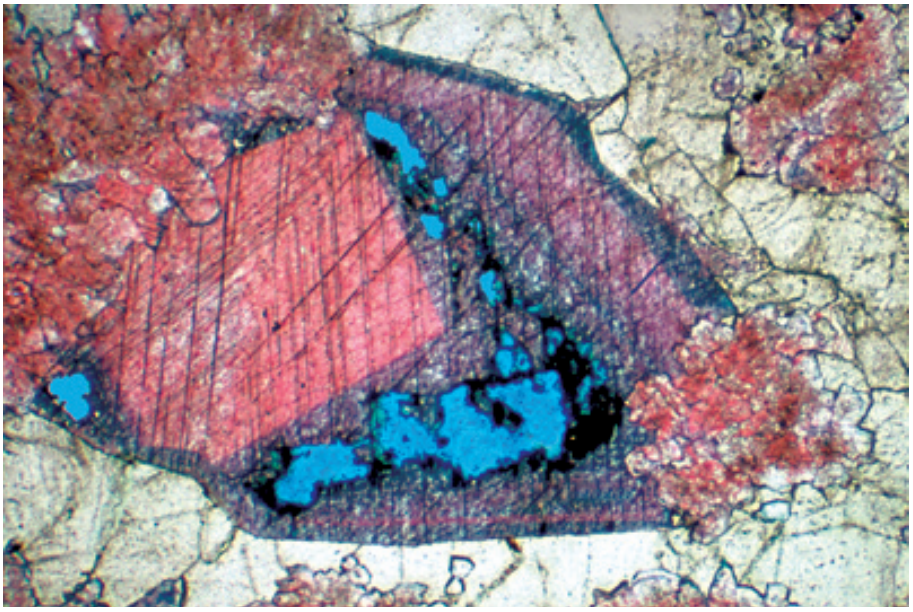

Another view showing how hydrocarbons can affect cementation. In this case, early non-ferroan calcite and a thin zone of ferroan calcite spar were followed by hydrocarbon migration into the rock. After some flushing, cementation continued with further precipitation of ferroan calcite and fluorite. The hydrocarbon residues were later largely removed, leaving irregular pore spaces and scattered asphaltic residues between cement generations.

PPL, AFeS, BSE, HA = 4.1 mm

Lo. Cretaceous (Barremian) Kharaib Fm., subsurface, offshore Qatar

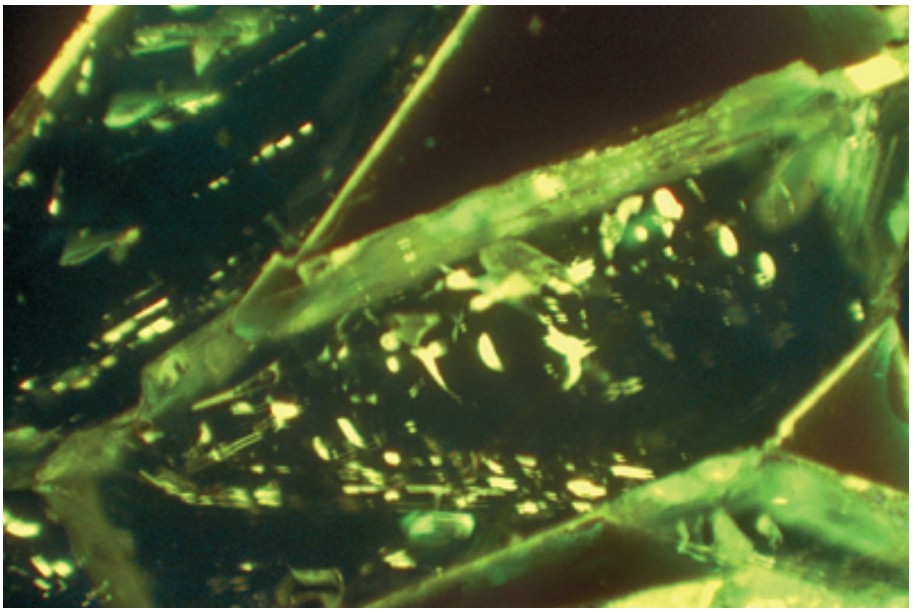

In this epi-fluorescence photomicrograph, hydrocarbon (mainly oil) inclusions are clearly visible as brightly fluorescent spots within dull to non-fluorescent calcite cements. Many of the inclusions formed along growth zones in the calcite cements; others appear to be more randomly distributed. The color and intensity of fluorescence can be used to identify oil types. Each "grade" has a color range in which it can be placed.

FL, HA =1.0 mm

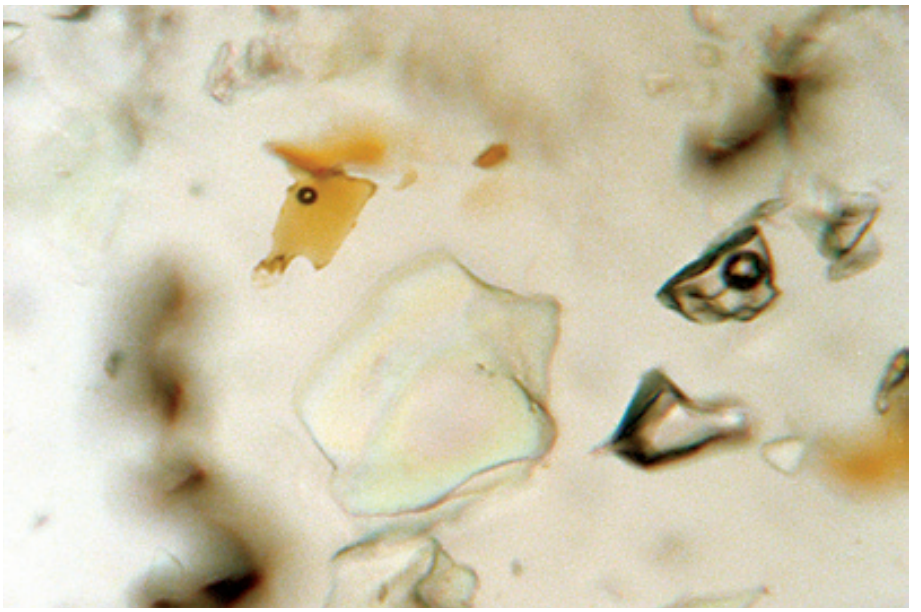

Up. Permian (Guadalupian) Yates Fm., Eddy Co., New Mexico

Hydrocarbon inclusions normally are brownish in color. Colorless hydrocarbon inclusions do occur, however, and epi-fluorescence petrography may be necessary to identify such inclusions. In this view, an authigenic quartz crystal in a limestone contains hydrocarbon, aqueous, and solid inclusions. All the fluid inclusions in this view are primary; the hydrocarbon inclusion is brown with a small vapor bubble, and the brine inclusion contains a large vapor bubble and is slightly darker than the host quartz crystal. The solid inclusions are remnants of anhydrite (indicating that the quartz has replaced an anhydrite nodule).

PPL, HA = 60 μm

Cited References and Additional Information Sources

Anderson, G. M., and G. Garven, 1987, Sulfate-sulfide carbonate associations in Mississippi Valley-type lead zinc deposits: Economic Geology, v. 82, p. 482-488.

Baker, P. A., and S. H. Bloomer, 1988, The origin of celestite in deep-sea carbonate sediments: Geochimica et Cosmochimica Acta, v. 52, p. 335-339.

Berner, R. A., 1970, Sedimentary pyrite formation: American Journal of Science, v. 268, p. 1-24.

Berner, R. A., 1984, Sedimentary pyrite formation: an update: Geochimica et Cosmochimica Acta, v. 48, p. 605-615.

Brodtkorb, M. K., de, V. Ramos, M. Barbieri, and S. Ametrano, 1982, The evaporitic celestite-barite deposits of Neuquen, Argentina: Mineralium Deposita (Berlin), v. 17, p. 423-436.

Burruss, R. C., K. R. Cercone, and P. M. Harris, 1985, Timing of hydrocarbon migration: evidenced from fluid inclusions in calcite cements, tectonics and burial history, *in* N. Schneidermann, and P. M. Harris, eds., Carbonate Cements: Tulsa, OK, SEPM Special Publication No. 36, p. 277-289.

Carlson, E. H., 1987, Celestite replacements of evaporites in the Salina Group: Sedimentary Geology, v. 54, p. 93-112.

Carson, G. A., and S. F. Crowley, 1993, The glauconite-phosphate association in hardgrounds: examples from the Cenomanian of Devon, southwest England: Cretaceous Research, v. 14, p. 69-89.

Church, T. M., 1979, Marine barite, *in* R. G. Burns, ed., Marine Minerals: Washington, D.C., Mineralogical Society of America Short Course Notes, Vol. 6, p. 175-209.

D'Angeljan, B. F., 1968, Phosphate diagenesis of marine carbonates as a mode of in situ formation of marine phosphorites. Observations in a core from the eastern Pacific: Canadian Journal of Earth Sciences, v. 5, p. 81-87.

Evans, G., and D. J. Shearman, 1964, Recent celestite from the sediments of the Trucial Coast of the Persian Gulf: Nature, v. 202, p. 385-386.

Field, M. E., and O. H. Pilkey, 1970, Lithification of deep sea sediments by pyrite: Nature, v. 226, p. 836-837.

Frazier, W. J., 1975, Celestite in the Mississippian Pennington Formation, central Tennessee: Southeastern Geology, v. 16, p. 241-248.

Graber, K. K., and H. S. Chafetz, 1990, Petrography and origin of bedded barite and phosphate in the Devonian Slaven Chert of central Nevada: Journal of Sedimentary Petrology, v. 60, p. 897-911.

Harwood, G. M., 1983, The application of cathodoluminescence in relative dating of barite mineralization in the Lower Magnesian Limestone (Upper Permian), United Kingdom: Economic Geology, v. 78, p. 1022-1027.

Heydari, E., 1997, The role of burial diagenesis in hydrocarbon destruction and H_2S accumulation, Upper Jurassic Smackover Formation, Black Creek Field, Mississippi: American Association of Petroleum Geologists Bulletin, v. 81, p. 26-45.

Honjo, S., A. G. Fischer, and R. E. Garrison, 1965, Geopetal pyrite in fine-grained limestones: Journal of Sedimentary Petrology, v. 35, p. 480-488.

Kastner, M., 1971, Authigenic feldspars in carbonate rocks: American Mineralogist, v. 56, p. 1403-1442.

Krajewski, K. P., 1984, Early diagenetic phosphate cements in the Albian condensed glauconitic limestone of the Tatra Mountains, Western Carpathians: Sedimentology, v. 31, p. 443-470.

Love, L. G., 1971, Early diagenetic polyframboidal pyrite, primary and redeposited, from the Wenlockian Denbigh Grit Group, Conway, North Wales, UK: Journal of Sedimentary Petrology, v. 41, p. 1038-44.

McConchie, D. M., and D. W. Lewis, 1978, Authigenic, perigenic and allogenic glauconites from the Castle Hill Basin, North Canterbury, New Zealand: New Zealand Journal of Geology and Geophysics, v. 21, p. 199-214.

Olaussen, S., 1981, Formation of celestite in the Wenlock, Oslo region Norway — evidence for evaporitic depositional environments: Journal of Sedimentary Petrology, v. 51, p. 37-46.

Raiswell, R., and R. A. Berner, 1985, Pyrite formation in euxinic and semi-euxinic sediments: American Journal of Science, v. 285, p. 710-725.

Sassano, G. P., and K. Schrijver, 1989, Framboidal pyrite: early diagenetic, late diagenetic, and hydrothermal occurrences from the Acton Vale Quarry, Cambro-Ordovician, Quebec: American Journal of Science, v. 289, p. 167-179.

Scholle, P. A., L. Stemmerik, and O. Harpøth, 1990, Origin of major karst-associated celestite mineralization in Karstryggen, central East Greenland: Journal of Sedimentary Petrology, v. 60, p. 397-410.

Spötl, C., M. Kralik, and M. J. Kunk, 1996, Authigenic feldspar as an indicator of paleo-rock/water interactions in Permian carbonates of the Northern Calcareous Alps, Austria: Journal of Sedimentary Research, Section A: Sedimentary Petrology and Processes, v. 66, p. 139-146.

Wilson, H. H., 1977, "Frozen-in" hydrocarbon accumulations or diagenetic traps — exploration targets: American Association of Petroleum Geologists Bulletin, v. 61, p. 483-491.

Facing Page: A cathodoluminescence (CL) photomicrograph showing a calcite-cemented skeletal limestone. CL reveals multiple generations of cement filling pores. Permian (Kazanian?) Wegener Halvø Fm., Jameson Land, East Greenland. HA = ~34 mm.

Analytical Techniques

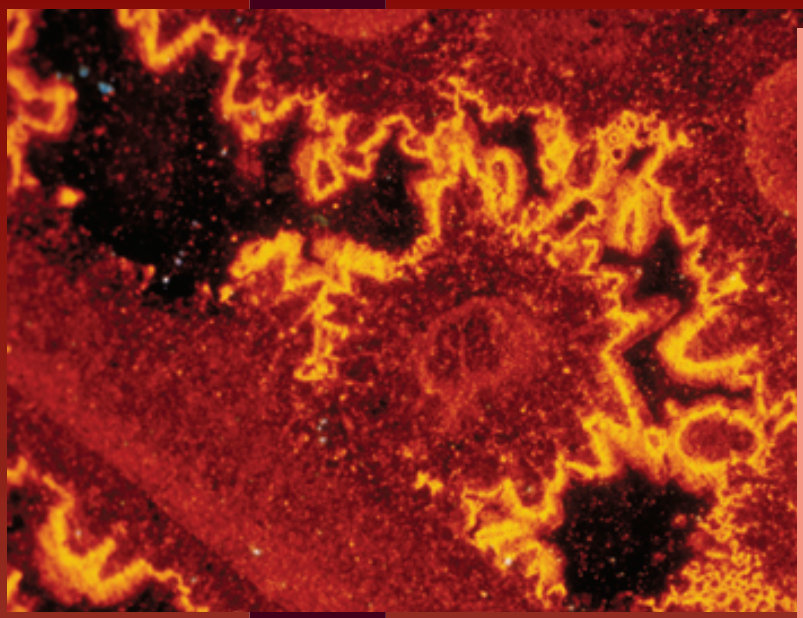

CHAPTER 30

- Staining
- Reflectance
- Cathodoluminescence
- Epi-fluorescence
- Fluid inclusion geothermometry
- Electron microprobe analysis
- X-ray diffraction
- C, O, and Sr isotopic geochemistry

INTRODUCTION TO TECHNIQUES

Although light-microscope petrography is an extremely valuable tool for the identification of minerals and their textural interrelationships, it is best used, in many cases, in conjunction with other techniques.

Precise mineral determinations are greatly aided by staining of thin sections or rock slabs, by x-ray analysis, or by microprobe examination. Where noncarbonate constituents are present in carbonate rocks, they often are better analyzed in acid-insoluble residues than in thin section. Where detailed understanding of the trace element chemistry of the sediments is essential, x-ray fluorescence, inductively coupled plasma mass spectrometry, ion microprobe, electron microprobe, atomic absorption or cathodoluminescence techniques may be applicable; and where it is desirable to know the temperatures, water sources, and/or pore fluid compositions involved in cementation, fluid inclusion geothermometry, stable isotope geochemistry, strontium isotope geochemistry and a number of other analytical techniques may provide useful information.

In addition, many sediments may be too fine-grained for adequate examination with the light microscope. The practical limit of resolution of the best light microscopes is in the 1-2 μm range. Many carbonate and non-carbonate matrix constituents fall within or below this size range. Furthermore, because most standard thin sections are about 30 μm thick, a researcher typically sees 10 or 20 such small grains stacked on top of one another in a micritic limestone, with obvious loss of resolution. Smear mounts or strew mounts (slides with individual, disaggregated grains smeared or settled out onto the slide surface) are an aid in examining small grains where the material can be disaggregated into individual components. In most cases, however, scanning and transmission electron microscopy have proved to be the most effective techniques for the detailed examination of fine-grained sediments.

The bibliography for this chapter (and those in many previous chapters as well) provides references to techniques useful in supplementing standard petrographic analysis. Although many of the techniques require sophisticated and expensive equipment, others, such as thin-section staining, production of acetate peels, or concentration of insoluble residues, can be done in any laboratory and at very little cost.

Because of the potential desirability of supplemental techniques, it is often useful to prepare epoxy-cemented thin sections without coverslips. These sections can be examined under a light microscope, either by placing a drop of water and a coverslip on the sample during viewing, or by using mineral oil or index of refraction oils with or without coverslips. Such examination involves some loss of resolution, but does allow the cleaning and drying of the surface of the section and subsequent staining, cathodoluminescence, or microprobe examination. One can even partially or completely immerse the thin section in acetic or hydrochloric acid and decalcify the section, thereby sometimes enhancing organic structures or insoluble-mineral fabrics. Finally, uncovered thin sections can be ground thinner in cases where examination of very fine-grained sediments is needed.

Clearly, one can spend years analyzing a single sample using all possible techniques. Efficient study requires a thorough understanding of all available tools and proper application of the most useful and productive of these.

QUALITATIVE TECHNIQUES

Staining techniques are among the fastest, simplest, and cheapest methods for getting reliable mineralogical, and some qualitative elemental, data on carbonate phases. The following list of minerals and their diagnostic stains is derived from the work of Friedman (1959), Dickson (1965 and 1966), Milliman (1974), and others. The original papers, listed in the bibliography, will provide details about the exact application and methods.

Aragonite **- can be distinguished from calcite by the use of Feigel's Solution. Aragonite turns black whereas calcite remains colorless for some time. Mixing Feigel's Solution requires 7.1 g of $MnSO_4 \cdot H_2O$; 2 to 3 g of Ag_2SO_4; 100 cc of distilled water and a 1% NaOH solution. Difficult to prepare and store.**

Calcite **- can be distinguished from dolomite with a simple stain of Alizarin Red S in a 0.2% HCl solution (cold). Calcite and aragonite turn red, whereas dolomite remains colorless.**

Dolomite **- can be distinguished from calcite by the above method or one can stain specifically for dolomite with a number of organic stains including Titan yellow, Trypan Blue, and Safranine O. All these stains require careful boiling of the sample in a concentrated NaOH solution.**

High-Mg calcite **- can be distinguished from aragonite and low-Mg calcite with a Clayton Yellow stain, made by adding 0.5 g of Titan Yellow, 4.0 g of NaOH, and 2 g of EDTA to 500 ml of distilled water. The section is etched in dilute acetic acid for 30 seconds, and is then put in Clayton Yellow solution for 30 minutes. Mg-calcites stain pale pink to red with increasing Mg content. Mg-calcite can also be stained with Alizarin Red S in 30% NaOH; calcite remains colorless and Mg-calcite turns purple (see Choquette and Trusell, 1978).**

Ferroan calcite **- can be distinguished (along with ferroan dolomite) from normal calcite by the use of a potassium ferricyanide stain in a weak HCl solution (details in Dickson, 1966). Ferroan minerals turn pale to deep turquoise, and non-ferroan ones remain colorless. This is normally done in conjunction with Alizarin Red S staining of a thin section. The combined staining process requires initial etching in HCl, followed by staining in a combined solution of HCl, Alizarin Red S and potassium ferricyanide, and then a final staining in an HCl and Alizarin Red S mixture (see Dickson 1965, 1966). Although it sounds complex and must be done carefully, it is not difficult and can be accomplished in any laboratory with a sink and a fume hood.**

Most stains are easily damaged on uncovered sections, so they must be handled with care or they can be more robustly preserved with a covering of mineral oil or normal application of a glass cover slip.

Rock slabs can also be stained with these same solutions to see macroscopic mineralogical variations.

Acetate peels are fast, easy and cheap method to view details of carbonate rock fabric; they can even provide mineralogical information if staining is combined with pre-peel etching (see Katz and Friedman, 1965).

Variations in illumination methods, such as the "white card" technique of Folk (1987), can accentuate details and enhance recognition of subtle or largely obliterated features defined by organic or mineral residues.

Finally, visual estimation of percentages of grains, matrix, or porosity is enhanced by impregnation with dyed or fluorescent media and by the use of visual comparison charts, two of which are included as an appendix to this chapter. Computerized image analysis is now widely used for accurate percentage determinations.

Up. Cambrian Kittatiny Fm., northern New Jersey

Sometimes even very simple and inexpensive techniques can enhance petrographic observation. This image and the one below offer a comparison of textural details visible with standard transmitted light illumination and with "white card" incident lighting (Folk, 1987). In this view, one sees a dolomitized grainstone with probable organic-rich ooids along the margins of the image and smaller, more indistinct, possible skeletal fragments in the central area. Sample from F. B. Van Houten.

PPL, HA = 2.0 mm

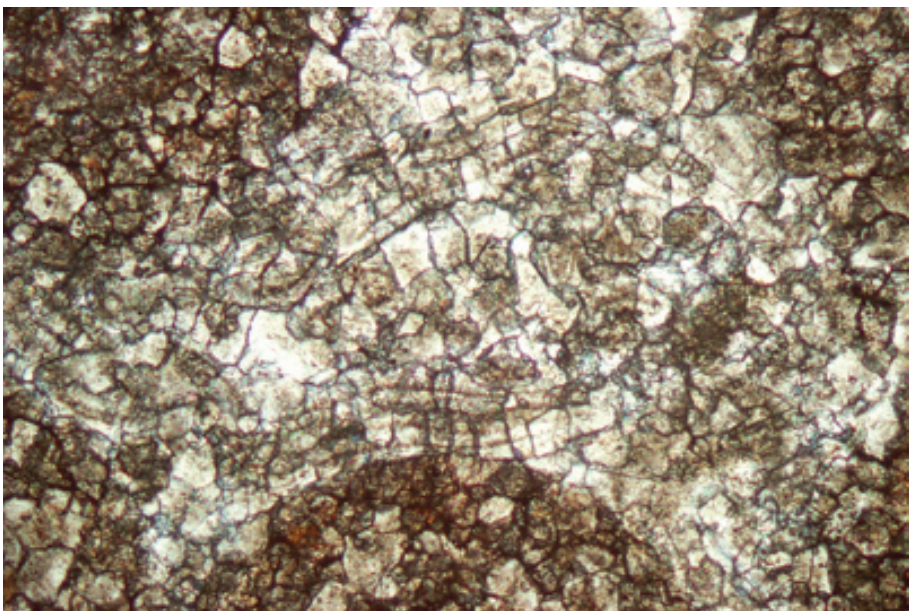

Up. Cambrian Kittatiny Fm., northern New Jersey

This image was taken with a white index card inserted on the stage below the thin section coupled with oblique illumination from a standard, relatively high-intensity light bulb. Under this illumination, the ooids are seen to have hematite (perhaps after pyrite) precipitated in the interstices between replacement dolomite crystals. In the central area, a number of skeletal grains and small, rounded peloids are visible. All in all, this is a much clearer image of relict fabric than that seen above and it reveals a less well sorted sediment than would have been inferred from the transmitted light view. Sample from F. B. Van Houten.

RL, HA = 2.0 mm

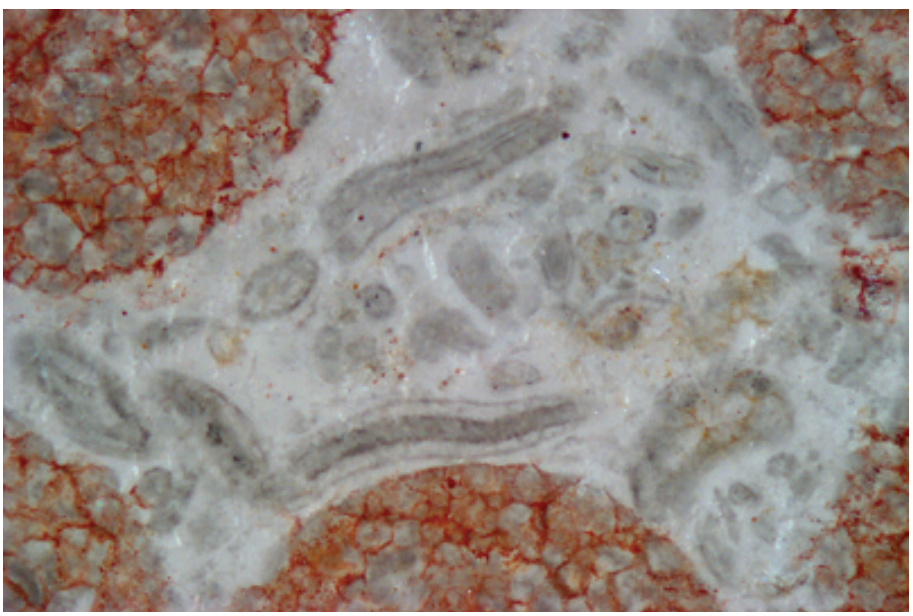

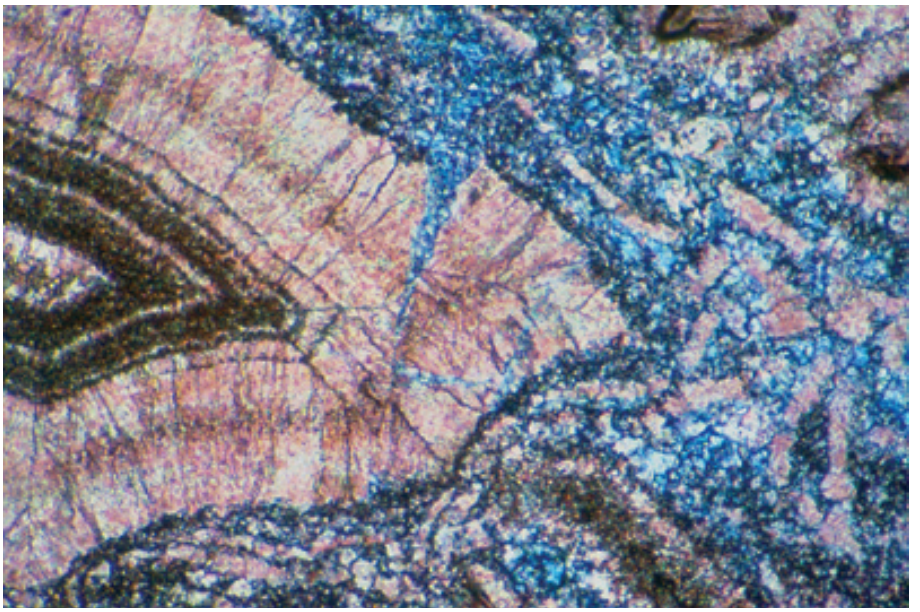

Up. Permian (Kazanian?) Wegener Halvø Fm., Jameson Land, East Greenland

An example of the utility of combined Alizarin Red S-potassium ferricyanide staining. In this case, selective dissolution of synsedimentary marine cements has led to collapse of some cement layers and formation of a collapse breccia of fragments of those cement crusts. The breccia fragments were then encased in late-stage ferroan calcite cement. In the absence of staining, this fabric would be virtually impossible to recognize or interpret.

PPL, AFeS, HA = 1.8 mm

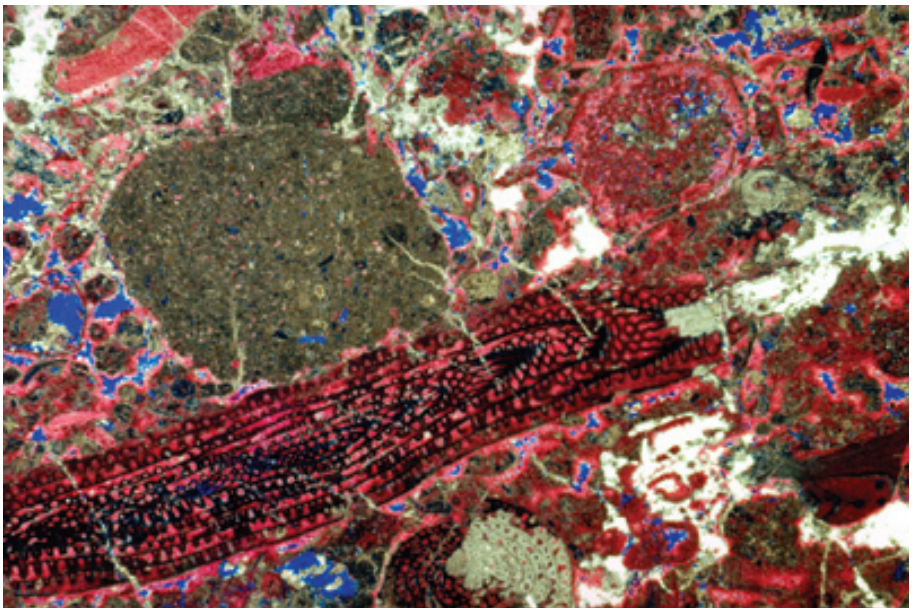

Up. Permian (Guadalupian), Capitan Fm., subsurface, Eddy Co., New Mexico

An example of Alizarin Red S staining of a partially dolomitized and fractured dolopackstone from a forereef slope deposit. Grains include fusulinids and small lithoclasts. Pores are lined by an isopachous rind of calcite (dark) and are filled with minor, finely crystalline dolomite (gray) and anhydrite (white). In the absence of staining, it would be almost impossible to accurately distinguish such aphanocrystalline dolomite.

PPL, AS, BSE, HA = 16 mm

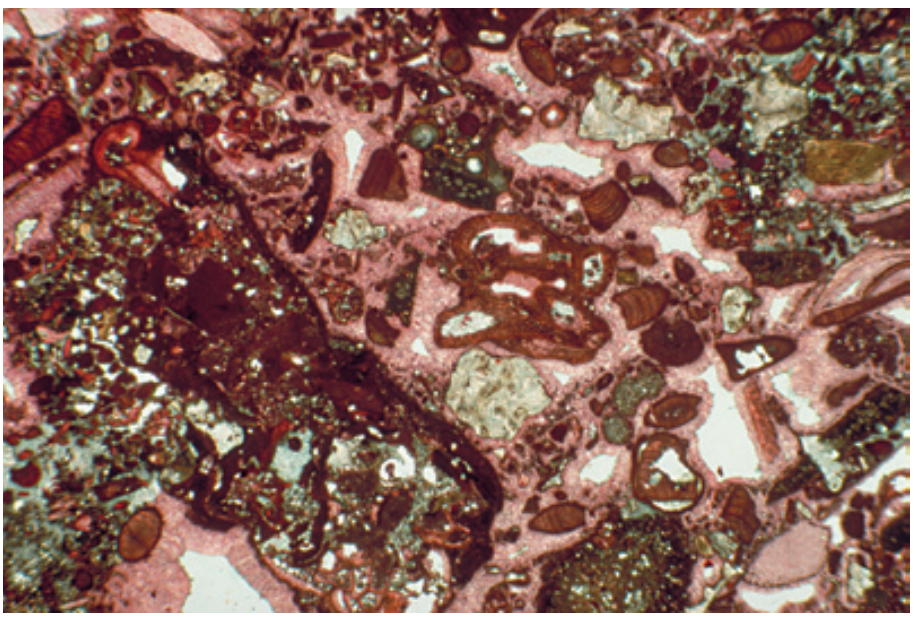

Holocene reef-wall limestone, Belize

This section is stained with Clayton Yellow. It shows a skeletal grainstone cemented by isopachous rinds of fibrous Mg-calcite (stained pink) with patchy areas of aragonitic grains and cement (unstained). In the absence of staining, it would be very difficult to distinguish, with complete accuracy, these two mineralogies. Photograph courtesy of Noel P. James.

PPL, CYS, HA = 2.0 mm

Up. Permian (Kazanian?) Wegener Halvø Fm., Jameson Land, East Greenland

Staining of carbonate minerals can be done on cut and etched rock surfaces (even naturally etched outcrop surfaces). Here, a slabbed but unpolished core was lightly etched and stained with potassium ferricyanide. Late-stage ferroan calcite cements (stained bright blue) are clearly visible and are graphically distinguished from the primary (unstained) constituents without the need to cut a thin section.

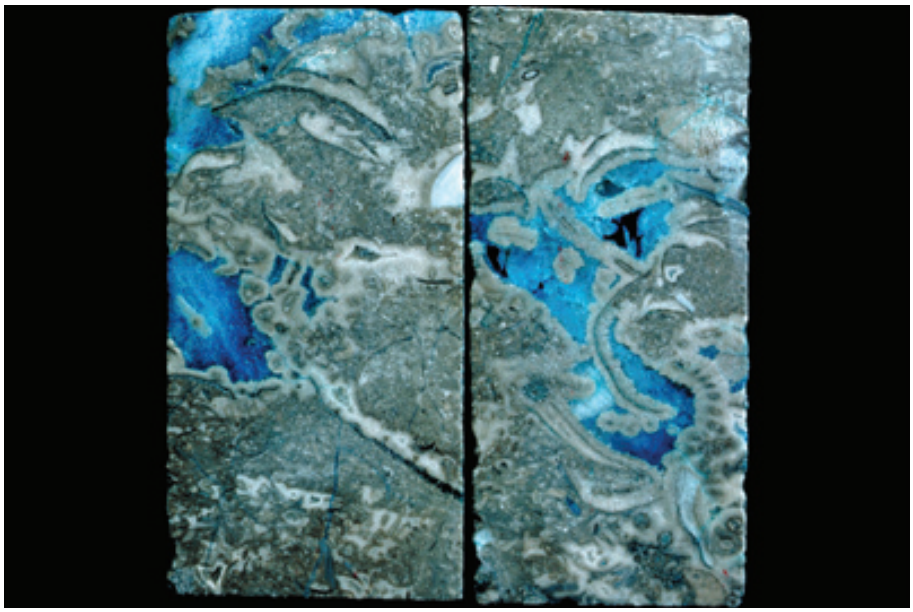

Mac, AFeS, HA = ~12 cm

Mid. Jurassic (Bathonian) Cajarc Fm., Marcilhac Mbr., Aquitaine Basin, SW France

Acetate peels represent another simple method to get detailed observational data without cutting thin sections. Peels require only a cut, ground, and etched rock surface, and thus are fast and easy to prepare. This example shows pseudomorphs after crystals of secondary anhydrite. The pseudomorphs are filled with geopetal sediment, but the roof of unreplaced relicts is very thin and the calcite-cemented void is even thinner. Photograph courtesy of David N. Clark.

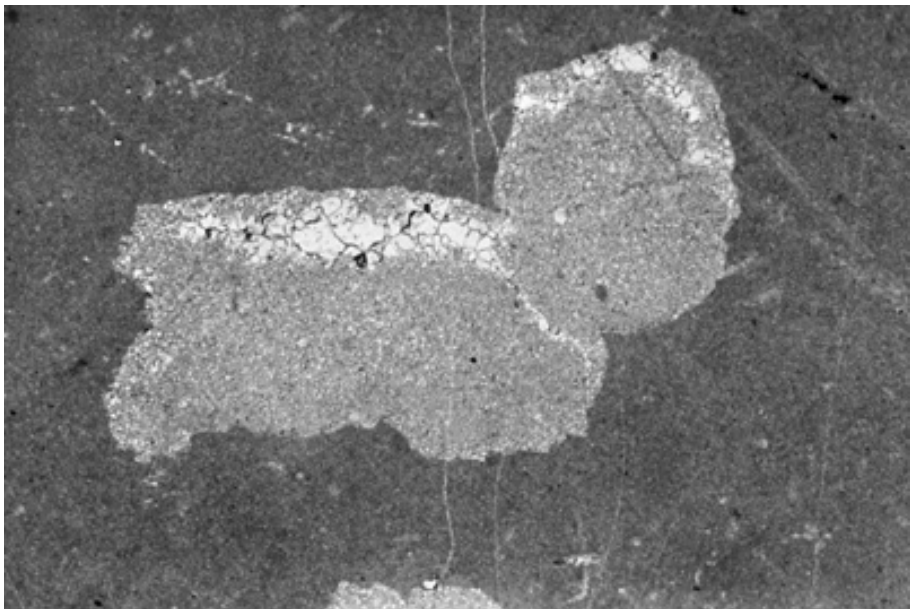

PPL, HA = 2.1 mm

Devonian limestone, Reefton, Westland, New Zealand

This is an example of an acetate peel made from a coral-stromatoporoid limestone. The fidelity of reproduction of the limestone fabric is excellent and allows clear observation of the both grains and matrix. Although mineralogic studies are more difficult with peels, one can stain the rock first and then make a peel that incorporates part of the stain. This at least allows recognition of those mineralogies for which stains are available (Bissell, H., 1957; Katz and Friedman, 1965; Davies and Roger, 1968). Photograph courtesy of Doug W. Lewis.

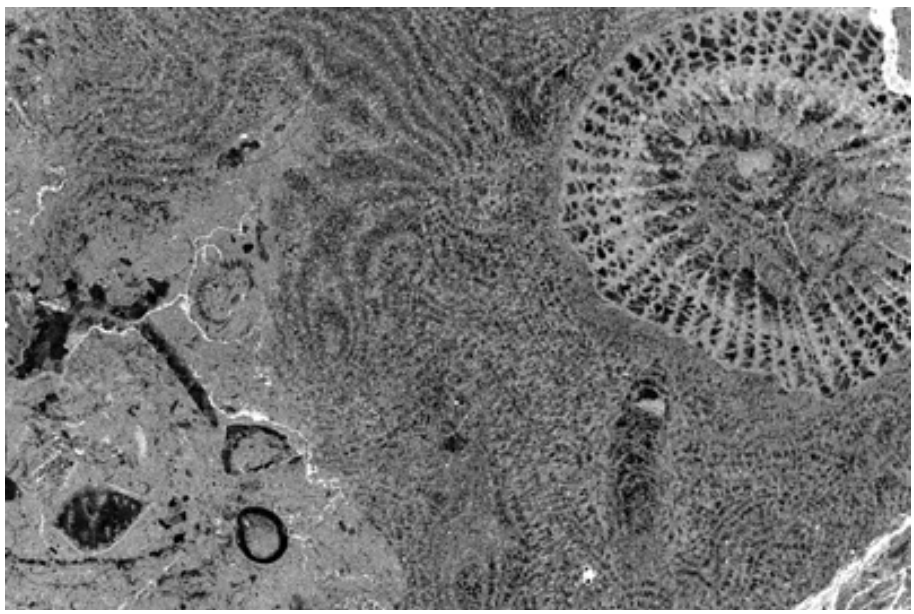

PPL, HA = ~20 mm

Pennsylvanian Francis Creek Shale, Mazon Creek, Illinois

This is an acetate peel of plant remains in partially silicified sediment. The peel was made using HF acid etching (a process requiring extreme care and specialized equipment to handle caustic fumes and hazardous chemicals). Note the excellent preservation of replaced cellular material along with ray structure and concentric growth banding in this member of the extinct order, Lepidodendrales. Acetate peels like this commonly show more structure than thin sections because of the effects of etching. Serial peels can be made with little material wastage, allowing examination of structures in three dimensions (e.g., Honjo, 1963).

PPL, HA = 12.5 mm

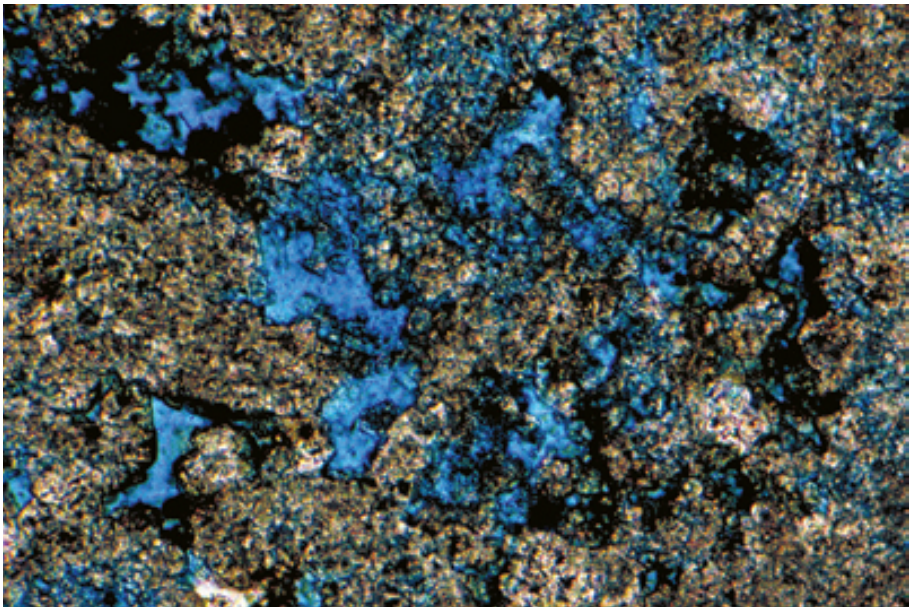

Up. Permian (Guadalupian) Grayburg-Up. San Andres Fms., 3,103 ft (946 m) depth, Crane Co., Texas

Recognition of porosity in carbonate rocks is greatly facilitated by impregnation with dyed epoxy prior to cutting and grinding thin sections. Colored epoxy allows distinction of real porosity from porosity created by plucking or fracturing of material during section preparation. It also helps to reveal microporosity, as in this dolomitized shallow shelf deposit. Fluorescent dyes can be used to further aid in quantification of porosity distributions (e.g., Ali and Weiss, 1968). Photograph courtesy of Susan Longacre.

PPL, BSE, HA = ~0.25 mm

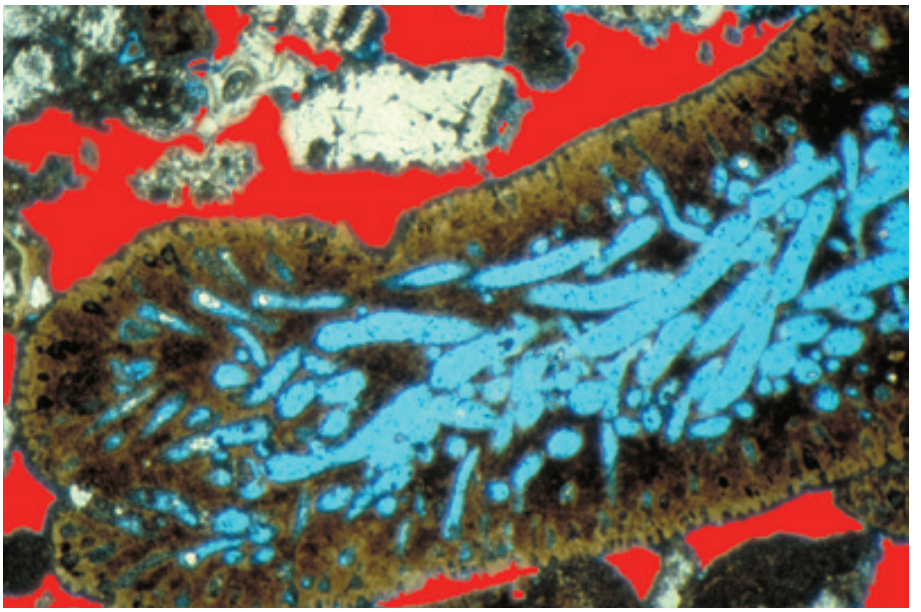

Recent sediment, Grand Cayman, Cayman Islands, B.W.I.

This thin section of a modern shelf limestone (containing a large grain of the green alga, *Halimeda*) has been impregnated with blue-dyed epoxy. The interparticle porosity was distinguished from intraparticle porosity by computer enhancement. Such computer manipulation of porosity types can help to quantify porosity information in carbonate rocks through automated image analysis.

PPL, BSE+, HA = 2.4 mm

SEMI-QUANTITATIVE AND QUANTITATIVE TECHNIQUES

Although many highly specialized techniques exist, only a few of those most commonly used will be covered here — cathodoluminescence, epi-fluorescence, fluid inclusion geothermometry, SEM backscattered electron imaging, microprobe analysis, x-ray diffraction, and isotope geochemistry. It is beyond the scope of this book to provide details of any of these techniques, so only basic principles and examples of major uses are provided.

CATHODOLUMINESCENCE MICROSCOPY

Cathodoluminescence (CL) can be an invaluable tool in petrographic studies. It provides information on the spatial distribution of trace elements, particularly Fe^{2+} and Mn^{2+}, in calcite, dolomite and other grains and cements. Regional mapping of cement zones relative to unconformities has been used to determine the timing and origin of some cements (e.g., Meyers, 1974).

Analysis can be done using polished rock chips, polished thin sections, or even unpolished and uncovered thin sections. The equipment needed costs about the same as a moderately priced polarizing microscope and can be installed on virtually any microscope (see Marshall, 1988; Miller, 1988).

CL responses are normally described as brightly luminescent, dully luminescent, or nonluminescent, although modern equipment allows more detailed measurement of intensities and spectral information on CL. In general, incorporation of Mn^{2+} into the calcite lattice stimulates luminescence and incorporation of Fe^{2+} reduces or quenches luminescence.

As noted earlier in this book, qualitative interpretation of CL assigns nonluminescent response to oxidizing environments in which the reduced forms of both Mn and Fe are unavailable for incorporation into the crystal lattices of calcite or dolomite precipitates. Oxidized forms of these elements are not incorporated into calcite or dolomite crystals and, thus, there is nothing in the crystals to excite luminescence. Bright luminescence is associated with crystals with relatively high Mn/Fe trace element ratios, typically achieved under reducing conditions during early to intermediate stages of burial diagenesis. Dull luminescence occurs where lower Mn/Fe trace element ratios are present in carbonate crystals, typical in cements or replacements formed during intermediate to late stages of burial diagenesis.

These generalized comments are major simplifications, and the reader is urged to consult recent references on CL-related issues for more details (Frank et al., 1982; Machel, 1985; Marshall, 1988; Hemming et al., 1989; Barker and Kopp, 1991; Budd et al., 2000) In particular, there has been much discussion over the past two decades about whether or not other elements can supplement or moderate the effects of Mn^{2+} and Fe^{2+} enhancement or reduction of luminescence, but recent papers have largely discounted the importance of such influences (e.g., Budd et al., 2000).

Up. Permian (Kazanian?) Karstryggen Fm., Jameson Land, East Greenland

Cathodoluminescence (CL) allows the recognition, regional mapping, and correlation of subtle compositional variations in calcite or dolomite cements with little cost and effort. In this example from a calcite-filled fracture, CL reveals numerous geochemical fluctuations during cement precipitation. Field, petrographic and geochemical evidence suggest that these fluctuations probably reflect changes in redox conditions within an extensively fractured rock that underwent alteration beneath multiple subaerial exposure surfaces.

CL, HA = ~25 mm

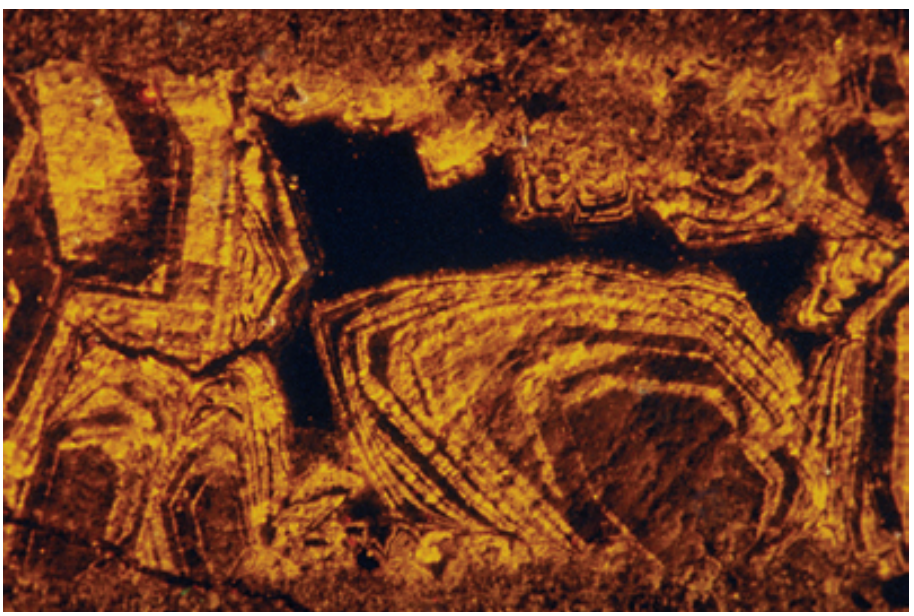

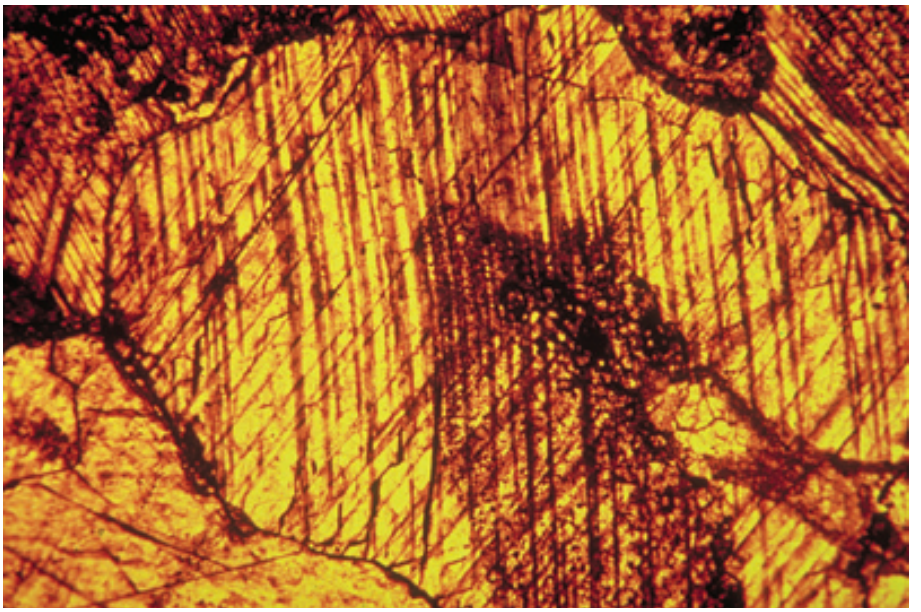

Lo. Mississippian Lake Valley Fm., Otero Co., New Mexico

This photograph and the one below show the same area in transmitted light and under cathodoluminescence. Both images depict a crinoidal biosparite with a large syntaxial overgrowth surrounding a crinoid (the speckled grain in the lower center of the photograph). From this transmitted light view, one can only discern a single undifferentiated overgrowth, recognizable from the twin lamellae that cross from the crinoid through the surrounding sparry calcite. Photograph courtesy of William J. Meyers.

PPL, HA = ~2.7 mm

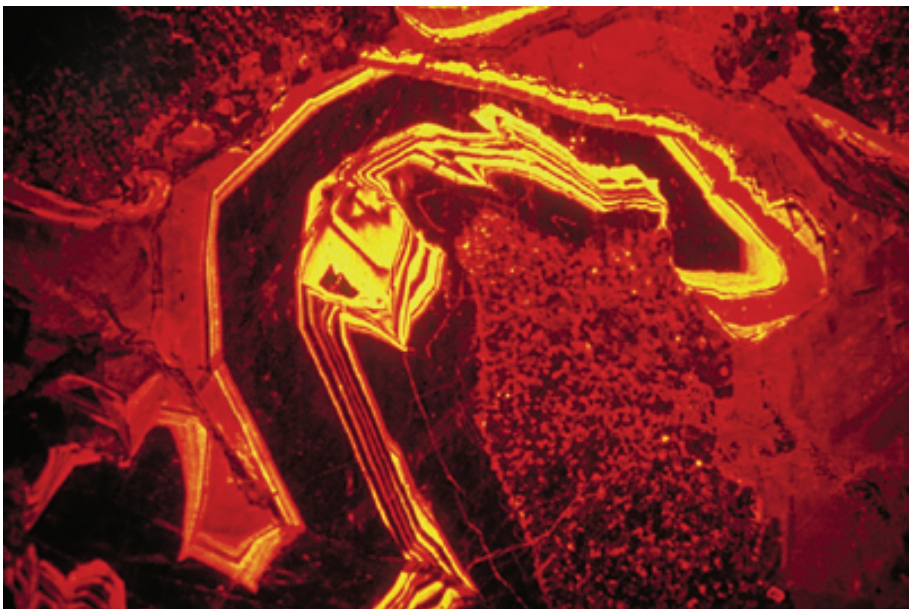

Lo. Mississippian Lake Valley Fm., Otero Co., New Mexico

A CL image of approximately the same area as shown in the image above. With cathodoluminescence, at least five major generations of cementation are visible, along with a number of minor events marked by thinner banding. The major cement generations have been correlated from sample to sample and were tied to a variety of tectonic and erosional events (see Meyers, 1974). Photograph courtesy of William J. Meyers.

CL, HA = ~2.7 mm

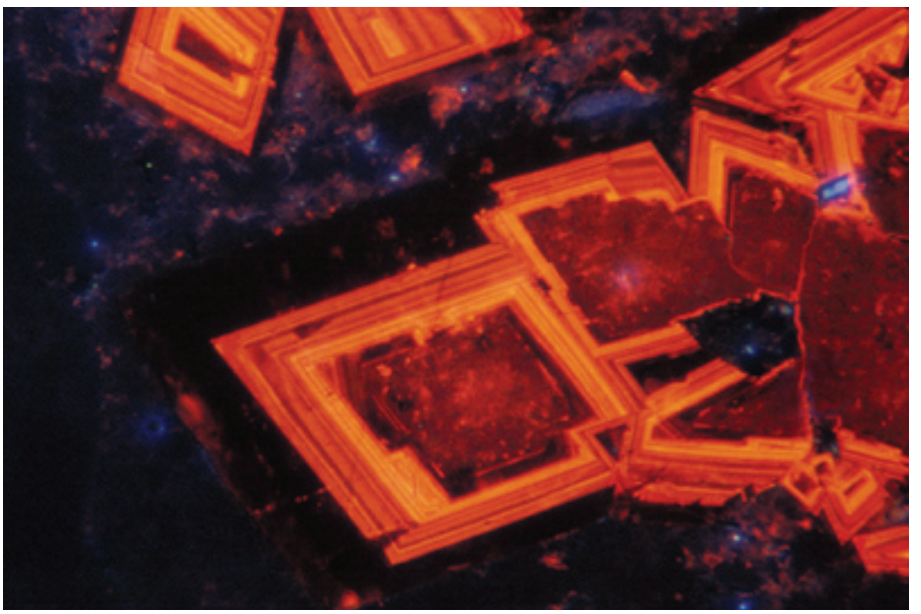

Cambrian Bonneterre Fm., near Viburnum, Missouri

A CL image of vug-filling dolomite cements and authigenic quartz (blue) in a carbonate mudstone. Note the clear definition of multiple compositional zones of alternating bright and dull luminescence in the dolomite cements and the consistency of that zonation from crystal to crystal. The zones with little or no luminescence tend to have elevated Fe^{2+} contents. Photograph courtesy of Jay M. Gregg.

CL, HA = 0.7 mm

Epi-fluorescence Microscopy

Epi-fluorescence microscopy (also termed incident light fluorescence microscopy) has a number of uses in medical, biological, and geological fields — uses that vary with the wavelength spectrum used to excite fluorescence. All uses depend on the emission of light (by a substance capable of producing fluorescence) that continues only during the absorption of the excitation-generating light beam (Rost, 1992).

The primary geological application of fluorescence is to facilitate the recognition of organic matter or "live" hydrocarbons present as inclusions within crystals or as residues in pore spaces. Indeed, with carefully calibrated fluorescence work, one can even determine the specific oil types present (see Dravis and Yurewicz, 1985). Fluorescence can also help to detect zonation within crystals, again on the basis of incorporated organic materials. It is an especially valuable tool when used in conjunction with fluid inclusion microscopy because it can help to distinguish hydrocarbon-filled inclusions from water-filled ones (a particular problem when working with low-maturity, nearly colorless hydrocarbons).

The equipment needed for fluorescence microscopy is relatively simple and can be mounted on any high-quality petrographic microscope. The specialized equipment required includes a high-intensity, mercury- or xenon-arc lighting system, filter packages for different wavelength bands, and specialized water- or oil-immersion reflected light objectives.

Lo. Permian (Leonardian) Bone Spring Ls., Delaware Basin, Eddy Co., New Mexico

Minute hydrocarbon inclusions within compositional zones of dolomite crystals as imaged using epi-fluorescence. Some of these hydrocarbons are present in fluid inclusions and some are found as pore-filling residues. Epi-fluorescence is an effective method for locating and typing non-asphaltic hydrocarbons in thin sections, especially because immature oil inclusions can be colorless, and thus easily confused with aqueous inclusions. Photograph courtesy of David Wiggins and Mitch Harris.

FL, HA = ~2.0 mm

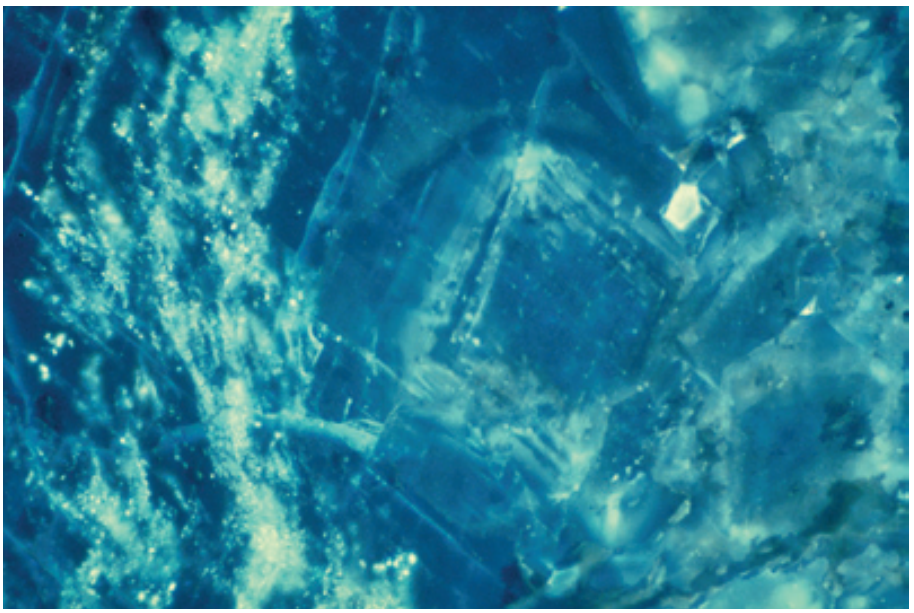

Up. Permian (Guadalupian) Yates Fm., Eddy Co., New Mexico

A view of a limestone under ultraviolet epi-fluorescence showing hydrocarbon and brine inclusions in replacement quartz crystals. Note the strong fluorescence of the hydrocarbon-bearing inclusions and the lack of fluorescence in aqueous inclusions. The inclusions in this view are all primary. The strength and color of the fluorescence provide information on hydrocarbon maturity and type.

FL, HA = 75 µm

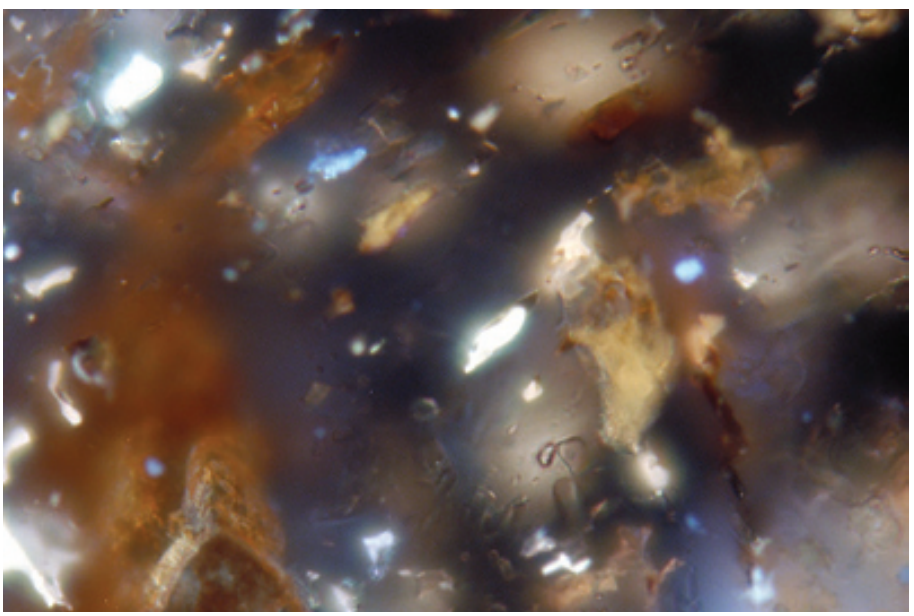

FLUID-INCLUSION MICROSCOPY

Fluid inclusions are present in virtually all crystals. They range in size from less than 1 μm to a few centimeters, although inclusions larger than 1 mm are uncommon. Most contain a fluid that represents a sample of waters trapped during inclusion formation, plus a gas or solid phase that may have separated during later cooling.

Petrographic study (using heating and freezing stages) is used to determine the composition and original temperature of the fluids involved in crystal formation. If interpreted in the broader context of known burial rates and temperature histories for a given basin, this can provide useful information on the timing and conditions of cementation or mineralization.

Finding fluid inclusions requires care and patience because they can occur at any level within a mineral (thus, requiring not just scanning along the X and Y axes of the mineral, but also continually focusing upward and downward along its Z axis as well. Care also must be taken to determine the exact relationships between the fluid inclusions and their host mineral — primary and pseudosecondary inclusions formed when the crystal was initially precipitated; secondary inclusions formed at a later date, perhaps when a crystal was fractured and healed. By distinguishing between these types of inclusions, it sometimes is possible to obtain data on several diagenetic events from a single suite of inclusions. Heating studies are used to determine temperatures at the time of cement precipitation; freezing point determinations on the inclusions can establish the salinities and approximate composition of the waters (or hydrocarbons and hydrocarbon gases) present at the time of inclusion entrapment.

Various minerals, however, give more or less reliable results from fluid inclusion studies. Calcite is an easily cleaved and deformable mineral, so continued heating during burial, to temperatures above those of initial mineral formation, can cause inclusions to stretch or leak, giving misleading temperatures or fluid compositions. Various studies have shown that temperatures only 15°C above those at the time of formation can lead to such re-equilibration in calcite (see summary of studies in Goldstein, 1992). Dolomite and quartz are less easily deformed and so give more reliable results on primary formation temperatures. It should be remembered, however, that even data from re-equilibrated inclusions, if properly interpreted as such, may yield useful information on the *maximum* burial paleotemperatures.

The compositions of fluid inclusions may also be analyzed directly. A number of analytical methods have been used for this type of work, including neutron activation analysis of the dried residuum left after crushing of inclusions, analysis by ion microprobe of liquid or frozen inclusions, or analysis by mass spectrometry of material emitted when inclusions are crushed.

Fluid inclusion microscopy is a complex subject that is both an art and a science — the interested user therefore is urged to read one or more of the books that have been written on this topic (Shepherd et al., 1985; and especially, Goldstein and Reynolds, 1994) and the papers cited in those volumes.

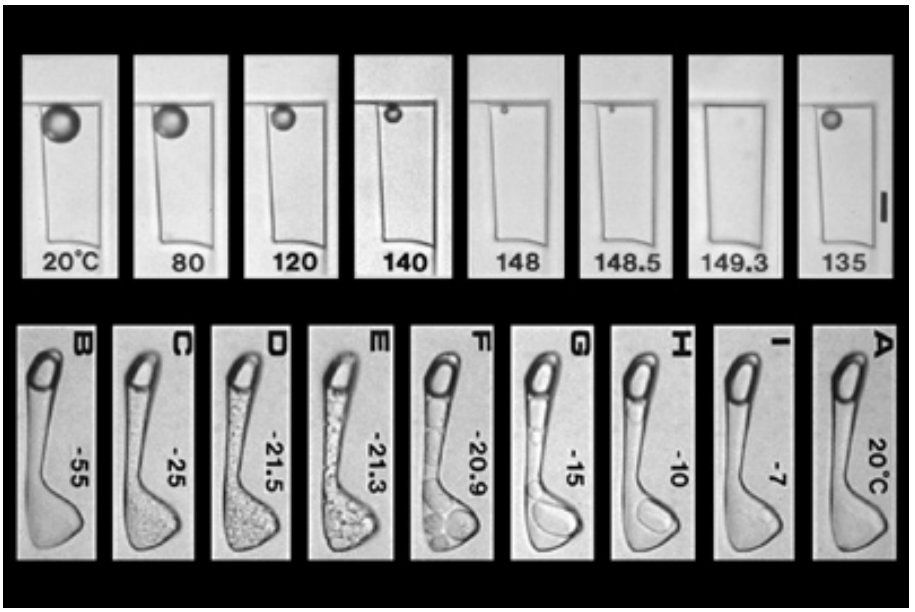

Top: A large inclusion in fluorite being heated to determine the homogenization temperature. The inclusion homogenizes at 149.3°C and must be undercooled to 135°C before the vapor bubble renucleates abruptly. Scale bar = 7 μm

Bottom: Cool/thaw run for synthetic H_2O-NaCl inclusion of 10 wt.% NaCl. A) Room temperature. B) Inclusion freezes to clear solid at about -55°C. C) First indication of crystals (recrystallization?) is at -25°C. D) At -21.5°C, brighter and darker crystal outlines are obvious. E) At 0.1°C below the eutectic. At eutectic, the brighter crystals (hydrohalite) instantly begin to disappear, and concomitantly the ice crystals change size. F) By just 0.3°C above eutectic there is obvious "clearing" (all hydrohalite has broken down). G-I) progressive loss of ice crystals. Photographs courtesy of Robert H. Goldstein (in Goldstein and Reynolds, 1994).

Mississippian limestone, southeastern Kansas

An assemblage of primary fluid inclusions in a calcite cement overgrowth (center) that formed on a crinoid fragment (below). Cloudy area in lower center is a growth-zone bounded area of fluid inclusions; most are two-phase with relatively consistent ratios of liquid to vapor and some are all liquid. Photograph courtesy of Robert H. Goldstein; from Goldstein and Reynolds (1994, Fig. 11.20).

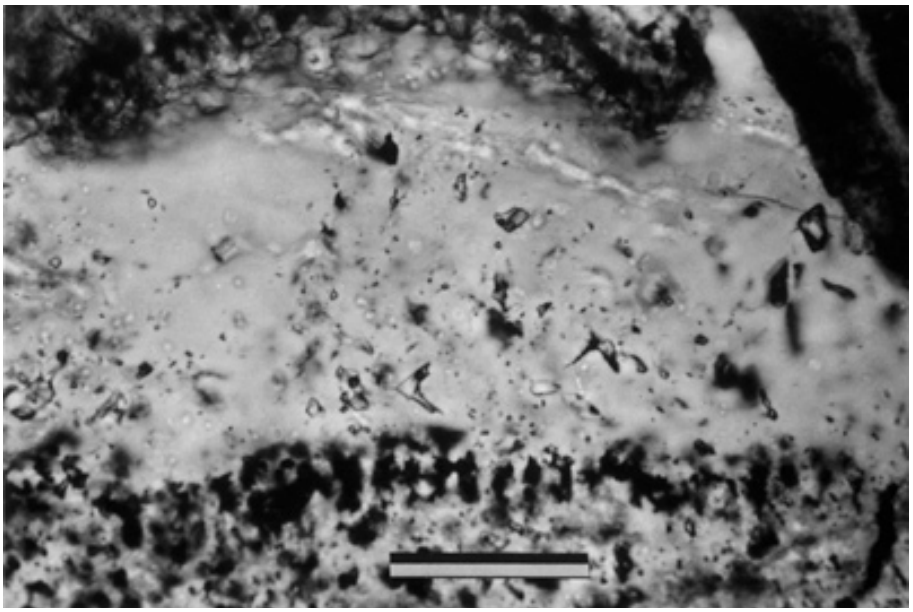

PPL, HA = 115 μm

Late Jurassic, Oxfordian Upper Smackover Fm., Gulf Coast, U.S.A.

A close-up view of numerous two-phase aqueous fluid inclusions in burial-stage calcite cement. To ascertain that the inclusions have not stretched (by overheating) or decreased in size during later diagenesis, it is important to demonstrate a consistent ratio of vapor bubble volume to total inclusion volume within the crystal. This limits possible sources of error during microthermometry. Many of these inclusions, for example, have consistent ratios and, therefore, would be good candidates for fluid inclusion geothermometry. Photograph courtesy of Clyde H. Moore.

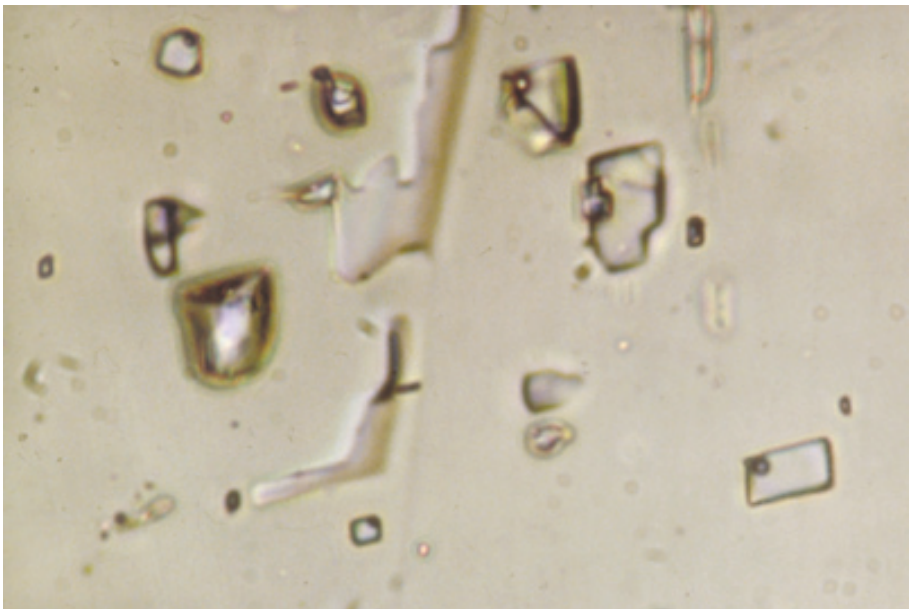

PPL, HA = ~95 μm

Lo. Cretaceous (Barremian) Kharaib Fm., 3,793 ft (1,156 m) depth, offshore Qatar

A view of lath-like calcite crystals filling a secondary vug in a shallow shelf limestone. The crystals contain abundant liquid hydrocarbon inclusions. These inclusions are pseudosecondary, because they have formed along crystal growth zones. Differentiating between secondary and pseudosecondary inclusions can be difficult since they both form linear trends. Detailed petrographic studies, in conjunction with fluid inclusion investigations, are important to help unravel these issues.

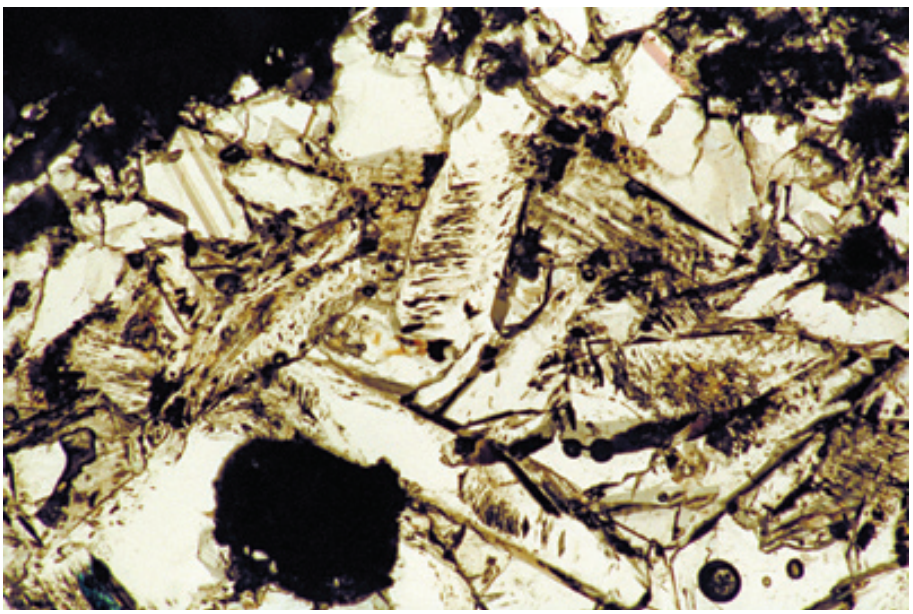

PPL, HA = 4.0 mm

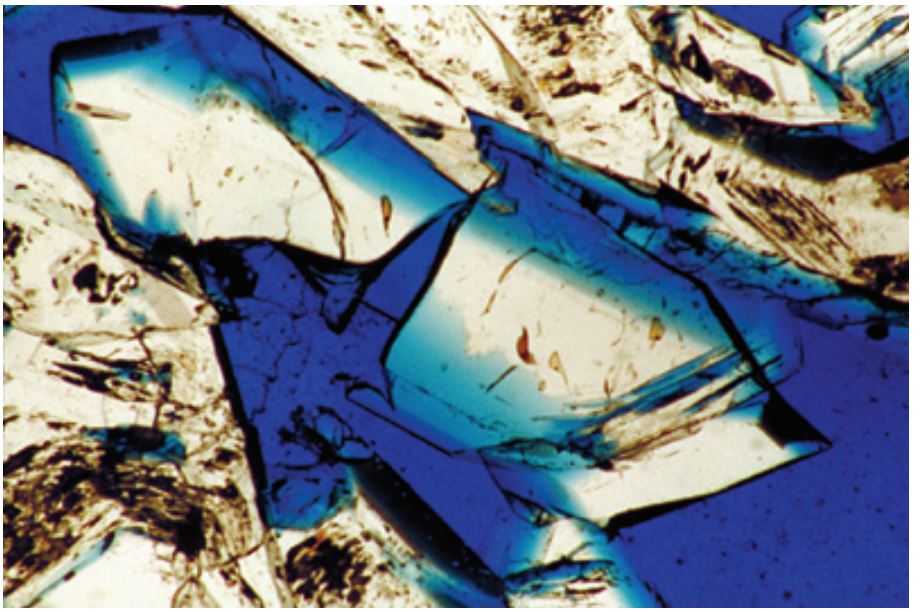

Lo. Cretaceous (Barremian) Kharaib Fm., 3,793 ft (1,156 m) depth, offshore Qatar

A close-up view of material from the same sample as shown in the previous photograph. It again shows calcite crystals filling a secondary vug; the crystals contain abundant and large liquid hydrocarbon inclusions. Note the hydrocarbon staining along growth zones. The calcite crystal morphology in this specimen is unusual in its lath-like shape; this may be due to poisoning of the lattice by the hydrocarbons.

PPL, BSE, HA = 3.0 mm

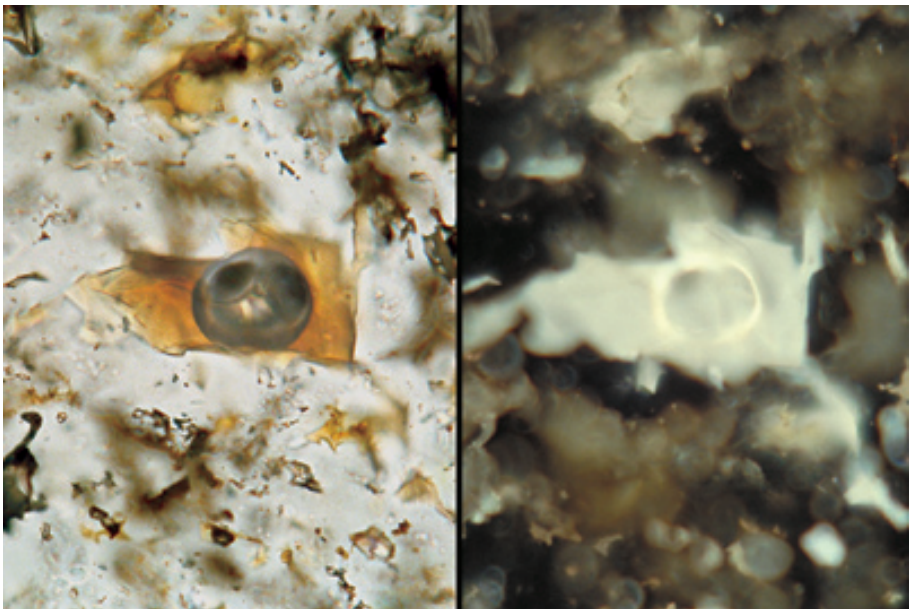

Up. Permian, (Guadalupian) Yates Fm., Eddy Co., New Mexico

A comparison of plane-polarized transmitted light (left) and ultraviolet epi-fluorescence (right) views of hydrocarbon and brine inclusions in replacement quartz crystals. Note the brownish color of the hydrocarbons in transmitted light and the vapor bubble in the oil. The hydrocarbons also are clearly distinguishable by their strong fluorescence.

PPL/FL, HA = 37 μm each

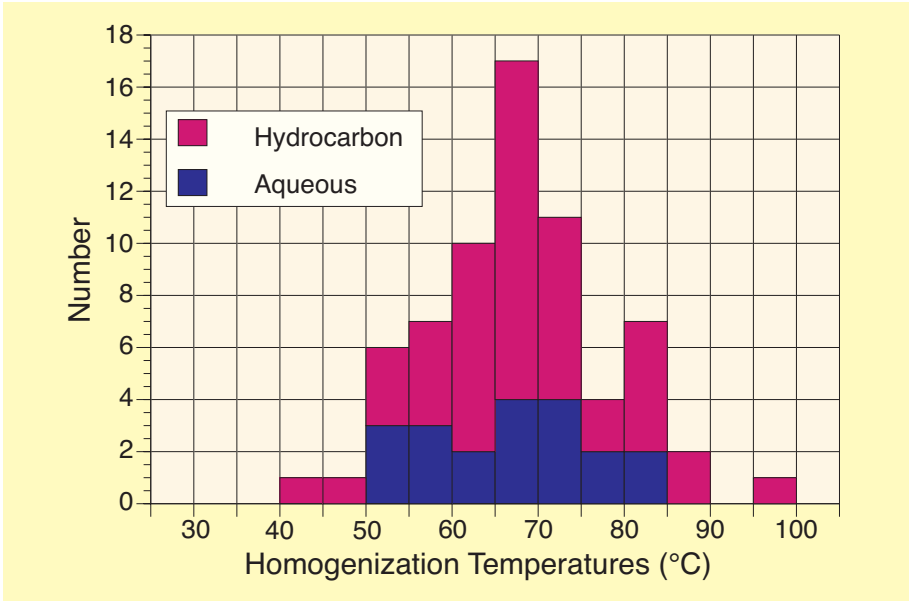

Up. Permian, (Guadalupian) Yates Fm., Eddy Co., New Mexico

Use of histograms is an effective way to illustrate the data gathered during fluid inclusion microthermometry studies. In this graph, aqueous and hydrocarbon inclusions in replacement quartz are plotted against their measured homogenization temperatures. Using histograms enables effective visual display of the data on the thermal history of multiple phases. Redrawn from Ulmer-Scholle et al. (1993).

SEM ENERGY-DISPERSIVE ANALYSIS

The utility of scanning electron microscopy in studying very small objects and three-dimensional grains has been shown throughout this book and in many other publications and needs no elaboration here. The scanning electron microscope, however, is useful not only for examining sediment textures, but when equipped with an energy dispersive analyzer, it also can be used for mineral identification and semi-quantitative chemical analysis. The analyses are rapid (seconds), require relatively little sample preparation, and can be used for very fine-grained sediment (in which staining may be unable to resolve fine-scale details). In most cases, small chips of the sample can be mounted on a small plug with no polishing or cutting required. The sample is then coated with a gold-palladium alloy (or other conductive material) and is inserted into the SEM.

Although energy-dispersive analysis on the SEM provides an excellent tool for mineral identification, it is not ideally suited for quantitative analytical work. Detailed determination of mineral composition or analysis of small crystals for trace element contents is best done using polished samples on an electron microprobe.

The examples below show accessory minerals in chalks from the Upper Cretaceous Atco Formation (Austin Group) of Texas. The upper pair of photographs illustrate pyrite crystals (about 60 µm in diameter) and a chemical analysis of the same area. Note the prominent iron and sulfur peaks highlighted in white. The lower pair of photographs shows a fragment of phosphatic skeletal material (circular depressions are about 100 µm across) with the highest peaks representing the phosphorous and calcium concentrations.

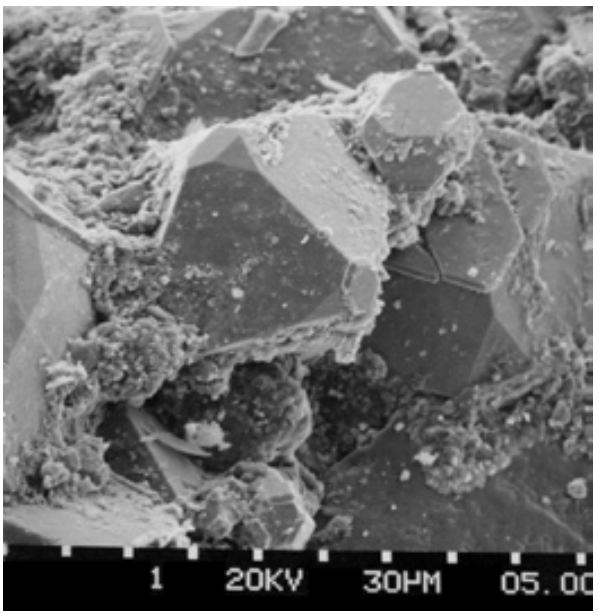

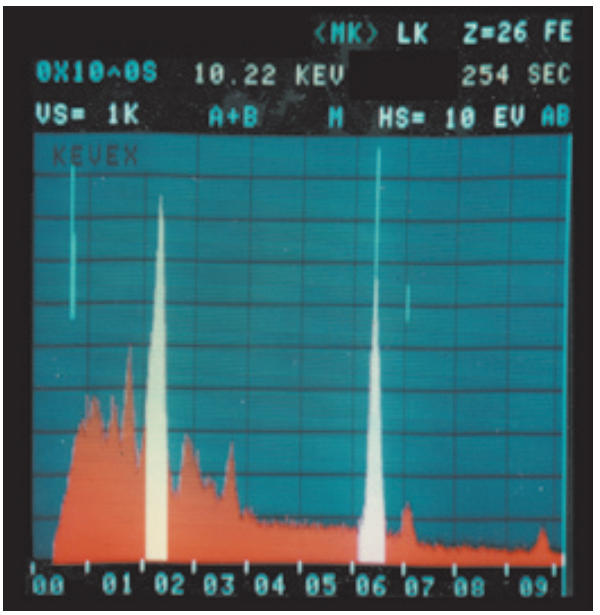

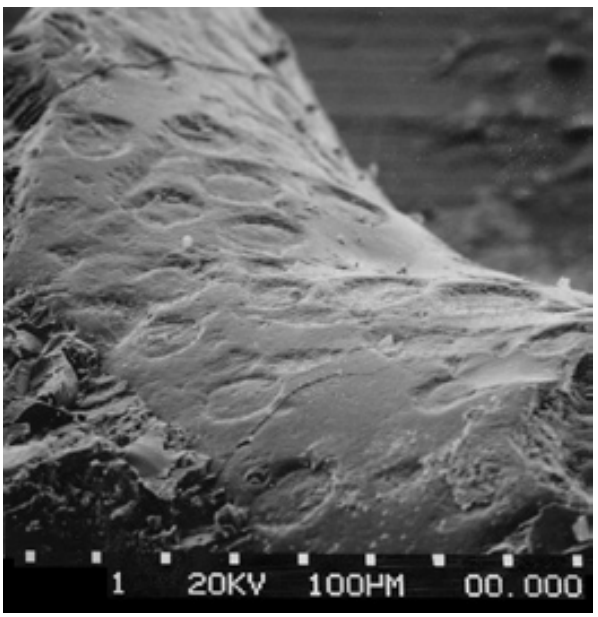

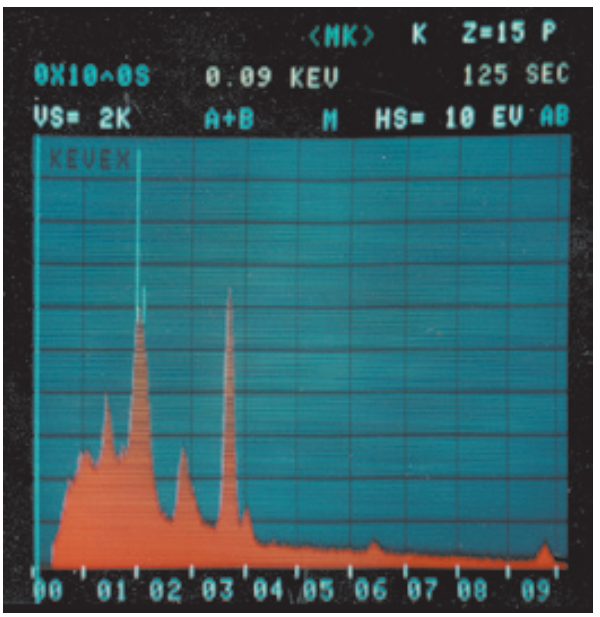

ELECTRON MICROPROBE ANALYSIS

The unique capability of the electron microprobe is the ability to provide quantitative geochemical analyses of areas as small as 1 μm on a polished sample surface. A single geochemical analysis can be produced in a matter of minutes once the machine is calibrated with well characterized reference materials. This type of analysis is valuable for assessing the composition of sample material, and is particularly useful in conjunction with backscattered electron imaging, through which subtle chemical variations or zonation can be easily identified.

A second, commonly-used application of the electron microprobe is production of chemical maps. These maps are made by rastering the electron beam over the sample surface, collecting the x-ray intensity for each image step, and combining this information to produce an image. These map images can be useful for identification of trace phases, examination of compositional zonation, and mineralogical identification. With current computerized image-processing techniques, the maps can be used to quickly produce the type of information that traditionally would be collected by point counting mineral grains.

The main disadvantages of electron microprobe analysis are cost, time required for sample preparation, need for well characterized standards (for quantitative analysis), and difficulty of analyzing trace elements that are present in low abundances.

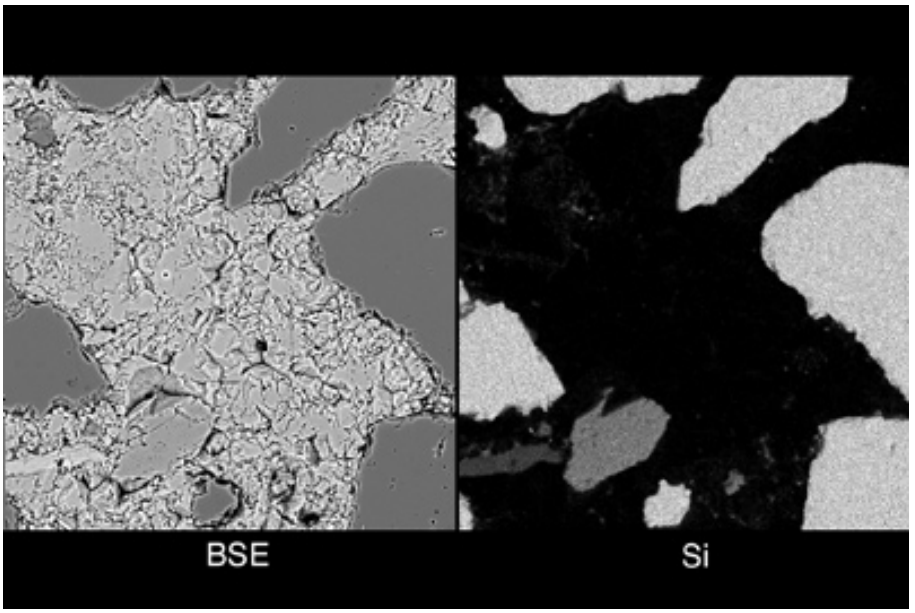

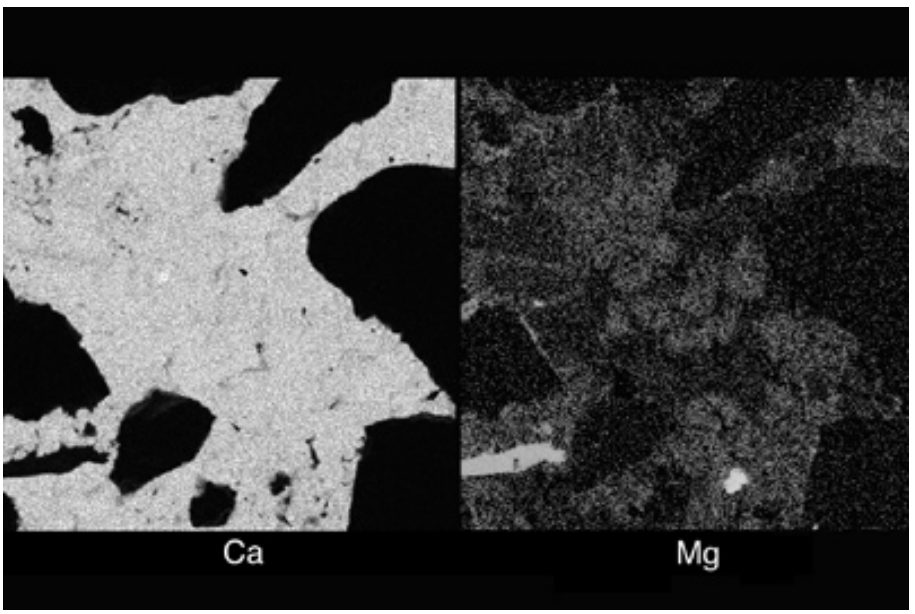

Plio-Pleistocene Santa Fe Gp., Socorro Co., New Mexico

The four images shown here (in two sets) are a backscattered electron (BSE) image and three chemical maps of a carbonate-cemented concretion. The chemical maps highlight the distribution of different chemical elements, in this case Si, Ca, and Mg, across the polished surface of a sample. The Ca chemical map shows that the cement in this concretion is Ca-bearing, and that the Ca content of the cement is relatively uniform over the 2.5 mm^2 area of this image. The Si chemical map shows that all of the clasts are silicate fragments, and based on the intensity of silica x-rays, at least three different minerals are present. The Mg map shows that the overall abundance of Mg in the carbonate matrix is low, but that there is some variability in the Mg abundance. Also, one of the silicate clasts is Mg-rich, and based on the platy shape, may be a mica. Photographs courtesy of Peter Mozely.

HA = 0.3 mm for each of the four photos

Tertiary terrigenous sediment, U.S.A.

This backscattered electron image from a prodeltaic, carbonate-cemented sandstone shows a variety of grains — quartz (dark, angular grains), K-feldspar (bright, elongate, broken clast), argillaceous rock fragments (lower left) and chert (upper right, with holes). The cement is dolomitic and the banding id due to variations in Ca/Mg ratios: the brighter areas contain more Ca than the darker areas due to the higher atomic number of Ca (20) relative to Mg (12).

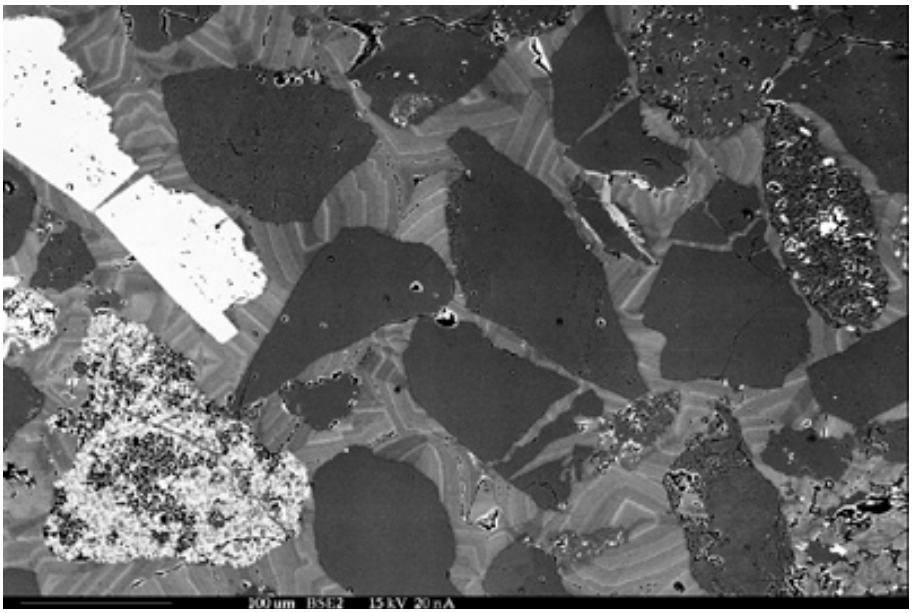

MP, HA = 0.59 mm

Detrital grain in Holocene surface sediment, Great Australian Bight, Australia

A backscattered electron image of a detrital crystal of Cenozoic dolomite reworked into Holocene sediment. The dolomite crystal has a high manganese stoichiometric core surrounded by a non-stoichiometric overgrowth. The light crystal at the very center, as well as other light areas, are low-Mg calcite. Photograph courtesy of Kurt Kyser.

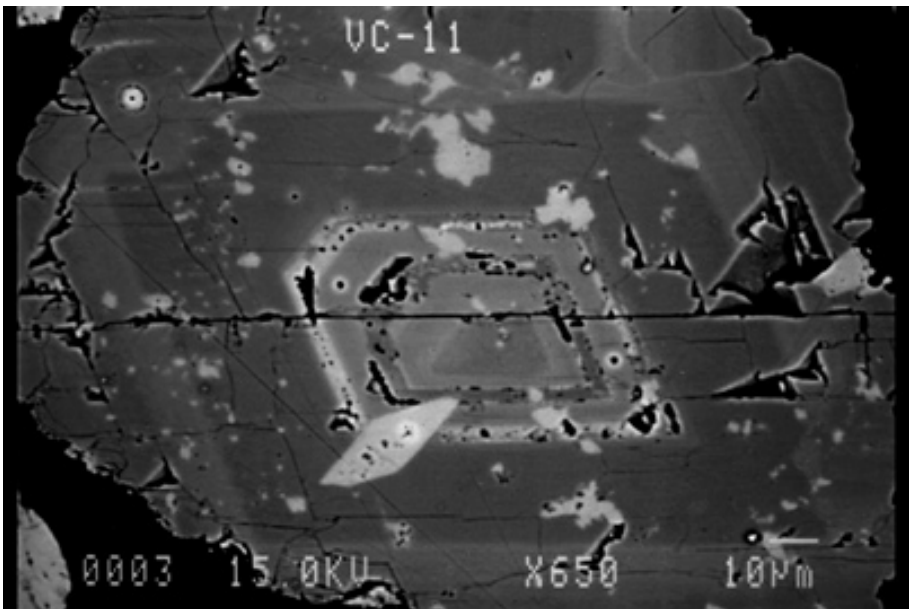

MP, HA = 0.18 mm

X-RAY DIFFRACTION ANALYSIS

In addition to being a fast, reliable, and relatively inexpensive method of determining the bulk mineralogy of carbonate rocks (aragonite, calcite, dolomite, siderite, etc.), x-ray diffraction allows fairly accurate determination of the amount of magnesium substitution in the calcite or dolomite lattice. For this, one needs to do careful, slow-speed scans. Including an internal standard that does not conflict with carbonate peaks, but that allows accurate calibration is important — galena (PbS) is a common standard for ancient carbonates and halite (NaCl) or fluorite (CaF_2) for modern sediments.

Using those methods, one can determine very accurately (in terms of the angle 2θ) the reflection peak positions representing the (112) plane of the calcite crystal lattice. By matching that data against the chart given in the following diagram (modified from Goldsmith et al., 1961) one can approximate the magnesium content of the lattice to about 0.5 mol%. Other cations besides magnesium, however, can cause lattice-spacing shifts, and this data should thus be checked occasionally with electron microprobe or atomic absorption analysis. Further information about x-ray analytical techniques suitable for carbonate rocks is available in Fang and Zevin (1985).

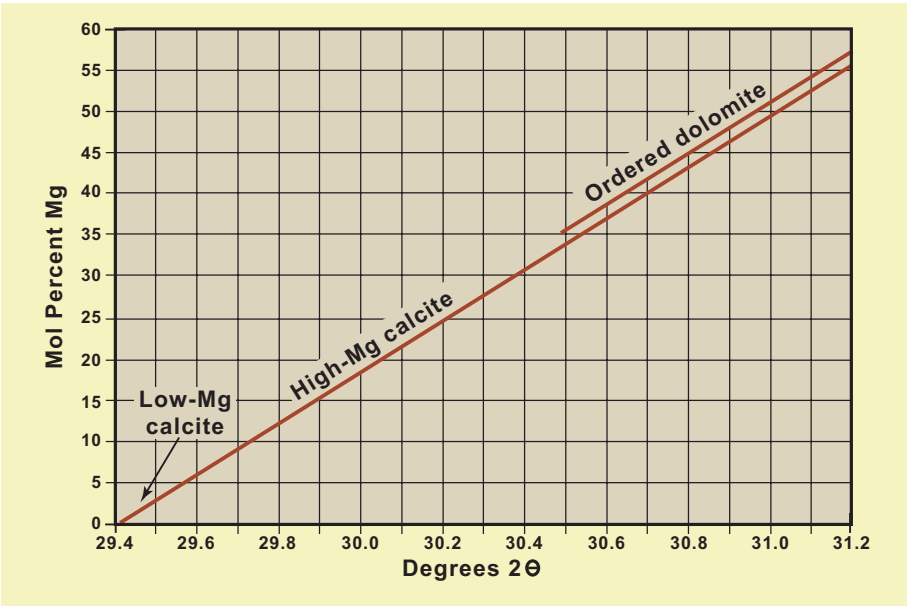

Chart for x-ray determination of Mg content in calcite and dolomite lattices

This chart can be used to convert x-ray peak angles to percentage of magnesium (in mol% Mg) in the calcite or dolomite lattice. Accurate determination of peak positions, however, depends on careful calibration and the use of admixed standards (galena, halite, or fluorite). After Goldsmith et al. (1961).

STABLE ISOTOPE ANALYSIS

Stable and radiometric isotopic geochemical analyses are not petrographic techniques, but they have become such natural adjuncts to petrography that it is impossible not to mention them in a book such as this. Only the briefest of summaries can be provided here, however, and the interested reader is encouraged to peruse the applicable literature for a fuller explanation (e.g., Arthur et al., 1983; and Hoefs, 1987).

Stable isotope geochemistry of carbonate rocks involves the measurement of $^{18}O/^{16}O$ and $^{13}C/^{12}C$ ratios, and comparing these to the ratios in a standard — typically PDB (a belemnite) for carbonate rocks and/or SMOW (standard mean ocean water) for waters and for some carbonate and silicate rocks. Isotopic results are given as delta values (δ) between the isotopic ratio of the analyzed sample and that of the standard.

Carbon and oxygen isotopic analyses require a mass spectrometer and so are moderately expensive. These analyses now can be done on extremely small samples, so sampling of cement zones or individual fossil constituents is feasible, although microsampling commonly is the most difficult part of isotopic study (Prezbindowski, 1980). Advances in laser ablation mass spectrometry allow in-situ sampling and analysis on a very small scale and should minimize sampling problems in the future.

Interpretation of stable isotopic data is inherently complex because there are more variables than knowns. The $^{18}O/^{16}O$ incorporated into a calcite or dolomite, for example, is a function of water temperature; higher temperatures yield precipitates with more ^{16}O relative to ^{18}O and thus "lighter" or more negative ratios relative to the PDB standard. Unfortunately the $^{18}O/^{16}O$ ratios of precipitated carbonates are also a function of the $^{18}O/^{16}O$ ratios in the waters from which they precipitate. Thus, carbonates precipitated from fresh meteoric waters will also have "light" or negative isotopic ratios relative to PDB. Further complications come from possible secular variations in the isotopic chemistry of seawater, from isotopic fractionation in the biological precipitation of tests and shells (fractionation that varies even down to the species level), and from a wide range of isotopic water compositions (resulting from isotopic fractionation during repeated evaporation events) and from other factors.

Carbon isotopic variation is less dependent on temperature, but does depend on biological fractionation processes, the carbon isotopic composition of water (which also shows secular variations), organic and inorganic decomposition of organic matter, and the possible introduction of plant- or soil-derived CO_2.

Despite all these complications, some useful patterns of stable isotopic geochemistry in carbonate rocks have emerged in the roughly 50 years that these analyses have been conducted. Such patterns are summarized in the diagrams that follow this text, and the reader is urged to read the original articles for full explanations. Basically, if the isotopic compositions of typical marine precipitates of a given age are known, meteoric products typically will have slightly lighter $^{18}O/^{16}O$ ratios and slightly to substantially lighter $^{13}C/^{12}C$ ratios. Burial diagenetic products may have lighter to much lighter $^{18}O/^{16}O$ ratios and variable $^{13}C/^{12}C$ ratios depending on the nature of organic decomposition processes active at the time of carbonate precipitation.

Diagenetic trends of carbon and oxygen isotopic ratios in limestones

These diagrams show generalized trends in the isotopic geochemistry of carbonate rocks and of CO_2 generated by the diagenesis of organic matter. The left-hand diagram (adapted from Lohmann, 1988) shows the effects of meteoric alteration in shifting rock chemistry to lighter $^{18}O/^{16}O$ ratios and variably lighter $^{13}C/^{12}C$ ratios (depending on the ratio of water to rock involved in the diagenesis). The "burial trend" arrow shows the extension of that alteration into the subsurface. The right-hand diagram (adapted from Irwin et al., 1977) shows the $^{13}C/^{12}C$ ratios in CO_2 liberated during burial diagenesis of organic matter. Some of that may be incorporated in burial-stage calcite cements.

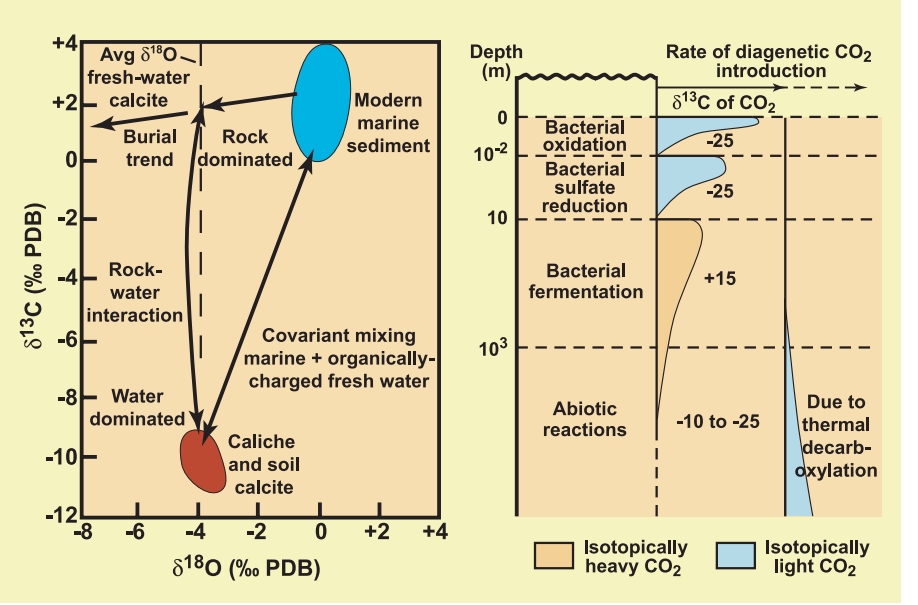

Up. Permian Wegener Halvø Fm., Jameson Land, East Greenland

This diagram shows the range of carbon and oxygen isotopic values for a variety of separately analyzed constituents in a Permian limestone. It illustrates the typical diagenetic trend to lighter carbon and oxygen isotopic values through burial diagenesis. Primary marine constituents have average $^{18}O/^{16}O$ ratios of about -5‰ and average $^{13}C/^{12}C$ ratios of about +5‰ in this area. The latest-stage cements, reflecting deep and high-temperature burial conditions, have average $^{18}O/^{16}O$ ratios of -18‰ and $^{13}C/^{12}C$ ratios of about 2‰. Although the specific values vary from area to area, the trend is consistent and aids in the recognition of burial-stage precipitates.

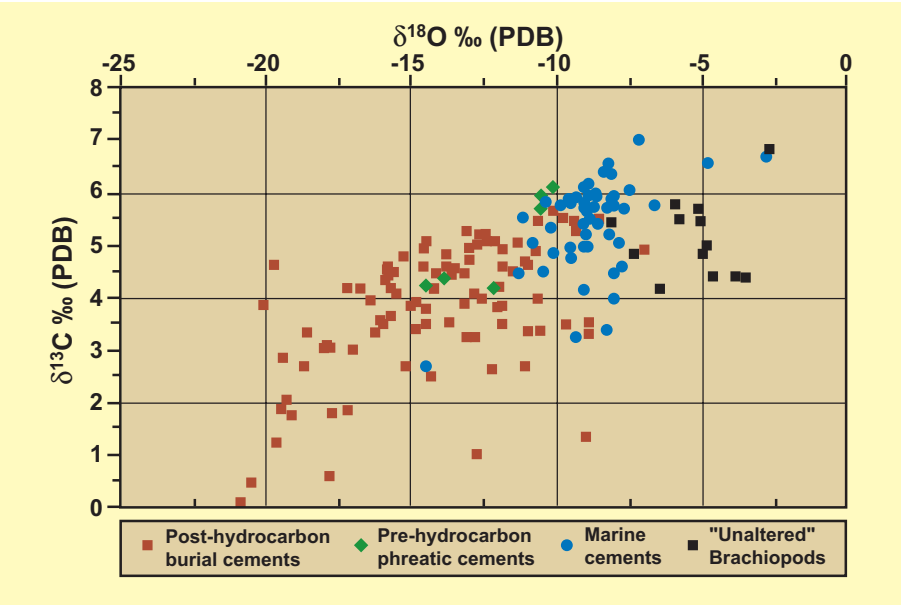

A simplified burial history plot for Permian strata of the Delaware Basin of west Texas-New Mexico

Determinations of temperatures of formation of cements using fluid-inclusion geothermometry or stable isotope geochemistry can be related to the geologic history of an area through petrographic studies (paragenesis), coupled with burial history plots (e.g. Burruss et al., 1985; Guidish et al., 1985). This plot shows an example of a simple burial history consisting of rapid early-stage burial, intermediate-stage stability, and late-stage uplift. Maximum burial depth and burial temperatures for any rock unit and time period can be visualized from this plot, a process that can help in the interpretation of petrographic and isotopic data. Diagram adapted from multiple sources.

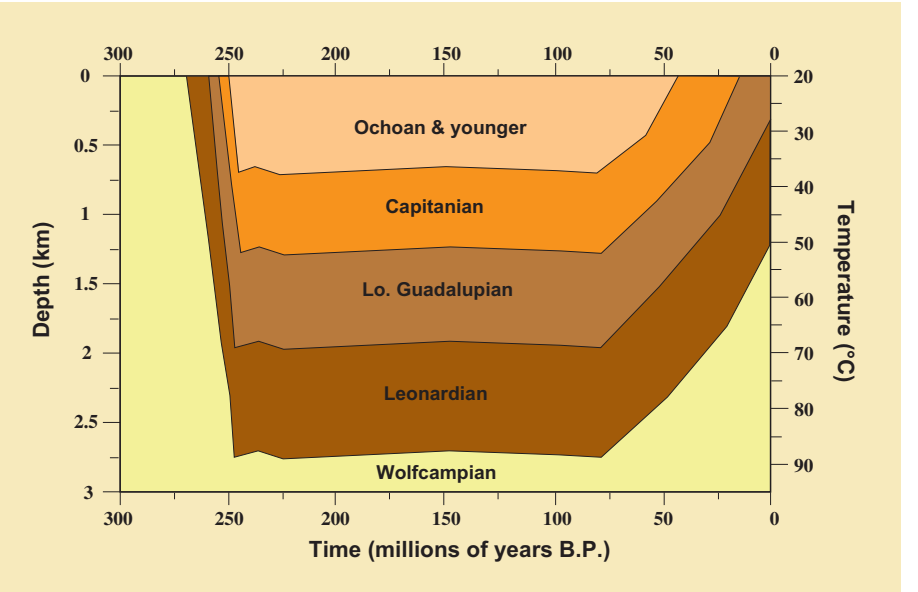

STRONTIUM ISOTOPE GEOCHEMISTRY

The fundamental concepts in strontium isotope geochemistry of carbonate rocks are that all ocean water is well mixed and has a uniform $^{87}Sr/^{86}Sr$ ratio, but that the $^{87}Sr/^{86}Sr$ ratio of seawater has varied significantly through geologic time. The Phanerozoic curve for secular variation of strontium was first compiled by Burke et al. (1982) and has subsequently been refined by a number of other workers (see, for example, Elderfield, 1986) and is depicted in the diagram below. The variations of seawater $^{87}Sr/^{86}Sr$ ratios through time result from temporal variations in the relative amounts of Sr inputs from continental and oceanic sources which have substantially different $^{87}Sr/^{86}Sr$ ratios (see diagram at bottom of page).

The measurement of $^{87}Sr/^{86}Sr$ in unaltered limestones (or in unaltered constituents within limestones) allows dating of samples, especially from intervals with long unidirectional trends of changing $^{87}Sr/^{86}Sr$ ratios (the Cenozoic, for example).

Other studies using $^{87}Sr/^{86}Sr$ ratios in carbonate rocks have tried to tie cementation or replacement processes to subsurface influx of waters from specific sources or ages. Deep basinal brines in continental sediments commonly are highly radiogenic because of uptake of strontium from feldspar dissolution or clay diagenesis. Refluxing evaporative marine fluids that percolate downward carry with them the $^{87}Sr/^{86}Sr$ ratios of seawater at the time of reflux, a signature that may be modified during rock-water interactions, but may also be used to determine the time of alteration (e.g., Denison et al., 1994; Land, 1992; Vahrenkamp and Swart, 1991).

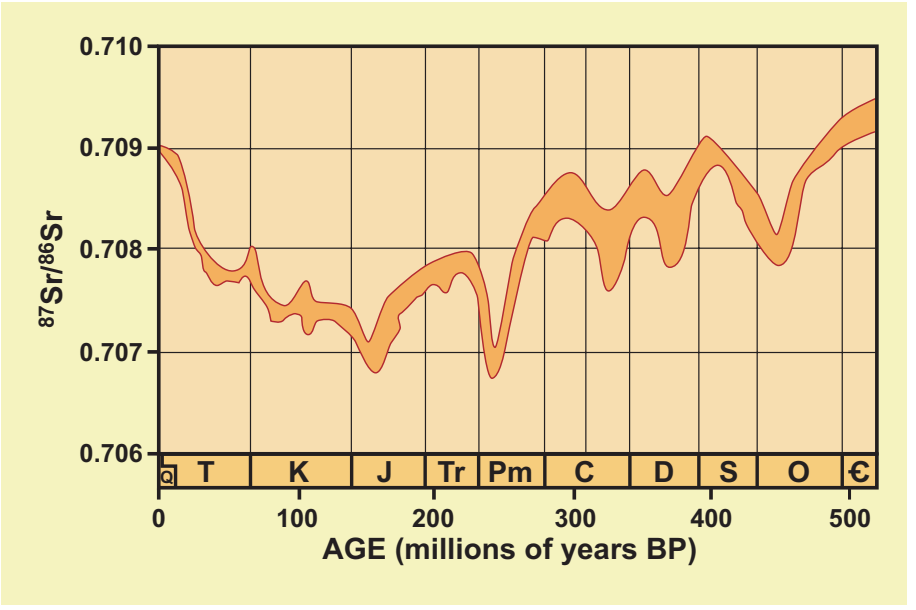

Phanerozoic secular variation curve of strontium isotopic ratios in seawater

The orange band on this diagram shows the best estimate fit for 786 strontium isotopic values measured from relatively unaltered Phanerozoic marine carbonate rocks — and thus, by inference, for variations in the Sr isotopic ratio of seawater through time (redrawn from Burke et al., 1982, as modified by Allan and Wiggins, 1993). Given a good knowledge of the expected $^{87}Sr/^{86}Sr$ ratio of seawater (and of primary carbonate rock constituents) for any given age allows the recognition of anomalies resulting from diagenetic alteration in waters of different isotopic ratios (marine, meteoric, or basinal). See cited papers for some of the many successful applications.

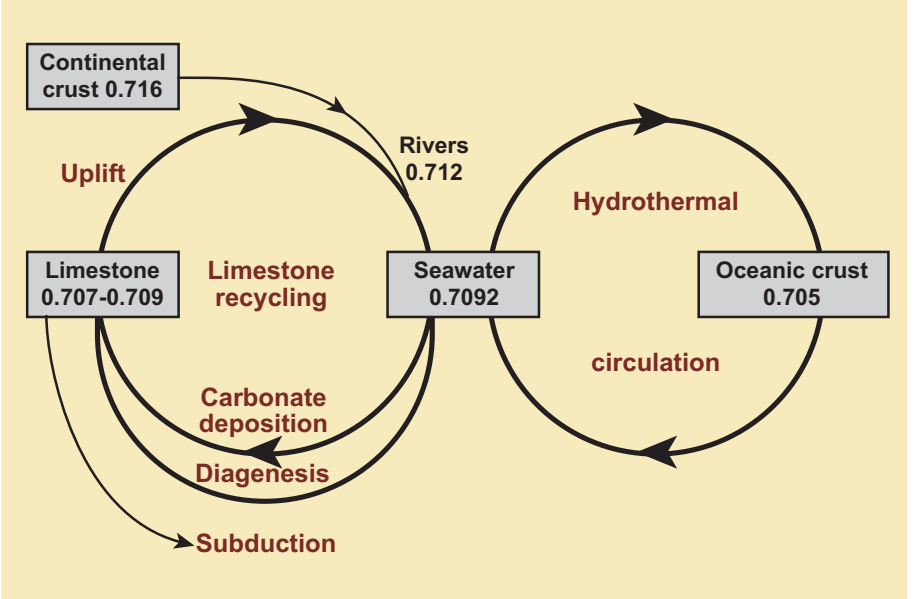

Reservoirs of strontium and cycles of inputs and output relative to seawater

A diagram depicting interactions between major reservoirs of radiogenic and non-radiogenic strontium and the geochemical cycles that control the variations in the $^{87}Sr/^{86}Sr$ ratios of seawater through time. Continental sources, in general, are radiogenic and oceanic sources are non-radiogenic. Changes in the relative inputs from those two major groups of sources are influenced by oceanic spreading rates, extent of continental exposure, uplift, and erosion, and many other factors. Adapted from Elderfield (1986).

Cited References and Additional Information Sources

Ali, S. A., and M. P. Weiss, 1968, Fluorescent dye penetrant technique for displaying obscure structures in limestone: Journal of Sedimentary Petrology, v. 38, p. 681-682.

Allan, J. R., and W. D. Wiggins, 1993, Dolomite reservoirs — geochemical techniques for evaluating origin and distribution: Tulsa, OK, AAPG Short Course Note Series No. 36, 129+ p.

Allen, J., 1956, Estimation of percentages in thin-sections — considerations in visual psychology: Journal of Sedimentary Petrology, v. 26, p. 160-161.

Amieux, P., 1982, La cathodoluminescence: méthode d'étude sédimentologique des carbonates: Bulletin des Centres de Recherches Exploration-Production Elf-Aquitaine, v. 6, p. 437-483.

Arthur, M. A., T. F. Anderson, I. R. Kaplan, J. Veizer, and L. S. Land, 1983, Stable Isotopes in Sedimentary Geology: Tulsa, OK, SEPM Short Course No. 10 (Dallas 1983), 435 p.

Baccelle, L. S., and A. Bosellini, 1965, Diagrammi per la stima visiva della composizione percentuale nelle rocce sedimentarie: Annali dell'Università di Ferrara, Nuove Serie, Sezione IX, Scienze Geologiche e Paleontologiche, v. 1, p. 59-62.

Banner, J. L., 1995, Application of the trace element and isotopic geochemistry of strontium to studies of carbonate diagenesis: Sedimentology, v. 42, p. 805-824.

Banner, J. L., and G. N. Hanson, 1990, Calculation of simultaneous isotopic and trace element variations during water-rock interaction with applications to carbonate diagenesis: Geochimica et Cosmochimica Acta, v. 54, p. 3123-3137.

Barker, C. E., and R. B. Halley, 1986, Fluid inclusion, stable isotope, and vitrinite reflectance evidence for the thermal history of the Bone Spring Limestone, southern Guadalupe Mountains, Texas, *in* D. L. Gautier, ed., Roles of Organic Matter in Sediment Diagenesis: Tulsa, OK, SEPM Special Publication No. 38, p. 189-203.

Barker, C. E., and O. C. Kopp, eds., 1991, Luminescence Microscopy and Spectroscopy: Qualitative and Quantitative Applications: Tulsa, OK, SEPM Short Course 25, 194 p.

Beckett, D., and B. W. Sellwood, 1991, A simple method for producing high-quality porecasts of carbonate rocks: Sedimentary Geology, v. 71, p. 1-4.

Bissell, H., 1957, Combined preferential staining and cellulose peel technique: Journal of Sedimentary Petrology, v. 27, p. 417-420.

Budd, D. A., U. Hammes, and W. B. Ward, 2000, Cathodoluminescence in calcite cements: new insights on Pb and Zn sensitizing, Mn activation, and Fe quenching at low trace-element concentrations: Journal of Sedimentary Research, v. 70, p. 217-226.

Burke, W. H., R. E. Denison, E. A. Hetherington, R. B. Koepnick, H. F. Nelson, and J. B. Otto, 1982, Variation of seawater $^{87}Sr/^{86}Sr$ throughout Phanerozoic time: Geology, v. 10, p. 516-519.

Burruss, R. C., K. R. Cercone, and P. M. Harris, 1985, Timing of hydrocarbon migration: evidenced from fluid inclusions in calcite cements, tectonics and burial history, *in* N. Schneidermann, and P. M. Harris, eds., Carbonate Cements: Tulsa, OK, SEPM Special Publication No. 36, p. 277-289.

Carver, R. E., 1971, Procedures in Sedimentary Petrology: New York, Wiley-Interscience, 672 p.

Choquette, P. W., and F. C. Trusell, 1978, A procedure for making the Titan-yellow stain for Mg calcite permanent: Journal of Sedimentary Petrology, v. 48, p. 639-641.

Davies, P. J., and T. Roger, 1968, Stained dry cellulose peels of ancient and recent impregnated carbonate sediments: Journal of Sedimentary Petrology, v. 38, p. 234-237.

Denison, R. E., R. B. Koepnick, A. Fletcher, M. W. Howell, and W. S. Callaway, 1994, Criteria for the retention of original seawater $^{87}Sr/^{86}Sr$ in ancient shelf limestones: Chemical Geology, v. 112, p. 131-143.

DePaolo, D. J., 1988, Neodymium Isotope Geochemistry: New York, Springer-Verlag, 187 p.

Dickson, J. A. D., 1965, A modified staining technique for carbonates in thin section: Nature, v. 205, p. 587.

Dickson, J. A. D., 1966, Carbonate identification and genesis as revealed by staining: Journal of Sedimentary Petrology, v. 36, p. 491-505.

Dorobek, S. L., J. F. Read, J. M. Niemann, T. C. Pong, and R. M. Haralick, 1987, Image analysis of cathodoluminescent-zoned calcite cements: Journal of Sedimentary Petrology, v. 57, p. 766-770.

Dravis, J. J., 1991, Carbonate petrography — update on new techniques and applications: Journal of Sedimentary Petrology, v. 61, p. 626-628.

Dravis, J. J., and D. A. Yurewicz, 1985, Enhanced carbonate petrography using fluorescence microscopy: Journal of Sedimentary Petrology, v. 55, p. 795-804.

Eby, D. E., and R. C. Hager, 1986, Fluorescence petrography of San Andres dolomites — H.O. Mahoney lease, Wasson Field, Yoakum Co., Texas, *in* D. G. Bebout, and P. M. Harris, eds., Hydrocarbon Reservoir Studies, San Andres/Grayburg Formations, Permian Basin: Midland, TX, Permian Basin Section-SEPM Publication 86-26, p. 37-38.

Elderfield, H., 1986, Strontium isotope stratigraphy: Palaeogeography, Palaeoclimatology, Palaeoecology, v. 57, p. 71-90.

Evamy, B. D., 1963, The application of a chemical staining technique to a study of dedolomitization: Sedimentology, v. 2, p. 164-170.

Evamy, B. D., 1969, The precipitational environment and correlation of some calcite cements deduced from artificial staining: Journal of Sedimentary Petrology, v. 39, p. 787-792.

Fairchild, I., G. Hendry, M. Quest, and M. Tucker, 1988, Chemical analysis of sedimentary rocks, *in* M. Tucker, ed., Techniques in Sedimentology: Oxford, Blackwell Scientific Publications, p. 274-354.

Fang, J. H., and L. Zevin, 1985, Quantitative x-ray diffractometry of carbonate rocks: Journal of Sedimentary Petrology, v. 55, p. 611-613.

Filippelli, G. M., and M. L. Delaney, 1992, Quantifying cathodoluminescent intensity with an on-line camera and exposure meter: Journal of Sedimentary Petrology, v. 62, p. 724-725.

Flügel, E., 1982, Microfacies Analysis of Limestones: New York, Springer-Verlag, 633 p.

Folk, R. L., 1951, A comparison chart for visual percentage estimation: Journal of Sedimentary Petrology, v. 21, p. 32-33.

Folk, R. L., 1987, Detection of organic matter in thin sections of carbonate rocks using a white card: Sedimentary Geology, v. 54, p. 193-200.

Frank, J. R., A. B. Carpenter, and T. W. Oglesby, 1982, Cathodoluminescence and composition of calcite cement in Taum Sauk Limestone (Upper Cambrian), southeast Missouri: Journal of Sedimentary Petrology, v. 52, p. 631-638.

Frank, R. M., 1965, An improved carbonate peel technique for high-powered studies: Journal of Sedimentary Petrology, v. 35, p. 499-500.

Frank, T. D., K. C. Lohmann, and W. J. Meyers, 1996, Chronostratigraphic significance of cathodoluminescence zoning in syntaxial cement: Mississippian Lake Valley Formation, New Mexico: Sedimentary Geology, v. 105, p. 29-50.

Friedman, G. M., 1959, Identification of carbonate minerals by staining methods: Journal of Sedimentary Petrology, v. 29, p. 87-97.

Gardner, K. L., 1980, Impregnation technique using colored epoxy to define porosity in petrographic thin sections: Canadian Journal of Earth Sciences, v. 17, p. 1104-1107.

Gensmer, R. P., and M. P. Weiss, 1980, Accuracy of calcite/dolomite ratios by x-ray diffraction and comparison with results from staining techniques: Journal of Sedimentary Petrology, v. 50, p. 626-629.

Goldsmith, J. R., D. L. Graf, and H. C. Heard, 1961, Lattice constants of the calcium-magnesium carbonates: American Mineralogist, v. 46, p. 453-457.

Goldstein, R. H., 1986, Reequilibration of fluid inclusions in low-temperature calcium-carbonate cement: Geology, v. 14, p. 792-795.

Goldstein, J. I., D. E. Newbury, P. Echlin, D. C. Joy, C. Fiori, and E. Lifshin, 1981, Scanning electron microscopy and X-ray microanalysis: a text for biologists, materials scientists, and geologists [2nd edition]: New York, NY, Plenum Press, 673 p.

Goldstein, R. H., and T. J. Reynolds, 1994, Systematics of Fluid Inclusions in Diagenetic Minerals: Tulsa, OK, SEPM Short Course 31, 198 p.

Gregg, J. M., and M. Karakus, 1991, A technique for successive cathodoluminescence and reflected light petrography: Journal of Sedimentary Petrology, v. 61, p. 613-635.

Guidish, T. M., C. G. St. C. Kendall, I. Lerche, D. J. Toth, and R. F. Yarzab, 1985, Basin evaluation using burial history calculations: an overview: AAPG Bulletin, v. 69, p. 92-105.

Guilhaumou, N., N. Szydlowskii, and B. Padier, 1990, Characterization of hydrocarbon fluid inclusions by infra-red and fluorescence microspectrometry: Mineralogical Magazine, v. 54, p. 311-324.

Halley, R. B., 1978, Estimating pore and cement volumes in thin section: Journal of Sedimentary Petrology, v. 48, p. 641-650.

Hemming, N. G., W. J. Meyers, and J. C. Grams, 1989, Cathodoluminescence in diagenetic calcites: the roles of Fe and Mn as deduced from electron probe and spectrophotometric measurements: Journal of Sedimentary Petrology, v. 59, p. 404-411.

Hoefs, J., 1987, Stable Isotope Geochemistry (Third Edition): New York, Springer-Verlag, 241 p.

Honjo, S., 1963, New serial micropeel technique: Lawrence, KS, Kansas Geological Survey Bulletin 165, part 6, p. 1-16.

Hutchison, C. S., 1974, Laboratory Handbook of Petrographic Techniques: New York, John Wiley & Sons, 527 p.

Irwin, H., C. Curtis, and M. Coleman, 1977, Isotopic evidence for source of diagenetic carbonates formed during burial of organic-rich sediments: Nature, v. 269, p. 209-213.

Katz, A., and G. M. Friedman, 1965, The preparation of stained acetate peels for the study of carbonate rocks: Journal of Sedimentary Petrology, v. 35, p. 248-249.

Klosterman, M. J., 1981, Applications of fluid inclusion techniques to burial diagenesis in carbonate rock sequences: Baton Rouge, Louisiana State University, Applied Carbonate Research Program, Technical Series Contribution No. 7, 101 p.

Land, L. S., 1992, The dolomite problem: stable and radiogenic isotope clues, *in* N. Clauer, and S. Chanduri, eds., Isotope Signatures and Sedimentary Records: Lecture Notes in Earth Science 43: Berlin, Springer-Verlag, p. 49-68.

Lewis, D. W., and D. McConchie, 1994, Analytical Sedimentology: New York, Chapman & Hall, 197 p.

Lindholm, R. C., and D. A. Dean, 1973, Ultra-thin sections in carbonate petrology: a valuable tool: Journal of Sedimentary Petrology, v. 43, p. 295-297.

Lindholm, R. C., and R. B. Finkelman, 1972, Calcite staining: semi-quantitative determination of ferrous iron: Journal of Sedimentary Petrology, v. 42, p. 239-242.

Lohmann, K. C., 1988, Geochemical patterns of meteoric diagenetic systems and their application to studies of paleokarst, *in* N. P. James, and P. W. Choquette, eds., Paleokarst: New York, Springer-Verlag, p. 58-80.

Machel, H. G., 1985, Cathodoluminescence in calcite and dolomite and its chemical interpretation: Geoscience Canada, v. 12, p. 139-147.

Machel, H. G., and E. A. Burton, 1991, Factors governing cathodoluminescence in calcite and dolomite and their implications for studies of carbonate diagenesis, *in* C. E. Barker, and O. C. Kopp, eds., Luminescence Microscopy and Spectroscopy: Qualitative and Quantitative Applications: Tulsa, OK, SEPM Short Course 25, p. 37-57.

Marshall, D. J., 1988, Cathodoluminescence of Geological Materials: Winchester, MA, Allen & Unwin, 128 p.

Marshall, D. J., 1991, Combined cathodoluminescence and energy dispersive spectroscopy, *in* C. E. Barker, and O. C. Kopp, eds., Luminescence Microscopy and Spectroscopy: Qualitative and Quantitative Applications: Tulsa, OK, SEPM Short Course 25, p. 27-36.

Martinez, B., and F. Plano, 1987, Quantitative X-ray diffraction of carbonate sediments: mineralogical analysis through fitting of Lorentzian profiles to diffraction peaks: Sedimentology, v. 34, p. 169-174.

Miller, J., 1988, Cathodoluminescence microscopy, *in* M. Tucker, ed., Techniques in Sedimentology: Oxford, Blackwell Scientific Publications, p. 174-190.

Miller, J., 1988, Microscopical techniques: I. Slices, slides, stains and peels, *in* M. Tucker, ed., Techniques in Sedimentology: Oxford, Blackwell Scientific Publications, p. 86-107.

Pittman, E. D., and R. W. Duschatko, 1970, Use of pore casts and scanning electron microscopy to study pore geometry: Journal of Sedimentary Petrology, v. 40, p. 1153-1157.

Potts, P. J., J. F. W. Bowles, S. J. B. Reed, and M. R. Cave, 1995, Microprobe Techniques in Earth Sciences, v. Mineralogical Society of America Vol. 6: London, Chapman and Hall, 419 p.

Prezbindowski, D. R., 1980, Microsampling technique for stable isotopic analyses of carbonates: Journal of Sedimentary Petrology, v. 50, p. 643-644.

Prezbindowski, D. R., and R. E. Larese, 1987, Experimental stretching of fluid inclusions in calcite — implications for diagenetic studies: Geology, v. 15, p. 333-336.

Ramseyer, K., J. Fischer, A. Matter, P. Eberhardt, and J. Geiss, 1989, A cathodoluminescence microscope for low intensity luminescence: Journal of Sedimentary Petrology, v. 59, p. 619-622.

Reed, S. J. B., 1989, Ion microprobe analysis — a review of geological applications: Mineralogical Magazine, v. 53, p. 3-24.

Reed, S. J. B., 1996, Electron Microprobe and Scanning Electron Microscopy in Geology, v. 1: Cambridge, Cambridge University Press, 201 p.

Riciputi, L. R., H. G. Machel, and D. R. Cole, 1994, An ion microprobe study of diagenetic carbonates in the Devonian Nisku Formation of Alberta, Canada: Journal of Sedimentary Research, v. A64, p. 115-127.

Roedder, E., 1984, Fluid inclusions: Washington, D.C., Mineralogical Society of America Reviews in Mineralogy, Vol. 12, 641 p.

Rost, F. W. D., 1992, Fluorescence Microscopy, v. 1: New York, Cambridge University Press, 253 p.

Russ, J. C., 1990, Computer-Assisted Microscopy: The Measurement and Analysis of Images: New York, Plenum Press, 543 p.

Ruzyla, K., and D. I. Jezek, 1987, Staining method for recognition of pore space in thin and polished sections: Journal of Sedimentary Petrology, v. 57, p. 777-778.

Shepherd, T. J., Rankin, A.H., and D. H. M. Alderton, 1985, A Practical Guide to Fluid Inclusion Studies: Glasgow, Blackie & Sons, 239 p.

Sippel, R. F., and E. D. Glover, 1965, Structures in carbonate rocks made visible by luminescence petrography: Science, v. 150, p. 1283-1287.

Smalley, P. C., C. N. Maile, M. L. Coleman, and J. E. Rouse, 1992, LASSIE (Laser Ablation Sampler for Stable Isotope Extraction) applied to carbonate minerals: Chemical Geology, v. 101, p. 43-52.

Smalley, P. C., D. E. Stijfhoorn, A. Råheim, H. Johansen, and J. A. D. Dickson, 1989, The laser microprobe and its application to the study of C and O isotopes in calcite and aragonite: Sedimentary Geology, v. 65, p. 211-222.

Swanson, R. G., 1981, Sample Examination Manual: Tulsa, OK, AAPG Methods in Exploration Series, 80 p.

Tickell, F. G., 1965, The Techniques of Sedimentary Mineralogy: New York, Elsevier Publ. Co., 220 p.

Tucker, M. E., ed., 1988, Techniques in Sedimentology: Palo Alto, CA, Blackwell Scientific Publications, 394 p.

Ulmer-Scholle, D. S., P. A. Scholle, and P. V. Brady, 1993, Silicification of evaporites in Permian (Guadalupian) back-reef carbonates of the Delaware Basin, west Texas and New Mexico: Journal of Sedimentary Petrology, v. 63, p. 955-965.

Vahrenkamp, V. C., and P. K. Swart, 1991, Episodic dolomitization of late Cenozoic carbonates in the Bahamas: evidence from strontium isotopes: Journal of Sedimentary Petrology, v. 61, p. 1002-1014.

Veizer, J., R. W. Hinton, R. N. Clayton, and A. Lerman, 1987, Chemical diagenesis of carbonates in thin-sections: Ion microprobe as trace element tool: Chemical Geology, v. 64, p. 225-237.

Wolf, K. H., A. J. Easton, and S. Warne, 1967, Techniques of examining and analysing carbonate skeletons, minerals and rocks, *in* G. V. Chilingar, H. J. Bissell, and R. W. Fairbridge, eds., Carbonate Rocks: Physical and Chemical Aspects: Developments in Sedimentology 9B: New York, Elsevier Publishing Co., p. 253-341.

Glossary of Petrographic Terms

Acicular - Describes a fibrous or needle-like growth form of calcite in which crystals have a length to width ratio greater than 6:1 and are less than 10 μm wide. Contrasts with the wider crystals of the "columnar" growth form.

Agglutinated - A term used to describe the wall composition of certain foraminifers, tintinnids and other groups where the shell is built of foreign particles (sand grains, carbonate fragments, sponge spicules, and others) bound together with an organic or calcareous cement.

Aggrading neomorphism - A kind of neomorphism in which the average crystal size has been increased as a consequence of diagenetic processes (Folk, 1965).

Allochem - A term used for one of several varieties of discrete and organized carbonate aggregates (skeletal fragments, pellets, peloids, intraclasts, ooids, and others) that serve as the coarser framework grains in most mechanically deposited limestones (coined by Folk, 1959).

Allochthonous - Refers to material formed or produced at a site other than its present location; material of foreign origin. In the context of carbonate strata, the term normally refers to grains produced in one environment that are later reworked to another setting through the action of storms, debris flows, or other transport processes.

Allogenic - A term meaning generated elsewhere; applied especially to rock constituents that came into existence outside of, and previous to, the rock of which they are now a part — for example, the pebbles of a limestone conglomerate (Holmes, 1928). Contrast with authigenic.

Alveolar texture - A term introduced by Esteban and Klappa (1983) for cylindrical to irregular pores which may or may not be filled with calcite cement, separated by a network of anastomosing micrite walls. Typically associated with a caliche or subaerial exposure surface. Pore diameters are typically 100-500 μm and walls are composed of banded calcite needle fibers.

Anhedral - Descriptive of a single crystal or crystal fabric that does not show well defined or typical crystallographic forms (i.e., crystal faces are absent). Coined by Pettijohn (1957); see also Friedman (1965).

Anhydrite - An orthorhombic evaporite mineral consisting of anhydrous calcium sulfate: $CaSO_4$. It represents gypsum without its water of hydration and it alters readily to gypsum.

Ankerite - A white, red, or grayish iron-rich mineral related to dolomite: $Ca(Fe,Mg,Mn)(CO_3)_2$. It is associated with iron ores and commonly forms as thin veins associated with coal seams.

Aphanocrystalline - Descriptive of an interlocking texture of a carbonate sedimentary rock having crystals whose diameters are in the range of 0.001-0.004 mm (1-4 μm) (Folk, 1959).

Aragonite - An orthorhombic variety of calcium carbonate ($CaCO_3$) that is trimorphous with calcite and vaterite. It is denser and harder than calcite and has less pronounced cleavage. It is a common inorganic marine precipitate and is the main skeletal material in many invertebrate groups (e.g., green algae, scleractinian corals, and mollusks). Aragonite is unstable in most nonmarine settings and thus is rare in pre-Tertiary rocks except in settings which preclude extensive contact with pore fluids (such as concretions or oil-saturated strata).

Arenaceous - A textural term for clastic sediments or sedimentary rocks of average grain size ranging from 1/16 to 2 mm. Also used to describe foraminifers and other organisms that agglutinate terrigenous sand grains to form their test or shell walls.

Argillaceous - Pertaining to a sediment or sedimentary rock containing clay-size particles; clayey or shaly.

Articulate - Refers to fossils having two or more parts joined together in their natural relationship, for example, the valves of bivalves (pelecypods) or brachiopods or the columnals of crinoids.

Authigenic - Rock constituents and minerals that have been not been transported or that crystallized locally at the spot where they are now found (Holmes, 1928). Contrast with allogenic.

Autochthonous - Formed or grown in the place where found. Contrast with "allochthonous."

Bafflestone - A term used by Embry and Klovan (1971) for a rock with abundant stalk-shaped (dendroid) fossil remains that are interpreted as having formed a baffle for matrix accumulation; matrix is volumetrically important; commonly poorly sorted.

Bahamite - Granular limestone composed largely of lumps (intraclasts) of cemented or agglutinated pellets, peloids and skeletal fragments (similar to those found on parts of the Bahama Platform). An outdated term that is non-descriptive and is no longer widely used.

Barite - A white, yellow, or colorless orthorhombic mineral: $BaSO_4$. It occurs in tabular crystals, in granular form, or in compact masses resembling marble, and it has a specific gravity of 4.5.

Baroque dolomite - Dolomite characterized by large crystal size, opaque white color, curving or saddle-shaped crystal faces, and undulose extinction. Typically formed at temperatures above 75-80°C. Also termed "saddle dolomite." See Folk and Assereto (1974).

Beachrock - A friable to well-cemented rock consisting of calcareous sand cemented by calcium carbonate crusts precipitated in the intertidal zone. Generally found as thin beds dipping seaward at less than 15 degrees.

Bindstone - A term used by Embry and Klovan (1971) for a rock with tabular-lamellar organisms binding and encrusting a large amount of matrix. No self-supporting organic fabric is present.

Bioclastic - Aspect of a material (sediment, rock, particle) alluding to its composition of broken remains of calcareous organisms.

Biolithite - A limestone made up of organic structures growing in place and forming a coherent, resistant mass during growth (Folk, 1959, 1962).

Biomicrite - A limestone composed predominantly of skeletal grains in a micrite matrix (Folk, 1959, 1962).

Biomicrudite - A biomicrite containing fossils or fossil fragments that are more than one millimeter in diameter (Folk, 1959, 1962).

Biosparite - A limestone composed predominantly of skeletal grains and sparry calcite cement (Folk, 1959, 1962).

Birdseyes - In sedimentary carbonates, the term is used for small but conspicuous, somewhat lens-shaped or globular masses of sparry calcite cement a few millimeters to one centimeter or more in size. Although the term normally refers to either the sparry carbonate features themselves or to the rock containing them (Folk, 1959), it has also been applied to voids of like sizes and shapes; hence, the expression "birdseye porosity" (Choquette and Pray, 1970, p. 244). Generally synonymous with "fenestral porosity"; sometimes spelled "bird's-eyes".

Birefringence - The property of a crystal to split a beam of light into two beams of unequal velocities based on the difference between the greatest and the least indices of refraction of that crystal. Under a polarizing microscope (in cross-polarized light), the degree of birefringence is manifest as "interference colors" which are a function of the mineral type, orientation and thickness as well as the nature of the light.

Bitumen - Generally, the spectrum of natural flammable hydrocarbons (petroleum, asphalt, mineral wax, etc.), including semisolid and solid admixtures with mineral matter.

Bladed - In reference to sparry calcite cement, defined as including crystals

with a length-to-width ratio between 1.5:1 and 6:1. See Folk (1965).

Boring/boring porosity - Openings created in relatively rigid rock, shell, or other material by boring organisms. The rigid host substrate is the feature that distinguishes borings from burrows; the latter are produced in unconsolidated sediment. Porosity created by boring organisms is not common in ancient carbonate rocks but such pores are recognized as a distinct, if minor, porosity type by Choquette and Pray (1970).

Botryoid/botryoidal - Having the curved form of a bunch of grapes. Commonly used for mineral deposits, such as aragonite, chalcedony, or hematite, which have a surface of spherical shapes. Also used for crystalline aggregates in which the spherical shapes are composed of radiating crystals, such as in some marine aragonite cements. An individual, rounded crystal cluster is termed a "botryoid".

Boudinage - A lenticular structure common in deformed sedimentary and metamorphic rocks, resulting from the stretching, thinning, and breaking of a competent bed within less competent strata resembling boudins (sausage) in cross-section.

Boundstone - A carbonate rock showing signs of grains being lithified or "bound" (by organisms) during deposition (Dunham, 1962).

Breccia - A rock structure marked by an accumulation of angular fragments, or of an ore texture showing mineral fragments without notable rounding. Major types of breccias in carbonate strata include fracture breccias associated with structural features or solution-collapse breccias typically associated with removal of associated evaporites or cavern formation and collapse in limestones.

Breccia porosity - the type of interparticle porosity in a breccia. Breccias are rather common in many carbonate facies, but breccia porosity is only locally of quantitative importance, especially along fracture zones (fracture breccias), dissolution features (solution breccias), or in debris flows (depositional breccias). See Choquette and Pray (1970, p. 244).

Burrow porosity - Feature created by organic burrowing in relatively unconsolidated sediment, in contrast to borings, which formed in rigid sedimentary particles or rock. Most burrows collapse, become filled with sediment, or are back-filled by the burrow-forming organism itself. Thus, burrows rarely form discrete macroporosity although they may affect interparticle pore space distribution (Choquette and Pray, 1970, p. 244).

Calcarenite - A limestone composed predominantly (more than 50 percent) of sand-sized calcium carbonate grains (a carbonate sand). Term was first introduced by Grabau (1904).

Calcilutite - A limestone consisting predominantly (more than 50 percent) of detrital calcite particles of silt and/or clay size; a lithified calcareous mud (lime mud). Term was first introduced by Grabau (1904).

Calcirudite - A limestone composed predominantly (more than 50 percent) of calcium carbonate fragments larger than sand size (carbonate conglomerate). Term was first introduced by Grabau (1904).

Calcispheres - Silt- or sand-sized spheres of clear (sparry) calcite, some with a discernible single or double wall and some without. Calcispheres are problematic grains that have, in most instances, no certain origin. Several types of calcispheres exist and most are attributed to algal sources. Mesozoic to Recent calcispheres are predominantly the remains of dinoflagellates.

Calcite - A common rock-forming material, composed of $CaCO_3$, that is the major constituent of limestones. This hexagonal mineral is trimorphous with aragonite and vaterite. It is usually white, colorless, or pale shades of gray; it has perfect rhombohedral cleavage, a hardness of 3 on the Mohs scale, and effervesces in cold dilute HCl. It is the most stable calcium carbonate mineral under most earth-surface conditions, including fresh water and burial diagenetic environments.

Calclithite - A rock formed chiefly of carbonate clasts (extraclasts) derived from older, lithified limestone, generally external to the contemporaneous depositional system. Commonly located along downthrown sides of fault scarps. Term coined by Folk (1959).

Calcrete - Surficial material such as sand-, gravel-, or cobble-sized materials that are cemented by calcium carbonate in arid climates as a result of evaporative concentration of $CaCO_3$ in surface pore waters. Often characterized by crusts, pisoids, reverse grading, autofracturing, and microstalactitic textures. Syn.: caliche.

Calcspar - A term used for coarsely crystalline calcite cement.

Caliche - Surficial material such as sand-, gravel-, or cobble-sized materials that are cemented by calcium carbonate in arid climates as a result of evaporative concentration of $CaCO_3$ in surface pore waters. Commonly characterized by crusts, pisoids, reverse grading, autofracturing, and microstalactitic textures.

Cathodoluminescence - The emission of characteristic visible luminescence by a substance when bombarded by an electron stream or ionized gas beam.

Cavern(ous) porosity - A pore system characterized by large openings or caverns. Although much cavernous porosity is of solution origin, the term is descriptive and not genetic. A practical lower size limit of "cavern" for outcrop studies is about the smallest opening an adult person can enter. Such pore space is too large to be identified in normal subsurface cores, but is recognizable during drilling by large drops (0.5 m or greater) of the drill bit. See Choquette and Pray (1970).

Celestite - An orthorhombic mineral: $SrSO_4$. It is commonly white with an occasional pale-blue tint. It often occurs in residual clays and in deposits of salt, gypsum, and associated dolomite and shale. Typically, it is associated with subaerially altered evaporites and/or carbonates with the strontium being derived from alteration of marine aragonite or detrital siliciclastic minerals (clays, feldspars).

Cellular limestone - A carbonate rock characterized by cellular openings (pores that are largely unconnected or may be only partially connected. A fabric in which calcitic veins or partitions intervene between large pores. This fabric is commonly formed through the alteration (dissolution) of nodular evaporites in a carbonate matrix. Syn.: rauhwacke.

Cellular porosity - "Cellular porosity" is term with diverse meanings; first used for solution-formed molds and other generally equidimensional solution vugs, as opposed to more elongate, channel-like openings in rocks. Also applied to intraparticle openings within fossils, particularly chambered organisms. The term is little used now and Choquette and Pray (1970, p. 244-5) advocated its abandonment.

Cement - Mineral material, typically precipitated, that occurs in the spaces between individual grains of a consolidated or partially consolidated sedimentary rock.

Chalcedony - A cryptocrystalline variety of silica, commonly microscopically fibrous, with lower indices of refraction and mineral density than quartz.

Chalk - A limestone that consists predominantly of the remains of calcareous nannoplankton (especially coccoliths) and microplankton (especially foraminifers). Chalks commonly are also considered to be soft and friable and "chalky" is used as a synonym for "porous and unconsolidated". Although many exposed chalks are indeed friable, burial and diagenetic alteration can lead to the complete lithification of chalks.

Chalky porosity - "Chalky" is a widely used surface-texture term denoting the distinctive dull and earthy character of fine-grained carbonate rocks and has also been applied to the porosity of such very finely textured rocks. It is useful where a more specific size or porosity-type designation such as "micropore," "micro-interparticle", or "micromold"

is not warranted (see Choquette and Pray, 1970, p. 245).

Channel (channel porosity) - A type of pore or pore system with marked elongation or continuity of pores in one or two dimensions relative to a third dimension (Choquette and Pray, 1970, p. 245). These authors recommend that the term be applied only to such pores and openings which show by their boundaries or continuity that they have developed indiscriminately with respect to texture or fabric elements in the host rock (i. e. they are non-fabric selective and are essentially elongate vugs).

Chert - A hard, dense, dull to semi-vitreous, cryptocrystalline sedimentary rock, composed of variable amounts of silica mainly in the form of microcrystalline quartz; may contain minor carbonate, iron oxide, or other impurities.

Chloralgal - A term proposed by Lees and Buller (1972) for the common association of skeletal grains in warm-water or low-latitude, elevated salinity, carbonate sediments; derived from a contraction of two of the skeletal groups typically present, and often dominant, in saline warm-water settings — Chlorophyta and algal species. These organisms reflect temperatures above 15°C and variable salinities that reach above 40 ppt. The term stands in contrast to the "foramol " or cold-water skeletal grain association and the "chlorozoan " warm-water, normal-salinity association.

Chlorozoan - A term proposed by Lees and Buller (1972) for the common association of skeletal grains in warm-water or low-latitude, normal salinity, carbonate sediments; derived from a contraction of the names of two of the skeletal groups typically present, and often dominant, in warm-water settings — Chlorophyta and Zoantharians. These organisms reflect temperatures above 15°C and salinities in the range of 32 to 40 ppt. The term stands in contrast to the "foramol " or cold-water skeletal grain association and the "chloralgal " warm-water, elevated-salinity association.

Circumgranular cracking - Irregular to globular masses of sediment separated by non-tectonic fractures and produced by alternate shrinkage and expansion are called circumgranular cracking (Swineford, et al., 1958; Esteban and Klappa, 1983). A common feature in soils in general and caliche in particular.

Clastic - As used by most sedimentary petrologists, composed of particles that have been mechanically transported, at least locally. Specifically includes limestones made up of fossils or other allochems that have been moved by waves or currents. (Note that most facies mappers use clastic for terrigenous rocks and not limestones).

Cleavage - The fracturing or breakage of a mineral along its crystallographic planes; cleavage is, therefore, a reflection of crystal structure.

Coalescive neomorphism - A term introduced by Folk (1965) for aggrading neomorphism in which small crystals are converted to large ones by gradual enlargement maintaining a uniform crystal size at all times.

Coarsely crystalline - Descriptive of an interlocking texture of a carbonate sedimentary rock having crystals whose diameters are in the range of 0.25-1.0 mm (Folk, 1959), or exceed 0.2 mm.

Coated grains - A general term for grains with coatings or rims of calcium carbonate; includes oolites and superficial oolites, pisolites, and algally coated grains (oncoids).

Collophane - A carbonate-hydroxyl-fluorapatite. This colorless, gray or yellowish brown to dark brown phosphate mineral is a common constituent of some skeletal materials and phosphatic marine sediments. It has extremely low birefringence (virtually isotropic) when viewed in thin section.

Columnar - Describes a form of fibrous calcite in which crystals have a length to width ratio greater than 6:1 and the crystals typically are more than 10 μm wide. Contrasts with the narrower crystals of the "acicular" growth form. Columnar calcites can occur as radial-fibrous, radiaxial-fibrous or fascicular-optic-fibrous varieties.

Compact - A surface-texture term applied to rocks that break along smooth to conchoidal faces and generally have little or no macro- or micro-porosity. The term was advocated in a classification of carbonate reservoir rocks by Archie (1952, p. 280) and has wide usage in this sense. "Compact" is useful as a gross indicator of low matrix porosity in a finely textured rock, and seems preferable to the somewhat synonymous term "dense," as it avoids connotations of mass (Choquette and Pray, 1970).

Coquina – Carbonate rock or sediment consisting entirely, or nearly so, of mechanically sorted skeletal debris. Most commonly applied to more or less cemented shell debris. For finer-grained shelly detritus of sand size or less, the term "microcoquina" is more appropriate (Pettijohn, 1957).

Cristobalite - A silica (SiO_2) polymorph of quartz that is stable only above 1470°C. It is a common intermediate stage in the diagenetic transition from Opal-A to quartz.

Crossed-lamellar microstructure - A common wall structure in mollusks (bivalves and gastropods). It is best developed in aragonitic shells (especially gastropods, bivalves, scaphopods and chitons), but may also be found in calcitic ones. It consists of a complex of micrometer-scale lamellae packed together in roughly parallel vertical sheets. Alternating orientations of crystals within adjacent lamellae yields a distinctive "zebra-striping" to the shell wall when viewed perpendicular to the banding.

Cryptocrystalline - Descriptive of a crystalline texture of a carbonate sedimentary rock having discrete crystals whose diameters are less than 0.001 mm.

Cutan - A pedological feature (crust or grain coating) which can be used as diagnostic indicator of paleo-soil formation when composed of clay minerals. Defined by Brewer (1964) as "a modification of the texture, structure or fabric at natural surfaces in soil materials due to the concentration of soil constituents or in-place modifications of the plasma (relatively unstable soil matrix)." See Esteban and Klappa (1983).

Decimicron-sized - Refers to a fabric in which the crystal diameters are 10-100 μm (microns). See Friedman (1965).

Dedolomite - The product of diagenetic conversion of dolomite to another mineral (typically calcite), a process that occurs most commonly during the dissolution of associated calcium sulfates or at high temperatures. Because the term does not specify the end product of conversion, it is less definitive than terms such as "calcitized dolomite".

Degrading neomorphism - A kind of neomorphism in which the crystal size decreases (Folk, 1965).

Detrital - Used in different ways by different authors and hence largely undefinable out of context. Sometimes synonymous with clastic, sometimes with terrigenous, and sometimes restricted to rocks composed of broken fragments of older rocks.

Diagenesis - Any physical or chemical changes in sediments or sedimentary rocks that occur after deposition, excluding processes involving high enough temperature and pressure to be called metamorphism.

Dismicrite - A disturbed micrite; a carbonate mud that contains stringers or "eyes" of sparry calcite resulting from filling of burrows, slump or shrinkage cracks, or other partial disruption on the sea floor (Folk, 1959, 1962).

Dolomite - A term used for both a mineral and a rock. Dolomite is a widespread, rock-forming, rhombohedral mineral consisting of $CaMg(CO_3)_2$. Part of the magnesium may be replaced by iron or manganese. Dolomite is typically colorless or white but may be tinted reddish, brown, yellow, etc. It has perfect cleavage and effervesces feebly in cold, dilute HCl. Dolomite occurs most commonly as a replacement of calcium carbonate minerals. The term is also used (following Kay, 1951) for a rock composed predominantly of the

mineral dolomite although the term "dolostone" is preferable.

Dolospar - A sparry dolomite crystal, generally of rather coarse size on the order of 100 μm (micrometers) or more.

Dolostone - A term employed for a sedimentary rock composed of the mineral dolomite.

Druse (drusy) - A crust or coating of crystals lining a cavity (druse) in a rock (specifically, sparry calcite lining the pores of a limestone, generally with crystal sizes increasing from the edges to the center of the pores).

Effective porosity - The "intercommunicating void space of a rock" (Muskat, 1949, p. 114). As it is usually the effective and not the total porosity of a rock that is measured in standard core-analysis procedures and that contributes to its permeability, in petroleum-engineering practice the term "porosity" normally means "effective porosity" (Choquette and Pray, 1970).

Encrinite - A crinoidal limestone, specifically one in which crinoidal grains constitute more than 50 percent of the volume of the rock (see Bissell and Chilingar, 1967).

Enfacial junction - A triple-junction (meeting place) between three adjacent crystals where one of the three angles is 180 degrees (Bathurst, 1964, p. 362, and 1971). An abundance of enfacial junctions in a sparry calcite mosaic has been interpreted as indicating precipitated (void filling) spar. It also may indicate two distinct generations of spar formation, with newly formed crystals of the second generation abutting against those of the earlier generation.

Eogenetic porosity - Porosity that formed in the eogenetic stage of diagenesis (term proposed by Choquette and Pray, 1970). Contrast with mesogenetic and telogenetic.

Eogenetic stage - A stage of diagenesis occurring during the time interval between final deposition and burial of the newly deposited sediment or rock below the depth of significant influence by processes that either operate from the surface or depend for their effectiveness on proximity to the surface. From Choquette and Pray (1970).

Epigenetic - Pertaining to sedimentary structures, minerals, and mineral deposits formed after deposition, at low temperature and pressure changes or transformations affecting sedimentary rocks subsequent to compaction (a definable stage of diagenesis).

Epitaxial - See "syntaxial."

Equant - In reference to sparry calcite cement it is defined as including crystals with a length to width ratio of less than 1.5:1.

Euhedral - Refers to a single crystal or crystal fabric that shows well defined typical crystallographic forms (i.e., the crystal is largely or completely bounded by crystal faces). See Friedman (1965).

Evaporite - A nonclastic sedimentary rock composed primarily of minerals produced from a saline solution as a result of extensive or total evaporation of the parent solution. Gypsum, anhydrite, and halite are the most common evaporite minerals in carbonate strata, but celestite, sylvite, and many other minerals also fall in this category.

Extraclast - A detrital grain of lithified carbonate sediment (lithoclast) derived from outside the depositional area of current sedimentation. The rock composed of these grains would be a calclithite. See also intraclast (Folk, 1959).

Fabric - The arrangement of grains and/or crystals in a rock in terms of their sizes, shapes and orientations.

Fabric selective - A term that refers to a dependent spatial relationship between pores or replacement crystals and primary or diagenetic fabric elements of the host rock. Term coined by Choquette and Pray (1970, with detailed discussion on p. 211-214).

Fascicular-optic fibrous calcite - A cavity-filling calcite mosaic consisting of fibrous crystals (and subcrystals) radiating away from the initial growth surface and allied to optic axes that diverge away from the wall. FOFC is characterized by curved cleavages, undulose extinction and irregular intergranular boundaries which distinguish this fabric from simple radial-fibrous calcite. Must also be distinguished from radiaxial-fibrous calcite (RFC): FOFC has twin planes that are concave downward relative to the substrate and extinction sweeps in the opposite direction from stage rotation; the opposite is true for RFC. See Kendall (1977, 1985).

Fenestrae (fenestral fabric) - Primary or penecontemporaneous gaps in rock framework larger than grain-supported interstices. Such features may be open pores or may have been partially or completely filled with internal sediment and/or sparry cement. Fenestrae occur as somewhat rounded features of spherical, lenticular, or more irregular shapes; their large size in comparison to normal interparticle openings and their multigranular roofs, floors, and other margins are key characteristics. Fenestrae are commonly somewhat flattened parallel with the laminae or stratigraphic planes of the rock. They may, however, be round or very irregular, and some are elongate in a vertical dimension. Although isolated fenestrae occur in sedimentary carbonates, it is more common to find many in close association. Fenestrae are commonly associated with microbial mats and can result from shrinkage, gas formation, organic decay, or other synsedimentary processes.

Ferroan dolomite - A mineral that is intermediate in composition between dolomite and ferrodolomite. That is, it has some degree of substitution of Fe for Mg in the dolomite lattice (typically from 1% to slightly more than 50%). Generally used as a synonym of ankerite.

Fibrous - In reference to sparry calcite cement it is defined as including crystals with length-to-width ratios greater than 6:1.

Finely crystalline - Descriptive of an interlocking texture of a carbonate sedimentary rock having crystals whose diameters are in the range of 0.016-0.062 mm (Folk, 1959).

Floatstone - A textural type of a limestone in which fragmented (mainly biogenic) constituents are not organically bound, are mostly greater than 2 mm in diameter, but are mud supported. See Embry and Klovan (1971).

Foliated microstructure - A common wall structure in brachiopods, bryozoans, some bivalves and gastropods and some calcified worms. This structure is always calcitic and consists of thin (1-2 μm) calcite lamellae. The lamellae may be long and uniformly oriented within layers or they may be short and randomly oriented.

Foramol - A term proposed by Lees and Buller (1972) for the common association of skeletal grains in cold-water or high-latitude carbonate sediments; derived from a contraction of two of the skeletal groups typically present, and often dominant, in cold-water settings — foraminifers and mollusks. The term stands in contrast to the "chlorozoan" or "chloralgal " skeletal grain associations of warmer waters.

Fracture porosity - Porosity formed by fracturing. The term is generally used for porosity occurring along breaks in a sediment or rock body where there has been little mutual displacement of the opposing blocks. Fracture porosity grades into breccia porosity with increasing dislocation or "chaos." In carbonate rocks, fractures and hence fracture porosity may originate in diverse ways, such as by collapse related to solution, slumping, or various kinds of tectonic deformation. See Choquette and Pray (1970, p. 246).

Framboid - Microscopic spheroidal clusters of pyrite grains commonly associated with bits of organic material.

Framestone - A term used by Embry and Klovan (1971) for a boundstone with in-situ massive fossils which construct a rigid framework; matrix, cement, or void space fills in the framework.

Frustule - The siliceous skeleton of a diatom.

Geopetal structure - Any internal structure or organization of a rock indicating original orientation such as top and bottom of strata. Common examples are internal sediment accumulating on the floor of a cavity which it partly fills or solution-collapse residue that has fallen to the bottom of a vug or cave. See Sander (1951).

Glaebule - A soil feature, usually equant, prolate, to irregular in shape, generally a nodule or concretion that has not precipitated in a pre-existing void space (see Esteban and Klappa, 1983, p. 28-29). In caliche profiles, glaebules consist of discrete, powdery to indurated concentrations of calcite, commonly with some degree of concentric structure (see also pisoids).

Grains - (1) solid particles whose physical limits may encompass many crystalline entities. Distinctions as between coarse grained and coarsely crystalline are not always observed but are fundamental; (2) the friable aggregates of silt-sized carbonate crystals that are formed from the partial cementation of crystals in contact with each other, as found in modern deposits of the Bahama platform and comparable areas; (3) a general term used to describe silt- and larger-sized carbonate sediment particles, including pellets, skeletal fragments, ooids, and intraclasts — see also: allochem.

Grain supported - Refers to the fabric of a rock in which the grains (allochems) are in contact with each other forming a framework, even though they may have a carbonate mud (micrite) matrix.

Grainstone - A carbonate rock composed of grains (allochems) that lacks carbonate mud in the interstices (coined by Dunham, 1962).

Grapestone - Sometimes used for aggregates of silt-sized carbonate crystals (or grains), but more properly applied to grape-like clusters of such aggregates.

Gravitational cement - A descriptive term for cements which are concentrated on the bottom sides of grains. Such textures generally form in meteoric vadose or upper intertidal areas (marine vadose settings) where pores are only partially water-filled and in which water droplets can hang from the undersides of grains. Syn.: pendant or microstalactitic cement.

Growth-framework porosity - Primary porosity created by the in-place growth of a carbonate rock framework. Term is specifically used for pore space of rock frameworks known or inferred to have grown in place as rigid or semi-rigid fabrics as a result of organic and/or inorganic processes (i.e., boundstones or biolithites). See Choquette and Pray (1970, p. 246-247).

Gypsum - An evaporite mineral consisting of hydrous calcium sulfate, $CaSO_4 \cdot 2H_2O$. It is the commonest sulfate mineral and is white or colorless when pure.

Halite - An evaporite mineral — sodium chloride, NaCl, (commonly termed "table salt" or "rock salt"). It occurs in massive granular, compact, or cubic-crystalline forms. Because of its great solubility, special care must be taken to preserve halite in thin sections, including cutting and grinding in oil.

Hardground - A zone at the sea floor, generally a few centimeters thick, in which the sediment was lithified to form a hardened surface; often encrusted, discolored, hardened by calcium carbonate, phosphate and/or glauconite impregnation and encrusted or bored by organisms; implies a slowdown or gap in sedimentation, and may be preserved stratigraphically as a disconformity. A softer, incipient hardground is sometimes termed a "firmground."

Heterozoan association - Used as a more generalized (less biologically restricted) synonym for a "foramol" association of skeletal organisms or grains typically found in cool- or deep-water area. This biotic assemblage contrasts with that of the photozoan association. Heterozoan assemblages can occur in warm water areas, but in such areas are generally found below the photic zone or in areas of elevated trophic resources. Defined by James (1997).

High-magnesium calcite - A variety of calcite: $CaCO_3$. It consists of randomly substituted magnesium ions in solid solution for calcium in the calcite structure. Different workers use different percentages of Mg substitution as the minimum cutoff for the use of this term but most definitions use 2 to 5 mol percent Mg as the minimum — the practical upper end of the range in modern carbonates is about 30 mol percent Mg. High-magnesium calcite (sometimes called simply "magnesium calcite" or abbreviated as "Mg-calcite" or "HMC") is a common constituent of modern carbonate sediments both in the form of marine cements and in shells/tests of many organisms (especially red algae and echinoderms). Generally unstable in fresh waters.

Homogeneous microstructure - A common wall structure in calcitic tests or shells of foraminifers, ostracodes and trilobites and in the aragonitic shells of some mollusks. It consists of an orderly arrangement of uniformly small microstructural elements of such size that the individual elements are not distinguishable with standard thin-sections and light-microscope magnifications. The uniform orientation of the crystal elements leads to a sweeping extinction as the grain is rotated under crossed polars.

Intercrystal porosity - Porosity between crystals. Although this simple definition could apply in a strict sense to almost all porosity in carbonates, "intercrystal" (or "intercrystalline") normally is restricted to the porosity between individual crystals of somewhat equant and equal size, as in many porous dolomites. Intercrystal porosity may be of either primary or secondary origin. See Choquette and Pray (1970, p. 247).

Intergrain porosity - Referring to pore spaces existing between individual grains or particles of a sedimentary rock. Intergrain porosity is the most commonly used term for between-grain porosity in sandstones and carbonates (cf. "interparticle porosity"), but it is not synonymous with primary porosity — it is a non-genetic term denoting only the relative position, not the time of formation, of the pores. See Choquette and Pray (1970, p. 247).

Interparticle porosity - Porosity between any types of sedimentary particles. Can even be used for pores between particles of silt and clay sizes where it isn't obvious that the particles are sedimentary or have been diagenetically modified (and thus this term differs somewhat from "intergrain porosity" or "intergranular porosity"). Interparticle porosity denotes position and not genesis. In clastic carbonates, interparticle porosity is generally of depositional (primary) origin, but it can also form by several post-depositional processes of which the predominant mechanism is selective dissolution of finer textured matrix from between larger particles. See Choquette and Pray (1970, p. 247).

Interstices - Technically, voids; but used mostly for areas that were voids in the initial sediment, though they are now filled.

Intraclast - A fragment of penecontemporaneous, commonly weakly consolidated, carbonate sediment that has been eroded and redeposited, generally nearby, within the same depositional sequence in which it formed (Folk, 1959, 1962). See also: extraclast.

Intracrystal porosity - Porosity within individual crystals — pores in large crystals of echinoderms, and fluid/gaseous inclusions form most of this category of porosity.

Intragrain porosity - The porosity existing within individual grains or particles of a rock, especially within skeletal material of a sedimentary carbonate rock. Despite wide usage of "intragrain" or "intragranular," Choquette and Pray (1970) prefer to use "intraparticle" as the general term for this type of porosity.

Intramicrite - A limestone containing at least 25 percent intraclasts and in which the carbonate-mud matrix (micrite) is more abundant than the sparry-calcite cement (Folk, 1959).

Intraparticle porosity - The porosity within individual particles or grains of a rock. (See also intragrain porosity). "Intraparticle porosity" as used here is a physical, positional, not a genetic porosity type. It is abundant in carbonate sediments and can be an important part of the preserved porosity in carbonate rocks. Much intraparticle porosity in carbonates forms before final deposition of the sedimentary particle or grain (predepositional porosity); some forms during or after final deposition. Internal chambers or other openings within individual or colonial skeletal organisms are the most commonly recognized intraparticle pores. However, an appreciable amount of the primary intraparticle porosity in carbonate sediments consists of pore space within individual pellets, intraclasts, ooids, and other nonskeletal grains (Choquette and Pray, 1970).

Intrasparite - A limestone containing at least 25 percent intraclasts and in which the sparry-calcite cement is more abundant than the carbonate-mud matrix (micrite) (Folk, 1959).

Inversion - The diagenetic transformation (replacement in the loose sense) of a mineral by its polymorph — specifically the transformation of aragonite to calcite. See Folk (1965).

Isopachous - A descriptive term for cement which has formed as a uniform-thickness coating around grains. Syn.: "grainskin".

Isotropic - In petrography, the term refers to a crystal whose optical properties do not vary according to crystallographic direction. Thus, light travels with the same speed in any direction through the crystal and the crystal shows no birefringence under crossed polars. Typical of cubic and amorphous substances.

Limestone - A carbonate rock composed of more than 50 percent by weight of calcium carbonate (in the form of calcite or aragonite). For practical petrographic work, areal percentages are used instead of weight percentages.

Limpid dolomite - A variety of dolomite crystal that is optically clear (essentially free of inclusions), generally less than 100 μm in size, and thought to have precipitated from relatively dilute pore waters.

Lithoclast - A mechanically formed and deposited fragment of a carbonate rock, normally > 2 mm in diameter, derived from an older limestone, dolomite, or other sedimentary rock stratum. Also termed an extraclast.

Lithographic - Refers to extremely fine-grained and uniform carbonate rock, usually with smooth conchoidal fracture.

Loferite - Carbonate rock containing a great abundance of shrinkage-type pores (a "birdseye" or fenestral limestone or dolomite). See Fischer (1964). A term now rarely used as the term "fenestral fabric" has become more widely applied.

Lumps - In modern sediments, irregular composite aggregates of silt- or sand-sized carbonate particles that are cemented together at points of contact: in ancient carbonates, similar-appearing lobate grains that are composed of carbonate mud (micrite). After Illing (1954).

Magnesite - A white to grayish, yellow or brown mineral: $MgCO_3$. It is isomorphous with siderite. Magnesite is generally found as earthly masses or irregular veins resulting from the altercation of dolomite rocks, or of rocks rich in magnesium silicates, by magmatic solutions. It is used chiefly in making refractories and magnesia. Syn: "giobertite."

Marine phreatic - A subsurface zone in which the interstitial pores are completely filled with fluids derived from the overlying marine water mass. Used specifically to refer to the environment of formation of marine cements such as botryoidal aragonite or peloidal high-magnesium calcite in near-surface settings where marine pore fluids are moved through sediments by wave- or tidal pumping, convection, or diffusion.

Marl - Soft, loose, earthy sediment or rock consisting chiefly of a mixture of clay and fine-grained calcium carbonate in varying proportions between 35 and 65% of each; formed under marine or freshwater conditions.

Matrix - Descriptive of the sedimentary, mechanically deposited material between grains. Includes carbonate mud or micrite as well as terrigenous mud or other fine-grained interstitial material.

Matrix porosity - The porosity of the matrix or finer portion of a carbonate sediment or rock, in contrast to porosity associated with the coarser particles or constituents; or the porosity of "blocks" of the rock in contrast to the porosity of the fractures (Choquette and Pray, 1970).

Medium crystalline - Descriptive of an interlocking texture of a carbonate sedimentary rock having crystals whose diameters fall in the range of 0.062-0.25 mm (Folk, 1959).

Megapore (megaporosity) - A size term proposed by Choquette and Pray (1970) for large pores. Megapore is the largest of three pore-size classes (along with mesopore and micropore). The "mega-" size designation is used for equant to equant-elongate pores whose average diameter is larger than 4 mm, and for tubular or platy pores whose average cross-sectional diameter or thickness, respectively, is larger than 4 mm. Megaporosity is the largest of three pore-size groupings (along with mesoporosity and microporosity).

Meniscus cement - Refers to a carbonate cement type formed during vadose diagenesis where cement crystals form only at or near grain contacts in the positions a water meniscus would occupy.

Mesogenetic - Occurring during the time interval in which rocks or sediments are buried at depth below the major influence of processes directly operating from or closely related to the surface. See Choquette and Pray (1970).

Mesopore (mesoporosity) - A size term proposed by Choquette and Pray (1970) for intermediate-size pores (as contrasted with megapore and micropore). The "meso-" size designation is used for equant to equant-elongate pores whose average diameter is between 4 and 1/16 mm, and for tubular or platy pores whose average cross-sectional diameter or least diameter, respectively is between 4 and 1/16 mm. Mesoporosity is dominated by intermediate-size pores (as contrasted with megaporosity and microporosity).

Meteoric environment - Zone at or near the earth's surface influenced or pervaded by waters of recent atmospheric origin. Typically divided into unsaturated (vadose) and saturated (phreatic) zones divided by a water table.

Micrite - An abbreviation of "microcrystalline calcite. The term is used both as a synonym for carbonate mud (or "ooze") and for a rock composed of carbonate mud (calcilutite). Micrite is defined as having crystals 1 to 4 μm in diameter and is formed as organic or inorganic precipitates or as the product of breakdown of coarser carbonate grains. Micrite is produced within the basin of deposition and shows little or no evidence of significant transport (Folk, 1959, 1962).

Micritization - Conversion of sand- or silt-sized sedimentary particles partly or completely to micrite-sized calcium carbonate, possibly due to microscopic boring algae and/or fungi.

Microcodium - Elongate, petal-shaped calcite prisms or ellipsoids, 1 mm or less in length and grouped in spherical, sheet or bell-like clusters. Typically associated with caliche crusts and other subaerial exposure surfaces. Currently thought to be formed by the calcification of microrhizae — symbiotic associations between soil fungi and cortical cells of higher plant roots (see Esteban and Klappa, 1983).

Microcrystalline - Texture of a rock consisting of or having crystals that are small enough to be visible only under the microscope.

Micron-sized - Refers to a fabric in which crystal diameters are 0-10 μm (micrometers).

Micropore - Size term proposed by Choquette and Pray (1970) for

microscopic pores or pores small enough to hold water against the pull of gravity and to inhibit the flow of water. Micropore is the smallest of three pore-size terms (with mesopore and megapore). The "micro-" designation is used for equant to equant-elongate pores whose average diameter is less than 1/16 mm and for tubular or platy pores whose average cross-sectional diameter or least diameter, respectively, is less than 1/16 mm.

Microspar - Generally 5- to 20-μm-sized calcite produced by recrystallization (neomorphism) of micrite; can be as coarse as 30 μm (Folk, 1965).

Microsparite - A term used by Folk (1959) for a limestone whose carbonate-mud matrix has recrystallized to microspar.

Microstalactitic cement - A descriptive term for cements which are concentrated on the bottom sides of grains. Such textures generally form in meteoric vadose or upper intertidal areas (marine vadose settings) where pores are only partially water-filled and in which water droplets can hang from the undersides of grains. Syn.: pendant or gravitational cement.

Microstylolite - A low-relief (less than 1 mm of relief) surface produced by tectonic of burial-related pressure dissolution of soluble carbonate, typically marked by the presence of clays, organic matter or other insoluble material. Often microstylolites form in groups or clusters, sometimes referred to as horse-tail seams. Syn.: solution seam; also see stylolite.

Microsucrosic - Microcrystalline texture of largely euhedral to subhedral calcite or dolomite crystal (mosaics) in the approximate size range of 5 to 50 μm.

Millimeter-sized - Refers to a fabric in which the crystal diameters are 1-10 mm (Friedman, 1965). Brit. usage - "millimetre-sized."

Mold - A mold is a pore formed by the selective removal of a former individual constituent of the sediment or rock. Most molds in sedimentary carbonates are created by the selective dissolution of various types of carbonate depositional particles. Especially common in limestones are molds of primary aragonitic constituents, notably ooids and molluscan shells. Molds in dolomite commonly formed by selective dissolution of either aragonite or calcite primary constituents, and less commonly by solution of anhydrite, gypsum, or halite. Brit. usage - "mould."

Moldic porosity - Descriptive of pores formed by the selective removal of a former individual constituent of the sediment or rock. Most moldic porosity in sedimentary carbonates is created by the selective dissolution of various types of carbonate depositional particles. Especially common in limestones are molds of primary aragonitic constituents, notably ooids and molluscan shells. Moldic pores in dolomite commonly formed by selective dissolution of either aragonite or calcite primary constituents, and less commonly by solution of anhydrite, gypsum, or halite (Choquette and Pray, 1970). Moldic is often used with modifying prefixes, including oomoldic or dolomoldic. Brit. usage - "mouldic."

Monomict - referring to a sedimentary rock containing clasts of just a single rock type, for example an intraclastic limestone bearing only clasts of laminated tidal flat sediment or one containing only beachrock fragments (Syn.: monomictic; contrast with polymict).

Mudstone - In referring to carbonates, a carbonate rock composed of carbonate mud with less than 10% allochems (Dunham, 1962).

Mud-supported - Refers to the fabric of a mudstone (micrite) in which the grains (allochems) are separated from each other by, and "float" in, a micrite matrix (Dunham, 1962).

Nacreous microstructure - A shell wall structure present only in mollusks (bivalves, gastropods and cephalopods). It consists of an orderly arrangement of numerous thin (tablet-like) aragonite laminae, each separated by a thin film of organic material of equal thickness and uniform orientation. Laminae may be parallel to the shell surface or parallel to growth lines. Nacre is easily recognized in hand sample as it shows pearly luster.

Neomorphism - A general "term of ignorance" for all diagenetic transformations between one mineral and itself or a polymorph, whether the new crystals are larger or smaller or simply differ in shape from the previous ones, or represent a new mineral species. Includes both inversion and recrystallization. See Folk (1965).

Neptunian dike - A body of sediment that cross-cuts beds in the manner of a dike, formed by sedimentation in submarine fissures. Sedimentation can include reworking of sediment from the seafloor downward into the fissure, growth of organisms on the walls of the fissure, or precipitation of cements from seawater circulating into the fissure.

Occlusion - The reduction or replacement of porosity by mineral growth or internal sediment infilling.

Oncoid - In North American usage, an oncoid is a coated grain of algal (but not red algal) or microbial origin that is coarser than 2 mm in diameter; a spheroidal form of a microbial/algal stromatolite showing a series of concentric (often irregular or scalloped) laminations. These unattached stromatolites are produced by mechanical turning or rolling, exposing new surfaces to algal growth. Common European usage is less genetic as a microbial/algal origin is not a prerequisite for using the term. Peryt (1981) divided oncoids into two groups: porostromate forms and spongiostromate forms.

Oncolite - A rock composed of oncoids. The term is often improperly used, however, as a synonym for an oncoid.

Ooid - A spherical to ellipsoidal grain, 0.25 to 2.00 mm in diameter, with a nucleus covered by one or more precipitated concentric coatings that have radial and/or concentric orientation of constituent crystals. Ooids can have calcareous, ferruginous (especially hematite or chamosite), siliceous, bauxitic, phosphatic, evaporitic (gypsum, halite) or other concentric coatings.

Oolite - A rock composed dominantly of ooids. The term commonly is misused to describe the constituent grains.

Oomicrite - A limestone composed dominantly of ooids in a matrix of micrite (Folk, 1959, 1962).

Oomold - A spheroidal pore or in a sedimentary rock resulting from the dissolution of an ooid. Oomoldic is the adjectival form, as used in the term "oomoldic porosity."

Oosparite - A limestone containing at least 25% ooliths and no more than 25% intraclasts and in which the sparry-calcite cement is more abundant than the carbonate-mud matrix (micrite) (Folk, 1959).

Opal-A - An amorphous form of silica ($SiO_2 \bullet nH_2O$), probably colloidal in origin, that composes the precipitated skeletal material of diatoms, radiolarians and siliceous sponges. The mineral is colorless to gray or brown, has high negative relief, and is isotropic in thin section. It can contain up to 20% water, but usually has 3-9%. Typically converts to opal-CT or quartz at higher temperatures during sediment burial.

Orthochemical - A rock constituent that is a normal chemical precipitate, as contrasted to fossils, ooids, or other mechanically or biologically deposited constituents (Folk, 1959, p. 7).

Ossicles - Individual calcareous skeletal components of echinoderms (e.g. plates). Echinoids or crinoids consist of numerous ossicles which typically disaggregate upon the death of the organism. Each ossicle effectively acts as a single crystal of calcite under the polarizing microscope; in reality, however, each ossicle actually consists of an agglomeration of numerous submicroscopic crystallites with nearly perfectly parallel c-axes and well aligned a-axes.

Overgrowth - Secondary material deposited in optical and crystallographic continuity around a crystal grain of the same mineral composition.

Packed - Containing sufficient grains (allochems) for the grains to be in contact and mutually supporting, as contrasted with rocks with grains "floating" in mud (Folk, 1959, 1962).

Packstone - A grain-supported carbonate rock with more than 10 percent interstitial carbonate mud matrix (cf. grainstone and wackestone; Dunham, 1962).

Palisade (-style) - A type of pore-lining calcium carbonate cement composed of markedly elongate crystals arranged picket-fence style on or around a grain or other substrate.

Paragenesis - A sequential order of mineral formation or transformation.

Paramorphism - The transformation of internal structure of a mineral without change of external form or of chemical composition.

Passive precipitation -The precipitation of cement in open spaces, as in between grains, in the body chambers of fossils or in fenestrae (Folk, 1965). To be distinguished from the growth of neomorphic spar and the growth of crystals by displacement.

Pellet - A pellet is a grain (allochem) composed of lime mud (micrite) generally lacking significant internal structure. Pellets commonly are rounded, spherical to elliptical or ovoid in shape and most are considered to be the fecal products of invertebrate organisms. As such, pellets are generally small (0.03 to 0.3 mm) and of uniform size and shape in any single sample. The related term "peloid" sometimes is used as a more inclusive term to describe micritic (or micritized) grains of uncertain origin.

Pelletal - Describing a rock containing a significant percentage of pellets.

Pelmatozoan - Any echinoderm, with or without a stem, that lives or lived attached to its substrate. A term for any attached echinoderm, most commonly crinoids. A modifier used to describe and echinoderm-rich limestone.

Pelmicrite - A limestone composed dominantly of peloids (or pellets) in a matrix of micrite (Folk, 1959, 1962).

Peloid - An allochem formed of cryptocrystalline or microcrystalline carbonate regardless of size or origin. This term (coined by McKee and Gutschick, 1969) allows reference to grains composed of micrite or microspar without the need to imply any particular mode of origin (can thus include pellets, some vague intraclasts, micritized fossils, degraded ooids, and other grains of problematic origin).

Pelsparite - A limestone composed dominantly of peloids (or pellets) in sparry calcite cement (Folk, 1959, 1962).

Pendant cement - See "microstalactitic" cement.

Penecontemporaneous - Generally referring to cements or replacement textures indicating that, in the opinion of the user, the feature or mineral formed at almost the same time as the original sediment was deposited, that is, close to the sediment-air or sediment-water interface. Syn: syndepositional.

Photozoan association - Used to describe shallow, warm-water, benthic calcareous communities and their resultant sediments. The term "emphasizes the light-dependent nature of the major biotic constituents" (including the influences of harbored photosymbionts). Contrasts with "heterozoan association". Defined by James (1997).

Phreatic - The zone of water saturation below the water table. There can be marine or meteoric phreatic zones. Sometimes termed the "saturated zone". Contrast with "vadose" or unsaturated zone".

Phylloid algae - a term coined by Pray and Wray (1963) to describe all Late Paleozoic calcareous algae with platy or leaf-like forms and a lack of sufficient internal fabric preservation to allow generic-level identification.

Pisoid - A small spheroidal particle with concentrically laminated internal structure, larger than 2 mm and (in some usages) less than 10 mm in diameter.

Pisolite - A rock containing abundant pisoids.

Poikilotopic (poikilitic) - Textural term denoting a condition in which small granular crystals or grains are irregularly scattered without common orientation in a larger crystal of another mineral (generally sand or silt grains in a single, coarse cement crystal). See Friedman (1965).

Polymict - referring to a sedimentary rock containing clasts of multiple rock types, for example an intraclastic limestone or calclithite with varied clast lithologies or fabric types. (Syn.: polymictic; contrast with monomict).

Polymorph - One of two or more crystalline forms of the same chemical substance. For example, calcite (rhombohedral), aragonite (orthorhombic) and vaterite (hexagonal) are polymorphs of calcium carbonate.

Poorly-washed - A rock which has sparry calcite cement but which also has one-third to one-half of all interstices filled with carbonate mud (i.e., a poorly sorted rock).

Porcelaneous microstructure - A calcareous wall type common in foraminifers and characterized by a dense, fine-grained calcite with a dull white luster. Resembles unglazed porcelain.

Porosity - The percentage of void (empty space), whether isolated or connected, in earth material such as soil or rock. For a classification of porosity types in carbonate rocks, see Choquette and Pray (1970).

Porphyritic - A textural term for the fabric of a sedimentary rock in which the crystals are of more than one size and in which larger crystals (porphyrotopes) are enclosed in a groundmass of smaller crystals: the term is restricted to carbonate rocks which have undergone neomorphism or are precipitates (Friedman, 1965).

Porphyroid neomorphism - A term introduced by Folk (1965) for aggrading neomorphism in which small crystals are converted to large ones by growth of a few large crystals in and replacing micritic matrix.

Primary porosity - Porosity formed during final sedimentation or present in the rock or sediment at the time of deposition. The term "primary porosity" includes all predepositional and depositional porosity of a particle, sediment, or rock. It also refers to any post-diagenetic remnant of primary pore space. (See Choquette and Pray, 1970, p. 249).

Prismatic microstructure - A wall structure common to the shells of a number of organisms and found in three varieties. **1. Normal prismatic** - consists of multiple single crystals of quadrangular or polygonal cross section, generally oriented with their long axis perpendicular or slightly inclined to the plane of the layer. This type can form in either aragonitic or calcitic shells and is especially common in molluscan shells. **2. Complex prismatic** - numerous units of quadrangular or polygonal cross section oriented as in normal prismatic shells. Found only in mollusks of either aragonitic or calcitic composition. Each unit, although it looks like a normal prism, consists of smaller crystals that radiate outward from the central axis. Transverse sections show a black extinction cross under crossed polars; longitudinal sections show a sweeping extinction as the stage is rotated. **3. Composite prismatic** - large units, each composed of small geometric prisms (normal or complex) radiating outward from a central axis. Generally oriented with the long dimension of the composite prism in the plane of the shell layer. Found only in mollusks of either aragonitic or calcitic composition.

Protodolomite - A crystalline calcium- magnesium carbonate with a disordered structure in which the two cations occur in the same

crystallographic layers instead of in alternate layers as in the dolomite mineral. The term is now rarely used.

Pseudomorph - A mineral whose outward crystal form is that of another mineral species; it has developed by alteration, substitution, encrustation, or paramorphism.

Pseudospar - A neomorphic (recrystallization) calcite fabric with average crystal size larger than 30-50 μm (Folk, 1965).

Radial-fibrous calcite - A descriptive term for a fabric of crystal fibers arranged with their long axes radiating from a center (opposite to tangential). Radial fibrous crystals also have unit extinction and straight twin planes. See also radiaxial-fibrous calcite and fascicular-optic fibrous calcite (Kendall, 1985).

Radiaxial-fibrous calcite - A cavity-filling calcite mosaic consisting of fibrous crystals (and subcrystals) radiating away from the initial growth surface and allied to optic axes that converge away from the wall. RFC is characterized by curved cleavages, undulose extinction and irregular intergranular boundaries which distinguish this fabric from simple radial-fibrous calcite. Must also be differentiated from fascicular-optic fibrous calcite (FOFC): RFC has twin planes that are concave upward relative to the substrate and extinction sweeps in the same direction as stage rotation; the opposite is true for FOFC. See Kendall (1985).

Rauhwacke - A German term (rauh = rough) for a carbonate rock characterized by cellular openings (pores that are largely unconnected or may be only partially connected). A fabric in which calcitic veins or partitions intervene between large pores. This fabric is commonly formed through the alteration (dissolution) of nodular evaporites in a carbonate matrix. Syn.: cellular limestone.

Recrystallization - The formation, essentially in the solid state, of new crystalline mineral grains in a rock. The new grains are generally larger than the original grains, and may have the same or a different mineralogical composition.

Replacement - In its general sense, the term refers to the transformation of one mineral to another — either a polymorph or a mineral of a different composition, In the strict, and more widely used, definition proposed by Folk (1965), the term refers to the replacement of a mineral by one of a different composition (e.g., silica or dolomite replacement of calcite).

Rhizoliths - Organosedimentary structures produced in roots by accumulation and/or cementation around, cementation within, or replacement of, higher plant roots by mineral matter (Klappa, 1980). Includes root casts, tubules, and molds as well as rhizocretions and root petrifications. Rhizoliths are typically millimeters to centimeters in diameter and centimeters to meters in length, occur just below hiatus surfaces, and may taper slightly. See Esteban and Klappa (1983).

Rhodoid (rhodolith) - An irregularly laminated calcareous nodule composed largely of encrusting coralline algae arranged in more or less concentric layers about a core; generally cream to pink, spheroidal but with a somewhat knobby surface, and up to several centimeters in diameter; forms in warm or cold, clear, shallow sea water down to depths of 150-200 m.

Rudstone - A textural type of coarse-grained limestone grain supported by fragmented constituents that are not organically bound and are mostly greater than 2 mm in diameter. See Embry and Klovan (1971).

Saccharoidal - A textural term, essentially synonymous with "sucrose," referring to a textural resemblance to common table sugar (see sucrose/sucrosic).

Saddle dolomite - A variety of dolomite that has a warped crystal lattice; it is characterized by curved crystal faces, curved cleavage, and sweeping extinction. Saddle dolomite is slightly enriched in calcium (typically 50-60 mol%) and, in many cases, iron (1-33 mol%). It occurs as either a cement or a replacement, is commonly associated with hydrothermal ore mineralization, sulfate-rich carbonates, and the presence of hydrocarbons. It has been interpreted to indicate formation through sulfate reduction at elevated temperatures (60-150° C). See Radke and Mathis (1980) and Folk and Assereto (1974). Syn.: baroque dolomite.

Sclerite - A hard, calcareous or chitinous plate, piece or spicule of any invertebrate. Commonly used for ossicles of holothurians and calcareous spicules in gorgonian octocorals.

Secondary porosity - A hard, calcareous or chitinous plate, piece or spicule of any invertebrate. Commonly used for ossicles of holothurians and calcareous spicules in gorgonian octocorals.

Septarian nodule - A hard, roughly spherical, diagenetic nodule or concretion formed of calcite, siderite, iron oxides, or other materials. The most distinctive characteristic is a complex network of intersecting radial and/or concentric fractures similar to shrinkage cracks. The fractures are typically filled with calcite cements, in many cases consisting of multiple generations of yellowish-brown to white, fibrous to bladed calcite. Syn.: septarium.

Shelter porosity - A type of primary interparticle porosity created by the sheltering effect of relatively large sedimentary particles which prevent the infilling of pore space beneath them by finer clastic particles. As shelter pores are commonly larger than most of the associated interparticle primary pores, they tend to be sites of preserved primary porosity in many rocks whose finer interparticle pores have been filled by cementation (Choquette and Pray, 1970, p. 249). (Syn: umbrella voids)

Shrinkage porosity - Porosity produced by sediment shrinkage. Drying commonly produces shrinkage porosity, but other processes can create contraction cracks (shrinkage porosity) in aqueous environments. Although most shrinkage porosity is a specialized type of fracture porosity, it can be formed by shrinkage of individual sedimentary particles (Schmidt, 1965; Choquette and Pray, 1970).

Siderite - A rhombohedral mineral of the calcite group: $FeCO_3$. It is isomorphous with magnesite and rhodochrosite, and commonly contains up to a few percent magnesium and manganese. Crystals usually are yellow-brown, brownish red, or brownish black, but sometimes can be white or gray; often found (impure) in beds or nodules in clays and calcareous shales, as a cement in sandstones, and as a directly precipitated deposit altered by iron oxides. Characterized in thin-section by flattened rhombs. A common early-diagenetic cement in areas of reducing, fresh to brackish pore fluids.

Single-crystal microstructure - A skeletal wall structure in which the shell layers or large segments of shell layers have the properties of a single crystal. A common feature of many echinoderms.

Siliciclastic - Pertaining to clastic noncarbonate rocks, or to sedimentary fragments of previous rocks, comprised dominantly of silicon-rich minerals such as quartz or feldspar.

Skeletal - Carbonate components (or the rocks they form) derived from hard material secreted directly by organisms. A substitute for the confusing term "organic" of some older literature.

Smear mount - A smear mount is a microscopic preparation in which individual grains (or thin pastes of muddy sediment) are spread or smeared across a glass slide. The material may be affixed with an adhesive or simply be allowed to dry. This preparation allows quick and inexpensive viewing of materials under the petrographic microscope and is especially valuable in examination of extremely small objects (such as coccoliths) that may be obscured by other material in standard (30 μm) thin sections.

Solution-collapse breccia - A collapse breccia formed where soluble material has been partly or wholly removed by dissolution, thereby

allowing the overlying rock to settle and become fragmented.

Solution-cavity fill - A phrase used by Folk (1965) to describe the process, common in carbonate rocks, where an unstable mineral is dissolved away, leaving a void space. After the passage of an indeterminate period of time, the void space is filled with a newly precipitated mineral that naturally contains no relict inclusions of the original material that once occupied the area.

Solution seam – A low-relief internal surface produced by subsurface pressure dissolution of soluble carbonate, typically marked by the presence of clays, organic matter or other insoluble material. Similar to stylolites but marked by lower relief and less obvious insoluble residue and generally occurring as closely spaced swarms of such dissolution surfaces. Syn. Horse-tail seam or microstylolite.

Spar - A common simplification of the term "sparry calcite."

Sparry calcite - A mosaic of calcite crystals, formed either as cement or by neomorphic processes, sufficiently coarsely crystalline to appear fairly transparent in thin section, as contrasted to dark, cloudy appearing carbonate mud or micrite (Folk, 1959, 1962). Commonly simply termed "spar."

Sparse – Refers to the scarcity of grains relative to muddy matrix — a situation in which allochems are sufficiently scarce so as to be separated from each other by carbonate mud and constitute less than 50% of the rock (Folk, 1959, 1962).

Spastolith - An ooid or other coated grain that has been deformed, generally by shearing the concentric laminations away from each other or from the nucleus.

Steinkern - A term derived from the German literature to describe the lithified internal sediment filling of a shell or articulated pair of shells (such as a bivalve), or the "fossil" generated by the subsequent dissolution of the shell mold and "liberation" of the lithified filling.

Strain recrystallization - Recrystallization in which a deformed mineral alters to a mosaic of undeformed crystals of the same mineral (e.g., strained to unstrained calcite). See Folk (1965).

Stromatactis - A cavity structure common in muddy carbonate sediments, typically 3 to 10 cm in diameter, characterized by a flat floor and an irregular roof. The floor of this former cavity typically is overlain by fine-grained internal sediment; the remaining void is filled with marine cement or later sparry cement. These poorly understood vugs have been attributed to the decay of unknown soft-bodied organisms, to gas formation in impermeable sediments, to gravity sliding and shear, to the alteration of sponges and sponge holdfasts, and to several other causes.

Stromatolite - An organosedimentary structure produced by sediment trapping, binding, and/or precipitation as a result of the growth and metabolic activity of microbial organisms, principally cyanophytes.

Stylolite - A jagged, columnar surface in carbonate rocks which may be at any orientation relative to bedding; produced by pressure-induced dissolution and grain interpenetration and often associated with large amounts of insoluble material accumulated as a result of such dissolution.

Subaerial - A term descriptive of location, of processes, or conditions operating in open air or immediately beneath land surfaces.

Subhedral - Descriptive of the shape of mineral crystals on which crystal faces are partially developed. Taken here to imply that a crystal is partly bounded by crystal faces.

Sucrosic/sucrose - Carbonate rocks that have appreciable intercrystal pore space and are composed dominantly of relatively equant, uniformly sized, euhedral to subhedral crystals that give the rock a "sugary" appearance. Most typically used to describe a dolomitized fabric.

Superficial ooid - An ooid (oolith) with an incomplete or very thin cortical coating; specifically one in which the thickness of the accretionary coating is less, commonly far less, than the radius of the nucleus.

Syndepositional - See "penecontemporaneous."

Syntaxial - Refers to overgrowths which are in optical continuity with their underlying grains such that the original crystal and the overgrowth form a single larger crystal, sharing the same crystallographic axes. Applied, for example, to overgrowths of calcite on echinoid grains (Bathurst, 1958). (Syn: optically continuous, epitaxial).

Telogenetic - Occurring in the time interval during which long-buried sediments or rocks are located near the surface again, as a result of crustal movement and erosion, and are influenced significantly by processes (e..g. karst development) associated with the formation of an unconformity (Choquette and Pray, 1970). Contrast with eogenetic and mesogenetic.

Terra rossa - A reddish-brown, residual soil found as a mantle over limestone bedrock. Also spelled "terra rosa."

Terrigenous - Derived from the land area and transported mechanically to the basin of deposition; commonly, essentially synonymous with "noncarbonate" (e.g. terrigenous sand vs. carbonate sand).

Test - An external shell of variable mineral composition and architecture secreted by invertebrates, especially protozoans of the order Foraminiferida.

Trabecular structure - A wall structure found in scleractinian corals in which a rod or column of radiating calcareous elements (fiber fascicles) forming a skeletal element in the structure of the septa and related parts of a coral wall. Also used for small skeletal elements in bryozoans, hexactinellid sponges, and holothurian sclerites.

Travertine - A relatively dense, banded deposit of $CaCO_3$ especially common in caverns and formed by the evaporation of spring or river water. (Pettijohn, 1957).

Tufa - A spongy, porous sedimentary rock (limestone or silica) deposited in or around springs, lakes and rivers from emerging ground waters charged with CO_2 and $CaCO_3$ or SiO_2, and thus typically of limited aerial extent. Commonly builds calcite deposits rich in algae and higher plant material. Tufa deposits can form around both cold- and hot-water springs. (Similar to travertine; calcareous tufa deposits are sometimes termed "calctufa").

Twinning - The development of a twin crystal (one with reversed or reflected crystal symmetry) by growth, transformation or gliding. A common feature in strained, unrecrystallized calcite crystals.

Umbrella void - A void (perhaps later filled with sparry calcite) produced by the presence of a large grain sheltering the underlying area by preventing infiltration of mud-sized grains. Also called shelter porosity.

Undulose (undulatory) extinction - A type of extinction of crystals under crossed polars that occurs successively in adjacent areas as the microscope stage is turned (Syn.: wavy extinction or sweeping extinction).

Unit extinction - A type of extinction behavior under crossed polars in which large segments of a fossil reach extinction at the same time as microscope stage is turned. Best exhibited by members of the Echinodermata, in which each shell segment (plate, spine, columnal, etc.) acts as a single crystal that extinguishes at the same time.

Vadoid - A coated grain (ooid or pisoid) that formed in a vadose setting. Vadoids include cave pearls, vadose soil or caliche pisolites, and coated grains from hot spring and travertine deposits (Peryt, 1983)

Vadose - Pertaining to that zone of partial or complete groundwater saturation subject to aeration and lying between the land surface and

the phreatic zone (above the groundwater table). That is, it is a zone in which both water and air may be present in pores.

Vadose diagenesis - Alteration, especially of carbonate strata, which occurs within the vadose zone. May be characterized by one or more specific fabrics such as karst topography, alveolar structure, soil glaebules, Microcodium, caliche, hardpan surfaces, pendant and meniscus cements, and others. (See Esteban and Klappa, 1983).

Vadose silt - A crystal silt, largely lacking clay-sized or sand-sized constituents as well as recognizable skeletal debris, deposited as internal sediment in voids within partially-cemented marine sediment. Interpreted by Dunham (1969) to be a product of vadose diagenesis during early emergence of marine carbonate sediments.

Vaterite - A rare hexagonal form of calcium carbonate. It is trimorphous with aragonite and calcite and is a relatively unstable form of $CaCO_3$. Although rare in nature, vaterite is a common artificial product in laboratory experiments.

Vug - A pore that is somewhat equant, is larger than 1/16 mm in diameter, and does not specifically conform in position, shape or boundary to particular fabric elements to the host rock (i.e., is not fabric selective). Generally formed by solution but the term is descriptive, not genetic (Choquette and Pray, 1970).

Wackestone - Carbonate rock composed of carbonate mud with over 10% allochems (grains) suspended in it (Dunham, 1962).

Zebra limestone - A limestone banded by parallel sheet cracks (generally filled with carbonate cement). Defined by Fischer (1964).

CITED REFERENCES

Archie, G. E., 1952, Classification of carbonate reservoir rocks and petrophysical considerations: American Association of Petroleum Geologists Bulletin, v. 36, p. 278-298.

Bathurst, R. G. C., 1958, Diagenetic fabrics in some British Dinantian limestones: Liverpool and Manchester Geological Journal, v. 2, p. 11-36.

Bathurst, R. G. C., 1964, The replacement of aragonite by calcite in the molluscan shell wall, *in* J. Imbrie, and N. D. Newell, eds., Approaches to Paleoecology: New York, John Wiley & Sons, p. 357-375.

Bathurst, R. G. C., 1971, The enfacial junction, *in* O. P. Bricker, ed., Carbonate Cements: Studies in Geology No. 19: Baltimore, MD, The Johns Hopkins Press, p. 296.

Bissell, H. J., and G. V. Chilingar, 1967, Classification of sedimentary carbonate rocks, *in* G. V. Chilingar, H. J. Bissell, and R. W. Fairbridge, eds., Carbonate Rocks — Origin, Occurrence and Classification: Developments in Sedimentology 9A: New York, Elsevier, p. 87-168.

Brewer, R., 1964, Fabric and Mineral Analysis of Soils: New York, Wiley, 470 p.

Choquette, P. W., and L. C. Pray, 1970, Geologic nomenclature and classification of porosity in sedimentary carbonates: American Association of Petroleum Geologists Bulletin, v. 54, p. 207-250.

Dunham, R. J., 1962, Classification of carbonate rocks according to their depositional texture, *in* W. E. Ham, ed., Classification of Carbonate Rocks: Tulsa, OK, American Association of Petroleum Geologists Memoir 1, p. 108-121.

Dunham, R. J., 1969, Vadose pisolite in the Capitan reef (Permian), New Mexico and Texas, *in* G. M. Friedman, ed., Depositional Environments in Carbonate Rocks: Tulsa, OK, SEPM Special Publication 14, p. 182-191.

Embry, A. F., and J. E. Klovan, 1971, A Late Devonian reef tract on northeastern Banks Island, N.W.T.: Bulletin of Canadian Petroleum Geology, v. 19, p. 730-781.

Esteban, M., and C. F. Klappa, 1983, Subaerial exposure environment, *in* P. A. Scholle, D. G. Bebout, and C. H. Moore, eds., Carbonate Depositional Environments: Tulsa, OK, American Association of Petroleum Geologists Memoir 33, p. 1-54.

Fischer, A. G., 1964, The Lofer cyclothems of the Alpine Triassic, *in* D. F. Merriam, ed., Symposium on Cyclic Sedimentation: Lawrence, KS, Kansas Geological Survey Bulletin 169, p. 107-149.)

Folk, R. L., 1959, Practical petrographic classification of limestones: American Association of Petroleum Geologists Bulletin, v. 43, p. 1-38.

Folk, R. L., 1962, Spectral subdivision of limestone types, *in* W. E. Ham, ed., Classification of Carbonate Rocks: Tulsa, OK, American Association of Petroleum Geologists Memoir 1, p. 62-84.

Folk, R. L., 1965, Some aspects of recrystallization in ancient limestones, *in* L. C. Pray, and R. S. Murray, eds., Dolomitization and Limestone Diagenesis: Tulsa, OK, SEPM Special Publication No. 13, p. 14-48.

Folk, R. L., and R. Assereto, 1974, Giant aragonite rays and baroque white dolomite in tepee-fillings, Triassic of Lombardy, Italy: American Association of Petroleum Geologists and Society of Economic Paleontologists and Mineralogists, Annual Meeting Abstracts, v. 1, p. 34-35.

Friedman, G. M., 1965, Terminology of crystallization textures and fabrics in sedimentary rocks: Journal of Sedimentary Petrology, v. 35, p. 643-655.

Grabau, A. W., 1904, On the classification of sedimentary rocks: American Geologist, v. 33, p. 228-247.

Holmes, A., 1928, The Nomenclature of Petrology [2nd Edition]: London, Thomas Murby, 284 p.

Illing, L. V., 1954, Bahaman calcareous sands: American Association of Petroleum Geologists Bulletin, v. 38, p. 1-95.

James, N. P., 1997, The cool-water carbonate depositional realm, *in* N. P. James, and A. D. Clarke, eds., Cool-Water Carbonates: Tulsa, OK, SEPM Special Publication No. 56, p. 1-20.

Kay, G. M., 1951, North American geosynclines: New York, Geological Society of America (GSA) Memoir 48, 143 p.

Kendall, A. C., 1977, Fascicular-optic calcite: a replacement of bundled acicular carbonate cements: Journal of Sedimentary Petrology, v. 47, p. 1056-1062.

Kendall, A. C., 1985, Radiaxial fibrous calcite: a reappraisal, *in* N. Schneidermann, and P. M. Harris, eds., Carbonate Cements: Tulsa, OK, SEPM Special Publication No. 36, p. 59-77.

Klappa, C. F., 1980, Rhizoliths in terrestrial carbonates: classification, recognition, genesis and significance: Sedimentology, v. 27, p. 613-629.

Lees, A., and A. T. Buller, 1972, Modern temperate-water and warm-water shelf carbonate sediments contrasted: Marine Geology, v. 13, p. M67-M73.

McKee, E. D., and R. C. Gutschick, 1969, History of the Redwall Limestone of northern Arizona: Boulder, CO, Geological Society of America Memoir 114, 726 p.

Muskat, M., 1949, Physical Principles of Oil Production: New York, McGraw-Hill, 922 p.

Peryt, T. M., 1981, Phanerozoic oncoids — an overview: Facies, v. 4, p. 197-214.

Peryt, T. M., 1983, Classification of coated grains, *in* T. M. Peryt, ed., Coated Grains: New York, Springer-Verlag, p. 3-6.

Pettijohn, F. J., 1957, Sedimentary Rocks (Second Edition): New York, Harper Brothers, 718 p.

Pray, L. C., and J. L. Wray, 1963, Porous algal facies (Pennsylvanian) Honaker Trail, San Juan Canyon, Utah, *in* R. O. Bass, and S. L. Sharps, eds., Shelf Carbonates, Paradox Basin (4th Field Conference Guidebook): Durango, Four Corners Geological Society, p. 204-234.

Radke, B. M., and R. L. Mathis, 1980, On the formation and occurrence of saddle dolomite: Journal of Sedimentary Petrology, v. 50, p. 1149-1168.

Sander, B. K., 1951, Contributions to the study of depositional fabrics - rhythmically deposited Triassic limestones and dolomites [translated from 1936 original by E.B. Knopf]: Tulsa, OK, American Association of Petroleum Geologists, 207 p.

Schmidt, V., 1965, Facies, diagenesis, and related reservoir properties in the Gigas Beds (Upper Jurassic), northwestern Germany, *in* L. C. Pray, and R. C. Murray, eds., Dolomitization and Limestone Diagenesis; a Symposium: Tulsa, OK, SEPM Special Publication No. 13, p. 124-168.

Swineford, A., A. B. Leonard, and J. C. Frye, 1958, Petrology of the Pliocene pisolitic limestone in the Great Plains: Lawrence, KS, Kansas Geological Survey Bulletin 130, Part 2, p. 97-116.